Functionalization of Thiosemicarbazones for Biomedical Applications



Doctoral thesis

for

the award of the doctoral degree

of the Faculty of Mathematics and Natural Sciences

of the University of Cologne

submitted by

Johannes Hohnsen

accepted in the year 2026

Abstract

Thiosemicarbazones (TSCs) are organosulfur compounds which are frequently investigated as multidentate ligands in coordination chemistry. The huge interest in these compounds is based on their biological activity which includes antimicrobial and antitumor properties. Especially the latter are often of interest since several TSCs have entered clinical trails in the past. However, most of the compounds have a limited selectivity and water solubility, which needs further optimization.

During this research a total of 83 new TSCs and 24 metal complexes (Cu(II), Pt(II) and Fe(III)) have been synthesized, whereby the *N*1 and *N*4 positions were functionalized. In addition, many new isothiocyanates and thiosemicarbazides have been synthesized. Beside this investigation of the ligand design, the idea of this work was to investigate concepts for improving the medical performance of TSCs: 1) by their conjugation to nanoparticles and 2) biomolecules, 3) their labeling with fluorescence markers, 4) their design towards amphiphilic structures, 5) increasing their coordination sphere to hexadentate ligands and 6) tuning the Fe(II)/(III) redox potential of α-pyridyl TSC as well as their conjugation to TiO_2 nanoparticles.

To synthesize TSC nanoconjugates, functional groups (amine, thiol, azide, alkyne, phosphonate, diol and isothiocyanates) have been attached to the *N*4 position and the TSCs were investigated by NMR, UV/Vis absorption and emission spectroscopy. Their cytotoxicity against HepG2 and HCT-116 was investigated, where Dipy(TSC)PhNCS, Dipy(TSC)PhNH$_2$ and Dipy(TSC)PhPO(OEt)$_2$ showed a significant inhibition. Their conjugation to SiO_2 and TiO_2 nanoparticles was investigated at some selected examples and investigated by UV/Vis absorption and FTIR spectroscopy as well as zeta, DLS and EDX measurements, which confirmed successful conjugation.

To investigate the application of TSCs in bioconjugation, TSCs derived from amino acids, glucose and cyclohexanol have been synthesized and characterized. The cytotoxicity of the amino acid derived TSCs was investigated against HT-29 and HFF1. The compounds showed a high toxicity, whereby the tumor cells were more affected than the healthy control. In addition, a time dependance of their toxicity was found. As an example of bioconjugation, Dipy(TSC)Val was successfully conjugated to the cell penetrating peptide sC18*.

Anthracene, carbazole, pyrene, fluorene and coumarin have been introduced at the *N*4 position of dipyridyl ketone TSCs as a fluorescence tag and their Pt(II) complexes have been synthesized and characterized. The ligands showed typical fluorescence of the chromophores which occurred in a range of 390-440 nm, and which was blue shifted for the Pt(II) complexes. Most of the Pt(II) complexes showed a second emission at longer wavelength which was attributed to the TSC function and related to its deprotonation and rigidification by metal complexation. The cytotoxicity of the Pt(II) complexes was investigated against A549, MDA-MB-321, MCF-7 and HT-29. [Pt(Dipy(TSC)Pyr)Cl] showed the highest toxicity in this series which was increased compared to cisplatin. [Pt(Dipy(TSC)Cbz)Cl] showed a selective toxicity against MDA-MB-32.

The synthesis of amphiphilic TSCs was investigated by introducing lipophilic groups at the *N*4 position (octyl, dodecyl, hexadecyl, cholesterol), while the *N*1 position was mostly functionalized with hydrophilic ketones (di(2-pyridyl)ketone, 2,5-dihydroxybenzaldehyde, 2,3,4-trimethoxybenzaldehyde and butane-2,3-dione). In addition, Pt(II) and Cu(II) complexes of the corresponding dipyridyl and bis-TSC were synthesized and characterized. Solubility studies in pentane, toluene, MeOH and H_2O showed that most of the compounds were soluble in polar (MeOH) and nonpolar solvents (toluene, pentane) but insoluble in H_2O. The solubility of the metal complexes was usually decreased compared to the ligands. The compounds showed a negative solvatochromism, which was investigated by UV/Vis absorption spectroscopy. In the last step, the cytotoxicity of the compounds was investigated against HepG2, HCT-116 and HEK-293. Dipy(TSC)Oct showed a high inhibition, which was reduced after the complexation of Pt(II) and Cu(II).

Hexadentate TSCs with bpy, phen, dppz, naph, DTT, tpy and pyphpy in their structure have been successfully synthesized and characterized by HR-ESI-MS, NMR spectroscopy and UV/Vis absorption and emission spectroscopy. Dppz(TSC)Ala*t*Bu, DTT(TSC)Ala*t*Bu, Phen(TSC)Ala*t*Bu and Naph(TSC)Ala*t*Bu showed a characteristic fluorescence assigned to their heterocyclic backbone. Their metal complexation was not discussed in this research.

α-Pyridyl TSCs with electron donating or withdrawing substituents (Me, *t*Bu, Ph, Py, COOMePh, CF_3Ph, OMePh, NO_2Ph) at the *N*1 position as well as their corresponding Fe(III) complexes have been successfully synthesized and characterized. It was found that the substituents significantly affect the Fe(II)/(III) redox potential, which is cathodically shifted for electron donating groups. In this way, [Fe(*t*BuPy(TSC)H_2)$_2$]ClO_4 showed the most negative potential (–0.63 V) and [Fe(NO_2PhPy(TSC)H_2)$_2$]ClO_4 the most positive potential (–0.40 V). After that, [Fe(Dipy(TSC)PhPO(OH)$_2$] was synthesized as well as [Ru(bipy)$_2$(bipy(PO(OH)$_2$)$_2$] as a photosensitizer and their conjugation on TiO_2 nanoparticles was investigated by UV/Vis absorption spectroscopy, FTIR spectroscopy and EDX measurements.

Table of content

1. State of Knowledge 1

1.1 Properties and synthesis of thiosemicarbazones and their metal complexes 1

1.2 Applications of thiosemicarbazones 3

1.3 Thiosemicarbazones for cancer treatment 5

1.4 α-Pyridyl TSCs in cancer therapy 5

1.5 α-Pyridyl TSCs – Examples and structure activity relationships 8

1.6 Strategies to improve the pharmacological potential of thiosemicarbazones 11

1.7 Nanoconjugation 11

1.7.1 Nanoparticles (NPs) and their functionalization 11

1.7.2 Nanoparticles for medical applications and drug transport and release 13

1.7.3 Thiosemicarbazones in nanochemistry 16

1.8 TSC-functionalization of TiO_2 NPs for photocatalytic applications 18

1.9 Bioconjugation 19

1.9.1 Drug delivery by bioconjugates 19

1.9.2 TSC-Bioconjugates 21

1.10 Fluorescence labeling 22

1.10.1 Fluorescence labeling for medical applications 22

1.10.2 Fluorescent thiosemicarbazones 23

1.11 Amphiphilic drugs 25

1.11.1 Amphiphilic metal complexes and their advantages in medicine 25

1.11.2 Amphiphilic thiosemicarbazones 26

1.12 Hexadentate Thiosemicarbazones and their complexes 26

2. Aims and concept 28

2.1 Conjugation of TSCs to nanoparticles for drug delivery 28

2.2 Conjugation of TSCs to biomolecules for drug delivery 29

2.3 Tuning the Fe(II)/(III) redox potential of α-pyridyl TSC Fe complexes and their immobilization onto TiO_2 NPs 30

2.4 Fluorescence labeling of TSCs 30

2.5 Synthesis of amphiphilic TSCs 31

2.6 Synthesis of hexadentate TSCs 32

3. Results and Discussion 33

3.1 Thiosemicarbazones for the covalent conjugation to nanoparticles 33

3.1.1 Synthesis of TSCs with functional groups at the *N*4 position 33
3.1.1.1 Synthesis of TSCs from primary amines 33
3.1.1.2 Synthesis of TSCs with isothiocyanate function 34
3.1.1.3 Synthesis of TSCs with thiol function 35
3.1.1.4 Synthesis of TSCs with alkyne function 35
3.1.1.5 Synthesis of TSCs with an azide function 36
3.1.1.6 Synthesis of TSCs with phosphonate function 37
3.1.1.7 Synthesis of TSCs with a catechol function 38
3.1.1.8 Unsuccessful attempts 38
3.1.2 Photophysical properties of *N*4 functionalized TSCs with functional groups 39
3.1.3 Cytotoxicity of *N*4 functionalized TSCs with functional groups 42
3.1.4 Conjugation of TSCs to nanoparticles 43
3.1.4.1 Molecular test reaction 44
3.1.4.2 Functionalization of SiO_2 nanoparticles with Dipy(TSC)PhNCS 49
3.1.4.3 Crosslinking of thiosemicarbazides to SiO_2 nanoparticles by glutaraldehyde 52
3.1.4.4 Functionalization of TiO_2 nanoparticles with TSCs having phosphonate anchor 54
3.1.5 Summary – TSCs for nanoconjugation 58
3.2 Tuning the Fe(II)/(III) redox potential of α-pyridyl TSC iron complexes and their conjugation to TiO_2 nanoparticles 59
3.2.1 Synthesis of α-pyridyl TSC iron complexes 59
3.2.1.1 α-pyridyl ketones 59
3.2.1.2 α-Pyridyl TSCs 60
3.2.1.3 α-Pyridyl TSC Fe(III) complexes 61
3.2.2 NMR studies of α-Pyridyl TSCs 62
3.2.3 UV/Vis absorption spectroscopy of α-Pyridyl TSCs and their iron complexes 63
3.2.4 Cyclovoltammetry of α-Pyridyl TSCs and their iron complexes 65
3.2.5 Functionalization of TiO_2 nanoparticles 70
3.2.6 Summary - α-pyridyl TSCs Fe(III) complexes and their conjugation to TiO_2 76
3.3 Thiosemicarbazones for the covalent conjugation to biomolecules 77
3.3.1 Synthesis of TSC for bioconjugation 77
3.3.1.1 Synthesis of TSCs derived from amino acids 77
3.3.1.2 Synthesis of TSCs derived sugars or analogues 79
3.3.2 UV/Vis absorption and photoluminescence spectroscopy 79

3.3.3 Cytotoxicity studies of glucose and cyclohexanol derived TSCs 81
3.3.4 Cytotoxicity studies of amino acid derived TSCs 81
3.3.5 Conjugation of Dipy(TSC)Val to sC18* 85
3.3.6 Summary – TSCs for bioconjugation 87
3.4 Fluorophore-tagged thiosemicarbazones and their Pt(II) complexes 88
3.4.1 Synthesis of fluorophore-tagged TSCs and their Pt(II) complexes 88
3.4.2 UV/Vis absorption and photoluminescnce spectroscopy of the tagged TSCs and their Pt(II) complexes 92
3.4.3 Cyclovoltammetry of the tagged TSCs and their Pt(II) complexes 96
3.4.4 Spectroelectrochemical measurements of the Pt(II) complexes of tagged TSCs 100
3.4.5 Cytotoxicity studies of tagged TSC Pt(II) complexes 102
4.4.6 Summary – tagged TSCs 103
3.5 TSCs with potential amphiphilic character and their Pt(II) and Cu(II) complexes 104
3.5.1 Synthesis of TSCs with lipophilic and hydrophilic groups 106
3.5.2 UV/Vis absorption spectroscopy of amphiphilic TSCs and their metal complexes 108
3.5.3 Cyclic voltammetry of amphiphilic TSCs and their metal complexes 111
3.5.4 Cytotoxicity of amphiphilic TSCs 113
3.5.5 Summary – Amphiphilic TSCs 114
3.6 Hexadentate bis-TSCs 115
3.6.1 Synthesis of hexadentate TSCs 115
3.6.2 UV/Vis absorption and emission spectroscopy of hexadentate TSCs 118
3.6.3 Summary – Hexadentate bis-TSCs 120
4. Summary and Outlook 121
5. Experimental part 127
5.1. Materials and Solvents 127
5.2. Methods 127
5.3 Synthesis 131
5.3.1 Synthesis of TSCs derived from amino acids 131
5.3.1.1 Synthesis of amino acid *tert*-butyl esters – general description 131
5.3.1.2 Synthesis of isothiocyanates – general description 132
5.3.1.3 Synthesis of thiosemicarbazides – general description 133
5.3.1.4 Synthesis of TSCs – general description 135
5.3.1.5 Transesterfication of di-2-pyridylketone TSC to methyl esters 139

5.3.1.6 Synthesis of 2-(1-[Bis(2-pyridyl)methylene]thiosemicarbazido)-3-methylbutyric acid 140
5.3.2 Synthesis of TSCs derived from diamines 140
5.3.2.1 Synthesis of mono-BOC-protected diamines 140
5.3.2.2 Synthesis of isothiocyanates – general description 141
5.3.2.3 Synthesis of thiosemicarbazides – general description 142
5.3.2.4 Synthesis of TSCs – general description 143
5.3.2.5 Deprotection of the TSCs with phenyl spacer 145
5.3.2.6 Conjugation of amino TSCs with isocyanates 146
5.3.2.7 Synthesis of TSCs with isothiocyanate function 146
5.3.2.8 Conjugation of isothiocyanate TSCs with amines 147
5.3.3 TSCs derived from acetobromo-α-D-glucose 147
5.3.3.1 Synthesis of β-D-glucopyranosyl isothiocyanate 147
5.3.3.2 Synthesis of *N*-(2,3,4,6-tetra-*O*-acetyl-β-D-glucopyranosyl)hydrazinecarbothioamide 147
5.3.3.3 Synthesis of TSCs – general description 148
5.3.4 Syntheses of TSCs derived from *trans*-4-hydroxycyclohexanol 149
5.3.4.1 Synthesis of *trans*-4-hydroxycyclohexyl isothiocyanate 149
5.3.4.2 Synthesis of 4-(trans-4-hydroxycyclohexyl)-thiosemicarbazide 149
5.3.4.3 Synthesis of TSCs – general description 149
5.3.5 TSCs derived from dopamine 150
5.3.5.1 Synthesis of 4-(2-isothiocyanatoethyl)benzene-1,2-diol 150
5.3.5.2 Synthesis of 4-[2-(hydrazidecarbothioamino)ethyl]benzene-1,2-diol 151
5.3.5.3 Synthesis of TSCs derived from dopamine 151
5.3.6 Synthesis of TSCs derived from amino thiols 152
5.3.6.1 Synthesis of 2-benzylsulfanyl ethylamine 152
5.3.6.2 Synthesis of 2-benzylsulfanylethyl isothiocyanate 152
5.3.6.3 Synthesis of 4-(2-benzylsulfanylethyl)thiosemicarbazide 152
5.3.6.4 Synthesis of TSCs – general description 153
5.3.7 Syntheses of TSCs with alkyne function 154
5.3.7.1 Synthesis of 4-[(trimethylsilyl)ethynyl]aniline 154
5.3.7.2 Synthesis of 4-[(trimethylsilyl)ethynyl] phenyl isothiocyanate 154
5.3.7.3 Synthesis of *N*-hydrazidecarbothio[4-(trimethylsilyl)ethynylphenyl]amine 154
5.3.7.4 Synthesis of TSCs – general description 155

5.3.7.5 Deprotection of the TMS group 156
5.3.7.6 Platinum complexes of the alkyne TSCs 157
5.3.8 Syntheses of TSCs with azide function 158
5.3.8.1 Synthesis of 4-(aminomethyl)benzyl alcohol 158
5.3.8.2 Synthesis of 4-(bromomethyl)benzylamine hydrobromide 158
5.3.8.3 Synthesis of 4-(azidomethyl)benzylamine 158
5.3.8.4 Synthesis of 1-(azidomethyl)-4-(isothiocyanatomethyl)benzene 158
5.3.8.5 Synthesis of 4-([*p*-(azidomethyl)phenyl]methyl)thiosemicarbazide 159
5.3.8.6 Synthesis of TSCs – general description 159
5.3.9 Synthesis of TSCs with phosphonate function 160
5.3.9.1 Synthesis of diethyl(4-nitrophenyl)phosphonate 160
5.3.9.2 Synthesis of diethyl(4-aminophenyl)phosphonate 160
5.3.9.3 Synthesis of diethyl (4-isothiocyanatophenyl)phosphonate 161
5.3.9.4 Synthesis of diethyl [4-(hydrazidecarbothioamino)phenyl] phosphonate 161
5.3.9.5 Synthesis of TSCs – general description 161
5.3.9.6 Deprotection of TSCs with phosphonate group – general description 162
5.3.9.7 Synthesis of $[Fe(Dipy(TSC)PhPO(OH)_2)_2]ClO_4$ 163
5.3.10 Synthesis of the $[Ru(bpy)_3]$ photosensitizer 163
5.3.10.1 Synthesis of di(diethylphosphonate)bispyridine 163
5.3.10.2 Synthesis of *cis*-dichlorobis(bipyridine)ruthenium(II) 163
5.3.10.3 Synthesis of Tribis(bipyridine)ruthenium(II)di(diethyl)phosphonate 164
5.3.10.4 Synthesis of Tribis(bipyridine)ruthenium(II)diphosphonate 164
5.3.11 Functionalization of nanoparticles with TSCs 164
5.3.11.1 Anchoring the TSC with phosphonate function on TiO_2 NPs 164
5.3.11.2 Anchoring $[Fe(Dipy(TSC)PhPO(OH)_2)_2]ClO_4$ on TiO_2 NPs 165
5.3.11.3 Anchoring tribis(bipyridine)ruthenium(II)diphosphonate on TiO_2 NPs 165
5.3.11.4 Synthesis of TiO_2@$[Fe(TSC)_2]$/$[Ru(bpy)_3]$ 165
5.3.11.5 Synthesis of SiO_2@APTMS 166
5.3.11.6 Synthesis of SiO_2@APTMS@Dipy(TSC)PhNCS 166
5.3.11.7 Synthesis of SiO_2@APTMS@GA 166
5.3.11.8 Synthesis of SiO_2@APTMS@GA@AntThio 166
5.3.12 Synthesis of TSCs with fluorophores 167
5.3.12.1 Synthesis of the amino precursors 167
5.3.12.2 Synthesis of the isothiocyanates with fluorophores 173

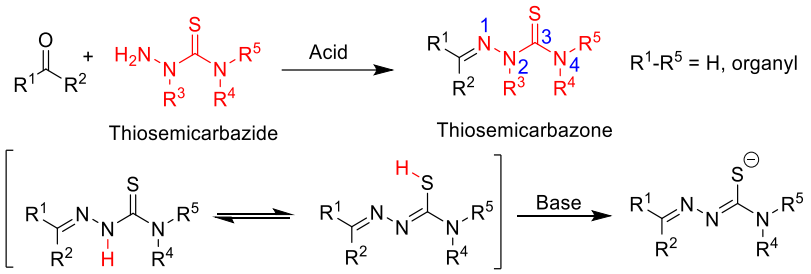
5.3.12.3 Synthesis of the thiosemicarbazides with fluorophores – general description 175
5.3.12.4 Synthesis of the dipyridyl ketone TSCs with fluorophores – general description 177
5.3.12.5 Synthesis of Pt(II) complexes with TSCs with fluorophores – general description 178
5.3.13 Synthesis of hexadentate bis-TSCs 179
5.3.13.1 Synthesis of the dialdehyde precursors 179
5.3.13.2 Synthesis of hexadentate bis-TSCs 184
5.3.13.3 Synthesis of Dipy(TSC)Tpy and Ant(TSC)Tpy 188
5.3.14 Synthesis of amphiphilic TSCs 191
5.3.14.1 Synthesis of cholesterol derived TSCs 191
5.3.14.2 Synthesis of octyl, dodecyl and hexadecyl isothiocyanates 193
5.3.14.3 Synthesis of octyl, dodecyl and hexadecyl thiosemicarbazides – general procedure 194
5.3.14.4 Synthesis of dipyridyl ketone TSCs – general procedure 195
5.3.14.5 Synthesis of 2,3,4-trimethoxybenzaldehyde TSCs – general procedure 195
5.3.14.6 Synthesis of 2,3-butadione bis-TSCs – general procedure 196
5.3.14.7 Synthesis of 2,5-dihydroxybenzaldehyde TSCs – general procedure 197
5.3.14.8 Synthesis of Pt(II) and Cu(II) bis-TSC complexes 198
5.3.14.9 Synthesis of Pt(II) and Cu(II) dipyridyl ketone TSC complexes 199
5.3.15 Synthesis of pyridyl ketones and their corresponding TSCs and their Fe(III) complexes 200
5.3.15.1 Synthesis of pyridyl ketones 200
5.3.15.2 Synthesis of TSCs – general approach 204
5.3.15.3 Synthesis of the TSC Fe(III) complexes – general description 206
6. Literature 209
7. Supporting Information 222
7.1 NMR Data 222
7.1.1 NMR data TSCs with functional groups at the *N*4 position 222
7.1.2 NMR data of the Ru(II) photosensitizer 333
7.1.3 NMR data of the tagged TSCs and their Pt(II) complexes 334
7.1.4 NMR data of hexadentate TSCs 368
7.1.5 NMR data of α-pyridyl TSCs 396
7.1.6 NMR data of amphiphile TSCs 405

7.2 High resolution electron spray ionization mass spectrometry (HR-ESI-MS) _____ 431
7.2.1 HR-ESI-MS of TSCs with functional groups at the *N*4 position _____ 431
7.2.2 HR-ESI-MS of hexadentate TSCs _____ 446
7.2.3 HR-ESI-MS of α-pyridyl TSCs and their Fe(III) complexes _____ 448
7.2.4 HR-ESI-MS of tagged TSCs _____ 453
7.2.5 HR-ESI-MS of amphiphilic TSCs _____ 457
7.3 UV/Vis absorption spectroscopy _____ 464
7.3.1 UV/Vis absorption spectra of *N*4 functionalized TSC with anchor groups for nano - and bioconjugation _____ 464
7.3.2 UV/Vis absorption spectra of amphiphilic TSCs _____ 465
7.3.3 UV/Vis absorption spectrum of tagged TSCs _____ 469
7.3.4 UV/Vis absorption spectra of α-pyridyl TSCs and their Fe(III) complexes _____ 470
7.3.5 UV/Vis absorption spectra of hexadentate TSCs _____ 471
7.4 Emission spectroscopy _____ 471
7.4.1 UV/Vis emission spectroscopy of *N*4 functionalized TSC for nano -and bioconjugation _____ 471
7.4.2 UV/Vis emission spectroscopy of tagged TSCs _____ 472
7.4.3 UV/Vis emission spectroscopy of hexadentate TSCs _____ 474
7.5 Cyclic voltammetry (CV) _____ 475
7.5.1 CV of α-pyridyl TSCs and their Fe(III) complexes _____ 475
7.5.2 CV of tagged TSCs and their Pt(II) complexes _____ 478
7.5.3 CV of amphiphilic TSCs _____ 482
7.6 DLS/Zeta potential measurements _____ 482
7.7 EDX/SEM measurements _____ 485

1. State of Knowledge

1.1 Properties and synthesis of thiosemicarbazones and their metal complexes

Thiosemicarbazones (TSCs) are hydrazine derived thioureas which are formed by an acid catalyzed condensation reaction of thiosemicarbazides with ketones or aldehydes (Scheme 1).[1,2] They are closely related to semicarbazones and selenosemicarbazones which are their oxygen and selenium analogues.[3-5] Depending on the pH and the functional groups attached to the *N*1, *N*2, and *N*4 position, tautomerism is observed in solution, if R^3 or R^4 = H.[5-9] The acidity of this proton and thus the thiol/thione equilibrium is influenced by residues R^1, R^2, and R^5. The addition of a base leads to the deprotonation of the hydrazone and a thiolate is formed.[7]



Scheme 1. Synthesis of TSCs by condensation of thiosemicarbazides with ketones/aldehydes (top) and their thiol/thione tautomerism (bottom).

TSCs can be considered as *Schiff bases* due to the azomethine group within the structure which is an important class of ligands in coordination chemistry.[10] In this way, TSCs have at least two donor functions namely the azomethine and the thione group.[7] With respect to the HSAB concept (hard and soft acids and bases), the combination of a soft (sulfur) and a hard (nitrogen) donor atom in the same ligand makes them suitable for the complexation of various metals from the p-, d-, or f-block.[7,11-16] TSCs can act as neutral ligands with a thione donor (Chart 1, Compound **1**) or as anionic ligands with a thiolate donor (Compound **2**).[7,17,18] Frequently, a bidentate (N^S) coordination is observed.[7,17,18] However, there are also some unusual examples of other coordination modes found in literature (Compounds **3–6)**.[19-22]

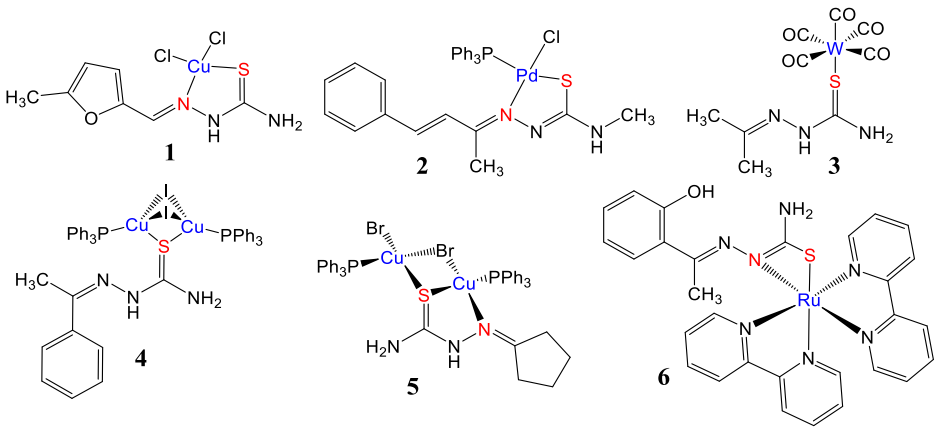


Chart 1. Different binding modes of TSCs at examples from literature. Adopted from Ref. [17-22].

Furthermore, the coordination sphere of TSCs can be extended with additional donor groups by functionalizing the *N*1 position with suitable substituents. In this way, TSCs with C^N^S (**7**), N^N^S (**8**) O^N^S (**9**), S^N^S (**10**), or P^N^S (**11**) donor sets have been reported (Chart 2, Compounds **7–11**).[23-27]

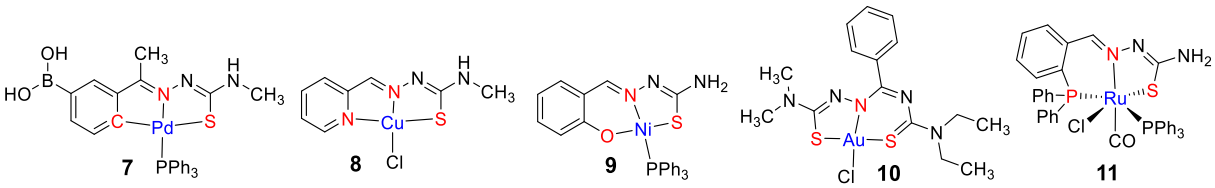


Chart 2. Examples of tridentate TSCs and their metal complexes with different sets of donor atoms. Adopted from Ref. [23-27].

The coordination sphere can be also increased to tetra- (**12**, **13**), penta- (**14**), or hexadentate (**15**) ligands (Chart 3).[28-32] Especially for the synthesis of large coordination spheres, bis-thiosemicarbazones (bis-TSCs), which are obtained from the reaction of dialdehydes/diketones with two equivalents of the thiosemicarbazide, are a good choice.[29,30]

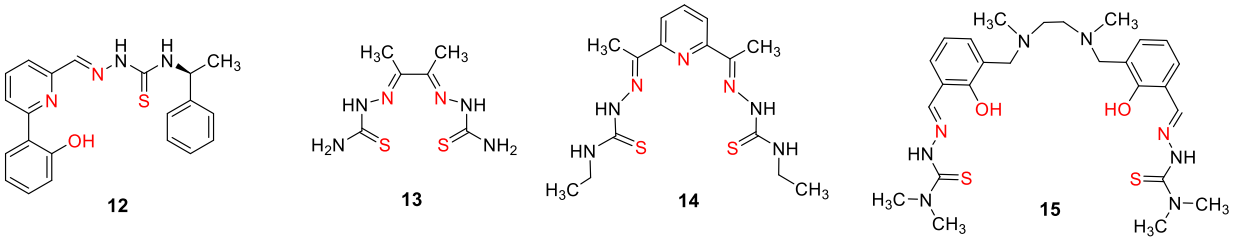
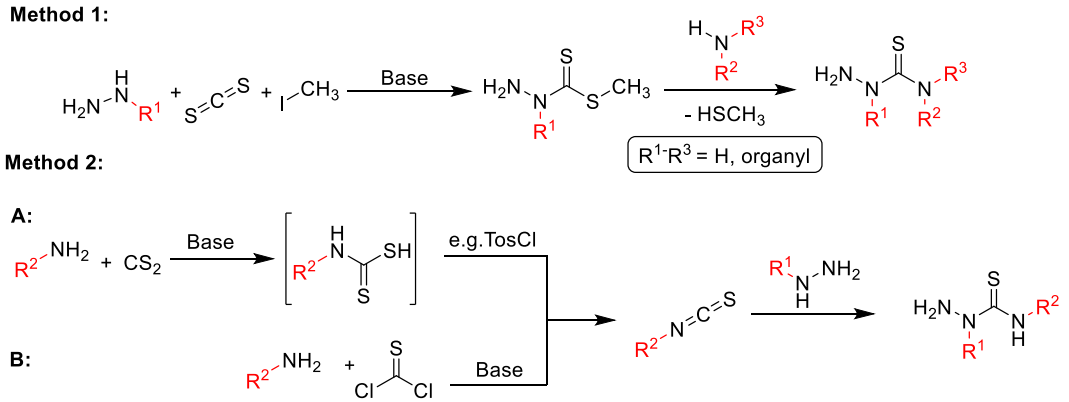


Chart 3. Examples of tetra-, penta-, and hexadentate TSCs from the literature. Adopted from Ref. [28-32].

An interesting aspect of TSCs is their modular synthesis which offers the opportunity to introduce functional groups at the *N*1, *N*2, and *N*4 positions.[33-37] The most frequently used position for derivatization is the *N*1 position where numerous commercially or synthetically available ketones and aldehydes can be introduced through condensation with thiosemicarbazides (Scheme 1, top).[32,34,38-40] Functional groups at the *N*2 and *N*4 position can be introduced during the synthesis of the thiosemicarbazide.[41] Two different methods are available for this purpose (Scheme 2). The first one starts with the reaction of a hydrazine derivative with CS_2 and CH_3I yielding a *S*-methyl dithiocarbazate (Scheme 1, Method 1).[2,42,43] In a second step, the *S*-methyl group is substituted with primary or secondary amines yielding the thiosemicarbazide. In this way, the *N*2 and *N*4 position of TSCs can be functionalized just by choosing different derivatives of hydrazine or amines. However, there might be limitations concerning the substrate scope.[2]



Scheme 2. Synthesis of thiosemicarbazides. Method 1 starts with hydrazine derivatives and Method 2 with primary amines.

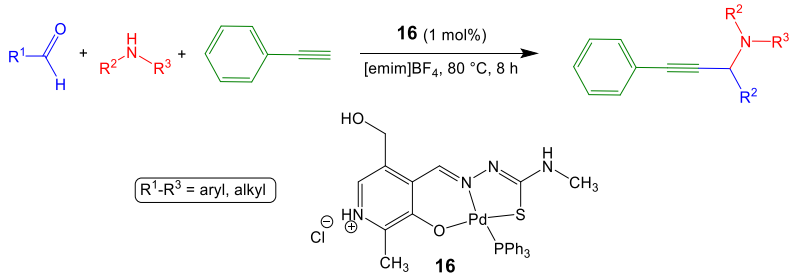
The second method starts with a primary amine which is converted to an isothiocyanate either by the reaction with thiophosgene (Scheme 2, Method 2A) or CS_2 (Scheme 2, 2B) under basic conditions.[44-47] In the case of the latter, a dithiocarbazate is formed as an intermediate, which must be decomposed to the isothiocyanate. This can be achieved by the addition of a desulfurization reagent like tosyl chloride (TosCl), NaClO, H_2O_2, or $POCl_3$.[47] Method 2A has the advantage that high yields can be achieved, due

to the high reactivity of thiophosgene. However, this high reactivity can also lead to side reactions and a high toxicity.[46,47] Especially nucleophilic groups, heterocycles and other functional groups neighboring the amine are usually not tolerated.[46] Method 2B has the advantage that CS_2 is less reactive. However, depending on the kind of used desulfurization reagent, side reactions are also possible. In addition, reaction yields can be poor depending on the nucleophilicity of the primary amine.[47] In the next step, the isothiocyanates are reacted with hydrazine derivatives yielding the thiosemicarbazide.[48] Method 2 offers the opportunity to functionalize the *N*2 and *N*4 position. However, the *N*4 position can be only monosubstituted (Scheme 2).

1.2 Applications of thiosemicarbazones

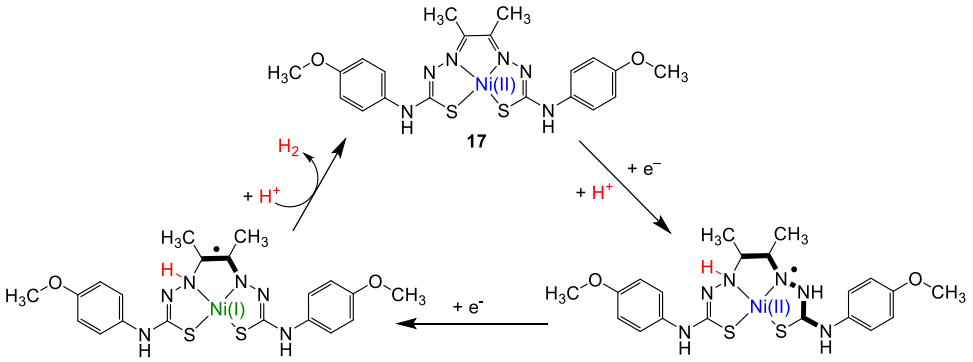
The huge number of possible functionalizations and the versatile coordination chemistry of TSCs have led to many applications, especially in bio-medical applications, but also in catalysis and metal sensing or metal recovery.[38,49,50]

TSC complexes of Pd(II), Ni(II), Ru(II) and Cu(II) have been used in catalysis for C–C and C–N type coupling reactions (e.g. *Heck*, *Suzuki*, *Sonogashira*, *Kumada*, *Buchwald-Hartwig* and other related reactions).[49,51-54] For example, the TSC Pd(II) complex **16** (Scheme 3) was used as a catalyst for the synthesis of propargylamines by a three-component coupling of aldehydes, amines and phenylacetylene.[55] The authors used the ionic liquid [emim]BF_4 (1-ethyl-3-methylimidazolium tetrafluoroborate) as the reaction medium and 1 mol% of the catalyst with yields of 81–96% for a large substrate scope. An interesting aspect of this catalyst is its reusability since the reaction products can be separated by extraction with Et_2O, while the catalyst stays in the ionic liquid, which can be reused after drying without any loss of efficiency.[55]



Scheme 3. Catalytic synthesis of propargyl amines using TSC Pd complex **16**. Adopted from Ref. [55].

Some TSC complexes of Ni(II) and Co(II) have been found to be efficient catalysts for H_2 evolution.[56-58] The bis-TSC Ni(II) complex **17** (Scheme 4) produces H_2 in DMF with trifluoro acetic acid (TFA) as a proton source.[57] The authors used electrochemical measurements and density functional calculations (DFT) to propose a mechanism which includes a ligand-centered radical species upon the first reduction. The reduced hydrazone function is protonated which is followed by a metal-centered reduction. A further protonation leads to the H_2 evolution.[57]



Scheme 4. Catalytic H_2 production by TSC Ni(II) complex **17**. Adopted from Ref. [57].

TSCs gained a lot of interest in the development of sensors for metal cations or for anions such as fluoride, cyanide, or acetate.[50] Advantages of TSCs in this field of research are the versatile coordination chemistry for metals and the possibility of forming multiple hydrogen bonds for anion recognition. The rational ligand design and the cheap synthesis of TSC are additional cons. TSCs have been used as sensor materials for colorimetry, fluorimetry, potentiometry, and voltammetry.[50] Some interesting examples from the literature are shown in Chart 4.[59-62] TSC **18** contains an azo dye at the *N*1 position and was used as a colorimetric anion sensor for acetate, which can be followed by eye. This compound showed selective acetate binding in the presence of other anions like halides with a detection limit of 0.71 μM.[60] An example for a fluorometric sensor is TSC **19**. This compound becomes fluorescent upon coordination of Zn(II). Remarkably, the compound was found to be cell-permeable and was used for the detection of intracellular Zn(II). Also, the monitoring of toxic metal ions was done with TSCs.[62] An example is the bis-TSC **20**, which contains a bianthracene motif. The complexation of Hg^{2+} leads to a quenching of the anthracene fluorescence. This allowed the detection of Hg^{2+} at very low concentrations down to 6.62×10^{-7} M.[59] TSC **21** was designed with an azide group at the *N*4 position. This allowed immobilization on an electrode using a Cu(I) catalyzed click reaction. The detection of Hg^{2+} with these functionalized electrodes was possible at a nanomolar level.[61]

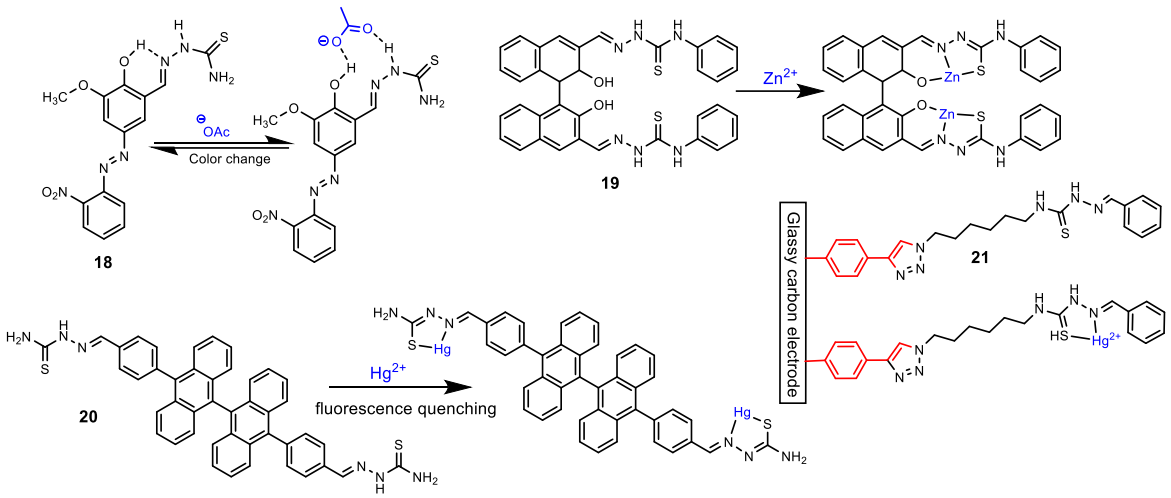


Chart 4. Examples of TSCs used for metal sensing. Adopted from Ref. [59-62].

The biological activity of TSCs was already discovered in the 1960s. An early example of a pharmaceutical application is methisazone (Chart 5, **22**) which was used for prophylaxes and therapy of smallpox. However, due to side effects this drug is not used anymore.[63,64] In the upcoming decades the cytotoxicity of TSCs was explored in more detail. Nowadays the antimicrobial activity of TSCs (e.g. antifungal, antibacterial, antiviral) is well described in literature.[65-67] Some TSCs have been also tested as antidiabetic reagents, since it was found that they are able to inhibit enzymes such as *α*-amylase and *α*-glucosidase.[68,69] An example is compound **23** (Chart 5) which showed promising antidiabetic activity in diabetes-induced Wistar rats. In addition to that, the compound has a very low toxicity.[69] TSC metal complexes with radionuclides such as ^{67}Ga, ^{99m}Tc, or ^{114m}In, ^{64}Cu, or ^{60}Cu have been used for applications in nuclear medicine.[30,70] For example, ^{64}Cu complexes of bis-TSCs such as **24** have been used in clinical trials for positron emission tomography (PET). An interesting aspect of these compounds is their increased retention in hypoxic tissue, making them promising candidates as hypoxia imaging agents.[30,70] Some TSCs were also tested for the treatment of neurodegenerative diseases like *Alzheimer*.[71,72] An example is compound **25** for which a high iron chelation efficacy, the inhibition of copper-mediated amyloid-*β* aggregation, the inhibition of acetylcholinesterase, and autophagic induction was observed. This makes the compound an interesting candidate for a multifunctional treatment of *Alzheimers disease*.[71]

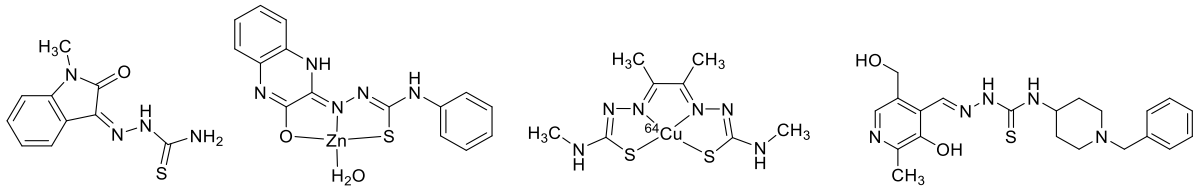


Chart 5. Examples of TSC tested or used for medical applications. Adopted from Ref. [30,63,69,71].

Probably the most frequently analyzed application of TSCs in medicine is their antitumor activity and many candidates have been tested in clinical trials for various kinds of tumors.[38,40,71] This aspect will be discussed in detail in the following chapters.

1.3 Thiosemicarbazones for cancer treatment

TSCs and their metal complexes are known in literature for their antitumor activity against different types of cancer such as leukemia, lung, breast, skin, prostate, ovarian, or bladder cancer.[73-78] Their mode of action, structure activity relationships, and the improvement of side effects are currently in the focus of research. Since TSCs with antitumor activity can have very different chemical structures, it is not possible to make general statements about their mode of action. Instead, this aspect must be considered for every subclass of TSCs individually. In addition, it was found that TSCs can be cytotoxic *via* different pathways at the same time.[38,40,76,79] The complexation of metal ions can improve cytotoxicity but there are also examples where it inhibits the activity.[80] It must be considered whether the metal center is involved in the mode of action (e.g. release of metal ions or redox activity) or to what extent water solubility and lipophilicity are influenced by complexation, which in turn influences their cellular uptake.[81-83] Some frequently investigated examples of TSC metal complexes contain Fe(III), Ni(II), Co(III), Cu(II), Zn(II), Pt(II), or Au(I).[84-89]

Within the field of TSCs in cancer therapy, there are three groups which are most frequently investigated namely tridentate TSCs with O^N^S donor set (**26**), tridentate α-pyridyl TSCs with N^N^S donor set (**27**) and tetradentate bis-TSCs and their metal complexes (e.g. Cu and Zn) (**28**) (Chart 6).[30,38,40,70]

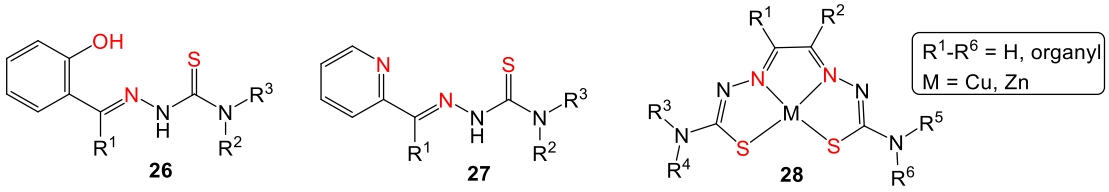


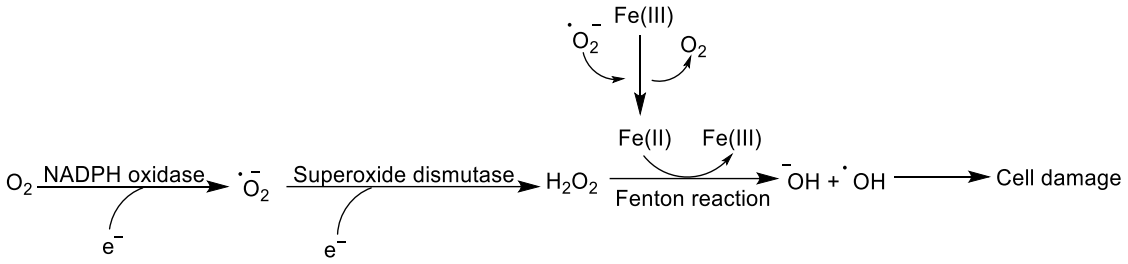
Chart 6. Group of TSCs tested for the treatment of cancer.

In general, the cytotoxic behavior of these three groups is very similar. However, the detailed mechanism is different, since different cellular components are damaged by these compounds (e.g. different enzymes or DNA). Nevertheless, they have in common that the complexation of intracellular metals such as Cu and Fe as well as the redox chemistry of these TSC complexes seem to play an important role in cytotoxicity. The mode of action will be discussed at the example of α-pyridyl TSCs in more detail.[30,38,40,70]

1.4 α-Pyridyl TSCs in cancer therapy

To understand the role of α-pyridyl TSCs in cancer therapy, it is important to understand the role of iron in biological processes. Iron was found to be an interesting target in cancer therapy, due to its outstanding role in essential biological processes such as cell growth and proliferation, oxygen transport, energy metabolism or DNA synthesis. For example, iron can be found in hemoglobin or different enzymes like ribonucleotide reductase which is involved in the rate-determining step of DNA

synthesis and repair.[38,40,90,91] The redox activity of iron plays an important role in these processes, since it can cycle between the Fe(II)/Fe(III) state by oxidation or reduction with intracellular reductants/oxidants. The regulation of Fe ions at a cellular level is called homeostatic regulation and is an essential process within the cells, since an excess of iron can lead to toxicity due to the formation of reactive oxygen species (ROS), while a deficit can lead to diseases.[40] The term ROS usually includes superoxide ($^{\bullet}O_2^-$), hydrogen peroxide (H_2O_2) and hydroxy radicals ($^{\bullet}OH$) which are naturally occurring in cells in small concentrations due to enzymatic processes (Scheme 5).[1] In addition, Fe(II) can catalyze the formation of $^{\bullet}OH$ from H_2O_2 which is known as the Fenton reaction (Scheme 5).[1] In this way, a high concentration of iron in the cytosol can increase the concentration of highly reactive $^{\bullet}OH$ and lead to harmful effects.[1,40]



Scheme 5. Formation of reactive oxygen species (ROS) in cells. Adopted from Ref. [1].

Iron is transported in the blood stream by transferrin (Tf), which can bind two Fe(III) ions (diferric Tf). When two of these diferric Tf bind to the transferrin receptor 1 (TfR1), the Tf-TfR1 complex can enter the cell within an endosome (Figure 1).[40] Fe is released from this complex due to a decrease in endosomal pH and it is reduced to Fe(II). In this way, it can be transported out of the endosome by the divalent metal transporter 1 (DMT1) into the labile iron pool of the cell.[40] The Fe concentration of this pool is controlled by Fe regulatory proteins (IPR) which control the expression of molecules involved in Fe uptake, utilization, and storage. In this way, Fe is for example incorporated into heme or stored in ferritin.[40]

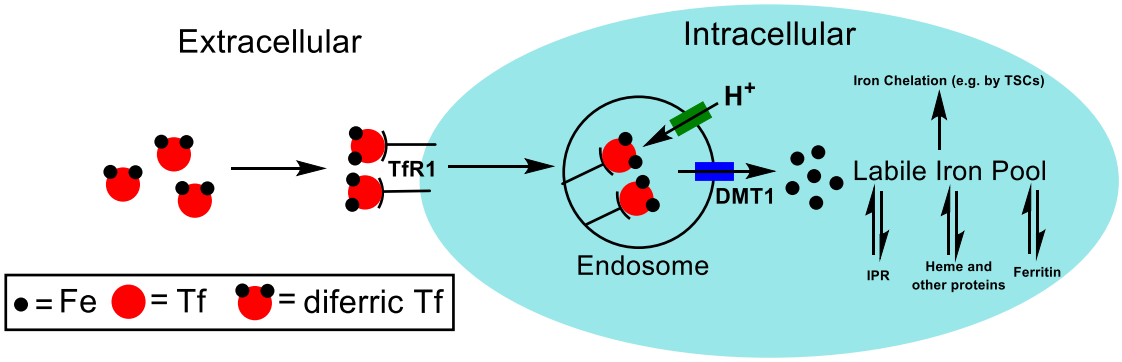
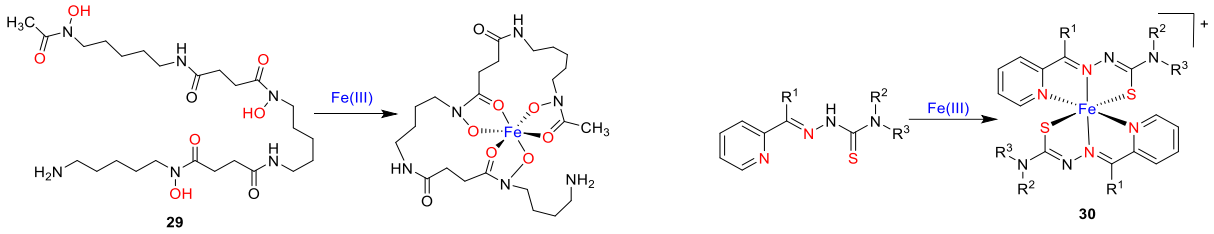


Figure 1. Cellular uptake of iron from the blood stream into the cytosol. Adopted from Ref. [40].

Cancer cells have an increased rate of proliferation and DNA synthesis. Thus, they have a high demand for iron, since it is important for enzymes in DNA synthesis and in the progression of cells by influencing the expression of molecules involved in cell cycle. In this way, the TfR1 is usually overexpressed compared to healthy cells.[38,40] Depletion of Fe in cells can lead to a decreased rate of DNA synthesis and to cell cycle arrest. This fact led to the idea, that chelators which can bind iron from the labile iron pool can be potent drugs for cancer treatment. A prominent example of an iron chelating drug is desferrioxamine (DFO, Scheme 6, **29**).[38,40,92,93] It is used for the treatment of iron overload diseases since it rapidly binds to Fe and stabilize the Fe(III) state. In this way, the ROS formation is suppressed. However, it was also found that DFO can be used as an anticancer agent.[40,92]



Scheme 6. Iron complexation of DFO and α-pyridyl TSCs.

Also, α-pyridyl TSCs have a very high affinity for the complexation of intracellular iron leading to the formation of octahedral complexes of the type $[Fe(TSC)_2]^+$ (Scheme 6). It was even found that the mixing of [Fe(DFO)] with an excess of an α-pyridyl TSCs lead to the formation of $[Fe(TSC)_2]^+$, underlining their high affinity to iron.[94] In this way, it is supposed that these TSCs lead to a depletion of iron in the cells by chelating the labile iron pool. However, a big difference compared to DFO is that the Fe(II)/Fe(III) redox potential is in the range of cellular oxidants and reductants (e.g. glutathione, ascorbate).[38,40] This means that the formed Fe-TSC complexes can catalyze ROS formation by Fenton reaction which leads to additional cell damage. This combination of iron depletion and the catalytic ROS formation is known as the double punch mechanism of TSCs (Figure 2) and leads to enhanced antitumor activity.[38,40] It is believed that these TSCs can follow the same mechanism with Cu instead of Fe. Moreover, the Cu complexes seem to be more potent in redox cycling and ROS formation than the corresponding Fe complexes.[95-97]

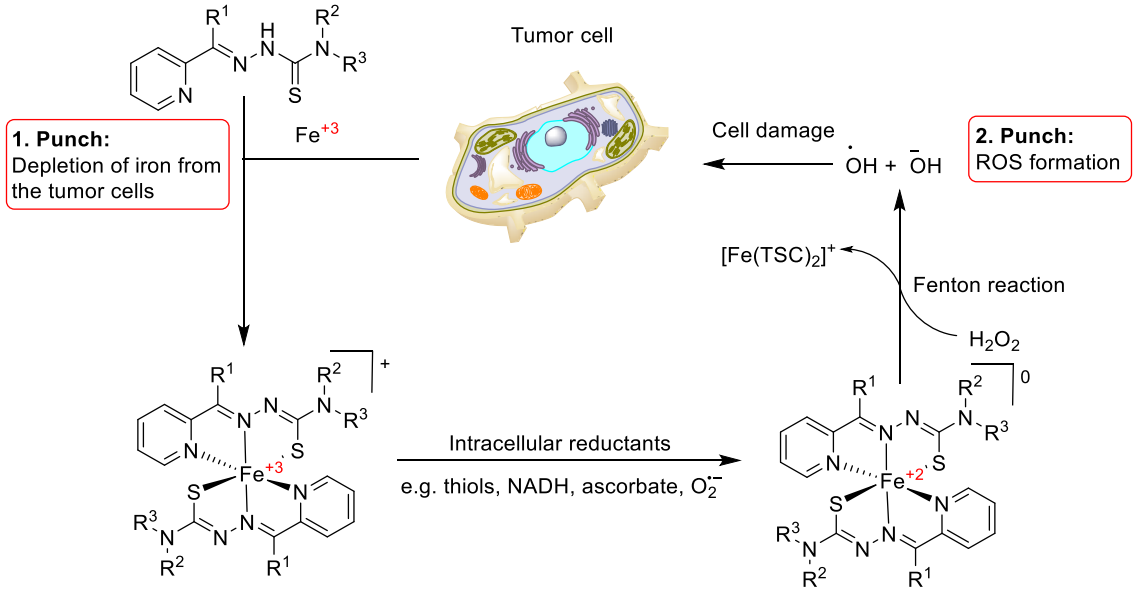


Figure 2. Double punch mechanism of α-pyridyl TSCs. Adopted from [38]. Cell template from *Chemdraw* (*Revvity Signals Software*).

It was found that TSCs damage and inhibit different components in the cells leading to apoptosis.[1,38,40] The formed iron and copper complexes can lead to ROS formation within the lysosomes which results in lysosomal membrane permeabilization and the release of lysosomal enzymes like cathepsin in the cytosol. This enzyme in turn can damage the mitochondrial membrane which leads to the release of *cytochrome c* and to apoptosis.[96-99] TSCs can also inhibit ribonucleotide reductase (RR) and topoisomerase II (topo II) which are both relevant in DNA synthesis and cell replication. The mechanism of this inhibition is still not clear, and controversy discussed in literature. The discussed double punch mechanism seems to play a role in inhibition, especially for the iron containing enzyme RR but also other mechanisms might contribute. Especially for topo II the picture seems to be more complex.[1,38,40] It was also found that α-pyridyl TSCs can lead to the upregulated expression of the protein ndrg-1 (N-myc downstream regulated gene 1) which suppresses the formation of metastases. Since it was found that ndrg-1 overexpression is observed when Fe depletion occurs within the cells, this observation seems

to be linked to the double-punch mechanism of TSCs.[1,40] In addition, Fe plays a role in the progression of cells by regulating the expression of molecules involved in cell cycle. In this way, it was also found that α-pyridyl TSCs lead to a cell cycle arrest which is also linked to the depletion of Fe in the cells.[1,40]

This interplay of different mechanisms inducing apoptosis makes α-pyridyl TSCs interesting compounds for cancer therapy because drug resistance becomes unlikely. In addition, their mode of action differs from established cytostatic agents, making them suitable for combinational therapies with other anticancer drugs.[100] In this way, many TSCs have entered clinical I/II trials in the past. However, there are several side effects which hampers their use in cancer therapy like the oxidation of oxy-myoglobin (oxy-Mb) and oxy-hemoglobin (oxy-Hb) due to the redox activity of these TSCs. Also, cardiotoxicity was observed for some of these TSCs at a high dosage.

1.5 α-Pyridyl TSCs – Examples and structure activity relationships

To find structure activity relationships and to reduce side effects, the derivatization of α-pyridyl TSCs was intensively studied. For example, the impact of substituents at the *N*1 and *N*2 position was investigated as well as the impact of metal chelation or substituting the thione group with a Selene group (Figure 3).[38,39,101,102]

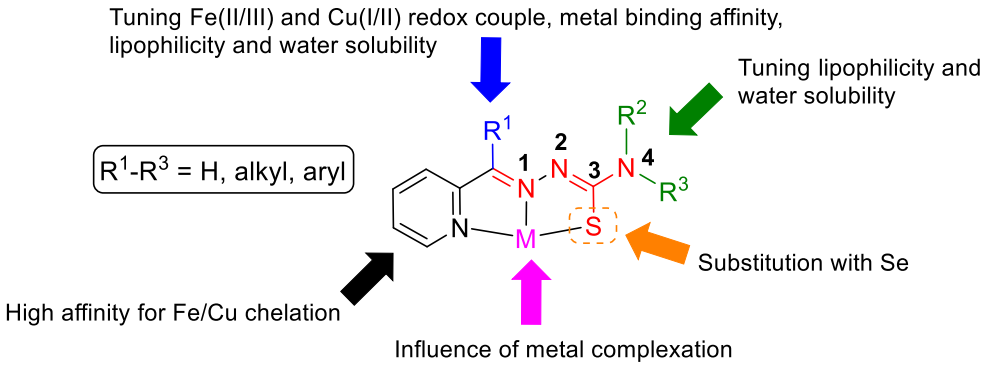


Figure 3. Possibilities for tuning the biological properties of α-pyridyl TSCs.

It was found that a pyridyl group at the *N*1 position is necessary for a high affinity for iron and copper chelation.[38] However, there are no detailed studies on the impact of substituents at the pyridyl group on the biological activity. This is probably since substitutions at this position can be synthetically challenging. An important example of a TSC bearing a substituent at the pyridyl group is triapine (**31**) (Chart 7). This compound has entered clinical trial II for the treatment of different kinds of cancer, but side effects have been observed like the oxidation of oxy-myoglobin and oxy-hemoglobin.[103,104]

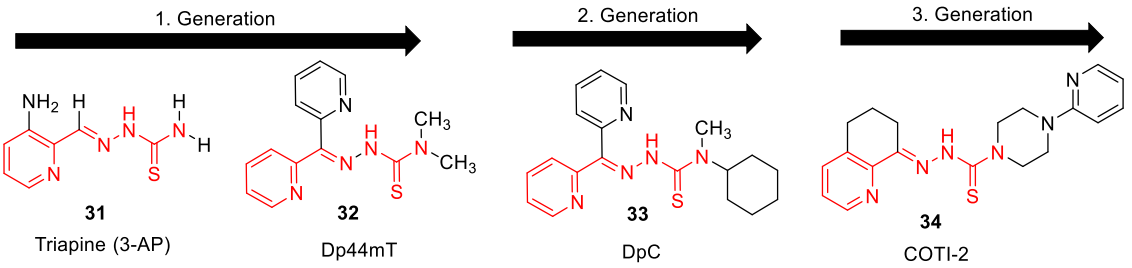


Chart 7. Examples of medical important α-pyridyl TSCs which have entered clinical trials.

The impact of substituent R^1 at the *N*1 position was studied in more detail in the past (Figure 4). It was found to have an influence on the metal binding affinity, the thiol/thione tautomerism, the lipophilicity, the water solubility and the redox potential of the corresponding Cu(I)/(II) and Fe(II)/(III) complexes.[38,40] In this way, the dipyridyl ketone (DpT), 2-acetylpyrdine (ApT), 2-benzoylpyridine (BpT) and different substituted 2-benzoylpyridine (RDpT) TSC series has been developed and studied in detail.[38-40,95,105,106] It was found for the corresponding iron complexes that the Fe(II)/(III) redox potential

can drastically differ between these series (Figure 4). However, it should be noted that the redox potential is also influenced by substituents at the *N*4 position with a smaller magnitude. Thus, a comparison between these series can be only made for same substituents at this position. Electron donating groups like methyl groups lead to lower redox potential (cathodic shift) while electron withdrawing groups like a nitro benzyl group lead to an increased potential (anodic shift).[38,39,95,105,106] This indeed has an impact on the effectiveness for ascorbate oxidation and ROS formation, which is increasing for decreasing redox potentials. This trend is in accordance with the cytotoxicity of these compounds where the ApT series has the highest toxicity in average, followed by the BpT and DpT series.[38] However, it should be noted that the picture is incomplete when cytotoxicity is only related to the Fe(II)/(III) redox potential. The substituents have also an impact on the lipophilicity and water solubility of the compounds and thus on the cellular uptake. This can maybe explain why the dipyridyl motif is often found in TSCs with high antitumor activity, since the pyridyl group leads to an increased water solubility. In addition, the second pyridyl group increases the affinity for binding intracellular metals.[38,40]

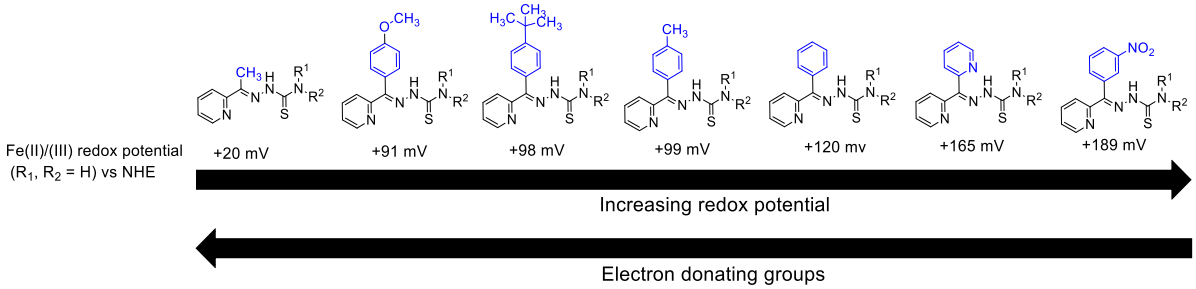


Figure 4. Influence of electron donating and withdrawing groups on the Fe(II)/(III) redox potential.[38,39,95,105,106]

The *N*4 position was mainly substituted to influence the lipophilicity of the TSCs. It was found that organic groups at this position can drastically increase cytotoxicity.[39,102] For example, Dp44mT (**32**) bearing two methyl groups at the *N*4 position has a drastically improved cytotoxicity compared to the corresponding derivative bearing a NH_2 function. By comparing the H_2O/octanol partition coefficient of these compounds, which is log p = 2.19 for Dp44mT and log p = 0.78 for the NH_2 derivative, the difference in lipophilicity becomes clear.[39] The increased lipophilicity of Dp44mT leads to higher cell permeability and an increased effectiveness of binding intracellular iron. Dp44mT has entered many clinical trials, but it was found to induce cardiotoxicity at high doses.[107] In this way a second generation of the DpT series was developed with DpC (**33**) as an important example. This TSC bears a cyclohexyl group at the *N*4 position and did not show cardiotoxicity.[102,107] The development was followed by a third generation of α-pyridyl TSCs, at which COTI-2 (**34**) must been mentioned. It is functionalized with a piperazine pyridyl unit at the *N*4 position.[107,108]

Metal complexation can lead to an enhanced cytotoxicity of α-pyridyl TSCs. Especially the corresponding complexes with Cu and Fe are in the focus of interest, since they can redox cycles within the cells leading to ROS formation.[38,40] The direct application of these complexes can have benefits compared to the intracellular formation of these complexes by application of the ligands. For the corresponding Zn complexes, it was found that the metal center can be substituted by Cu within the lysosomes of the cell (Figure 5).[97,109] An interesting aspect of this circumstance is that the Zn complexes are often non-toxic and thus can act as a prodrug. In this way, the cytotoxicity of the compound only occurs after a certain time within the cells after Zn is substituted by Cu.[109] This was found to reduce side effects. The impact of metal complexion and the role of intracellular substitution with Cu or Fe was studied later in more detail with further metals.[110]

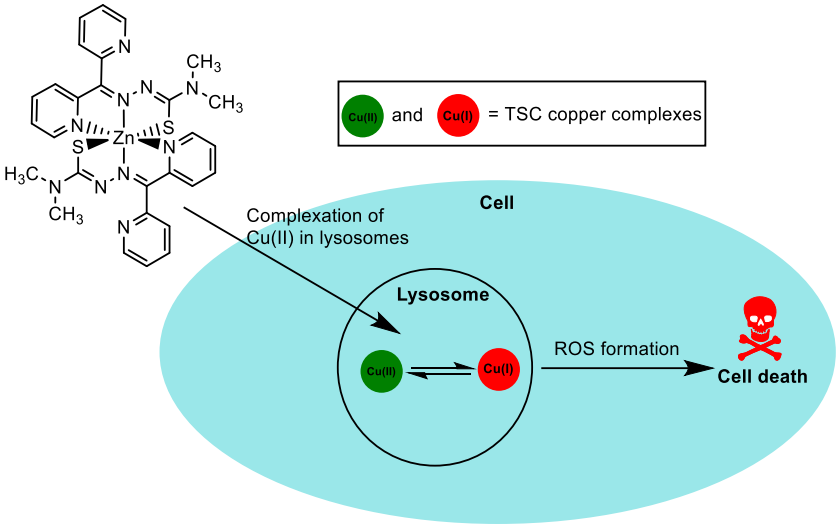
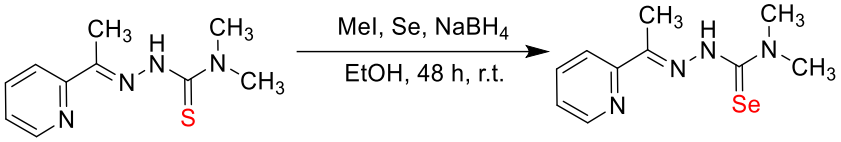


Figure 5. Zn(II) α-pyridyl TSCs complexes entering the lysosomes leading to a substitution with Cu and the formation of ROS. Adopted from Ref. [97].

The substitution of the thione with seleno group and the impact on medical properties has been investigated in detail in the last years (Scheme 7).[101,111] The replacement leads to a softer donor atom and to a higher affinity for soft metals. In this way, the compounds usually have a high affinity for binding intracellular Fe and Cu. It was also found that the Se analogues can have an increased selectivity to tumor cells and reduced side effects regarding the oxidation of oxy-myoglobin and oxy-hemoglobin. The latter is probably due to the reduced Fe(II)/(III) redox potential of the Se analogues. In this way, the Fe(III) state is stabilized which hampers the oxidation of oxy-myoglobin and oxy-hemoglobin. [101,111]



Scheme 7. Synthesis of selenosemicarbazones from TSCs.[101]

Very recently, the (*E*)-3-phenyl-1-(2-pyridinyl)-2-propen-1-one TSC series (PPPT) has been developed (Figure 6).[99,101,109,111] These TSCs have a styrene motif at the *N*1 position and reduced side effects concerning oxy-myoglobin and oxy-hemoglobin oxidation. In this way, this series has enhanced properties even compared to DpC and COTI-2. It is suggested that the styrene motif leads to a sterically hinderance for the interaction of the TSC iron complex with the heme-Fe(II) moiety of oxy-Hb and oxy-Mb. In addition, the electron donating styrene group lowers the Fe(II)/(III) redox potential, which also reduces the affinity for oxy-Hb and oxy-Mb oxidation.[99,101,109,111] These findings were combined with the observations for the selenosemicarbazones. By introducing a selenone instead of a thione group the Fe(II)/(III) redox potential becomes lower and side effect can be further reduced.[101,111]

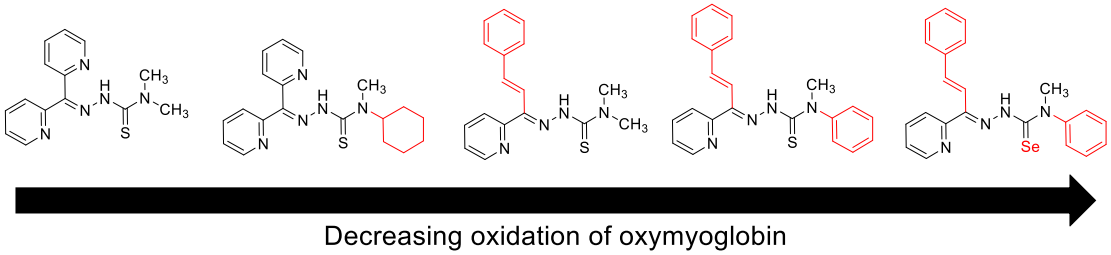


Figure 6. The development of the (*E*)-3-phenyl-1-(2-pyridinyl)-2-propen-1-one TSC series to suppress the oxidation of oxy-myoglobin and oxy-hemoglobin. The percentages are relative to negative control. Adopted from [111].

By additional fine tuning of substituents at the *N*4 position and at the styrene group, oxy-Hb and oxy-Mb oxidation was completely suppressed. However, this also led to increased lipophilicity, low water solubility and decreased cytotoxicity.[111] Thus, finding the perfect compromise between a high cytotoxicity without side effects is still in the focus of interest.

1.6 Strategies to improve the pharmacological potential of thiosemicarbazones

There are several problems that limit the application of TSCs in cancer therapy including side effects like the oxidation of oxy-myoglobin and oxy-hemoglobin, a poor selectivity to tumor cells as well as a high lipophilicity and poor water solubility, which decreases their cellular uptake. Different strategies have been studied in literature to improve the pharmacological potential of TSCs, by tuning the ligand design (Figure 7). These strategies include: 1) their conjugation to nanoparticles (NPs)[112] and 2) biomolecules,[113] 3) their labeling with fluorescence markers,[114] 4) their design towards amphiphilic structures,[115] 5) increasing their coordination sphere to hexadentate ligands,[116] and 6) their applications in photocatalysis.[117] The latter is not directly related to medical applications but could be used in this field in the future (Chapter 1.8). The background of these strategies will be discussed in the following in more detail.

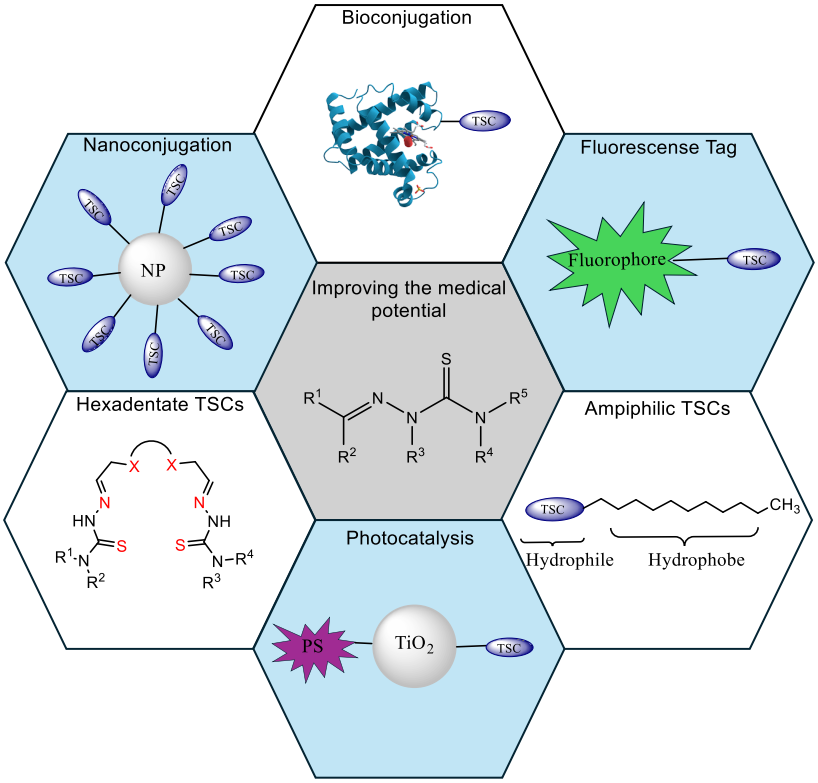


Figure 7. Selected strategies to improve the pharmacological performance of TSCs.

1.7 Nanoconjugation

1.7.1 Nanoparticles (NPs) and their functionalization

The term nanoparticle (NP) is used for particles which are smaller than 100 nm.[118] Their properties are strongly size and shape dependent and can drastically differ from the corresponding bulk material. This is usually due to their increased surface to volume ratio which leads to an increased number of atoms at the surface. In this way, NPs can have an increased reactivity or decreased melting point, but also other physical properties like optical (e.g. surface plasmon resonance) or magnetic (e.g. superparamagnetism) properties can change depending on the material.[119-123] Nanomaterials can be

synthesized by a top-down or bottom-up approach.[124,125] While the top-down approach starts from a bulk material, which is crushed into smaller structures by physical and mechanical methods, the bottom-up approach starts from molecular structures which build up the nanomaterial by chemical and physical processes.[124,125] The latter has the advantage that the size, shape and chemical composition can be controlled. In this way, for example core-shell, hollow, mesoporous or shaped NPs can be synthesized, which can be investigated by transmission electron microscopy (TEM) (Figure 8).[126-129]

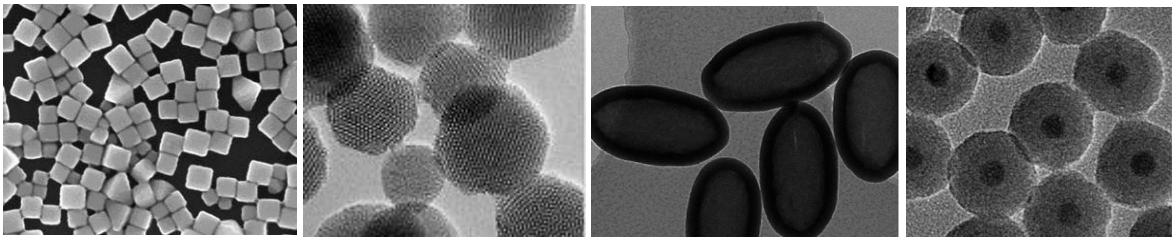
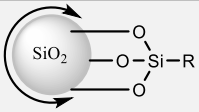
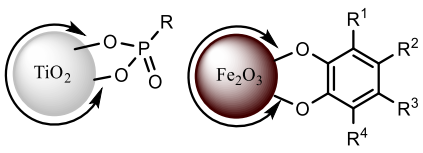
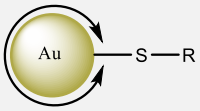


Figure 8. TEM images. From left to right: cube shaped Ag NPs, mesoporous silica NPs, hollow silica nano capsules and core-shell NPs (Fe_3O_4@SiO_2).[126-129]

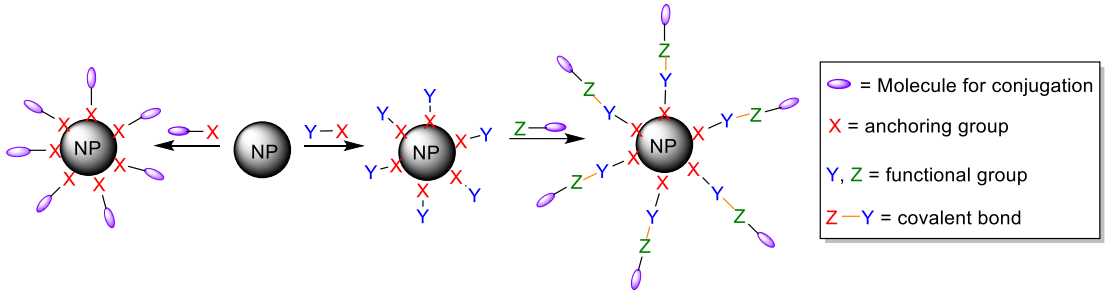
It can be distinguished between organic polymer or biomolecule NPs and inorganic metal oxide, -sulfide, -nitride, or -carbide NPs.[130-132] An important aspect of NPs is their surface functionalization, which is an important tool for tuning their properties for specific applications.[133] The surface functionalization can increase the stability in solutions since NP agglomeration can be circumvented by steric and electronic repulsion.[134] In addition, it can make the particles dispersible in different solvents, depending on the chemical nature (hydrophile or hydrophobic) of the surface ligands.[135] Functionalization can be achieved by covalent and non-covalent interactions including hydrogen bonds, electrostatic interactions, π–stacking *(e.g. π–π or CH–π)*, van der Waal forces and hydrophobic interactions.[135-137] Covalent interactions have usually the advantage of higher stability and are in the focus of this research. For this, specific functional groups are necessary that can bind to the surface, which are also called anchoring groups. It depends on the material, which functional groups are preferred for a strong binding, but the HSAB concept can be used to find ideal surface ligands (Table 1).[135]

SiO_2 and metal oxide NPs have hydroxy groups at their surface which are used for surface functionalization. SiO_2 NPs are usually functionalized with silanes which are condensed to the surface.[135,138] For TiO_2 NPs a higher stability is achieved by condensation of phosphonates to their surface.[135,139] Iron oxide NPs are often functionalized with ligands having a catechol motif in their structure for very strong Fe-binding on the NP surface.[140] Nobel metal NPs like gold are usually functionalized with thiols due to the strong S–Au bond.[135,141]

Table 1. Anchoring groups for different nanomaterials.[135]

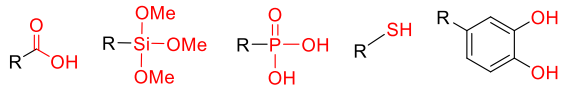
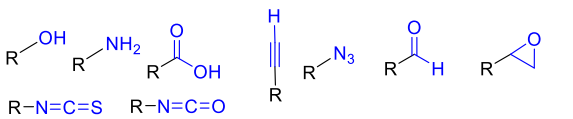
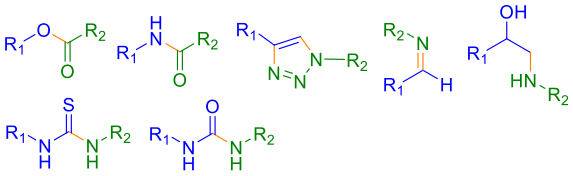
Nano material	Examples	Surface groups	Anchor groups	Examples of covalent binding
SiO_2	-	—Si—OH	Alkoxy-, hydrogeno-, halosilanes,	
Metal oxides	TiO_2, Al_2O_3, Fe_2O_3 Fe_3O_4	—M—OH	Silanes, carboxylates, phosphonates, catecholes	
Metals	Au, Ag, Pt, Hg	—M	thiols, disulfides, amines, nitriles, carboxylates, phosphines	

The conjugation of molecules to the NP surface is possible in two different ways (Scheme 8). If the molecule has an anchor group (X) within its structure, a direct attachment to the NP surface is possible (Method A). Another option is the pre-functionalization of the surface (Method B).[135,142] For this, a bifunctional linker can be used which has an anchor group (X) for binding to the NP surface and another functional group (Y) which can bind covalently to the molecule in a second step. These bifunctional linkers are often commercially available. In this way, the molecule needs a functional group (Z) which can react with the functional group (Y) at the particle surface.[135,142] It is important that the reaction between the molecule and the pre-functionalized NP can proceed in high yields and under mild reaction conditions. In this way, click reactions are often used like the Cu(I)-catalyzed azide-alkyne cycloaddition (CuAAC), the Diels-Alder reaction, the formation of ester and amides, the formation of ureas and thioureas, the addition to epoxides or the imine condensation. Some examples are summarized in Table 2. Which approach is preferred for conjugation depends on the functional groups available at the target molecule or which functional groups can be attached by derivatization.



Scheme 8. Conjugation of molecules to the surface of NPs. Adopted from Ref. [135,142].

Table 2. Examples of common functional groups for the attachment and crosslinking to NPs. [135,142]

Components of the conjugate	Examples
= molecule for conjugation	Drug, radiopharmaceutical, fluorophore, catalyst, photosensitizer, biomolecule
X = anchoring group	
Y, Z = functional group	
Z—Y = covalent bond	

1.7.2 Nanoparticles for medical applications and drug transport and release

A huge interest in NPs is due to their applications in medicine for the treatment, diagnostic and monitoring of different diseases like cancer. The size of NPs (1–100 nm) is usually in the range of large biomolecules and hundreds to thousands of times smaller than human cells.[143] It was found that NPs can penetrate cells *via* endocytosis where the particle is surrounded by the cell membrane and a vehicle is formed which is called endosome (Figure 9). In a second step the NPs are released from the endosomes into the cytosol.[144] It can be distinguished between phagocytosis, pinocytosis and receptor-mediated endocytosis.[145] Phagocytosis is usually found for larger particles and is a process of the immune system of the cells which leads to their removal. Pinocytosis is found for small NPs and molecules and lead to their cellular uptake.[146] The receptor-mediated endocytosis is a process where the endocytosis is triggered by the binding of a molecule to a receptor outside of the cell membrane.[145]

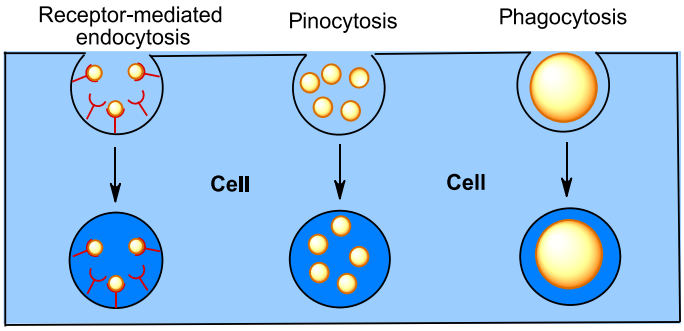


Figure 9. Different kinds of endocytosis (phagocytosis, pinocytosis and receptor-mediated endocytosis). Adopted from Ref. [145].

The cellular uptake of NPs depends on their chemical composition, their surface functionalization, their size and their shape. For example, it was found that large NPs (>200 nm), can be removed from the body by macrophages (phagocytosis) which decrease their cellular uptake.[146] A small particle size increases the surface to volume ratio and therefore the interaction area with the cell membrane which leads to a higher cellular uptake. It is usually suggested in literature that a particle size of approximately 25 nm is ideal for pinocytosis. Also, the shape (e.g. rods, disks, cubes, capsular shape) of the NPs can affect their behavior in the body. Non-spherical particles can for example escape the phagocytic system. In addition, shaped NPs can interact with the cell membrane in a different way (contact angle) which can lead to an increased cellular uptake compared to spherical particles which was for example found for capsular shaped NPs.[146,147] The surface charge of NPs is an important factor for their cellular uptake which can be influenced by surface functionalization. It was found that particles with a positive and negative zeta potential have often a higher cellular uptake compared to NPs with neutral potential. Especially, positive zeta potentials lead to an increased cellular uptake which is usually explained by the fact that the cell membrane is negatively charged.[146]

An important aspect of NPs is that they can target cancer cells, leading to a preferred accumulation in the tumor tissue. It can be distinguished between passive and active targeting (Figure 10).[148-151] Passive targeting uses the different properties of cancer cells compared to healthy cells. These have usually a high demand for nutrients due to their fast proliferation. It was found that the formation of new blood vessels (angiogenesis) is often increased for tumor cells to ensure a high supply of nutrients for cells. These blood vessels differ compared to those of healthy cells and have an increased permeability. In this way, NPs and large molecules can enter tumor cells more easily. In addition to that, NPs can accumulate in cancer cells because tumors have less effective lymphatic drainage. This is known as the enhanced permeability and retention (EPR) effect and usually explains the passive targeting of NPs.[152,153] An active targeting to tumor cells is possible by functionalizing their particle surface with targeting ligands.

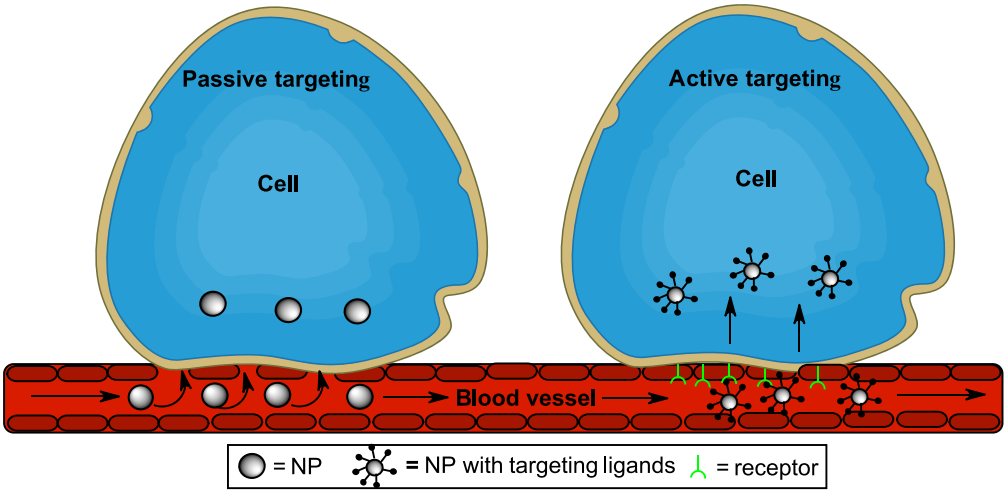


Figure 10. Active and passive targeting of cancer cells by NPs. Adopted from Ref. [149]. Cell template from *ChemDoodle* (2011-2015, *iChemLabs*, LLC).

These are molecules or biomolecules which can bind to receptors in the cell membrane. In this way the particles can enter the cells by a receptor mediated endocytosis.[148,151] An increased selectivity to tumor cells is achieved by the fact that tumor cells often overexpress specific receptors at their surface. Important examples of targeting ligands are antibodies, proteins (e.g. transferrin), polysaccharides, small molecules such as folic acid or anisamide and short nucleic acids (DNA and RNA) which are called aptamers.[148,151] It should be noted that the selectivity to tumor cells can be increased by active and passive targeting but there is usually no complete selectivity. In addition to that it always depends on the type of cancer if or to what extent the EPR effect or the overexpression of receptors is observed.[152,153]

The facility to target cancer cells by NPs made them frequently used as vehicles for the transport of drugs or diagnostic molecules to tumor cells to improve their selectivity. This in turn can reduce side effects because it is avoided that the drug damages healthy cells.[118,154,155] For diagnostic applications the increased selectivity to tumor cells can help to visualize them.

There are usually two different strategies for drug transport (Figure 11). The first option is to encapsulate the drug into NPs such as mesoporous SiO_2, polymer, or liposome NPs with the aim of drug-release from the NPs within the tumor cells.[128,156-159] An advantage of this method is that there is an increased capacity for drug loading due to the increased surface areas of mesoporous and hollow NPs.[128,160,161] In addition to that, the particle surface can be used as a platform to attach targeting ligands. However, it can be challenging to achieve a controlled drug release in the target tissue. In this way, the host-guest interactions between the particle surface and the drug are important factors. At the same time, surface functionalization can be used to slow down drug release.[160]

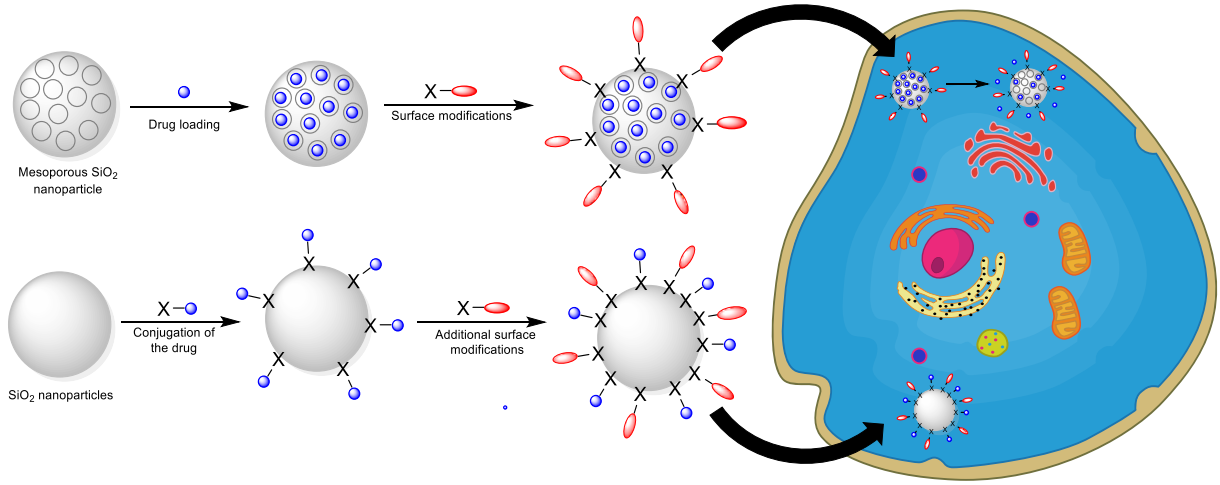


Figure 11. Drug delivery to tumor cells by NPs. Either, by mesoporous SiO_2 NPs, with the drug loaded into the pores or to SiO_2 NPs with the drug covalently attached to the surface. Cell template from *ChemDoodle* (2011-2015, *iChemLabs*, LLC).

The second option is to bind the drug to the NP surface. For this, usually covalent binding is used to avoid the loss of the drug during delivery to the target tissue. In this way, these drug delivery systems have the advantage of high stability.[162,163] Disadvantages of this method are a smaller drug loading capacity and the difficulty of attaching additional surface ligands to the NP (e.g. targeting ligands). At the same time, the medical potential of the drug can be reduced when it stays bound to the NP surface.[162]

For medical applications NPs usually consist of materials with high biocompatibility and low toxicity. Most frequently, inorganic SiO_2, Fe_2O_3, Fe_3O_4, Au, and Ag NPs are used.[154,160,164,165] A large interest is also in organic NPs made up from polymeric liposomes or micelles as well as in NPs based on biomolecules like proteins.[156-158]

1.7.3 Thiosemicarbazones in nanochemistry

The antitumor activity and the opportunity for chemical modifications make TSCs interesting candidates for nano conjugation or their loading into NPs. However, there are only a few examples found in the literature which combine these fields of research. These examples investigate the application of TSC nanoconjugates in medicine, catalysis and sensing.

Several publications are found about the encapsulation of TSCs into NPs. For example, polymeric block copolymer, poly(lactic-co-glycolic acid) (PLGA), polylactic acid (PLA) and poly-(ε-caprolactone) (PCL) NPs have been investigated by several authors for drug loading.[166-170] An example is the Pd(II) TSC complex (**35**) (Figure 12) which was encapsulated in PLGA NPs to increase its solubility and bioavailability. The high lipophilicity of this metal complex led to a high encapsulation efficacy (>90%) in the hydrophobic core of the particles. A slow drug release was found but the maximum amount of released TSCs was low (about 15%). This can be explained by its poor water solubility. Nevertheless, the cytotoxic potential of the TSC loaded NPs was high against ovarian cancer cells since only small concentrations (1 μM) are necessary for toxicity. In addition, the loaded NPs had an improved cytotoxicity compared to the non-encapsulated TSC.[168]

Other examples in literature investigate the loading of TSCs into liposomes.[171-173] For example, triapine was tried to load into liposomes to improve its plasma half-time, its cellular uptake and its selectivity to tumor cells. However, the authors found a poor stability of the triapine loaded liposomes which led to a burst release and a comparable toxicity as for non-encapsulated triapine.[171,173] By that reason, the authors chemically modified the triapine by the addition of a lipophilic tail and a primary amine group at the *N*4 position (**36**) (Figure 12). This modification led to stable liposomes and continuous drug release. This clearly shows the importance of the chemical structure of the drug for loading and release from liposomes. The authors showed that side effects associated by triapine like the oxidation of oxy-hemoglobin were circumvented by the drug transport.[171]

Another strategy is the loading of TSCs into NPs of biomolecules, typically proteins such as albumin, lactoferrin or lipoproteins, but also NPs coated with red-blood cell membranes have been reported.[174-180] There are several publications on using albumin NPs for drug delivery of TSCs, which is a plasma protein. It has the advantage that these NPs are nontoxic, biocompatible and biodegradable. Different TSC complexes with Pt, In, Cu, and Fe (e.g. **37**) (Figure 12) have been loaded into these particles.[174,177,178,180] In most cases, an improved cytotoxicity and increased selectivity to tumor cells was found.

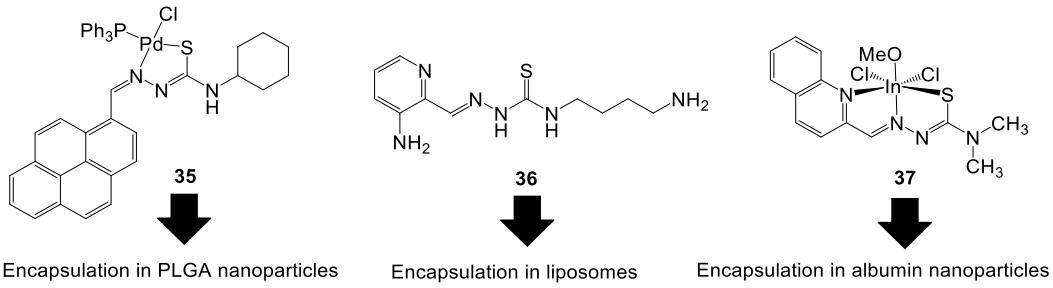


Figure 12. Examples of TSCs encapsulated into polymeric NPs, liposomes or NPs consisting of biomolecules. Adopted from Refs. [168,171,180].

Furthermore, the covalent conjugation of TSCs to NPs has been published. TSCs have been used as surface ligands for the stabilization of Au and Ag NPs, since they have donor atoms which can bind to their surface (e.g. thione and azomethine group). These functionalized particles have been tested for the sensing of Hg^{2+} and Cu^{2+} ions in solutions using the conjugate **38** (Chart 8).[181,182] Other authors used glutamate for crosslinking TSCs to different metal oxide NPs such as CuO, NiO, ZnO, or Fe_3O_4.[183-186] While one of the carboxylate groups can bind to the particle surface the other carboxylate group can bin to the TSC. For this, the authors left the *N*4 position of the TSCs unsubstituted so that the amine function

can react with the carboxylate group at the particle surface to form the conjugate **39** (Chart 8).[186] These nanoconjugates have been tested against different cancer cell lines and showed a high toxicity and improved selectivity to tumor cells.[183-186] Another example from literature is TSC nanoconjugate **40** (Chart 8) which was tested as a multi diagnostic tool (Chart 8).[112] For this purpose, Fe_3O_4 NPs have been coated with dextran, which was oxidized, leading to aldehyde functions at the surface. The aldehyde groups were on the one hand reacted with biotin hydrazide to attach a targeting ligand and on the other hand with thiosemicarbazide, which led to the formation of TSCs at the surface. The TSC ligands were labeled with ^{68}Ga which can be used for PET. In addition, the Fe_3O_4 particles can be used for magnetic particle imaging (MPI). A preferred accumulation of the particles was found in cancer cells which overexpress the biotin receptor.[112]

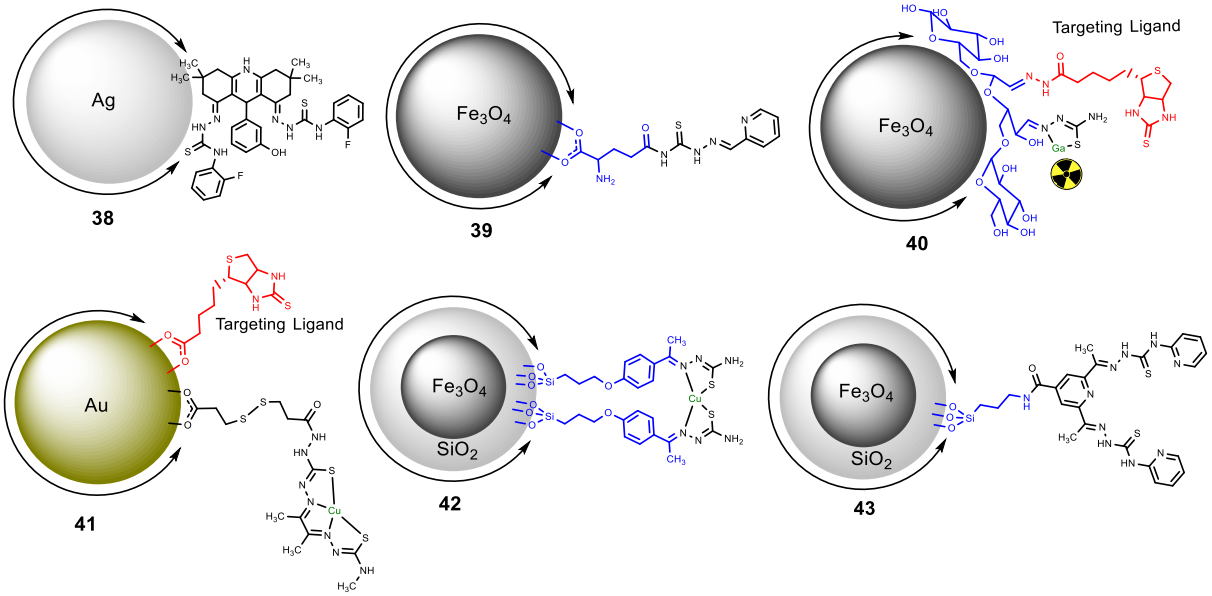


Chart 8. Examples of TSC nanoconjugates. Adopted from Ref. [112,182,186-189].

A quite similar concept was published with Au NPs which were functionalized with biotin as well as a tetradentate bis-TSC Cu complex (**41**) (Chart 8), which were anchored to the surface by carboxy groups.[189] The combination of biotin as a targeting ligand and the bis-TSC complex as an antitumor drug led to interesting anticancer properties. The most interesting feature in this compound is the disulfide bridge within the TSC structure, which is redox cleavable by glutathione leading to a drug release from the surface.[189]

For the synthesis of the TSC nanoconjugate **42** (Chart 8) functionalized silica coated Fe_3O_4 NPs with (3-chloropropyl)trimethoxysilane were synthesized.[188,190,191] This was followed by a nucleophilic substitution reaction with hydroxy acetophenone, which leads to acetyl groups at the surface which were reacted with thiosemicarbazide to the corresponding TSC. Finally, the corresponding copper complex has been synthesized by adding $CuSO_4$. The authors tested these conjugates for Cu(I) catalyzed azide-alkyne cycloaddition and Ullmann-type *N*-arylation of *N*-heterocycles.[188,190] The magnetic properties of the particles make them separable and reusable. Our research group recently published the immobilization of pentadentate TSCs to SiO_2 and SiO_2-coated Fe_3O_4 NPs **43** (Chart 8).[187,192] These compounds have been tested for the adsorption of heavy metal ions from solutions.[193] The corresponding Pd(II) complex has been used as C–C coupling catalyst. Covalent attachment was achieved by the formation of an amide bond. For this, a carboxylate function was introduced in the backbone of the TSC which can react with (3-aminopropyl)triethoxysilane (APTES) functionalized NPs.

1.8 TSC-functionalization of TiO_2 NPs for photocatalytic applications

TiO_2 is a semiconductor with a wide band gap in the UV region (3.2 eV), which has high chemical and physical stability.[194] Starting from the 1970s TiO_2 has been used as catalyst for water splitting.[195,196] Furthermore, its application as a catalyst material for ROS formation was observed, which can be used in medicine.[197] However, the photocatalytic efficiency of TiO_2 is low due to its large band gap and a fast electron-hole recombination. To increase its efficiency, TiO_2 nanomaterials can be used which have an increased surface area and thus an increased efficiency for catalytic processes at their surface.[198] A strategy to face the problem of a large bad gap is to modify their surface with a photosensitizer (PS) which can absorb light in the visible range and inject an electron into the conduction band of TiO_2.[199] To prevent a fast electron-hole recombination, a catalyst can be attached to the TiO_2 surface, which can capture the electron and prevents recombination. The reduced catalyst in turn can catalyze the reaction.[199] An example from literature, which combines these strategies is shown in Figure 13. Here, TiO_2 NPs have been functionalized by the $[Ru(bpy)_3]^{2+}$ (bpy = 2,2'-bipyridine) photosensitizer (Ru-P) and a cobalt complex as a catalyst (Co-P) for H_2 production. Both are covalently attached to the surface by phosphonate groups (P). Triethanolamine (TEOA) is used as a sacrificial electron donor.[199]

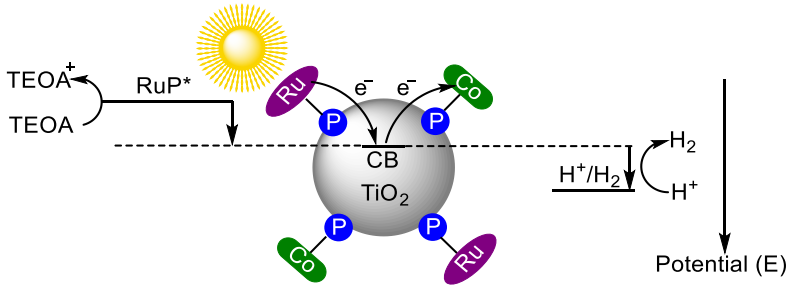
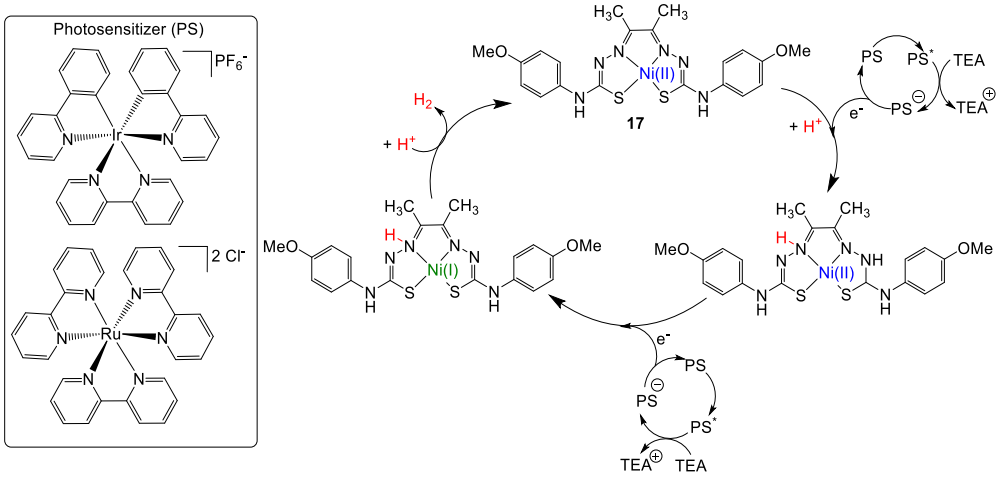


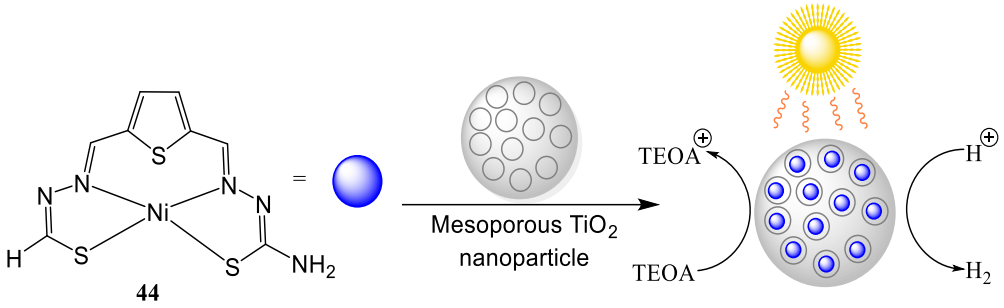
Figure 13. Photochemical production of H_2 by TiO_2 NPs functionalized with a Ru photosensitizer (Ru-P) and a cobalt complex (Co-P) as catalyst. Adopted from Ref. [199].

Moreover, TSCs can be used as redox catalysts. An example is the catalytic ROS formation by α-pyridyl TSC complexes of Cu and Fe (Chapter 1.4) but also the catalytic formation of H_2 by Ni(II) complexes of bis-TSCs (Chapter 1.2).[38,57] This can open the question if also a photocatalyst can be synthesized with TSCs. Two independent publications follow this question for bis-TSC Ni(II) complexes which can catalytically produce H_2 (Figure 13).[117,200] The TSC **17** was mixed by the authors with different PS like $[Ir(ppy)_2(bpy)]PF_6$ (Hppy = phenyl-pyridine) or $[Ru(bpy)_3]Cl_2$ (bpy = bipyridine) which can be excited by light and transfer an electron to the TSC catalyst. In addition, triethylamine (TEA) was used as an electron donor to regenerate the PS. The proposed catalytic mechanism is shown in Scheme 9, which is similar to the mechanism discussed in Chapter 1.2 but with the additional contribution of the PS.[200]



Scheme 9. Photocatalytic H_2 production by TSC complex **17** in combination with a photosensitizer. Adopted from Ref. [200].

Other authors used the TSC Ni(II) complex **44** as a catalyst which was loaded into mesoporous TiO_2 NPs. Also, this compound was found to produce H_2 after irradiation with light (Scheme 10).[117] A quite related work was carried out using N-doped carbon dots functionalized with a Co(II) bis-TSC complex to produce H_2.[201] Also here, semiconducting NPs act as the PS. However, no information was provided in which way the TSC catalysts binds to the particle surface.



Scheme 10. Photocatalytic H_2 production using the TSC Ni(II) complex **44,** incorporated into mesoporous TiO_2 NPs. Adopted from Ref. [117].

An interesting target in the future could be the combination of the two mentioned approaches by immobilizing a TSC catalyst and a PS on the surface of TiO_2 NPs to create similar catalytic systems published by *Reisner* and coworkers (Figure 13). An advantage of using TSCs in this context is their modular ligand design which might allow the attachment of functional groups for anchoring to TiO_2 NPs. In addition, their redox potential can be tuned by functionalization which was already discussed in Chapter 1.5 at the example of α-N-pyridyl TSC Fe(III) complexes. In this way, a very modular photocatalyst to produce ROS can be formed.

1.9 Bioconjugation

1.9.1 Drug delivery by bioconjugates

The underlining principle of bioconjugation is very similar to that of nano conjugation. A drug, medical imaging agent or biosensor is covalently linked to a biomolecule for (targeted) drug delivery to specific cells or even to specific cell organelles.[202] Typically used biomolecules are antibodies, proteins, enzymes and peptides but also nucleic acids, oligo -and polysaccharides or lipids.[202-207] In this way, the term bioconjugation usually refers to the conjugation to large biomolecules or biopolymers. The linkage to bio monomers (e.g. amino acids, saccharides) or other small biomolecules is usually not included in this field of research.[208] Currently, this topic has gained an increased interest since it can improve some of the disadvantages of nano conjugation like high costs, low stability in biological systems or poor reproducibility. In addition, the large pool of natural occurring or synthetically available biomolecules can be used to create a customized therapy for the patient.[202] For this, the development of specific reactions is necessary which link the drug to the biomolecule by choosing a suitable crosslinker.[209-212] In this way, bioconjugation can be divided into different groups depending on which conjugation process is used like amine reactions, thiol reactions, carboxylate reactions, hydroxyl reactions, aldehyde and ketone reactions, photochemical reactions or cycloaddition reactions (e.g. alkyne-azide cycloaddition, Diels-Alder reaction) (Figure 14).[213]

There are several challenges for the synthesis of bioconjugates, which depend on the class of biomolecules.[208,211] Firstly, bioconjugation is usually performed in aqueous media which requires a certain H_2O solubility of the drug. In addition, conjugation usually does not allow harsh reaction conditions since the chemical structure of the biomolecule (e.g. a protein) can be destroyed. Hence the reaction should proceed at neutral pH and room temperature.[208] Biomolecules like proteins must be chemically modified by linker groups which allow their attachment to the drug. This functionalization can also change the structure and properties of the biomolecule which should be avoided because it can affect the application in drug delivery. In addition, it can be very challenging to achieve homogeneous

products because the functionalization should be chemo and site selective to address one target group of the biomolecule. [208,211] This means for proteins a specific group, at a specific amino acid side chain which is almost impossible in practice. Most frequently, the functionalization of proteins is done at lysine and cysteine side chains since the amine or rather the thiol group are the most nucleophilic groups within proteins.[208,211] However, there are also approaches which use the hydroxy group of tyrosine for chemical modifications.[214] Other functional groups like the carbon acid function in aspartic and glutamic acid are less favored since the formed esters have a low stability under biological conditions. An advantage of cysteine modifications is the low biological abundance in proteins, which reduces the amount of target sides within the structure.[208]

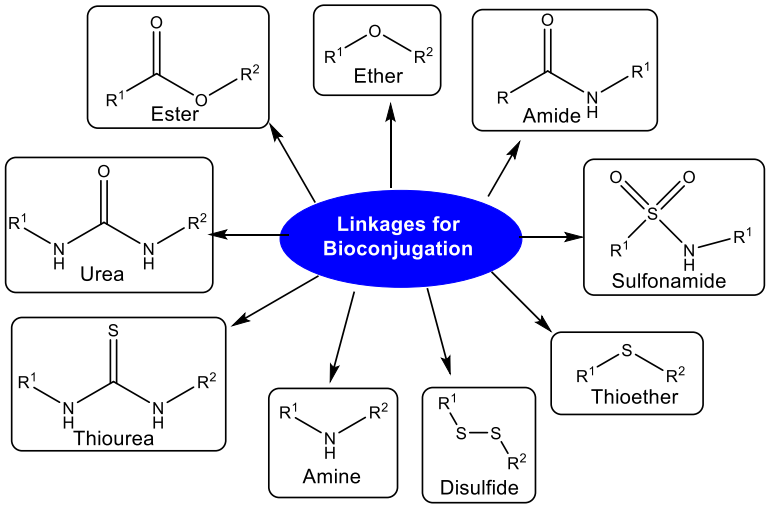


Figure 14. Overview of bioconjugation linkages. Adopted from Ref. [213].

Bioconjugation becomes easier for peptides, which usually consist of 10-40 amino acids and do not have a complex, three-dimensional structure as proteins. This usually leads to higher stability and allows harsher reaction conditions. In addition, the smaller size leads to a smaller number of accessible residues for chemical modifications which can improve the site specificity. Another advantage is that peptides are synthetically accessible by the solid-phase peptide synthesis.[208] In this way bioactive peptides can be designed for specific applications in drug delivery. In this context, cell penetrating peptides (CPPs) are an important class of compounds which can penetrate cell membranes *via* energy dependent or independent mechanisms without binding to specific receptors.[215-218] As an example, octaarginin (R8) is shown in Figure 15 which is conjugated to the anticancer drug oxaliplatin.[219]

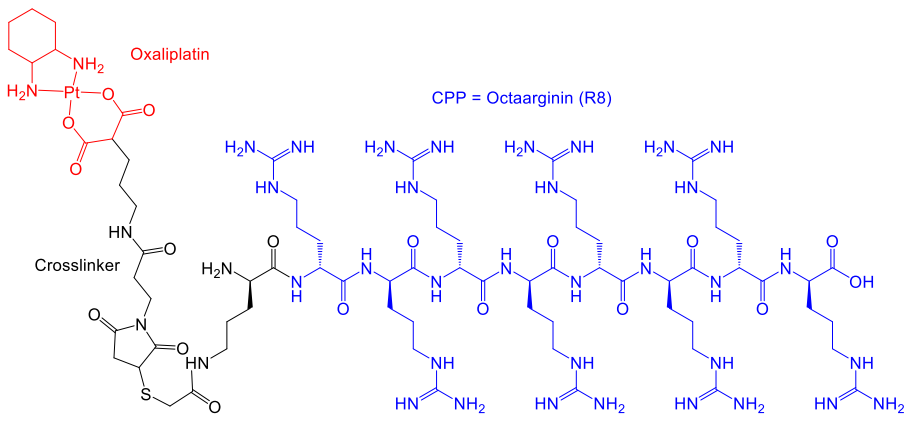


Figure 15. Bioconjugate of oxaliplatin with the cell penetrating peptide octaarginin. Adopted from Ref. [219].

CPPs can enter cells *via* different pathways like direct penetration or endocytosis. In addition, CPPs often differ in their chemical structure, at which three subgroups can be defined. The first group is represented by cationic peptides with a positive net charge resulting from basic amino acids like

arginine and lysine. The second one are amphipathic peptides which have hydrophilic amino acids (arginine, lysine) and hydrophobic amino acids such as alanine, valine, or phenylalanine in their structure. The third one are hydrophobic peptides with low net charge.[215-217] The challenge of using CPPs conjugates for drug delivery is their often-limited selectivity to specific cells. However, much research has been done in this field to overcome this problem and today there are examples found in literature which have an improved selectivity to tumor cells or even to specific intracellular targets like mitochondria, endoplasmic reticulum, or lysosomes.[215]

1.9.2 TSC-Bioconjugates

Bioconjugation has also found applications for TSCs. There are many examples in the literature incorporating structures or subunits of biologically relevant molecules in the TSC backbone.[220-227] These compounds are not bioconjugates in a classical sense but still fulfill the criteria that a biomolecule and a drug are covalently connected to each other. Usually, these derivatizations are done due to the expectation that biological relevant structures within TSCs can improve medical performance or lead to site-directing effects.[224] Some examples are shown in Chart 9, which have steroids (**45**), sugars (**46**), amino acids (**47**) or other biological relevant structures (**48** and **49**) in their backbone.[221,222,224-226]

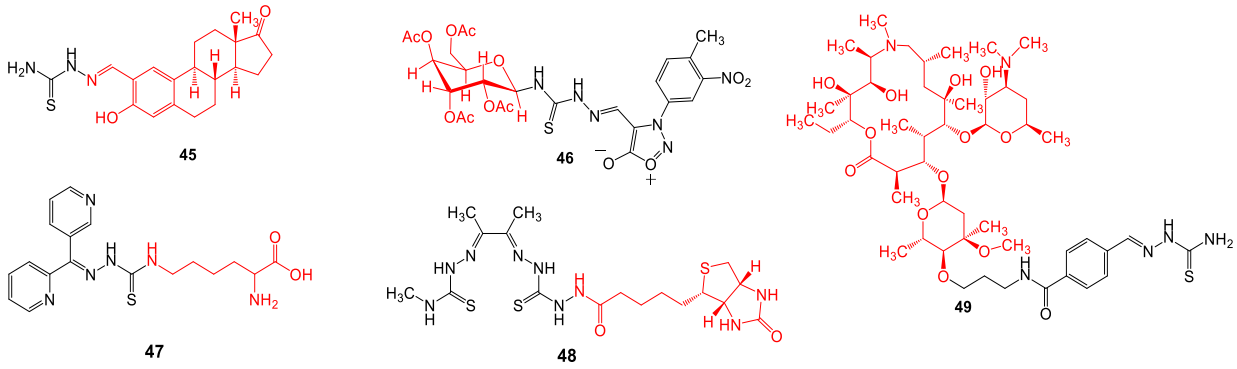
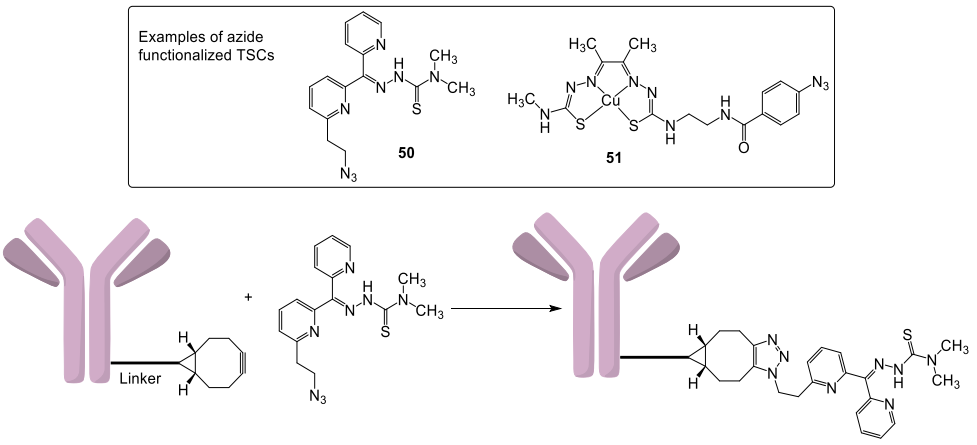


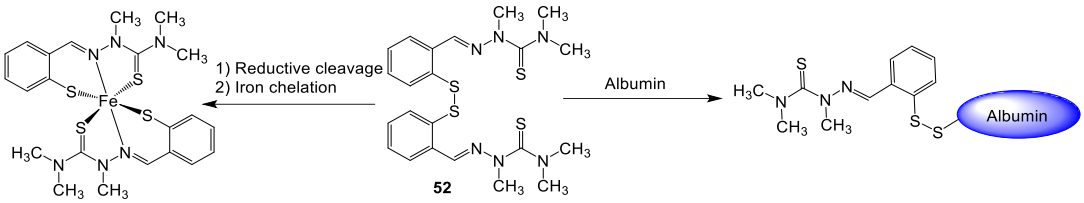
Chart 9. Example of TSCs having biological relevant substructures in their backbone. Adopted from Refs. [221,222,224-226].

In addition to that, TSCs have been successfully conjugated to antibodies, cellulose, proteins, enzymes and peptides.[30,113,220-237] The conjugation strategies strongly depend on the functional groups accessible at the biomolecule. Some examples in literature have introduced an azide function into the TSC (Scheme 11, **50** and **51**) which can be clicked to biomolecules in a second step.[113,229] For example, a Cu-free click reaction via a strain-promoted alkyne–azide (SPAAC) reaction has been carried out to link the TSC **50** to an antibody (Scheme 11).[113]



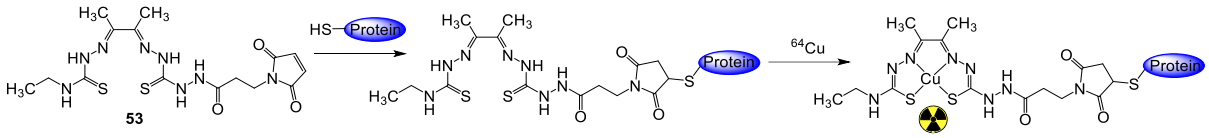
Scheme 11. Conjugation of a TSC to an antibody by strain-promoted alkyne–azide click reaction. Adopted from Refs. [113,229]. Antibody template from *ChemDoodle* (2011-2015, *iChemLabs*, LLC).

Other authors synthesized a bis-TSC which is bridged by a disulfide group (Scheme 12, **52**).[236] The TSC was found to be a prochelator at which its affinity to bind intracellular iron increases after the reductive cleavage of the disulfide group leading to tridentate ligands with an S^N^S donor set. In addition, the compound can form conjugates with albumin by a disulfide exchange reaction with a cysteine residue at the protein.[236]



Scheme 12. Conjugation of a TSC to albumin by disulfide linkage.[236]

Another example is bis-TSC copper complex **53** which has a maleimide group in the structure (Scheme 13). Maleimide groups are frequently used for bioconjugation to proteins because they can easily react with thiol groups of cysteine. In this way the authors were able to bind the bis-TSC to a protein domain and to label the compound with ^{64}Cu for diagnostic application in PET.[231]



Scheme 13. Conjugation of a bis-TSC to a protein *via* a maleimide group.[231]

Several examples are found in literature which conjugate TSCs to peptides, especially CCPs.[30,230,232-234,237] Also, our research group published the conjugation of a lysine derived TSC **54** to cell penetrating peptide sC18.[222] In general, the conjugation of TSCs to peptides follows a similar approach in literature, whereby the TSC is functionalized with an amine or carbon acid function which can bind to the peptide by the formation of an amid bond. Some examples of these TSCs are shown in Chart 10 (**54**, **55** and **56**).[222,232,234]

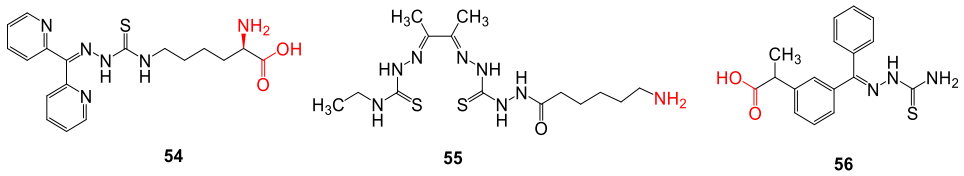


Chart 10. Examples of TSCs with carbon acid or amine function which were successfully bound to peptides *via* an amid bond.[222,232,234]

1.10 Fluorescence labeling

1.10.1 Fluorescence labeling for medical applications

Visualization of biological processes is very important to understand biodistribution in the cells. To do so, a frequently used tool is fluorescence labeling at which a fluorophore (fluorescence tag) is bound to specific compounds in the cells which become visible by fluorescence imaging (e.g. fluorescence microscopy or spectroscopy).[238-241] For fluorescence imaging, the tissue or the cells are irradiated with a specific excitation wavelength, at which most of the light is reflected, scattered or absorbed by molecules in the cells.[238] The penetration depth in the tissue depends on the used wavelength and increases with increasing wavelength (Figure 15).[242] The light can also excite the fluorescence tag within the cells, which in turn emits light of a specific, longer wavelength (*Stokes* shift).[238] This is based on *Kasha's* rule which founds that the emission originates from the lowest vibrational state of the excited state (Figure 15).[243] The emitted light can be detected by highly sensitive detectors to localize the

emission. Most frequently, fluorescence imaging is used for *in-vitro* studies (e.g. fluorescence microscopy), but also *in-vivo* applications have gained an increased interest. However, for *in-vivo* studies, the fluorescence tag should absorb light of a long wavelength, ideally in the near infrared (700-1000 nm), to guarantee a high penetration depth.[238-241]

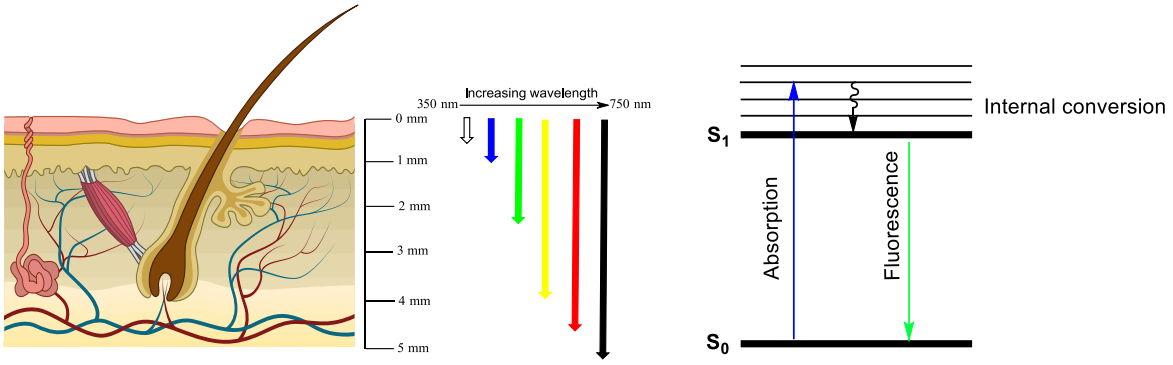


Figure 15. Left: Dependency of the wavelength on the penetration depth into the tissue. Right: *Jablonski* scheme of absorption and fluorescence. Adopted from Ref. [242,243]. Skin template from *ChemDoodle* (2011-2015, *iChemLabs*, LLC).

Different fluorescent tags can be used for labeling like fluorescent proteins or dyes. Some examples of dye-based fluorescence markers are shown in Figure 16, which have functional group in their structure for linkage.[244] Fluorescence labeling is usually used for tagging specific biomolecules and components in cells.[238-241] In this way, this field of research is strongly connected to the topic of bioconjugation discussed before (Chapter 1.9). In addition, this topic is also important for nano conjugation because the fluorescence labeling of NPs has been used to analyze their biodistribution.[245]

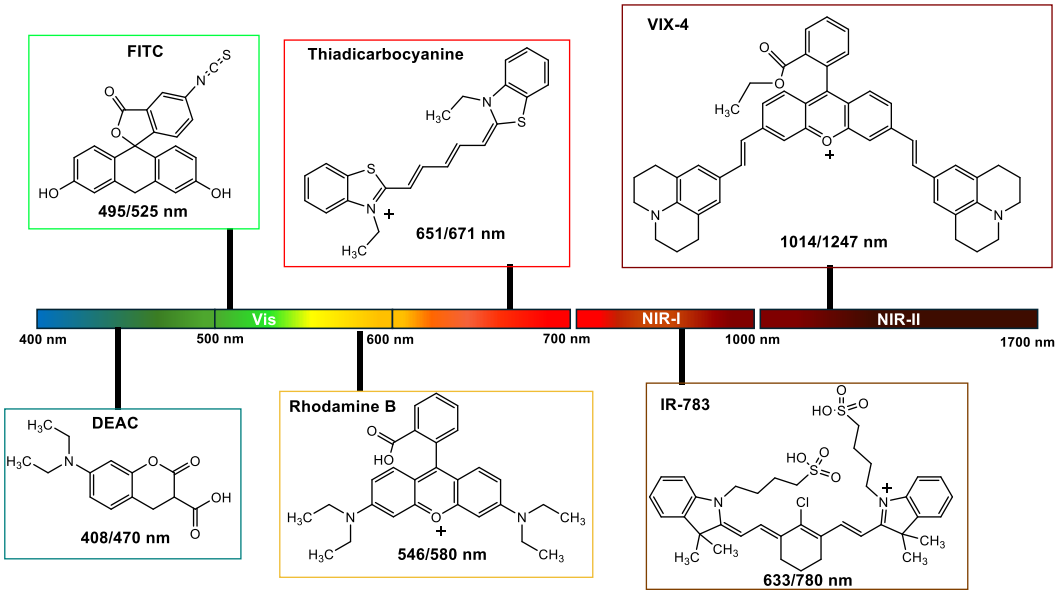


Figure 16. Emission and absorption wavelength of some frequently used fluorescent dyes for labeling. Adopted from Ref. [244].

Another strategy is the fluorescence labeling of drugs to visualize their biological processes. However, this method has the disadvantage that the labeling can drastically change their properties, since large organic dyes are linked to usually small drugs. A better option are drugs which are auto-fluorescent without labeling, which makes fluorescent groups in their structure necessary. A very prominent example is doxorubicin which is a fluorescent anticancer drug.[246]

1.10.2 Fluorescent thiosemicarbazones

TSCs are usually not fluorescent but it is possible to introduce fluorophores in their structure or to use metal complexation to induce fluorescence. In this way, this property can be used for visualization of

their biological distribution. A challenge can be to achieve fluorescence and a high cytotoxicity at the same time, since most fluorophores are aromatic and lipophilic groups which can reduce the H_2O solubility and cellular uptake of the TSC. Some examples of fluorescent TSCs are shown in Chart 11 (**57-64**). In most cases, the fluorescent group was introduced at the *N*1 position of the TSC, due to the high availability of ketone- or aldehyde-functionalized chromophores.[98,114,247-255]

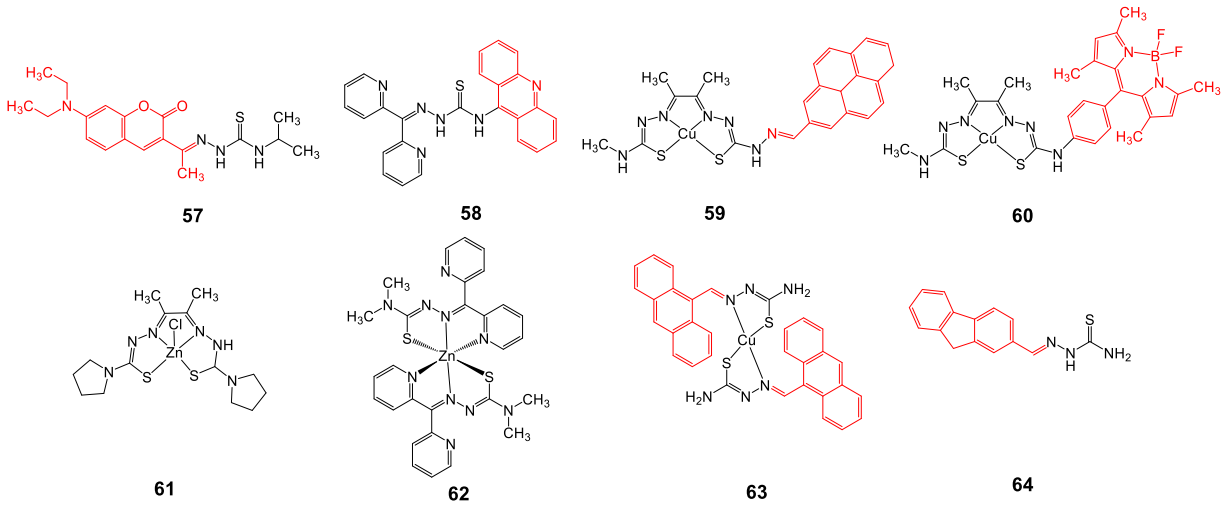


Chart 11. Examples of fluorescent TSCs. Adopted from Ref. [98,109,114,249,251-253,255].

TSC **57**, having a coumarin group in its structure, was found to be an intracellular sensor for Zn(II) ions. The complexation leads to a change of the emitted wavelength compared to the ligand which can be tracked by living cell imaging.[253] Another example is TSC **58** with an *N*-acridine group at the *N*4 position. On the one hand the authors introduced this group because it is known for targeting and entrapping into lysosomes, which is favorable for the cytotoxicity of TSCs (Chapter 1.4). On the other hand, it shows fluorescence which can be used for tracking. The authors were able to prove the accumulation of the TSC in lysosomes by fluorescence microscopy. In addition, the TSC showed a high cytotoxicity.[98] TSCs **59** and **60** are examples for the fluorescence labeling of bis-TSC copper complexes known for their high cytotoxicity and application in PET. Pyrene and BODIPY were successfully introduced into the backbone of the structure in the past and their biodistribution was analyzed by fluorescence microscopy.[114,249]

Also, zinc complexes of mono -and bis-TSCs are found to be fluorescent, while TSC complexes with other metals show fluorescence quenching (**61** and **62**). This fact can be used for imaging, having the advantage that the introduction of fluorophores in the structure is not necessary. For example, *R. Cowley* and coworkers were able to visualize the successful cellular uptake of a TSC Zn(II) complexes into prostate cancer cells by fluorescence microscopy (Figure 17).[247,250,254] The fluorescence of the zinc complexes is usually attributed to intra ligand transitions. Coordination with Zn(II) leads to a chelation enhanced fluorescence since it increases the rigidity of the molecule and can stabilize the excited state.[256]

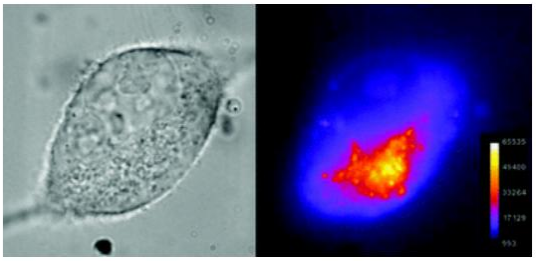


Figure 17. Fluorescence image of a prostate cancer cell after loading with TSC Zn(II) complex **61**. From A. R. Cowley, J. Davis, J. R. Dilworth, P. S. Donnelly, R. Dobson, A. Nightingale, J. M. Peach, B. Shore, D. Kerr, Len Seymour, *Chem Commun*. **2005**, 845-847. Ref. [247].

1.11 Amphiphilic drugs

1.11.1 Amphiphilic metal complexes and their advantages in medicine

In the last decades an increased interest was found in amphiphilic metal complexes, also called metallosurfactants, and their applications in medicine.[257] These compounds usually have a hydrophilic group (hydrophilic head) which consists of a metal complex and a hydrophobic part (hydrophobic tail) which consist of an alkyl chain. An interesting aspect of these metal complexes are their interaction with biomolecules such as proteins, DNA or membranes but also their self-assembling to form aggregates such as micelles (Figure 18).[257-261] It depends on the ratio between the volume of the hydrophilic and the hydrophobic group whether micelles are formed or other structures such as rods or bilayers. Self-aggregation is concentration-depended and usually starts after reaching the critical aggregation concentration.[257] In some case self-aggregation of metallosurfactants is only possible if a surfactant support is added, whereby the amphiphilic metal complex is embedded into the micellular structure.[257,262]

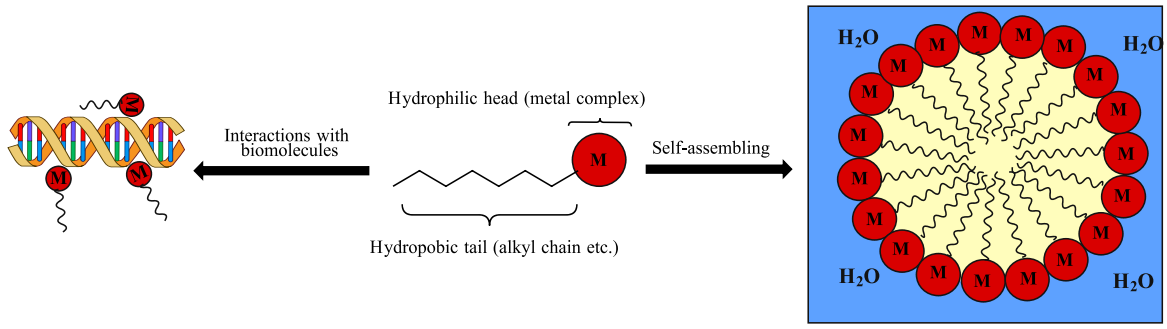


Figure 18. Generalized structure of amphiphilic metal complexes and their ability to form micelles or to interact with biomolecules. DNA template from *ChemDoodle* (2011-2015, *iChemLabs*, LLC).

Most important part of metallosurfactants is the ligand which has a hydrophobic tail within its backbone. This ligand binds to the metal center and connects the hydrophobic and hydrophilic part of the compound. A polydentate ligand is favored for this since it leads to a high stability of the metal complex. Some examples from literature are found in Chart 12 (**65–67**).[263-265]

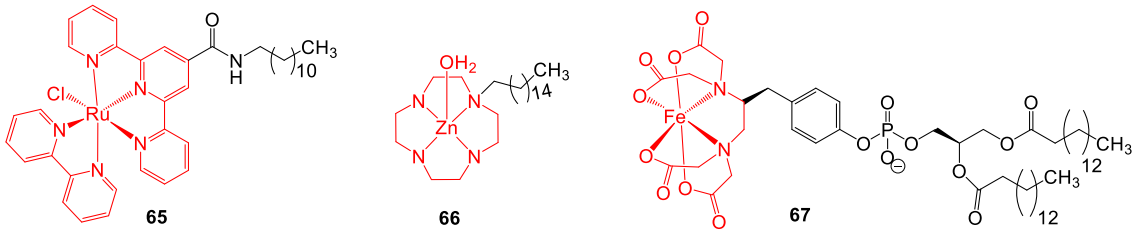


Chart 12. Examples of amphiphilic metal complexes from literature. Adopted from Refs. [263-265].

For the interaction of metallosurfactants with biomolecules often an increased binding affinity is found. For example, the hydrophobic part of the compounds can interact with hydrophobic subdomains of a protein, while the hydrophilic part can interact with hydrophilic domains. In addition, these compounds have an increased interaction with cell membranes which can improve their penetration into the cells.[257] In some cases, these compounds were found to be embedded into the cell membrane.[263] Especially the interaction of micelle structures with biomolecules was found to be interesting and can lead to the unfolding of protein structures.[257,265] Since the metal center of these metallosurfactants is usually not innocent and can have a certain reactivity due to *Lewis*'s acidity, ligand exchange reactions or redox reactions, these compounds can exhibit interesting biological activity and cytotoxicity. For example, amphiphilic metal complexes were found to lead to an improved hydrolytic cleavage of DNA and proteins compared to non-amphiphilic analogues.[257]

1.11.2 Amphiphilic thiosemicarbazones

The flexible ligand design of TSCs can offer the opportunity to synthesize amphiphilic structures.[32,115,266-275] On the one hand, aliphatic groups can be attached to the backbone of the TSC. On the other hand, the TSC function is a polar and hydrophilic group, which can form inter -and intramolecular hydrogen bonds. In addition, a multidentate binding to metal ions is possible. It was found that TSCs with hydrophilic as well as hydrophobic groups can have improved biological properties. For example, a certain lipophilicity is necessary to increase their cellular uptake.[39,102] Other authors recognized that TSCs with an amphiphilic character have improved interactions with specific biomolecules (Chart 13, **68-76**). An example is TSC **68**, which binds selectively to albumin. The TSC shows a weak fluorescence which drastically increases after binding to the protein which can be used for sensing.[115]

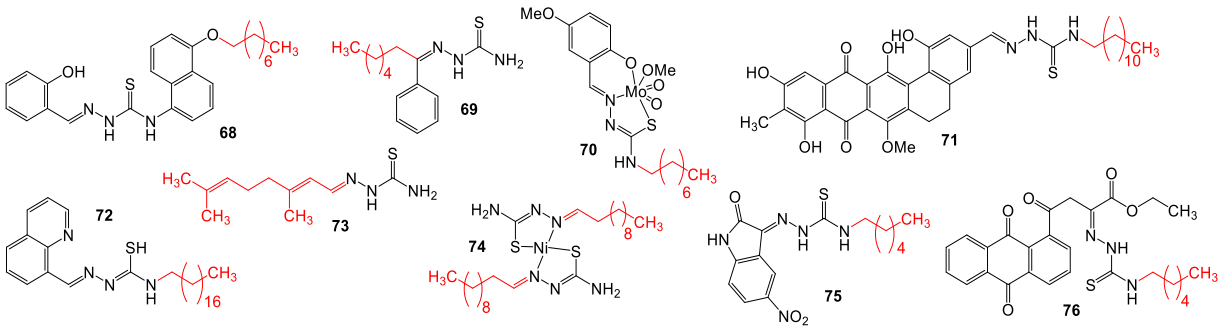
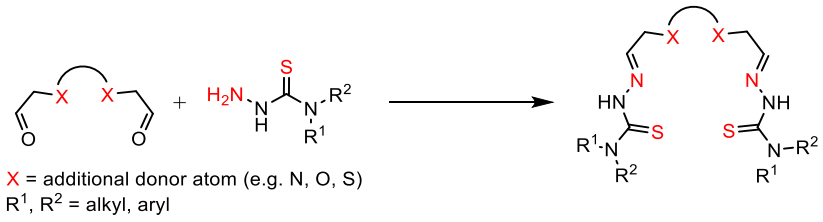


Chart 13. Examples of TSCs with amphiphilic structure from literature. Adopted from Refs. [115,266-268,270,273-275].

The TSC **69** was synthesized by authors with a lipophilic group for inhibiting tyrosinase which has a lipophilic binding pocket. The compound was found to inhibit the enzyme by a reversible, competitive mode.[275] The TSC Mo(VI) complex **70** showed strong interactions with DNA. In addition, the inhibition of α-amylase and glucosidase was observed. The authors recognized stronger interactions with these biomolecules for TSCs with an octyl chain compared to their analogues with a methyl group.[268] Further examples of amphiphilic TSCs are shown in Chart 13. Except for these, the research on amphiphilic TSC is quite rare. Therefore, their ability to form aggregates like micelles has not been tested yet.

1.12 Hexadentate Thiosemicarbazones and their complexes

Hexadentate TSCs are rare in literature compared to tri-, tetra- and pentadentate TSCs.[32,116,269,272,276-279] However, hexadentate TSCs might have several advantages which can make them interesting for medical applications. First, the binding affinity to metals should be increased due to six coordination sites. This can make them interesting compounds for binding intracellular metals like copper and iron but also for radiolabeling, since stable metal complexes with radionuclides should be rapidly formed. In addition, they are suitable ligands for various metals and can also bind to metal ions which prefer a high coordination numbers like lanthanides and actinides.[280,281] The formation of bimetallic complexes by using hexadentate TSCs is also possible.[116,276,279] Most examples of hexadentate TSCs in literature are bis-TSCs but also hexadentate tristhiosemicarbazones (tris-TSC) are known in literature.[32,116,269,272,276-279] In this way, the starting point of their synthesis are dialdehydes or diketones which should have two additional donor sites to synthesize hexadentate ligands (Scheme 14).



Scheme 14. Generalized synthesis of hexadentate bis-TSCs.

TSC **77** was synthesized with two S^N^O doner sets (Chart 14). Radiolabeling with ^{111}In was successful and its biodistribution in mice was analyzed for which a preferred accumulation in liver and intestine was observed. In this way, this compound was found to be an interesting alternative to other frequently used ligands for radiolabeling like 1,4,7,10-tetraazacyclododecane-1,4,7,10-tetraacetic acid (DOTA).[32] A quite similar study was done with the TSC complex **78**, which has two sets of N^N^S donors and which was labeled with ^{99m}Tc (Chart 14). In addition, the authors changed the functional groups at the *N*4 position which range from hydrophilic to lipophilic groups to tune their biodistribution. They found that hydrophilic compounds had a higher uptake in kidneys while the lipophilic compounds accumulated in the liver.[272] The example shows that hexadentate TSCs have many options for fine tuning their properties due to their easy derivatization which might be an advantage over other established chelators for radionuclides.

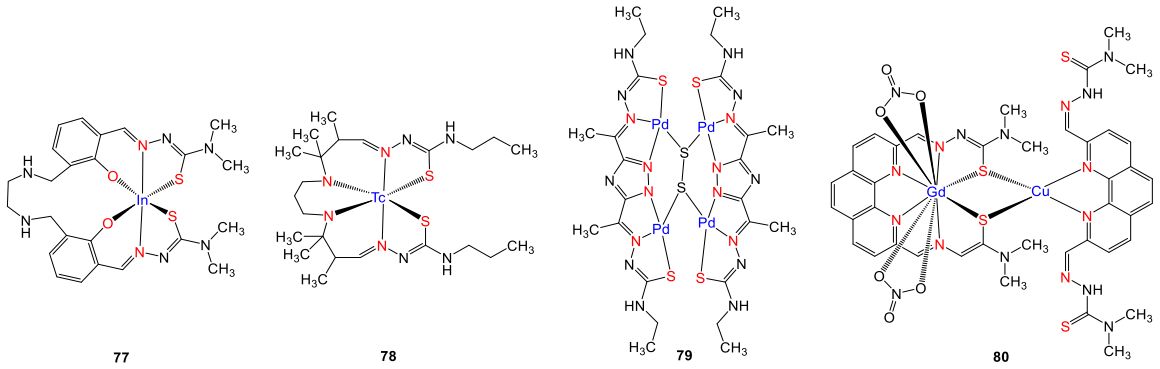


Chart 14. Examples of hexadentate TSCs and their metal complexes from literature. Adopted from Refs. [32,116,272,276].

The hexadentate TSC **79** has two sets of N^N^S donors and was derived from 3,5-diacetyl 1,2,4-triazole.[276] The authors were able to synthesize a tetranuclear Pd(II) complex which consists of two TSC ligands which bind two Pd(II) respectively and which are bridged by a disulfide (Chart 14).

Another interesting example from literature is the heterometallic Gd(III)/Cu(I) TSC complex **80** (Chart 14).[116] The authors synthesized a hexadentate TSC with two N^N^S donor sets and a phenanthroline backbone and formed the corresponding Gd(III) complex. By reacting this complex with $Cu(NO_3)$ and another equivalent of the TSC the authors obtained the bimetallic complex **80** with Gd(III) and Cu(I) metal centers and studied its theranostic properties. While the Gd center can be used for MRI (magnetic resonance imaging) the Cu center can lead to an increased cytotoxicity. Thereby, the authors found a significant cytotoxicity and anti-metastasis ability against breast cancer cells. To improve the selectivity to tumor cells the authors developed a delivery system where they encapsulated the complex into apoferritin NPs thus improving the MRI and cytotoxicity of the complex *in-vitro* and *in-vivo*.[116]

2. Aims and concept

General strategies to improve the pharmacological potential of TSCs have been shown in Figure 7 (Chapter 1.7). These strategies are followed in this research but with new specific targets.

This work has two general tasks. The first one is to explore the derivatization of TSCs for targeted ligand design. For this, especially the *N*4 position is functionalized, to investigate limitations and problems during the synthesis. It was found that functionalization at this position is relatively rare in literature, or functionalization was only done with simple aliphatic and aromatic groups. Introducing more complex functions to this position might open new opportunities for TSCs. The second task is to improve the medical properties of TSCs to overcome problems like side effects, poor selectivity to tumor cells as well as a high lipophilicity and poor H_2O solubility. For this, the six different strategies discussed before are explored in more detail: 1) Conjugation of TSCs to NPs, 2) conjugation of TSCs to biomolecules, 3) tuning the Fe(II)/(III) redox potential of α-pyridyl TSC iron complexes and their immobilization on TiO_2 NPs 4) fluorescence labeling of TSCs, 5) synthesis of amphiphilic TSCs and 6) synthesis of hexadentate bis-TSCs (Figure 19). The structure of the TSCs will be designed to match specific criteria for each strategy. Another general aim is to analyze the cytotoxicity of the synthesized TSC against various cancer cell lines.

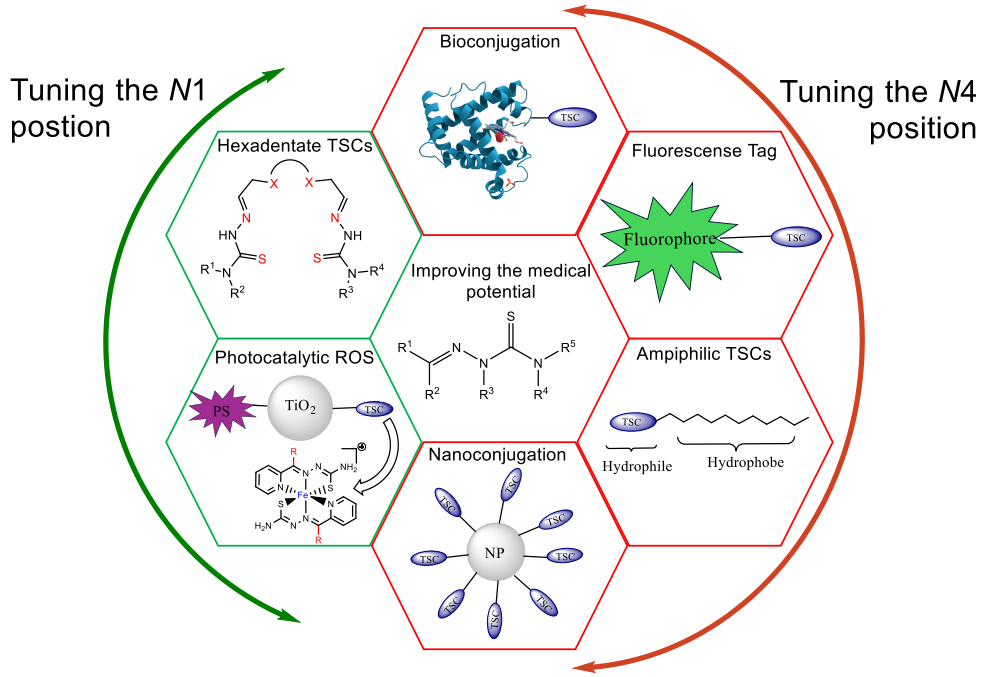


Figure 19. Strategies to improve the pharmacological performance of TSCs. Derivatization at the *N*1 and *N*4 positions is used to design the TSC structure for each concept.

2.1 Conjugation of TSCs to nanoparticles for drug delivery

Nanoconjugation can be used to improve the selectivity of a drug to tumor cells due to the EPR effect or for the transport of lipophilic drugs with poor H_2O solubility. This strategy can be also applied to TSCs to improve their antitumor activity. In this work, the aim is to achieve covalent conjugation of TSCs to the surface of NPs and to investigate these nanoconjugates in detail. For this, mainly SiO_2 and TiO_2 NPs are used as a platform to test conjugation strategies. To do so, the TSCs must have functional groups which can directly bind to the particle surface or react with prefunctionalized NPs (Figure 20). Targets are TSCs with carbon acid, azide, alkyne, amine, hydroxy, thiol, phosphonate, halide, alkoxysilane and isothiocyanate groups. This leads to flexibility for the synthesis of various nanoconjugates in a second step. The functional group should be attached to the *N*4 position of the TSC. In this way, the *N*1 position can be used for late-stage functionalization with ketones and aldehydes to tune the properties of the TSC (e.g. coordination sphere, fluorescence, cytotoxicity). The *N*1 position will

be mainly functionalized with dipyridyl ketone which was found to lead to improved cytotoxicity or with 9-anthraldeyde as a fluorescence tag. The anchor group and the TSC should be separated by a linker unit to reduce the impact of this group on the properties of the TSC. The generalized structure of the target compounds is shown in Figure 20.

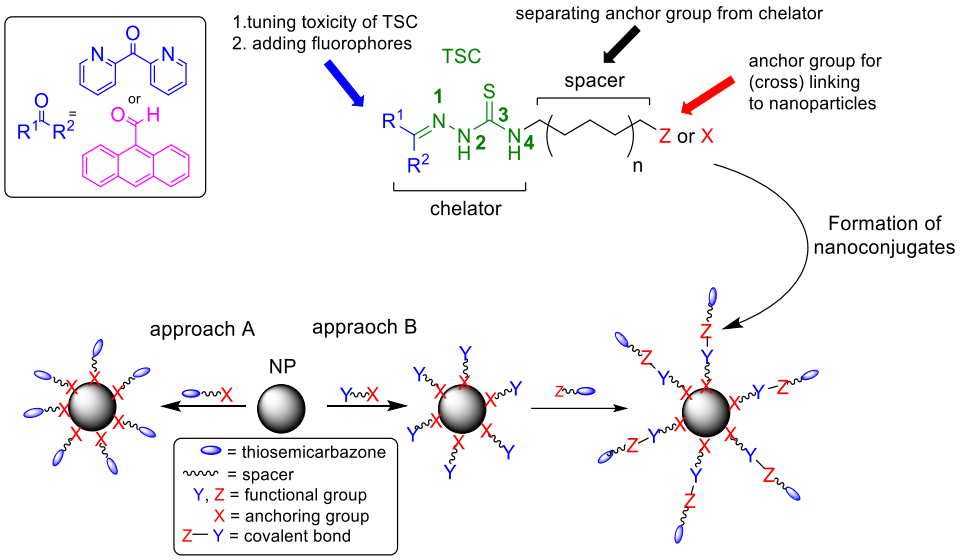
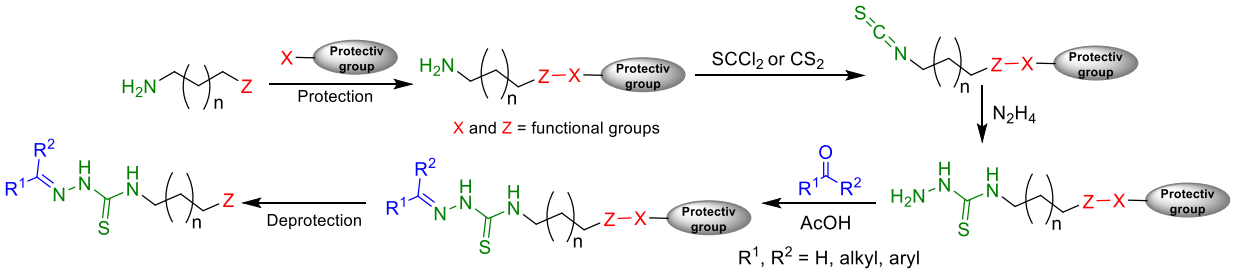


Figure 20. General structure of TSCs for covalent binding to NPs.

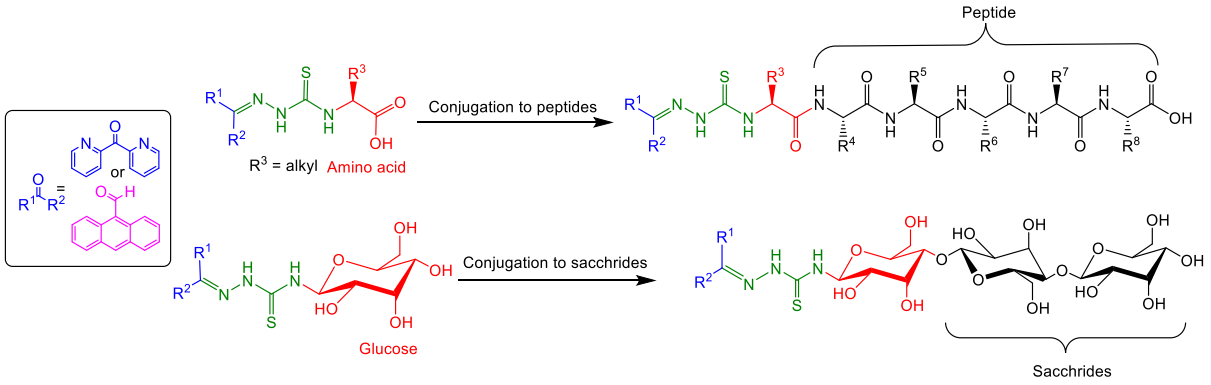
These TSCs are synthetically available from bifunctional, primary amines which have a space group between the amine and the functional group. Depending on the nature of the functional groups, protecting groups should be used to avoid side reactions with thiophosgene/CS_2 and hydrazine during the synthesis of the corresponding thiosemicarbazide (Scheme 15).



Scheme 15. Synthesis of TSCs with functional groups at the *N*4 position starting from bifunctional, primary amines.

2.2 Conjugation of TSCs to biomolecules for drug delivery

Bioconjugation is another strategy for drug delivery. However, a certain biocompatibility and H_2O solubility of the drug is usually necessary to synthesize bioconjugates. Thus, the strategy is used to introduce the chemical structure of bio monomers like amino acids or sugars into the backbone of the TSC. This improves the H_2O solubility of the TSC and in addition the compounds have suitable functional groups to link them to the corresponding biopolymers (peptides and polysaccharides). Again, the structure of the bio monomers will be attached to the *N*4 position, while the *N*1 position will be used for the functionalization with dipyridyl ketone and 9-anthraaldehyde. Starting point for the synthesis of amino acid derived TSCs will be the pool of proteinogenic amino acids at which the TSC is built up at the amine function. The impact of variations in the amino acid backbone on the cytotoxicity of the TSC will be investigated. In case of the sugar derived TSCs, glucose is attached to the TSC backbone. The synthesis of TSC conjugates with peptides will be explored in more detail. The target compounds are shown in Scheme 16.



Scheme 16. Geneal concept for the synthesis of TSC bioconjugates with peptides and saccharides.

2.3 Tuning the Fe(II)/(III) redox potential of α-pyridyl TSC Fe complexes and their immobilization onto TiO_2 NPs

It is well known that Fe(III) complexes of α-pyridyl TSC can catalyze the formation of ROS, which is part of their cytotoxicity. In addition, it was found that the Fe(II)/Fe(III) redox potential is tunable by electron donating or withdrawing substituents at the *N*1 position, which has an impact on catalytic efficiency. These findings will be investigated in more detail during this research. For this, new substituents will be introduced at the *N*1 position and their impact on the redox potential will be analyzed. The aim is to determine the gap between the highest and lowest Fe(II)/Fe(III) redox potential which can be achieved by derivatization. The results of this research can be used to develop a photocatalyst for the formation of ROS. To do so, the Fe(III) α-pyridyl TSC complex as well as the photosensitizer $[Ru(bpy)_3]^{2+}$ can be covalently attached to TiO_2 NPs (Figure 21). Phosphonate groups should be used for the attachment of the catalysts and the photosensitizer, since they lead to a high stability for TiO_2 nanoconjugates. Variating the Fe(II)/Fe(III) redox potential of the attached complexes by derivatization can be used to improve the catalytic performance.

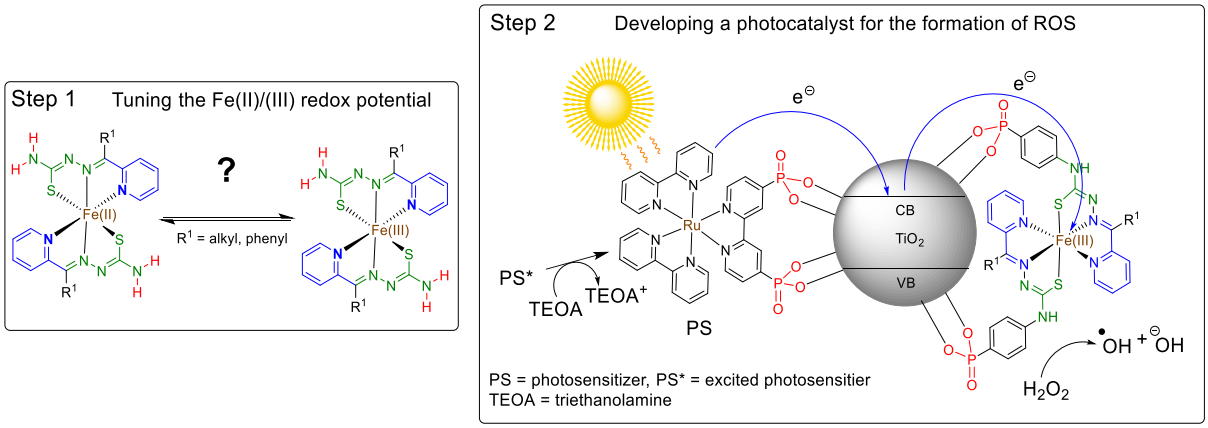


Figure 21. Step 1: Tuning the Fe(II)/Fe(III) redox potential of α-pyridyl TSC iron complexes. Step 2: Synthesis of a photocatalyst to produce ROS, based on TiO_2 NPs, $[Ru(bpy)_3]^{2+}$, and α-pyridyl TSC iron complexes.

2.4 Fluorescence labeling of TSCs

Fluorescent TSCs can be used for monitoring their biodistribution in the cells to get more details about their mode of action. In this work, fluorescent TSCs will be synthesized by attaching fluorophores to the *N*4 position of the TSC (Figure 22). In this way the *N*1 position can be used to tune the cytotoxicity of the compound. For this, dipyridyl ketone will be attached which is known for a high cytotoxicity. Starting point of the synthesis will be the amino derivatives of the fluorophores to build up the TSC at this function. Pyrene, fluorene, anthracene, coumarin, carbazole, tetraphenyl porphyrin, naphthalimide and fluoresceine will be used as the fluorophores. On the one hand this will give the facility to choose

between different dyes with different excitation wavelengths. On the other hand, the impact of different fluorophores on the cytotoxicity of the TSC is unclear and must be investigated. In the next step the corresponding TSC Pt(II) complexes will be synthesized to investigate the impact on the electrochemical and photochemical properties as well as on the cytotoxicity.

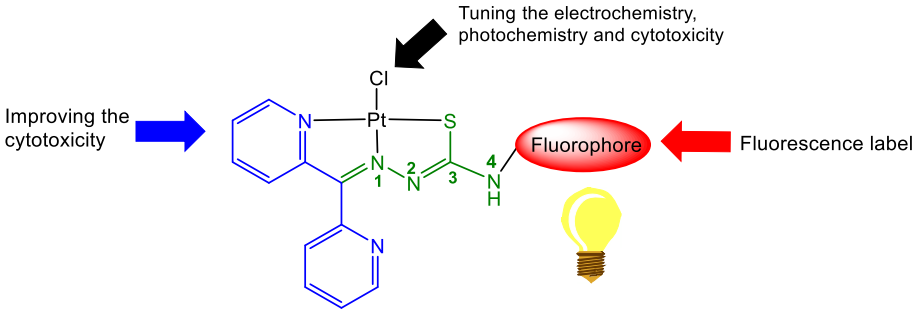


Figure 22. General structure of TSCs with fluorophores.

2.5 Synthesis of amphiphilic TSCs

Amphiphilic metal complexes have often improved biological properties due to their interactions with biomolecules or the ability to form micelles. The aim of this work will be the synthesis of amphiphilic TSCs and their corresponding metal complexes to investigate their antitumor potential. For this the hydrophobic tail will be attached to the *N*4 position. Octylamine, dodecyl amine and hexadecyl amine are used as the starting materials (Figure 23, Targets A). In this way, the lipophilicity can be tuned by varying the aliphatic chain length. In addition, other lipophilic structures with biological relevance such as steroids might be attached. For this purpose, cholesterol might be used as a precursor. The hydrophilic part of the molecule will form the TSC unit. The hydrophilicity can be tuned by attaching polar groups to the *N*1 position. For example, hydroxy and methoxy benzaldehydes could be used but also dipyridyl ketone is again in the focus of interest.

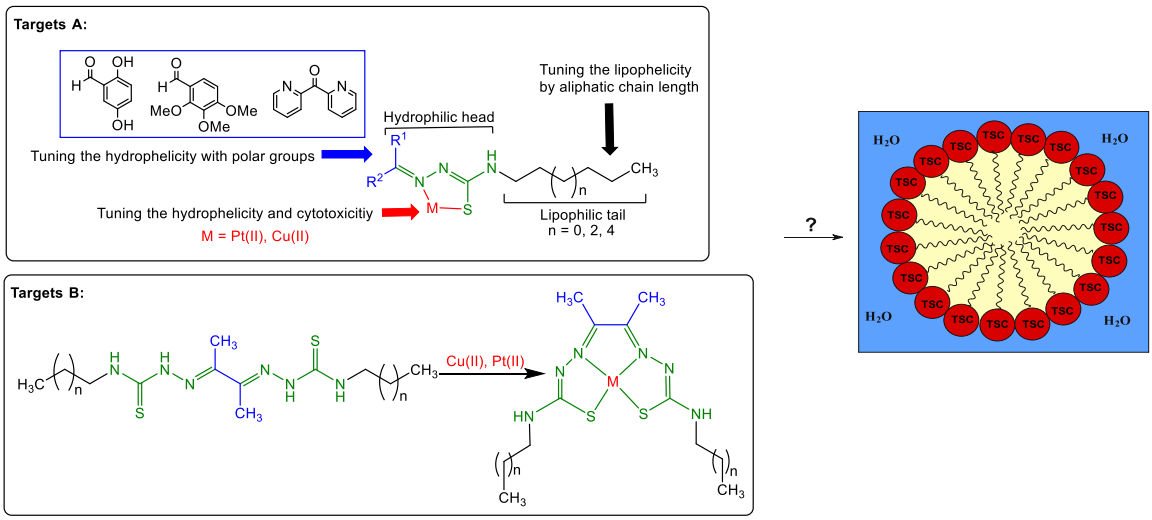


Figure 23. General targets for the synthesis of amphiphilic TSCs.

In addition, bis-TSCs will be synthesized (Figure 23, Targets B). These compounds will have two aliphatic tails in their structure. Metal complexation will direct the aliphatic chains in the same direction due to their square planar geometry. This will be necessary for the formation of micelles later. Complexation will be done with Pt(II) and Cu(II) which might improve the hydrophilicity of the TSC. In addition, the antitumor properties might be improved. In a final step, the affinity to form micelles will be tested as well as the cytotoxicity of the compounds.

2.6 Synthesis of hexadentate TSCs

Hexadentate TSCs have the advantage of a high binding affinity to various metals. In this way they can be used for radiolabeling, the binding of intracellular metals or the synthesis of bimetallic complexes. Herein the synthesis of hexadentate bis-TSCs is investigated. Some restrictions are made on their structure to design their properties for medical applications. The first one is that the ligands should have functional groups for conjugation to form bio -and nanoconjugates. The second one is a heteroaromatic backbone with N and S donors, which contribute to the ligand sphere. In an ideal case they have an extended π system and show a certain fluorescence which simplifies to investigate their biodistribution and the formation of conjugates. The third requirement is high solubility, ideally in H_2O. Since the heteroaromatic backbone will probably decrease their solubility, this might be challenging. By that reason thiosemicarbazides derived from amino acids will be condensed to the dialdehydes. This leads to carbon acid functions in the TSC structure for conjugation and improves their solubility. Starting point of this project will be the synthesis of heteroaromatic dialdehydes/diketones derived from bipyridine (bpy), phenanthroline (phen), diyrido[3,2-a:2′,3′-c]phenazine (dppz), naphthyridine (naph) or dithieno[3,2-b:2′,3′-d]thiophen (DTT). In a second step the corresponding TSCs are synthesized and characterized (Chart 15).

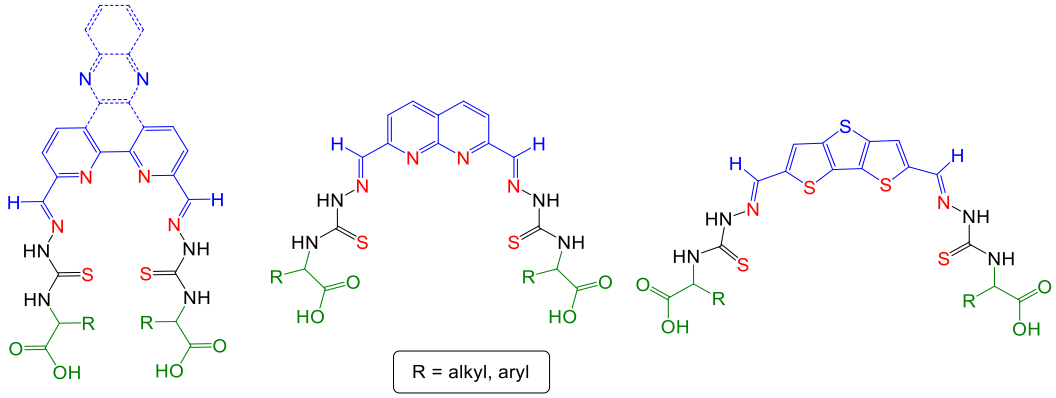


Chart 15. Hexadentate bis-TSCs derived from heteroaromatic dialdeyhdes.

3. Results and Discussion

3.1 Thiosemicarbazones for the covalent conjugation to nanoparticles

3.1.1 Synthesis of TSCs with functional groups at the *N*4 position

Several TSCs for nano conjugation have been synthesized during this research, bearing amine, thiol, azide, alkyne, phosphonate, diol and isothiocyanate functions. Some of these compounds have been first reported during the master thesis of the author which includes TSCs with amine and thiol function. Their synthesis and characterization have been optimized during PhD studies. The successfully synthesized TSCs and their overall yields are summarized in Chart 16. Their synthesis and properties have been published recently.[142] All products were found to be stable under ambient conditions for at least several months to years. However, some of the TSCs with anthracenyl group were sensitive to light and should be stored in darkness, which is mentioned later.

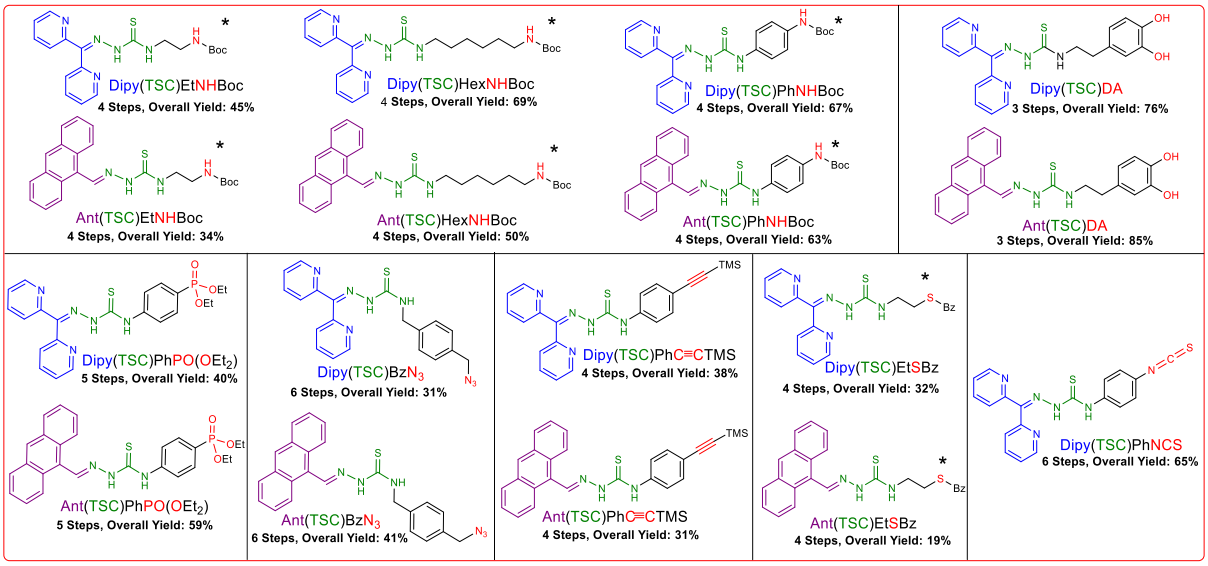


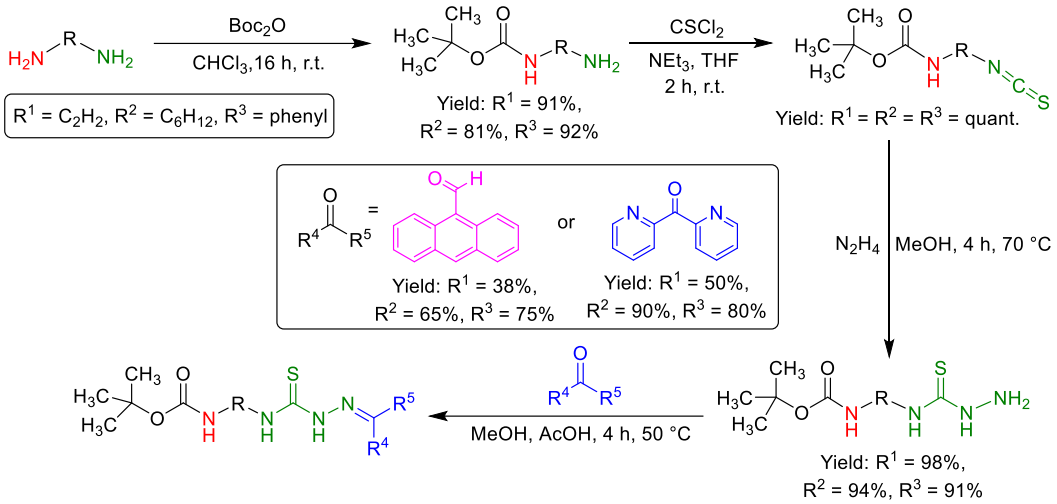
Chart 16. Summary of synthesized TSCs with functional groups at the *N*4 position for their conjugation to NPs. *Compounds have been first reported during master studies.

Their solubility depends on the functional groups attached, but all of them are soluble in polar, organic solvents. The H_2O solubility for most of these TSCs is poor. Exceptions are the di(2-pyridyl)ketone TSCs with diole, amine, and phosphonate group which showed improved solubility after deprotection of their functional groups. In case of the amine derivatives, the corresponding hydrochlorides can be synthesized which shows excellent H_2O solubility. In general, the di(2-pyridyl)ketone TSCs are at least soluble in small concentrations (< 1 mg in 30 mL). The anthracenyl group at the TSCs decreases the H_2O solubility due to its hydrophobic character. Since their solubility in DMSO is excellent, the TSCs are also soluble in mixtures of DMSO/H_2O which is an important criterion to investigate their cytotoxicity later. The synthesis of the TSCs is discussed in the following in more detail. All products were characterized using ^1H and ^{13}C nuclear magnetic resonance (NMR) spectroscopy, electron-spray-ionization mass spectrometry (ESI-MS), UV/Vis absorption and in part, photoluminescence spectroscopy.

3.1.1.1 Synthesis of TSCs from primary amines

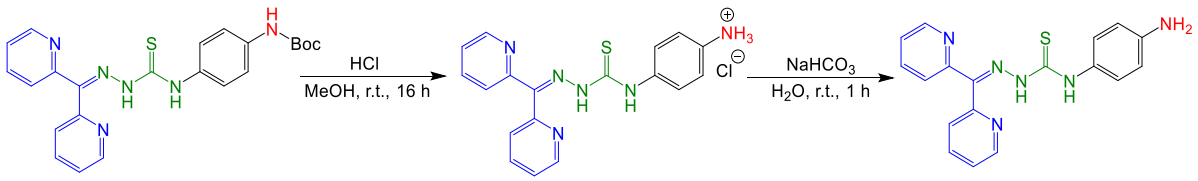
Primary amines are an important functional group for nano conjugation. They can act as surface ligands for noble metal NPs or can be used for crosslinking *via* an amid or urea/thiourea group.[282] Starting point of their synthesis are diamines, whereby the spacer function varies between an ethyl, hexyl or phenyl group. In this way, the flexibility and lipophilicity of the TSCs and their nanoconjugates can be tuned.

In the first step, one of the amine groups was BOC (*tert*-butyloxycarbonyl) protected by methods form literature leading to high yields (81-92%).[283-285] This was followed by the synthesis of the isothiocyanates using thiophosgene and thiosemicarbazides using hydrazine hydrate (Scheme 17). Both steps led to excellent yields (91-100%). In the final step, di(2-pyridyl)ketone and 9-anthraldehyde were condensed to the thiosemicarbazides by sonicating the reaction mixture for 4 h at 50 °C using AcOH as a catalyst. The yields range from 38-80%. Thus, this reaction seems to be a key step to improve the overall yields of the synthesis. Variating the reaction conditions (e.g. solvent, temperature, time and catalyst) will probably lead to further improvements in the future.



Scheme 17. Synthesis of TSCs with amino function, derived from diamines.

The deprotection of the amine by cleaving the BOC function is usually achieved by strong acids like HCl and TFA and was tested at the example of Dipy(TSC)PhNHBoc. Finding the ideal concentration of the acid was found to be important because the TSC starts to decompose at high concentrations of HCl. It was found that 23.0 eq. of HCl are ideal for deprotection. The rection leads to the Dipy(TSC)PhNH$_2$ hydrochloride, which has an excellent H$_2$O solubility. Deprotonation of the amine can be achieved with NaHCO$_3$ (Scheme 18).

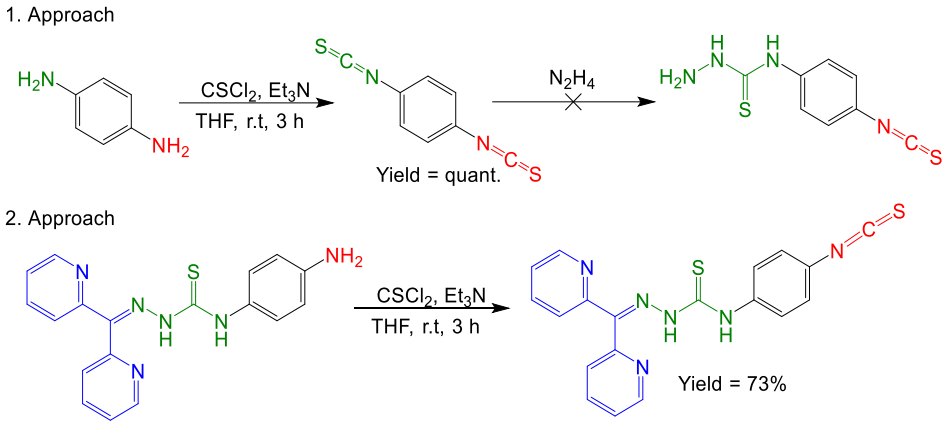


Scheme 18. Deprotection of Dipy(TSC)PhNHBoc using HCl.

3.1.1.2 Synthesis of TSCs with isothiocyanate function

Isothiocyanate functions are important groups for crosslinking because they rapidly form thioureas by their reaction with amines.[282,286] To synthetize TSCs with isothiocyanate group, again diamines were used as the starting material. In the first approach, *p*-phenylenediamine was reacted with thiophosgene yielding the diisothiocyanate in quantitative yields (Scheme 19). However, the next reaction step was found to be problematic because the reaction of hydrazine hydrate with the diisothiocyanate probably leads to a mixture of mono thiosemicarbazide, dithiosemicarbazide, diisothiocyanate as well as polythioureas. Especially the latter is difficult to remove from the mixture. In addition, there was no chance to control the reaction *via* temperature, the equivalents or the addition rate to increase the yield of the mono thiosemicarbazide due to the high reactivity of both reaction partners. As an alternative approach, Dipy(TSC)PhNH$_2$ (Chapter 3.1.1.1) was reacted with thiophosgene. The reaction leads to moderate yields of Dipy(TSC)PhNCS and side reactions with the TSC function were observed but

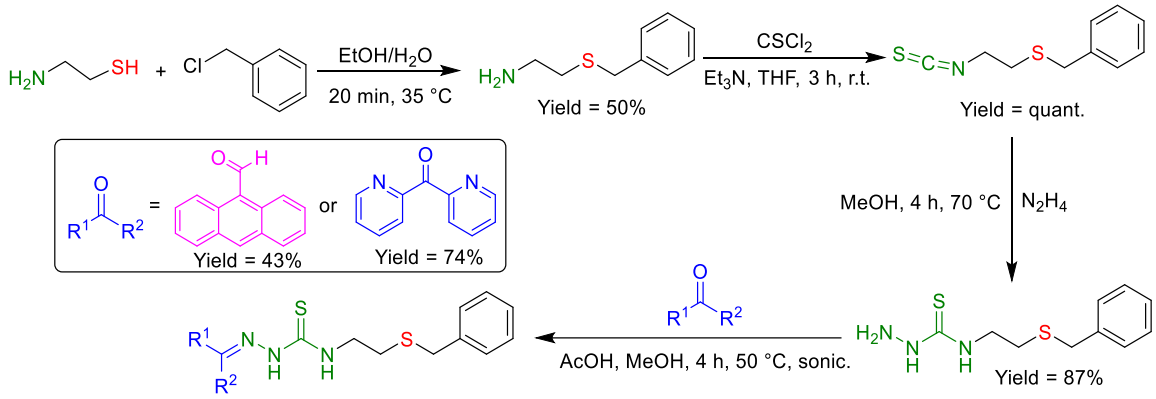
purification of the product was possible. This leads to a total of 5 reaction steps to synthesize TSCs with isothiocyanate function.



Scheme 19. Synthesis of TSCs with isothiocyanate function. Top: Synthetic approach via a diisothiocyanate. Bottom: Synthesis starting from Dipy(TSC)PhNH2.

3.1.1.3 Synthesis of TSCs with thiol function

Thiols are important surface ligands of noble metal NPs.[287] The synthesis of TSCs with thiol function started from 2-aminoethanthiol which was reacted with benzyl chloride to protect the thiol.[288] The benzyl thioether was obtained in poor yields of 50%. This was followed by the synthesis of the TSC by similar methods discussed before. High yields were obtained for most of the reaction steps (Scheme 20).



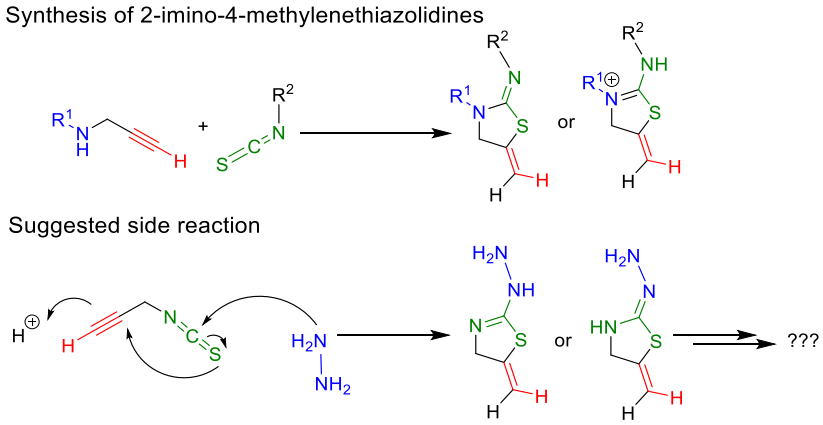
Scheme 20. Synthesis of TSCs with thiol function starting from 2-aminoethanthiol.

Deprotection of the thiol was not successful, since it usually requires harsh reaction conditions like strong acids and bases or reductive and oxidative agents (e.g. alkali metals) which are not tolerated by the TSC group. Some methods have been reported in literature which are using softer reaction conditions, which could be explored in the future.[289] Alternately, the protective group must be changed to other ethers which can be cleaved easier.

3.1.1.4 Synthesis of TSCs with alkyne function

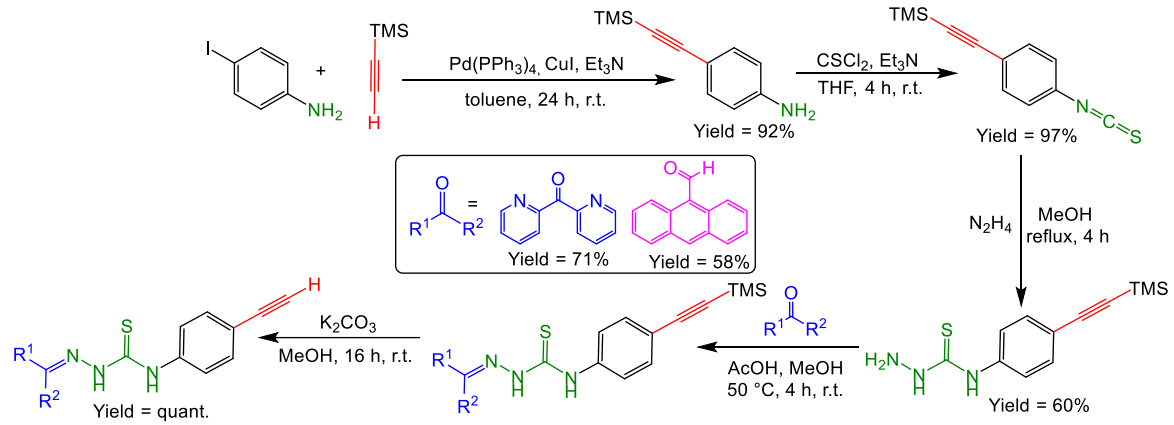
Introducing alkyne functions into the TSC structure is a key step to using them in Cu(I) catalyzed azide-alkyne cycloaddition, which is one of the most prominent methods for nano -and bioconjugation.[290] Starting point of the synthesis was propargylamine. The synthesis of the corresponding isothiocyanate led to high yields. However, the synthesis of the thiosemicarbazide was unsuccessful due to side reactions. It was already published in literature that propargylamine can react with isothiocyanates to 2-imino-4-methylenethiazolidines or 2-amino-4-methylenethiazolines. By that reason, the addition of

hydrazine to propargyl isothiocyanate might trigger similar, intramolecular reactions (Scheme 21). However, it was not possible to identify the side products in detail.



Scheme 21. Top: Reaction of propargylamine with isothiocyanates to 2-imino-4-methylenethiazolidines or 2-amino-4-methylenethiazolines. Bottom: Suggested side reaction of propargyl isothiocyanate with hydrazine.

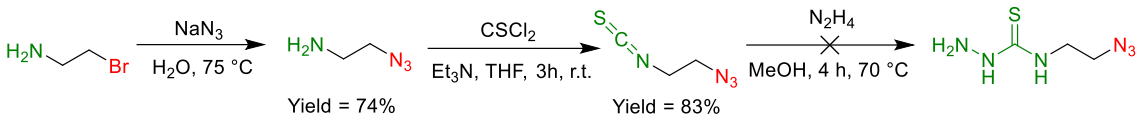
To circumvent intramolecular cyclization, the spacer function between the isothiocyanate and the alkyne was changed to a more rigid phenyl group by using 4-[(trimethylsilyl)ethynyl]aniline as a starting material (Scheme 22). This in turn was synthesized from 4-iodoaniline by *Sonogashira* coupling with trimethylsilyl acetylene (Yield: 92%).[291] The alkyne group is protected by a trimethylsilyl (TMS) function. In this way, the synthesis of the corresponding TSCs was possible in high yields. Cleavage of the TMS group was achieved in quantitative yields under basic conditions using two equivalents of K_2CO_3.



Scheme 22. Synthesis of TSCs with alkyne group using 4-[(trimethylsilyl)ethynyl]aniline as the starting material.

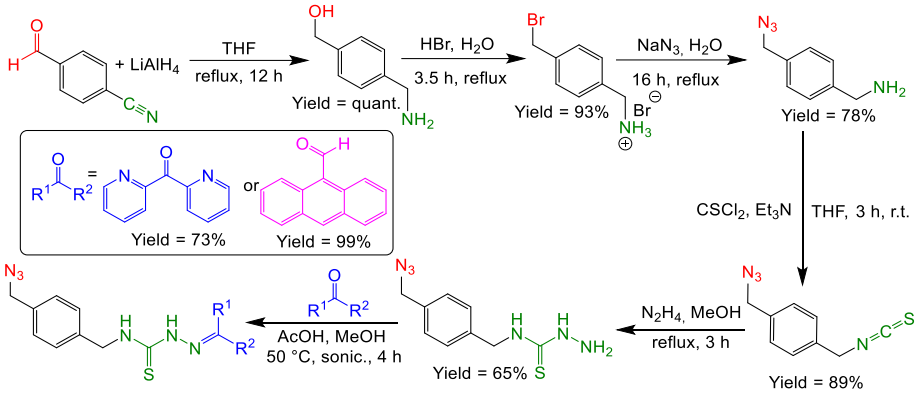
3.1.1.5 Synthesis of TSCs with an azide function

Azide functions are the counterpart to alkynes in Cu(I) catalyzed azide-alkyne cycloaddition and were also attached to the structure of TSCs. At the beginning, 2-azidoethylamine was used as the starting material. While the synthesis of the isothiocyanate was successful (Yield: 83%), the synthesis of the corresponding thiosemicarbazide was not possible (Scheme 23). This was related to side reaction, but the underlying mechanism was not clarified during this research. A plausible explanation could be the decomposition of the compound, since organic azides are often unstable and explosive. Heating the 2-azidoethylisothiocyanate under reflux in MeOH might lead to its decomposition. If the thiosemicarbazide is formed during the reaction, this compound might be even more unstable than the starting material since it contains six nitrogen atoms and only four carbon or sulfur atoms. Another problem might be the flexibility of the spacer function, which was already found for the alkynes.



Scheme 23. Synthetic approach to synthesize thiosemicarbazides with azide function starting from 2-azidoethylamine.

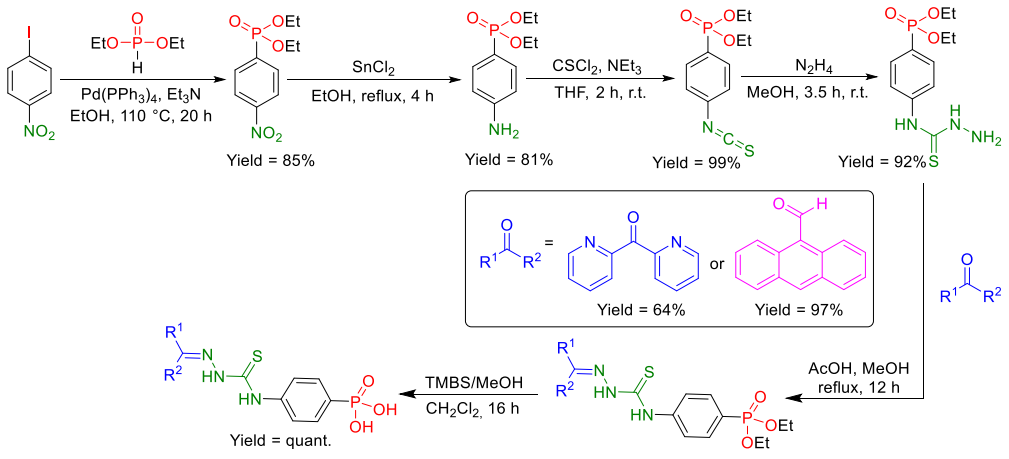
For this reason, 4-(azidomethyl)benzenemethanamine was chosen as a new starting point which was synthesized from 4-cyanobenzaldehyde in three reaction steps (Scheme 24).[292-294] The content of nitrogen is smaller in this molecule, which should increase its stability. In addition, the rigid spacer function can prevent intramolecular side reactions. In this way, the synthesis of the corresponding TSCs was possible in high yields, following the typical approach discussed before. This example shows again the importance of the chemical structure of the spacer group for designing TSCs with functional groups.



Scheme 24. Synthesis of TSCs with azide function derived from 4-(azidomethyl)benzenemethanamine.

3.1.1.6 Synthesis of TSCs with phosphonate function

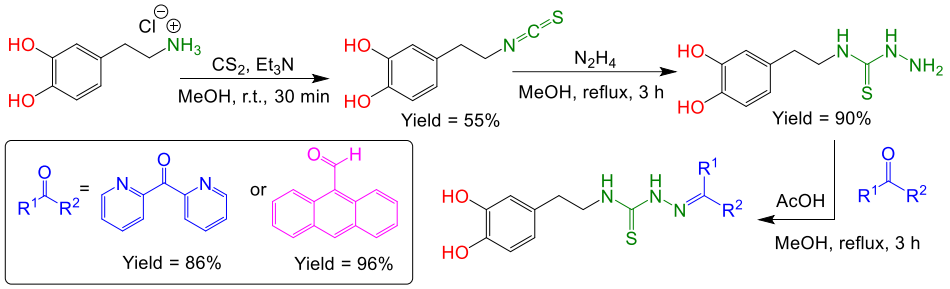
Phosphonates are important anchor groups for the functionalization of TiO_2 NPs.[295,296] Diethyl(4-aminophenyl)phosphonate was used as a starting point for the TSC synthesis, which was synthesized from 4-iodo-nitrobenzene by phosphonylation (Yield: 85%), followed by the reduction of the nitro group (Yield: 81%) (Scheme 25).[297,298] After that, the TSC function was synthesized by similar methods discussed before. The synthesis of the thiosemicarbazide needed some improvement. Reflux of the reaction mixture in the presence of hydrazine led to the decomposition of the phosphonate function. However, performing the reaction at room temperature gave quantitative yields. In this way, the synthesis of the TSCs was possible in high overall yields of 59-40% after five steps. Deprotection of the phosphonate was done with bromotrimethylsilane, yielding the phosphonic acid function in quantitative yields.



Scheme 25. Synthesis of TSCs with phosphonate group starting from diethyl(4-aminophenyl)phosphonate.

3.1.1.7 Synthesis of TSCs with a catechol function

Catechol groups are important surface ligands for iron oxide NPs.[140,299] Dopamine was found to be an ideal precursor for the TSC synthesis since it has a high biological relevance and a catechol as well as primary amine group in its structure. The synthesis of isothiocyanates with hydroxy function has the general problem that side reactions with thiophosgene or CS_2 are observed. By that reason, the alcohol function can be protected by standard methods. However, the reaction can be also performed without any protection since the amine is usually a better nucleophile than the OH group. In this way, reasonable yields can be achieved without protection. Thus, it depends on the yield of protection and deprotection which approach should be used. Using CS_2 instead of thiophosgene is usually the better choice for the synthesis because it is less reactive. The dopamine isothiocyanate was synthesized by a protocol from literature using CS_2 at which 55% yield was obtained (Scheme 26).[300]



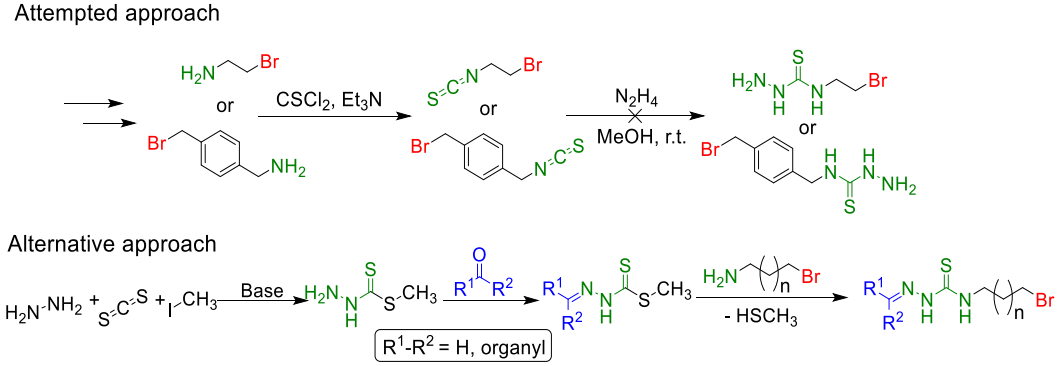
Scheme 26. Synthesis of TSCs with catechol group starting from dopamine.

Synthesis of the corresponding thiosemicarbazide and TSCs was possible in high yields (86-96%). For the di(2-pyridyl) ketone TSC a limited stability in DMSO was observed.

3.1.1.8 Unsuccessful attempts

Some unsuccessful attempts were made during this research to synthesize TSCs with primary bromide, alkoxy silane or sulfonic acid function.

In case of the bromide function, the synthesis of thiosemicarbazide was unsuccessful (Scheme 27). Different spacer units were tested, namely an ethyl as well as a benzyl group. In both cases, side reactions were observed but it was not possible to clarify the mechanism or to identify the side products. Since the reaction was also unsuccessful with rigid spacer groups, a cyclisation reaction is probably not the origin. Instead, it is expected that the bromide can be substituted by hydrazine yielding an alkyl hydrazine. This can be followed by further reactions of this hydrazine derivative. An alternative approach for the synthesis of the thiosemicarbazide could be used in the future. For example, a *S*-methyl dithiocarbazate could be synthesized and reacted with a ketone/aldehyde. In the final step, the *S*-methyl group is substituted by an amino alkyl bromide (Scheme 27). In this way, the *N*4 position is functionalized in the final step and harsh reaction conditions are avoided.



Scheme 27. Top: Synthetic approach, tested during this research. Bottom: Suggested approach for further research in the future.

Also, the attempt to synthesize TSCs with alkoxysilane function was unsuccessful, at which APTMS (3-aminopropyl trimethoxy silane) was used as the starting material. While the synthesis of the corresponding isothiocyanate was again successful, the synthesis of the thiosemicarbazide failed. Decomposition of the trimethoxy silane group was observed due to hydrolysis. Since it is not possible to avoid H_2O during this reaction or polar, protic solvents, this approach was found to be unsuitable. Instead, a late-stage introduction of the silane group could be tested in the future as discussed for the primary bromide function before.

To introduce a sulfonic acid function into the structure of TSCs, sulfanilic acid was used as the starting material. However, the synthesis of the corresponding TSC has the problem that this functional group increases the solubility in H_2O, which makes the purification of the intermediates difficult during the synthesis. In this way, already the synthesis of the corresponding isothiocyanate failed. In the future, it will be probably necessary to synthesize sulfonic esters to mask the properties of the acid function during the TSC synthesis. Again, a late-state functionalization of the *N*4 position would be a better choice.

3.1.2 Photophysical properties of *N*4 functionalized TSCs with functional groups

UV/Vis absorption spectra of the *N*4 functionalized TSCs with anthracenyl group showed three maxima at around 255 nm (intense), 300 nm and 390 nm (Figure 24, left). The exact absorption maxima and extinction coefficients are summarized in Table 3. The shape of the spectrum is in accordance with the typical spectrum of anthracene, which is dominant for the anthracenyl TSCs.[301] The absorption maxima are not significantly shifted between different residues at the *N*4 position since both groups are spatially separated. However, there are differences in the shape of the absorption band around 390 nm. For some of the TSCs (e.g. Anth(TSC)DA), the absorption band shows a pronounced vibrational fine structure, which is typical for anthracene. However, for most of the TSC, this was not observed which indicates interactions of the TSCs in solution. In principle, π–π stacking of the anthracenyl group or hydrogen bonding between the TSCs function might be possible. The functional group at the *N*4 position might have an impact on these interactions, due to sterically repulsion or further attractive interactions caused by functional groups at this position (e.g. OH).

The TSCs with dipyridyl ketone residue at the *N*1 position show three absorption maxima (Figure 24, right and Table 3) around 235 nm, 275 nm and 340 nm, which are related to a related to n → π* and π → π* transitions. These results are in accordance with literature.[302,303] The long wavelength absorption was attributed to an intra-ligand charge transfer (ILCT) of the thione group to the dipyridyl ketone unit in literature.[302]

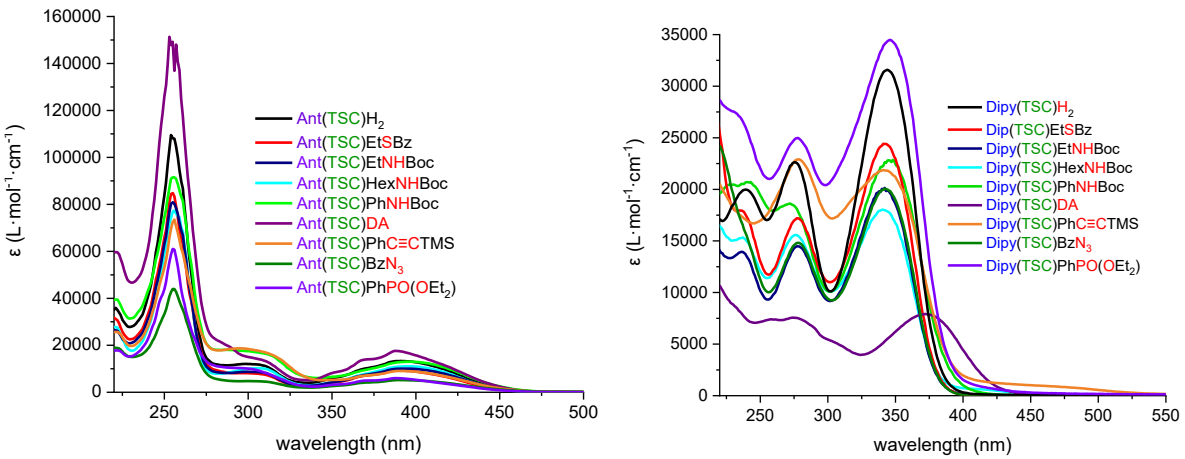


Figure 24. UV/Vis absorption spectra of *N*4 functionalized TSCs with anthracenyl groups (left) and dipyridyl groups (right) measured in MeCN.

It is known that the absorption properties of dipyridyl ketone TSCs are very sensitive to its surroundings because they can form intra -and intermolecular hydrogen bonds. An additional factor is the thiol/thione tautomerism in solution and the pH sensitivity due to the acidity of the hydrazone proton, which can affect the absorption properties.[302] The solvent sensitivity is also in accordance with DFT calculations from literature, which locate the LUMO at the imine and pyridine unit and the HOMO at the thione.[2,302] Since these functionalities are also involved in hydrogen bonding or protonation and deprotonation processes, their energy is affected by the solvent. The absorption spectra of the synthesized dipyridyl ketone TSCs show small shifts between the mentioned absorption maxima (Table 3). Again, the residues on the *N*4 position might have an impact on the interactions of the TSCs in solution.

Table 3. Absorption maxima of the *N*4 functionalized TSC.[a]

Compound	λ_1 [nm], ε [L·mol^{-1}·cm^{-1}]	λ_2 [nm], ε [L·mol^{-1}·cm^{-1}]	λ_3 [nm], ε [L·mol^{-1}·cm^{-1}]
Ant(TSC)H_2	255, 108110	299, 12090	388, 13250
Ant(TSC)EtSBz	254, 84390	298, 8160	390, 9070
Ant(TSC)EtNHBoc	255, 80920	300, 8730	393, 10070
Ant(TSC)HexNHBoc	256, 77350	307, 9250	395, 11070
Ant(TSC)PhNHBoc	255, 91530	295, 17680	397, 13000
Ant(TSC)DA	255, 149230	302, 14750	388, 17620
Ant(TSC)PhC≡CTMS	256, 73520	296, 18650	390, 9070
Ant(TSC)BzN_3	256, 43980	300, 4740	390, 5190
Ant(TSC)PhPO$(OEt)_2$	255, 61040	298, 10250	388, 6010
Dipy(TSC)H_2	239, 19970	276, 22630	344, 31590
Dipy(TSC)EtSBz	236, 17950	277, 17200	342, 24390
Dipy(TSC)EtNHBoc	236, 13950	278, 14480	341, 18010
Dipy(TSC)HexNHBoc	237, 15340	276, 15570	342, 20050
Dipy(TSC)PhNHBoc	240, 20710	272, 18620	346, 22790
Dipy(TSC)DA	258, 7410	275, 7560	372, 7919
Dipy(TSC)PhC≡CTMS	-	278, 22910	341, 21840
Dipy(TSC)BzN_3	-	278, 14820	342, 20050
Dipy(TSC)PhPO(OEt_2)	229, 27570	278, 24970	346, 34490

[a] Measured in MeCN.

TSCs with anthracenyl group showed a characteristic fluorescence in acetonitrile (MeCN) (Figure 25). A broad maximum is usually found between 490-508 nm (Table 4), depending on the residue at the *N*4 position. In addition, two shoulders around 410 nm and 440 nm are observed.

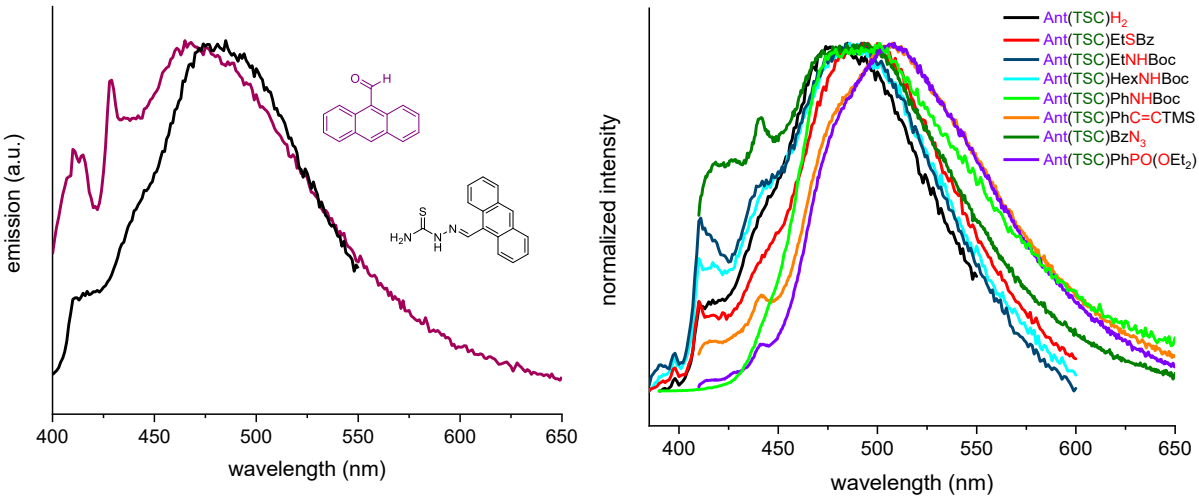


Figure 25. Left: Normalized emission spectrum of 9-anthraldehyde and Ant(TSC)H_2 in MeCN upon irradiation at 365 nm. Right: Normalized emission spectra of *N*4 functionalized TSCs with anthracenyl group in MeCN upon irradiation at 365 nm.

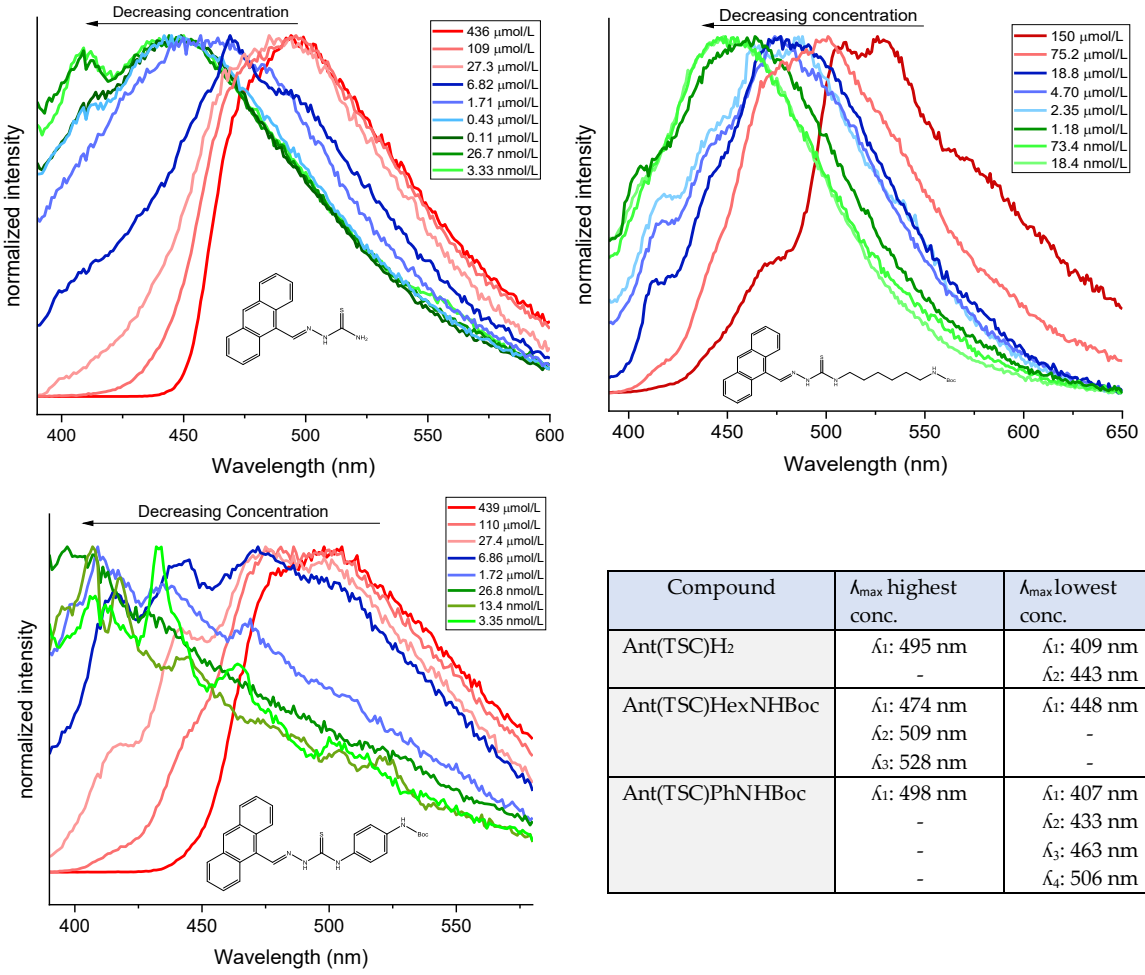
Depending on the residue at the *N*4 position, these shoulders are pronounced with a different magnitude. This observation is in accordance with literature for other TSCs with anthracenyl group.[251] Again, the measurements indicate the presence of aggregates in solutions like excimers or exciplexes and support the finding of UV/Vis absorption spectroscopy.

Table 4. Emission maxima of *N*4 functionalized TSCs with anthracenyl group.[a]

Compound	λ_1 [nm]	λ_2 [nm]	λ_3 [nm]
Ant(TSC)H_2	418	-	480
Ant(TSC)EtSBz	410	-	494
Ant(TSC)EtNHBoc	411	442 (s)	487
Ant(TSC)HexNHBoc	410	444 (s)	487
Ant(TSC)PhNHBoc	-	-	489
Ant(TSC)PhC≡CTMS	416	442	506
Ant(TSC)BzN_3	418	441	484
Ant(TSC)PhPO(OEt_2)	-	441	508

[a] Measured in MeCN upon irradiation at 365 nm.

To investigate these interactions in more detail, concentration dependent fluorescence measurements were performed (Figure 26). To analyze the impact of different residues at the *N*4 position, this experiment was performed with Ant(TSC)H_2, Ant(TSC)PhNHBoc and Ant(TSC)HexNHBoc. In this way, residues with different sterically demand can be compared to each other. In all cases, the emission maximum shifts to lower wavelength upon dilution.



Compound	λ_{max} highest conc.	λ_{max} lowest conc.
Ant(TSC)H_2	λ_1: 495 nm -	λ_1: 409 nm λ_2: 443 nm
Ant(TSC)HexNHBoc	λ_1: 474 nm λ_2: 509 nm λ_3: 528 nm	λ_1: 448 nm - -
Ant(TSC)PhNHBoc	λ_1: 498 nm - - -	λ_1: 407 nm λ_2: 433 nm λ_3: 463 nm λ_4: 506 nm

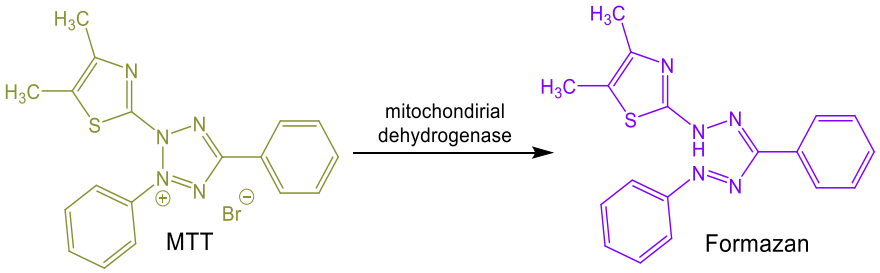
Figure 26. Concentration dependent, normalized emission spectroscopy of Ant(TSC)H_2 (Top, left), Ant(TSC)HexNHBoc (Top, right) and Ant(TSC)HexNHBoc (Bottom, left) in MeCN at room temperature. Bottom, right: Summary of the emission maxima at the highest and lowest concentration in MeCN. Excitation at 365 nm.

In case of Ant(TSC)H_2, the absorption maximum is located at 495 nm for the highest concentration (436 µmol/L). Upon dilution, the formation of two maxima is found at 409 nm and 443 nm. In this way, the maximum is shifting by 86 nm or rather 52 nm. The transformation of this spectral shape was observed stepwise upon dilution. After reaching a concentration of 26.7 nmol/L, the shape did not change anymore. For intermediate concentrations, the maximum was very broad, which indicates a mixture of different species. It remains unclear, if the formation of aggregates was completely prevented upon dilution. In case of Ant(TSC)HexNHBoc, the compound shows a broad emission maximum for the highest concentration (150.0 µmol/L) consisting of three maxima at 474, 509 and 525 nm. Upon dilution, the maximum shifts to 448 nm. In addition, a small shoulder at 410 nm is observed. This shape was observed for a concentration of 73.4 nmol/L and did not change upon further dilution. The Ant(TSC)PhNHBoc showed a broad maximum at 489 nm for the highest concentration. Dilution to concentrations around 13.4 nmol/L led to a pronounced vibrational fine structure at 407, 433, 463 and 506 nm.

From these results it becomes clear that the emission properties of these TSCs are extremely concentration dependent. It seems that aggregation can be at least reduced upon dilution. By comparing the emission spectra of these TSCs at similar concentrations, it is found that they drastically differ in their shape, which also shows the impact of the residue at the *N*4 position. Since aggregation is also found at very small concentrations, it can be suggested that the interactions between the TSCs are quite strong. This would mean that hydrogen bonding is probably more important than π–π stacking, since it is stronger. These investigations could be extended in the future by performing concentration depending UV/Vis absorption spectroscopy. In this way, also concentration dependency of the dipyridyl ketone TSCs could be investigated. However, the results are already pointing out that the absorption and emission properties of TSCs can be much more complex than expected, which is related to their interactions with their surroundings.

3.1.3 Cytotoxicity of *N*4 functionalized TSCs with functional groups

To explore the cytotoxicity of the *N*4 functionalized TSCs, MTT (3-(4,5-dimethylthiazol-2-yl)-2,5-diphenyl tetrazolium bromide) assays have been performed to determine the cell viability after incubation for 24 h with the respective TSC. In this assay, the reduction of the yellow, H_2O soluble MTT to the violet, H_2O insoluble formazan by mitochondrial dehydrogenases is followed by UV/Vis absorption spectroscopy (Scheme 28). The enzyme activity is correlated to the cell viability, which is used to calculate the % inhibition (Equation 1 and 2).[304]



Scheme 28. Principal of the MTT assay: MTT is reduced to formazan by mitochondrial dehydrogenases. The conversion is followed by UV/Vis absorption spectroscopy.

The toxicity was tested against three different cell lines namely HepG2 (huma liver cancer cell line), HCT-116 (human colon cancer cell line) and HEK-293 (human embryonic kidney cell line). The latter was used as a reference cell line to check for possible tumor selectivity. The TSCs were dissolved in 1% DMSO (in H_2O). As a positive and negative reference 50 µM cisplatin and 1% DMSO were used respectively. For the tested TSC, the % inhibition was determined at a concentration of 50 µM (Equation 2), which is shown in Table 5.

$$\text{cell viability} = \frac{\text{absorbance (control)} - \text{absorbance (test)}}{\text{absorbance (control)}} \cdot 100 \quad \textbf{(1)}$$

$$\%\ \text{Inhibition} = 100 - \textit{cell viability} \quad \textbf{(2)}$$

Table 5. % Inhibition of the tested TSCs at a concentration of 50 µM.[a]

Compounds	HepG2	HCT-116	HEK-293
	% Inhibition at 50 µM±SD		
Dipy(TSC)PhNH$_2$	70.51 ± 1.42	89.14 ± 1.00	71.66 ± 1.21
Dipy(TSC)PhC≡CH	42.69 ± 0.32	39.50 ± 0.13	71.36 ± 0.32
Dipy(TSC)DA	55.95 ± 0.87	57.91 ± 0.64	80.14 ± 2.41
Dipy(TSC)PhNCS	94.90 ± 1.21	92.03 ± 1.12	78.74 ± 1.31
Dipy(TSC)BzN$_3$	52.57 ± 1.03	47.88 ± 1.31	95.71 ± 1.54
Dipy(TSC)EtSBz	57.67 ± 2.22	43.43 ± 1.54	70.58 ± 2.26
Dipy(TSC)PhPO(OEt)$_2$	70.88 ± 1.32	83.55 ± 1.54	72.35 ± 0.92
Dipy(TSC)PhPO(OH)$_2$	60.56 ± 1.25	67.01 ± 1.82	85.40 ± 2.41
Cisplatin	67.32 ± 2.12	75.32 ± 1.24	97.33 ± 2.31

[a] The values were determined in an MTT assay.

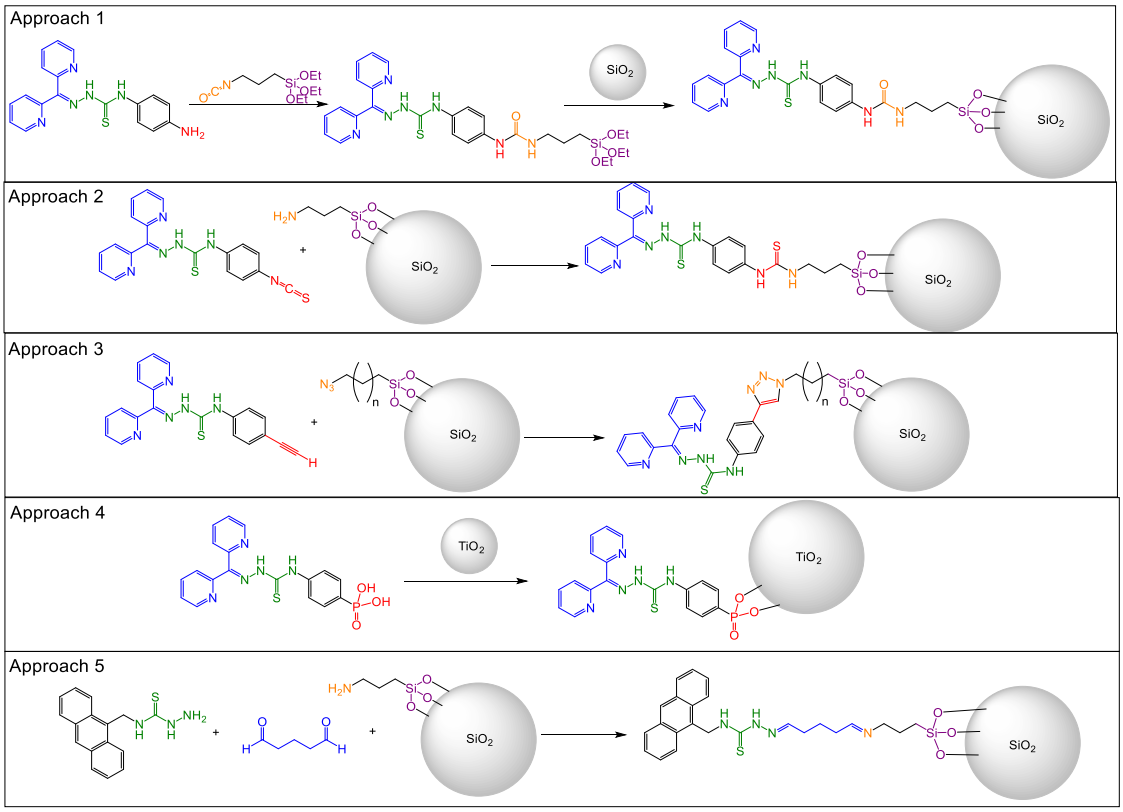
For all the tested TSCs a significant % inhibition was observed after 24 h incubation. For most of the TSCs, the highest inhibition was observed against HEK-293, which indicates no selectivity to the tested tumor cell lines. However, the same observation was made for the positive control cisplatin. In case of the Dipy(TSC)PhNCS, Dipy(TSC)PhNH$_2$ and Dipy(TSC)PhPO(OEt)$_2$, the % inhibition against the cancer cells was to some extent higher compared to HEK-293. At the same time, these compounds showed the highest inhibition against HepG2 and HCT-116 of all the tested compounds, which was 70-95%. Interestingly, the deprotection of Dipy(TSC)PhPO(OEt)$_2$, led to a reduced cytotoxicity (60-67%). For most of the other compounds, the % inhibition ranges between 40% to 60%. In this way, the % inhibition was smaller, compared to cisplatin. The differences in the cytotoxicity are maybe attributed to differences in their cellular uptake, which is often related to the residue at the *N*4 position.[39]

The results give some interesting first insights into the cytotoxicity of the newly synthesized TSCs. In the future, these investigations should be done in more detail, which include concentration and time-dependent measurements of the cytotoxicity and the determination of IC_{50} values. Especially, the time dependency of the cytotoxicity is a factor, which should not be underestimated, and which is discussed in more detail in Chapter 3.3.4. By that reason, also longer incubation times should be explored (e.g. 48 h and 72 h).

3.1.4 Conjugation of TSCs to nanoparticles

Some TSCs were selected to investigate their conjugation to nanoparticles (NPs). An overview of the tested approaches is shown in Scheme 29. In the first approach TSCs with amine group are linked to silica NPs *via* the formation of a urea function. 3-(triethoxysilyl)propyl isocyanate can be used for crosslinking which is reacted with the amino TSC to form a urea, followed by its condensation to SiO_2 NPs. In the second approach TSCs with isothiocyanate function are linked to APTMS (3-aminopropyl)trimethoxysilane) functionalized SiO_2 NPs by forming a thiourea group. In the third approach TSCs with alkyne group are connected by click reaction to prefunctionalized SiO_2 NPs, having azide groups at their surface. In the fourth approach TSCs with phosphonate group are directly attached to the surface of TiO_2 NPs. In the last approach, it was tested to conjugate thiosemicarbazides to the

surface of SiO_2 NPs by the formation of a TSC. For this, the particles are prefunctionalized with APTMS and glutaraldehyde to have aldehyde functions at the particle surface.



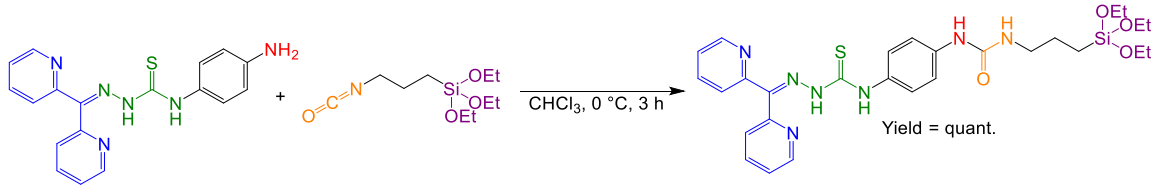
Scheme 29. Tested approaches for the functionalization of SiO_2 and TiO_2 NPs with TSCs.

3.1.4.1 Molecular test reaction

Before nanoconjugates are synthesized, it is important to test the conjugation at the example of molecular test reactions. This has the advantage that it is much easier to determine success, yield and purity of the conjugate at a molecular level than for functionalized NPs. For the latter, it is usually necessary to use different analytical techniques to prove a successful conjugation. In addition, it can be difficult to distinguish between covalent attachment and adsorption. In this way, the reaction conditions should be optimized for molecular reactions, before they are used for nanoconjugation.

Reaction of amino TSCs with 3-(triethoxysilyl)propylisocyanat

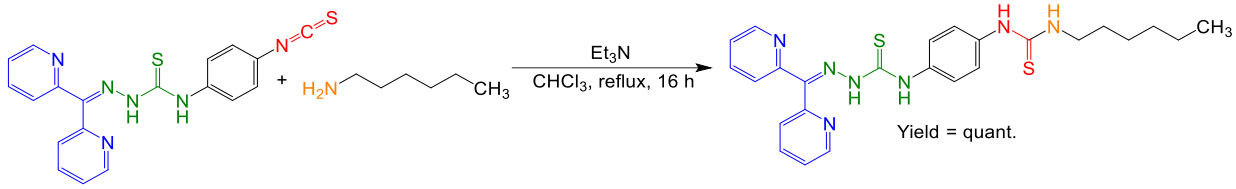
To link Dipy(TSC)PhNH$_2$ to SiO_2 NPs *via* a urea function it must be reacted with 3-(triethoxysilyl)propylisocyanate. The reaction product can be condensed to the particle surface in a second step. It was found that their reaction at room temperature leads to decomposition due to the high reactivity of the isocyanate. By slowly adding the isocyanate at 0 °C to the TSC, the reaction gave quantitative yields (Scheme 30). The reaction and the product should be handled under inert conditions to avoid hydrolysis of the triethoxysilyl group.



Scheme 30. Conjugation of Dipy(TSC)PhNH$_2$ to 3-(triethoxysilyl)propylisocyanate.

Reaction of isothiocyanate TSCs with primary amines

The reaction of Dipy(TSC)PhNCS with primary amines like 1-hexylamine needed increased temperature (reflux $CHCl_3$) and the addition of a Et_3N as a catalyst (Scheme 31). Reaction at room temperature, without a base led to no reaction conversion, which is quite surprising because isothiocyanates are usually quite reactive at room temperature.



Scheme 31. Conjugation of Dipy(TSC)PhNCS to 1-hexylamine.

It is suggested that the TSC and the amine can interact in solutions *via* hydrogen bonding which maybe slows down the reaction of the amine with the isocyanate function at room temperature. The decreased reactivity of nucleophiles due to hydrogen bonding has been already described in literature.[305] Hydrogen bonding was confirmed by ^{1}H NMR spectroscopy after mixing of 1-hexylamine with Dipy(TSC)H_2 (Figure 27). The disappearance of the NH and NH_2 signals of the TSC was observed, while a broad signal around 3 ppm appears. This observation was reversible after removing the 1-hexylamine.

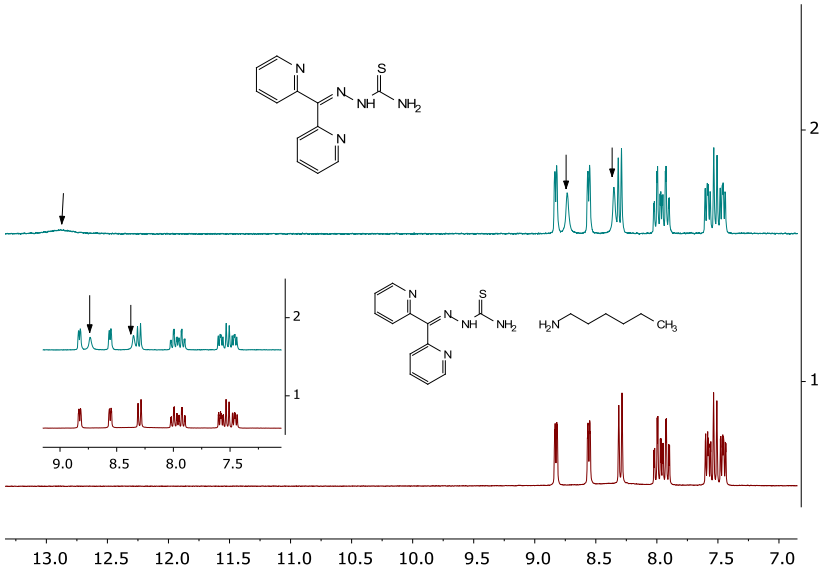
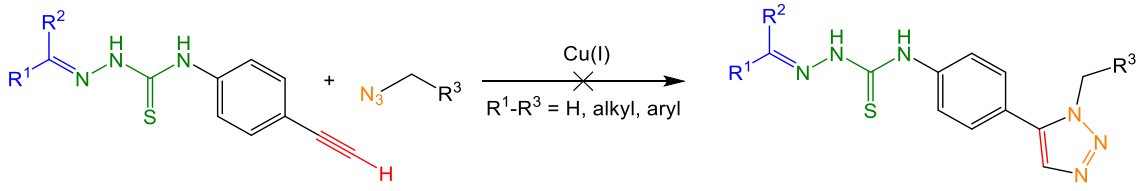


Figure 27. ^{1}H NMR spectrum at 300 MHz in DMSO-d_6. Top: Dipy(TSC)H_2. Bottom: Mixture of Dipy(TSC)H_2 and 1-hexylamine.

Cu(I) catalyzed azide-alkyne click reaction with TSCs having azide and alkyne groups

The Cu(I) catalyzed azide-alkyne click reaction of TSCs with alkyne function and organic azides was found to be unsuccessful. (Scheme 32).



Scheme 32. General reaction scheme for the Cu(I) catalyzed azide-alkyne click reaction of TSCs with alkyne function.

By that reason, various reaction conditions, catalysts and starting materials (**A1-A6**, **B1-B3**) have been tested (Table 6 and 7). However, all the tested approaches failed. Control experiments for the coupling of phenyl acetylene and 1-azidopentane were successful, which proved that there might be a specific problem of TSCs as a substrate in this reaction.

Tabel 6. Overview about the used starting materials for screening the Cu(I) catalyzed azide-alkyne click reaction.

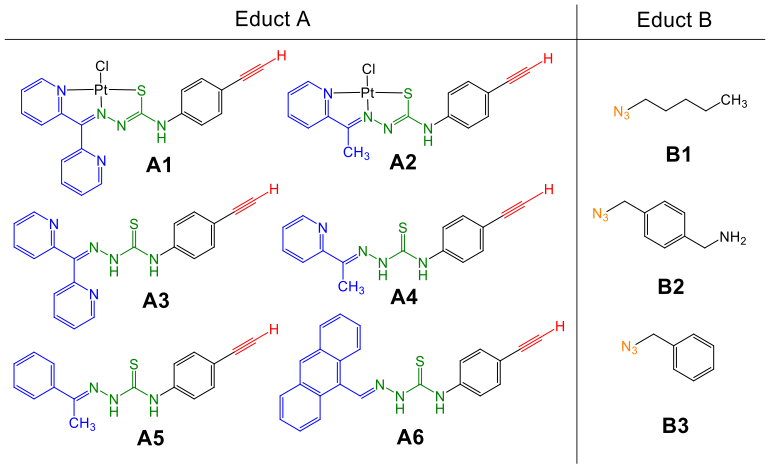


Table 7. Tested reaction conditions for Cu(I) catalyzed azide-alkyne click reaction of TSCs with alkyne function.[a]

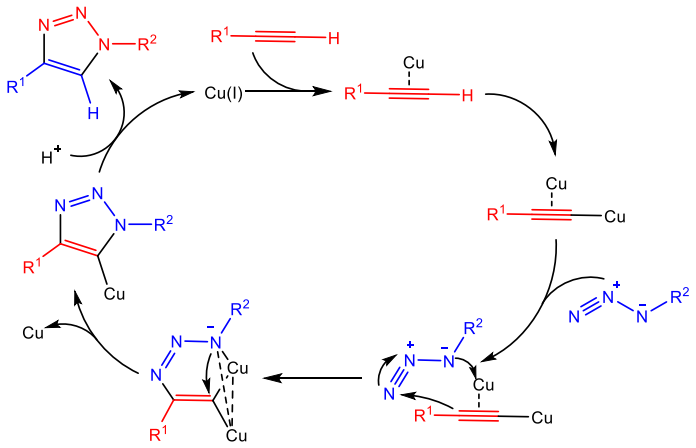
Educt A	Educt B	Cu(I) catalyst [mol%]	Stabilizing Ligand [mol%]	Solvent	T [°C]	Outcome
A1	B1	$CuSO_4$ (4 mol%), sodium ascorbate (10 mol%)	-	EtOH/H_2O (9:1)	r.t.	Starting material
A1	B1	$CuSO_4$ (5 mol%), sodium ascorbate (20 mol%)	-	THF/H_2O (17:1)	r.t.	Starting material
A1	B1	$CuSO_4$ (5 mol%), sodium ascorbate (20 mol%)	-	DMF/H_2O (3:1)	r.t.	Starting material
A1	B1	$CuSO_4$ (10 mol%), sodium ascorbate (30 mol%)	-	DMF/H_2O (3:1)	90	Decomposed
A1	B1	$CuSO_4$ (5 mol%), sodium ascorbate (20 mol%)	Histidine (5 mol%)	DMF/H_2O (1.67:1)	r.t.	Starting material
A1	B1	CuBr (10 mol%), DIPA (1.00 eq.)	-	DMF	r.t.	Starting material
A1	B2	$CuSO_4$ (5 mol%), sodium ascorbate (20 mol%)	-	DMF/H_2O (3:1)	r.t.	Starting material
A2	B1	$CuSO_4$ (10 mol%), sodium ascorbate (30 mol%)	-	DMF/H_2O (3:1)	90	Decomposed
A2	B3	$CuSO_4$ (5 mol%), sodium ascorbate (20 mol%)	-	DMF/H_2O (3:1)	r.t.	Starting material
A2	B3	$CuSO_4$ (5 mol%), sodium ascorbate (20 mol%)	TBTA (5 mol%)	DMF/H_2O (3:1)	r.t.	Starting material
A2	B3	$[Cu(CH_3CN)_4]PF_6$ (5 mol%)	TBTA (5 mol%)	DMF	r.t.	Starting material
A3	B2	$CuSO_4$ (5 mol%), sodium ascorbate (20 mol%)	-	DMF/H_2O (3:1)	r.t.	Starting material
A3	B1	$CuSO_4$ (5 mol%), sodium ascorbate (20 mol%)	Histidine (5 mol%)	DMF/H_2O (1.67:1)	r.t.	Starting material
A3	B2	$CuSO_4$ (5 mol%), sodium ascorbate (20 mol%)	-	H_2O/*t*BuOH (1:1)	r.t.	Starting material
A3	B1	$[CuBr(PPh_3)_3]$ (2.00 eq.), Et_3N (1.00 mL)	-	DMF	r.t.	Side reaction
A3	B2	$[CuBr(PPh_3)_3]$ (2.00 eq.), Et_3N (1.00 mL)	-	DMF	r.t.	Side reaction

A3	B1	CuBr (10 mol%), Et_3N (1.00 mL)	-	DMF	r.t	Starting material
A3	B1	$CuSO_4$ (5 mol%), sodium ascorbate (20 mol%)	-	DMF/H_2O (3:1)	90	Starting material
A4	B1	$CuSO_4$ (10 mol%), sodium ascorbate (30 mol%)	-	DMF/H_2O (3:1)	r.t.	Starting material
A5	B1	$CuSO_4$ (10 mol%), sodium ascorbate (30 mol%)	-	DMF/H_2O (3:1)	r.t.	Starting material
A6	B1	$CuSO_4$ (10 mol%), sodium ascorbate (30 mol%)	-	DMF/H_2O (3:1)	r.t.	Starting material

[a] Procedure: 10 mg of TSC was used for each approach as well as 2 mL of the solvent (mixtures). Reactions were stirred for 16 h.

In the first step, the impact of the chemical structure of the TSC on the outcome of the reaction was investigated. Since TSCs are multidentate ligands, they have several donor sites which can bind to the Cu(I) catalyst and can have an impact on catalysis. For example, the redox potential of Cu(I)/(II) can be changed by complexation and lead to a stabilization of the undesired Cu(II) state. In addition, complexation potentially leads to sterically hindrance, which hinders the Cu(I) center to participate in the catalytic cycle (Scheme 33). The Dipy(TSC)PhC≡C (**A3**) has four donor sites namely two pyridine groups, one azomethine group and one thione group. By that reason, the substrate scope from Chapter 3.1.1.4 was extended, with the goal to reduce the amount of donor functions stepwise. While TSC **A4** has three donor functions, TSCs **A5** and **A6** have only two sites left. In case of TSC **A6**, the anthracenyl group of the TSC leads to an additional sterically hinderance. By metal complexation with Pt(II), the coordination sites can be blocked for Cu(I) later, which led to the synthesis of the TSC Pt(II) complexes **A1** and **A2**. However, for all these substrates no reaction conversion was observed, and the starting material was recovered.

In addition to that, the substrate scope of the azide was varied (**B1-B3**), which were freshly synthesized before use. Again, the outcome of the reaction did not change, and the starting materials were recovered.



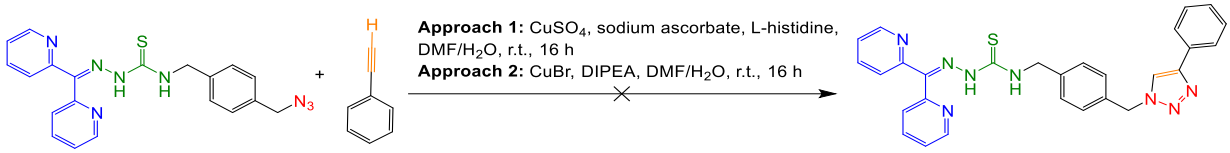
Scheme 33. Proposed mechanism of the Cu(I) catalyzed azide-alkyne dick reaction. Adopted from.[306]

Another factor which was investigated are the reaction conditions. Different solvent systems were tested to achieve a high solubility of all reaction compounds, namely EtOH/H_2O, THF/H_2O, *t*BuOH/H_2O and DMF/H_2O. It was found that DMF/H_2O led to the best solubility of the TSCs. However, changing the solvent did not change the reaction outcome. Most of the reactions were performed at room temperature, which is usually reported for click reactions in literature. Increasing the temperature to 90 °C led to the decomposition of the TSCs. In this way, there is still a huge temperature range which can be tested in the future to improve the reaction.

The last factor, which varied, is the catalyst. The typical catalyst for this reaction is $CuSO_4$ and sodium ascorbate which reduces Cu(II) to Cu(I). The amount of $CuSO_4$ and sodium ascorbate was varied. In addition, a fresh batch of ascorbate was used since it decomposes over time. Since this catalytic system

was not successful, different Cu(I) salts have been used namely CuBr, [CuBr(PPh$_3$)$_3$] and [Cu(CH$_3$CN)$_4$]PF$_6$. In addition, a base like Et$_3$N and DIPEA (N,N-diisopropylethylamine) was added for the deprotonation of the alkyne. The addition of ligands which can stabilize the Cu(I) state and accelerate the reaction was also tested using L-histidine and TBTA (tris(benzyltriazolylmethyl)amine). All approaches were found to be unsuccessful.

The click reaction was also tested the other way round, by means that Dipy(TSC)BzN$_3$ was reacted with phenylacetylene using CuSO$_4$/sodium ascorbate/L-histidine or CuBr/DIPEA as the catalyst (Scheme 34). Again, only the starting material was recovered.



Scheme 34. Synthetic approach for the click reaction of Dipy(TSC)BzN$_3$ with phenylacetylene.

The results of the reaction screening clearly show that TSCs are problematic substrates for the Cu(I) catalyzed azide-alkyne click reaction. This was shown for various, different substrates. Complexation of the copper catalyst by TSCs might be a problem but it is in contradiction to the finding that also TSCs with all coordination site blocked are unsuccessful in this reaction. However, a recently published example from literature (Figure 28) proves that Cu(I) can still coordinate to the *N*2 position in the backbone of the TSC.[307] In this way, the binding of TSCs to Cu(I) was probably not completely prevented. However, it is unclear if the coordination of the cooper catalyst to the TSC can really prevent the catalysis. Some TSC Cu(II) complexes have been reported in literature to catalyze azide-alkyne click reactions, which support these doubts.[190,308,309]

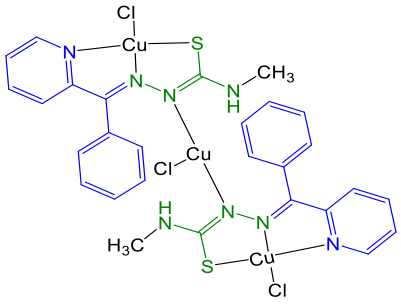
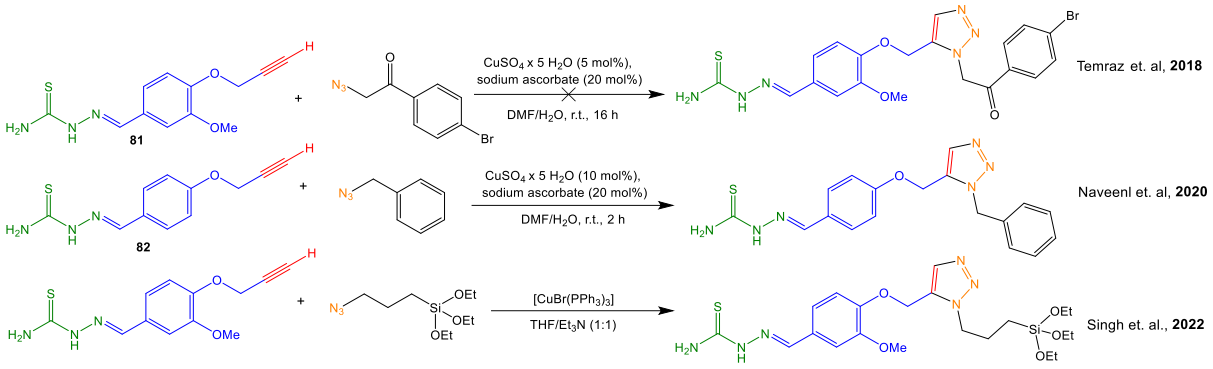


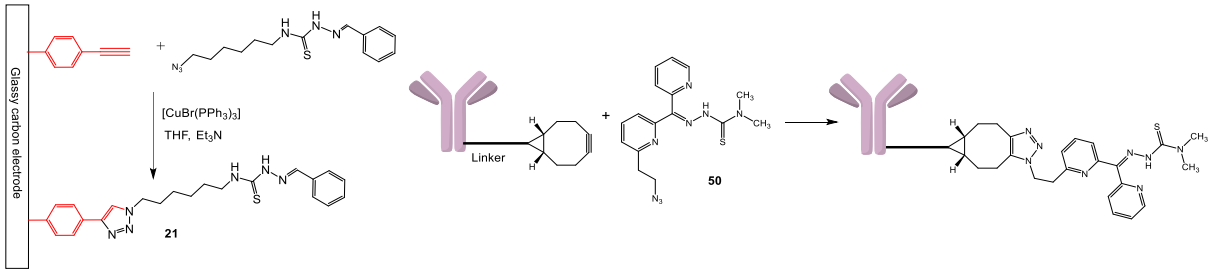
Figure 28. Solid state structure of two α-pyridyl TSC Cu(II) complexes which are bridged by a Cu(I) center, which coordinates to the *N*2 position of the TSC. Adopted from Ref. [307]

There are some publications which report TSCs as substrates in click reaction which can be compared to the results of this research (Scheme 35).[61,310-313] Some authors tried to click TSC **81** with different azides, which was found to be unsuccessful. They used CuSO$_4$ · 5 H$_2$O (5 mol %) and sodium ascorbate (20 mol %) as a catalyst in DMF/H$_2$O at room temperature overnight.[313] These findings are in accordance with our research. Later, other authors used a similar TSC substrate but reported a successful click reaction. However, they used very similar reaction conditions as the authors before namely CuSO$_4$ · 5 H$_2$O (10 mol%), sodium ascorbate (20 mol %), DMF/H$_2$O (8:2), 2 h, room temperature.[311] Further authors used the same TSC substrate and again reported a successful click reaction. They used [CuBr(PPh$_3$)$_3$] as a catalyst in a mixture of THF/Et$_3$N (1:1).[312] These findings can lead to the assumption that small differences in the reaction protocol can have a significant difference in the reaction outcome. This means that the reaction of this research should be analyzed in much more detail in the future. However, very similar reaction conditions to that from literature have been already tested (Table 7). In addition, the reactivity of the substrate from literature should be significantly higher, due to the ether function, which makes a comparison difficult.



Scheme 35. Cu(I) catalyzed azide-alkyne click reaction of TSCs with alkyne function and azides, reported in literature.[311-313]

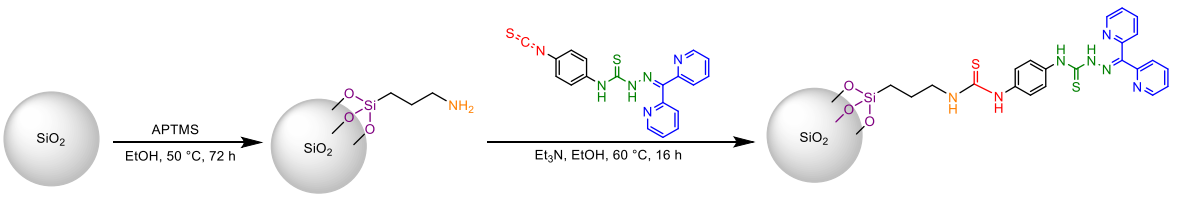
Also, TSCs with azide function were reported in azide-alkyne click reaction. One example was already shown in Chapter 1.2, at which TSC **21** was clicked to the surface of functionalized electrodes (Scheme 36). They used [CuBr(PPh3)3] as a catalyst in a mixture of THF/Et3N. However, since the author did not analyze the reaction on a molecular level, it is difficult to prove if their approach was successful or just let to the adsorption of the TSC to the electrode.[61] Another TSC with azide function was discussed in Chapter 1.9.2, which was linked to antibodies by a strain-promoted azide-alkyne click reaction (Scheme 36).[113] By that reason, it might be interesting to test the TSCs of this research also in strain-promoted azide-alkyne in the future, as an alternative to the Cu(I) catalyzed approach.



Scheme 36. Left: Cu(I) catalyzed azide-alkyne click reaction of TSC with azide function reported in literature. Right: Strain-promoted azide-alkyne click reaction of TSC with azide function reported in literature. Adopted from Ref. [61,113].

3.1.4.2 Functionalization of SiO_2 nanoparticles with Dipy(TSC)PhNCS

The used SiO_2 NPs had a size of 80-100 nm, determined by SEM. In the first step, the particles were functionalized with APTMS (3-aminopropyl)trimethoxysilan), which was condensed to the particle surface in EtOH at 50 °C for 72 h. The particles were purified by three times washing with EtOH (Scheme 37).



Scheme 37. Functionalization of SiO_2 NPs by Dipy(TSC)PhNCS.

In the second step, the particles (10.0 mg) were reacted with Dipy(TSC)PhNCS (5.0 mg) in EtOH at 60 °C for 16 h. Et3N was used as the catalyst. The particles were washed with EtOH until the supernatant was colorless, which was confirmed by UV/Vis absorption spectroscopy. After the functionalization, the particles were slightly yellow, which is shown in Figure 29.

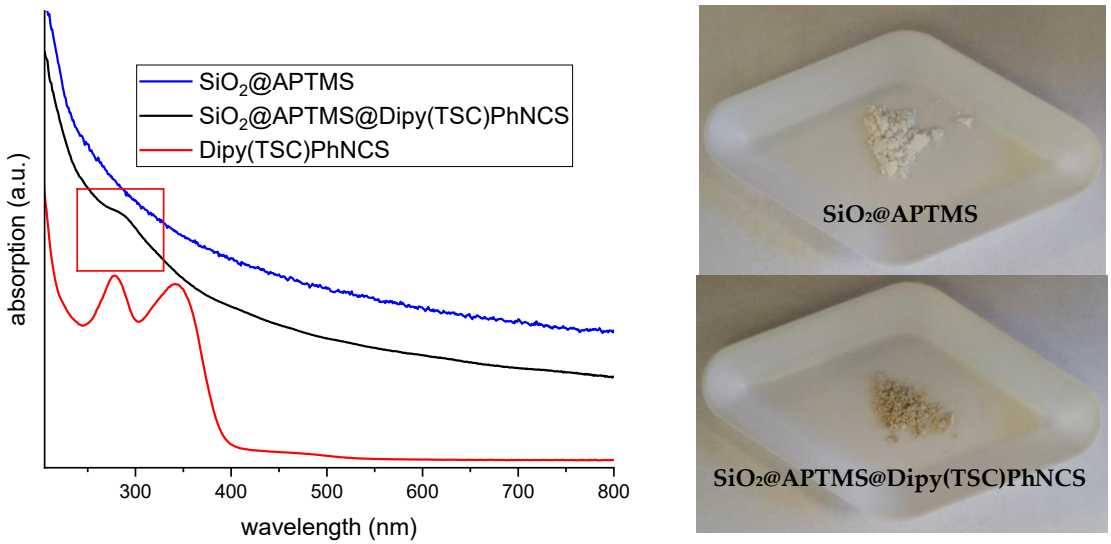


Figure 29. Left: UV/Vis absorption spectra of SiO_2@APTMS, SiO_2@APTMS@Dipy(TSC)PhNCS and Dipy(TSC)PhNCS measured in MeOH. Right: Photographs of SiO_2@APTMS (Top) and SiO_2@APTMS@Dipy(TSC)PhNCS (Bottom).

UV/Vis absorption spectra of the particles were recorded in MeOH (Figure 29). The absorption spectrum of SiO_2@APTMS shows a ramp shape typically found for NPs, which originates from the wavelength dependency of scattering. For SiO_2@APTMS@Dipy(TSC)PhNCS a shoulder at 280 nm is observed, which matches the absorption bands of Dipy(TSC)PhNCS. The results give a first evidence for successful functionalization.

In addition to that, the particles were analyzed by FTIR spectroscopy. Figure 30 shows a comparison of the SiO_2 and SiO_2@APTMS NPs. Both particles show the typical vibrational bands of SiO_2 at 1060 cm^{-1} (υ_{as} Si–O–Si stretch), 950 cm^{-1} (υ Si–OH stretch), 795 cm^{-1} (υ Si–O–Si bending) and 440 cm^{-1} (υ_s Si–O–Si stretch).[314] The band at 3350 cm^{-1} can be assigned to the stretching vibration of H_2O and the band at 1630 cm^{-1} to the corresponding bending vibration and clearly show the adsorption of H_2O to the particle surface.[314] A closeup to the region of 4000-1200 cm^{-1} gives more details about the differences between SiO_2 and SiO_2@APTMS (Figure 30, right). For SiO_2@APTMS, two additional vibrations at 2983 and 2905 cm^{-1} are observed which can be assigned to C–H stretching vibrations. At 1485, 1450 and 1396 cm^{-1} further vibrational bands are observed which are related to C–H bending vibrations.[286] The intensity of these bands is low, which can be explained by the fact that the amount of SiO_2 is much higher than for the surface ligand. In the future, smaller SiO_2 NPs could be used to increase the surface area and the amount of attached surface ligand. However, the results are in accordance with the literature and indicate a successful functionalization with APTMS.[286]

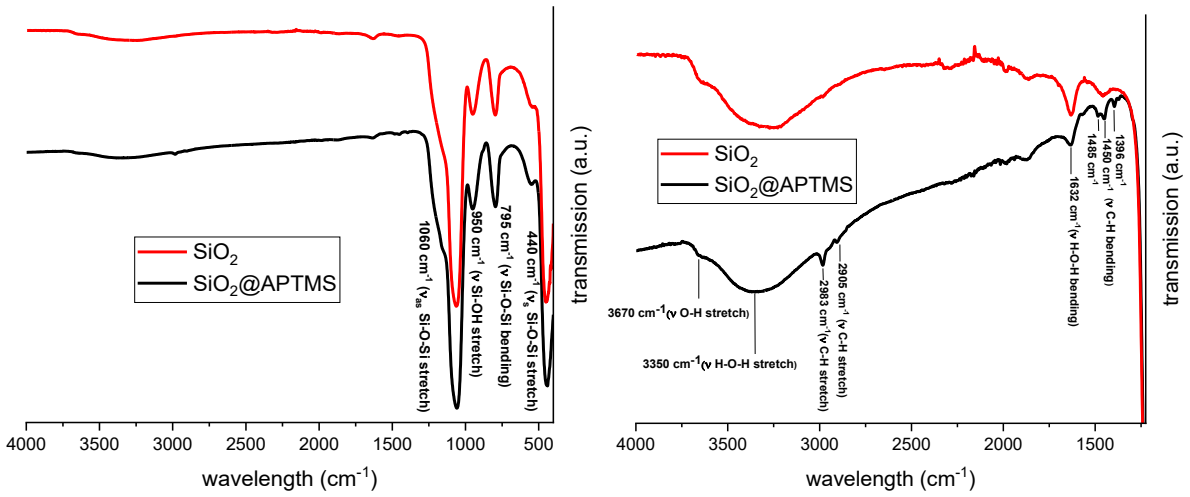


Figure 30. Left: FTIR spectra of SiO_2 and SiO_2@APTMS NPs. Right: Closeup to the region of 4000-1200 cm^{-1}.

For SiO_2@APTMS@Dipy(TSC)PhNCS, the relative intensity of the C–H stretching and bending vibrations are increasing (Figure 31). In addition to that, the relative intensity and energy of these vibrational bands fit perfectly with the FTIR spectrum of Dipy(TSC)PhNCS. For the TSC, an intense and broad vibration is found around 2000-2200 cm^{-1} which is in the typical region of isothiocyanates.[315] After the functionalization, this band is missing which is an indication for the successful reaction of the isothiocyanate to the corresponding thiourea. Since the typical vibrations of thioureas (e.g. C=S) are in the region of 1600-1400 cm^{-1}, they are overlapping with the vibrations of TSCs, which makes a distinct assignment of the vibrational bands difficult.[316] Nevertheless, the results indicate a covalent attachment of the TSCs to the surface and not just its adsorption.

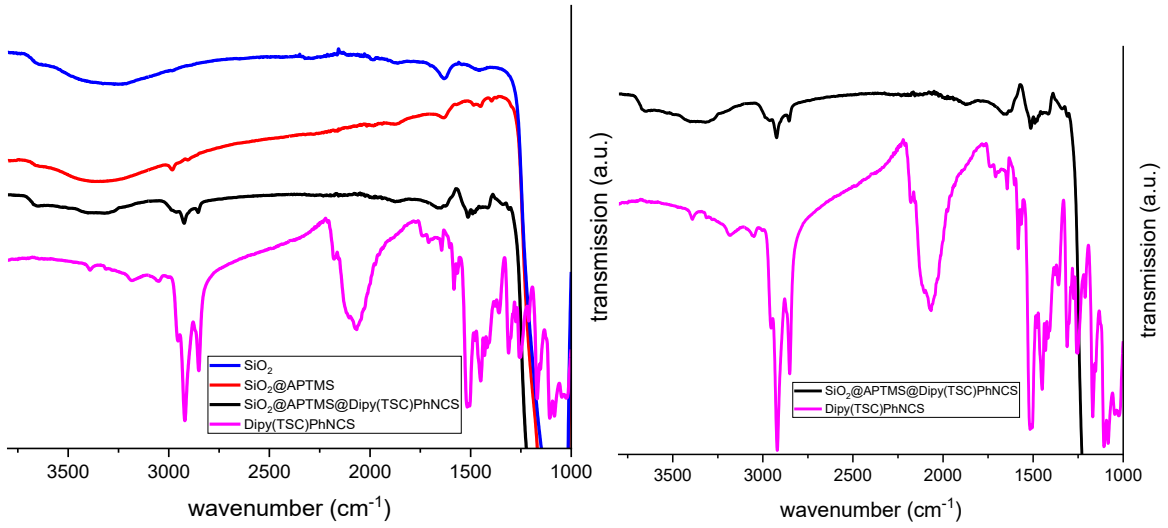


Figure 31. Left: FTIR spectra of SiO_2, SiO_2@APTMS, SiO_2@APTMS@Dipy(TSC)PhNCS and Dipy(TSC)PhNCS. Right: Closeup to the region of 3800-1000 cm^{-1}.

In addition to these experiments, DLS and zeta potential measurements were performed (Table 8). For the SiO_2 NPs, a hydrodynamic radius of 215 nm and a negative zeta potential of –35.7 mV was observed. After the surface functionalization with APTMS the hydrodynamic radius increases to 230 nm and the zeta potential changes drastically to a positive value of 51.2 mV which indicates the presence of amino groups at the surface.[317] The functionalization of the NPs with the TSC led to a decrement of the zeta potential to 20.6 mV. The hydrodynamic radius increased to 289 nm. However, also the polydispersity index increased significantly (0.65), which indicates and increment of agglomeration of the particles.

Table 8. Hydrodynamic radius and zeta potential of SiO_2, SiO_2@APTMS and SiO_2@APTMS@Dipy(TSC)PhNCS NPs.[a]

	SiO_2	SiO_2@APTMS	SiO_2@APTMS@Dipy(TSC)PhNCS
Z-Average (nm)	215	230	289
Zeta potential (mV)	–35.7	51.2	20.6
Polydispersity index	0.18	0.35	0.65

[a] Measured in H_2O (pH = 7.0) at room temperature.

In the next step EDX (energy dispersive x-ray spectroscopy) measurements of SiO_2@APTMS@Dipy(TSC)PhNCS have been prepared (Figure 32). Besides the expected signals of Si and O, related to the SiO_2 NPs, also the presence of N, C and S was confirmed. The results are in line with a successful functionalization of the NPs with TSC. A quantification of the elements was not possible, due to the overlapping of signals and the fact that carbon tape was used as a carrier material, which distorts the amount of carbon. The mapping images are found in the appendix.

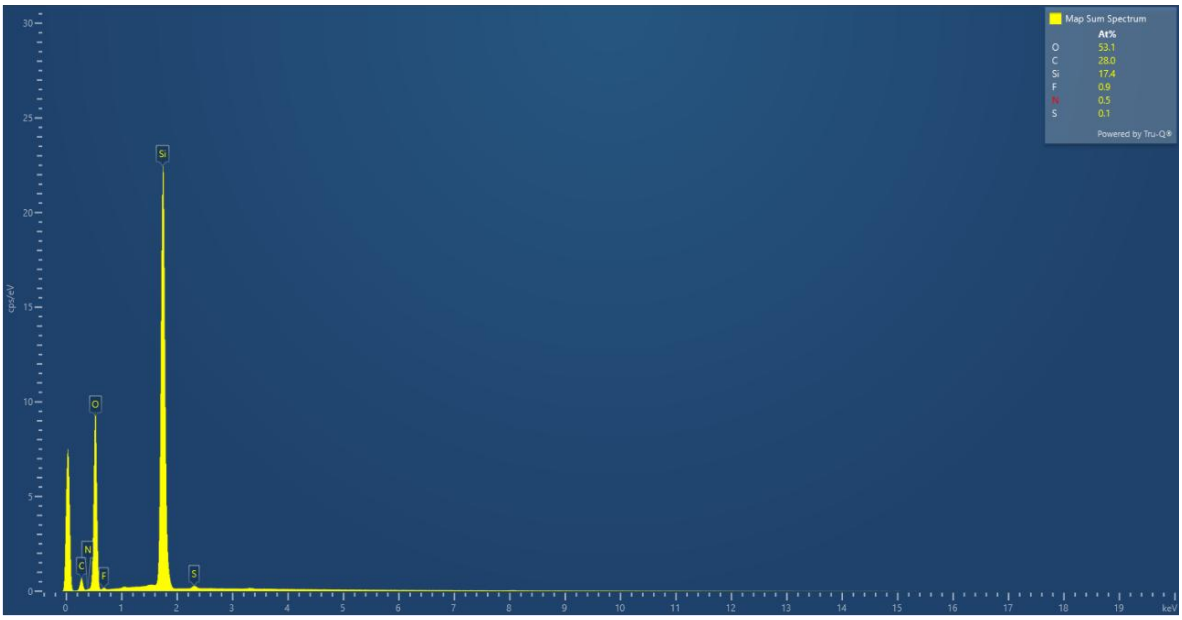
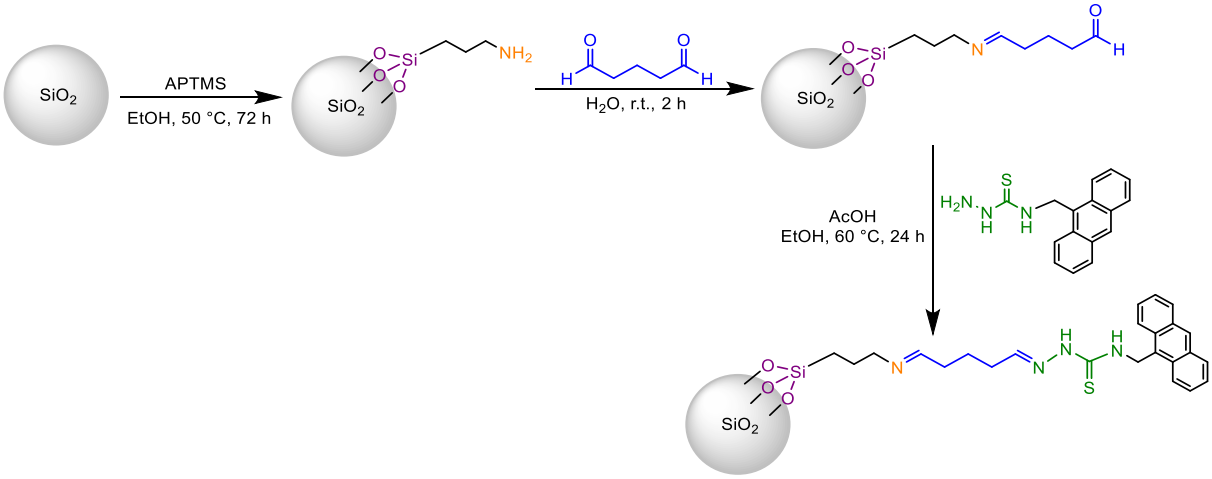


Figure 32. EDX spectrum of SiO_2@APTMS@Dipy(TSC)PhNCS. The particles were spread onto a carbon tape, and the measurement was performed on large nanoaggregates to get a reliable intensity of the elements. The corresponding mapping images are found in the appendix.

3.1.4.3 Crosslinking of thiosemicarbazides to SiO_2 nanoparticles by glutaraldehyde

The idea of crosslinking thiosemicarbazides to APTMS functionalized SiO_2 NPs is inspired from literature, where glutaraldehyde (GA) is a typical reagent for crosslinking of amines under the formation of an imine.[317] In a first step the SiO_2@APTMS NPs were reacted with glutaraldehyde in H_2O at room temperature for 2 h (Scheme 38). After that, the particles were washed with H_2O to remove an excess of glutaraldehyde, which is important to avoid side reactions later, due to crosslinking of two thiosemicarbazides. It should be noted that also a crosslinking between the particles might be possible in the first step, which was tried to avoid statistically by using a large excess of GA. After that, the particles were subsequently reacted with anthracene thiosemicarbazide (Chapter 3.4.1), under the formation of a TSC, which has the advantage of an anthracene tag, which simplifies the particle characterization. The reaction was performed in EtOH at 60 °C for 24 h using AcOH as a catalyst. The particles were washed with EtOH until the supernatant was colorless, which was confirmed by UV/Vis absorption spectroscopy.



Scheme 38. Crosslinking of SiO_2@APTMS NPs to anthracene thiosemicarbazide under the formation of a TSC.

The synthesized particles had a yellowish color, which is shown in Figure 33. UV/Vis absorption spectroscopy of the particles clearly showed the characteristic absorption bands of anthracene at 250 nm as well as at 350, 370 and 385 nm. In this way, the anthracene tag helped to identify its presence on the particle surface.

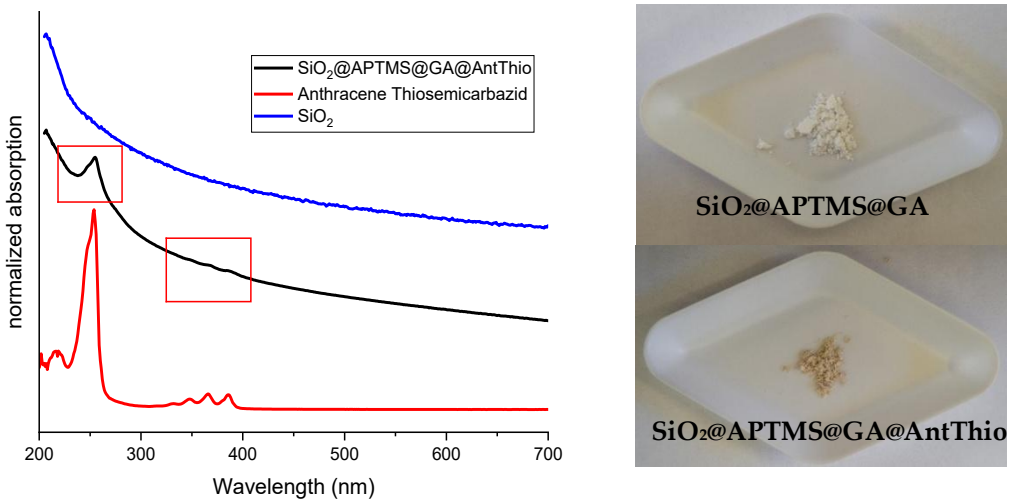


Figure 33. Left: UV/Vis absorption spectra of SiO_2@APTMS@GA, SiO_2@APTMS@GA@AntThio and anthracene thiosemicarbazide for comparison, measured in MeOH. Right: Photographs of SiO_2@APTMS@GA (Top) and SiO_2@APTMS@GA@AntThio (Bottom).

FTIR spectroscopy of the particles showed an increment of the intensity of the C–H stretching (2923 and 2845 cm^{-1}) and deformation vibrations (1500-1325 cm^{-1}) after functionalizing SiO_2@APTMS with glutaraldehyde (Figure 34). In addition, the bands of the C–H stretching vibrations are shifting to lower wavenumber. Unfortunately, the characteristic C=O vibration of the aldehyde was not detectable, since it probably overlaps with the deformation vibration of H_2O. Between SiO_2@APTMS@GA and SiO_2@APTMS@GA@AntThio, the C–H stretching vibration have gained some intensity and an additional vibration is visible at 2985 nm. While a vibration at 3160 cm^{-1} is found for the anthracene thiosemicarbazide, which can be assigned to the stretching vibration of its amine group, this band is missing for the functionalized particles, indicating a successful reaction between the thiosemicarbazide and the aldehyde functions at the particle surface.

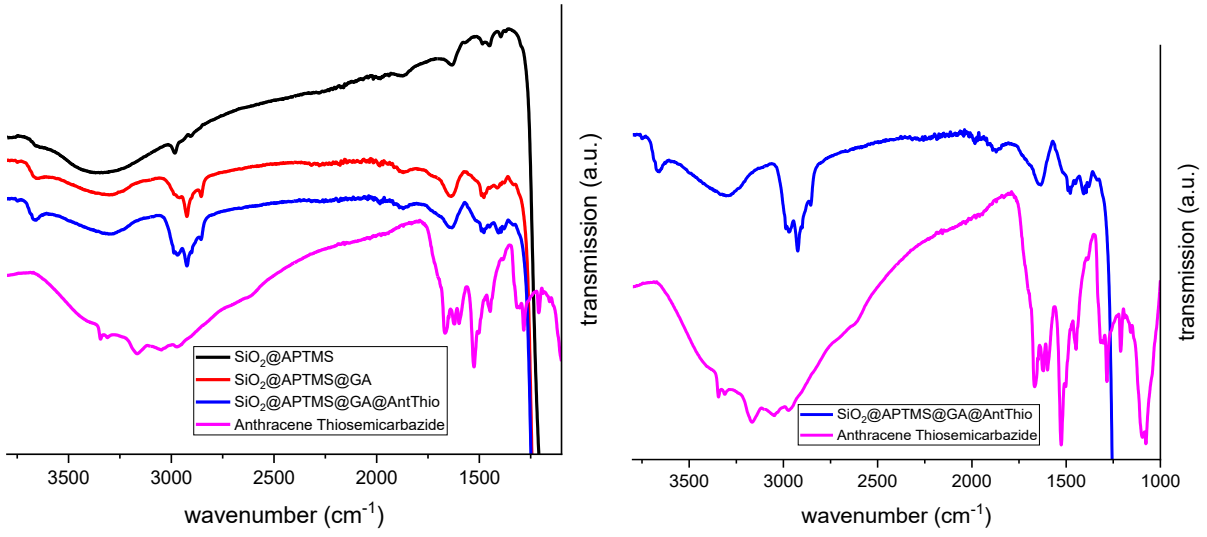


Figure 34. Left: FTIR spectrum of SiO_2@APTMS, SiO_2@APTMS@GA, SiO_2@APTMS@GA@AntThio and anthracene thiosemicarbazide. Right: Closeup to the region of 3800-1000 cm^{-1}. The transmission of the anthracene thiosemicarbazide is divided by 2 for a better comparison.

Also, DLS and zeta potential measurements have been performed for the functionalized NPs (Table 9). After functionalization of SiO_2@APTMS with glutaraldehyde the hydrodynamic radius decreased significantly. Since also the polydispersity index decreased, it seems that the particles are more stabilized, and agglomeration is prevented leading to a smaller average size. The zeta potential decreased from 51.3 to 44.5 mV which is in accordance with results from literature.[317] For SiO_2@APTMS@GA@AntThio the zeta potential is further decreased to 22.94 mV. The hydrodynamic radius and the polydispersity index are again increasing.

Table 9. Hydrodynamic radius and zeta potential of SiO_2, SiO_2@APTMS, SiO_2@APTMS@GA and SiO_2@APTMS@GA@AntThio NP.[a]

	SiO_2	SiO_2@APTMS	SiO_2@APTMS@GA	SiO_2@APTMS@GA@AntThio
Z-Average (nm)	215	230	141.4	261.2
Zeta potential (mV)	–35.7	51.2	44.5	22.94
Polydispersity index	0.18	0.35	0.16	0.37

[a] Measured in H_2O (pH = 7.0) at room temperature.

The results of the EDX measurements of SiO_2@APTMS@GA@AntThio are in line with the observations from Chapter 3.1.4.2 and confirm the presence of C, N and S (Figure 35). For the same reasons discussed before, a reliable quantification of the signals is not possible. The mapping images are found in the appendix.

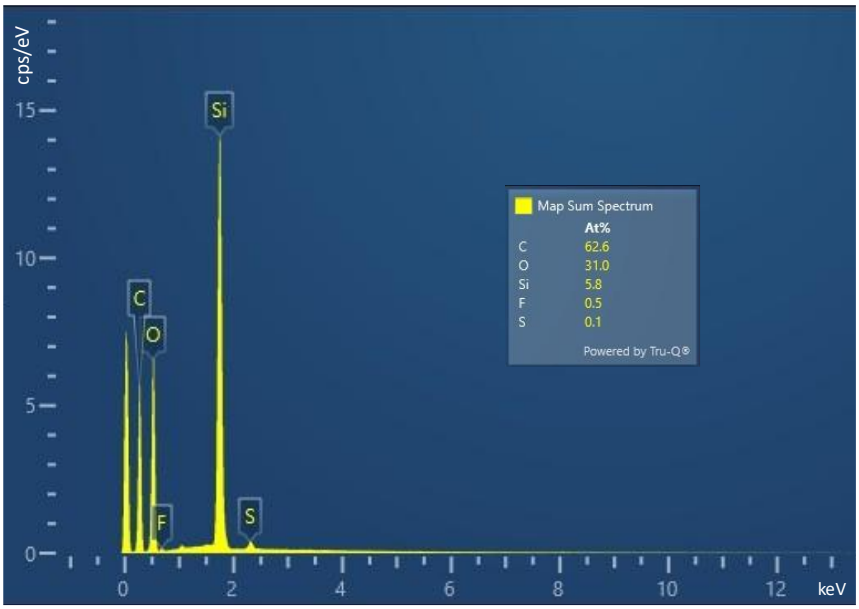
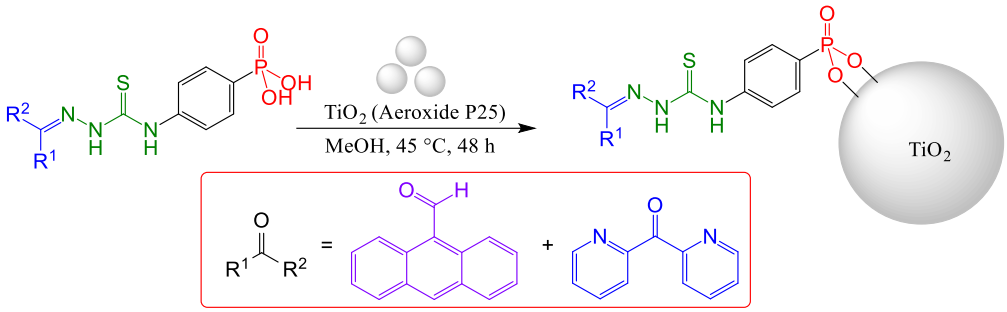


Figure 35. EDX spectrum of SiO_2@APTMS@GA@AntThio. The particles were spread onto a carbon tape, and the measurement was performed on large nanoaggregates to get a reliable intensity of the elements. The corresponding mapping images are found in the appendix.

3.1.4.4 Functionalization of TiO_2 nanoparticles with TSCs having phosphonate anchor

The used TiO_2 NPs (*Aeroxide P25, Evonik*) are commercially available and were synthesized by a gas phase reaction of $TiCl_4$ with oxygen and hydrogen at temperatures of 1000-2400 °C. The particles have an average size of 21 nm and an average surface area of approximately 50 m^2/g. In solution, the particles tend to form larger aggregates. The content of anatase in these particles is 80-90% by weight (the rest is rutile).[318] To attach the Dipy(TSC)PhPO$(OH)_2$ and Ant(TSC)PhPO$(OH)_2$ to the surface, the corresponding TSC (5 mg) and the NPs (10 mg) were reacted in MeOH at 45 °C for 48 h (Scheme 39). The functionalized NPs were washed with MeOH until the supernatant was colorless, which was confirmed by UV/Vis absorption spectroscopy.



Scheme 39. Surface functionalization of TiO_2 NPs with Dipy(TSC)PhPO(OH)$_2$ and Ant(TSC)PhPO(OH)$_2$.

While the TiO_2@Dipy(TSC)PhPO(OH)$_2$ particles had a brownish color, the Ant(TSC)PhPO(OH)$_2$ functionalized particles showed a yellow color (Figure 36). The particles were investigated by UV/Vis absorption spectroscopy. For the TiO_2 particles, a characteristic absorption band at 345 nm is observed, which is in accordance with the optical band gap of TiO_2.[318] For the TiO_2@Dipy(TSC)PhPO(OH)$_2$ particles an additional maximum is observed at 270 nm, which is in accordance with the absorption spectrum of the TSC. Also, for the TiO_2@Ant(TSC)PhPO(OH)$_2$ particles an additional absorption maximum at 255 nm is found, which matches the characteristic absorption of the anthracene function at the TSC. The results indicate successful functionalization.

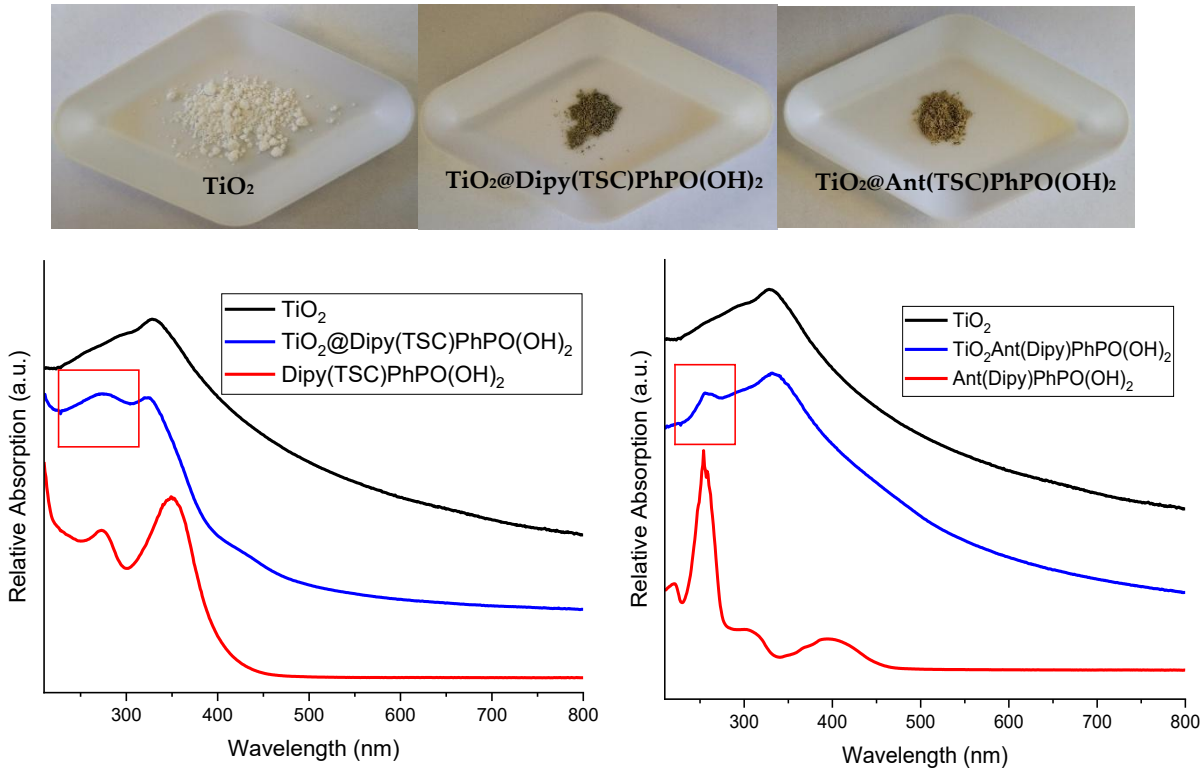


Figure 36. Top: Photographs of TiO_2 (left), TiO_2@Dipy(TSC)PhPO(OH)$_2$ (middle) and TiO_2@Ant(TSC)PhPO(OH)$_2$ (right). Bottom: UV/Vis absorption spectra of TiO_2@Dipy(TSC)PhPO(OH)$_2$ (left) and TiO_2@Dipy(TSC)PhPO(OH)$_2$ (right) compared to TiO_2 NPs and the corresponding TSCs, measured in MeOH.

In addition, the TiO_2@Ant(TSC)PhPO(OH)$_2$ particles were investigated by emission spectroscopy, whereby the particles showed the characteristic emission of the anthracene motif (Figure 37). The shape of the emission band indicates an aggregation (Chapter 3.1.2) which can be related to interactions of the TSC with the particle surface or to interactions between different TSCs at the surface.

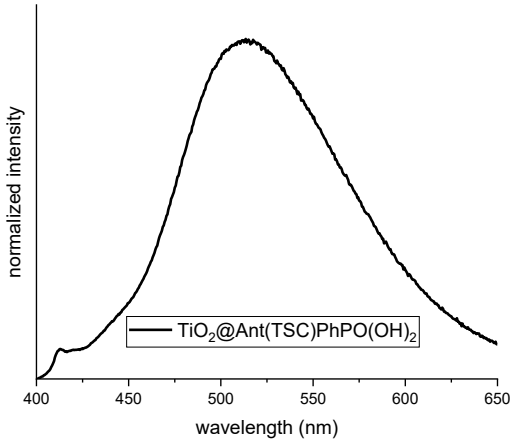


Figure 37. Normalized emission spectrum of TiO_2@Ant(TSC)PhPO(OH)$_2$ in MeOH at room temperature.

In the next step, the particles were investigated by FTIR spectroscopy (Figure 38). For the functionalized NPs, additional vibrational bands are observed between 1500-700 cm^{-1}, which are clearly related to the TSC at the particle surface. In case of the unattached TSCs, vibrational bands at 3000-3500 cm^{-1} are observed which are related to O–H vibrations of the phosphonic acid, which are missing for the nanoconjugate, indicating a successful condensation to the particle surface. In addition, the P–O region of the ligand (1300-800 cm^{-1}) changes significantly after the functionalization. The vibrational band at 1045 cm^{-1} can be assigned to the Ti–O–P vibration in accordance with literature, which confirms a successful, covalent conjugation to the particle surface.[295,319,320]

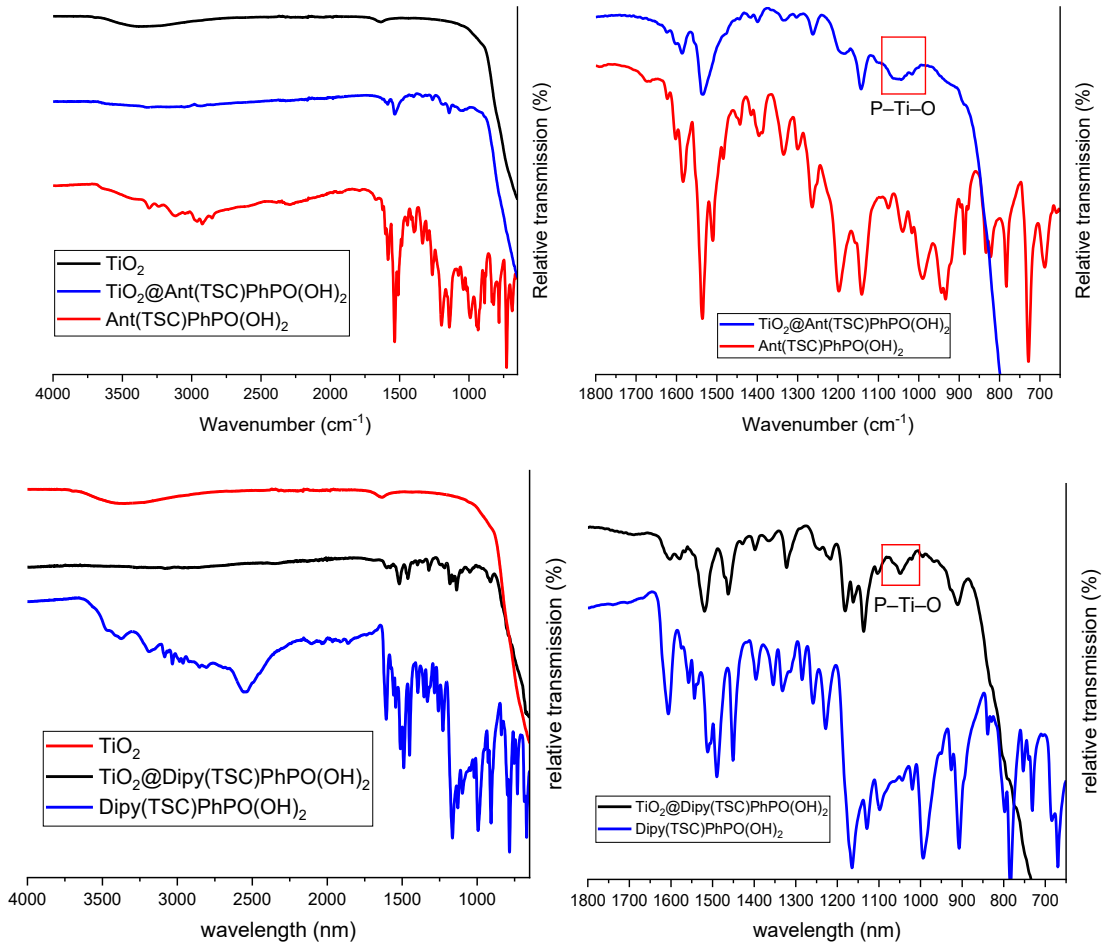


Figure 38. FTIR spectrum of TiO_2@Ant(TSC)PhPO(OH)$_2$ (Top, left) and TiO_2@Dipy(TSC)PhPO(OH)$_2$ (Bottom, left) in comparison to TiO_2 and the corresponding TSCs. Top/Bottom, right: Closeup to the region of 1800-650 cm^{-1} (the intensity of the functionalized NPs was increased by a factor of 2.5 for a better comparison).

Zeta potential and DLS measurements of the TiO_2 NPs showed a huge tendency of the particles to agglomerate which is supported by a polydispersity index of 0.72 and a hydrodynamic radius of 537 nm (Table 10). The findings are in accordance with the declarations of the manufacturer of the particles.[321] The zeta potential of the particles was –10.3 mV, which is also in accordance with measurements from literature.[321] The functionalization of the particles with the TSCs led to a decrement of the zeta potential to –19.4 (Dipy(TSC)PhPO(OH)$_2$) and –35.7 mV (Ant(TSC)PhPO(OH)$_2$). Also, the hydrodynamic radius and the polydispersity index decreased after the functionalization, which indicates an increased stability of the particles.

Table 10. Hydrodynamic radius and zeta potential of TiO_2 TiO_2@Dipy(TSC)PhPO(OH)$_2$ and TiO_2@Ant(TSC)PhPO(OH)$_2$ NPs.

	TiO_2	TiO_2@Dipy(TSC)PhPO(OH)$_2$	TiO_2@ Dipy(TSC)PhPO(OH)$_2$
Z-Average (nm)	537	185	275
Zeta potential (mV)	–10.3	–19.4	–35.7
Polydispersity index	0.72	0.266	0.252

[a] Measured in H_2O (pH = 7.0) at room temperature.

EDX measurements of TiO_2@Dipy(TSC)PhPO(OH)$_2$ showed the presence of the expected elements Ti, O, N, P and S (Figure 39). In addition to that, contamination with Na was observed, which might originate from an impurity of the TSC, or solvents used for the particle syntheses and purification. Again, the quantification of the elements was not possible for similar reasons discussed before but the results indicate a successful surface functionalization.

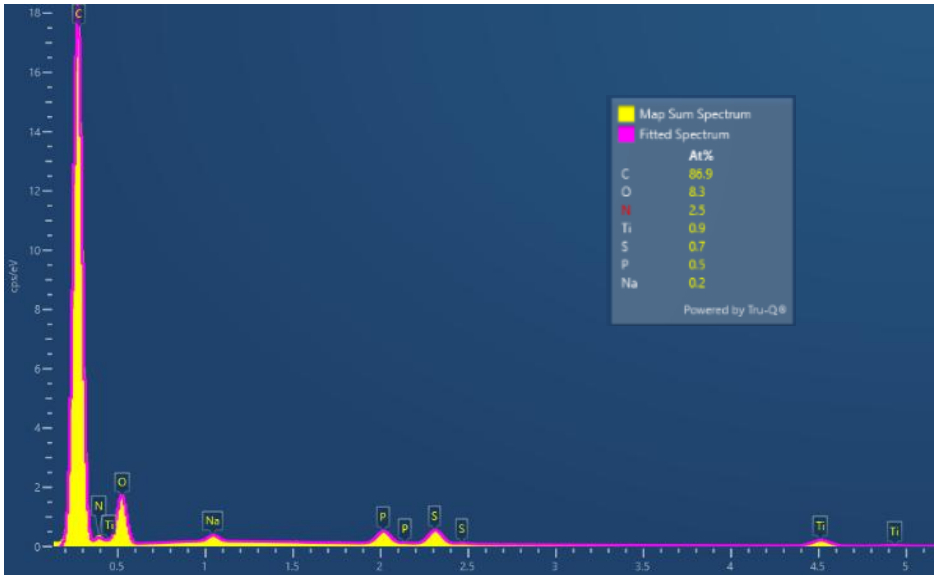


Figure 39. EDX spectrum of TiO_2@Dipy(TSC)PhPO(OH)$_2$. The particles were spread onto a carbon tape, and the measurement was performed on large nanoaggregates to get a reliable intensity of the elements. The corresponding mapping images are found in the appendix.

SEM (scanning electron microscopy) images of the nano aggregates and the corresponding elemental EDX mapping are shown in Figure 40. The results show an equal distribution of the elements within the measured aggregates and indicate a homogeneous surface functionalization.

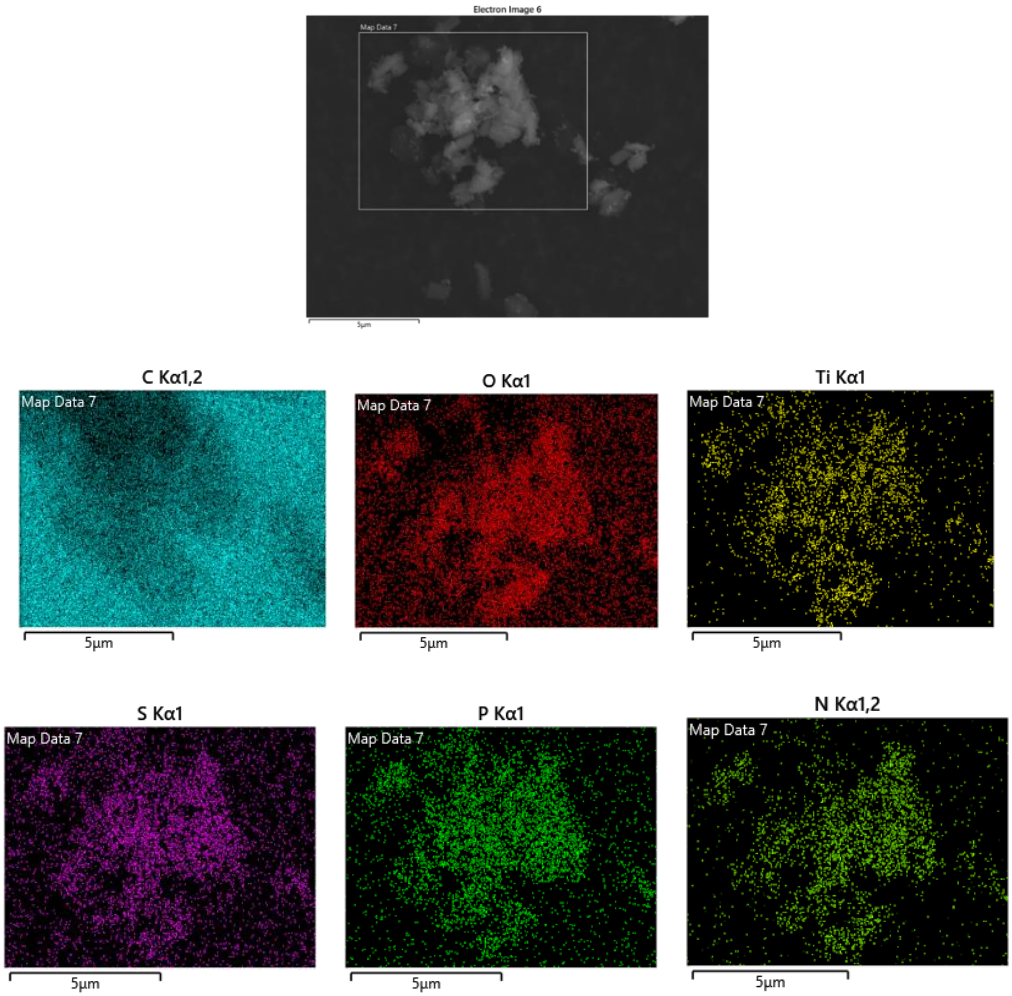


Figure 40. SEM image of TiO_2@Dipy(TSC)PhPO(OH)$_2$ and the corresponding elemental mapping of the EDX measurements.

3.1.5 Summary – TSCs for nanoconjugation

TSCs with amine, thiol, azide, alkyne, phosphonate, diol and isothiocyanate function were successfully synthesized. It was found for their synthesis that rigid spacers between the TSC and the functional group were often necessary to avoid side reactions. The synthesis of TSCs with primary bromide, sulfonate and alkoxy silane function remained unsuccessful due to side reaction during the synthesis of the thiosemicarbazides. UV/Vis absorption and emission spectroscopy showed no significant impact of residues at the *N*4 position on the photophysical properties. However, a concentration dependency of the emission properties was found for the anthracenyl derivatives, due to interactions of TSCs in solution. Cytotoxicity studies of the TSCs showed strong inhibition of HepG2 and HCT-116 by Dipy(TSC)PhNCS, Dipy(TSC)PhNH$_2$ and Dipy(TSC)PhPO(OEt)$_2$ which was even higher, compared to cisplatin. Conjugation of the TSCs was tested at the example of molecular reactions. While the amino and isothiocyanate functionalized TSCs were successfully crosslinked by the formation of a urea/thiourea function, the Cu(I) catalyzed click reaction with azide and alkyne functionalized TSCs was unsuccessful. In a finals step, the attachment of TSCs with phosphonate or isothiocyanate function to TiO_2 and SiO_2 NPs was investigated in detail. In addition, the crosslinking of thiosemicarbazides to APTMS functionalized SiO_2 NPs using glutaraldehyde was investigated. FTIR and UV/Vis absorption spectroscopy as well as Zeta, DLS and EDX measurements indicate successful functionalization. In the future the synthesis of further nanoconjugations as well as the investigation of their cytotoxicity should be investigated in more detail to analyze if nanoconjugation can improve the medical performance of TSCs.

3.2 Tuning the Fe(II)/(III) redox potential of α-pyridyl TSC iron complexes and their conjugation to TiO_2 nanoparticles

During this research, several α-pyridyl TSC Fe(III) complexes have been successfully synthesized (Chart 17). All compounds are stable under ambient conditions and soluble in polar, organic solvents like MeOH, MeCN or DMSO. In addition, all of them are at least soluble in small concentrations in H_2O or in mixtures of DMSO and H_2O. The R^1 group at the *N*1 position has been substituted with different electron donating or withdrawing groups to investigate the impact on the electrochemical properties. Introduction of a CF_3 and C_6F_5 group remained unsuccessful. For comparison, also some literature known TSCs have been synthesized.[39,95,105,106] In the first step, the *N*4 position was left unsubstituted since it also influences the electrochemical properties in a small magnitude. Later, phosphonate anchors were attached to this position for their conjugation to TiO_2 NPs (Chapter 3.2.5).

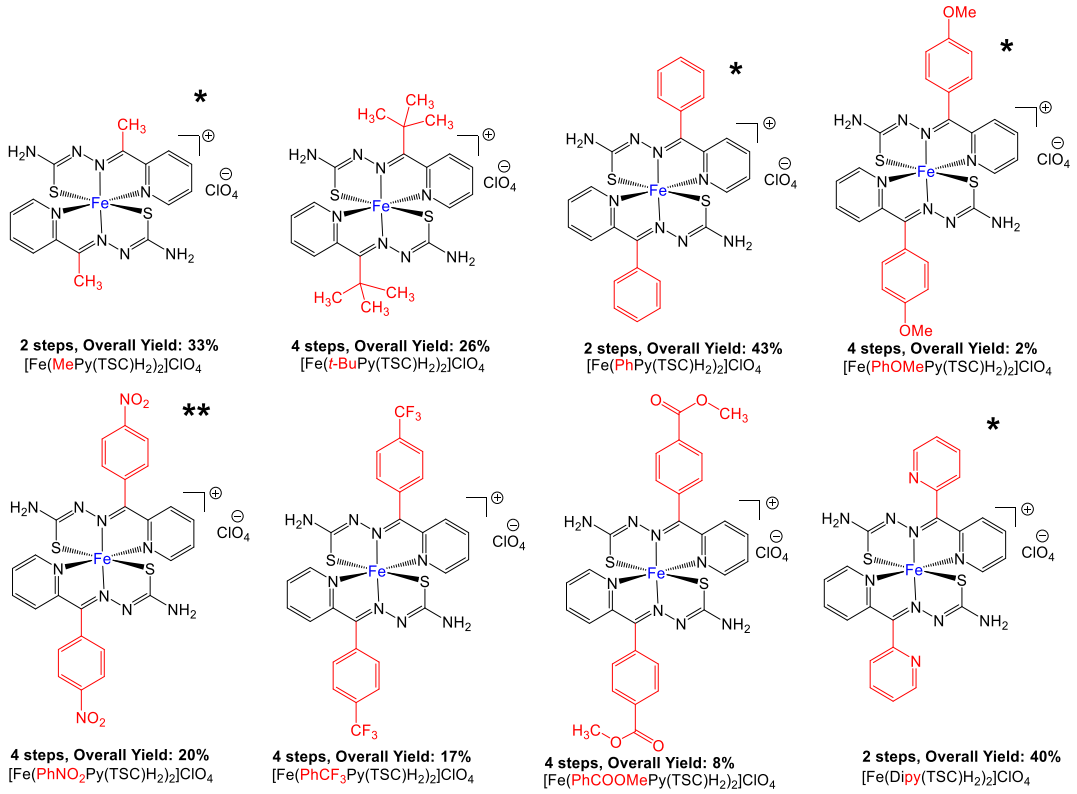


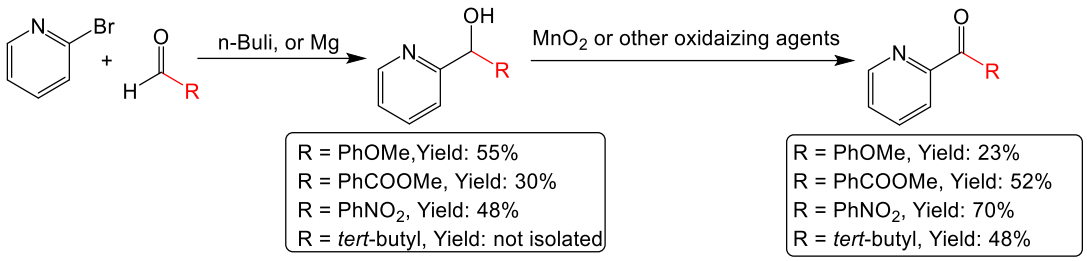
Chart 17. Overview of synthesized α-pyridyl TSC iron complexes. *Compound was described in literature.[39,95,106] **Comparable compounds were described in literature.[105]

3.2.1 Synthesis of α-pyridyl TSC iron complexes

3.2.1.1 α-pyridyl ketones

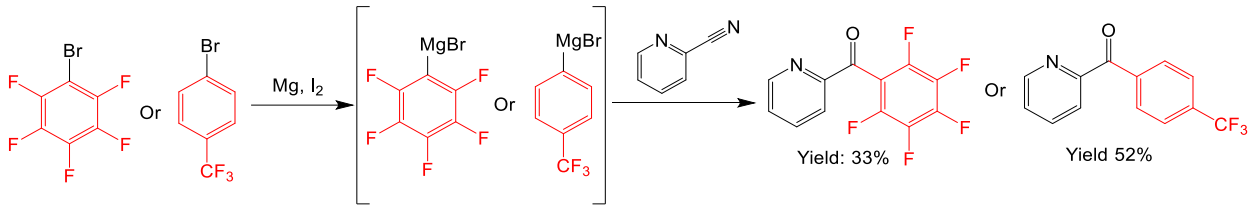
Starting point for the synthesis of α-pyridyl TSC Fe(III) complexes was the synthesis of α-pyridyl ketones to introduce different substituents. Di(2-pyridyl)ketone, phenyl 4-pyridyl ketone and 2-acetyl pyridine were commercially available. All other ketones were synthesized by literature known protocols.[322-327]

α-pyridyl ketones with 4-methoxyphenyl, 4-methoxycarbonylphenyl, 4-nitrophenyl and *tert*-butyl group were synthesized in two steps (Scheme 40). In the first step, 2-bromopyridine was lithiated or the corresponding *Grignard* reagent was synthesized, which was reacted with different aldehydes yielding the secondary alcohols in moderate yields. In the second step, the alcohol was oxidized to the corresponding ketones using MnO_2 or other oxidizing reagents.[322-325] Again, most of the yields were poor or moderate.



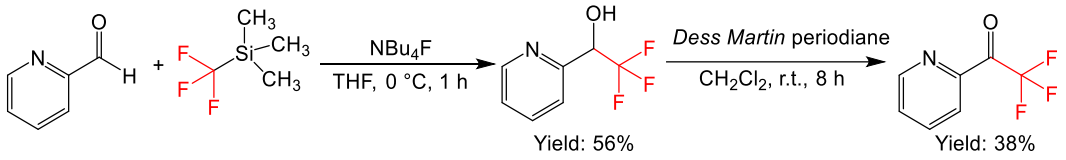
Scheme 40. Synthesis of α-pyridyl ketones with 4-methoxyphenyl, 4-methoxycarbonylphenyl, 4-nitrophenyl and *tert*-butyl group.

For the synthesis of α-pyridyl ketones with pentafluoro phenyl or 4-trifluoromethyl phenyl group, the corresponding bromides were reacted with Mg to form the *Grignard* reagents. These were directly reacted with pyridine-2-carbonitrile yielding the ketones in moderate or low yields (Scheme 41).[327]



Scheme 41. Synthesis of α-pyridyl ketones with pentafluoro phenyl and 4-trifluoromethyl phenyl group.

2,2,2-trifluoro-1-(2-pyridinyl)ethenone was synthesized in two steps (Scheme 42). First, 2-pyridinecarboxaldehyde was fluorinated with (trifluoromethyl)trimethylsilane, yielding the secondary alcohol in 56% yield. After that, the alcohol was oxidized to the ketone.



Scheme 42. Synthesis of 2,2,2-trifluoro-1-(2-pyridinyl)ethenone.

Here, it was found that oxidation with MnO_2 or CrO_3 was not successful, due to the low reactivity of alcohol due to the electron withdrawing CF_3 group. However, oxidation with *Dess Martin* periodinane was successful with 38% yield.[326] A summary of all α-pyridyl ketones is shown in Chart 18.

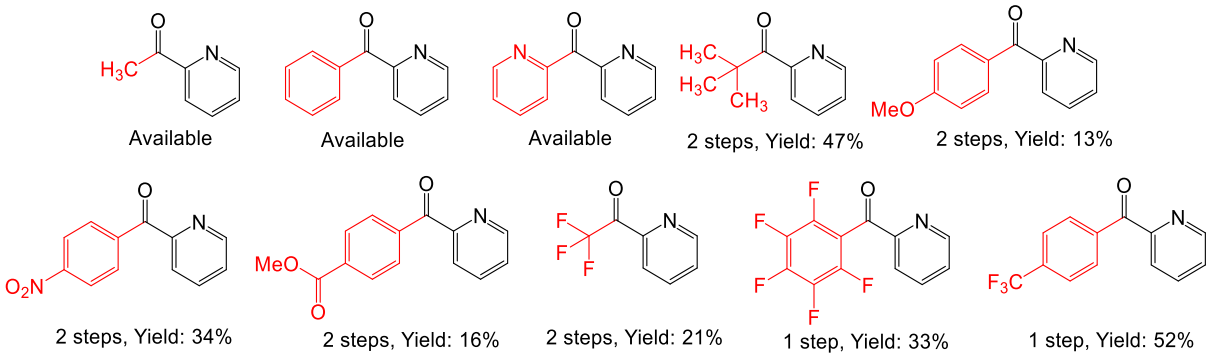
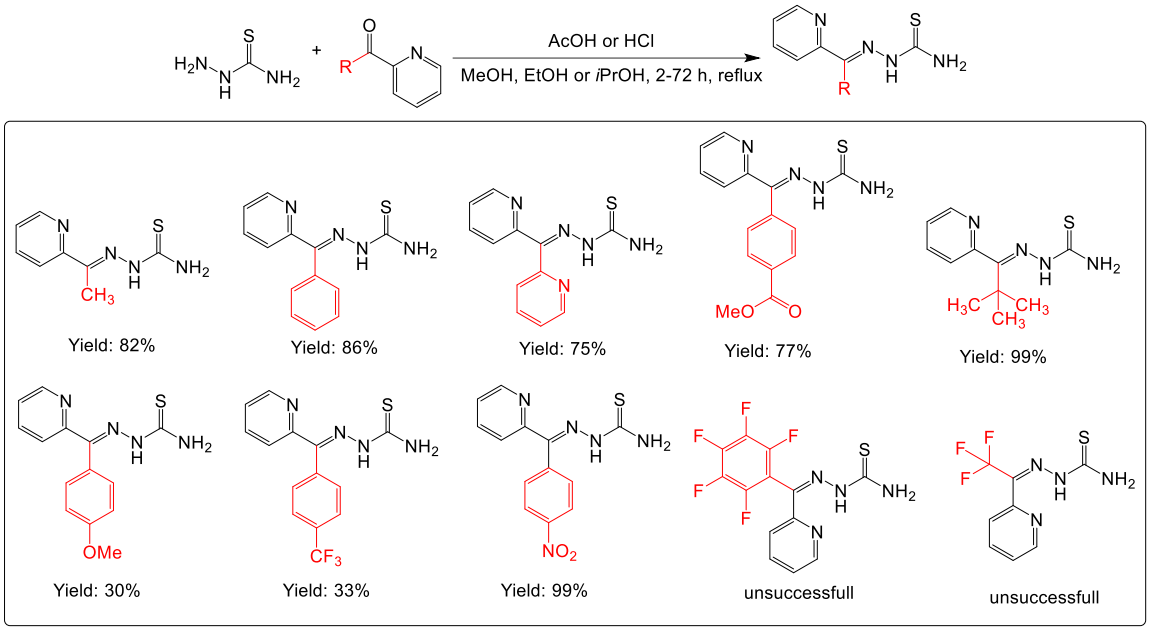


Chart 18. Overview of the α-pyridyl ketones, used for the synthesis of TSCs.

3.2.1.2 α-Pyridyl TSCs

The α-pyridyl ketones were reacted with thiosemicarbazide using AcOH or HCl as a catalyst, yielding the TSCs in 30-99% (Scheme 43).



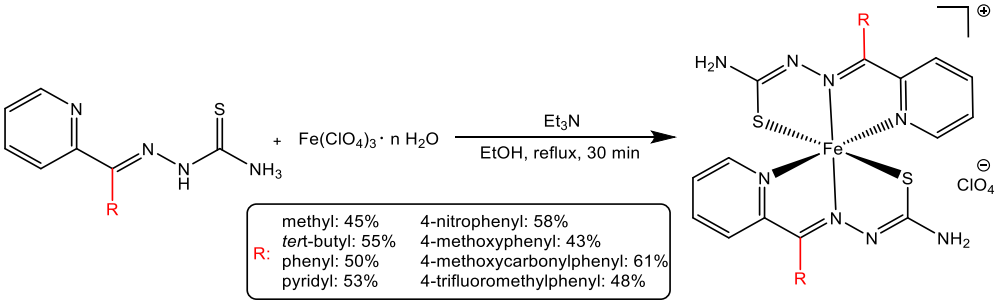
Scheme 43. Synthesis of α-pyridyl ketones TSCs by the acid catalyzed condensation of α-pyridyl ketones with thiosemicarbazide.

The reactions involving 2,2,2-trifluoro-1-(2-pyridinyl)ethenone and (2,3,4,5,6-pentafluorophenyl)-2-pyridinylmethanone were found to be unsuccessful for different tested catalysts and reaction conditions. When using AcOH as a catalyst, no reaction conversion was observed and only starting material was reisolated. By that reason, HCl was used as a catalyst due to its increased acidity. In case of (2,3,4,5,6-pentafluorophenyl)-2-pyridinylmethanone, again the starting material was isolated. In case of 2,2,2-trifluoro-1-(2-pyridinyl)ethenone a decomposition was observed. The results are unexpected because highly electron withdrawing groups should increase the electrophilicity of the carbonyl function and speed up the reaction. However, experimental observation is exactly the opposite. This observation is probably related to the fact that strong electron-withdrawing groups are leading to an increased reactivity of the TSC, which in turn can hydrolyze and react back to the starting materials. This observation is in accordance with results from literature, which reported that imines with perfluoroalkyl or perfluoro aryl groups in α-position quickly hydrolyze under weakly acidic conditions.[328] In addition to that, this limited stability was also reported for TSCs in literature. *Richardson* and co-authors recognized the hydrolyzation of a *meta*-nitro benzyl substituted TSCs during its synthesis. In addition, they mentioned that the rection needed anhydrous conditions to obtain high yields.[105]

In the future, the reaction conditions could be changed to a base catalyzed condensation reaction. In addition, H_2O should be avoided in the reaction, which requires a *Dean-Stark* setup to remove the released H_2O during the condensation reaction. However, these TSC are probably not interesting for medical applications, due to their sensitivity. In this way, a synthetic limitation was found for the TSC design, since electron-withdrawing groups limit the stability. This in turn limits the possibilities to tune the Fe(II)/(III) redox potential later.

3.2.1.3 α-Pyridyl TSC Fe(III) complexes

The α-pyridyl TSCs Fe(III) complexes were synthesized by a protocol from literature.[39] Two equivalents of the TSC were reacted with one equivalent of $Fe(ClO_4)_3$ under reflux and basic conditions (Et_3N) for 30 min (Scheme 44). The reaction yields were moderate to low. This can be explained by the fact that workup of the reaction can lead to massive losses in yield because the solubility of the ligand and the iron complex are often quite similar. However, it was possible to synthesize enough material for further investigations.



Scheme 44. Synthesis of α-Pyridyl TSCs Fe(III) complexes.

3.2.2 NMR studies of α-Pyridyl TSCs

The proton signal of the hydrazone function of TSCs is usually shifted downfield in the ^{1}H NMR spectrum, which leads to a characteristic signal, often found around 12 ppm. This circumstance is related to the acidity of the proton, which in turn is affected by substituents at the *N*1 position. For electron donating substituents, the signal is usually highfield shifted, while for electron withdrawing substituents a downfield shift is observed.[39,302,329] This behavior was also found for α-pyridyl TSCs synthesized in this research, which is shown in Figure 41 and Table 11. For the TSC with *tert*-butyl function, the signal is the most highfield shifted in this series and found at 8.68 ppm. For the methyl substituent, the signal is significantly shifted to 10.30 ppm. A further shift to 12.10 ppm is found for the phenyl group. Substituents at the phenyl ring only led to small differences in the chemical shift, which should not be overinterpreted. The highest chemical shift is found for the dipyridyl ketone TSC (12.97 ppm).

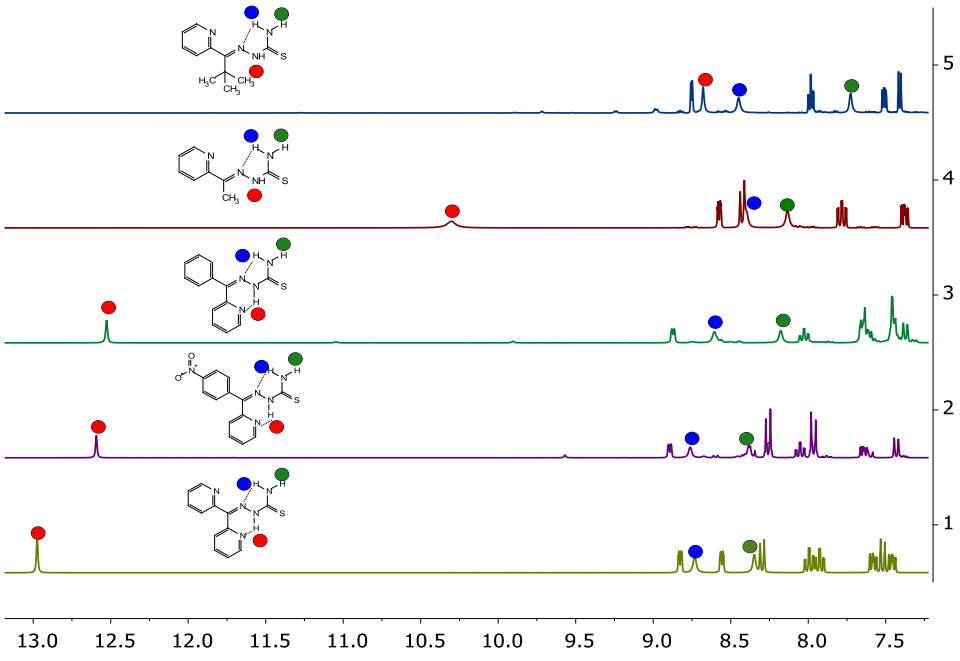
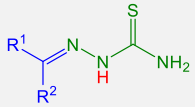


Figure 41. ^{1}H NMR spectra of some selected α-pyridyl ketone TSCs measured in DMSO-d$_6$ at 499 MHz.

Table 11. Chemical shifts of the hydrazone proton of α-pyridyl TSCs measured in DMSO-*d*$_6$ at 499 MHz.

R^1 + R^2 at *N*1	*t*BuPy	MePy	OMePhPy	COOMePhPy	PhPy	NO$_2$PhPy	CF$_3$PhPy	Dipy
 Chemical shift NH [ppm]	8.68	10.30	12.10	12.48	12.53	12.59	12.72	12.97

However, interpreting the chemical shifts solely on the basis of electronic factors caused by different substituents is too simple. This is evident from the fact that the differences in the chemical shifts are very significant, meaning that other factors must also play a role. An important factor in NMR spectroscopy is the chemical environment, whereby the configuration of TSCs in solutions is significantly influenced by intramolecular hydrogen bonds. The proton at the *N*4 position can form a hydrogen bond with nitrogen *N*1, which is found in crystal structures from literature but also by ^{1}H NMR spectroscopy since the NH_2 function splits into two singlets (Figure 42).[39,105,329]

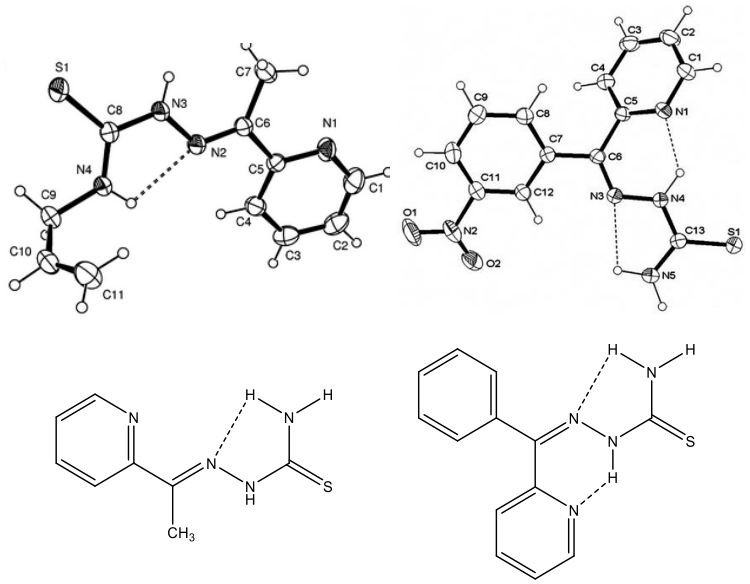


Figure 42. Hydrogen bonding in α-pyridyl TSCs. The crystal structure is obtained from literature: Ref. [105,329].

Another hydrogen bond is often observed between the pyridine nitrogen and the proton at the *N*2 position. However, it depends on the acidity of the proton, if this hydrogen bond is formed, which in turn is determined by residues at the *N*1 position. For strongly electron-donating substituents such as *t*Bu and Me, the proton at *N*2 is probably not acidic and no hydrogen bonding is observed. A comparison with crystal structures of acetylpyridine TSCs confirms this assumption, where this hydrogen bond is missing (Figure 42).[329] In the case of a benzyl substituent, the acidity at *N*2 position seems to be increased. In the corresponding crystal structure, hydrogen bonding is found between the pyridine and the proton at the *N*2 position (Figure 42).[105] The strong shift between MePy(TSC)H_2 and PhPy(TSC)H_2 can be explained in this way. However, the significant difference in the chemical shift between MePy(TSC)H_2 and *t*BuPy(TSC)H_2 cannot be explained by this image. One explanation could be a hydrophobic and steric shielding of the proton at the *N*2 position by the *tert*-butyl function which should be significantly decreased for the methyl substituent. This circumstance could contribute to the large difference of the chemical shifts, in addition to the electronic impact caused by different substituents.

The ^{1}H NMR spectrum gives first evidence about the electronic situation of the TSCs. However, it should be noted that the ^{1}H NMR spectrum is also massively influenced by interactions of the TSC with its surroundings, which is quite pronounced for TSCs. For example, the solvent and the concentration of the TSC might affect these interactions. Often, the solvents used for NMR spectroscopy can have different contents of H_2O. This is especially true for DMSO, which is hygroscopic. This limits a detailed interpretation of the exact chemical shifts and only general trends can be estimated.

3.2.3 UV/Vis absorption spectroscopy of α-Pyridyl TSCs and their iron complexes

The α-pyridyl TSCs were analyzed by UV/Vis absorption spectroscopy, which was measured in MeCN (Figure 43). The TSC exhibits two or three maxima, which are significantly shifted, depending on the

residue at the *N*1 position (Table 12). A trend can be clearly identified by comparing the maximum of their lowest energy transition:

tBuPy(TSC)H$_2$ (**278 nm**) < MePy(TSC)H$_2$ (**312 nm**) < OMePhPy(TSC)H$_2$ (**334 nm**) < PhPy(TSC)H$_2$ (**336 nm**) < Dipy(TSC)H$_2$ (**342 nm**) = CF$_3$PhPy(TSC)H$_2$ (**342 nm**) < COOMePhPy(TSC)H$_2$ (**354 nm**) < NO$_2$PHPy(TSC)H$_2$ (**356 nm**).

Electron donating groups are leading to a hypochromic shift of their absorption maximum, while electron withdrawing groups lead to bathochromic shifts. Between tBuPy(TSC)H$_2$, which is most blue shifted and NO$_2$PhPy(TSC)H$_2$, which is the reddest shifted compound, a difference of 78 nm occurs. The shifts between different substituted phenyl groups are less pronounced but still obvious. As mentioned before, DFT calculations from literature showed that the LUMO of the TSCs is located at the imine group.[2] By that reason, it is not surprising that functional groups, directly attached to the imine have a significant impact on the absorption properties. In contradiction to that, substituents at the *N*4 position do not affect the absorption properties significantly as described in Chapter 3.1.2. As shown by the results from NMR spectroscopy, the acidity of the hydrazone motif is also affected by substituents. This in turn can influence the thiol/thione tautomerism which can also influence the absorption properties in protic solvents. These solvent dependent effects could be investigated in the future in more detail.

The optical HOMO-LUMO gaps were calculated, by determining the onset wavelength of the lowest energy transition. The values are summarized in Table 12 and follow a similar trend as observed for the absorption maxima. Here, the *t*BuPy(TSC)H$_2$ and MePy(TSC)H$_2$ have the largest HOMO-LUMO gaps. The HOMO-LUMO gaps of Dipy(TSC)H$_2$, PhPy(TSC)H$_2$, CF$_3$PhPy(TSC)H$_2$ and OMePhPy(TSC)H$_2$ are in a very similar range, and differences are less pronounced than it was observed for the absorption maxima. The smallest HOMO-LUMO gaps are found for NO$_2$PhPy(TSC)H$_2$ and COOMePhPy(TSC)H$_2$.

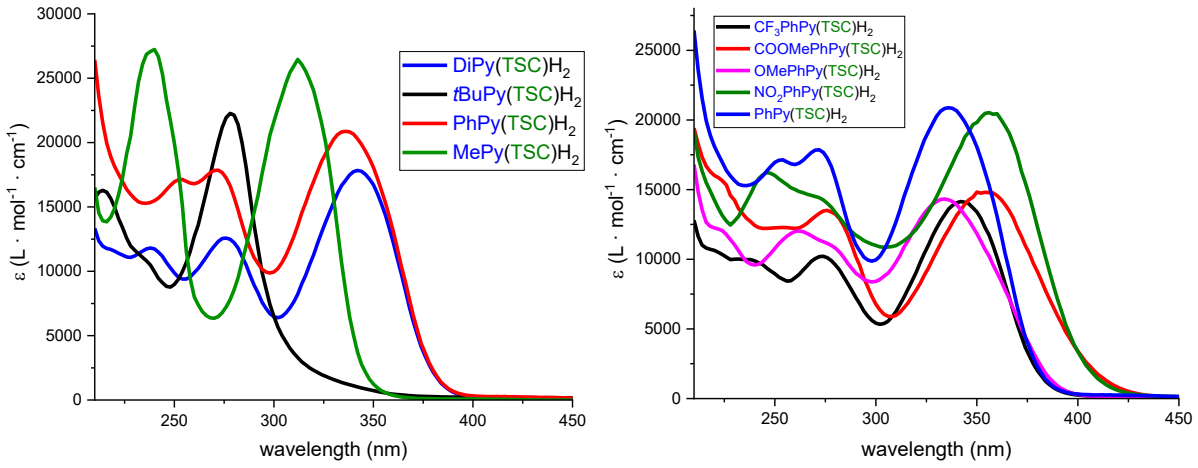


Figure 43. UV/Vis absorption spectra of α-pyridyl TSCs in MeCN.

Table 12. UV/Vis absorption data of α-pyridyl TSCs.[a]

Compound	λ$_1$ [nm], ε [L · mol^{-1} · cm^{-1}]	λ$_2$ [nm], ε [L · mol^{-1} · cm^{-1}]	λ$_3$ [nm], ε [L · mol^{-1} · cm^{-1}]	ΔE$_{opt}$ [eV]
Dipy(TSC)H$_2$	238, 11810	274, 12580	342, 17840	3.23
*t*BuPy(TSC)H$_2$	214, 16290	236 (sh), 11070	278, 22270	4.04
PhPy(TSC)H$_2$	252, 17110	272, 17860	336, 20880	3.24
MePy(TSC)H$_2$	240, 27240	312, 26460	-	3.56
CF$_3$PhPy(TSC)H$_2$	238, 9970	274, 10190	342, 14140	3.24
COOMePhPy(TSC)H$_2$	222 (sh), 15860	276, 13510	354, 14810	3.01
OMePhPy(TSC)H$_2$	222 (sh), 12170	262, 12030	334, 14810	3.18
NO$_2$PhPy(TSC)H$_2$	246, 16340	272 (sh), 14420	356, 2530	3.05

[a] Measured in MeCN. λ = absorption maxima, sh = shoulder. ΔE$_{opt}$ [eV] = optical HOMO-LUMO gap.

The corresponding Fe(III) complexes show less pronounced absorption maxima, compared to the ligands (Figure 44). An exception is [Fe(Dipy(TSC)H$_2$)$_2$]ClO$_4$ and [Fe(OMePhPy(TSC)H$_2$)$_2$]ClO$_4$, which show the characteristic maxima of the ligand as well as an additional broad shoulder around 450 nm. For the other compounds, one sharp maximum is found around 240 nm, while the other maxima are fused to several shoulders. All compounds have in common that they show an additional absorption band around 400-500 nm, compared to the ligands. The maxima are summarized in Table 13. Also, for the complexes, the optical HOMO-LUMO gaps have been determined. It is found that the differences in their HOMO-LUMO gaps are less pronounced compared to the ligands (2.41-2.29 eV). The highest gap is found for [Fe(COOMePhPy(TSC)H$_2$)$_2$]ClO$_4$ and [Fe(COOMePhPy(TSC)H$_2$)$_2$]ClO$_4$ (2.41 eV and 2.39 eV). This is followed by [Fe(NO$_2$PhPy(TSC)H$_2$)$_2$]ClO$_4$ (2.37 eV), [Fe(OMePhPy(TSC)H$_2$)$_2$]ClO$_4$ (2.36 eV) and [Fe(PhPy(TSC)H$_2$)$_2$]ClO$_4$ (2.35 eV). The smallest gaps are found for [Fe(CF$_3$PhPy(TSC)H$_2$)$_2$]ClO$_4$ (2.31 eV), [Fe(*t*BuPy(TSC)H$_2$)$_2$]ClO$_4$ (2.30 eV), [Fe(Dipy(TSC)H$_2$)$_2$]ClO$_4$ (2.29 eV) and [Fe(MePy(TSC)H$_2$)$_2$]ClO$_4$ (2.27 eV).

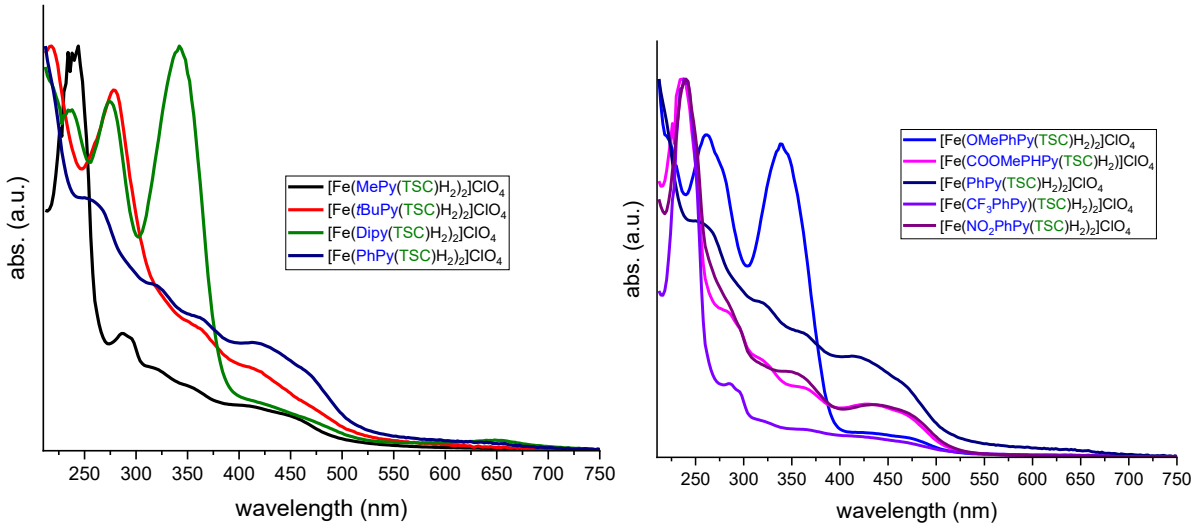


Figure 44. UV/Vis absorption spectra of α-pyridyl TSC Fe(III) complexes in MeCN.

Table 13. UV/Vis absorption data of α-pyridyl TSC Fe(III) complexes.

Compound	λ_1 [nm]	λ_2 [nm]	λ_3 [nm]	λ_4 [nm]	λ_5 [nm]	ΔE_{opt} [eV]
[Fe(Dipy(TSC)H$_2$)$_2$]ClO$_4$	236	274	342	440	-	2.29
[Fe(*t*BuPy(TSC)H$_2$)$_2$]ClO$_4$	218	280	356 (sh)	416	-	2.30
[Fe(PhPy(TSC)H$_2$)$_2$]ClO$_4$	258	316 (sh)	358 (sh)	416	464 (sh)	2.35
[Fe(MePy(TSC)H$_2$)$_2$]ClO$_4$	240	288	318 (sh)	354 (sh)	412	2.41
[Fe(CF$_3$PhPy(TSC)H$_2$)$_2$]ClO$_4$	240	288	322 (sh)	364 (sh)	440	2.31
[Fe(COOMePhPy(TSC)H$_2$)$_2$]ClO$_4$	238	284 (sh)	320 (sh)	362 (sh)	440	2.39
[Fe(OMePhPy(TSC)H$_2$)$_2$]ClO$_4$	260	338	433	-	-	2.36
[Fe(NO$_2$PhPy(TSC)H$_2$)$_2$]ClO$_4$	240	346	440	-	-	2.37

[a] Measured in MeCN. λ = absorption maxima, sh = shoulder. ΔE_{opt} [eV] = optical HOMO-LUMO gap.

3.2.4 Cyclovoltammetry of α-Pyridyl TSCs and their iron complexes

The electrochemistry of the ligands was investigated by cyclic voltammetry (CV) measurements in MeCN (Referenced to FeCp$_2$/FeCp$_2^+$). The measurements of the literature unknown TSCs *t*BuPy(TSC)H$_2$, CF$_3$PhPy(TSC)H$_2$, COOMePhPy(TSC)H$_2$ and NO$_2$PhPy(TSC)H$_2$ are shown in Figure 45 (all data in the appendix). All potentials are summarized in Table 14.

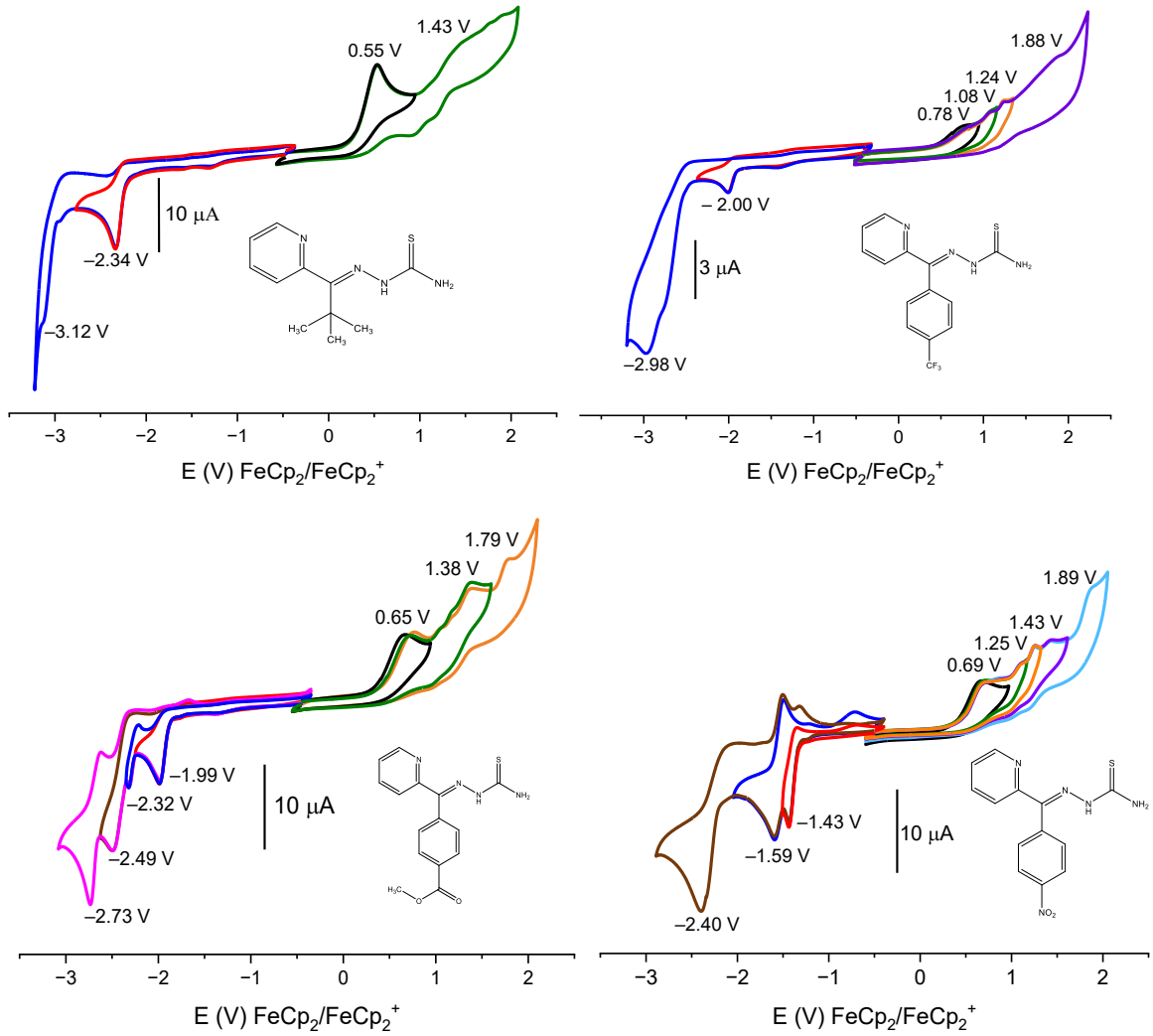


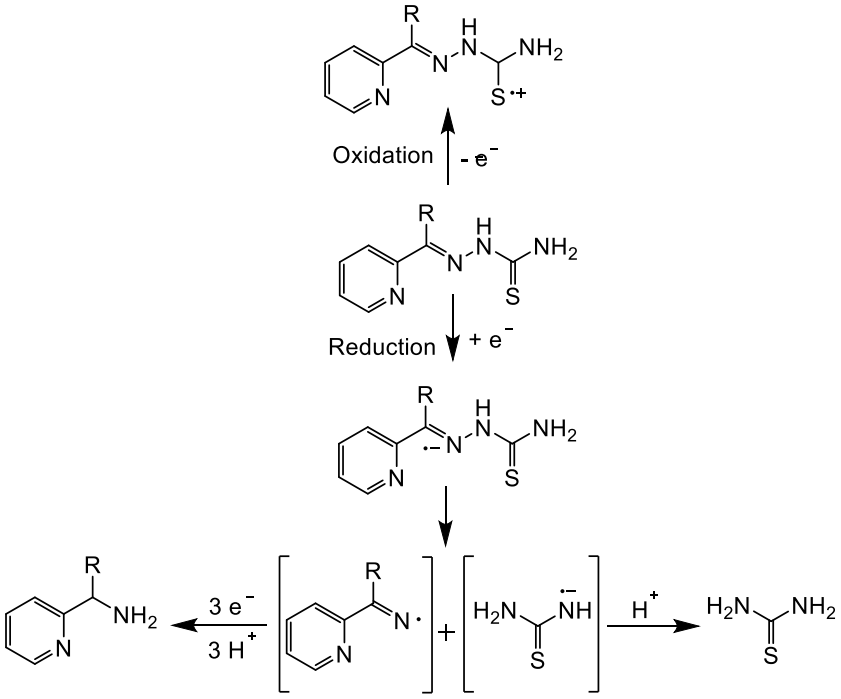
Figure 45. CVs of *t*BuPy(TSC)H$_2$ (Top, left), CF$_3$PhPy(TSC)H$_2$ (Top, right), COOMePhPy(TSC)H$_2$ (Bottom, left) and NO$_2$PhPy(TSC)H$_2$ (Bottom, right), measured in 0.1 M solution of *n*Bu$_4$NPF$_6$ in MeCN at a scan rate of 100 mV/s, referenced against FeCp$_2$/FeCp$_2^+$.

Table 14. Redox potentials of α-pyridyl TSCs.[a]

	Ox 4 (V)	Ox 3 (V)	Ox 2 (V)	Ox 1 (V)	Red 1 (V)	Red 2 (V)	Red 3 (V)	Red 4 (V)
*t*BuPy(TSC)H$_2$	-	-	1.43	0.55	–2.34	–3.12	-	-
MePy(TSC)H$_2$	-	-	1.38	0.63	–2.27	–2.92		
OMePhPy(TSC)H$_2$	-	-	1.12	0.69	–2.13	–3.00	–3.27	-
PhPy(TSC)H$_2$	-	-	1.10	0.62	–2.10	–2.89	-	-
Dipy(TSC)H$_2$	-	-	1.40	0.85	–2.02	–2.93	-	-
CF$_3$PhPy(TSC)H$_2$	1.88	1.24	1.08	0.78	–2.00	–2.98	-	-
COOMePhPy(TSC)H$_2$	-	1.79	1.38	0.65	–1.99	–2.32	–2.49	–2.73
NO$_2$PhPy(TSC)H$_2$	1.89	1.43	1.25	0.69	–1.43	–1.59	–2.40	-

[a] Measured in 0.1 M solution of *n*Bu$_4$NPF$_6$ in MeCN at a scan rate of 100 mV/s, referenced against FeCp$_2$/FeCp$_2^+$.

Most of the TSCs typically show two irreversible reductions. The first one is usually attributed to an imine centered reduction in literature, since the LUMO is usually located at this position. It is expected that the reduction will lead to a cleavage of the TSC at the imine group (Scheme 45) under the formation of an imine radical and urea.[302]



Scheme 45. Suggested mechanism for the electrochemical oxidation and reduction of *α*-pyridyl TSC. Adopted from Ref. [302].

The cleaved imine radical can be further reduced (3 e^-, 3 H^+) to an amine, which is usually in accordance with the second reduction observed in the CV of these compounds. Depending on the functional groups at the *N*1 position, further reduction processes are observed, which was the case for OMePhPy(TSC)H_2, COOMePhPy(TSC)H_2 and NO_2PhPy(TSC)H_2. The processes are probably attributed to these functional groups. By that reason, it is unclear for these compounds, if the first reduction is imine centered or at one of the functional groups. Especially for NO_2PhPy(TSC)H_2, the first reduction is probably related to the reduction of the nitro function. In this way, it is more likely that the second reduction is imine centered. However, it should be considered that the second reduction is the reduction of a reduced species, which makes an assignment more complicated.

For most of the TSCs, two irreversible oxidations are found. DFT calculations from literature usually show, that the HOMO is located at the thione function.[302] In this way, the first oxidation is maybe attributed to the formation of a thio radical, which directly starts decomposing (Scheme 45). Again, the oxidation processes become more complex, if functional groups are in the TSC structure. This was the case for CF_3PhPy(TSC)H_2, COOMePhPy(TSC)H_2 and NO_2PhPy(TSC)H_2.

By comparing the potential of the first reduction, it is found that they are cathodically shifted for electron donating substituents (Figure 46). This means that TSCs with electron withdrawing groups become easier to reduce. The trends are consistent with the observation from ^{1}H NMR spectroscopy as well as UV/Vis absorptions spectroscopy and are demonstrating the impact of residues at the *N*1 position on the LUMO of the TSC. Also, the potential of the first oxidation differs between the different TSCs. However, these shifts do not follow the same trend. The electrochemical HOMO-LUMO gaps are in general smaller than the optical HOMO-LUMO gaps, which were determined in Chapter 3.2.3. Nevertheless, the trend remains the same with the *t*BuPy(TSC)H_2 and MePy(TSC)H_2 having the largest gaps and NO_2PhPy(TSC)H_2 and COOMePhPy(TSC)H_2 having the smallest gaps.

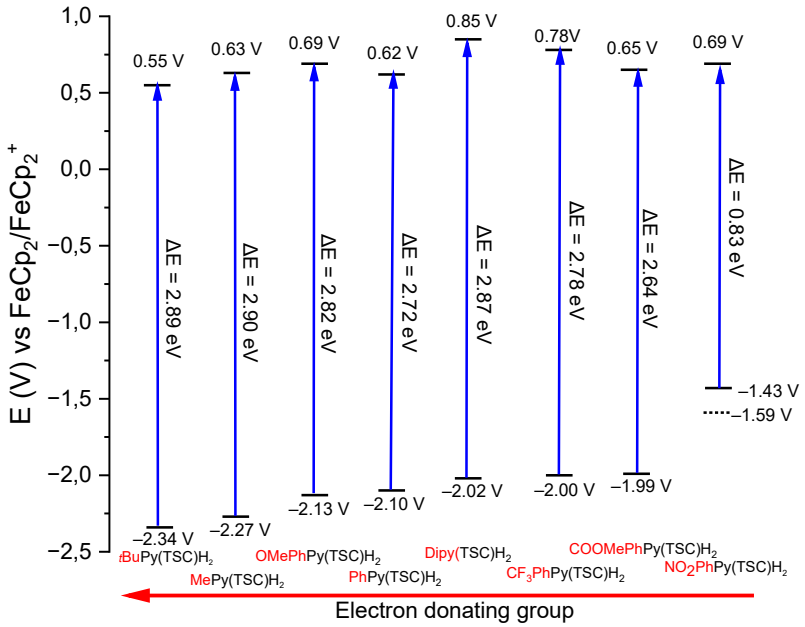


Figure 46. Redox potentials of the first oxidation and reduction as well as the electrochemical HOMO-LUMO gap of the α-pyridyl TSCs. For $NO_2PhPy(TSC)H_2$ the second reduction is shown, since the first reduction is probably centered at the NO_2 function. The potentials are measured in 0.1 M solution of nBu$_4$NPF$_6$ in MeCN at a scan rate of 100 mV/s and referenced against $FeCp_2/FeCp_2^+$.

In the next step, the corresponding Fe(III) complexes have been studied by CV. As an example, the results of $[Fe(CF_3PhPy(TSC)H_2)_2]ClO_4$ are shown in Figure 47 (all data in the appendix). In addition to that, the results of the other complexes are shown in Table 15. For all the complexes, a reversible reduction is found, which is assigned to the Fe(II)/(III) redox potential, in accordance with literature.[39] By comparing this redox potential between the different Fe(III) complexes, a significant shift is observed (Figure 47).

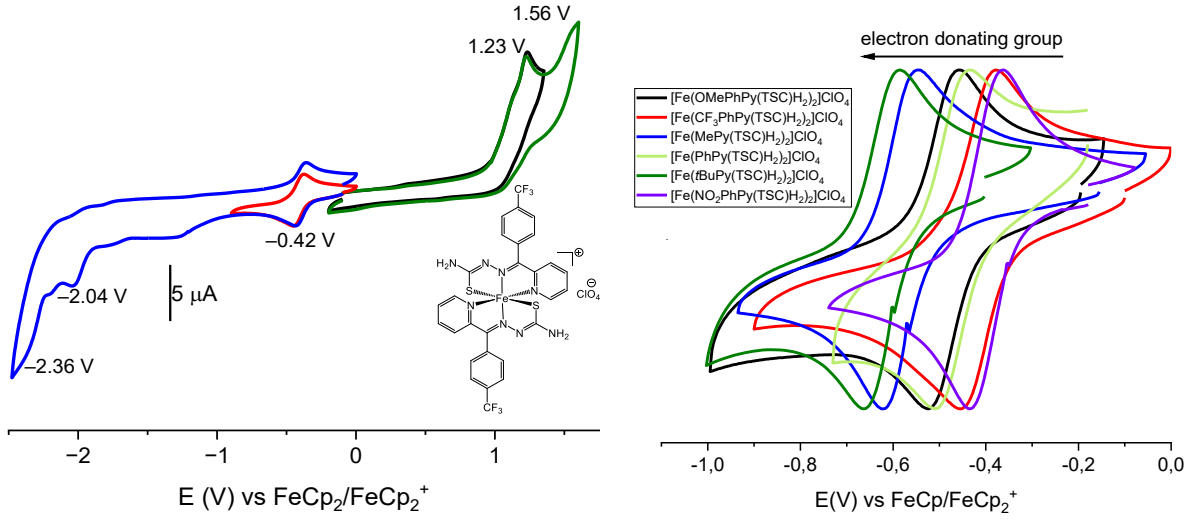


Figure 47. Left: CVs of $[Fe(CF_3PhPy(TSC)H_2)_2]ClO_4$ measured in 0.1 M solution of nBu$_4$NPF$_6$ in MeCN at a scan rate of 100 mV/s, referenced against $FeCp_2/FeCp_2^+$. Right: CVs of the first reduction of $[Fe(OMePhPy(TSC)H_2)_2]ClO_4$, $[Fe(CF_3PhPy(TSC)H_2)_2]ClO_4$, $[Fe(MePy(TSC)H_2)_2]ClO_4$, $[Fe(PhPy(TSC)H_2)_2]ClO_4$, $[Fe(t$BuPy$(TSC)H_2)_2]ClO_4$ and $[Fe(NO_2PhPy(TSC)H_2)_2]ClO_4$ measured in 0.1 M solution of nBu$_4$NPF$_6$ in MeCN at a scan rate of 100 mV/s, referenced against $FeCp_2/FeCp_2^+$.

The results completely fulfill the expectations of the ligand design and are in accordance with examples from literature.[40] Electron donating groups at the *N*1 position led to a cathodically shift. This means that the iron center becomes more difficult to reduce, and the Fe(III) state is stabilized. Electron

withdrawing substituents lead to an anodically shift of the redox potential and the complexes become easier to reduce. Here, the Fe(II) state is stabilized. The [Fe(NO$_2$PhPy(TSC)H$_2$)$_2$]ClO$_4$ shows the most anodically shifted redox potential (–0.40 V), followed by [Fe(CF$_3$PhPy(TSC)H$_2$)$_2$]ClO$_4$ (–0.42 V). The results are in accordance with observations from literature, which measured a similar TSC with nitro function in *meta* position.[105] The most anodically shifted redox potential was found for [Fe(*t*BuPy(TSC)H$_2$)$_2$]ClO$_4$ (–0.63 V). The redox potential was significantly shifted compared to literature known [Fe(MePy(TSC)H$_2$)$_2$]ClO$_4$ (–0.58 V), which has the second most negative redox potential.

The impact of the redox potential on their cytotoxicity is unclear and should be investigated in the future to get a deeper understanding of structure-activity relationships. Although, it was found in literature that the average toxicity was increasing for electron donating substituents ([Fe(Dipy(TSC)H$_2$)$_2$]ClO$_4$ < [Fe(PhPy(TSC)H$_2$)$_2$]ClO$_4$ < [Fe(MePy(TSC)H$_2$)$_2$]ClO$_4$), it is questionable what happens, if the potential is further shifted to even more negative values. An important requirement for the cytotoxicity of TSCs is to cycle between the Fe(II) and Fe(III) state. If the Fe(III) or the Fe(II) state becomes more stabilized, the redox cycling will be maybe less favored.

Table 15. Redox potentials of α-pyridyl TSC Fe(III) complexes.[a]

	Ox 4 (V)	Ox 3 (V)	Ox 2 (V)	Ox 1 (V)	Red 1 (V)	Red 2 (V)	Red 3 (V)	Red 4 (V)
[Fe(tBuPy(TSC)H$_2$)$_2$]ClO$_4$	1.71	1.17	1.05	0.35	–0.63	–1.37	–2.30	–2.80
[Fe(MePy(TSC)H$_2$)$_2$]ClO$_4$	-	-	1.48	1.00	–0.58	–2.26	–2.59	-
[Fe(OMePhPy(TSC)H$_2$)$_2$]ClO$_4$	-	1.34	1.14	0.54	–0.50	–2.11	–2.39	–2.88
[Fe(PhPy(TSC)H$_2$)$_2$]ClO$_4$	-	-	1.14	0.47	–0.47	–2.14	–2.56	-
[Fe(Dipy(TSC)H$_2$)$_2$]ClO$_4$	-	-		0.64	–0.45	–2.03	–2.81	-
[Fe(CF$_3$PhPy(TSC)H$_2$)$_2$]ClO$_4$	-	-	1.56	1.23	–0.42	–2.04	–2.36	-
[Fe(COOMePhPy(TSC)H$_2$)$_2$]ClO$_4$	1.93	1.54	1.26	1.13	–0.44	–2.00	–2.36	-
[Fe(NO$_2$PhPy(TSC)H$_2$)$_2$]ClO$_4$	-	-	1.60	1.13	–0.40	–1.46	–2.47	–3.09

[a] Measured in 0.1 M solution of *n*Bu$_4$NPF$_6$ in MeCN at a scan rate of 100 mV/s, referenced against FeCp$_2$/FeCp$_2^+$.

The redox potential of the first oxidation does not follow the trend observed for the first reduction (Figure 48).

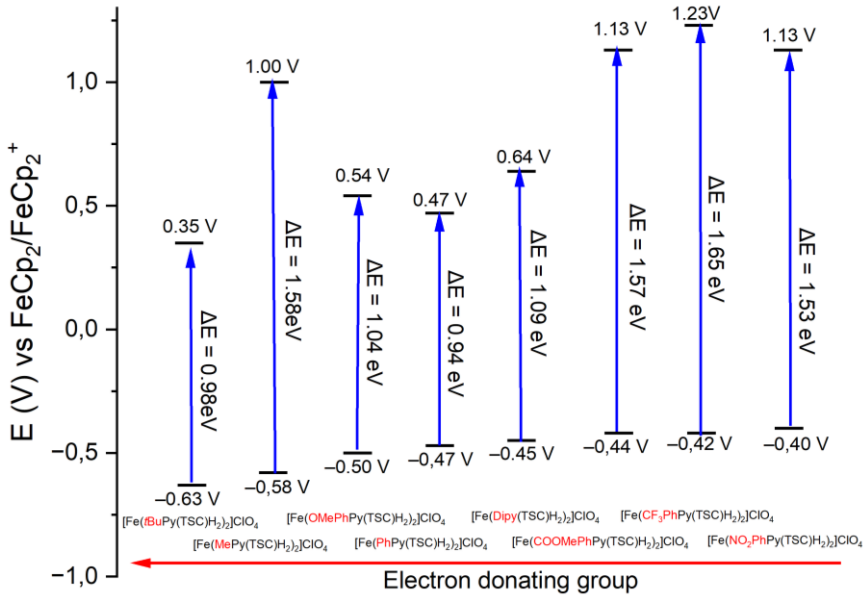
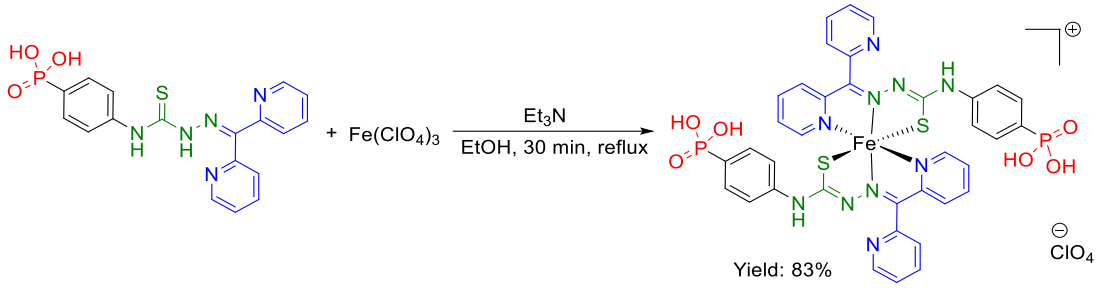


Figure 48. Redox potentials of the first oxidation and reduction as well as the electrochemical HOMO-LUMO gap of the α-pyridyl TSCs Fe(III) complexes. The potentials are measured in 0.1 M solution of *n*Bu$_4$NPF$_6$ in MeCN at a scan rate of 100 mV/s and referenced against FeCp$_2$/FeCp$_2^+$.

The electrochemical HOMO-LUMO gaps were found to be smaller than the optical HOMO-LUMO gaps from Chapter 3.2.3. The largest gap was determined for $[Fe(CF_3PhPy(TSC)H_2)_2]ClO_4$ (1.65 eV), followed by $[Fe(MePy(TSC)H_2)_2]ClO_4$ (1.58 eV), $[Fe(COOMePhPy(TSC)H_2)_2]ClO_4$ (1.57 eV) and $[Fe(NO_2PhPy(TSC)H_2)_2]ClO_4$ (1.53 eV). Significant smaller HOMO-LUMO gaps are found for the other complexes (0.64 to 0.34 eV).

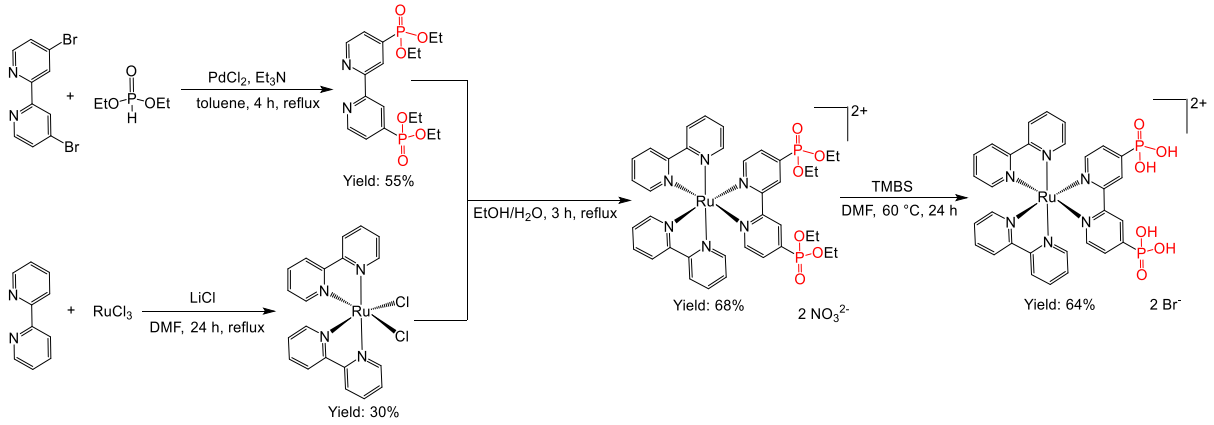
3.2.5 Functionalization of TiO_2 nanoparticles

In the next step, the idea was to covalently attach a TSC Fe(III) complex and a photosensitizer on the surface of TiO_2 NPs to synthesize a potential photocatalyst for the production of ROS. Dipy(TSC)PhPO(OH)$_2$ (Chapter 3.1.1.6) was used as the ligand and reacted with $Fe(ClO_4)_3$ in EtOH for 30 min under reflux using Et_3N as a base. The corresponding Fe(III) complex was obtained in high yields of 83% (Scheme 46).



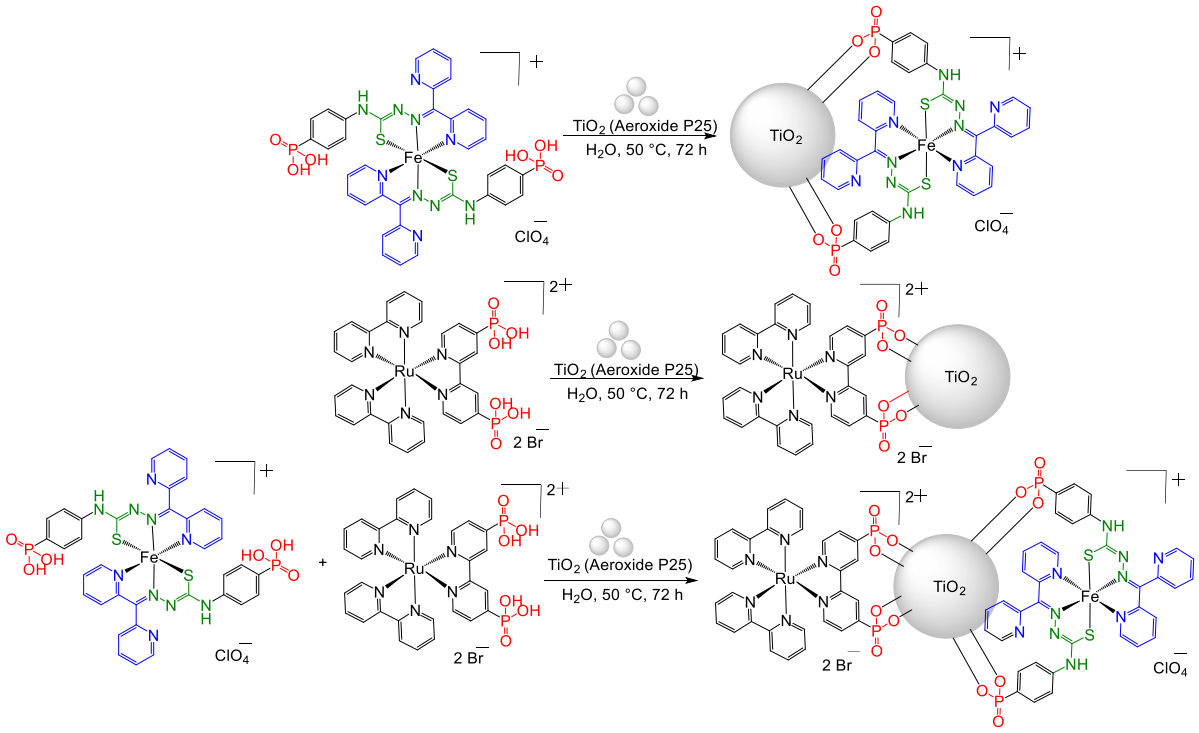
Scheme 46. Synthesis of $[Fe(Dipy(TSC)PhPO(OH)_2)_2]ClO_4$.

As a photosensitizer, the literature known $[Ru(bpy)_2(bpy(PO(OH)_2)_2)]Br_2$ was synthesized (Scheme 47).[330,331] In a first step bis(diethylphosphonate)bipyridine was synthesized by a P–C coupling reaction of dibromobispyridine and diethylphosphonate using $PdCl_2$ and Et_3N as the catalyst. After that, $[Ru(bpy)_2Cl_2]$ was synthesized by the reaction of $RuCl_3$, LiCl and bpy in DMF. The reaction of $[Ru(bpy)_2Cl_2]$ and bis(diethylphosphonate)bipyridine gave $[Ru(bpy)_2(bpy(PO(OEt)_2)_2)](NO_3)_2$ which was deprotected using TMBS yielding $[Ru(bpy)_2(bpy(PO(OH)_2)_2)]Br_2$.



Scheme 47. Synthesis of $[Ru(bpy)_2(bpy(PO(OH)_2)_2)]Br_2$.

With these two compounds at hand, the functionalization of TiO_2 (*Aeroxide P25, Evonik*) NPs with $[Fe(Dipy(TSC)PhPO(OH)_2)_2]$, $[Ru(bpy)_2(bpy(PO(OH)_2)_2)]$ and both compounds together was investigated (Scheme 48). The respective compounds (5.0 mg) were reacted with the particles (10.0 mg) in H_2O at 50 °C for 72 h. To attach both compounds together to the surface, 2.5 mg of both compounds (= 1.09 eq. $[Ru(bpy)_3]$, 1.00 eq. $[Fe(TSC)_2]$) were mixed in H_2O and added to the particle dispersion. The nanoconjugates were washed with H_2O and EtOH until the supernatant was colorless, which was confirmed by UV/Vis absorption spectroscopy.



Scheme 48. Overview of the tested functionalization reactions of TiO_2 NPs with [Fe(Dipy(TSC)PhPO(OH)$_2$)$_2$] and [Ru(bpy)$_2$(bpy(PO(OH)$_2$)$_2$)].

The TiO_2@[Ru(bpy)$_3$] particles had an orange color, while the TiO_2@[Fe(TSC)$_2$] particles were brown (Figure 49). Also, the TiO_2@[Ru(bpy)$_3$]/[Fe(TSC)$_2$] particles showed a brown color.



Figure 49. Photographs of TiO_2, TiO_2@[Ru(bpy)$_3$] and TiO_2@[Fe(TSC)$_2$] NPs.

The functionalized NPs were investigated by UV/Vis absorption spectroscopy (Figure 50). For the TiO_2@[Fe(TSC)$_2$] particles the absorption maxima related to [Fe(Dipy(TSC)PhPO(OH)$_2$)$_2$] are clearly visible at 285 and 320 nm, which can be seen by comparison with the spectra of TiO_2 and the TSC Fe(III) complex. In addition, a weak shoulder around 400 nm is found. Also, the absorption spectrum of TiO_2@[Ru(bpy)$_3$] showed characteristics of the Ru(II) complex. While the TiO_2 NPs showed a typical ramp shape, the absorption of TiO_2@[Ru(bpy)$_3$] starts to increase significantly around 500-250 nm, where the absorptions maxima of the ruthenium complex are located. Two maxima are clearly visible at 265 and 295 nm, which can be assigned to the Ru(II) photosensitizer.

The absorption spectrum of TiO_2@[Ru(bpy)$_3$]/[Fe(TSC)$_2$] is very similar to that of TiO_2@[Fe(TSC)$_2$]. The maxima of the Ru(II) complex are not visible. Since the extinction coefficients of [Ru(bpy)$_2$(bpy(PO(OH)$_2$)$_2$)] are very high, it opens the question whether both compounds are attached to the surface or if it is mainly functionalized with the TSC Fe(III) complex. This would mean that the affinity of the TSC complex to the particle surface is higher than for the Ru(II) complex. An explanation could be the fact that the Ru(II) complex has two positive charges while the TSC complex has one positive charge. This could lead to more repulsion at the particle surface for the [Ru(bpy)$_3$] complex. Since both compounds compete for a place on the particle surface, different affinities have a significant impact. Therefore, the functionalization conditions should be changed in the future. A possible

approach could be to functionalize the surface with [Ru(bpy)$_2$(bpy(PO(OH)$_2$)$_2$)] first, while the TSC complex is added in a second step. A question that needs to be clarified here is whether the Ru(II) complex can be displaced from the surface by TSC Fe(III) complex once it has been bound. If not, the concentration of [Ru(bpy)$_2$(bpy(PO(OH)$_2$)$_2$)] at the surface must be carefully adjusted so that there is enough space left to attach the TSC complex in a second step. This requires much optimization of the reaction conditions in the future, especially of the concentrations of the surface ligands.

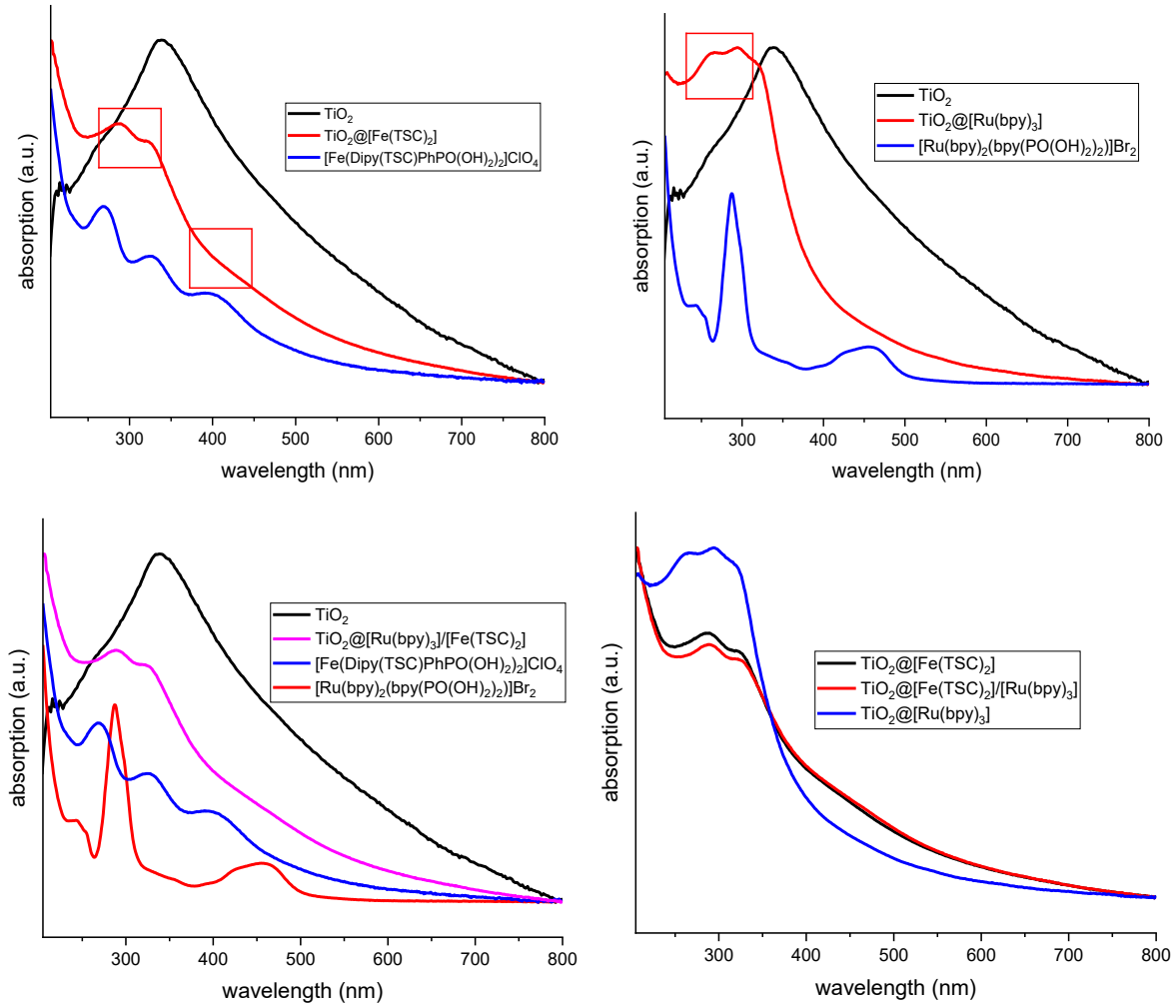


Figure 50. UV/Vis absorption spectra measured in MeOH. Top, left: TiO_2, [Fe(Dipy(TSC)PhPO(OH)$_2$)$_2$]ClO_4 and TiO_2@[Fe(TSC)$_2$]. Top, right: TiO_2, [Ru(bpy)$_2$(bpy(PO(OH)$_2$)$_2$)]Br_2, TiO_2@[Ru(bpy)$_3$]. Bottom, left: TiO_2, [Fe(Dipy(TSC)PhPO(OH)$_2$)$_2$]ClO_4, [Ru(bpy)$_2$(bpy(PO(OH)$_2$)$_2$)]Br_2 and TiO_2@[Ru(bpy)$_3$]/[Fe(TSC)$_2$]. Bottom, right: TiO_2@[Ru(bpy)$_3$], TiO_2@[Fe(TSC)$_2$] and TiO_2@[Ru(bpy)$_3$]/[Fe(TSC)$_2$].

FTIR measurements of the particles support the assumptions of the UV/Vis absorption spectroscopy (Figure 51). For the TiO_2@[Fe(TSC)$_2$] particles, additional vibrations are found in the region of 1600-900 cm^{-1}, which are related to the TSC Fe(III) complex at the particle surface. Especially the changes in the P–O region of the spectrum (1200-900 cm^{-1}) are indicating a successful functionalization. As already discussed in Chapter 3.1.4.4, the vibration band at 1045 cm^{-1} is probably assigned to the Ti–O–P vibration.

Also, for the TiO_2@[Ru(bpy)$_3$] particles, additional vibrations are found between 1600-800 cm^{-1}. However, the relative intensity of these signals, is very low, compared to TiO_2@[Fe(TSC)$_2$], which provides some evidence for a lower affinity to bind to the particle surface. Again, the vibrational band at 1045 cm^{-1} indicates a successful, covalent attachment.

The TiO_2@[Ru(bpy)$_3$]/[Fe(TSC)$_2$] particles, show additional vibrational bands in the region of 1600-800 cm^{-1}. A comparison to the FTIR spectra of [Fe(Dipy(TSC)PhPO(OH)$_2$)$_2$]ClO_4 and [Ru(bpy)$_2$(bpy(PO(OH)$_2$)$_2$)]Br_2, shows that these vibrations can be assigned to [Fe(Dipy(TSC)PhPO(OH)$_2$)$_2$]ClO_4. As already found for the UV/Vis absorption spectroscopy, the characteristic signals of [Ru(bpy)$_2$(bpy(PO(OH)$_2$)$_2$)]Br_2 are not observed indicating that the particles are at least mostly functionalized with the TSCs iron complex, while no or only a small concentration of [Ru(bpy)$_2$(bpy(PO(OH)$_2$)$_2$)]Br_2 is present at the surface.

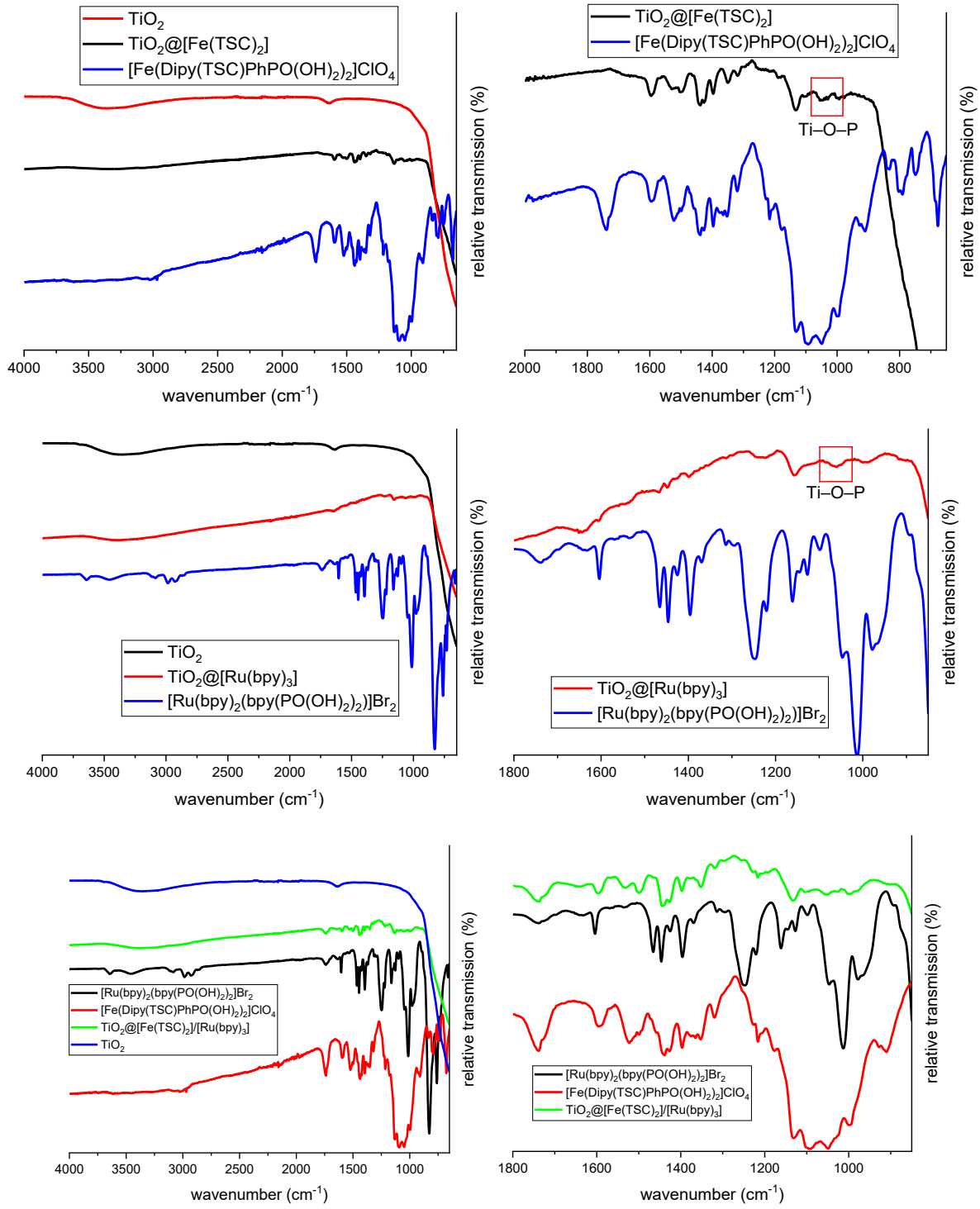


Figure 51. Normalized FTIR spectra of TiO_2@[Fe(TSC)$_2$] (top), TiO_2@[Ru(bpy)$_3$] (middle) and TiO_2@[Ru(bpy)$_3$]/[Fe(TSC)$_2$] (bottom) compared to TiO_2 and the metal complexes. Left side shows the full FTIR spectrum while on the right side a closeup to the region of 200-750 cm^{-1} is found. The intensity of the functionalized NPs is increased in the closeup by a factor of 2.5 for a better comparison.

The EDX spectrum of TiO_2@[Ru(bpy)$_3$] is shown in Figure 52. The signals of Ti, O and C are dominating in the spectrum, resulting from the TiO_2 NPs and the carbon tape used as a carrier material for measurements. Since the signal of N overlaps with Ti, it is not visible in the spectrum. However, the additional signals of P, Ru and Br are in accordance with a successful functionalization. The detection of Br is related to bromide, which is the anion of the Ru(II) complex. The signal of Ru was very weak. In addition to that, a detection of S is observed, which is probably related to an impurity. Quantification of the signals is not possible by similar reasons discussed in Chapter 3.1.4.4.

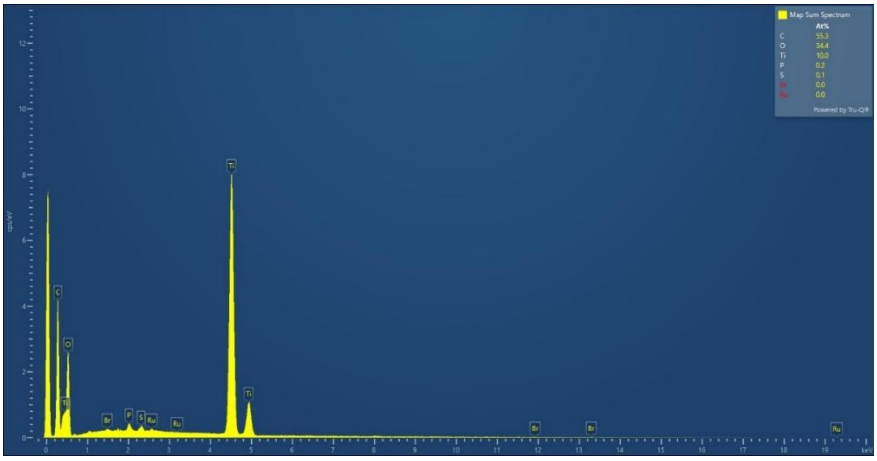


Figure 52. EDX spectrum of TiO_2@[Ru(bpy)$_3$]. The particles were spread onto a carbon tape, and the measurement was performed on large nanoaggregates to get a reliable intensity of the elements. The corresponding mapping images are found in the appendix.

The EDX spectrum of TiO_2@[Fe(TSC)$_2$] is shown in Figure 53. Besides the signals of Ti, O and C, also the presence of P, S and Fe is found which is in line with a successful functionalization. However, the detection of Si, Na and Br was not expected in this sample and must originate from an impurity. Since TMBS (trimethylsilyl bromide) was used for the deprotection of the phosphonate ester, it could be the source of Br and Si. In addition to that, the contamination with silica gel from column chromatography might be an option. However, the origin of this impurity must be clarified in the future.

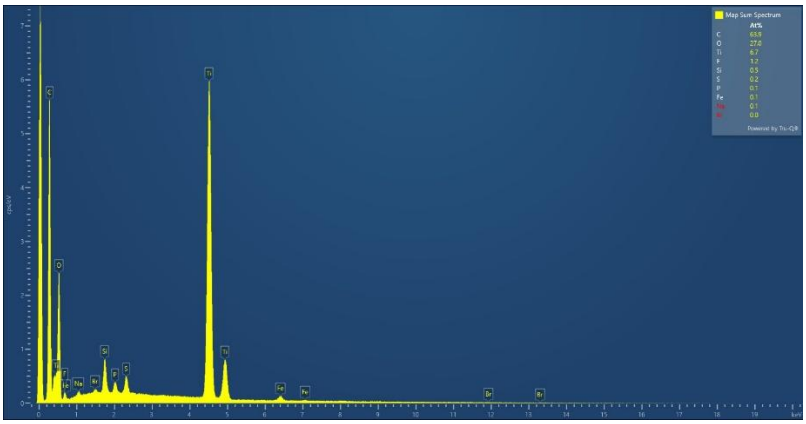


Figure 53. EDX spectrum of TiO_2@[Fe(TSC)$_2$]. The particles were spread onto a carbon tape, and the measurement was performed on large nanoaggregates to get a reliable intensity of the elements. The corresponding mapping images are found in the appendix.

The EDX data of TiO_2@[Ru(bpy)$_3$]/[Fe(TSC)$_2$] (Figure 54) shows similar signals discussed for TiO_2@[Fe(TSC)$_2$] but also the detection of Ru was observed. Although, a quantitative analysis of the signals is not possible in detail, the results indicate a higher concentration of the TSC Fe(III) complex on the surface than of the Ru(II) complex. Figure 54 shows the percentual amount of the elements (at%), whereby C, N and O are not included in this calculation since these signals overlap with other signals or are part of the carrier material (carbon tape). From this calculation, the ratio between Fe (1.0%) and

Ru (0.2%) is 5:1 and supports the assumptions from IR and UV/Vis spectroscopy that the TSC complex is dominant at the surface. On the other hand, the ratio of Fe (1.0%), P (2.2%) and S (2.4%) are close to the expectation and in line with the ratio of elements in the TSC Fe(III) complex.

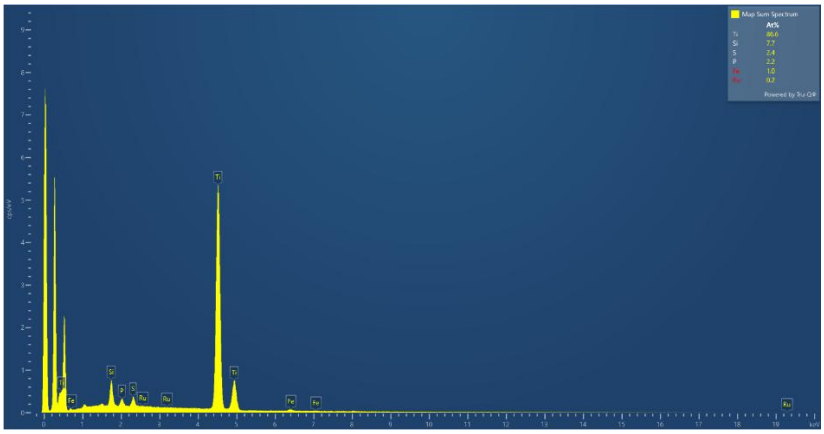


Figure 54. EDX spectrum of TiO_2@[Ru(bpy)$_3$]/[Fe(TSC)$_2$]. The particles were spread onto a carbon tape, and the measurement was performed on large nanoaggregates to get a reliable intensity of the elements. The corresponding mapping images are found in Figure 55.

The images of the elemental EDX mapping are shown in Figure 55 and confirm a homogenous distribution of the elements within the measured aggregates.

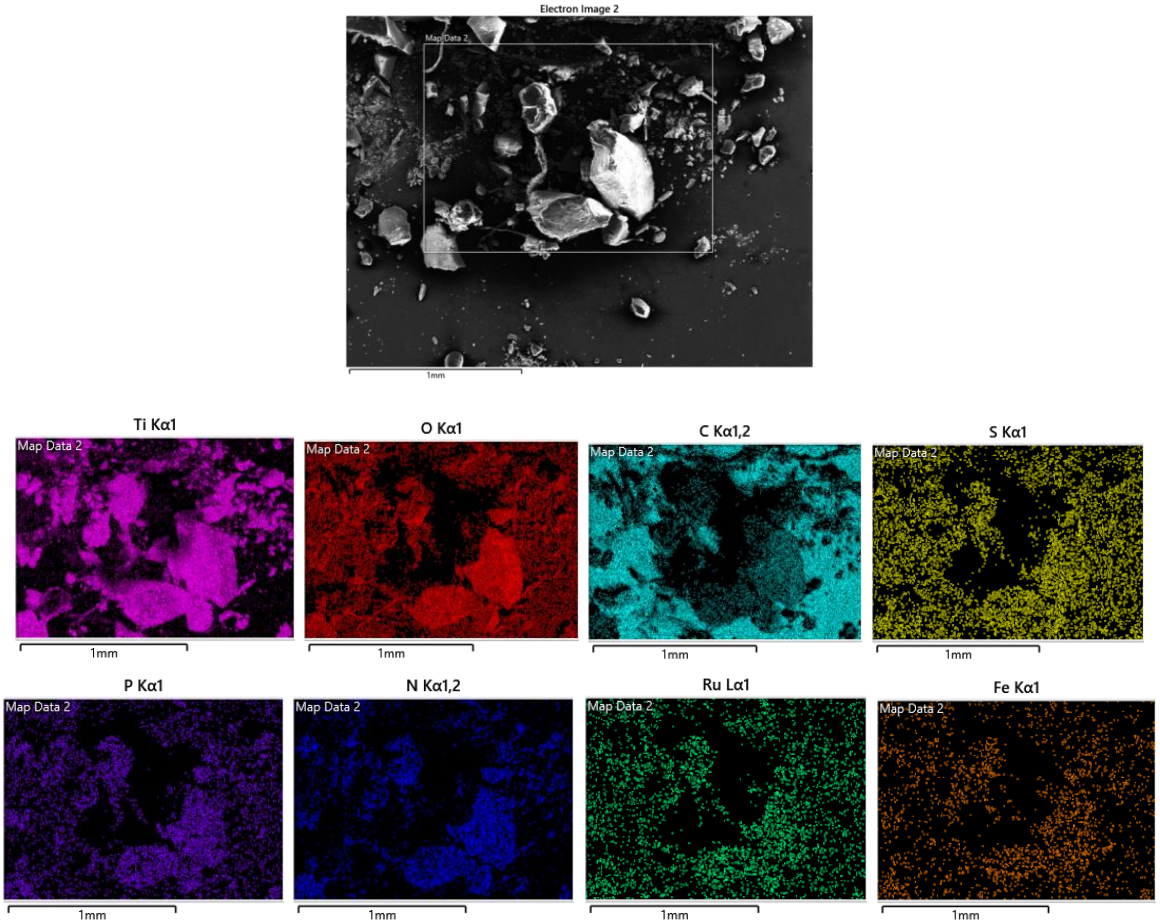


Figure 55. SEM image of TiO_2@[Ru(bpy)$_3$]/[Fe(TSC)$_2$] and the corresponding elemental mapping of the EDX measurements.

3.2.6 Summary - α-pyridyl TSCs Fe(III) complexes and their conjugation to TiO_2

New as well as literature known α-pyridyl TSCs have been successfully synthesized, having different electron donating or withdrawing substituents at the *N*1 position (Me, *t*Bu, Ph, Py, COOMePh, CF_3Ph, OMePh, NO_2Ph). In addition to that, the corresponding Fe(III) complexes were synthesized. The introduction of strongly electron withdrawing groups at the *N*1 position, namely CF_3 and C_6F_5 was unsuccessful. The results indicate a reduced stability of these TSCs. ^{1}H NMR spectroscopy, UV/Vis absorption spectroscopy as well as cyclic voltammetry of the ligands showed a significant impact of the substituents on the LUMO of the TSCs. Electron withdrawing substituents led to an anodically shift of the first reduction potential. Similar observations were made for the corresponding Fe(III) complexes, where the Fe(III)/Fe(II) redox potential was cathodically shifted for electron donating groups. In this way, $[Fe(t\text{BuPy(TSC)H}_2)_2]ClO_4$ showed the most negative potential (–0.63 V) and $[Fe(NO_2\text{PhPy(TSC)H}_2)_2]ClO_4$ the most positive potential (–0.40 V).

In the second step, $[Fe(\text{Dipy(TSC)PhPO(OH)}_2]$ was synthesized and immobilized on TiO_2 NPs. In addition, the photosensitizer $[Ru(bpy)_2(bpy(PO(OH)_2)]^{2+}$ was synthesized and immobilized on TiO_2 NPs. In the final step, the TSC Fe(III) complex as well as the photosensitizer were immobilized together on TiO_2 NPs. The nanoconjugates were investigated by FTIR and UV/Vis absorption spectroscopy as well as zeta, DLS and EDX measurements. While the synthesis of TiO_2@$[Fe(TSC)_2]$ and TiO_2@$[Ru(bpy)_3]$ was successful, the condensation of both compounds together to the particle led to the assumption that the TSC Fe(III) complex has a higher affinity to the particle surface than the Ru(II) complex, which requires some optimization of the reaction conditions in the future.

3.3 Thiosemicarbazones for the covalent conjugation to biomolecules

To synthesize TSCs for applications in bioconjugation, the biological structure of bio monomers like amino acids or sugars was introduced into their backbone (Chart 19). In case of the amino acid derived TSCs, L-alanine, L-valine, L-phenylalanine, L-leucine, L-isoleucine, L-tyrosine and L-aspartic acid have been successfully introduced into the structure. The carbon acid function was protected by a *tert*-butyl ester. The protected TSCs have a low H_2O solubility but they are soluble in mixtures of DMSO/H_2O (< 1% DMSO). After deprotection of the carbon acid function, the TSCs become H_2O soluble, which is an important requirement for their bioconjugation. In addition, they are soluble in polar, organic solvents. The TSCs are stable under ambient conditions, for months or several years. However, the amino acid TSCs with anthracenyl group are sensitive to light and can decompose after several weeks. They should be stored in darkness.

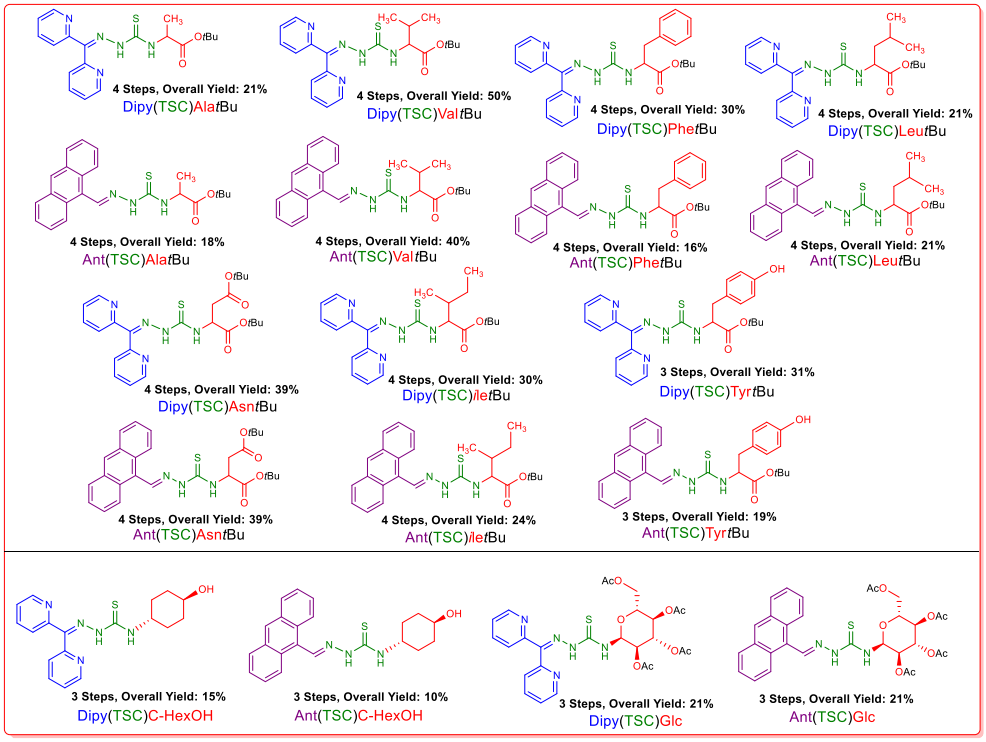


Chart 19. Overview of TSCs synthesized for applications in bioconjugation. The compounds are derived from amino acids, glucose or cyclohexanol.

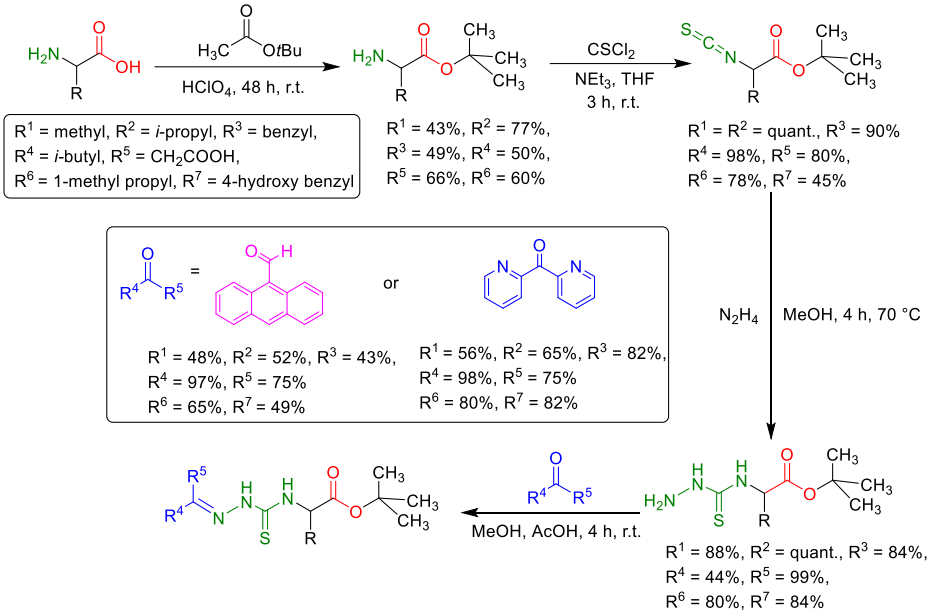
In addition to that, TSCs derived from glucose as well as cyclohexanol have been synthesized. The latter is structurally related to hexoses. Also, these compounds were soluble in H_2O or DMSO/H_2O mixtures. In addition, they are stable under ambient conditions.

3.3.1 Synthesis of TSC for bioconjugation

3.3.1.1 Synthesis of TSCs derived from amino acids

In the first step the carbon acid function of the used amino acids was protected by a *tert*-butyl ester (Scheme 49). It was found in the past that a sterically demanding ester group is necessary for this synthesis. Methyl esters have a limited stability because the thiosemicarbazides can cyclize intramolecular under cleavage of the ester group.[2] For protection, a protocol from literature is used where the amino acid is dissolved in *tert*-butyl acetate and perchloric acid is used as a catalyst.[332] This reaction usually leads to moderate yields and limits the overall yield of the TSC synthesis. In addition, this protocol was found to be unsuccessful for some of the tested amino acids like L-histidine, L-glutamic acid, L-methionine or L-tryptophane. This observation was mainly attributed to the low solubility of these amino acids in *tert*-butyl acetate. These compounds could be protected by other

methods in the future, or the stability of other ester groups could be tested to increase the substrate scope.



Scheme 49. Synthesis of TSCs derived from amino acids.

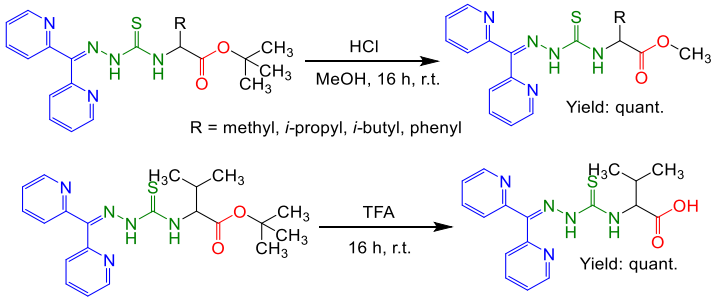
After protection of the amino acids, the synthesis of the TSCs followed the same protocol discussed before. The yields of each reaction step were high for most of the substrates, ending up with high overall yields after four reaction steps (Scheme 49). It was tested whether the chirality at the stereocenter of the amino acid remains the same during the synthesis or if racemization is observed. For this, the specific rotation of the compounds was measured (Table 16). Since the values are ≠ 0, there was no evidence of racemization.

Tabel 16. Specific optical rotation values for the TSCs derived from amino acids.[a]

	Phenyl-alanine	Alanine	Leucin	*Iso*-leucine	Valin	Aspartic acid	Tyrosine
Conc. [g/100cm³]	0.1160	0.1170	0.1000	0.1045	0.1040	0.1150	0.1045
$[\alpha]_{546}^{20}$	+35.6	–	+5.0	+23.9	+29.3	–9.7	+20.1
$[\alpha]_{579}^{20}$	+30.5	+15.1	+5.0	+22.6	+29.5	–7.5	+18.5
$[\alpha]_{589}^{20}$	+29.3	+13.4	+4.7	+22.0	+25.3	–6.4	+18.8

[a] Measured at 20 °C in $CHCl_3$ at λ = 546, 579 or 589 nm. Accuracy: ±0.1.

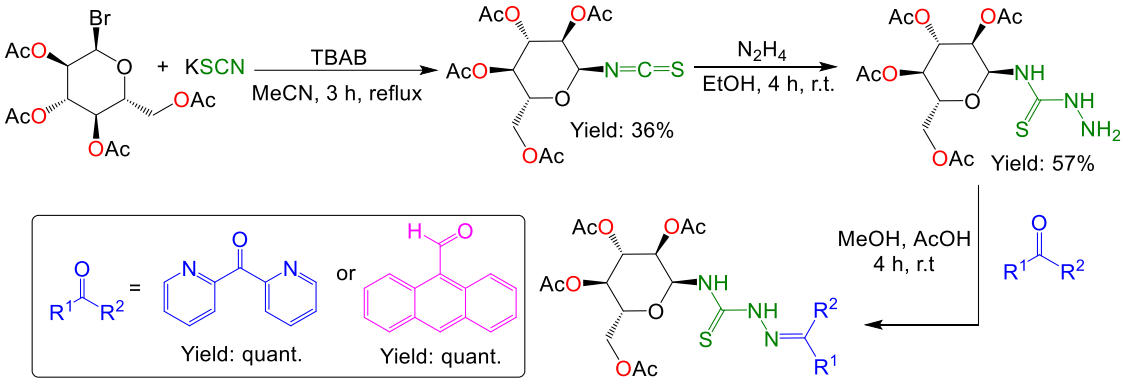
Deprotection of the TSCs was tested at some selected examples. In pure, conc. HCl the decomposition of the TSCs was observed. By that reason, deprotection was tested in in diluted, methanolic solutions of HCl. However, these conditions led to a selective transesterification of the *tert*-butyl esters to the methyl esters. In the end, deprotection was successful in pure TFA, in quantitative yields (Scheme 50).



Scheme 50. Top: Transesterification of the *tert*-butyl esters to methyl esters. Bottom: Deprotection of TSCs derived from amino acids using TFA.

3.3.1.2 Synthesis of TSCs derived sugars or analogues

The synthesis of TSCs derived from glucose was started from 2,3,4,6-tetra-O-acetyl-α-D-glucopyranosyl bromide. The bromide function was substituted with KSCN using a protocol from literature, yielding the isothiocyanate in 36%.[333-335] After that, the thiosemicarbazide (Yield: 57%) and the corresponding TSCs (Yield: quant.) have been synthesized (Scheme 51).



Scheme 51. Synthesis of TSCs derived from 2,3,4,6-tetra-O-acetyl-α-D-glucopyranosyl bromide.

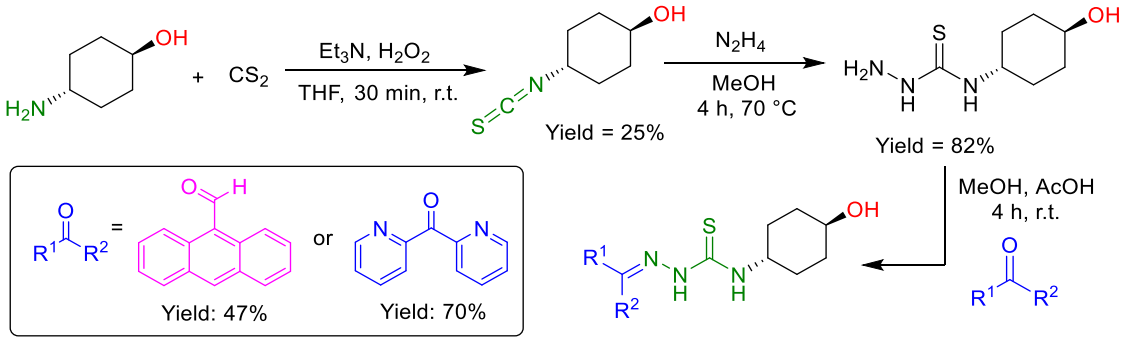
The specific rotation of Dipy(TSC)Glc was measured, which showed no evidence of racemization, indicating that the stereocenters were retained during the synthesis (Table 17).

Tabel 17. Specific optical rotation values for Dipy(TSC)Glc.[a]

Conc. [g/100cm³]	$[\alpha]_{546}^{20}$	$[\alpha]_{579}^{20}$	$[\alpha]_{589}^{20}$
0.1165	+95.3	+77.0	+74.7

[a] Measured at 20 °C in $CHCl_3$ at λ = 546, 579 or 589 nm. Accuracy: ±0.1.

The synthesis of TSCs with cyclohexanol group was started from 4-aminocyclohexanol. The synthesis of the isothiocyanate was done by a protocol from literature, using CS_2 (Scheme 52).[336] A low yield of 25% was obtained for this step, which can be attributed to side reactions with the OH group. Synthesis of the thiosemicarbazide was possible in 82% yield. The TSCs were obtained in moderate to high yields of 47 to 70%.



Scheme 52. Synthesis of TSCs derived from 4-aminocyclohexanol.

3.3.2 UV/Vis absorption and photoluminescence spectroscopy

The results of the UV/Vis absorption spectroscopy of the anthracenyl and dipyridyl TSCs are similar to that from Chapter 3.1.2. The absorption spectra are summarized in Figure 56 and the maxima are summarized in Table 18.

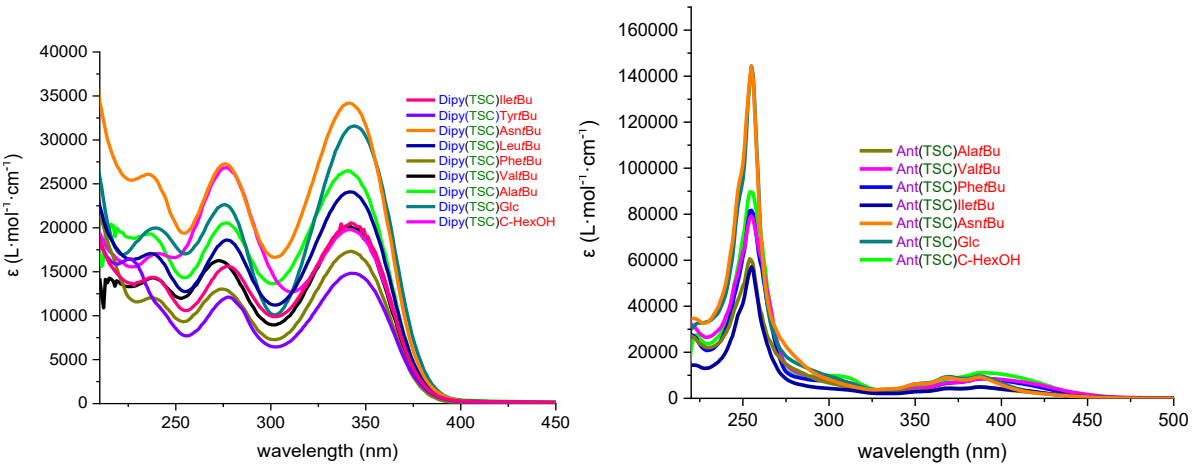


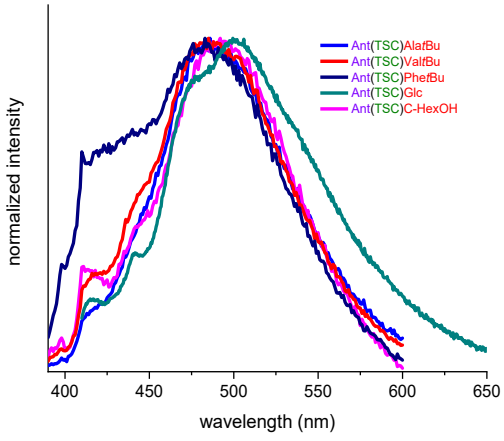
Figure 56. UV/Vis absorption spectra of dipyridyl and anthracenyl functionalized TSCs derived from amino acids, glucose and cyclohexanol in MeCN.

Table 18. UV/Vis absorption maxima of dipyridyl and anthracenyl functionalized TSCs.[a]

Compound	λ_1 [nm], ε [L·mol^{-1}·cm^{-1}]	λ_2 [nm], ε [L·mol^{-1}·cm^{-1}]	λ_3 [nm], ε [L·mol^{-1}·cm^{-1}]
Dipy(TSC)Ile*t*Bu	238, 14380	278, 15660	340, 26470
Dipy(TSC)Tyr*t*Bu	226, 16470	278, 12120	343, 14810
Dipy(TSC)Asn*t*Bu	235, 26100	276, 27290	341, 34180
Dipy(TSC)Leu*t*Bu	237, 17080	277, 18610	342, 24070
Dipy(TSC)Phe*t*Bu	238, 11900	278, 12120	342, 14810
Dipy(TSC)Val*t*Bu	238, 14380	272, 16280	342, 20120
Dipy(TSC)Ala*t*Bu	236, 19290	276, 20530	340, 26470
Dipy(TSC)Glc	239, 19970	275, 22610	344, 31590
Dipy(TSC)C-HexOH	240, 16990	276, 26720	342, 19780
Ant(TSC)Ala*t*Bu	254, 57160	-	385, 4900
Ant(TSC)Val*t*Bu	255, 8200	-	395, 8080
Ant(TSC)Phe*t*Bu	254, 57160	-	385, 4900
Ant(TSC)Ile*t*Bu	255, 80200	-	395, 8080
Ant(TSC)Asn*t*Bu	255, 144280	-	369, 9000
Ant(TSC)Glc	255, 144280	-	369, 9000
Ant(TSC)C-HexOH	254, 89740	305, 9700	390, 11100

[a] TSCs derived from amino acids, glucose and cyclohexanol in MeCN. Measured in MeCN.

Also, the emission spectra show the expected shape, like the results discussed before (Figure 57 and Table 19).



Compound	λ_1 [nm]	λ_2 [nm]	λ_3 [nm]
Ant(TSC)Ala*t*Bu	414 (s)	-	486
Ant(TSC)Val*t*Bu	414 (s)	443 (s)	485
Ant(TSC)Phe*t*Bu	411 (s)	-	484
Ant(TSC)Glc	415 (s)	441 (s)	501
Ant(TSC)C-HexOH	410 (s)	445 (s)	490

Figure 57. Normalized emission spectra of Ant(TSC)Ala*t*Bu, Ant(TSC)Val*t*Bu, Ant(TSC)Phe*t*Bu, Ant(TSC)Glc and Ant(TSC)C-HexOH in MeCN upon irradiation at 365 nm. **Table 19.** Summary of the corresponding emission maxima.

3.3.3 Cytotoxicity studies of glucose and cyclohexanol derived TSCs

The cytotoxicity of Dipy(TSC)C-HexOH and Dipy(TSC)Glc was analyzed by MTT assays. The experiments were performed in a similar way described in Chapter 3.1.3 and are shown in Table 20.

Table 20. % Inhibition of the tested TSCs at a concentration of 50 µM.[a]

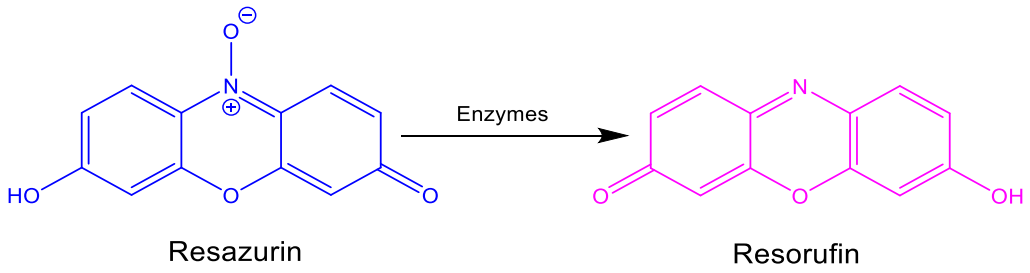
Compounds	HepG2	HCT-116	HEK-293
	% Inhibition at 50 µM±SD		
Dipy(TSC)C-HexOH	53.62 ± 1.62	57.70 ± 3.90	83.06 ± 1.50
Dipy(TSC)Glc	49.81 ± 2.20	22.64 ± 0.37	69.85 ± 1.60
Cisplatin	67.32 ± 2.12	75.32 ± 1.24	97.33 ± 2.31

[a] Values were determined in an MTT assay.

Compared to the results from Chapter 3.1.3, the % inhibition of HepG2, HCT-116 and HEK-293 by Dipy(TSC)C-HexOH and Dipy(TSC)Glc was smaller. In addition, the healthy HEK-293 cells are more affected by the TSCs compared to the cancer cell lines.

3.3.4 Cytotoxicity studies of amino acid derived TSCs

The cytotoxicity of the *tert*-butyl esters of the amino acid derived TSCs was analyzed by a resazurin assay, where the blue resazurin is reduced to pink resorufin by enzymes. In this way, the color change can be analyzed by UV/Vis absorption spectroscopy and corelated to the enzyme activity which is in turn related to the cell viability (Scheme 53).[222]



Scheme 53. Principle of the resazurin assay.

The experiments were performed with HT-29, which is a human colon cancer cell line and HFF1, which are fibroblasts. The latter acts as a control, to analyze the toxicity against healthy cells for comparison. The TSCs were dissolved in DMSO as a stock solution, which was diluted with the medium to a concentration of 1% DMSO. The concentration of the TSC was 100, 50, 25 and 10 µM respectively. As a negative control, the cells were incubated with the medium and 1% DMSO. As a positive control, the cells were incubated with 70% EtOH. The incubation time was 24 h.

The TSCs showed no significant toxicity after 24 h incubation against the tested cell lines (Figure 58). In case of HT-29, the cell viability was 80-95% even at high concentrations of the TSCs (100 µM). For HFF1, the toxicity was also low but at least slightly increased compared to the cancer cells. At the highest concentration, the cell viability was 58-60% for the most toxic TSCs, namely Dipy(TSC)Ala*t*Bu, Dipy(TSC)Val*t*Bu and Dipy(TSC)Leu*t*Bu. The results were quite surprising, because it was expected that the amino acid function will improve the biocompatibility, while the dipyridyl ketone motif should lead to a high toxicity.

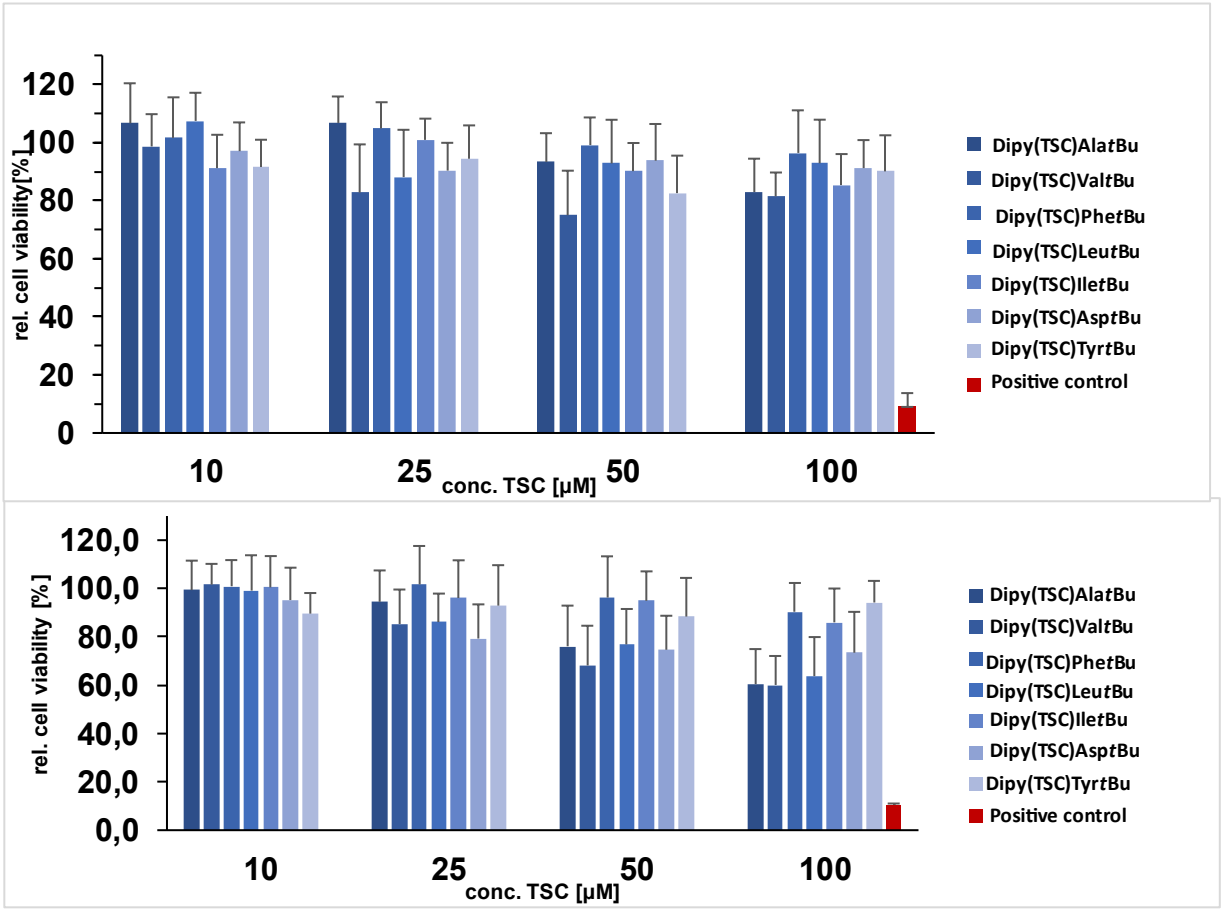


Figure 58. Top: Relative cell viability of HT-29 after 24 h. Bottom: Relative cell viability of HFF-1 after 24 h.

For comparison, the methyl esters of the alanine, valine, phenylalanine and leucine derived TSCs were tested to check if the cytotoxicity changes. However, the results were quite similar (Figure 59).

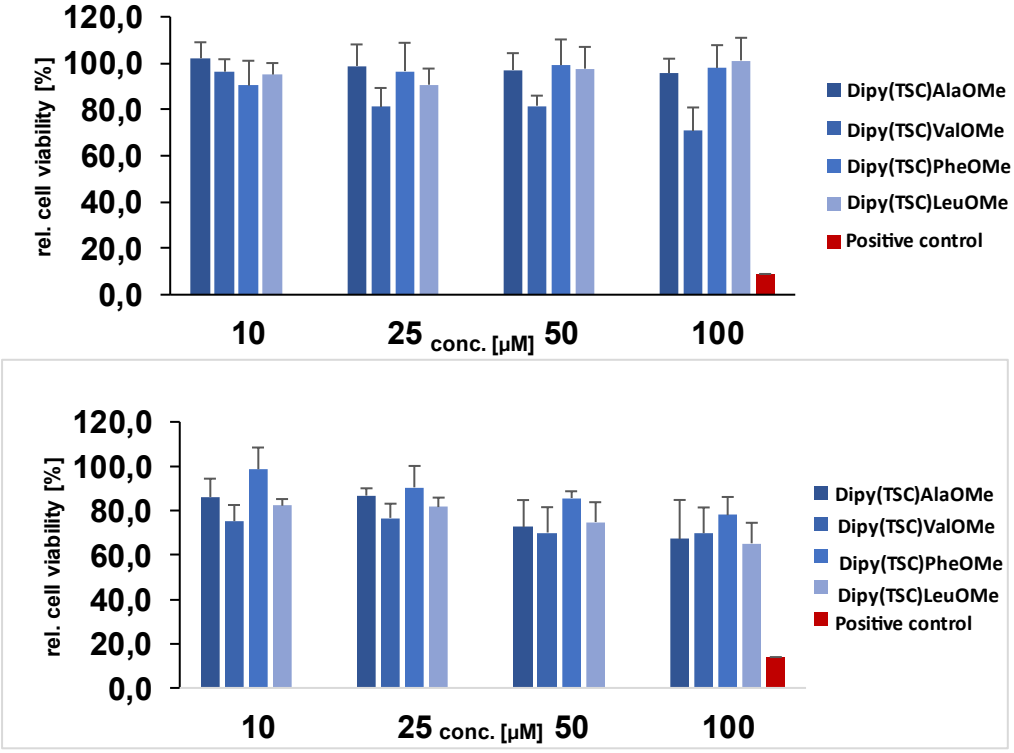


Figure 59. Top: Relative cell viability of HT-29 after 24 h. Bottom: Relative cell viability of HFF-1 after 24 h.

In the next step, the incubation time was increased, and the relative cell viability was determined after 48 h and 96 h. The experiments were performed with the *tert*-butyl esters of the TSCs and clearly showed a time-dependency of the cytotoxicity. After 48 h, the relative cell viability of HT-29 was 30-40% at low concentrations of the TSCs (10 µM). Interestingly, an increasing concentration did not increase the cytotoxicity (Figure 60).

The cytotoxicity against HFF-1 was lower than for HT-29. At low concentrations (10 µM), the relative cell viability was 70-80%. The highest toxicity was found for Dipy(TSC)Ile (57% relative cell viability at 10 µM). In this way, the time-dependency of the cytotoxicity is less pronounced for the healthy cells. Again, an increasing TSC concentration did not significantly increase cytotoxicity.

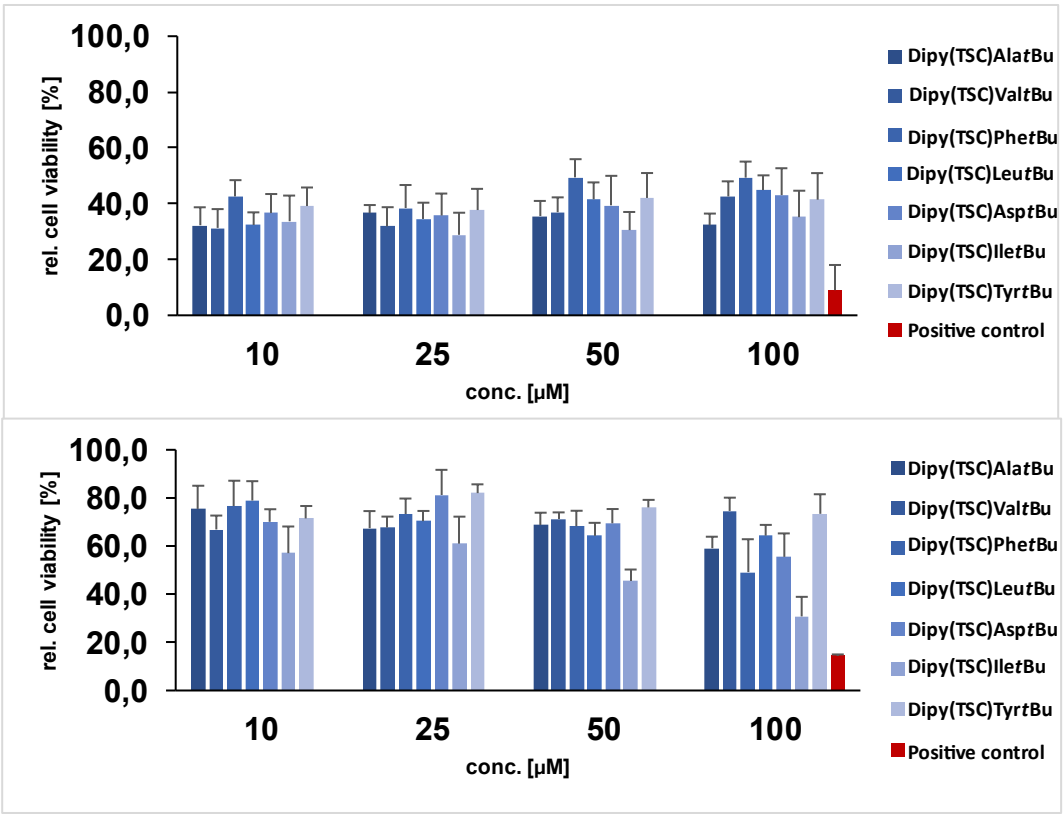


Figure 60. Top: Relative cell viability of HT-29 after 48 h. Bottom: Relative cell viability of HFF-1 after 48 h.

The effects were also found after 96 h of incubation (Figure 61 and 62). In case of HT-29, the relative cell viability was around 10% for the tested TSCs. Again, the concentration did not affect the cytotoxicity.

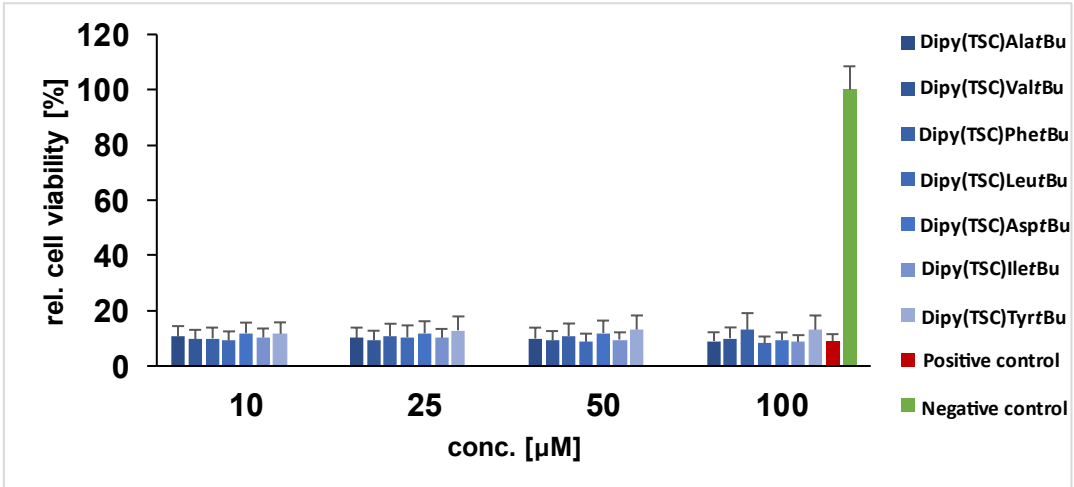


Figure 61. Relative cell viability of HT-29 after 96 h.

HFF-1 was less affected and showed a relative cell viability of 30% for most of the TSCs. After 48 h, the relative cell viability of HT-29 was decreased by a factor of 2, compared to HFF1. After 96 h, the cell viability was three times lower for HT-29. However, after 96 h, the healthy cells are also significantly damaged. Anyway, the results indicate that there might be a therapeutic window, at which the cancer cells are more damaged than the healthy cells.

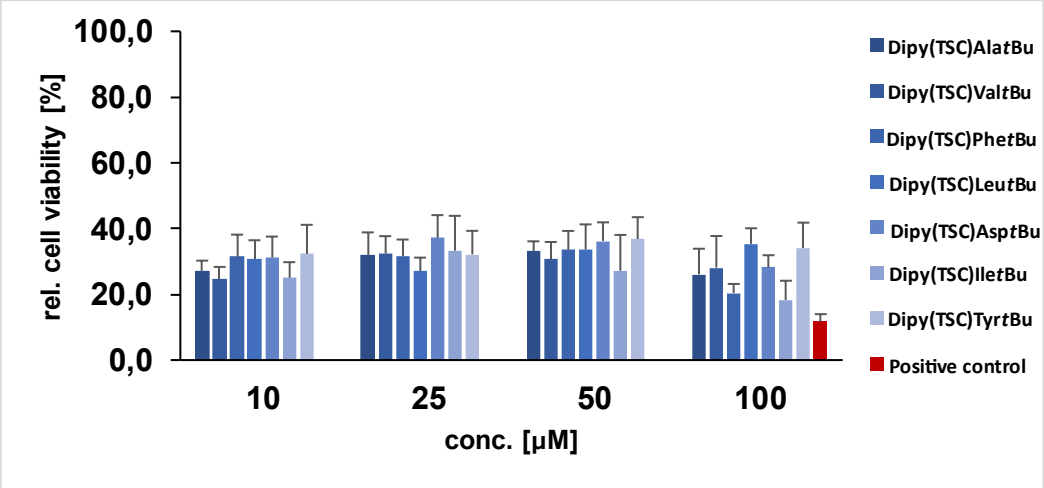


Figure 62. Relative cell viability of HFF1 after 96 h.

In the next step, the cytotoxicity of Dipy(TSC)Val*t*Bu was investigated at lower concentration (0.025 µM, 0.05 µM, 0.1 µM, 0.25 µM, 0.5 µM, 1 µM, 2.5 µM, 5 µM and 10 µM) and compared to Dp44mT as an example of a highly toxic TSC from literature. After 24 h of incubation, HT-29 was not significantly affected by both TSCs (Figure 63). The HFF1 cell were slightly more affected by Dp44mT compared to Dipy(TSC)Val*t*Bu. However, the relative cell viability was still 74% at a concentration of 10 µM of Dp44mT.

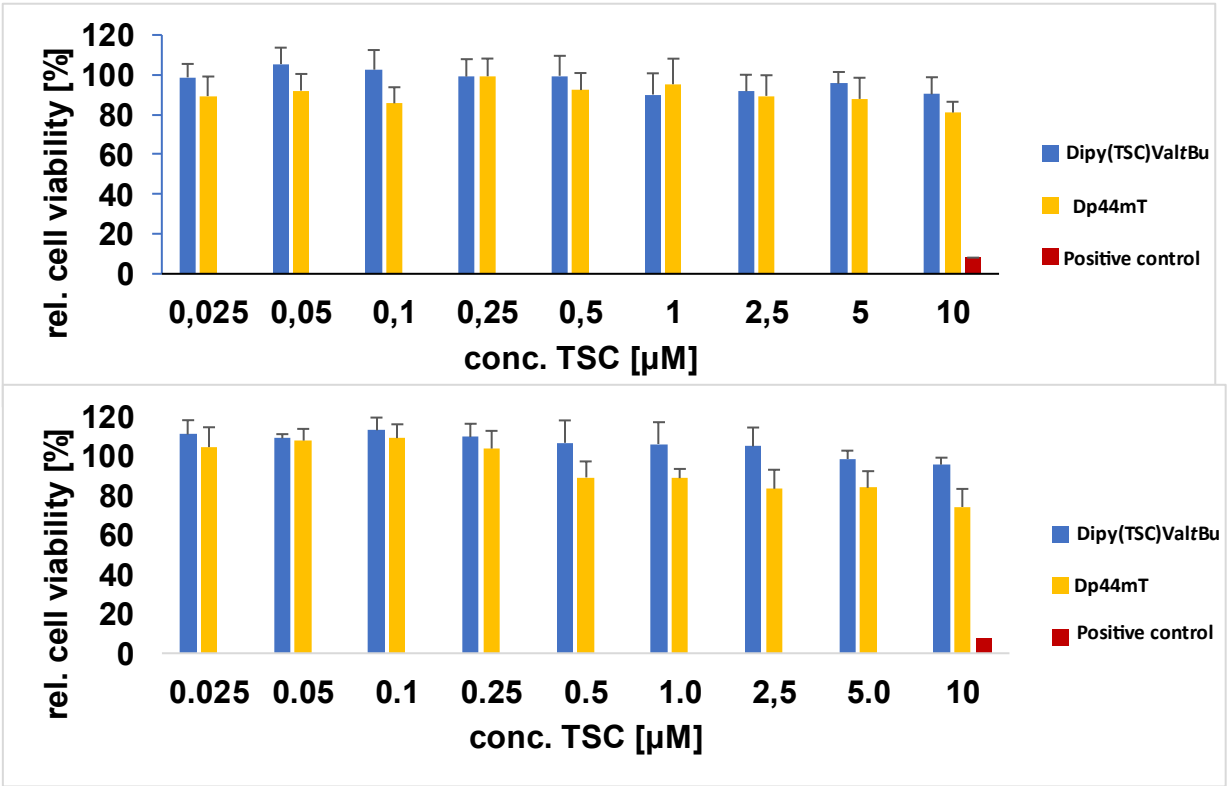


Figure 63. Top: Relative cell viability of HT-29 after 24 h. Bottom: Relative cell viability of HFF-1 after 24 h.

After 48 h of incubation, the toxicity again significantly increased (Figure 64). In this way, Dp44mT shows a similar time dependency of its cytotoxicity as observed for the amino acid derived TSCs. This time-dependency might originate from the double-punch mechanism of TSCs since it probably takes some time until the TSC has entered the cells and starts to bind intracellular iron to form ROS.[38] The toxicity of Dp44mT is significantly higher compared to Dipy(TSC)Val*t*Bu. The IC_{50} value against HT-29 is approximately 0.025 µM for Dp44mT and 5 µM for Dipy(TSC)Val*t*Bu. At an increasing concentration, the toxicity is increasing for both TSCs but the increment is higher for Dipy(TSC)Val*t*Bu. This leads to the fact that their toxicity at high concentrations is quite similar.

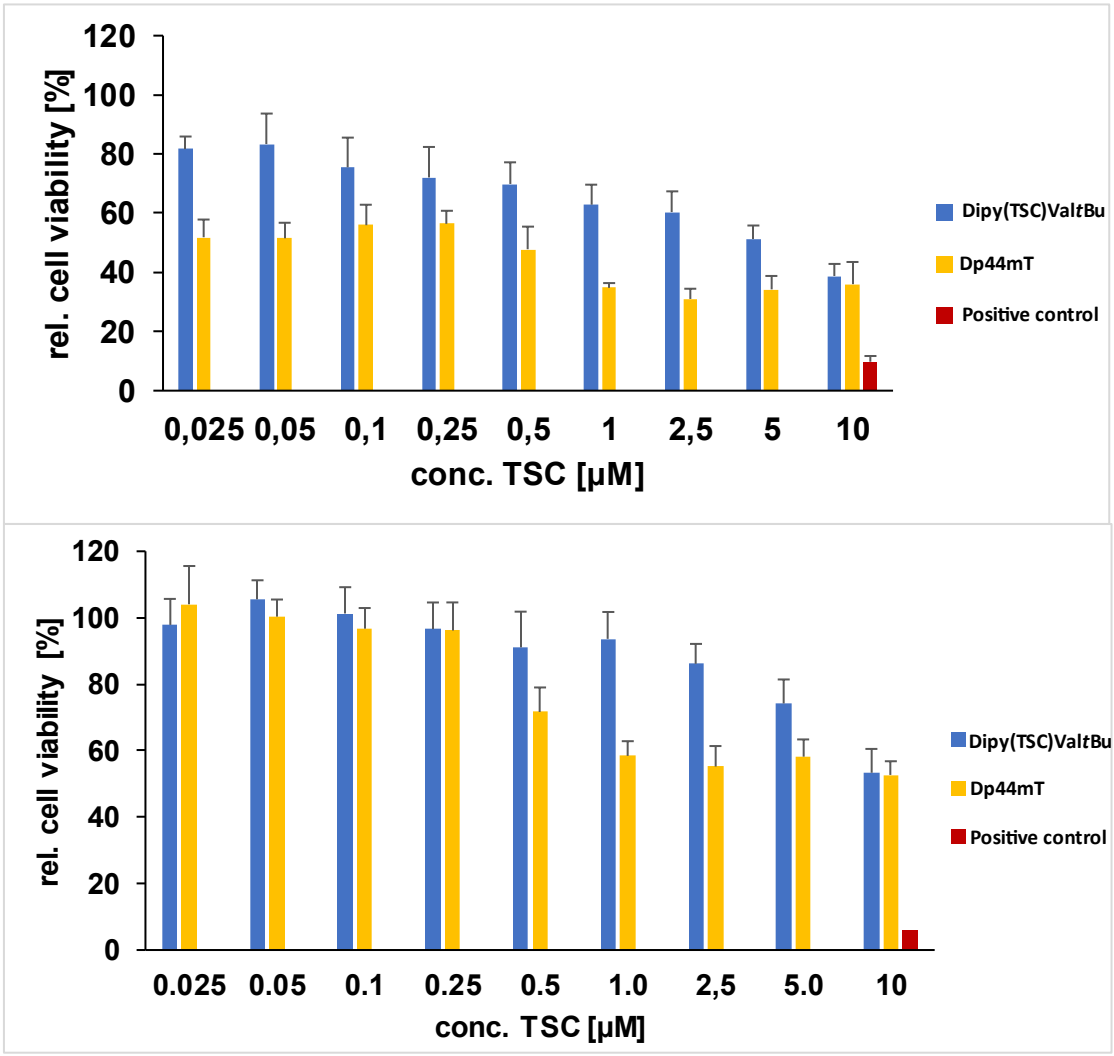


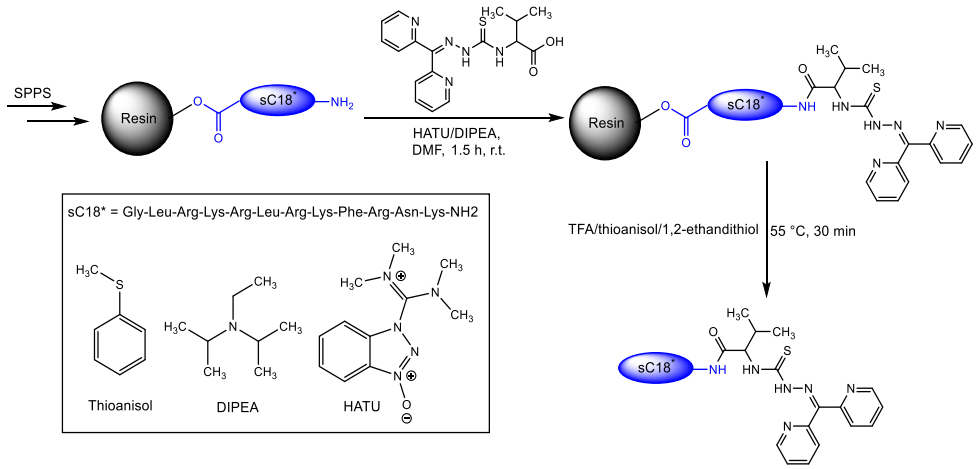
Figure 64. Top: Relative cell viability of HT-29 after 48 h. Bottom: Relative cell viability of HFF-1 after 48 h.

The toxicity against HFF1 is smaller but also increases with increasing concentration. For small concentrations of Dp44mT (0.025 to 0.25 µM) the cells are almost not affected. In this way, the TSC shows a selectivity to the cancer cells. For Dipy(TSC)Val*t*Bu, this selectivity is less pronounced.

3.3.5 Conjugation of Dipy(TSC)Val to sC18*

In the next step it was tried to attach Dipy(TSC)Val to the cell penetrating peptide sC18*. The peptide sC18* is a shorter version of sC18 (the last four amino acids are missing), which was used for TSC coupling experiments in the past.[222,337] It consists of the amino acid sequency [Gly-Leu-Arg-Lys-Arg-Leu-Arg-Lys-Phe-Arg-Asn-Lys-NH_2] and was synthesized by a solid-phase peptide synthesis (SPPS). It was tried to couple the TSC terminally to the peptide, which was bound on a resin. Hexafluorophosphate azabenzotriazole tetramethyl uronium (HATU) and *N*,*N*-diisopropylethylamine (DIPEA) have been used as coupling reagents (HATU/DIPEA/TSC, 2.00 eq. respectively, 1.5 h, r.t.)

(Scheme 54). The product was cleaved from the resin by a mixture of TFA, thioanisol and 1,2-ethandithiol (90:7:3) at 55 °C for 30 min, which also leads to the cleavage of the protective groups at the peptide. Thioanisol and 1,2-ethandithiol are used as a scavenger in this reaction, to protect the cleaved amino acids from side reactions.



Scheme 54. Synthesis of the Dipy(TSC)Val-sC18* conjugate.

HPLC-ESI-MS measurements (High-performance liquid chromatography electrospray ionization mass spectrometry) have been used to verify the experiments (Figure 65).

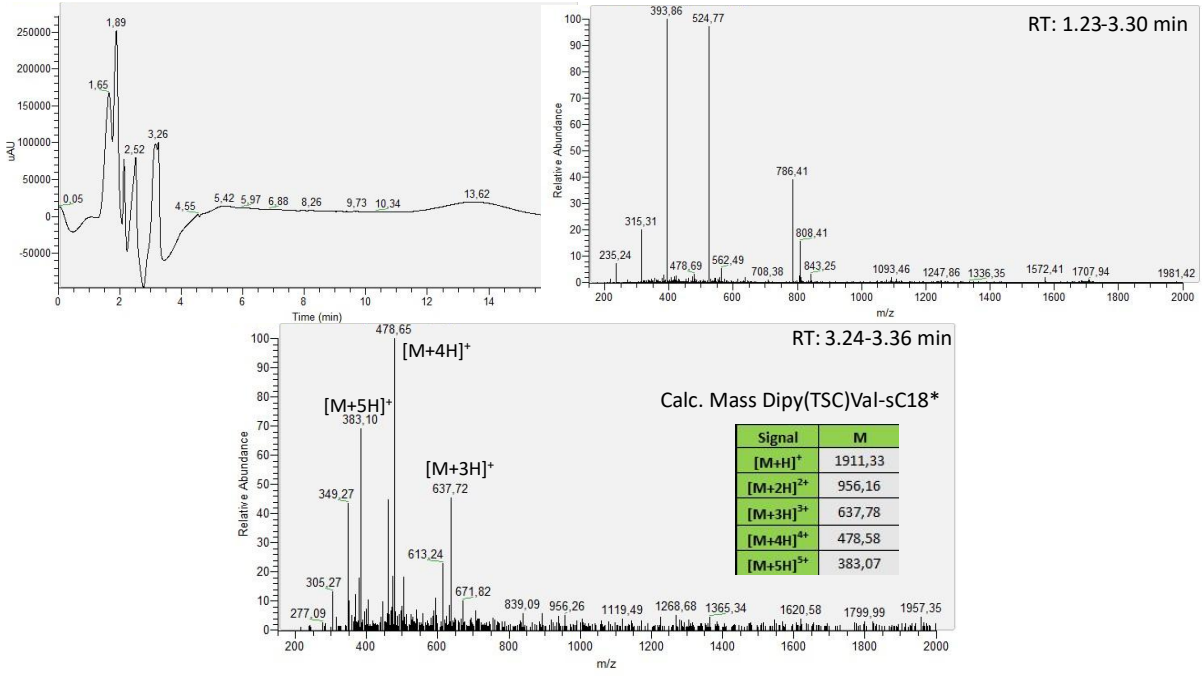


Figure 65. HPLC analysis and ESI-MS measurements for different retention time.

The results are indicating the successful formation of the conjugate, since different protonated species of Dipy(TSC)Val-sC18* ([M+3H]+, [M+4H]+ and [M+5H+]) are detected in the mass spectrum. However, it seems that side products are formed, and the yield of the conjugate is poor. Currently, the purification of the conjugate as well as the optimization of the coupling conditions are studied in more detail to get enough material for investigating the biological properties of the conjugate in detail.

3.3.6 Summary – TSCs for bioconjugation

TSCs derived from different amino acids as well as glucose and cyclohexanol have been successfully synthesized. Their photophysical properties are similar to other *N*4 functionalized TSCs from Chapter 3.1.2, which was confirmed by UV/Vis absorption and emission spectroscopy. The cytotoxicity of Dipy(TSC)Glc and Dipy(TSC)C-HexOH against HepG2 and HCT-116 was low, compared to other results from Chapter 3.1.3 and were below expectation. However, the amino acid derived TSCs showed a high toxicity against HT-29 cells. An interesting aspect of these compounds was the time dependency of this toxicity, which increased after 48 h. In addition, the cancer cells were more affected by the TSCs compared to the healthy HFF-1 cells. To investigate an example of bioconjugation, Dipy(TSC)Val was deprotected and successfully conjugated to the cell penetrating peptide sC18*. However, the obtained yields seem to be poor, and further optimization is currently in progress.

3.4 Fluorophore-tagged thiosemicarbazones and their Pt(II) complexes

During this research, it was attempted to introduce several fluorophores at the *N*4 position of TSCs, namely anthracene, fluorene, pyrene, carbazole, coumarin, tetraphenyl porphyrin, fluorescein and naphthalimide. In addition, the aim was to synthesize their Pt(II) complexes. Chart 20 shows a summary of all the successfully synthesized TSC complexes. The compounds are stable under ambient conditions and soluble in organic solvents like DMSO, DMF, MeCN or THF. The coumarin derivative has the poorest solubility of all these compounds. The metal complexes as well as the corresponding ligands are not soluble in H_2O. However, it is possible to dissolve them in mixtures of DMSO or DMF/H_2O (< 1% DMSO).

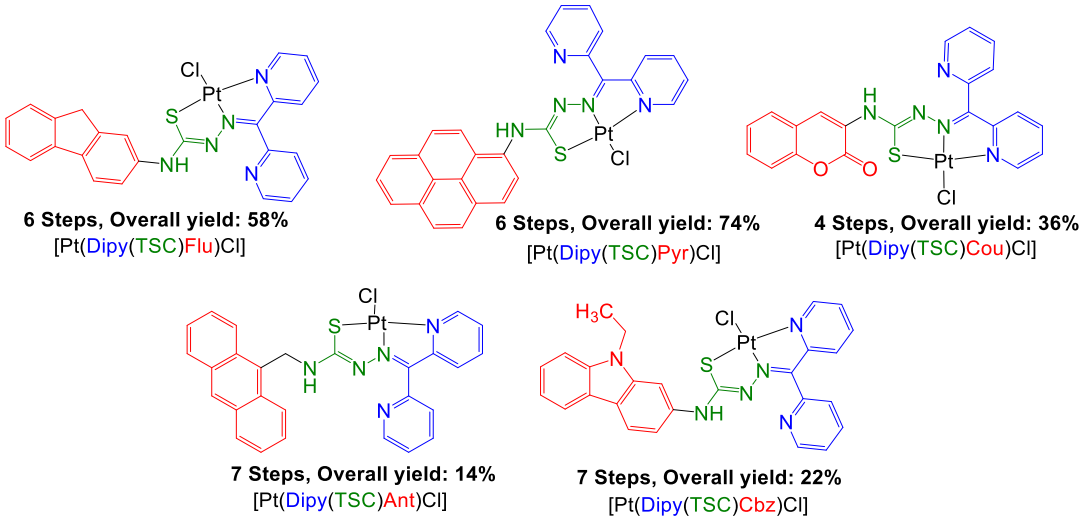
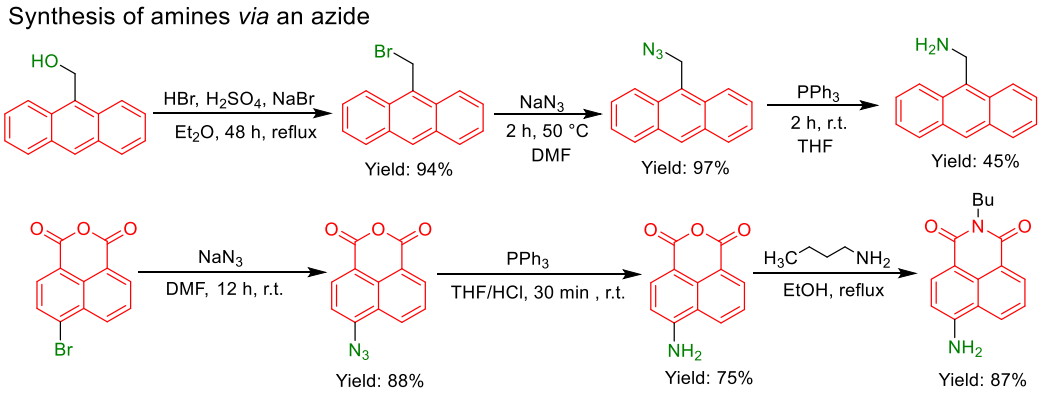


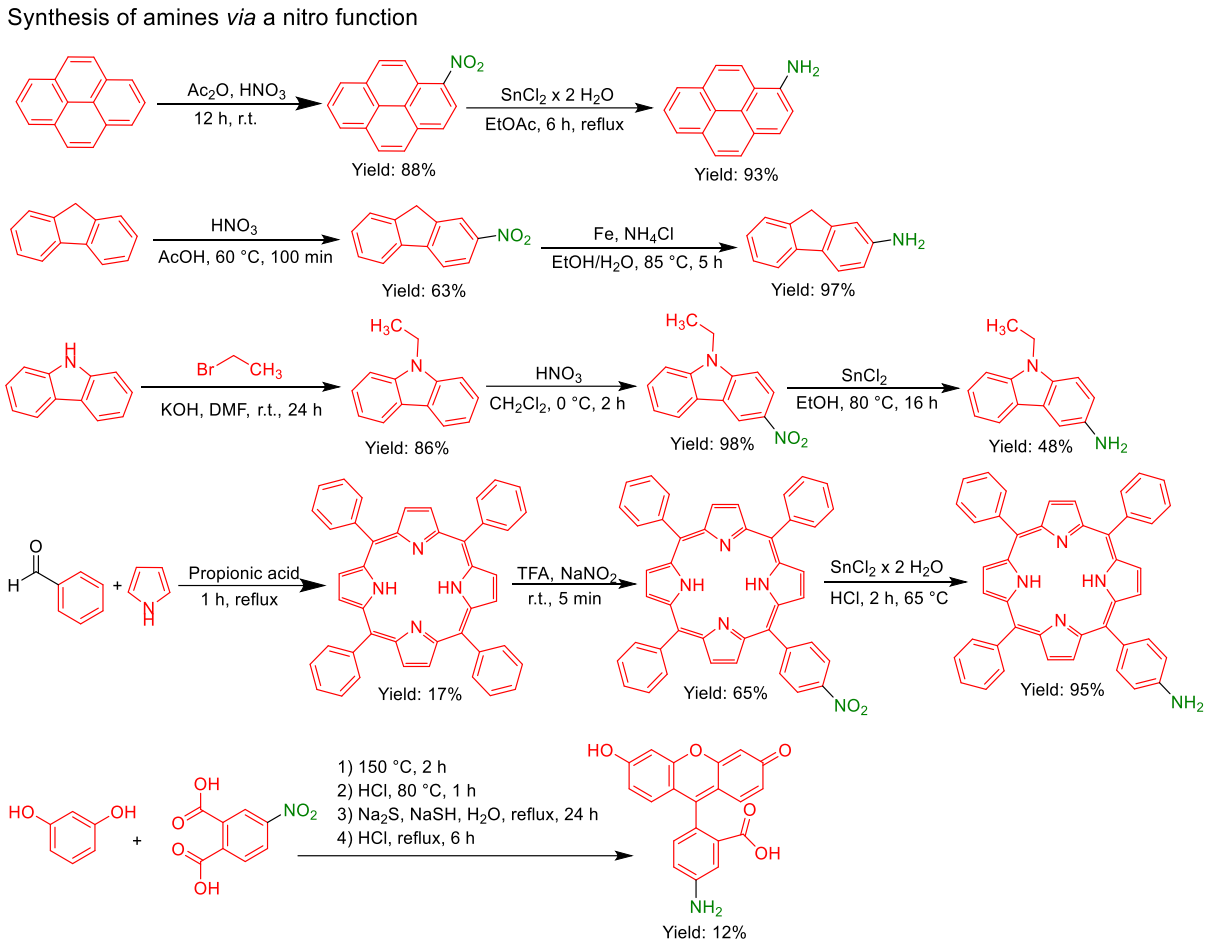
Chart 20. Overview of the successfully synthesized TSC Pt(II) complexes with fluorophores at the *N*4 position.

3.4.1 Synthesis of fluorophore-tagged TSCs and their Pt(II) complexes

The synthesis of the TSCs starts from the corresponding amino derivative of the fluorophore. These are commercially available or can be synthesized by literature known approaches.[338-343] Scheme 55 summarizes the synthesis of the amino fluorophores used in this research.

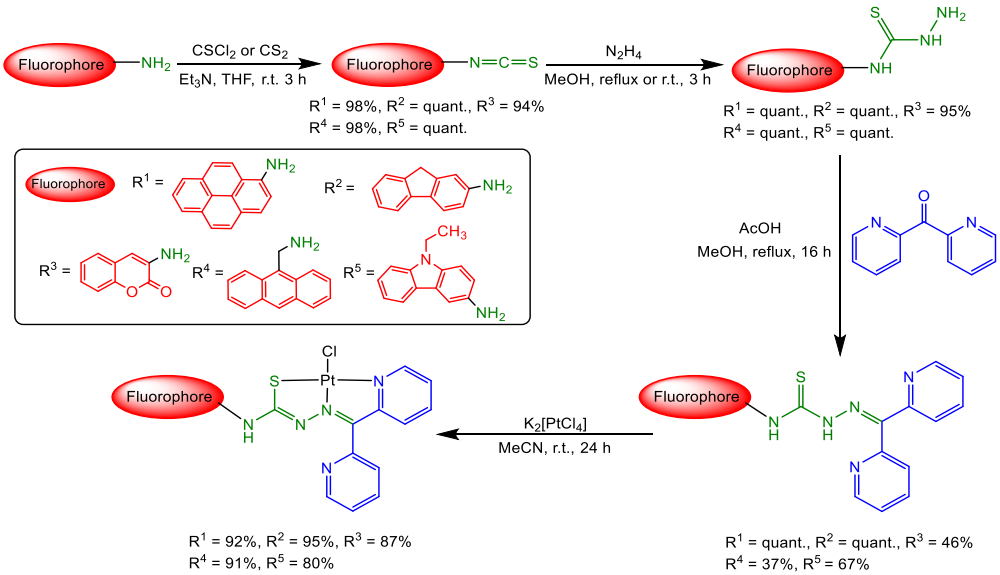
Two different general approaches have been used. The first one starts with the bromide derivative of the fluorophore, which is substituted by an azide, followed by its reduction to the amine. The second approach starts with nitro derivatives, or the nitro group is introduced by aromatic nitration. After that, the nitro group is reduced to the amine. These reactions usually led to high yields (Scheme 55).





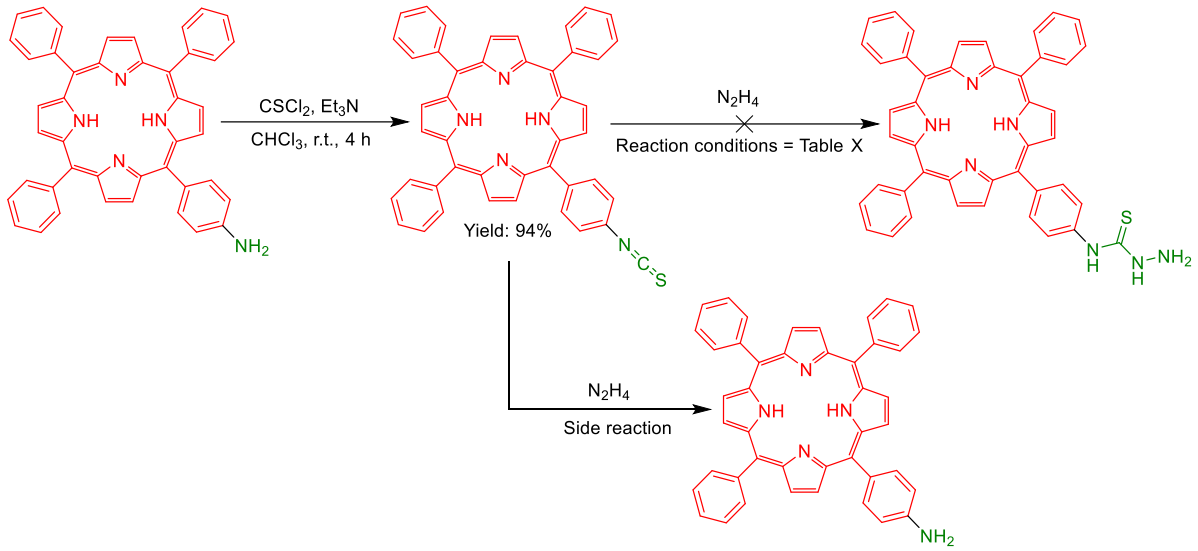
Scheme 55. Overview of the synthesis of fluorophores with amine function, which can be used as precursors for the synthesis of TSCs.

With the amino derivatives at hand, the TSCs have been synthesized in excellent yields by similar approaches discussed before (Scheme 56). In this way, anthracene, fluorene, pyrene, carbazole and coumarin have been successfully introduced at the *N*4 position of the TSC. For the synthesis of the corresponding Pt(II) complexes, the ligands were mixed with $K_2[PtCl_4]$ in MeCN at room temperature. The TSC Pt(II) complexes were obtained in high yields.



Scheme 56. Synthesis of TSC Pt(II) complexes with fluorophores at the *N*4 position.

The synthesis of TSCs derived from 5-(4-aminophenyl)10,15,20-triphenylporphine, 5-amino fluorescein and 4-amino-*N*-butyl-1,8-naphthalimide was not successful. In case of the tetraphenyl porphyrin, the synthesis of the isothiocyanate was successful (Yield: 94%), while the synthesis of the thiosemicarbazide failed (Scheme 57).



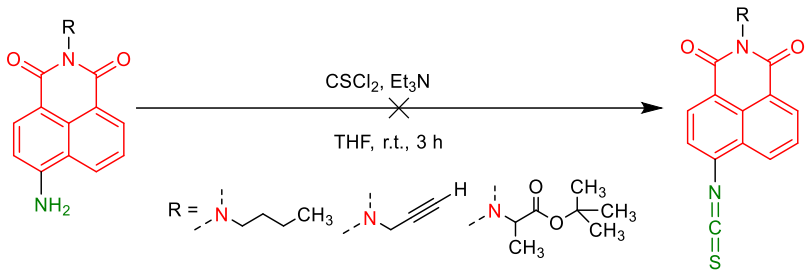
Scheme 57. Synthetic attempt to synthesize TSCs with tetraphenyl porphyrin function at the *N*4 position. The synthesis of the corresponding thiosemicarbazide failed. The formation of 5-(4-aminophenyl)10,15,20-triphenylporphine was observed during the synthesis as a side reaction.

Different reaction conditions have been tested, which are summarized in Table 21. The best solvent mixture was DCM/MeOH since it dissolves the porphyrin as well as the hydrazine hydrate. However, the formation of the thiosemicarbazide was not successful for all the tested approaches. Instead, decomposition was observed. One of the side products was found to be 5-(4-aminophenyl)10,15,20-triphenylporphine, which was confirmed by ^{1}H NMR spectroscopy and HI ESI-MS (High-resolution electrospray ionization mass spectrometry). However, the mechanism of this side reaction is unclear. Decomposition was also observed under inert reaction conditions and cooling to –78 °C.

Table 21. Tested reaction conditions for the synthesis of the porphyrin thiosemicarbazide.

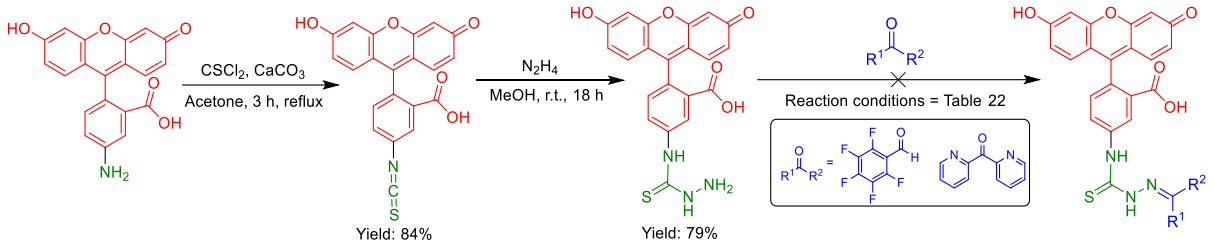
Solvent	Inert conditions	Temperature	Time [h]	Outcome
THF	No	r.t.	2	Educt
MeOH/THF	No	r.t.	2	Decomposition
MeOH/DCM	No	reflux	3	Decomposition
MeOH/DCM	Yes	r.t.	5	Decomposition
MeOH/DCM	Yes	–78 °C	5	Decomposition

Also, the synthesis of TSCs derived from 4-amino-*N*-butyl-1,8-naphthalimide failed because the synthesis of the corresponding isothiocyanate was not successful. Addition of thiophosgene led to the decomposition of the naphthalimide group. However, also starting material was reisolated, which indicates a poor nucleophilicity of the amine function, due to the electron withdrawing character of the naphthalimide. In this way, side reactions seem to be faster than the reaction of thiophosgene with the amine group. Changing substituents at the imide function, had no impact on the reaction outcome and was also unsuccessful (Scheme 58).



Scheme 58. Synthetic attempt to synthesize the isothiocyanate of different *N*-substituted amino naphthalimides.

The synthesis of fluoresceine thiosemicarbazide was successful (Scheme 59). This compound, as well as the isothiocyanate, has been already described in literature as a fluorescence marker.[344,345] However, it was found that the thiosemicarbazide is sensitive and decomposes quickly. Also, the exclusion of light did not prevent decomposition.



Scheme 59. Synthetic attempt to synthesize TSCs derived from 5-amino fluorescein.

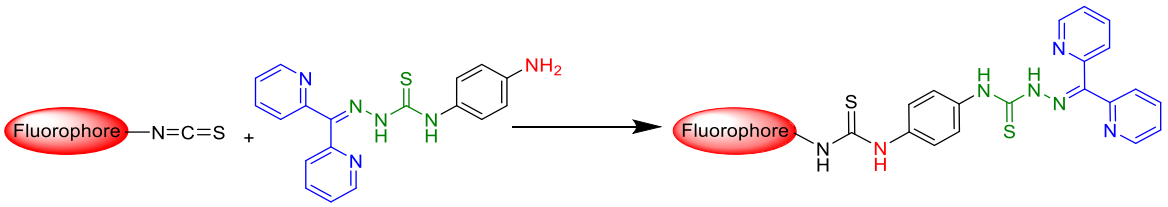
The synthesis of the corresponding TSC with di(2-pyridyl)ketone was not successful, whereby different conditions have been tested (Table 22). Especially, for harsher reaction conditions, the compound decomposes. Instead of di(2-pyridyl)ketone also pentafluoro benzaldehyde was used as a substrate, which is more electrophile and should rapidly react with the thiosemicarbazide. However, this approach was also not successful.

Table 22. Tested reaction conditions for the synthesis of TSCs with fluorescein at the *N*4 position.[a]

Ketone/Aldehyde	Catalyst	Temperature	Time [h]	Outcome
Di(2-pyridyl)ketone	AcOH	reflux	8	Decomposition
Di(2-pyridyl)ketone	AcOH	sonication, 50 °C	5	Decomposition
Di(2-pyridyl)ketone	HCl	reflux	7	Decomposition
Pentafluorobenzaldehyde	AcOH	sonication, 50 °C	5	Decomposition

[a] Reaction were performed in MeOH.

The synthesis of TSCs with tetraphenyl porphyrin, fluorescein and naphthalimide group could be repeated in the future using a different approach. Since the synthesis of tetraphenyl porphyrin and fluorescein with isothiocyanate function was successful, they could be conjugated to TSC with primary amine groups from Chapter 3.1.1.1 (Scheme 60).



Scheme 60. Alternative approach for the synthesis of TSCs with tetraphenyl porphyrin and fluorescein group at the *N*4 position. The corresponding isothiocyanates of the fluorophore are conjugated to Dipy(TSC)PhNH2 under the formation of a thiourea.

3.4.2 UV/Vis absorption and photoluminescnce spectroscopy of the tagged TSCs and their Pt(II) complexes

UV/Vis absorption and emission spectroscopy of the TSCs and their corresponding Pt(II) complexes have been measured in MeCN and are shown in Figures 66-70. Their maxima are summarized in Table 23 and 24.

Dipy(TSC)Cou shows an intense maximum at 239 nm as well as two additional maxima at 285 and 350 nm (Figure 66, left). Interestingly, the typical absorption maxima of the chromophore are not dominant in the absorption spectra of the TSC, which shows a comparison with the corresponding coumarin thiosemicarbazide. Instead, the spectrum shows more characteristics of Dipy(TSC)H_2, which is shown for comparison (Figure 66). The absorption maxima of Dipy(TSC)Cou are bathochromic shifted compared to Dipy(TSC)H_2. In addition, the maxima are hyperchromic shifted, especially for the absorption maximum at 239 nm. Complexation of Pt(II) leads to the disappearance of the absorption maximum at 350 nm, which is typically observed for dipyridyl ketone TSCs after metal complexation or deprotonation at the hydrazone.[302] An additional maximum appears for the Pt(II) complex at 420 nm, which is probably attributed to a metal to ligand charge transfer (MLCT).[222]

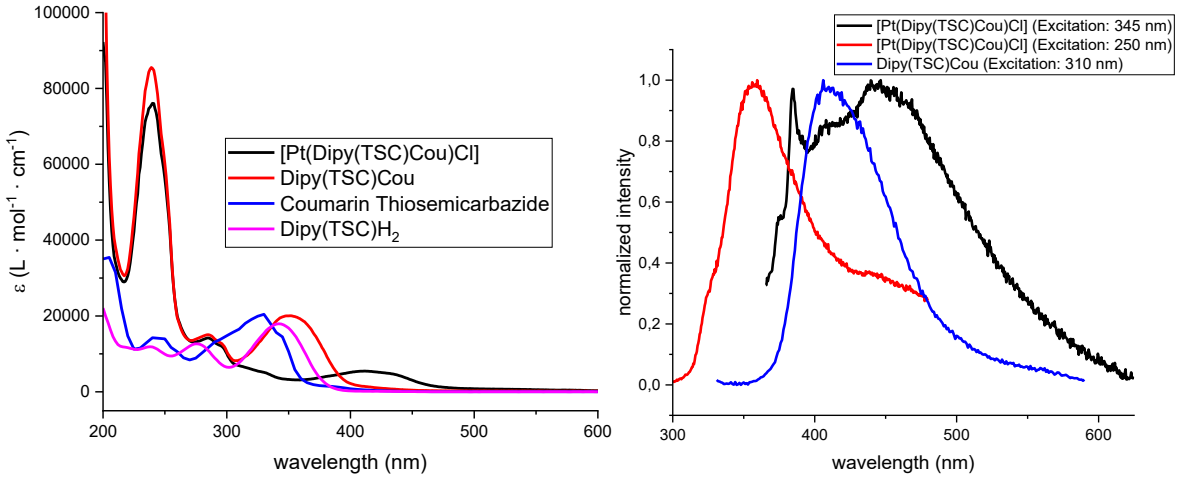


Figure 66. Left: UV/Vis absorption spectra of [Pt(Dipy(TSC)Cou)Cl], Dipy(TSC)Cou, coumarin thiosemicarbazide and Dipy(TSC)H_2 in MeCN. Right: Normalized emission spectra of Dipy(TSC)Cou and [Pt(Dipy(TSC)Cou)Cl] in MeCN at room temperature.

The emission maximum of Dipy(TSC)Cou is observed at 411 nm, which is blue shifted to 365 nm for the corresponding Pt(II) complex (Figure 67, right). An additional shoulder was found around 440 nm. By changing the excitation wavelength, from 250 to 345 nm, the shoulder at 440 nm becomes more intense and forms a new maximum. Two additional maxima are found at 409 and 385 nm, which are probably related to different vibrational states. Interestingly, this second emission was most intense after excitation at 345 nm, which correlates with an absorption maximum of the corresponding ligand. This absorption maximum is typically observed for dipyridyl ketone TSC and was assigned to an intra-ligand charge transfer (ILCT) of the thione group to the dipyridyl ketone unit.[302] For the metal complex, the maximum disappeared and the absorption at this wavelength is weak. Nevertheless, it was the ideal excitation wavelength for the emission at 440 nm, which is confirmed by their excitation spectra in the appendix. In this way, [Pt(Dipy(TSC)Cou)Cl] shows a kind of dual emission behavior. The first emission is probably related to the coumarin. The ideal excitation wavelength for this emission is 250 nm, where the coumarin unit has exactly an absorption maximum. The second emission maximum might be related to the TSC unit, since the ideal excitation wavelength is 345 nm, where the ligand shows a maximum attributed to a TSC centered transition (ILCT of the thione group to the dipyridyl ketone unit). The fact that the Pt(II) complex shows an additional emission, compared to the ligand, is probably related to the deprotonation of the hydrazone function, which increases the π-system and the rigidification of the compound due to metal coordination.

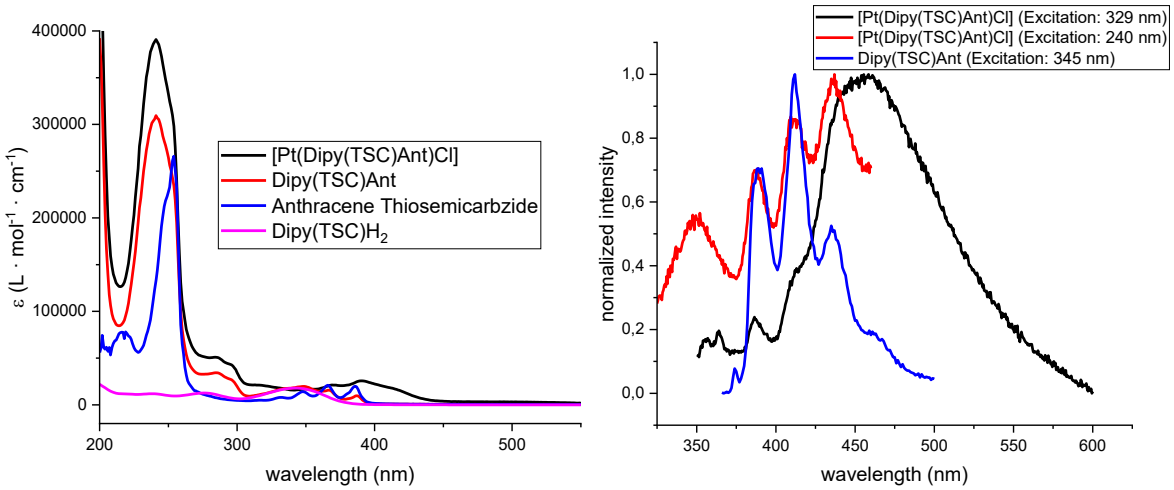


Figure 67. Left: UV/Vis absorption spectra of [Pt(Dipy(TSC)Ant)Cl], Dipy(TSC)Ant, anthracene thiosemicarbazide and Dipy(TSC)H_2 in MeCN. Right: Normalized emission spectra of Dipy(TSC)Ant and [Pt(Dipy(TSC)Ant)Cl] in MeCN at room temperature.

Dipy(TSC)Ant shows an intense maximum at 242 nm with a shoulder at 250 nm (Figure 67, left). By comparing with the absorption spectrum of anthracene thiosemicarbazide and Dipy(TSC)H_2, it seems that the maximum is related to an overlap of anthracene and dipyridyl TSC centered transitions. The Dipy(TSC)Ant shows an additional maximum at 285 nm, which was also observed for the Dipy(TSC)Cou. Thus, the maximum is probably related to dipyridyl TSC centered transitions. The TSC shows four additional weak maxima at 333, 349, 367 and 386 nm, which are attributed to the anthracene group and related to different vibrational states.[301] Interestingly, Dipy(TSC)Ant shows a pronounced vibrational fine structure, which was not observed for TSCs with an anthracene function at the *N*1 position (Ant(TSC)H_2) (Chapter 3.1.2). This was related to interactions of the TSCs in solution. In case of Dipy(TSC)Ant, these interactions either play a minor role, or the different behavior is related to the fact that the anthracene function is electronically separated from the TSC unit, due to the methylene bridge in between. After complexation of Pt(II), an additional absorption is found at 415 nm, which is related to the MLCT transition.

Also, in the emission spectrum of Dipy(TSC)Ant, the vibrational fine structure of the anthracene emission is clearly visible (Figure 67, right). In this way, the emission band exhibits four maxima at 390, 410, 436 and 462 nm. Compared to the corresponding Pt(II) complex, these maxima are not shifted, which again shows the electronic separation of the anthracene and TSC group. In case of the Pt(II) complex, an additional maximum is found at 350 nm. It is unclear if this emission is also found for the ligand since the measurement window is not the same due to different excitation wavelengths. By changing the excitation wavelength from 240 to 329 nm, again a second emission is found at 455 nm. It is expected that it has the same origin as discussed for the coumarin derivatives.

The Dipy(TSC)Cbz shows four maxima at 239, 268, 296 and 346 nm (Figure 68, left). The shape and energy of the transitions are very similar to that of Dipy(TSC)Cou. Again, the shape of the spectrum has more similarities to that of Dipy(TSC)H_2 than with the corresponding thiosemicarbazide. Complexation of Pt(II) leads again to the disappearance of the maxima at 346 nm and a MLCT transition is observed at 460 nm.

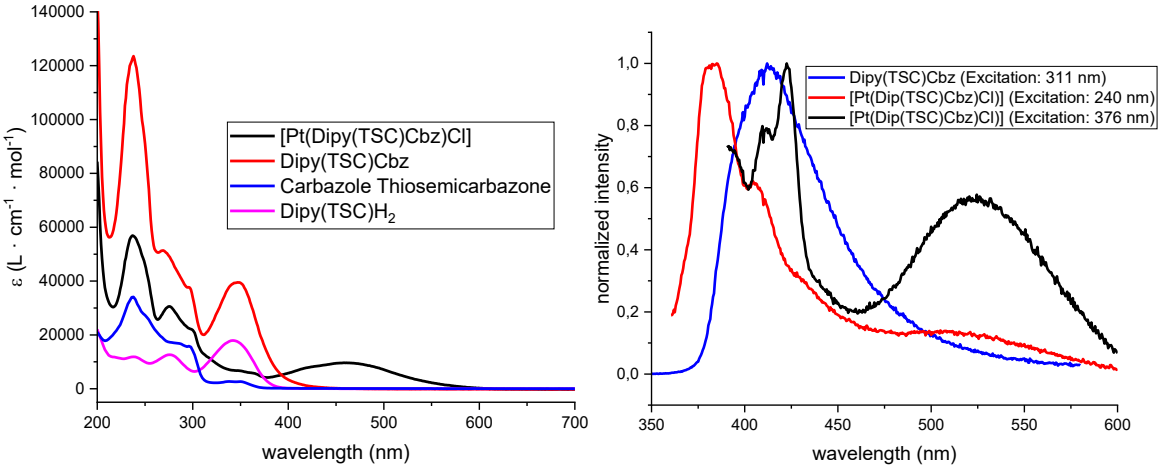


Figure 68. Left: UV/Vis absorption spectra of [Pt(Dipy(TSC)Cbz)Cl], Dipy(TSC)Cbz, carbazole thiosemicarbazide and Dipy(TSC)H_2 in MeCN. Right: Normalized emission spectra of Dipy(TSC)Cbz and [Pt(Dipy(TSC)Cbz)Cl] in MeCN at room temperature.

The emission maximum of the ligand is located at 412 nm (Figure 69, right). For the Pt(II) complex, the maximum is blue shifted to 383 nm. Two additional shoulders are observed at 405 nm and 426 nm. In addition to that, a second weak maximum was observed at 516 nm, which became more intense after changing the excitation wavelength from 240 to 376 nm. In this way, the compound also exhibits the dual emission behavior discussed before. The complex was used as an example, to investigate if this emission maxima has a triplet character. For this, the sensitivity to oxygen was tested. Since the intensity of the emission maximum was not affected by O_2, it seems that it is not related to phosphorescence. Instead, it supports the assumption of a ligand centered fluorescence.

The absorption and emission properties of Dipy(TSC)Flu and [Pt(Dipy(TSC)Flu)Cl] follow similar trends discussed before (Figure 69). The absorption and emission maxima are summarized in Table 23 and 24.

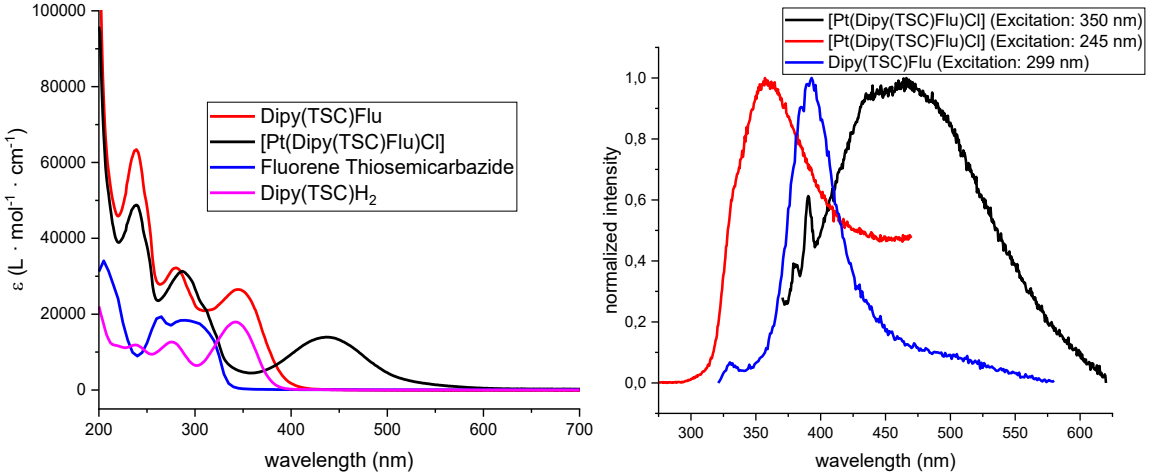


Figure 69. Left: UV/Vis absorption spectra of [Pt(Dipy(TSC)Flu)Cl], Dipy(TSC)Flu, fluorene thiosemicarbazide and Dipy(TSC)H_2 in MeCN. Right: Normalized emission spectra of Dipy(TSC)Cbz and [Pt(Dipy(TSC)Cbz)Cl] in MeCN at room temperature.

On the other hand, Dipy(TSC)Pyr and the corresponding Pt(II) complex shows some different behavior. The TSC exhibits four maxima at 239, 276, 330 and 344 nm and has a comparable shape to the corresponding thiosemicarbazide (Figure 70, left). Also, for the Pt(II) complex, the shape remains similar, but an additional maximum is found at 420 nm. The maximum at 330 nm decreases in intensity.

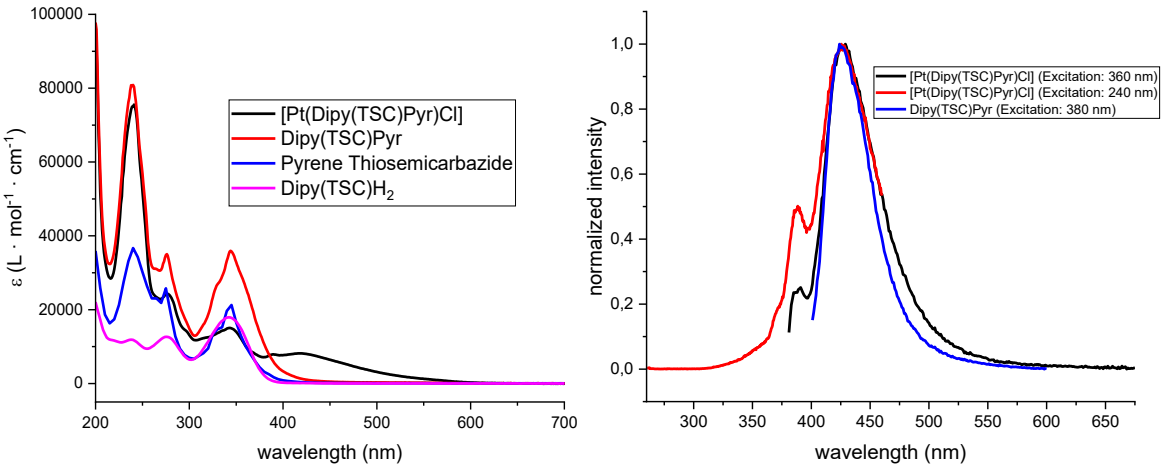


Figure 70. Left: UV/Vis absorption spectra of [Pt(Dipy(TSC)Pyr)Cl], Dipy(TSC)Pyr, carbazole thiosemicarbazide and Dipy(TSC)H_2 in MeCN. Right: Normalized emission spectra of Dipy(TSC)Pyr and [Pt(Dipy(TSC)Pyr)Cl] in MeCN at room temperature.

Another interesting aspect is that the emission maximum of the ligand and the complex are at the same wavelength (425 nm) (Figure 70, right). In addition to that, the compound shows no dual emission, after changing the excitation wavelength from 240 to 360 nm. This can be probably explained by the fact that the absorption maximum of pyrene is overlapping with the absorption maximum of the TSC unit. By that reason, the excitation at this wavelength probably leads to an excitation of the pyrene functionality.

Table 23. UV/Vis absorption maxima of the tagged TSCs and their corresponding Pt(II) complexes.[a]

	λ_1 [nm], ε [L·mol^{-1}·cm^{-1}]	λ_2 [nm], ε [L·mol^{-1}·cm^{-1}]	λ_3 [nm], ε [L·mol^{-1}·cm^{-1}]	λ_4 [nm], ε [L·mol^{-1}·cm^{-1}]	λ_5 [nm], ε [L·mol^{-1}·cm^{-1}]	λ_6 [nm], ε [L·mol^{-1}·cm^{-1}]	λ_7 [nm], ε [L·mol^{-1}·cm^{-1}]	ΔE_{opt} [eV]
Dipy(TSC)Cou	239, 85300	285, 15050	295 (sh), 12700	350, 20060	-	-	-	3.13
[Pt(Dipy(TSC)Cou)Cl]	240, 76070	285, 14190	294 (sh), 12160	-	420, 5260	-	-	2.59
Dipy(TSC)Ant	241, 305590	285, 34340	295, 27410	333, 17310	349, 19640	367, 15680	386, 9710	3.15
[Pt(Dipy(TSC)Ant)Cl]	241, 390860	285, 50880	295, 42760	368, 21120	390, 25630	415, 16860	-	2.77
Dipy(TSC)Cbz	239, 123530	268, 51370	296, 37510	346, 39420	-	-	-	3.17
[Pt(Dipy(TSC)Cbz)Cl]	239, 56450	275, 30590	299, 22050	-	460, 9640	-	-	2.18
Dipy(TSC)Pyr	239, 80580	276, 35040	330 (s), 26880	344, 35930	-	-	-	3.14
[Pt(Dipy(TSC)Pyr)Cl]	239, 75040	276, 24280	-	343, 15020	420, 8160	-	-	2.25
Dipy(TSC)Flu	238, 63220	279, 32200	344, 26480	-	-	-	-	3.16
[Pt(Dipy(TSC)Flu)Cl]	238, 48800	287, 30190	-	440, 13930	-	-	-	2.37

[a] Measured in MeCN. Sh = shoulder.

The optical HOMO-LUMO gaps were calculated by determining the onset of the low-energy transition (Table 23). In case of the ligands, the energy of the HOMO-LUMO gaps was almost identical. It supports the finding that the shape of the absorption spectra remains similar, independently of the respective chromophore at the *N*4 position. For the corresponding Pt(II) complexes the HOMO-LUMO gaps differ more significantly which can be directly seen by the shifts of their MLCT absorption bands. In this way, the chromophore seems to have an impact on this transition, which can be explained by the deprotonation of the ligand, which leads to an extended, conjugated π-system. The highest HOMO-LUMO gap is found for [Pt(Dipy(TSC)Ant)Cl], which fits to this observation quite well, since the

anthracene chromophore is separated by a methylene group from the TSC. The smallest HOMO-LUMO gap is observed for the [Pt(Dipy(TSC)Cbz)Cl].

Table 24. UV/Vis emission maxima of the tagged TSCs and their corresponding Pt(II) complexes.[a]

	λ_1 [nm]	λ_2 [nm]	λ_3 [nm]	λ_4 [nm]
Dipy(TSC)Cou (Excitation: 310 nm)	410	-	-	-
[Pt(Dipy(TSC)Cou)Cl] (Excitation: 250 nm)	357	-	-	-
[Pt(Dipy(TSC)Cou)Cl] (Excitation: 345 nm)	385	412	450	-
Dipy(TSC)Ant (Excitation: 345 nm)	390	412	436	-
[Pt(Dipy(TSC)Ant)Cl] (Excitation: 240 nm)	350	388	411	436
[Pt(Dipy(TSC)Ant)Cl] (Excitation: 329 nm)	386	415 (s)	456	-
Dipy(TSC)Cbz (Excitation: 311 nm)	412	-	-	-
[Pt(Dipy(TSC)Cbz)Cl] (Excitation: 240 nm)	382	403 (s)	427 (s)	508 (s)
[Pt(Dipy(TSC)Cbz)Cl] (Excitation: 376 nm)	411	422	524	-
Dipy(TSC)Pyr (Excitation: 380 nm)	426	-	-	-
[Pt(Dipy(TSC)Pyr)Cl] (Excitation: 240 nm)	387	426	-	-
[Pt(Dipy(TSC)Pyr)Cl] (Excitation: 380 nm)	387	426	-	-
Dipy(TSC)Flu (Excitation: 299 nm)	391	-	-	-
[Pt(Dipy(TSC)Flu)Cl] (Excitation: 245 nm)	358	-	-	-
[Pt(Dipy(TSC)Flu)Cl] (Excitation: 350 nm)	380	391	460	-

[a] Measured in MeCN at room temperature.

3.4.3 Cyclovoltammetry of the tagged TSCs and their Pt(II) complexes

The electrochemistry of the tagged TSCs and their Pt(II) complexes was investigated by CV in different solvents, namely MeCN, DMF and THF. The main reason for this was the solubility of the compounds, which was poor in MeCN, leading to a poor quality of the CV data. In THF the solubility was increased except for the coumarin derivatives, while in DMF all compounds showed high solubility. Since it was possible to determine the redox potential in all these solvents, a comparison of the solvent dependent redox properties is possible. The data of the measurements in MeCN and THF are shown in the appendix. The data in DMF is shown in Figure 71-75, summarized in Table 25 and discussed in the following.

Dipy(TSC)Ant shows a first reduction at –2.07 V, which is irreversible (Figure 71, left). The reduction occurs in a similar range, as for other pyridyl ketone TSCs discussed before (Chapter 3.2.4). By that reason, it might be related to an imine centered reduction. A second reduction is found at –2.45 V, which is reversible. Since this reversible reduction was not found in Dipy(TSC)H_2 and not for other tagged dipyridyl ketone TSCs, it might be related to an anthracene centered reduction. This would be in accordance with other electrochemical studies of anthracene derivatives in literature.[222,346] Two additional, irreversible reductions are found at –2.99 and –3.12 V. In addition to that, the ligand shows two irreversible oxidations at 0.38 and 0.82 V.

After complexation of Pt(II), the redox properties change significantly (Figure 71, right). The first reduction is anodically shifted to –1.51 V and becomes reversible. This first reduction was assigned in literature to a ligand centered reduction, at the pyridine ring, were the LUMO of dipyridyl ketone Pt(II) complexes is located.[2,222] In this way, the metal coordination stabilizes the reduction of the ligand. A second, reversible reduction occurs at –2.11 V. The origin of the second reduction is unclear and might be attributed to a second ligand centered reduction.[2,28,222] A third reversible reduction is found at –2.40 V, which might be attributed to the same reduction process found for the ligand at –2.45, probably centered on the anthracene group. The complex shows an irreversible oxidation at 0.86 V. DFT calculations from literature show that the HOMO of dipyridyl ketone Pt(II) complexes is located at the Pt(II) center (d_{xy} orbital), the thiolate S atom and on a minor contribution on the chloride co-ligand.[2,222] In this way, the first oxidation might be attributed to the oxidation of Pt(II) to Pt(III). However, it should be considered that there might be also oxidative processes located at the chromophore. In this way, the

results should be complemented with specific DFT calculations of the ligand and the metal complex in the future. The electrochemical HOMO-LUMO gap of the ligand was 2.45 and 2.37 eV for the Pt(II) complex.

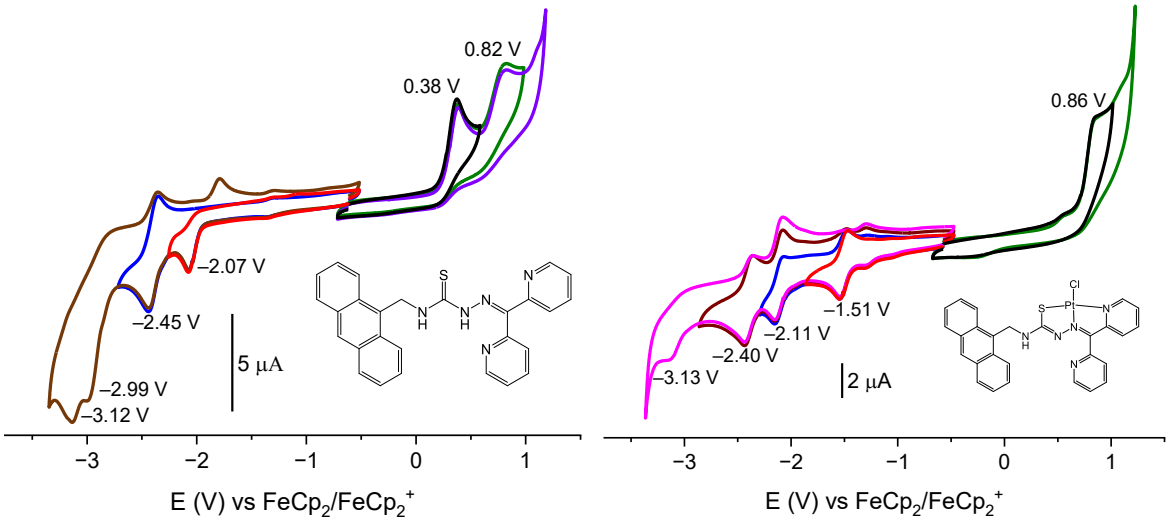


Figure 71. CVs of Dipy(TSC)Ant (left) and [Pt(Dipy(TSC)Ant)Cl] (right) measured in 0.1 M solution of *n*Bu4NPF6 in DMF at a scan rate of 100 mV/s, referenced against $FeCp_2/FeCp_2^+$.

Dipy(TSC)Cou shows three irreversible reductions at –1.84, –2.49 and –3.18 V and a reversible reduction at –2.77 V (Figure 72, left). Two irreversible oxidations are found at 0.87 and 1.14 V. The corresponding Pt(II) complex shows three reversible reductions at –1.26, –1.85 and –2.68 V (Figure 72, right). Two irreversible oxidations are found at 0.90 V and 0.98 V. In this way, the shape of the CVs of the Pt(II) complex has many similarities to that of the anthracene derivative. It is expected that the first two reductions are related to ligand centered reductions as discussed before. The third reduction might be located at the coumarin, since also the ligand shows a reversible reduction in a similar range. The electrochemical HOMO-LUMO gap of the ligand was 2.71 and 2.16 eV for the Pt(II) complex.

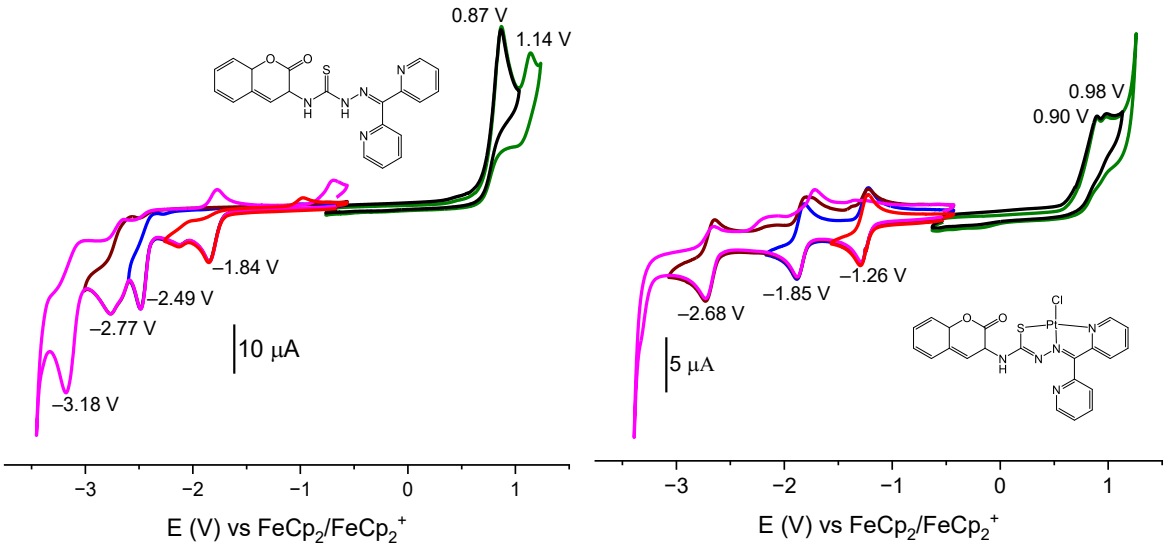


Figure 72. CVs of Dipy(TSC)Cou (left) and [Pt(Dipy(TSC)Cou)Cl] (right) measured in 0.1 M solution of *n*Bu4NPF6 in DMF at a scan rate of 100 mV/s, referenced against $FeCp_2/FeCp_2^+$.

Dipy(TSC)Carb shows two irreversible reductions at –2.02 and –2.85 V and three irreversible oxidations at 0.57, 0.82 and 1.02 V. The Pt(II) complex shows again two characteristic, reversible reductions at –1.45

and –2.06 V as well as an irreversible reduction at –3.32 V. Two irreversible oxidations are found at 0.49 V and 0.73 V (Figure 73).

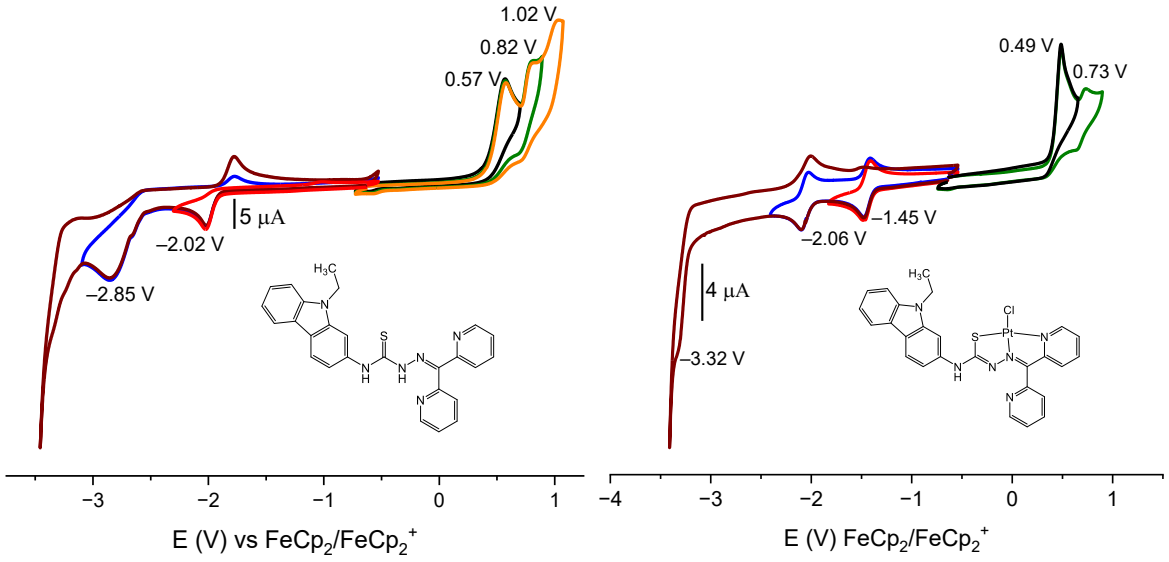


Figure 73. CVs of Dipy(TSC)Cbz (left) and [Pt(Dipy(TSC)Cbz)Cl] (right) measured in 0.1 M solution of *n*Bu4NPF6 in DMF at a scan rate of 100 mV/s, referenced against FeCp2/FeCp2+.

Similar, results are found for the fluorene derivatives, which are shown in Figure 74. The ligand has a electrochemical HOMO-LUMO gap of 2.81 eV, which decreases for the Pt(II) complex to 2.16 eV.

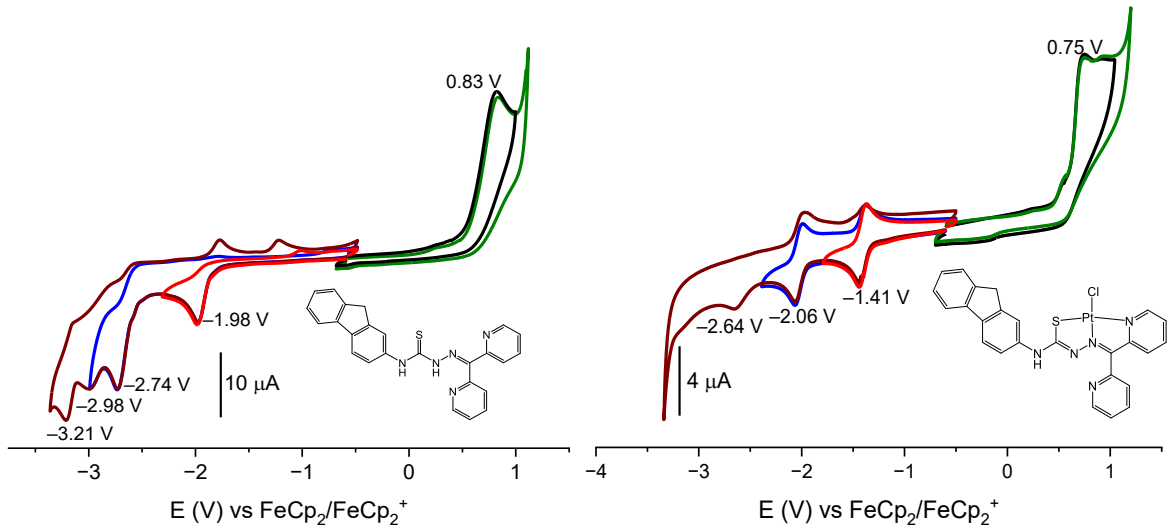


Figure 74. CVs of Dipy(TSC)Flu (left) and [Pt(Dipy(TSC)Flu)Cl] (right) measured in 0.1 M solution of *n*Bu4NPF6 in DMF at a scan rate of 100 mV/s, referenced against FeCp2/FeCp2+.

The pyrene derivative shows four irreversible reductions at –1.94, –2.52, –2.87 and –3.20 V as well as one irreversible oxidation at 0.69 V (Figure 75, left). For the corresponding Pt(II) complex one reversible reduction is found at –1.94 V. Interestingly, the second reduction is found to be irreversible, which is a difference compared to the other derivatives discussed before (Figure 75, right). One explanation could be that a reduction of the pyrene function occurs at similar voltage. The broadening of the first reduction wave around –1.95 to –2.40 V in the ligand, compared to the other derivatives supports this assumption, that two different reductive processes might overlap in this region. The electrochemical HOMO-LUMO gap of the ligand was 2.63 eV and 2.06 eV for the Pt(II) complex.

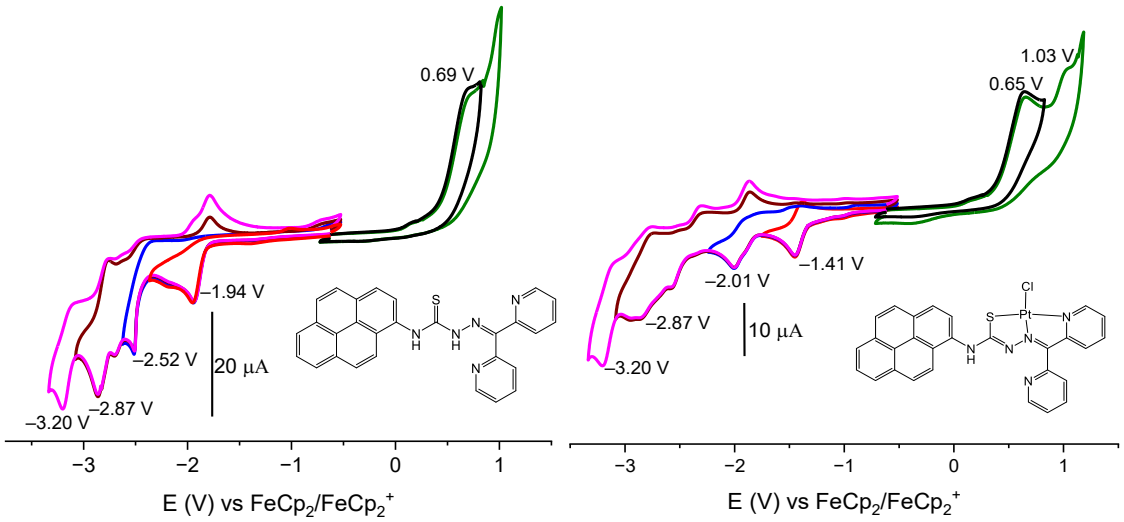


Figure 75. CVs of Dipy(TSC)Pyr (left) and [Pt(Dipy(TSC)Pyr)Cl] (right) measured in 0.1 M solution of nBu$_4$NPF$_6$ in DMF at a scan rate of 100 mV/s, referenced against FeCp$_2$/FeCp$_2^+$.

Table 25. Redox potentials of tagged TSCs and their corresponding Pt(II) complexes.[a]

	Red 4 (V)	Red 3 (V)	Red 2 (V)	Red 1 (V)	Ox 1 (V)	Ox 2 (V)	Ox 3 (V)	ΔE (eV)
Dipy(TSC)Ant	–3.12	–2.99	–2.45	–2.07	0.38	0.82	-	2.45
[Pt(Dipy(TSC)Ant)Cl]	–3.13	–2.40	–2.11	–1.51	0.86	-	-	2.37
Dipy(TSC)Carb	-	-	–2.85	–2.02	0.57	0.82	1.02	2.59
[Pt(Dipy(TSC)Carb)Cl]	-	–3.32	–2.06	–1.45	0.49	0.73	-	1.94
Dipy(TSC)Cou	–3.18	–2.77	–2.49	–1.84	0.87	1.14	-	2.71
[Pt(Dipy(TSC)Cou)Cl]	-	–2.68	–1.85	–1.26	0.90	0.98	-	2.16
Dipy(TSC)Flu	–3.21	–2.98	–2.74	–1.98	0.83	-	-	2.81
[Pt(Dipy(TSC)Flu)Cl]	-	–2.64	–2.06	–1.41	0.75	-	-	2.16
Dipy(TSC)Pyr	–3.20	–2.87	–2.52	–1.94	0.69	-	-	2.63
[Pt(Dipy(TSC)Pyr)Cl]	–3.20	–2.87	–2.01	–1.41	0.65	1.03	-	2.06

[a] Measured in 0.1 M solution of nBu$_4$NPF$_6$ in DMF at a scan rate of 100 mV/s, referenced against FeCp$_2$/FeCp$_2^+$.

Table 26 shows a comparison of the first reduction and oxidation in different solvents (DMF, MeCN and THF) as well as their HOMO-LUMO gaps. For the Pt(II) complex, also the second reduction is considered. In general, it is found that the redox potential and electrochemical HOMO-LUMO gaps are strongly solvent dependent.

Table 26. Redox potentials of tagged TSCs and their corresponding Pt(II) complexes.[a]

	DMF				MeCN				THF			
	Red2 (V)	Red1 (V)	Ox1 (V)	ΔE (ev)	Red2 (V)	Red1 (V)	Ox1 (V)	ΔE (ev)	Red2 (V)	Red1 (V)	Ox1 (V)	ΔE (ev)
Dipy(TSC)Ant	-	–2.07	0.38	2.45	-	–1.96	0.50	2.46	-	–2.18	0.47	2.65
[Pt(Dipy(TSC)Ant)Cl]	–2.11	–1.51	0.86	2.37	–2.03	–1.45	1.00	2.45	–2.46	–1.55	0.99	2.54
Dipy(TSC)Cbz	-	–2.02	0.57	2.59	-	–2.62	0.54	3.16	-	–2.26	0.82	3.08
[Pt(Dipy(TSC)Cbz)Cl]	–2.06	–1.45	0.49	1.94	–2.98	–1.40	0.64	2.04	–2.05	–1.42	0.69	2.11
Dipy(TSC)Cou	-	–1.84	0.87	2.71	-	–2.45	0.95	3.40	-	–2.02	1.42	3.44
[Pt(Dipy(TSC)Cou)Cl]	–1.85	–1.26	0.90	2.16	–1.62	–1.19	0.93	2.12	–1.39	–1.39	-	-
Dipy(TSC)Flu	-	–1.98	0.83	2.81	-	–2.66	0.70	3.36	-	–2.15	1.01	3.16
[Pt(Dipy(TSC)Flu)Cl]	–2.06	–1.41	0.75	2.16	–1.92	–1.36	0.97	2.33	–1.46	–1.46	0.95	2.41
Dipy(TSC)Pyr	-	–1.41	0.65	2.06	-	–1.92	0.79	2.71	-	–2.11	0.77	2.88
[Pt(Dipy(TSC)Pyr)Cl]	–2.52	–1.94	0.69	2.63	–1.88	–1.17	0.69	1.86	–1.51	–1.51	0.82	2.33

[a] Measured in 0.1 M solution of nBu$_4$NPF$_6$ in DMF, MeCN or THF at a scan rate of 100 mV/s, referenced against FeCp$_2$/FeCp$_2^+$.

In DMF, the HOMO-LUMO gaps are usually the smallest, while in THF they are the largest, with some exceptions. The first oxidation is usually cathodically shifted in DMF. In MeCN the potential becomes more anodically shifted, whereby this shift increases in THF. The first reduction in DMF is usually anodically shifted compared to THF. For the second reduction, no clear trends are visible.

3.4.4 Spectroelectrochemical measurements of the Pt(II) complexes of tagged TSCs

Spectroelectrochemical measurements have been performed for the five Pt(II) complexes to gain a deeper understanding about the redox processes. The [Pt(Dipy(TSC)Ant)Cl], [Pt(Dipy(TSC)Carb)Cl] and [Pt(Dipy(TSC)Flu)Cl] have been measured in THF and are shown in Figure 76.

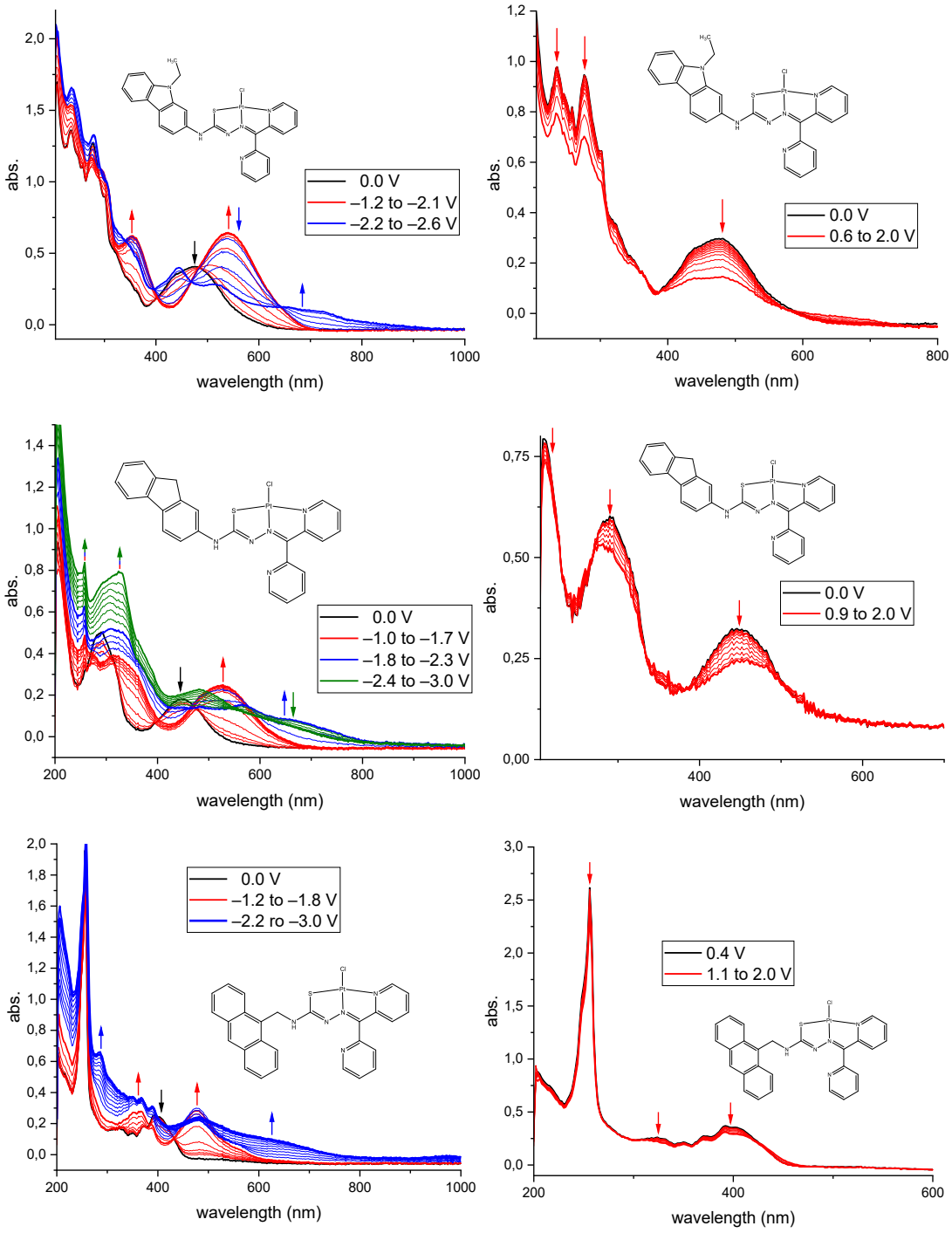


Figure 76. UV/Vis absorption spectra of [Pt(Dipy(TSC)CBz)Cl] (Top), [Pt(Dipy(TSC)Flu)Cl] (middle) and [Pt(Dipy(TSC)Ant)Cl] (bottom) during their stepwise reduction (left) or oxidation (right) in a solution of 0.1 M nBu$_4$NPF$_6$ in THF. The potential was reduced or decreased in 0.1 V steps and the UV/Vis absorption spectra were recorded after 30 s.

The complexes show quite similar behavior, which supports the assumptions that the redox processes have a similar origin. After the first reduction, the absorption maximum around 400-430 nm, which was assigned to a MLCT transition, is bathochromic shifted to 440-550 nm and the intensity is increasing. In addition to that, a second maximum is formed around 350 nm. The absorption maxima in the UV region of the spectrum are also affected, whereby their intensity is increasing. The observations are in accordance with the literature and support the assignment to a ligand centered reduction.[2,28,222] During the second reduction, the absorption band at 440-550 nm is decreasing and the formation of a broad, long-wavelength absorption is observed which reaches up to 800-900 nm in the near infrared reagion. For [Pt(Dipy(TSC)Ant)Cl] an additional weak maximum is found around 950-1000 nm. In the UV region of the spectrum, the intensity of the absorption bands is increasing again, which is especially pronounced for [Pt(Dipy(TSC)Ant)Cl]. Since the newly formed absorption bands are observed in the near infrared region, their assignment to π^*-π^* transitions might be most plausible, which supports the assignment to a second, ligand centered reduction.[2,28,222] For [Pt(Dipy(TSC)Flu)Cl] it was possible to follow a third reductive process, whereby the absorption maxima at 220, 260 and 440 nm increased in intensity. The oxidation of the complexes led to a constant decrement of the absorption maxima over time. In this way, it seems that the oxidized species was not soluble in THF.

[Pt(Dipy(TSC)Cou)Cl] and [Pt(Dipy(TSC)Pyr)Cl] were measured in DMF due to the increased solubility in this solvent (Figure 77). The general trends remain similar compared to the other compounds. The first reduction led to the formation of two new maxima around 350 and 520 nm. For the second reduction the formation of a very intense absorption band around 630 to 710 nm is observed as well as an absorption up to 1000 nm. During the third reduction these formed maxima are decreasing again.

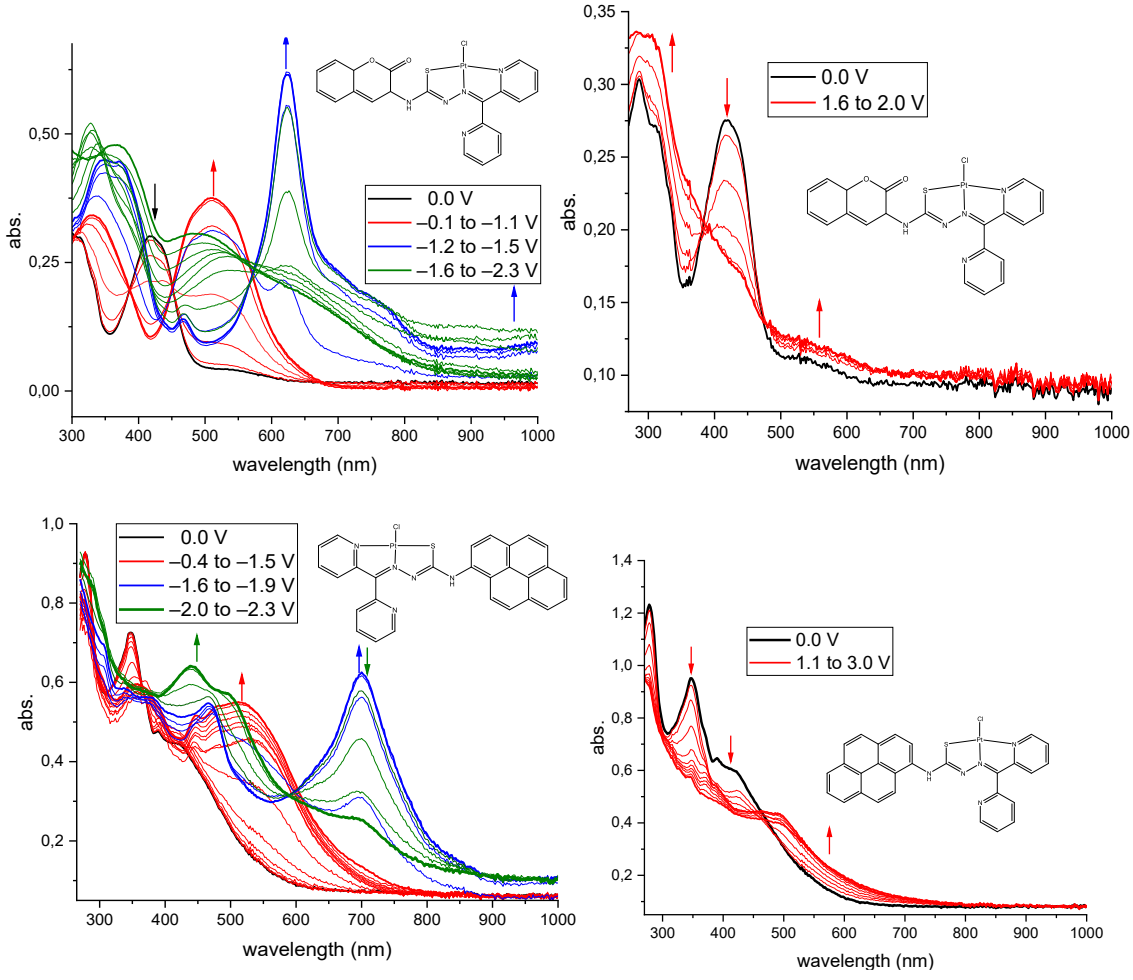


Figure 77. UV/Vis absorption spectra of [Pt(Dipy(TSC)Cou)Cl] (Top) and [Pt(Dipy(TSC)Pyr)Cl] (Bottom) during their stepwise reduction (left) or oxidation (right) in a solution of 0.1 M nBu$_4$NPF$_6$ in DMF. The potential was reduced or decreased in 0.1 V steps and the UV/Vis absorption spectra were recorded after 30 s.

Also, the oxidation of the complexes can be investigated since the solubility of the oxidized species was increased in DMF. The absorption band, assigned to the MLCT transition was decreasing during the oxidation and a weak absorption band around 550-600 nm formed. Since both complexes with different chromophores are acting similar, this observation might support the assignment to a metal centered oxidation discussed before and not to oxidative processes at the chromophore.

3.4.5 Cytotoxicity studies of tagged TSC Pt(II) complexes

The cell viability was determined by a crystal violet straining assay and the IC_{50} values were determined as the concentration that caused 50% inhibition of cell proliferation compared to an untreated control.[347] The crystal violet assay is based on the principle that the dye binds to healthy cells which can be used for their quantification. The TSCs were tested against different cancer cell lines namely A549 (lung carcinoma cells), MDA-MB-321 (metastatic breast adenocarcinoma), MCF-7 (breast adenocarcinoma) and HT-29 (colorectal adenocarcinoma). Vero E6 are African green monkey kidney cells which were used as a reference cell line to check for possible tumor selectivity. The incubation time was 72 h. As a reference cisplatin was used, which is one of the most established platinum cytostatic agents.

Most of the TSC Pt(II) complexes showed no significant toxicity against the cell lines (IC_{50} > 50 µM) (Table 27). One exception is [Pt(Dipy(TSC)Cbz)Cl] which showed a certain cytotoxicity against metastatic breast adenocarcinoma (MDA-MB-321) with an IC_{50} of 26.0 µM. Interestingly, this compound was not toxic for all the other cancer cell lines as well as the healthy Vero E6 cells. Since the TSC seems to selectively address the metastatic tumor cells, it might be an interesting candidate for further research, although the IC_{50} value is high, compared to cisplatin. To understand why only MDA-MB-321 cells are affected, will be a task for the future.

Table 27. IC_{50} values, determined for the tagged TSC Pt(II) complexes against A549, MDA-MB-321, MCF-7, HT-29 and Vero E6.

Compound	IC_{50}, µM ± SD				
	A549	MDA-MB-321	MCF-7	HT-29	Vero E6
[Pt(Dipy(TSC)Flu)Cl]	> 50	> 50	> 50	> 50	> 50
[Pt(Dipy(TSC)Cbz)Cl]	> 50	$26.0^{\pm 3.9}$	> 50	> 50	> 50
[Pt(Dipy(TSC)Ant)Cl]	> 50	> 50	> 50	> 50	> 50
[Pt(Dipy(TSC)Pyr)Cl]	$1.71^{\pm 0.08}$	$0.46^{\pm 0.01}$	$0.89^{\pm 0.04}$	$1.03^{\pm 0.08}$	$1.97^{\pm 0.09}$
[Pt(Dipy(TSC)Cou)Cl]	> 50	> 50	> 50	> 50	> 50
Cisplatin	$1.46^{\pm 0.36}$	$1.96^{\pm 0.17}$	$2.66^{\pm 0.6}$	$4.52^{\pm 0.69}$	$1.28^{\pm 0.06x}$

The [Pt(Dipy(TSC)Pyr)Cl] complex showed a remarkably cytotoxicity against the tested cancer cell lines. In this way, this compound is by far the most toxic compound of this series. The determined IC_{50} values are quite low, namely 1.71 µM for A549, 0.46 µM for MDA-MB-321, 0.89 µM for MCF-7 and 1.03 µM for HT-29. In case of the MDA-MB-321, MCF-7 and HT29 cells, the compound is three or even four times more toxic than cisplatin. Against Vero E6 cells, an IC_{50} value of 1.97 µM was determined. Although, the toxicity against these healthy cells is high, it is at least lower than for cisplatin (1.28 µM). In addition, the IC_{50} values against the cancer cells were lower by a factor of two (MCF-7 and HT-29) or even four (MDA-MB-321). This might be evidence that there is a facility of a therapeutic window, where the damage against the tumor cells is higher than for healthy ones.

The results open the question, which mechanism is related to the cytotoxicity of [Pt(Dipy(TSC)Pyr)Cl] and [Pt(Dipy(TSC)Cbz)Cl]. It cannot be assumed that it is the same as for typical α-pyridyl TSC and their iron or copper complexes, since the Pt(II) center probably remains bound to the TSC within the cells. In this way, the coordination side is blocked for binding intracellular metals. In addition, the Pt(II) complexes will be not able to redox cycle and to produce ROS. Since these complexes are planar, they might be able to intercalate between DNA, which is a typical mechanism found for other cytostatic agents.[348] To check this assumption, DNA binding studies could be performed in the future. However, since all the compounds are planar, this should be also possible for the other derivatives. This opens the

question, why only the pyrene and carbazole derivatives are cytotoxic. One explanation could be a different cellular uptake. Determining their H_2O /octanol partition coefficient might help to analyze their lipophilicity, which in turn affects the cellular uptake. Since the compounds are designed for their fluorescence, this will be an additional tool in the future to investigate their biodistribution and to figure out their mission of action.

Additional biological tests are currently in progress, which includes cytotoxicity studies of the corresponding Dipy(TSC)Pyr ligand, as well as antiviral tests with the inactive TSC Pt(II) complexes.

4.4.6 Summary – tagged TSCs

TSCs with anthracene, carbazole, pyrene, fluorene and coumarin group at the *N*4 position as well as their corresponding Pt(II) complexes have been successfully synthesized. Unfortunately, attempts for the synthesis of TSCs derived from fluoresceine, naphthaliminde or tetraphenyl porphyrin were unsuccessful, due to side reactions. Although different chromophores were attached to the TSCs, the UV/Vis absorption spectra were quite similar and showed many characteristics of dipyridyl ketone TSCs. For the Pt(II) complexes an MLCT absorption band was observed, which was shifted depending on the chromophore (415-460 nm). The ligands showed the typical fluorescence of the chromophores which occurred in a range of 390-440 nm. Complexation of Pt(II) usually led to a blue shift of the emission. However, for most of the compounds a second emission was observed which is probably attributed to the TSC function and related to the deprotonation and rigidification of the ligand by metal complexation. The electrochemical properties were investigated by CV. Again, the compounds showed many similarities. For the Pt(II) complexes, the compounds showed a set of two characteristic, reversible reduction, which are probably ligand centered. The results were supported by spectroelectrochemical measurements.

In a last step, the cytotoxicity of the Pt(II) complexes was investigated. Thereby, [Pt(Dipy(TSC)Pyr)Cl] showed a high toxicity against A549, MDA-MB-321, MCF-7 and HT-29, which was even higher than for cisplatin. In addition, [Pt(Dipy(TSC)Cbz)Cl] showed a selective toxicity against MDA-MB-321. In this way, some of the TSCs fulfill the idea of a cytotoxic TSC with a fluorescence tag. This circumstance could be used in the future to investigate their mission of action by fluorescence microscopy.

3.5 TSCs with potential amphiphilic character and their Pt(II) and Cu(II) complexes

Several TSCs consisting of a lipophilic and hydrophilic group have been synthesized (Chart 21). The *N*4 position was successfully functionalized with aliphatic residues, namely an octyl, dodecyl and hexadecyl group as well as with cholesterol. On the other hand, hydrophilic residues have been introduced at the *N*1 position of the TSC by condensation of the corresponding thiosemicarbazides with di(2-pyridyl)ketone, 2,5-dihydroxybenzaldehyde, 2,3,4-trimethoxybenzaldehyde and butane-2,3-dione. For the dipyridyl ketone TSCs and bis-TSC, the corresponding metal complexes with Cu(II) and Pt(II) have been synthesized.

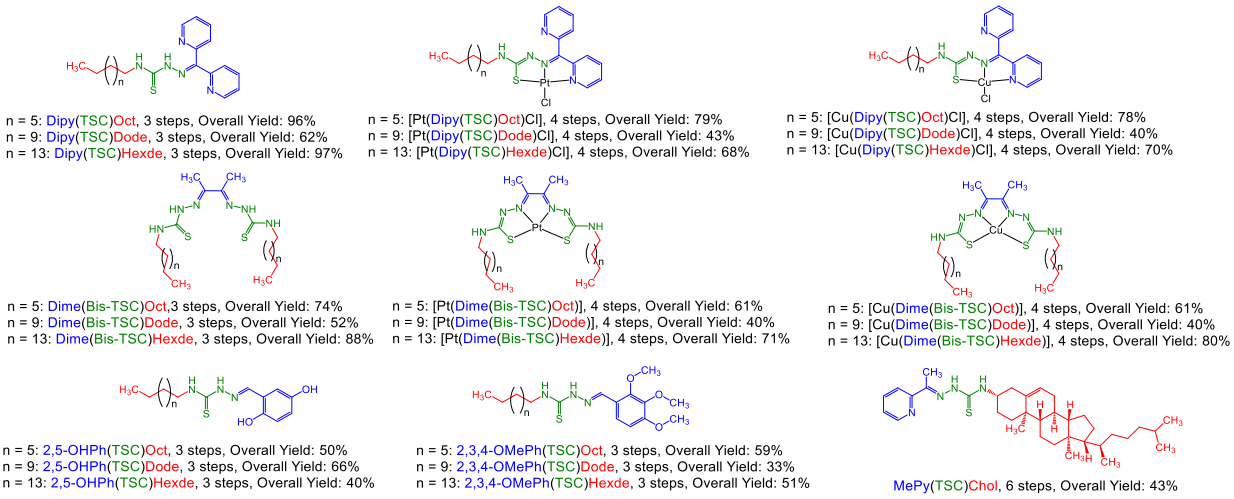


Chart 21. Overview about the synthesized amphiphilic TSCs and their corresponding metal complexes.

The compounds are stable under ambient conditions, at least for several months. Their solubility in pentane, toluene, MeOH and H_2O were investigated to analyze if they have an amphiphilic character. UV/Vis absorption spectroscopy was used to estimate the solubility of the compounds. For this, 2.0 mg of the compound were dissolved in 25 mL of the respective solvent. If no absorption was detected, the compounds are considered as insoluble. If an absorption was detectable but a precipitate was observed, the compounds are considered as poorly soluble. In case that > 5.0 mg of the compound is soluble without any precipitation, the TSC is considered as soluble. The maximum amount, which is soluble in the respective solvent was not determined. In this way, the results can just give a qualitative picture of the solubility of the compounds. The results are summarized in Table 28.

It was found that none of the compounds were soluble in H_2O, but some exceptions are at least poorly soluble like Dipy(TSC)Oct, Dipy(TSC)Dode and 2,5-OHPh(TSC)Oct. As expected, the lipophilicity of the TSCs is increasing for long alkyl chains and reduces their solubility in H_2O. Complexation of Cu(II) and Pt(II) seems to not improve the H_2O solubility which becomes even worse. This could be explained by the fact that the polarity of the TSC group is not increased for these neutral complexes. At the same time, the metal ion reduces the facility of the TSC to form hydrogen bonds because the donor atoms are blocked. However, their solubility in mixture of DMSO/H_2O was high enough to determine their cytotoxic potential. Due to the poor solubility in H_2O, the formation of micelles was not possible. Nevertheless, the compounds might be interesting candidates for nano formulation, where the drug is incorporated into liposomes or micelles.

Table 28. Solubility of TSCs with lipophilic and hydrophilic groups in pentane, toluene, MeOH and H_2O.[a]

Compound	Pentane	Toluene	MeOH	H_2O
Octyl thiosemicarbazide		-		
Dodecyl thiosemicarbazide		-		
Hexadecyl thiosemicarbazide		-		
Dipy(TSC)Oct				
Dipy(TSC)Dode				
Dipy(TSC)Hexde				
[Pt(Dipy(TSC)Oct)Cl]				
[Pt(Dipy(TSC)Dode)Cl]				
[Pt(Dipy(TSC)Hexde)Cl]				
[Cu(Dipy(TSC)Oct)Cl]				
[Cu(Dipy(TSC)Dode)Cl]				
[Cu(Dipy(TSC)Hexde)Cl]				
Dime(bis-TSC)Oct				
Dime(bis-TSC)Dodec				
Dime(bis-TSC)Hexdec				
[Pt(Dime(bis-TSC)Oct)Cl]				
[Pt(Dime(bis-TSC)Dode)Cl]				
[Pt(Dime(bis-TSC)Hexde)Cl]				
[Cu(Dime(bis-TSC)Oct)Cl]				
[Cu(Dime(bis-TSC)Dode)Cl]				
[Cu(Dime(bis-TSC)Hexde)Cl]				
2,5-OHPh(TSC)Oct				
2,5-OHPh(TSC)Dode				
2,5-OHPh(TSC)Hexde				
2,3,4-OMePh(TSC)Oct				
2,3,4-OMePh(TSC)Dode				
2,3,4-OMePh(TSC)Hexde				

[a] Color code: soluble (> 5 mg in 25 mL), poorly soluble (< 2 mg in 25 mL), insoluble (no detection by UV/Vis absorption spectroscopy).

Most of the compounds were found to be poorly soluble in pentane. Again, the metal complexes have a decreased solubility, compared to the corresponding ligands. Interestingly, it was found that an increasing alkyl chain length did not increase their solubility in this solvent. Most of the compounds were soluble in toluene and MeOH. In this way, the ligands have at least some kind of amphiphilic character. From all the tested compounds, Dipy(TSC)Oct and Dipy(TSC)Dode showed the best solubility in the tested solvents. The bis-TSCs had the poorest solubility and are probably not suitable for biological applications. The two alkyl chains in their structure make them a way too lipophilic, while the TSC unit is not hydrophile enough to develop an amphiphilic behavior.

In general, the ideal balance between hydrophobic and hydrophilic groups in the TSC structure was not found during this research. However, some general things can be learned from these results. The first thing is that metal complexation can decrease the H_2O solubility of the TSCs, which is probably related to the facility of hydrogen bonding for the free ligand. The second finding is that the hydrophilicity of the TSC function was not high enough. To optimize this property, it will be necessary to have a positive or negative charge at this function. There will be two options to do so. The first one is the complexation of a metal ion to form charged complexes. Depending on the TSC, they can offer one ($N\text{^}N\text{^}\boldsymbol{S}^-$) or even two negative charges ($\boldsymbol{O}^-\text{^}N\text{^}\boldsymbol{S}^-$), which must be considered for the choice of the metal valency and the co-ligands to synthesize charged compounds. For the dipyridyl ketone TSCs, Au(III) complexes are

suitable candidates, since it is a trivalent metal ion which prefers a square planar coordination. The second option could be the introduction of functional groups like sulfonic acids, carbon acids or amines which can be protonated or deprotonate to generate a charge (Chart 22).

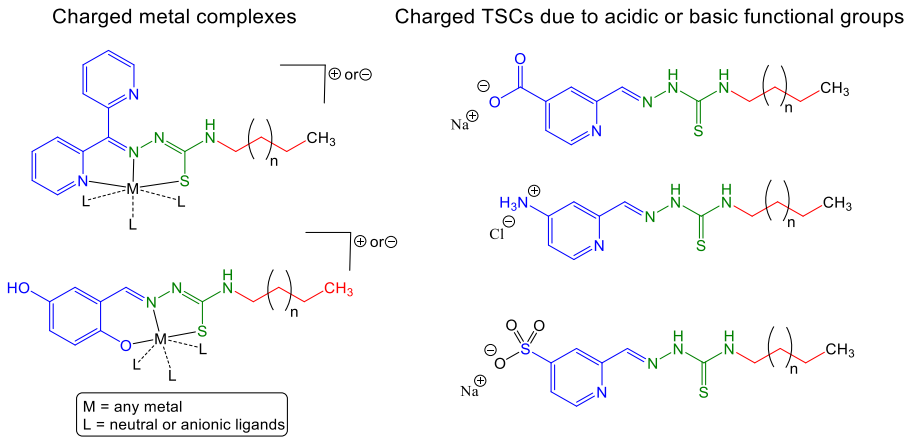
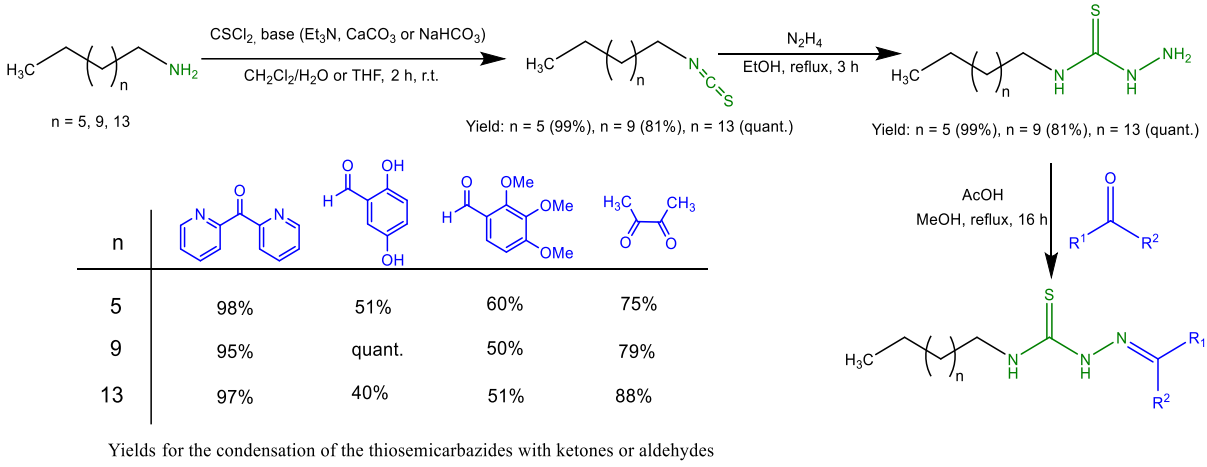


Chart 22. Strategies to synthesize charged TSCs to increase their amphiphilic behavior.

3.5.1 Synthesis of TSCs with lipophilic and hydrophilic groups

Starting point of the synthesis was the corresponding alkyl amines namely 1-aminooctane, 1-aminododecane and 1-aminohexadecane. By using the typical approach discussed before, the corresponding thiosemicarbazides have been synthesized in high yields (Scheme 61).[349,350] This was followed by the AcOH catalyzed condensation with ketones or aldehydes (di(2-pyridyl)ketone, 2,5-dihydroxybenzaldehyde, 2,3,4-trimethoxybenzaldehyde and butane-2,3-dione) yielding the TSCs or bis-TSCs. The products were obtained in moderate to high yields.

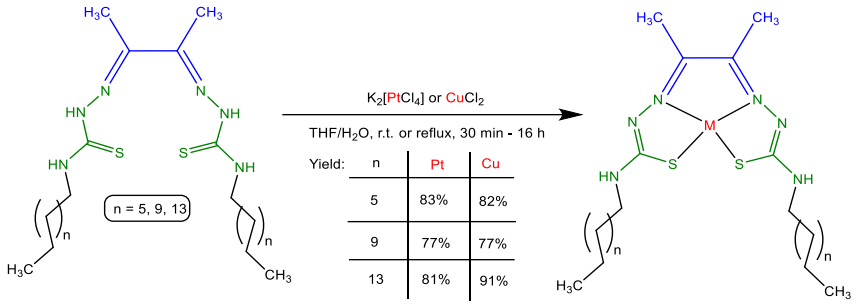


n				
5	98%	51%	60%	75%
9	95%	quant.	50%	79%
13	97%	40%	51%	88%

Yields for the condensation of the thiosemicarbazides with ketones or aldehydes

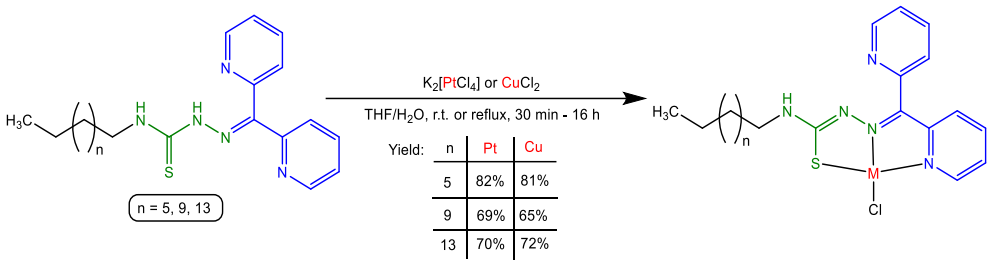
Scheme 61. Synthesis of TSCs with aliphatic chain at the *N*4 position.

The bis-TSCs were used in a second step to synthesize their corresponding Pt(II) and Cu(II) complexes (Scheme 62). For this, $K_2[PtCl_4]$ or $CuCl_2$ were reacted with the ligands in a mixture of THF/H_2O under reflux or at room temperature. It was found that the metal complexes can decompose under increased temperature, which usually requires a short reaction time, if the mixture was refluxed. Otherwise, the reaction can be performed at room temperature. However, the hexadecyl derivatives need increased temperature due to their poor solubility in the solvent mixture. The metal complexes were obtained in high yields.



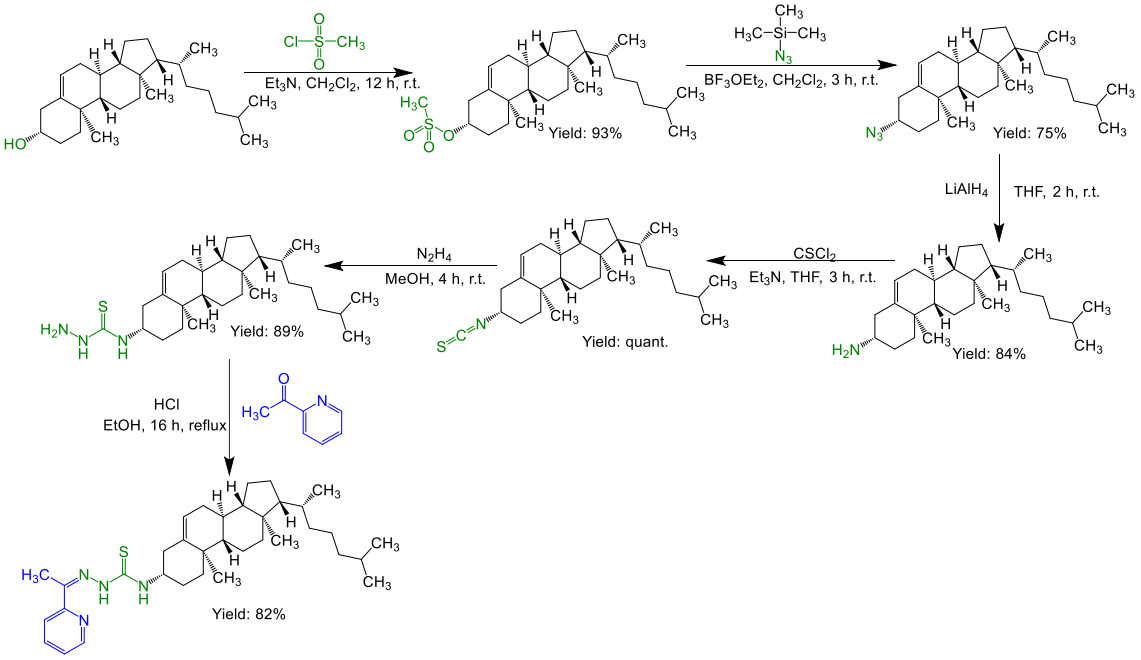
Scheme 62. Synthesis of bis-TSC complex Cu(II) and Pt(II).

For the synthesis of Pt(II) and Cu(II) complexes with di(2-pyridyl)ketone TSCs, the same reaction conditions were used (Scheme 63). Again, the metal complexes were obtained in high yields.



Scheme 63. Synthesis of di(2-pyridyl)ketone TSC complexs Cu(II) and Pt(II).

Besides these aliphatic TSCs, the structure of steroids was introduced at the *N*4 position. For this, cholesterol was used as the starting material (Scheme 64). First part of the synthesis was the substitution of the hydroxy function by an amine, which was successful in three reaction steps, following a protocol from literature.[351] First, a methyl sulfonyl ester is synthesized to introduce an appropriate leaving group, which is replaced by an azide in a second step. Finally, the azide is reduced to the amine, giving the amino steroid in high yields, which was used to synthesize the thiosemicarbazide using a similar protocol discussed before. The synthesis of the TSC needed some optimization. While the usage of AcOH as the catalyst led to no reaction conversion, HCl was a better choice which led to high yields for the condensation with 2-acetylpyridine (Scheme 64). However, the derivatization with di(2-pyridyl)ketone was not successful. Maybe, steric hindrance plays a role during the reaction.



Scheme 64. Synthesis of TSC with cholesterol at the *N*4 position.

3.5.2 UV/Vis absorption spectroscopy of amphiphilic TSCs and their metal complexes

As expected, the residue at the *N*4 position (octyl, dodecyl, hexadecyl) has no impact on the absorption properties of the compound (see appendix). By that reason, the absorption properties are discussed at the example of the octyl derivatives. The UV/Vis absorption spectra in MeOH are shown in Figure 78 and are summarized in Table 29.

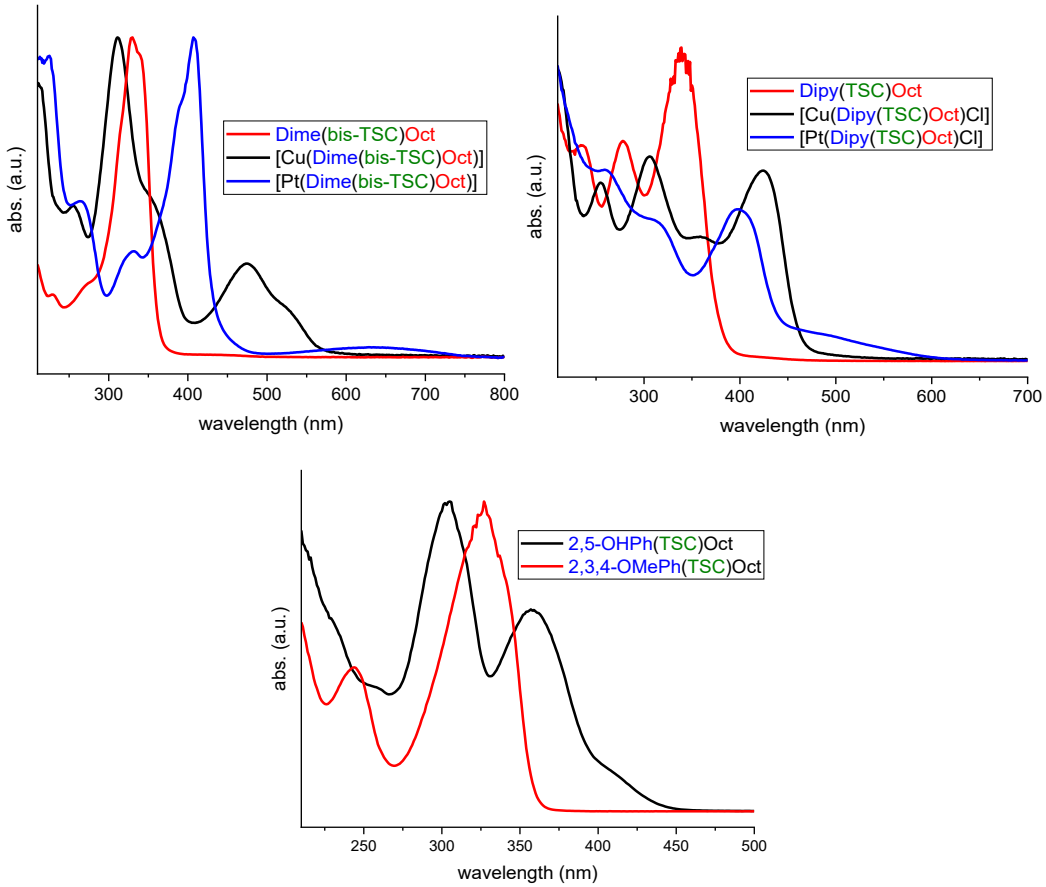


Figure 78. UV/Vis absorption spectra of dime(TSC)Oct and the corresponding Cu(II) and Pt(II) complexes (Top, left); Dipy(TSC)Oct and the corresponding Cu(II) and Pt(II) complexes (Top, right) and 2,5-OHPh(TSC)Oct and 2,3,4-OMePh(TSC)Oct (Bottom) in MeOH.

Table 29. UV/Vis absorption maxima of the amphiphilic TSCs and their metal complexes.[a]

Compound	λ_1 (nm)	λ_2 (nm)	λ_3 (nm)	λ_4 (nm)	λ_5 (nm)	λ_6 (nm)
Dime(bis-TSC)Oct	230	274 (s)	330	340 (s)	-	-
[Cu(Dime(bis-TSC)Oct)]	253	312	352 (s)	474	517 (s)	-
[Pt(Dime(bis-TSC)Oct)]	226	263	331	391 (s)	410	630
Dipy(TSC)Oct	235	277	340	-	-	-
[Cu(Dipy(TSC)Oct)Cl]	255	307	368	425	-	-
[Pt(Dipy(TSC)Oct)Cl]	260	307	398	490	-	-
2,5-OHPh(TSC)Oct	303	358	407 (s)	-	-	-
2,3,4-OMePh(TSC)Oct	243	473	-	-	-	-

[a] Measured in MeOH.

Dime(bis-TSC)Oct shows a broad maximum at 330 nm as well as a shoulder at 340 nm. In addition, a small maximum at 230 nm and an additional shoulder at 274 nm are observed. The spectrum is comparable to similar TSCs in literature (e.g. diacetyl bis(4,4-dimethyl-3-thiosemicarbazone).[352,353] The complexation of Cu(II) leads to a blue shift of the absorption bands, leading to two maxima at 253 and 312 nm as well as a shoulder at 352 nm. In addition to that, an additional absorption maximum at

474 nm as well as a shoulder at 517 nm are observed. This long-wavelength absorption was assigned to d-d transitions in literature.[352,353] In case of the corresponding Pt(II) complex, the absorption bands at short wavelength are bathochromic shifted. Here, four maxima at 226, 263, 331 and 410 nm are observed as well as a shoulder at 391 nm. In addition to that, a weak absorption maximum is found at 630 nm.

The Dipy(TSC)Oct shows the typical absorption spectra of dipyridyl ketone TSCs, which was already discussed in Chapter 3.1.2. The absorption maxima are found at 235, 277 and 340 nm. The UV/Vis absorption spectrum of the corresponding Cu(II) complex is in accordance with comparable compounds from literature.[354] The maxima are blue shifted in the metal complex, which are found at 255 and 307 nm. An additional maximum is found at 425 nm, which was assigned in the literature to a S → Cu(II) transitions (ligand to metal charge transfer, LMCT).[354] The absorption spectrum of the Pt(II) complex is in accordance with published results from our research group of comparable complexes.[222] The long wavelength absorption at 490 nm can be assigned to a MLCT. The absorption band in the UV region originate from π–π^* transitions of the ligand and are bathochromic shifted (260, 307 and 398 nm) compared to the ligand.

The absorption spectrum of 2,5-OHPh(TSC)Oct shows two maxima at 303 and 358 nm as well as a shoulder at 407 nm. The 2,3,4-OMePh(TSC)Oct has two maxima at 243 and 473 nm (Figure 78).

Since the synthesized compounds are soluble in polar and nonpolar solvents, their absorption properties can be analyzed in different solvents (pentane, toluene, methanol and H_2O) to investigate solvatochromic effects (Figure 79-81 and Table 30). In case of Dipy(TSC)Oct, a negative solvatochromism was found for the long-wavelength absorption which means that the absorption maximum is bathochromic shifted for nonpolar solvents: 360 nm (Pentane), 357 nm (Toluene), 337 nm (MeOH). In H_2O, the shape of the spectra differs most significantly. Here, it seems that the maximum is further shifted to 294 nm. Another weak absorption appears around 400 nm (Figure 79).

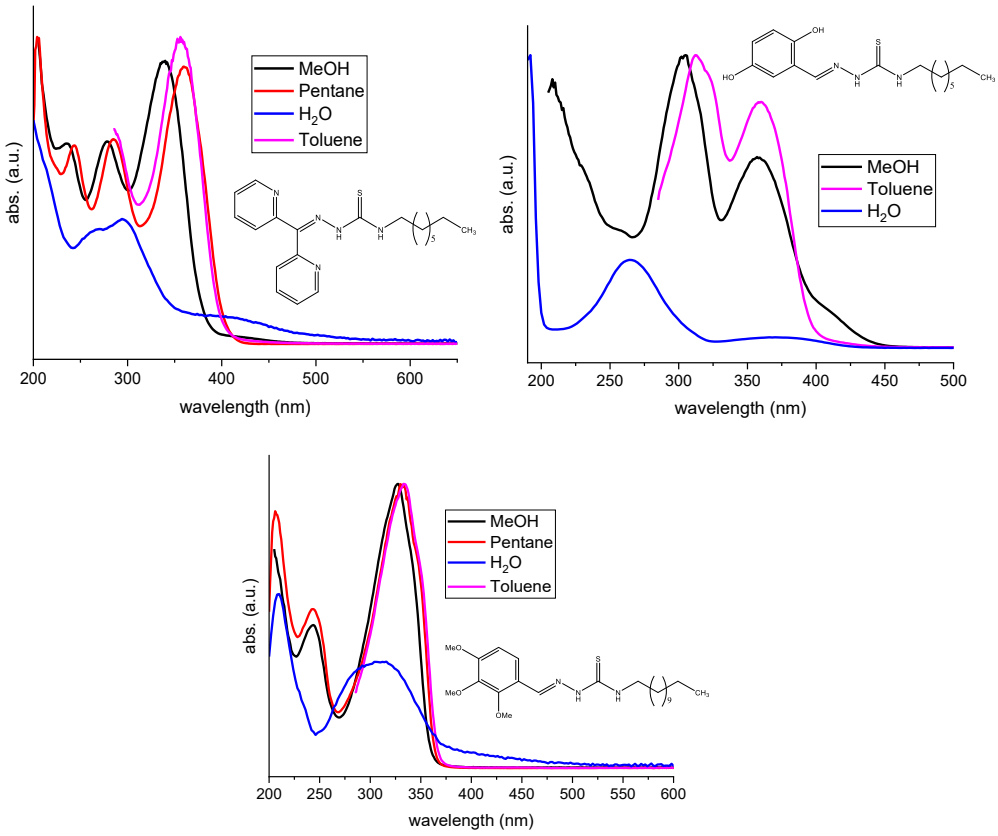


Figure 79. Top, left: UV/Vis absorption spectra of Dipy(TSC)Oct in MeOH, pentane, toluene and H_2O. Top, right: UV/Vis absorption spectra of 2,5-OHPh(TSC)Oct in MeOH, toluene and H_2O. Bottom: UV/Vis absorption spectra of 2,3,4OMePh(TSC)Dode in MeOH, pentane, toluene and H_2O.

The solvatochromism of the 2,5-OHPh(TSC)oct was less pronounced but again a hypsochromic shift of the two absorption maxima is found in MeOH (358 nm, 303 nm) compared to toluene (359 nm, 312 nm). In H_2O, the absorption spectrum differs significantly. One absorption maximum is found at 264 nm and an additional weak absorption at 370 nm (Figure 79).

Table 30. UV/Vis absorption maxim of the amphiphilic TSCs and their metal complexes.[a]

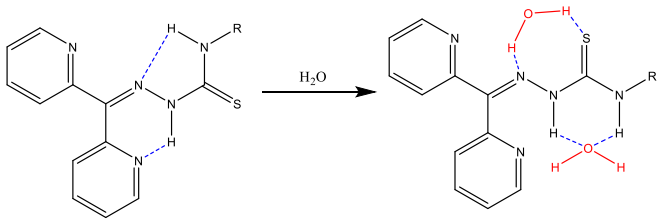
Compound	Pentane	Toluene	MeOH	H_2O
Dipy(TSC)Oct	244, 284, 360	355	235, 278, 339	268, 294, 405
2,5-OHPh(TSC)Oct	229, 257, 360	312, 359	230 (s), 257 (s), 303, 358	264, 370
2,3,4-OMePh(TSC)Dode	206, 243, 332	334	243, 327	210, 306
[Pt(Dipy(TSC)Dode)Cl]	-	329, 388 (s), 407, 534	259 (s), 310 (s), 399, 486	-
[Cu(Dipy(TSC)Dode)Cl]	-	303, 360, 442	254, 306, 423	205, 270, 298 (s), 390
[Pt(Dime(bis-TSC)Oct)]	225 (s), 277, 326, 378 (s), 390, 414, 663	335, 389, 410, 646	219, 264, 331, 392 (s), 407, 625	-
[Cu(Dime(bis-TSC)Oct)]	210, 259, 311, 358, 492, 545 (s)	315, 354 (s), 485, 536 (s)	210, 256, 311, 351 (s), 474, 520 (s)	-

[a] Measured in MeOH, pentane, toluene or H_2O.

The 2,3,4-OMePh(TSC)Dode shows the weakest solvatochromism of the analyzed ligands. Here, the maximum of the low energy absorption band is located at 332 nm (pentane), 334 (toluene) and 327 nm (MeOH). Again, the absorption properties in H_2O differ most significantly, with two maxima found at 210 nm and 306 nm (Figure 79).

A negative solvatochromism is usually explained by the fact that the electronic ground state is more polar than the excited state of the molecule. This means that the ground state has a higher dipole moment than the excited state. Thus, the stabilization of the ground state is increased in polar solvents, which leads to an increasing HOMO-LUMO gap and a blue shift.[355,356] The solvatochromism is more pronounced for charge transfer transitions. As mentioned in Chapter 3.1.2, the long wavelength transition is assigned to an intraligand charge transfer of the thione to the pyridine function of the TSC and can explain its sensitivity to different solvents. In addition, hydrogen bonding can affect the absorption properties of TSCs, which might explain the different behavior between these TSCs. While hydrogen bonding is probably more pronounced for the TSCs with pyridine or hydroxy functions, it is less favored for the TSCs with methoxy functions.

In H_2O, the absorptions properties change most drastically, since intermolecular hydrogen bonding will be most pronounced and intramolecular hydrogen bonds will be probably destroyed (Scheme 65). In MeOH, where hydrogen bonding is weaker compared to H_2O, a mixture of different species is probably found. This is supported by the fact that a weak shoulder is found around 420 nm in this solvent.



Scheme 65. Possible destruction of intramolecular hydrogen bonds by H_2O under the formation of intermolecular hydrogen bonds.

The bis-TSC complexes with Pt(II) and Cu(II) were measured in MeOH, toluene and pentane (Figure 80).

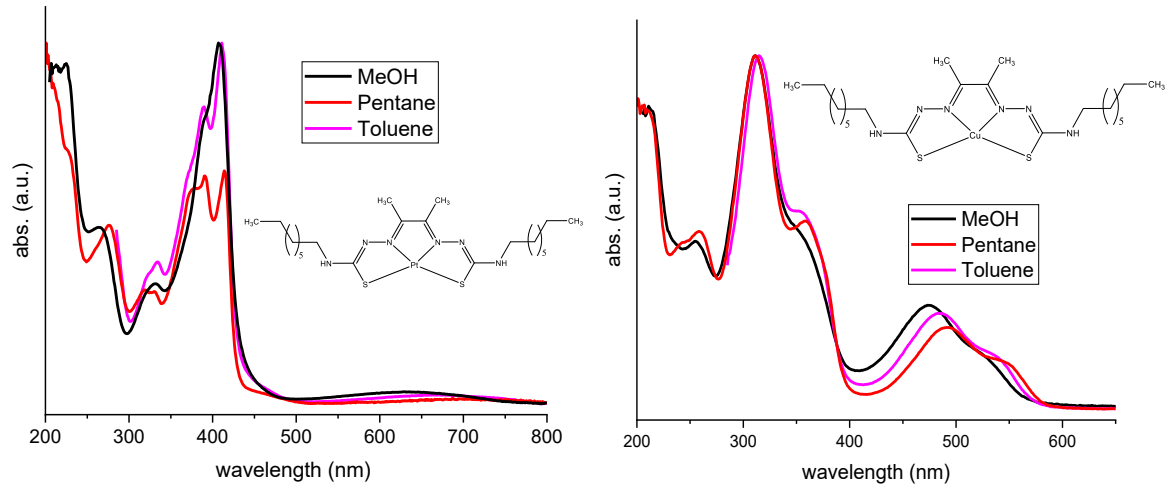


Figure 80. UV/Vis absorption spectra of [Pt(Dime(bis-TSC)Oct)] (left) and [Cu(Dime(bis-TSC)Oct)] (right) in MeOH, pentane and toluene.

Also, for these compounds a negative solvatochromism was observed (Table 30), for the low energy transitions around 650 nm ([Pt(Dime(bis-TSC)Oct)]) or rather 480 nm ([Cu(Dime(bis-TSC)Oct)]), which is in accordance with their charge transfer character. The intraligand transitions showed no significant solvatochromism. Similar results are found for the dipyridyl ketone TSC complexes with Cu(II) and Pt(II) (Figure 81).

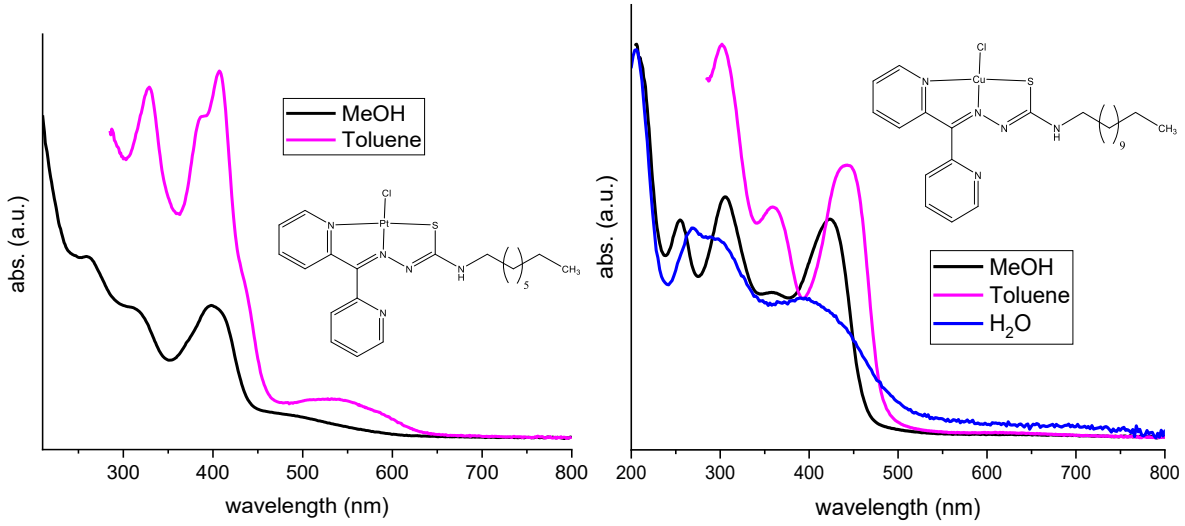


Figure 81. UV/Vis absorption spectra of [Pt(Dipy(TSC)Oct)Cl] (left) and [Cu(Dipy(TSC)Oct)Cl] (right) in MeOH, toluene and H_2O.

3.5.3 Cyclic voltammetry of amphiphilic TSCs and their metal complexes

The electrochemical properties were analyzed by CV. The bis-TSC shows three irreversible reductions in THF at –1.65 V, –2.67 V and –3.46 V (Referenced to $FeCp_2/FeCp_2^+$) (Figure 82). The first reduction is probably centered on the imine group, where the LUMO of the TSC is usually localized. The first oxidation is found at 0.89 V. After the complexation of Cu(II), a reversible reduction is found at –1.29 V which is attributed to the Cu(I)/Cu(II) redox couple (Figure 82).[357] The broadening of the reduction wave is probably related to a conformational rearrangement of the Cu(I) species to a tetrahedral conformation. A second, irreversible reduction is found at –3.19 V. The first oxidation is located at 0.20 V, which is reversible and attributed to the Cu(II)/Cu(III) redox pair. Compared to the first reduction, no broadening of the oxidation wave is found, which is in accordance with the exception, that the

conformation is not significantly changing for the Cu(III) species. A second, irreversible oxidation is at 0.89 V. The electrochemical properties of the TSC indicate that the compound will be able to redox cycle, which is an important requirement for its toxicity. The results are similar to the literature known Cu(II) atsm bis-TSC (diacetyl-bis(N4-methylthiosemicarbazone)), which is known for its cytotoxicity. As expected, the increasing alkyl chain length at the *N*4 position seems to not affect the redox properties of the TSC significantly, which is in accordance with the UV/Vis absorption measurements. Thus, tuning the lipophilicity by varying the length of the alkyl chain and tuning the redox properties by changing the substituents at the *N*1 position can be done independently.

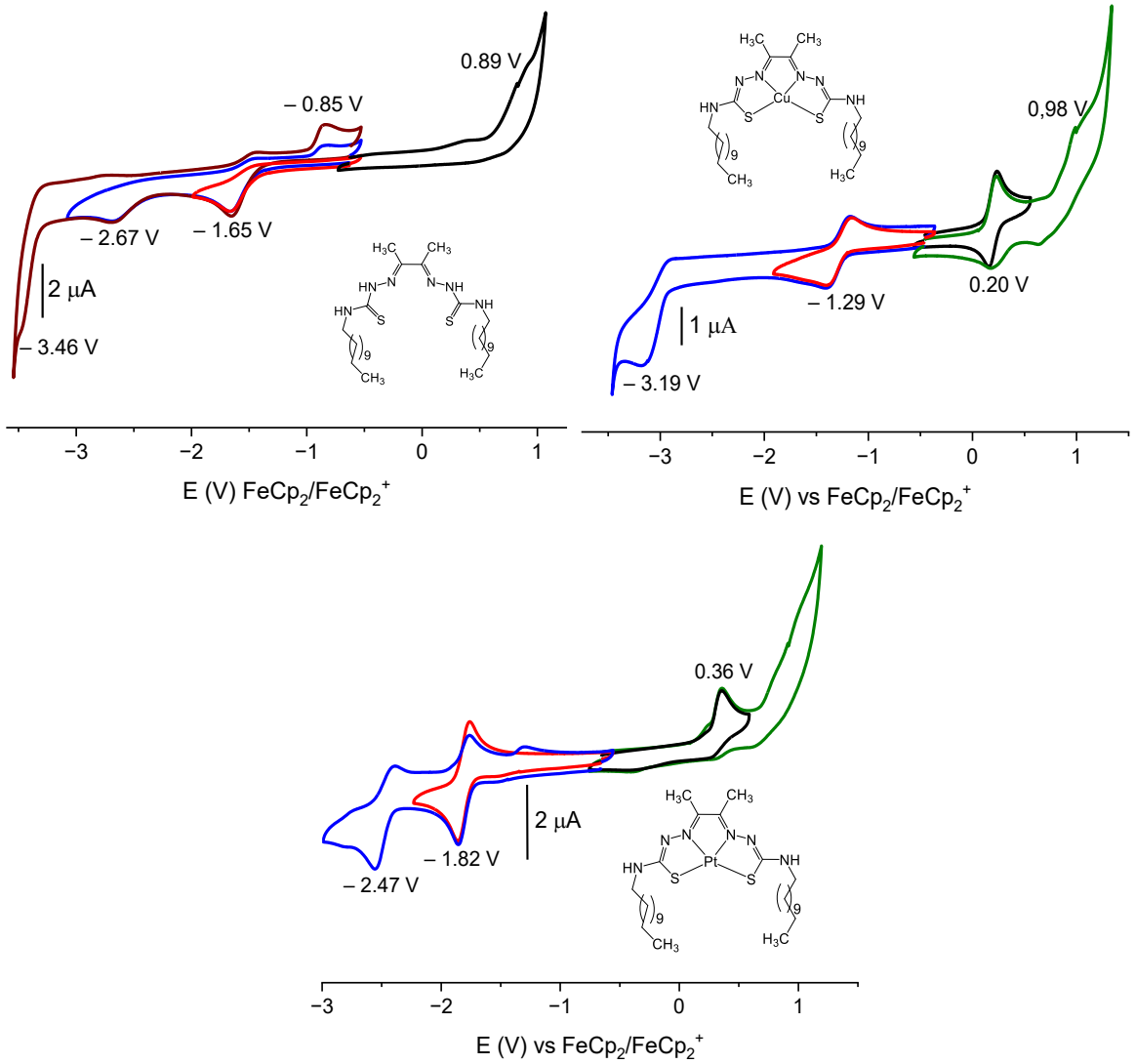


Figure 82. CVs of Dime(bis-TSC)Dode (Top, left), [Cu(Dime(bis-TSC)Dode)] (Top, right) and [Cu(Dime(bis-TSC)Dode)] (Bottom) measured in 0.1 M solution of nBu$_4$NPF$_6$ in THF at a scan rate of 100 mV/s, referenced against FeCp$_2$/FeCp$_2^+$.

The Pt(II) complex of the bis-TSC has two reversible reductions at –1.82 V and –2.47 V (Figure 82). However, for the second reduction, the process seems to be not fully reversible. The first oxidation is found at 0.36 V, which is irreversible. Surprisingly, examples of such bis-TSC Pt(II) complexes in literature are rare and their electrochemical properties were not analyzed yet.[358] However, by comparing with other bis-TSC complexes or other TSC complexes with Pt(II) it is expected that the first reduction is ligand centered and located at the imine. The second reduction might be also ligand centered, as already discussed for other Pt(II) complexes before (Chapter 3.4.3).

Dipy(TSC)Oct shows three irreversible reductions at –1.76, –2.38 and –2.85 V and an irreversible oxidation at 1.35 V (Figure 83). The observation is in accordance with literature and other results from

this research of dipyridyl ketone TSCs (Chapter 3.2.4). Again, the first reduction is probably located at the imine group. After complexation of Cu(II), four irreversible reductions are observed at –1.07, –2.23, –2.72 and –3.17 V. The first reduction can be assigned to the Cu(I)/Cu(II) redox couple, which seems to be partially reversible, and which is in accordance with literature.[95]An irreversible oxidation was found at 0.67 V. The corresponding Pt(II) complex shows two reversible reductions at –1.60 V and –2.20 V as well as two irreversible oxidations at 0.84 V and 0.47 V. The observations are in accordance with Pt(II) complexes in Chapter 3.4.3.

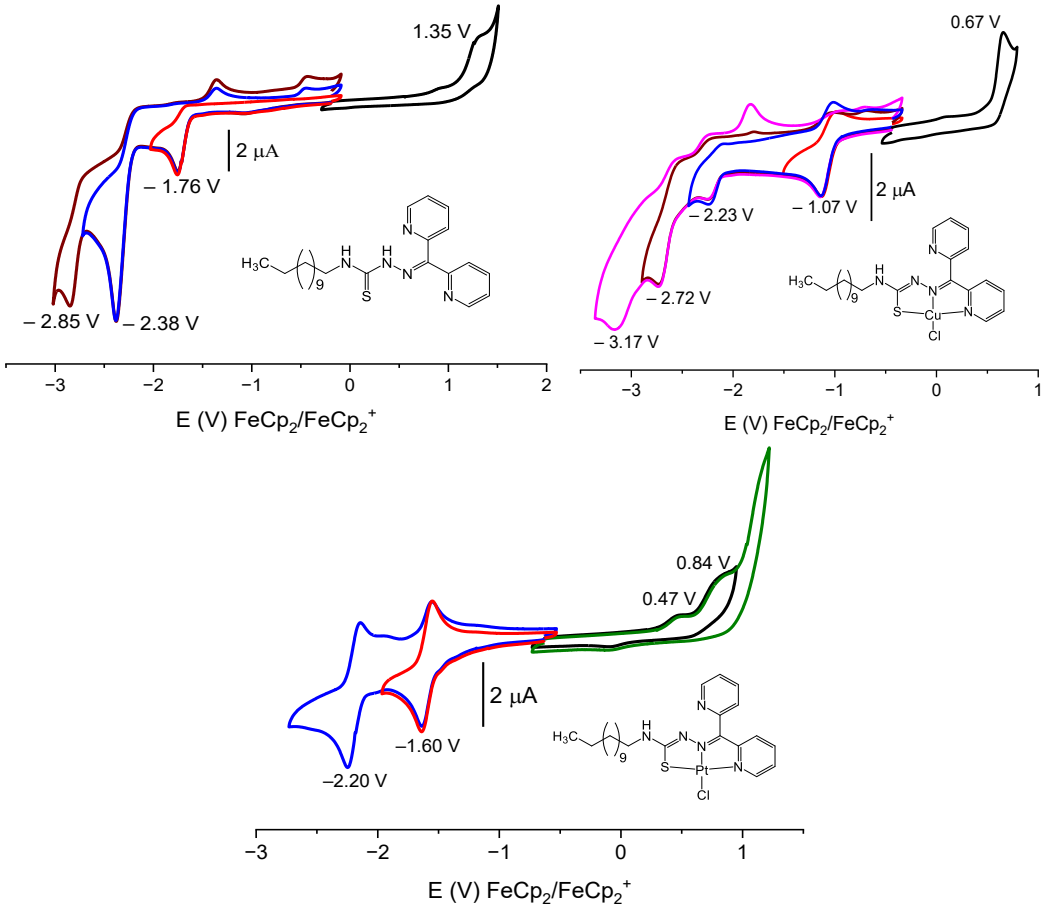


Figure 83. CVs of Dipy(TSC)Dode (Top, left), [Cu(Dipy(TSC)Dode)Cl] (Top, right) and [Pt(Dipy(TSC)Dode)Cl] (Bottom) measured in 0.1 M solution of nBu$_4$NPF$_6$ in THF at a scan rate of 100 mV/s, referenced against FeCp$_2$/FeCp$_2^+$.

The cyclic voltammograms of the 2,5-OHPh(TSC)Dode and 2,3,4-OMePh(TSC)Dode are shown in the appendix.

3.5.4 Cytotoxicity of amphiphilic TSCs

The cytotoxicity of the octyl and cholesterol derivatives was analyzed by MTT assays. The experiments were performed in a similar way described in Chapter 3.1.3. The % inhibition of HepG2, HCT-116 and HEK-293 at a concentration of 50 µM is shown in Table 31. The highest % inhibition of the cells was found for Dipy(TSC)Oct. Against HepG2 and HCT-116 the inhibition was even higher than for cisplatin, which was used as a positive control. However, also the healthy HEK-293 cells are affected by this compound, but the inhibition was at least smaller than for cisplatin. For the corresponding Pt(II) complex, the toxicity against HepG2 and HCT-116 was significantly reduced, while the toxicity against HEK-293 remained in a similar magnitude.

Table 31. % Inhibition of HepG2, HCT-116 and HEK-293 by the tested TSCs at a concentration of 50 µM.[a]

Compounds	HepG2	HCT-116	HEK-293
	% Inhibition at 50 µM±SD		
Dipy(TSC)Oct	77.51 ± 2.03	93.38 ± 1.32	87.80 ± 1.06
[Pt(Dipy(TSC)Oct)Cl]	54.36 ± 1.42	41.36 ± 1.32	88.31 ± 2.8
[Cu(Dipy(TSC)Oct)Cl]	67.26 ± 1.13	47.67 ± 1.71	87.06 ± 3.21
[Cu(Dime(bis-TSC)Oct]	43.48 ± 1.88	42.50 ± 1.14	76.26 ± 1.72
[Pt(Dime(bis-TSC)Oct]	39.25 ± 1.22	30.50 ± 0.96	73.08 ±1.55
2,5-OHPh(TSC)Oct	43.30 ± 1.52	42.91 ± 1.20	79.71 ± 2.21
2,3,4-OMePh(TSC)Oct	45.27 ± 1.18	47.77 ± 0.734	87.06 ± 2.27
MePy(TSC)Chol	57.24 ± 1.07	47.67 ± 1.03	69.40 ± 1.41
Cisplatin	67.32 ± 2.12	75.32 ± 1.24	97.33 ± 2.31

[a] The values were determined in an MTT assay.

A similar observation was made for the corresponding Cu(II). However, the inhibition against HepG2 was comparable to that of cisplatin (67.26%). For all the other tested TSCs, the % inhibition of HepG2 and HCT-116 was significantly lower which ranges between 57-30%. Unfortunately, the HEK-293 cells are more affected by these compounds with % inhibitions of 87-69%. In the future detailed investigations of the cytotoxicity will be necessary including increased incubation times and the determination of IC_{50} values.

3.5.5 Summary – Amphiphilic TSCs

TSCs with lipophilic groups at the *N*4 position (octyl, dodecyl, hexadecyl, cholesterol) have been successfully synthesized. Their *N*1 position was functionalized with di(2-pyridyl)ketone, 2,5-dihydroxybenzaldehyde, 2,3,4-trimethoxybenzaldehyde and butane-2,3-dione and Pt(II) and Cu(II) complexes with the corresponding dipyridyl and bis-TSC were synthesized. Their solubility in pentane, toluene, MeOH and H_2O were explored to investigate if they show an amphiphilic behavior. Most of the TSCs were soluble in polar (MeOH) and nonpolar (toluene) solvents but had a limited solubility in H_2O. In the future, a second generation of TSCs should be synthesized which have a charge at the TSC function to improve their H_2O solubility. UV/Vis absorption spectra were measured in pentane, toluene, MeOH and H_2O. Depending on the TSC, it was possible to record spectra in all these solvents and their solvatochromism was investigated. Most of them showed a pronounced negative solvatochromism. Their electrochemistry was explored by CV. The Cu(II) and P(II) showed the characteristic redox process, discussed in the literature before. In the last step, the cytotoxicity of the compounds was investigated against HepG2, HCT-116 and HEK-293. Thereby, Dipy(TSC)Oct showed a remarkable cytotoxicity, which was reduced after the complexation of Pt(II) and Cu(II).

3.6 Hexadentate bis-TSCs

Several hexadentate bis-TSCs and TSCs have been synthesized during this research, which are stable under ambient conditions. By synthesizing the corresponding diketones or dialdehydes, bipyridine (Bipy), phenanthroline (Phen), diyrido[3,2-a:2′,3′-c]phenazine (DPPZ), naphthyridine (Naph), dithieno[3,2-b:2′,3′-d]thiophen (DTT) and 2,2′-(1,3-phenylene)bis[pyridine] (PyPhPy) have been successfully introduced into their structure (Chart 22). Thiosemicarbazides, derived from amino acids (Chapter 3.3.1), have been reacted with these dialdehydes/ketones to synthesize their bis-TSCs. The amino acid function at the *N*4 position drastically increased their solubility in organic solvents, compared to the dialdehydes/ketones. Deprotection of their carbon acid function can give them the opportunity to use them for nano -or bioconjugation which was not tested during this research. Another TSC has been synthesized which has a terpyridine (Tpy) function at the *N*4 position, while the *N*1 position was functionalized with di(2-pyridyl)ketone (Chart 22). This compound is an example of a hexadentate TSC, which is not a bis-TSC, and which offers two different binding pockets namely a *S^N^N* and a *N^N^N* pocket.

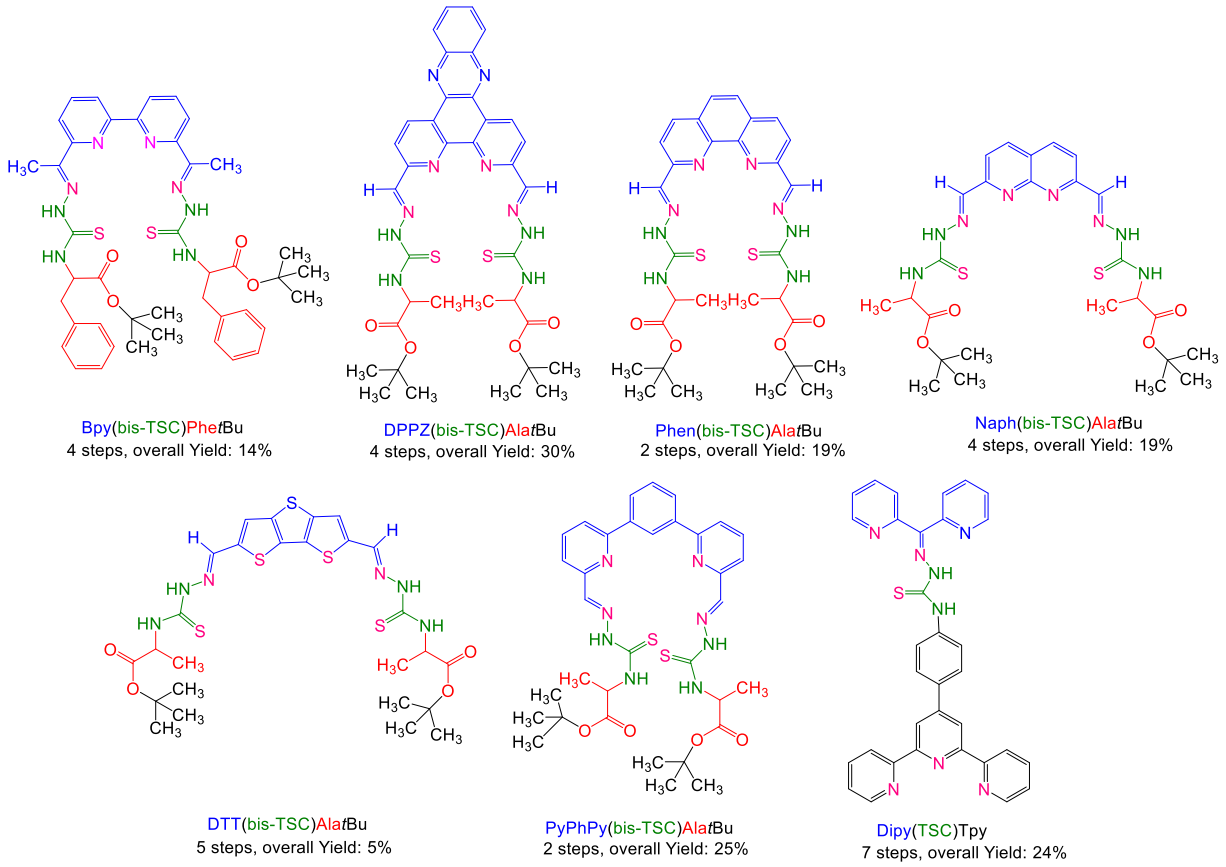


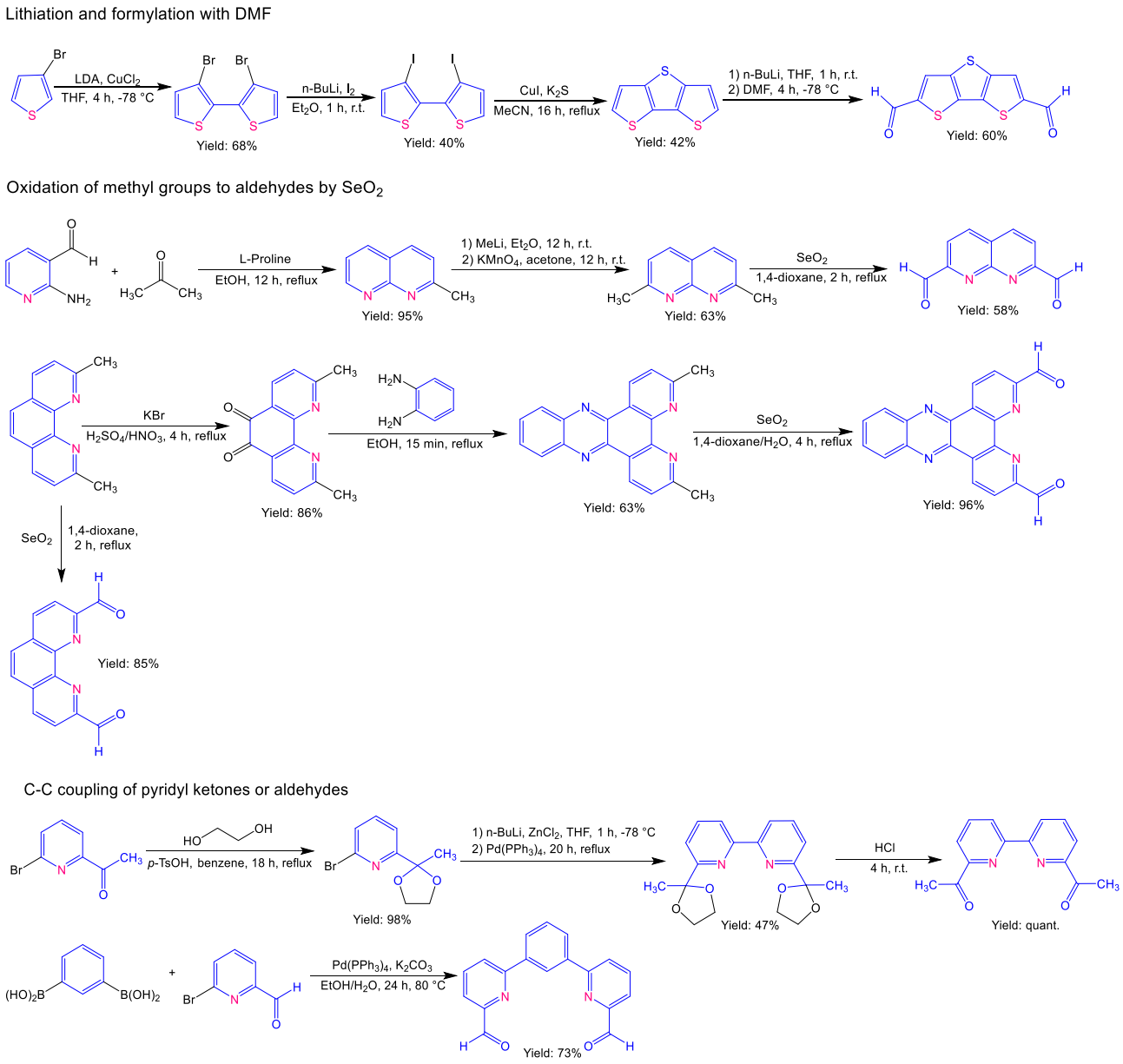
Chart 22. Overview about the successfully synthesized hexadentate TSCs.

Their metal complexes were not in the focus of this research. Instead, the ligand design and their characterization were in the focus of this research.

3.6.1 Synthesis of hexadentate TSCs

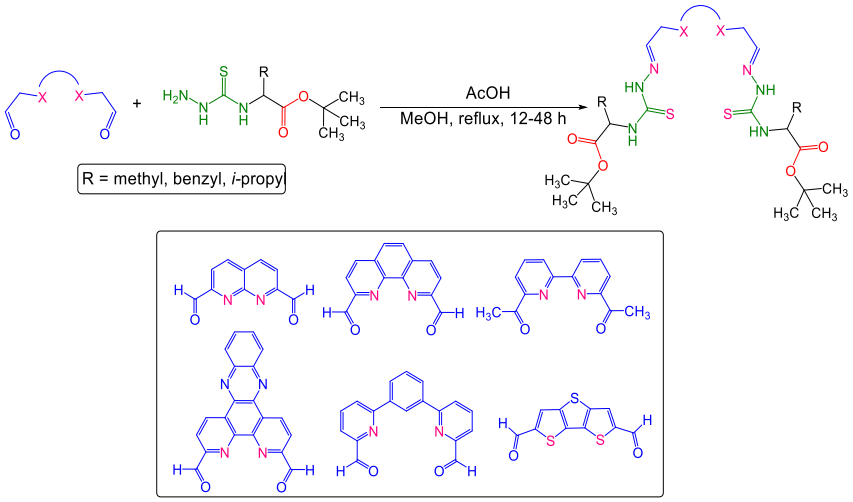
First step during the synthesis of hexadentate bis-TSCs was the synthesis of dialdehydes or diketones, which offer two additional coordination sites in α-position. For this, protocols from literature were used.[359-363] The key step during their synthesis is always the introduction of aldehyde functions which can be divided into three general methods (Scheme 66). The first one is the lithiation of heteroaromates at the α-position, which is followed by a formylation using DMF. This method was used for DTT. The

second method is a *Riley* oxidation which oxidizes methyl groups at the α-position of *N*-heteroaromates, using SeO_2. This method was used for Naph, Phen and DPPZ. The third method is the C—C cross coupling of pyridyl ketones and aldehydes, which was used for Bpy and PyPhPy.



Scheme 66. Overview about the synthesis of diketones and dialdehydes with donor atoms at the α-position.

The dialdehydes have been reacted with alanine, valine or phenylalanine thiosemicarbazide using AcOH as a catalyst (Scheme 67). When HCl was used instead of AcOH, the carbon acid function can be directly deprotected in one step. However, this was found to be a disadvantage for the condensation reaction and should be done in a separate step. The corresponding bis-TSC were obtained in moderate or poor yields (Table 32). It is expected that also the mono TSCs are formed as a side product in this reaction, which can be favored due to steric hindrance. By that reason, this step will need some optimization of the reaction conditions in the future.

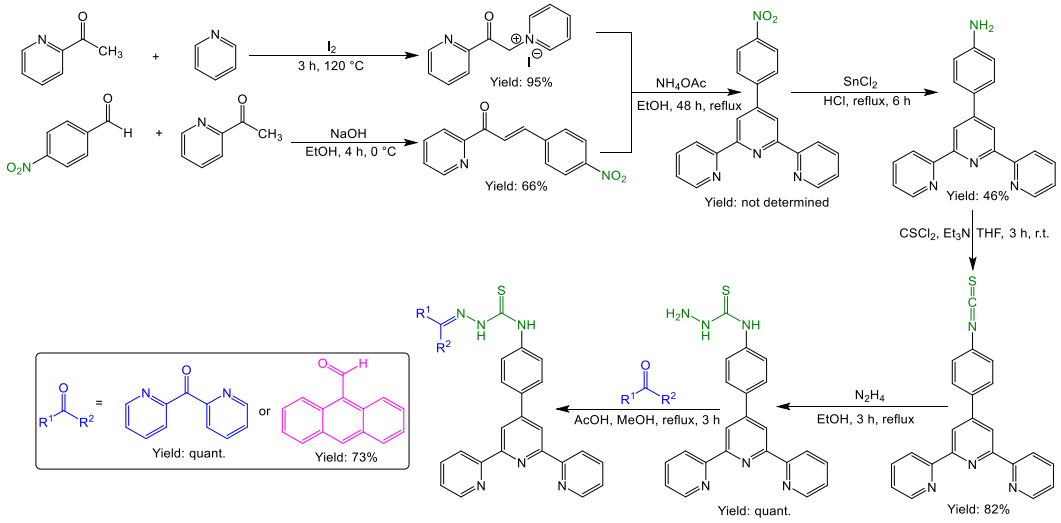


Scheme 67. Synthesis of hexadentate bis-TSC from dialdehydes/diketones and alanine, valine or phenylalanine thiosemicarbazide.

Table 32. Yields for the synthesis of hexadentate bis-TSCs

	Naph	Phen	Bpy	DPPZ	PyPhPy	DTT
Alanin thiosemicarbazide	37%	22%	-	58%	34%	78%
Valin thiosemicarbazide	40%	-	-	-	39%	-
Phenylalanine thiosemicarbazide	-	-	30%	-	-	-

For the synthesis of TSCs with Tpy residue at the *N*4 position, 4-[2,2′:6′,2″-terpyridin]-4′-ylbenzenamine was used as a precursor which was synthetized in four reaction steps (Scheme 68).[364] Firstly, 1-[2-oxo-2-(2-pyridyl)ethyl]pyridinium iodide was synthesized by the reaction of 2-acetylpyridine and I_2 in pyridine, which was obtained in 95% yield. After that, 3-(4-nitrophenyl)-1-(2-pyridinyl)-2-propen-1-one was synthesized by an aldol condensation of 4-nitrobenzaldehyde and 2-acetylpyridine using NaOH as a catalyst (Yield: 66%). Both precursors were reacted in a *Kröhnke* pyridine synthesis yielding the 4′-(4-nitrophenyl)-2,2′:6′,2″-terpyridine, which was directly reduced to the amine using $SnCl_2$ (Yield: 46%). The amino terpyridine was reacted with thiophosgene yielding isothiocyanate in 82%, followed by its reaction with hydrazine, giving the thiosemicarbazide in quantitative yields. In a final step, the thiosemicarbazide was reacted with di(2-pyridyl)ketone (Yield: quant) or 9-antraaldehyde (Yield: 73%) to the TSCs.



Scheme 68. Synthesis of Dipy(TSC)Tpy and Anth(TSC)Tpy *via* 4-[2,2′:6′,2″-terpyridin]-4′-ylbenzenamine.

3.6.2 UV/Vis absorption and emission spectroscopy of hexadentate TSCs

The TSCs have been analyzed by UV/Vis absorption spectroscopy (Figure 84 and Table 33). The Bpy(bis-TSC)Phe*t*Bu has a pyidyl and methyl group at the *N*1 position. In this way, it is structurally related to PyMe(TSC)NH_2 discussed in Chapter 3.2.3. This is in accordance with the absorption properties of this compound which also shows two absorption bands at 230 nm and 325 nm. Another, structural related compound in this series is the PyPhPy(TSC)Ala*t*Bu. Here, the pyridine units are not directly connected to each other (as for Bpy) but instead by a phenyl spacer. This compound shows two absorption maxima around 240 nm and 260 nm and a broad shoulder between 300-350 nm.

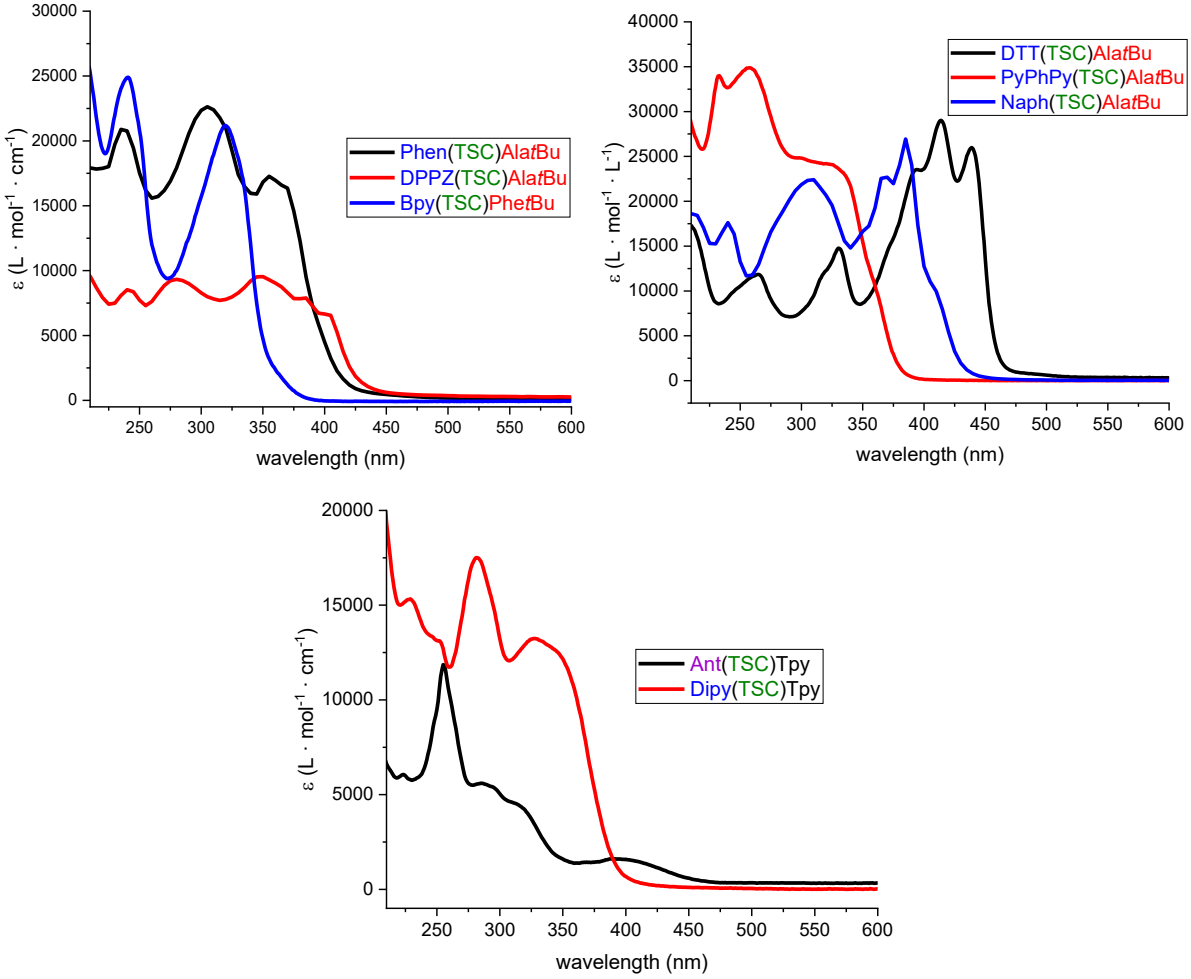


Figure 84. UV/Vis absorption spectra of Phen(TSC)Ala*t*Bu, DPPZ(TSC)Ala*t*Bu and Bpy(TSC)Ala*t*Bu (Top, left); DTT(TSC)Ala*t*Bu, PyPhPy(TSC)Ala*t*Bu and Naph(TSC)Ala*t*Bu (Top, right) and Dipy(TSC)Tpy and Ant(TSC)Tpy (Bottom) measured in MeCN.

Table 33. UV/Vis absorption maxima of the hexadentate TSCs.[a]

Compound	λ_1 (nm), ε (L · cm^{-1} · mol^{-1})	λ_2 (nm), ε (L · cm^{-1} · mol^{-1})	λ_3 (nm), ε (L · cm^{-1} · mol^{-1})	λ_4 (nm), ε (L · cm^{-1} · mol^{-1})	λ_5 (nm), ε (L · cm^{-1} · mol^{-1})
Phen(bis-TSC)Ala*t*Bu	240, 20760	305, 22630	355, 17270	370 (sh), 16360	-
DPPZ(bis-TSC)Ala*t*Bu	240, 8540	280, 9330	350, 9540	385 (sh), 7890	405 (sh), 6550
Bpy(bis-TSC)Phe*t*Bu	239, 24890	320, 21190	-	-	-
DTT(bis-TSC)Ala*t*Bu	266, 11780	330, 14590	394, 23540	415, 28900	440, 25840
PyPhPy(bis-TSC)Ala*t*Bu	233, 34000	257, 34890	322 (sh), 24180	-	-
Naph(bis-TSC)Ala*t*Bu	240, 17620	310, 22410	370, 22680	385, 26940	410 (sh), 9960
Anth(TSC)Tpy	223, 6030	255, 11860	288 (sh), 5560	314 (sh), 4520	396, 1590
Dipy(TSC)Tpy	228, 15270	249 (sh), 13130	283, 17510	327, 13240	344 (sh), 12510

[a] Measured in MeCN. Sh = shoulder.

The Phen(bis-TSC)Ala*t*Bu can be also considered as a structural expansion of Bpy(bis-TSC)Phe*t*Bu, where the two pyridine rings are merged by a phenyl ring in the backbone. In comparison, this compound has an additional absorption maximum and a shoulder around 365-375 nm. In case of DPPZ(bis-TSC)Ala*t*Bu the π-system is further expanded compared to Phen(bis-TSC)Ala*t*Bu. It seems that the absorption maxima around 365-375 nm are bathochromic shifted to 390 nm and 420 nm for this compound. An additional maximum is found at 350 nm.

The DTT(bis-TSC)Ala*t*Bu and Naph(bis-TSC)Ala*t*Bu have a completely different backbone making them difficult to compare with the other bis-TSCs. The DTT(bis-TSC)Ala*t*Bu shows five absorption maxima at 266, 330, 394, 415 and 440 nm. The Naph(bis-TSC)Ala*t*Bu has four maxima at 240, 310, 370 and 385 nm as well as a shoulder at 410 nm.

The last group of TSCs prepared have a Tpy unit at the *N*4 position, while the *N*1 position was functionalized with di(2-pyridyl) ketone or 9-anthraldehyde. The Dipy(TSC)Tpy shows three maxima at 228, 283 and 327 nm and two additional shoulders at 249 nm and 344 nm. The shape of the spectra of Ant(TSC)Tpy has some similarities. The compound has three maxima at 223, 255 and 396 nm and two shoulders at 288 nm and 314 nm. The maximum at 396 nm can be assigned to the anthracene motif.

The TSCs with DPPZ, DTT, Phen and Naph motif in the backbone were analyzed by UV/Vis emission spectroscopy since these groups are known in literature to show fluorescence (Figure 85 and Table 34).[365-367] The maximum of Phen(bis-TSC)Ala*t*Bu at 456 nm is the bluest shifted emission of all the compounds. This is followed by Naph(bis-TSC)Ala*t*Bu (465 nm) and DTT(bis-TSC)Ala*t*Bu (466 nm and 484 nm). The emission of DPPZ(bis-TSC)Ala*t*Bu is the most bathochromic emission in this series with a maximum located at 552 nm.

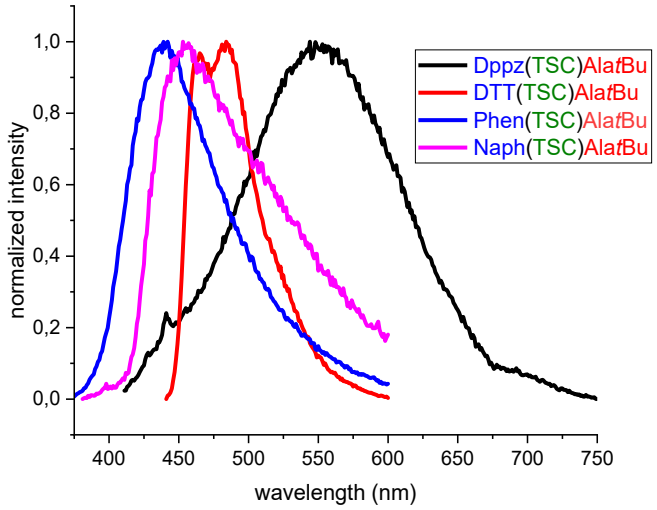


Figure 85. Normalized emission spectra of DPPZ(TSC)Ala*t*Bu (Excitation: 390 nm), DTT(TSC)Ala*t*Bu (Excitation: 420 nm), Phen(TSC)Ala*t*Bu (Excitation: 340 nm) and Naph(TSC)Ala*t*Bu (Ecitation: 365 nm) in MeCN at room temperature

Table 34. Emission maxima of DPPZ(TSC)Ala*t*Bu, DTT(TSC)Ala*t*Bu, Phen(TSC)Ala*t*Bu and Naph(TSC)Ala*t*Bu.[a]

Compound	Dppz(bis-TSC)Ala	DTT(bis-TSC)Ala	Phen(bis-TSC)Ala	Naph(bis-TSC)Ala
λ_1 (nm)	552	466	441	456
λ_2 (nm)	-	484	-	-

[a] Measured in MeCN at room temperature.

3.6.3 Summary – Hexadentate bis-TSCs

New hexadentate TSCs with Bpy, Phen, DPPZ, Naph, DTT, Tpy and PyPhPy in their structure have been successfully synthesized and characterized by HR-ESI-MS, NMR spectroscopy and UV/Vis absorption and emission spectroscopy. Thereby, DPPZ(TSC)Ala*t*Bu, DTT(TSC)Ala*t*Bu, Phen(TSC)Ala*t*Bu and Naph(TSC)Ala*t*Bu showed a characteristic fluorescence assigned to their heterocyclic backbone. Metal complexation of these ligands is not discussed in this research but is currently explored in bachelor and master thesis in the research group of Prof. Dr. Axel Klein. The complexation of bio abundant metals like Cu, Zn or Fe as well as the synthesis of bimetallic complex using these ligands are two examples for further research in the future.

4. Summary and Outlook

A total of 83 new TSCs and 24 TSC metal complexes (Cu(II), Pt(II) and Fe(III)) have been synthesized, which underlines the focus on ligand design in this work. In addition to that, many new isothiocyanates and thiosemicarbazides have been synthesized as intermediates. Especially the number of 27 new thiosemicarbazides is an important goal, since it offers the opportunity to synthesize countless numbers of new TSCs by condensation with ketones or aldehydes. A huge focus of this work was on the derivatization of the *N*4 position of the TSC, which was done to a minor extent in the literature before. Here, it was possible to introduce functional groups for bio and nanoconjugation, aliphatic groups for tuning the lipophilicity and fluorophores as a tag. On the other hand, the *N*1 position was derivatized with anthracene aldehyde as a fluorescence tag, hydrophilic aldehydes to modify the hydrophilicity of the TSCs, heteroaromatic dialdehydes to tune the denticity of the TSCs and α-pyridyl ketones to tune the cytotoxicity and redox potential of the corresponding Fe(III) complexes (Figure 86).

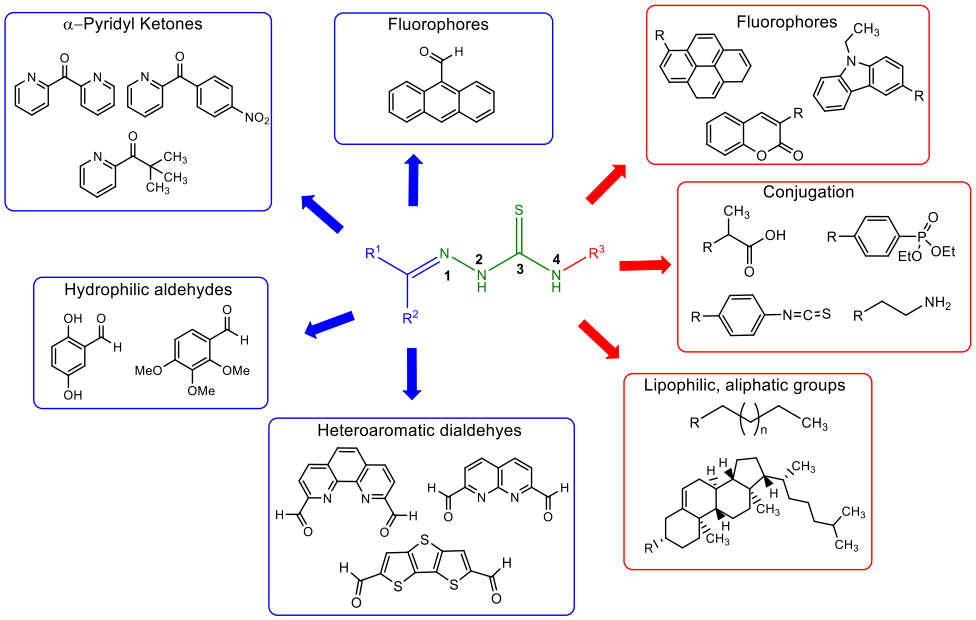


Figure 86. Overview of the functionalization of the *N*1 and *N*4 position of TSCs, which was explored in detail during this research.

In this way, a certain expertise on the synthesis of TSCs was developed during this research, which ended up in some important recommendations for their synthesis and ligand design:

1) The synthesis of isothiocyanates as intermediates using thiophosgene, usually leads to quantitative yields. Nucleophilic groups should be protected to avoid side reactions.

2) The reaction of isothiocyanates with hydrazine to thiosemicarbazide can be a key step. Side reactions with hydrazine are often observed. Therefore, the reaction should be performed at room temperature. Also, the stability of the thiosemicarbazide can have limitations.

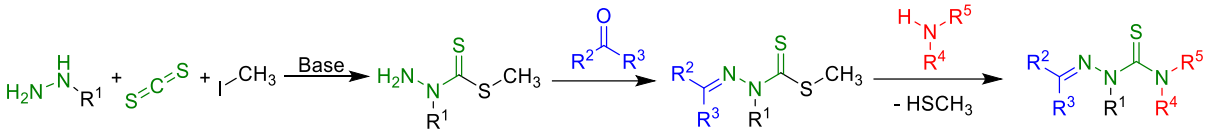
3) For the condensation of thiosemicarbazides and ketones/aldehydes, the choice of the acid catalyst (e.g. AcOH, HCl) can have a huge impact on the yield.

4) Aliphatic and aromatic groups can be usually attached to the *N*4 position, without any limitations except for the poor solubility of lipophilic residues.

5) For introducing functional groups at the *N*4 position, a rigid spacer function between the TSC and the functional group is often necessary.

6) The condensation of highly electrophilic ketones with thiosemicarbazides can fail, due to a limited stability of the TSC.

Although the functionalization of the *N*4 position worked quite well for many different residues, some limitations were found (e.g. bromide, alkoxysilanes, sulfonic acids, porphyrin, fluoresceine), which did not tolerate the reaction conditions (thiophosgene and hydrazine). In the future, a different approach could be used, which starts with the synthesis of a *S*-methyl dithiocarbazate, followed by the condensation with ketones and aldehydes (Scheme 69). In the final step, the S-methyl group can be substituted with amines. In this way, the residue at the *N*4 position is introduced in the last step and harsh reaction conditions can be avoided.



Scheme 69. Alternative approach for the synthesis of TSCs in the future. The *N*4 position is functionalized in the final step.

Beside this general investigation of the ligand design, the idea of this work was to investigate concepts for improving the medical performance of TSCs (Chapter 2): 1) by their conjugation to nanoparticles and 2) biomolecules, 3) their labeling with fluorescence markers, 4) their design towards amphiphilic structures, 5) increasing their coordination sphere to hexadentate ligands and 6) tuning the Fe(II)/(III) redox potential of α-pyridyl TSC as well as their conjugation to TiO_2 nanoparticles (Figure 87).

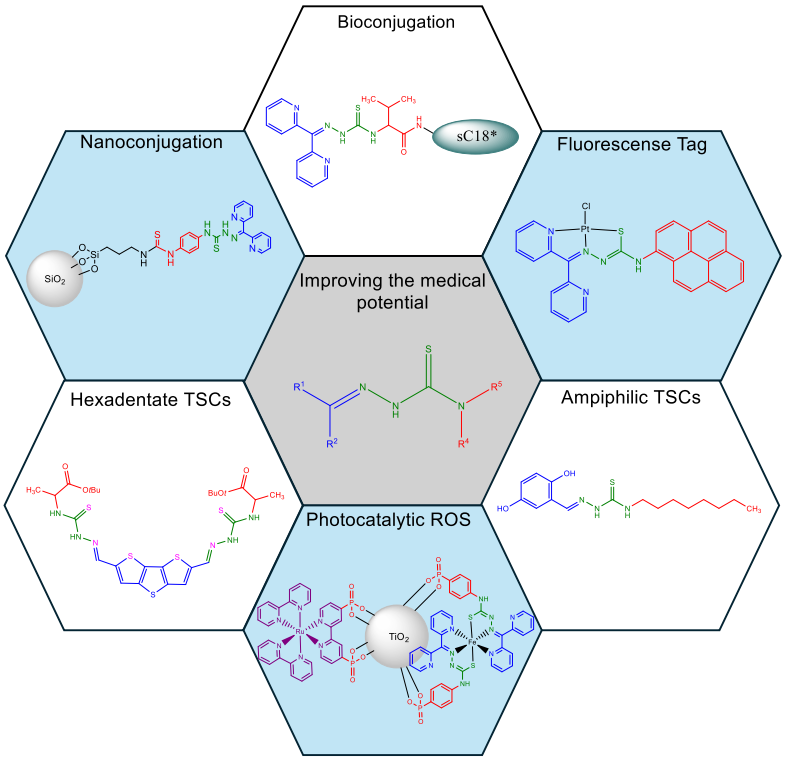


Figure 87. Overview of the investigated concepts to improve the medical performance of TSCs.

To link TSCs covalently to nanoparticles, several functional groups have been attached to the *N*4 position in their structure. In this way, amine, thiol, azide, alkyne, phosphonate, diol and isothiocyanate functions were successfully introduced. The compounds were characterized by NMR, UV/Vis absorption and emission spectroscopy as well as HR-ESI-MS. In addition, their cytotoxicity was investigated, where Dipy(TSC)PhNCS, Dipy(TSC)PhNH$_2$ and Dipy(TSC)PhPO(OEt)$_2$ showed the strongest inhibition of HepG2 and HCT-116, which was even higher than for cisplatin. Their conjugation was tested at the example of molecular reactions. Dipy(TSC)PhNCS and Dipy(TSC)PhNH$_2$ showed a successful conjugation to isocyanates or amines by the formation of a urea or thiourea. The Cu(I)

catalyzed click reaction with azide and alkyne functionalized TSCs was unsuccessful and starting material was reisolated, whereby several substrates and reaction conditions have been tested. In the future, this reaction should be investigated in more detail to find optimizations. In a final step, several nanoconjugates with SiO_2 and TiO_2 particles have been synthesized and characterized by FTIR and UV/Vis absorption spectroscopy as well as Zeta, DLS and EDX measurements. In this way, frame conditions for the synthesis of TSC nanoconjugates have been successfully developed, which includes the synthesis of linkable TSCs and their spectroscopic and cytotoxic characterization. In addition, methods for their conjugation have been successfully developed. To answer the question, if nanoconjugation can improve their medical performance, further characterization of the nanoconjugates will be necessary in the future, which includes cytotoxicity studies (Figure 88).

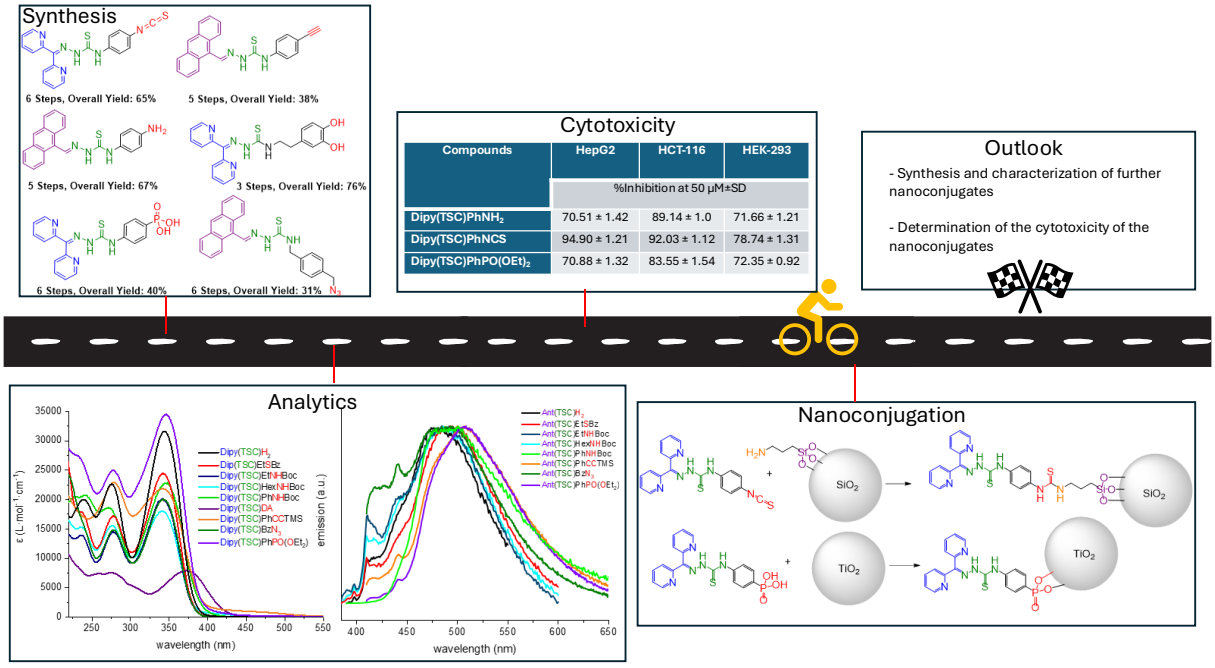


Figure 88. Overview of the progress for the application of TSCs in nano conjugation including upcoming tasks for the future.

To investigate how the Fe(II)/(III) redox potential is affected by the ligand design, α-pyridyl TSCs with electron donating or withdrawing substituents (Me, *t*Bu, Ph, Py, COOMePh, CF_3Ph, OMePh, NO_2Ph) at the *N*1 position have been successfully synthesized, as well as their corresponding Fe(III) complexes. The compounds were characterized by NMR and UV/Vis absorption spectroscopy as well as cyclic voltammetry. It was found that the substituents significantly affect the Fe(II)/(III) redox potential, which is cathodically shifted for electron donating substituents, while electron withdrawing groups lead to an anodic shift. In this way, $[Fe(tBuPy(TSC)H_2)_2]ClO_4$ showed the most negative potential (–0.63 V) and $[Fe(NO_2PhPy(TSC)H_2)_2]ClO_4$ the most positive potential (–0.40 V). In the future, the cytotoxicity of these compounds should be investigated in more detail. After that, $[Fe(Dipy(TSC)PhPO(OH)_2]$ was synthesized as well as $[Ru(bipy)_2(bipy(PO(OH)_2)_2]$ as a photosensitizer and their immobilization on TiO_2 NPs was investigated. The nanoconjugates were analyzed by FTIR and UV/Vis absorption spectroscopy as well as EDX measurements. While the synthesis of TiO_2@$[Fe(TSC)_2]$ and TiO_2@$[Ru(bpy)_3]$ was successful, the attempt to condensate both compounds together to the particle surface indicated that the TSC Fe(III) has a higher affinity to bind to the surface. In this way, the functionalization needs some optimization in the future. In addition to that, the conjugates should be investigated towards their applications as catalyst for the formation of ROS (Figure 89).

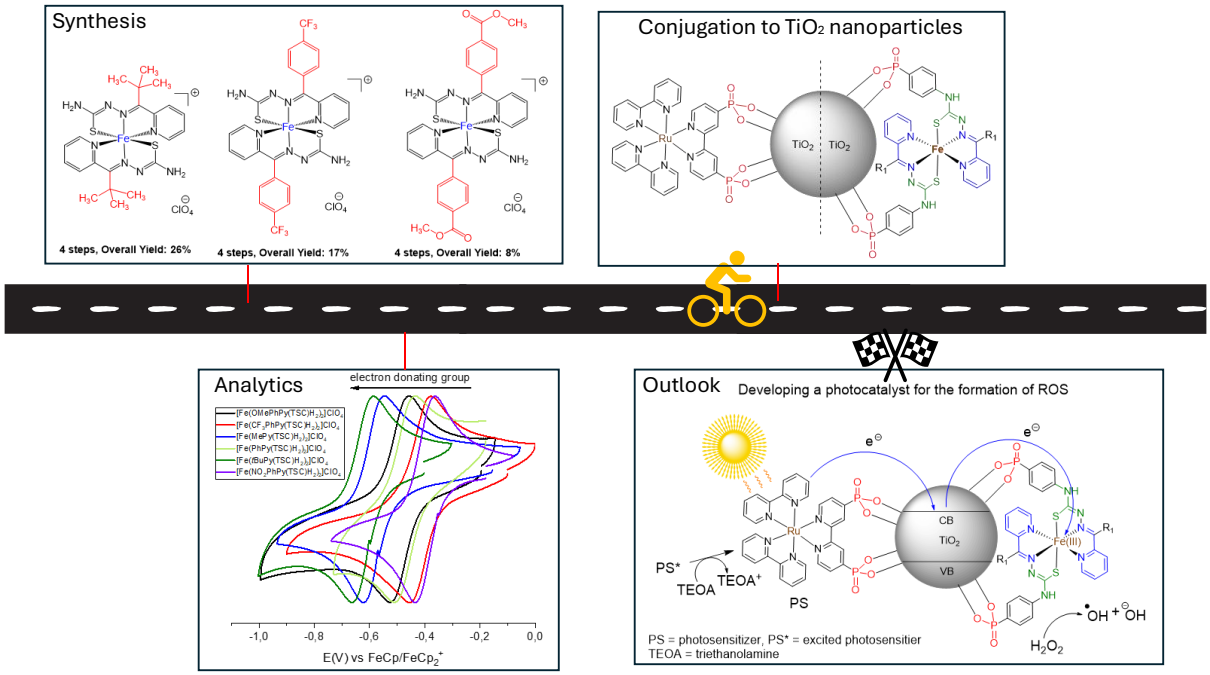


Figure 89. Overview of the progress made for the synthesis and characterization of α-pyridyl TSC to tune the redox potential of the corresponding Fe(III) complexes as well as their conjugation to TiO_2 NPs. In the future their application as a photocatalyst could be explored in more detail.

To investigate the application of TSCs in bioconjugation, TSCs derived from amino acids, glucose and cyclohexanol have been synthesized and characterized, which offer the opportunity to link them to biomolecules. The cytotoxicity of the amino acid derived TSC against HT-29 cancer cells was investigated in detail. An interesting aspect of these compounds was the time dependency of their toxicity, which increased after 48 h. In addition, the cancer cells were more affected by the TSCs compared to the healthy HFF-1. As an example of bioconjugation, Dipy(TSC)Val was successfully conjugated to the cell penetrating peptide sC18*. Optimalization of the conjugation, the purification of the conjugate and the investigation of its biomedical properties are the focus of interest in the future. In addition, the complexation of radio nuclides could be of interest to find applications in radio diagnostics (e.g. ^{68}Ga, ^{111}In or ^{64}Cu) (Figure 90).

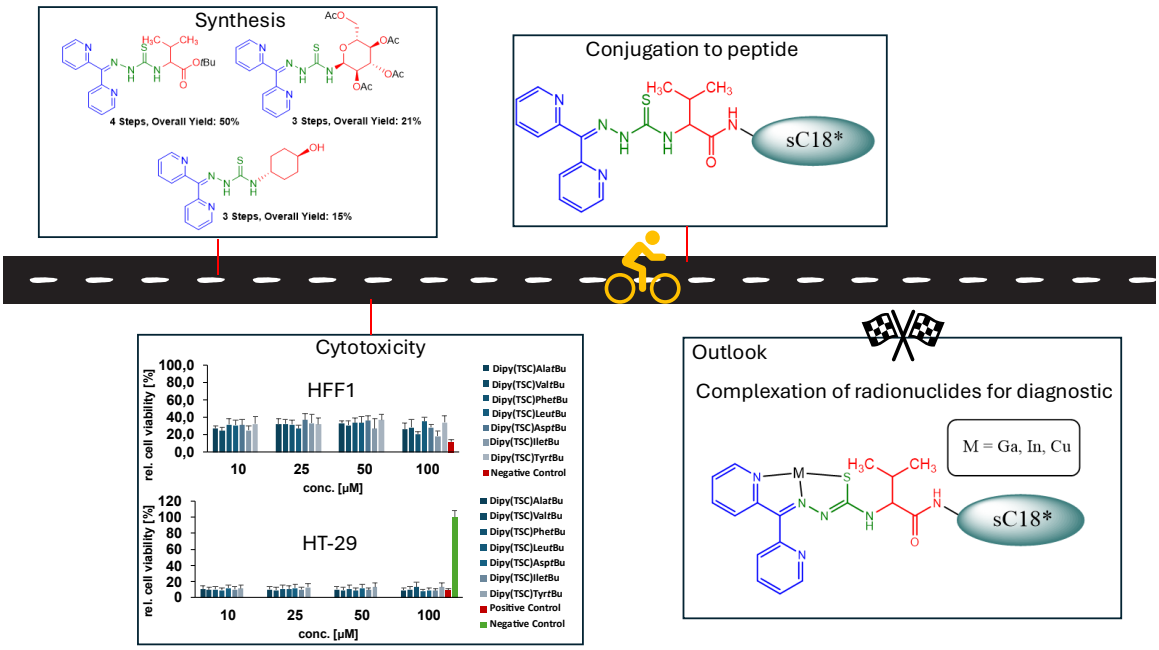


Figure 90. Overview of the progress for the application of TSCs in bioconjugation including upcoming tasks for the future.

To introduce a fluorescence tag in the structure of TSCs, different chromophores have been attached to the *N*4 position namely anthracene, carbazole, pyrene, fluorene and coumarin. After that, the corresponding Pt(II) complexes have been synthesized and characterized by NMR, UV/Vis absorption and emission spectroscopy, cyclic voltammetry and spectroelectrochemical measurements. Thereby, the compounds had many similarities in their properties. The ligands showed the typical fluorescence of the chromophores which occurred in a range of 390-440 nm. Complexation of Pt(II) usually led to a blue shift of the emission. In addition, most of the compounds showed a second emission at longer wavelength which is probably attributed to the TSC function and related to the deprotonation and rigidification of the ligand by metal complexation. In a last step, the cytotoxicity of the Pt(II) complexes was investigated against A549, MDA-MB-321, MCF-7 and HT-29. For the tested compounds, [Pt(Dipy(TSC)Pyr)Cl] showed the highest toxicity which was even higher than for cisplatin. [Pt(Dipy(TSC)Cbz)Cl] showed a selective toxicity against MDA-MB-321 but the LC_{50} value was higher. The TSCs fulfill the concept of a cytotoxic TSC with a fluorescence tag. This circumstance could be used in the future to investigate their mission of action by fluorescence microscopy. DNA binding studies might help to understand their cytotoxicity since it is expected that these compounds can intercalate DNA (Figure 91).

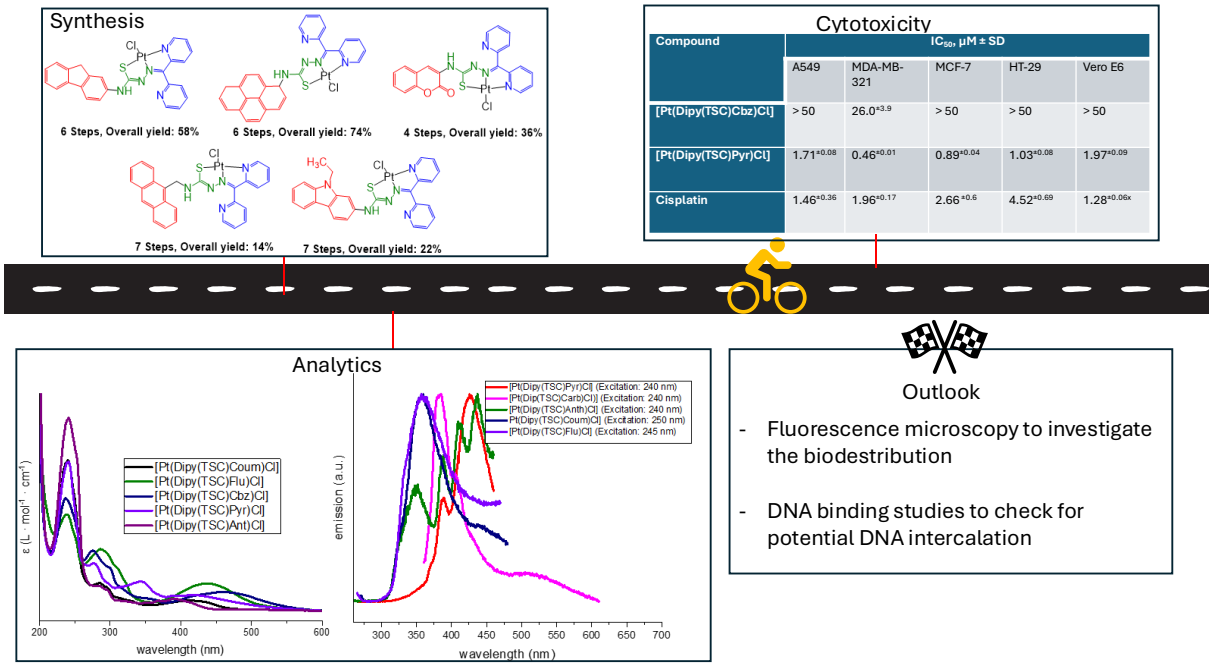


Figure 91. Overview of the progress made for the synthesis and characterization of TSCs with a fluorescence Tag. In the future their biodistribution could be explored in more detail using fluorescence microscopy.

To investigate the possibility to synthesize amphiphilic TSCs, lipophilic groups have been introduced to the *N*4 position (octyl, dodecyl, hexadecyl, cholesterol), while the *N*1 position was mostly functionalized with hydrophilic ketones (di(2-pyridyl)ketone, 2,5-dihydroxybenzaldehyde, 2,3,4-trimethoxybenzaldehyde and butane-2,3-dione). In addition, Pt(II) and Cu(II) complexes of the corresponding dipyridyl and bis-TSC were synthesized, and characterized by HR-ESI-MS, NMR and UV/Vis absorption spectroscopy as well as cyclic voltammetry. Solubility studies in pentane, toluene, MeOH and H_2O showed that most of the compounds were soluble in polar (MeOH) and nonpolar solvents (toluene, pentane) but insoluble in H_2O. The solubility of the metal complexes was usually decreased compared to the ligands. The compounds showed a negative solvatochromism, which was investigated by UV/Vis absorption spectroscopy. In the last step, the cytotoxicity of the compounds was investigated against HepG2, HCT-116 and HEK-293. Dipy(TSC)Oct showed a high cytotoxicity, which was reduced after the complexation of Pt(II) and Cu(II). In the future, the H_2O solubility should be improved to get closer to the goal of amphiphilic TSCs, which might be able to form micelles. For this, a second generation of TSCs should be synthesized, having a charge at the TSC group, which can be

achieved by metal complexation (e.g. Au(III) or functional groups (e.g. carbon acid, sulfonic acid). As an alternative, it could be tried to mix the TSCs with a tenside to incorporate them into micelles or liposomes (Figure 92).

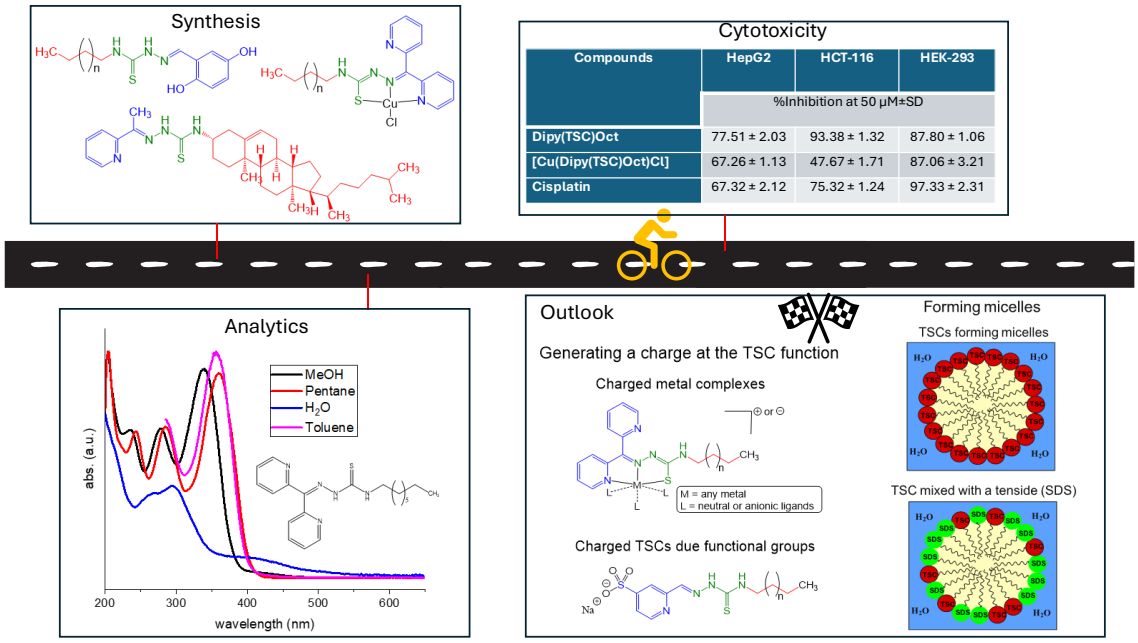


Figure 92. Overview of the progress made for the synthesis and characterization of amphiphilic TSCs. Improving their H_2O solubility will be a task for the future.

Hexadentate TSCs with Bpy, Phen, DPPZ, Naph, DTT, Tpy and PyPhPy in their structure have been successfully synthesized and characterized by HR-ESI-MS, NMR spectroscopy and UV/Vis absorption and emission spectroscopy. Thereby, DPPZ(TSC)Ala*t*Bu, DTT(TSC)Ala*t*Bu, Phen(TSC)Ala*t*Bu and Naph(TSC)Ala*t*Bu showed a characteristic fluorescence assigned to their heterocyclic backbone. Metal complexation of these ligands was not discussed in this research but is currently explored in bachelor and master thesis in the research group of Prof. Dr. Axel Klein. The complexation of bio abundant metals like Cu, Zn or Fe as well as the synthesis of bimetallic complex are two examples for further research in the future (Figure 93).

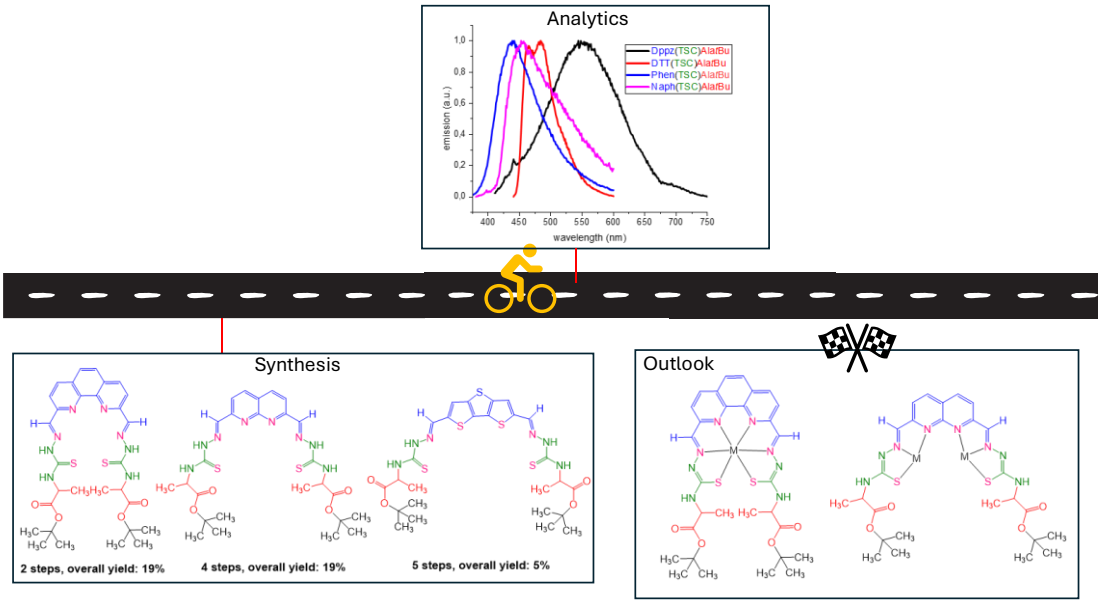


Figure 93. Overview of the progress made for the synthesis and characterization of hexadentate TSCs. The synthesis of their metal complexes will be investigated in the future.

5. Experimental part

5.1. Materials and Solvents

All chemicals were purchased from Sigma-Aldrich (St. Louis, USA), Thermo Fisher Scientific (Waltham, USA), Carbolution (St. Ingbert, Germany), BLDpharm (Reinbek, Germany), Janssen Chimica (Beerse, Belgium), Alfa Aeser (Thermo Fisher Scientific), Acros (Thermo Fisher Scientific) or Biosynth (Staad, Switzerland) and used without further purification: Thiophosgene (85%, Thermo Scientific), *tert*-butyl-acetate (> 99.0%, TCI), *L*-alanine (98%, Sigma-Aldrich), *L*-valine (99%, Acros), *L*-phenylalanine (98%, Sigma-Aldrich), *L*-leucine (98%, Biosynth), *L*-isoleucine (98%, Sigma-Aldrich), *L*-aspartic acid (97%, Alfa Aeser), *L*-tyrosine-*tert*-butyl ester (99%, BLDpharm), hydrazine hydrate (100%, ThermoFisher), ethylenediamine (99%, Alfa Aeser), hexamethylene diamine (98%, Sigma-Aldrich), 1,4-phenylene diamine (98%, Sigma-Aldrich), di-*tert*-butyl dicarbonate (98%, Carbolution), acetobromo-α-D-Glucose (98%, BLDpharm), 9-antracene aldehyde (99%, Acros), di(2-pyridyl)ketone (97%, BLDpharm), *trans*-4-hydroxycyclohexanol (98%, BLDpharm), dopamine hydrochloride (99%, Sigma Aldrich), cysteamine hydrochloride (98%, BLDpharm), benzyl chloride (99%, Janssen Chimica), 4-Iodoaniline (98%, Sigma-Aldrich), trimethylsilyl acetylene (98%, BLDpharm), $Pd(PPh_3)_4$ (99%, ThermoFisher), 4-cyanobenzaldehyde (97%, BLDpharm), 1-Iodo-nitrobenzene (98%, Sigma-Aldrich), diethylphosphite (98%, Sigma-Aldrich), bromtrimethylsilan (97%, carbolution), titanium(IV) oxide *Aeroxide P25* (thermos scientific) pyrene (98%, Sigma-Aldrich), fluorene (97%, bayer), 9-anthracenemethanol (98%, Alfa Aeser), carbazole (99%, Sigma), Resorcinol (98%, TCI), 4-nitrophthalic acid (97%, TCI), 4-bromo-1,8-naphthalic anhydride (96%, BLDpharm), 3-aminocoumarine (98%, Sigma), $K_2[PtCl_4]$ (98%, BLDpharm), 3-bromothiophen (95%, Alfa Aeser), 2-aminonicotinaldehyde (97%, BLDpharm), 2,9-dimethyl-1,10-phenanthroline (98%, BLDpharm), 6-acetyl-2-bromopyridine (95%, ABCR), cholesterol (98%, ABCR), octylamine (97%, Sigma Aldrich), dodecylamine (98%, BLDPharm), hexadecylamine (98%, BLDpharm), 2,3,4-trimethoxybenzaldehyde (95%, across), 2,3-butadione (98%, Alfa Aeser), 2,5-dihydroxybenzaldehyde (98%, Sigma Aldrich).

All solvents used for synthesis had HPLC grade and were used without further purification. Dry THF was freshly distilled over Na/K (alloy 3:7) before use. Other dry solvents were obtained from AcroSeal bottles from Thermo Fisher Scientific.

5.2. Methods

NMR-spectroscopy
NMR spectra were recorded at 280 K by a *Brunker Avance II* 300 spectrometer (300 MHz) with a *L.T. BBO ATM* 5 mm z-gradient probe head or a *Brunker Acance III* 500 spectrometer (499 MHz) with a *TCI Prodigy* 5 mm z-gradient probe head. The assignment of signals is based on 2D NMR experiments which were performed using standard pulse sequences from the *Bruker* pulse program library. The measurements were performed in deuterated $CDCl_3$ or DMSO-d_6 with 0.03 wt% TMS (tetramethyl silane) as an internal standard. The chemical shifts are in relation to residual solvent signals or TMS (chloroform-d_1: 7.26 ppm, DMSO-d_6: 2.50 ppm). The data was analyzed with the software *MestReNova (*Version: *12.0.0-20080)*.

UV/Vis absorption spectroscopy
UV/Vis absorption spectra were recorded in solution at room temperature on a *Varian Cary50 Scan* UV/Vis spectrometer. The used quartz cuvettes had a diameter of 1 cm. The spectra were baseline corrected and analyzed with the software *Origin Pro* 2025.

Fourier-transform infrared spectrometer (FTIR)
FTIR measurements were performed at a *Perkin Elmer Spektrum Two* spectrometer in ambient conditions. The data was analyzed by *Origin Pro* 2025.

Emission spectrometry
Fluorescence spectroscopy was performed at a spectrometer from *Edinburgh Instruments* with a 450 W xenon light source. The spectrometer was equipped with a PMT-900 detector and a double-grating *Czerny-Turner* monochromator. All measurements were performed at room temperature in MeCN. The data was analyzed by *Origin Pro* 2025.

High resolution mass spectrometry (HR-ESI-MS)
High resolution mass spectra were recorded with a LC/MS (Liquid Chromatography/Mass spectrometry) approach at a *THERMO Scientific LTQ Orbitrap XL* spectrometer equipped with a FTMS analyzer in a positive ion mode. Electron spray ionization (ESI) was used as an ionization method.

Cyclic voltammetry
Cyclic voltammetry measurements were performed in 0.1 M solutions of nBu_4NPF_6 in THF, MeCN or DMF at room temperature. An oven-dried three-necked flask was used with three electrodes, namely a glazed carbon working electrode, a platinum counter electrode and a Ag/AgCl reference electrode. The sweep potential rate was 100 mV/s. A *Metrohm µStat400* potentiate was used to apply the voltage. The measurements were referenced to Ferrocene/Ferrocenium. The data was analyzed by *Origin Pro* 2025.

Spectroelectrochemical measurements
Spectroelectrochemical measurements were performed in an OTTLE cell (optically transparent thin layer electrochemical cell) in a 0.1 M solution of nBu_4PF_6 in dry MeCN or DMF. The applied potential was increased or decreased stepwise (steps of 0.1 V). After 30 s at the respective potential, a UV/Vis absorptions spectrum was measured using a *Varian Cary50 Scan* UV/Vis spectrometer. The data was analyzed by *Origin Pro* 2025.

Dynamic light scattering DLS/Zeta potential measurements
Dynamic light scattering DLS/Zeta potential measurements were carried out on a *Malvern Zetasizer Ultra* (Malvern Panalytical, Malvern, UK) in H_2O, at room temperature and a pH of 7.

SEM/EDX measurements
The elemental distribution of the bulk material was analyzed with a *Zeiss Sigma 300 VP RISE* field emission scanning electron microscope (FESEM) with integrated energy-dispersive X-ray spectrometer (EDX, *Oxford instruments Xplore 30*). The samples have been spread onto a carbon tape for each measurement.

Specific optical rotation
Specific optical rotation was measured on an *Anton Paar* (Graz, Austria, MCP 200) polarimeter, in $CHCl_3$ solutions at 20 °C and λ = 365 nm, 436 nm, 546 nm, 579 nm, and 589 nm.

Working under-inert conditions
Some reactions were performed under inert conditions, which is mentioned in the experimental procedure. Thereby, the *Schlenk* technique was used, with argon (99.998% form *Linde*) as an inert gas. The used glassware was heated three times to 650 °C under vacuum by a heat gun, for removing residual H_2O.

Chromatography
Column chromatography was performed with silica (0.035-0.070 mm 60 A form *Merck*) as a stationary phase. Solvent mixtures of ethyl acetate and cyclohexane or methanol and dichloromethane were used as eluents. Thin layer chromatography was performed with silica gel 60 plates from the company Merck.

Conjugation to peptides

The conjugation of Dipy(TSC)Val to cell penetrating peptides was performed in the research group of Prof. Ines Neundorf at the institute of biochemistry at the University of Cologne. The experiments were performed by Philipp Holz. The cell-penetrating peptide sC18* was synthesized by an automated solid phase peptide synthesis at a Syro I peptide synthesizer (MultiSynTech). Dipy(TSC)Val (2.00 eq.) was coupled manually to the resin using 2.00 eq. HATU (*O*-(7-azabenzotriazol-1-yl)-*N*,*N*,*N*′,*N*′-tetramethyluronium hexafluorophosphate) and 2.00 eq. DIPEA (*N*,*N*-diisopropylethylamine) in DMF for 2 h at room temperature. The resulting conjugate was cleaved from the resin with trifluoroacetic acid/thioanisol/1,2-Ethandithiol (90 : 7 : 3) at 55 °C for 30 min. HPLC chromatograms were recorded on an *Agilent 1260 HPLC system* (column: Nucleodur C18ec; 100-5; Macherey-Nagel; gradient: 10-60% MeCN in H_2O (incl. 0.1 % formic acid) over 15 min; 0.6 mL/min flow rate). ESI-MS(+) spectra were performed on a *LTQ-XL* mass spectrometer *via* electron spray ionization.

Antiproliferative activity

Variant 1

The cytotoxicity of the TSCs was determined by a resazurin assay and tested against HT-29 (human colon cancer cell line) and HFF1 (fibroblasts). The cells were loaded into a 96-well plate and incubated at 37 °C for 24 h in a CO_2 incubator. The TSCs were dissolved in DMSO as a stock solution, which was diluted with the medium to a concentration of 1% DMSO. The concentration of the TSCs was 100 µM, 50 µM, 25 µM and 10 µM respectively. For Dp44mT and Dipy(TSC)Val*t*Bu, additional concentrations of 0.025, 0.05, 0.10, 0.25, 0.50, 0.50, 1.00, 2.50, 5.00, and 10.00 µM have been tested. As a negative control, the cells were incubated with the medium and 1% DMSO. As a positive control, the cells were incubated with 70% EtOH. The incubation time was 24, 48 and 96 h. Antiproliferative activity was determined by photospectrometric measurements. The conversion of resazurin (λ_{ex}=550 nm) into the resorufin (λ_{ex}=595 nm) was measured on a *Tecan infinite M200* plate reader (Tecan Group AG). The Data was normalized to untreated control cells (100% viability). Results were calculated as the means of three independent experiments.[222]

Variant 2

The cytotoxicity was determined by a crystal violet assay. The TSCs were tested against different cancer cell lines namely A549 (lung carcinoma cells), MDA-MB-321 (metastatic breast adenocarcinoma), MCF-7 (breast adenocarcinoma) and HT-29 (colorectal adenocarcinoma). Vero E6 are African green monkey kidney cells which were used as a reference cell line to check for possible tumor selectivity. The cells were loaded into a 96-well plate and incubated at 37 °C in 5% CO_2 for 24 h. Stock solutions of the TSCs in dimethylformamide (DMF) were freshly prepared and diluted with the respective cell culture medium to graded concentrations (final concentration of DMF: 0.1% v/v). After 72 h of incubation, the cell biomass was determined by crystal violet staining using an *X4 Victor Perkin Elmer* plate reader at 595 nm, and the IC_{50} value was determined as the concentration that caused 50% inhibition of cell proliferation compared to an untreated control. Results were calculated as the means of three independent experiments.[347]

Variant 3

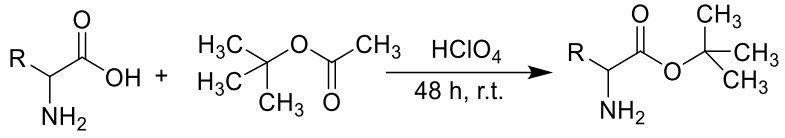
A MTT (3-(4,5-dimethylthiazol-2-yl)-2,5-diphenyl tetrazolium bromide) assay was used to determine the cell viability of the synthesized TSCs. The compounds were tested against HepG2 (huma liver cancer cell line), HCT-116 (human colon cancer cell line) and HEK-293 (human embryonic kidney cell line). The cells were loaded in a sterile 96-well plate and incubated for 24 h in CO_2 incubator at 37 °C. The media was discarded, and the cells were washed with PBS (phosphate buffered saline). After that, the TSCs were loaded at a concentration of 50 µM/well in triplicates. 1% DMSO and 50 µM cisplatin were used as negative control or positive control. A blank that contained only serum free media served as the reference. The 96 well plate was further incubated for 24 h in 5% CO_2 incubator at 37 °C. Then, 100 µL of MTT was added to achieve a final concentration of 0.2 mg/mL. The cells were placed in an incubator

for further 2 to 4 h until insoluble formazan has formed. The media was aspirated, and 100 µL/well solubilizing agent (SDS solution) were added. Subsequently, the plates were shaken for 30 min to ensure complete dissolution of the formazan. The absorbance was measured with a microplate reader (*FLUOstar Omega*, BMG LABTECH GmbH, Germany) at 570 nm for the formazan and at 630 nm for the background signal. The conversion of MTT reagent to formazan crystals by mitochondrial dehydrogenases was related to the relative cell viability.[304]

5.3 Synthesis

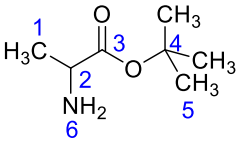
5.3.1 Synthesis of TSCs derived from amino acids

5.3.1.1 Synthesis of amino acid *tert*-butyl esters – general description

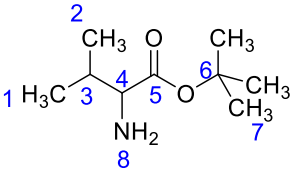


The amino acid (1.00 eq.) was suspended in *tert*-butyl acetate (amino acid/*tert*-butyl acetate approx. 1:30) and cooled to 0 °C. To this mixture, $HClO_4$ (70% in H_2O, 1.5 eq.) was added dropwise, which lead to the formation of a clear solution, which was stirred for 48 h at room temperature. Then, the reaction mixture was washed with 150 mL of distilled H_2O and 75 mL of 1 M HCl and the combined aqueous phase was adjusted to pH 9 by using K_2CO_3. A white precipitate formed, which was filtered off. The aqueous solution was extracted with CH_2Cl_2 (3 x 100 mL) and the organic phase was dried over Na_2SO_4. The solvent was removed under reduced pressure yielding the product as colorless oil.[332]

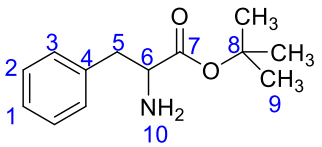
***L*-alanine *tert*-butyl ester** from 6.24 g (70.0 mmol) *L*-alanine, 90 mL (666 mmol) *tert*-butyl acetate, 8.40 mL (106.0 mmol) perchloric acid. The product was obtained as colorless oil. Yield: 4.37 g (30.1 mmol, 43%). $C_7H_{15}NO_2$ (145.20 g/mol). ^{1}H NMR (499 MHz, $CDCl_3$) δ [ppm] = 3.36 (q, *J* = 7.0 Hz, 1H, H-2), 1.51 (s, 2H, H-6), 1.42 (s, 9H, H-5), 1.26 (d, *J* = 7.1 Hz, 3H, H-1). ^{13}C NMR (499 MHz, $CDCl_3$) δ [ppm] = 175.90 (C-3), 80.67 (C-4), 50.55 (C-2), 27.97 (C-5), 20.66 (C-1).



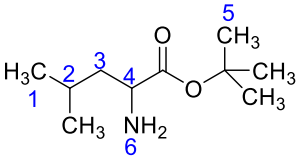
***L*-valine *tert*-butyl ester** from 5.00 g (42.7 mmol) *L*-valine, 90 mL (666 mmol) *tert*-butyl acetate, 5.30 mL (64.1 mmol) perchloric acid. The product was obtained as colorless oil. Yield: 5.71 g (32.9 mmol, 77%). $C_9H_{19}NO_2$ (173.26 g/mol). ^{1}H NMR (499 MHz, $CDCl_3$) δ [ppm] = 3.13 (d, *J* = 4.6 Hz, 1H, H-4), 1.93 (m, 1H, H-3), 1.49 (s, 2H, H-8), 1.44 (s, 9H, H-7), 0.95 (d, *J* = 6.7 Hz, 3H, H-1/H-2), 0.87 (d, *J* = 6.7 Hz, 3H, H-1/H-2). ^{13}C NMR (499 MHz, $CDCl_3$) δ [ppm] = 174.69 (C-5), 80.73 (C-6), 60.18 (C-4), 32.07 (C-3), 28.01 (C-7), 19.18 (C-1/C-2), 17.02 (C-1/C-2).



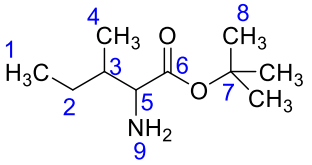
***L*-phenylalanine *tert*-butyl ester** from 4.95 g (30.0 mmol) L-phenylalanine, 90 mL (666.0 mmol) *tert*-butyl acetate, 3.90 mL (47.2 mmol) perchloric acid. The product was obtained as colorless oil. Yield: 3.22 g (14.5 mmol, 49%). $C_{13}H_{19}NO_2$ (221.30 g/mol). ^{1}H NMR (499 MHz, $CDCl_3$) δ [ppm] = 7.28 (m, 2H, H-3), 7.21 (m, 3H, H-1, H-2), 3.58 (m, 1H, H-6), 3.04 (m, 1H, H-5), 2.81 (m, 1H, H-5), 1.52 (s, 2H, H-10), 1.42 (s, 9H, H-9). ^{13}C NMR (499 MHz, $CDCl_3$) δ [ppm] = 174.88 (C-7), 138.60 (C-4), 129.30 (C-1/C-2), 128.32 (C-3), 125.39 (C-1/C-2), 82.00 (C-8), 56.35 (C-6), 41.40 (C-5), 27.52 (C-9).



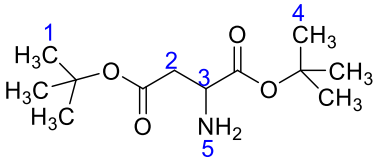
***L*-leucine *tert*-butyl ester** from 2.00 g (15.0 mmol) L-leucine, 50 mL (500.5 mmol) *tert*-butyl acetate, 1.94 mL (22.5 mmol) perchloric acid. The product was obtained as colorless oil. Yield: 1.40 g (7.5 mmol, 50%). $C_{10}H_{21}NO_2$ (187.28 g/mol). ^{1}H NMR (499 MHz, $CDCl_3$) δ [ppm] = 3.26 (m, 1H, H-4), 1.71 (m, 1H, H-2), 1.44-1.29 (m, 13H, H-5, H-3, H-6), 0.86 (t, *J* = 6.8 Hz, 6H, H-1).



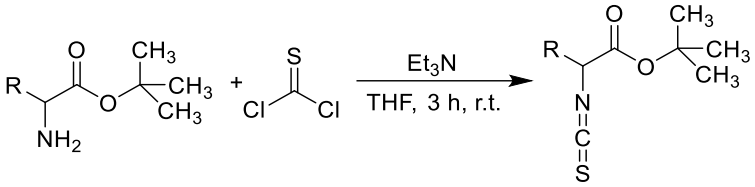
***L*-Isoleucine *tert*-butyl ester** from 2.00 g (15.2 mmol) L-isoleucine, 50 mL (500.5 mmol) *tert*-butyl acetate, 1.96 mL (22.9 mmol) perchloric acid. The product was obtained as colorless oil. Yield: 1.71 g (9.1 mmol, 60%). $C_{10}H_{21}NO_2$ (187.28 g/mol). ^{1}H NMR (499 MHz, $CDCl_3$) δ [ppm] = 3.28 (d, *J* = 4.5 Hz, 1H, H-5), 2.87 (s, 2H, H-9), 1.70 (m, 1H, H-3), 1.43-1.34 (m, 10H, H-2, H-8), 1.14 (m, 1H, H-2), 0.89-0.84 (m, 6 H, H-1, H-4). ^{13}C NMR (499 MHz, $CDCl_3$) δ [ppm] = 173.64 (C-6), 81.30 (C-7), 58.93 (C-5), 38.88 (C-3), 28.00 (C-8), 24.89 (C-2), 15.36 (C-1/C-4), 11.73 (C-1/C-4).



***L*-aspartic acid *tert*-butyl ester** from 0.81 g (6.1 mmol) L-aspartic acid, 50 mL (500.5 mmol) *tert*-butyl acetate, 0.60 mL (7.0 mmol) perchloric acid. The product was obtained as colorless oil. Yield: 1.00 g (4.1 mmol, 66%). $C_{12}H_{23}NO_4$ (245.32 g/mol). ^{1}H NMR (499 MHz, $CDCl_3$) δ [ppm] = 3.68 (m, 1H, H-3), 2.70 (m, 2H, H-2), 2.04 (s, 2H, H-5), 1.45 (s, 18H, H-1, H-5).



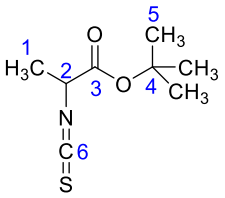
5.3.1.2 Synthesis of isothiocyanates – general description



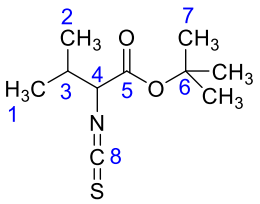
R = benzyl, *i*propyl, methyl, *i*butyl, $CH_2COOtBu$, 1-methyl propyl, 4-hydroxy benzyl

The reaction was performed under inert conditions. The amino acid *tert*-butyl ester (1.00 eq.) and Et_3N (3.00 eq.) were dissolved in 50 mL of THF and thiophosgene (85%, 1.00 to 1.10 eq.) was slowly added at 0 °C. The reaction mixture was stirred for 3 h at room temperature, which lead to the formation of a brown suspension. The reaction was quenched by adding 100 mL of distilled H_2O and the product was extracted with Et_2O (3 x 100 mL). The organic phase was dried over Na_2SO_4, and the solvent was removed under reduced pressure, yielding the isothiocyanates.

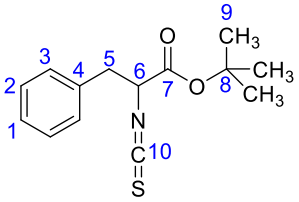
(*S*)-*tert*-butyl 2-isothiocyanatopropanoate from 1 g (6.9 mmol) alanine *tert*-butyl ester, 0.7 mL (7.6 mmol) thiophosgene, 2.86 mL (20.7 mmol) NEt_3. The product was obtained as brown oil. Yield: 1.34 g (7.1 mmol, quant.). $C_8H_{13}NO_2S$ (187.26 g/mol). ^{1}H NMR (499 MHz, $CDCl_3$) δ [ppm] = 4.17 (q, *J* = 7.2 Hz, 1H, H-2), 1.53 (d, *J* = 7.4 Hz, 3H, H-1), 1.49 (s, 9H, H-5). ^{13}C NMR (499 MHz, $CDCl_3$) δ [ppm] = 167.56 (C-3), 137.35 (C-6), 83.59 (C-4), 55.34 (C-2), 27.74 (C-5), 19.38 (C-1).



(*S*)-*tert*-butyl 2-isothiocyanato-3-metylbutanoate from 2 g (11.5 mmol) valine *tert*-butyl ester, 1.10 mL (12.7 mmol) thiophosgene, 4.80 mL (34.6 mmol) NEt_3. The product was obtained as brown oil. Yield: 2.51 g (11.5 mmol, quant.). $C_{10}H_{17}NO_2S$ (215.31 g/mol). ^{1}H NMR (499 MHz, $CDCl_3$) δ [ppm] = 3.98 (d, *J* = 4.6 Hz, 1H, H-4), 2.28 (m, 1H, H-3), 1.50 (s, 9H, H-7), 1.05 (d, *J* = 7.4 Hz, 3H, H-1/H-2), 0.96 (d, *J* = 7.4 Hz, 3H, H-1/H-2). ^{13}C NMR (499 MHz, $CDCl_3$) δ [ppm] = 166.95 (C-5), 135.86 (C-8), 83.45 (C-6), 64.54 (C-4), 32.56 (C-3), 28.06 (C-7), 19.62 (C-1/C-2), 16.57 (C-1/C-2).

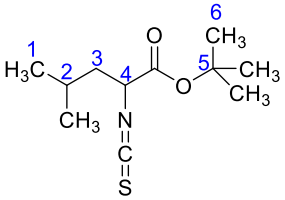


(*S*)-*tert*-butyl 2-isothiocyanato-3-phenylpropanoate from 3 g (13.5 mmol) phenylalanine *tert*-butyl ester, 1.2 mL (13.5 mmol) thiophosgene, 5.6 mL (40.7 mmol) NEt_3. The product was obtained as brown oil. Yield: 3.20 g (12.1 mmol, 90%). $C_{14}H_{17}NO_2S$ (263.36 g/mol). ^{1}H NMR (499 MHz, $CDCl_3$) δ [ppm] = 7.32 (m, 2H, H-2), 7.27 (m, 1H, H-1), 7.23 (m, 2H, H-3), 4.29 (m, 1H, H-6), 3.17 (m, 1H, H-5), 3.09 (m, 1H, H-5), 1.44 (s, 9H, H-9). ^{13}C NMR (499 MHz, $CDCl_3$) δ [ppm]

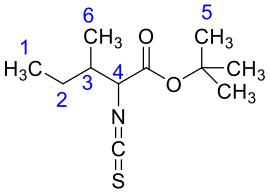


= 165.82 (C-7), 136.50 (C-10), 135.95 (C-4), 129.51 (C-3), 128.67 (C-2), 127.67 (C-1), 83.38 (C-8), 60.99 (C-6), 39.09 (C-5), 28.09 (C-9).

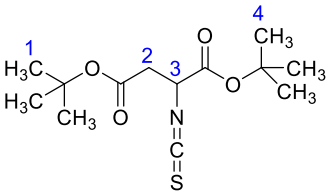
(*S*)-*tert*-butyl 2-isothiocyanato-4-methylpentanoate from 1.40 g (7.5 mmol) leucine *tert*-butyl ester, 0.68 mL (7.5 mmol) thiophosgene, 3.11 mL (22.4 mmol) NEt_3. The product was obtained as brown oil. Yield: 1.69 g (7.4 mmol, 98%). $C_{11}H_{19}NO_2S$ (229.34 g/mol). ^1H NMR (300 MHz, $CDCl_3$) δ [ppm] = 4.13 (m, 1H, H-4), 1.88-1.60 (m, 3H, H-2, H-3), 1.50 (s, 9H, H-6), 0.97 (m, 6H, H-1).



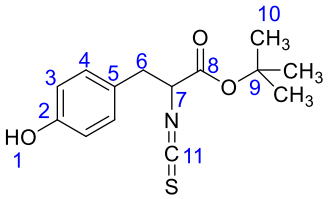
(*S*)-*tert*-butyl 2-isothiocyanato-3-methylpentanoate from 0.50 g (2.7 mmol) isoleucine *tert*-butyl ester, 0.24 mL (2.7 mmol) thiophosgene, 1.12 mL (8.0 mmol) NEt_3. The product was obtained as brown oil. Yield: 0.48 g (2.1 mmol, 78%). $C_{11}H_{19}NO_2S$ (229.34 g/mol). ^1H NMR (300 MHz, $CDCl_3$) δ [ppm] = 4.53 (d, *J* = 3.9 Hz, 1H, H-4), 2.02 (m, 1H, H-3), 1.46 (s, 9H, H-5), 1.42-1.13 (m, 2H, H-2), 0.97 (d, *J* = 6.8 Hz, 3H, H-6), 0.89 (t, *J* = 7.4 Hz, 3H, H-1).



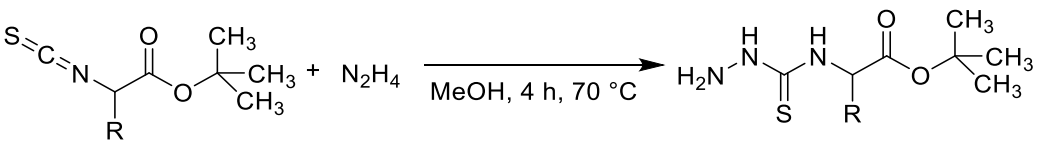
(S)-di-*tert*-butyl 2-isothiocyanatobutanedioate from 1.00 g (4.4 mmol) L-aspartic acid *tert*-butyl ester, 0.39 mL (4.4 mmol) thiophosgene, 1.82 mL (13.1 mmol) NEt_3. The product was purified by column chromatography (EOAc) and obtained as brown oil. Yield: 1.02 g (3.5 mmol, 80%). $C_{13}H_{21}NO_4S$ (287.37 g/mol). ^1H NMR (499 MHz, $CDCl_3$) δ [ppm] = 4.48 (m, 1H, H-3), 2.76 (m, 2H, H-2), 1.50 (s, 9H, H-1/H-4), 1.48 (s, 9H, H-1/H-4).



***Tert*-butyl 3-(4-hydroxyphenyl)-2-isothiocyanatopropanoate** from 0.50 g (2.1 mmol) L-tyrosine *tert*-butyl ester, 0.19 mL (2.1 mmol) thiophosgene, 0.88 mL (6.3 mmol) NEt_3. The reaction was cooled down to –78 °C. The product was purified by column chromatography (c-hexane/EOAc 4:1 v/v) and obtained as brown oil. Yield: 0.25 g (0.9 mmol, 42%). $C_{14}H_{17}NO_3S$ (279.35 g/mol). ^1H NMR (300 MHz, $CDCl_3$) δ [ppm] = 7.31 (d, *J* = 8.3 Hz, 2H, H-3), 7.20 (d, *J* = 8.3 Hz, 2H, H-4), 4.35 (s, 1H, H-7), 3.20 (m, 2H, H-6), 1.44 (s, 9H, H-10). ^{13}C NMR (499 MHz, $CDCl_3$) δ [ppm] = 166.29 (C-8), 153.07 (C-2), 138.73 (C-11), 133.79 (C-5), 130.75 (C-3), 122.30 (C-2), 84.62 (C-9), 60.60 (C-7), 39.18 (C-6), 27.83 (C-10).



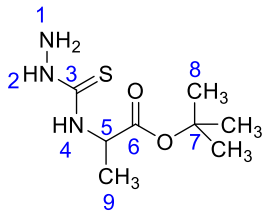
5.3.1.3 Synthesis of thiosemicarbazides – general description



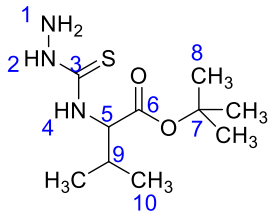
R = bezyl, ipropyl or methyl, *i*butyl, $CH_2COOtBu$, 1-methyl propyl, 4-hydroxy benzyl

Hydrazine monohydrate (1.00 eq.) was dissolved in 30 mL of MeOH and heated to 70 °C. The isothiocyanate (1.00 eq.) was dissolved in 100 mL of MeOH and added to the hydrazine solution over the course of 1 h. The reaction mixture was stirred for an additional 3 h, then the solvent was removed under reduced pressure. The crude product was dissolved in 10 mL of $CHCl_3$ and poured into boiling petrol ether. A precipitate was formed, which was separated by decantation or filtration and the obtained product was dried under ambient conditions.

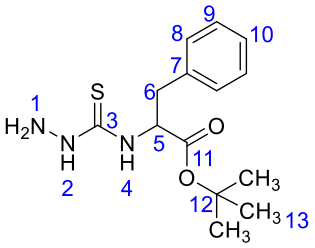
4-((*S*)-*Tert*-butyl propanoate)thiosemicarbazide from 1.29 g (6.9 mmol) (*S*)-*tert*-butyl 2-isothiocyanatopropanoate, 0.33 mL (6.9 mmol) hydrazine hydrate. The product was obtained as brownish solid. Yield: 1.35 g (6.1 mmol, 88%). $C_8H_{17}N_3O_2S$ (219.30 g/mol). ^{1}H NMR (499 MHz, DMSO-d_6) δ [ppm] = 8.90 (s, 1H, H-2), 7.83 (s, 1H, H-3), 4.75 (m, 1H, H-5), 4.56 (s, 2H, H-1), 1.42 (s, 9H, H-8), 1.33 (d, *J* = 7.5 Hz, 3H, H-9). ^{13}C NMR (499 MHz, $CDCl_3$) δ [ppm] = 181.04 (C-3), 171.41 (C-6), 81.33 (C-7), 52.30 (C-5), 28.09 (C-8), 18.80 (C-9). HR-ESI-MS: m/z $[M+H]^+$ = 220.1117, m/z $[M+Na]^+$ = 242.0937.



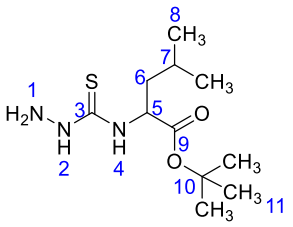
4-((*S*)-*Tert*-butyl 3-metylbutanoate)thiosemicarbazide from 2.48 g (11.5 mmol) (*S*)-*tert*-butyl 2-isothiocyanato-3-metylbutanoate, 0.55 mL (11.5 mmol) hydrazine hydrate. The product was obtained as brown solid**.** Yield: 3.02 g (12.2 mmol, quant.). $C_{10}H_{21}N_3O_2S$ (247.36 g/mol). ^{1}H NMR (499 MHz, DMSO-d_6) δ [ppm] = 8.96 (s, 1H, H-2), 7.84 (s, 1H), 4.75 (m, 1H, H-4), 4.75 (m, 1H, H-5), 4.63 (s, 2H, H-1), 2.13 (m, 1H, H-9), 1.43 (s, 9H, H-8), 0.88 (m, 6H, H-10). ^{13}C NMR (499 MHz, $CDCl_3$) δ [ppm] = 181.49 (C-3), 171.09 (C-6), 81.60 (C-7), 62.93 (C-5), 31.51 (C-9), 28.16 (C-8), 18.64 (C-10). HR-ESI-MS: m/z $[M+H]^+$ = 248.1430, m/z $[M+Na]^+$ = 270.1251.



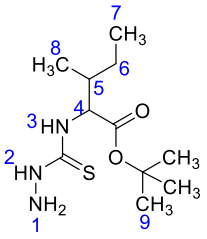
4-((*S*)-*Tert*-butyl 3-phenylpropanoate)thiosemicarbazide from 3.20 g (12.1 mmol) (*S*)-*tert*-butyl 2-isothiocyanato-3-phenylpropanoate, 0.60 mL (2.1 mmol) hydrazine hydrate. The product was obtained as brown solid. Yield: 3.01 g (10.2 mmol, 84%). $C_{14}H_{21}N_3O_2S$ (295.40 g/mol). ^{1}H NMR (499 MHz, DMSO-d_6) δ [ppm] = 8.99 (s, 1H, H-2), 7.83 (s, 1H, H-4), 7.30 (m, 2H, H-8), 7.23 (m, 1H, H-10), 7.19 (m, 2H, H-9), 5.06 (m, 1H, H-5), 4.56 (s, 2H, H-1), 3.07 (m, 2H, H-6), 1.30 (s, 9H, H-13). ^{13}C NMR (499 MHz, $CDCl_3$) δ [ppm] = 181.00 (C-3) 170.42 (C-11), 136.67 (C-7), 129.30 (C-9), 128.21 (C-8), 126.61 (C-10), 81.17 (C-12), 57.08 (C-5), 37.08 (C-6), 27.55 (C-13). HR-ESI-MS: m/z $[M+H]^+$ = 296.1432, m/z $[M+Na]^+$ = 318.1252.



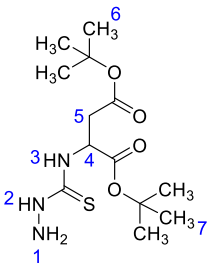
4-((*S*)-*Tert*-butyl 4-methylpentonate)thiosemicarbazide from 1.69 g (7.4 mmol) (*S*)-*tert*-butyl 2-isothiocyanato-4-methylpentanoate, 0.36 mL (7.4 mmol) hydrazine hydrate. The product was obtained as brown solid. Yield: 0.84 g (3.2 mmol, 44%). $C_{11}H_{23}N_3O_2S$ (261.38 g/mol). ^{1}H NMR (499 MHz, DMSO-d_6) δ [ppm] = 8.88 (s, 1H, H-2), 7.72 (d, *J* = 7.9 Hz, 1H, H-4), 4.84 (m, 1H, H-5), 4.56 (s, 2H, H-1), 1.70-1.49 (m, 4H, H-6, H-7), 1.41 (s, 9H, H-11), 0.90 (t, *J* = 5.7 Hz, 6H, H-8). ^{13}C NMR (499 MHz, DMSO-d_6) δ [ppm] = 181.60 (C-3), 172.37 (C-9), 81.18 (C-10), 55.23 (C-5), 41.41 (C-6), 28.12 (C-11), 24.89 (C-7), 23.13 (C-8), 22.47 (C-8). HR-ESI-MS: m/z $[M+H]^+$ = 262.1585 , m/z $[M+Na]^+$ = 284.1405.



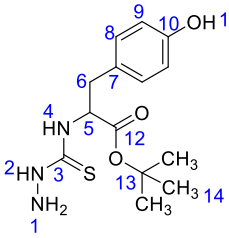
(*S*)-*Tert*-butyl 2-(hydrazidecarbothioamino)-3-methylpentanoate from 0.43 g (1.9 mmol) (*S*)-*tert*-butyl 2-isothiocyanato-3-methylpentanoate, 0.09 mL (1.9 mmol) hydrazine hydrate. The product was obtained as brown solid. Yield: 0.45 g (1.7 mmol, 90%). $C_{11}H_{23}N_3O_2S$ **(**261.38 g/mol). ^{1}H NMR (499 MHz, DMSO-d_6) δ [ppm] = 7.99 (s, 1H, H-2), 7.90 (d, *J* = 8.4 Hz, 1H, H-3), 4.88 (m, 1H, H-4), 3.88 (s, 2H, H-1), 1.99 (m, 1H, H-5), 1.56-1.12 (m, 11H, H-6, H-9), 0.98-0.89 (m, 6H, H-7/-H8).



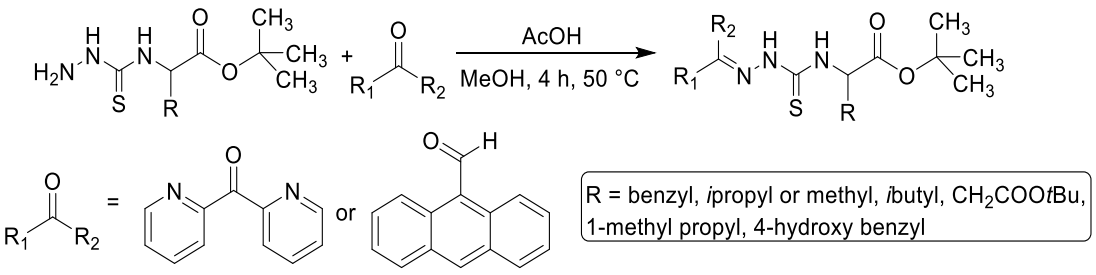
(*S*)-Di-*tert*-butyl 2-(hydrazidecarbothioamino)butanedioate from 0.43 g (1.7 mmol) (*S*)-di-*tert*-butyl 2-isothiocyanatobutanedioate, 0.08 mL (1.7 mmol) hydrazine hydrate. The product was obtained as brown solid. Yield: 0.55 g (1.7 mmol, 99%). $C_{13}H_{25}N_3O_4S$ (319.42 g/mol). ^{1}H NMR (300 MHz, DMSO-d_6) δ [ppm] = 9.01 (s, 1H, H-2), 8.11 (d, *J* = 8.0 Hz, 1H, H-3), 5.10 (m, 1H, H-4), 4.59 (s, 2H, H-1), 2.80 (m, 2H, H-5), 1.42-1,40 (m, 18H, H-6, H-7). HR-ESI-MS: m/z $[M+H]^+$ = 320.1639, m/z $[M+Na]^+$ = 342.1460.



(*S*)-*Tert*-butyl 2-(hydrazidecarbothioamino)-3-(4-hydroxyphenyl)propanoate from 0.16 g (0.6 mmol) *tert*-butyl-3 (4-hydroxyphenyl)-2-isothiocyanatopropanoate, 0.03 mL (0.6 mmol) hydrazine hydrate. The product was obtained as brown solid. Yield: 0.15 g (0.5 mmol, 88%). $C_{14}H_{21}N_3O_3S$ (311.40 g/mol). ^{1}H NMR (300 MHz, DMSO-d_6) δ [ppm] = 8.95 (s, 1H, H-2), 7.77 (d, *J* = 7.4 Hz, 1H, H-4), 6.96 (d, *J* = 8.5 Hz, 2H, H-9), 6.68 (d, *J* = 8.4 Hz, 2H, H-8) 4.96 (m, 1H, H-5), 4.55 (s, 2H, H-1), 2.97 (m, 2H, H-6), 1.35 (s, 9H, H-14). ^{13}C NMR (300 MHz, DMSO-d_6) δ [ppm] = 180.75 (C-3) 170.92 (C-12), 156.53 (C-10), 130.72 (C-9), 126.96 (C-7), 115.48 (C-8), 81.52 (C-13), 57.75 (C-5), 37.44 (C-6), 28.03 (C-14). HR-ESI-MS: m/z $[M+H]^+$ = 312.1375, m/z $[M+Na]^+$ = 334.1195.

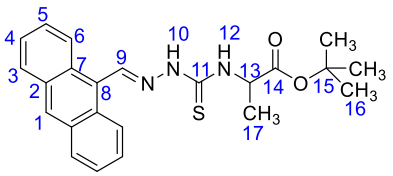


5.3.1.4 Synthesis of TSCs – general description



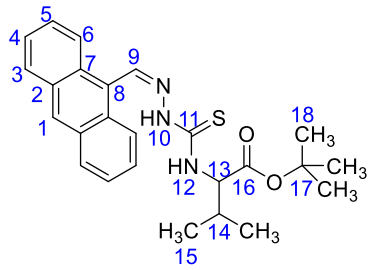
The thiosemicarbazide (1.00 eq.) and antracene-9-carbaldehyde or di-(2-pyridyl) ketone (1.00 eq.) were dissolved in a minimum amount of MeOH. A few drops of glacial AcOH or HCl were added, and the reaction mixture was sonicated at 50 °C for 4 h or refluxed overnight. The solvent was removed under reduced pressure, and the crude product was purified by column chromatography.

9-Anthraldehyde-4-((*S*)-*tert*-butylpropanoate)-3-thiosemicarbazone from 0.30 g (1.4 mmol) 4-((*S*)-*tert*-butylpropanoate)thiosemicarbazide, 0.28 g (1.4 mmol) antracene-9-carbaldehyde. The reaction mixture was sonicated for 4 h. The product was purified by column chromatography (c-hexane/EOAc 8:1 v/v) and obtained as yellow solid. Yield: 0.27 g (0.7 mmol, 48%). $C_{23}H_{25}N_3O_2S$ (407.53 g/mol). ^{1}H NMR (499 MHz, DMSO-d_6) δ [ppm] = 11.94 (s, 1H, H-10), 9.34 (s, 1H, H-9), 8.73 (s, 1H, H-1), 8.52 (d, *J* = 8.3 Hz, 2H, H-6), 8.21 (d, *J* = 8.3 Hz, 1H, H-12), 8.15 (d, *J* = 8.5 Hz, 2H, H-3), 7.65-7.57 (m, 4H, H-4, H-5), 4.87 (m, 1H, H-13), 1.44-1.42 (m, 12H, H-16, H-17). ^{13}C NMR (499 MHz, DMSO-d_6) δ [ppm] = 177.28 (C-11), 170.75 (C-14), 142.43 (C-9), 131.25 (C-2), 130.04 (C-1), 129.87 (C-7), 129.46 (C-3), 127.87 (C-5), 126.05 (C-4), 125.54 (C-8), 124.96 (C-6), 82.50 (C-15), 53.03 (C-13), 28.76 (C-16), 18.36 (C-17).

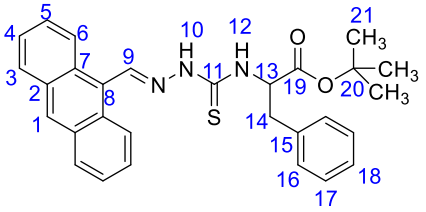


9-Anthraldehyde-4-((*S*)-*tert*-butyl 3-metylbutanoate)-3-thiosemicarbazone from 0.30 g (1.2 mmol) 4-((*S*)-*tert*-butyl-3-metylbutanoate)thiosemicarbazide, 0.25 g (1.2 mmol) antracene-9-carbaldehyde. The reaction mixture was sonicated for 4 h. The product was purified by column chromatography (c-

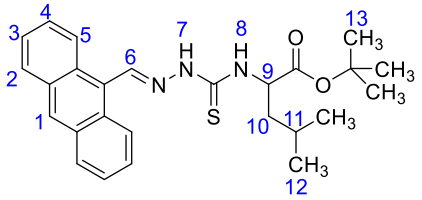
hexane/EOAc 6:1 v/v) and obtained as orange solid. Yield: 0.27 g (0.6 mmol, 52%). $C_{25}H_{29}N_3O_2S$ (435.59 g/mol). ^{1}H NMR (499 MHz, DMSO-*d*$_6$) δ [ppm] = 12.09 (s, 1H, H-10), 9.38 (s, 1H, H-9), 8.74 (s, 1H, H-1), 8.57 (d, *J* = 7.4 Hz, 2H, H-6), 8.16 (d, *J* = 7.4 Hz, 2H, H-3), 7.90 (d, *J* = 7.9 Hz, 1H, H-12), 7.60 (m, 4H, H-4, H-5), 4.81 (m, 1H, H-13), 2.27 (m, 1H, H-14), 1.45 (s, 9H, H-18), 0.97 (m, 6H, H-15) ^{13}C NMR (499 MHz, DMSO-*d*$_6$) δ [ppm] = 177.92 (C-11), 170.52 (C-16), 142.55 (C-9), 131.72 (C-2), 130.28 (C-2), 130.06 (C-7), 129.47 (C-3), 127.66 (C-4/C-5), 125.96 (C-4/C-5), 125.10 (C-8), 124.74 (C-6), 82.10 (C-17), 62.29 (C-13), 32.67 (C-14), 27.49 (C-18), 18.11 (C-15).



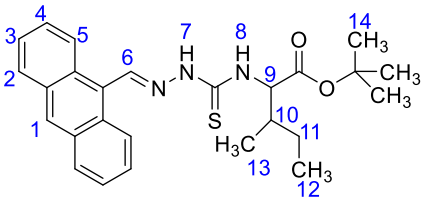
9-Anthraldehyde-4-((*S*)-*tert*-butyl 4-methylbutanoate)-3-thiosemicarbazone from 0.30 g (1.0 mmol) 4-((*S*)-*tert*-butyl-3-phenylpropanoate)thiosemicarbazide, (0.20 g, 1.0 mmol) antracene-9-carbaldehyde. The product was purified by column chromatography (c-hexane/EOAc 8:1 v/v) and obtained as yellow solid. Yield: 0.21 g (0.4 mmol, 43%). $C_{29}H_{29}N_3O_2S$ (483.63 g/mol). ^{1}H NMR (499 MHz, DMSO-*d*$_6$) δ [ppm] = 12.01 (s, 1H, H-10), 9.33 (s, 1H, H-9), 8.73 (s, 1H, H-1), 8.47 (m, 2H, H-6), 8.15 (m, 2H, H-3), 8.08 (d, *J* = 6.6 Hz, 1H, H-12), 7.58 (m, 4H, H-4, H-5), 7.25 (m, 4H, H-16, H-17), 7.22 (m, 1H, H-18), 5.13 (m, 1H, H-13), 3.24 (m, 2H, H-14), 1.36 (s, 9H, H-21). ^{13}C NMR (499 MHz, DMSO-*d*$_6$) δ [ppm] = 177.39 (C-11), 169.86 (C-19), 142.77 (C-9), 137.02 (C-15), 131.39 (C-2), 130.10 (C-7), 130.01 (C-1), 129.61 (C-3), 129.06 (C-16, C-17), 127.73 (C-4/C-5), 127.51 (C-18), 126.02 (C-4/C-5), 125.26 (C-8), 124.98 (C-6), 82.59 (C-20), 58.14 (C-13), 37.18 (C-14), 28.01 (C-21).



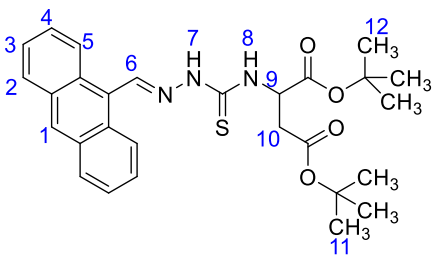
9-Anthraldehyde-4-((*S*)-*tert*-butyl 4-methylpentonate)-3-thiosemicarbazone from 0.20 g (0.8 mmol) 4-((*S*)-*tert*-butyl-4-methylpentonate)thiosemicarbazide, 0.16 g (0.8 mmol) antracene-9-carbaldehyde. The product was obtained as yellow solid. Yield: 0.36 g (0.8 mmol, 100%). $C_{26}H_{31}N_3O_2S$ (449.61 g/mol). ^{1}H NMR (499 MHz, DMSO-*d*$_6$) δ [ppm] = 11.99 (s, 1H, H-7), 9.34 (s, 1H, H-6), 8.72 (s, 1H, H-1), 8.52 (d, *J* = 8.0 Hz, 2H, H-5), 8.14 (m, 3H, H-2), 7.58 (m , 4H, H-3, H-4), 4.96 (m, 1H, H-9), 1.86-1.62 (m , 3H, H-10, H-11), 1.42 (s, 9H, H-13), 0.93 (m, 6H, H-12). HR-ESI-MS: m/z $[M+H]^+$ = 450.2214, m/z $[M+Na]^+$ = 472.2032.



***Tert*-butyl-2-([(1*E*)-(anthracen-9-yl)methylideneaminocarbamthioyl]amino)-3-methylpentanoate** from 0.10 g (0.4 mmol) (*S*)-*tert*-butyl-2-(hydrazidecarbothioamino)-3-methylpentanoate, 0.08 g (0.4 mmol) antracene-9-carbaldehyde. The product was obtained as yellow solid. Yield: 0.15 g (0.34 mmol, 90%). $C_{26}H_{31}N_3O_2S$ (449.61 g/mol). ^{1}H NMR (499 MHz, DMSO-*d*$_6$) δ [ppm] = 12.11 (s, 1H, H-7), 9.39 (s, 1H, H-6), 8.76 (s, 1H, H-1), 8.61 (m, 2H, H-5), 8.18 (m, 2H, H-2), 8.04 (d, *J* = 8.7 Hz, 1H, H-8), 7.62 (m, 4H, H-3, H-4), 5.04 (m, 1H, H-9), 2.05 (m, 1H, H-10), 1.46 (s, 9H, H-14), 1.23 (m, 2H, H-11), 0.92 (m, 6H, H-12, H-13).

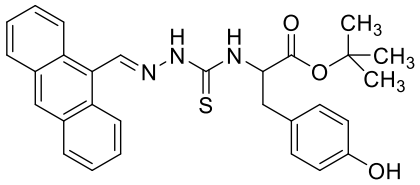


Di-*tert*-butyl-2-([(1*E*)-(anthracen-9-yl)methylideneaminocarbamthioyl]amino) butanedioate from 0.20 g (0.8 mmol) (*S*)-di-*tert*-butyl-2-(hydrazide-carbothioamino)butanedioate, 0.16 g (0.8 mmol). antracene-9-carbaldehyde. The product was obtained as yellow solid. Yield: 0.29 g (0.6 mmol, 75%). $C_{28}H_{33}N_3O_4S$ (507.65 g/mol). ^{1}H NMR (499 MHz, DMSO-*d*$_6$) δ [ppm] = 12.06 (s, 1H, H-7), 9.38 (s, 1H, H-6), 8.74 (s, 1H, H-1), 8.58 (d, *J* = 8.4 Hz, 2H, H-5), 8.41 (d, J = 8.3 Hz, 1H, H-2), 8.17 (d, *J* = 7.7 Hz, 2H, H-8), 7.61 (p, *J* = 5.8 Hz, 4H,

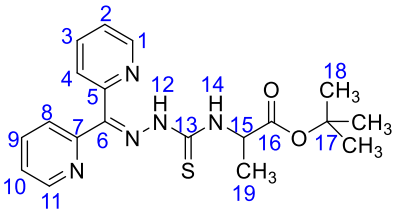


H-3, H-4), 5.21 (m, 1H, H-9), 2.91 (d, *J* = 4.6 Hz, 2H, H-10), 1.41 (s, 9H, H-11/H-12), 1.29 (s, 9H, H-11/H-12). HR-ESI-MS: m/z $[M+H]^+$ = 508.2274, m/z $[M+Na]^+$ = 530.2084.

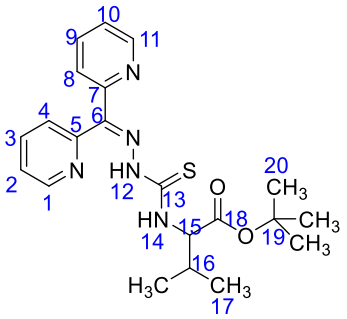
***Tert*-butyl-2-[(2*E*)-2-[(anthracen-9-yl)methylidene]hydrazinocarbamthioyl]-3-(4-hydroxyphenyl) propanoate** from 0.10 g (0.32 mmol) (*S*)-*tert*-butyl-2-(hydrazidecarbothioamino)-3-(4-hydroxyphenyl) propanoate, 0.07 g (0.32 mmol) antracene-9-carbaldehyde. The product was purified by column chromatography (c-hexane/EOAc 4:1) and obtained as yellow solid. Yield: 0.07 g (0.14 mmol, 45%). $C_{29}H_{29}N_3O_3S$ (499.63 g/mol). ^{1}H NMR (499 MHz, DMSO-d_6) δ [ppm] = 11.99 (s, 1H), 9.34 (s, 1H), 9.25 (s, 1H), 8.74 (s, 1H), 8.74 (m, 2H), 8.16 (m, 2H), 7.99 (d, *J* = 7.9 Hz, 1H), 7.04 (d, *J* = 8.3 Hz, 2H), 6.64 (d, *J* = 8.4, 2H), 5.04 (m, 1H), 3.13 (m, 2H), 1.36 (s, 9H).



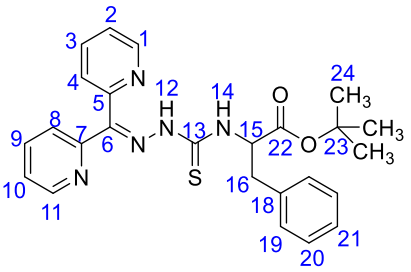
Di-2-pyridylketone-4-((*S*)-*tert*-butyl propanoate)-3-thiosemicarbazone from 0.30 g (1.4 mmol) 4-((*S*)-*tert*-butylpropanoate)thiosemicarbazide, 0.25 g (1.4 mmol) di-pyridyl ketone. The product was purified by column chromatography (c-hexane/EOAc 1:2 v/v) and obtained as orange solid. Yield: 0.30 g (0.8 mmol, 56%). $C_{19}H_{23}N_5O_2S$ (385.49 g/mol). ^{1}H NMR (499 MHz, DMSO-d_6) δ [ppm] = 13.53 (s, 1H, H-12), 8.82 (d, *J* = 4.4 Hz, 1H, H-1), 8.72 (d, *J* = 8.6 Hz, 1H, H-14), 8.59 (d, *J* = 4.3 Hz, 1H, H-11), 8.14 (d, *J* = 7.4 Hz, 1H, H-4), 7.98 (m, 2H, H-3, H-3, H-9), 7.59 (m, 1H, H-10), 7.49 (m, 2H, H-2, H-8), 4.88 (m, 1H), 1.48 (d, *J* = 7.3 Hz, 3H), 1.43 (s, 9H). ^{13}C NMR (499 MHz, DMSO-d_6) δ [ppm] = 178.11 (C-13), 171.48 (C-16), 155.47 (C-7), 151.50 (C-5), 148.95 (C-11), 148.65 (C-1), 142.33 (C-6), 138.10 (C-3), 137.67 (C-9), 127.65 (C-8), 125.43 (C-10), 124.58 (C-2), 124.29 (C-4), 82.24 (C-17), 62.63 (C-15), 28.11 (C-18), 19.10 (C-19). HR-ESI-MS: m/z $[M+H]^+$ = 386.1650, m/z $[M+Na]^+$ = 408.1469.



Di-2-pyridylketone-4-((*S*)-*tert*-butyl 3-metylbutanoate)-3-thiosemicarbazone from 0.30 g (1.2 mmol) 4-((*S*)-*tert*-butyl-3-metylbutanoate)thiosemicarbazide, 0.22 g (1.2 mmol) di-pyridyl ketone. The product was purified by column chromatography (c-hexane/EOAc 1:3 v/v) and obtained as yellowish solid. Yield: 0.32 g (0.8 mmol, 65%). $C_{21}H_{27}N_5O_2S$ (413.54 g/mol). ^{1}H NMR (499 MHz, DMSO-d_6) δ [ppm] = 13.59 (s, 1H, H-12), 8.84 (m, 1H, H-1), 8.62 (m, 1H, H-11), 8.36 (m, 1H, H-14), 8.00 (m, 3H, H-3, H-8, H-9), 7.60 (m, 1H, H-2), 7.52 (m, 2H, H-4, H-10), 4.74 (m, 1H, H-15), 2.30 (m, 1H, H-16), 1.44 (s, 9H, H-20), 0.95 (m, 6H, H-17). ^{13}C NMR (499 MHz, DMSO-d_6) δ [ppm] = 178.26 (C-13), 170.26 (C-18), 155.49 (C-7), 151.51 (C-5), 149.11 (C-11), 148.71 (C-1), 142.33 (C-6), 138.22 (C-3), 137.87 (C-9), 127.67 (C-10), 125.38 (C-2), 124.48 (C-4), 123.78 (C-8), 82.03 (C-19), 62.59 (C-15), 31.14 (C-16), 28.61 (C-19), 18.93 (C-17). HR-ESI-MS: m/z $[M+H]^+$ = 414.1961, m/z $[M+Na]^+$ = 436.1782.

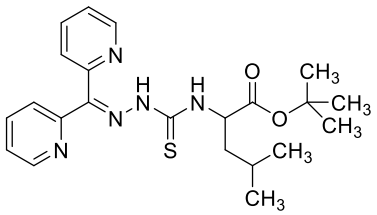


Di-2-pyridylketone-4-((*S*)-*tert*-butyl 3-phenylbutanoate)-3-thiosemicarbazone from 0.30 g (1.0 mmol) 4-((*S*)-*tert*-butyl-3-phenylpropanoate)thiosemicarbazide, 0.18 g (1.0 mmol) di-pyridyl ketone. The product was purified by column chromatography (c-hexane/EOAc 1:2 v/v) and obtained as colorless solid. Yield: 0.38 g (0.8 mmol, 82%). $C_{25}H_{27}N_5O_2S$ (461.58 g/mol). ^{1}H NMR (499 MHz, DMSO-d_6) δ [ppm] = 13.57 (s, 1H, H-12), 8.81 (d, *J* = 4.2 Hz, 1H, H-1), 8.61 (d, *J* = 4.4 Hz, 1H, H-11), 8.53 (d, *J* = 7.9 Hz, 1H, H-14), 8.05-7.93 (m , 3H, H-3, H-8, H-9), 7.61-7.48 (m, 3H, H-2, H-4, H-10), 7.32-7.21 (m, 5H, H-19,H-20, H-21), 5.08 (m, 1H, H-15), 3.28 (m, 2H, H-16), 1.38 (s, 9H, H-24). ^{13}C NMR (499 MHz, DMSO-d_6) δ [ppm] = 178.18 (C-13), 170.14 (C-21), 155.44 (C-7), 151.29 (C-5), 149.00 (C-11), 148.57 (C-1), 142.10 (C-6), 138.12 (C-3/C-8/C-9), 137.63 (C-3/C-8/C-9), 137.17 (C-18), 129.85 (C-18/C-19/C-20), 128.86 (C-18/C-19/C-20), 127.74 (C-

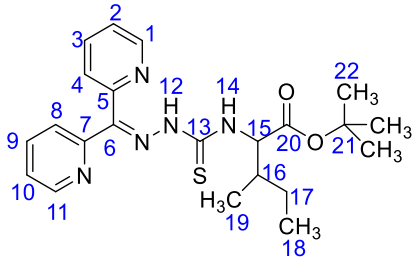


2/C-4/C-10), 127.68 (C-18/C-19/C-20), 125.40 (C-2/C-4/C-10), 124.50 (C-2/C-4/C-10), 124.00 (C-3/C-8/C-9), 82.16 (C-23), 59.19 (C-15), 37.06 (C-16), 27.86 (C-24). HR-ESI-MS: m/z $[M+H]^+$ = 462.1961, m/z $[M+Na]^+$ = 484.1780.

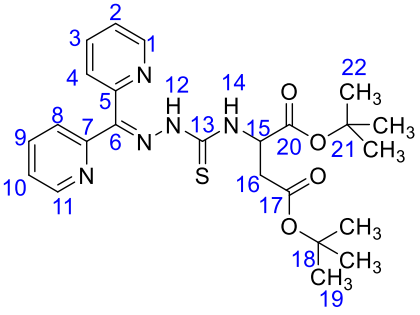
Di-2-pyridylketone-4-((*S*)-*tert*-butyl-4-methylpentanoate)-3-thiosemicarbazone from 0.20 g (0.8 mmol) 4-((*S*)-*tert*-butyl-4-methylpentonate)thiosemicarbazide, 0.14 g (0.8 mmol) di-pyridyl ketone. The product was obtained as brown oil. Yield: 0.34 g (0.8 mmol, quant.). $C_{22}H_{29}N_5O_2S$ (427.57 g/mol). ^{1}H NMR (499 MHz, DMSO-d_6) δ [ppm] = 13.42 (s, 1H), 11.94, (s, 1H), 8.84 (d, *J* = 4.1 Hz, 1H), 8.69 (d, *J* = 8.3 Hz, 1H), 8.60 (d, *J* = 3.9 Hz, 1H), 8.17 (d, *J* = 7.8 Hz, 1H), 8.00 (t, *J* = 7.5 Hz, 2H), 7.62 (m, 1H), 7.52 (m, 2H), 4.94 (m, 1H), 3.17 (m, 1H), 1.67 (m, 2H), 1.43 (s, 9H), 0.93 (t, *J* = 5.6 Hz, 6H). HR-ESI-MS: m/z $[M+H]^+$ = 428.2116, m/z $[M+Na]^+$ = 450.1936.



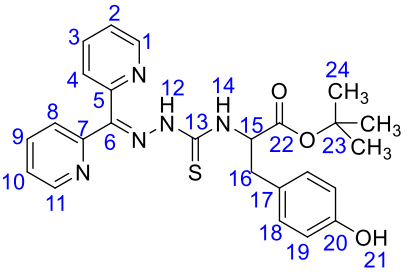
***Tert*-butyl 2-(2-[bis(pyridin-2-yl)methylidene]hydrazinocarbamthioyl)-3-methylpentanoate** from 0.10 g (0.5 mmol) (*S*)-*tert*-butyl-2-(hydrazidecarbothioamino)-3-methylpentanoate, 0.14 g (0.5 mmol) di(2-pyridyl) ketone. The product was purified by column chromatography (c-hexane/EOAc 1:2 v/v) and obtained as brown oil. Yield: 0.17 g (0.4 mmol, 80%). $C_{22}H_{29}N_5O_2S$ (427.57 g/mol). ^{1}H NMR (499 MHz, DMSO-d_6) δ [ppm] = 13.64 (s, 1H, H-12), 8.85 (d, *J* = 4.3 Hz, 1H, H-1), 8.62 (d, *J* = 4.6 Hz, 1H, H-11), 8.38 (d, *J* = 8.2 Hz, 1H, H-14), 8.00 (m, 3H, H-3, H-8, H-9), 7.60 (m, 1H, H-2), 7.50 (m, 2H, H-4, H-10), 4.83 (m, 1H, H-15), 2.09 (m, 1H, H-16), 1.53 (m, 1H), 1.44 (s, 9H, H-22), 1.30 (m, 2H, H-17), 0.33 (m, 6H, H-18, H-19). ^{13}C NMR (499 MHz, DMSO-d_6) δ [ppm] = 177.78 (C-13), 170.43 (C-20), 155.53 (C-7), 151.61 (C-5), 149.08 (C-11), 148.67 (C-1), 142.35 (C-6), 138.17 (C-3/C-8/C-9), 137.89 (C-3/C-8/C-9), 127.64 (C-4/C-10), 125.40 (C-2), 124.56 (C-4/C-10), 123.75 (C-3/C-8/C-9), 81.75 (C-21), 61.26 (C-15), 37.46 (C-16), 28.10 (C-22), 26.14 (C-17), 11.71 (C-18/C-19), 15.55 (C-18/C-19). HR-ESI-MS: m/z $[M+H]^+$ = 428.2116, m/z $[M+Na]^+$ = 450.1936.



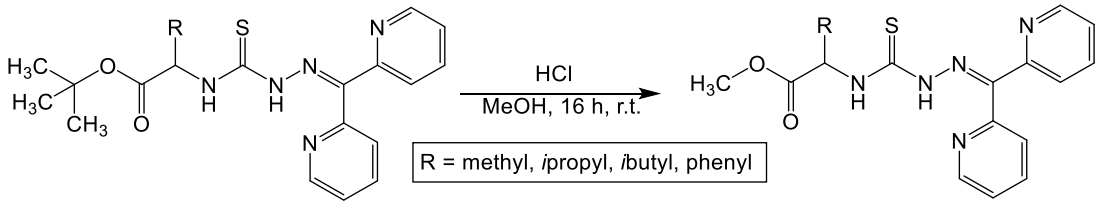
Di-*tert*-butyl 2-([bis(pyridin-2-yl)methylideneaminocarbamthioyl]amino)butanedioate from 0.20 g (0.8 mmol) (*S*)-di-*tert*-butyl-2-(hydrazide-carbothioamino)butanedioate, 0.15 g (0.8 mmol) di(2-pyridyl ketone. The product was purified by column chromatography (c-hexane/EOAc 1:2 v/v) and obtained as brown oil. Yield: 0.30 g (0.6 mmol, 75%). $C_{24}H_{31}N_5O_4S$ (485.60 g/mol). ^{1}H NMR (499 MHz, DMSO-d_6) δ [ppm] = 13.69 (s, 1H, H-12), 8.86 (d, *J* = 4.2 Hz, 1H, H-1), 8.79 (d , *J* = 8.5 Hz, 1H, H-14), 8.62 (d, *J* = 4.7 Hz, 1H, H-11), 7.99 (m, 3H, H-3, H-8, H-9), 7.62 (m, 1H, H-2), 7.51 (m, 2H, H-4, H-10), 5.18 (m, 1H, H-15), 2.92 (d, *J* = 5.3 Hz, 2H, H-16), 1.43 (s, 9H, H-19/H-22), 1.36 (s, 9H, H-19/H-22). ^{13}C NMR (499 MHz, DMSO-d_6) δ [ppm] = 178.16 (C-13), 169.94 (C-17/C-20), 169.38 (C-17/C-20), 155.63 (C-7), 151.52 (C-5), 149.65 (C-11), 148.65 (C-1), 142.47 (C-6), 138.21 (C-3/C-8/C-9), 137.70 (C-3/C-8/C-9), 127.59 (C-4/C-10), 125.34 (C-2), 124.41 (C-4/C-10), 123.93 (C-3/C-8/C-9), 82.30 (C-18/C-21), 81.18 (C-18/C-21), 53.75 (C-15), 37.18 (C-16), 28.03 (C-19, C-22). HR-ESI-MS: m/z $[M+H]^+$ = 486.2173, m/z $[M+Na]^+$ = 508.1994.



***Tert*-butyl 2-(2-[bis(pyridin-2-yl)methylidene]hydrazinocarbamthioyl)-3-(4-hydroxyphenyl)-propanoate** from 0.10 g (0.3 mmol) (*S*)-*tert*-butyl-2-(hydrazidecarbothioamino)-3-(4-hydroxyphenyl) propanoate, 0.07 g (0.3 mmol) di(2-pyridyl) ketone. The product was purified by column chromatography (c-hexane/EOAc 1:3 v/v) and obtained as brown oil. Yield: 0.12 g (0.25 mmol, 82%). $C_{25}H_{27}N_5O_3S$ (477.58 g/mol). ^{1}H NMR (499 MHz, DMSO-d_6) δ [ppm] = 13.53 (s, 1H, H-12), 9.30 (s, 1H, H-21), 8.84 (d, *J* = 6.6 Hz, 1H, H-1), 8.61 (d, *J* = 5.6 Hz, 1H, H-11), 8.39 (d, *J* = 8.5 Hz, 1H, H-14), 8.00 (m, 3H, H-3, H-8, H-9), 7.59 (m, 1H, H-2), 7.52 (m, 2H, H-4, H-10), 7.07 (d, *J* = 8.5 Hz, 2H, H-18), 6.69 (d, *J* = 8.5, 2H, H-19), 4.95 (m, 1H, H-15), 3.10 (m, 2H, H-16), 1.40 (s, 9H, H-24). ^{13}C NMR (499 MHz, DMSO-d_6) δ [ppm] = 177.67 (C-13), 169.14 (C-22), 156.76 (C-17), 155.59 (C-7), 151.25 (C-5), 148.94 (C-11), 148.54 (C-1), 141.98 (C-6), 138.12 (C-3/C-8/C-9), 137.73 (C-3/C-8/C-9), 130.44 (C-18) 127.73 (C-4/C-10), 126.67 (C-20), 125.44 (C-2), 124.37 (C-4/C-10), 123.96 (C-3/C-8/C-9), 115.88 (C-20), 81.87 (C-23), 58.78 (C-15), 36.15 (C-16), 28.07 (C-24). HR-ESI-MS: m/z $[M+H]^+$ = 478.1911, m/z $[M+Na]^+$ = 500.1733.

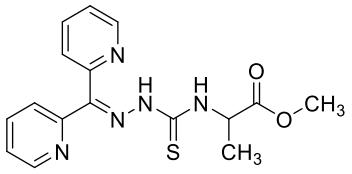


5.3.1.5 Transesterfication of di-2-pyridylketone TSC to methyl esters

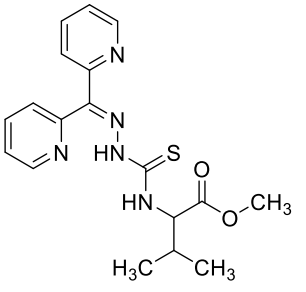


The TSC (1.00 eq.) was dissolved in 10 mL of MeOH and cooled down to 0 °C. Afterwards, conc. HCl (200.00 eq.) was added dropwise. The reaction mixture was stirred overnight at room temperature. Then, the solvent was removed under reduced pressure and the crude product was redissolved in 20 mL of EtOAc. The solution was washed three times with 30 mL of sat. Na_2CO_3 solution and two times with 30 mL brine. The organic phase was dried over $MgSO_4$ and the solvent was removed under reduced pressure yielding the product.

Methyl 2-(2-[bis(pyridin-2-yl)methylidene]hydrazinocarbamthioyl) propanoate from 50.0 mg (0.13 mmol) di-2-pyridylketone-4-((*S*)-*tert*-butyl propanoate)-3-thiosemicarbazone and 2.16 mL (26.00 mmol) conc. HCl. The product was obtained as a green solid. Yield: 40.8 mg (0.12 mmol, 95%). $C_{16}H_{17}N_5O_2S$ (343.41 g/mol). ^{1}H NMR (300 MHz, DMSO-d_6) δ [ppm] = 13.44 (s, 1H), 8.96 (d, *J* = 8.0 Hz, 1H), 8.84 (d, *J* = 4.2 Hz, 1H), 8.60 (d, *J* = 4.2 Hz, 1H), 8.20 (d, *J* = 7.9 Hz, 1H), 8.01 (m, 2H), 7.60 (m, 1H), 7.50 (d, *J* = 8.1 Hz, 2H), 5.08 (p, *J* = 7.2 Hz, 1H), 3.68 (s, 3H), 1.49 (d, *J* = 7.2 Hz, 3H). ^{13}C NMR (499 MHz, DMSO-d_6) δ [ppm] = 172.72, 151.46, 148.92, 148.65, 138.10, 137.63, 127.67, 125.33, 124.49, 124.34, 52.98, 52.60, 17.35.

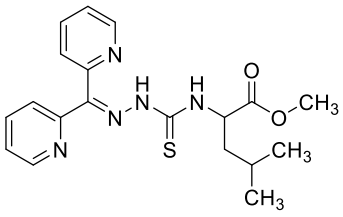


Methyl 2-(2-[bis(pyridin-2-yl)methylidene]hydrazinocarbamthioyl)-3-methylbutanoate from 100.0 mg (0.24 mmol) di-2-pyridylketone-4-((*S*)-*tert*-butyl 3-metylbutanoate)-3-thiosemicarbazone and 4.02 mL (48.40 mmol) conc. HCl. The product was obtained as a green solid. Yield: 71.5 mg (0.20 mmol, 83%). $C_{18}H_{21}N_5O_2S$ (371.46 g/mol). ^{1}H NMR (300 MHz, DMSO-d_6) δ [ppm] = 13.57 (s, 1H), 8.84 (d, *J* = 4.9 Hz, 1H), 8.61 (d, *J* = 4.7 Hz, 1H), 8.54 (d, *J* = 8.3 Hz, 1H), 8.09-7.97 (m, 3H), 7.61 (ddd, *J* = 7.6, 5.0, 1.0 Hz, 1H), 7.51 (m, 2H), 4.85 (dd, *J* = 8.3, 6.3 Hz, 1H), 3.71 (s, 3H), 2.34 (m, 1H), 0.97 (t, *J* = 6.4 Hz, 6H). ^{13}C

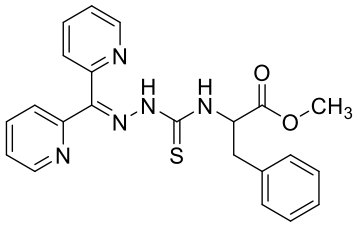


NMR (499 MHz, DMSO-d_6) δ [ppm] = 178.66, 172.19, 155.91, 151.53, 148.59, 148.17, 140.80, 137.26, 136.96, 126.83, 124.26, 123.78, 123.70, 61.75, 52.21, 31.62, 29.69, 18.71, 18.52, 1.02

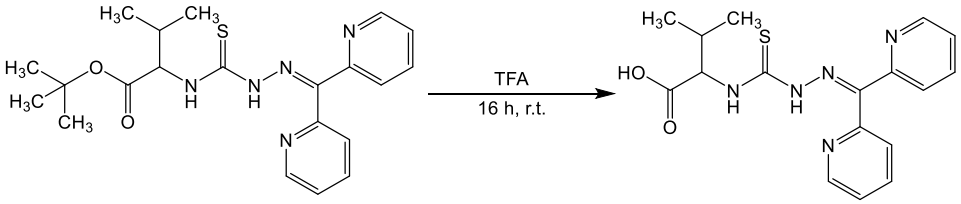
Methyl 2-(2-[bis(pyridin-2-yl)methylidene]hydrazinocarbamthioyl)-4-methylpentanoate from di-2-pyridylketone-4-((*S*)-*tert*-butyl-4-methylpentanoate)-3-thiosemicarbazone 50.0 mg (0.12 mmol) and 1.95 mL (23.40 mmol) conc. HCl. The product was obtained as a green solid. Yield: 43.7 mg (0.11 mmol, 98%). $C_{19}H_{23}N_5O_2S$ (385.49 g/mol). ^{1}H NMR (300 MHz, DMSO-d_6) δ [ppm] = 13.21 (s, 1H), 8.86 (m, 1H), 8.69 (m, 1H), 8.15 (m, 4H), 7.65 (m, 3H), 5.04 (m, 1H), 3.67 (s, 3H), 2.74 (m, 1H), 2.17 (m, 2H), 0.92 (m, 6H).



Methyl 2-(2-[bis(pyridin-2-yl)methylidene]hydrazinocarbam thioyl)-3-phenylpropanoate from 50.0 mg (0.11 mmol) di-2-pyridylketone-4-((*S*)-*tert*-butyl-3-phenylbutanoate)-3-thiosemi carbazone and 1.80 mL (21.71 mmol) conc. HCl. The product was obtained as a green solid. Yield: 40.0 mg (0.09 mmol, 88%). $C_{22}H_{21}N_5O_2S$ (419.50 g/mol). ^{1}H NMR (300 MHz, DMSO-d_6) δ [ppm] = 13.32 (s, 1H), 8.76 (m, 1H), 8.57 (m, 1H), 7.96 (m, 3H), 7.76 (m, 1H), 7.50 (m, 4H), 7.19 (m, 6H), 4.53 (m, 1H), 3.68 (s, 3H), 2.29 (m, 2H).



5.3.1.6 Synthesis of 2-(1-[Bis(2-pyridyl)methylene]thiosemicarbazido)-3-methylbutyric acid

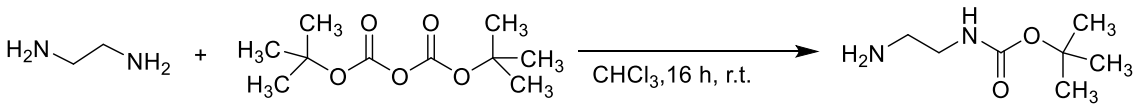


50.0 mg of the TSC (0.12 mmol) was dissolved in 5 mL of TFA and the reaction mixture was stirred overnight at room temperature. After that, the solvent was removed under reduced pressure yielding the product in quantitative yield. Yield: 43.0 mg (quant., 0.12 mmol,). $C_{17}H_{19}N_5O_2S$ (357.43 g/mol). ^{1}H NMR (300 MHz, DMSO-d_6) δ [ppm] = 13.52 (s, 1H), 8.88 (d, J = 4.5 Hz, 1H), 8.66 (d, J = 4.4 Hz, 1H), 8.45 (d, J = 6.0 Hz, 1H), 8.06 (m, 3H), 7.59 (m, 3H), 4.86 (m, 1H), 2.33 (m, 1H), 0.96 (m, 6H).

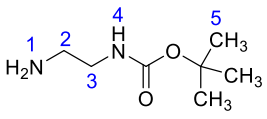
5.3.2 Synthesis of TSCs derived from diamines

5.3.2.1 Synthesis of mono-BOC-protected diamines

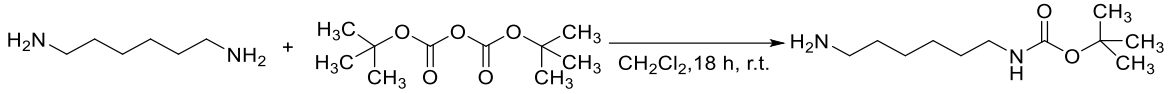
***Tert*-butyl *N*-(2-aminoethyl)carbamate**



1,2-diaminoethane (28.00 mL, 419.3 mmol, 10.00 eq.) was dissolved in 400 mL of $CHCl_3$ and a solution of di-*tert*-butyldicarbonate (9.14 g, 41.9 mmol, 1.00 eq.) in 200 mL of $CHCl_3$ was added dropwise at 0 °C over a period of 3 h. The reaction mixture was stirred for an additional 16 h at room temperature. Then, the solution was washed with brine (6 x 100 mL) and H_2O (1 x 100 mL), dried over $MgSO_4$ and the solvent was removed under reduced pressure. The product was obtained as colorless oil.[283] Yield: 6.09 g (38.0 mmol, 91%). $C_7H_{16}N_2O_2$ (160.22 g/mol). ^{1}H NMR (300 MHz, $CDCl_3$) δ [ppm] = 4.98 (s, 1H, H-4), 3.13 (m, 2H, H-2/H-3), 2.77 (t, J = 5.8 Hz, 2H, H-2/H-3), 1.42 (s, 9H, H-5), 1.28 (s, 2H, H-1).

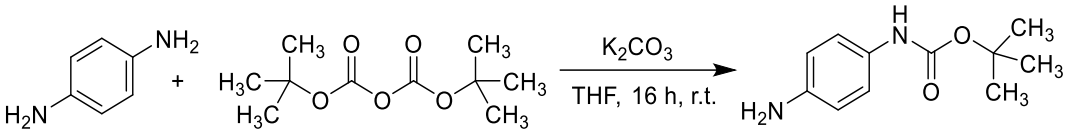


***Tert*-butyl *N*-(6-aminohexyl)carbamate**

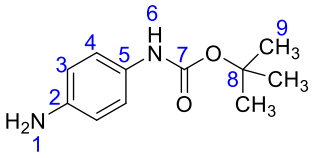


1,6-Hexadiamine (11.70 g, 101.0 mmol, 1.00 eq.) was dissolved in 100 mL of CH_2Cl_2 and the solution was cooled to 0 °C. A solution of di-*tert*-butyl dicarbonate (4.40 g, 20.2 mmol, 0.20 eq.) in 30 mL of CH_2Cl_2 was added dropwise, which lead to the formation of a colorless precipitate. The reaction mixture was stirred for 1 h at 0 °C and for an additional 18 h at room temperature. The precipitate was filtered off, washed with CH_2Cl_2 and the solvent was removed under reduced pressure. The crude product was dissolved in ethyl acetate (EtOAc) and washed with brine solution (3 x 50 mL). The organic phase was separated, dried over $MgSO_4$ and the solvent was removed under reduced pressure, yielding the product as colorless oil.[284] Yield: 3.50 g (16.4 mmol, 81%). $C_{11}H_{24}N_2O_2$ (216.33 g/mol). ^{1}H NMR (300 MHz, DMSO-d_6) δ [ppm] = 4.81 (s, 1H), 2.99 (m, 2H), 2.56 (m, 2H), 1.38 (m, 4H), 1.32 (s, 9H), 1.11 (s, 2H).

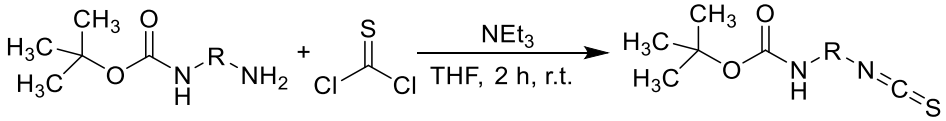
***Tert*-butyl (4-aminophenyl)carbamate**



p-Aminoaniline (9.72 g, 90.0 mmol, 1.00 eq.) and K_2CO_3 (4.56 g, 33.0 mmol, 0.33 eq.) were dissolved in 100 mL of THF and a solution of di-*tert*-butyl dicarbonate (6.54 g, 30.0 mmol, 1.00 eq.) in 30 mL of THF was added dropwise over the course of 1.5 h. The reaction mixture was stirred at room temperature for 16 h. The solution was diluted with 200 mL distilled H_2O and extracted with CH_2Cl_2 (4 x 100 mL). The combined organic phase was washed with brine (2 x 100 mL), dried over Na_2SO_4, and the solvent was removed under reduced pressure. The crude product was purified by column chromatography (petroleum ether/EOAc 2:1 v/v) yielding the product as yellow solid.[285] Yield: 5.75 g (27.6 mmol, 92%). $C_{11}H_{16}N_2O_2$ (208.26 g/mol). ^{1}H NMR (499 MHz, DMSO-d_6) δ [ppm] = 8.76 (s, 1H, H-6), 7.06 (m, 2H, H-4), 6.46 (d, J = 7.6 Hz, 2H, H-3), 4.71 (s, 2H, H-1), 1.44 (s, 9H, H-9). ^{13}C NMR (499 MHz, DMSO-d_6) δ [ppm] = 144.29 (C-5), 129.56 (C-2), 120.73 (C-4), 114.44 (C-2), 79.67 (C-8), 28.62 (C-9).



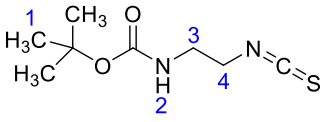
5.3.2.2 Synthesis of isothiocyanates – general description



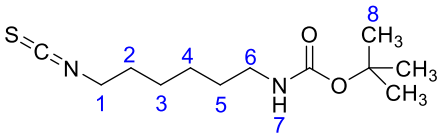
R = C_2H_4, C_6H_{12}, C_6H_4

The reaction was performed under inert conditions. The *boc*-protected amine (1.00 eq.) and Et_3N (3.00 eq.) were dissolved in 200 mL of THF and thiophosgene (85%, 1.40 eq.) was slowly added at 0 °C. The reaction mixture was stirred for 2 h at room temperature, which lead to the formation of a brown suspension. The reaction was quenched by adding 200 mL of H_2O and the product was extracted with Et_2O (3 x 150 mL). The organic phase was dried over Na_2SO_4, and the solvent was removed under reduced pressure, yielding the isothiocyanates.

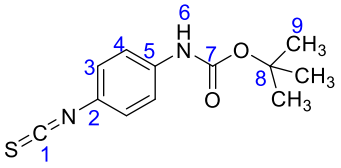
***Tert*-butyl(2-isothiocyanatoethyl)carbamate** from 6.00 g (37.4 mmol) *tert*-butyl-*N*-(2-aminoethyl) carbamate, 4.60 mL (52.4 mmol) thiophosgene, 15.60 mL (112.3 mmol) triethylamine. The product was obtained as brown oil. Yield: 8.19 g (40.5 mmol, quant.). $C_8H_{14}N_2O_2S$ (202.27 g/mol). ^{1}H NMR (300 MHz, $CDCl_3$) δ [ppm] = 4.94 (s, 1H, H-2), 3.63 (t, J = 5.5 Hz, 2H, H-4), 3.36 (q, J = 5.7 Hz, 2H, H-3), 1.44 (s, 9H, H-1).



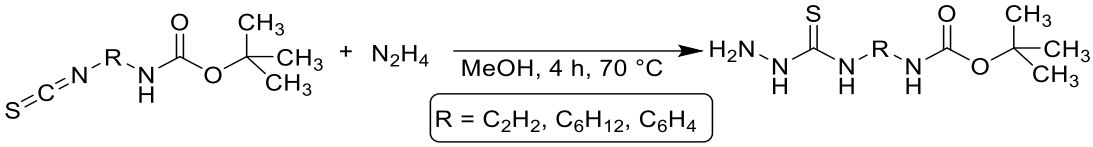
***Tert*-butyl(6-isothiocyanatohexyl)carbamate** from 3.55 g (16.4 mmol) *tert*-butyl-*N*-(6-aminohexyl) carbamate, 1.80 mL (23.0 mmol) thiophosgene, 6.80 mL (49.0 mmol) triethylamine. The product was obtained as brown oil. Yield: 4.26 g (16.4 mmol, quant.). $C_{12}H_{22}N_2O_2S$ (258.38 g/mol). ^{1}H NMR (300 MHz, $CDCl_3$) δ [ppm] = 4.64 (s, 1H, H-7), 3.52 (t, *J* = 6.6 Hz, 2H, H-1), 3.10 (q, *J* = 6.4 Hz, 2H, H-6), 1.71 (m, 2H, H-2), 1.50 (m, 2H, H-5), 1.44 (s, 9H, H-8), 1.35 (m, 4H, H-3, H-4).



***Tert*-butyl(4-isothiocyanatophenyl)carbamate** from 3.00 g (14.4 mmol) *tert*-butyl(4-aminophenyl) carbamate, 1.40 mL (15.8 mmol) thiophosgene, 6.00 mL (43.2 mmol) triethylamine. The product was obtained as brown solid. Yield: 3.72 g (18.4 mmol, quant.). $C_{12}H_{14}N_2O_2S$ (250.32 g/mol). ^{1}H NMR (499 MHz, DMSO-d_6) δ [ppm] = 7.35 (d, *J* = 8.5 Hz, 2H, H-4), 7.14 (m, 2H, H-3), 6.69 (s, 1H, H-6), 1.50 (s, 9H, H-9). ^{13}C NMR (499 MHz, DMSO-d_6) δ [ppm] = 137.86 (C-2), 126.27 (C-3), 119.28 (C-5), 119.23 (C-4), 81.85 (C-8), 28.17 (C-9).

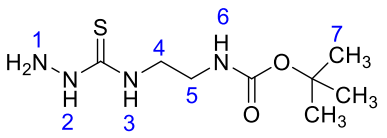


5.3.2.3 Synthesis of thiosemicarbazides – general description

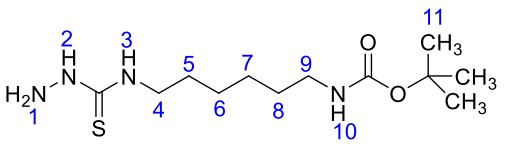


Hydrazine monohydrate (1.80 eq.) was dissolved in 50 mL of MeOH and heated to 70 °C. The isothiocyanate (1.00 eq.) was dissolved in 100 mL of MeOH and slowly added to the hydrazine solution over the course of 1 h. The reaction mixture was stirred for an additional 3 h, then the solvent was removed under reduced pressure, yielding a brown oil. The crude product was dissolved in 10 mL of $CHCl_3$ and poured into boiling petrol ether. A precipitate formed, which was separated by decantation or filtration and the obtained product was dried under ambient conditions.

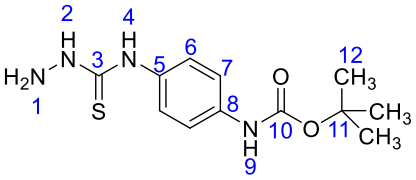
4-(2-*Tert*-butoxycarbonylamino-ethyl)thiosemicarbazide from 7.56 g (37.4 mmol) *ter*t-butyl(2-isothiocyanatoethyl)carbamate, 3.30 mL (67.3 mmol) hydrazine hydrate. The product was obtained as brown solid. Yield: 8.03 g (36.8 mmol, 98%). $C_8H_{18}N_4O_2S$ (234.32 g/mol). ^{1}H NMR (300 MHz, DMSO-d_6) δ [ppm] = 8.67 (s, 1H, H-2), 7.94 (s, 1H, H-3), 6.83 (s, 1H, H-6), 4.44 (s, 2H, H-1), 3.48 (q, *J* = 5.9 Hz, 2H, H-4/H-5), 3.05 (q, *J* = 5.9 Hz, 2H, H-4/H-5), 1.37 (s, 9H, H-7). ^{13}C NMR (300 MHz, DMSO-d_6) δ [ppm] = 181.82, 156.19, 78.15, 43.23, 40.39, 28.69. HR-ESI-MS: m/z $[M+Na]^+$ = 257.1044.



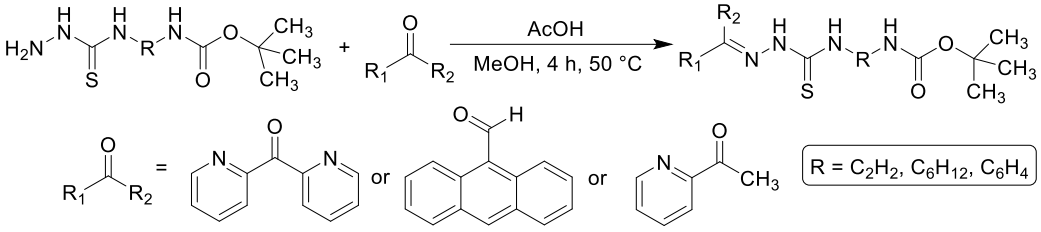
4-(6-*Tert*-butoxycarbonylamino-hexyl)thiosemicarbazide from 4.26 g (16.4 mmol) *tert*-butyl(6-isothiocyanatohexyl)carbamate, 2.20 mL (29.5 mmol) hydrazine hydrate. The product was obtained as brown solid. Yield: 4.46 g (15.4 mmol, 94%). $C_{12}H_{26}N_4O_2S$ (290.43 g/mol). ^{1}H NMR (300 MHz, DMSO-d_6) δ [ppm] = 8.51 (s, 1H, H-2), 7.78 (s, 1H, H-3), 6.74 (s, 1H, H-10), 4.43 (s, 2H, H-1), 2.86 (q, *J* = 6.1 Hz, 2H, H-4), 3.39 (q, *J* = 6.1 Hz, 2H, H-9), 1.47 (m, 2H, H-5), 1.36 (s, 9H, H-8, H-11), 1.23 (m, 4H, H-6, H-7). ^{13}C NMR (300 MHz, DMSO-d_6) δ [ppm] = 181.61, 156.04, 77.74, 40.23, 43.28, 39.66, 29.92, 29.56, 28.73, 26.53. HR-ESI-MS: m/z $[M+H]^+$ = 291.1851, m/z $[M+Na]^+$ = 313.1671.



4-(4-*Tert*-butoxycarbonylamino-phenyl)thiosemicarbazide from 3.72 g (14.8 mmol) *tert*-butyl(4-isothiocyanatophenyl)carbamate, 1.1 mL (23.7 mmol) hydrazine hydrate. The product was obtained as brown solid. Yield: 3.78 g (13.4 mmol, 91%). $C_{12}H_{18}N_4O_2S$ (282.36 g/mol). ^{1}H NMR (499 MHz, DMSO-d_6) δ [ppm] = 9.53 (s, 1H, H-2), 9.27 (s, 1H, H-4), 9.01 (s, 1H, H-9), 7.43 (d, J = 8.5 Hz, 2H, H-7), 7.36 (d, J = 7.8 Hz, 2H, H-6), 4.73 (s, 2H, H-1), 1.47 (s, 9H, H-12). ^{13}C NMR (499 MHz, DMSO-d_6) δ [ppm] = 153.28 (C-10), 136.39 (C-8), 134.02 (C-5), 124.73 (C-6), 118.29 (C-7), 79.36 (C-11), 28.60 (C-12). HR-ESI-MS: m/z $[M+H]^+$ = 283.1218, m/z $[M+Na]^+$ = 305.1038.

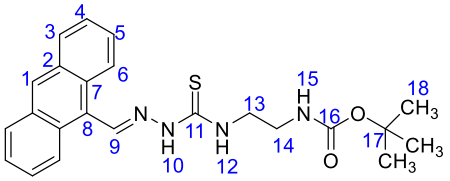


5.3.2.4 Synthesis of TSCs – general description

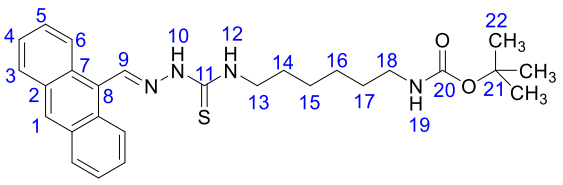


The thiosemicarbazide (1.00 eq.) and the ketone or aldehyde (1.00 eq.) were dissolved in a minimum amount of MeOH. 0.1 mL of glacial AcOH was added, and the reaction mixture was sonicated at 50 °C for 4 h. In case a precipitate was formed during the reaction, the product was filtered off, washed with cold MeOH and dried under ambient conditions. If the product did not precipitate, the solvent was removed under reduced pressure, and the crude product was purified by column chromatography.

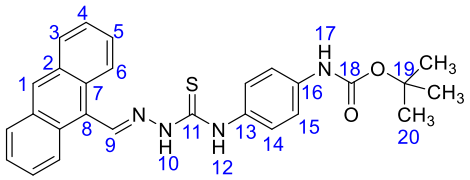
9-Anthraldehyde-4-(2-*tert*-butoxycarbonylamino-ethyl)-3-thiosemicarbazone form 0.20 g (0.8 mmol) 4-(2-*tert*-butoxycarbonylamino-ethyl)thiosemicarbazide, 0.18 g (0.8 mmol) antracene-9-carbaldehyde. The product precipitated as orange solid. Yield: 0.12 g (0.3 mmol, 38%). $C_{23}H_{26}N_4O_2S$ (422.55 g/mol). ^{1}H NMR (499 MHz, DMSO-d_6) δ [ppm] = 11.76 (s, 1H, H-10), 9.29 (s, 1H, H-9), 8.71 (s, 1H, H-1), 8.52 (d, J = 8.4 Hz, 2H, H-6), 8.35 (m, 1H, H-12), 8.14 (d, J = 6.9 Hz, 2H, H-3), 7.65 (t, J = 7.0 Hz, 2H, H-5), 7.58 (t, J = 7.8 Hz, 2H, H-4), 6.89 (m, 1H, H-15), 3.65 (q, J = 5.7 Hz, 2H, H-13), 3.18 (q, J = 5.1 Hz, 2H, H-14), 1.28 (s, 9H, H-18). ^{13}C NMR (499 MHz, DMSO-d_6) δ [ppm] = 176.68 (C-11), 155.95 (C-16), 1.42.16 (C-9), 131.28 (C-2), 130.05 (C-7), 129.69 (C-1), 129.28 (C-3), 127.62 (C-5), 126.02 (C-4), 125.78 (C-8), 124.24 (C-6), 78.77 (C-17), 43.92 (C-13), 39.72 (C-14), 28.52 (C-18). HR-ESI-MS: m/z $[M+H]^+$ = 423.1854, m/z $[M+Na]^+$ = 445.1673.



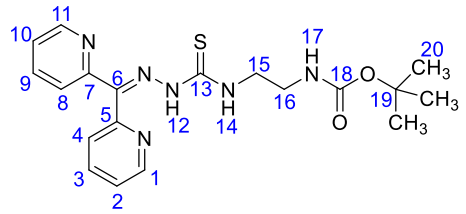
9-Anthraldehyde-4-(6-*tert*-butoxycarbonylamino-hexyl)-3-thiosemicarbazone from 0.30 g (10.0 mmol) 4-(6-*tert*-butoxycarbonylamino-hexyl) thiosemicarbazide, 0.21 g (10.0 mmol) antracene-9-carbaldehyde. The product precipitated as yellow solid. Yield: 0.31 g (6.5 mmol, 65%). $C_{27}H_{34}N_4O_2S$ (478.66 g/mol). ^{1}H NMR (499 MHz, DMSO-d_6) δ [ppm] = 11.66 (s, 1H, H-10), 9.28 (s, 1H, H-9), 8.70 (s, 1H, H-1), 8.50 (d, J = 8.16 Hz, 2H, H-6), 8.31 (m, 1H, H-12), 8.14 (d, J = 8.3 Hz, 2H, H-3), 7.62 (t, J = 6.7 Hz, 2H, H-5), 7.57 (t, J = 7.7 Hz, 2H, H-4), 6.76 (m, 1H, H-19), 3.57 (q, J = 6.7 Hz, 2H, H-13), 2.88 (q, J = 6.7 Hz, 2H, H-18), 1.57 (m, 2H, H-14), 1.36 (s, 11H, H-17, H-22), 1.27 (m, 4H, H-15, H-16). ^{13}C NMR (499 MHz, DMSO-d_6) δ [ppm] = 177.92 (C-11), 155.58 (C-20), 141.74 (C-9), 131.34 (C-2), 130.05 (C-7), 129.62 (C-1), 129.28 (C-3), 127.59 (C-5), 125.98 (C-4), 125.92 (C-8), 125.24 (C-6), 77.78 (C-21), 43.93 (C-13), 40.31 (C-18), 30.05 (C-17), 29.07 (C-14), 28.72 (C-21), 26.59 (C-15, C-16). HR-ESI-MS: m/z $[M+H]^+$ = 479.2480, m/z $[M+Na]^+$ = 501.2301.



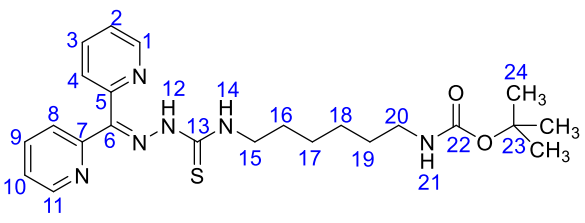
9-anthraldehyde-4-(4-*tert*-butoxycarbonylamino-phenyl)-3-thiosemicarbazone from 0.30 g (1.1 mmol) 4-(4-*tert*-butoxycarbonylamino-phenyl) thiosemicarbazide, 0.22 g, (1.1 mmol) antracene-9-carbaldehyde. The product precipitated as yellow solid. Yield: 0.39 g (0.8 mmol, 75%). $C_{27}H_{26}N_4O_2S$ (470.59 g/mol). ^{1}H NMR (499 MHz, DMSO-d_6) δ [ppm] = 11.98 (s, 1H, H-10), 9.89 (s, 1H, H-12), 9.39 (s, 1H, H-17), 9.34 (s, 1H, H-9), 8.73 (s, 1H, H-1), 8.58 (d, *J* = 9.0 Hz, 2H, H-6), 8.15 (d, *J* = 9.0 Hz, 2H, H-3), 7.66 (t, *J* = 8.0 Hz, 2H, H-5), 7.59 (t, *J* = 7.2 Hz, 2H, H-4), 7.41 (m, 4H, H-14, H-15), 1.48 (s, 9H, H-20). ^{13}C NMR (499 MHz, DMSO-d_6) δ [ppm] = 176.62 (C-11), 153.28 (C-18), 142.50 (C-9), 137.15 (C-13/C-16), 133.72 (C-13/C-16), 131.33 (C-2), 130.19 (C-7), 130.02 (C-1), 129.22 (C-3), 127.69 (C-5), 126.40 (C-14/C-15), 126.05 (C-4), 125.72 (C-8), 125.22 (C-6), 118.05 (C-14/C-15), 78.87 (C-19), 28.33 (C-20). HR-ESI-MS: m/z $[M+H]^+$ = 471.1853, m/z $[M+Na]^+$ = 493.1674.



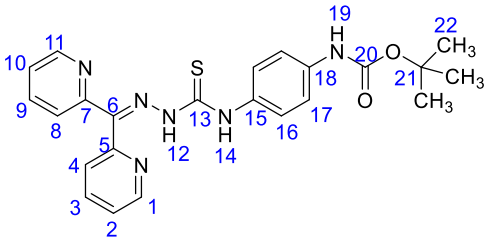
Di-2-pyridylketone-4-(2-*tert*-butoxycarbonylamino-ethyl)-3-thiosemicarbazone from 0.20 g (0.8 mmol) 4-(2-*tert*-butoxycarbonylamino-ethyl) thiosemicarbazide, 0.16 g (0.8 mmol) di-pyridyl ketone. The product was purified by column chromatography (c-hexane/EOAc 1:3 v/v) and obtained as pale orange solid. Yield: 0.17 g (0.4 mmol, 50%). $C_{19}H_{24}N_6O_2S$ (400.50 g/mol). ^{1}H NMR (499 MHz, DMSO-d_6) δ [ppm] = 13.23 (s, 1H, H-12), 8.91 (m, 1H, H-14), 8.82 (d, *J* = 4.6 Hz, 1H, H-1), 8.58 (d, *J* = 4.5 Hz, 1H, H-11), 8.26 (d, *J* = 8.0 Hz, 1H, H-8), 8.00-7.93 (m, 2H, H-3, H-9), 7.56 (m, 1H, H-2), 7.51-7.46 (m, 2H, H-4, H-10), 7.04 (m, 1H, H-17), 3.64 (m, 2H, H-15), 3.21 (m, 2H, H-16), 1.34 (s, 9H, H-20). ^{13}C NMR (499 MHz, DMSO-d_6) δ [ppm] = 177.55 (C-13), 155.58 (C-18), 155.40 (C-7), 151.71 (C-5), 148.80 (C-11), 148.58 (C-1), 141.64 (C-6), 137.98 (C-3/C-9), 137.36 (C-3/C-9), 127.57 (C-4/C-10), 125.14 (C-2), 124.33 (C-4/C-10), 124.18 (C-8), 78.95 (C-19), 45.09 (C-15), 39.37 (C-16), 28.59 (C-20). HR-ESI-MS: m/z $[M+H]^+$ = 401.1758, m/z $[M+Na]^+$ = 423.1577.



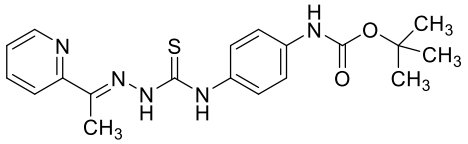
Di-2-pyridylketone-4-(6-*tert*-butoxycarbonylamino-hexyl)-3-thiosemicarbazone from 0.30 g (1.0 mmol) 4-(6-*tert*-butoxycarbonylamino-hexyl)thiosemicarbazide, 0.18 g (1.0 mmol) di-pyridyl ketone. The product was purified by column chromatography (CH_2Cl_2/MeOH 95:5 v/v) and obtained as orange oil. Yield: 0.40 g (0.9 mmol, 90%). $C_{23}H_{32}N_6O_2S$ (456.61 g/mol). ^{1}H NMR (499 MHz, DMSO-d_6) δ [ppm] = 13.14 (s, 1H, H-12), 8.88 (t, *J* = 5.8 Hz, 1H, H-14), 8.82 (d, *J* = 7.9 Hz, 1H, H-1), 8.57 (d, *J* = 4.1 Hz, 1H, H-11), 8.23 (d, *J* = 7.9 Hz, 1H, H-8), 7.98 (m, 2H, H-3, H-9), 7.57 (m, 1H, H-2), 7.49 (m , 2H, H-4, H-10), 6.75 (m, 1H, H-21), 3.59 (q, *J* = 6.5 Hz, 2H, H-15), 2.90 (q, *J* = 6.2 Hz, 2H, H-20), 1.60 (m, 2H, H-16), 1.36 (s, 11H, H-19, H-24), 1.28 (m, 4H, H-16, H-17). ^{13}C NMR (499 MHz, DMSO-d_6) δ [ppm] = 177.49 (C-13), 156.13 (C-22), 155.57 (C-7), 151.41 (C-5), 148.77 (C-11), 148.56 (C-1), 141.51 (C-6), 137.93 (C-3/C-9), 137.46 (C-3/C-9), 127.55 (C-4/C-10), 125.10 (C-2), 124.32 (C-4/C-10), 124.23 (C-8), 77.22 (C-23), 44.34 (C-15), 40.22 (C-20), 29.93 (C-19), 29.09 (C-16), 28.74 (C-24), 26.47 (C-17, C-18). HR-ESI-MS: m/z $[M+H]^+$ = 457.2384, m/z $[M+Na]^+$ = 479.2201.



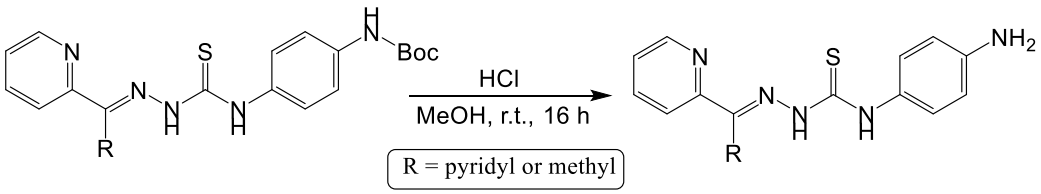
Di-2-pyridylketone-4-(4-*tert*-butoxycarbonylamino-phenyl)-3-thiosemicarbazone from 0.30 g (1.0 mmol) 4-(4-*tert*-butoxycarbonylamino-phenyl) thiosemicarbazide, 0.19 g (1.0 mmol) di-pyridyl ketone. The product was purified by column chromatography (c-hexane/EOAc 1:3 v/v) and obtained as colorless solid. Yield: 0.38 g (0.8 mmol, 80%). $C_{23}H_{24}N_6O_2S$ (448.55 g/mol). ^{1}H NMR (499 MHz, DMSO-d_6) δ [ppm] = 13.45 (s, 1H, H-12), 10.34 (s, 1H, H-14), 9.40 (s, 1H, H-19), 8.84 (m, 1H, H-1), 8.58 (m, 1H, H-11), 8.40 (m, 1H, H-8), 8.01 (m, 1H, H-3), 7.95 (m, 1H, H-9), 7.60 (m, 1H, H-2), 7.54 (m, 1H, H-4), 7.47 (H-10, H-16/H-17), 7.41 (H-16/H-17), 1.48 (s, 9H, H-22). ^{13}C NMR (499 MHz, DMSO-d_6) δ [ppm] = 178.48 (C-13), 155.42 (C-7), 153.38 (C-20), 151.40 (C-5), 148.76 (C-11), 148.59 (C-1), 142.24 (C-6), 138.02 (C-3), 137.50 (C-15/C-18), 137.50 (C-9), 133.43 (C-15/C-18), 127.73 (C-4), 126.94 (C-16/C-17), 125.24 (C-2), 124.60 (C-8), 124.40 (C-10), 118.23 (C-16/C-17), 78.58 (C-21), 28.65 (C-22). HR-ESI-MS: m/z $[M+H]^+$ = 449.1757, m/z $[M+Na]^+$ = 471.1575.



***p*-[(*E*)-1-[1-(2-Pyridyl)ethylidene]thiosemicarbazido]phenyl 2-methyl-2-propanecarbamate** from 0.60 g (2.1 mmol) 4-(4-*tert*-butoxycarbonylamino-phenyl)thiosemicarbazide, 0.24 mL (2.12 mmol) 2-acetylpyridine. The product was purified by column chromatography (c-hexane/EOAc 1:2 v/v) and obtained as colorless solid. Yield: 0.78 g (2.0 mmol, 95%). $C_{19}H_{23}N_5O_2S$ (385.49 g/mol). ^{1}H NMR (499 MHz, DMSO-d_6) δ [ppm] = 10.61 (s, 1H), 10.11 (s, 1H), 9.38 (s, 1H), 8.62 (d, J = 4.5 Hz, 1H), 8.56 (d, J = 8.0 Hz, 1H), 7.83 (m, 1H), 7.43 (d, J = 8.6 Hz, 2H), 7.38 (d, J = 8.6 Hz, 2H), 2.46 (s, 3H), 1.49 (s, 9H).

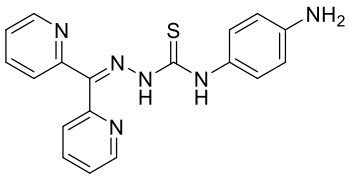


5.3.2.5 Deprotection of the TSCs with phenyl spacer

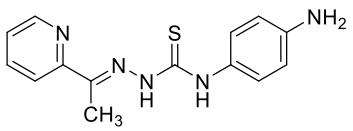


The TSC (1.00 eq.) was dissolved in 50 mL of $CHCl_3$. A solution of 0.42 mL conc. HCl (23.00 eq.) in 10 mL of MeOH was added at 0 °C for 15 minutes. After that, the reaction was stirred for 16 h at room temperature. The solvent was removed under reduced pressure, and the crude product was redissolved in 20 mL of EtOAc. The organic phase was washed two times with 20 mL of H_2O, two times with 20 mL of conc. $NHCO_3$ solution and dried over $MgSO_4$. The solvent was removed under reduced pressure yielding the product as yellowish solid. Yield: 65.5 mg (0.19 mmol, 94%).

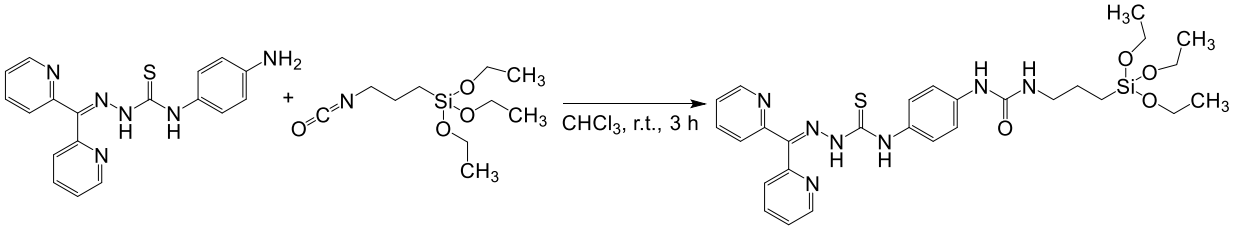
***p*-(1-[Bis(2-pyridyl)methylene]thiosemicarbazido)aniline** from 100.0 mg (0.22 mmol) di-2-pyridylketone-4-(4-*tert*-butoxycarbonylamino-phenyl)-3-thiosemicarbazone, 0.42 mL (5.1 mmol) conc. HCl. The product was obtained as a yellow solid. Yield: 65.5 mg (0.19 mmol, 94%). $C_{18}H_{16}N_6S$ (348.43 g/mol). ^{1}H NMR (499 MHz, DMSO-d_6) δ [ppm] = 13.38 (s, 1H), 11.06 (s, 1H), 8.82 (d, J = 4.5 Hz, 1H), 8.29 (d, J = 5.0 Hz, 1H), 8.25 (m, 2H), 8.14 (m, 1H), 7.77 (m, 4H), 7.40 (d, J = 8.7 Hz, 2H), 5.29 (s, 2H).



***p*-[(*E*)-1-[1-(2-Pyridyl)ethylidene]thiosemicarbazido]aniline** from 0.74 g (1.9 mmol) *p*-[(*E*)-1-[1-(2-pyridyl)ethylidene]thiosemicarbazido]phenyl 2-methyl-2-propanecarbamate, 3.67 mL (4.4 mmol) conc. HCl. The product was obtained as a yellow solid. Yield: 0.53 g (1.8 mmol, 98%). $C_{14}H_{15}N_5S$ (285.37 g/mol). ^{1}H NMR (499 MHz, DMSO-d_6) δ [ppm] = 11.05 (s, 1H), 10.75 (s, 1H), 8.73 (d, *J* = 4.8 Hz, 1H), 8.49 (d, *J* = 8.0 Hz, 1H), 8.22 (m, 1H), 7.67 (d, *J* = 8.6 Hz, 2H), 7.37 (d, *J* = 8.6 Hz, 2H), 4.05 (s, 2H), 2.45 (s, 3H).

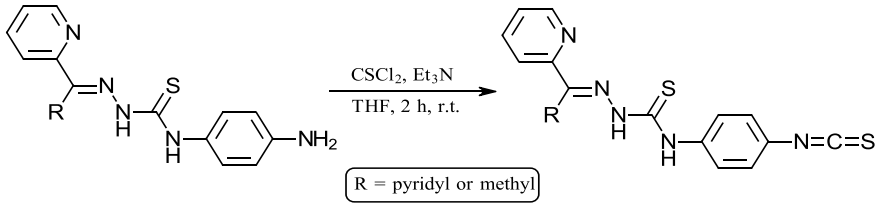


5.3.2.6 Conjugation of amino TSCs with isocyanates



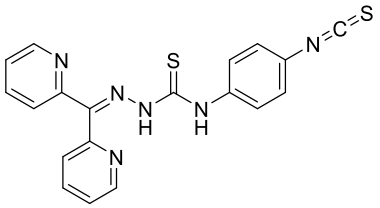
50.0 mg (0.14 mmol, 1.00 eq.) of the TSC was dissolved in 50 mL of dry $CHCl_3$ under inert conditions. After that, a solution of 35.5 µL 3-(triethoxysilyl)propylisocyanat (0.14 mmol, 1.00 eq.) in 10 mL $CHCl_3$ was added at 0 °C. The reaction was stirred 30 min at 0 °C and 3 h at room temperature. After that, the solvent was removed under reduced pressure, yielding the product as a colorless solid. Yield: g (0.14 mmol, quant.). $C_{28}H_{37}N_7O_4SSi$ (595.79 g/mol). ^{1}H NMR (499 MHz, DMSO-d_6) δ [ppm] = 14.55 (s, 1H), 9.46 (s, 1H), 8.87 (m, 1H), 8.69 (m, 1H), 7.85 (m, 2H), 7.60 (t, *J* = 5.0 Hz, 2H), 7.43 (m, 2H), 7.35 (m, 3H), 6.40 (s, 1H), 4.98 (t, *J* = 4.0 Hz, 1H), 3.83 (m, 6H), 1.70 (m, 2H), 1.24 (t, *J* = 5.0 Hz, 9H), 0.87 (m, 2H), 1.44 (m, 2H).

5.3.2.7 Synthesis of TSCs with isothiocyanate function

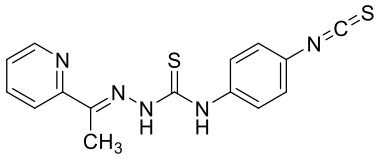


The TSC (1.00 eq.) and triethylamine (4.00 eq.) were dissolved in 70 mL of THF and thiophosgene (85%, 1.00 eq.) were added at 0 °C. The reaction was stirred for 2 h at room temperature. After that, 100 mL of H_2O was added, and the reaction mixture was extracted with Et_2O (3 x100 mL). The combined organic layer was dried over $MgSO_4$, and the solvent was removed under reduced pressure. The crude product was purified by column chromatography.

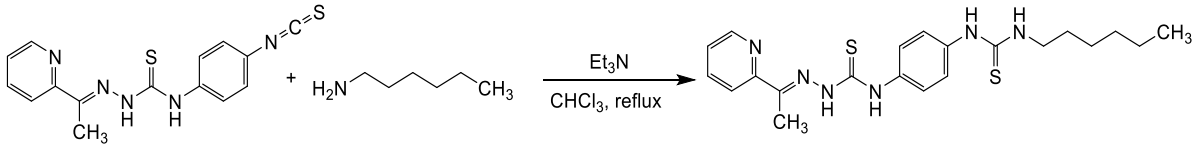
1-[Bis(2-pyridyl)methylene]-4-(*p*-isothiocyanatophenyl)thiosemicarbazide from 77.0 mg (0.22 mmol) *p*-(1-[Bis(2-pyridyl)methylene]thiosemicarbazido)aniline, 0.12 mL (0.88 mmol) triethylamine, 20.0 µL (0.22 mmol) thiophosgene. The product was purified by column chromatography (2:1 c-hexane/EtOAc) and obtained as a colorless solid. Yield: 62.7 mg (0.16 mmol, 73%). $C_{19}H_{14}N_6S_2$ (390.49 g/mol). ^{1}H NMR (300 MHz, DMSO-d_6) δ [ppm] = 13.69 (s, 1H), 10.52 (s, 1H), 8.85 (d, *J* = 4.5 Hz, 1H), 8.60 (d, *J* = 4.4 Hz, 1H), 8.35 (d, *J* = 7.9 Hz, 1H), 8.00 (dt, *J* = 14.1, 7.0 Hz, 2H), 7.72 (d, *J* = 8.7 Hz, 2H), 7.65-7.44 (m, 5H).



(*E*)-4-(*p*-Isothiocyanatophenyl)-1-[1-(2-pyridyl)ethylidene]thiosemicarbazide from 0.30 g (1.0 mmol) *p*-[(*E*)-1-[1-(2-pyridyl)ethylidene]thiosemicarbazido]aniline, 0.60 mL (4.0 mmol) triethylamine, 93.3 µL (1.0 mmol) thiophosgene. The product was purified by column chromatography (2:1 c-hexane/EtOAc) and obtained as a colorless solid. Yield: 0.21 g (0.65 mmol, 65%). $C_{15}H_{13}N_5S_2$ (327.42 g/mol). ^{1}H NMR (300 MHz, DMSO-d_6) δ [ppm] = 10.84 (s, 1H), 10.26 (s, 1H), 8.62 (d, *J* = 4.5 Hz), 8.50 (d, *J* = 8.0 Hz, 1H), 7.83 (m, 1H), 7.69 (d, *J* = 8.6 Hz, 2H), 7.44 (d, *J* = 8.6 Hz, 2H), 2.47 (s, 3H).



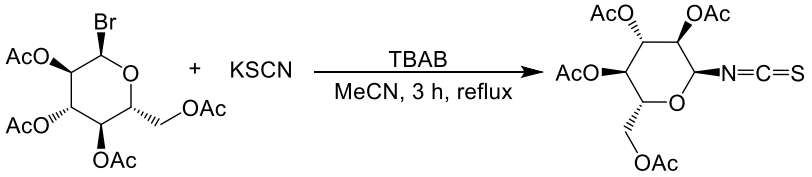
5.3.2.8 Conjugation of isothiocyanate TSCs with amines



6.0 µL Hexylamine (46.0 µmol, 1.00 eq.) and 15.0 mg (46.0 µmol, 1.00 eq.) of the TSC was dissolved in 5 mL $CHCl_3$ and 1 drop of triethylamine was added. The reaction was refluxed for 16 h. After that, the solvent was removed under reduced pressure, and the residue was washed with H_2O and c-hexane. Yield: 19.7 mg (46.0 µmol, quant.). $C_{21}H_{28}N_6S_2$ (428.62 g/mol). ^{1}H NMR (300 MHz, DMSO-d_6) δ [ppm] = 10.65 (s, 1H), 10.14 (s, 1H), 9.47 (s, 1H), 8.62 (d, *J* = 4.5 Hz, 1H), 8.51 (d, *J* = 8.0 Hz), 7.83 (m, 2H), 7.44 (m, 5H), 3.46 (m, 2H), 2.47 (s, 3H), 1.55 (m, 4H), 1.24 (m, 4H), 0.88 (m, 3H).

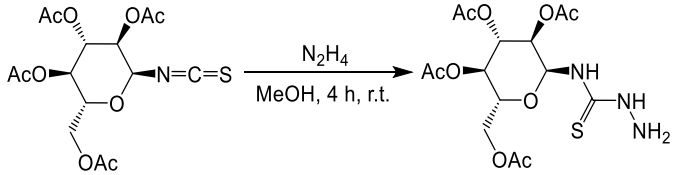
5.3.3 TSCs derived from acetobromo-α-D-glucose

5.3.3.1 Synthesis of β-D-glucopyranosyl isothiocyanate



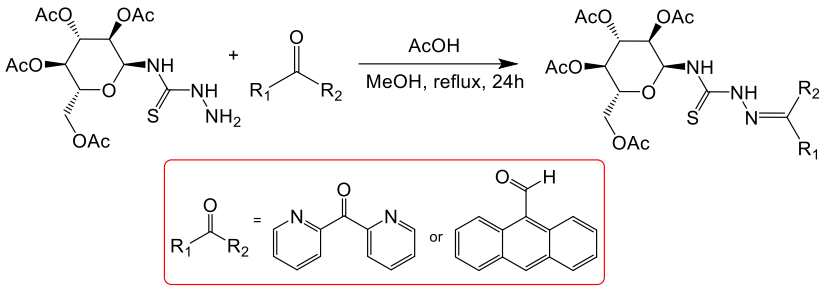
KSCN (0.40 g, 4.0 mmol, 2.00 eq.) and TBAB (0.64 g, 2.0 mmol, 1.00 eq.) were dissolved in 200 mL of dry MeCN and molecular sieves (4 Å, 3.00 g) were added. The reaction mixture was stirred for 3 h. Then, acetobromo-α-D-glucose (0.85 g, 2.0 mmol, 1.00 eq.) was added, and the reaction was refluxed for an additional 3 h. The reaction mixture was filtrated, and the solvent was removed under reduced pressure. The crude product was purified by column chromatography (c-hexane/EOAc 3:2). The product was obtained as colorless solid.[334] Yield: 0.28 g (0.7 mmol, 36%). $C_{15}H_{19}NO_9S$ (389.38 g/mol). ^{1}H NMR (499 MHz, DMSO-d_6) δ [ppm] = 5.26-5.02 (m, 4H), 4.29-4.13 (m, 2H), 3.75 (m, 1H), 2.12 (s, 6H), 2.03 (d, *J* = 3.9 Hz, 6H).

5.3.3.2 Synthesis of *N*-(2,3,4,6-tetra-*O*-acetyl-β-D-glucopyranosyl)hydrazinecarbothioamide



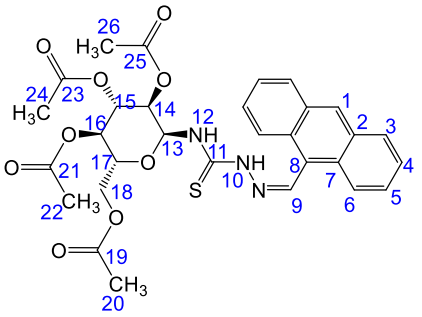
Hydrazine monohydrate (0.035 mL, 0.7 mmol, 1.00 eq.) was dissolved in 20 mL of EtOH. β-D-glucopyranosyl isothiocyanate (0.28 g, 0.7 mmol, 1.00 eq.) was dissolved in 20 mL of EtOH and slowly added to the hydrazine solution over the course of 1 h. The reaction mixture was stirred for an additional 3 h. The formed precipitate was filtered off and washed with cold EtOH. The product was obtained as colorless solid. Yield: 0.16 g (0.4 mmol, 57%). $C_{15}H_{23}N_3O_9S$ (421.42 g/mol). ^{1}H NMR (499 MHz, DMSO-d_6) δ [ppm] = 9.27 (s, 1H), 8.18 (s, 1H), 5.82 (m, 1H), 5.37 (t, *J* = 9.5, 1H), 5.09 (t, *J* = 9.4 Hz, 1H), 4.92 (t, *J* = 9.8 Hz, 1H), 4.61 (s, 2H), 4.20-4.11 (m, 1H), 4.02-3.93 (m, 2H), 2.03-1.92 (m, 12H).

5.3.3.3 Synthesis of TSCs – general description

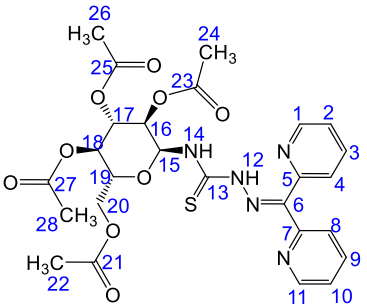


9-anthracene aldehyde or di(2-pyridyl) ketone (1.00 eq.) and *N*-(2,3,4,6-tetra-*O*-acetyl-β-D-glucopyranosyl)hydrazinecarbothioamide (1.00 eq.) were dissolved in 10 mL of MeOH and 0.1 mL of glacial AcOH were added. The reaction mixture was refluxed for 24 h. The solvent was removed under reduced pressure, yielding the product in quantitative yields.

9-Anthraldehyde-4-(2,3,4,6-Tetra-*O*-acetyl-β-D-glucopyranosyl)-3-thiosemicarbazone from 0.070 g (0.17 mmol) *N*-(2,3,4,6-Tetra-*O*-acetyl-β-D-gluco-pyranosyl) hydrazine carbothioamide, 0.035 g (0.17 mmol) 9-antracene aldehyde. The product was obtained as colorless solid. Yield: 0.105 g (0.17 mmol, quant.). $C_{30}H_{31}N_3O_9S$ (609.65 g/mol). ^{1}H NMR (499 MHz, DMSO-d_6) δ [ppm] = 12.16 (s, 1H, H-10), 9.38 (s, 1H), 8.75 (s, 1H, H-9), 8.75 (s, 1H, H-1), 8.54 (t, *J* = 9.1 Hz, 3H, H-6, H-12), 8.17 (d, *J* = 8.3 Hz, 2H, H-3), 7.69 (m, 2H, H-5), 7.60 (m, 2H, H-4), 5.98 (m, 1H, H-13), 5.45 (t, *J* = 9.5 Hz, 1H, H-15), 5.26 (t, *J* = 9.3 Hz, 1H, H-14), 4.92 (t, *J* = 9.7 Hz, 1H, H-16), 4.18 (m, 1H, H-18), 4.10 (m, 1H, H-17), 3.99 (m, 1H, H-18), 2.04 (s, 3H, H-26), 2.00 (s, 3H, H-22), 1.98 (s, 3H, H-24), 1.97 (s, H-25). ^{13}C NMR (499 MHz, DMSO-d_6) δ [ppm] = 179.32 (C-11), 170.45 (C-19), 170.14 (C-25), 169.99 (C-23), 169.79 (C-21), 144.00 (C-9), 131.34 (C-2), 130.32 (C-1), 130.20 (C-7), 129.44 (C-3), 128.22 (C-5), 126.07 (C-4), 124.85 (C-8), 81.73 (C-13), 72.95 (C-15), 72.62 (C-17), 71.10 (C-14), 68.33 (C-16), 62.05 (C-18), 20.99 (C-20/C-22/C-24/C-26), 20.94 (C-20/C-22/C-24/C-26), 20.89 (C-20/C-22/C-24/C-26), 20.82 (C-20/C-22/C-24/C-26). HR-ESI-MS: m/z $[M+H]^+$ = 610.1860, m/z $[M+Na]^+$ = 632.1680.

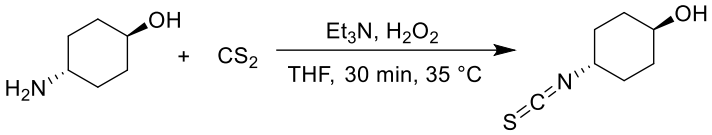


Di-2-pyridylketone-4-(2,3,4,6-Tetra-*O*-acetyl-β-D-glucopyranosyl)-3-thiosemicarbazone from 0.070 g (0.17 mmol) *N*-(2,3,4,6-Tetra-*O*-acetyl-β-D-gluco-pyranosyl) hydrazine carbothioamide, 0.031 g (0.17 mmol) di(2-pyridyl) ketone. The product was obtained as colorless solid. Yield: 0.10 g (0.17 mmol, quant.). $C_{26}H_{29}N_5O_9S$ (587.60 g/mol). ^{1}H NMR 499 MHz, DMSO-d_6) δ [ppm] = 13.61 (s, 1H, H-12), 9.14 (d, *J* = 9.0, 1H, H-14), 8.84 (d, *J* = 4.4 Hz, 1H, H-1), 8.60 (d, *J* = 4.2 Hz, 1H, H-11), 8.27 (d, *J* = 7.8 Hz, 1H, H-8), 7.99 (m, 2H, H-3, H-9), 7.61 (m, 1H, H-2), 7.53 (m, 2H, H-4, H-10), 5.98 (t, *J* = 9.1 Hz, 1H, H-15), 5.47 (t, *J* = 9.5 Hz, 1H, H-17), 5.38 (t, *J* = 8.9 Hz, 1H, H-16), 4.98 (t, *J* = 9.7 Hz, 1H, H-18), 4.24 (m, 1H, H-20), 4.14 (m, 1H, H-19), 4.01 (d, *J* = 11.3 Hz, 1H, H-20), 2.01 (s, 3H, H-22/H-24/H-26/H-28), 1.98 (s, 3H, H-22/H-24/H-26/H-28), 1.95 (s, 3H, H-22/H-24/H-26/H-28), 1.92 (s, 3H, H-22/H-24/H-26/H-28). ^{13}C NMR (499 MHz, DMSO-d_6) δ [ppm] = 179.44 (C-13), 170.48 (C-21), 170.08 (C-23), 170.01 (C-25), 169.84 (C-27), 155.20 (C-7), 151.22 (C-5), 148.87 (C-11), 148.65 (C-1), 143.09 (C-6), 138.10 (C-3/C-9), 137.54 (C-3/C-9), 127.87 (C-4/C-10), 125.49 (C-2), 124.64 (C-4/C-10), 124.55 (C-8), 82.15 (C-21), 72.99 (C-17), 72.68 (C-19), 71.27 (C-16), 68.27 (C-18), 62.12 (C-20), 21.03 (C-22/C-24/C-26/C-28), 20.89 (C-22/C-24/C-26/C-28), 20.87 (C-22/C-24/C-26/C-28), 20.81 (C-22/C-24/C-26/C-28). HR-ESI-MS: m/z $[M+H]^+$ = 588.1762, m/z $[M+Na]^+$ = 610.1582.

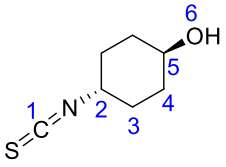


5.3.4 Syntheses of TSCs derived from *trans*-4-hydroxycyclohexanol

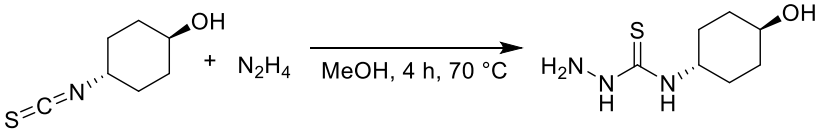
5.3.4.1 Synthesis of *trans*-4-hydroxycyclohexyl isothiocyanate



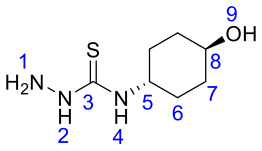
The reaction was performed under inert conditions. *Trans*-4-hydroxycyclohexanol (4.00 g, 34.7 mmol, 1.00 eq.) was dissolved in 35 mL of THF and CS_2 (10.50 mL, 173.5 mmol, 5.00 eq.) as well as Et_3N (0.50 mL, 3.5 mmol, 0.10 eq.) were added dropwise. The mixture was stirred for 30 min at room temperature. Then, the reaction was cooled to 0 °C and conc. H_2O_2 (9.90 mL, 97.2 mmol, 2.80 eq.) was slowly added. The solution was subsequently acidified with conc. HCl and concentrated under reduced pressure to 15 mL. The suspension was filtered, and the filtrate was extracted with EtOAc (3 x 50 mL). The combined organic phase was dried over $MgSO_4$ and the solvent was removed under reduced pressure. The crude product was extracted with $CHCl_3$ and insoluble residues were filtered off. The product was obtained as yellow oil.[336] Yield: 1.38 g (8.8 mmol, 25%). $C_7H_{11}NOS$ (157.23 g/mol). ^1H NMR (499 MHz, $CDCl_3$) δ [ppm] = 3.78 (m, 1H, H-5), 3.67 (m, 1H, H-2), 2.10 (m, 2H, H-3), 1.96 (m, 3H, H-4), 1.62 (m, 2H, H-3), 1.41 (m, 2H, H-4). ^{13}C NMR (499 MHz, DMSO-d_6) δ [ppm] = 130.18 (C-1), 67.67 (C-5), 54.61 (C-2), 31.50 (C-4), 29,69 (C-3).



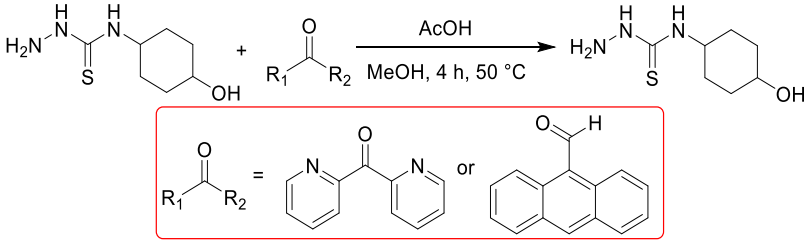
5.3.4.2 Synthesis of 4-(trans-4-hydroxycyclohexyl)-thiosemicarbazide



Hydrazine monohydrate (0.40 mL, 8.7 mmol, 1.00 eq.) was dissolved in 20 mL of MeOH and heated to 70 °C. *trans*-4-hydroxycyclohexyl isothiocyanate (1.38 g, 8.7 mmol, 1.00 eq.) was dissolved in 50 mL of MeOH and slowly added to the hydrazine solution over the course of 1 h. The reaction mixture was stirred for an additional 3 h, then the solvent was removed under reduced pressure, yielding a brown oil. The crude product was dissolved in 10 mL of $CHCl_3$ and poured into boiling petrol ether. The formed precipitate was filtered off and dried under ambient conditions. The product was obtained as colorless solid. Yield: 1.35 g (7.1 mmol, 82%). $C_7H_{15}N_3OS$ (189.28 g/mol). ^1H NMR (499 MHz, DMSO-d_6) δ [ppm] = 8.55 (s, 1H, H-2), 7.43 (d, J = 8.8 Hz, 1H, H-4), 4.52 (s, 1H, H-9), 4.43 (s, 2H, H-1), 3.99 (m, 1H, H-5), 3.37 (m, 2H, H-8), 1.82 (m, 4H, H-7/H-6), 1.28 (m, 2H, H-6), 1.17 (m, 2H, H-7). ^{13}C NMR (499 MHz, DMSO-d_6) δ [ppm] = 180.60 (C-3), 68.54 (C-8), 51.65 (C-5), 34.58 (C-7), 30.56 (C-6). HR-ESI-MS: m/z $[M+H]^+$ = 190.1011.

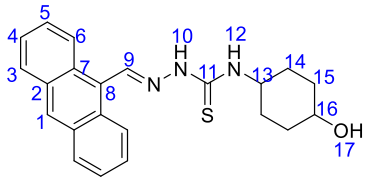


5.3.4.3 Synthesis of TSCs – general description

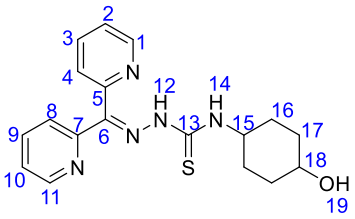


4-(*Trans*-4-hydroxycyclohexyl)-thiosemicarbazide (1.00 eq.) and antracene-9-carbaldehyde or di(2-pyridyl) ketone (1.00 eq.) were dissolved in a minimum amount of MeOH. 0.1 mL of glacial AcOH was added, and the reaction mixture was sonicated at 50 °C for 4 h. The solvent was removed under reduced pressure, and the crude product was purified by column chromatography.

9-Anthraldehyde-4-(*trans*-4-hydroxycyclohexyl)-3-thiosemicarbazone from 0.30 g (1.6 mmol) 4-(*trans*-4-hydroxycyclohexyl)thiosemicarbazide, (0.32 g, 1.6 mmol) antracene-9-carbaldehyde. The product was purified by column chromatography (c-hexane/EOAc 1:2 v/v) and obtained as yellow solid. Yield: 0.28 g (0.7 mmol, 47%). $C_{22}H_{23}N_3OS$ (377.51 g/mol). ^{1}H NMR (499 MHz, DMSO-d_6) δ [ppm] = 11.72 (s, 1H, H-10), 9.28 (s, 1H, H-9), 8.70 (s, 1H, H-1), 8.47 (d, *J* = 9.1 Hz, 2H, H-6), 8.14 (d, *J* = 8.3 Hz, 2H, H-3), 7.83 (d, *J* = 8.3 Hz, 1H, H-12), 7.62 (m, 2H, H-5), 7.52 (m, 2H, H-4), 4.55 (s, 1H, H-17), 4.16 (m, 1H, H-13), 3.37 (m, 1H, H-16), 1.91 (m, 2H, H-14), 1.80 (m, 2H, H-15), 1.40 (m, 2H, H-14), 1.25 (m, 2H, H-15). ^{13}C NMR (499 MHz, DMSO-d_6) δ [ppm] = 176.63 (C-11), 141.85 (C-9), 131.34 (C-2), 130.02 (C-7), 129.66 (C-1), 129.42 (C-3), 127.63 (C-4/C-5), 125.90 (C-4/C-5), 125.85 (C-8), 124.88 (C-6), 68.37 (C-16), 52.54 (C-13), 34.37 (C-15), 29.92 (C-14). HR-ESI-MS: m/z $[M+H]^+$ = 378.1637, m/z $[M+Na]^+$ = 400.1457.

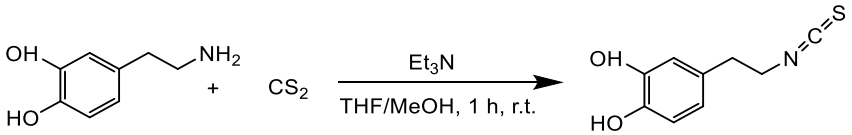


Di-2-pyridylketone-4-(*trans*-4-hydroxycyclohexyl)-3-thiosemicarbazone from 0.30 g (1.6 mmol) 4-(*trans*-4-hydroxycyclohexyl)thiosemicarbazide, 0.29 g (1.6 mmol) di(2-pyridyl) ketone. The product was purified by column chromatography (CH_2Cl_2/MeOH 95:5 v/v) and obtained as pale orange solid. Yield: 0.40 g (1.1 mmol, 70%). $C_{18}H_{21}N_5O_2S$ (355.46 g/mol). ^{1}H NMR (499 MHz, DMSO-d_6) δ [ppm] = 13.20 (s, 1H, H-13), 8.81 (d, *J* = 4.3 Hz, 1H, H-1), 8.56 (d, *J* = 5.1 Hz, 1H, H-11), 8.33 (d, *J* = 9.4 Hz, 1H, H-14), 8.17 (d, *J* = 8.3 Hz, 1H, H-8), 7.96 (m, 2H, H-3, H-9), 7.58 (m, 1H, H-2), 7.47 (m, 2H, H-4, H-10), 4.57 (s, 1H, H-19), 4.17 (d, *J* = 4.4 Hz, 1H, H-15), 3.39 (m, 1H, H-18), 1.87 (m, 4H, H-16, H-17), 1.52 (m, 2H, H-16), 1.23 (m, 2H, H-17). ^{13}C NMR (499 MHz, DMSO-d_6) δ [ppm] = 176.84 (C-13), 155.51 (C-7), 151.57 (C-5), 148.84 (C-11), 148.58 (C-1), 141.78 (C-6), 137.99 (C-3/C-9), 137.58 (C-3/C-9), 127.53 (C-4/C-10), 125.16 (C-2), 124.34 (C-4/C-10, C-8), 68.64 (C-18), 53.41 (C-15), 34.63 (C-17), 29.89 (C-16). HR-ESI-MS: m/z $[M+H]^+$ = 356.1543, m/z $[M+Na]^+$ = 378.1361.

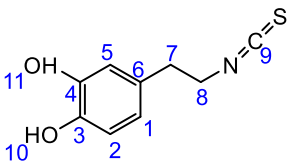


5.3.5 TSCs derived from dopamine

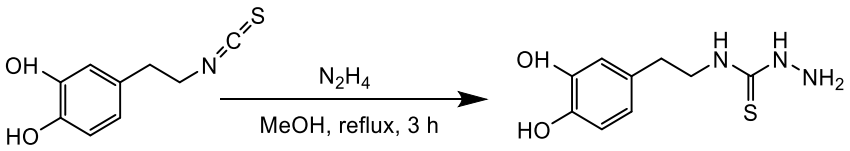
5.3.5.1 Synthesis of 4-(2-isothiocyanatoethyl)benzene-1,2-diol



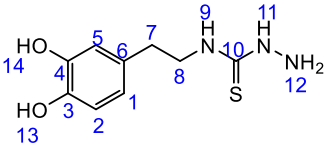
The reaction was performed under inert conditions. Dopamine hydrochloride (2 g, 10.5 mmol, 1 eq.) was suspended 26 mL of THF and Et_3N (1.62 mL, 11.6 mmol, 1.10 eq.) was added under stirring. 21 mL of MeOH were slowly added to form a clear solution. Then, CS_2 (3.17 mL, 52.7 mmol, 5 eq.) was added, and the mixture was stirred for 1 h at room temperature. The reaction was cooled to 0 °C and H_2O_2 (30% in H_2O, 0.94 mL) was added dropwise. The mixture was acidified (pH 2) using conc. HCl and the solution was concentrated under reduced pressure. The formed precipitate was filtered off and the filtrate was diluted with 15 mL of H_2O. Then, the filtrate was extracted with EtOAc (3 x 50 mL). The combined organic phase was dried over $MgSO_4$ and the solvent was removed under reduced pressure. The product was obtained as colorless solid.[300] Yield: 1.13 g (5.8 mmol, 55%). $C_9H_9NO_2S$ (195.24 g/mol). ^{1}H NMR (499 MHz, DMSO-d_6) δ [ppm] = 6.82 (d, *J* = 8.1 Hz, 1H, H-2), 6.74 (d, *J* = 2.0 Hz, 1H, H-5), 6.65 (dd, *J* = 8.1 Hz, 2.0 Hz, 1H, H-1), 5.74-4.65 (s, 2H, H-10, H-11), 3.66 (t, *J* = 6.8 Hz, 2H, H-8), 2.86 (t, *J* = 6.8 Hz, 2H, H-7), ^{13}C NMR (499 MHz, DMSO-d_6) δ [ppm] = 143.70 (C-3), 142.60 (C-4), 130.12 (C-6), 121.45 (C-1), 115.99 (C-5), 115.74 (C-2), 46.57 (C-8), 35.84 (C-7).



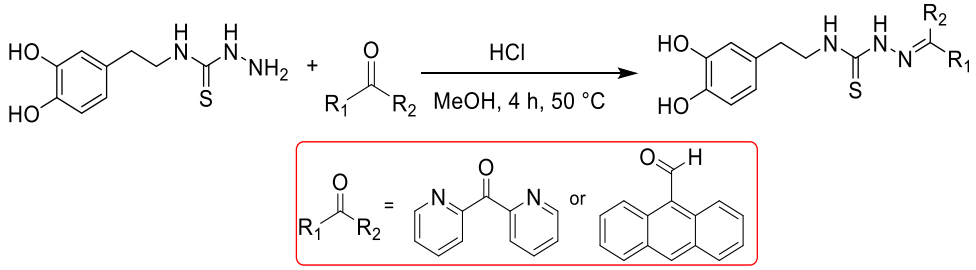
5.3.5.2 Synthesis of 4-[2-(hydrazidecarbothioamino)ethyl]benzene-1,2-diol



Hydrazine monohydrate (0.28 mL, 5.8 mmol, 1.00 eq.) was dissolved in 50 mL of MeOH and heated to 70 °C. 4-(2-isothiocyanatoethyl)benzene-1,2-diol (1.13 g, 5.8 mmol, 1.00 eq.) was dissolved in 50 mL of MeOH and slowly added to the hydrazine solution over the course of 1 h. The reaction mixture was stirred for an additional 3 h, then the solvent was removed under reduced pressure. The product was obtained as colorless solid. Yield: 1.18 g (5.2 mmol, 90%). $C_9H_{13}N_3O_2S$ (227.28 g/mol). ^{1}H NMR (499 MHz, DMSO-d_6) δ [ppm] = 8.59 (s, 1H, H-11), 7.81 (s, 1H, H-9), 6.66-6.59 (m, 2H, H-2, H-5), 6.47 (dd, J = 8.20, 2.0 Hz, 1H, H-1), 4.41 (s, 2H, H-12), 3.58 (m, 3H, H-8), 2.62 (m, 2H, H-7). ^{13}C NMR (499 MHz, DMSO-d_6) δ [ppm] = 145.56 (C-4), 143.99 (C-3), 130.56 (C-6), 119.68 (C-1), 116.38 (C-2/C-5), 116.01 (C-2/C-5), 45.20 (C-8), 35.04 (C-7). HR-ESI-MS: m/z $[M+H]^+$ = 228.0800.

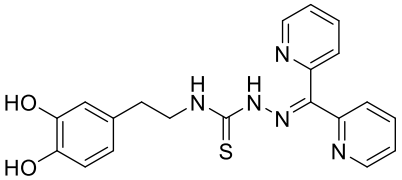


5.3.5.3 Synthesis of TSCs derived from dopamine

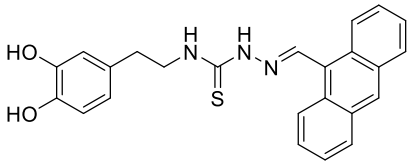


9-anthracene aldehyde or di(2-pyridyl) ketone (1.00 eq.) and 4-[2-(hydrazidecarbothioamino)ethyl] benzene-1,2-diol (1.00 eq.) were dissolved in a minimum amount of MeOH and a few droplets of conc. HCl were added. The reaction mixture was refluxed for 72 h. The solvent was removed under reduced pressure and the crude product was purified by column chromatography.

[Bis(pyridin-2-yl)methylideneamino][2-(3,4-dihydroxyphenyl)ethylamino] carbothioamide from 0.10 g (0.44 mmol) 4-[2-(hydrazidecarbothioamino)ethyl] benzene-1,2-diol, 0.08 g (0.44 mmol) dipyridyl ketone. The product was purified by column chromatography (c-hexane/EOAc 1:2 v/v) and obtained as colorless solid. Yield: 0.16 g (0.40 mmol, 90%). $C_{20}H_{19}N_5O_2S$ (393.47 g/mol). ^{1}H NMR (499 MHz, DMSO-d_6) δ [ppm] = 12.81 (s, 1H), 9.66 (t, J = 4.7 Hz, 1H), 8.91 (d, J = 4.5 Hz, 1H), 8.81 (d, J = 4.6 Hz, 1H), 8.34 (t, J = 8.6 Hz, 1H), 8.18-8.06 (m, 2H), 7.83 (m, 1H), 7.76-7.68 (m, 2H), 6.65 (m, 2H), 6.51 (dd, J = 8.0, 1.9 Hz, 1 H), 3.70 (m, 2H), 2.78 (m, 2H). HR-ESI-MS: m/z $[M+H]^+$ = 394.1331 m/z, $[M+Na]^+$ = 416.1151.

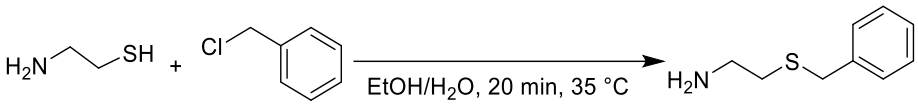


[(1*E*)-(anthracen-9-yl)methylideneamino][2-(3,4 dihydroxyphenyl)ethylamino] carbothioamide from 0.10 g (0.44 mmol) 4-[2-(hydrazidecarbothioamino)ethyl] benzene-1,2-diol, 0.09 g (0.44 mmol) dipyridyl ketone. The product was purified by column chromatography (c-hexane/EOAc 6:1 v/v) and obtained as yellow solid. Yield: 0.16 g (0.38 mmol, 87%). $C_{24}H_{21}N_3O_2S$ (415.51 g/mol). ^{1}H NMR (499 MHz, DMSO-d_6) δ [ppm] = 11.71 (s, 1H), 9.29 (s, 1H), 8.71 (s, 1H), 8.47 (d, J = 8.7 Hz, 2H), 8.27 (t, J = 5.7 Hz, 1H), 8.15 (d, J = 8.9 Hz, 2H), 7.61 (m, 4H), 6.65 (m, 2H), 6.50 (dd, J = 8.0, 2.0 Hz, 1H), 3.71 (q, J = 6.3 Hz, 2H), 2.73 (t, J = 7.5 Hz, 2H). HR-ESI-MS: m/z $[M+H]^+$ = 416.1433 m/z, $[M+Na]^+$ = 438.1251.

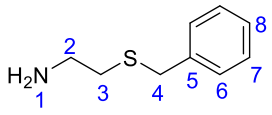


5.3.6 Synthesis of TSCs derived from amino thiols

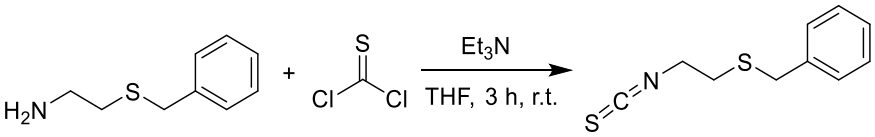
5.3.6.1 Synthesis of 2-benzylsulfanyl ethylamine



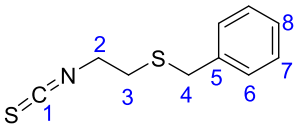
LiOH (0.49 g, 20.4 mmol, 2.00 eq.) was dissolved in a mixture of 10 mL of distilled H_2O and 30 mL of EtOH and the resulting solution was transferred to a flask containing cysteamine hydrochloride (1.14 g, 10.0 mmol, 1.00 eq.). Then, benzyl chloride (1.15 mL, 10.0 mmol, 1.00 eq.) was added dropwise to the solution and the reaction mixture was stirred for 20 min at 35 °C. Then, the EtOH was removed under reduced pressure and 40 mL of distilled H_2O was subsequently added. The aqueous solution was extracted with CH_2Cl_2 (3 x 60 mL), dried over anhydrous Na_2SO_4 and the solvent was removed under reduced pressure. The product was obtained as yellowish oil.[288] Yield: 0.84 g (5.0 mmol, 50%). $C_9H_{13}NS$ (167.27 g/mol). ^{1}H NMR (499 MHz, $CDCl_3$) δ [ppm] = 7.23 (m, 4H, H-6, H-7) 7.14 (m, 1H, H-8), 3.62 (s, 2H, H-4), 2.73 (t, *J* = 6.5 Hz, 2H, H-2), 2.43 (t, *J* = 6.3 Hz, 2H, H-3), 1.40 (s, 2H, H-1). ^{13}C NMR (499 MHz, DMSO-*d*$_6$) δ [ppm] = 138.12 (C-5), 128.61 (C-6, C-7), 127.08 (C-8), 40.95 (C-2), 35.90 (C-4), 35.42 (C-3).



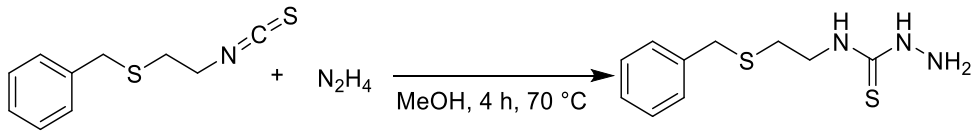
5.3.6.2 Synthesis of 2-benzylsulfanylethyl isothiocyanate



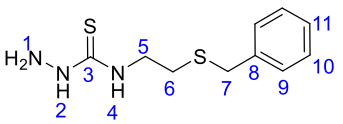
The reaction was performed under inert conditions. The protected cysteamine (0.8 g, 4.8 mmol, 1.00 eq.) and Et_3N (2.00 mL, 14.3 mmol, 3.00 eq.) were dissolved in 30 mL of THF. Thiophosgene (0.46 mL, 4.8 mmol, 1.00 eq.) was slowly added at 0 °C and the reaction mixture was stirred for 3 h at room temperature, which lead to the formation of a brown suspension. The reaction was quenched by adding 100 mL of distilled H_2O and the product was extracted with Et_2O (3 x 100 mL). The organic phase was dried over Na_2SO_4 and the solvent was removed under reduced pressure, yielding the product as brown oil. Yield: 1.00 g (4.8 mmol, quant.). $C_{10}H_{11}NS_2$ (209.33 g/mol). ^{1}H NMR (499 MHz, $CDCl_3$) δ [ppm] = 7.33 (m, 4H, H-6, H-7), 7.28 (m, 1H, H-8), 3.77 (s, 2H, H-4), 3.54 (t, *J* = 7.5 Hz, 2H, H-2), 2.69 (t, *J* = 7.5 Hz, 2H, H-3). ^{13}C NMR (499 MHz, DMSO-*d*$_6$) δ [ppm] = 137.09 (C-5), 132.59 (C-1), 128.72 (C-6, C-7), 127.51 (C-8), 44.47 (C-2), 36.44 (C-4), 30.77 (C-3).



5.3.6.3 Synthesis of 4-(2-benzylsulfanylethyl)thiosemicarbazide

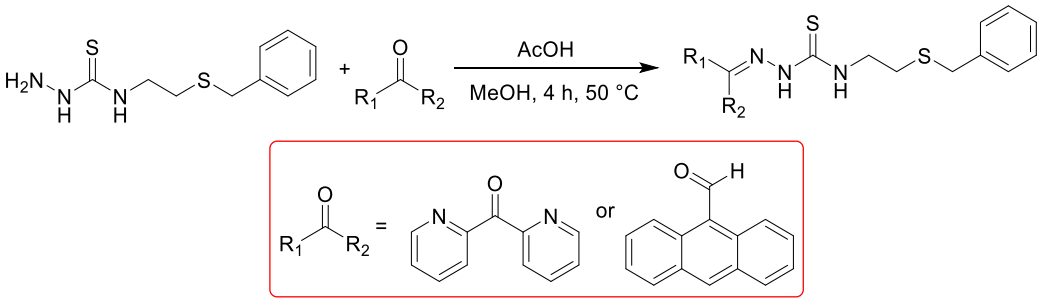


Hydrazine monohydrate (65% aqueous solution, 0.23 mL, 4.8 mmol, 1.00 eq.) was dissolved in 20 mL of MeOH and heated to 70 °C. Then, the isothiocyanate (1.00 g, 4.8 mmol, 1.00 eq.) was dissolved in 50 mL of MeOH and slowly added to the hydrazine solution over 1 h. The reaction mixture was stirred for an additional 3 h, then, the solvent was removed under reduced pressure, yielding a brown oil. The crowd product was dissolved in 10 mL of $CHCl_3$ and poured into boiling petrol ether. The oily precipitate was separated by decantation and dried under ambient conditions. The product was obtained as brown oil. Yield: 1.01 g (4.2 mmol, 87%). $C_{10}H_{15}N_3S_2$ (241.37 g/mol). ^{1}H NMR (499 MHz, DMSO-*d*$_6$) δ [ppm] = 8.69 (s, 1H, H-2), 8.04 (s, 1H, H-4), 7.35 (m, 2H, H-9), 7.30 (m, 2H, H-10), 7.23 (m, 1H, H-11), 4.47 (s, 2H, H-1), 3.77 (s, 2H, H-7), 3.64 (q, *J* = 8.1 Hz, 2H, H-5), 2.57 (t, *J* = 7.3 Hz, 2H, H-6). ^{13}C NMR (499 MHz, DMSO-*d*$_6$) δ



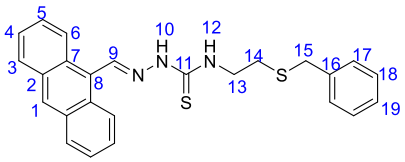
[ppm] = 181.44 (C-3), 139.24 (C-8), 129.37 (C-9), 128.80 (C-10), 127.22 (C-11), 42.73 (C-5), 35.20 (C-7), 30.64 (C-6). HR-ESI-MS: m/z $[M+H]^+$ = 242.0781.

5.3.6.4 Synthesis of TSCs – general description

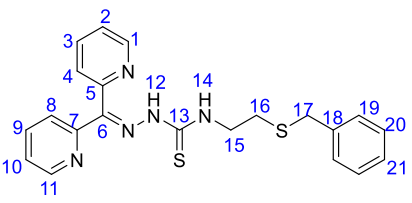


4-(2-Benzylsulfanylethyl)thiosemicarbazide (1.00 eq.) and antracene-9-carbaldehyde or di(2-pyridyl) ketone (1.00 eq.) were dissolved in a minimum amount of MeOH. Then, 0.1 mL of glacial AcOH were added, and the reaction mixture was sonicated at 50 °C for 4 h. Then, the solvent was removed under reduced pressure, and the crude product was purified by column chromatography.

9-Anthraldehyde-4-(2-benzylsulfanylethyl)-3-thiosemicarbazone from 0.30 g (1.2 mmol) 4-(2-benzylsulfanylethyl)-thiosemicarbazide, 0.25 g (1.2 mmol) antracene-9-carbaldehyde. The product was purified by column chromatography (c-hexane/EOAc 4:1 v/v) and obtained as yellow solid. Yield: 0.22 g (0.5 mmol, 43%). $C_{25}H_{23}N_3S_2$ (429.60 g/mol). ^{1}H NMR (499 MHz, DMSO-d_6) δ [ppm] = 11.80 (s, 1H, H-10), 9.31 (s, 1H, H-9), 8.71 (s, 1H, H-1), 8.51 (m, 3H, H-6, H-12), 8.14 (d, *J* = 8.4 Hz, 2H, H-3), 7.59 (m, 4H, H-4, H-5), 7.34 (d, *J* = 6.9 Hz, 2H, H-17), 7.27 (m, 2H, H-18), 7.21 (m, 1H, H-19), 3.80 (m, 4H, H-13, H-15), 2.68 (t, *J* = 7.2 Hz, 2H, H-14). ^{13}C NMR (499 MHz, DMSO-d_6) δ [ppm] = 177.60 (C-11), 142.30 (C-9), 139.13 (C-16), 131.33 (C-2), 130.07 (C-7), 129.76 (C-1), 129.40 (C-3), 129.35 (C-17), 128.79 (C-18), 127.70 (C-4/C-5), 127.24 (C-19), 126.05 (C-4/C-5), 125.76 (C-8), 125.24 (C-6), 43.30 (C-13), 35.24 (C-15), 30.33 (C-14). HR-ESI-MS: m/z $[M+H]^+$ = 430.1410, m/z $[M+Na]^+$ = 452.1229.

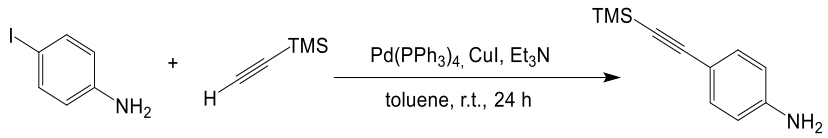


Di-2-pyridylketone-4-(2-benzylsulfanylethyl)-3-thiosemicarbazone from 0.30 g (1.2 mmol) 4-(2-benzylsulfanylethyl)thiosemicarbazide, 0.23 g (1.2 mmol) di(2-pyridyl) ketone. The product was purified by column chromatography (c-hexane/EOAc 1:3 v/v) and obtained as colorless solid. Yield: 0.36 g (0.9 mmol, 74%). $C_{21}H_{21}N_5S_2$ (407.55 g/mol). ^{1}H NMR (499 MHz, DMSO-d_6) δ [ppm] = 13.32 (s, 1H, H-12), 9.00 (t, *J* = 5.9 Hz, 1H, H-14), 8.84 (d, *J* = 4.4 Hz, 1H, H-1), 8.59 (d, *J* = 4.4 Hz, 1H, H-11), 8.20 (d, *J* = 8.0 Hz, 1H, H-8), 7.97 (m, 2H, H-3, H-9), 7.58 (m, 1H, H-2), 7.49 (m, 2H, H-4, H-10), 7.36 (d, *J* = 7.3 Hz, 2H, H-19), 7.30 (t, *J* = 6.5 Hz, 2H, H-20), 7.23 (m, 1H, H-21), 3.82 (m, 4H, H-15, H-17), 2.70 (t, *J* = 7.2 Hz, 2H, H-16). ^{13}C NMR (499 MHz, DMSO-d_6) δ [ppm] = 177.90 (C-13), 155.50 (C-7), 151.48 (C-5), 148.87 (C-11), 148.61 (C-1), 141.85 (C-6), 139.11 (C-18), 138.01 (C-3/C-9), 137.54 (C-3/C-9), 129.36 (C-19), 128.82 (C-20), 127.60 (C-4/C-10), 127.27 (C-21), 125.22 (C-2), 124.39 (C-4/C-10), 124.27 (C-8), 43.88 (C-15), 35.40 (C-17), 30.03 (C-16). HR-ESI-MS: m/z $[M+H]^+$ = 408.1314 m/z $[M+Na]^+$ = 430.1133.



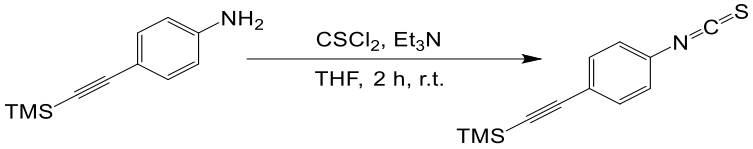
5.3.7 Syntheses of TSCs with alkyne function

5.3.7.1 Synthesis of 4-[(trimethylsilyl)ethynyl]aniline



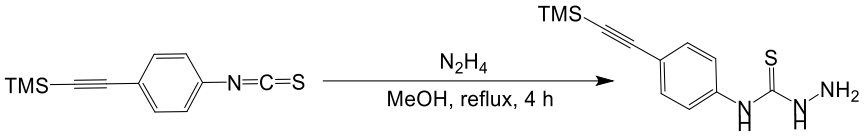
The reaction was performed under inert conditions. [Pd(PPh$_3$)$_4$] (0.28 g, 0.2 mmol, 0.03 eq.), CuI (0.14 g, 0.7 mmol, 0.09 eq.), 4-iodobenzene amine (1.75 g, 8.0 mmol, 1.00 eq.), trimethylsilyl acetylene (1.20 mL, 8.6 mmol, 1.08 eq.) and Et$_3$N (1.40 mL, 10.0 mmol, 1.25 eq.) were dissolved in 20 mL of toluene and the reaction mixture was stirred for 24 h at room temperature. Then, the solvent was removed under reduced pressure, and the product was purified by column chromatography (c-hexane/EOAc 8:1 → 5:1 → 3:1 → 2:1 → EOAc v/v). The product was obtained as yellow solid.[291] Yield: 1.39 g (7.3 mmol, 92%). $C_{11}H_{15}NSi$ (189.33 g/mol). ^{1}H NMR (499 MHz, DMSO-*d*$_6$) δ [ppm] = 7.28 (d, *J* = 7.9 Hz, 2H), 6.61 (d, *J* = 8.4 Hz, 2H), 3.80 (s, 2H), 0.24 (s, 9H).

5.3.7.2 Synthesis of 4-[(trimethylsilyl)ethynyl] phenyl isothiocyanate

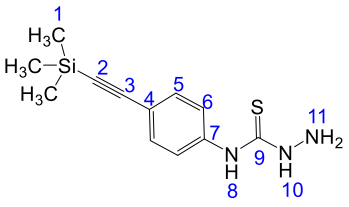


The reaction was performed under inert conditions. 4-[(trimethylsilyl)ethynyl]aniline (1.00 g, 5.3 mmol, 1.00 eq.) and Et$_3$N (2.20 mL, 15.8 mmol, 3.00 eq.) were dissolved in 50 mL of THF and thiophosgene (0.44 mL, 5.8 mmol, 1.10 eq.) was slowly added at 0 °C. The reaction mixture was stirred for 2 h at room temperature, which lead to the formation of a brown suspension. The reaction was quenched by adding 100 mL of distilled H_2O and the product was extracted with Et_2O (3 x 100 mL). The organic phase was dried over Na_2SO_4, and the solvent was removed under reduced pressure. The product was obtained as brown oil. Yield: 1.20 g (5.2 mmol, 98%). $C_{12}H_{13}NSSi$ (231.39 g/mol). ^{1}H NMR (499 MHz, DMSO-*d*$_6$) δ [ppm] = 7.43 (d, *J* = 8.4 Hz, 2H), 7.16 (d, *J* = 8.4 Hz, 2H), 0.26 (s, 9H)

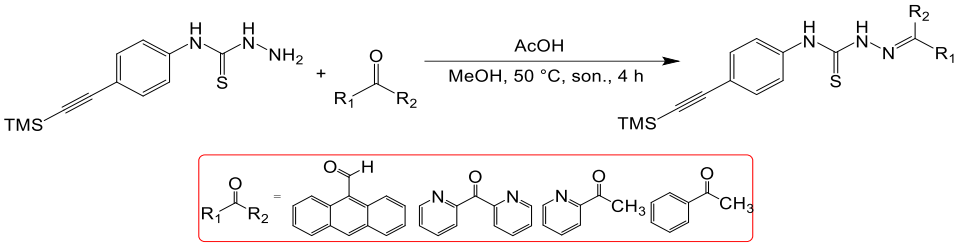
5.3.7.3 Synthesis of *N*-hydrazidecarbothio[4-(trimethylsilyl)ethynylphenyl]amine



Hydrazine monohydrate (0.26 mL, 5.3 mmol, 1.00 eq.) was dissolved in 50 mL of MeOH and heated to 70 °C. Then, 4-[(trimethylsilyl)ethynyl] phenyl isothiocyanate (1.20 g, 5.3 mmol, 1.00 eq.) was dissolved in 50 mL of MeOH and slowly added to the hydrazine solution over the course of 1 h. The reaction mixture was stirred for an additional 3 h followed by the removal of the solvent under reduced pressure, yielding a brown oil. The crude product was purified by column chromatography (c-hexane/EOAc 3:1 → EOAc v/v) and obtained as pale-yellow solid. Yield: 0.81 g (3.1 mmol, 60%). $C_{12}H_{17}N_3SSi$ (263.43 g/mol). ^{1}H NMR (499 MHz, DMSO-*d*$_6$) δ [ppm] = 9.26 (s, 1H, H-10), 7.83-7.68 (m, 3H, H-6, H-7), 7.37 (d, *J* = 8.0 Hz, 2H, H-5), 0.22 (s, 9H, H-1). ^{13}C NMR (499 MHz, DMSO-*d*$_6$) δ [ppm] = 179.23 (C-9), 140.50 (C-4), 131.91 (C-5), 122.83 (C-6), 105.96 (C-3), 93.64 (C-2), 0.47 (C-1). HR-ESI-MS: m/z [M+H]$^+$ = 264.0986.

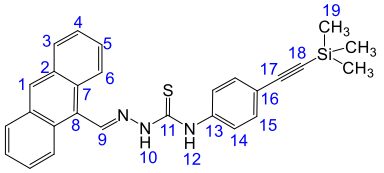


5.3.7.4 Synthesis of TSCs – general description

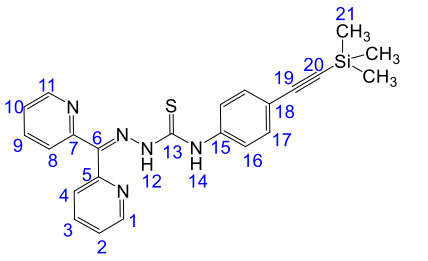


9-anthracene aldehyde or di(2-pyridyl) ketone (1.00 eq.) and *N*-hydrazidecarbothio[4-(trimethylsilyl) ethynylphenyl]amine (1.00 eq.) was dissolved in 50 mL of MeOH and 0.1 mL of glacial AcOH were added. The reaction mixture was sonicated at 50 °C for 4 h. The solvent was removed under reduced pressure, and the crude product was purified by column chromatography.

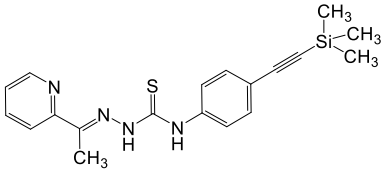
[(1*E*)-(anthracen-9-yl)methylideneamino][4-(trimethylsilyl)ethynylphenylamino] carbothioamide from 0.20 g (0.8 mmol) *N*-hydrazidecarbothio[4-(trimethylsilyl)ethynylphenyl]amine, 0.16 g (0.8 mmol) antracene-9-carbaldehyde. The formed precipitate was filtered off and washed with cold MeOH. The product was obtained as yellow solid. Yield: 0.20 g (0.4 mmol, 58%). $C_{27}H_{25}N_3SSi$ (451.66 g/mol). ^{1}H NMR (499 MHz, DMSO-*d*$_6$) δ [ppm] = 12.16 (s, 1H, H-10), 10.13 (s, 1H, H-12), 9.45 (s, 1H, H-9), 8.72 (s, 1H, H-1), 8.57 (d, *J* = 8.8 Hz, 2H, H-6), 8.16 (d, *J* = 8.3 Hz, 2H, H-3), 7.71 (d, *J* = 8.5 Hz, 2H, H-14), 7.65 (t, *J* = 8.0 Hz, 2H, H-4/H-5), 7.58 (t, *J* = 8.0 Hz, 2H, H-4/H-5), 7.44 (d, *J* = 8.5 Hz, 2H, H-15), 0.23 (s, 9H, H-19). ^{13}C NMR (499 MHz, DMSO-*d*$_6$) δ [ppm] = 176.01 (C-11), 143.38 (C-9), 140.17 (C-16), 131.93 (C-15), 131.34 (C-2), 130.18 (C-7), 130.03 (C-1), 129.42 (C-3), 127.80 (C-4/C-5), 126.10 (C-4/C-5), 125.55 (C-8), 125.31 (C-6), 125.02 (C-14), 118.78 (C-13), 105.70 (C-17), 94.18 (C-18), 0.44 (C-19). HR-ESI-MS: m/z $[M+H]^+$ = 452.1615, m/z $[M+Na]^+$ = 474.1433.



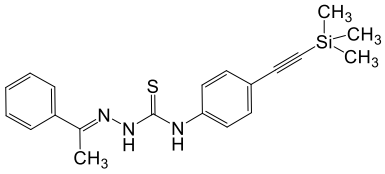
[Bis(pyridin-2-yl)methylideneamino][4-(trimethylsilyl)ethynylphenylamino] carbothioamide from 0.20 g (0.8 mmol) *N*-hydrazidecarbothio[4-(trimethylsilyl)ethynylphenyl]amine, 0.14 g (0.8 mmol) dipyridyl ketone. The product was purified by column chromatography (c-hexane/EOAc 4:1 v/v) and obtained as brownish solid. Yield: 0.23 g (0.5 mmol, 71%). $C_{23}H_{23}N_5SSi$ (429.62 g/mol). ^{1}H NMR (499 MHz, DMSO-*d*$_6$) δ [ppm] = 13.70 (s, 1H, H-12), 10.51 (s, 1H, H-14), 8.86 (d, *J* = 4.2 Hz, 1H, H-1), 8.60 (d, *J* = 4.2 Hz, 1H, H-11), 8.37 (d, *J* = 8.0 Hz, 1H, C-8), 8.02 (m, 2H, H-3, H-9), 7.68 (m, 2H, H-16), 7.62 (m, 1H, H-2), 7.56 (m, 2H, H-4, H-10), 7.52 (m, 2H, H-17), 0.24 (s, 1H, H-21). ^{13}C NMR (499 MHz, DMSO-*d*$_6$) δ [ppm] = 176.63 (C-13), 155.28 (C-7), 151.41 (C-5), 148.81 (C-11), 148.63 (C-1), 142.61 (C-6), 139.75 (C-18), 138.13 (C-3/C-9), 137.58 (C-3/C-9), 132.05 (C-4/C-10, C-17), 125.66 (C-2), 125.43 (C-16), 124.71 (C-8), 124.55 (C-4), 119.43 (C-15), 105.52 (C-19), 94.47 (C-20), 0.41 (C-21). HR-ESI-MS: m/z $[M+H]^+$ = 430.1520, m/z $[M+Na]^+$ = 452.1339.



Trimethyl(2-(*p*-[(*E*)-1-[1-(2-pyridyl)ethylidene]thiosemicarbazido]phenyl)ethynyl)silane from 0.30 g (1.2 mmol) *N*-hydrazidecarbothio[4-(trimethylsilyl)ethynylphenyl]-amine, 135.0 µL (1.2 mmol) 2-acetylpyridine. The product was purified by column chromatography (c-hexane/EOAc 2:1 v/v) and obtained as a colorless solid. Yield: 0.41 g (1.1 mmol, 95%). $C_{19}H_{22}N_4SSi$ (366.56 g/mol). ^{1}H NMR (499 MHz, DMSO-*d*$_6$) δ [ppm] = 10.81 (s, 1H), 10.25 (s, 1H), 8.60 (s, 1H), 8.51 (d, *J* = 4.5 Hz, 1H), 7.83 (m, 1H), 2.14 (d, *J* = 8.7 Hz, 2H), 7.45 (m, 2H), 2.48 (s, 3H), 0.24 (s, 9H).

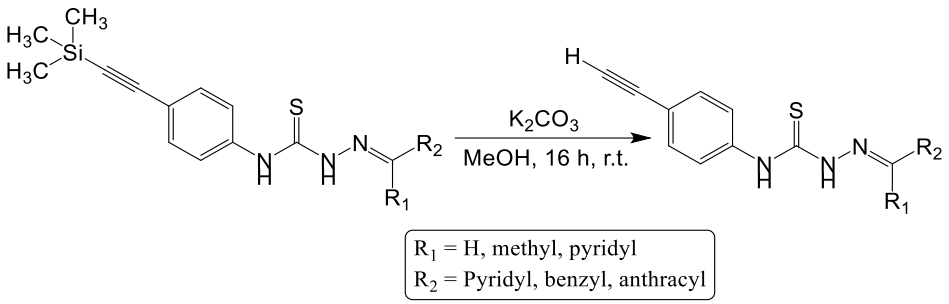


[(1*E*)-1-phenyleth-1-ylideneamino][4-(trimethylsilyl)ethynylphenylamino]carbothioamide



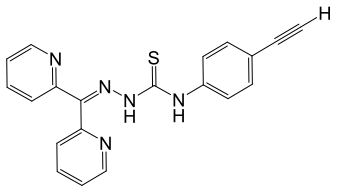
From 0.30 g (1.2 mmol) *N*-hydrazidecarbothio[4-(trimethylsilyl)ethynylphenyl]-amine, 141.0 µL (1.2 mmol) acetophenon. The product was purified by column chromatography (c-hexane/EOAc 2:1 v/v) and obtained as a colorless solid. Yield: 0.37 g (1.0 mmol, 81%). $C_{20}H_{23}N_3SSi$ (365.57 g/mol). ^{1}H NMR (499 MHz, DMSO-d_6) δ [ppm] = 10.72 (s, 1H), 10.13 (s, 1H), 7.99 (m, 4H), 7.69 (m, 2H), 7.43 (m, 4H), 2.39 (s, 3H), 0.24 (s, 9H).

5.3.7.5 Deprotection of the TMS group



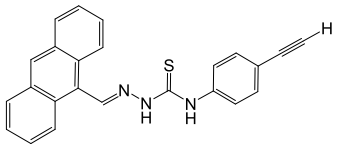
The TSC (1.00 eq.) was dissolved in MeOH and K_2CO_3 (2.00 eq.) was added. The reaction was stirred at room temperature for 16 h. After that, the solvent was removed under reduced pressure and the crude product was redissolved in 20 mL of EtOAC. The solution was washed three times with 20 mL of H_2O, dried over $MgSO_4$ and the solvent was removed under reduced pressure, yielding the product.

1-[Bis(2-pyridyl)methylene]-4-(*p*-ethynylphenyl)thiosemicarbazide



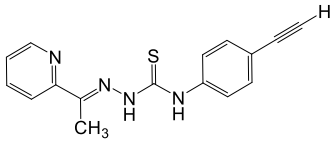
from 50.0 mg (0.12 mmol) [bis(pyridin-2-yl)methylideneamino][4-(trimethylsilyl)ethynyl phenylamino] carbothioamide, 32.3 mg (0.23 mmol) K_2CO_3. The product was obtained as a beige solid. Yield: 43.0 mg (0.12 mmol, quant.). $C_{20}H_{15}N_5S$ (357.44 g/mol). ^{1}H NMR (499 MHz, DMSO-d_6) δ [ppm] = 14.63 (s, 1H), 9.58 (s, 1H), 8.85 (d, *J* = 4.8 Hz, 1H), 8.68 (d, *J* = 4.8 Hz, 1H), 7.90-7.74 (m, 5H), 7.58-7.49 (m, 3H), 7.41 (m, 1H), 3.07 (s, 1H).

(*E*)-1-[(9-Anthryl)methylene]-4-(*p*-ethynylphenyl)thiosemicarbazide



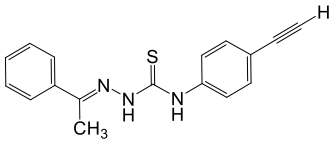
from 100.0 mg (0.22 mmol) [(1*E*)-(anthracen-9-yl)methylideneamino][4-(trimethylsilyl)ethynyl phenylamino] carbothioamide, 30.6 mg (0.22 mmol) K_2CO_3. The product was obtained as a beige solid. Yield: 84.0 mg (0.22 mmol, quant.). $C_{24}H_{17}N_3S$ (379.48 g/mol). ^{1}H NMR (499 MHz, DMSO-d_6) δ [ppm] = 12.14 (s, 1H), 10.10 (s, 1H), 9.42 (s, 1H), 8.74 (s, 1H), 8.58 (d, *J* = 5.0 Hz, 2H), 8.16 (d, *J* = 7.0 Hz, 2H), 7.72-7.59 (m, 6H), 7.46 (d, *J* = 7.0 Hz, 2H).

(*E*)-4-(*p*-Ethynylphenyl)-1-[1-(2-pyridyl)ethylidene]thiosemicarbazide

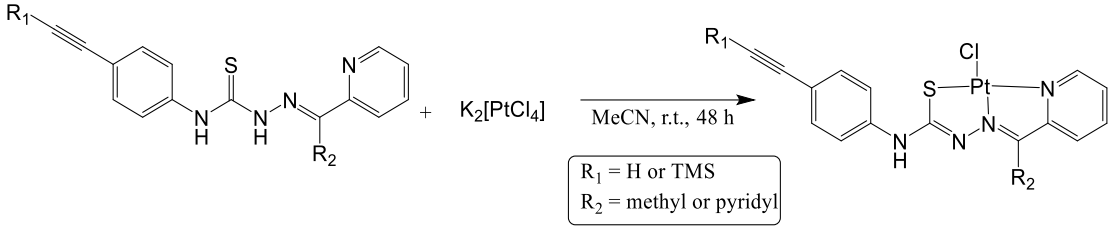


from 100.0 mg (0.27 mmol) trimethyl(2-(*p*-[(*E*)-1-[1-(2-pyridyl)ethylidene]thiosemicarbazido]phenyl) ethynyl)silane, 37.7 mg (0.27 mmol) K_2CO_3. The product was obtained as a beige solid. Yield: 80.3 mg (0.27 mmol, quant.). $C_{16}H_{14}N_4S$ (294.38 g/mol). ^{1}H NMR (499 MHz, DMSO-d_6) δ [ppm] = 10.81 (s, 1H), 10.25 (s, 1H), 8.62 (d, *J* = 4.5 Hz, 1H), 8.53 (d, *J* = 8.0 Hz), 7.83 (m, 1H), 7.65 (d, *J* = 8.6 Hz, 2H), 7.51 (d, *J* = 8.6 Hz, 2H), 2.44 (m, 1H), 2.47 (s, 3H).

(*E*)-4-(*p*-Ethynylphenyl)-1-(1-phenylethylidene)thiosemicarbazide from 100.0 mg (0.27 mmol) [(1*E*)-1-phenyleth-1-ylideneamino][4-(trimethylsilyl)ethynylphenylamino] carbothioamide, 37.8 mg (0.27 mmol) K_2CO_3. The product was obtained as a beige solid. Yield: 80.0 mg (0.27 mmol, quant.). $C_{17}H_{15}N_3S$ (293.39 g/mol). ^1H NMR (499 MHz, DMSO-d_6) δ [ppm] = 9.49 (s, 1H), 8.77 (s, 1H), 7.78 (d, *J* = 9.0 Hz, 3H), 7.53 (d, *J* = 9.0 Hz, 2H), 7.46 (m, 3H), 3.10 (s, 1H), 2.38 (s, 3H).

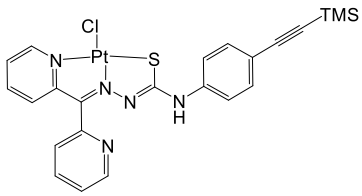


5.3.7.6 Platinum complexes of the alkyne TSCs

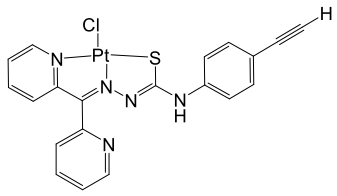


The TSC (1.00 eq.) and $K_2[PtCl_4]$ (1.00 eq.) were suspended in 70 mL of MeCN and the reaction was stirred for 48 h at room temperature. The formed precipitate was filtered off and washed with H_2O and c-hexane, yielding the product.

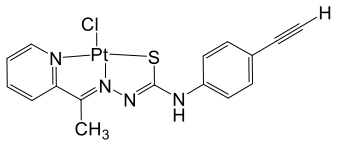
[Pt(TMSC≡CPhTSCdipy)Cl] from 100.0 mg (0.23 mmol) [bis(pyridin-2-yl)methylideneamino][4-(trimethylsilyl)ethynylphenylamino] carbothioamide, 95.0 mg (0.23 mmol) $K_2[PtCl_4]$. The product was obtained as a red solid. Yield: 146.0 mg (0.22 mmol, 95%). $C_{23}H_{22}ClN_5PtSSi$ (659.14 g/mol). ^1H NMR (499 MHz, DMSO-d_6) δ [ppm] = 10.65 (s, 1H), 8.94 (d, *J* = 4.5 Hz, 1H), 8.83 (d, *J* = 4.4 Hz, 1H), 8.19 (m, 2H), 7.92 (d, *J* = 6.0 Hz, 1H), 7.82 (m, 1H), 7.68 (m, 1H), 7.46 (d, *J* = 6.0 Hz, 1H), 7.32 (d, *J* = 8.0 Hz, 2H), 7.25 (d, *J* = 8.0 Hz, 2H), 0.22 (s, 9H).



[Pt(HC≡CPhTSCdipy)Cl] from 100.0 mg (0.28 mmol) 1-[bis(2-pyridyl)methylene]-4-(*p*-ethynylphenyl)thiosemicarbazide, 116.0 mg (0.28 mmol) $K_2[PtCl_4]$. The product was obtained as a red solid. Yield: 161.0 mg (0.27 mmol, 98%). $C_{20}H_{14}ClN_5PtS$ (586.96 g/mol). ^1H NMR (499 MHz, DMSO-d_6) δ [ppm] = 10.65 (s, 1H), 8.92 (d, *J* = 4.5 Hz), 8.82 (d, *J* = 4.4 Hz, 1H), 8.17 (m, 2H), 7.95 (d, *J* = 6.0 Hz), 7.84 (m, 1H), 7.67 (m, 1H), 7.46 (d, *J* = 6.0 Hz, 1H) 7.33 (d, *J* = 8.0 Hz, 2H), 7.28 (d, *J* = 8.0 Hz, 2H), 4.11 (s, 1H).

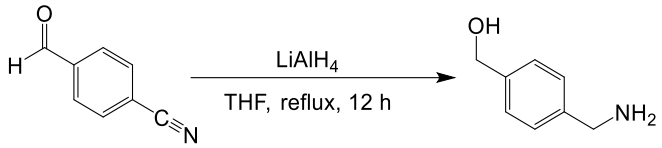


[Pt(HC≡CPhTSCacpy)Cl] from 100.0 mg (0.34 mmol) (*E*)-4-(*p*-ethynylphenyl)-1-[1-(2-pyridyl)ethylidene]thiosemicarbazide, 141.0 mg (0.34 mmol) $K_2[PtCl_4]$. The product was obtained as a red solid. Yield: 160.2 mg (0.30 mmol, 90%). $C_{16}H_{13}ClN_4PtS$ (523.90 g/mol). ^1H NMR (499 MHz, DMSO-d_6) δ [ppm] = 10.47 (s, 1H), 8.84 (d, *J* = 4.5 Hz, 1H), 8.24 (m, 1H), 7.93 (d, *J* = 7.0 Hz, 1h), 7.78 (m, 1H), 7.64 (d, *J* = 9.0 Hz, 2H), 7.48 (d, *J* = 7.48 Hz, 2H), 4.11 (s, 1H), 2.47 (s, 3H).



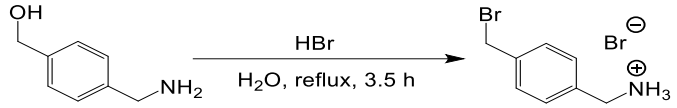
5.3.8 Syntheses of TSCs with azide function

5.3.8.1 Synthesis of 4-(aminomethyl)benzyl alcohol



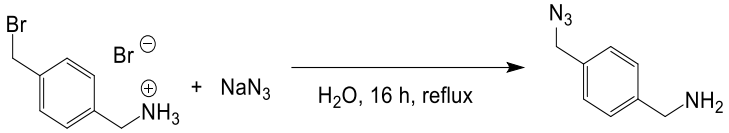
The reaction was performed under inert conditions. 4-Cyanobenzaldehyde (5.11 g, 39.1 mmol, 1.00 eq.) was dissolved in 40 mL of THF and added to a solution of $LiAlH_4$ (5.93 g, 156.0 mmol, 4.00 eq.) in 120 mL of THF at 0 °C. The reaction mixture was refluxed for 12 h. Then, the reaction was quenched with 20 mL of H_2O, and the mixture was filtered over *Celite* and washed with EtOAc (150 mL). The solvent was removed under reduced pressure yielding the product as colorless solid.[368] Yield: 5.4 g (39.0 mmol, quant.). $C_8H_{11}NO$ (137.18 g/mol). ^1H NMR (499 MHz, $CDCl_3$) δ [ppm] = 7.54 (s, 2H), 6.85 (s, 2H), 3.62 (m, 2H), 3.02 (m, 2H), 2.81 (m, 2H).

5.3.8.2 Synthesis of 4-(bromomethyl)benzylamine hydrobromide



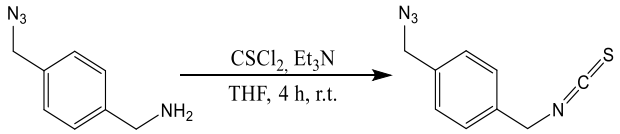
4-(Aminomethyl)benzyl alcohol (5.4 g, 39.0 mmol, 1 eq.) was dissolved in 60 mL of H_2O and 95 mL of HBr (46% aqueous solution). The reaction mixture was refluxed for 3.5 h. Then, the solvent was removed under reduced pressure, and the crude product was washed with 50 mL of Et_2O and dried under ambient conditions. The product was obtained as colorless solid.[369] Yield: 10.15 g (36.1 mmol, 93%). $C_8H_{10}BrN{\cdot}HBr$ (280.99 g/mol). ^1H NMR (499 MHz, DMSO-d_6) δ [ppm] = 8.27 (s, 3H), 7.48 (s, 4H), 4.72 (s, 2H), 4.02 (m, 2H).

5.3.8.3 Synthesis of 4-(azidomethyl)benzylamine



4-(Bromomethyl)benzylamine hydrobromide (5.00 g, 17.8 mmol, 1.00 eq.) was suspended in 50 mL of H_2O and a solution of NaN_3 (3.47 g, 53.4 mmol, 3.00 eq.) in 70 mL of H_2O was added. The reaction mixture was refluxed for 16 h. Then, half of the volume was removed under reduced pressure and 20 mL of Et_2O was added. The mixture was cooled to 0 °C, 5.00 g KOH was added, and the mixture was stirred for 20 min. The organic phase was separated, and the aqueous phase was extracted with Et_2O (3 x 50 mL). The combined organic phase was dried over $NaSO_4$, and the solvent was removed under reduced pressure. The product was obtained as colorless solid.[294] Yield: 2.26 g (13.9 mmol, 78%). $C_8H_{10}N_4$ (162.20 g/mol). ^1H NMR (499 MHz, DMSO-d_6) δ [ppm] = 7.29 (m, 4H), 4.30 (m, 2H), 3.86 (m, 2H), 1.59 (m, 2H).

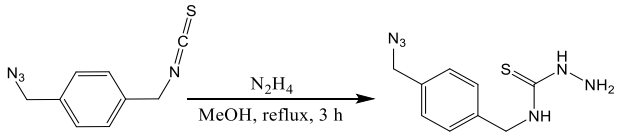
5.3.8.4 Synthesis of 1-(azidomethyl)-4-(isothiocyanatomethyl)benzene



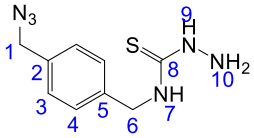
The reaction was performed under inert conditions. 4-(Azidomethyl)benzylamine (1.00 g, 6.2 mmol, 1.00 eq.) and Et_3N (2.60 mL, 18.6 mmol, 3.00 eq.) were dissolved in 50 mL of THF and thiophosgene (0.60 mL, 6.8 mmol, 1.10 eq., 85 %) was slowly added at 0 °C. The reaction mixture was stirred for 2 h at room temperature, which lead to the formation of a brown suspension. The reaction was quenched by

adding 100 mL of distilled H_2O and the product was extracted with Et_2O (3 x 100 mL). The organic phase was dried over Na_2SO_4 and the solvent was removed under reduced pressure. The product was obtained as brownish solid and used without further purification. Yield: 1.13 g (5.5 mmol, 89%). $C_9H_8N_4S$ (204.25 g/mol). ^{1}H NMR (499 MHz, DMSO-*d*$_6$) δ [ppm] = 7.35 (s, 4H), 4.73 (s, 2H), 4.36 (s, 2H).

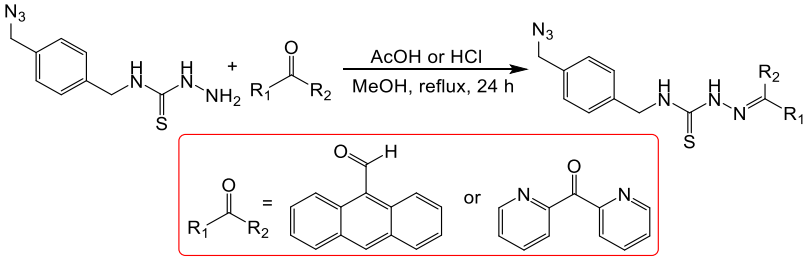
5.3.8.5 Synthesis of 4-([*p*-(azidomethyl)phenyl]methyl)thiosemicarbazide



Hydrazine monohydrate (0.27 mL, 5.5 mmol, 1.00 eq.) was dissolved in 50 mL of MeOH and heated to 70 °C. 1-(azidomethyl)-4-(isothiocyanatomethyl)benzene (1.13 g, 5.5 mmol, 1.00 eq.) was dissolved in 50 mL of MeOH and slowly added to the hydrazine solution over the course of 1 h. The reaction mixture was stirred for an additional 3 h, then, the solvent was removed under reduced pressure. The crude product was purified by column chromatography (c-hexane/EOAc 1:3 v/v). The product was obtained as brownish solid. Yield: 0.84 g (3.6 mmol, 65%). $C_9H_{12}N_6S$ (236.30 g/mol). ^{1}H NMR (499 MHz, DMSO-*d*$_6$) δ [ppm] = 8.75 (s, 1H, H-9), 8.33 (s, 1H, H-7), 7.32 (m, 4H, H-3, H-4), 4.72 (d, *J* = 6.0 Hz, 2H, H-6), 4.51 (s, 2H, H-10), 4.41 (s, 1H, H-1).^{13}C NMR (499 MHz, DMSO-d$_6$) δ [ppm] = 182.00 (C-8), 140.32 (C-5), 134.32 (C-2), 128.78 (C-3/C-4), 128.11 (C-3/C-4), 53.87 (C-1), 46.32 (C-6). HR-ESI-MS: m/z $[M+H]^+$ = 237.0918.

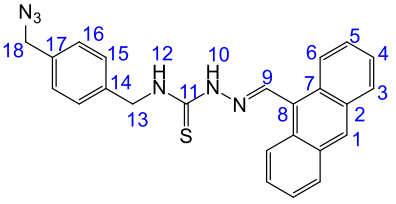


5.3.8.6 Synthesis of TSCs – general description

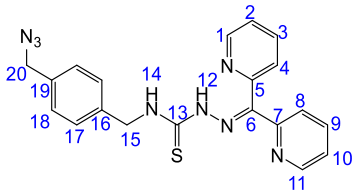


9-Anthracene aldehyde or di(2-pyrdyl) ketone (1.00 eq.) and 4-([*p*-(azidomethyl)phenyl]methyl) thiosemicarbazide (1.00 eq.) were dissolved in a minimum amount of MeOH and a few droplets of glacial AcOH or conc. HCl were added. The reaction mixture was refluxed for 24 h. If the product precipitates during the reaction, the solid was filtered off and washed with cold MeOH. Otherwise, the solvent was removed under reduced pressure, and the compound was purified by column chromatography.

[(2*E*)-2-[(Anthracen-9-yl)methylidene]hydrazino]-[4-(azidomethyl)phenyl]ethanethioamide from 0.20 g (0.8 mmol) 4-([*p*-(azidomethyl)phenyl]methyl) thiosemicarbazide, 0.17 g (0.8 mmol) antracene-9-carbaldehyde., conc. HCl. The product was washed with cold EtOH and obtained as yellow solid. Yield: 0.34 g (0.8 mmol, 100%). $C_{24}H_{20}N_6S$ (424.53 g/mol). ^{1}H NMR (499 MHz, DMSO-*d*$_6$) δ [ppm] = 11.83 (s, 1H, H-10), 9.32 (s, 1H, H-9), 8.92 (m, 1H, H-12), 8.70 (s, 1H, H-1), 8.52 (d, *J* = 8.1 Hz, 2H, H-6), 8.14 (d, *J* = 7.5 Hz, H-3), 7.59 (m, 4H, H-4, H-5), 7.37 (m, 4H, H-15, H-16), 4.85 (d, *J* = 5.5 Hz, 2H, H-13), 4.40 (s, 2H, H-18). ^{13}C NMR (499 MHz, DMSO-*d*$_6$) δ [ppm] = 178.11 (C-11), 142.34 (C-9), 139.88 (C-14), 134.73 (C-17), 131.26 (C-2), 130.02 (C-7), 129.72 (C-1), 129.34 (C-3), 128.87 (C-15/C-16), 128.04 (C-15/C-16), 127.63 (C-4/C-5), 126.01 (C-4/C-5), 125.85 (C-8), 125.27 (C-6), 53.94 (C-18), 47.01 (C-13). HR-ESI-MS: m/z $[M+H]^+$ = 425.1543, m/z $[M+Na]^+$ = 447.1364.

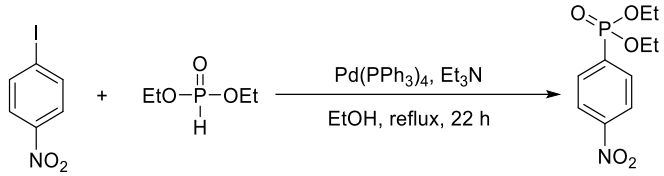


(2-[Bis(pyridin-2-yl)methylidene]hydrazine)-[4-(azidomethyl)phenyl]ethanethioamide from 0.2 g (0.8 mmol) 4-([*p*-(azidomethyl)phenyl]methyl) thiosemicarbazide, (0.15 g, 0.8 mmol) dipyridyl ketone, glacial AcOH. The product was purified by column chromatography (c-hexane/EOAc 1:3 v/v) and obtained as colorless solid. Yield: 0.25 g (0.6 mmol, 73%). $C_{20}H_{18}N_8S$ (402.48 g/mol). ^{1}H NMR (499 MHz, DMSO-*d*$_6$) δ [ppm] = 13.32 (s, 1H, H-12), 9.46 (t, *J* = 6.2 Hz, 1H, H-14), 8.85 (d, *J* = 4.9 Hz, 1H, H-1), 8.58 (d, *J* = 4.8 Hz, 1H, H-11), 8.26 (d, *J* = 7.9 Hz, 1H, H-8), 7.97 (dtd, *J* = 15.6, 7.8, 1.8 Hz, 2H, H-3, H-9), 7.58 (m, 1H, H-2), 7.52 (m, 1H, H-4), 7.47 (H-10), 7.35 (m, 4H, H-17, H-18), 4.90 (d, *J* = 6.2 Hz, 2H, H-15), 4.41 (s, 2H, H-20), ^{13}C NMR (499 MHz, DMSO-*d*$_6$) δ [ppm] = 178.58 (C-13), 155.47 (C-7), 151.50 (C-5), 148.80 (C-11), 148.60 (C-1), 142.04 (C-6), 139.41 (C-16), 138.01 (C-3/C-9), 137.48 (C-3/C-9), 134.51 (C-19), 128.89 (C-17/C-18), 127.98 (C-17/C-18), 127.66 (C-4), 125.21 (C-2), 124.37 (C-10), 124.35 (C-8), 53.85 (C-20), 47.29 (C-15). HR-ESI-MS: m/z $[M+H]^+$ = 403.1451, m/z $[M+Na]^+$ = 425.1269.

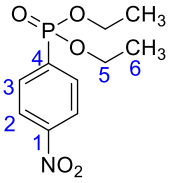


5.3.9 Synthesis of TSCs with phosphonate function

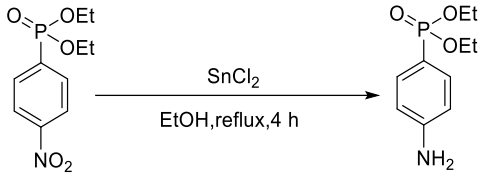
5.3.9.1 Synthesis of diethyl(4-nitrophenyl)phosphonate



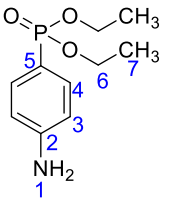
The reaction was performed under inert conditions. 1-Iodo-nitrobenzene (3.59 g, 14.4 mmol, 1.00 eq.) was dissolved in 70 mL of EtOH and diethylphosphite (2.04 mL, 15.9 mmol, 1.10 eq.), Et_3N (8.04 mL, 57.7 mmol, 4.00 eq.) and $[Pd(PPh_3)_4]$ (0.50 g, 0.43 mmol, 0.03 eq.) were added. The mixture was stirred at room temperature for 10 min and refluxed for 22 h. The solvent was removed under reduced pressure, and the crude product was purified by column chromatography (*c*-hexane/EOAc 1:1 v/v → EOAc), yielding the product as brownish oil. Yield: 3.19 g (12.3 mmol, 85%). $C_{10}H_{14}NO_5P$ (259.20 g/mol). ^{1}H NMR (499 MHz, DMSO-*d*$_6$) δ [ppm] = 8.35 (dd, *J* = 8.8, 3.2 Hz, H-6, 2H, H-3), 7.99 (dd, *J* = 12.5, 8.8 Hz, H-5, 2H, H-2), 4.16-3.98 (m, H-2, 4H, H-5), 1.25 (t, *J* = 7.0 Hz, H-1, 6H, H-6). ^{13}C NMR (499 MHz, DMSO-*d*$_6$) δ [ppm] = 149.92 (C-1), 136.20 (C-4), 132.85 (C-2), 123.62 (C-3), 62.39 (C-5), 16.18 (C-6).



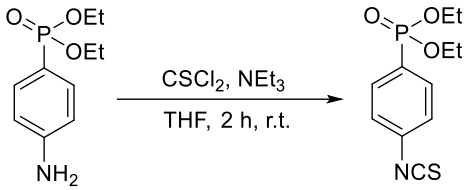
5.3.9.2 Synthesis of diethyl(4-aminophenyl)phosphonate



A solution of diethyl(4-nitrophenyl)phosphonate (0.50 g, 1.9 mmol, 1.00 eq.) and $SnCl_2$ x 2 H_2O (1.74 g, 7.7 mmol, 4.00 eq.) in 20 mL of EtOH was refluxed for 4 h. The solvent was removed under reduced pressure and 20 mL of NaOH solution (2 M) was added to the residue. The precipitate was filtered off and washed with EtOAc. Then, the aqueous layer was extracted with EtOAc (3 x 50 mL) and the combined organic layers were washed with brine (2 x 50 mL). The organic phase was dried over Na_2SO_4 and the solvent was removed under reduced pressure leaving the product as pale-yellow solid. Yield: 0.42 g (1.8 mmol, 94%).[297] $C_{10}H_{16}NO_3P$ (229.22 g/mol). ^{1}H NMR (499 MHz, DMSO-*d*$_6$) δ [ppm] = 7.32 (dd, *J* = 12.5, 8.5 Hz, 2H, H-3), 6.60 (dd, *J* = 8.5, 3.8 Hz, 2H, H-4), 5.80 (s, 2H, H-1), 4.03-3.77 (m, 4H, H-6), 1.19 (t, *J* = 7.0 Hz, 6H, H-7). ^{13}C NMR (499 MHz, DMSO-*d*$_6$) δ [ppm] = 153.03 (C-2), 133.42 (C-3), 113.38 (C-4), 113.30 (C-5), 61.32 (C-6), 16.63 (C-7).

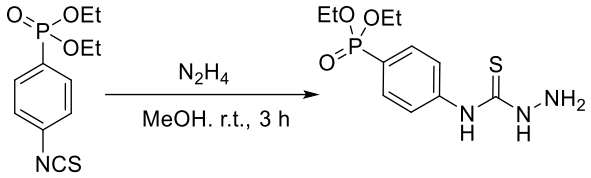


5.3.9.3 Synthesis of diethyl (4-isothiocyanatophenyl)phosphonate



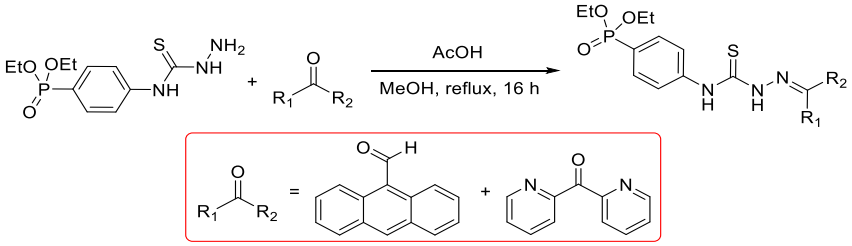
The reaction was performed under inert conditions. A solution of diethyl(4-aminophenyl)phosphonate (1.00 g, 4.4 mmol, 1.00 eq.) and Et_3N (1.82 mL, 13.1 mmol, 3.00 eq.) in 50 mL of THF was cooled to 0 °C and thiophosgene (0.39 mL, 4.4 mmol, 1.00 eq., 85%) was added slowly. The reaction was stirred for 2 h at room temperature, followed by quenching with the addition of 100 mL of H_2O. The aqueous phase was extracted with Et_2O (3 x 100 mL) and the combined organic layers were dried over Na_2SO_4. The solvent was removed under reduced pressure, and the crude product was purified by column chromatography (EOAc), yielding the product as dark reddish oil. Yield: 1.18 g (4.4 mmol, 99%). $C_{11}H_{14}NO_3PS$ (271.27 g/mol). ^{1}H NMR (300 MHz, DMSO-*d*$_6$) δ [ppm] = 7.76 (dd, *J* = 12.8, 8.4 Hz, 2H), 7.57 (dd, *J* = 8.4, 3.4 Hz, 2H), 4.18-3.88 (m, 4H), 1.23 (t, *J* = 7.0 Hz, 6H).

5.3.9.4 Synthesis of diethyl [4-(hydrazidecarbothioamino)phenyl] phosphonate



To a stirring solution of hydrazine hydrate (0.29 mL, 1.1 mmol, 1.00 eq.) in 50 mL of MeOH was added a solution of diethyl(4-isothiocyanatephenyl)phosphonate (0.30 g, 1.1 mmol, 1.00 eq.) in 20 mL of MeOH over the course of 1.5 h. Then, the reaction was stirred for an additional 2 h at room temperature. The solvent was removed under reduced pressure yielding the product as yellowish oil, which was used without further purification. Yield: 0.22 g (1.1 mmol, quant.). $C_{11}H_{18}N_3O_3PS$ (303.32 g/mol). ^{1}H NMR (300 MHz, DMSO-*d*$_6$) δ [ppm] = 7.93 (m, H-6, 2H), 7.60 (dd, *J* = 12.7, 8.6 Hz, H-5, 2H), 4.15-3.82 (m, H-2, 4H), 1.29 (t, *J* = 7.1 Hz, H-1, 6H).

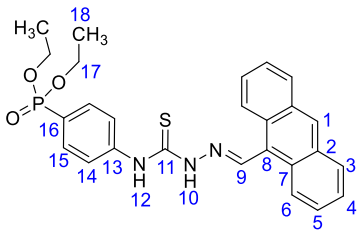
5.3.9.5 Synthesis of TSCs – general description



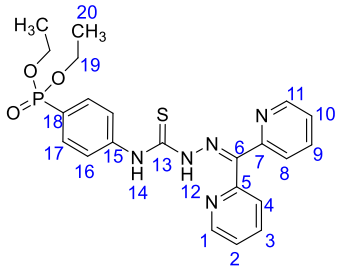
To a stirred solution of diethyl(4-thiosemicarbazidephenyl)phosphonate (1.00 eq.) in 50 mL of MeOH was added di-2-pyridylketone or 9-anthracene aldehyde (1.00 eq.) and a few droplets of glacial AcOH. The reaction mixture was refluxed for 16 h. If the product precipitates during the reaction, the solid was filtered off and washed with cold MeOH. Otherwise, the solvent was removed under reduced pressure, and the compound was purified by column chromatography.

[(2*E*)-2-[(Anthracen-9-yl)methylidene]hydrazino]-4-(diethoxyphosphoryl)benzene-1-carbothioamide from 0.22 g (0.7 mmol) diethyl [4-(hydrazidecarbothioamino)phenyl] phosphonate, 0.15 g (0.73 mmol) 9-anthraaldehyde. The product was filtered off, washed with cold MeOH and obtained as yellow solid. Yield: 0.35 g (0.7 mmol, 97%). $C_{26}H_{26}N_3O_3PS$ (491.55 g/mol). ^{1}H NMR (499 MHz, DMSO-*d*$_6$) δ [ppm] = 12.21 (s, 1H, H-10), 10.23 (s, 1H, H-12), 9.43 (s, 1H, H-9), 8.74 (s, 1H, H-1), 8.58 (dd, *J* = 8.7, 1.2 Hz, 2H, H-6), 8.19 (m, 2H, H-3), 7.87 (dd, *J* = 8.6, 3.7 Hz, 2H, H-14/H-15), 7.77-7.34

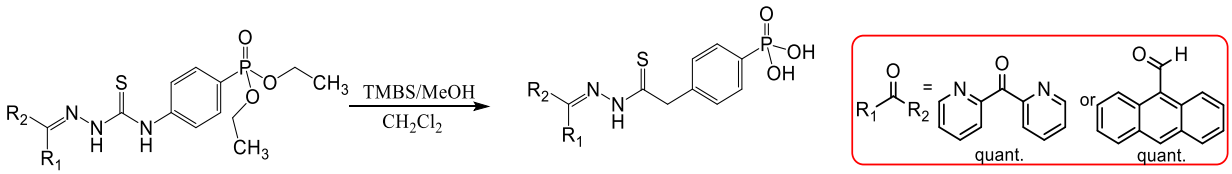
(m, 6H, H-14/H-15, H-4/H-5), 4.15-3.76 (m, 4H, H-17), 1.23 (t, *J* = 7.0 Hz, 6H, H-18). ^{13}C NMR (499 MHz, DMSO-*d*$_6$) δ [ppm] = 176.18 (C-11), 143.63 (C-9), 143.36 (C-16), 131.89 (C-14/C-15), 131.34 (C-2), 130.20 (C-7), 130.11 (C-1), 129.45 (C-3), 127.84 (C-4/C-5), 126.12 (C-4/C-5), 125.49 (C-7), 125.29 (C-6), 124.85 (C-14/C-15), 123.80 (C-13), 62.05 (C-17), 16.64 (C-18). HR-ESI-MS: m/z $[M+H]^+$ = 492.1509, m/z $[M+Na]^+$ = 514.1333.



(2-[Bis(pyridin-2-yl)methylidene]hydrazine)-4-(diethoxyphosphoryl)benzene-1-carbothioamide from 0.22 g (0.7 mmol) diethyl [4-(hydrazidecarbothioamino)phenyl] phosphonate, 0.14 g (0.7 mmol) dipyridyl ketone. The product was purified by column chromatography (CH_2Cl_2/MeOH, 95:5) and obtained as yellow solid. Yield: 0.22 g (0.5 mmol, 64%). $C_{22}H_{24}N_5O_3PS$ (469.50 g/mol). ^{1}H NMR (499 MHz, DMSO-*d*$_6$) δ [ppm] = 13.76 (s, H-10, 1H, H-12), 10.58 (s, H-8, 1H, H-14), 8.85 (d, *J* = 4.0 Hz, 1H, H-1), 8.60 (d, *J* = 4.5 Hz, 1H, H-11), 8.34 (d, *J* = 7.9 Hz, 2H, H-8), 8.00 (dtd, *J* = 14.6, 7.8, 1.8 Hz, 2H, H-3, H-9), 7.85 (dd, *J* = 8.4, 3.6 Hz, 2H, H-16/H-17), 7.72 (dd, *J* = 12.8, 8.4 Hz,2H, H-16/H-17), 7.61 (m, 1H, H-2), 7.55 (m, 1H, H-4), 7.51 (m, H-10), 4.17-3.87 (m, 4H, H-19), 1.24 (t, *J* = 7.0 Hz, 6H, H-20). ^{13}C NMR (499 MHz, DMSO-*d*$_6$) δ [ppm] = 176.89 (C-13), 155.21 (C-7), 151.38 (C-5), 148.84 (C-11), 148.63 (C-1), 143.03 (C-15/C-18), 142.81 (C-6), 138.19 (C-3/C-9), 137.66 (C-3/C-9), 131.94 (C-4, C-16/C-17), 126.47 (C-2), 126.10 (C-15/C-18), 125.60 (C-16/C-17), 124.73 (C-10), 124.62 (C-8), 62.21 (C-19), 16.63 (C-20). HR-ESI-MS: m/z $[M+H]^+$ = 470.1413, m/z $[M+Na]^+$ = 492.1232.

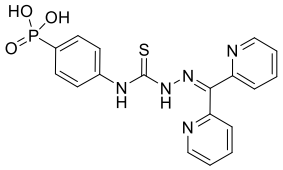


5.3.9.6 Deprotection of TSCs with phosphonate group – general description

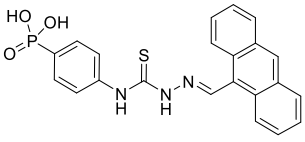


The reaction was performed under inert conditions. To a solution of the TSC (1.00 eq.) in dry DCM (30 mL) was added trimethylsilanbromide (7.0 eq.). The reaction mixture was stirred at room temperature for 24 h. After that, the solvent was removed under reduced pressure, and the residue was redissolved in MeOH. After stirring for 3 additional hours at room temperature, the solvent was removed under reduced pressure, and the product was dried under high vacuum for 10 h at 50 °C.

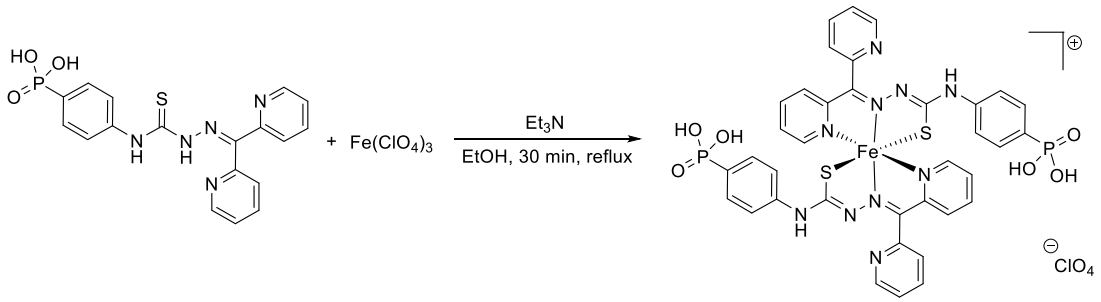
(4-([bis(pyridin-2-yl)methylideneaminocarbamthioyl]amino)phenyl)phosphonic acid from 0.10 g (0.21 mmol) (2-[Bis(pyridin-2-yl)methylidene]hydrazine)-4-(diethoxy phosphoryl)benzene-1-carbothio-amide, 0.19 mL (1.50 mmol) trimethylsilanbromid. The product was obtained as an orange solid. Yield: 0.08 g (0.21 mmol, quant.). $C_{18}H_{16}N_5O_3PS$ (413.39 g/mol). ^{1}H NMR (499 MHz, DMSO-*d*$_6$) δ [ppm] = 13.46 (s, 1H), 10.66 (s, 1H), 8.93 (d, *J* = 4.3 Hz, 1H), 8.74 (d, J = 5.1 Hz, 1H), 8.36 (d, J = 8.0 Hz, 2H), 8.17 (m, 2H), 7.71 (m, 7H).



[(2*Z*)-2-[(anthracen-9-yl)methylidene]hydrazino]-4-phosphonobenzene-1-carbothioamide from 0.06 g (0.12 mmol) [(2*E*)-2-[(Anthracen-9-yl)methylidene]hydrazino]-4-(diethoxyphosphoryl)benzene-1-carbothioamide, 0.11 mL (0.85 mmol) trimethylsilanbromid. The product was obtained as a yellow solid. Yield: 0.05 g (0.12 mmol, quant.). $C_{22}H_{18}N_3O_3PS$ (435.55 g/mol). ^{1}H NMR (499 MHz, DMSO-*d*$_6$) δ [ppm] = 12.15 (s, 1H), 10.14 (s, 1H), 8.75 (s, 1H), 8.57 (d, J = 8.7 Hz, 2H), 8.17 (d, J = 8.0 Hz, 2H), 7.62 (m, 7H).



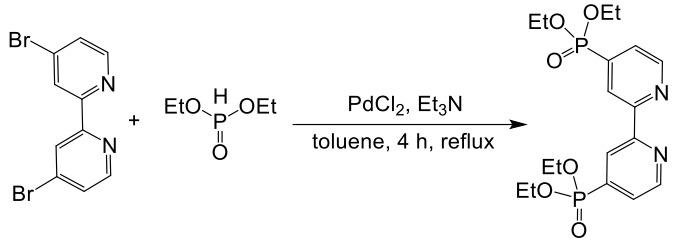
5.3.9.7 Synthesis of [Fe(Dipy(TSC)PhPO(OH)$_2$)$_2$]ClO$_4$



The TSC (0.10 g, 0.24 mmol, 2.00 eq.) was dissolved in EtOH and Et$_3$N (34.0 µL, 0.24 mmol, 2.00 eq.) was added. After that, Fe(ClO$_4$)$_3$ · 6 H$_2$O (55.0 mg, 0.12 mmol, 1.00 eq.) was added and the mixture was refluxed for 30 min, which lead to the formation of a brown suspension. The mixture was cooled to room temperature, and the precipitate was filtered off and washed with EtOH and Et$_2$O yielding the product as a brown solid. Yield: 98.0 mg (0.10 mmol, 83%). [C$_{36}$H$_{30}$FeN$_{10}$O$_6$P$_2$S$_2$]ClO$_4$ (980.06 g/mol). HR-ESI-MS: m/z [M–ClO$_4$]$^+$ = 880.0628.

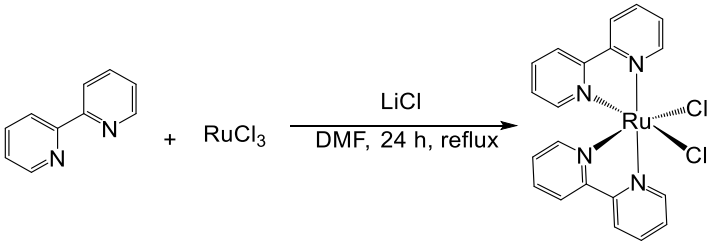
5.3.10 Synthesis of the [Ru(bpy)$_3$] photosensitizer

5.3.10.1 Synthesis of di(diethylphosphonate)bispyridine



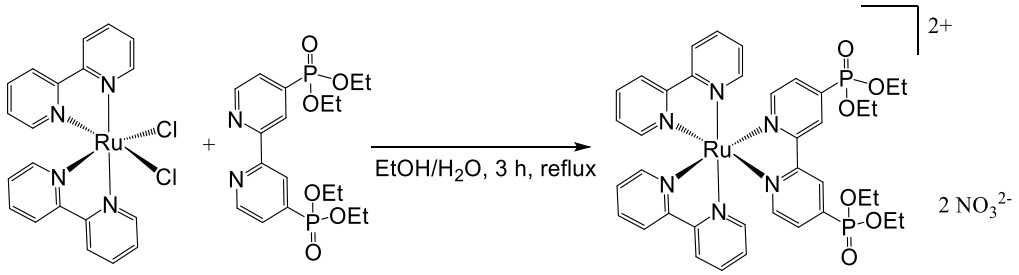
Under an argon atmosphere, dibromobispyridine (800 mg, 2.55 mmol, 1.00 eq.) and PdCl$_2$ (274 mg, 0.25 mmol, 0.10 eq.) were dissolved in 30 mL of dry toluene. After that, dry Et$_3$N (0.75 mL, 5.61 mmol, 2.20 eq.) and diethylphosphonate (0.75 mL, 5.61 mmol, 2.20 eq.) were added and the reaction mixture was stirred for 4 h at 110 °C. The reaction was filtered hot, and the solvent was removed under reduced pressure. The crude product was purified by column chromatography (EtOAc) leaving the product as a colorless solid.[331] Yield: 606 mg (1.40 mmol, 55%). C$_{18}$H$_{26}$N$_2$O$_6$P$_2$ (428.36 g/mol). ^{1}H NMR (499 MHz, CDCl$_3$) δ [ppm] = 8.91-8.69 (m, 4H), 7.76 (dd, *J* = 4.8, 1.4 Hz, 1H), 7.72 (dd, *J* = 4.8, 1.4 Hz, 1H), 4.56-3.82 (m, 8H), 1.39 (t, *J* = 7.0 Hz, 12H).

5.3.10.2 Synthesis of *cis*-dichlorobis(bipyridine)ruthenium(II)



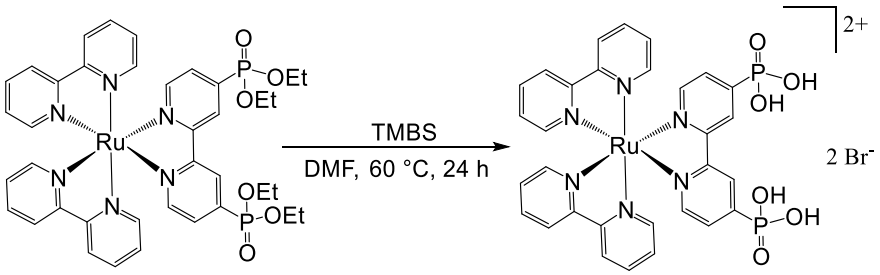
Under inert atmosphere RuCl$_3$ (1.00 g, 4.82 mmol, 1.00 eq.), LiCl (1.39 g, 32.8 mmol, 6.80 eq.) and 2,2´-dipyridine (1.51 g, 9.64 mmol, 2.0 eq.) were dissolved in 30 mL DMF and refluxed for 24 h. The dark purple mixture was filtered and washed several times with H$_2$O and Et$_2$O. The solid was dried under ambient conditions yielding the product as green crystals.[370] Yield: 0.70 g (1.44 mmol, 30%). C$_{17}$H$_{21}$N$_4$O$_3$PS (392.41 g/mol). ^{1}H NMR (499 MHz, DMSO-*d*$_6$) δ [ppm] = 9.98 (d, *J* = 5.6 Hz, 2H), 8.64 (d, *J* = 8.1 Hz, 2H), 8.48 (d, *J* = 8.1 Hz, 2H), 8.07 (td, *J* = 7.9, 1.6 Hz, 2H), 7.77 (t, *J* = 6.8 Hz, 2H), 7.68 (t, *J* = 7.4 Hz, 2H), 7.52 (d, *J* = 5.9 Hz, 2H), 7.10 (t, *J* = 6.7 Hz, 2H).

5.3.10.3 Synthesis of Tribis(bipyridine)ruthenium(II)di(diethyl)phosphonate



To a solution of diphosphonatebispyridine (214 mg, 0.50 mmol, 1.00 eq.) in 50 mL of a mixture of EtOH and H_2O (9:1) was added *cis*-dichlorobis(bipyridine)ruthenium(II) (312 mg, 0.60 mmol, 1.20 eq.) and the reaction mixture was refluxed for 3 h under argon atmosphere in the dark. After that, the solvent was removed under reduced pressure and the red solid was dissolved in a small amount of an acetone/H_2O solvent mixture (9:1) and purified by column chromatography (acetone/H_2O 8:2, then acetone/H_2O /KNO_3, 8:2, 10 drops). The product was obtained as a dark red solid.[371] Yield: 330 mg (0.34 mmol, 68%). $[C_{38}H_{42}N_6O_6P_2Ru](NO_3)_2$ (966.83 g/mol). ^{1}H NMR (499 MHz, acetonitrile-d_3) δ [ppm] = 8.86 (s, 1H), 8.82 (s, 1H), 8.59 – 8.50 (m, 4H), 8.11 (tt, *J* = 7.9, 1.3 Hz, 4H), 7.94 (dd, *J* = 5.7, 3.9 Hz, 2H), 7.78 – 7.69 (m, 4H), 7.68 – 7.58 (m, 2H), 7.48 – 7.38 (m, 4H), 4.27 – 4.04 (m, 8H), 1.35 (t, *J* = 7.0 Hz, 12H).

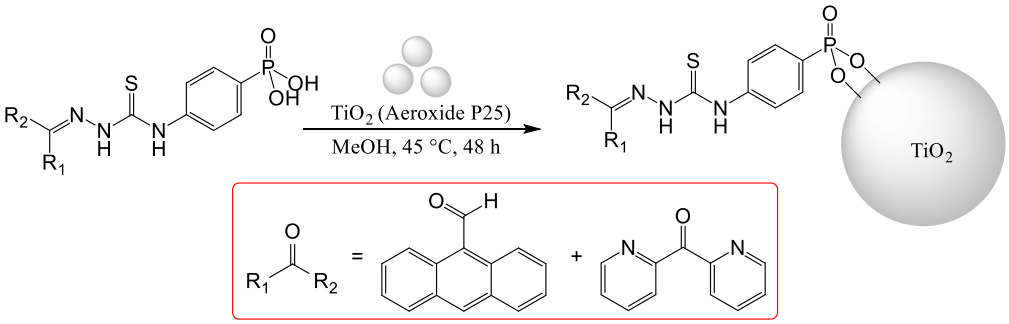
5.3.10.4 Synthesis of Tribis(bipyridine)ruthenium(II)diphosphonate



To a solution of tribis(bipyridine)ruthenium(II)di(diethyl)phosphonate (0.30 g, 0.31 mmol, 1.00 eq.) in 20 mL of dry DMF was added trimethylsilanbromide (0.60 mL, 4.00 mmol, 13.00 eq.) under argon atmosphere in the dark. The reaction mixture was stirred at 60 °C for 24 h. After that, the solvent and the excess of TMBS were removed under reduced pressure using a liquid nitrogen trap. After that, the residue was dissolved in MeOH and stirred for 3 additional hours at room temperature. The solvent was removed under reduced pressure, yielding the product as a red solid.[371] Yield: 200 mg (0.2 mmol, 64%). $[C_{30}H_{26}N_6O_6P_2Ru](Br)_2$ (889.39 g/mol). ^{1}H NMR (499 MHz, DMSO-d_6) δ [ppm] = 8.86 (m, 4H), 8.75 (m, 2H), 8.19 (m, 4H), 7.90 (m, 2H), 7.77 (m, 2H), 7.70-7.64 (m, 4H), 7.53 (m, 4H).

5.3.11 Functionalization of nanoparticles with TSCs

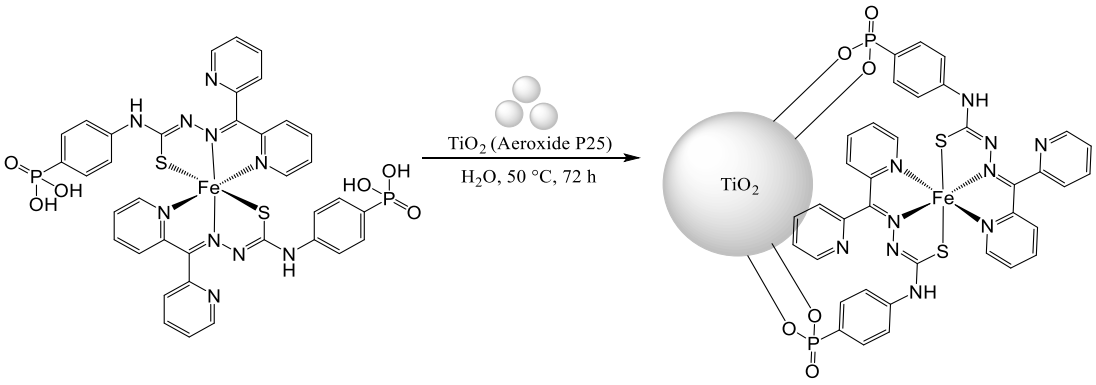
5.3.11.1 Anchoring the TSC with phosphonate function on TiO_2 NPs



10 mg of TiO_2 NP (*Aeroxid* P25) were dispersed in 2 mL of MeOH using ultrasound. After 15 min, a solution of the TSC in 3 mL of MeOH was added and the mixture was stirred for 48 h at 45 °C. The

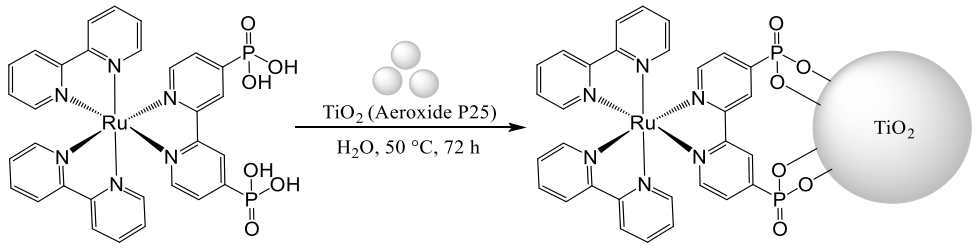
particles were separated by centrifugation (5 min, 12000 rpm) and washed 5 times with MeOH until the supernatant was colorless. The functionalized particles were dried in a drying oven (45 °C) for 16 h.

5.3.11.2 Anchoring $[Fe(Dipy(TSC)PhPO(OH)_2)_2]ClO_4$ on TiO_2 NPs



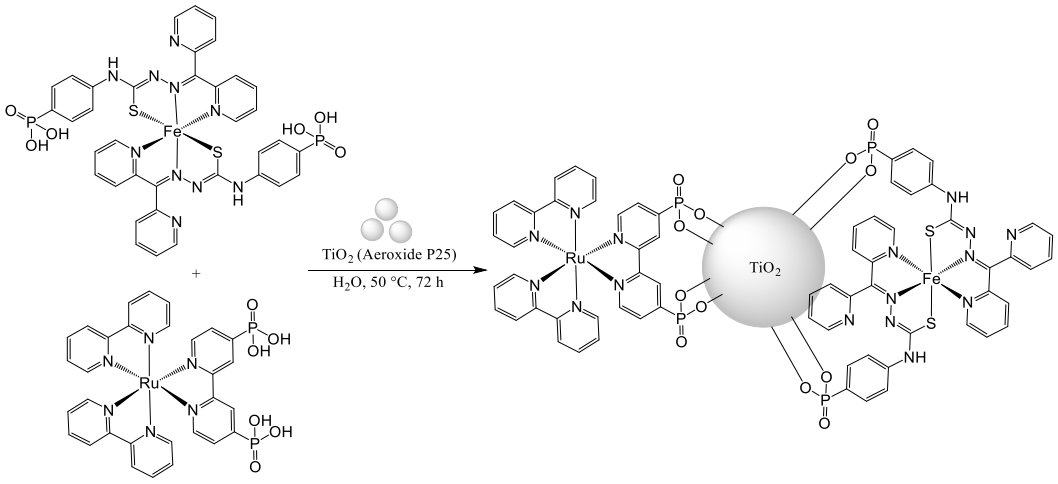
10 mg TiO_2 NPs were dispersed in 2 mL H_2O by sonicating for 30 min. After that, a solution of 5 mg $[Fe(Dipy(TSC)PhPO(OH)_2)]ClO_4$ in 3 mL H_2O was added dropwise under stirring. The mixture was heated to 60 °C and stirred for 48 h. The particles were separated by centrifugation (5 min, 12000 rpm) and washed 7 times with H_2O until the supernatant was colorless. The functionalized particles were dried in a drying oven (45 °C) for 16 h.

5.3.11.3 Anchoring tribis(bipyridine)ruthenium(II)diphosphonate on TiO_2 NPs



10 mg TiO_2 NPs were dispersed in 2 mL of H_2O by sonicating for 30 min. After that, a solution of 5 mg of $[Ru(Bipy)_3]Br$ in 2 mL H_2O was added under stirring. The mixture was stirred at 50 °C for 3 days under the exclusion of light. The particles were separated by centrifugation (5 min, 12000 rpm) and washed 3 times with H_2O until the supernatant was colorless. The functionalized particles were dried in a drying oven (45 °C) for 16 h.

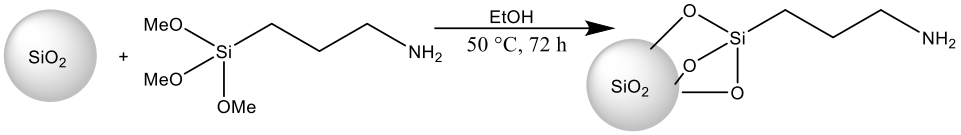
5.3.11.4 Synthesis of TiO_2@$[Fe(TSC)_2]$/$[Ru(bpy)_3]$



10 mg TiO_2 NPs were dispersed in 2 mL H_2O by sonicating for 30 min. After that, a solution of 2.5 mg $[Fe(Dipy(TSC)PhPO(OH)_2)]$ and 2.5 mg $[Ru(bpy)_3]$ in 4 mL H_2O was added dropwise under stirring.

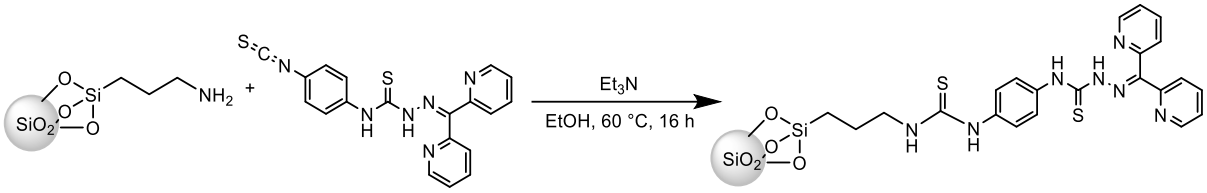
The mixture was stirred at 60 °C for 1 day under the exclusion of light. The particles were separated by centrifugation (5 min, 12000 rpm) and washed 5 times with H_2O until the supernatant was colorless. The functionalized particles were dried in a drying oven (45 °C) for 16 h.

5.3.11.5 Synthesis of SiO_2@APTMS



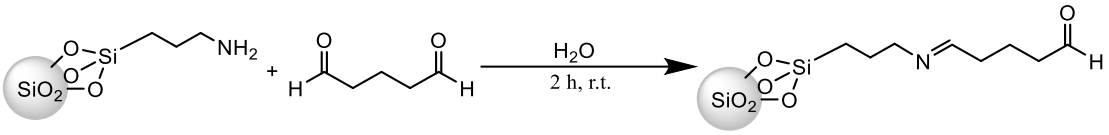
100 mg SiO_2 NPs were dispersed in 20 mL of EtOH by sonicating for 15 min. The suspension was stirred and heated to 50 °C. After that, 1.50 mL 3-aminopropyltriethoxysilane (APTMS) was added dropwise under nitrogen and the reaction mixture was stirred 72 h at 50 °C. After that, the particles were separated by centrifugation and washed three times with 30 mL EtOH (10 min, 11000 rpm). The functionalized particles were dried in a drying oven (45 °C) for 16 h.

5.3.11.6 Synthesis of SiO_2@APTMS@Dipy(TSC)PhNCS



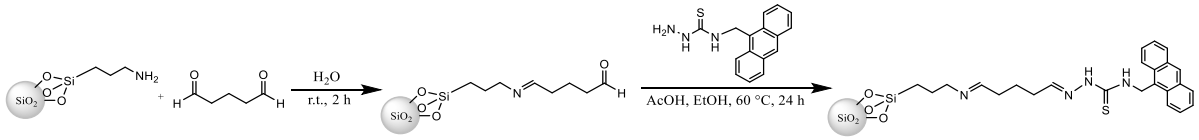
10 mg of SiO_2@APTMS NPs were dispersed in 1 mL of EtOH by sonicating for 30 min. After that, a solution of 5.4 mg of the TSC in 2 mL EtOH was added at 60 °C. Then, 3 drops of Et_3N were added and the reaction was stirred for 16 h at 60 °C. After that, the particles were separated by centrifugation and washed four times with 10 mL EtOH (10 min, 11000 rpm) until the supernatant was colorless. The functionalized particles were dried in a drying oven (45 °C) for 16 h.

5.3.11.7 Synthesis of SiO_2@APTMS@GA



10 mg of the SiO_2@APTMS NPs were dispersed in 1 mL distilled H_2O by sonicating for 30 min. After that, 100 µL glutaraldehyde (25 % in H_2O) was added and the reaction was stirred for 2 h at room temperature. After that, the particles were separated by centrifugation and washed three times with 10 mL H_2O (10 min, 11000 rpm). The functionalized particles were dried in a drying oven (45 °C) for 16 h.

5.3.11.8 Synthesis of SiO_2@APTMS@GA@AntThio



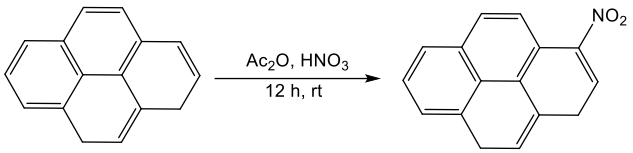
10 mg of the SiO_2@APTMS NPs were dispersed in 1 mL distilled H_2O by sonicating for 30 min. After that, 100 µL glutaraldehyde (25 % in H_2O) was added and the reaction was stirred for 2 h. The particles were separated by centrifugation and washed three times with H_2O (10 min, 11000 rpm). After that, the particles were dispersed in 1 mL of EtOH and a solution of the thiosemicarbazide (5 mg) in 3 mL EtOH was added, as well as 3 droplets of AcOH. The reaction was stirred at 60 °C for 24 h. After that, the particles were separated by centrifugation and washed four times with 10 mL EtOH until the

supernatant was colorless (10 min, 11000 rpm). The functionalized particles were dried in a drying oven (45 °C) for 16 h.

5.3.12 Synthesis of TSCs with fluorophores

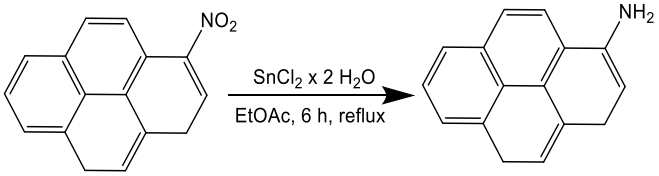
5.3.12.1 Synthesis of the amino precursors

Synthesis of 1-nitropyrene



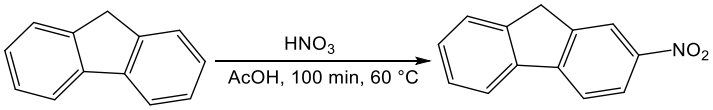
5.39 g Pyrene (26.7 mmol, 1.00 eq.) were dissolved in 15 mL of Ac_2O and 1.8 mL of conc. HNO_3 (24.0 mmol, 0.90 eq.) was added. The mixture was stirred at room temperature for 12 h. After that, the formed precipitate was filtered off, washed with H_2O and dried under ambient conditions to give the product as a yellow solid.[372] Yield: 5.68 g (22.8 mmol, 85%). $C_{16}H_{11}NO_2$ (249.27 g/mol). ^{1}H NMR (300 MHz, $CDCl_3$) δ [ppm] = 8.82 (m, 1H), 8.61 (m, 1H), 8.40-7.99 (m, 7H).

Synthesis of 1-aminopyrene



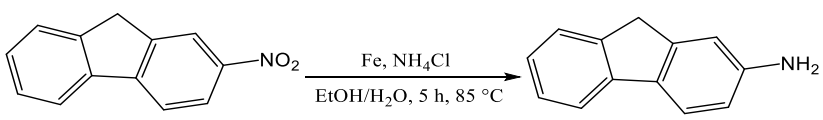
5.68 g 1-Nitropyrene (22.8 mmol, 1.00 eq.) and 24.70 g $SnCl_2 \cdot 2\ H_2O$ (109.4 mmol, 4.80 eq.) were suspended in 300 mL of EtOAc and the mixture was refluxed for 6 h. After that, the reaction was cooled to room temperature, and the mixture was basified to pH 8.0 using an aqueous Na_2CO_3 solution (20% m/v). After stirring the reaction for one more hour, the organic phase was extracted with EtOAc (3 x 100 mL) and dried over $MgSO_4$. The solvent was removed under reduced pressure yielding the product as light green solid.[373] Yield: 4.64 g (0.0212 mol, 93%). $C_{16}H_{11}N$ (219.29 g/mol). ^{1}H NMR (300 MHz, DMSO-d_6) δ [ppm] = 8.30 (d, *J* = 9.2 Hz, 1H), 7.98 (m, 3H), 7.93 (d, *J* = 9.2 Hz, 1H), 7.88 (m, 2H), 7.71 (d, *J* = 8.8 Hz, 1H), 7.40 (d, *J* = 8.3 Hz, 1H), 6.36 (s, 2H).

Synthesis of 2-nitrofluorene



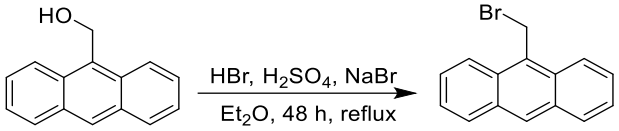
6.00 g Fluorene (36.1 mmol, 1.00 eq.) was dissolved in 100 mL of glacial AcOH and heated to 60 °C. After that, 15 mL of conc. HNO_3 were added dropwise, and the reaction was stirred for 100 min at 60 °C. The mixture was poured into 600 mL of H_2O, and the precipitate was filtered off and washed with H_2O. The crude product was recrystallized from 200 mL MeCN yielding the product as a yellowish solid.[374] Yield: 4.81 g (22.8 mmol, 63%). $C_{13}H_9NO_2$ (211.22 g/mol). ^{1}H NMR (300 MHz, $CDCl_3$) δ [ppm] = 8.34 (m, 1H), 8.26 (m, 1H), 7.81 (m, 2H), 7.58 (m, 1H), 7.43 (m, 2H), 3.93 (s, 2H).

Synthesis of 2-aminofluorene



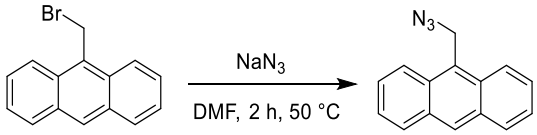
4.81 g 2-Nitro-9H-fluorene (22.8 mmol, 1.00 eq.), 2.55 g iron powder (45.6 mmol, 2.00 eq.) and 1.58 g NH_4Cl (29.6 mmol, 1.30 eq.) were dissolved in a mixture of 150 mL EtOH and 50 mL H_2O and heated to 85 °C for 5 h. After that, the reaction was cooled to room temperature and 50 mL of saturated aqueous sodium bicarbonate solution was added to the reaction mixture. The formed precipitate was filtered off and the solvent of the filtrate was removed under reduced pressure, yielding the product as colorless solid.[374] Yield: 1.67g (9.2 mmol, 40%). $C_{13}H_{11}N$ (181.24 g/mol). ^{1}H NMR (300 MHz, $CDCl_3$) δ [ppm] = 7.61 (m, 3H), 7.31 (d, *J* = 6.5 Hz, 2H), 6.82 (d, *J* = 7.8 Hz, 2H), 3.84 (s, 2H), 3.76 (s, 2H).

Synthesis of 9-(bromomethyl)anthracene



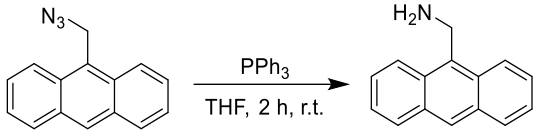
1.65 g 9-Anthracenemethanol (7.9 mmol, 1.00 eq.) was dissolved in 250 mL of Et_2O and stirred for 1 h at 45 °C. After that, 4.00 mL HBr (48%, 35.1 mmol, 4.40 eq.), 0.80 mL H_2SO_4 (95%, 14.9 mmol, 1.90 eq.) and 1.00 g NaBr (9.7 mmol, 1.20 eq.) were slowly added, and the reaction mixture was refluxed for 48 h. After cooling to room temperature, the solution was neutralized by adding a saturated solution of K_2CO_3 and the aqueous phase was extracted with CH_2Cl_2 (3 x 25 mL). The combined organic phase was washed with H_2O (3 x 25 mL), dried over Na_2SO_4 and the solvent was removed under reduced pressure. The product was obtained as a yellow solid.[375] Yield: 2.00 g (7.4 mmol, 94%). $C_{15}H_{11}Br$ (271.16 g/mol). ^{1}H NMR (300 MHz, $CDCl_3$) δ [ppm] = 8.49 (s, 1H), 8.29 (d, *J* = 9.13 Hz, 2H), 8.03 (d, *J* = 8.7 Hz, 2H), 7.65 (t, *J* = 7.0 Hz, 2H), 7.51 (t, *J* = 7.0 Hz, 2H), 5.54 (s, 2H).

Synthesis of 9-(azidomethyl)anthracene



2.00 g 9-(Bromomethyl)anthracene (7.3 mmol, 1.00 eq.) and 1.92 g NaN_3 (29.5 mmol, 4.00 eq.) were dissolved in 30 mL of DMF, and the suspension was stirred for 2 h at 50 °C. After that, 50 mL of distilled H_2O were added, and the solution was cooled to room temperature. The reaction mixture was extracted with Et_2O (2 x 50 mL) and the combined organic phase was washed with H_2O (3 × 50 mL), dried over Na_2SO_4 and the solvent was removed under reduced pressure. The product was obtained as a yellow solid.[376] Yield: 1.65 g (7.1 mmol, 97%). $C_{15}H_{11}N_3$ (233.27 g/mol). ^{1}H NMR (300 MHz, $CDCl_3$) δ [ppm] = 8.50 (s, 1H), 8.28 (d, *J* = 8.8 Hz, 2H), 8.03 (d, *J* = 7.5 Hz, 2H), 7.60 (t, *J* = 6.9 Hz, 2H), 7.52 (d, *J* = 8.0 Hz, 2H), 5.31 (s, 2H).

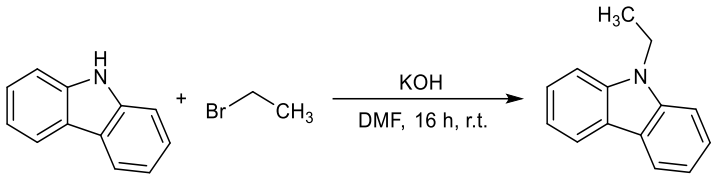
Synthesis of 9-(aminomethyl)anthracene



The reaction was performed under inert conditions. 1.40 g triphenylphosphine (6.0 mmol, 1.00 eq.) was added in a *Schlenk*-flask and cooled to 0 °C. After that, a solution of 2.52 g 9-(azidomethyl)anthracene (9.6 mmol, 1.60 eq.) in 10 mL of THF was slowly added and the reaction was stirred for 2 h at room temperature. Then, 1 mL of distilled H_2O was added, and the reaction was stirred for an additional hour. The reaction mixture was poured into a beaker and 50 mL of Et_2O were added. After that, the solution was acidified by the addition of 20 mL of 5 M HCl and a yellow precipitate formed, which was filtered

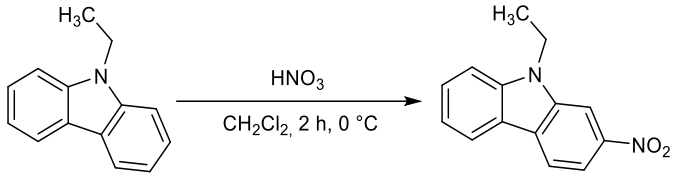
off and washed with 10 mL of an ice-cold mixture of H_2O and acetone (50:50). The solid was suspended in 60 mL EtOAc, cooled to 0 °C and basified by the addition of concentrated aqueous ammonia solution. The resulting solution was washed with 100 mL of H_2O and the aqueous layer was extracted with EtOAc (2 x 50 mL). The combined organic phase was washed with H_2O (2 x 50 mL), dried over Na_2SO_4 and the solvent was removed under reduced pressure. The product was obtained as a pale-yellow solid.[377] Yield: 0.90 g (4.3 mmol, 45%). $C_{15}H_{13}N$ (207.28 g/mol). ^{1}H NMR (300 MHz, $CDCl_3$) δ [ppm] = 8.39 (s, 1H), 8.32 (d, *J* = 4.8 Hz, 2H), 7.50 (m, 6H), 4.82 (s, 2H), 1.74 (s, 2H).

Synthesis of N-ethyl carbazole



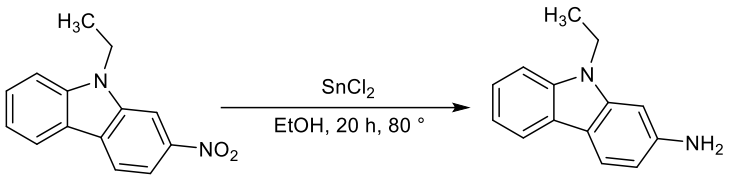
21.00 g (375.0 mmol, 6.25 eq.) KOH was dissolved in 100 mL DMF and 9.90 g (60.0 mmol, 1.00 eq.) carbazole was added. The mixture was stirred for 40 min at room temperature. After that, a solution of 6.72 mL (90.0 mmol, 1.50 eq.) bromoethane in 25 mL DMF was added dropwise and the mixture was stirred at room temperature for 16 h. The reaction mixture was poured in 500 mL H_2O, and the formed precipitate was filtered off and washed with cold H_2O (150 mL). The crude product was recrystallized from EtOH, yielding the product as a colorless solid.[378] Yield: 10.03 g (4.3 mmol, 45%). $C_{14}H_{13}N$ (195.27 g/mol). ^{1}H NMR (300 MHz, $CDCl_3$) δ [ppm] = 8.14 (d, *J* = 7.8 Hz, 2H), 7.53-7.42 (m, 4H), 7.30-7.27 (m, 1H), 7.26-7.22 (m, 1H), 4.41 (q, *J* = 7.2 Hz, 2H), 1.47 (t, *J* = 7.2 Hz, 3H).

Synthesis of 2-nitro-9-ethylcarbazole



10.00 g (51.2 mmol, 1.00 eq.) *N*-Ethyl carbazole were dissolved in 100 mL CH_2Cl_2 and cooled to 0 °C. After that, 4.34 mL (68.1 mmol, 1.33 eq.) HNO_3 (70%) was added dropwise to the mixture and the reaction was stirred for 2 h at 0 °C. After that, the reaction was warmed up to room temperature and the precipitate was filtered off and washed with EtOH (50 mL) and H_2O (50 mL). The product was obtained as a colorless solid.[379] Yield: 12.03 g (50.1 mmol, 99%). $C_{14}H_{12}N_2O_2$ (240.26 g/mol). ^{1}H NMR (300 MHz, $CDCl_3$) δ [ppm] = 9.19 (s, 1H), 8.42 (d, *J* = 7.8 Hz, 1H), 8.35 (dd, *J* = 9.1, 2.0 Hz, 1H), 7.81 (d, *J* = 9.1 Hz, 1H), 7.75 (d, *J* = 8.2 Hz, 1H), 7.59 (t, *J* = 7.6 Hz, 1H), 7.35 (t, *J* = 7.4 Hz, 1H), 4.54 (q, *J* = 7.1 Hz, 2H), 1.35 (t, *J* = 7.2 Hz, 3H).

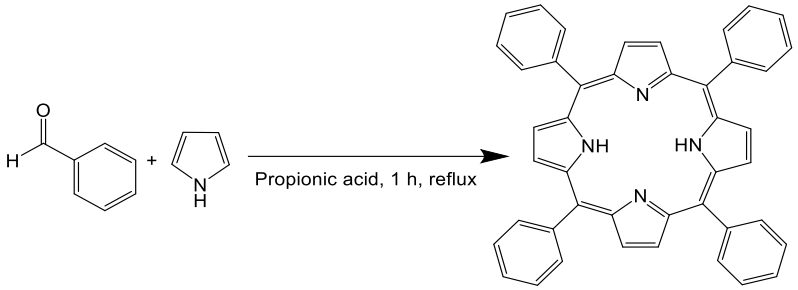
Synthesis of 2-amino-9-ethylcarbazole



12.03 g (50.1 mmol, 1.00 eq.) 9-Ethyl-3-nitro-9*H*-carbazole and 56.41 g (250.5 mmol, 5.00 eq.) $SnCl_2 \cdot 2\ H_2O$ were dissolved in 250 mL EtOH and heated to 70 °C for 20 h. After that, the mixture was cooled to room temperature and poured onto ice/saturated aqueous $NaHCO_3$ (200 mL). The mixture was extracted with EtOAc (3 x 100 mL) and the combined organic phase was washed with H_2O (100 mL) and

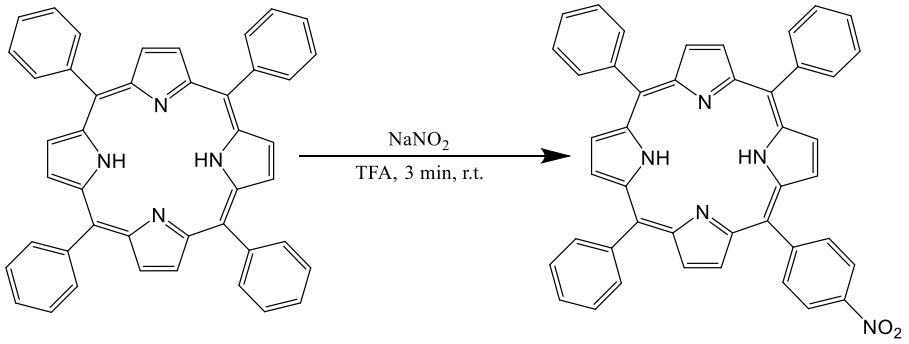
brine (100 mL). The organic phase was dried over $MgSO_4$ and the solvent was removed under reduced pressure. The crude product was purified by column chromatography (c-Hexane/EtOAc 3:1 → 2:1 → 100% EtOAc), yielding the product as a brownish solid.[379] Yield: 5.00 g (24.0 mmol, 48%). $C_{14}H_{14}N_2$ (210.28 g/mol). ^{1}H NMR (300 MHz, $CDCl_3$) δ [ppm] = 8.01 (s, 1H), 7.42 (d, *J* = 21.9 Hz, 2H), 7.22 (d, *J* = 25.1 Hz, 2H), 6.94 (d, *J* = 8.5 Hz, 1H), 4.32 (m, 2H), 1.42 (m, 3H).

Synthesis of tetraphenylporphyrin



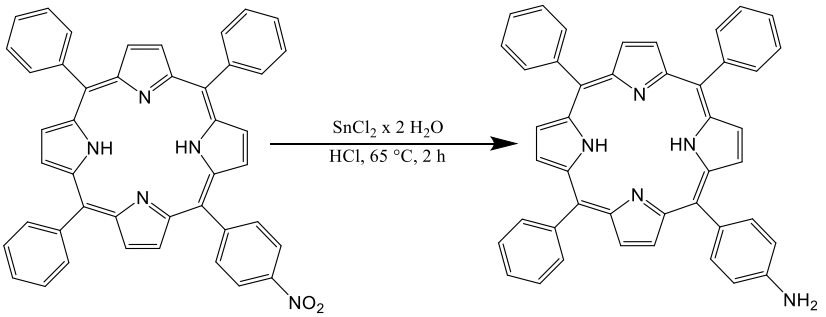
16.60 mL (164.0 mmol, 1.10 eq.) Benzaldehyde was dissolved in 300 mL propionic acid and the mixture was refluxed for 15 min. After that, 10.30 mL (149.0 mmol, 1.00 eq.) of freshly distilled pyrrole was added dropwise, and the reaction was refluxed for an additional hour. The mixture was cooled to room temperature and 400 mL of MeOH was added. The mixture was stirred at room temperature for 16 h. Then, the precipitate was filtered off, and the residue was washed with hot MeOH (500 mL), yielding the product as a purple solid.[380] Yield: 4.10 g (6.7 mmol, 18%). $C_{44}H_{30}N_4$ (614.75 g/mol). ^{1}H NMR (300 MHz, $CDCl_3$) δ [ppm] = 8.84 (s, 8H), 8.21 (dd, *J* = 7.6, 1.6 Hz, 8H), 7.74 (m, 12H).

Synthesis of 5-(p-nitrophenyl)-10,15,20-triphenylporphyrin



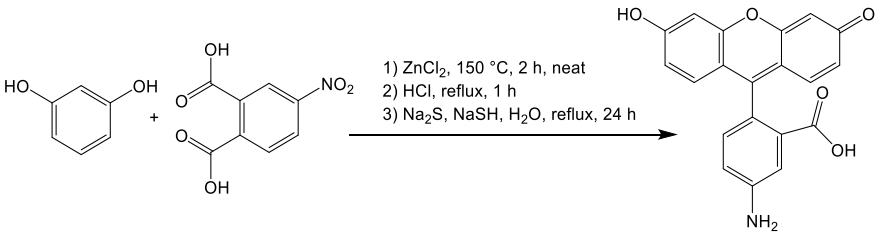
2.00 g (3.3 mmol, 1.00 eq.) Tetraphenylporphyrin was dissolved in 50 mL TFA, and the solution was stirred for 10 min. After that, 0.40 g (5.9 mmool, 1.80 eq.) $NaNO_2$ was added, and the reaction was stirred for 3 min at room temperature and directly poured into ice-cold H_2O (300 mL). $NaHCO_3$ was slowly added to the mixture, and the product was extracted with CH_2Cl_2 (5 x 100 mL). After that, the combined organic layer was washed three times with conc. $NaHCO_3$ solution. The organic layer was dried over Na_2SO_4 and the solvent was removed under reduced pressure. The crude product was purified by column chromatography (1:1 CH_2Cl_2/n-hexane -> 2:1 PE/CH_2Cl_2-> 3:1 EtOAc/c-hexane), yielding the product as a purple solid.[381] Yield: 1.40 g (2.1 mmol, 65%). $C_{44}H_{29}N_5O_2$ (659.73 g/mol). ^{1}H NMR (300 MHz, $CDCl_3$) δ [ppm] = 8.88 (m, 6H), 8.77 (d, J = 4.63 Hz, 2H), 8.65 (d, J = 8.17 Hz, 2H), 8.44 (d, J = 8.18 Hz, 2H), 8.25 (d, J = 7.16 Hz, 6H), 7.80 (m, 9H).

Synthesis of 5-(4-aminophenyl)-10,15,20-triphenylporphyrin



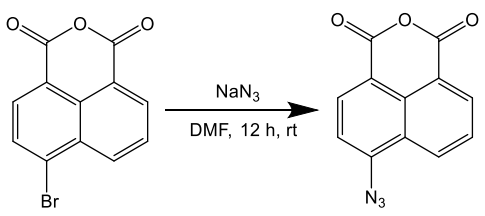
11.60 g (51.4 mmol, 24.00 eq.) $SnCl_2 \cdot 2\ H_2O$ was added to a suspension of 1.40 g (2.1 mmol, 1.00 eq.) 5-(p-nitrophenyl)-10,15,20-triphenylporphyrin in 230 mL conc. HCl and the mixture was heated to 65 °C for 2 h. The reaction was cooled to room temperature and poured into 150 mL ice-cold H_2O. After that, conc. ammonia was added to adjust pH = 8 and the suspension was filtered over celite. The aqueous layer was extracted with CH_2Cl_2 (5 x 50 mL) and the combined organic extracts were dried over Na_2SO_4. The solvent was removed under reduced pressure, and the crude product was purified by column chromatography (CH_2Cl_2) yielding the product as a purple solid.[343] Yield: 1.27 g (2.01 mmol, 95%). $C_{44}H_{31}N_5$ (629.77 g/mol). ^{1}H NMR (300 MHz, $CDCl_3$) δ [ppm] = 8.97-8.87 (m, 8H), 8.22 (m, 8H), 7.99 (d, *J* = 5.0 Hz, 2H), 7.75 (m, 9H), 7.04 (d, *J* = 5.0 Hz, 2H), 4.03 (s, 2H, NH_2).

Synthesis of 5-aminoflourescein



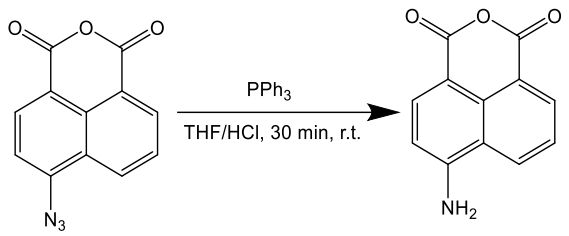
8.28 g (75.0 mmol, 2.50 eq.) Resorcinol, 6.33 g (30.0 mmol, 1.00 eq.) 4-nitrophthalic acid and 9.00 g (66.0 mmol, 2.30 eq.) $ZnCl_2$ were heated to 120 °C until its molten. Then, the temperature increased to 150 °C and the mixture was stirred for 2 h. After that, the reaction was cooled to 80 °C, 150 mL HCl (1 M) was added, and the mixture was refluxed for an additional hour. After cooling to room temperature, the precipitate was filtered off and dried in vacuo. The crude product was redissolved in 240 mL H_2O and 33.40 g (139.0 mmol, 4.60 eq.) $Na_2S \cdot 9\ H_2O$ and 5.90 g (80.0 mmol, 2.70 eq.) $NaSH \cdot H_2O$ were added. The reaction mixture was refluxed for 24 h. Afterwards, AcOH was added and the solid was filtered off and dried in vacuo. The crude product was dissolved in 300 mL HCl (1 M) and refluxed for 6 h. After cooling down to room temperature, the solid was filtered off and the product was precipitated from the filtrate by storing at 5 °C for 18 h. The crude product was purified via column chromatography (CH_2Cl_2/methanol, 15:1), yielding the product as a dark red solid.[340] Yield: 1.22 g (3.5 mmol, 12%, 2 steps). $C_{20}H_{13}NO_5$ (347.33 g/mol). ^{1}H NMR (300 MHz, $CDCl_3$) δ [ppm] = 10.06 (s, 1H), 6.98 (m, 2H), 6.86 (d, 1H), 6.63-6.55 (m,6H), 5.74 (d, 2H)

Synthesis of 4-nitro-1,8-naphthalic anhydride



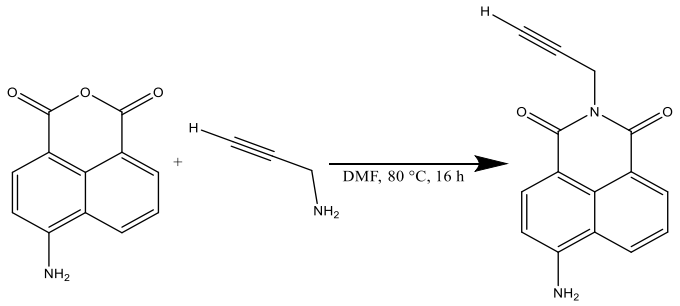
To a solution of 3.00 g (10.8 mmol, 1.00 eq.) 4-bromo-1,8-naphthalic anhydride in 30 mL DMF was added 1.05 g (16.1 mmol, 1.50 eq.) NaN_3 and the mixture was stirred at room temperature for 12 h. After that, 180 mL H_2O was added and the precipitate was collected by filtration, washed with 50 mL H_2O and dried in vacuo. The product was obtained as a pale-yellow solid.[382] Yield: 2.27 g (9.5 mol, 88%). $C_{12}H_5N_3O_3$ (239.19 g/mol). ^{1}H NMR (300 MHz, $CDCl_3$) = 8.66 (m, 3H), 7.85 (m, 3H), 7.85 (m, 1H), 7.56 (m, 1H).

Synthesis of 4-amino-1,8-naphthalic anhydride



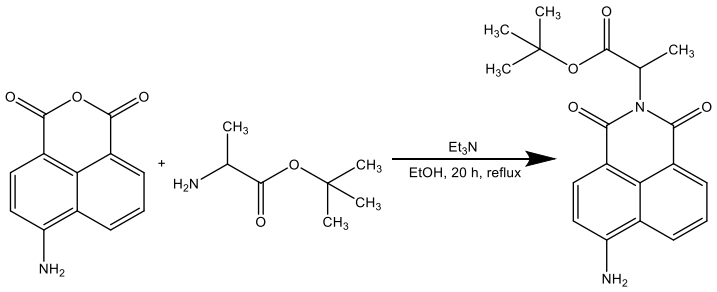
2.27 g (9.5 mmol, 1.00 eq.) 4-Nitro-1,8-naphthalic anhydride was suspended in a mixture of THF (150 mL) and 0.5 M HCl (30 mL), and 2.50 g (9.5 mmol, 1.00 eq.) PPh_3 was slowly added to the suspension. The reaction was stirred for 30 min at room temperature. After that, the mixture was basified with 10 mL of 2 M NaOH and the THF was removed under reduced pressure. The resulting mixture was diluted with EtOAc (40 mL) and the precipitate was filtered off. The solid was washed with EtOAc and H_2O and dried in vacuo yielding the product as an orange solid.[383] Yield: 1.50 g (7.0 mol, 75%). $C_{12}H_7NO_3$ (213.19 g/mol). ^{1}H NMR (300 MHz, $CDCl_3$) δ [ppm] = 8.65 (d, *J* = 8.1 Hz, 1H), 8.39 (d, *J* = 6.9 Hz, 1H), 8.15 (d, *J* = 8.2 Hz, 1H), 7.76 (s, 2H), 7.65 (t, *J* = 7.5 Hz, 1H), 6.84 (d, *J* = 8.3 Hz, 1H).

Synthesis of 6-amino-2-(prop-2-ynyl)-2-aza-1*H*-phenalene-1,3(2*H*)-dione



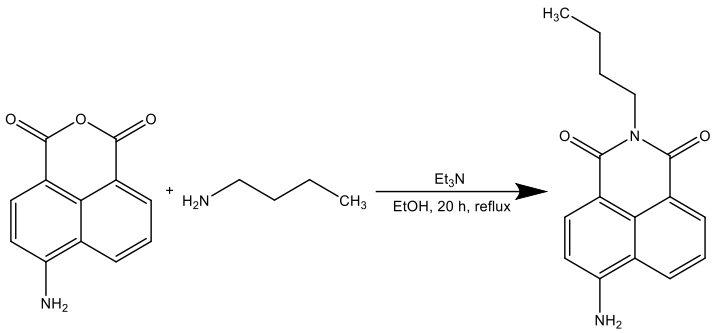
1.50 g (7.0 mmol, 1.00 eq.) 4-Amino-1,8-naphthalic anhydride and 0.90 mL (14.0 mmol, 2.00 eq.) propargylamine were dissolved in 20 mL DMF and heated to 80 °C for 16 h. After cooling to room temperature, the mixture was poured into 400 mL of ice-cold H_2O and the precipitate was filtered off, washed with H_2O and dried in vacuo. The product was obtained as a yellowish solid. Yield: 1.15 g (5.7 mmol, 81%). $C_{15}H_{10}N_2O_2$ (250.26 g/mol). ^{1}H NMR (300 MHz, $CDCl_3$) δ [ppm] = 8.65 (d, *J* = 7.3 Hz, 1H), 8.46 (d, *J* = 8.1 Hz, 1H), 8.13 (d, *J* = 8.4 Hz, 1H), 7.68 (t, *J* = 7.5 Hz, 1H), 6.90 (d, *J* = 8.1 Hz, 1H), 4.98 (s, 2H), 4.95 (d, *J* = 2.4 Hz, 2H), 1.26 (s, 1H).

Synthesis of *tert*-butyl 2-[6-amino-1,3-dioxo-2-aza-3*H*-phenalen-2(1*H*)-yl]propanoate



6-Amino-2-(prop-2-ynyl)-2-aza-1*H*-phenalene-1,3(2*H*)-dione (0.15 g, 0.69 mmol, 1.00 eq.) and tert-butyl 2-aminopropanoate (0.20 g, 1.38 mmol, 2.00 eq.) were dissolved in 25 mL of EtOH and Et_3N (0.48 mL, 3.44 mmol, 5.00 eq.) was added. The reaction mixture was refluxed for 20 h. After that, the solvent was removed under reduced pressure and the crude product was purified by column chromatography (3:1, c-hexane/EtOAc). The product was obtained as a yellow solid.[384] Yield: 0.21 g (0.61 mmol, 88%). $C_{19}H_{20}N_2O_4$ (340.38 g/mol). ^{1}H NMR (300 MHz, $CDCl_3$) δ [ppm] = 8.68 (m, 1H), 8.43 (m, 1H), 8.17 (m, 1H), 7.80 (m, 2H), 7.66 (m, 1H), 3.61 (m, 1H), 1.43 (s, 9H), 1.25 (m, 3H).

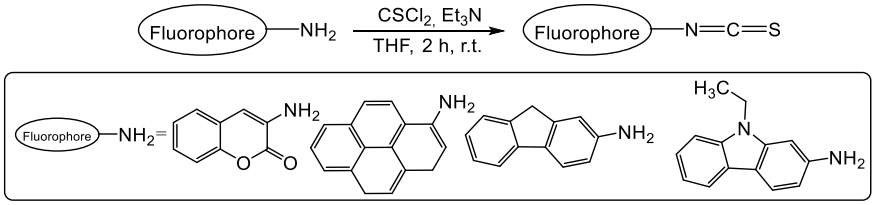
Synthesis of 6-amino-2-butyl-2-aza-1H-phenalene-1,3(2H)-dione



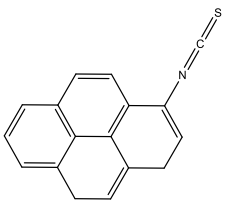
6-Amino-2-(prop-2-ynyl)-2-aza-1*H*-phenalene-1,3(2*H*)-dione (0.50 g, 2.35 mmol, 1.00 eq.) and butan-1-amine (0.47 mL, 4.69 mmol, 2.00 eq.) were dissolved in 25 mL of EtOH and Et_3N (2.00 mL, 14.30 mmol, 6.12 eq.) was added. The reaction mixture was refluxed for 20 h. After that, the solvent was removed under reduced pressure and the crude product was purified by column chromatography (1:1, c-hexane/EtOAc). The product was obtained as a yellow solid.[385] Yield: 0.52 g (1.94 mmol, 83%). $C_{16}H_{26}N_2O_2$ (268.32 g/mol).^{1}H NMR (300 MHz, $CDCl_3$) δ [ppm] = 8.61 (dd, *J* = 8.4, 1.0 Hz, 1H), 8.42 (dd, *J* = 7.3, 1.0 Hz, 1H), 8.19 (d, *J* = 8.4 Hz, 1H), 7.65 (dd, *J* = 8.3, 7.4 Hz, 1H), 7.42 (s, 2H), 6.84 (d, *J* = 8.4 Hz, 1H), 4.00 (m, 2H), 1.58 (m, 2H), 1.34 (m, 2H), 0.91 (t, *J* = 7.3 Hz, 3H).

5.3.12.2 Synthesis of the isothiocyanates with fluorophores

Synthesis of coumarin, pyrene, fluorene and carbazole isothiocyanates

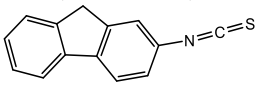


The reaction was performed under inert conditions. The fluorophore with amine function (1.00 eq.) and Et_3N (3.00 eq.) were dissolved in 50 mL of THF and thiophosgene (85%, 1.10 eq.) slowly added at 0 °C. The reaction mixture was stirred for 2 h at room temperature, which led to the formation of a brown suspension. The reaction was quenched by adding 100 mL of distilled H_2O and the product was extracted with Et_2O (3 x 100 mL). The organic phase was dried over Na_2SO_4, and the solvent was removed under reduced pressure, yielding the product.

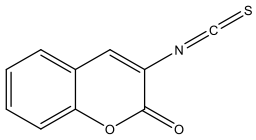


1-Isothiocyanatopyrene from 1.00 g (4.6 mmol) 1-aminopyrene, 1.90 mL (13.7 mmol) Et_3N and 0.46 mL (5.1 mmol) thiophosgene. The product was obtained as a brownish solid. Yield: 1.17 g (4.5 mmol, 98%). $C_{17}H_9NS$ (261.34 g/mol). ^{1}H NMR (300 MHz, $CDCl_3$) δ [ppm] = 8.13 (m, 2H), 8.05-7.94 (m, 4H), 7.88 (m, 2H), 7.69 (m, 1H).

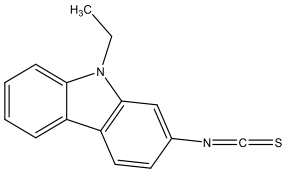
2-Isothiocyanato-9H-fluorene from 1.00 g (5.5 mmol) 2-amino-9H-fluorene, 2.30 mL (16.5 mmol) Et_3N and 0.53 mL (6.00 mmol) thiophosgene. The product was obtained as a brownish solid. Yield: 1.23 g (5.5 mmol, quant.). $C_{14}H_9NS$ (223.29 g/mol). ^1H NMR (300 MHz, $CDCl_3$) δ [ppm] = 7.76 (m, 2H), 7.57 (d, *J* = 7.3 Hz, 1H), 7.44-7.33 (m, 3H), 7.27 (m, 1H), 3.90 (s, 2H).



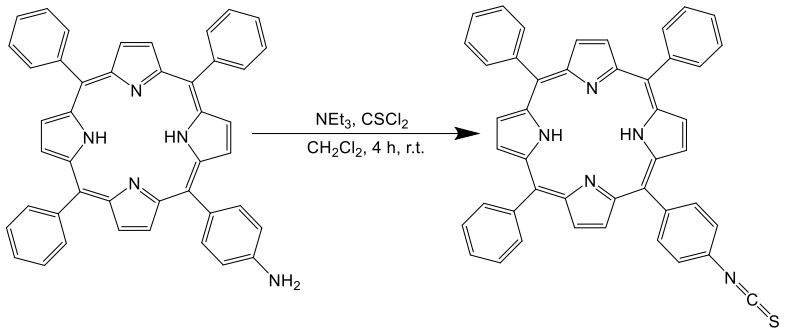
3-Isothiocyanatocumarine from 0.37 g (2.3 mmol) 3-aminocumarine, 0.97 mL (6.9 mmol) Et_3N and 0.23 mL (2.5 mmol) thiophosgene. The product was obtained as a brownish solid. 0.44 g (2.2 mmol, 94%). $C_{10}H_5NO_2S$ (203.22 g/mol). ^1H NMR (300 MHz, DMSO-d_6) δ [ppm] = 8.06 (s, 1H), 7.73-7.61 (m, 2H), 7.49-7.38 (m, 2H).



2-isothiocyanato-9-ethylcarbazole from 0.50 g (2.4 mmol) 2-amino-9-ethylcarbazole, 1.00 mL (7.1 mmol) Et_3N and 0.22 mL (2.40 mmol) thiophosgene. The product was obtained as a brownish solid. Yield: 0.61 g (2.42 mmol, quant.). $C_{15}H_{12}N_2S$ (252.34 g/mol). ^1H NMR (300 MHz, $CDCl_3$) δ [ppm] = 8.05 (dt, *J* = 7.8, 1.0 Hz, 1H), 7.96 (t, *J* = 1.3 Hz, 1H), 7.51 (ddd, *J* = 8.2, 7.1, 1.2 Hz, 1H), 7.42 (dt, *J* = 8.3, 1.0 Hz, 1H), 7.34 (d, *J* = 1.3 Hz, 2H), 7.26 (dd, *J* = 14.9, 1.1 Hz, 2H), 4.36 (q, *J* = 7.2 Hz, 2H), 1.43 (t, *J* = 7.3 Hz, 3H). ^{13}C NMR (126 MHz, DMSO-d_6) δ [ppm] = 140.75, 138.69, 131.83, 127.20, 123.98, 123.04, 121.93, 121.45, 121.10, 119.90, 118.81, 110.69, 110.07, 37.67, 30.89, 14.16. HR-EI-MS: $[M+H]^+$ m/z = 252.0714.

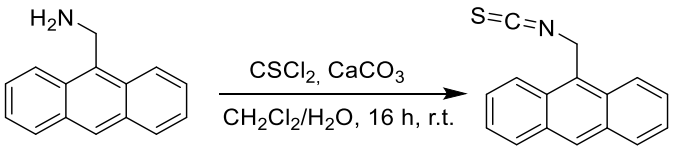


Synthesis of 5-(4-isothiocyanatophenyl)-10,15,20- triphenylporphyrin



0.20 g (0.32 mmol, 1.00 eq.) 5-(4-Aminophenyl)-10,15,20-triphenylporphyrin was dissolved in 10 mL dry CH_2Cl_2 and 0.75 mL (5.37 mmol, 16.9 eq.) dry NEt_3 was added. The reaction mixture was cooled to 0 °C and 72.9 µL (0.95 mmol, 3.00 eq.) thiophosgene was added dropwise. After that, the resulting solution was stirred for 15 minutes at 0 °C and then 4 h at room temperature. The solvent was removed under reduced pressure, and the residue was purified by column chromatography (CH_2Cl_2), yielding the product as a purple solid. Yield: 0.20 g (0.30 mmol, 94%). $C_{45}H_{29}N_5S$ (671.82 g/mol). ^1H NMR (500 MHz, $CDCl_3$) δ [ppm] = 8.88 (s, 2H), 8.25 – 8.22 (m, 8H), 8.07 (s, 1H), 7.81 – 7.73 (m, 15H), 7.63 (d, *J* = 8.4 Hz, 3H). ^{13}C NMR (126 MHz, $CDCl_3$) δ [ppm] = 142.06, 141.49, 134.59, 131.14, 127.84, 127.82, 126.77, 126.75, 124.13, 120.62, 120.43, 118.13. EI-MS: $[M+H]^+$ m/z = 672.22169, $[M+Na]^+$ m/z = 694.20368.

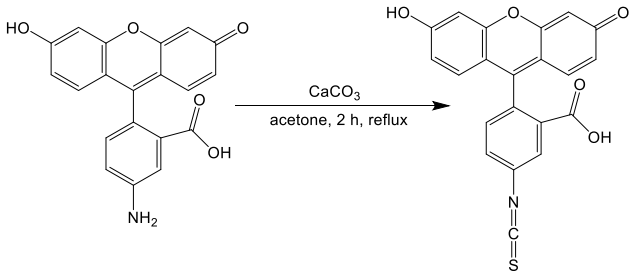
Synthesis of 9-(isothiocyanatomethyl)anthracene



0.41 g Anthracen-9-ylmethanamine (2.0 mmol, 1.00 eq.) was dissolved in 20 mL of CH_2Cl_2 and 0.52 g $CaCO_3$ (5.2 mmol, 1.40 eq.) as well as 20 mL of H_2O were added. The reaction mixture was stirred for 20 min at 0 °C and 0.25 mL thiophosgene (85%, 2.8 mmol, 1.40 eq.) was slowly added. After that, the solution was stirred for additional 16 h at room temperature. Then, the reaction mixture was neutralized by the addition of sat. Na_2CO_3 solution and the organic phase was separated. The aqueous layer was extracted with CH_2Cl_2 (2 x 50 mL) and the combined organic solution was dried over Na_2SO_4. The

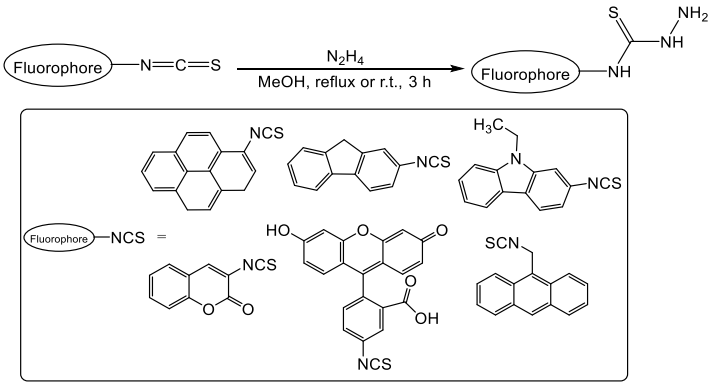
solvent was removed under reduced pressure yielding the product as yellow solid. Yield: 0.49 g (1.9 mmol, 98%). $C_{16}H_{11}NS$ (249.33 g/mol). ^{1}H NMR (300 MHz, $CDCl_3$) δ [ppm] = 8.53 (s, 1H), 8.24 (d, *J* = 9.3 Hz, 2H), 8.07 (d, *J* = 7.6 Hz, 2H), 7.64 (m, 2H), 7.55 (m, 2H), 5.59 (s, 2H).

Synthesis of fluoresceine-5-isothiocyanate



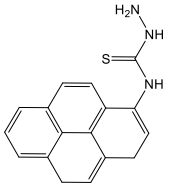
0.20 g (0.58 mmol, 1.00 eq.) 5-Aminofluoresceine was dissolved in 10 mL of acetone and 0.20 g (2.04 mmol, 3.51 eq.) $CaCO_3$ was added. After that, 50.7 µL (0.66 mmol, 1.14 eq.) thiophosgene was added and the mixture was stirred for 1 h at room temperature and refluxed for 2 h. The reaction mixture was filtered hot, and the residue was washed with boiling acetone. The filtrate was concentrated, and petroleum ether was added. The precipitate was filtered off and washed with petroleum ether, yielding the product as an orange solid.[344] Yield: 0.19 g (0.49 mmol, 84%). $C_{21}H_{11}NO_5S$ (389.38 g/mol). ^{1}H NMR (500 MHz, DMSO-d_6) δ [ppm] = 8.03 (d, *J* = 1.5 Hz, 1H), 7.80 (dd, *J* = 8.2, 1.8 Hz, 1H), 7.35 (d, *J* = 8.2 Hz, 1H), 6.69 (d, *J* = 2.1 Hz, 2H), 6.61 (d, *J* = 8.7 Hz, 2H), 6.55 (dd, *J* = 8.7, 2.3 Hz, 2H). ^{13}C NMR (126 MHz, DMSO-d_6) δ [ppm] = 167.78, 160.17, 152.33, 151.37, 136.17, 133.85, 132.53, 129.63, 128.30, 126.19, 122.24, 113.16, 109.39, 102.76. EI-MS: $[M+H]^+$ m/z = 390.04308, $[M+Na]^+$ m/z = 412.02525.

5.3.12.3 Synthesis of the thiosemicarbazides with fluorophores – general description

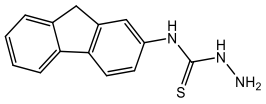


$N_2H_4 \cdot H_2O$ (1.00 eq.) was dissolved in 10 mL of MeOH and heated to reflux (or stirred at room temperature). After that, a solution of the isothiocyanate (1.00 eq.) in 40 mL of MeOH was slowly added to the hydrazine solution over the course of 1 h. The reaction mixture was refluxed reflux (or stirred at room temperature) for an additional 3 h, after that, the solvent was removed under reduced pressure, yielding the product.

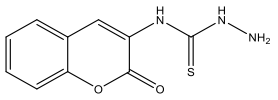
4-(3,6-Dihydro-1-pyrenyl)thiosemicarbazide from 1.12 g (4.3 mmol) 1-isothiocyanatopyrene, 0.21 mL (4.3 mmol) $N_2H_4 \cdot H_2O$. The reaction was refluxed. The product was obtained as a brownish solid. Yield: 1.26 g (4.3 mmol, quant.). $C_{17}H_{13}N_3S$ (293.39 g/mol). ^{1}H NMR (300 MHz, DMSO-d_6) δ [ppm] = 9.34 (s, 1H), 8.34-8.04 (m, 10H), 3.45 (s, 2H). ^{13}C NMR (126 MHz, DMSO-d_6) δ [ppm] = 182.06, 134.03, 131.17, 130.97, 129.35, 127.68, 127.62, 127.29, 127.08, 126.91, 126.78, 125.71, 125.47, 124.90, 124.78, 124.37, 122.97.



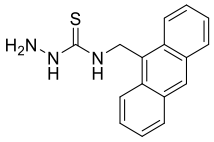
4-(9*H*-Fluoren-2-yl)thiosemicarbazide from 1.04 g (4.7 mmol) 2-isothiocyanato-9H-fluorene, 0.23 mL (4.7 mmol) $N_2H_4 \cdot H_2O$. The reaction was refluxed. The product was obtained as a brownish solid. Yield: 1.20 g (4.7 mmol, quant.). $C_{14}H_{13}N_3S$ (255.34 g/mol). ^{1}H NMR (499 MHz, DMSO-d_6) δ [ppm] = 9.70 (s, 1H), 9.11 (s, 1H), 7.96 (s, 1H), 7.82 (m, 1H), 7.57 (m, 1H), 7.39-7.25 (m, 2H), 4.79 (s, 2H), 3.90 (s, 2H). ^{13}C NMR (126 MHz, DMSO-d_6) δ [ppm] = 179.78, 143.41, 141.41, 138.73, 137.75, 127.24, 126.71, 125.53, 122.92, 120.72, 120.08, 119.94, 36.94.



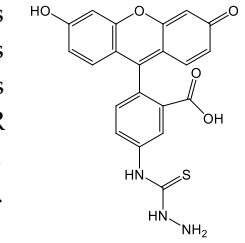
4-(3-Coumarinyl)thiosemicarbazide from 0.44 g (2.2 mmol) 3-isothiocyanatocumarine, 0.11 mL (2.2 mmol) $N_2H_4 \cdot H_2O$. The reaction was stirred at room temperature. The product was purified by column chromatography (1:1 EtOAc/c-hexane) and obtained as a yellowish solid. Yield: 0.44 g (2.2 mmol, 95%). $C_{10}H_9N_3O_2S$ (235.26 g/mol). ^{1}H NMR (300 MHz, DMSO-d_6) δ [ppm] = 9.68 (s, 1H), 9.47 (s, 1H), 7.70 (dd, *J* = 7.7, 1H), 7.54-7.33 (m, 4H), 5.05 (s, 2H). ^{13}C NMR (126 MHz, DMSO-d_6) δ [ppm] = 178.45, 159.12, 149.67, 129.88, 128.24, 125.59, 125.47, 121.60, 119.83, 116.40.



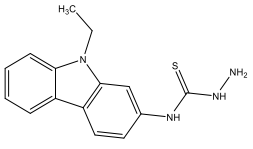
***N*4-9-Metyhlantracene thiosemicarbazide** from 0.49 g (2.0 mmol, 1.00 eq.) 9-(isothiocyanatomethyl)anthracene, 0.27 mL (3.5 mmol, 1.80 eq.) $N_2H_4 \cdot H_2O$. The reaction was refluxed. The product was purified by recrystallisation ($CHCl_3$/petroleum ether) and obtained as a yellowish solid. Yield: 0.58 g (2.0 mmol, quant.). $C_{16}H_{15}N_3S$ (281.38 g/mol). ^{1}H NMR (300 MHz, DMSO-d_6) δ [ppm] = 8.92 (s, 1H), 8.65 (s, 1H), 8.46 (d, *J* = 8.3 Hz, 2H), 8.12 (d, *J* = 7.4 Hz, 2H), 7.68 (s, 1H), 7.58 (m, 4H), 5.69 (d, *J* = 3.3 Hz, 2H), 4.39 (s, 2H).



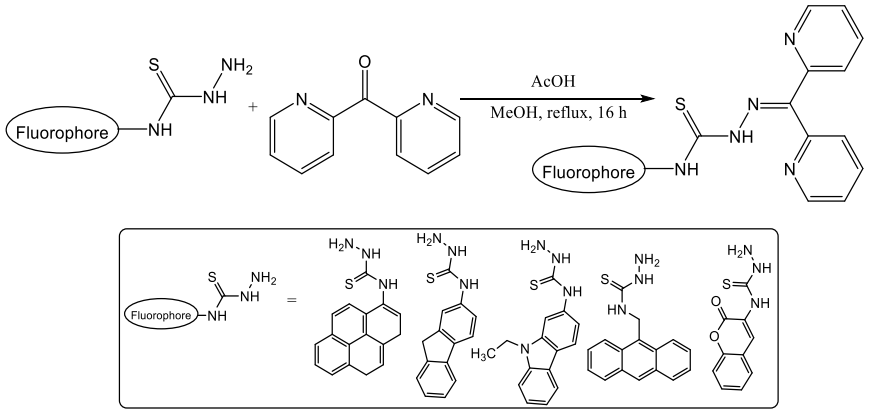
2-(6-Hydroxy-3-oxo-3*H*-xanthen-9-yl)-5-thiosemicarbazidobenzoic acid from 70.0 mg (0.18 mmol) fluoresceine-5-isothiocyanate, 9.0 µL (0.18 mmol) $N_2H_4 \cdot H_2O$. The reaction was stirred at room temperature under the exclusion of light. The product was purified by column chromatography (CH_2Cl_2/MeOH 10:2 -> 1:1) and obtained as a yellow solid. 60.0 mg (0.14 mmol, 79%). $C_{21}H_{15}N_3O_5S$ (421.43 g/mol). ^{1}H NMR (500 MHz, Methanol-d_4) δ [ppm] = 8.32 (s, 1H), 7.97 (d, *J* = 8.1 Hz, 1H), 7.17 (dd, *J* = 11.4, 8.2 Hz, 1H), 6.88 – 6.79 (m, 2H), 6.70 – 6.66 (m, 2H), 6.59 – 6.56 (m, 2H). EI-MS: $[M+H]^+$ m/z = 422.08065.



4-(9-Ethyl-2-carbazolyl)thiosemicarbazide from 0.61 mg (2.40 mmol) 2-isothiocyanato-9-ethylcarbazole, 0.12 mL (2.40 mmol) $N_2H_4 \cdot H_2O$. The reaction was stirred at room temperature. The product was obtained as a brownish solid. Yield: 0.68 g (2.4 mmol, quant.). $C_{15}H_{16}N_4S$ (284.38 g/mol). ^{1}H NMR (500 MHz, Methanol-d_4) δ [ppm] = 9.01 (s, 1H), 8.21 (s, 1H), 8.09 (d, *J* = 7.7 Hz, 1H), 7.62 – 7.51 (m, 3H), 7.44 (ddd, *J* = 8.3, 7.0, 1.2 Hz, 1H), 7.18 (t, *J* = 7.3 Hz, 1H), 4.76 (s, 1H), 4.43 (q, *J* = 7.1 Hz, 2H), 1.31 (t, *J* = 7.0 Hz, 3H). ^{13}C NMR (126 MHz, DMSO-d_6) δ [ppm] = 148.26, 140.40, 137.57, 131.43, 126.17, 124.51, 122.51, 122.11, 120.78, 119.06, 117.23, 109.61, 108.82, 37.46, 14.20. EI-MS: $[M+H]^+$ m/z = 285.11718, $[M+Na]^+$ m/z = 307.09918.

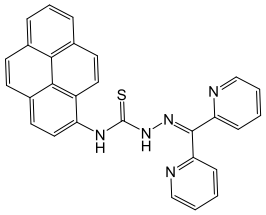


5.3.12.4 Synthesis of the dipyridyl ketone TSCs with fluorophores – general description

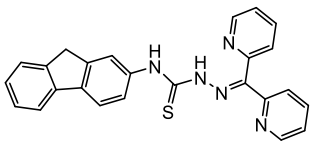


Dipyridyl ketone (1.00 eq.) and the thiosemicarbazide (1.00 eq.) were dissolved in a minimum amount of MeOH and 0.1 ml glacial AcOH were added. The reaction was refluxed for 16 h. After that, the solvent was removed under reduced pressure, and the crude product was purified by column chromatography.

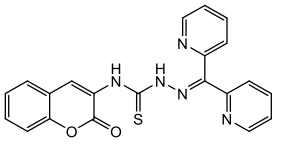
1-[Bis(2-pyridyl)methylene]-4-(4,8-dihydro-1-pyrenyl)thiosemicarbazide from 0.20 g (0.7 mmol) 4-(3,6-dihydro-1-pyrenyl)thiosemicarbazide, 0.12 g (0.7 mmol) dipyridyl ketone. The product was obtained as a brownish solid without further purification. Yield: 0.32 g (0.7 mmol, quant.). $C_{28}H_{19}N_5S$ (457.56 g/mol). ^{1}H NMR (300 MHz, DMSO-d_6) δ [ppm] = 13.65 (s, 1H), 11.10 (s, 1H), 8.88 (s, 1H), 8.62 (d, *J* = 4.4 Hz, 1H), 8.55 (d, *J* = 8.0 Hz, 1H), 8.39-8.29 (m, 3H), 8.27-8.19 (m, 3H), 8.17-8.01 (m, 4H), 7.96 (m, 1H), 7.64 (d, *J* = 7.7 Hz, 2H), 7.50 (m, 1H). ^{13}C NMR (126 MHz, DMSO-d_6) δ [ppm] = 179.22, 172.50, 155.31, 151.48, 148.72, 142.66, 138.10, 137.55, 133.74, 131.11, 130.94, 130.29, 128.08, 127.93, 127.89, 127.68, 126.97, 126.00, 125.83,125.36, 125.23, 124.78, 124.73, 124.53, 124.25, 123.35.



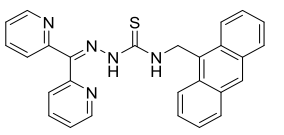
1-[Bis(2-pyridyl)methylene]-4-(9*H*-fluoren-2-yl)thiosemicarbazide from 0.20 g (0.8 mmol) 4-(9*H*-fluoren-2-yl)thiosemicarbazide, 0.14 g (0.8 mmol) dipyridyl ketone. The product was obtained as a brownish solid without further purification. Yield: 0.34 g (0.8 mmol, quant.). $C_{25}H_{19}N_5S$ (421.52 g/mol). ^{1}H NMR (300 MHz, DMSO-d_6) δ [ppm] = 13.56 (s, 1H), 10.51 (s, 1H), 8.86 (d, *J* = 3.8 Hz, 1H), 8.60 (d, *J* = 3.8 Hz, 1H), 8.42 (d, *J* = 7.7 Hz, 1H), 8.06-7.79 (m, 5H), 7.59 (m, 4H), 7.52 (m, 1H), 7.42-7.28 (m, 2H), 3.96 (s, 2H). ^{13}C NMR (126 MHz, DMSO-d_6) δ [ppm] = 177.01, 155.37, 151.49, 148.78, 148.63, 143.65, 143.49, 142.34, 141.17, 139.23, 138.09, 137.57, 127.82, 127.31, 127.10, 125.62, 125.35, 125.11, 124.67, 124.49, 122.97, 120.43, 120.03, 36.91.



1-[Bis(2-pyridyl)methylene]-4-(3-coumarinyl)thiosemicarbazide from 50.0 mg (0.21 mmol) 4-(3-coumarinyl)thiosemicarbazide, 40.0 mg (0.21 mmol) dipyridyl ketone. The product was purified by column chromatography (3:1 EtOAc/c-hexane) and obtained as a yellow solid. Yield: 40.0 mg (0.10 mmol, 46%). $C_{21}H_{15}N_5O_2S$ (401.44 g/mol). ^{1}H NMR (300 MHz, DMSO-d_6) δ [ppm] = 14.18 (s, 1H), 10.46 (s, 1H), 9.18 (s, 1H), 8.90 (d, *J* = 4.10 Hz, 1H), 8.66 (d, *J* = 4.63 Hz, 1H), 8.13-8.02 (m, 4H), 7.78 (dd, *J* = 7.81 Hz, 1.32 Hz, 1H), 7.62-7.53 (m, 5H). HR-ESI-MS: m/z = $[M+H]^+$ 402.10207, m/z = $[M+Na]^+$ 424.08407.

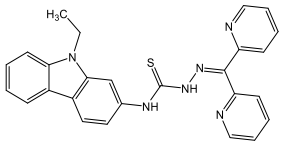


4-[(9-Anthryl)methyl]-1-[bis(2-pyridyl)methylene]thiosemicarbazide from 100.0 mg (0.3 mmol) *N*$_4$-9-metyhlantracene thiosemicarbazide, 60.0 mg (0.3 mmol) dipyridyl ketone. The product was purified by column chromatography (2:1 EtOAc/c-hexane) and obtained as a yellow solid. Yield: 60.1 mg (0.1 mmol, 37%). $C_{27}H_{21}N_5S$ (447.56 g/mol). ^{1}H NMR (300 MHz, DMSO-d_6) δ [ppm] = 13.47 (s, 1H), 8.91 (m, 1H), 8.82 (d, *J* = 4.0 Hz, 1H), 8.64 (s, 1H), 8.54 (d, *J* = 9.2 Hz, 2H), 8.46 (d, *J* = 5.0 Hz, 1H), 8.11 (d, *J* = 9.2 Hz, 2H), 7.95 (m, 1H), 7.83 (d, *J* = 7.7 Hz, 1H), 775 (m, 1H), 7.56 (m, 5H), 7.37 (m, 2H), 5.86 (d, *J* = 5.3 Hz, 2H). ^{13}C

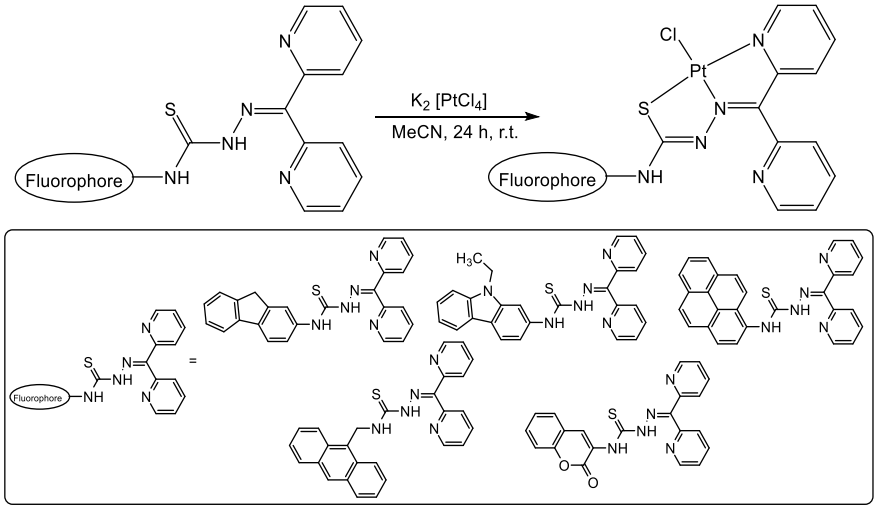


NMR (126 MHz, DMSO-d_6) δ [ppm] = 155.38, 151.51, 148.82, 148.66, 138.05, 137.46, 131.56, 130.79, 129.45, 129.32, 128.33, 127.49, 126.89, 125.74, 125.23, 125.14, 124.28, 124.02, 41.53. HR-ESI-MS: m/z = $[M+H]^+$ 448.15927, m/z = $[M+Na]^+$ 470.14102.

1-[Bis(2-pyridyl)methylene]-4-(9-ethyl-2-carbazolyl)thiosemicarbazide from 0.20 g (0.7 mmol) 4-(9-ethyl-2-carbazolyl)thiosemicarbazide, 0.13 g (0.7 mmol) dipyridyl ketone. The product was purified by column chromatography (2:1 c-hexane/EtOAc) and obtained as a yellowish solid. Yield: 0.21 g (0.5 mmol, 67%). $C_{26}H_{22}N_6S$ (450.56 g/mol). ^{1}H NMR (500 MHz, DMSO-d_6) δ [ppm] = 13.44 (s, 1H), 10.59 (s, 1H), 8.87 (s, 1H), 8.59 (d, *J* = 4.3 Hz, 1H), 8.48 (d, *J* = 6.6 Hz, 1H), 8.22 (s, 1H), 8.15 (d, *J* = 7.8 Hz, 1H), 8.02 (d, *J* = 7.3 Hz, 1H), 7.96 (t, *J* = 7.7 Hz, 1H), 7.63 (s, 1H), 7.61 (s, 2H, H-2), 7.58 (d, *J* = 7.6 Hz, 1H), 7.56 (s, 1H), 7.49 (d, *J* = 5.3 Hz, 1H), 7.46 (d, *J* = 7.8 Hz, 1H), 7.20 (t, *J* = 7.4 Hz, 1H), 4.47 (q, *J* = 6.9 Hz, 2H), 1.34 (t, *J* = 7.1 Hz, 3H). ^{13}C NMR (126 MHz, DMSO-d_6) δ [ppm] = 155.44, 151.53, 148.75, 148.64, 142.21, 140.47, 138.04, 137.49, 127.77, 126.34, 125.69, 125.27, 124.61, 124.43, 122.54, 122.26, 120.93, 119.28, 118.99, 109.73, 108.98, 37.55, 14.20. HR-ESI-MS: $[M+H]^+$ m/z = 451.17013, $[M+Na]^+$ m/z = 473.15186.

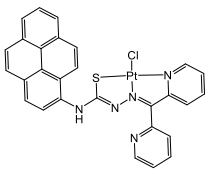


5.3.12.5 Synthesis of Pt(II) complexes with TSCs with fluorophores – general description

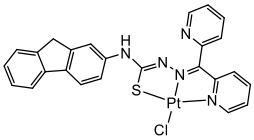


The TSC (1.00 eq.) and $K_2[PtCl_4]$ (1.00 eq.) were dissolved in 70 mL MeCN and stirred for 24 h at ambient temperature. The solvent was removed under reduced pressure, and the residue was washed with H_2O, toluene and Et_2O.

[Pt(PyrTSCDiPy)Cl] from 100.0 mg (0.22 mmol) 1-[bis(2-pyridyl)methylene]-4-(4,8-dihydro-1-pyrenyl)thiosemicarbazide, 91.0 mg (0.22 mmol) $K_2[PtCl_4]$. The product was obtained as a red solid. Yield: 139.1 mg (0.20 mmol, 92%). $C_{28}H_{18}ClN_5PtS$ (687.08 g/mol). ^{1}H NMR (500 MHz, DMSO-d_6) δ [ppm] = 11.05 (s, 1H), 8.90 (s, 1H), 8.62 (s, 1H), 8.32-8.05 (m, 11 H), 7.75 (m, 2H), 7.39 (m, 2H). ^{13}C NMR (126 MHz, DMSO-d_6) δ [ppm] = 147.31, 141.07, 136.45, 136.33, 131.17, 130.85, 128.13, 128.08, 127.58, 127.03, 126.05, 125.73, 125.06, 125.01, 124.53, 124.15, 122.84. HR-ESI-MS: m/z = $[M-Cl]^+$ 652.09281, m/z = $[M+H]^+$ 688.07006.

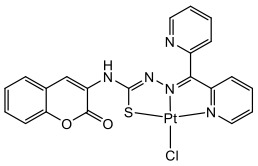


[Pt(FluTSCDiPy)Cl] from 100.0 mg (0.24 mmol) 1-[bis(2-pyridyl)methylene]-4-(9*H*-fluoren-2-yl)thiosemicarbazide, 100.0 mg (0.24 mmol) $K_2[PtCl_4]$. The product was obtained as a red solid. Yield: 148.4 mg (0.23 mmol, 95%). $C_{25}H_{18}ClN_5PtS$ (651.05 g/mol). ^{1}H NMR (500 MHz, DMSO-d_6) δ [ppm] = 10.61 (s, 1H), 8.92 (s, 1H), 8.87 (s, 1H), 8.22 (m, 1H), 8.12 (m, 1H), 7.99 (d, *J* = 5.2 Hz, 1H), 7.78 (m, 2H), 7.70 (m, 2H), 7.66 (s, 1H), 7.54 (d, *J* = 4.0 Hz, 1H), 7.41 (d, *J* = 4.0 Hz, 1H), 7.32 (m, 2H), 7.26 (m, 1H), 3.72 (s, 2H). ^{13}C NMR (126 MHz, DMSO-d_6) δ [ppm] = 159.08, 150.19, 149.22, 147.41, 143.94, 143.39, 141.14, 141.10, 139.32,

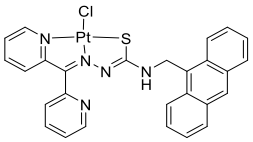


137.52, 137.19, 128.01, 127.75, 127.64, 127.22, 126.77, 125.54, 125.49, 120.24, 120.13, 36.97. HR-ESI-MS: m/z = $[M-Cl]^+$ 614.08949, m/z = $[M+H]^+$ 650.06776, m/z = $[M+Na]^+$672.04946.

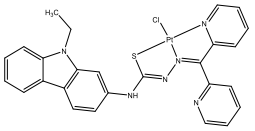
[Pt(CoumTSCDiPy)Cl] from 50.0 mg (0.12 mmol) 1-[bis(2-pyridyl)methylene]-4-(3-coumarinyl)thiosemicarbazide, 52.0 mg (0.12 mmol) $K_2[PtCl_4]$. The product was obtained as a red solid. Yield: 65.9 mg (0.10 mmol, 87%). $C_{21}H_{14}ClN_5O_2PtS$ (630.97 g/mol). ^{1}H NMR (500 MHz, DMSO-d_6) δ [ppm] = 9.73 (s, 1H), 8.93 (d, *J* = 4.5 Hz, 1H), 8.86 (d, *J* = 4.4 Hz, 1H), 8.15 (m, 2H), 8.00 (d, *J* = 7.0 Hz, 1 H), 7.84 (m, 1H), 7.76 (s, 1H), 7.70 (m, 1H), 7.51 (m, 1H), 7.38 (m, 3H), 7.16 (d, *J* = 7.0 Hz, 1H). HR-ESI-MS: m/z = $[M+H]^+$ 630.02619, m/z = $[M+Na]^+$ 652.00784.



[**Pt(AntTSCDiPy)Cl]** from 70.0 mg (0.16 mmol) 4-[(9-anthryl)methyl]-1-[bis(2-pyridyl)methylene]thiosemicarbazide, 65.0 mg (0.16 mmol) $K_2[PtCl_4]$. The product was obtained as a red solid. Yield: 98.5 mg (0.14 mmol, 91%). $C_{27}H_{20}ClN_5PtS$ (677.09 g/mol). ^{1}H NMR (500 MHz, DMSO-d_6) δ [ppm] = 8.89 (m, 8.63 (m, 1H), 8.24 (m, 2H), 8.10 (m, 5H), 7.75 (m, 1H), 7.53 (m, 6H), 5.46 (m, 2H). HR-ESI-MS: m/z = $[M+H]^+$ 676.08465, m/z = $[M+Na]^+$ 698.06528.



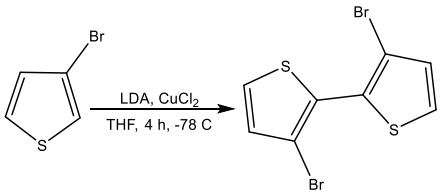
[Pt(CarbTSCDiPy)Cl] from 50.0 mg (0.11 mmol) 1-[bis(2-pyridyl)methylene]-4-(9-ethyl-2-carbazolyl)thiosemicarbazide, 46.0 mg (0.11 mmol) $K_2[PtCl_4]$. The product was obtained as a red solid. Yield: 59.9 mg (0.1 mmol, 80%). $C_{26}H_{21}ClN_6PtS$ (680.09 g/mol). ^{1}H NMR (500 MHz, DMSO-d_6) δ [ppm] = 10.58 (s, 1H), 8.94 (m, 1H), 8.83 (d, *J* = 4.5 Hz, 1H), 8.11 (m, 2H), 8.00 (m, 2H), 7.78 (m, 1H), 7.68 (m, 1H), 7.62 (m, 2H), 7.50-7.42 (m, 3H), 7.33 (m, 1H), 7.23 (t, *J* = 6.0 Hz, 1H), 4.40 (q, *J* = 6.2 Hz, 2H), 1.28 (t, *J* = 6.9 Hz, 3H). HR-ESI-MS: m/z = $[M+H]^+$ 679.09439, m/z = $[M+Na]^+$ 701.07624.



5.3.13 Synthesis of hexadentate bis-TSCs

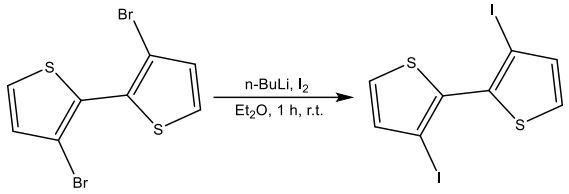
5.3.13.1 Synthesis of the dialdehyde precursors

Synthesis of 3,3'-dibromo-2,2'-bithiophene



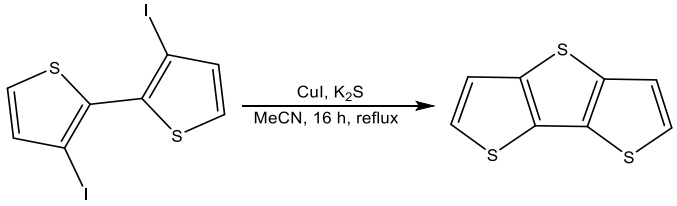
The reaction was performed under inert conditions. 20.00 mL n-Buli (2.5 M, 50.0 mmol, 1.00 eq.) were added dropwise to a solution of 7.70 mL diisopropylamine (55.0 mmol, 1.10 eq.) in 25 mL of anhydrous THF at – 78 °C. The formed LDA solution was warmed up to room temperature and added dropwise to a solution of 4.70 mL 3-bromothiophene (50.0 mmol, 1.00 eq.) in 50 mL of anhydrous THF at – 78 °C. The reaction was stirred for 1 h at – 78 °C. After that, 7.06 g $CuCl_2$ (53.0 mmol, 1.06 mmol) was added and the reaction mixture was warmed up to room temperature. 50 mL of conc. HCl was added, and the organic phase was separated. The aqueous phase was extracted four times with 50 mL of Et_2O and the combined organic phase was dried over Na_2SO_4, and the solvent was removed under reduced pressure. The crude product was purified by column chromatography (hexane) yielding the product as a colorless solid.[386] Yield: 5.50 g (17.0 mmol, 68%). $C_8H_4Br_2S_2$ (324.05 g/mol). ^{1}H NMR (300 MHz, $CDCl_3$) δ [ppm] = 7.43 (m, 2H), 7.10 (m, 2H).

Synthesis of 3,3'-diiodo-2,2'-bithiophene



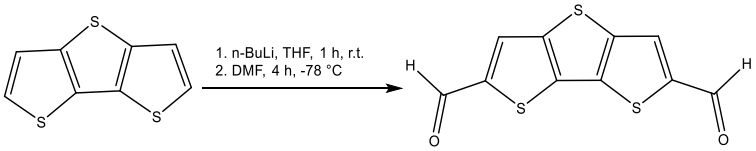
The reaction was performed under inert conditions. 5.19 g 3,3′-Dibromo-2,2′-bithiophene (16.0 mmol, 1.00 eq.) was dissolved in 125 mL of anhydrous Et_2O and 14.0 mL n-BuLi (2.5 M, 35.0 mmol, 2.20 eq.) was added dropwise at –78°C. The reaction mixture was stirred for 1 h at – 78 °C. After that, a solution of 8.93 g I_2 (35.0 mmol, 2.20 eq.) in 30 mL of anhydrous Et_2O was added dropwise to the reaction and the mixture was warmed to room temperature and stirred for another hour. In the next step, 120 mL sat. aqu. $Na_2S_2O_3$ solution was added, and the organic phase was separated. The aqueous phase was extracted with Et_2O (2 × 100 mL). The combined organic phase was washed with brine, dried over $MgSO_4$ and the solvent was removed under reduced pressure. The crude product was recrystallized from hexanes/toluene (2:1), yielding the product as a colorless solid.[387] Yield: 2.7 g (6.5 mmol, 40%). $C_8H_4S_2I_2$ (418.05 g/mol). ^{1}H NMR (300 MHz, CD_2Cl_2) δ [ppm] = 7.49 (d, *J* = 5.3 Hz, 2H), 7.23 (d, *J* = 5.3 Hz, 2H).

Synthesis of dithieno[3,2-b:2′,3′-d]thiophene



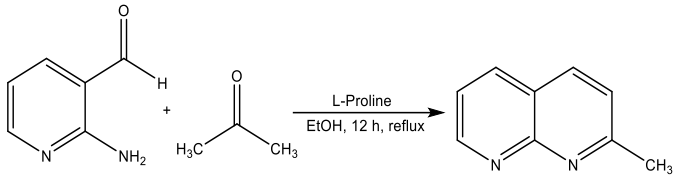
The reaction was performed under inert conditions. 1.50 g 3,3'-Diiodo-2,2'-bithiophene (3.6 mmol, 1.00 eq.) was dissolved in 42 mL of dry MeCN and 69.0 mg CuI (0.36 mmol, 0.10 eq.) as well as 0.79 g K_2S (7.2 mmol, 2.00 eq.) was added. The mixture was refluxed for 16 hours. After cooling to room temperature, the reaction was quenched with 50 mL of H_2O, and the resulting mixture was extracted three times with 50 mL of Et_2O. The combined organic phase was dried over Na_2SO_4, and the solvent was removed under reduced pressure. The crude product was purified by column chromatography (n-hexane) yielding the product as a colorless solid.[388] Yield: 0.30 g, 1.5 mmol, 42%). $C_8H_4S_3$ (196.30 g/mol). ^{1}H NMR (300 MHz, CD_2Cl_2) δ [ppm] = 7.37 (d, *J* = 5.3 Hz, 2H), 7.32 (d, *J* = 5.3 Hz, 2H).

Synthesis of 3,7,11-trithiatricyclo[6.3.0.0^{2,6}]undeca-1(8),2(6),4,9-tetraene-4,10-dicarbaldehyde



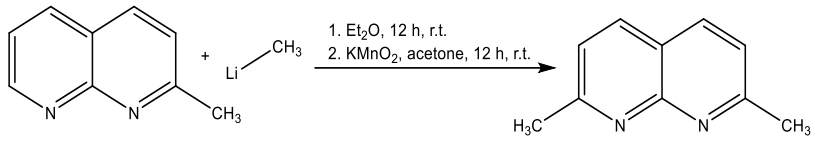
The reaction was performed under inert conditions. 0.30 g Dithieno[3,2-b:2′,3′-d]thiophene (1.5 mmol, 1.00 eq.) were dissolved in 40 mL of anhydrous THF and 1.92 mL n-BuLi (1.6 M, 3.1 mmol, 2.00 eq.) were added dropwise. The mixture was stirred for 1 h at room temperature. After that, the reaction was cooled to –78 °C and 0.60 mL (9.2 mmol, 6.00 eq.) DMF were added slowly. The mixture was stirred for 1.5 h at –78 °C and 2 h at room temperature. The reaction was quenched by adding diluted HCl. The formed precipitate was filtered off, washed with H_2O and dried under ambient conditions, yielding the product as a brownish solid.[359] Yield: 0.23 g (0.9 mmol, 60%). $C_{10}H_4O_2S_3$ (252.32 g/mol). ^{1}H NMR (300 MHz, DMSO-*d*$_6$) δ [ppm] = 10.06 (s, 2H), 8.54 (s, 2H). ^{13}C NMR (126 MHz, DMSO-*d*$_6$) δ [ppm] = 185.69, 185.06, 146.36, 146.03, 136.07, 133.23, 132.72, 132.02, 122.32.

Synthesis of 2-methyl-1,8-naphthyridine



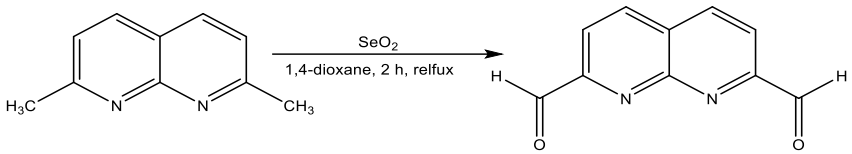
To a suspension of 2.00 g 2-aminonicotinaldehyde (16.4 mmol, 1.00 eq.) and 3.19 g L-proline (16.4 mmol, 1.00 eq.) in 70 mL of EtOH was added 23.00 mL acetone (492.0 mmol, 30.00 eq.). The reaction was refluxed for 12 h. After that, the solvent was removed under reduced pressure, and the residue was washed with 100 mL H_2O and extracted with CH_2Cl_2 (3 x 50 mL). The combined organic phase was washed with brine (50 mL), dried over Na_2SO_4 and the solvent was removed under reduced pressure. The crude product was purified by column chromatography (1:5 EtOAc/petrol ether) yielding the product as colorless solid.[389] Yield: 2.46 g (15.6 mol, 95 %). $C_9H_8N_2$ (114.18 g/mol). ^{1}H NMR (300 MHz, $CDCl_3$) δ [ppm] = 9.02 (m, 1H), 8.11 (d, *J* = 8.1 Hz, 1H), 8.02 (d, *J* = 8.3 Hz, 1H), 7.38 (m, 1H), 7.33 (d, *J* = 8.3 Hz, 1H), 2.77 (s, 1H).

Synthesis of 2,7-dimethyl-1,8-naphthyridine



The reaction was performed under inert conditions. 2.46 g 2-Methyl-1,8-naphthyridine (17.1 mmol, 1.00 eq.) was dissolved in 50 mL anhydrous Et_2O and cooled to –78 °C. After that, 16.00 mL methyllithium (1.6 M, 25.6 mmol, 1.50 eq.) was added dropwise. The reaction was stirred 2 h at –78 °C and for an additional 12 h at room temperature. The reaction was quenched by the addition of H_2O, and the organic layer was separated, dried over Na_2SO_4 and concentrated in vacuo. The resulting orange solid was added to a solution of $KMnO_4$ in acetone and stirred for another 12 h. The solution was filtered, dried over Na_2SO_4, and the solvent was removed under reduced pressure yielding the product as a colorless solid.[390] Yield: 1.70 g (10.7 mmol, 63%). $C_{10}H_{10}N_2$ (158.20 g/mol). ^{1}H NMR (300 MHz, $CDCl_3$) δ [ppm] = 8.00 (d, *J* = 8.2 Hz, 2H), 7.29 (d, *J* = 8.3 Hz, 2H), 2.77 (s, 6H).

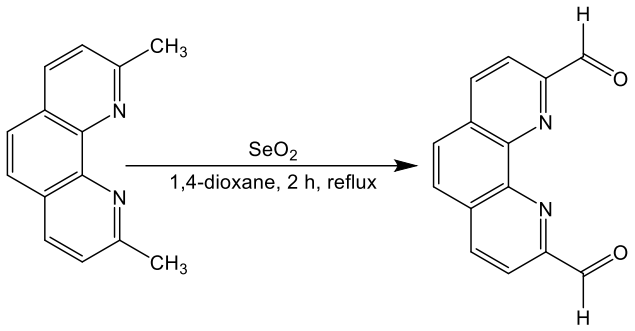
Synthesis of 1,8-diazanaphthalene-2,7-dicarbaldehyde



3.83 g SeO_2 (34.5 mmol, 3.21 eq.) and 1.00 g molecular sieve (4 Å) were added into 130 mL of 1,4-dioxane and the mixture was refluxed. After that, a solution of 1.70 g 2,7-dimethyl-1,8-naphthyridine (10.7 mmol, 1.00 eq.) in 30 mL of 1,4-dioxane was slowly added *via* a dropping funnel. The reaction mixture was refluxed for 2 h. The formed, black suspension was filtered hot, and the precipitate was washed with hot 1,4-dioxane. The filtrate was concentrated under reduced pressure to a volume of 60 mL and diluted with 60 mL of $CHCl_3$. The organic phase was washed with H_2O (3 x 100 mL) and the combined aqueous phase was extracted with $CHCl_3$ (3 x 100 mL). The combined organic phase was washed with 5% $NaHCO_3$ (300 mL), dried over $MgSO_4$, and the solvent was evaporated to yield a brownish solid. The solid was redissolved in hot EtOAc (85 mL), and the precipitate was filtered hot and washed with hot EtOAc (3 x 50 mL). The filtrate was evaporated under reduced pressure yielding the product as pale brown solid.[360] Yield: 1.17 g (6.28 mmol, 58%). $C_{10}H_6N_2O_2$ (186.17 g/mol). ^{1}H NMR (300 MHz, DMSO-

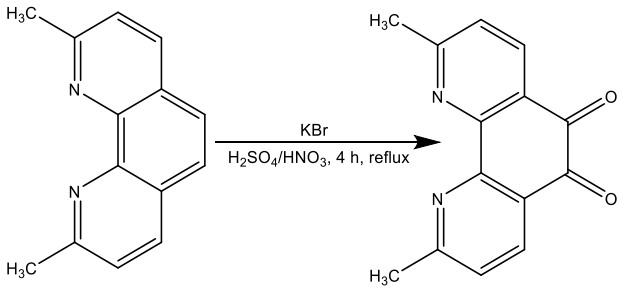
*d*6) δ [ppm] = 10.21 (s, 2H), 8.84 (d, *J* = 8.46 Hz, 2H), 8.24 (d, *J* = 8.40, 2H). ^{13}C NMR (126 MHz, DMSO-*d*6) δ [ppm] = 193.96, 156.23, 155.12, 140.65, 127.71, 120.37.

Synthesis of 4,5-diazaphenanthrene-3,6-dicarbaldehyde



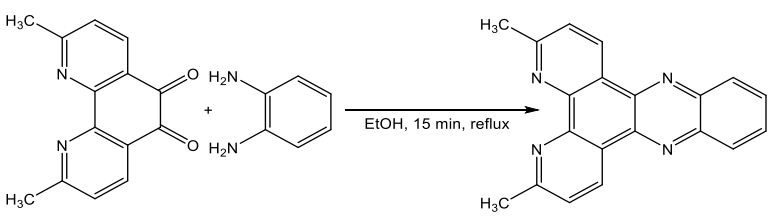
1.00 g 2,9-Dimethyl-1,10-phenanthroline (4.8 mmol, 1.00 eq.) was dissolved in 65 mL of a mixture of 1,4-dioxane and H_2O (96:4 v/v) and 2.40 g SeO_2 (21.6 mmol, 4.50 eq.) was added. The reaction mixture was refluxed for 3 h. After that, the hot suspension was filtered over celite, the precipitate was washed with hot 1,4-dioxane and the filtrate was evaporated. The crude product was redissolved in a minimum amount of EtOH and Et_2O was added to precipitate the product, which was separated by filtration. The product was obtained as a beige solid.[362] Yield: 0.96 g (4.1 mmol, 85%). $C_{14}H_8N_2O_2$ (236.23 g/mol). ^{1}H NMR (300 MHz, DMSO-*d*6) δ [ppm] = 10.34 (s, 2H), 8.77 (d, *J* = 8.3 Hz, 2H), 8.29 (d, *J* = 8.2 Hz, 2H), 8.26 (s, 2H).

Synthesis of 2,9-dimethyl-1,10-phenanthroline-5,6-dione



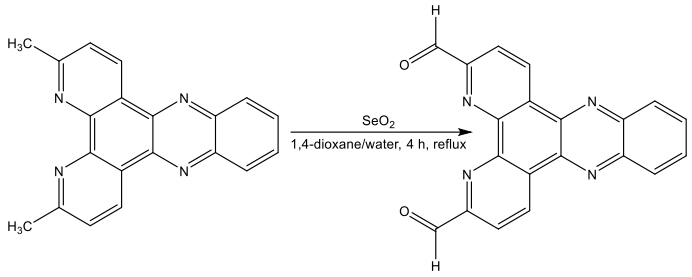
2.00 g 2,9-Dimethyl-1,10-phenanthroline (9.6 mmol, 1.00 eq.) and 10.30 g KBr (86.4 mmol, 9.00 eq.) were dissolved in a mixture of 40 mL conc. H_2SO_4 and 20 mL of conc. HNO_3 at 0 °C. The mixture was slowly heated to 80 °C and refluxed for 4 h. The resulting solution was cooled to room temperature, diluted with 400 mL H_2O and neutralized with $NaHCO_3$. The aqueous phase was extracted with CH_2Cl_2 (3 x 100 mL) and the combined organic layer was dried over $MgSO_4$ and the solvent was removed under reduced pressure. After that, n-hexane was added which led to the precipitation of the product as a yellow solid, which was separated by filtration.[361] Yield: 1.97 g (8.3 mmol, 86%). $C_{14}H_{10}N_2O_2$ (238.25 g/mol). ^{1}H NMR (300 MHz, $CDCl_3$) δ [ppm] = 8.38 (d, *J* = 8.0 Hz, 2H), 7.42 (d, *J* = 8.0 Hz, 2H), 2.85 (s, 6 H).

Synthesis of 3,6-dimethyldipyrido[3,2-a:2,3-c]phenazine



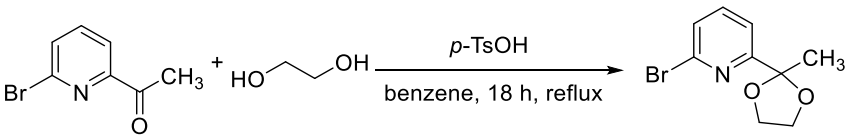
1.97 g 2,9-Dimethyl-1,10-phenanthroline-5,6-dione (8.3 mmol, 1.00 eq.) was dissolved in 150 mL of EtOH and the mixture was refluxed for 10 min. After that, 0.89 g 1,2-phenylenediamine (8.3 mmol, 1.00 eq.) was added and the reaction was refluxed for 15 min. The solution was cooled to room temperature and put into a freezer (–25 °C) for 12 h. The formed precipitate was filtered off, washed with Et_2O and dried under ambient conditions. The product was obtained as a yellow solid.[361] Yield: 1.60 g (5.2 mmol, 63%). $C_{20}H_{14}N_4$ (310.36 g/mol). ^{1}H NMR (300 MHz, $CDCl_3$) δ [ppm] = 9.58 (d, *J* = 8.3 Hz, 2H), 8.36 (dd, *J* = 6.5, 3.5 Hz, 2H), 7.91 (dd, *J* = 6.6, 3.4 Hz, 2H), 7.69 (d, *J* = 8.3 Hz, 2H), 3.03 (s, 6H).

Synthesis of 4,5-diazaphenanthrene-3,6-dicarbaldehyde



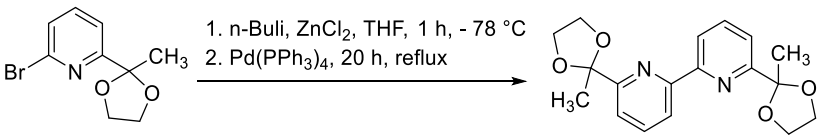
2.15 g SeO_2 (19.3 mol, 3.75 eq.) was dissolved in 100 mL of a mixture of 1,4-dioxane/H_2O (96:4 v/v) and a solution of 1.60 g 3,6-dimethyldipyrido[3,2-a:2,3-c]phenazine (5.16 mmol, 1.00 eq) in 300 mL of 1,4-dioxane/H_2O (96:4 v/v) was slowly added. The reaction mixture was refluxed for 4 h. After that, the suspension was filtered hot over Celite, and the precipitate was washed several times with hot 1,4-dioxane. After that, the filtrate was evaporated, yielding the product as a light-yellow solid.[361] Yield: 1.67 g (4.9 mmol, 96%). $C_{20}H_{10}N_4O_2$ (338.33 g/mol). ^{1}H NMR (300 MHz, DMSO-d_6) δ [ppm] = 10.40 (s, 2H), 9.88 (d, *J* = 8.32 Hz, 2H), 8.49 (d, *J* = 8.23 Hz, 4H), 8.17 (dd, *J* = 9.89 Hz, 3.15 Hz 2H). HR-ESI-MS (m/z) $[M+H]^+$ 741.27524 (Calc: 741.2748176), $[M+Na]^+$ 763.25741 (Calc: 763.2567623).

Synthesis of 2-bromo-6-(2-methyl-1,3-dioxolan-2-yl)pyridine



2.20 g 6-Acetyl-2-bromopyridine (11.0 mmol, 1.00 eq.), 0.89 mL ethylene glycol (15.9 mmol, 1.45 eq.), and 0.21 g *p*-toluenesulfonic acid monohydrate (1.1 mmol, 0.1 eq.) were dissolved in 12.5 mL of benzene and heated under reflux in a *Dean-Stark* apparatus for 18 h. The mixture was cooled to room temperature and poured into 12.5 mL of a 0.5 M NaOH solution. The phases were separated, and the aqueous phase was extracted with EtOAc (2 x 25 mL). The combined organic extracts were washed with 0.5 M aqueous NaOH (2 x 15 mL), H_2O (2 x 15 mL), brine (1 x 15 mL) and dried over $MgSO_4$. The solvent was removed under reduced yielding the product as a yellow oil.[391] Yield: 2.64 g (10.8 mmol, 98%). $C_9H_{10}BrNO_2$ (244.09 g/mol). ^{1}H NMR (300 MHz, CDCl3) δ [ppm] = 7.56-7.41 (m, 2H), 7.39-7.33 (m, 1H), 4.09-3.99 (m, 2H), 3.89-3.78 (m, 2H), 1.66 (s, 3H). ^{13}C NMR (75 MHz, CDCl3) δ [ppm] = 162.44, 141.94, 138.83, 127.48, 118.22, 107.93, 65.04, 25.06.

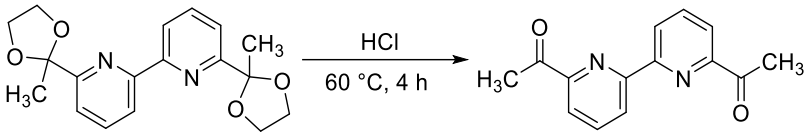
Synthesis of 6,6′-bis(2-methyl-1,3- dioxolan-2-yl)-2,2′-bipyridine



The reaction was performed under inert conditions. 2.23 mL *n*-BuLi (2.5 M, 5.6 mmol, 1.19 eq.) were diluted with 6 mL of dry THF and cooled to –78°C. A solution of 1.36 g 2-bromo- 6-(2-methyl-1,3-dioxolan-2-yl)pyridine (5.6 mmol, 1.19 eq.) in 4 mL of dry THF was added dropwise and the reaction

was stirred for 30 min at – 78 °C. After that, a solution of 0.82 g zinc chloride (6.0 mmol, 1.27 eq.) in 6 mL Et_2O was added dropwise. The reaction was warmed to 0 °C and 0.11 g $Pd(PPh_3)_4$ (2.00 mol%) as well as 1.14 g 2-bromo-6-(2-methyl-1,3-dioxolan-2-yl)pyridine (4.7 mmol, 1.00 eq.) were added. The reaction mixture was stirred at 0 °C for 30 min and then refluxed for 20 h. The reaction mixture was stored at –18 °C for 12 h and the formed precipitate was filtered off and washed with cold THF. The precipitate was added to 30 mL of an aqueous, saturated $NaHCO_3$ solution and 25 mL of an aqueous, saturated Na_2EDTA solution were added. The aqueous phase was extracted with CH_2Cl_2 (3 x 50 mL). and the combined organic phase was washed with 100 mL brine and dried over Na_2SO_4. The solvent was removed under reduced pressure yielding the product as a yellow solid.[363] Yield: 0.71 g (2.16 mmol, 47%). $C_{18}H_{20}N_2O_4$ (328.37 g/mol). ^{1}H NMR (300 MHz, CDCl3) δ [ppm] = 8.45 (d, *J* = 7.8 Hz, 2H), 7.80 (t, *J* = 7.8 Hz, 2H), 7.55 (d, *J* = 7.8 Hz, 2H), 4.19-4.08 (m, 4H), 4.02-3.93 (m, 4H), 1.84 (s, 6H).

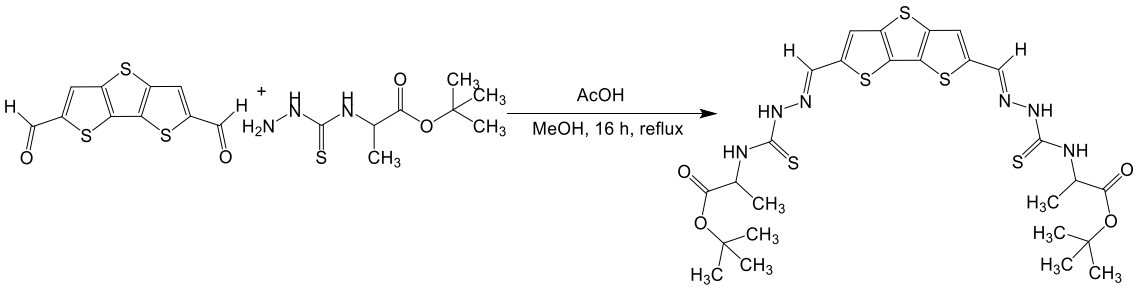
Synthesis of 6,6′-bis(2-acetyl)-2,2′-bipyridine



0.70 g 6,6′-Bis(2-methyl-1,3-dioxolan- 2-yl)-2,2′-bipyridine (2.1 mmol, 1.00 eq.) was dissolved in 10 mL of 4 M HCl and stirred at 60 °C for 4 h. The mixture was cooled to room temperature, diluted with 20 mL EtOAc and neutralized with 4 M NaOH. The aqueous phase was separated and extracted with EtOAc (3 x 20 mL). The combined organic phase was washed with saturated $NaHCO_3$ solution, brine and dried over $MgSO_4$. The solvent was removed under reduced pressure yielding the product as a colorless solid.[363] Yield: 0.55 g (2.1 mmol, quant.). $C_{14}H_{12}N_2O_2$ (240.26 g/mol). ^{1}H NMR (500 MHz, $CDCl_3$) δ [ppm] = δ 8.73 (dd, *J* = 7.8, 1.2 Hz, 2H), 8.10 (dd, *J* = 7.7, 1.2 Hz, 2H), 8.01 (t, *J* = 7.8 Hz, 2H), 2.84 (s, 6H). ^{13}C NMR (126 MHz, $CDCl_3$) δ [ppm] = 200.05, 154.64, 153.04, 137.96, 124.33, 121.88, 25.77. HR-ESI-MS (m/z) $[M+H]^+$ 240.0894.

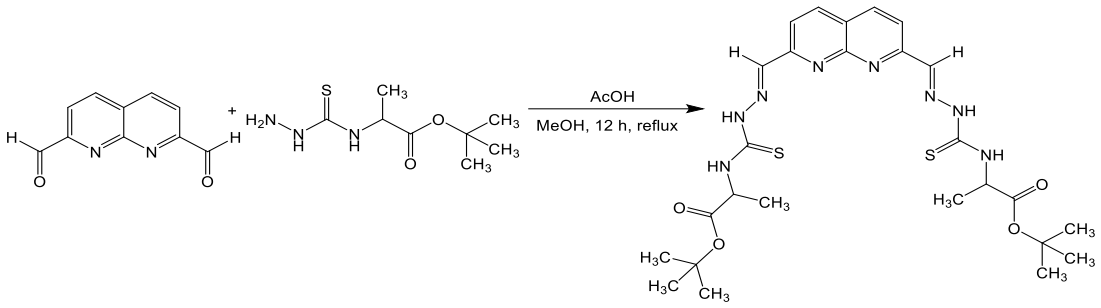
5.3.13.2 Synthesis of hexadentate bis-TSCs

Synthesis of DTT(bis-TSC)Ala*t*Bu



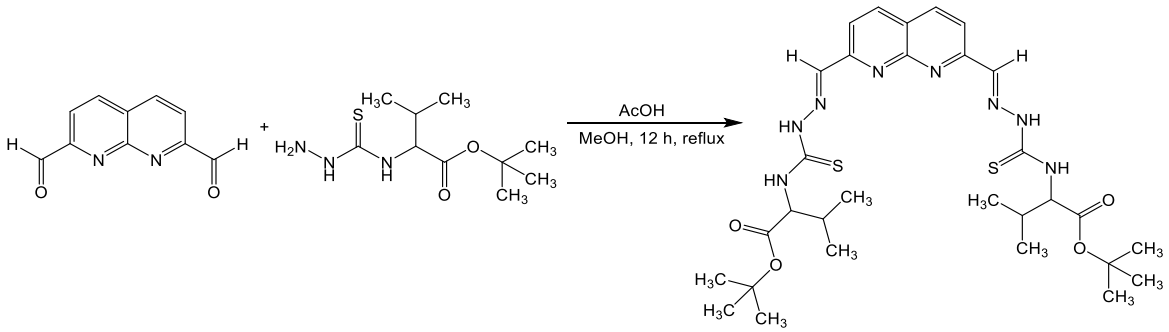
0.10 g of the dialdehyde (0.4 mmol, 1.00 eq.) and 0.17 g of the thiosemicarbazide (0.8 mmol, 2.00 eq.) were dissolved in a minimum amount of MeOH and 0.1 mL AcOH were added. The mixture was refluxed for 16 h and cooled to room temperature. The solvent was removed under reduced pressure to yield the product as a brown powder. Yield: 0.20 g (0.3 mmol, 78%). $C_{26}H_{34}N_6O_4S_5$ (654.90 g/mol). ^{1}H NMR (300 MHz, DMSO-d_6) δ [ppm] = 11.90 (s, 2H), 8.34 (s, 2H), 8.03 (d, *J* = 7.75 Hz, 2H), 7.92 (s, 2H), 4.82 (q, 2H), 1.46 (s, 18H), 1.42 (s, 6H). ^{13}C NMR (126 MHz, DMSO-d_6) δ [ppm] = 176.76, 171.86, 143.43, 141.12, 138.31, 131.60, 125.59, 81.75, 52.98, 28.13, 18.22.

Synthesis of Naph(bis-TSC)Ala*t*Bu



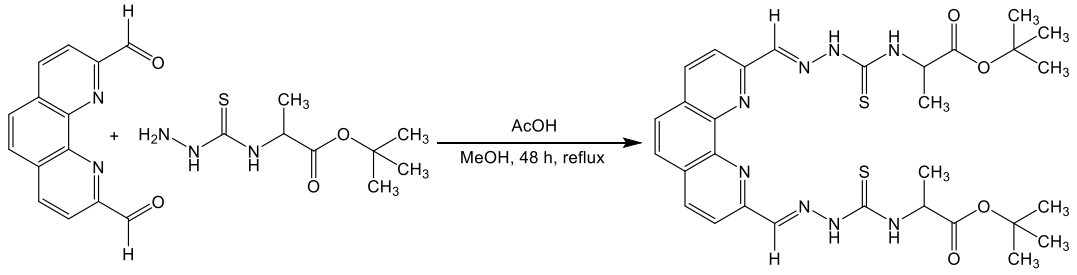
0.10 g of the dialdehyde (0.54 mmol, 1.00 eq.) and 0.24 g of the thiosemicarbazide (1.10 mmol, 2.00 eq) were dissolved in a minimum amount of MeOH and 0.1 mL AcOH were added. The mixture was refluxed for 48 h and cooled to room temperature. The solvent was removed under reduced pressure, and the crude product was purified by column chromatography (5:1 EtOAc/c-hexane). The product was obtained as a brown solid. Yield: 0.12 g (0.20 mmol, 37%). $C_{21}H_{15}N_5O_2S$ (401.44 g/mol). ^{1}H NMR (300 MHz, DMSO-d_6) δ [ppm] = 12.12 (s, 2H), 8.77(d, *J* = 7.95 Hz, 2H), 8.54 (dd, *J* = 7.70 Hz, 4H), 8.32 (s, 2H), 4.93 (q, 2H), 1.49 (d, *J* = 7.30 Hz, 6H), 1.46 (s, 18H). HR-ESI-MS (m/z) $[M+H]^+$ 589.23753 (Calc: 589.2373695), $[M+Na]^+$ 611.21949 (Calc: 611.2193142).

Synthesis of Naph(bis-TSC)Val*t*Bu



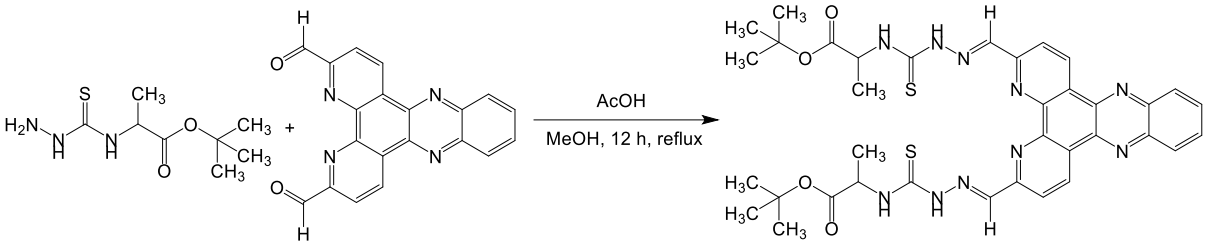
0.20 g 1,8-Naphthyridine-2,7-dicarboxaldehyde (1.1 mmol, 1.00 eq.) and 0.53 g of the thiosemicarbazide (2.2 mmol, 2.00 eq.) were dissolved in 10 mL MeOH and a few drops of glacial AcOH were added. The mixture was refluxed for 12 h and cooled to room temperature. The solvent was removed under reduced pressure, and the crude product was purified by column chromatography (c-hexane/EtOAc 5:1) yielding the product as a yellow solid. Yield: 0.28 g (0.4 mmol, 40%). $C_{30}H_{44}N_8O_4S_2$ (644.85 g/mol). ^{1}H NMR (499 MHz, $CDCl_3$) δ [ppm] = 9.64 (s, 2H), 8.36 (s, 2H, H-13, H-15), 8.24 (d, *J* = 8.4 Hz, 2H), 8.18 (d, *J* = 8.4 Hz, 2H), 8.14 (d, *J* = 8.4 Hz, 2H), 5.00 (dd, J = 8.5, 4.2 Hz, 2H), 2.45 (dd, J = 11.1, 6.9 Hz, 2H), 1.54 (s, 18H), 1.12 (d, J = 7.0 Hz, 6H), 1.05 (d, J = 6.9 Hz, 6H). ^{13}C NMR (499 MHz, $CDCl_3$) δ [ppm] = = 177.66, 170.59, 156.58, 155.81, 142.51, 137.41, 123.41, 119.19, 82.66, 62.31, 31.90, 28.18, 18.71, 18.32. HRMS (ESI): m/z = 645.30057 $[M+H]^+$. m/z = 667.28252 $[M+Na]^+$.

Synthesis of Phen(bis-TSC)Ala*t*Bu



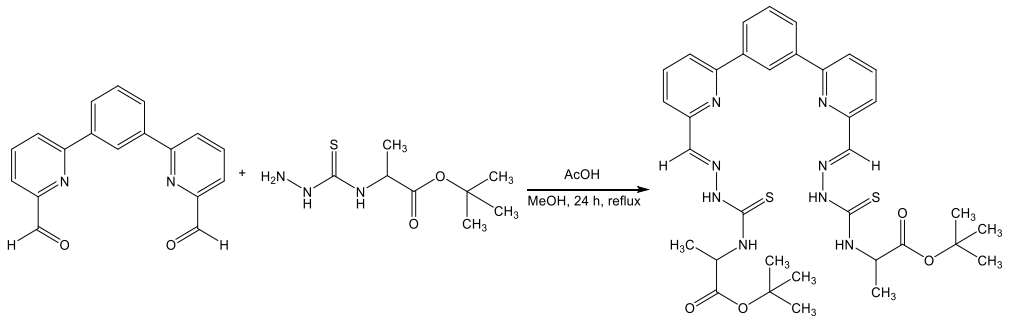
0.10 g phenanthroline aldehyde (0.42 mmol, 1.00 eq.) and 0.19 g of the thiosemicarbazide (0.85 mmol, 2.00 eq.) were dissolved in a minimum amount of MeOH and 0.1 mL glacial AcOH were added. The mixture was refluxed for 48 h and cooled to room temperature. The solvent was removed under reduced pressure, and the crude product was purified by column chromatography (2:1 EtOAc/c-hexane) yielding the product as a brown solid. Yield: 0.06 g (0.09 mmol, 22%). $C_{30}H_{38}N_8O_4S_2$ (638.81 g/mol). ^{1}H NMR (300 MHz, DMSO-d_6) δ [ppm] = 12.19 (s, 2H), 8.75 (d, J = 8.00 Hz, 2H), 8.69 (d, J = 8.45 Hz), 8.58 (d, J = 8.45, 2H), 8.50 (s, 2H), 8.06 (s, 2H), 4.95 (m, 2H), 1.52 (d, J = 7.30 Hz, 6H), 1.47 (s, 18H

Synthesis of DPPZ(bis-TSC)Ala*t*Bu



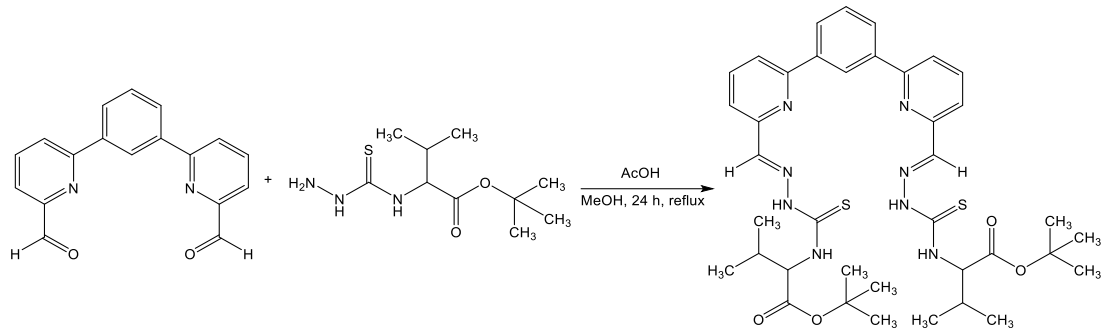
0.10 g of the dialdehyde (0.30 mmol, 1.00 eq.) and 0.13 g of the thiosemicarbazide (0.60 mmol, 2.00 eq.) were dissolved in a minimum amount of MeOH and 0.1 mL of glacial AcOH were added. The mixture was refluxed for 16 h and cooled to room temperature. The solvent was removed under reduced pressure, and the crude product was purified by column chromatography (5:1 EtOAc/c-hexane). The product was obtained as a brownish solid. Yield: 0.13 g (0.18 mmol, 58%). $C_{36}H_{40}N_{10}O_4S_2$ (740.90 g/mol). ^{1}H NMR (499 MHz, DMSO-d_6) δ [ppm] = 12.24 (s, 2H), 9.42 (d, J = 8.40 Hz, 2H), 8.75 (m, 4H), 8.44 (s, 2H), 8.35 (m, 2H), 8.04 (m, 2H), 4.97 (q, J = 15.02 Hz, 2H), 1.57 (d, J = 7.25 Hz, 6H), 1.50 (s, 18H). ^{13}C NMR (126 MHz, DMSO-d_6) δ [ppm] = 177.96, 171.81, 155.83, 147.55, 142.20, 140.71, 127.32, 81.47, 53.42, 28.21, 17.77.

Synthesis of NCN(bis-TSC)Ala*t*Bu



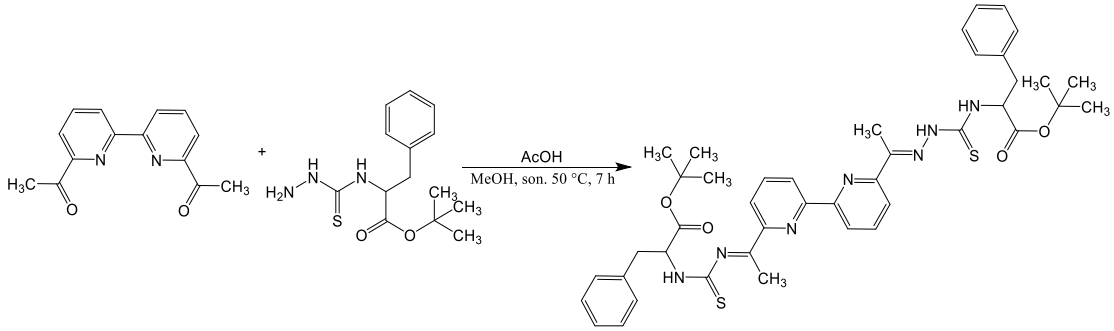
0.10 g of the dialdehyde (0.35 mmol, 1.00 eq.) and the 0.15 g of the thiosemicarbazide (0.70 mmol, 2.00 eq.) were dissolved in 10 mL of EtOH and a few droplets of glacial AcOH were added. The mixture was refluxed for 16 h and cooled to room temperature. The solvent was removed under reduced pressure, and the crude product was purified by column chromatography (2:1, EtOAc/c-hexane). The product was obtained as a colorless solid. Yield: 0.08 g (0.12 mmol, 34%). $C_{34}H_{42}N_8O_4S_2$ (690.88 g/mol). ^{1}H NMR (300 MHz, $CDCl_3$) δ [ppm] = 14.69 (s, 2H), 8.54 (m, 1H), 8.25-8.15 (m, 6H), 7.90 (t, J = 7.9 Hz, 2H), 7.66 (t, J = 7.8 Hz, 1H), 7.36 (d, J = 7.6 Hz, 2H), 7.18 (s, 2H), 5.04 (q, J = 7.3 Hz, 2H), 1.59 (d, J = 7.1 Hz, 6H), 1.53 (s, 18H). ^{13}C NMR (126 MHz, DMSO-d_6) δ [ppm] = 177.70, 172.19, 156.31, 151.69, 143.46, 138.42, 138.37, 133.51, 133.23, 130.18, 129.75, 129.14, 125.57, 124.38, 122.54, 121.33, 82.46, 82.16, 60.41, 53.36, 52.97, 28.00, 18.70, 14.21.

Synthesis of NCN(bis-TSC)Val*t*Bu



The dialdehyde (0.20 g, 0.69 mmol, 1.00 eq.) and the thiosemicarbazide (0.34 g, 1.39 mmol, 2.00 eq) were dissolved in 10 mL of MeOH and a few droplets of glacial AcOH were added. The mixture was refluxed for 16 h and cooled to room temperature. The solvent was removed under reduced pressure, and the crude product was purified by column chromatography (1:2 cHex/EtOAc). The product was obtained as a colorless solid. Yield: 0.20 g (0.27 mmol, 39%), $C_{38}H_{50}N_8O_4S_2$ (746.99 g/mol). ^{1}H NMR (300 MHz, $CDCl_3$) δ [ppm] = 14.74 (s, 2H), 9.36 (s, 2H), 8.28-8.24 (m, 4H), 8.02 (s, 1H), 7.95 (t, *J* = 7.9 Hz, 2H), 7.73 (t, *J* = 7.8 Hz, 1H), 7.38 (d, *J* = 7.6 Hz, 2H), 7.20 (s, 2H), 5.05 (dd, *J* = 8.8, 4.5 Hz, 2H), 2.43-2.39 (m, 2H), 1.52 (d, *J* = 6.5 Hz, 18H), 1.09-1.05 (m, 12H). ^{13}C NMR (126 MHz, DMSO-d_6) δ [ppm] = 178.48, 177.70, 170.78, 170.53, 157.09, 156.34, 152.44, 151.69, 143.11, 139.26, 133.53, 130.18, 129.17, 125.54, 124.37, 122.55, 118.85, 82.51, 82.15, 62.31, 61.97, 31.87, 31.80, 28.17, 28.15, 18.64, 18.59, 18.53, 18.40. HR-ESI-MS (m/z) $[M+H]^+$ 747.3473, $[M+Na]^+$ 769.3289.

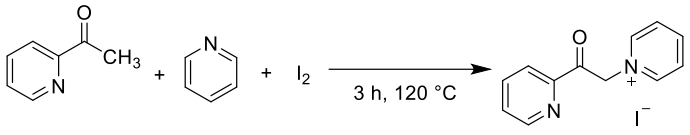
Synthesis of bpy(bis-TSC)Phe*t*Bu



The aldehyde (50.0 mg, 0.21 mmol, 1.00 eq.) and the thiosemicarbazide (122.9 mg, 0.42 mmol, 2.00 eq.) were dissolved in 5 mL MeOH and a few drops of AcOH were added. The mixture sonicated at 50 °C for 7 h. The solvent was removed under reduced pressure, and the residue was purified by column chromatography (7:1 cHex/EtOAc) yielding the bis-TSC as yellow solid. Yield: 50.0 mg (0.06 mmol, 30%). $C_{42}H_{50}N_8O_4S_2$ (795.03 g/mol). ^{1}H NMR (300 MHz, $CDCl_3$) δ [ppm] = 8.82 (s, 2H), 8.48 (dd, *J* = 7.2, 1.6 Hz, 2H), 8.12 (d, *J* = 8.0 Hz, 2H), 7.87-7.80 (m, 4H), 7.32 – 7.27 (m, 8H), 7.25-7.23 (m, 2H), 5.36-5.28 (m, 2H), 3.38 (dd, *J* = 13.9, 4.6 Hz, 2H), 3.30 (dd, *J* = 13.8, 6.8 Hz, 2H), 2.53 (s, 6H), 1.43 (s, 18H). ^{13}C NMR (126 MHz, DMSO-d_6) δ [ppm] = 177.25, 170.10, 154.66, 153.65, 147.79, 137.32, 136.04, 129.73, 128.47, 127.03, 121.09, 120.46, 82.68, 58.09, 38.05, 28.02, 11.25. HR-ESI-MS (m/z) $[M+H]^+$ 795.3474, $[M+Na]^+$ 817.3292.

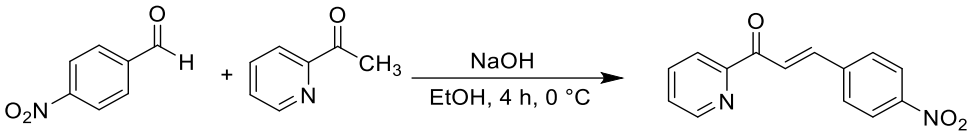
5.3.13.3 Synthesis of Dipy(TSC)Tpy and Ant(TSC)Tpy

Synthesis of 1-[2-oxo-2-(2-pyridyl)ethyl]-1-pyridinium iodide



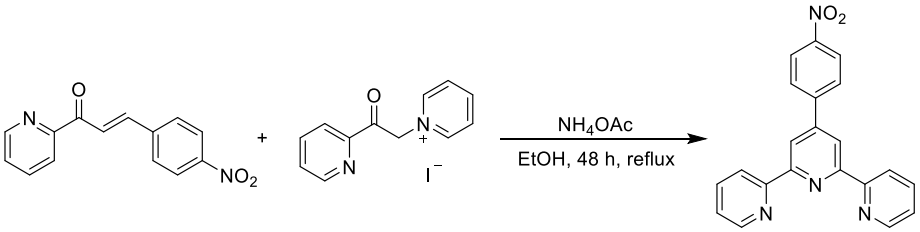
5.55 mL 2-acetylpyridin (46.8 mmol, 1.00 eq.) was dissolved in 60 mL pyridine and 11.90 g I_2 (46,8 mmol, 1.00 eq.) was added. The reaction mixture was heated to 120 °C for 3 h, leading to a black precipitate. After cooling to room temperature, the solid was filtered off, washed with pyridine, and dried under ambient conditions. The product was obtained as a black solid.[392] Yield: 9.69 g (29.7 mmol, 55%). $C_{12}H_{11}N_2OI$ (326.14 g/mol). ^{1}H NMR (300 MHz, DMSO-d_6) δ [ppm] = 8.99 (m, 2H), 8.87 (m, 1H), 8.80 (m, 1H), 8.73 (m, 1H), 8.27 (m, 1H), 8.17-8.05 (m, 2H), 7.83 (m, 2H), 6.51 (s, 2H).

Synthesis of 3-(4-nitrophenyl)-1-(2-pyridyl)-2-propen-1-one



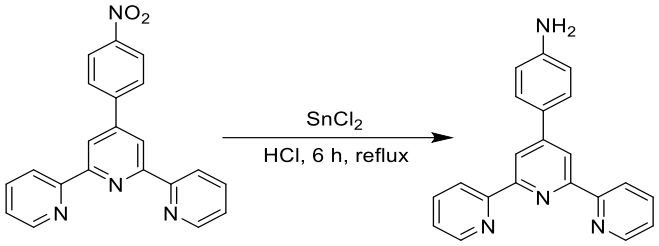
6.25 g 4-Nitrobenzaldehyde (41.4 mmol, 1.00 eq.) was suspended in 50 mL of EtOH and 2.50 mL of an aqueous solution of 10% NaOH was added. After that, the reaction mixture was cooled to 0 °C and 4.63 mL 2-acetylpyridin (41.2 mmol, 1.00 eq.) was slowly added for 2 h. The reaction mixture was stirred for an additional 2 h at 0 °C, which led to the formation of a pale-yellow precipitate. The solid was filtered off and washed with EtOH, yielding the product as a yellowish solid.[393] Yield: 6.85 g (27.0 mmol, 66%).$C_{14}H_{10}N_2O$ (254.26 g/mol). ^{1}H NMR (300 MHz, CDCl3) δ [ppm] = 8.78 (d, *J* = 5.00 Hz, 1H), 8.47, (d, *J* = 4.90 Hz, 1H), 8.35-8.17 (m, 3H), 8.97-8.87 (m, 4H), 7.54 (m, 1H)

Synthesis of 4'-(4-nitrophenyl)-2,2':6',2''-terpyridine



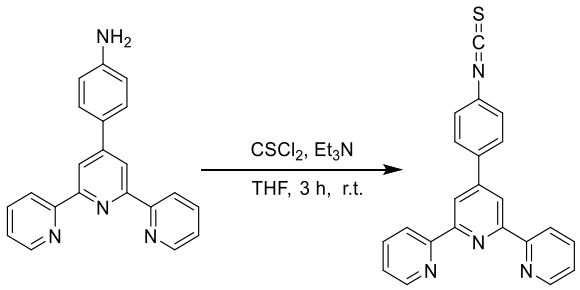
3.00 g of the *Kröhnke*-reagent (9.0 mmol, 1.00 eq.) and 2.34 g of the chalcone (9.0 mmol, 1.00 eq.) were dissolved in 60 mL of a solution of NH_4OAc in EtOH (10 %). The reaction mixture was refluxed for 48 h and the solved was removed under reduced pressure, yielding a black solid, which was redissolved in 50 mL of $CHCl_3$ and washed with H_2O (3 x 50 mL). The solvent was removed under reduced pressure yielding the product as a brownish solid, which was used directly in the next reaction step without further purification or analyzation.[364]

Synthesis of 4-([2,2':6',2''-terpyridin]-4'-yl)phenylamine



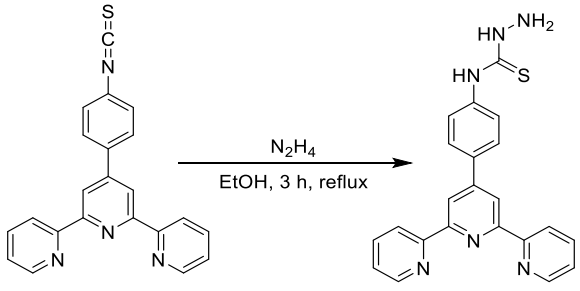
3.19 g 4-Nitrophenyl terpyridine (9.0 mmol, 1.00 eq.) was dissolved in 90 mL of conc. HCl and 12.70 g $SnCl_2 \cdot H_2O$ (56.3 mmol, 6.26 eq.) was added. The reaction mixture was stirred for 6 h at 70 °C. After that, the reaction was cooled to room temperature, and the grey precipitate was filtered off and stirred in 50 mL of an aqueous NaOH solution (10%) for 1 h at room temperature. Again, the solid was filtered off and washed with H_2O. After that, the crude product was dissolved in $CHCl_3$, at which insoluble components were separated by filtration. The solvent was removed under reduced pressure yielding the product as a yellow solid.[364] Yield: 1.32 g (4.1 mmol, 46%). $C_{21}H_{16}N_4$ (324.39 g/mol). ^{1}H NMR (300 MHz, DMSO-d_6) δ [ppm] = 8.73-8.64 (m, 6H), 7.86 (d, 2H), 7.79 (d, 2H), 7.34 (m, 2H), 6.81 (m, 2H), 5.56 (s, 2H).

Synthesis of 4'-(4-isothiocyanatophenyl)-2,2':6',2''-terpyridine



The reaction was performed under inert conditions. 0.30 g 4-Aminophenyl terpyridine (0.9 mmol, 1.00 eq.) and 0.38 mL Et_3N (2.8 mmol, 3.00 eq.) were dissolved in 50 mL of THF and 0.09 mL thiophosgene (85%, 0.9 mmol, 1.00 eq.) slowly added at 0 °C. The reaction mixture was stirred for 2 h at room temperature, which led to the formation of a brown suspension. The reaction was quenched by adding 100 mL of distilled H_2O and the product was extracted with Et_2O (3 x 100 mL). The organic phase was dried over Na_2SO_4, and the solvent was removed under reduced pressure. The product was obtained as a brownish solid. Yield: 0.27 g (0.7 mmol, 82%). $C_{22}H_{14}N_4S$ (366.44 g/mol).^{1}H NMR (300 MHz, $CDCl_3$) δ [ppm] = 8.71 (m, 6H), 7.91 (m, 4H), 7.38 (m, 4H). ^{13}C NMR (126 MHz, DMSO-d_6) δ [ppm] = 156.07, 155.92, 149.10, 148.76, 137.47, 137.07, 136.24, 131.98, 128.55, 126.31, 124.05, 121.45, 118.66.

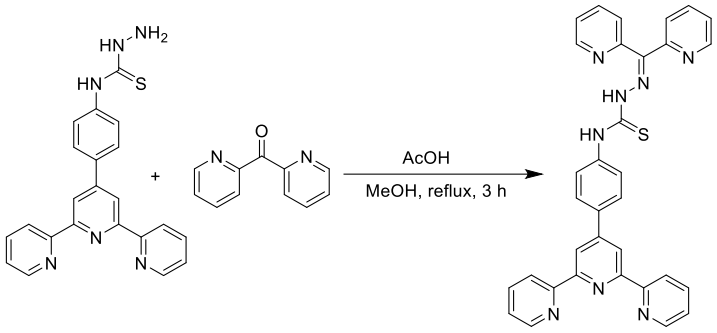
Synthesis of *N*-hydrazidecarbothio[4-([2,2':6',2''-terpyridin]-4'-yl)phenyl]amine



36.0 µL Hydrazine monohydrate (0.74 mmol, 1.00 eq.) was dissolved in 20 mL of EtOH and heated to reflux. After that, 0.27 g of the isothiocyanate (0.74 mmol, 1.00 eq.) was dissolved in 20 mL of EtOH and

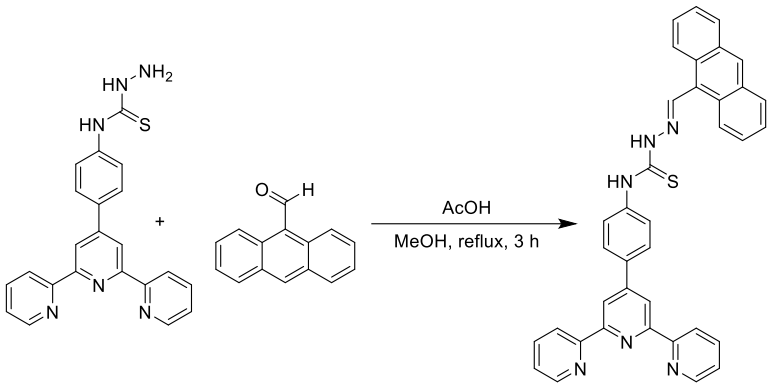
slowly added to the hydrazine solution over the course of 1 h. The reaction mixture was stirred for an additional 3 h, after that, the solvent was removed under reduced pressure. The product was obtained as a brownish solid. Yield: 0.30 g (0.74 mmol, quant.). $C_{22}H_{18}N_6S$ (398.49 g/mol). ^{1}H NMR (499 MHz, DMSO-d_6) δ [ppm] = 9.31 (s, 1H), 8.77 (d, J = 4.0 Hz, 1H), 8.71 (s, 2H), 8.67 (d, J = 7.9 Hz, 1H), 8.04 (td, J = 7.8, 1.7 Hz, 2H), 7.97 (m, 2H), 7.88 (d, J = 8.5 Hz, 2H), 7.53 (m, 2H), 4.93 (s, 2H). ^{13}C NMR (126 MHz, DMSO-d_6) δ [ppm] = 156.09, 155.50, 149.80, 149.50, 137.91, 127.10, 124.96, 121.40, 117.99. HR-ESI-MS (m/z) $[M+H]^+$ 399.1389, $[M+Na]^+$ 421.1209.

Synthesis of 4'-(4-([bis(pyridin-2-yl)methylideneaminocarbamthioyl]amino)phenyl)-2,2':6',2''-terpyridine



46.0 mg dipyridyl ketone (0.25 mmol, 1.00 eq.) and 100.0 mg of the thiosemicarbazide (0.25 mmol, 1.00 eq.) were dissolved in a minimum amount of MeOH and a few droplets of glacial AcOH were added. The reaction mixture was refluxed for 48 h. After that, the solvent was removed under reduced pressure yielding the product as a beige solid. Yield: 140.0 mg (0.25 mmol, quant.). $C_{33}H_{24}N_8S$ (564.67 g/mol). ^{1}H NMR (499 MHz, DMSO-d_6) δ [ppm] = 13.70 (s, 1H), 10.61 (s, 1H), 8.88 (d, J = 4.2 Hz, 1H), 8.78 (d, J = 4.5 Hz, 2H), 8.75 (s, 2H), 8.69 (d, J = 8.0 Hz, 2H), 8.61 (d, J = 5.5 Hz, 1H), 8.41 (d, J = 7.9 Hz, 1H), 8.08-7.97 (m, 6H), 7.89 (d, J = 8.6 Hz, 1H), 7.65-7.49 (m, 5H). ^{13}C NMR (126 MHz, DMSO-d_6) δ [ppm] = 156.13, 149.78, 148.78, 148.66, 140.58, 138.15, 137.67, 134.90, 127.84, 127.28, 126.56, 125.05, 124.74, 124.56, 121.48, 118.25. HR-ESI-MS (m/z) $[M+H]^+$ 565.1916, $[M+Na]^+$ 587.1736.

Synthesis of (*E*)-1-[(9-anthryl)methylene]-4-[*p*-(2,2':6',2''-terpyridin-4'-yl)phenyl]thiosemi-carbazide



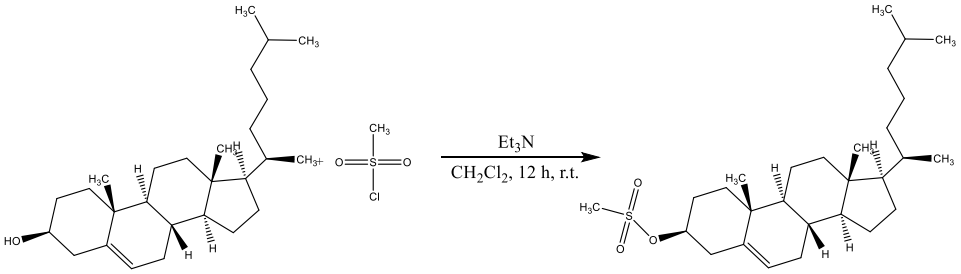
9-anthracenaldehyde (0.052 g, 0.25 mmol, 1.00 eq.) and the thiosemicarbazide (0.10 g, 0.25 mmol, 1.00 eq.) were dissolved in a minimum amount of MeOH and 10 drops of AcOH were added. The reaction mixture was refluxed overnight. The solvent was evaporated under reduced pressure, and the residue was purified with column chromatography (7% MeOH in CH_2Cl_2) yielding the product as an orange solid. Yield: 0.11 g, (0.19 mmol, 75%). $C_{37}H_{26}N_6S$ (586.71 g/mol). ^{1}H NMR (499 MHz, DMSO-d_6) δ [ppm] = 12.18 (s, 1H), 10.23 (s, 1H), 9.45 (s, 1H), 8.78 (m, 3H), 8.73 (s, 2H), 8.67 (d, J = 7.0 Hz, 2H), 8.61 (d, J = 7.2 Hz, 2H), 8.17 (d, J = 8.4 Hz, 2H), 8.05 (td, J = 7.8, 1.8 Hz, 2H), 7.92 (m, 4H), 7.68 (m, 2H), 7.62 (m, 2H), 7.54 (ddd, J = 7.5, 4.8, 1.1 Hz, 2H). ^{13}C NMR (126 MHz, DMSO-d_6) δ [ppm] = 176.25, 156.18, 155.48,

149.85, 149.48, 143.32, 140.91, 137.96, 134.27, 131.36, 130.20, 130.03, 129.45, 127.83, 127.15, 126.13, 125.95, 126.61, 125.34, 125.02, 121.44, 118.16. HR-ESI-MS (m/z) $[M+H]^+$ 587.2010, $[M+Na]^+$ 609.1830.

5.3.14 Synthesis of amphiphilic TSCs

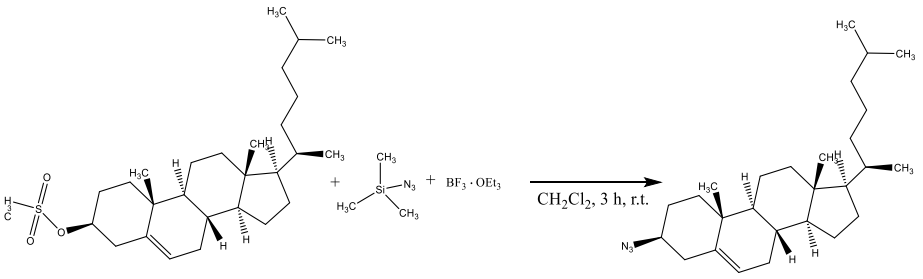
5.3.14.1 Synthesis of cholesterol derived TSCs

Synthesis of (1*S*,2*R*,5*S*,10*S*,11*S*,14*R*,15*R*)-14-[(1*R*)-1,5-dimethylhexyl]-5-(methanesulfonyloxy) -2,15-dimethyltetracyclo[8.7.0.0^{2,7}.0^{11,15}]heptadec-7-ene



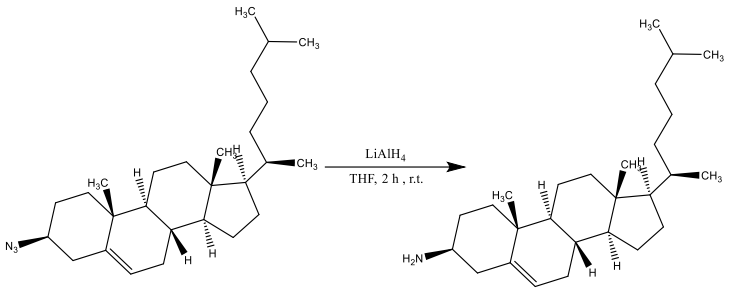
The reaction was performed under inert conditions. 5.00 g of cholesterol (13.0 mmol, 1.00 eq.) was dissolved in 50 mL of anhydrous CH_2Cl_2 and 2.70 mL of freshly distilled Et_3N (19.5 mmol, 1.50 eq.) was added. The mixture was cooled to 0 °C and a solution of 1.07 mL MsCl (13.7 mmol, 1.05 eq.) in 5 mL of anhydrous CH_2Cl_2 was added. The reaction was stirred 30 min at 0 °C and 12 h at room temperature. The solvent was removed under reduced pressure, and the residue was purified by recrystallisation from CH_2Cl_2/MeOH. The product was obtained as a colorless solid.[394] Yield: 5.62 g (12.1 mmol, 93%). $C_{28}H_{48}O_3S$ (464.75 g/mol). ^{1}H NMR (300 MHz, $CDCl_3$) δ [ppm] = 5.42 (s, 1H), 4.52 (m, 1H), 3.00 (s, 3H), 2.50 (m, 2H), 2.04-0.85 (m, 38H), 0.68 (s, 3H).

Synthesis of (1*S*,2*R*,5*S*,10*S*,11*S*,14*R*,15*R*)-5-azido-14-[(1*R*)-1,5-dimethylhexyl]-2,15-dimethyl tetracyclo [8.7.0.0^{2,7}.0^{11,15}]heptadec-7-ene



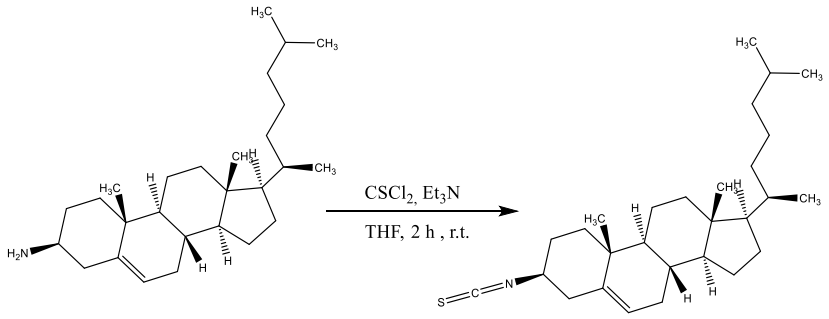
The reaction was performed under inert conditions. 5.59 g 3β-Methanesulfonyl-5-cholestene (12.0 mmol, 1.00 eq.) was dissolved in 150 mL of anhydrous CH_2Cl_2 and 1.76 mL $TMSN_3$ (13.2 mmol, 1.10 eq.) as well as 3.05 mL $BF_3{\cdot}OEt_2$ (24.1 mmol, 2.00 eq.) was added. The reaction was stirred for 3 h at room temperature. After that, the reaction mixture was poured into 25 mL of aqueous NaOH (2.0 M) and stirred for 5 min. The organic phase was separated, and the aqueous layer was extracted with 40 mL CH_2Cl_2. The combined organic phase was washed with 30 mL brine, dried over Na_2SO_4 and the solvent was removed under reduced pressure. The crude product was purified by column chromatography (n-hexane) yielding the product as a colorless solid.[394] Yield: 3.70 g (9.0 mmol, 75%). $C_{27}H_{45}N_3$ (411.68 g/mol). ^{1}H NMR (300 MHz, $CDCl_3$) δ [ppm] = 5.38 (m, 1H), 3.20 (m, 1H), 2.30 (m, 2H), 2.04-0.84 (m, 38H), 0.68 (s, 3H).

Synthesis of (1*S*,2*R*,5*S*,10*S*,11*S*,14*R*,15*R*)-14-[(1*R*)-1,5-dimethylhexyl]-2,15-dimethyltetracyclo [8.7.0.0^{2,7}.0^{11,15}]heptadec-7-en-5-ylamine



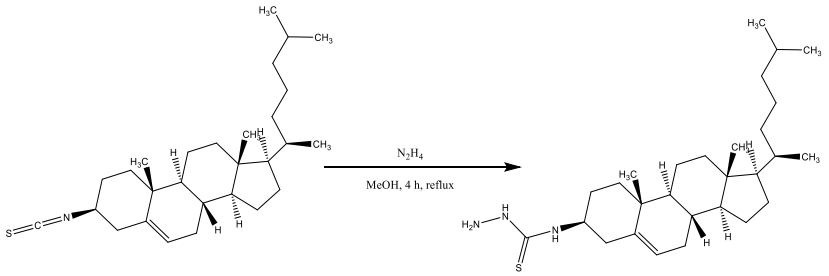
The reaction was performed under inert conditions. 0.70 g of the steroid (1.7 mmol, 1.00 eq.) was dissolved in 10 mL of anhydrous THF and a solution of 0.10 g $LiAlH_4$ (2.6 mmol, 1.50 eq.) in 5 mL THF was added dropwise. The reaction was stirred at room temperature for 2 h. After that, the reaction was cooled to 0 °C and quenched with 10 mL H_2O and 5 mL aqueous NaOH (1 M). The formed suspension was filtered over celite and washed with Et_2O. The filtrate was extracted with Et_2O (3 x 25 mL) and the combined organic phase was washed with 25 mL brine and dried over Na_2SO_4. The solvent was removed under reduced pressure yielding the product as a colorless solid.[394] Yield: 0.57 g (1.5 mmol, 88%). $C_{27}H_{47}N$ (385.68 g/mol). ^{1}H NMR (300 MHz, $CDCl_3$) δ [ppm] = 5.28 (m, 1H), 2.57 (m, 1H), 2.12 (m, 1H), 2.05-1.93 (m, 3H), 1.81-1.77 (m, 2H), 1.67 (m, 1H), 1.60-0.83 (m, 35H), 0.65 (s, 3H).

Synthesis of (1*S*,2*R*,5*S*,10*S*,11*S*,14*R*,15*R*)-14-[(1*R*)-1,5-dimethylhexyl]-5-isothiocyanato-2,15-dimethyl tetracyclo[8.7.0.0^{2,7}.0^{11,15}]heptadec-7-ene



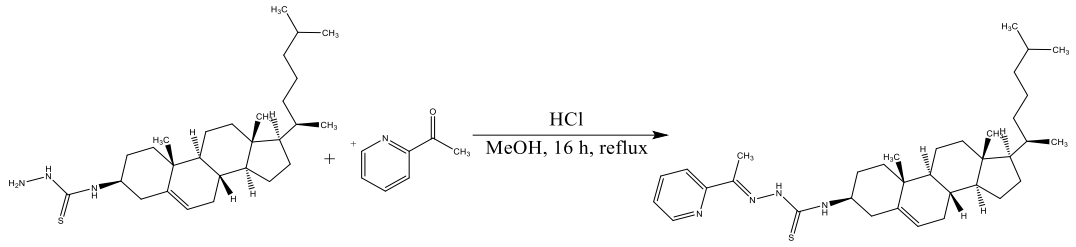
The reaction was performed under inert conditions. 0.10 g of the steroid (0.26 mmol, 1.00 eq.) and 0.11 mL Et_3N (0.78 mmol, 3.00 eq.) were dissolved in 5 mL of THF and 24 µL thiophosgene (0.26 mmol, 1.00 eq.) was added at 0 °C. The reaction mixture was stirred for 2 h at room temperature, which led to the formation of a brown suspension. The reaction was quenched by adding 20 mL of distilled H_2O and the product was extracted with Et_2O (3 x 20 mL). The organic phase was dried over Na_2SO_4, and the solvent was removed under reduced pressure. The product was obtained as a beige solid. Yield: 0.11 g (0.26 mmol, quant.). $C_{28}H_{45}NS$ (427.74 g/mol). ^{1}H NMR (300 MHz, $CDCl_3$) δ [ppm] = 5.39 (m, 1H), 3.42 (m, 1H), 2.41 (m, 1H), 1.99 (m, 3H), 1.85 (m, 3H), 1.58-0.86 (m, 40H), 0.67 (s, 3H). ^{13}C NMR (126 MHz, DMSO-*d*$_6$) δ [ppm] = 138.89, 123.37, 77.03, 56.82, 56.68, 56.14, 49.98, 42.30, 39.98, 39.67, 39.52, 37.25, 36.49, 36.18, 35.78, 31.73, 30.33, 30.02, 28.22, 28.02, 28.02, 24.26, 23.83, 22.83, 22.57, 20.93, 19.22, 18.72, 11.86.

Synthesis of *N*-hydrazidecarbothio[(1*S*,2*R*,5*S*,10*S*,11*S*,14*R*,15*R*)-14-[(1*R*)-1,5-dimethylhexyl]-2,15-dimethyltetracyclo[8.7.0.0^{2,7}.0^{11,15}]heptadec-7-en-5-yl]amine



11.3 µL Hydrazine monohydrate (0.23 mmol, 1.00 eq.) was dissolved in 10 mL of MeOH and heated to reflux. After that, 0.10 g of the isothiocyanate (0.23 mmol, 1.00 eq.) was dissolved in 20 mL of MeOH and slowly added to the hydrazine solution over the course of 1 h. The reaction mixture was stirred for an additional 3 h under reflux, after that, the solvent was removed under reduced pressure. The product was obtained as a colorless solid. Yield: 0.10 g (0.23 mmol, 1.00 eq.). $C_{28}H_{49}N_3S$ (459.78 g/mol). ^{1}H NMR (300 MHz, $CDCl_3$) δ [ppm] = 7.30 (s, 1H), 7.01 (s, 1H), 5.41 (m, 1H), 4.16 (m, 1H), 3.71 (s, 2H), 2.46 (m, 1H), 1.84, m, 3H), 1.58 (m, 2H), 1.49-0.86 (m, 36H), 0.68 (s, 3H). ^{13}C NMR (126 MHz, DMSO-*d*$_6$) δ [ppm] = 139.99, 122.26, 77.03, 56.69, 56.12, 54.04, 50.08, 42.31, 39.74, 39.53, 39.01, 37.75, 36.58, 36.19, 35.81, 31.89, 28.97, 28.25, 28.03, 24.30, 23.83, 22.84, 22.58, 20.99, 19.40, 18.73, 11.88. HR-ESI-MS (m/z) $[M+H]^+$ 460.3724.

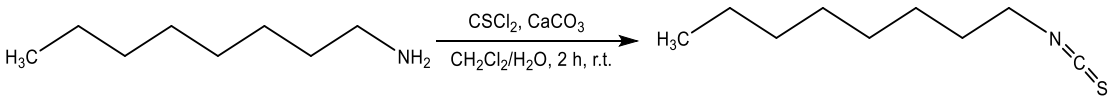
Synthesis of [(1*S*,2*R*,5*S*,10*S*,11*S*,14*R*,15*R*)-14-[(1*R*)-1,5-dimethylhexyl]-2,15-dimethyltetracyclo [8.7.0.0^{2,7}.0^{11,15}]heptadec-7-en-5-ylamino][(1*Z*)-1-(pyridin-2-yl)eth-1-ylideneamino]carbothioamide



34.0 µL 2-Acetylpyridine (0.30 mmol, 1.00 eq.) and 139.0 mg of the thiosemicarbazide (0.30 mmol, 1.00 eq.) were dissolved in 50 mL MeOH and a few droplets of conc. HCl were added. The reaction mixture was refluxed for 16 h. The solvent was removed under reduced pressure yielding the product as a colorless solid. Yield: 167.0 mg (0.30 mmol, quant.). $C_{35}H_{54}N_4S$ (562.90 g/mol). ^{1}H NMR (300 MHz, $CDCl_3$) δ [ppm] = 9.94 (s, 1H), 9.02 (s, 1H), 8.85 (m, 1H), 8.37 (m, 1H), 7.90 (d, *J* = 6.0 Hz, 1H, 7.79 (m, 1H), 5.37 (m, 1H), 4.39 (m, 1H), 2.95 (m, 1H), 2.39-0.85 (m, 42H), 0.69 (s, 3H). HR-ESI-MS (m/z) $[M+H]^+$ 563.4140, $[M+Na]^+$ 585.3959.

5.3.14.2 Synthesis of octyl, dodecyl and hexadecyl isothiocyanates

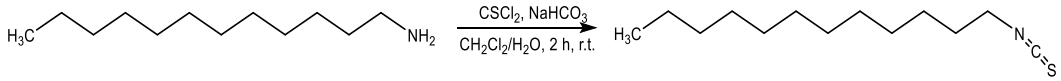
Synthesis of 1-isothiocyanatooctane



1.28 mL Octylamine (7.75 mmol, 1.00 eq.) was dissolved in 5 mL of CH_2Cl_2 and a solution of 4.65 g $CaCO_3$ (46.5 mmol, 6.00 eq.) in 25 mL of H_2O was added. The reaction mixture was cooled to 0 °C and 1.40 mL thiophosgene (1.95 eq., 15.10 mmol) was added dropwise. The reaction was stirred for 2 h at room temperature. After that, the organic layer was separated, and the aqueous phase was extracted

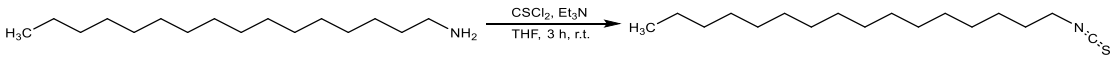
with CH_2Cl_2 (3 x 50mL). The combined organic phase was dried over $MgSO_4$ and the solvent was removed under reduced pressure yielding the product as a yellowish oil.[395] Yield: 1.23 g (7.2 mmol, 99%). $C_9H_{17}NS$ (171.31 g/mol). ^{1}H NMR (300 MHz, $CDCl_3$) δ [ppm] = 3.48 (t, *J* = 6.6 Hz, 2H), 1.67 (p, *J* = 6.7 Hz, 2H), 1.39 (m, 2H), 1.26 (m, 8H), 0.86 (m, 3H). ^{13}C NMR (126 MHz, $CDCl_3$) δ [ppm] = 129.49, 45.09, 31.71, 29.99, 29.07, 28.78, 26.56, 22.61, 14.07.

Synthesis of 1-isothiocyanatododecane



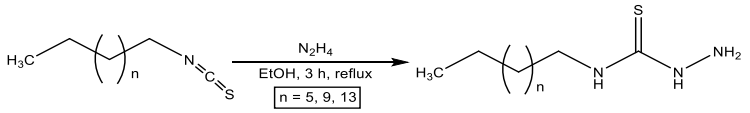
1.98 g Dodecylamine (10.8 mmol, 1.00 eq.) was dissolved in 5 mL of CH_2Cl_2 and 10 mL of a sat. aq. $NaHCO_3$ solution was added. The mixture was cooled to 0 °C and a solution of 1.07 mL thiophosgene (85%, 11.8 mmol, 1.10 eq.) in 5 mL of CH_2Cl_2 was added dropwise. The reaction was stirred for 2 h at room temperature. After that, the organic phase was separated and washed three times with 10 mL H_2O. The organic layer was dried over Na_2SO_4 and the solvent was removed under reduced pressure yielding the product as a yellowish oil.[396] Yield: 1.97 g (8.7 mmol, 81%). $C_{13}H_{25}NS$ (227.41 g/mol). ^{1}H NMR (300 MHz, $CDCl_3$) δ [ppm] = 3.52 (t, *J* = 6.6 Hz, 2H), 1.72 (p, *J* = 6.7 Hz, 2H), 1.42 (m, 2H), 1.28 (m, 16H), 0.89 (t, *J* = 6.6 Hz, 3H). ^{13}C NMR (126 MHz, $CDCl_3$) δ [ppm] = 129.54, 45.08, 31.92, 29.99, 29.62, 29.52, 29.41, 29.35, 28.83, 26.57, 22.70, 14.13.

Synthesis of 1-isothiocyanatohexadecane



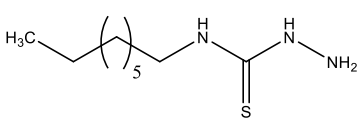
1.00 g Hexadecylamine (4.1 mmol, 1.00 eq.) and 1.72 mL Et_3N (12.4 mmol, 3.00 eq.) were dissolved in 10 mL of THF and 0.38 mL thiophosgene (85%, 4.1 mmol, 1.00 eq.) was slowly added at 0 °C. The reaction was stirred for 2 h at room temperature. After that, the reaction was quenched by adding 20 mL of distilled H_2O and the product was extracted with Et_2O (3 x 20 mL). The organic phase was dried over Na_2SO_4, and the solvent was removed under reduced pressure. The product was obtained as a beige solid. Yield: 1.15 g (4.1 mmol, quant.). $C_{17}H_{33}NS$ (283.52 g/mol). ^{1}H NMR (300 MHz, $CDCl_3$) δ [ppm] = 3.52 (t, *J* = 6.6 Hz, 2H), 1.71 (p, *J* = 6.7 Hz, 2H), 1.42 (m, 2H), 1.27 (m, 24H), 0.90 (m, 3H).

5.3.14.3 Synthesis of octyl, dodecyl and hexadecyl thiosemicarbazides – general procedure

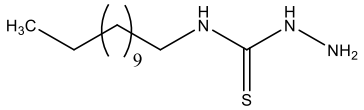


Hydrazine monohydrate (1.00 eq.) was dissolved in 20 mL EtOH and heated to reflux. After that the isothiocyanate (1.00 eq.) was dissolved in 20 mL EtOH and added dropwise to this solution. The mixture was refluxed for 3 h. After that, the solvent was removed under reduced pressure yielding the product in quantitative yield, which was used without further purification.

4-Octylthiosemicarbazide from 1.17 g 1-isothiocyanatohexadecane (4.1 mmol), 0.20 mL hydrazine hydrate (4.1 mmol). The product was obtained as a beige solid. Yield: 0.59 g (2.9 mmol, quant.). $C_9H_{21}N_3S$ (203.35 g/mol). ^{1}H NMR (300 MHz, $CDCl_3$) δ [ppm] = 7.64 (s, 1H), 7.44 (s, 1H), 3.77 (s, 2H), 3.61 (m, 2H), 1.63 (m, 2H), 1.29 (m, 10H), 0.89 (m, 3H). ^{13}C NMR (126 MHz, $CDCl_3$) δ [ppm] = 182.06, 60.42, 44.15, 31.80, 29.29, 29.22, 26.93, 22.65, 14.10.

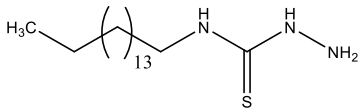


4-Dodecylthiosemicarbazide from 0.50 g 1-isothiocyanato-dodecane (2.2 mmol), 0.11 mL hydrazine hydrate (2.2 mmol). The product was obtained as a beige solid. Yield: 0.57 g (2.2 mmol, quant.). $C_{13}H_{29}N_3S$ (259.46 g/mol). ^{1}H NMR (300 MHz, $CDCl_3$) δ [ppm] = 7.43 (s, 1H), 6.99 (s, 1H), 3.74 (s, 2H), 3.65 (m, 2H), 1.62

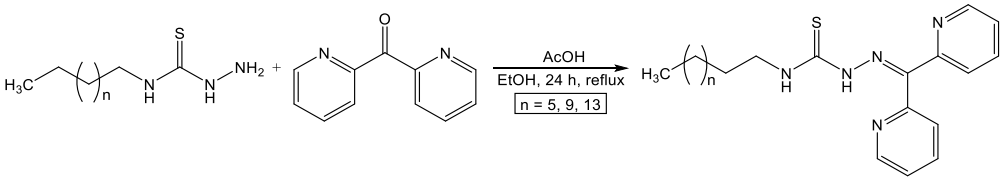


(m, 6H), 1.35 (m, 3H), 1.28 (m, 11H), 0.90 (m, 3H). ^{13}C NMR (126 MHz, $CDCl_3$) δ [ppm] = 182.40, 60.42, 44.24, 31.93, 29.66, 29.64, 29.60, 29.56, 29.36, 29.34, 29.28, 26.94, 22.70.

4-Hexadecylthiosemicarbazide from 0.50 g 1-isothiocyanato-octane (2.9 mmol), 0.14 mL hydrazine hydrate (2.9 mmol). The product was obtained as a beige solid. Yield: 1.30 g (4.1 mmol, quant.). $C_{17}H_{37}N_3S$ (315.56 g/mol). ^{1}H NMR (300 MHz, $CDCl_3$) δ [ppm] = 8.52 (s, 1H), 7.77 (s, 1H), 4.42 (s, 2H), 3.42 (q, *J* = 6.6 Hz, 2H), 1.48 (m, 2H), 1.24 (m, 25H), 0.86 (t, *J* = 7.1 Hz, 3H). ^{13}C NMR (126 MHz, $CDCl_3$) δ [ppm] = 181.43, 43.22, 31.77, 29.59, 29.53, 29.48, 29.32, 29.18, 26.83, 22.57, 14.42.

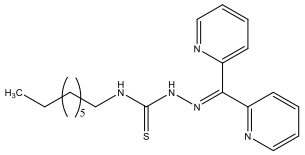


5.3.14.4 Synthesis of dipyridyl ketone TSCs – general procedure

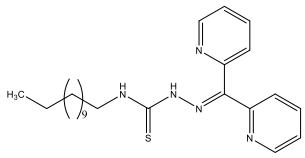


Di(2-pyridyl)ketone (1.00 eq.) and the thiosemicarbazide (1.00 eq.) were dissolved in 20 mL of EtOH. After that, a few droplets of glacial AcOH were added and the reaction mixture was refluxed for 24 h. The solvent was removed under reduced pressure, yielding the product in quantitative yields, without further purification.

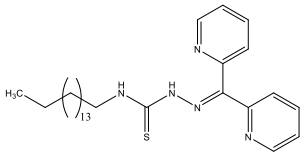
1-[Bis(2-pyridyl)methylene]-4-octylthiosemicarbazide from 0.15 g 4-octylthiosemicarbazide (0.7 mmol) and 0.14 g di(2-pyridyl)ketone (0.7 mmol). The product was obtained as a brown solid. Yield: 0.26 g (0.7 mmol, quant.). $C_{20}H_{27}N_5S$ (369.53 g/mol). ^{1}H NMR (300 MHz, $CDCl_3$) δ [ppm] = 13.13 (s, 1H), 8.88 (t, *J* = 5.9 Hz, 1H), 8.82 (d, *J* = 4.2 Hz, 1H), 8.58 (d, *J* = 5.4 Hz, 1H), 8.23 (d, *J* = 7.9 Hz, 1H), 7.98 (qd, *J* = 8.1, 1.7 Hz, 2H), 7.58 (m, 1H), 7.48 (m, 2H), 3.59 (q, *J* = 6.5 Hz, 2H), 1.61 (m, 2H), 1.25 (m, 10H), 0.85 (m, 3H).



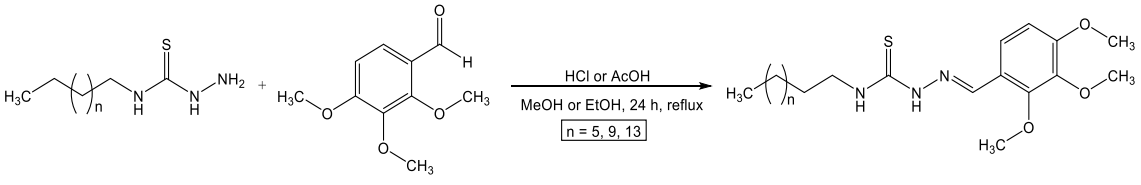
1-[Bis(2-pyridyl)methylene]-4-dodecylthiosemicarbazide from 0.15 g 4-dodecylthiosemicarbazide (0.6 mmol) and 0.11 g di(2-pyridyl)ketone (0.6 mmol). The product was obtained as a brown solid. Yield: 0.26 g (0.6 mmol, quant.). $C_{24}H_{35}N_5S$ (425.64 g/mol). ^{1}H NMR (300 MHz, $CDCl_3$) δ [ppm] = 13.15 (s, 1H), 8.87 (t, *J* = 5.8 Hz, 1H), 8.82 (d, *J* = 4.8 Hz, 1H), 8.57 (d, *J* = 4.6 Hz, 1H), 8.23 (d, *J* = 7.9 Hz, 1H), 7.97 (qd, *J* = 8.3, 1.6 Hz, 2H), 7.57 (m, 1H), 7.49 (m, 2H), 3.58 (m, 2H), 1.60 (m, 2H), 1.23 (m, 18H), 0.84 (m, 3H).



1-[Bis(2-pyridyl)methylene]-4-hexadecylthiosemicarbazide from 0.15 g 4-hexadecylthiosemicarbazide (0.5 mmol) and 0.09 g di(2-pyridyl)ketone (0.5 mmol). The product was obtained as a brown solid. Yield: 0.24 g (0.5 mmol, quant.). $C_{28}H_{43}N_5S$ (481.75 g/mol). ^{1}H NMR (300 MHz, $CDCl_3$) δ [ppm] = 13.14 (s, 1H), 8.87 (t, *J* = 5.9 Hz, 1H), 8.82 (d, *J* = 6.4 Hz, 1H), 8.57 (d, *J* = 4.8 Hz, 1H), 7.97 (qd, *J* = 7.9, 1.8 Hz, 2H), 7.58 (m, 1H), 7.49 (m, 2H), 3.58 (q, *J* = 6.4 Hz, 2H), 1.60 (m, 2H), 1.22 (m, 26H), 0.85 (m, 3H).

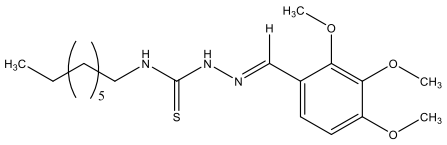


5.3.14.5 Synthesis of 2,3,4-trimethoxybenzaldehyde TSCs – general procedure

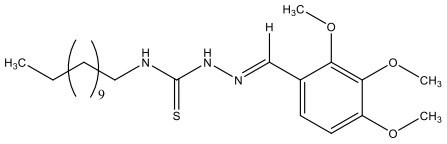


2,3,4-Trimethoxybenzaldehyde (1.00 eq.) and the thiosemicarbazide (1.00 eq.) were dissolved in 40 mL of MeOH or EtOH. After that, a few droplets of conc. HCl or glacial AcOH were added and the reaction mixture was refluxed for 24-48 h. The solvent was removed under reduced pressure, and the product was purified by column chromatography.

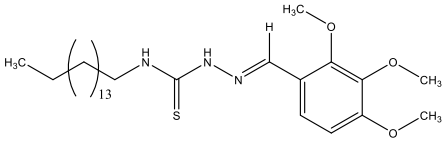
(*E*)-4-Octyl-1-[(2,3,4-trimethoxyphenyl)methylene]thiosemicarbazide from 100.0 mg 4-octyl-thiosemicarbazide (0.50 mmol), 98.0 mg 2,3,4-trimethoxybenzaldehyde (0.50 mmol) and conc. HCl. The reaction was refluxed 48 h and purified by column chromatography (4:1 c-hexane/EtOAc). The product was obtained as a beige solid. Yield: 105.0 mg (0.3 mmol, 60%). $C_{19}H_{31}N_3O_3S$ (381.54 g/mol). ^{1}H NMR (300 MHz, DMSO-d_6) δ [ppm] = 11.29 (s, 1H), 8.40 (t, *J* = 5.8 Hz, 1H), 8.27 (s, 1H), 7.82 (d, *J* = 8.9 Hz, 1H), 6.87 (d, *J* = 8.9 Hz, 1H), 3.85 (s, 3H), 3.79 (s, 3H), 3.76 (s, 3H), 3.53 (m, 2H), 1.58 (m, 2H), 1.29 (m, 10H), 0.86 (m, 3H). HR-ESI-MS (m/z) $[M+H]^+$ 382.2161, $[M+Na]^+$ 404.1980.



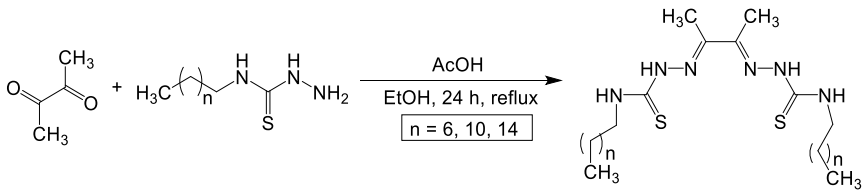
(*E*)-4-Dodecyl-1-[(2,3,4-trimethoxyphenyl)methylene]-thiosemicarbazide from 100.0 mg 4-dodecyl-thiosemicarbazide (0.40 mmol), 80.0 mg 2,3,4-trimethoxybenzaldehyde (0.40 mmol) and conc. HCl. The reaction was refluxed 48 h and purified by column chromatography (4:1 c-hexane/EtOAc). The product was obtained as a beige solid. Yield: 84.0 mg (0.2 mmol, 50%). $C_{23}H_{39}N_3O_3S$ (437.64 g/mol). ^{1}H NMR (300 MHz, DMSO-d_6) δ [ppm] = 11.28 (s, 1H), 8.40 (t, *J* = 5.5 Hz, 1H), 8.26 (s, 1H), 7.82 (d, *J* = 8.9 Hz, 1H), 6.87 (d, *J* = 8.9 Hz, 1H), 3.84 (s, 3H), 3.79 (s, 3H), 3.76 (s, 3H), 3.53 (q, *J* = 6.5 Hz, 2H), 1.57 (m, 2H), 1.24 (m, 18H), 0.85 (m, 3H). ^{13}C NMR (126 MHz, DMSO-d_6) δ [ppm] = 177.06, 155.37, 153.12, 142.00, 138.26, 121.48, 120.92, 109.00, 62.28, 60.95, 56.51, 43.89, 31.77, 29.53, 29.49, 29.47, 29.34, 29.27, 29.19, 26.80, 22.57, 14.43. HR-ESI-MS (m/z) $[M+H]^+$ 438.2785, $[M+Na]^+$ 460.2606.



(*E*)-4-Hexadecyl-1-[(2,3,4-trimethoxyphenyl)methylene]-thiosemicarbazide from 150.0 mg 4-hexadecyl-thiosemicarbazide (0.48 mmol), 93.0 mg 2,3,4-trimethoxybenzaldehyde (0.48 mmol) and glacial AcOH. The reaction was refluxed 24 h and purified by column chromatography (5:1 c-hexane/EtOAc). The product was obtained as a beige solid. Yield: 121.0 mg (0.24 mmol, 51%). $C_{27}H_{47}N_3O_3S$ (493.75 g/mol). ^{1}H NMR (300 MHz, DMSO-d_6) δ [ppm] = 11.29 (s, 1H), 8.39 (t, *J* = 5.6 Hz, 1H), 8.27 (s, 1H), 7.82 (d, *J* = 8.9 Hz, 1H), 6.87 (d, *J* = 8.9 Hz, 1H), 3.84 (s, 3H), 3.79 (s, 3H), 3.76 (s, 3H), 3.53 (q, *J* = 6.3 Hz, 2H), 1.57 (m, 2H), 1.23 (m, 26H), 0.85 (m, 3H). ^{13}C NMR (126 MHz, DMSO-d_6) δ [ppm] = 177.07, 155.38, 153.13, 142.01, 138.26, 121.48, 120.92, 108.99, 62.26, 60.94, 56.50, 43.89, 31.76, 29.52, 29.18, 26.81, 22.56, 14.41.

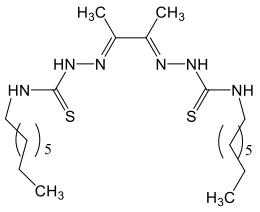


5.3.14.6 Synthesis of 2,3-butadione bis-TSCs – general procedure

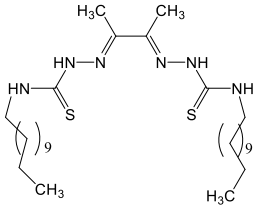


2,3-Butadione (1.00 eq.) and the thiosemicarbazide (2.00 eq.) were dissolved in a minimum amount of EtOH or MeOH. After that, a few droplets of glacial AcOH were added and the reaction mixture was refluxed for 24 h. The mixture was cooled to 0 °C and the formed precipitate was filtered off and washed with cold EtOH, yielding the product as a colorless solid.

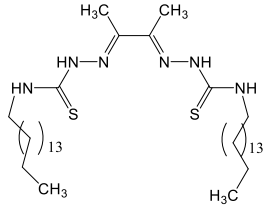
(*E*)-1-[1-Methyl-2-(4-octylthiosemicarbazidoidene)propylidene]-4-octylthiosemi-carbazide from 0.20 g 4-octylthiosemicarbazide (1.0 mmol) and 42.0 µL 2,3-butadione (0.5 mmol) in MeOH. The product was obtained as a colorless solid. Yield: 0.17 g (0.4 mmol, 75%). $C_{22}H_{44}N_6S_2$ (456.76 g/mol). ^{1}H NMR (300 MHz, $CDCl_3$) δ [ppm] = 8.70 (s, 2H), 7.46 (m, 2H), 3.73 (q, *J* = 6.9 Hz, 4H), 2.14 (s, 6H), 1.68 (m, 4H), 1.30 (m, 20H), 0.90 (m, 6H).



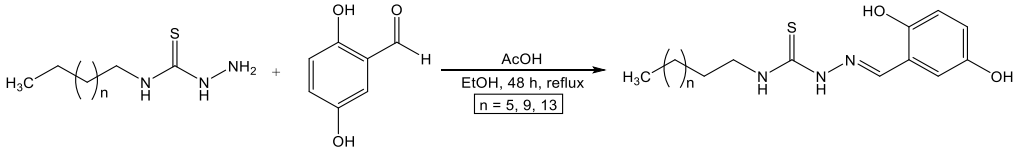
(*E*)-1-[1-Methyl-2-(4-dodecylthiosemicarbazidoidene)propylidene]-4-dodecylthio-semicarbazide from 0.30 g 4-dodecyllthiosemicarbazide (1.2 mmol) and 50.0 µL 2,3-butadione (0.6 mmol) in EtOH. The product was obtained as a colorless solid. Yield: 0.27 g (0.5 mmol, 79%). $C_{30}H_{60}N_6S_2$ (568.97 g/mol). ^{1}H NMR (300 MHz, $CDCl_3$) δ [ppm] = 8.70 (s, 2H), 7.46 (t, *J* = 5.5 Hz, 2H), 3.73 (q, *J* = 6.7 Hz, 4H), 2.15 (s, 6H), 1.70 (m, 4H), 1.35 (m, 36H), 0.90 (m, 6H).



(*E*)-1-[1-Methyl-2-(4-hexadecylthiosemicarbazidoidene)propylidene]-4-hexadecyl-thiosemicarbazide from 0.30 g 4-hexadecylthiosemicarbazide (1.0 mmol) and 41.0 µL 2,3-butadione (0.5 mmol) in EtOH. The product was obtained as a colorless solid. Yield: 0.30 g (0.4 mmol, 88%). $C_{38}H_{76}N_6S_2$ (681.19 g/mol). ^{1}H NMR (300 MHz, $CDCl_3$) δ [ppm] = 8.66 (s, 2H), 7.46 (m, 2H), 3.72 (m, 4H), 2.14 (s, 6H), 1.72 (m, 4H), 1.28 (m, 52H), 0.90 (m, 6H).

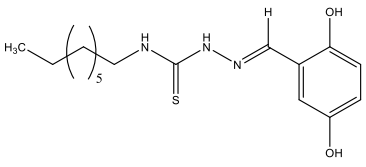


5.3.14.7 Synthesis of 2,5-dihydroxybenzaldehyde TSCs – general procedure

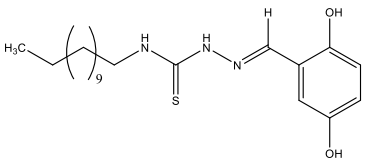


2,5-Dihydroxybenzaldehyde (1.00 eq.) and the thiosemicarbazide (1.00 eq.) were dissolved in 20 mL of EtOH. After that, a few droplets of glacial AcOH were added and the reaction mixture was refluxed for 48 h. The solvent was removed under reduced pressure, and the product was purified by column chromatography or directly obtained in quantitative yields.

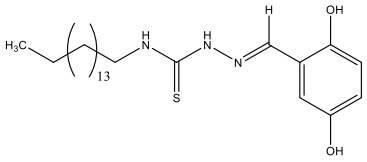
2-[(*E*)-(4-Octylthiosemicarbazidoidene)methyl]hydroquinone from 100.0 mg 4-octylthiosemi-carbazide (0.5 mmol) and 69.0 mg 2,5-dihydroxybenzaldehyde (0.5 mmol). The product was purified by column chromatography (95:5 CH_2Cl_2/MeOH) and obtained as a colorless solid. Yield: 83.0 mg (0.3 mmol, 51%). $C_{16}H_{25}N_3O_2S$ (323.46 g/mol). ^{1}H NMR (300 MHz, $CDCl_3$) δ [ppm] = 11.30 (s, 1H), 9.22 (s, 1H), 8.82 (s, 1H), 8.37 (t, *J* = 5.2 Hz, 1H), 8.29 (s, 1H), 7.26 (s, 1H), 6.68 (s, 2H), 3.52 (q, *J* = 6.2 Hz, 2H), 1.57 (m, 2H), 1.29 (m, 10H), 0.86 (m, 3H). ^{13}C NMR (126 MHz, DMSO-d_6) δ [ppm] = 150.37, 149.94, 121.20, 119.04, 117.20, 60.23, 43.93, 31.73, 29.36, 29.27, 29.13, 26.84, 22.57, 14.44. HR-ESI-MS (m/z) $[M+H]^+$ 324.1746.



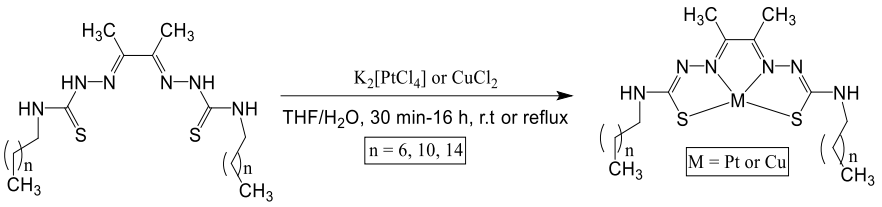
2-[(*E*)-(4-Dodecylthiosemicarbazidoidene)methyl]hydroquinone from 100.0 mg 4-dodecylthio-semicarbazide (0.4 mmol) and 55.0 mg 2,5-dihydroxybenzaldehyde (0.4 mmol). The product was obtained as a colorless solid. Yield: 150.0 mg (0.4 mmol, quant.). $C_{20}H_{33}N_3O_2S$ (379.56 g/mol). ^{1}H NMR (300 MHz, $CDCl_3$) δ [ppm] = 11.29 (s, 1H), 9.19 (s, 1H), 8.81 (s, 1H), 8.35 (t, *J* = 5.6 Hz, 1H), 8.29 (s, 1H), 7.25 (s, 1H), 6.68 (s, 2H), 3.52 (q, *J* = 6.5 Hz, 2H), 1.56 (m, 2H), 1.24 (m, 18H), 0.85 (m, 3H). ^{13}C NMR (126 MHz, DMSO-d_6) δ [ppm] = 177.07, 150.38, 149.91, 140.04, 121.21, 119.04, 117.19, 112.32, 60.22, 43.93, 31.78, 29.50, 29.20, 26.83, 22.58, 14.43.



2-[(*E*)-(4-Hexadecylthiosemicarbazidoidene)methyl]-hydroquinone from 200.0 mg 4-hexadecylthiosemicarbazide (0.8 mmol) and 110.0 mg 2,5-dihydroxybenzaldehyde (0.8 mmol). The product was purified by column chromatography (95:5 CH_2Cl_2/MeOH) and obtained as a colorless solid. Yield: 141.0 mg (0.3 mmol, 40%). $C_{24}H_{41}N_3O_2S$ (435.67 g/mol). ^{1}H NMR (300 MHz, $CDCl_3$) δ [ppm] = 11.29 (s, 1H), 9.18 (s, 1H), 8.80 (s, 1H), 8.38 (m, 1H), 8.29 (s, 1H), 7.26 (s, 1H), 6.68 (s, 2H), 3.54 (q, *J* = 6.5 Hz, 2H), 1.58 (m, 2H), 1.24 (m, 26H), 0.85 (m, 3H). ^{13}C NMR (126 MHz, DMSO-d_6) δ [ppm] = 150.38, 194.90, 121.22, 119.04, 117.19, 31.77, 29.51, 29.18, 26.83, 22.56, 14.43.

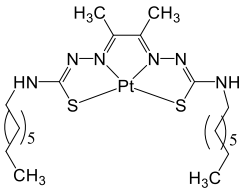


5.3.14.8 Synthesis of Pt(II) and Cu(II) bis-TSC complexes

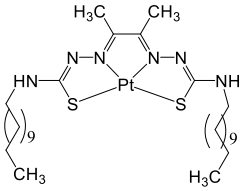


The bis-TSCs (1.00 eq.) was dissolved in 20-30 mL of THF and a solution of $K_2[PtCl_4]$ or $CuCl_2$ (1.00 eq.) in 2-3 mL of H_2O was added dropwise. The reaction mixture was refluxed for 30 min or stirred at room temperature for 4-16 h. The solvent was removed under reduced pressure and the residue was washed with ca. 50 mL of H_2O and ca. 20 mL of Et_2O. The product was dried under ambient conditions, yielding the respective metal complexes.

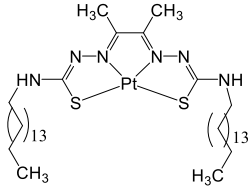
[Pt(Octyl-bisthiosemicarbazone)] from 50.0 mg (*E*)-1-[1-Methyl-2-(4-octylthiosemi-carbazidoidene)-propylidene]-4-octylthiosemi-carbazide (0.110 mmol) and 46.0 mg $K_2[PtCl_4]$ (0.110 mmol). The reaction was stirred at room temperature for 16 h. The product was obtained as a green solid. Yield: 60.0 mg (0.091 mmol, 83%). $C_{22}H_{42}N_6PtS_2$ (649.82 g/mol). ^{1}H NMR (300 MHz, $CDCl_3$) δ [ppm] = 5.12 (s, 2H), 3.50 (m, 4H), 2.02 (s, 6H), 1.56 (m, 4H), 1.30 (m, 20H), 0.90 (m, 6H). HR-ESI-MS (m/z) $[M+H]^+$ 649.2612, $[M+Na]^+$ 671.2431.



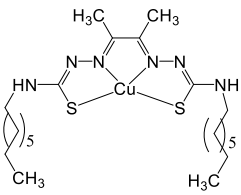
[Pt(Dodecyl-bisthiosemicarbazone)] from 50.0 mg (*E*)-1-[1-Methyl-2-(4-dodecylthiosemicarbazido-idene)propylidene]-4-octylthiosemi-carbazide (0.090 mmol) and 37.0 mg $K_2[PtCl_4]$ (0.090 mmol). The reaction was stirred at room temperature for 4 h. The product was obtained as a green solid. Yield: 53.0 mg (0.069 mmol, 77%). $C_{30}H_{58}N_6PtS_2$ (762.04 g/mol). ^{1}H NMR (300 MHz, $CDCl_3$) δ [ppm] = 5.15 (s, 2H), 3.50 (q, *J* = 6.4 Hz, 4H), 2.92 (s, 6H), 1.60 (m, 4H), 1.28 (m, 36H), 0.90 (m, 6H). HR-ESI-MS (m/z) $[M+H]^+$ 761.3864, $[M+Na]^+$ 783.3683.



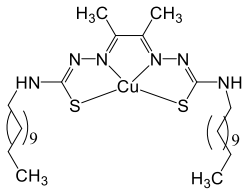
[Pt(Hexadecyl-bisthiosemicarbazone)] from 50.0 mg (*E*)-1-[1-Methyl-2-(4-hexadecylthiosemi-carbazidoidene)propylidene]-4-octylthiosemi-carbazide (0.070 mmol) and 30.5 mg $K_2[PtCl_4]$ (0.070 mmol). The reaction was refluxed for 30 min. The product was obtained as a green solid. Yield: 49.8 mg (0.057 mmol, 81%). $C_{38}H_{74}N_6PtS_2$ (874.26 g/mol). ^{1}H NMR (300 MHz, $CDCl_3$) δ [ppm] = 5.11 (s, 2H), 3.48 (q, *J* = 6.8 Hz, 4H), 2.00 (s, 6H), 1.55 (m, 4H), 1.25 (m, 52H), 0.88 (m, 6H). HR-ESI-MS (m/z) $[M+Na]^+$ 895.4935.



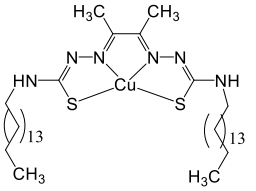
[Cu(Octyl-bisthiosemicarbazone)] from 50.0 mg (*E*)-1-[1-Methyl-2-(4-octylthiosemi-carbazidoidene)-propylidene]-4-octylthiosemi-carbazide (0.110 mmol) and 15.0 mg $CuCl_2$ (0.110 mmol). The reaction was stirred at room temperature for 4 h. The product was obtained as a brown solid. Yield: 47.0 mg (0.090 mmol, 82%). $C_{22}H_{42}N_6CuS_2$ (518.29 g/mol). HR-ESI-MS (m/z) $[M+H]^+$ 518.2269, $[M+Na]^+$ 540.2093.



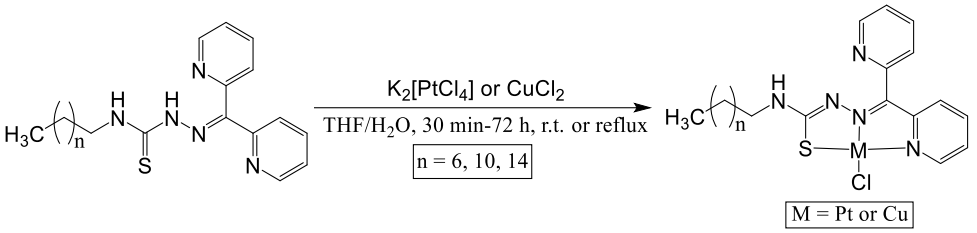
[Cu(Dodecyl-bisthiosemicarbazone)] from 30.0 mg (*E*)-1-[1-Methyl-2-(4-dodecylthiosemi-carbazidoidene)propylidene]-4-octylthiosemi-carbazide (0.050 mmol) and 7.0 mg $CuCl_2$ (0.050 mmol). The reaction was stirred at room temperature for 16 h. The product was obtained as a brown solid. Yield: 23.9 mg (0.038 mmol, 77%). $C_{38}H_{74}N_6CuS_2$ (630.50 g/mol). HR-ESI-MS (m/z) $[M+H]^+$ 630.3522, $[M+Na]^+$ 652.3351.



[Cu(Hexadecyl-bisthiosemicarbazone)] from 50.0 mg (*E*)-1-[1-Methyl-2-(4-hexadecyl-thiosemicarbazido-idene)propylidene]-4-octylthiosemi-carbazide (0.070 mmol) and 10.0 mg $CuCl_2$ (0.070 mmol). The reaction was refluxed for 30 min. The product was obtained as a brown solid. Yield: 47.5 mg (0.064 mmol, 91%). $C_{38}H_{74}N_6CuS_2$ (742.72 g/mol). HR-ESI-MS (m/z) $[M+H]^+$ 742.4776, $[M+Na]^+$ 764.4594.

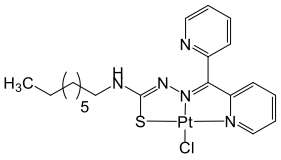


5.3.14.9 Synthesis of Pt(II) and Cu(II) dipyridyl ketone TSC complexes

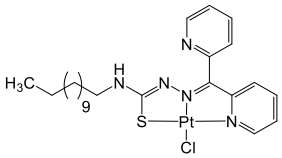


The thiosemicarbazide (1.00 eq.) was dissolved in 20 mL of THF. After that, a solution of $CuCl_2$ or $K_2[PtCl_4]$ in 5 mL H_2O was added dropwise. The reaction was stirred at room temperature for 5-72 h or under reflux for 30 min. After that, the solvent was removed under reduced pressure, and the residue was washed with 50 mL of H_2O and 20 mL of n-hexane. The solid was redissolved in acetone to separate insoluble components, and the solvent was removed under reduced pressure yielding the respective metal complexes.

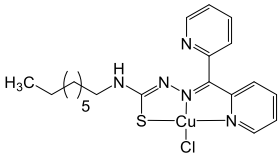
[Pt(Octyl-Dipy-TSC)] from 50.0 mg 1-[Bis(2-pyridyl)methylene]-4-octylthiosemicarbazide (0.14 mmol) and 58.0 mg $K_2[PtCl_4]$ (0.14 mmol). The reaction was refluxed for 30 min. The product was obtained as a red solid. Yield: 69.0 mg (0.11 mmol, 82%). $C_{20}H_{26}ClPtN_5S$ (599.06 g/mol). ^1H NMR (300 MHz, $CDCl_3$) δ [ppm] = 9.09 (s, 1H), 8.78 (m, 1H), 7.90-2.39 (m, 8H), 3.37 (m, 2H), 1.37 (m, 2H), 1.27 (m, 10H), 0.91 (m, 3H). HR-ESI-MS (m/z) $[M+H]^+$ 598.1301, $[M+Na]^+$ 620.1119.



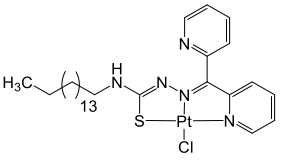
[Pt(Dodecyl-Dipy-TSC)] from 50.0 mg 1-[Bis(2-pyridyl)methylene]-4-dodecylthiosemicarbazide (0.12 mmol) and 50.0 mg $K_2[PtCl_4]$ (0.12 mmol). The reaction was refluxed for 30 min. The product was obtained as a red solid. Yield: 54.3 mg (0.08 mmol, 69%). $C_{24}H_{34}ClPtN_5S$ (655.17 g/mol). ^1H NMR (300 MHz, $CDCl_3$) δ [ppm] = 9.10 (s, 1H), 8.73 (m, 1H), 8.20-7.27 (m, 6H), 3.33 (m, 2H), 1.20 (m, 20H), 0.89 (m, 3H). HR-ESI-MS (m/z) $[M+H]^+$ 654.1929, $[M+Na]^+$ 676.1745.



[Pt(Hexadecyl-Dipy-TSC)] from 50.0 mg 1-[Bis(2-pyridyl)methylene]-4-hexadecylthiosemicarbazide (0.10 mmol) and 43.0 mg $K_2[PtCl_4]$ (0.10 mmol). The reaction was stirred at room temperature for 72 h. The product was obtained as a red solid. Yield: 50.0 mg (0.07 mmol, 70%). $C_{28}H_{42}ClPtN_5S$ (711.27 g/mol). ^1H NMR (300 MHz, $CDCl_3$) δ 8.85 (t, *J* = 5.9 Hz, 1H), 8.80 (d, *J* = 6.4 Hz, 1H), 8.52 (d, *J* = 4.8 Hz, 1H), 7.90 (qd, *J* = 7.9, 1.8 Hz, 2H), 7.56 (m, 1H), 7.49 (m, 2H), 3.58 (q, *J* = 6.4 Hz, 2H), 1.60 (m, 2H), 1.22 (m, 27H), 0.85 (m, 3H). HR-ESI-MS (m/z) $[M+H]^+$ 710.2555, $[M+Na]^+$ 732.2377.

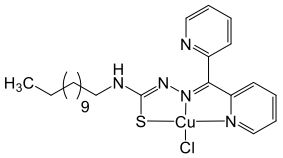


[Cu(Octyl-Dipy-TSC)] from 50.0 mg 1-[Bis(2-pyridyl)methylene]-4-octylthiosemicarbazide (0.14 mmol) and 18.0 mg $CuCl_2$ (0.14 mmol). The reaction was stirred at room temperature for 5 h. The product was obtained

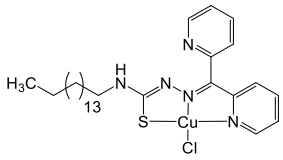


as a brown solid. Yield: 53.0 mg (0.11 mmol, 81%). $C_{20}H_{26}ClCuN_5S$ (467.52 g/mol). HR-ESI-MS (m/z) $[M+H]^+$ 467.0966, $[M+Na]^+$ 489.0786, $[M–Cl]^+$ 431.1199.

[Cu(Dodecyl-Dipy-TSC)] from 50.0 mg 1-[Bis(2-pyridyl)methylene]-4-dodecylthiosemi-carbazide (0.12 mmol) and 16.0 mg $CuCl_2$ (0.12 mmol). The reaction was stirred at room temperature for 5 h. The product was obtained as a brown solid. Yield: 41.9 mg (0.08 mmol, 65%). $C_{24}H_{34}ClCuN_5S$ (523.63 g/mol). HR-ESI-MS (m/z) $[M+H]^+$ 523.1590, $[M+Na]^+$ 545.1410, $[M–Cl]^+$ 487.1822.



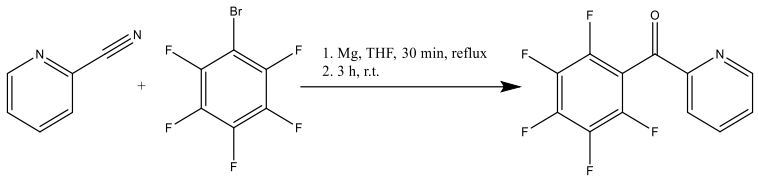
[Cu(Hexadecyl-Dipy-TSC)] from 50.0 mg 1-[Bis(2-pyridyl)methylene]-4-hexadecylthiosemicarbazide (0.100 mmol) and 14.0 mg $CuCl_2$ (0.100 mmol). The reaction was stirred at room temperature for 72 h. The product was obtained as a brown solid. Yield: 41.7 mg (0.072 mmol, 72%). $C_{28}H_{42}ClCuN_5S$ (579.74 g/mol). HR-ESI-MS (m/z) $[M+H]^+$ 579.2217, $[M+Na]^+$ 601.2039, $[M–Cl]^+$ 543.2450.



5.3.15 Synthesis of pyridyl ketones and their corresponding TSCs and their Fe(III) complexes

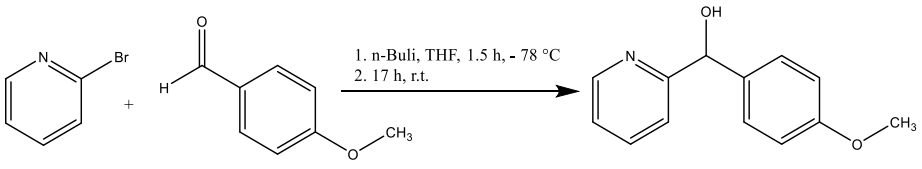
5.3.15.1 Synthesis of pyridyl ketones

Synthesis of pentafluorophenyl(pyridin-2-yl)methanone



The reaction was performed under inert conditions. 2.15 mL Bromopentafluorobenze (17.3 mmol, 1.20 eq.) was dissolved in 30 mL of anhydrous THF and added to a suspension of 1.40 g magnesium turnings (67.6 mmol, 4.00 eq.) in 10 mL of THF at 70 °C. The reaction was refluxed for 30 min, leading to the formation of the *Grignard* reagent. The solution was cooled to room temperature and slowly added into a solution of 1.50 g 2-cyanopyridine (14.4 mmol, 1.00 eq.) in 20 mL of THF at 0 °C. The reaction was stirred for 3 h at room temperature and quenched by the addition of 100 mL of sat. NH_4Cl solution. The organic layer was separated, and the aqueous phase was extracted with CH_2Cl_2 (2 x 100 mL). The combined organic phase was evaporated to dryness, and the residue was redissolved into 300 mL Et_2O. After that, 60 mL of 6 M HCl was added, and the mixture was stirred for 30 min at room temperature. The organic phase was separated, and the aqueous phase was basified by the addition of sat. $NaHCO_3$ solution. The aqueous phase was extracted with CH_2Cl_2 (3 x 100 mL) and the combined organic phase was dried over Na_2SO_4 and evaporated under reduced pressure. The crude product was purified by column chromatography (2:1 C-Hex/EtOAc -> 1:1 C-Hex/EtOAc -> EtOAc). The product was obtained as a colorless solid. Yield: 1.60 g (5.8 mmol, 33%). $C_{12}H_4F_5NO$ (273.16 g/mol). ^1H NMR (300 MHz, $CDCl_3$) δ [ppm] = 8.66 (m, 1H), 8.19 (d, *J* = 7.8 Hz, 1H), 7.94 (td, *J* = 7.7, 1.7 Hz, 1H), 7.56 (ddd, *J* = 7.6, 4.7, 1.2 Hz, 1H). HR-ESI-MS: m/z $[M+H]^+$ = 274.0285, m/z $[M+Na]^+$ = 296.0105.

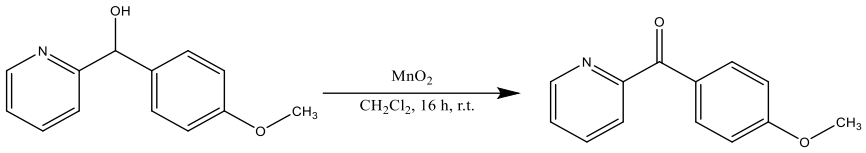
Synthesis of α-(4-methoxyphenyl)-2-pyridinemethanol



The reaction was performed under inert conditions. 31.25 mL n-Buli (1.6 M, 50.0 mmol, 1.10 eq.) was added dropwise to a solution of 4.24 mL 2-bromopyridine (43.5 mmol, 1.00 eq.) in 45 mL of anhydrous

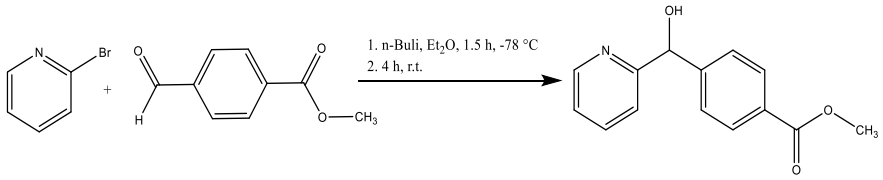
THF at – 78 °C. The reaction was stirred for 1,5 h at – 78 °C, after that, 5.65 mL 4-methoxybenzaldehyde (46.5 mmol, 1.10 eq.) was added. The reaction was stirred for 17 h at room temperature, followed by quenching with 30 mL H_2O. The reaction mixture was extracted with EtOAc (4 x 30 mL) and the combined organic phase was dried over Na_2SO_4 and the solvent was removed under reduced pressure. The product was obtained as a colorless solid.[397] Yield: 5.15 g (23.9 mmol, 55%). $C_{13}H_{13}NO_2$ (215.25 g/mol). ^{1}H NMR (300 MHz, $CDCl_3$) δ [ppm] = 8.58 (d, *J* = 4.8 Hz, 1H), 7.63 (td, *J* = 7.7 Hz, 1.7 Hz, 1H), 7.36-7.26 (m, 2H), 7.21 (dd, *J* = 7.0, 5.0 Hz, 1H), 7.15 (d, *J* = 7.9 Hz, 1H), 6.97-6.79 (m, 2H), 5.73 (s, 1H), 5.22 (s, 1H), 3.81 (s, 3H).

Synthesis of (4-methoxyphenyl)(pyridin-2-yl)methanone



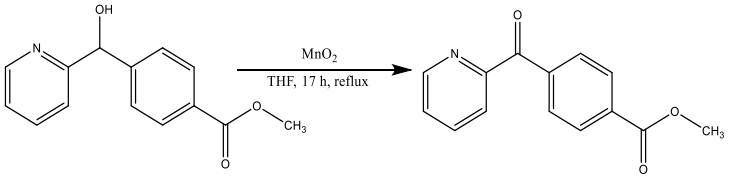
2.00 g α-(4-Methoxyphenyl)-2-pyridinemethanol (9.3 mmol, 1.00 eq.) was dissolved in 50 mL of CH_2Cl_2 and 3.31 g MnO_2 (38.1 mmol, 4.10 eq.) was added. The reaction mixture was stirred at room temperature for 16 h. The suspension was filtered over celite, and the precipitate was washed with CH_2Cl_2. The filtrate was evaporated, and the residue was purified by column chromatography (3:1 n-hexane/EtOAc), yielding the product as a colorless solid.[397] Yield: 0.45 g (2.1 mmol, 23%). $C_{13}H_{11}NO_2$ (213.24 g/mol). ^{1}H NMR (300 MHz, $CDCl_3$) δ [ppm] = 8.73 (ddd, *J* = 4.8, 1.6, 0.9 Hz, 1H), 8.20-8.10 (m, 2H), 8.01 (dt, *J* = 7.8, 1.0 Hz, 1H), 7.90 (td, *J* = 7.7, 1.7 Hz, 1H), 7.48 (ddd, *J* = 7.5, 4.8, 1.3 Hz, 1H), 7.06-6.93 (m, 2H), 3.90 (s, 3H).

Synthesis of methyl 4-[hydroxy(pyridin-2-yl)methyl]benzene-1-carboxylate



The reaction was performed under inert conditions. 1.76 mL 2-Bromopyridine (18.0 mmol, 1.00 eq.) was dissolved in 200 mL of anhydrous Et_2O and 15.60 mL n-Buli (1.6 M, 25.0 mmol, 1.39 eq.) was slowly added over the period of 1 h at –78 °C. The reaction was stirred for 30 min at –78 °C and a solution of 4.10 g methyl 4-formylbenzoate (25.0 mmol, 1.39 eq.) in 50 mL of anhydrous Et_2O was added dropwise. The reaction was stirred for 2 h at –78 °C and for an additional 2 h at room temperature. After that, the reaction was quenched by the addition of 70 mL brine and 30 mL H_2O and the organic layer was separated. The aqueous phase was extracted with CH_2Cl_2 (3 x 150 mL) and the combined organic phase was dried over $MgSO_4$ and evaporated under reduced pressure. The crude product was recrystallized from MeOH, yielding the product as a colorless solid. Yield: 1.36 g (5.6 mmol, 30%), $C_{14}H_{13}NO_3$ (243.26 g/mol). ^{1}H NMR (300 MHz, $CDCl_3$) δ [ppm] = 8.56 (d, *J* = 4.7 Hz, 1H), 8.01 (d, *J* = 8.3 Hz, 2H), 7.63 (td, *J* = 7.7, 1.7 Hz, 1H), 7.48 (d, *J* = 8.2 Hz, 2H), 7.23-7.13 (m, 2H), 5.81 (s, 1H), 5.44 (s, 1H), 3.90 (s, 3H).

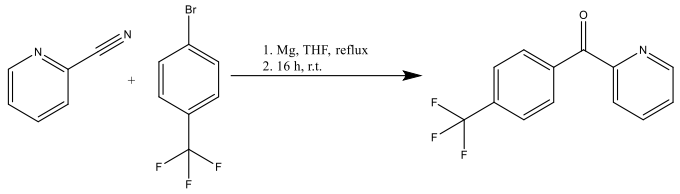
Synthesis of methyl 4-[(pyridin-2-yl)methanoyl]benzene-1-carboxylate



1.36 g 4-(Hydroxy-2-pyridinylmethyl)benzoate (5.6 mmol, 1.00 eq.) and 5.44 g activated MnO_2 (62.6 mmol, 11.18 eq.) were suspended in 70 mL of THF, and the reaction was refluxed for 17 h. After

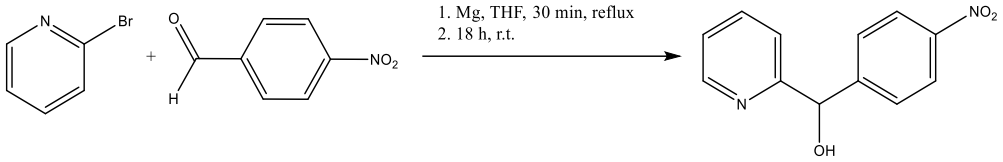
that, the reaction mixture was filtered over celite, and the precipitate was washed with 50 mL THF. The filtrate was evaporated under reduced pressure, and the crude product was purified by column chromatography (4:1 c-hexane/EtOAc).[397] Yield: 0.70 g (2.9 mmol, 52%). $C_{14}H_{11}NO_3$ (241.25 g/mol). ^{1}H NMR (300 MHz, $CDCl_3$) δ [ppm] = 8.74 (d, *J* = 6.4 Hz, 1H), 8.17-8.09 (m, 5H), 7.93 (td, *J* = 7.7, 1.7 Hz, 1H), 7.52 (ddd, *J* = 7.6, 4.8, 1.2 Hz, 1H), 3.96 (s, 3H).

Synthesis of (pyridin-2-yl)[4-(trifluoromethyl)phenyl]methanone



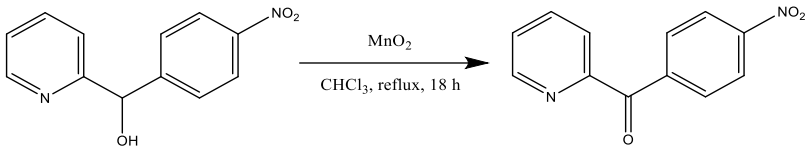
The reaction was performed under inert conditions. 3.40 mL 4-Brombenzotrifluorid (24.0 mmol, 1.20 eq.) was dissolved in 30 mL of anhydrous THF and added to a suspension of 2.32 g magnesium turnings (96.0 mmol, 4.00 eq.) in 10 mL of THF at 70 °C. The reaction was refluxed for 30 min, leading to the formation of the *Grignard* reagent. The solution was cooled to room temperature and slowly added into a solution of 2.00 mL 2-cyanopyridine (20.0 mmol, 1.00 eq.) in 20 mL of THF at 0 °C. The reaction was stirred for 16 h at room temperature and quenched by the addition of 100 mL of sat. NH_4Cl solution. The organic layer was separated, and the aqueous phase was extracted with CH_2Cl_2 (2 x 100 mL). The combined organic phase was evaporated to dryness, and the residue was redissolved into 300 mL Et_2O. After that, 60 mL of 6 M HCl was added, and the mixture was stirred for 30 min at room temperature. The organic phase was separated, and the aqueous phase was basified by the addition of sat. $NaHCO_3$ solution. The aqueous phase was extracted with CH_2Cl_2 (3 x 100 mL) and the combined organic phase was dried over Na_2SO_4 and evaporated under reduced pressure. The residue was purified by column chromatography (8:1 -> 5:1 -> 3:1 c-hexane/EtOAc) yielding the product as a colorless solid.[398] Yield: 2.60 g (10.3 mmol, 52%), $C_{13}H_8F_3NO_2$ (251.21 g/mol). ^{1}H NMR (300 MHz, $CDCl_3$) δ [ppm] = 8.73 (ddd, *J* = 4.7, 1.5, 0.8 Hz, 1H), 8.21-8.12 (m, 3H), 7.94 (td, *J* = 7.7, 1.7 Hz, 1H), 7.75 (d, *J* = 8.2 Hz, 2H), 7.53 (ddd, *J* = 7.6, 4.8, 1.2 Hz, 1H).

Synthesis of (4-nitrophenyl)(pyridin-2-yl)methanol



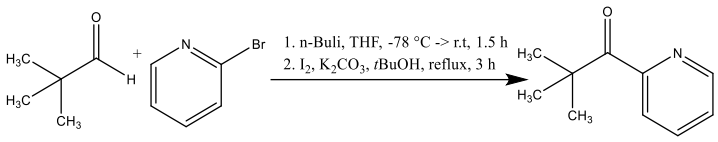
The reaction was performed under inert conditions. 3.00 g Mg powder (123.0 mmol, 4.10 eq.) was suspended in 20 mL of anhydrous THF and a solution of 2.90 mL 2-bromopyridine (30.0 mmol, 1.20 eq.) in 30 mL THF was added dropwise at 70 °C. The reaction was refluxed for 30 min, and the formed *Grignard* solution was added dropwise to a solution of 3.60 g 4-nitrobenzaldehyde (25.0 mmol, 1.00 eq.) in 30 mL THF at 0 °C. The reaction was stirred for 18 h at room temperature. After that, the solvent was removed under reduced pressure, and the residue was redissolved in $CHCl_3$. The organic phase was washed with 30 mL of a saturated NH_4Cl solution and two times with 30 mL H_2O. After drying over Na_2SO_4, the solvent was removed under reduced pressure, and the crude product was purified by column chromatography (3:1 -> 2:1 n-hexane/EtOAc). The product was obtained as a colorless solid.[324] Yield: 2.48 g (10.8 mmol, 48%). $C_{12}H_{10}N_2O_3$ (230.22 g/mol). ^{1}H NMR (300 MHz, $CDCl_3$) δ [ppm] = 8.59 (d, *J* = 4.8 Hz, 1H), 8.27-8.11 (m, 2H), 7.68 (td, *J* = 7.7, 1.7 Hz, 1H), 7.65-7.53 (m, 2H), 7.28-7.18 (m, 2H), 5.87 (s, 1H), 5.44 (s, 1H).

Synthesis of (4-nitrophenyl)(pyridin-2-yl)methanone



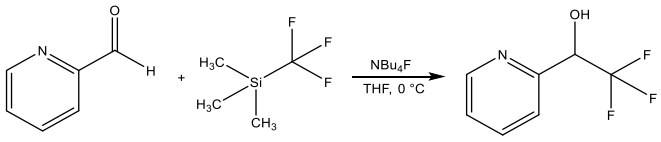
6.00 g activated MnO_2 (69.0 mmol, 5.00 eq.) and 2.00 g α-(4-nitrophenyl)-2-pyridinemethanol (8.7 mmol, 1.00 eq.) were dissolved in 80 mL $CHCl_3$ and refluxed for 48 h. The reaction was cooled to room temperature, filtered over celite and the precipitate was washed with $CHCl_3$ (3 x 30 mL). The filtrate was evaporated under reduced pressure, and the residue was purified by column chromatography (3:1 c-hexane/EtOAc). The product was obtained as a colorless solid.[397] Yield: 1.40 g (70%). $C_{12}H_8N_2O_3$ (6.1 mmol, 228.21 g/mol). ^{1}H NMR (300 MHz, $CDCl_3$) δ [ppm] = 8.73 (m, 1H), 8.36-8.21 (m, 4H), 8.18 (d, *J* = 7.9 Hz, 1H), 7.96 (t, *J* = 7.6 Hz, 1H), 7.56 (m, 1H). HR-ESI-MS: m/z $[M+H]^+$ = 229.0608, m/z $[M+Na]^+$ = 251.0429.

Synthesis of 2,2-dimethyl-1-(pyridin-2-yl)propan-1-one



The reaction was performed under inert conditions. 2.00 g 2-bromopyridine (12.7 mmol, 1.00 eq.) was dissolved in 30 mL of anhydrous THF and 8.73 mL n-Buli (1.6 M, 14.0 mmol, 1.10 eq.) was slowly added at –78 °C over the course of 30 min. The mixture was stirred at –78 °C for 30 min, after that, 1.44 mL pivaaldehyde (13.3 mmol, 1.05 eq.) was added. The reaction was stirred for 1 h at room temperature. The solvent was removed under reduced pressure, and the residue was redissolved in 25 mL *t*BuOH. After that, 5.15 g I_2 (20.3 mmol, 1.60 eq.) and 5.26 g K_2CO_3 (38.1 mmol, 3.00 eq.) were added, and the reaction was refluxed for 3 h. 50 mL of saturated Na_2SO_3 was added to the reaction and the phases were separated. The aqueous phase was extracted with $CHCl_3$ (3 x 100 mL) and the combined organic phase was dried over Na_2SO_4 and evaporated to dryness. The residue was purified by column chromatography (1:3 n-hexane/$CHCl_3$). The product was obtained as a brownish oil.[325] Yield: 1.00 g (6.1 mmol, 48%). $C_{10}H_{13}NO$ (163.22 g/mol). ^{1}H NMR (300 MHz, $CDCl_3$) δ [ppm] = 8.61 (d, *J* = 3.1 Hz, 1H), 7.90 (d, *J* = 7.8 Hz, 1H), 7.78 (m, 1H), 7.37 (m, 1H), 1.45 (s, 9H).

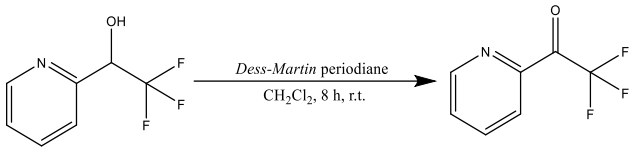
Synthesis of 2,2,2-trifluoro-1-(pyridin-2-yl)ethan-1-ol



The reaction was performed under inert conditions. 2.85 mL 2-pyridinecarboxyaldehyde (30.0 mmol, 1.00 eq.) was dissolved in 60 mL of anhydrous THF and 5.31 mL trifluoromethyltrimetylsilane (36.0 mmol, 1.20 eq.) and 1.50 mL NBu_4F (1 M in THF, 1.5 mmol, 0.05 eq.) were added dropwise at 0 °C. The reaction was stirred for 1 h at 0 °C and 16 h at room temperature. After that, 20 mL of 1 M HCl was added and the reaction was stirred 2 h at room temperature. The mixture was basified to pH 8 using 1 M aqueous NaOH and the product was extracted with EtOAc (4 x 50 mL). The combined organic phase was dried over Na_2SO_4 and the solvent was removed under reduced pressure. The crude product was purified by column chromatography (1:3, EtOAc/n-hexane). The product was obtained as a colorless solid.[326] Yield: 1.00 g (5.6 mmol, 56%). $C_7H_6F_3NO$ (177.12 g/mol). ^{1}H NMR (300 MHz, $CDCl_3$) δ [ppm] =

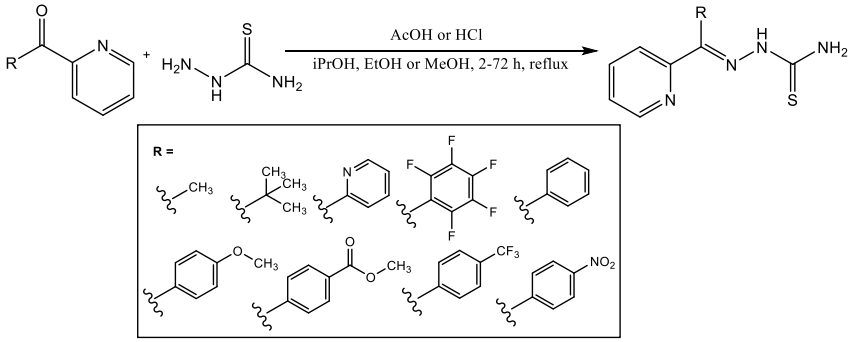
8.65 (d, *J* = 4.8 Hz, 1H), 7.81 (td, *J* = 7.7, 1.7 Hz, 1H), 7.47-7.38 (m, 2H), 5.52 (d, *J* = 6.8 Hz, 1H), 5.05 (p, *J* = 6.6 Hz, 1H).

Synthesis of 2,2,2-trifluoro-1-(pyridin-2-yl)ethan-1-one



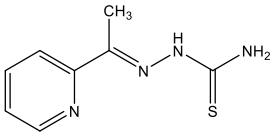
1.27 g 2,2,2-Trifluoro-1-(pyridin-2-yl)ethanol (7.2 mmol, 1.00 eq.) was dissolved in 50 mL CH_2Cl_2 and 3.66 g *Dess-Martin* periodiane (8.6 mmol, 1.20 eq.) was carefully added. The reaction was stirred for 8 h at room temperature. After that, the solvent was removed under reduced pressure and the residue was purified by column chromatography (1:3 EtOAc/n-hexane), followed by recrystallisation from CH_2Cl_2/n-hexane. The product was obtained as a colorless solid.[326] Yield: 0.48 g (2.7 mmol, 38%). $C_7H_4F_3NO$ (175.11 g/mol). ^{1}H NMR (300 MHz, $CDCl_3$) δ [ppm] = 8.62-8.54 (m, 1H), 7.93-7.85 (m, 1H), 7.83-7.77 (m, 1H), 7.48-7.42 (m, 1H).

5.3.15.2 Synthesis of TSCs – general approach

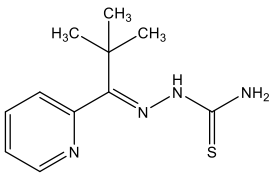


Thiosemicarbazide (1.00 eq.) and the pyridyl ketone (1.00 eq.) were dissolved in MeOH, *i*PrOH, EtOH or EtOH/H_2O. After that, a few drops of glacial AcOH or conc. HCl were added. The reaction was refluxed for 2-72 h. After that, the reaction was cooled to room temperature. The mixture was cooled down to 0 °C and the product was separated by filtration, or the solvent was removed under reduced pressure, and the product was purified by column chromatography.

(*E*)-1-[1-(2-Pyridyl)ethylidene]thiosemicarbazide from 0.64 g thiosemicarbazide (7.0 mmol) and 0.85 g 2-acetylpyridine (7.0 mmol). The educts were dissolved in *i*PrOH, a few drops of glacial AcOH were added and the mixture was refluxed for 5 h. The mixture was cooled to 0 °C, the product was separated by filtration and washed with n-hexane. The product was obtained as a colorless solid. Yield: 1.11 g (5.7 mmol, 82%). $C_6H_{10}N_4S$ (194.26 g/mol). ^{1}H NMR (300 MHz, $CDCl_3$) δ [ppm] = 10.30 (s, 1H), 8.57 (ddd, *J* = 4.8,1.8,0.9 Hz, 1H), 8.43 (d, *J* = 8.1 Hz, 2H), 8.13 (s, 1H), 7.78 (ddd, *J* = 8.1, 7.5, 1.8 Hz, 1H), 7.38 (ddd, *J* = 7.4, 4.8, 1.1 Hz, 1H), 2.38 (s, 3H).

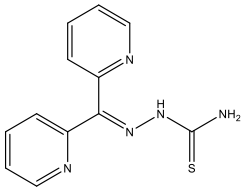


(*E*)-1-[2,2-Dimethyl-1-(2-pyridyl)propylidene]thiosemicarbazide from 0.34 g thiosemicarbazide (3.7 mmol) and 0.60 g trimethyl-2-pyridylketone (3.7 mmol). The educts were dissolved in MeOH, a few drops of glacial AcOH were added and the mixture was refluxed for 16 h. The solvent was removed under reduced pressure, yielding the product as a colorless solid. Yield: 0.88 g (3.7 mmol, quant.). $C_{11}H_{16}N_4S$ (236.34 g/mol). ^{1}H NMR (300 MHz, $CDCl_3$) δ [ppm] = 8.78 – 8.71 (m, 1H), 8.66 (s, 1H), 8.45 (s, 1H), 7.98 (td, *J* = 7.8, 1.8 Hz, 1H), 7.72 (s, 1H), 7.50 (ddd, *J* = 7.7, 4.9, 1.2 Hz, 1H), 7.40 (dt, *J* = 7.9, 1.1 Hz, 1H), 1.16 (s, 9H). ^{13}C NMR (126 MHz, DMSO-d_6) δ [ppm] =

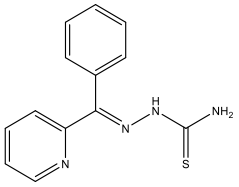


178.74, 158.36, 151.98, 150.65, 137.93, 124.66, 124.27, 38.31, 28.97. HR-ESI-MS: m/z $[M+H]^+$ = 237.1167, m/z $[M+Na]^+$ = 262.2378.

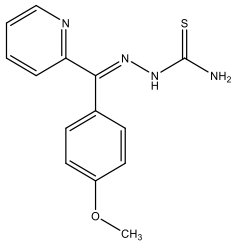
1-[Bis(2-pyridyl)methylene]thiosemicarbazide from 0.15 g thiosemicarbazide (1.62 mmol) and 0.30 g di-2-pyridyl ketone (1.62 mmol). The educts were dissolved in EtOH/H_2O (1:1), a few drops of glacial AcOH were added and the mixture was refluxed for 5 h. The mixture was cooled to 0 °C, the product was separated by filtration and washed with cold EtOH and Et_2O. The product was obtained as a yellow solid. Yield: 0.31 g (1.2 mmol, 75%). $C_{12}H_{11}N_5S$ (257.32 g/mol). ^{1}H NMR (300 MHz, $CDCl_3$) δ [ppm] = 12.97 (s, 1H), 8.83 (ddd, *J* = 4.9, 1.7, 0.9 Hz, 1H), 8.73 (s, 1H), 8.56 (ddd, *J* = 4.8, 1.7, 0.9 Hz, 1H), 8.35 (s, 1H), 8.30 (dt, *J* = 7.9, 0.9 Hz, 1H), 8.02-7.89 (m, 2H), 7.61-7.44 (m, 3H).



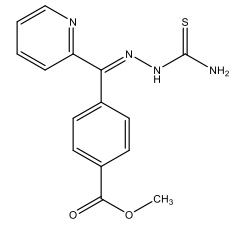
(*E*)-1-[Phenyl(2-pyridyl)methylene]thiosemicarbazide from 0.46 g thiosemicarbazide (5.0 mmol) and 0.92 g phenyl 3-pyridyl ketone (5.0 mmol). The educts were dissolved in EtOH, a few drops of glacial AcOH were added, and the mixture was refluxed for 5 h. The solvent was removed under reduced pressure and the product was purified by column chromatography (3:1 c-hexane/EtOAc -> EtOAc). The product was obtained as a colorless solid. Yield: 1.10 g (4.3 mmol, 86%). $C_{13}H_{12}N_4S$ (256.33 g/mol). ^{1}H NMR (300 MHz, DMSO-d_6) δ [ppm] = 12.53 (s, 1H), 8.87 (d, *J* = 4.7 Hz, 1H), 8.61 (s, 1H), 8.16 (s, 1H), 8.03 (td, *J* = 7.9, 1.7 Hz, 1H), 7.64 (m, 3H), 7.46 (m, 3H), 7.37 (d, *J* = 8.0 Hz, 1H).



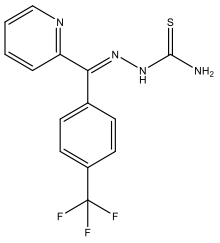
(*E*)-1-[(*p*-Methoxyphenyl)(2-pyridyl)methylene]thiosemicarbazide from 0.13 g thiosemicarbazide (1.4 mmol) and 0.30 g (4-methoxyphenyl)(pyridin-2-yl)methanone (1.4 mmol). The educts were dissolved in EtOH, a few drops of glacial AcOH were added and the mixture was refluxed for 72 h. The solvent was removed under reduced pressure and the product was purified by column chromatography (1:1 c-hexane/EtOAc). The product was obtained as a colorless solid. Yield: 0.12 g (0.4 mmol, 30%). $C_{14}H_{14}N_4OS$ (286.35 g/mol). ^{1}H NMR (300 MHz, DMSO-d_6) δ [ppm] = 12.11 (s, 1H), 8.86 (d, *J* = 4.6 Hz, 1H), 8.56 (s, 1H), 8.16 (s, 1H), 8.02 (m, 1H), 7.60 (s, *J* = 8.8 Hz, 3H), 7.39 (d, *J* = 8.0 Hz, 1H), 6.98 (d, *J* = 8.8 Hz, 2H), 3.81 (s, 3H). HR-ESI-MS: m/z $[M+H]^+$ = 287.0963, m/z $[M+Na]^+$ = 309.0784.



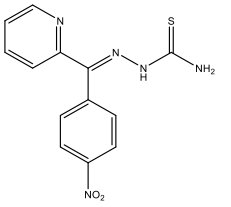
Methyl *p*-[(*E*)-(2-pyridyl)thiosemicarbazidoidenemethyl]benzoate from 0.11 g thiosemicarbazide (1.2 mmol) and 0.30 g methyl 4-[(pyridin-2-yl)methanoyl]benzene-1-carboxylate (1.2 mmol). The educts were dissolved in MeOH, a few drops of glacial AcOH were added and the mixture was refluxed for 6 h. The solvent was removed under reduced pressure, and the product was purified by column chromatography (3:1 c-hexane/EtOAc). The product was obtained as a colorless solid. Yield: 0.30 g (0.9 mmol, 77%). $C_{15}H_{14}N_4O_2S$ (314.26 g/mol). ^{1}H NMR (300 MHz, DMSO-d_6) δ [ppm] = 12.52 (s, 1H), 8.88 (m, 1H), 8.70 (s, 1H), 8.30 (m, 1H), 7.99 (d, *J* = 7.0 Hz, 2H), 7.83 (d, *J* = 7.5 Hz, 2H), 7.63 (m, 1H), 7.48 (m, 1H), 7.40 (m, 1H), 3.89 (s, 3H). HR-ESI-MS: m/z $[M+H]^+$ = 315.0913, m/z $[M+Na]^+$ = 337.0734.



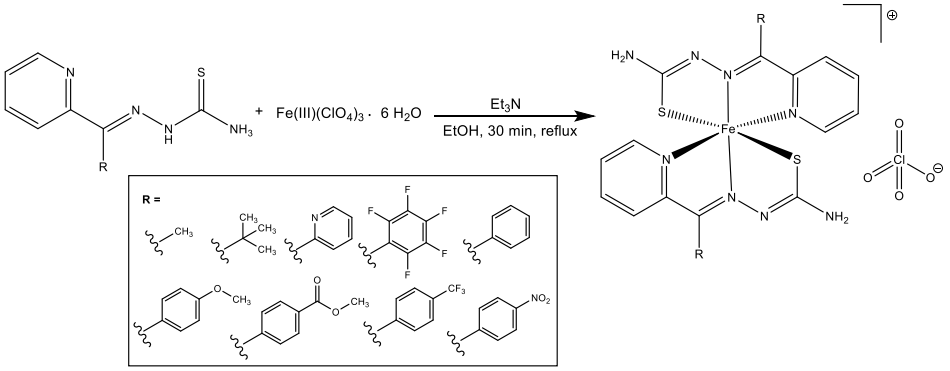
(*E*)-1-[(2-Pyridyl)[*p*-(trifluoromethyl)phenyl]methylene]thiosemicarbazide from 0.11 g thiosemicarbazide (1.2 mmol) and 0.30 g 2-pyridinyl[4-(trifluoromethyl) phenyl] methanone (1.2 mmol). The educts were dissolved in MeOH, a few drops of glacial AcOH were added and the mixture was refluxed for 8 h. The solvent was removed under reduced pressure, and the product was purified by column chromatography (3:1 -> 2:1 -> 1:1 c-hexane/EtOAc -> EtOAc). The product was obtained as a colorless solid. Yield: 0.13 g (0.4 mmol, 33%). $C_{14}H_{11}F_3N_4S$ (324.33 g/mol). ^{1}H NMR (300 MHz, DMSO-d_6) δ [ppm] = 12.73 (s, 1H), 8.89 (d, *J* = 4.6 Hz, 1H), 8.70 (s, 1H), 8.30 (s, 1H), 8.03 (td, *J* = 8.2, 1.7 Hz, 1H), 7.90 (d, *J* = 8.0 Hz, 2H), 7.79 (d, *J* = 8.3 Hz, 2H), 7.63 (dd, *J* = 7.3, 5.1 Hz, 1H), 7.41 (d, *J* = 8.1 Hz, 1H). HR-ESI-MS: m/z $[M+H]^+$ = 325.0729, m/z $[M+Na]^+$ = 347.0554.



(*E*)-1-[(*p*-Nitrophenyl)(2-pyridyl)methylene]thiosemicarbazide from 0.12 g thiosemicarbazide (1.3 mmol) and 0.30 g (4-nitrophenyl)(pyridin-2-yl)methanone (1.3 mmol). The educts were dissolved in MeOH, a few drops of glacial AcOH were added and the mixture was refluxed for 6 h. The mixture was cooled to 5 °C for 16 h and the product was separated by filtration and washed with Et_2O. The product was obtained as a yellow solid. Yield: 0.40 g (1.3 mmol, quant.). $C_{13}H_{11}N_5O_2S$ (301.32 g/mol). ^{1}H NMR (300 MHz, DMSO-d_6) δ [ppm] = 12.59 (s, 1H), 8.89 (ddd, *J* = 4.8, 1.6, 0.8 Hz, 1H), 8.76 (s, 1H), 8.37 (m, 1H), 8.26 (d, *J* = 9.0 Hz, 2H), 8.05 (td, *J* = 7.8, 1.8 Hz, 1H), 7.97 (d, *J* = 9.0 Hz, 2H), 7.64 (ddd, *J* = 7.7, 4.9, 1.0 Hz, 1H), 7.43 (d, *J* = 8.0 Hz, 1H). HR-ESI-MS: m/z $[M+H]^+$ = 302.0710, m/z $[M+Na]^+$ = 324.0527.

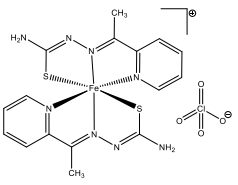


5.3.15.3 Synthesis of the TSC Fe(III) complexes – general description

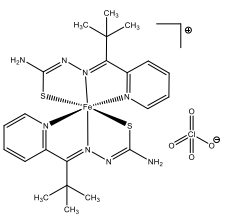


The appropriate TSC (2.00 eq.) was dissolved in EtOH and Et_3N (2.00 eq.) was added. After that, $Fe(ClO_4)_3 \cdot 6\ H_2O$ (1.00 eq.) was added and the mixture was refluxed for 30 min, which lead to the formation of a brown suspension. The mixture was cooled to room temperature, and the precipitate was filtered off and washed with EtOH and Et_2O.[39]

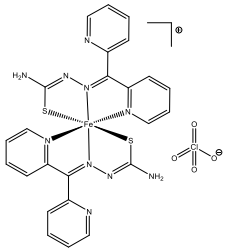
[Fe(MePy(TSC)H$_2$)$_2$]ClO$_4$ from 0.35 g (*E*)-1-[1-(2-Pyridyl)ethylidene] thiosemicarbazide (1.8 mmol), 0.25 mL Et_3N (1.8 mmol) 0.42 g $Fe(ClO_4)_3 \cdot 6\ H_2O$ (0.9 mmol). The product was obtained as a brown solid. Yield: 0.44 g (0.8 mmol, 45%). $[C_{16}H_{18}FeN_8S_2]ClO_4$ (541.79 g/mol). HR-ESI-MS: m/z $[M–ClO_4]^+$ = 442.0438.



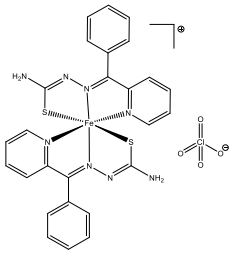
[Fe(*t*BuPy(TSC)H$_2$)$_2$]ClO$_4$ from 100.0 mg (*E*)-1-[2,2-Dimethyl-1-(2-pyridyl) propylidene]thiosemicarbazide (0.42 mmol), 59.0 µL Et_3N (0.42 mmol) and 98 mg $Fe(ClO_4)_3 \cdot 6\ H_2O$ (0.21 mmol). The product was obtained as a brown solid. Yield: 144.6 mg (0.23 mmol, 55%). $[C_{22}H_{30}FeN_8S_2]ClO_4$ (625.95 g/mol). HR-ESI-MS: m/z $[M–ClO_4]^+$ = 526.1376.



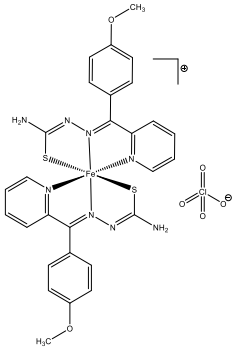
[Fe(Dipy(TSC)H$_2$)$_2$]ClO$_4$ from 0.14 g 1-[Bis(2-pyridyl)methylene]thiosemicarbazide (0.6 mmol), 0.07 mL Et$_3$N (0.6 mmol) and 0.14 g Fe(ClO$_4$)$_3$ · 6 H$_2$O (0.3 mmol). The product was obtained as a brown solid. Yield: 0.21 g (0.32 mmol, 53%). [C$_{24}$H$_{20}$FeN$_{10}$S$_2$]ClO$_4$ (667.91 g/mol).



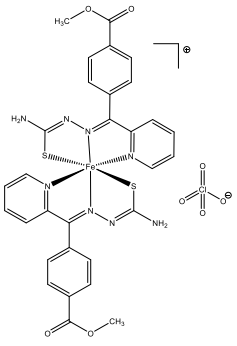
[Fe(PhPy(TSC)H$_2$)$_2$]ClO$_4$ from 0.35 g (*E*)-1-[Phenyl(2-pyridyl)methylene] thiosemicarbazide (1.4 mmol), 0.20 mL Et$_3$N (1.4 mmol) and 0.32 g Fe(ClO$_4$)$_3$ · 6 H$_2$O (0.7 mmol). The product was obtained as a brown solid. Yield: 0.47 g (0.70 mmol, 50%). [C$_{26}$H$_{22}$FeN$_8$S$_2$]ClO$_4$ (665.93 g/mol). HR-ESI-MS: m/z [M–ClO$_4$]$^+$ = 566.0748.



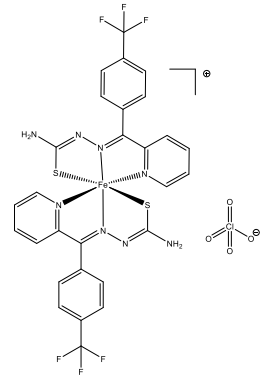
[Fe(MeOPhPy(TSC)H$_2$)$_2$]ClO$_4$ from 100.0 mg (*E*)-1-[(*p*-Methoxyphenyl)(2-pyridyl)-methylene]thiosemicarbazide (0.35 mmol), 50.0 µL Et$_3$N (0.35 mmol) and 78.6 mg Fe(ClO$_4$)$_3$ · 6 H$_2$O (0.17 mmol). The product was obtained as a brown solid. Yield: 109.2 mg (0.15 mmol, 43%). [C$_{28}$H$_{26}$FeN$_8$O$_2$S$_2$]ClO$_4$ (725.99 g/mol). HR-ESI-MS: m/z [M–ClO$_4$]$^+$ = 626.0959.



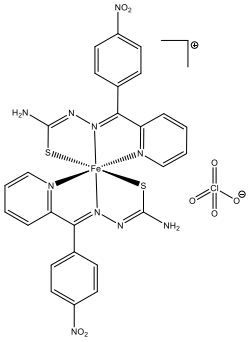
[Fe(COOMePhPy(TSC)H$_2$)$_2$]ClO$_4$ from 100.0 mg Methyl-*p*-[(*E*)-(2-pyridyl)thiosemi-carbazidoidenemethyl]benzoate (0.32 mmol), 44.0 µL Et$_3$N (0.32 mmol) and 74.0 mg Fe(ClO$_4$)$_3$ · 6 H$_2$O (0.16 mmol). The product was obtained as a brown solid. Yield: 153.1 mg (0.19 mmol, 61%). [C$_{30}$H$_{26}$FeN$_8$O$_4$S$_2$]ClO$_4$ (782.01 g/mol). HR-ESI-MS: m/z [M–ClO$_4$]$^+$ = 682.0863.



[Fe(CF$_3$PhPy(TSC)H$_2$)$_2$]ClO$_4$ from 100.0 mg (*E*)-1-[(2-Pyridyl)[*p*-(trifluoromethyl) phenyl]methylene]thiosemicarbazide (0.31 mmol), 43 µL Et$_3$N (0.31 mmol) and 74.0 mg Fe(ClO$_4$)$_3$ · 6 H$_2$O (0.16 mmol). The product was obtained as a brown solid. Yield: 120.0 mg (0.15 mmol, 48%). [C$_{28}$H$_{20}$F$_6$FeN$_8$S$_2$]ClO$_4$ (801.93 g/mol). HR-ESI-MS: m/z [M–ClO$_4$]$^+$ = 702.0505.



[Fe(NO$_2$PhPy(TSC)H$_2$)$_2$]ClO$_4$ from 100.0 mg (*E*)-1-[(*p*-Nitrophenyl)(2-pyridyl)methylene]-thiosemicarbazide (0.33 mmol), 46 µL Et$_3$N (0.33 mmol) and 77.0 mg Fe(ClO$_4$)$_3$ · 6 H$_2$O (0.17 mmol). The product was obtained as a brown solid. Yield: 145.1 mg (0.19 mmol, 58%). [C$_{26}$H$_{20}$FeN$_{10}$O$_4$S$_2$]ClO$_4$ (755.93 g/mol). HR-ESI-MS: m/z [M–ClO$_4$]$^+$ = 656.0458.



6. Literature

[1] B. Shakya & P. N. Yadav, *Mini Rev. Med. Chem.* **2020**, *20*, 638-661.

[2] A. Haseloer, Dissertation thesis, Universität zu Köln **2021**.

[3] A. Ibanez-Escribano, C. Fonseca-Berzal, M. Martinez-Montiel, M. Alvarez-Marquez, M. Gomez-Nunez, M. Lacueva-Arnedo, T. Espinosa-Buitrago, T. Martin-Perez, J. A. Escario, P. Merino-Montiel, S. Montiel-Smith, A. Gomez-Barrio, O. Lopez & J. G. Fernandez-Bolanos, *J. Enzyme Inhib. Med. Chem.* **2022**, *37*, 781-791.

[4] I. A. Mir, Q. U. Ain, T. Qadir, A. Q. Malik, S. Jan, S. Shahverdi & S. A. Nabi, *J. Mol. Struct.* **2024**, *1295*, 136216.

[5] M. Rubio-Hernández, T. R. Teixeira, T. P. Nguyen, M. Shingyoji, E. B. da Silva, A. J. O'Donoghue, C. R. Caffrey, S. Pérez-Silanes & N. Martínez-Sáez, *ACS Omega* **2025**, *10*, 24872-24886.

[6] E. G. Jayasree & S. Sreedevi, *Int. J. Quantum Chem.* **2017**, *117*, e25427.

[7] T. S. Lobana, R. Sharma, G. Bawa & S. Khanna, *Coord. Chem. Rev.* **2009**, *253*, 977-1055.

[8] S. Padhyé & G. B. Kauffman, *Coord. Chem. Rev.* **1985**, *63*, 127-160.

[9] K. N. Zelenin, O. B. Kuznetsova, V. V. Alekseev, I. Y. Kalvin'sh & L. Y. Leitis, *Chem. Heterocycl. Compd.* **1994**, *30*, 107-109.

[10] M. S. More, P. G. Joshi, Y. K. Mishra & P. K. Khanna, *Mater. Today Chem.* **2019**, *14*, 100195.

[11] V. B. Arion, M. A. Jakupec, M. S. Galanski, P. Unfried & B. K. Keppler, *J. Inorg. Biochem.* **2002**, *91*, 298-305.

[12] M. Cindrić, V. Vrdoljak, N. Strukan & B. Kamenar, *Polyhedron* **2005**, *24*, 369-376.

[13] G. F. de Sousa, L. C. C. Manso, E. S. Lang, C. C. Gatto & B. Mahieu, *J. Mol. Struct.* **2007**, *826*, 185-191.

[14] N. Kumari, S. Singh, M. Baral, D. Kumar & B. K. Kanungo, *J. Photochem. Photobiol. A Chem.* **2024**, *454*.

[15] M. Shebl, H. S. Seleem & B. A. El-Shetary, *Spectrochim. Acta A* **2010**, *75*, 428-436.

[16] A. Sreekanth, S. Sivakumar & M. R. Prathapachandra Kurup, *J. Mol. Struct.* **2003**, *655*, 47-58.

[17] E. M. Jouad, A. Riou, M. Allain, M. A. Khan & G. M. Bouet, *Polyhedron* **2001**, *20*, 67-74.

[18] M. A. Lima, V. A. Costa, M. A. Franco, G. P. de Oliveira, V. M. Deflon & F. V. Rocha, *Inorg. Chem. Comm.* **2020**, *112*.

[19] T. S. Lobana, G. Bawa, R. J. Butcher, B.-J. Liaw & C. W. Liu, *Polyhedron* **2006**, *25*, 2897-2903.

[20] T. S. Lobana, S. Khanna, R. J. Butcher, A. D. Hunter & M. Zeller, *Inorg. Chem.* **2007**, *46*, 5826-5828.

[21] T. S. Lobana, P. Kumari & R. J. Butcher, *Inorg. Chem. Comm.* **2008**, *11*, 11-14.

[22] J. Valdés-Martínez, A. Sierra-Romero, C. Alvarez-Toledano, R. A. Toscano & H. García-Tapia, *J. Organomet. Chem.* **1988**, *352*, 321-326.

[23] E. Bermejo, R. Carballo, A. Castiñeiras, R. Domínguez, C. Maichle-Mössmer, J. Strähle & D. X. West, *Polyhedron* **1999**, *18*, 3695-3702.

[24] F. Lucio-Martinez, L. A. Adrio, P. Polo-Ces, J. M. Ortigueira, J. J. Fernandez, H. Adams, M. T. Pereira & J. M. Vila, *Dalton Trans.* **2016**, *45*, 17598-17601.

[25] P. I. Maia, Z. A. Carneiro, C. D. Lopes, C. G. Oliveira, J. S. Silva, S. de Albuquerque, A. Hagenbach, R. Gust, V. M. Deflon & U. Abram, *Dalton Trans.* **2017**, *46*, 2559-2571.

[26] J. Patole, S. Padhye, M. S. Moodbidri & N. Shirsat, *Eur. J. Med. Chem.* **2005**, *40*, 1052-1055.

[27] R. Ramachandran, G. Prakash, S. Selvamurugan, P. Viswanathamurthi, J. G. Malecki & V. Ramkumar, *Dalton Trans.* **2014**, *43*, 7889-7902.

[28] A. Haseloer, L. M. Denkler, R. Jordan, M. Reimer, S. Olthof, I. Schmidt, K. Meerholz, G. Horner & A. Klein, *Dalton Trans.* **2021**, *50*, 4311-4322.

[29] K. Nomiya, K. Sekino, M. Ishikawa, A. Honda, M. Yokoyama, N. Chikaraishi Kasuga, H. Yokoyama, S. Nakano & K. Onodera, *J. Inorg. Biochem.* **2004**, *98*, 601-615.

[30] B. M. Paterson & P. S. Donnelly, *Chem. Soc. Rev.* **2011**, *40*, 3005-3018.

[31] R. Pedrido, A. M. Gonzalez-Noya, M. J. Romero, M. Martinez-Calvo, M. Vazquez Lopez, E. Gomez-Forneas, G. Zaragoza & M. R. Bermejo, *Dalton Trans.* **2008**, 6776-6787.
[32] V. S. Prado, R. C. F. Leitao, F. Silva, L. Gano, I. C. Santos, F. L. N. Marques, A. Paulo & V. M. Deflon, *Dalton Trans.* **2021**, *50*, 1631-1640.
[33] S. Carradori, D. Secci, M. D'Ascenzio, P. Chimenti & A. Bolasco, *J. Heterocycl. Chem.* **2014**, *51*, 1856-1861.
[34] A. A. Hassan, A. M. Shawky & H. S. Shehatta, *J. Heterocycl. Chem.* **2011**, *49*, 21-37.
[35] W. X. Hu, W. Zhou, C. N. Xia & X. Wen, *Bioorg. Med. Chem. Lett.* **2006**, *16*, 2213-2218.
[36] M. Islam, A. Khan, M. T. Shehzad, M. Khiat, S. A. Halim, A. Hameed, S. R. Shah, R. Basri, M. U. Anwar, J. Hussain, R. Csuk, A. Al-Harrasi & Z. Shafiq, *Bioorg. Chem.* **2021**, *109*, 104691.
[37] A. E. Stacy, D. Palanimuthu, P. V. Bernhardt, D. S. Kalinowski, P. J. Jansson & D. R. Richardson, *J. Med. Chem.* **2016**, *59*, 8601-8620.
[38] D. S. Kalinowski, P. Quach & D. R. Richardson, *Future Med. Chem.* **2009**, *1*, 1143-1151.
[39] D. R. Richardson, P. C. Sharpe, D. B. Lovejoy, D. Senaratne, D. S. Kalinowski, M. Islam & P. V. Bernhardt, *J. Med. Chem.* **2006**, *49*, 6510-6521.
[40] Y. Yu, D. S. Kalinowski, Z. Kovacevic, A. R. Siafakas, P. J. Jansson, C. Stefani, D. B. Lovejoy, P. C. Sharpe, P. V. Bernhardt & D. R. Richardson, *J. Med. Chem.* **2009**, *52*, 5271-5294.
[41] M. A. Metwally, S. Bondock, H. El-Azap & E.-E. M. Kandeel, *J. Sulfur Chem.* **2011**, *32*, 489-519.
[42] A. Basu, B. N. Sinha, P. Saiko & T. Szekeres, *Bioorg. Med. Chem. Lett.* **2012**, *22*, 4934-4938.
[43] J. Easmon, G. Purstinger, G. Heinisch, T. Roth, H. H. Fiebig, W. Holzer, W. Jager, M. Jenny & J. Hofmann, *J. Med. Chem.* **2001**, *44*, 2164-2171.
[44] K. Eschliman & S. H. Bossmann, *Synthesis* **2019**, *51*, 1746-1752.
[45] B. Maeda & K. Murakami, *Chem. Commun. (Camb)* **2024**, *60*, 2839-2864.
[46] A. K. Mukerjee & R. Ashare, *Chem. Rev.* **1991**, *91*, 1-24.
[47] R. Wong & S. J. Dolman, *J. Org. Chem.* **2007**, *72*, 3969-3971.
[48] A. P. d. Silva, G. de Freitas Gauze, N. P. Coelho, C. C. da Silva & E. A. Basso, *Tetrahedron Lett.* **2011**, *52*, 62-64.
[49] I. D. Kostas & B. R. Steele, *Catalysts* **2020**, *10*.
[50] O. Özbek & C. Berkel, *Polyhedron* **2023**, *238*.
[51] P. Anitha, R. Manikandan & P. Viswanathamurthi, *J. Coord. Chem.* **2015**, *68*, 3537-3550.
[52] I. D. Kostas, F. J. Andreadaki, D. Kovala-Demertzi, P. Christos & M. A. Demertzis, *Tetrahedron Lett.* **2005**, *46*, 1967-1970.
[53] P. Paul, S. Datta, S. Halder, R. Acharyya, F. Basuli, R. J. Butcher, S.-M. Peng, G.-H. Lee, A. Castineiras, M. G. B. Drew & S. Bhattacharya, *J. Mol. Catal. A Chem.* **2011**, *344*, 62-73.
[54] S. Priyarega, P. Kalaivani, R. Prabhakaran, T. Hashimoto, A. Endo & K. Natarajan, *J. Mol. Struct.* **2011**, *1002*, 58-62.
[55] R. Manikandan, P. Anitha, P. Viswanathamurthi & J. G. Malecki, *Polyhedron* **2016**, *119*, 300-306.
[56] J. Mehrez, A. Barrozo, L. Delmotte, R. Hardre, M. Papadakis & M. Orio, *Dalton Trans.* **2025**, *54*, 8113-8122.
[57] T. Straistari, J. Fize, S. Shova, M. Réglier, V. Artero & M. Orio, *ChemCatChem* **2016**, *9*, 2262-2268.
[58] T. Straistari, R. Hardre, J. Fize, S. Shova, M. Giorgi, M. Reglier, V. Artero & M. Orio, *Chemistry* **2018**, *24*, 8779-8786.
[59] Z. E. Chen, H. Zhang & Z. Iqbal, *Spectrochim. Acta A. Mol. Biomol. Spectrosc.* **2019**, *215*, 34-40.
[60] W. Radchatawedchakoon, W. Sangsuwan, S. Kruanetr & U. Sakee, *Spectrochim. Acta A* **2014**, *121*, 306-312.
[61] M. D. Raicopol, N. A. Chira, A. M. Pandele, A. Hanganu, A. A. Ivanov, V. Tecuceanu, I. G. Bugean & G.-O. Buica, *Sens. Actuators B Chem.* **2020**, *313*.
[62] L. Tang, Z. Huang, Z. Zheng, K. Zhong & Y. Bian, *J. Fluoresc.* **2016**, *26*, 1535-1540.
[63] D. J. Bauer & P. W. Sadler, *Br. J. Pharmacol. Chemother.* **1960**, *15*, 101-110.
[64] B. Woodson & W. K. Joklik, *Proc. Natl. Acad. Sci. U. S. A.* **1965**, *54*, 946-953.
[65] G. Korkmaz, *J. New Results Sci.* **2024**, *13*, 61-83.

[66] P. Padmanabhan, S. Khaleefathullah, K. Kaveri, G. Palani, G. Ramanathan, S. Thennarasu & U. Tirichurapalli Sivagnanam, *J. Med. Virol.* **2017**, *89*, 546-552.
[67] E. Pahontu, F. Julea, T. Rosu, V. Purcarea, Y. Chumakov, P. Petrenco & A. Gulea, *J. Cell Mol. Med.* **2015**, *19*, 865-878.
[68] E. A. Fayed, A. Thabet, S. M. A. El-Gilil, H. M. A. Elsanhory & Y. A. Ammar, *J. Mol. Struct.* **2024**, *1301*.
[69] N. V. Kulkarni, V. K. Revankar, B. N. Kirasur & M. H. Hugar, *Med. Chem. Res.* **2011**, *21*, 663-671.
[70] G. L. Parrilha, R. G. dos Santos & H. Beraldo, *Coord. Chem. Rev.* **2022**, *458*.
[71] D. Palanimuthu, R. Poon, S. Sahni, R. Anjum, D. Hibbs, H. Y. Lin, P. V. Bernhardt, D. S. Kalinowski & D. R. Richardson, *Eur. J. Med. Chem.* **2017**, *139*, 612-632.
[72] S. Zaib, R. Munir, M. T. Younas, N. Kausar, A. Ibrar, S. Aqsa, N. Shahid, T. T. Asif, H. O. Alsaab & I. Khan, *Molecules* **2021**, *26*.
[73] X. G. Bai, Y. Zheng & J. Qi, *Front. Pharmacol.* **2022**, *13*, 1018951.
[74] S. Guler, H. A. Kayali, E. O. Sadan, B. Sen & E. Subasi, *Front. Pharmacol.* **2022**, *13*, 882756.
[75] Z. X. He, J. L. Huo, Y. P. Gong, Q. An, X. Zhang, H. Qiao, F. F. Yang, X. H. Zhang, L. M. Jiao, H. M. Liu, L. Y. Ma & W. Zhao, *Eur. J. Med. Chem.* **2021**, *210*, 112970.
[76] A. I. Matesanz & P. Souza, *Mini Rev. Med. Chem.* **2009**, *9*, 1389-1396.
[77] D. C. Reis, M. C. Pinto, E. M. Souza-Fagundes, S. M. Wardell, J. L. Wardell & H. Beraldo, *Eur. J. Med. Chem.* **2010**, *45*, 3904-3910.
[78] N. Shahi, P. N. Yadav, U. Chaudhary, M. Saad, K. Mahiya, A. Khan, S. Shafi & Y. R. Pokharel, *ACS Omega* **2023**, *8*, 31998-32016.
[79] J. R. Dilworth & R. Hueting, *Inorg. Chim. Acta* **2012**, *389*, 3-15.
[80] C. R. Kowol, R. Trondl, P. Heffeter, V. B. Arion, M. A. Jakupec, A. Roller, M. S. Galanski, W. Berger & B. K. Keppler, *J. Med. Chem.* **2009**, *52*, 5032-5043.
[81] V. Jevtovic, A. K. Alshamari, D. Milenkovic, J. Dimitric Markovic, Z. Markovic & D. Dimic, *Int. J. Mol. Sci.* **2023**, *24*.
[82] N. P. Prajapati & H. D. Patel, *Synt. Commun.* **2019**, 1-38.
[83] M. Suleymanoglu, B. Kaya, S. Erdem-Kuruca & B. Ulkuseven, *J. Biochem. Mol. Toxicol.* **2019**, *33*, e22383.
[84] A. Q. Ali, S. G. Teoh, N. E. Eltayeb, M. B. K. Ahamed & A. A. Majid, *J. Coord. Chem.* **2014**, *67*, 3380-3400.
[85] Y. Gou, J. Wang, S. Chen, Z. Zhang, Y. Zhang, W. Zhang & F. Yang, *Eur. J. Med. Chem.* **2016**, *123*, 354-364.
[86] A. P. King, H. A. Gellineau, J. E. Ahn, S. N. MacMillan & J. J. Wilson, *Inorg. Chem.* **2017**, *56*, 6609-6623.
[87] J. A. Lessa, J. C. Guerra, L. F. de Miranda, C. F. Romeiro, J. G. Da Silva, I. C. Mendes, N. L. Speziali, E. M. Souza-Fagundes & H. Beraldo, *J. Inorg. Biochem.* **2011**, *105*, 1729-1739.
[88] A. I. Matesanz, I. Leitao & P. Souza, *J. Inorg. Biochem.* **2013**, *125*, 26-31.
[89] J. Shao, Z. Y. Ma, A. Li, Y. H. Liu, C. Z. Xie, Z. Y. Qiang & J. Y. Xu, *J. Inorg. Biochem.* **2014**, *136*, 13-23.
[90] E. Baruffini, R. Ruotolo, F. Bisceglie, S. Montalbano, S. Ottonello, G. Pelosi, A. Buschini & T. Lodi, *Sci. Rep.* **2020**, *10*, 10524.
[91] V. A. Rao, S. R. Klein, K. K. Agama, E. Toyoda, N. Adachi, Y. Pommier & E. B. Shacter, *Cancer Res.* **2009**, *69*, 948-957.
[92] P. N. Dayani, M. C. Bishop, K. Black & P. M. Zeltzer, *J. Neurooncol.* **2004**, *67*, 367-377.
[93] H. Kang, M. Han, J. Xue, Y. Baek, J. Chang, S. Hu, H. Nam, M. J. Jo, G. El Fakhri, M. P. Hutchens, H. S. Choi & J. Kim, *Nat. Commun.* **2019**, *10*, 5134.
[94] P. V. Bernhardt, P. C. Sharpe, M. Islam, D. B. Lovejoy, D. S. Kalinowski & D. R. Richardson, *J. Med. Chem.* **2009**, *52*, 407-415.
[95] P. J. Jansson, P. C. Sharpe, P. V. Bernhardt & D. R. Richardson, *J Med Chem* **2010**, *53*, 5759-5769.
[96] B. Kaya, H. Smith, Y. Chen, M. G. Azad, T. M. Russell, V. Richardson, M. Dharmasivam & D. R. Richardson, *Inorg. Chem.* **2024**, *63*, 20840-20858.

[97] A. E. Stacy, D. Palanimuthu, P. V. Bernhardt, D. S. Kalinowski, P. J. Jansson & D. R. Richardson, *J. Med. Chem.* **2016**, *59*, 4965-4984.
[98] B. Kaya, H. Smith, Y. Chen, M. G. Azad, M. R. T, V. Richardson, P. V. Bernhardt, M. Dharmasivam & D. R. Richardson, *Chem. Sci.* **2024**, *15*, 15109-15124.
[99] T. P. Wijesinghe, B. Kaya, M. A. Gonzalvez, J. R. Harmer, M. Gholam Azad, P. V. Bernhardt, M. Dharmasivam & D. R. Richardson, *J. Med. Chem.* **2023**, *66*, 15453-15476.
[100] C. A. Kunos, E. Chu, J. H. Beumer, M. Sznol & S. P. Ivy, *Cancer Chemother. Pharmacol.* **2016**, *79*, 201-207.
[101] B. Kaya, M. Gholam Azad, M. Suleymanoglu, J. R. Harmer, T. P. Wijesinghe, V. Richardson, X. Zhao, P. V. Bernhardt, M. Dharmasivam & D. R. Richardson, *J. Med. Chem.* **2024**, *67*, 12155-12183.
[102] D. B. Lovejoy, D. M. Sharp, N. Seebacher, P. Obeidy, T. Prichard, C. Stefani, M. T. Basha, P. C. Sharpe, P. J. Jansson, D. S. Kalinowski, P. V. Bernhardt & D. R. Richardson, *J. Med. Chem.* **2012**, *55*, 7230-7244.
[103] F. J. Giles, P. M. Fracasso, H. M. Kantarjian, J. E. Cortes, R. A. Brown, S. Verstovsek, Y. Alvarado, D. A. Thomas, S. Faderl, G. Garcia-Manero, L. P. Wright, T. Samson, A. Cahill, P. Lambert, W. Plunkett, M. Sznol, J. F. DiPersio & V. Gandhi, *Leuk. Res.* **2003**, *27*, 1077-1083.
[104] J. J. Knox, S. J. Hotte, C. Kollmannsberger, E. Winquist, B. Fisher & E. A. Eisenhauer, *Invest. New Drugs* **2007**, *25*, 471-477.
[105] D. S. Kalinowski, Y. Yu, P. C. Sharpe, M. Islam, Y. T. Liao, D. B. Lovejoy, N. Kumar, P. V. Bernhardt & D. R. Richardson, *J. Med. Chem.* **2007**, *50*, 3716-3729.
[106] C. Stefani, P. J. Jansson, E. Gutierrez, P. V. Bernhardt, D. R. Richardson & D. S. Kalinowski, *J. Med. Chem.* **2013**, *56*, 357-370.
[107] V. Sestak, J. Stariat, J. Cermanova, E. Potuckova, J. Chladek, J. Roh, J. Bures, H. Jansova, P. Prusa, M. Sterba, S. Micuda, T. Simunek, D. S. Kalinowski, D. R. Richardson & P. Kovarikova, *Oncotarget* **2015**, *6*, 42411-42428.
[108] N. L. Silver, A. A. Osman, A. A. Patel, N. Tanaka, L. Tang, G. Zhou & J. N. Myers, *Int. J. Radiat. Oncol. Biol. Phys.* **2016**, *94*, 942.
[109] M. Dharmasivam, B. Kaya, T. Wijesinghe, M. Gholam Azad, M. A. Gonzalvez, M. Hussaini, J. Chekmarev, P. V. Bernhardt & D. R. Richardson, *J. Med. Chem.* **2023**, *66*, 1426-1453.
[110] M. Dharmasivam, B. Kaya, T. P. Wijesinghe, V. Richardson, J. R. Harmer, M. A. Gonzalvez, W. Lewis, M. G. Azad, P. V. Bernhardt & D. R. Richardson, *Chem. Sci.* **2024**, *15*, 974-990.
[111] M. Dharmasivam, S. Zhang, X. Zhao, V. Richardson, T. P. Wijesinghe, M. Suleymanoglu, M. Gholam Azad, P. V. Bernhardt, B. Kaya & D. R. Richardson, *J. Med. Chem.* **2025**, *68*, 9594-9622.
[112] N. Gholipour, M. Akhlaghi, A. Mokhtari Kheirabadi, P. Geramifar & D. Beiki, *Int. J. Biol. Macromol.* **2020**, *148*, 932-941.
[113] N. Sheernaly, I. Shajan, A. Steinbrueck, B. Albada & N. Metzler-Nolte, *RSC Med. Chem.* **2025**, *16*, 3512-3521.
[114] S. Lim, K. A. Price, S. F. Chong, B. M. Paterson, A. Caragounis, K. J. Barnham, P. J. Crouch, J. M. Peach, J. R. Dilworth, A. R. White & P. S. Donnelly, *J. Biol. Inorg. Chem.* **2010**, *15*, 225-235.
[115] H. Pervez, N. Manzoor, M. Yaqub & K. M. Khan, *J. Enzyme Inhib. Med. Chem.* **2014**, *29*, 628-632.
[116] X.-Y. Man, M.-H. Zhu, S.-H. Li, W.-J. Li, G. Xu, Z.-L. Zhang, X.-Y. Wu, H. Liang & F. Yang, *Rare Metals* **2025**, *44*, 2589-2604.
[117] M. Papadakis, G. Landrou, M. Poisson, L. Delmotte, K. Achileos, S. Bertaina, R. Hardré, K. Ladomenou, A. G. Coutsolelos & M. Orio, *Eur. J. Inorg. Chem.* **2023**, *26*.
[118] K. Riehemann, S. W. Schneider, T. A. Luger, B. Godin, M. Ferrari & H. Fuchs, *Angew. Chem. Int. Ed. Engl.* **2009**, *48*, 872-897.
[119] H. Jiang, K.-s. Moon, H. Dong, F. Hua & C. P. Wong, *Chem. Phys. Lett.* **2006**, *429*, 492-496.
[120] K. L. Kelly, E. Coronado, L. L. Zhao & G. C. Schatz, *J. Phys. Chem. B* **2002**, *107*, 668-677.
[121] A. G. Kolhatkar, A. C. Jamison, D. Litvinov, R. C. Willson & T. R. Lee, *Int. J. Mol. Sci.* **2013**, *14*, 15977-16009.
[122] G. Schmid & U. Simon, *Chem. Commun. (Camb)* **2005**, 697-710.
[123] F. Vines, J. R. Gomes & F. Illas, *Chem. Soc. Rev.* **2014**, *43*, 4922-4939.

[124] N. Abid, A. M. Khan, S. Shujait, K. Chaudhary, M. Ikram, M. Imran, J. Haider, M. Khan, Q. Khan & M. Maqbool, *Adv. Colloid. Interface Sci.* **2022**, *300*, 102597.
[125] B. K. Teo & X. H. Sun, *J. Clust. Scie.* **2006**, *17*, 529-540.
[126] H. L. Ding, Y. X. Zhang, S. Wang, J. M. Xu, S. C. Xu & G. H. Li, *Chem. Mater.* **2012**, *24*, 4572-4580.
[127] I. Gessner, E. Krakor, A. Jurewicz, V. Wulff, L. Kling, S. Christiansen, N. Brodusch, R. Gauvin, L. Wortmann, M. Wolke, G. Plum, A. Schauss, J. Krautwurst, U. Ruschewitz, S. Ilyas & S. Mathur, *RSC Adv.* **2018**, *8*, 24883-24892.
[128] Z. Li, J. C. Barnes, A. Bosoy, J. F. Stoddart & J. I. Zink, *Chem. Soc. Rev.* **2012**, *41*, 2590-2605.
[129] S. E. Skrabalak, L. Au, X. Li & Y. Xia, *Nat. Protoc.* **2007**, *2*, 2182-2190.
[130] J. Allouche, in *Nanomaterials: A Danger or a Promise? A Chemical and Biological Perspective* (Eds.: Roberta Brayner, Fernand Fiévet, & Thibaud Coradin), Springer London, London, **2013**, pp. 27-74.
[131] K. A. Altammar, *Front. Microbiol.* **2023**, *14*, 1155622.
[132] A. C. Anselmo & S. Mitragotri, *AAPS J.* **2015**, *17*, 1041-1054.
[133] R. Mout, D. F. Moyano, S. Rana & V. M. Rotello, *Chem. Soc. Rev.* **2012**, *41*, 2539-2544.
[134] A. M. El Badawy, K. G. Scheckel, M. Suidan & T. Tolaymat, *Sci. Total Environ.* **2012**, *429*, 325-331.
[135] M.-A. Neouze & U. Schubert, *Monatsh. Chem.* **2008**, *139*, 183-195.
[136] G. Sanita, B. Carrese & A. Lamberti, *Front. Mol. Biosci.* **2020**, *7*, 587012.
[137] R. Thiruppathi, S. Mishra, M. Ganapathy, P. Padmanabhan & B. Gulyas, *Adv. Sci. (Weinh)* **2017**, *4*, 1600279.
[138] A. Liberman, N. Mendez, W. C. Trogler & A. C. Kummel, *Surf. Sci. Rep.* **2014**, *69*, 132-158.
[139] J. Xie, X. Pan, M. Wang, J. Ma, Y. Fei, P. N. Wang & L. Mi, *Colloids Surf. B* **2016**, *143*, 148-155.
[140] S. Ilyas, N. K. Ullah, M. Ilyas, K. Wennhold, M. Iqbal, H. A. Schlosser, M. S. Hussain & S. Mathur, *ACS Biomater. Sci. Eng.* **2020**, *6*, 6138-6147.
[141] Y. Chen, Y. Xianyu & X. Jiang, *Acc. Chem. Res.* **2017**, *50*, 310-319.
[142] J. Hohnsen, L. Rryci, D. Obretenova, J. Friedel, S. Jouchaghani & A. Klein, *Molecules* **2024**, *29*.
[143] W. Cai, T. Gao, H. Hong & J. Sun, *Nanotechnol. Sci. Appl.* **2008**, *1*, 17-32.
[144] S. A. Smith, L. I. Selby, A. P. R. Johnston & G. K. Such, *Bioconjug. Chem.* **2019**, *30*, 263-272.
[145] C. Pathak, F. U. Vaidya, B. N. Waghela, P. K. Jaiswara, V. K. Gupta, A. Kumar, B. K. Rajendran & K. Ranjan, *Int. J. Mol. Sci.* **2023**, *24*.
[146] K. Ozturk, M. Kaplan & S. Calis, *Int. J. Pharm.* **2024**, *666*, 124799.
[147] X. Liu, F. Wu, Y. Tian, M. Wu, Q. Zhou, S. Jiang & Z. Niu, *Sci. Rep.* **2016**, *6*, 24567.
[148] M. F. Attia, N. Anton, J. Wallyn, Z. Omran & T. F. Vandamme, *J. Pharm. Pharmacol.* **2019**, *71*, 1185-1198.
[149] M. Mahmoudi, S. Sant, B. Wang, S. Laurent & T. Sen, *Adv. Drug Deliv. Rev.* **2011**, *63*, 24-46.
[150] M. Wang & M. Thanou, *Pharmacol. Res.* **2010**, *62*, 90-99.
[151] J. Yoo, C. Park, G. Yi, D. Lee & H. Koo, *Cancers* **2019**, *11*.
[152] M. Bjornmalm, K. J. Thurecht, M. Michael, A. M. Scott & F. Caruso, *ACS Nano* **2017**, *11*, 9594-9613.
[153] J. Fang, H. Nakamura & H. Maeda, *Adv. Drug Deliv. Rev.* **2011**, *63*, 136-151.
[154] A. Z. Mirza & F. A. Siddiqui, *Int. Nano Lett.* **2014**, *4*.
[155] J. Shi, P. W. Kantoff, R. Wooster & O. C. Farokhzad, *Nat. Rev. Cancer* **2017**, *17*, 20-37.
[156] A. Kumari, S. K. Yadav & S. C. Yadav, *Colloids Surf. B* **2010**, *75*, 1-18.
[157] A. Samad, Y. Sultana & M. Aqil, *Curr. Drug Deliv.* **2007**, *4*, 297-305.
[158] M. Tarhini, H. Greige-Gerges & A. Elaissari, *Int. J. Pharm.* **2017**, *522*, 172-197.
[159] U. Wais, A. W. Jackson, T. He & H. Zhang, *Nanoscale* **2016**, *8*, 1746-1769.
[160] M. Gisbert-Garzaran, M. Manzano & M. Vallet-Regi, *Bioeng.* **2017**, *4*.
[161] A. Watermann & J. Brieger, *Nanomater.* **2017**, *7*.
[162] C. Ding & Z. Li, *Mater Sci. Eng. C Mater. Biol. Appl.* **2017**, *76*, 1440-1453.
[163] A. Imantay, N. Mashurov, B. A. Zhaisanbayeva & E. A. Mun, *Nanomater.* **2025**, *15*.

[164] A. K. A. Silva, A. Espinosa, J. Kolosnjaj-Tabi, C. Wilhelm & F. Gazeau, in *Iron Oxides*, **2016**, pp. 425-472.
[165] L. Vigderman & E. R. Zubarev, *Adv. Drug Deliv. Rev.* **2013**, *65*, 663-676.
[166] E. A. Britta, C. C. da Silva, A. F. Rubira, C. V. Nakamura & R. Borsali, *Mater. Sci. Eng. C Mater. Biol. Appl.* **2016**, *69*, 1159-1166.
[167] Q. Miao, D. Xu, Z. Wang, L. Xu, T. Wang, Y. Wu, D. B. Lovejoy, D. S. Kalinowski, D. R. Richardson, G. Nie & Y. Zhao, *Biomater.* **2010**, *31*, 7364-7375.
[168] C. G. Oliveira, L. F. Dalmolin, R. T. C. Silva, R. F. V. Lopez, P. I. S. Maia & J. A. Moreto, *New J. Chem.* **2020**, *44*, 14928-14935.
[169] R. T. C. Silva, L. F. Dalmolin, J. A. Moreto, C. G. Oliveira, A. E. H. Machado, R. F. V. Lopez & P. I. S. Maia, *J. Nanopart. Res.* **2020**, *22*.
[170] G. Spadola, V. Sanna, J. Bartoli, M. Carcelli, G. Pelosi, F. Bisceglie, F. M. Restivo, F. Degola & D. Rogolino, *Environ. Sci. Pollut. Res. Int.* **2020**, *27*, 20125-20135.
[171] B. Fischer, K. Kryeziu, S. Kallus, P. Heffeter, W. Berger, C. R. Kowol & B. K. Keppler, *RSC Adv.* **2016**, *6*, 55848-55859.
[172] A. A. Khan, A. M. Alanazi, N. Alsaif, N. Algrain, T. A. Wani & M. A. Bhat, *Pharm.* **2021**, *13*.
[173] M. Mathuber, S. Hager, B. K. Keppler, P. Heffeter & C. R. Kowol, *Dalton Trans.* **2021**, *50*, 16053-16066.
[174] F. Danışman-Kalındemirtaş, S. Erdem-Kuruca, G. E. Cilasun, E. Sert, D. Özerkan, T. B. Demirci, B. Ülküseven & İ. A. Kariper, *J. Taibah Univ. Sci.* **2024**, *18*.
[175] M. Ismail, W. Yang, Y. Li, Y. Wang, W. He, J. Wang, P. Muhammad, T. B. Chaston, F. U. Rehman, M. Zheng, D. B. Lovejoy & B. Shi, *Biomater.* **2022**, *289*, 121760.
[176] L. Jaragh-Alhadad, M. Samir, T. J. Harford & S. Karnik, *Drug Deliv.* **2022**, *29*, 2206-2216.
[177] M. Jiang, Z. Zhang, W. Li, X. Man, H. Sun, H. Liang & F. Yang, *J. Med. Chem.* **2022**, *65*, 9447-9458.
[178] S. Xu, W. Luo, M. Zhu, L. Zhao, L. Gao, H. Liang, Z. Zhang & F. Yang, *Mol. Pharm.* **2024**, *21*, 346-357.
[179] J. Zhang, R. Fang, Y. Li, J. Jin, F. Yang & J. Chen, *Mol. Pharm.* **2023**, *20*, 3632-3644.
[180] Z. Zhang, T. Yang, J. Zhang, W. Li, S. Li, H. Sun, H. Liang & F. Yang, *J. Med. Chem.* **2022**, *65*, 5392-5406.
[181] I. Ali, I. O. Isaac, F. Ahmed, F. Aslam, S. Ali, M. Imran, R. D. Alharthy, M. R. Shah, M. I. Malik & A. Hameed, *ChemistrySelect* **2019**, *4*, 8757-8763.
[182] D. S. Franciscato, T. A. Matias, J. Shinohara, J. M. Goncalves, N. P. Coelho, C. S. Fernandes, E. A. Basso, H. S. Nakatani, K. Araki, H. E. Toma & V. R. de Souza, *Spectrochim. Acta. A* **2018**, *204*, 174-179.
[183] M. Badrooh, F. Shokrollahi, S. Javan, T. Ghasemipour, S. Rezaei Mojdehi, H. Farahnak, M. Jahani Sayyad Noveiri, M. Hedayati & A. Salehzadeh, *Mol. Biol. Rep.* **2022**, *49*, 2217-2226.
[184] M. Hosseinkhah, R. Ghasemian, F. Shokrollahi, S. R. Mojdehi, M. J. S. Noveiri, M. Hedayati, M. Rezaei & A. Salehzadeh, *J. Clust. Sci.* **2021**, *33*, 2045-2053.
[185] I. Shafiei, S. P. Tavassoli, H. R. Rahmatollahi, R. Ghasemian & A. Salehzadeh, *J. Clust. Sci.* **2021**, *33*, 2697-2706.
[186] E. Veg, S. Joshi & T. Khan. *Eng. Proc.* **2024**, *67*, 46.
[187] E. T. Anthony, M. Wilhelm & A. Klein, *ACS Appl. Nano Mater.* **2025**, *8*, 5841-5852.
[188] N. Kaviani, S. Behrouz, A. A. Jafari & M. N. Soltani Rad, *RSC Adv.* **2023**, *13*, 30293-30305.
[189] A. K. Pramanik, Siddikuzzaman, D. Palanimuthu, K. Somasundaram & A. G. Samuelson, *Bioconjug. Chem.* **2016**, *27*, 2874-2885.
[190] N. Kaviani, S. Behrouz, A. A. Jafari & M. N. Soltani Rad, *J. Organomet. Chem.* **2024**, *1007*.
[191] Mohammad N. Soltani Rad, S. Behrouz, J. Mohammadtaghi-Nezhad, E. Zarenezhad & M. Agholi, *Appl. Organomet. Chem.* **2019**, *33*.
[192] E. Tobechukwu Anthony, S. Olthof, S. Roitsch, K. Meerholz, S. Mathur & A. Klein, *Eur. J. Inorg. Chem.* **2025**, *28*.
[193] E. T. Anthony & A. Klein, *Chem. Afr.* **2025**.
[194] S. Bagheri, N. Muhd Julkapli & S. Bee Abd Hamid, *Sci. World J.* **2014**, *2014*, 727496.

[195] A. Fujishima & K. Honda, *Nature* **1972**, *238*, 37-38.
[196] M. Ni, M. K. H. Leung, D. Y. C. Leung & K. Sumathy, *Renew. Sustain. Energy Rev.* **2007**, *11*, 401-425.
[197] K. Lee, S. Shin, W. J. Lee, D. Choi, Y. Ahn, M. Park, D. Seo & K. Seo, *Nano Lett.* **2021**, *21*, 6998-7004.
[198] L. Sang, Y. Zhao & C. Burda, *Chem. Rev.* **2014**, *114*, 9283-9318.
[199] F. Lakadamyali & E. Reisner, *Chem. Commun. (Camb)* **2011**, *47*, 1695-1697.
[200] S. Panagiotakis, G. Landrou, V. Nikolaou, A. Putri, R. Hardre, J. Massin, G. Charalambidis, A. G. Coutsolelos & M. Orio, *Front. Chem.* **2019**, *7*, 405.
[201] A. Santarelli, C. A. Brandl, C. N. Cechin, T. Bortolotto, N. d. F. Daudt, R. A. Burrow, E. S. Lang, B. Tirloni & G. N. Ledesma, *Mol. Catal.* **2024**, *566*.
[202] P. Elzahhar, A. S. F. Belal, F. Elamrawy, N. A. Helal & M. I. Nounou, *Methods Mol. Biol.* **2019**, *2000*, 125-182.
[203] D. A. Fulton & J. F. Stoddart, *Bioconjug. Chem.* **2001**, *12*, 655-672.
[204] R. S. Gamage, J. L. Chasteen & B. D. Smith, *Bioconjug. Chem.* **2023**, *34*, 961-971.
[205] P. L. Patel, N. K. Rana, M. R. Patel, S. D. Kozuch & D. Sabatino, *ChemMedChem* **2016**, *11*, 252-269.
[206] W. M. Rockey, L. Huang, K. C. Kloepping, N. J. Baumhover, P. H. Giangrande & M. K. Schultz, *Bioorg. Med. Chem.* **2011**, *19*, 4080-4090.
[207] K. M. Stewart, K. L. Horton & S. O. Kelley, *Org. Biomol. Chem.* **2008**, *6*, 2242-2255.
[208] J. Cardinale, C. Giammei, N. Jouini & T. L. Mindt, in Radiopharmaceutical Chemistry (Eds.: Jason S. Lewis, Albert D. Windhorst, & Brian M. Zeglis), Springer International Publishing, Cham, **2019**, pp. 449-466.
[209] K. Nwe & M. W. Brechbiel, *Cancer Biother. Radiopharm.* **2009**, *24*, 289-302.
[210] J. Ravasco, H. Faustino, A. Trindade & P. M. P. Gois, *Chemistry* **2019**, *25*, 43-59.
[211] N. Stephanopoulos & M. B. Francis, *Nat. Chem. Biol.* **2011**, *7*, 876-884.
[212] C. Zhang, E. V. Vinogradova, A. M. Spokoyny, S. L. Buchwald & B. L. Pentelute, *Angew. Chem. Int. Ed. Engl.* **2019**, *58*, 4810-4839.
[213] R. Bansal & A. Suryan, *ACS Bio. Med. Chem. Au.* **2022**, *2*, 340-369.
[214] P. A. Szijj, K. A. Kostadinova, R. J. Spears & V. Chudasama, *Org. Biomol. Chem.* **2020**, *18*, 9018-9028.
[215] R. A. Bottens & T. Yamada. *Cancers* **2022**, *14*, 5546.
[216] D. M. Copolovici, K. Langel, E. Eriste & U. Langel, *ACS Nano* **2014**, *8*, 1972-1994.
[217] G. Guidotti, L. Brambilla & D. Rossi, *Trends Pharmacol. Sci.* **2017**, *38*, 406-424.
[218] M. Zhou, X. Zou, K. Cheng, S. Zhong, Y. Su, T. Wu, Y. Tao, L. Cong, B. Yan & Y. Jiang, *Clin. Transl. Med.* **2022**, *12*, e822.
[219] T. Singh, D. H. Kang, T. W. Kim, H. J. Kong, J. S. Ryu, S. Jeon, T. S. Ahn, D. Jeong, M. J. Baek & J. Im, *Int. J. Pharm.* **2021**, *606*, 120904.
[220] E. A. Akam & E. Tomat, *Bioconjug. Chem.* **2016**, *27*, 1807-1812.
[221] I. Grgicevic, I. Mikulandra, M. Bukvic, M. Banjanac, V. Radovanovic, I. Habinovec, B. Bertosa & P. Novak, *Int. J. Antimicrob. Agents* **2020**, *56*, 106147.
[222] A. Haseloer, T. Lutzenburg, J. P. Strache, J. Neudorfl, I. Neundorf & A. Klein, *Chembiochem* **2021**, *22*, 694-704.
[223] M. P. Heng, S. K. Sinniah, W. Y. Teoh, K. S. Sim, S. W. Ng, Y. K. Cheah & K. W. Tan, *Spectrochim. Acta A* **2015**, *150*, 360-372.
[224] T. V. Petrasheuskaya, M. A. Kiss, O. Dömötör, T. Holczbauer, N. V. May, G. Spengler, A. Kincses, A. Čipak Gašparović, É. Frank & É. A. Enyedy, *New J. Chem.* **2020**, *44*, 12154-12168.
[225] S. Singh, A. K. Tiwari, R. Varshney, R. Mathur, G. Shukla, N. Bag, B. Singh & A. K. Mishra, *Spectrochim. Acta A* **2016**, *153*, 566-571.
[226] N. D. Thanh, V. N. Toan, D. N. Toan & V. M. Trang, *Med. Chem. Res.* **2024**, *34*, 476-495.
[227] H. T. K. Van, N. D. Thanh & D. T. Nguyet, *Med. Chem. Res.* **2025**, *34*, 1746-1770.

[228] X. Dong, H. Wang, H. Zhang, M. Li, Z. Huang, Q. Wang & X. Li, *Carbohydr. Polym.* **2022**, *294*, 119839.
[229] D. F. Earley, J. Esteban Flores, A. Guillou & J. P. Holland, *Dalton Trans.* **2022**, *51*, 5041-5052.
[230] R. Hueting, M. Christlieb, J. R. Dilworth, E. Garcia Garayoa, V. Gouverneur, M. W. Jones, V. Maes, R. Schibli, X. Sun & D. A. Tourwe, *Dalton Trans.* **2010**, *39*, 3620-3632.
[231] R. Hueting, R. Tavare, J. R. Dilworth & G. E. Mullen, *J. Inorg. Biochem.* **2013**, *128*, 108-111.
[232] P. Ledwon, W. Goldeman, K. Haldys, M. Jewginski, G. Calamai, J. Rossowska, A. M. Papini, P. Rovero & R. Latajka, *J. Enzyme Inhib. Med. Chem.* **2023**, *38*, 2193676.
[233] M. L. Low, L. Maigre, P. Dorlet, R. Guillot, J. M. Pages, K. A. Crouse, C. Policar & N. Delsuc, *Bioconjug. Chem.* **2014**, *25*, 2269-2284.
[234] B. M. Paterson, J. A. Karas, D. B. Scanlon, J. M. White & P. S. Donnelly, *Inorg. Chem.* **2010**, *49*, 1884-1893.
[235] N. Salvarese, B. Spolaore, S. Marangoni, A. Pasin, A. Galenda, S. Tamburini, G. Cicoria, F. Refosco & C. Bolzati, *J. Inorg. Biochem.* **2018**, *183*, 18-31.
[236] Y. S. Sung, W. Wu, M. A. Ewbank, R. D. Utterback, M. T. Marty & E. Tomat, *ChemMedChem* **2021**, *16*, 2764-2768.
[237] Z. Zhang, P. Yu, Y. Gou, J. Zhang, S. Li, M. Cai, H. Sun, F. Yang & H. Liang, *J. Med. Chem.* **2019**, *62*, 10630-10644.
[238] T. Etrych, H. Lucas, O. Janouskova, P. Chytil, T. Mueller & K. Mader, *J. Control Release* **2016**, *226*, 168-181.
[239] M. S. Goncalves, *Chem. Rev.* **2009**, *109*, 190-212.
[240] J. Rao, A. Dragulescu-Andrasi & H. Yao, *Curr. Opin. Biotechno.l* **2007**, *18*, 17-25.
[241] A. Refaat, M. L. Yap, G. Pietersz, A. P. G. Walsh, J. Zeller, B. Del Rosal, X. Wang & K. Peter, *J Nanobiotechnology* **2022**, *20*, 450.
[242] J. Gao, Z. Chen, X. Li, M. Yang, J. Lv, H. Li & Z. Yuan, *Int. J. Mol. Sci.* **2022**, *23*.
[243] S. Gull, M. H. Jamil, X. Zhang, H. S. Kwok & G. Li, *ChemistryOpen* **2022**, *11*, e202100285.
[244] T. Sun, H. Zhao, L. Hu, X. Shao, Z. Lu, Y. Wang, P. Ling, Y. Li, K. Zeng & Q. Chen, *Acta. Pharm. Sin. B.* **2024**, *14*, 2428-2446.
[245] H. Chen, Q. Hu, W. Li, X. Cai, L. Mao & R. Li, *Environ. Health* **2023**, *1*, 75-89.
[246] K. K. Karukstis, E. H. Thompson, J. A. Whiles & R. J. Rosenfeld, *Biophys. Chem.* **1998**, *73*, 249-263.
[247] A. R. Cowley, J. Davis, J. R. Dilworth, P. S. Donnelly, R. Dobson, A. Nightingale, J. M. Peach, B. Shore, D. Kerr & L. Seymour, *Chem. Commun. (Camb)* **2005**, 845-847.
[248] S. Gu, P. Yu, J. Hu, Y. Liu, Z. Li, Y. Qian, Y. Wang, Y. Gou & F. Yang, *Eur. J. Med. Chem.* **2019**, *164*, 654-664.
[249] J. L. Hickey, J. L. James, C. A. Henderson, K. A. Price, A. I. Mot, G. Buncic, P. J. Crouch, J. M. White, A. R. White, T. A. Smith & P. S. Donnelly, *Inorg. Chem.* **2015**, *54*, 9556-9567.
[250] J. P. Holland, P. J. Barnard, S. R. Bayly, H. M. Betts, G. C. Churchill, J. R. Dilworth, R. Edge, J. C. Green & R. Hueting, *Eur. J. Inorg. Chem.* **2008**, *2008*, 1985-1993.
[251] A. N. Kate, A. A. Kumbhar, A. A. Khan, P. V. Joshi & V. G. Puranik, *Bioconjug. Chem.* **2014**, *25*, 102-114.
[252] S. S. Marufa, T. Rahman, M. M. Rahman, M. M. Rahman, S. J. Khan, R. Jahan, H. Nishino, M. S. Alam & M. A. Haque, *RSC Adv.* **2024**, *14*, 35198-35214.
[253] Meenakshi, A. Bera, A. Kumar, M. Kumar & R. P. John, *Spectrochim. Acta A* **2025**, *336*, 126006.
[254] S. I. Pascu, P. A. Waghorn, T. D. Conry, H. M. Betts, J. R. Dilworth, G. C. Churchill, T. Pokrovska, M. Christlieb, F. I. Aigbirhio & J. E. Warren, *Dalton Trans.* **2007**, 4988-4997.
[255] V. N. Vadakkedathu Palakkeezhillam, J. Haribabu, V. S. Kumar, J. F. Santibanez, V. Manakkadan, P. Rasin, M. Garg, N. Bhuvanesh & A. Sreekanth, *Organometallics* **2024**, *43*, 242-260.
[256] R. Diana & B. Panunzi, *Molecules* **2020**, *25*.
[257] C. Schattschneider, S. Doniz Kettenmann, S. Hinojosa, J. Heinrich & N. Kulak, *Coord. Chem. Rev.* **2019**, *385*, 191-207.

[258] M. T. Carter, M. Rodriguez & A. J. Bard, *J. Am. Chem. Soc.* **2002**, *111*, 8901-8911.
[259] G. R. Chaudhary, P. Singh, G. Kaur, S. K. Mehta, S. Kumar & N. Dilbaghi, *Inorg. Chem.* **2015**, *54*, 9002-9012.
[260] P. Garg, G. Kaur, G. R. Chaudhary, S. Kaur, S. L. Gawali & P. A. Hassan, *Colloids Surf. B.* **2018**, *164*, 116-124.
[261] K. Nagaraj & S. Arunachalam, *New J. Chem.* **2014**, *38*, 366-375.
[262] B. Gruber, E. Kataev, J. Aschenbrenner, S. Stadlbauer & B. Konig, *J. Am. Chem. Soc.* **2011**, *133*, 20704-20707.
[263] G. Grasso & S. Bonnet, *Metallomics* **2014**, *6*, 1346-1357.
[264] E. Kimura, T. Shiota, T. Koike, M. Shiro & M. Kodama, *J. Am. Chem. Soc.* **2002**, *112*, 5805-5811.
[265] B. Siewert, M. Langerman, Y. Hontani, J. T. M. Kennis, V. H. S. van Rixel, B. Limburg, M. A. Siegler, V. Talens Saez, R. E. Kieltyka & S. Bonnet, *Chem. Commun. (Camb)* **2017**, *53*, 11126-11129.
[266] M. Belicchi Ferrari, F. Bisceglie, G. Pelosi, M. Sassi, P. Tarasconi, M. Cornia, S. Capacchi, R. Albertini & S. Pinelli, *J. Inorg. Biochem.* **2002**, *90*, 113-126.
[267] M. Belicchi-Ferrari, F. Bisceglie, G. Pelosi, S. Pinelli & P. Tarasconi, *Polyhedron* **2007**, *26*, 5150-5161.
[268] S. Eğlence-Bakır, M. Şahin, M. Zahoor, E. Dilmen-Portakal & B. Ülküseven, *Polyhedron* **2020**, *190*.
[269] O. A. El-Gammal, A. A. El-Bindary, A. M. Eldesoky & I. M. Abd Al-Gader, *J. Mol. Struct.* **2025**, *1322*.
[270] P. Jutten, W. Schumann, A. Hartl, L. Heinisch, U. Grafe, W. Werner & H. Ulbricht, *Bioorg. Med. Chem. Lett.* **2002**, *12*, 1339-1342.
[271] C. Kar, B. Ojha & G. Das, *Luminescence* **2013**, *28*, 339-344.
[272] C. A. A. Kelderman, P. Davey, M. T. Ma, M. de Veer, E. Salimova, P. S. Donnelly & B. M. Paterson, *Dalton Trans.* **2022**, *51*, 14064-14078.
[273] R. J. Laverick, N. Zhang, E. Reid, J. Kim, K. J. Kilpin & J. A. Kitchen, *J. Coord. Chem.* **2021**, *74*, 321-340.
[274] V. Markovic, A. Janicijevic, T. Stanojkovic, B. Kolundzija, D. Sladic, M. Vujcic, B. Janovic, L. Joksovic, P. T. Djurdjevic, N. Todorovic, S. Trifunovic & M. D. Joksovic, *Eur. J. Med. Chem.* **2013**, *64*, 228-238.
[275] S. Song, A. You, Z. Chen, G. Zhu, H. Wen, H. Song & W. Yi, *Eur. J. Med. Chem.* **2017**, *139*, 815-825.
[276] A. I. Matesanz, C. Pastor & P. Souza, *Inorg. Chem. Comm.* **2007**, *10*, 97-100.
[277] B. M. Paterson, J. M. White & P. S. Donnelly, *Dalton Trans.* **2010**, *39*, 2831-2837.
[278] V. V. Pavlishchuk, S. V. Kolotilov, A. W. Addison, R. J. Butcher & E. Sinn, *J. Chem. Soc., Dalton Trans.* **2000**, 335-341.
[279] M. J. Romero, M. Martinez-Calvo, M. Maneiro, G. Zaragoza, R. Pedrido & A. M. Gonzalez-Noya, *Inorg. Chem.* **2019**, *58*, 881-889.
[280] S. A. Cotton & P. R. Raithby, *Coord. Chem. Rev.* **2017**, *340*, 220-231.
[281] D. W. Keogh, in *Encycl. Inorg. Bioinorg. Chem.*, **2011**.
[282] Y. Lyu, L. M. Becerril, M. Vanzan, S. Corni, M. Cattelan, G. Granozzi, M. Frasconi, P. Rajak, P. Banerjee, R. Ciancio, F. Mancin & P. Scrimin, *Adv. Mater.* **2024**, *36*, e2211624.
[283] A. Butikofer & P. Chen, *Inorg. Chem.* **2023**, *62*, 4188-4196.
[284] C. Kiaku, J. M. Walsh, M. C. Leech, D. L. Poole, J. Mason, I. C. A. Goodall, P. Devo & K. Lam, *Org. Lett.* **2023**, *25*, 1147-1150.
[285] W. D. J. Tremlett, J. D. Crowley, L. J. Wright & C. G. Hartinger, *Dalton Trans.* **2024**, *53*, 14742-14751.
[286] H.-S. Jung, D.-S. Moon, J.-K. Lee & H. C. Gu, *J. Nanomater.* **2012**, *2012*.
[287] P. Ghosh, G. Han, M. De, C. K. Kim & V. M. Rotello, *Adv. Drug Deliv. Rev.* **2008**, *60*, 1307-1315.
[288] S. Ghosh & G. P. Tochtrop, *Tetrahedron Lett.* **2009**, *50*, 1723-1726.
[289] A. Akao, N. Nonoyama & N. Yasuda, *Tetrahedron Lett.* **2006**, *47*, 5337-5340.
[290] M. Meldal & C. W. Tornoe, *Chem. Rev.* **2008**, *108*, 2952-3015.
[291] R. C. Chadwick, U. Khan, J. N. Coleman & A. Adronov, *Small* **2013**, *9*, 552-560.

[292] J. A. Gavin, M. E. Garcia, A. J. Benesi & T. E. Mallouk, *J. Org. Chem.* **1998**, *63*, 7663-7669.
[293] J. Schoning, L. Rosner, D. A. Depke, S. Huwel, A. Kukhar, M. Schafers & A. Rentmeister, *Bioconjug. Chem.* **2025**, *36*, 34-43.
[294] Y. Yang & R. Kluger, *Chem. Commun. (Camb)* **2010**, *46*, 7557-7559.
[295] N. Bou Orm, Q. A. Trieu & S. Daniele, *Molecules* **2018**, *23*.
[296] S. Yamashita, T. Sudo, H. Kamiya & Y. Okada, *ChemistrySelect* **2021**, *6*, 2923-2927.
[297] G. Nemeth, Z. Greff, A. Sipos, Z. Varga, R. Szekely, M. Sebestyen, Z. Jaszay, S. Beni, Z. Nemes, J. L. Pirat, J. N. Volle, D. Virieux, A. Gyuris, K. Kelemenics, E. Ay, J. Minarovits, S. Szathmary, G. Keri & L. Orfi, *J. Med. Chem.* **2014**, *57*, 3939-3965.
[298] M. K. Urlam, R. Pireddu, Y. Ge, X. Zhang, Y. Sun, H. R. Lawrence, W. C. Guida, S. M. Sebti & N. J. Lawrence, *Medchemcomm* **2013**, *4*, 932-941.
[299] M. D. Shultz, J. U. Reveles, S. N. Khanna & E. E. Carpenter, *J. Am. Chem. Soc.* **2007**, *129*, 2482-2487.
[300] E. Belmonte-Reche, M. Martinez-Garcia, P. Penalver, V. Gomez-Perez, R. Lucas, F. Gamarro, J. M. Perez-Victoria & J. C. Morales, *Eur. J. Med. Chem.* **2016**, *119*, 132-140.
[301] Z. Kausar, A. Mansha & S. Asim, *J. Fluoresc.* **2024**, *34*, 1365-1378.
[302] M. Bakir & O. Brown, *J. Mol. Struct.* **2011**, *1006*, 402-408.
[303] J. K. Swearingen & D. X. West, *Transit. Met. Chem.* **2001**, *26*, 252-260.
[304] F. Rashid, S. Zaib, A. Ibrar, S. A. Ejaz, A. Saeed, J. Iqbal & I. Khan, *Anticancer Agents Med. Chem.* **2021**, *21*, 1082-1091.
[305] X. Chen & J. I. Brauman, *J. Am. Chem. Soc.* **2008**, *130*, 15038-15046.
[306] S. Shenoi-Perdoor, A. Noureddine, F. Dubois, M. Wong Chi Man & X. Cattoën, in *Handbook of Sol-Gel Science and Technology: Processing, Characterization and Applications* (Eds.: Lisa Klein, Mario Aparicio, & Andrei Jitianu), Springer International Publishing, Cham, **2018**, pp. 3001-3040.
[307] A. Li, K. Huang, W. Pan, Y. Wu, Y. Liang, Z. Zhang, D. Wu, L. Ma & Y. Gou, *J. Med. Chem.* **2024**, *67*, 9091-9103.
[308] L. Liang & D. Astruc, *Coord. Chem. Rev.* **2011**, *255*, 2933-2945.
[309] X. Man, W. Li, M. Zhu, S. Li, G. Xu, Z. Zhang, H. Liang & F. Yang, *Angew. Chem.* **2024**, *136*.
[310] H. Abdelbaki, A. Djemoui, M. R. Ouahrani, M. Messaoudi, I. Ben Amor, H. Alsaeedi, D. Cornu, M. Bechelany & A. Barhoum, *J. Mol. Struct.* **2025**, *1324*.
[311] Naveen, R. K. Tittal, V. D. Ghule, N. Kumar, L. Kumar, K. Lal & A. Kumar, *J. Mol. Struct.* **2020**, *1209*.
[312] G. Singh, Sushma, Priyanka, Diksha, Mohit, S. Gupta, M. Angeles Esteban, C. Espinosa-Ruíz & D. González-Silvera, *J. Mol. Struct.* **2022**, *1255*.
[313] M. G. Temraz, P. A. Elzahhar, A. B. A. El-Din, A. A. Bekhit, H. F. Labib & A. S. F. Belal, *Eur. J. Med. Chem.* **2018**, *151*, 585-600.
[314] Y. Yang, Y. Yang & C. Ni, *J. Inorg. Organomet. Polym. Mater.* **2022**, *32*, 4359-4372.
[315] N. S. Ham & J. B. Willis, *Spectrochim. Acta* **1960**, *16*, 279-301.
[316] D. M. Wiles, B. A. Gingras & T. Suprunchuk, *Can. J. Chem.* **1967**, *45*, 469-473.
[317] E. Krakor, I. Gessner, M. Wilhelm, V. Brune, J. Hohnsen, L. Frenzen & S. Mathur, *MRS Commun.* **2021**, *11*, 363-371.
[318] T. Zuccheri, M. Colonna, I. Stefanini, C. Santini & D. D. Gioia, *Mater.* **2013**, *6*, 3270-3283.
[319] A. Bachinger & G. Kickelbick, *Appl. Catal. Gen.* **2011**, *409-410*, 122-132.
[320] C. Queffelec, M. Petit, P. Janvier, D. A. Knight & B. Bujoli, *Chem. Rev.* **2012**, *112*, 3777-3807.
[321] S. Ortelli, A. L. Costa, I. Zanoni, M. Blosi, O. Geiss, I. Bianchi, D. Mehn, F. Fumagalli, G. Ceccone, G. Guerrini & L. Calzolai, *Colloids Surf. B Biointerfaces* **2021**, *207*, 112037.
[322] E. Goya-Jorge, C. Rampal, N. Loones, S. J. Barigye, L. E. Carpio, R. Gozalbes, C. Ferroud, M. Sylla-Iyarreta Veitia & R. M. Giner, *Eur. J. Med. Chem.* **2020**, *207*, 112777.
[323] T. Hirayama, S. Ueda, T. Okada, N. Tsurue, K. Okuda & H. Nagasawa, *Chemistry* **2014**, *20*, 4156-4162.

[324] B. Mravec, S. Budzak, M. Medved, L. F. Pasteka, C. Slavov, T. Sassmannshausen, J. Wachtveitl, J. Kozisek, L. Hegedusova, J. Filo & M. Cigan, *J. Org. Chem.* **2021**, *86*, 11633-11646.
[325] S. Ushijima, S. Dohi, K. Moriyama & H. Togo, *Tetrahedron* **2012**, *68*, 1436-1442.
[326] C. Wang, J. Qin, X. Shen, R. Riedel, K. Harms & E. Meggers, *Angew. Chem. Int. Ed. Engl.* **2016**, *55*, 685-688.
[327] K. Zeng, J. Ye, X. Meng, S. Dechert, M. Simon, S. Gong, R. A. Mata & K. Zhang, *Chemistry* **2022**, *28*, e202200648.
[328] D. O. Berbasov, I. D. Ojemaye & V. A. Soloshonok, *J. Fluor. Chem.* **2004**, *125*, 603-607.
[329] D. R. Richardson, D. S. Kalinowski, V. Richardson, P. C. Sharpe, D. B. Lovejoy, M. Islam & P. V. Bernhardt, *J. Med. Chem.* **2009**, *52*, 1459-1470.
[330] S. A. Archer, T. Keane, M. Delor, E. Bevon, A. J. Auty, D. Chekulaev, I. V. Sazanovich, M. Towrie, A. Meijer & J. A. Weinstein, *Chemistry* **2017**, *23*, 18239-18251.
[331] M. R. Norris, J. J. Concepcion, C. R. Glasson, Z. Fang, A. M. Lapides, D. L. Ashford, J. L. Templeton & T. J. Meyer, *Inorg. Chem.* **2013**, *52*, 12492-12501.
[332] E. Taschner, A. Chimiak, B. Bator & T. Sokołowska, *Justus Liebigs Ann. Chem.* **2006**, *646*, 134-136.
[333] F. Bisceglie, M. Tavone, F. Mussi, S. Azzoni, S. Montalbano, S. Franzoni, P. Tarasconi, A. Buschini & G. Pelosi, *J. Inorg. Biochem.* **2018**, *179*, 60-70.
[334] S. Ghosh, A. K. Misra, G. Bhatia, M. M. Khan & A. K. Khanna, *Bioorg. Med. Chem. Lett.* **2009**, *19*, 386-389.
[335] A. C. Tenchiu Deleanu, I. D. Kostas, D. Kovala-Demertzi & A. Terzis, *Carbohydr. Res.* **2009**, *344*, 1352-1364.
[336] H. Tajima & G. Li, *Synlett* **1997**, *1997*, 773-774.
[337] J. Grabeck, T. Lutzenburg, P. Frommelt & I. Neundorf, *Molecules* **2022**, *27*.
[338] J. Copko, L. Ludvikova & T. Slanina, *Chemistry* **2025**, *31*, e202500678.
[339] L. Cui, Z. Peng, C. Ji, J. Huang, D. Huang, J. Ma, S. Zhang, X. Qian & Y. Xu, *Chem. Commun. (Camb)* **2014**, *50*, 1485-1487.
[340] N. Diesendorf, P. Wenisch, J. Oppl & M. R. Heinrich, *Org. Lett.* **2023**, *25*, 76-81.
[341] S. Goswami & S. Jana, *Lett. Org. Chem.* **2010**, *7*, 399-405.
[342] S. Gundogdu, H. E. Duran, M. Arslan, B. D. Cetinkaya & C. Turkes, *Bioorg. Chem.* **2025**, *163*, 108689.
[343] Z. Zhou, S. Liu, L. Yang, Q. Kuang, H. Zhou, C. Zhuo & X. Wang, *ACS Catal.* **2023**, *13*, 15116-15125.
[344] M. Tomasch, J. S. Schwed, K. Kuczka, S. Meyer Dos Santos, S. Harder, R. M. Nusing, A. Paulke & H. Stark, *ACS Med. Chem. Lett.* **2012**, *3*, 774-779.
[345] Y. Zhang, Z. Wang, X. Zhang, W. Zhou & L. Huang, *Carbohydr. Res.* **2011**, *346*, 2156-2164.
[346] E. Cheng, T. C. Sun & Y. Oliver Su, *J. Chin. Chem. Soc.* **2013**, *40*, 551-555.
[347] U. Basu, A. Wilsmann, S. Turck, H. Hoffmeister, M. Schiedel, G. Gasser & I. Ott, *RSC Med. Chem.* **2025**, *16*, 2663-2676.
[348] N. J. Wheate, C. R. Brodie, J. G. Collins, S. Kemp & J. R. Aldrich-Wright, *Mini Rev. Med. Chem.* **2007**, *7*, 627-648.
[349] G. Kaur, G. Hedouin, R. Mandal, J. B. Jasinski, X. He, M. Su, J. Liu, X. Guo, J. R. Walensky, G. A. Baker, F. Gallou & S. Handa, *ACS Catal.* **2024**, *14*, 15645-15653.
[350] D. Li, Y. Shu, P. Li, W. Zhang, H. Ni & Y. Cao, *Med. Chem. Res.* **2012**, *22*, 3119-3125.
[351] H. J. Kim, T. Ishii, M. Zheng, S. Watanabe, K. Toh, Y. Matsumoto, N. Nishiyama, K. Miyata & K. Kataoka, *Drug Deliv. Transl. Res.* **2014**, *4*, 50-60.
[352] R. Anjum, D. Palanimuthu, D. S. Kalinowski, W. Lewis, K. C. Park, Z. Kovacevic, I. U. Khan & D. R. Richardson, *Inorg. Chem.* **2019**, *58*, 13709-13723.
[353] G. R. Walke & S. Ruthstein, *ACS Omega* **2019**, *4*, 12278-12285.
[354] T. S. Lobana, M. Kaushal, R. Bala, L. Nim, K. Paul, D. S. Arora, A. Bhatia, S. Arora & J. P. Jasinski, *J. Inorg. Biochem.* **2020**, *212*, 111205.
[355] A. Marini, A. Munoz-Losa, A. Biancardi & B. Mennucci, *J. Phys. Chem. B* **2010**, *114*, 17128-17135.
[356] S. Spange & T. G. Mayerhofer, *Chemphyschem* **2022**, *23*, e202200100.

[357] W.-X. Jiang, W.-X. Liu, C.-L. Wang, S.-Z. Zhan & S.-P. Wu, *New J. Chem.* **2020**, *44*, 2721-2726.
[358] D. Radomska, O. K. Szewczyk-Roszczenko, K. Marciniec, M. Ksiazek, J. Kusz, P. Roszczenko, A. Szymanowska, D. Radomski, K. Bielawski & R. Czarnomysy, *Bioorg. Chem.* **2024**, *148*, 107486.
[359] R. Chen, X. Yang, H. Tian, X. Wang, A. Hagfeldt & L. Sun, *Chem. Mater.* **2007**, *19*, 4007-4015.
[360] M. J. Behlen & C. Uyeda, *J. Am. Chem. Soc.* **2020**, *142*, 17294-17300.
[361] D. S. Beaudoin & S. O. Obare, *Tetrahedron Lett.* **2008**, *49*, 6054-6057.
[362] R. Adam, R. Ballesteros-Garrido, O. Vallcorba, B. Abarca, R. Ballesteros, F. R. Leroux, F. Colobert, J. M. Amigó & J. Rius, *Tetrahedron Lett.* **2013**, *54*, 4316-4319.
[363] W. Harnying & A. Berkessel, *Chemistry* **2015**, *21*, 6057-6061.
[364] M. Trigo-López, A. Muñoz, S. Ibeas, F. Serna, F. C. García & J. M. García, *Sens. Actuators B Chem.* **2016**, *226*, 118-126.
[365] J. Frey, A. D. Bond & A. B. Holmes, *Chem. Commun. (Camb)* **2002**, 2424-2425.
[366] T. Phillips, I. Haq, A. J. Meijer, H. Adams, I. Soutar, L. Swanson, M. J. Sykes & J. A. Thomas, *Biochem.* **2004**, *43*, 13657-13665.
[367] Q. Zhang & Z. Cao, *J. Phys. Chem. B* **2021**, *125*, 3005-3013.
[368] S. Leng, Q. Qiao, L. Miao, W. Deng, J. Cui & Z. Xu, *Chem. Commun. (Camb)* **2017**, *53*, 6448-6451.
[369] S. Vassiliou, E. Weglarz-Tomczak, L. Berlicki, M. Pawelczak, B. Nocek, R. Mulligan, A. Joachimiak & A. Mucha, *J. Med. Chem.* **2014**, *57*, 8140-8151.
[370] G. Kumar, R. S. Pillai, N.-u. H. Khan & S. Neogi, *Appl. Catal. B-Environ.* **2021**, *292*.
[371] I. Gillaizeau-Gauthier, F. Odobel, M. Alebbi, R. Argazzi, E. Costa, C. A. Bignozzi, P. Qu & G. J. Meyer, *Inorg. Chem.* **2001**, *40*, 6073-6079.
[372] N. Niamnont, N. Kimpitak, K. Wongravee, P. Rashatasakhon, K. K. Baldridge, J. S. Siegel & M. Sukwattanasinitt, *Chem. Commun. (Camb)* **2013**, *49*, 780-782.
[373] A. Kamal, G. Ramesh, O. Srinivas & P. Ramulu, *Bioorg Med Chem Lett* **2004**, *14*, 471-474.
[374] H. Rahimi, R. Hosseinzadeh & M. Tajbakhsh, *J. Photochem. and Photobiol. A Chem.* **2021**, *407*.
[375] C. M. Álvarez, H. Barbero & D. Miguel, *Eur. J. Org. Chem.* **2015**, *2015*, 6631-6640.
[376] M. B. Sims, J. J. Lessard, L. Bai & B. S. Sumerlin, *Macromol.* **2018**, *51*, 6380-6386.
[377] J. Singh, N. Steck, D. De, A. Hofer, A. Ripp, I. Captain, M. Keller, P. A. Wender, R. Bhandari & H. J. Jessen, *Angew. Chem. Int. Ed. Engl.* **2019**, *58*, 3928-3933.
[378] J. Chen, S. Ko, L. Liu, Y. Sheng, H. Han & X. Li, *New J. Chem.* **2015**, *39*, 2889-2900.
[379] D. Rennison, S. M. Gueret, O. Laita, R. J. Bland, I. A. Sutherland, I. K. Boddy & M. A. Brimble, *Aust. J. Chem.* **2016**, *69*, 1268-1276.
[380] M. K. Peters, F. Rohricht, C. Nather & R. Herges, *Org. Lett.* **2018**, *20*, 7879-7883.
[381] R. Luguya, L. Jaquinod, F. R. Fronczek, M. G. H. Vicente & K. M. Smith, *Tetrahedron* **2004**, *60*, 2757-2763.
[382] L. Fang, G. Trigiante, R. Crespo-Otero, C. S. Hawes, M. P. Philpott, C. R. Jones & M. Watkinson, *Chem. Sci.* **2019**, *10*, 10881-10887.
[383] H. Lu, H. Zeng, W. Wei, Y. Chen, Z. Zhou, X. Ning & P. Hu, *Theranostics* **2024**, *14*, 7589-7603.
[384] C. Yang, K. Chen, M. Chen, X. Hu, S. Y. Huan, L. Chen, G. Song & X. B. Zhang, *Anal. Chem.* **2019**, *91*, 2727-2733.
[385] Z. Shi, Q. Song, R. Göstl & A. Herrmann, *CCS Chem.* **2021**, *3*, 2333-2344.
[386] M. SasiKumar, G. Maddala, M. Ambapuram, M. Subburu, J. R. Vaidya, S. N. Babu, P. Chetti, R. Mitty & S. Pola, *Sustain. Energy Fuels* **2020**, *4*, 4754-4767.
[387] K. Kolanji & M. Baumgarten, *Chemistry* **2020**, *26*, 3626-3632.
[388] P. O. Schwartz, S. Fortsch, A. Vogt, E. Mena-Osteritz & P. Bauerle, *Beilstein J. Org. Chem.* **2019**, *15*, 1379-1393.
[389] W. Wang, X. Feng & H. Du, *Org. Biomol. Chem.* **2016**, *14*, 6683-6686.
[390] W. Ma, F. Chen, Y. Liu, Y. M. He & Q. H. Fan, *Org. Lett.* **2016**, *18*, 2730-2733.
[391] D. M. Lyubov, G. K. Fukin, A. V. Cherkasov, A. S. Shavyrin, A. A. Trifonov, L. Luconi, C. Bianchini, A. Meli & G. Giambastiani, *Organometallics* **2009**, *28*, 1227-1232.
[392] R. Karki, C. Park, K. Y. Jun, T. M. Kadayat, E. S. Lee & Y. Kwon, *Eur. J. Med. Chem.* **2015**, *90*, 360-378.

[393] F. Tessore, D. Roberto, R. Ugo, M. Pizzotti, S. Quici, M. Cavazzini, S. Bruni & F. De Angelis, *Inorg. Chem.* **2005**, *44*, 8967-8978.
[394] C. B. Lan & K. Auclair, *J. Org. Chem.* **2023**, *88*, 10086-10095.
[395] K. D. Nam, M. Han, J. Yoon, E.-A. Kim, S.-W. Cho & H.-G. Hahn, *Bull. Korean Chem. Soc.* **2013**, *34*, 271-274.
[396] L. Tei, Z. Baranyai, M. Botta, L. Piscopo, S. Aime & G. B. Giovenzana, *Org. Biomol. Chem.* **2008**, *6*, 2361-2368.
[397] Y. Shi, A. V. Gulevich & V. Gevorgyan, *Angew. Chem. Int. Ed. Engl.* **2014**, *53*, 14191-14195.
[398] H. Yang, N. Huo, P. Yang, H. Pei, H. Lv & X. Zhang, *Org. Lett.* **2015**, *17*, 4144-4147.

7. Supporting Information

7.1 NMR Data

7.1.1 NMR data TSCs with functional groups at the *N*4 position

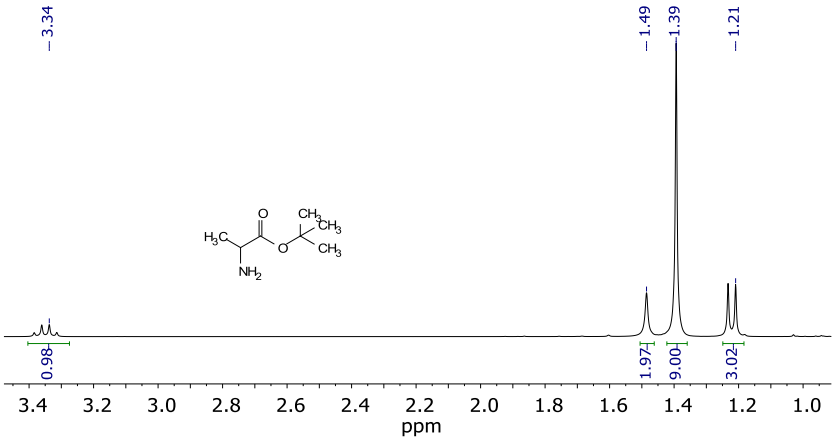


Figure 94. ^{1}H NMR spectrum of *L*-alanine *tert*-butyl ester in $CDCl_3$ at 499 MHz.

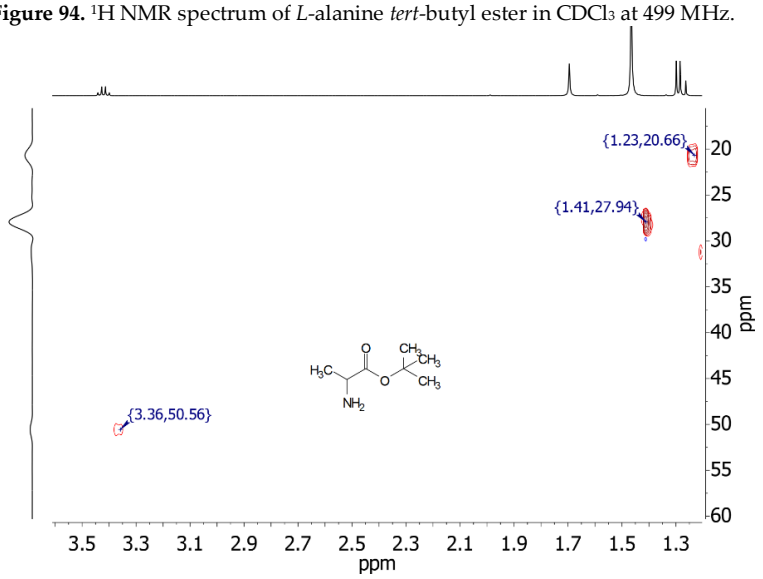


Figure 95. ^{1}H,^{13}C HMQC/HSQC NMR spectrum of *L*-alanine *tert*-butyl ester in $CDCl_3$ at 499 MHz.

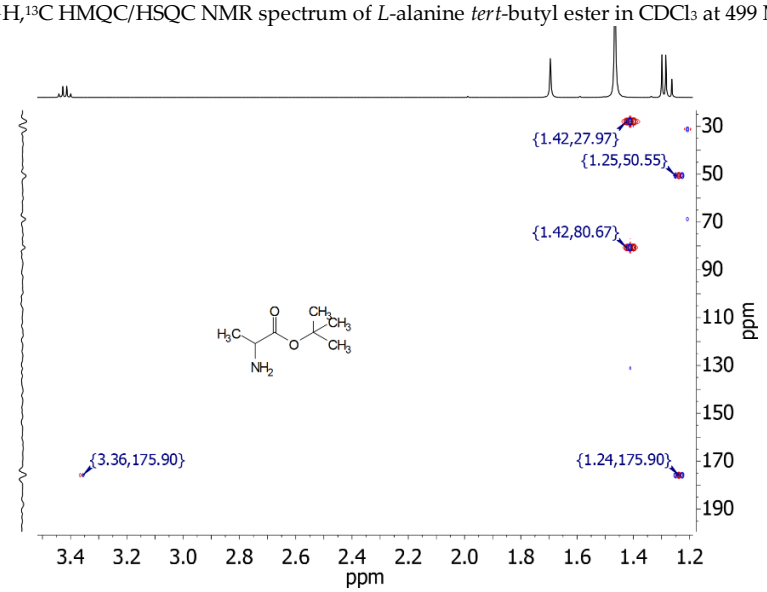


Figure 96. ^{1}H,^{13}C HMBC NMR spectrum of *L*-alanine *tert*-butyl ester in $CDCl_3$ at 499 MHz.

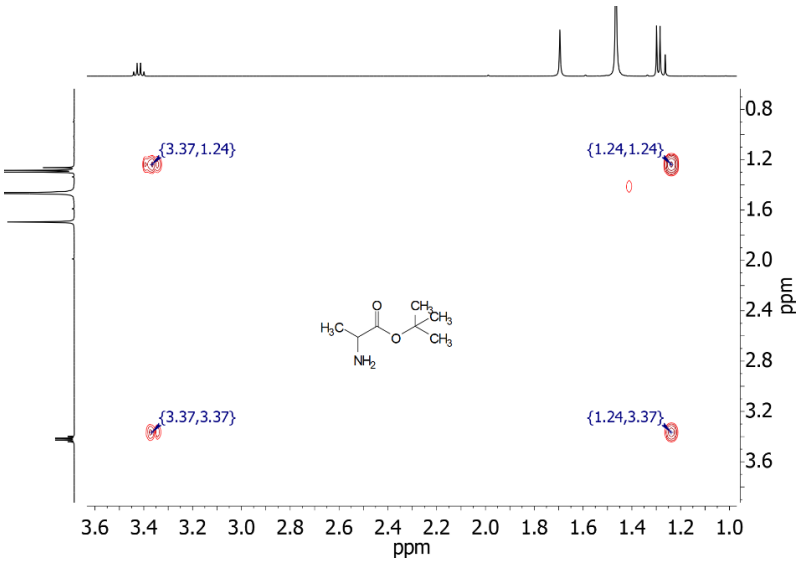


Figure 97. $^{1}H,^{1}H$ COSY NMR spectrum of *L*-alanine *tert*-butyl ester spectrum in $CDCl_3$ at 499 MHz.

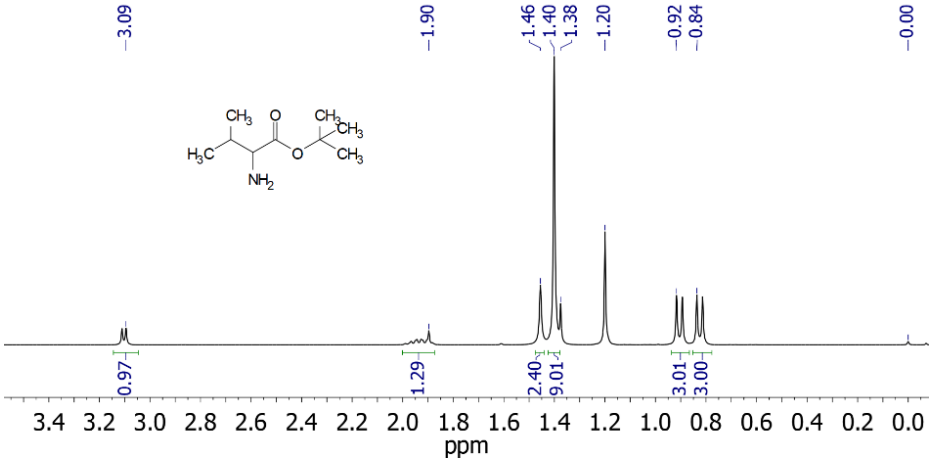


Figure 98. ^{1}H NMR spectrum of *L*-valine *tert*-butyl ester in $CDCl_3$ at 300 MHz.

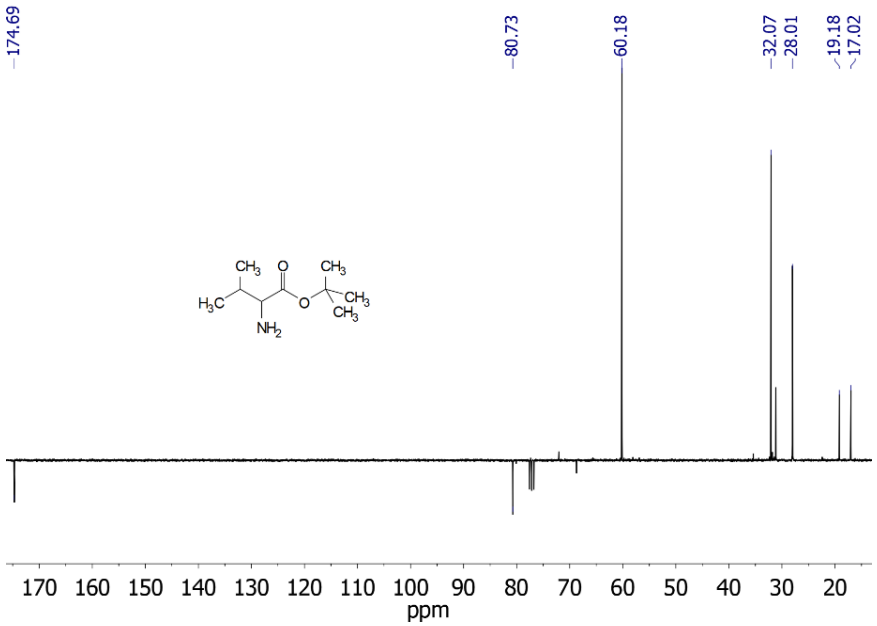


Figure 99. ^{13}C-DEPTQ NMR spectrum of *L*-valine *tert*-butyl ester in $CDCl_3$ at 300 MHz.

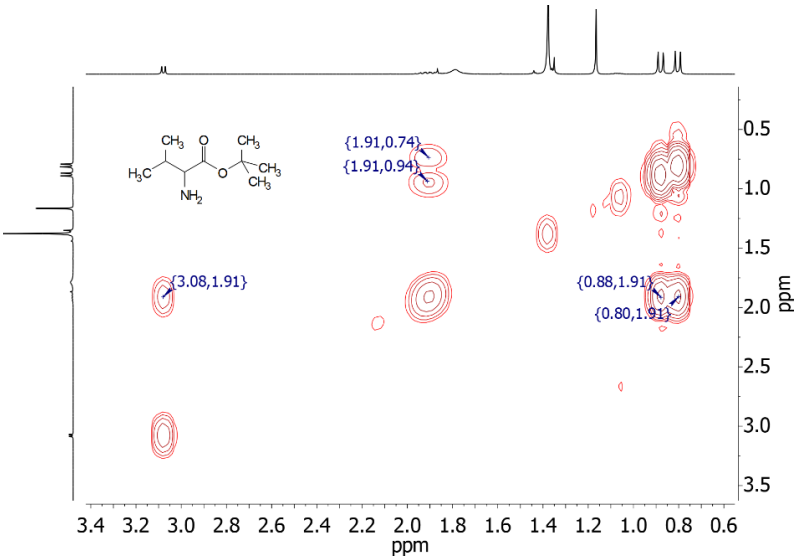


Figure 100. $^{1}H,^{1}H$ COSY NMR spectrum of *L*-valine *tert*-butyl ester in $CDCl_3$ at 300 MHz.

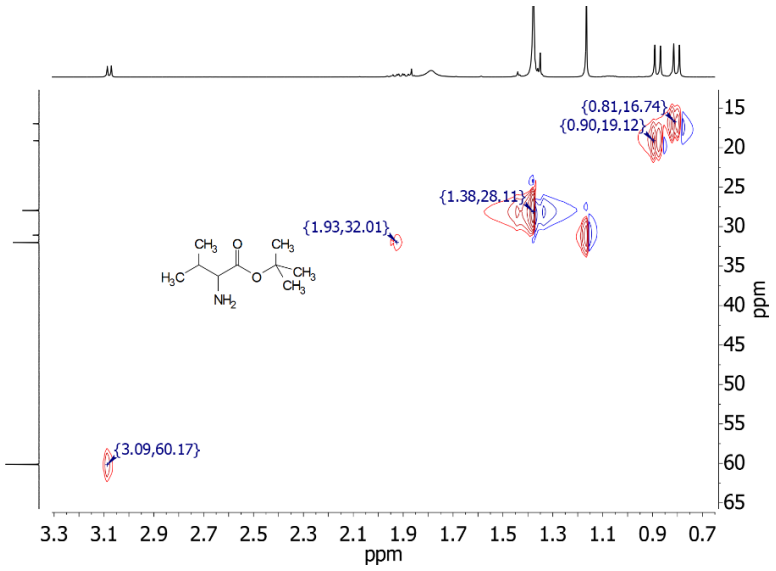


Figure 101. $^{1}H\ ^{13}C$ HMQC/HSQC NMR spectrum of *L*-valine *tert*-butyl ester in $CDCl_3$ at 300 MHz.

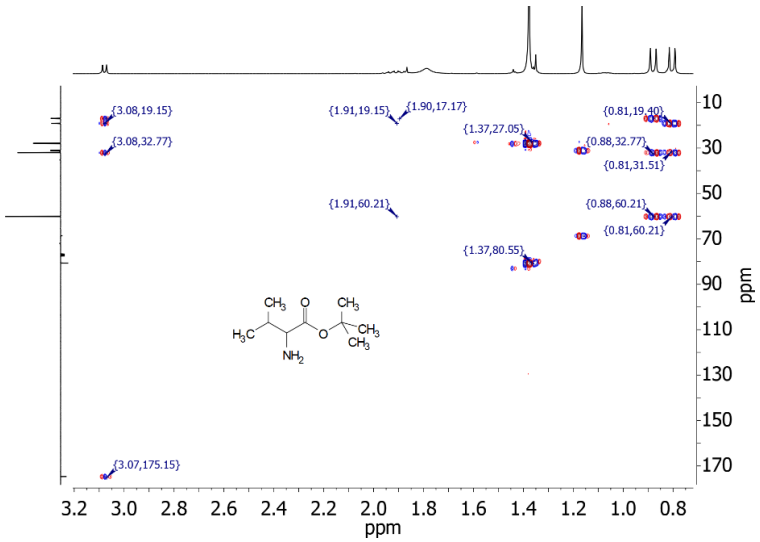


Figure 102. $^{1}H,^{13}C$ HMBC NMR spectrum of *L*-valine *tert*-butyl ester in $CDCl_3$ at 300 MHz.

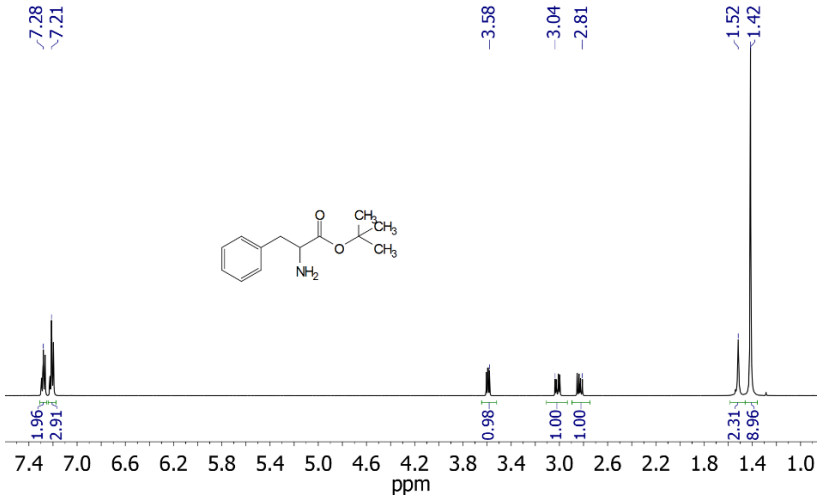


Figure 103. ^{1}H NMR spectrum of *L*-phenylalanine *tert*-butyl ester in $CDCl_3$ at 499 MHz.

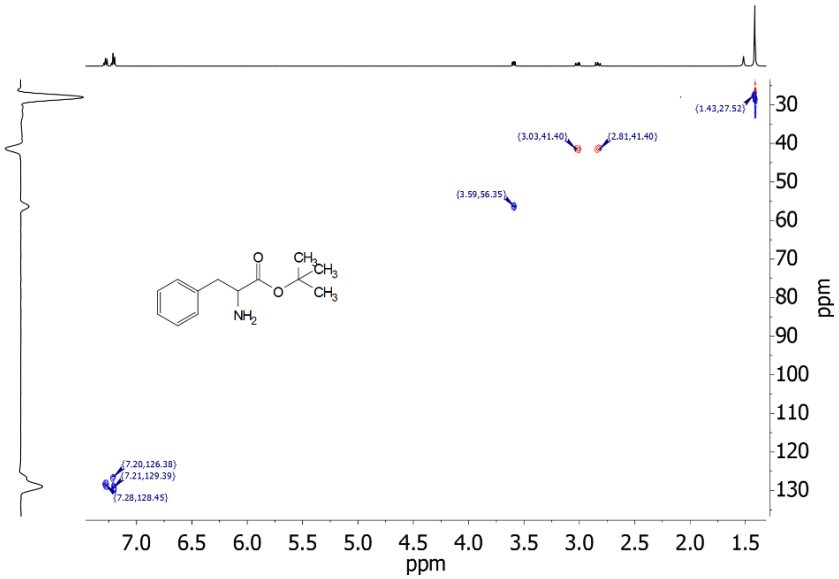


Figure 104. $^{1}H,^{13}C$ HMQC/HSQC NMR spectrum of *L*-phenylalanine *tert*-butyl ester in $CDCl_3$ at 499 MHz.

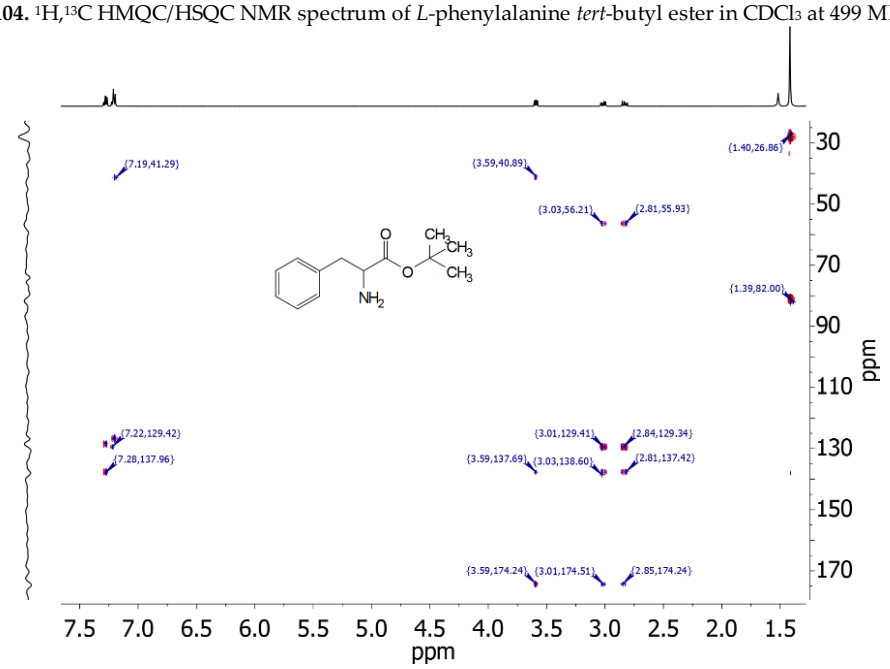


Figure 105. $^{1}H,^{13}C$ HMBC NMR spectrum of *L*-phenylalanine *tert*-butyl ester in $CDCl_3$ at 499 MHz.

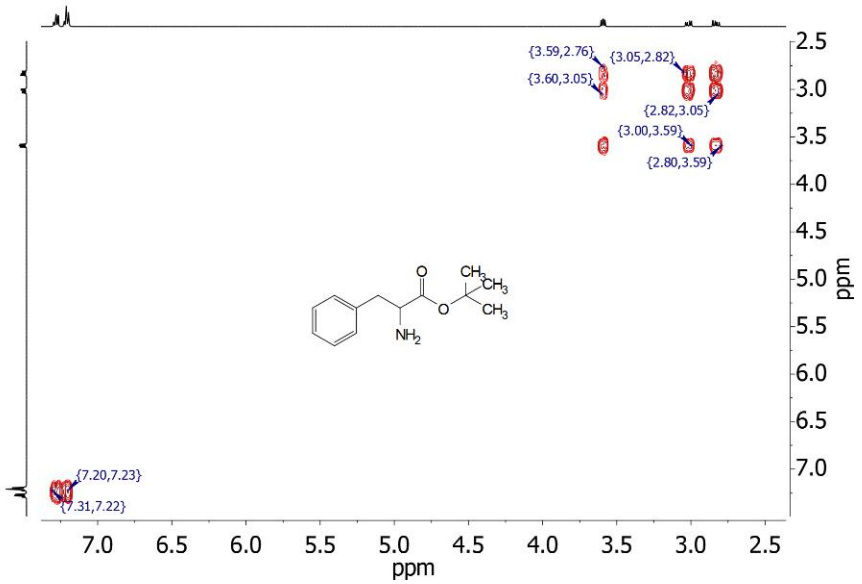


Figure 106. $^{1}H,^{1}H$ COSY NMR spectrum of *L*-phenylalanine *tert*-butyl ester in $CDCl_3$ at 499 MHz.

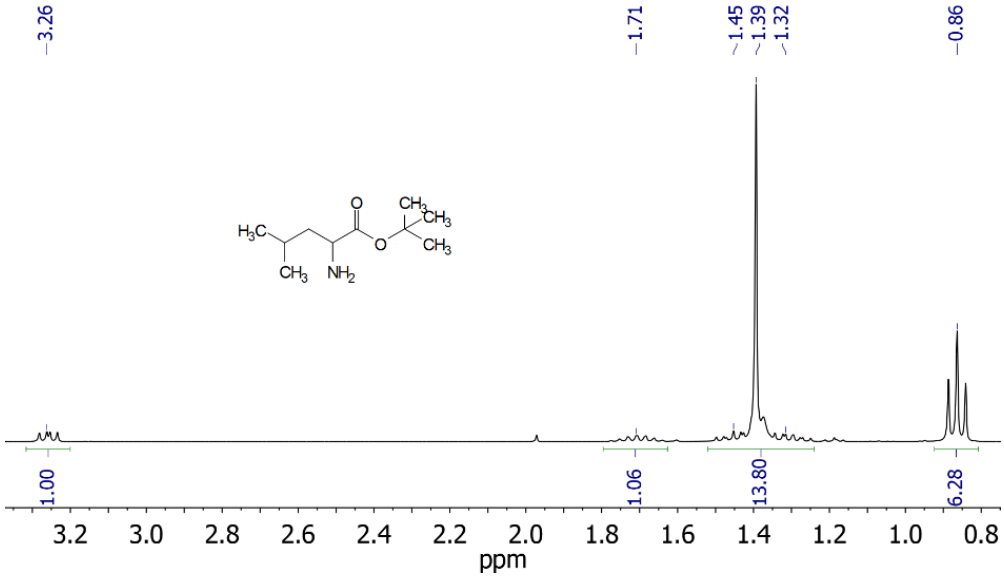


Figure 107. ^{1}H NMR spectrum of *L*-leucine *tert*-butyl ester in $CDCl_3$ at 499 MHz.

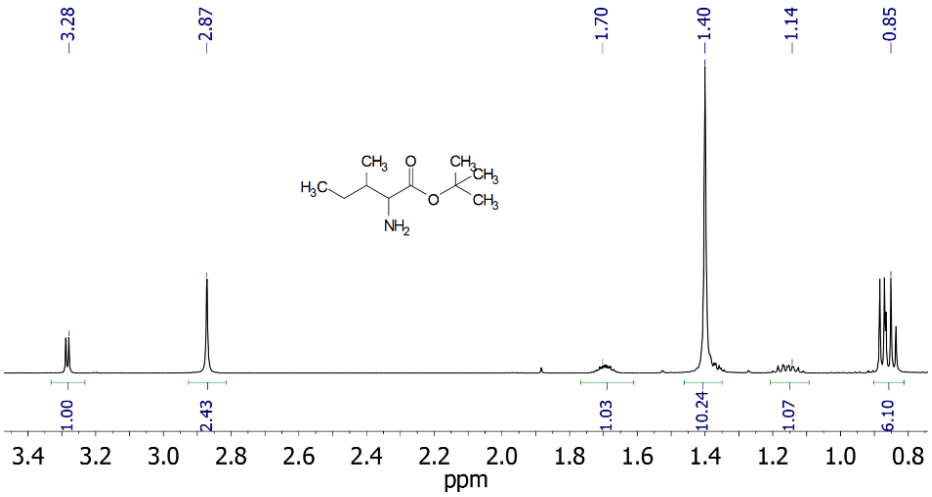


Figure 108. ^{1}H NMR spectrum of *L*-isoleucine *tert*-butyl ester in $CDCl_3$ at 499 MHz.

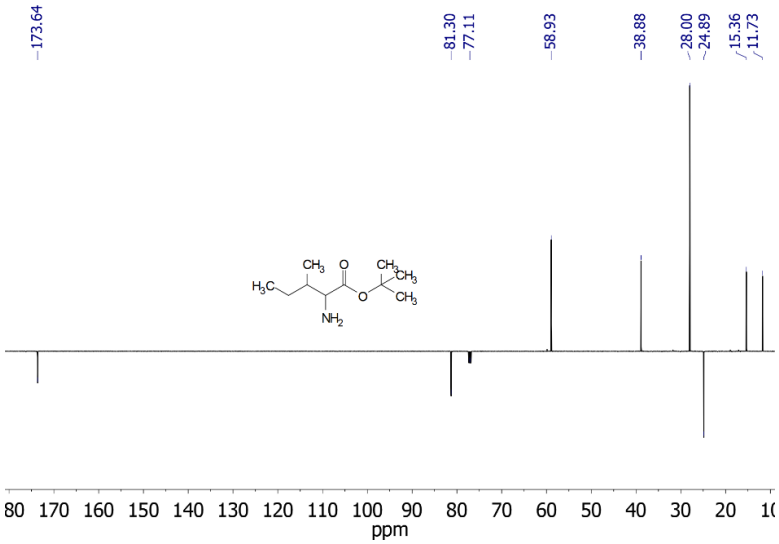


Figure 109. ^{13}C APT NMR spectrum of *L*-isoleucine *tert*-butyl ester in $CDCl_3$ at 499 MHz.

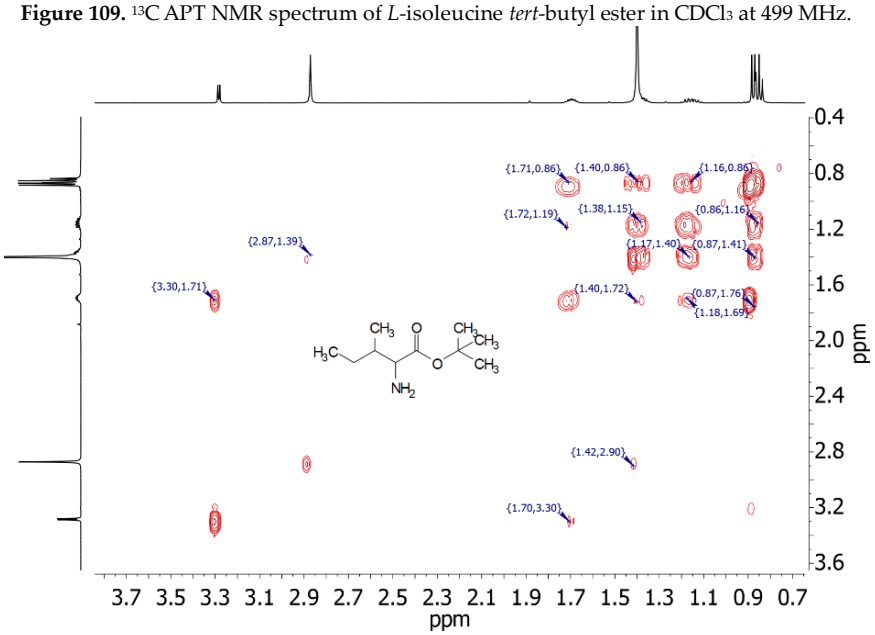


Figure 110. ^{1}H,^{1}H COSY NMR spectrum of *L*-isoleucine *tert*-butyl ester in $CDCl_3$ at 499 MHz.

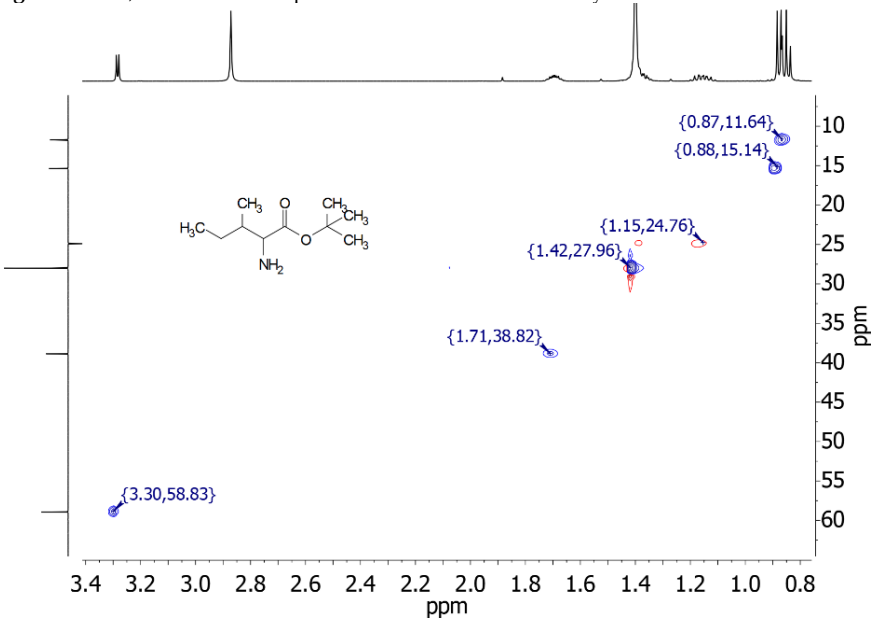


Figure 111. ^{1}H,^{13}C HMQC/HSQC NMR spectrum of *L*-isoleucine *tert*-butyl ester in $CDCl_3$ at 499 MHz.

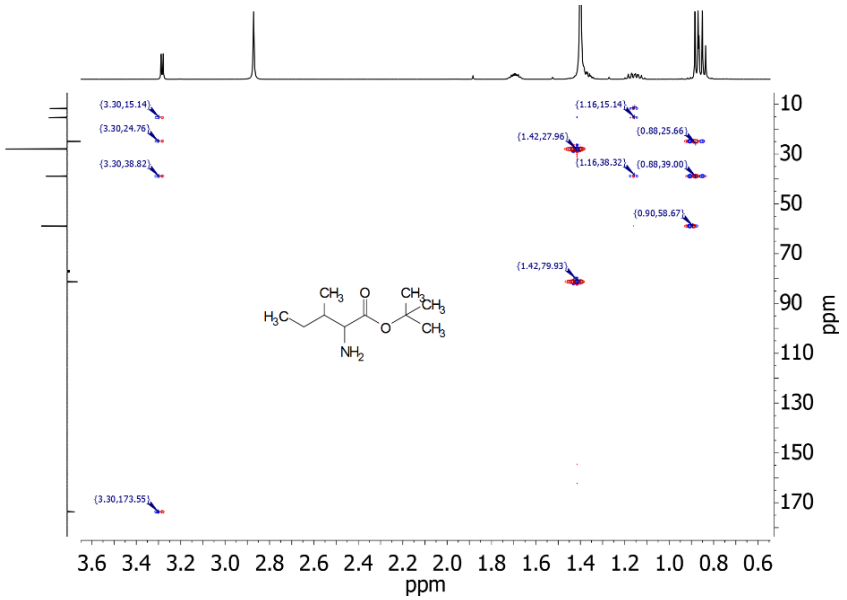


Figure 112. $^{1}H,^{13}C$ HMBC NMR spectrum of *L*-isoleucine *tert*-butyl ester in $CDCl_3$ at 499 MHz.

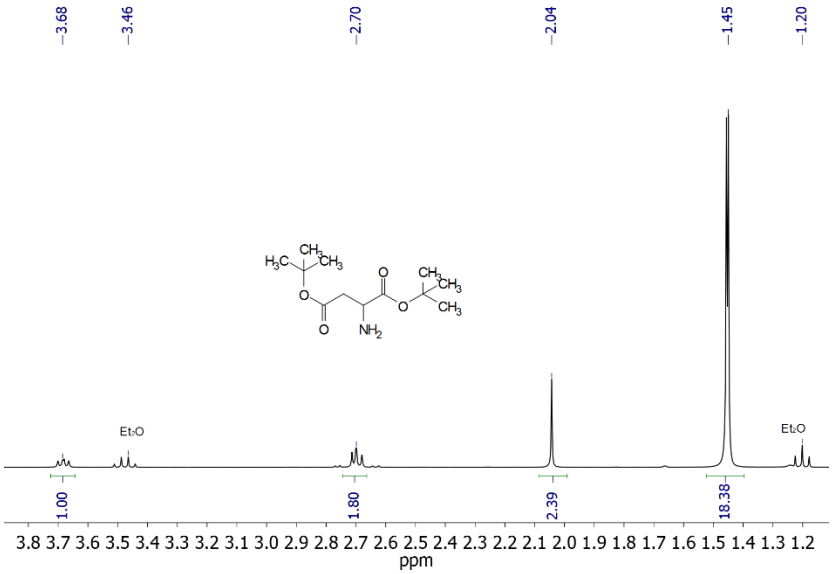


Figure 113. ^{1}H NMR spectrum of *L*-aspartic acid *tert*-butyl ester in $CDCl_3$ at 499 MHz.

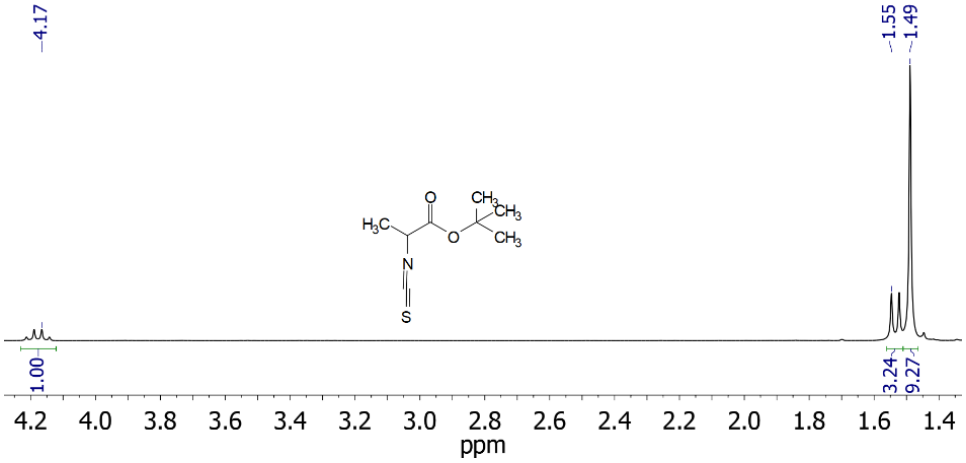


Figure 114. ^{1}H NMR spectrum of (*S*)-*tert*-butyl 2-isothiocyanatopropanoate in $CDCl_3$ at 499 MHz.

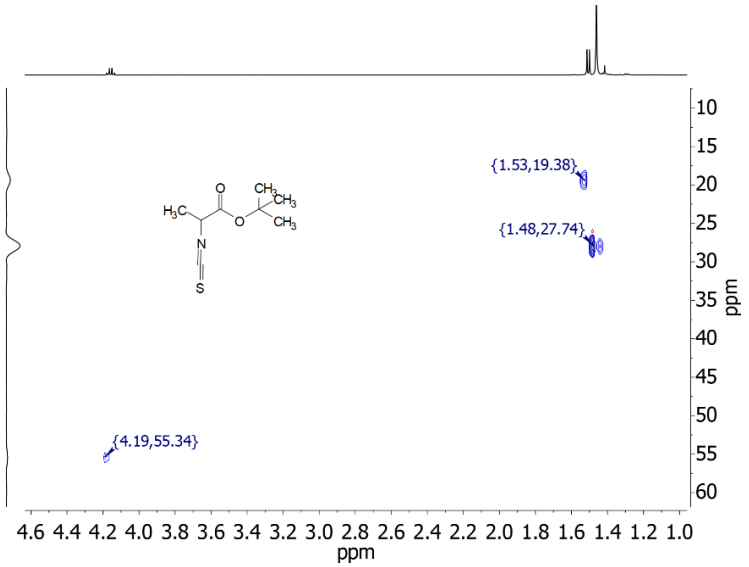


Figure 115. $^{1}H,^{13}C$ HMQC/HSQC NMR spectrum of (*S*)-*tert*-butyl 2-isothiocyanatopropanoate in $CDCl_3$ at 499 MHz.

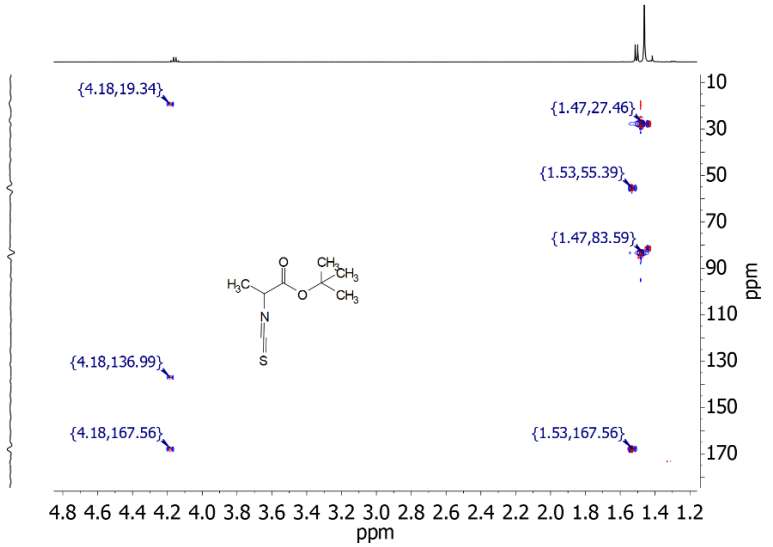


Figure 116. $^{1}H,^{13}C$-HMBC NMR spectrum of (*S*)-*tert*-butyl 2-isothiocyanatopropanoate in $CDCl_3$ at 499 MHz.

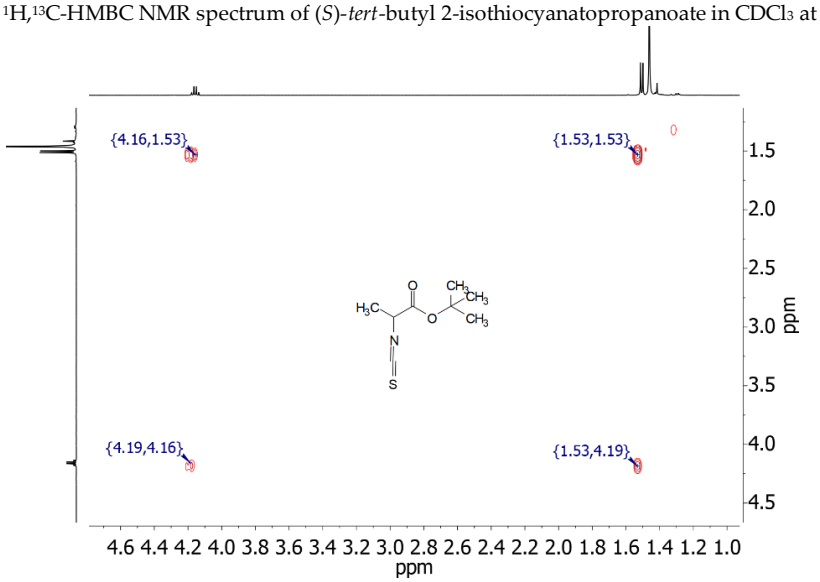


Figure 117. $^{1}H,^{1}H$ COSY NMR spectrum of (*S*)-*tert*-butyl 2-isothiocyanatopropanoate in $CDCl_3$ at 499 MHz.

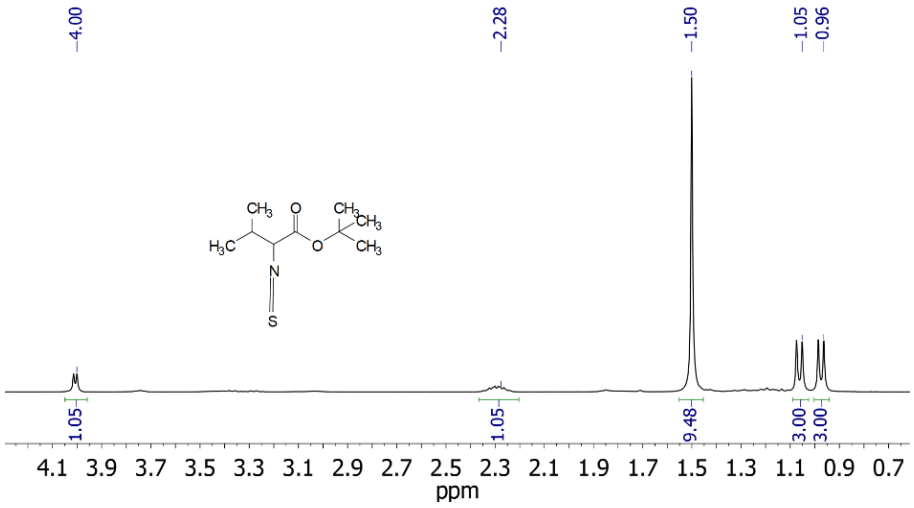


Figure 118. ^{1}H NMR spectrum of (*S*)-*tert*-butyl 2-isothiocyanato-3-metylbutanoate in $CDCl_3$ at 499 MHz.

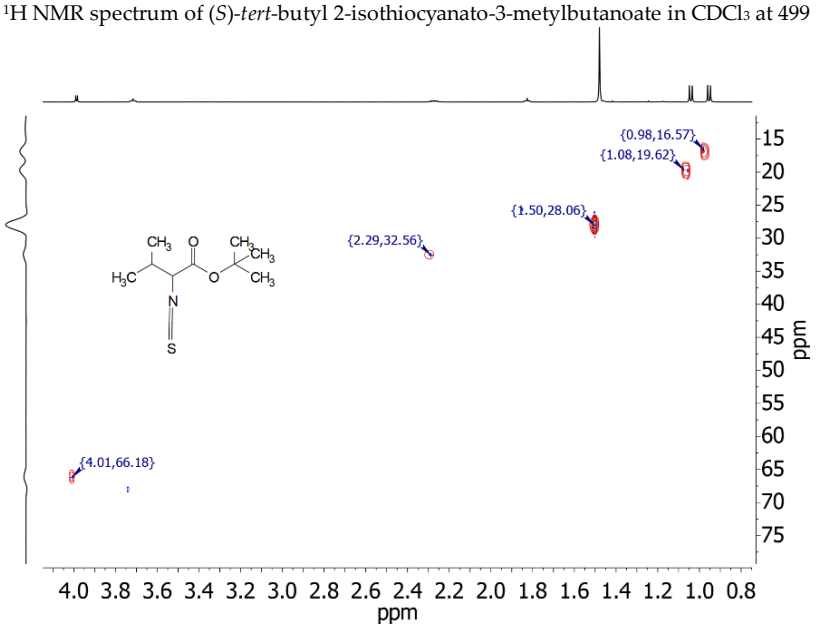


Figure 119. ^{1}H,^{13}C HMQC/HSQC NMR spectrum of (*S*)-*tert*-butyl 2-isothiocyanato-3-metylbutanoate in $CDCl_3$ at 499 MHz.

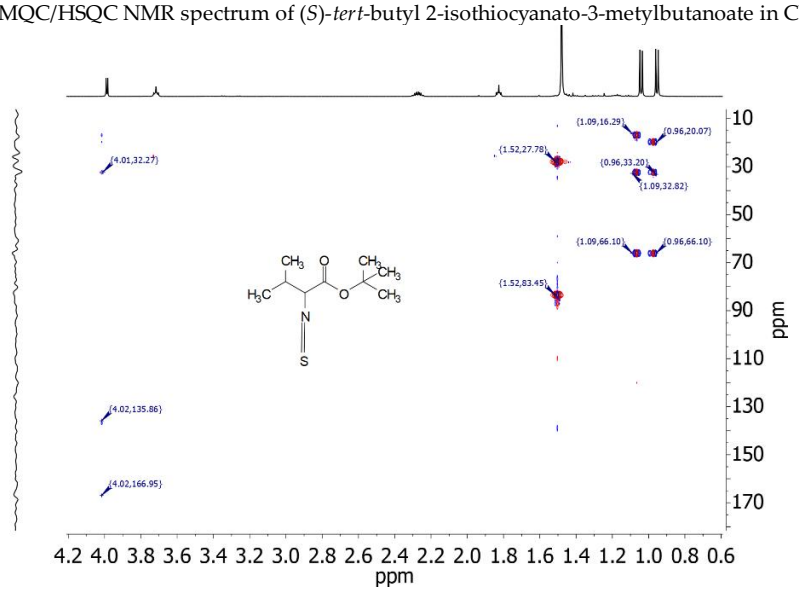


Figure 120. ^{1}H,^{13}C HMBC NMR spectrum of (*S*)-*tert*-butyl 2-isothiocyanato-3-metylbutanoate in $CDCl_3$ at 499 MHz.

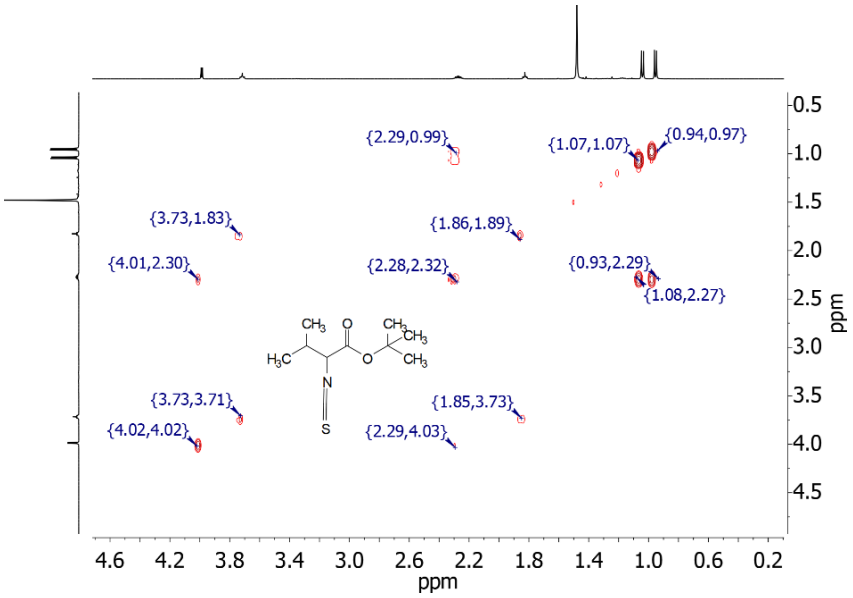


Figure 121. $^{1}H,^{1}H$ COSY-NMR spectrum of (*S*)-*tert*-butyl 2-isothiocyanato-3-metylbutanoate in $CDCl_3$ at 499 MHz.

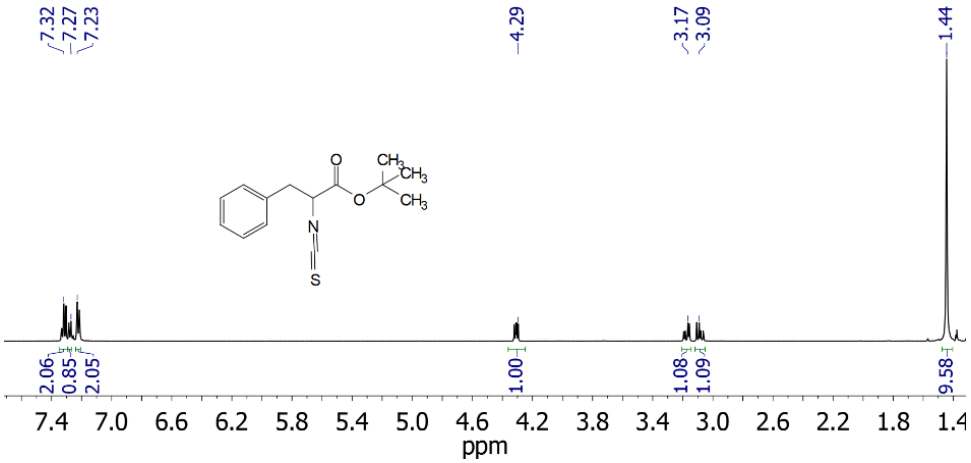


Figure 122. ^{1}H NMR spectrum of (*S*)-*tert*-butyl 2-isothiocyanato-3-phenylpropanoate in $CDCl_3$ at 499 MHz.

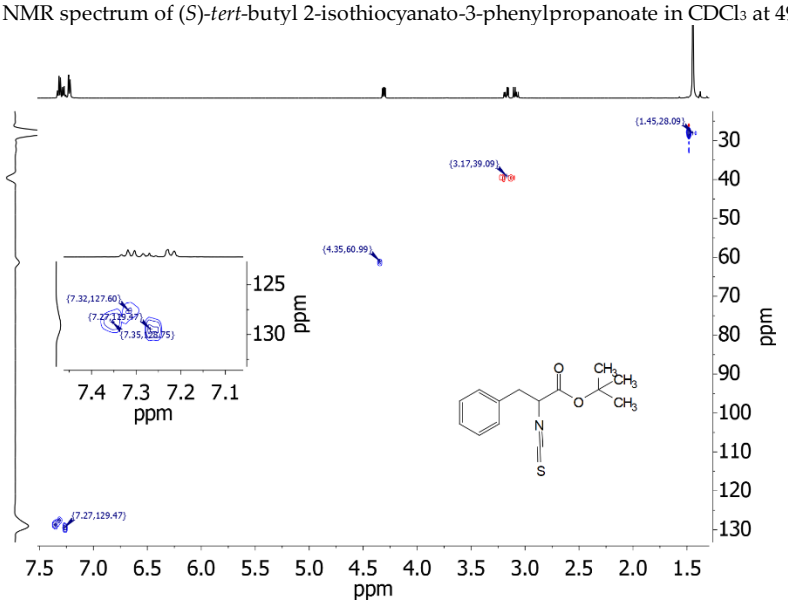


Figure 123. $^{1}H,^{13}C$ HMQC/HSQC NMR spectrum of (*S*)-*tert*-butyl 2-isothiocyanato-3-phenyl propanoate in $CDCl_3$ at 499 MHz.

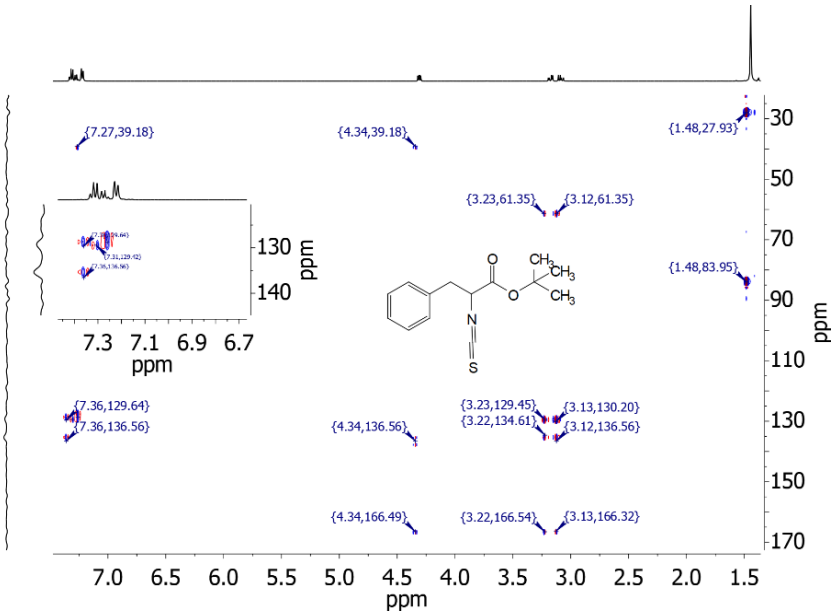


Figure 124. $^{1}H,^{13}C$ HMBC NMR spectrum of (*S*)-*tert*-butyl 2-isothiocyanato-3-phenylpropanoate in $CDCl_3$ at 499 MHz.

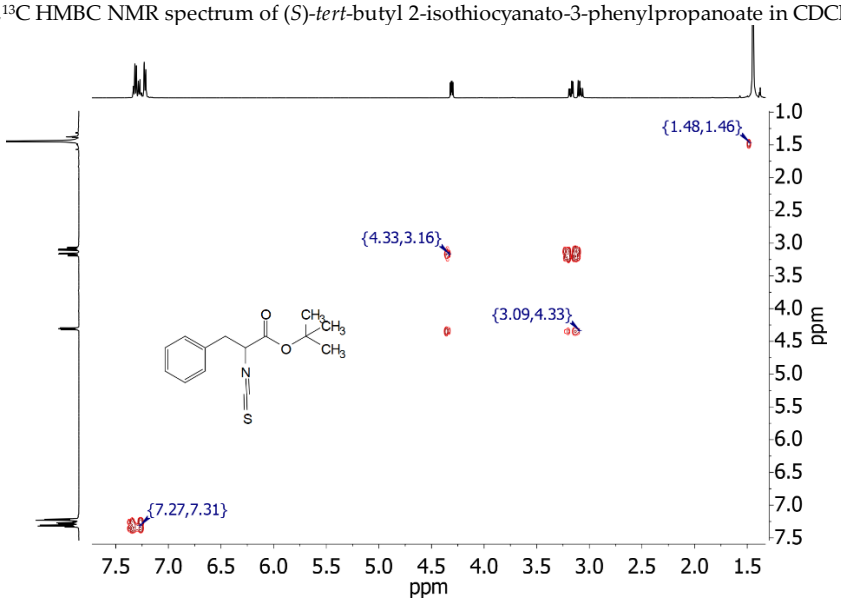


Figure 125. $^{1}H,^{1}H$ COSY NMR spectrum of (*S*)-*tert*-butyl 2-isothiocyanato-3-phenylpropanoate in $CDCl_3$ at 499 MHz.

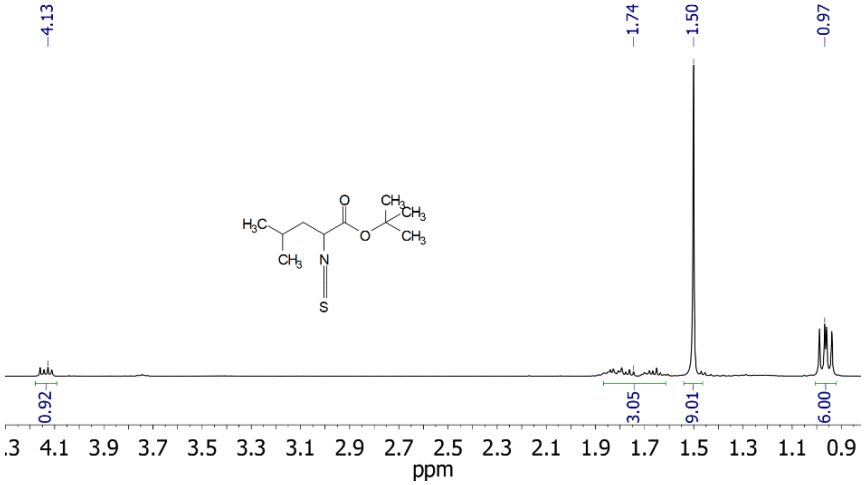


Figure 126. ^{1}H NMR spectrum of (*S*)-*tert*-butyl 2-isothiocyanato-4-methylpentanoate in $CDCl_3$ at 300 MHz.

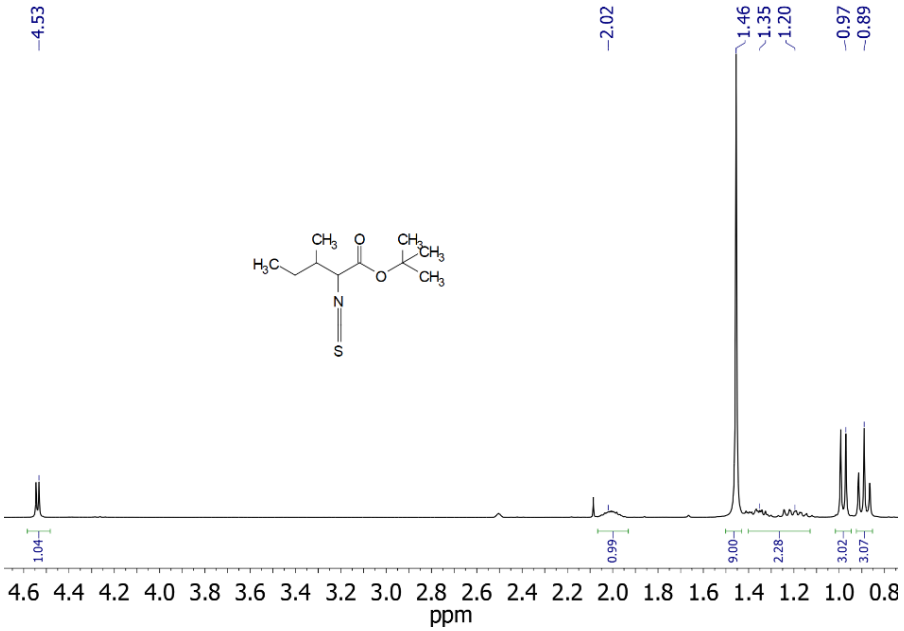


Figure 127. ^{1}H NMR spectrum of (*S*)-*tert*-butyl 2-isothiocyanato-3-methylpentanoate in $CDCl_3$ at 499 MHz.

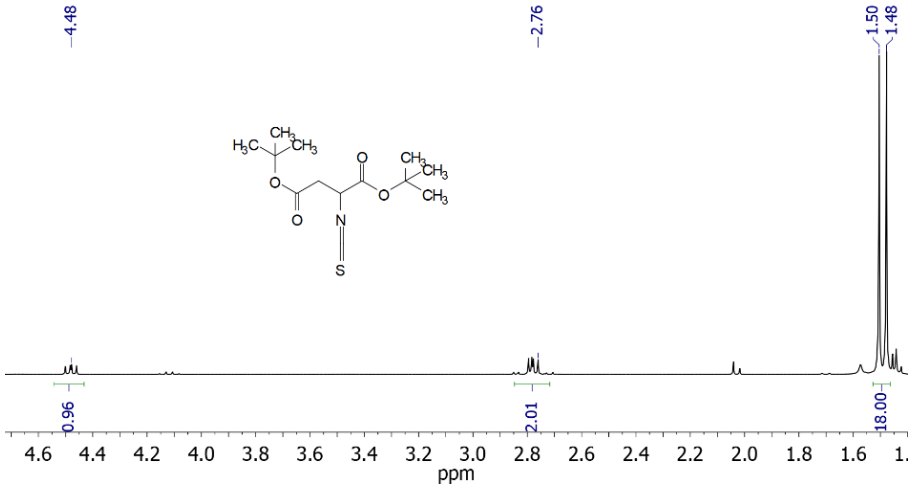


Figure 128. ^{1}H NMR spectrum of (*S*)-di-*tert*-butyl 2-isothiocyanatobutanedioate in $CDCl_3$ at 300 MHz.

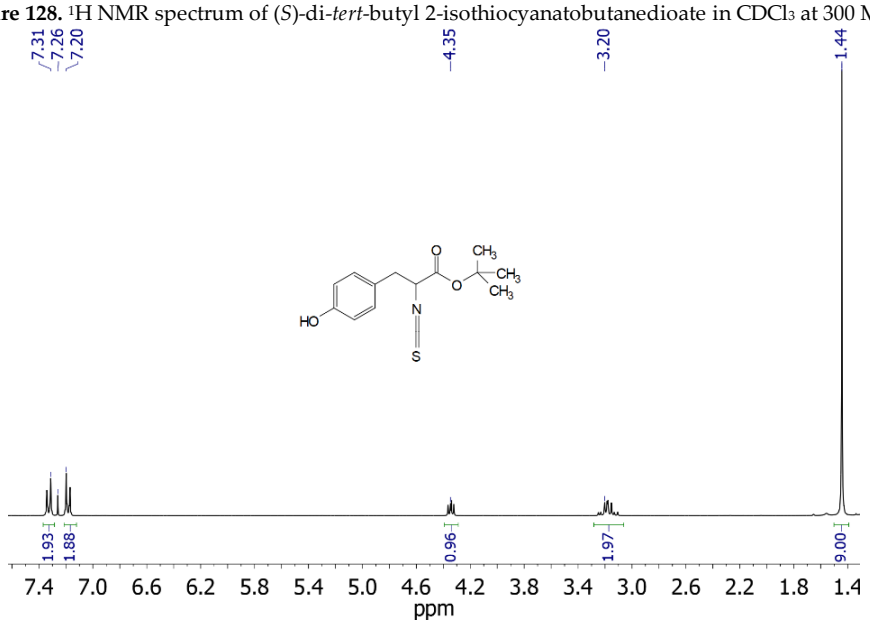


Figure 129. ^{1}H NMR spectrum of *tert*-butyl 3-(4-hydroxyphenyl)-2-isothiocyanatopropanoate in $CDCl_3$ at 499 MHz.

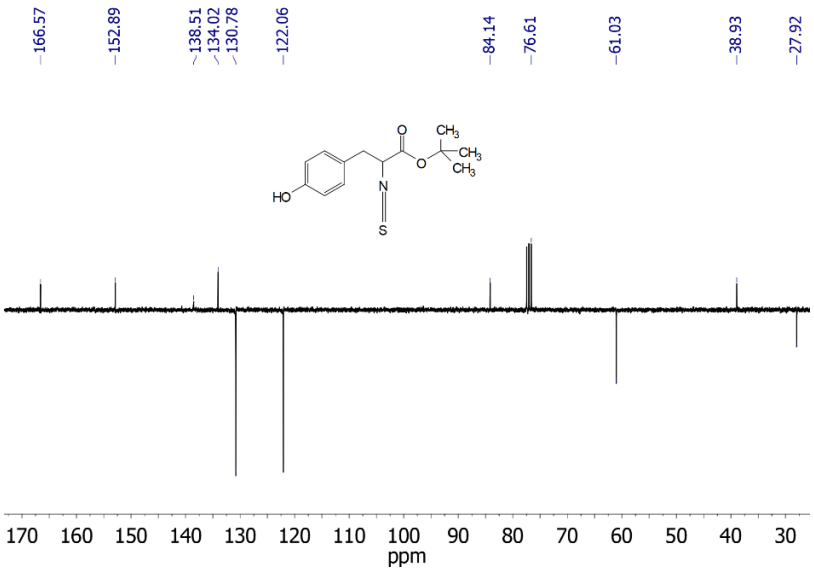


Figure 130. ^{13}C DEPTQ NMR spectrum of *tert*-butyl 3-(4-hydroxyphenyl)-2-isothiocyanatopropanoate in $CDCl_3$ at 499 MHz.

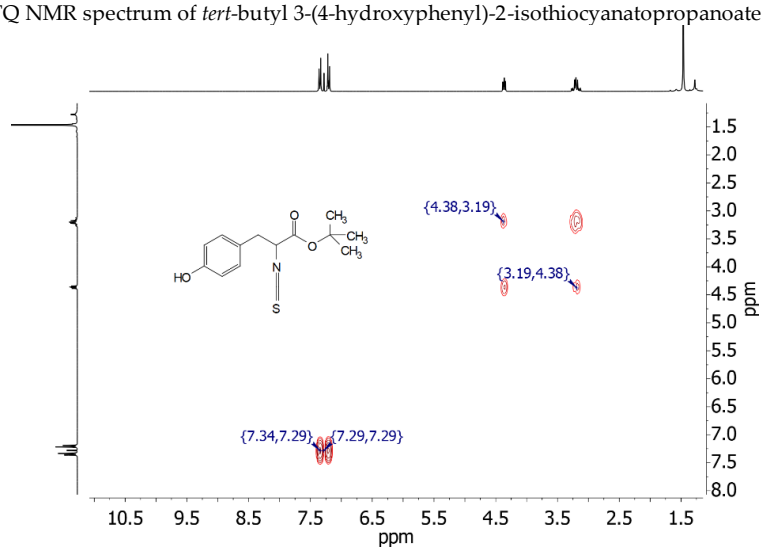


Figure 131. $^{1}H,^{1}H$ COSY NMR spectrum of *tert*-butyl 3-(4-hydroxyphenyl)-2-isothiocyanato-propanoate in $CDCl_3$ at 499 MHz.

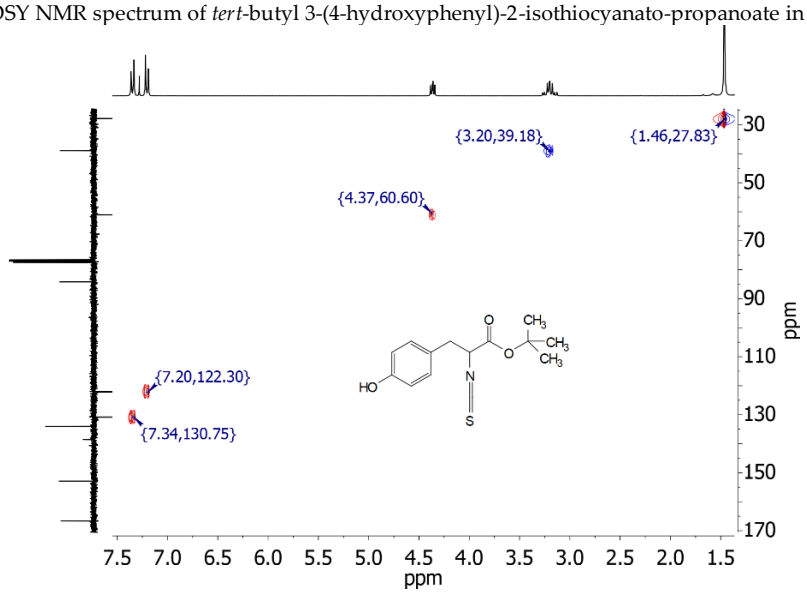


Figure 132. $^{1}H,^{13}C$ HMQC/HSQC NMR spectrum of *tert*-butyl 3-(4-hydroxyphenyl)-2-isothiocyanato-propanoatein $CDCl_3$ at 499 MHz.

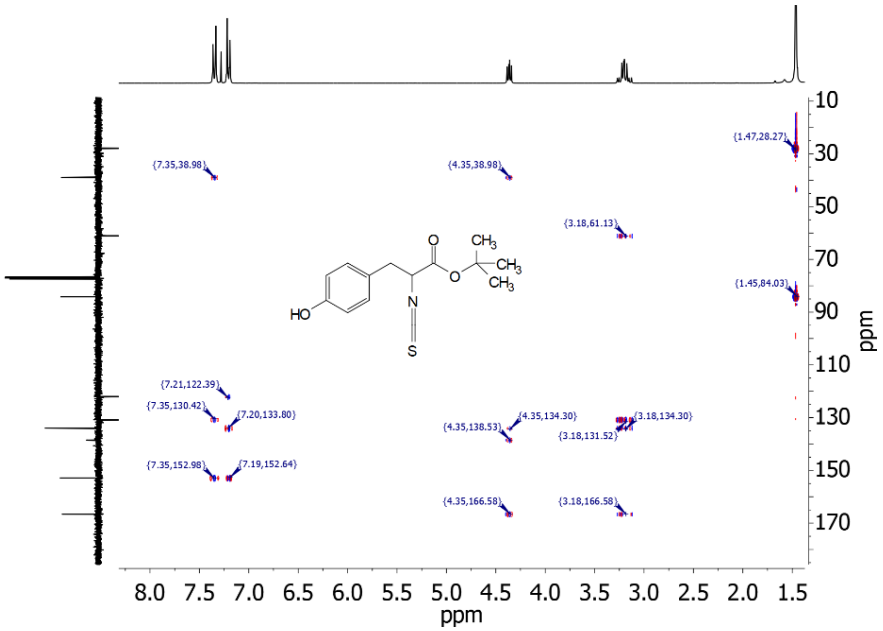


Figure 133. $^{1}H,^{13}C$ HMBC NMR spectrum of *tert*-butyl 3-(4-hydroxyphenyl)-2-isothiocyanato-propanoate in $CDCl_3$ at 499 MHz.

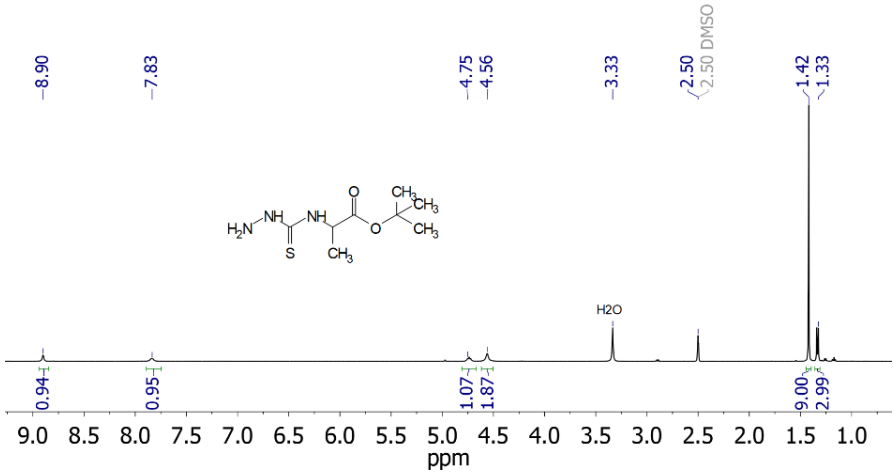


Figure 134. ^{1}H NMR spectrum of 4-((*S*)-*tert*-butylpropanoate)thiosemicarbazide in DMSO-d_6 at 499 MHz.

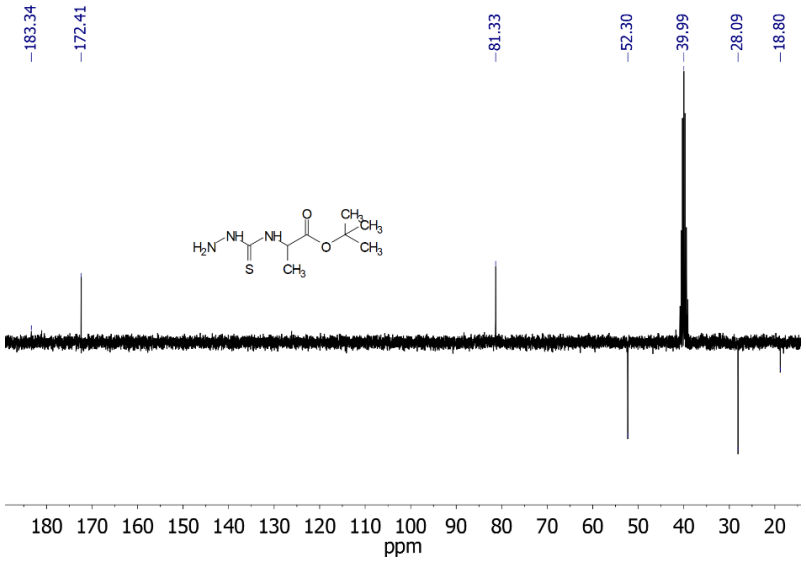


Figure 135. ^{13}C DEPTQ NMR spectrum of 4-((*S*)-*tert*-butylpropanoate)thiosemicarbazide in DMSO-d_6 at 300 MHz.

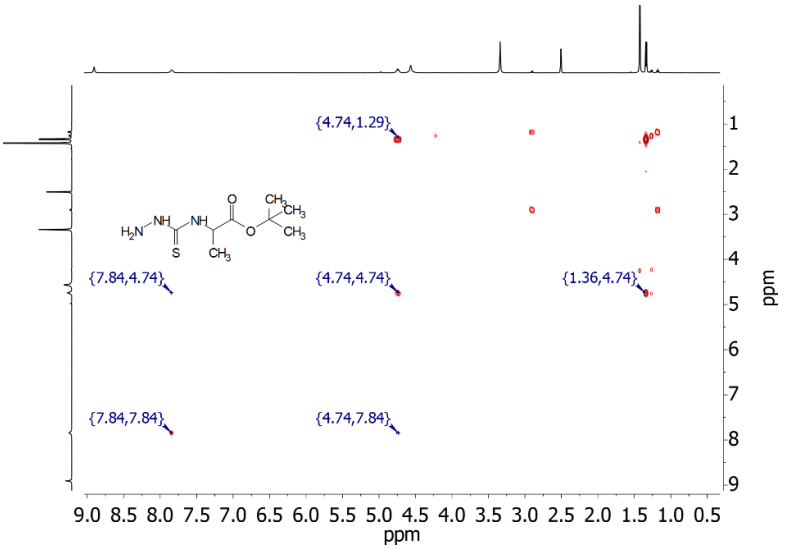


Figure 136. $^{1}H,^{1}H$ COSY NMR spectrum of 4-((*S*)-*tert*-butylpropanoate)thiosemicarbazide in DMSO-d_6 at 499 MHz.

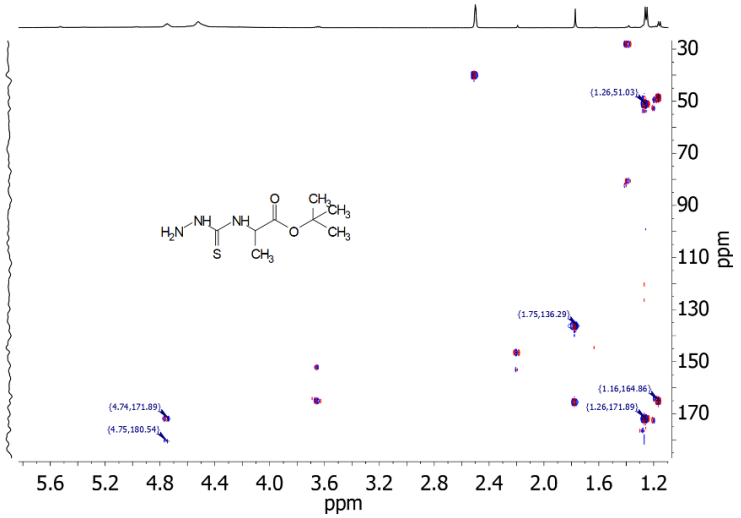


Figure 137. $^{1}H,^{13}C$ HMBC NMR spectrum of 4-((*S*)-*tert*-butylpropanoate)thiosemicarbazide in DMSO-d_6 at 499 MHz.

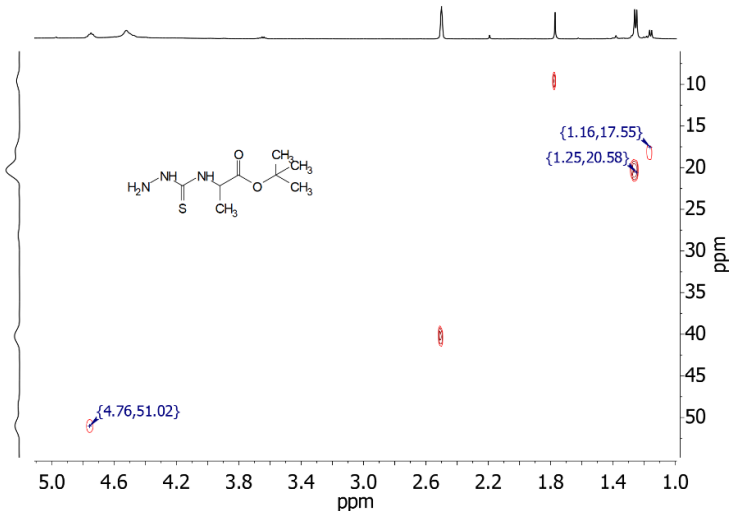


Figure 138. $^{1}H,^{13}C$ HMQC/HSQC NMR spectrum of 4-((*S*)-*tert*-butylpropanoate)thiosemicarbazide in DMSO-d_6 at 499 MHz.

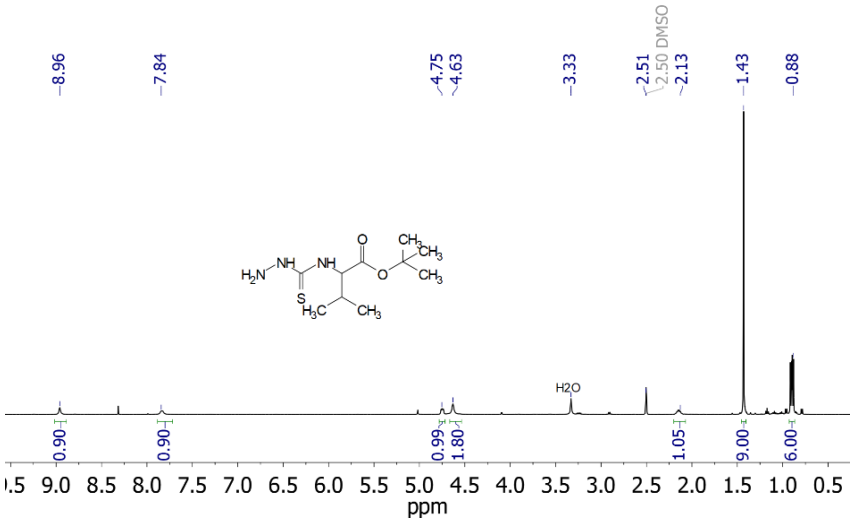


Figure 139. [1]H NMR spectrum of 4-((*S*)-*tert*-butyl-3-metylbutanoate)thiosemicarbazide in DMSO-*d*$_6$ at 499 MHz.

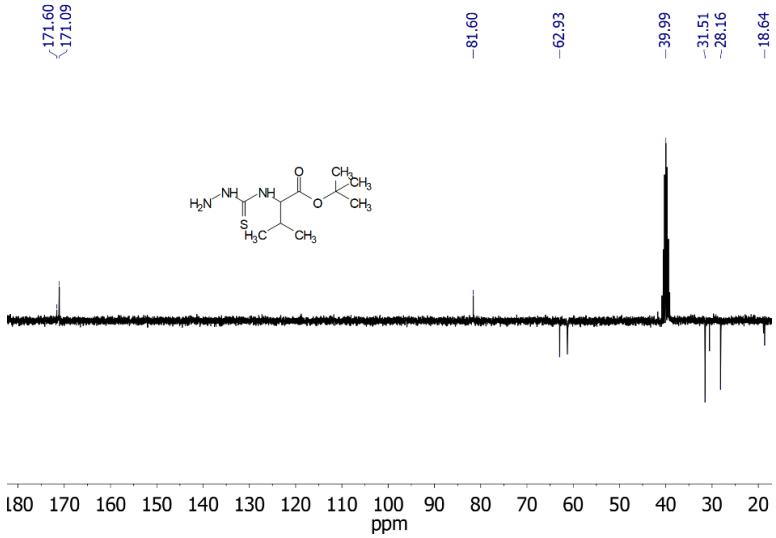


Figure 140. [13]C DEPTQ NMR spectrum of 4-((*S*)-*tert*-butyl-3-metylbutanoate)thiosemicarbazide in DMSO-*d*$_6$ at 300 MHz.

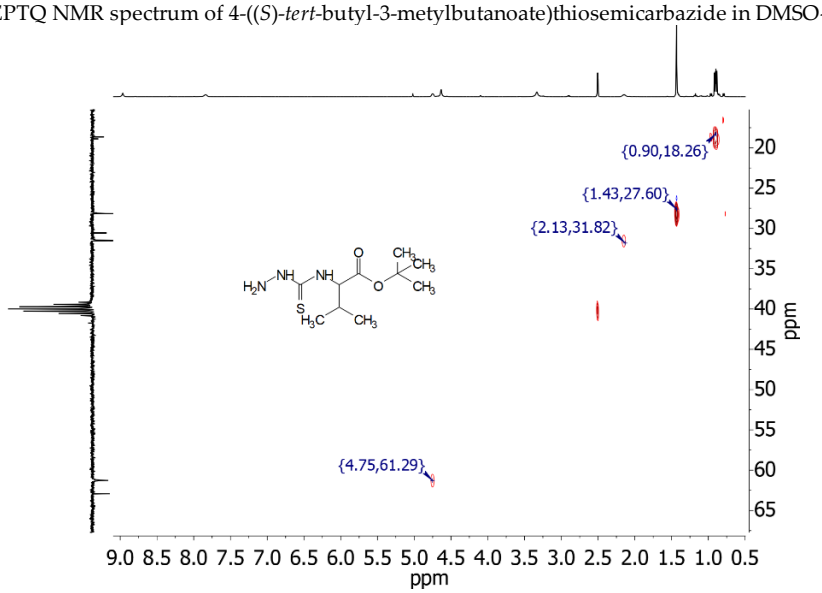


Figure 141. [1]H,[13]C HMQC/HSQC NMR spectrum of 4-((*S*)-*tert*-butyl-3-metylbutanoate)thiosemi-carbazide DMSO-*d*$_6$ at 499 MHz.

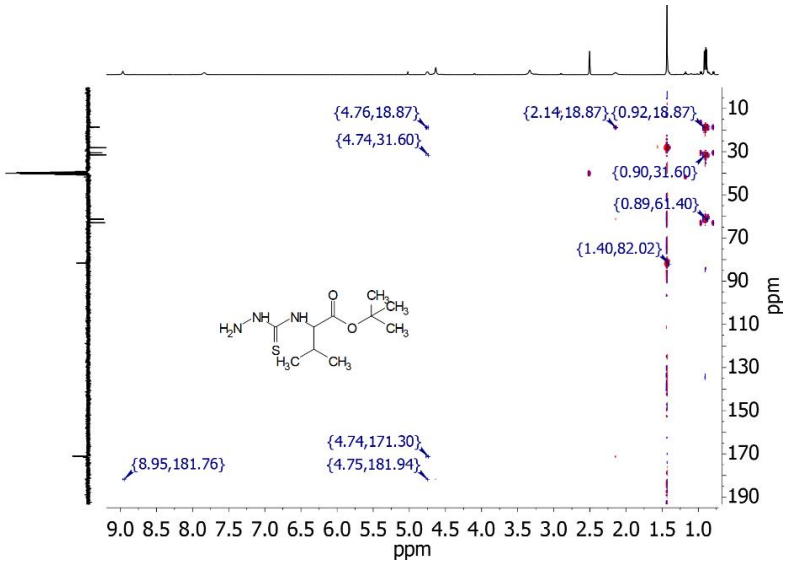


Figure 142. $^{1}H,^{13}C$ HMBC NMR spectrum of 4-((*S*)-*tert*-butyl-3-metylbutanoate)thiosemicarbazide in DMSO-d_6 at 499 MHz.

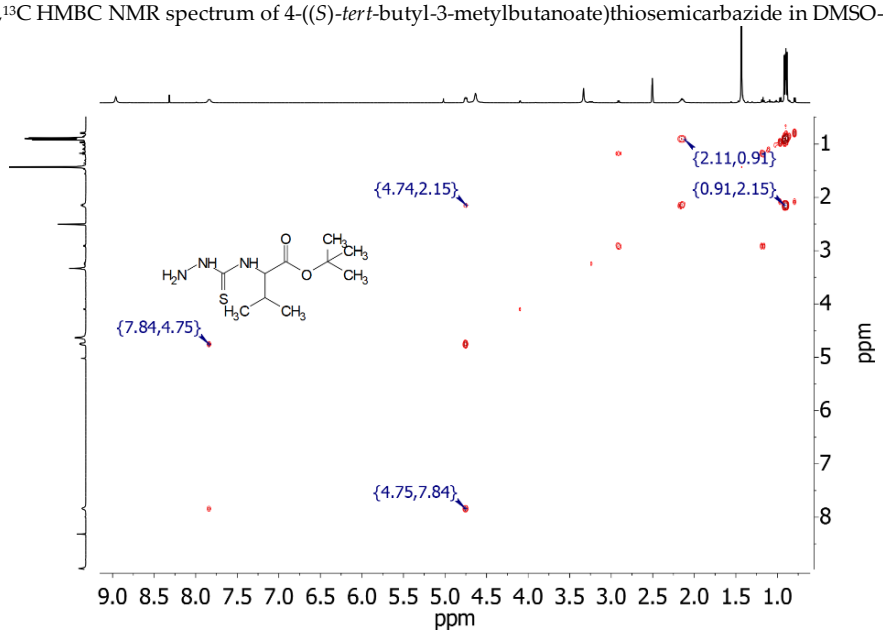


Figure 143. $^{1}H,^{1}H$ COSY NMR spectrum of 4-((*S*)-*tert*-butyl-3-metylbutanoate)thiosemicarbazide in DMSO-d_6 at 499 MHz.

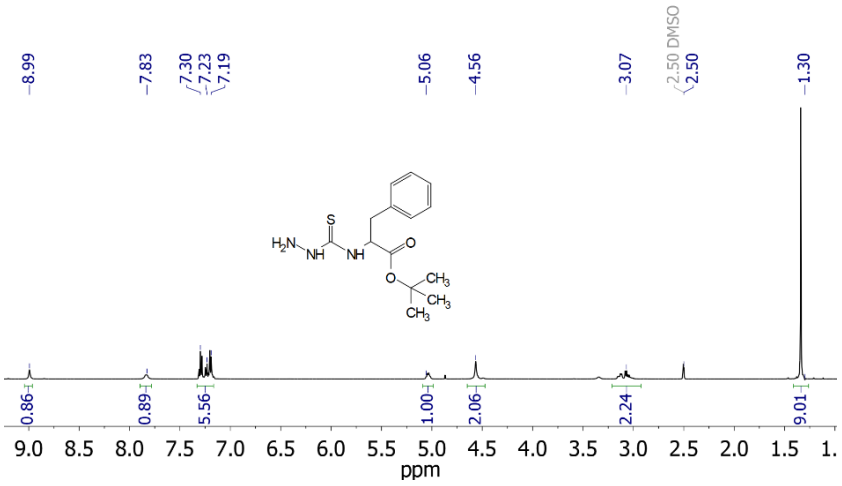


Figure 144. ^{1}H NMR spectrum of 4-((*S*)-*tert*-butyl-3-phenylpropanoate)thiosemicarbazide in DMSO-d_6 at 300 MHz.

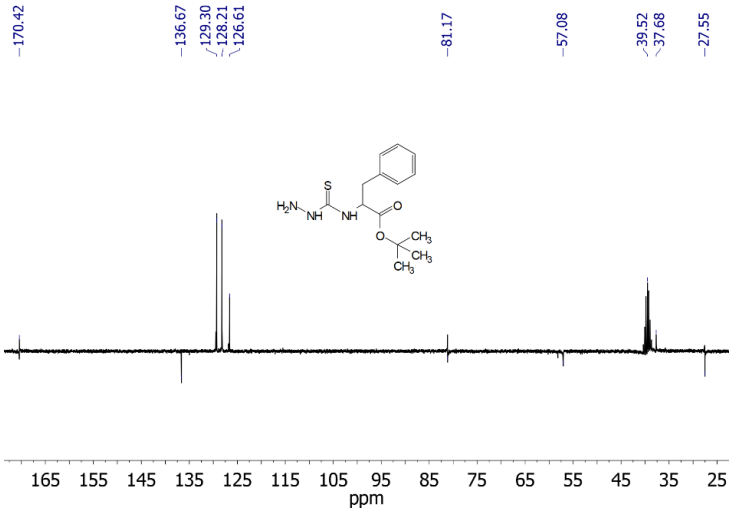


Figure 145. ^{13}C DEPTQ NMR spectrum of 4-((*S*)-*tert*-butyl-3-phenylpropanoate)thiosemicarbazide in DMSO-d_6 at 499 MHz.

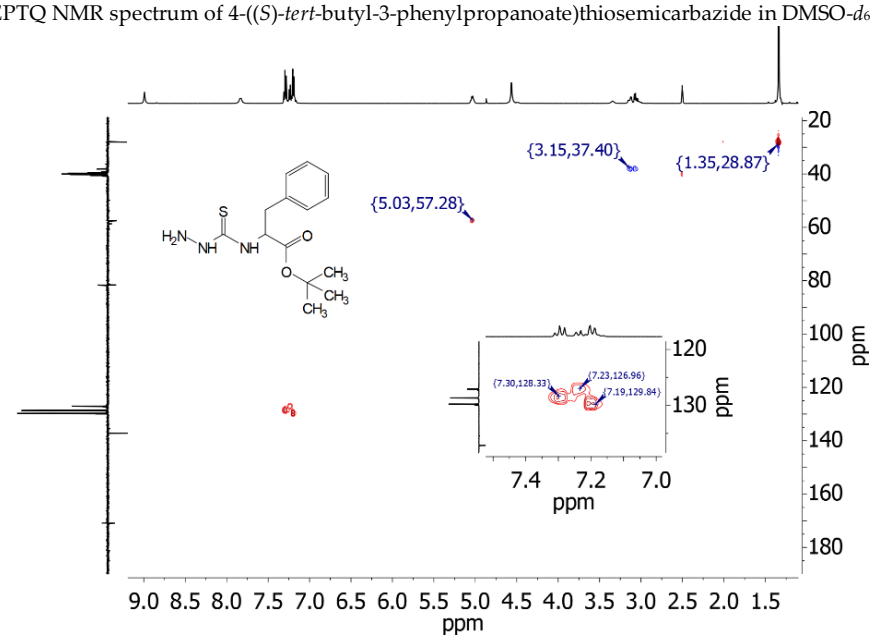


Figure 146. ^{1}H,^{13}C HMQC/HSQC NMR spectrum of 4-((*S*)-*tert*-butyl-3-phenylpropanoate)thiosemi-carbazide in DMSO-d_6 at 499 MHz.

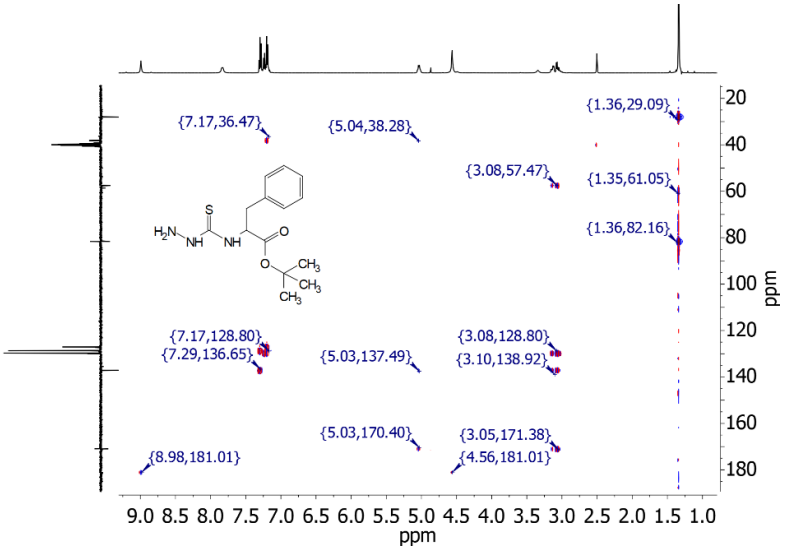


Figure 147. ^{1}H,^{13}C HMBC NMR spectrum of 4-((*S*)-*tert*-butyl-3-phenylpropanoate)thiosemicarbazide DMSO-d$_6$ at 499 MHz.

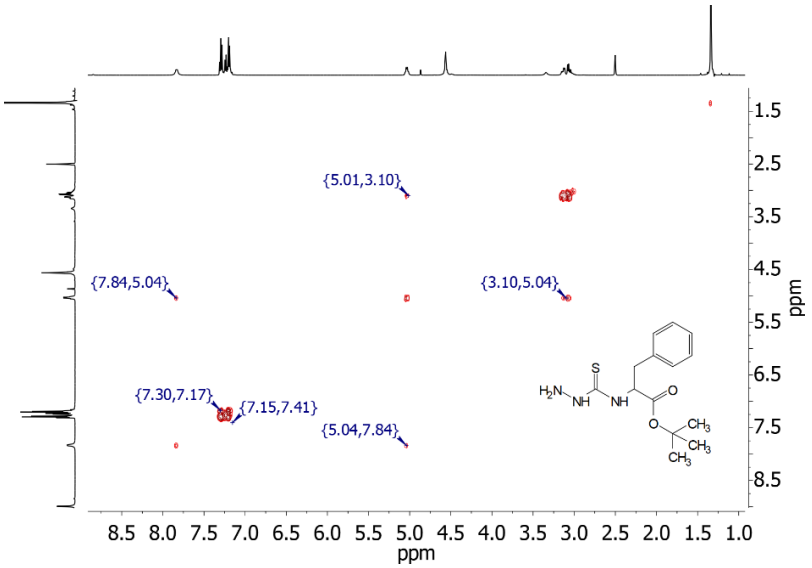


Figure 148. $^{1}H,^{1}H$ COSY-NMR spectrum of 4-((*S*)-*tert*-butyl-3-phenylpropanoate)thiosemicarbazide in DMSO-d_6 at 499 MHz.

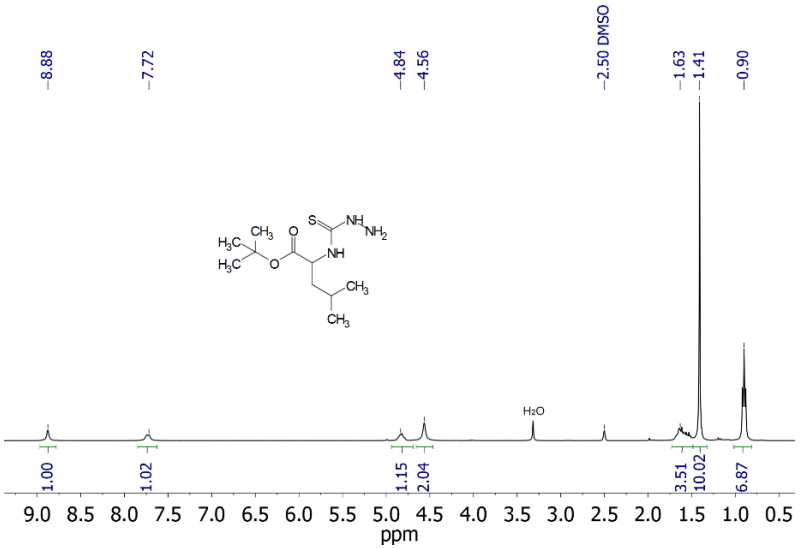


Figure 149. ^{1}H NMR spectrum of 4-((*S*)-*tert*-butyl-4-methylpentonate)thiosemicarbazide in DMSO-d_6 at 499 MHz.

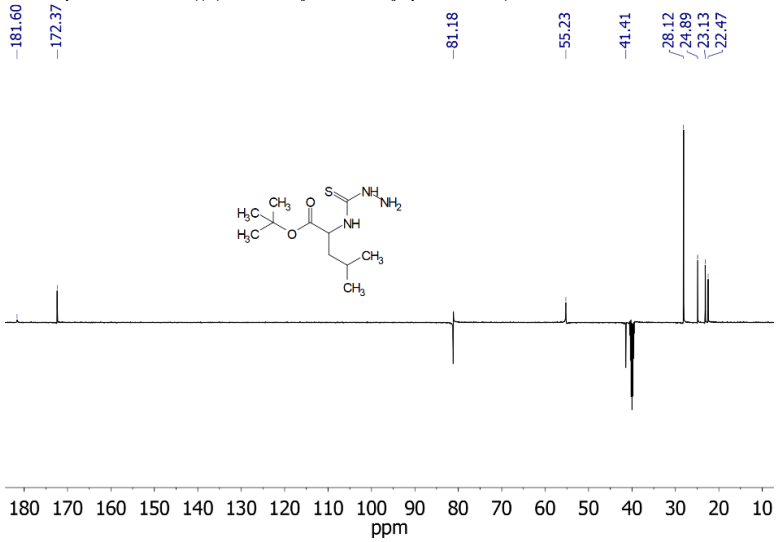


Figure 150. ^{13}C APT NMR spectrum of 4-((*S*)-*tert*-butyl-4-methylpentonate)thiosemicarbazide in DMSO-d_6 at 499 MHz.

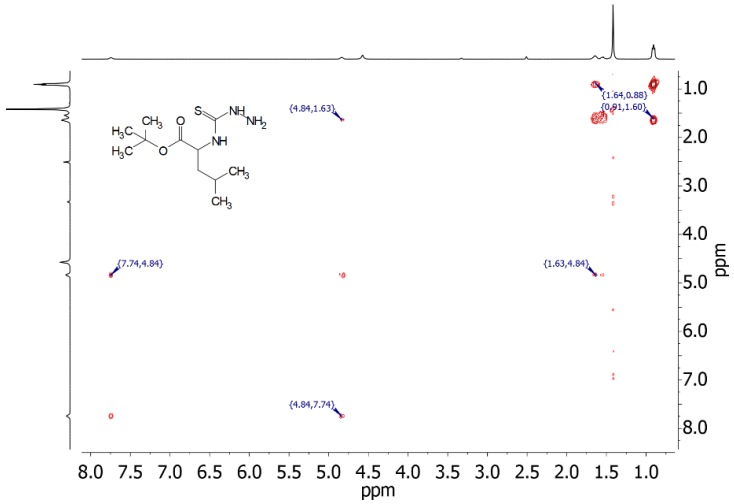


Figure 151. $^{1}H,^{1}H$ COSY NMR spectrum of 4-((*S*)-*tert*-butyl-4-methylpentonate)thiosemicarbazide in DMSO-d_6 at 499 MHz.

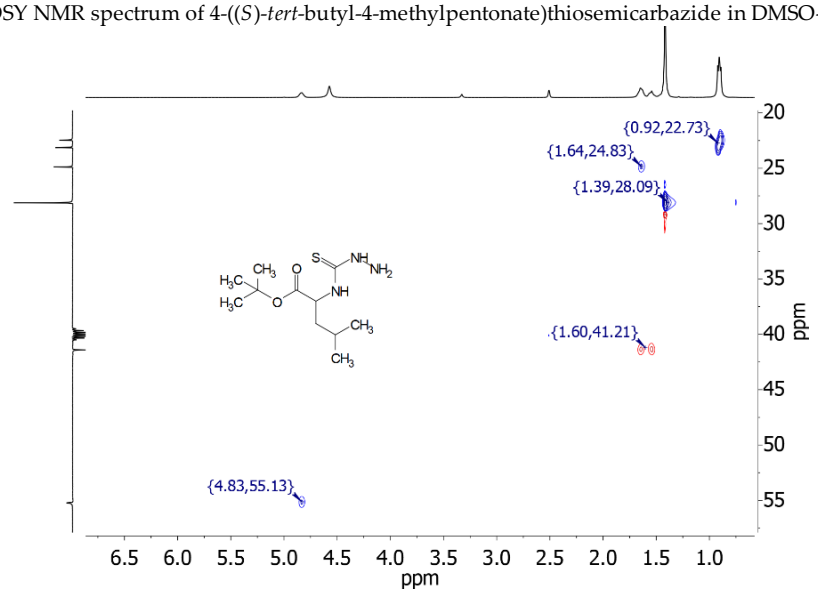


Figure 152. $^{1}H,^{13}C$ HMQC/HSQC NMR spectrum of 4-((*S*)-*tert*-butyl-4-methylpentonate)thiosemicarbazide in DMSO-d_6 at 499 MHz.

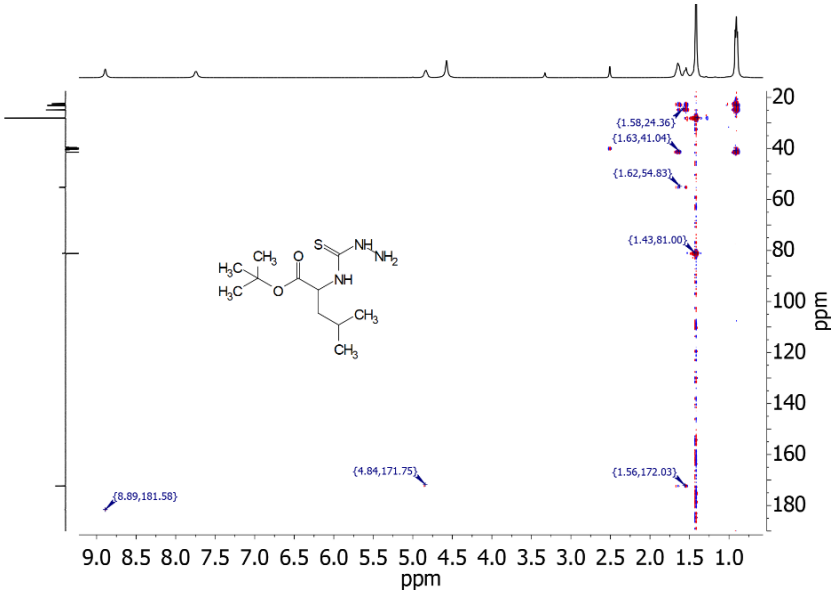


Figure 153. $^{1}H,^{13}C$ HMBC NMR spectrum of 4-((*S*)-*tert*-butyl-4-methylpentonate)thiosemicarbazide in DMSO-d_6 at 499 MHz.

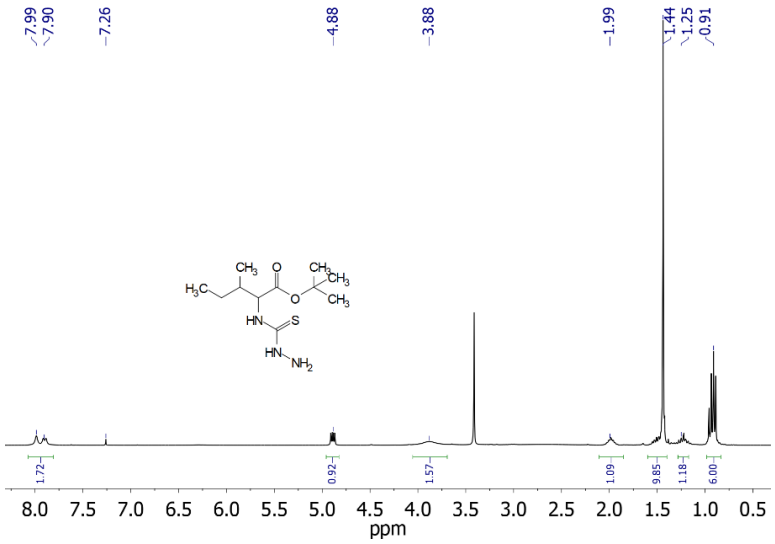


Figure 154. [1]H NMR spectrum of (*S*)-*tert*-butyl 2-(hydrazidecarbothioamino)-3-methylpentanoate in DMSO-d_6 at 300 MHz.

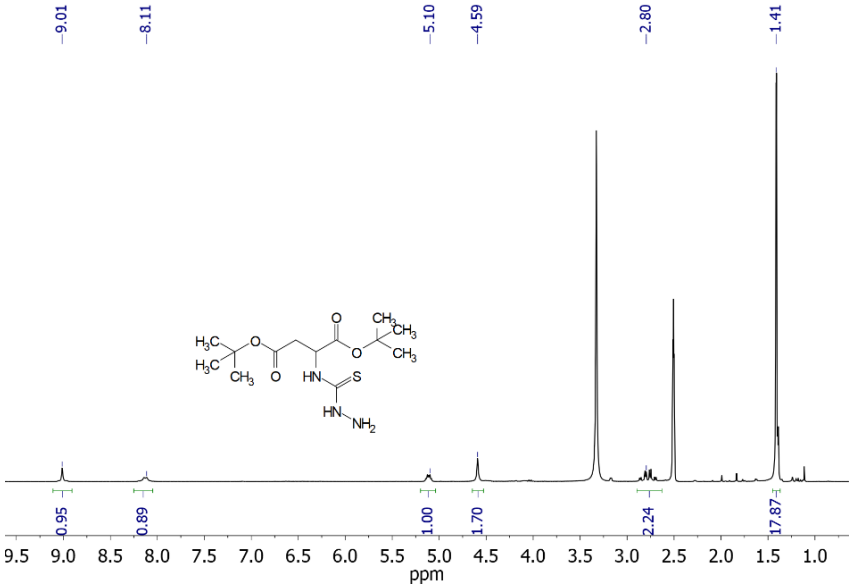


Figure 155. [1]H NMR spectrum of (*S*)-Di-*tert*-butyl 2-(hydrazidecarbothioamino)butanedioate in DMSO-d_6 at 300 MHz.

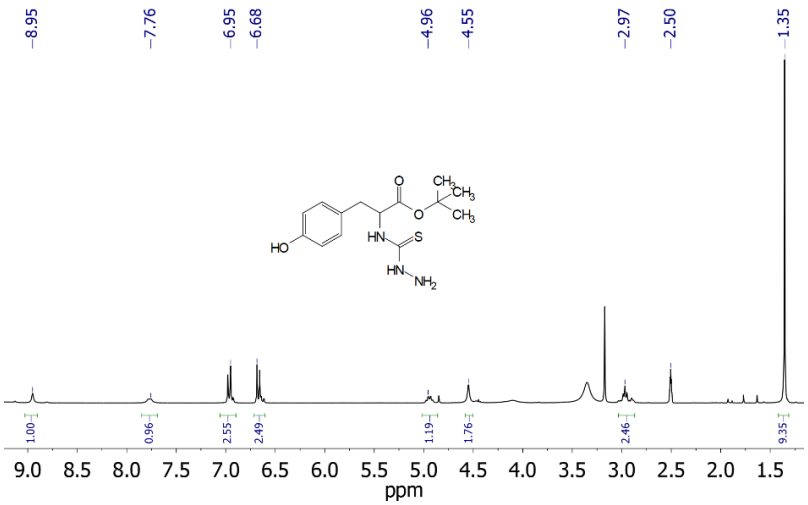


Figure 156. [1]H NMR spectrum of (*S*)-*tert*-butyl-2-(hydrazidecarbothioamino)-3-(4-hydroxyphenyl) propanoate in DMSO-d_6 at 300 MHz.

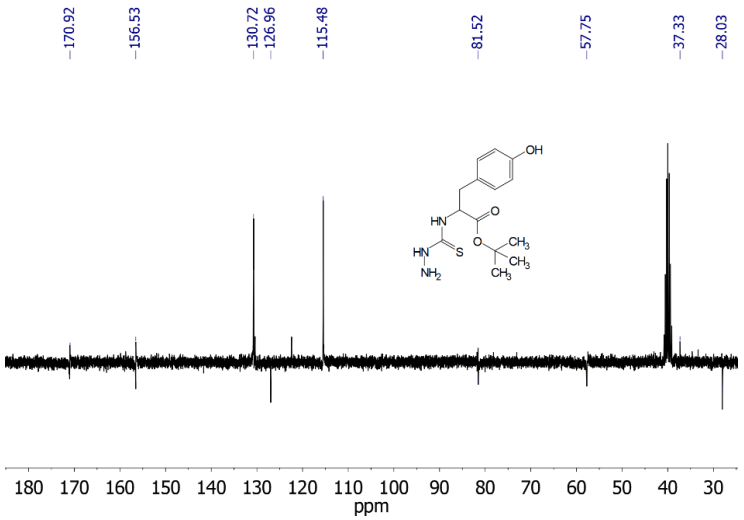


Figure 157. ^{13}C DEPTQ NMR spectrum of (*S*)-*tert*-butyl-2-(hydrazidecarbothioamino)-3-(4-hydroxyphenyl)propanoate in DMSO-d_6 at 300 MHz.

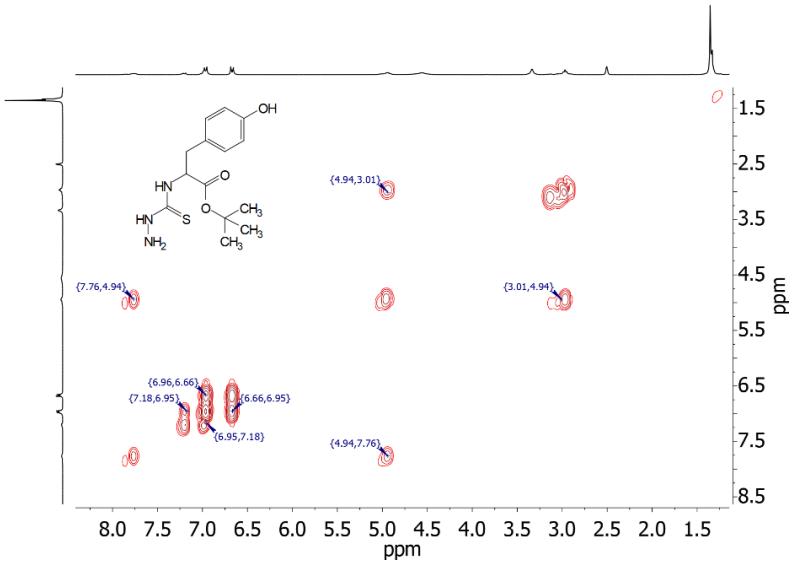


Figure 158. ^{1}H,^{1}H COSY NMR spectrum of (*S*)-*tert*-butyl-2-(hydrazidecarbothioamino)-3-(4-hydroxyphenyl)propanoate in DMSO-d_6 at 300 MHz.

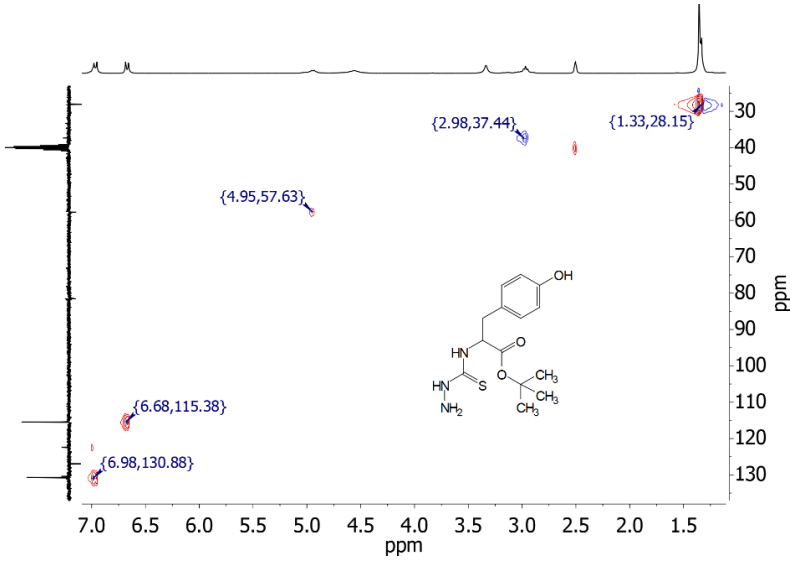


Figure 159. ^{1}H,^{13}C HMQC/HSQC NMR spectrum of (*S*)-*tert*-butyl-2-(hydrazidecarbothioamino)-3-(4-hydroxyphenyl)propanoate in DMSO-d_6 at 300 MHz.

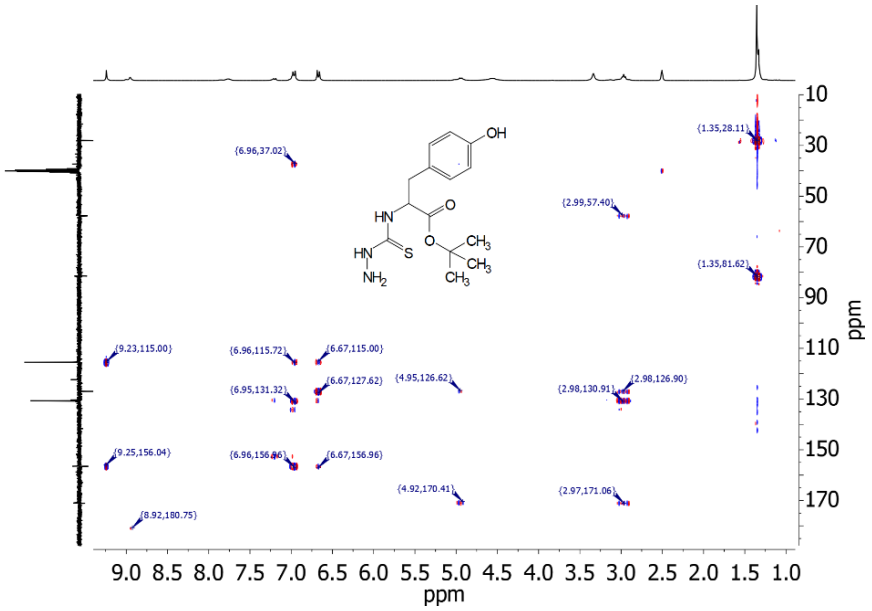


Figure 160. $^{1}H,^{13}C$ HMBC NMR spectrum of (*S*)-*tert*-butyl-2-(hydrazidecarbothioamino)-3-(4-hydroxyphenyl)propanoate in DMSO-d_6 at 300 MHz.

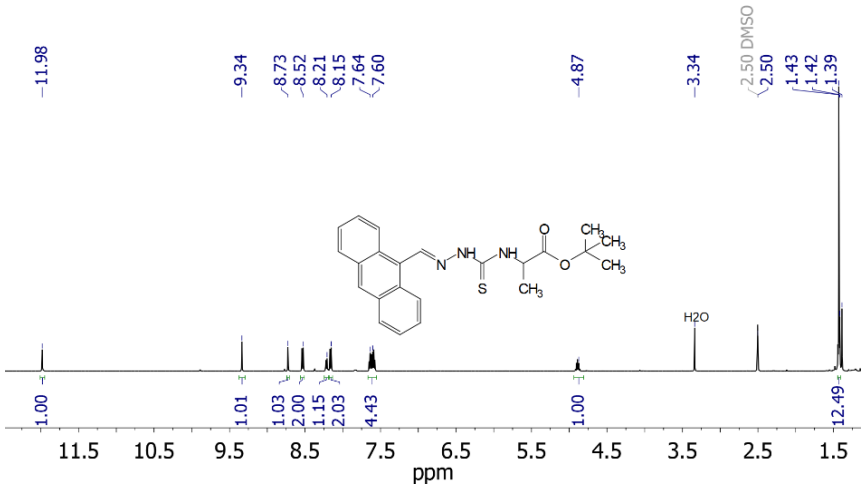


Figure 161. ^{1}H NMR spectrum of 9-anthraldehyde-4-((*S*)-*tert*-butylpropanoate)-3-thiosemicarbazone DMSO-d_6 at 499 MHz.

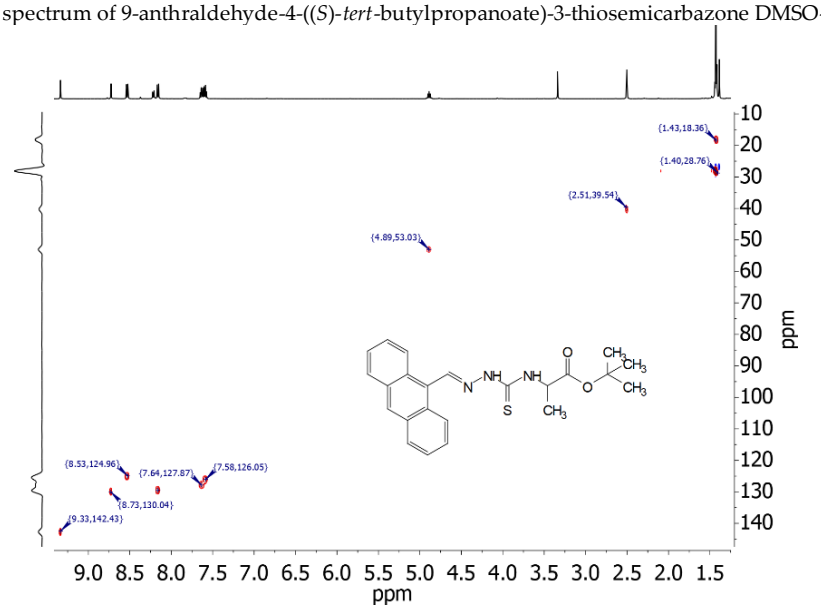


Figure 162. $^{1}H,^{13}C$ HMQC/HSQC NMR of 9-anthraldehyde-4-((*S*)-*tert*-butylpropanoate)-3-thiosemicarbazone spectrum in DMSO-d_6 at 499 MHz.

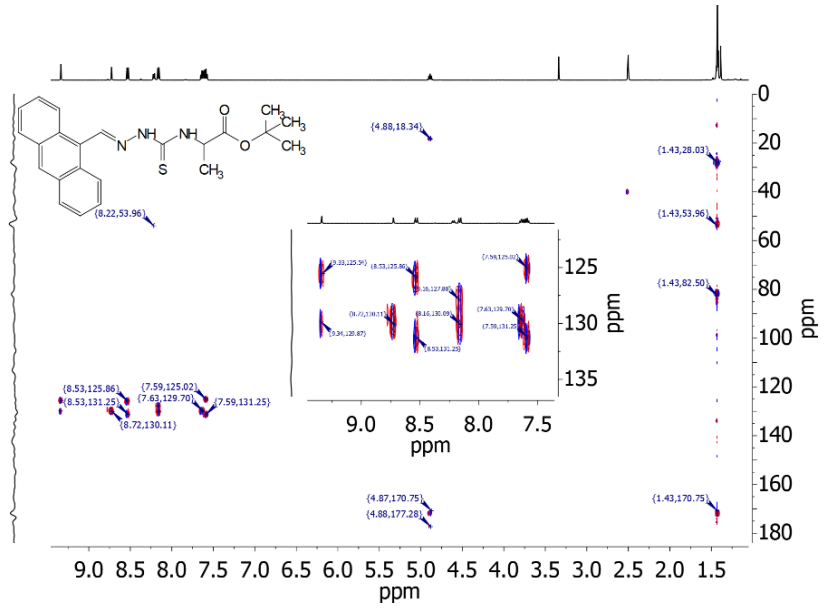


Figure 163. $^{1}H,^{13}C$ HMBC NMR spectrum of 9-anthraldehyde-4-((*S*)-*tert*-butylpropanoate)-3-thiosemicarbazone DMSO-d_6 at 499 MHz.

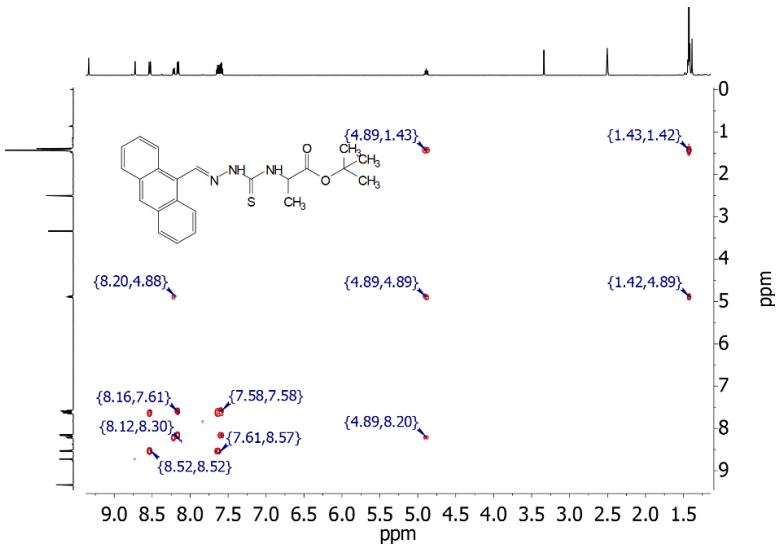


Figure 164. $^{1}H,^{1}H$ COSY NMR spectrum of 9-anthraldehyde-4-((*S*)-*tert*-butylpropanoate)-3-thiosemicarbazone in DMSO-d_6 at 499 MHz.

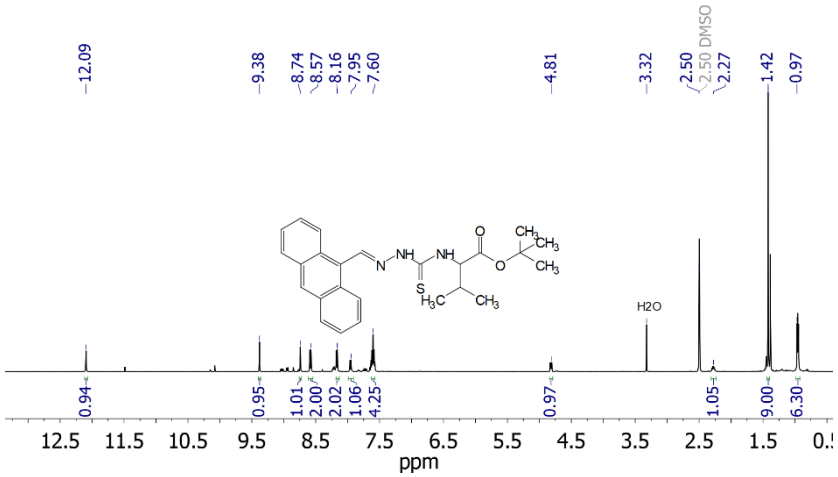


Figure 165. ^{1}H NMR spectrum of 9-anthraldehyde-4-((*S*)-*tert*-butyl 3-metylbutanoate)-3-thiosemicarbazone in DMSO-d_6 at 499 MHz.

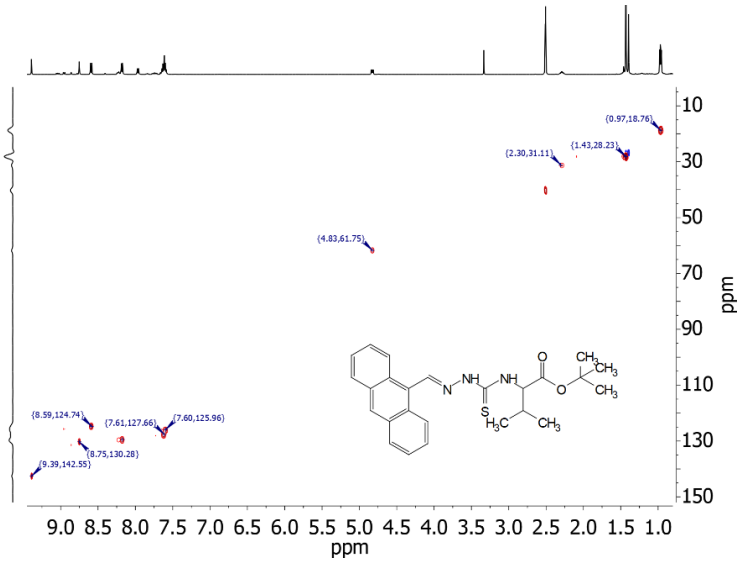


Figure 166. $^{1}H,^{13}C$ HMQC/HSQC NMR spectrum of 9-anthraldehyde-4-((*S*)-*tert*-butyl-3-metyl-butanoate)-3-thiosemicarbazone in DMSO-d_6 at 499 MHz.

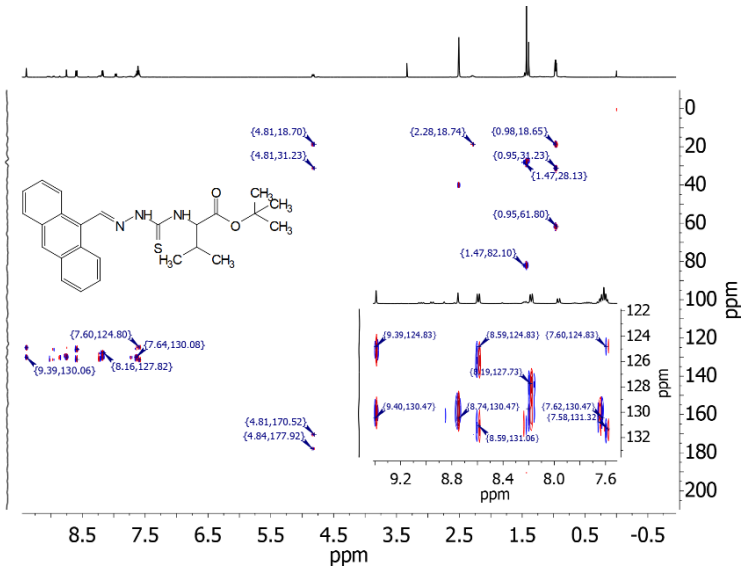


Figure 167. $^{1}H,^{13}C$ HMBC NMR spectrum of 9-anthraldehyde-4-((*S*)-*tert*-butyl 3-metylbutanoate)-3-thiosemicarbazone in DMSO-d_6 at 499 MHz.

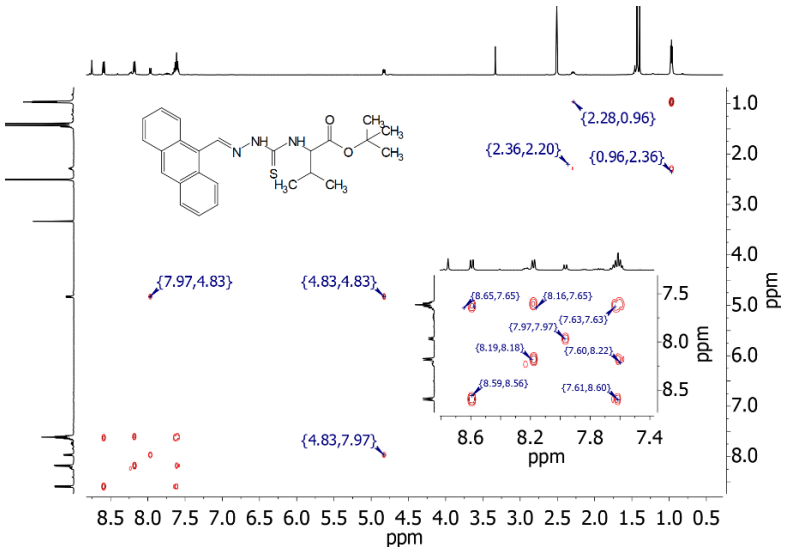


Figure 168. $^{1}H,^{1}H$ COSY NMR spectrum of 9-anthraldehyde-4-((*S*)-*tert*-butyl 3-metylbutanoate)-3-thiosemicarbazone in DMSO-d_6 at 499 MHz.

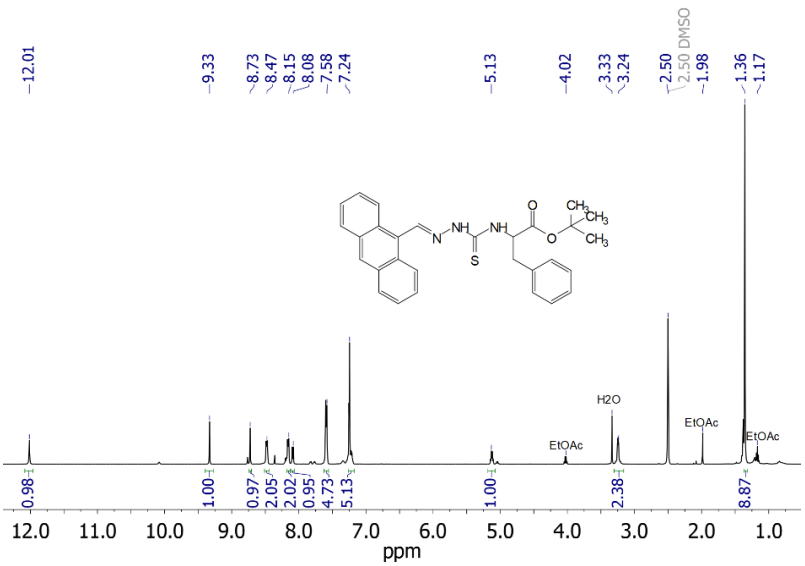


Figure 169. ^{1}H NMR spectrum of 9-anthraldehyde-4-((*S*)-*tert*-butyl 3-metylbutanoate)-3-thiosemicarbazone in DMSO-d_6 at 499 MHz.

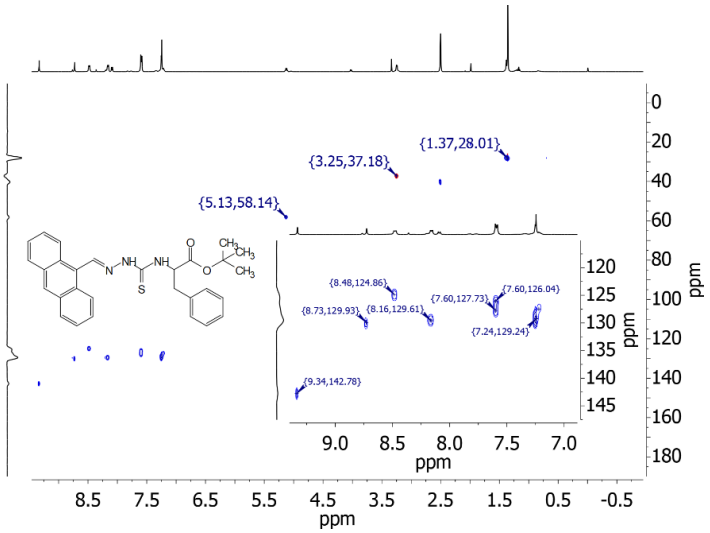


Figure 170. ^{1}H,^{13}C HMQC/HSQC NMR spectrum of 9-anthraldehyde-4-((*S*)-*tert*-butyl 3-metylbutanoate)-3-thiosemicarbazone in DMSO-d_6 at 499 MHz.

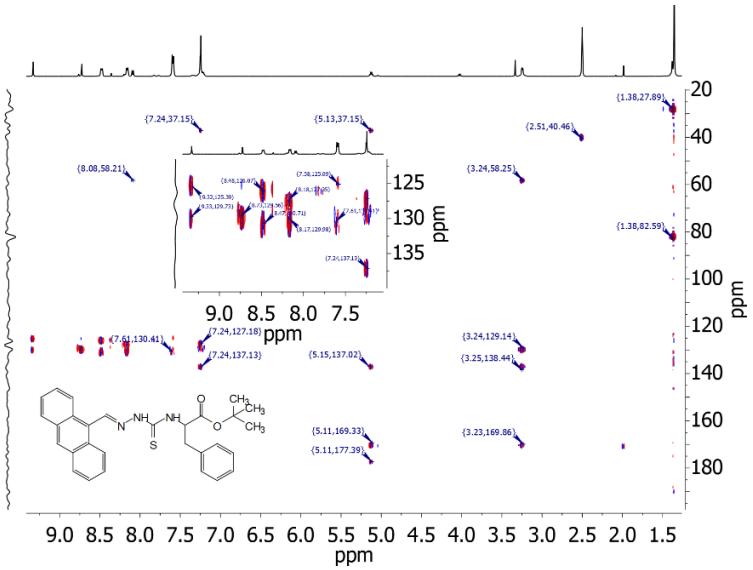


Figure 171. ^{1}H,^{13}C HMBC NMR spectrum of 9-anthraldehyde-4-((*S*)-*tert*-butyl 3-metylbutanoate)-3-thiosemicarbazone in DMSO-d_6 at 499 MHz.

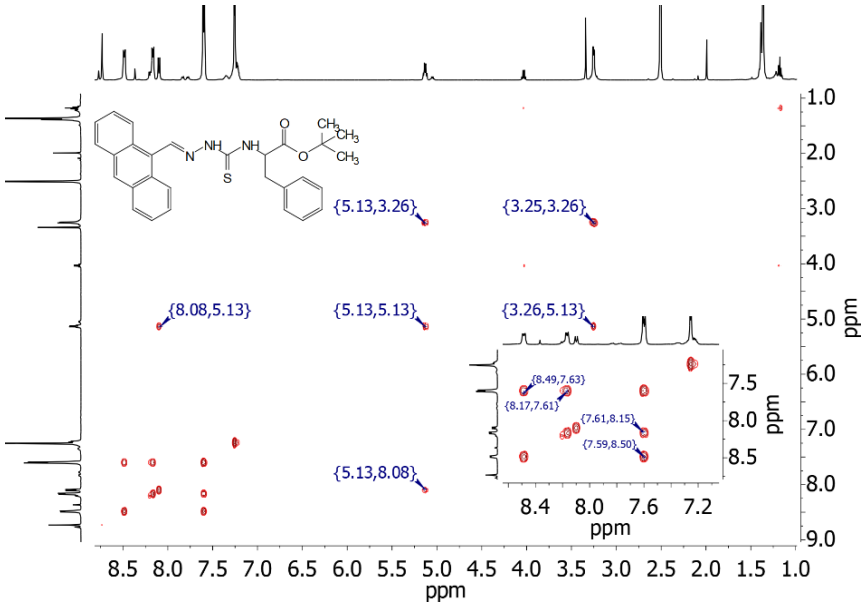


Figure 172. ^{1}H,^{1}H COSY NMR spectrum of 9-anthraldehyde-4-((*S*)-*tert*-butyl 3-metylbutanoate)-3-thiosemicarbazone DMSO-d_6 at 499 MHz.

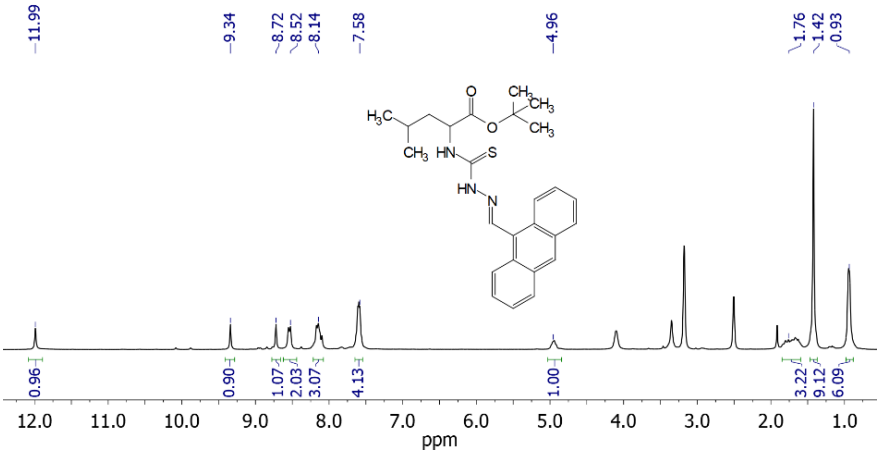


Figure 173. ^{1}H NMR spectrum of 9-anthraldehyde-4-((*S*)-*tert*-butyl 4-methylpentonate)-3-thiosemicarbazone in DMSO-d_6 at 300 MHz.

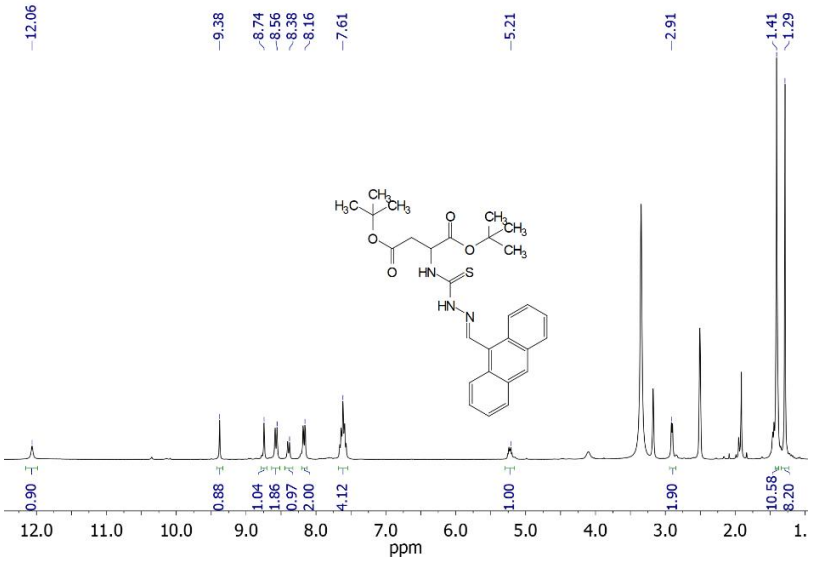


Figure 174. ^{1}H NMR spectrum of di-*tert*-butyl 2-8([(1*E*)-(anthracen-9-yl)methylideneamino-carbamthioyl]amino) butanedioate in DMSO-d_6 at 300 MHz.

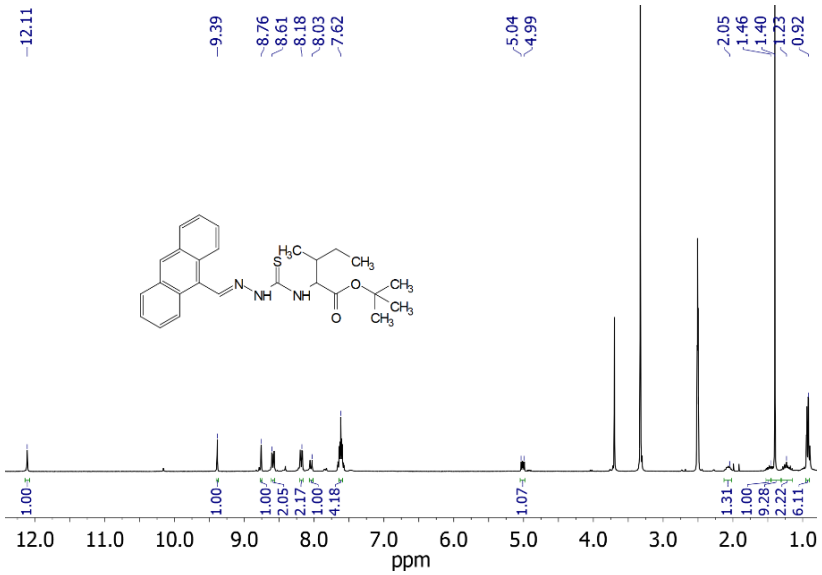


Figure 175. ^{1}H NMR spectrum of *tert*-butyl-2-([(1*E*)-(anthracen-9-yl)methylideneaminocarbam-thioyl]amino)-3-methyl pentanoate in DMSO-d_6 at 300 MHz.

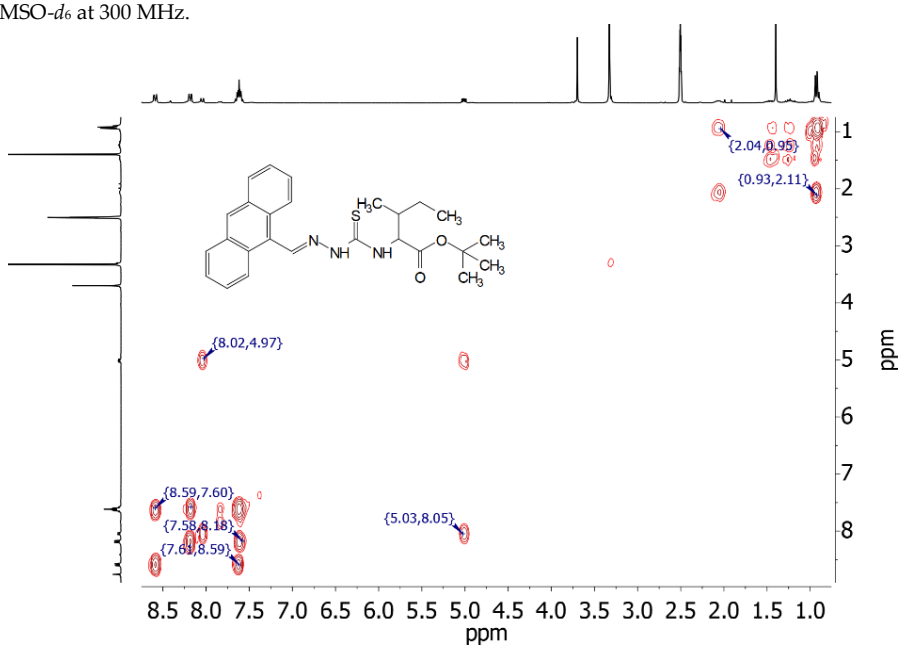


Figure 176. ^{1}H,^{1}H COSY NMR spectrum of *tert*-butyl-2-([(1*E*)-(anthracen-9-yl)methylideneamino-carbamthioyl]amino)-3-methyl pentanoate in DMSO-d_6 at 300 MHz.

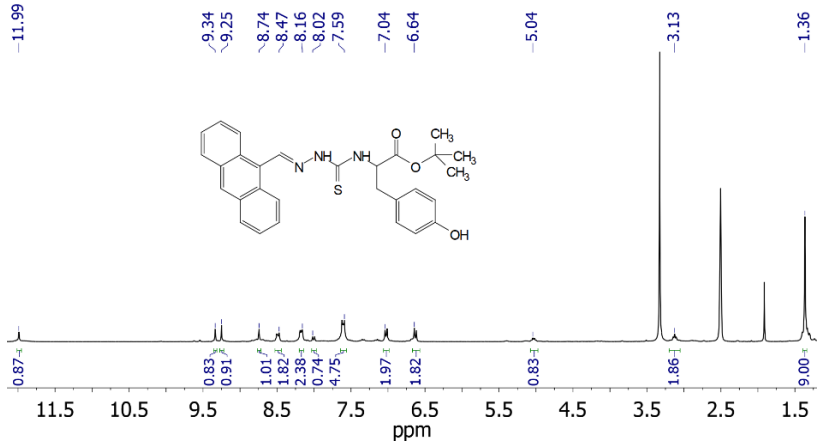


Figure 177. ^{1}H NMR spectrum of *tert*-butyl-2-[(2*E*)-2-[(anthracen-9-yl)methylidene]hydrazine-carbamthioyl]-3-(4-hydroxyphenyl)propanoate in DMSO-d_6 at 300 MHz.

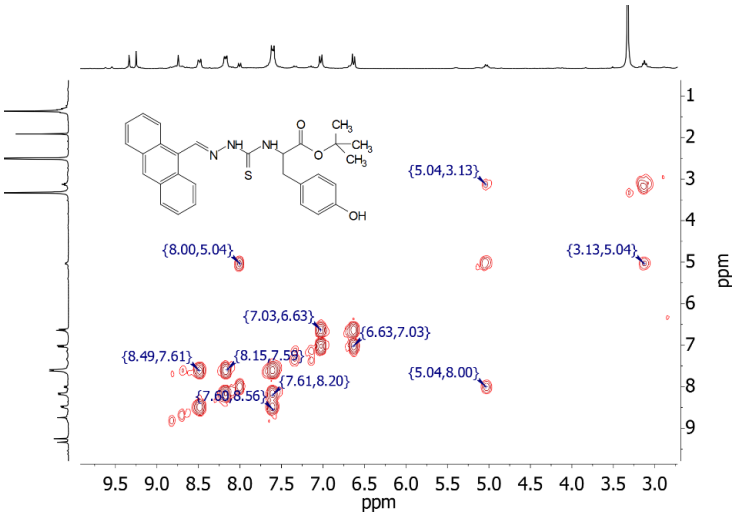


Figure 178. $^{1}H,^{1}H$ COSY NMR spectrum of *tert*-butyl-2-[(2*E*)-2-[(anthracen-9-yl)methylidene]-hydrazinecarbamthioyl]-3-(4-hydroxyphenyl) propanoate in DMSO-d_6 at 300 MHz.

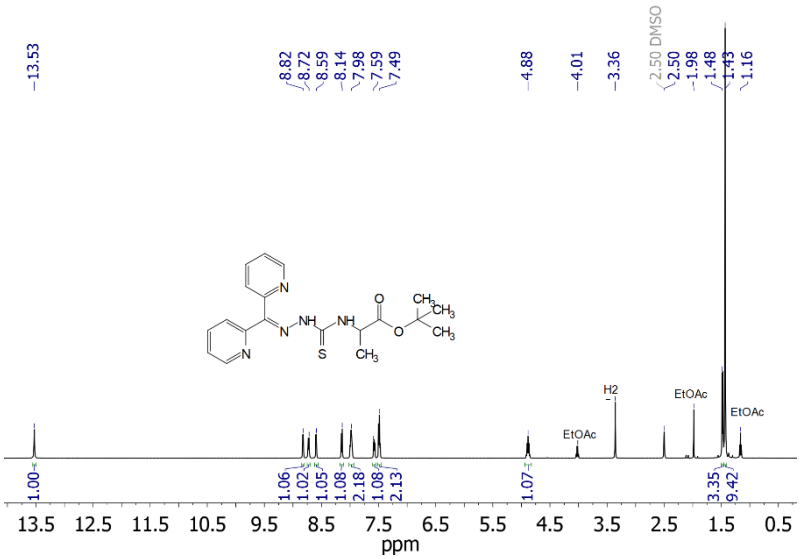


Figure 179. ^{1}H NMR spectrum of di-2-pyridylketone-4-((*S*)-*tert*-butyl propanoate)-3-thiosemi-carbazone in DMSO-d_6 at 499 MHz.

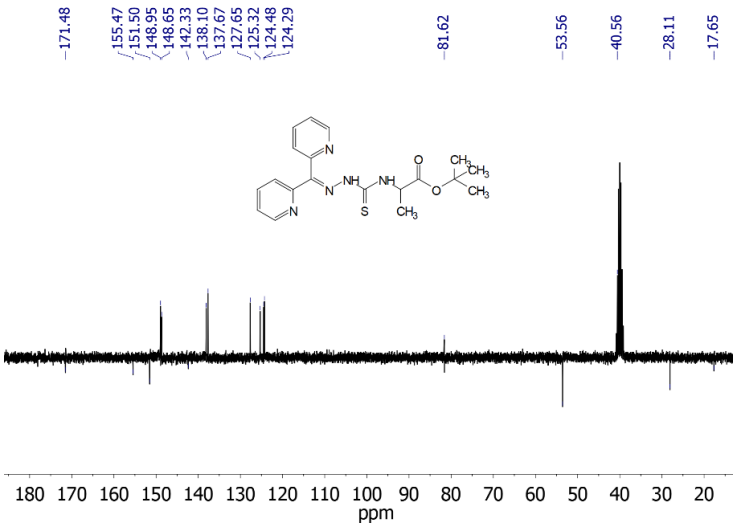


Figure 180. ^{13}C DEPTQ NMR spectrum of di-2-pyridylketone-4-((*S*)-*tert*-butyl propanoate)-3-thiosemicarbazone in DMSO-d_6 at 300 MHz.

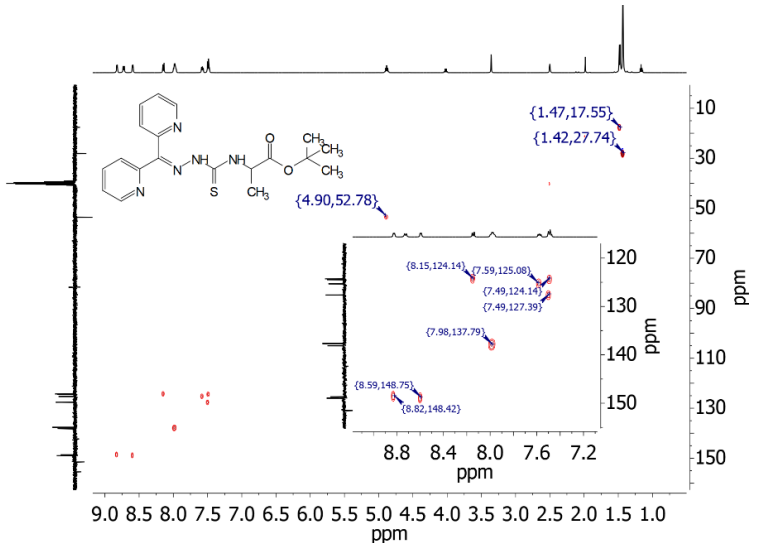


Figure 181. $^{1}H,^{13}C$ HMQC/HSQC NMR spectrum of di-2-pyridylketone-4-((*S*)-*tert*-butyl propanoate)-3-thiosemicarbazone in DMSO-d_6 at 499 MHz.

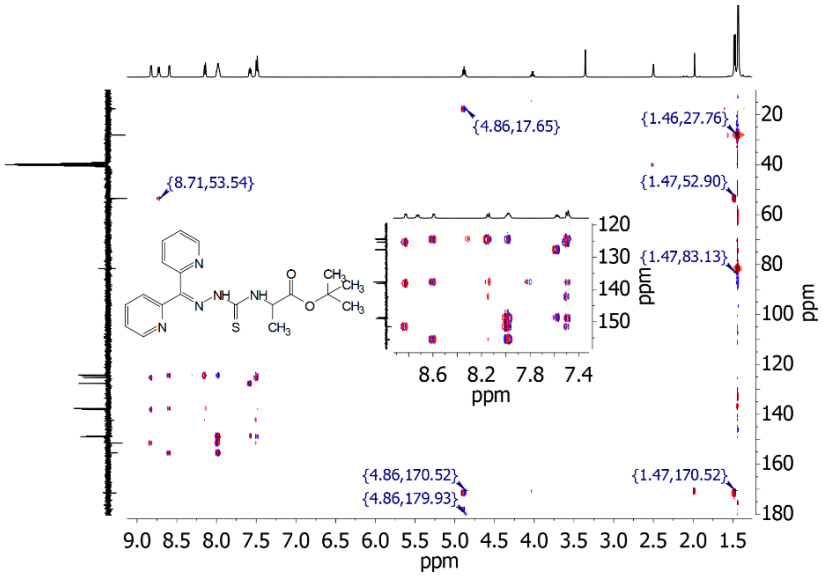


Figure 182. $^{1}H,^{13}C$ HMBC NMR spectrum of di-2-pyridylketone-4-((*S*)-*tert*-butyl propanoate)-3-thiosemicarbazone in DMSO-d_6 at 499 MHz.

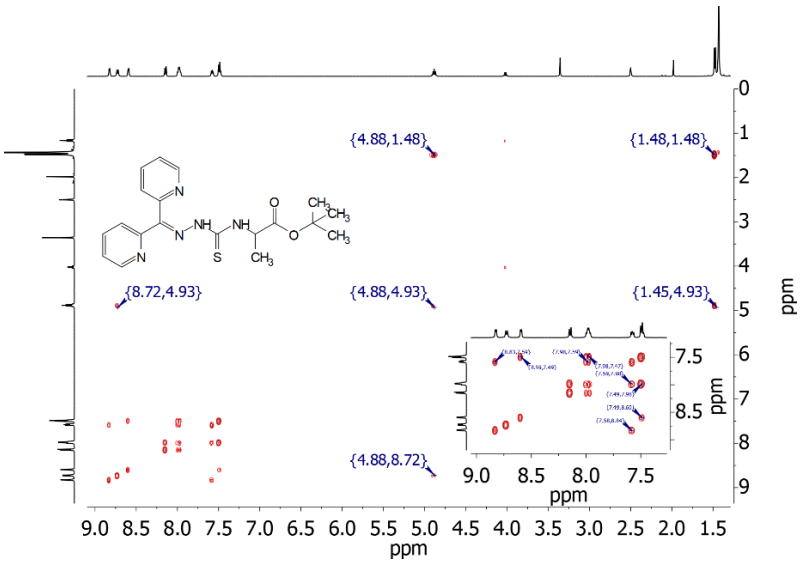


Figure 183. $^{1}H,^{1}H$ COSY NMR spectrum of di-2-pyridylketone-4-((*S*)-*tert*-butyl propanoate)-3-thiosemicarbazone in DMSO-d_6 at 499 MHz.

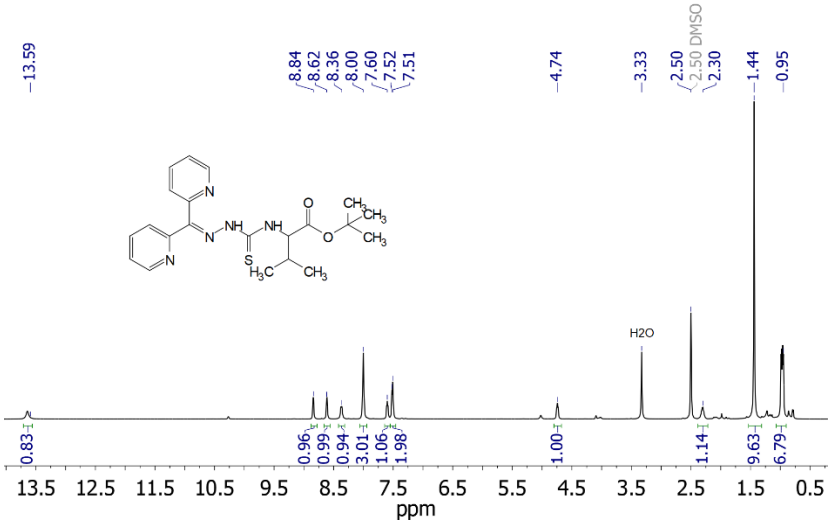


Figure 184. ^{1}H NMR spectrum of di-2-pyridylketone-4-((*S*)-*tert*-butyl 3-metylbutanoate)-3-thiosemicarbazone DMSO-d_6 at 499 MHz.

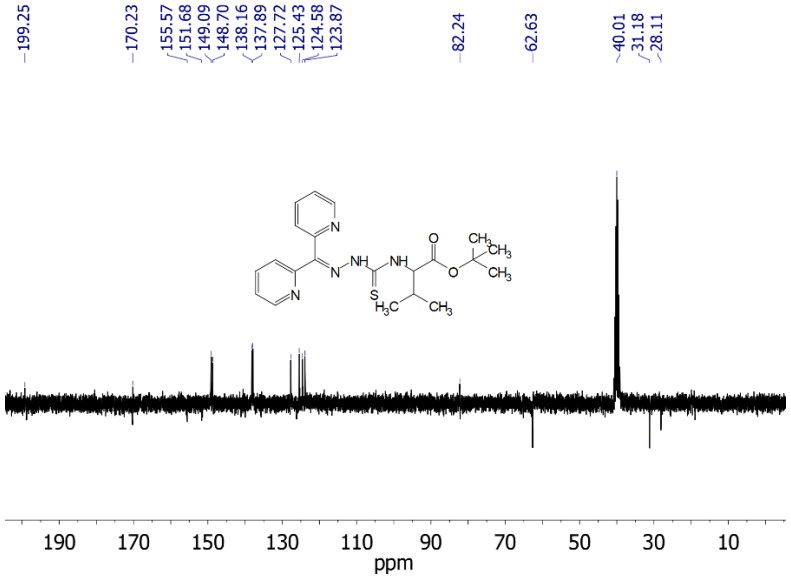


Figure 185. ^{13}C DEPTQ NMR spectrum of di-2-pyridylketone-4-((*S*)-*tert*-butyl 3-metylbutanoate)-3-thiosemicarbazone in DMSO-d_6 at 300 MHz.

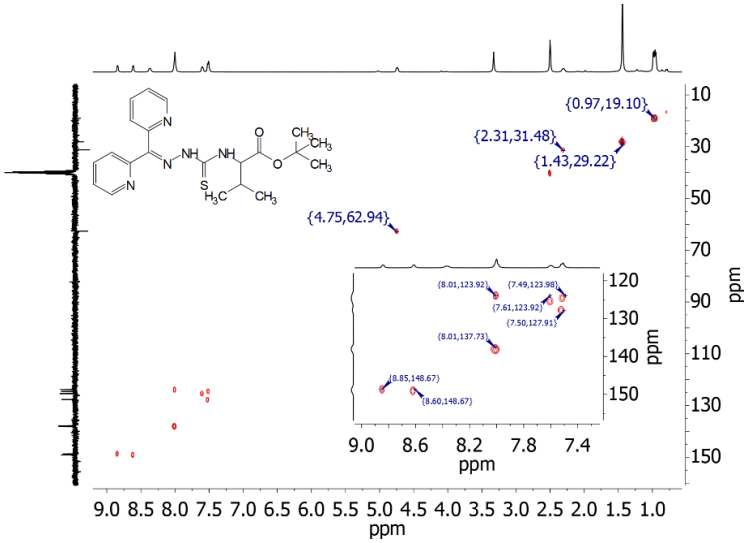


Figure 186. ^{1}H,^{13}C HMQC/HSQC NMR spectrum of di-2-pyridylketone-4-((*S*)-*tert*-butyl 3-metyl-butanoate)-3-thiosemicarbazone in DMSO-d_6 at 499 MHz.

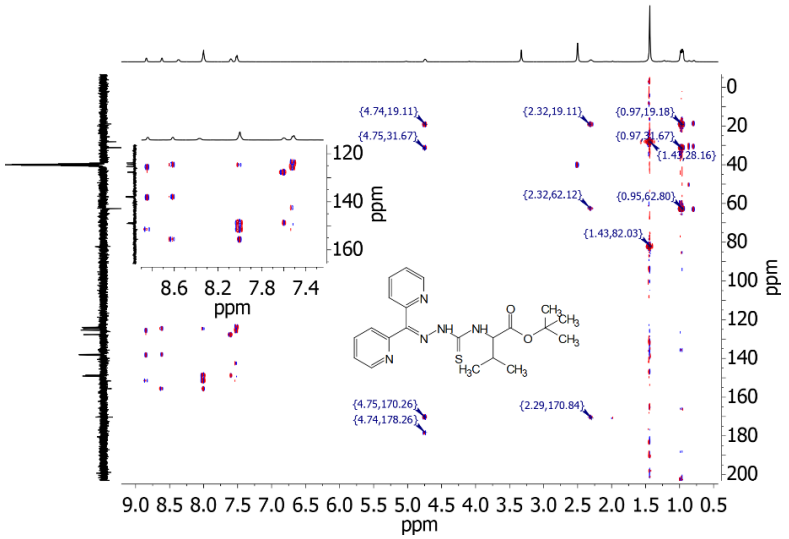


Figure 187. $^{1}H,^{13}C$ HMBC NMR spectrum of di-2-pyridylketone-4-((*S*)-*tert*-butyl 3-metylbutanoate)-3-thiosemicarbazone in DMSO-d_6 at 499 MHz.

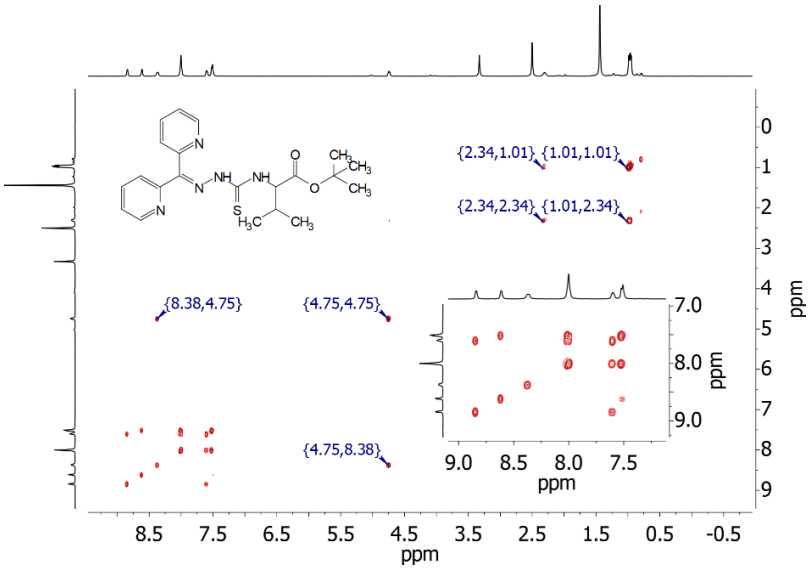


Figure 188. $^{1}H,^{1}H$ COSY NMR spectrum of di-2-pyridylketone-4-((*S*)-*tert*-butyl 3-metylbutanoate)-3-thiosemicarbazone in DMSO-d_6 at 499 MHz.

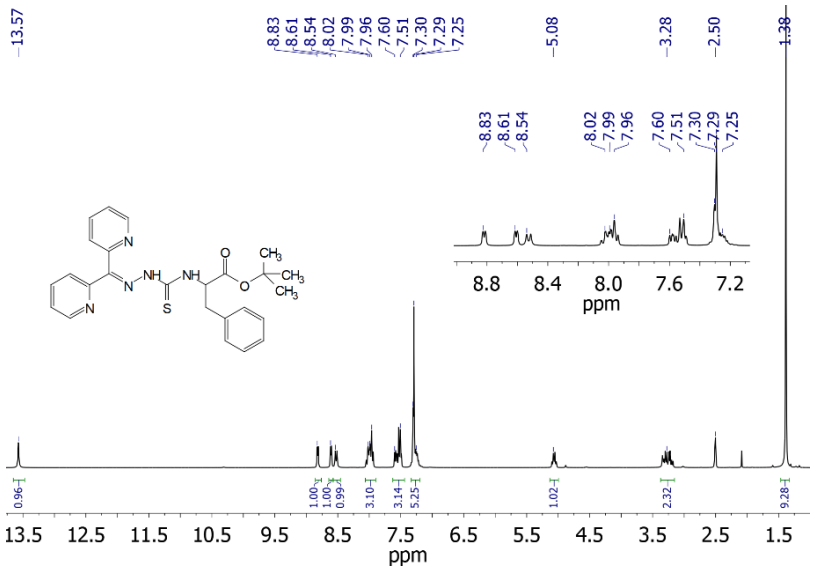


Figure 189. ^{1}H NMR spectrum of di-2-pyridylketone-4-((*S*)-*tert*-butyl 3-phenylbutanoate)-3-thiosemi-carbazone in DMSO-d_6 at 499 MHz.

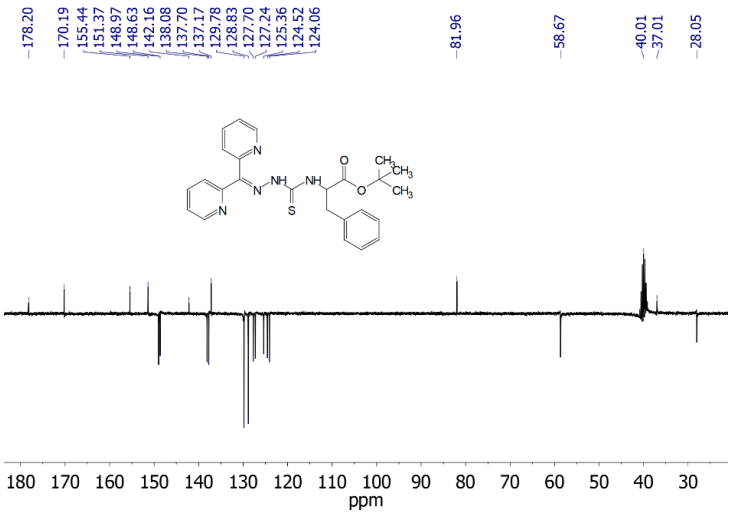


Figure 190. ^{13}C DEPTQ NMR spectrum of di-2-pyridylketone-4-((*S*)-*tert*-butyl 3-phenylbutanoate)-3-thiosemicarbazone in DMSO-d_6 at 300 MHz.

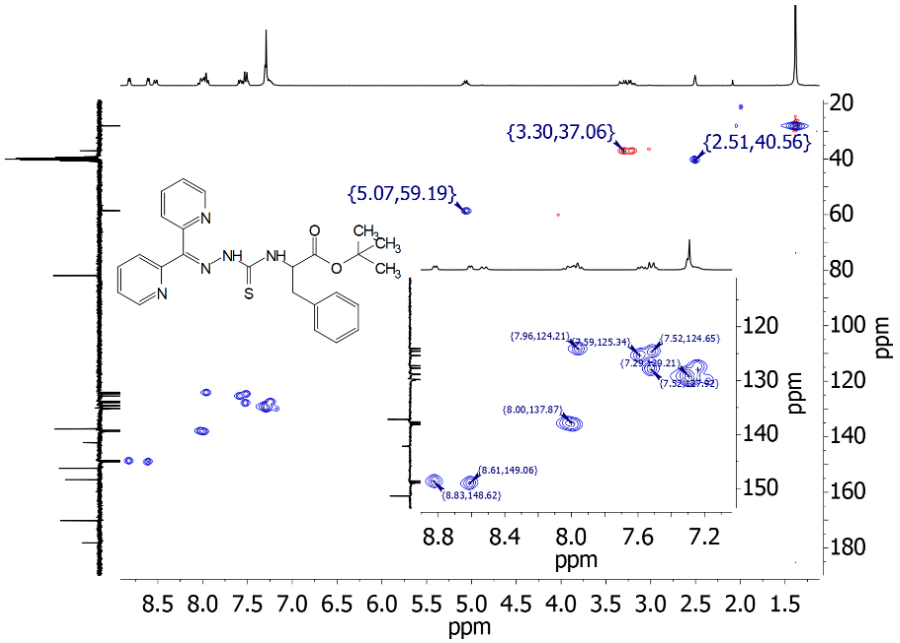


Figure 191. ^{1}H,^{13}C HMQC/HSQC NMR spectrum of di-2-pyridylketone-4-((*S*)-*tert*-butyl 3-phenylbutanoate)-3-thiosemicarbazone in DMSO-d_6 at 499 MHz.

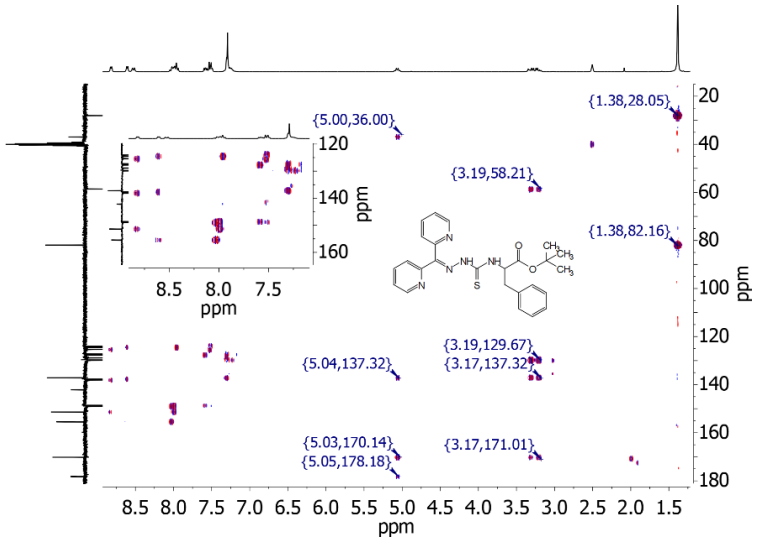


Figure 192. ^{1}H,^{13}C HMBC NMR spectrum of di-2-pyridylketone-4-((*S*)-*tert*-butyl 3-phenylbutanoate)-3-thiosemicarbazonein DMSO-d_6 at 499 MHz.

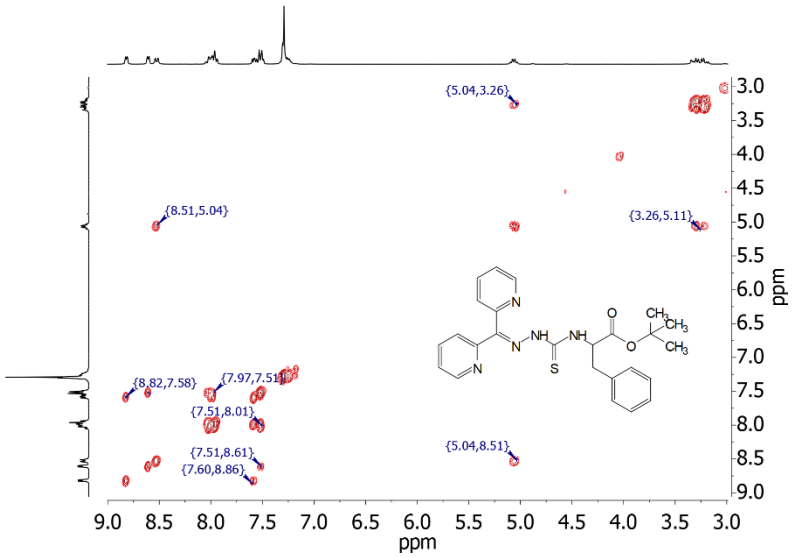


Figure 193. $^{1}H,^{1}H$ COSY NMR spectrum of di-2-pyridylketone-4-((*S*)-*tert*-butyl 3-phenylbutanoate)-3-thiosemicarbazone in DMSO-d_6 at 499 MHz.

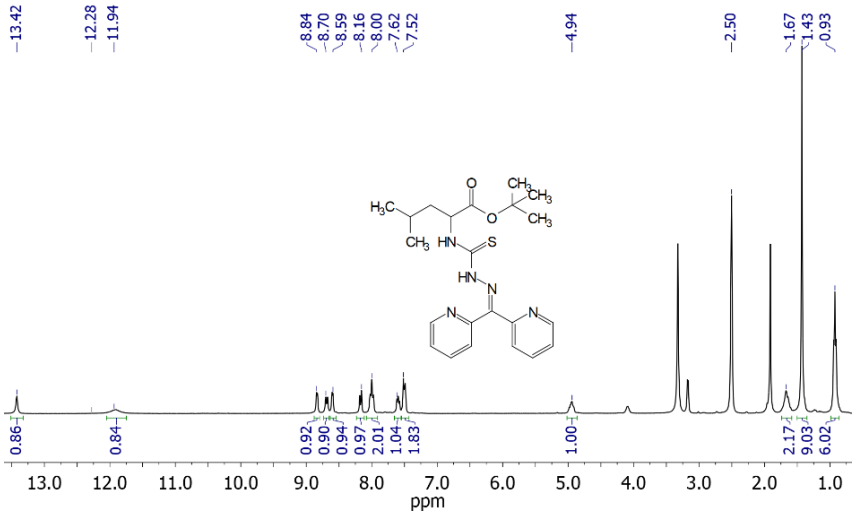


Figure 194. ^{1}H NMR spectrum of di-2-pyridylketone-4-((*S*)-*tert*-butyl-4-methylpentanoate)-3-thiosemicarbazone in DMSO-d_6 at 300 MHz.

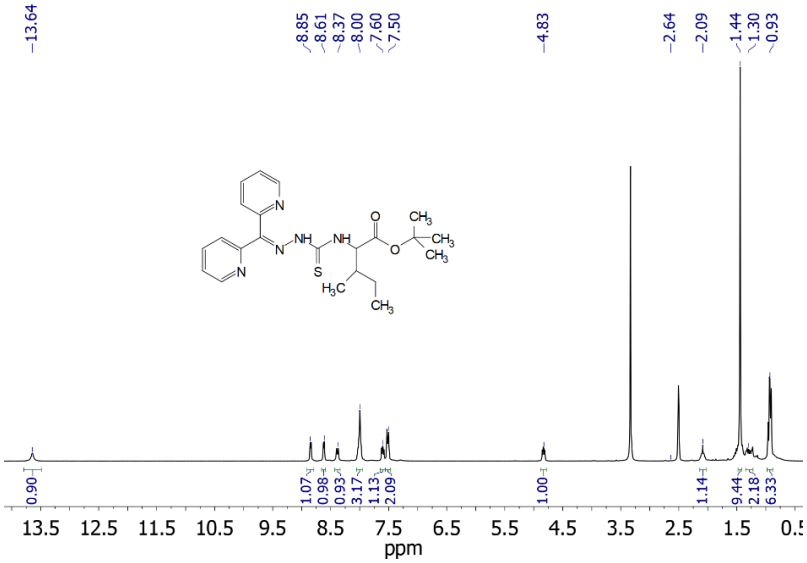


Figure 195. ^{1}H NMR spectrum of *tert*-butyl 2-(2-[bis(pyridin-2-yl)methylidene]hydrazine-carbamthioyl)-3-methylpentanoate in DMSO-d_6 at 300 MHz.

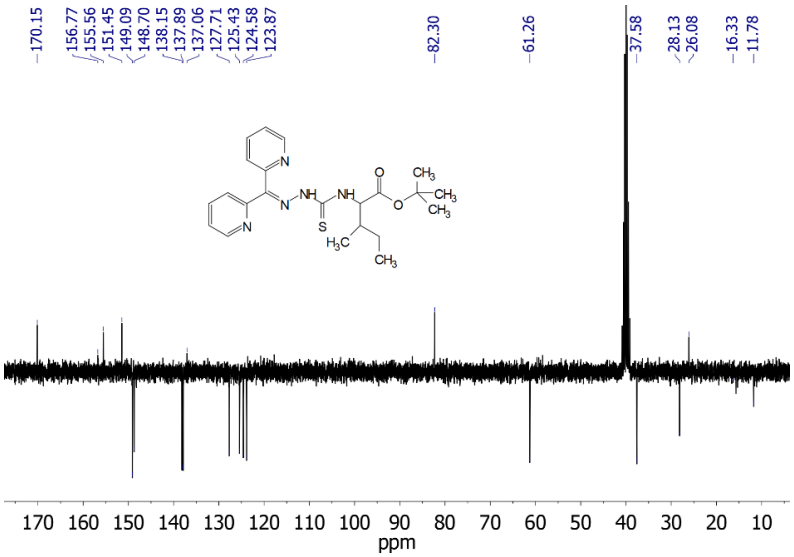


Figure 196. ^{13}C DEPTQ NMR spectrum of *tert*-butyl 2-(2-[bis(pyridin-2-yl)methylidene]hydrazine-carbamthioyl)-3-methylpentanoate in DMSO-d_6 at 300 MHz.

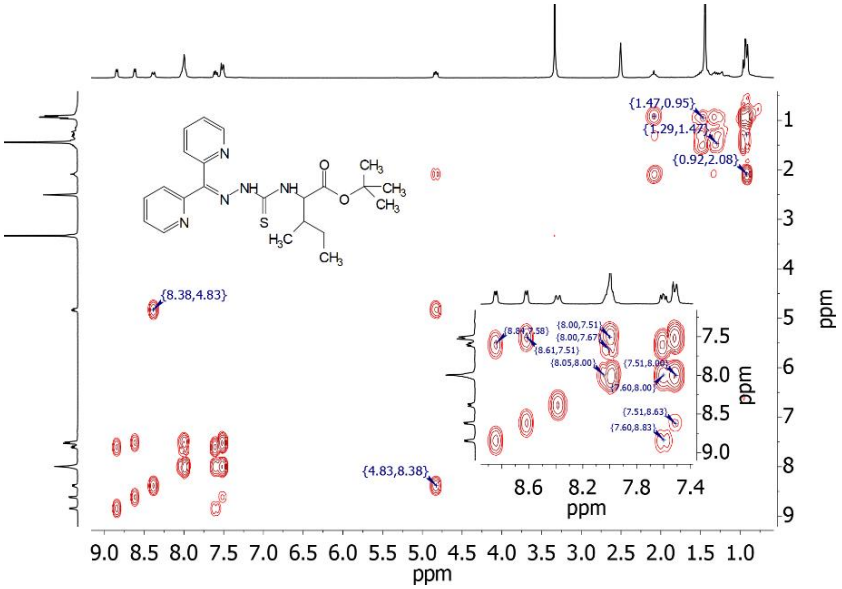


Figure 197. $^{1}H,^{1}H$ COSY NMR spectrum of *tert*-butyl 2-(2-[bis(pyridin-2-yl)methylidene]hydrazine-carbamthioyl)-3-methylpentanoate in DMSO-d_6 at 300 MHz.

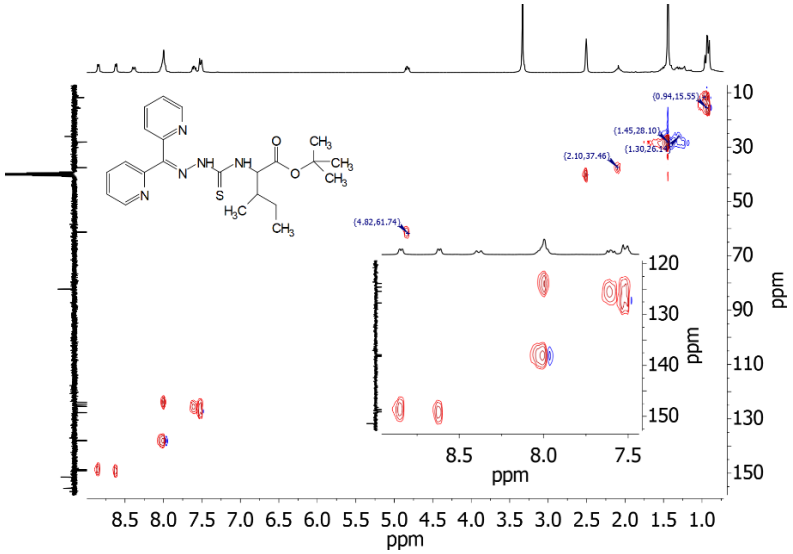


Figure 198. $^{1}H,^{13}C$ HMQC/HSQC spectrum of *tert*-butyl 2-(2-[bis(pyridin-2-yl)methylidene]-hydrazinecarbamthioyl)-3-methylpentanoate in DMSO-d_6 at 300 MHz.

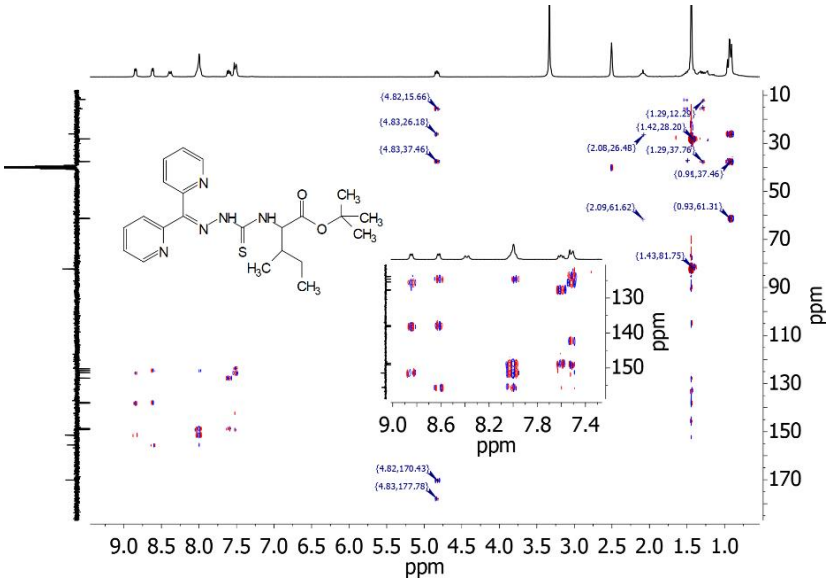


Figure 199. $^{1}H,^{13}C$ HMBC NMR spectrum of *tert*-butyl 2-(2-[bis(pyridin-2-yl)methylidene]hydrazine-carbamthioyl)-3-methylpentanoate in DMSO-d_6 at 300 MHz.

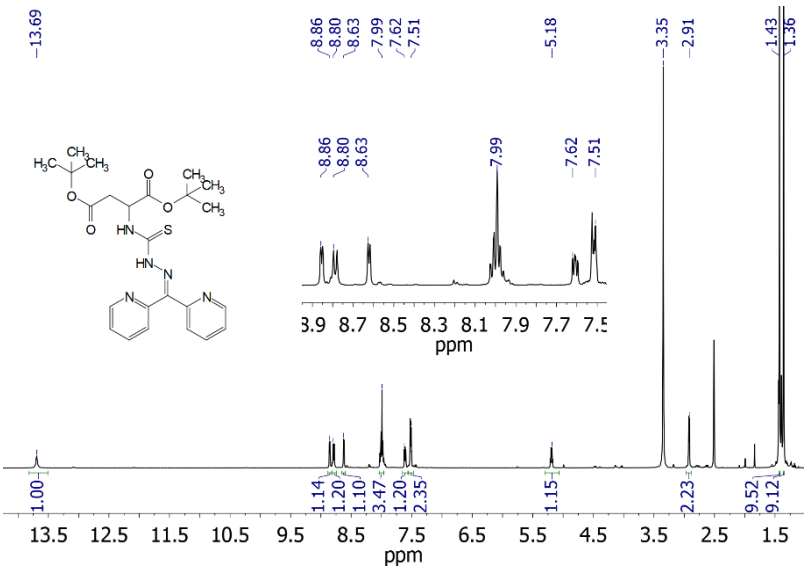


Figure 200. ^{1}H NMR spectrum of di-*tert*-butyl 2-([bis(pyridin-2-yl)methylideneamino-carbamthioyl]-amino)butanedioate in DMSO-d_6 at 499 MHz.

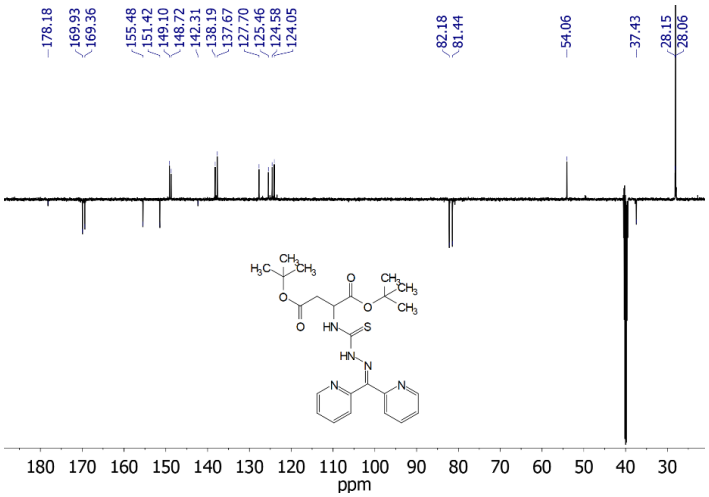


Figure 201. ^{13}C APT NMR spectrum of di-*tert*-butyl 2-([bis(pyridin-2-yl)methylideneaminocarbam-thioyl]amino)butanedioate in DMSO-d_6 at 499 MHz.

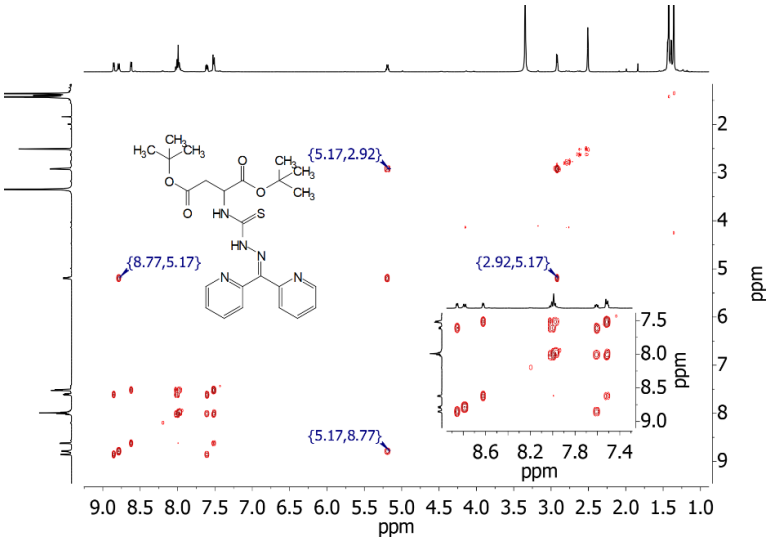


Figure 202. $^{1}H,^{1}H$ COSY NMR spectrum of di-*tert*-butyl 2-([bis(pyridin-2-yl)methylideneamino-carbamthioyl]amino) butanedioate in DMSO-d_6 at 499 MHz.

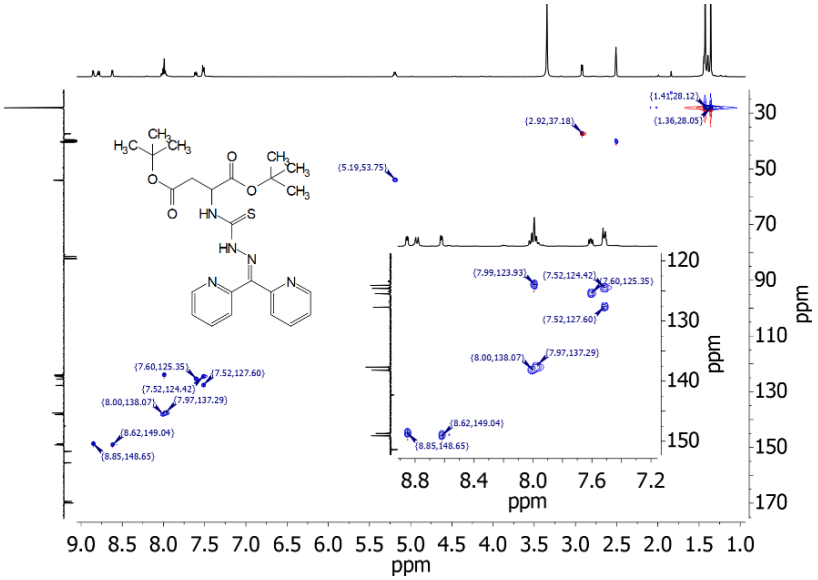


Figure 203. $^{1}H,^{13}C$ HMQC/HSQC NMR spectrum of di-*tert*-butyl 2-([bis(pyridin-2-yl)methylidene-aminocarbamthioyl]amino) butanedioate in DMSO-d_6 at 499 MHz.

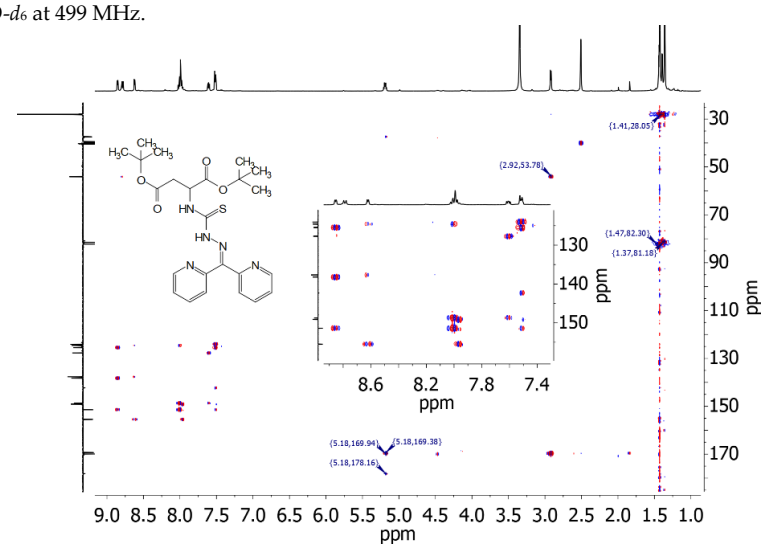


Figure 204. $^{1}H,^{13}C$ HMBC NMR spectrum of di-*tert*-butyl 2-([bis(pyridin-2-yl)methylideneamino-carbamthioyl]amino) butanedioate in DMSO-d_6 at 499 MHz.

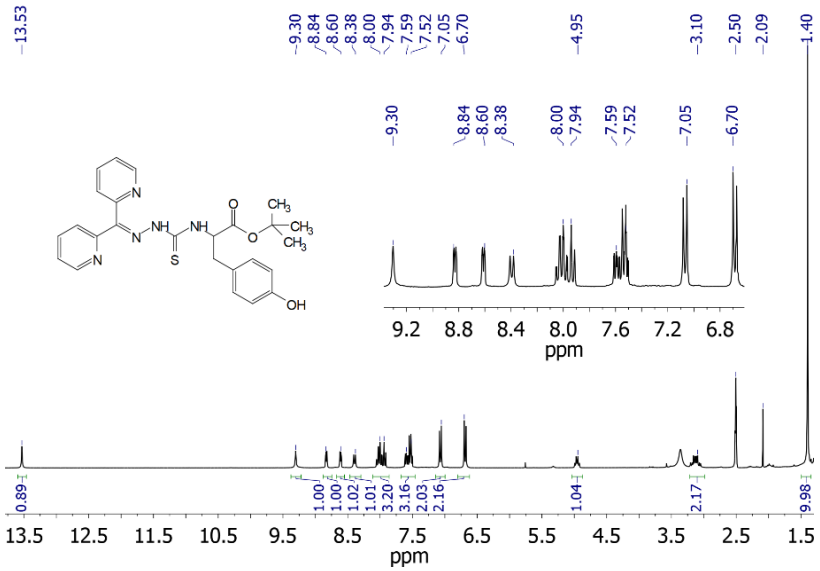


Figure 205. ^{1}H NMR spectrum of *tert*-butyl-2-(2-[bis(pyridin-2-yl)methylidene]hydrazine-carbamthioyl)-3-(4-hydroxyphenyl)-propanoate in DMSO-d_6 at 300 MHz.

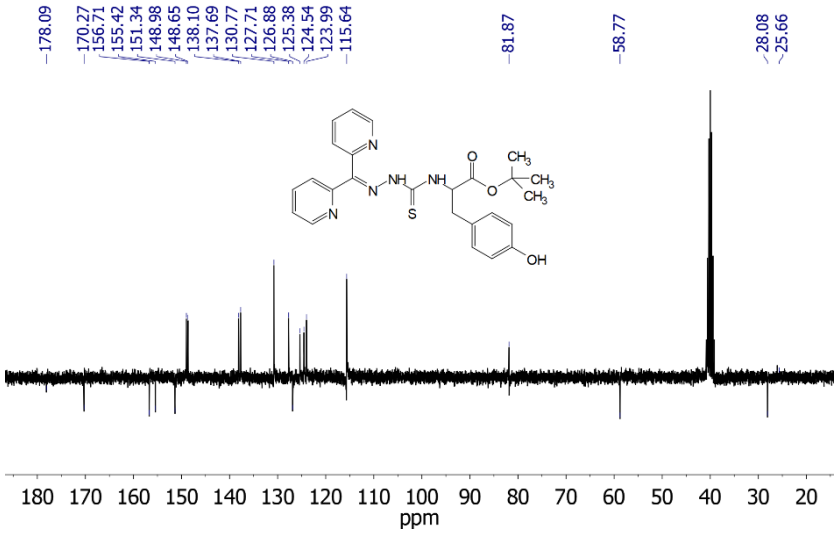


Figure 206. ^{13}C DEPTQ NMR spectrum of *tert*-butyl-2-(2-[bis(pyridin-2-yl)methylidene]hydrazine-carbamthioyl)-3-(4-hydroxyphenyl)propanoate in DMSO-d_6 at 300 MHz.

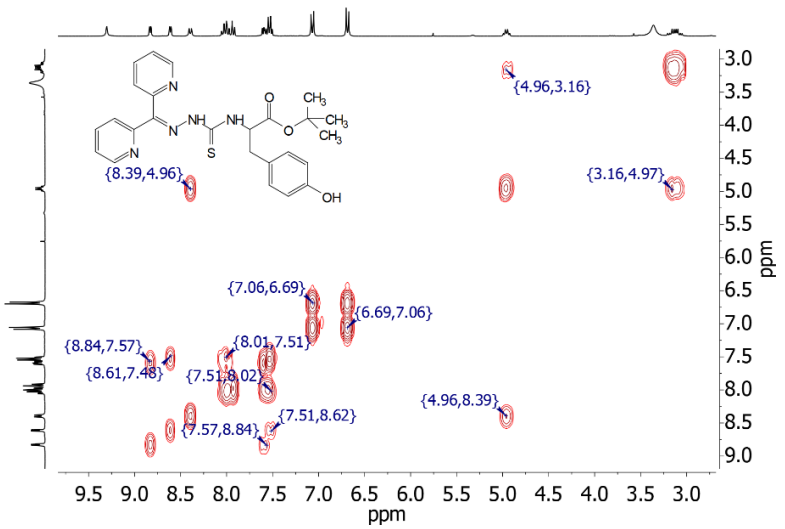


Figure 207. ^{1}H,^{1}H COSY NMR spectrum of *tert*-butyl-2-(2-[bis(pyridin-2-yl)methylidene]hydrazine-carbamthioyl)-3-(4-hydroxyphenyl)propanoate in DMSO-d_6 at 300 MHz.

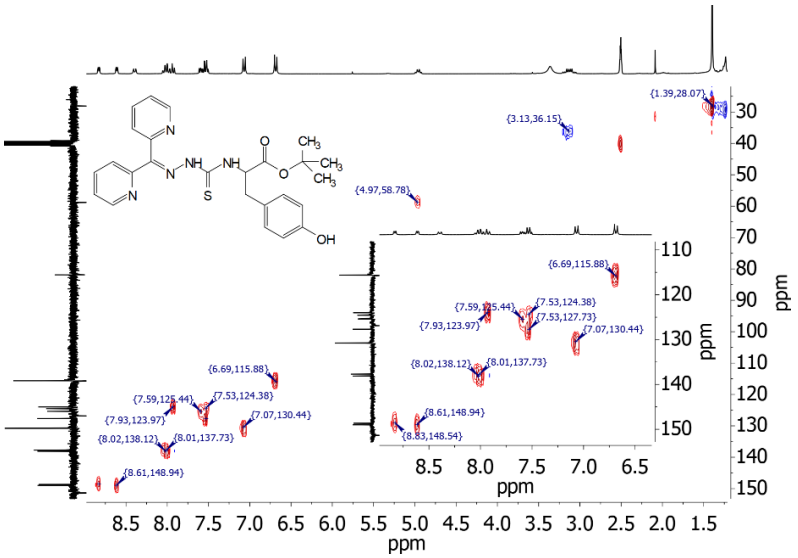


Figure 208. $^{1}H,^{13}C$ HMQC/HSQC NMR spectrum of *tert*-butyl-2-(2-[bis(pyridin-2-yl)methylidene]-hydrazinecarbamthioyl)-3-(4-hydroxyphenyl)-propanoate in DMSO-d_6 at 300 MHz.

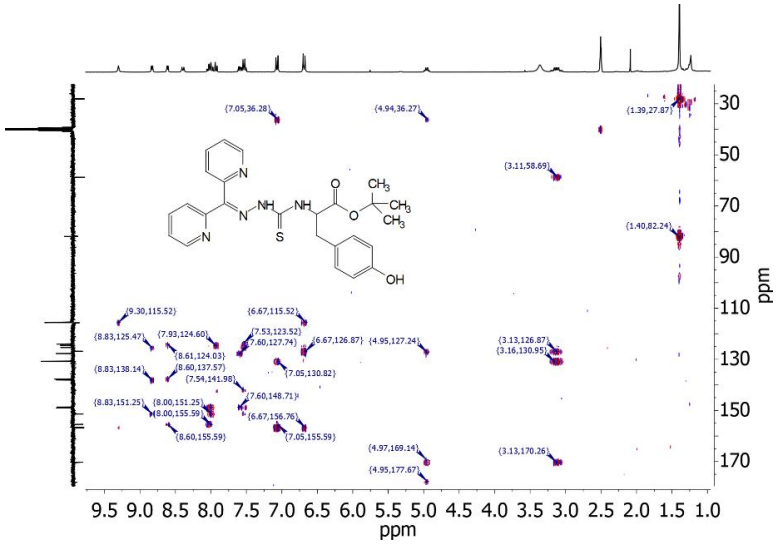


Figure 209. $^{1}H,^{13}C$ HMBC NMR spectrum of *tert*-butyl-2-(2-[bis(pyridin-2-yl)methylidene]hydrazine-carbamthioyl)-3-(4-hydroxyphenyl)-propanoate in DMSO-d_6 at 300 MHz.

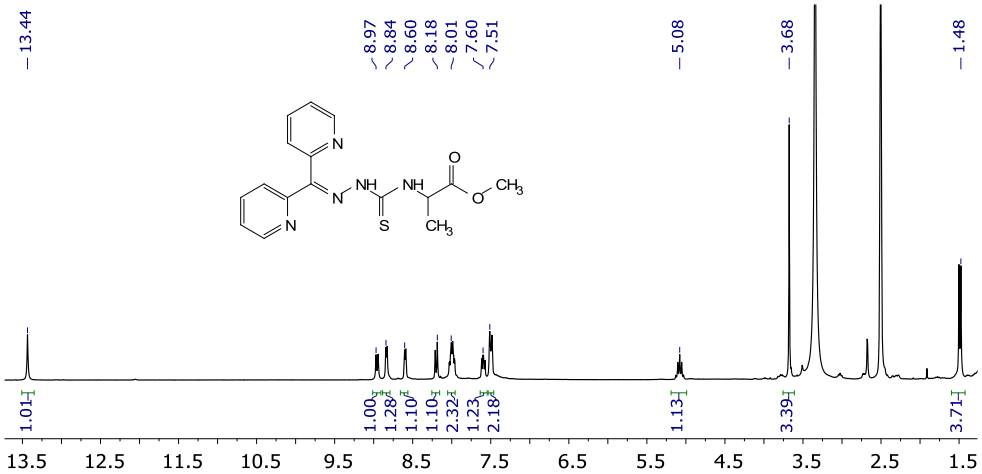


Figure 210. ^{1}H NMR spectrum of methyl 2-(2-[bis(pyridin-2-yl)methylidene]hydrazinocarbamthioyl) propanoate in DMSO-d_6 at 499 MHz.

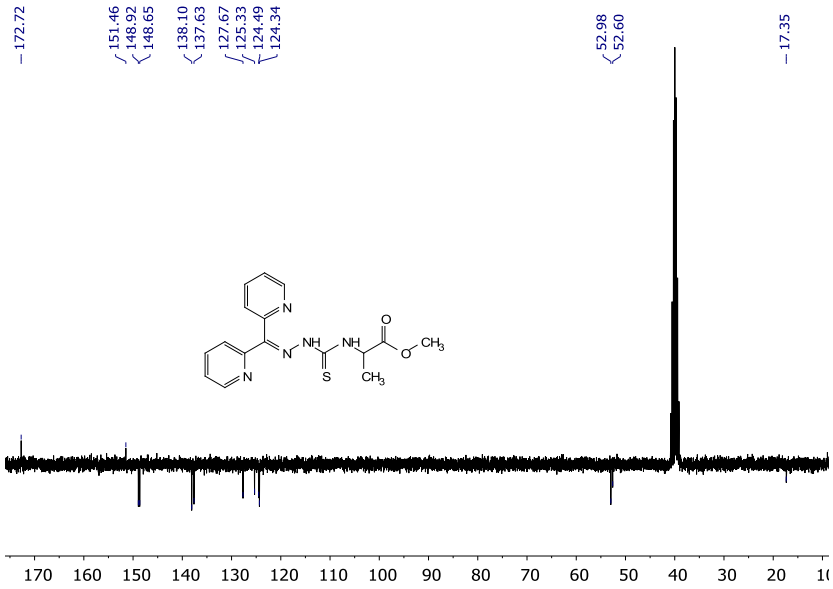


Figure 211. ^{13}C DEPTQ NMR spectrum of methyl 2-(2-[bis(pyridin-2-yl)methylidene]hydrazinocarbamthioyl) propanoate in DMSO-d_6 at 499 MHz.

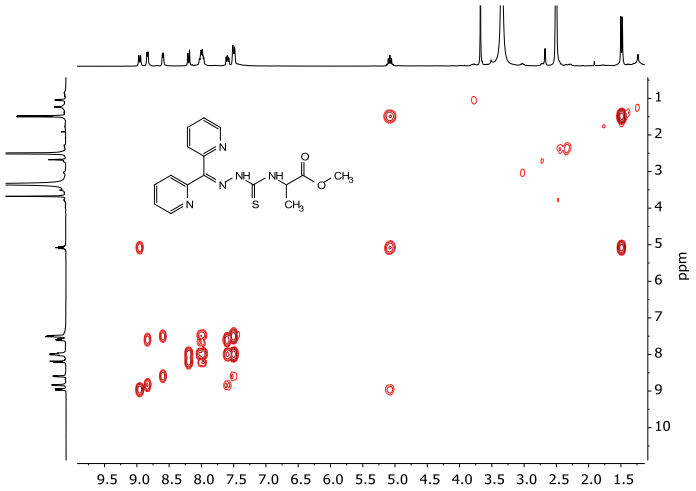


Figure 212. $^{1}H,^{1}H$ COSY NMR spectrum of methyl 2-(2-[bis(pyridin-2-yl)methylidene]hydrazinocarbamthioyl) propanoate in DMSO-d_6 at 499 MHz.

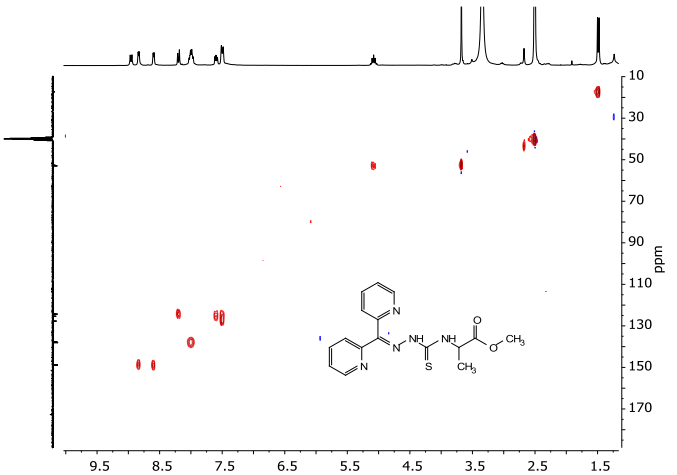


Figure 213. $^{1}H,^{13}C$ HMQC/HSQC NMR spectrum of methyl 2-(2-[bis(pyridin-2-yl)methylidene]hydrazinocarbamthioyl) propanoate in DMSO-d_6 at 499 MHz.

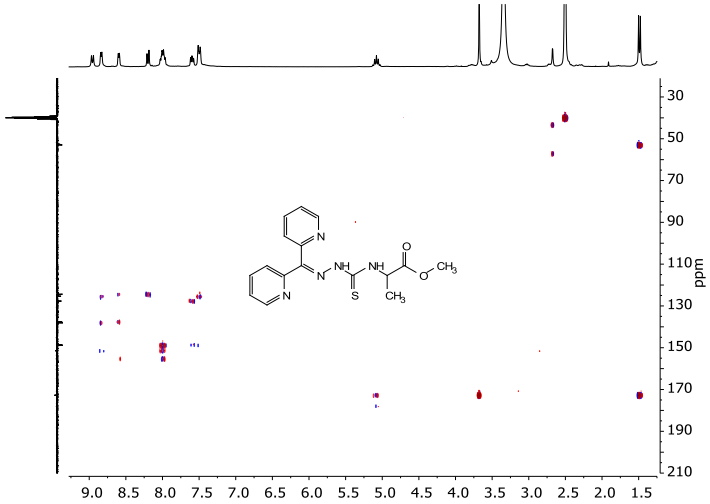


Figure 214. $^{1}H,^{13}C$ HMBC NMR spectrum of methyl 2-(2-[bis(pyridin-2-yl)methylidene]hydrazinocarbamthioyl) propanoate in DMSO-d_6 at 499 MHz.

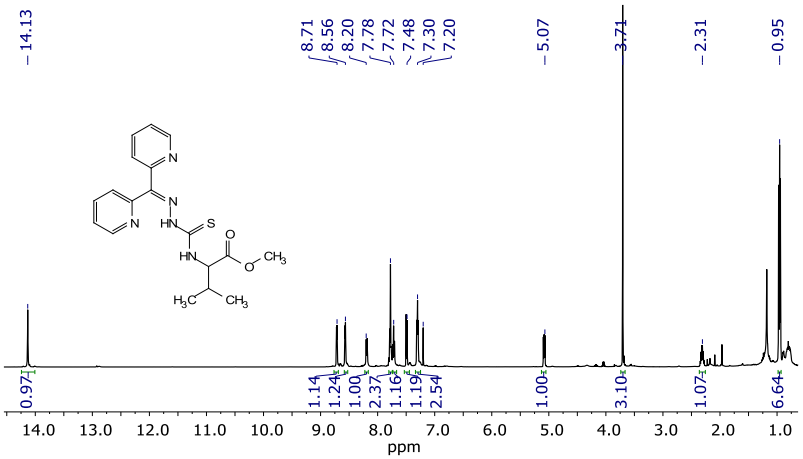


Figure 215. ^{1}H NMR spectrum of methyl 2-(2-[bis(pyridin-2-yl)methylidene]hydrazinocarbamthioyl)-3-methylbutanoate in DMSO-d_6 at 499 MHz.

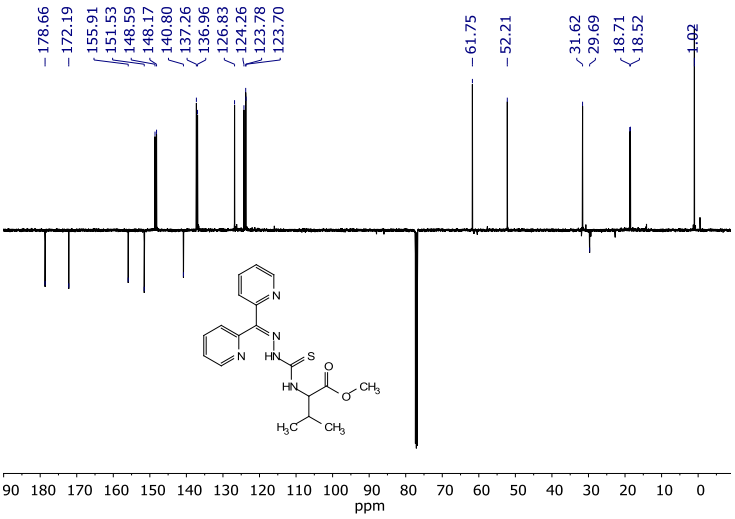


Figure 216. ^{13}C DEPTQ NMR spectrum of methyl 2-(2-[bis(pyridin-2-yl)methylidene]hydrazinocarbamthioyl)-3-methylbutanoate in DMSO-d_6 at 499 MHz.

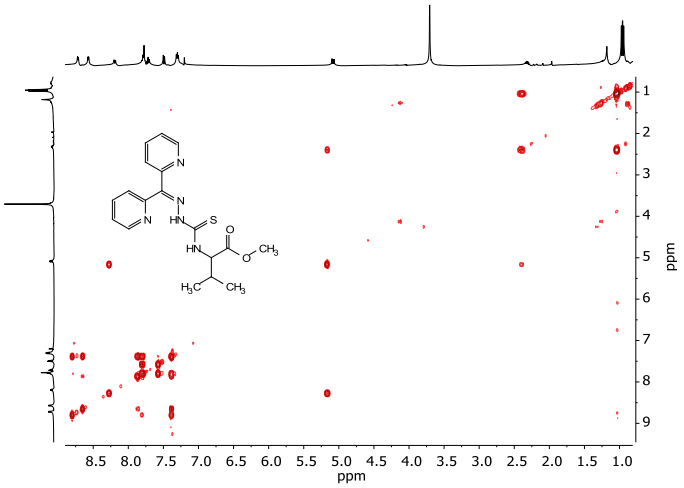


Figure 217. $^{1}H,^{1}H$ COSY NMR spectrum of methyl 2-(2-[bis(pyridin-2-yl)methylidene]hydrazinocarbamthioyl)-3-methylbutanoate in DMSO-d_6 at 499 MHz.

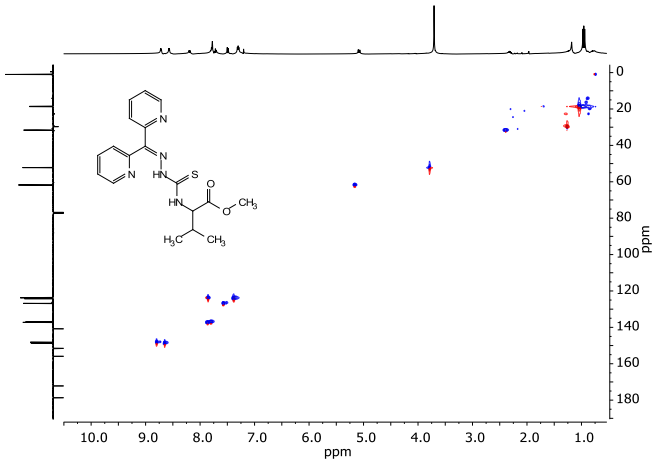


Figure 218. $^{1}H,^{13}C$ HMQC/HSQC NMR spectrum of methyl 2-(2-[bis(pyridin-2-yl)methylidene]hydrazinocarbamthioyl)-3-methylbutanoate in DMSO-d_6 at 499 MHz.

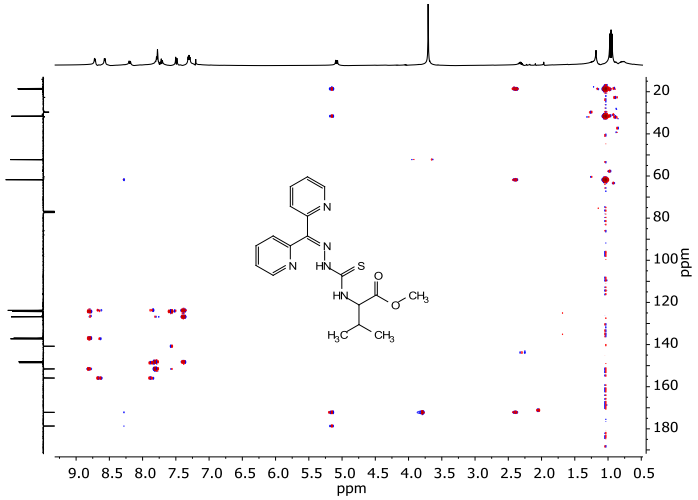


Figure 219. $^{1}H,^{13}C$ HMBC NMR spectrum of methyl 2-(2-[bis(pyridin-2-yl)methylidene]hydrazinocarbamthioyl)-3-methylbutanoate in DMSO-d_6 at 499 MHz.

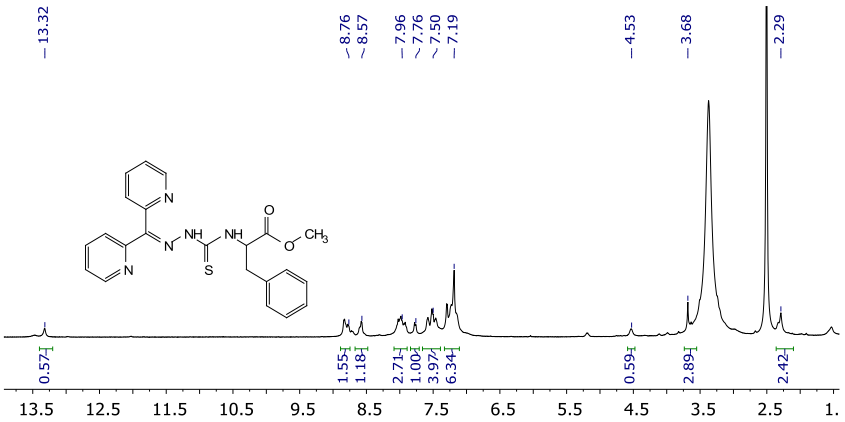


Figure 220. ^{1}H NMR spectrum of methyl 2-(2-[bis(pyridin-2-yl)methylidene]hydrazinocarbamthioyl)-3-phenylpropanoate in DMSO-d_6 at 499 MHz.

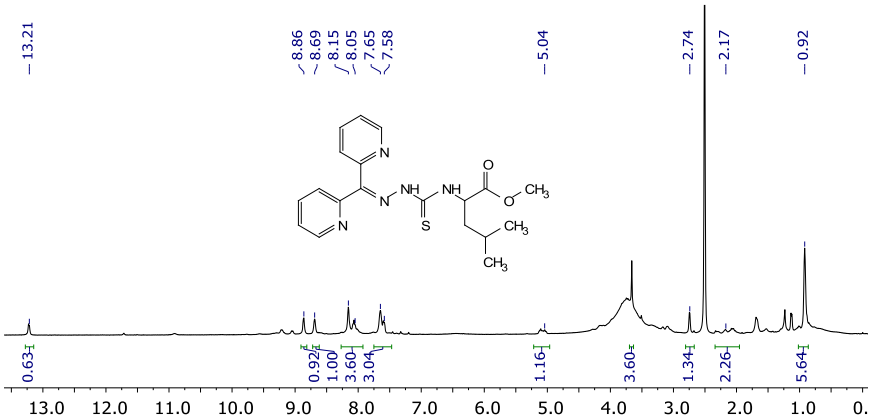


Figure 221. ^{1}H NMR spectrum of methyl 2-(2-[bis(pyridin-2-yl)methylidene]hydrazinocarbamthioyl)-4-methylpentanoate in DMSO-d_6 at 499 MHz.

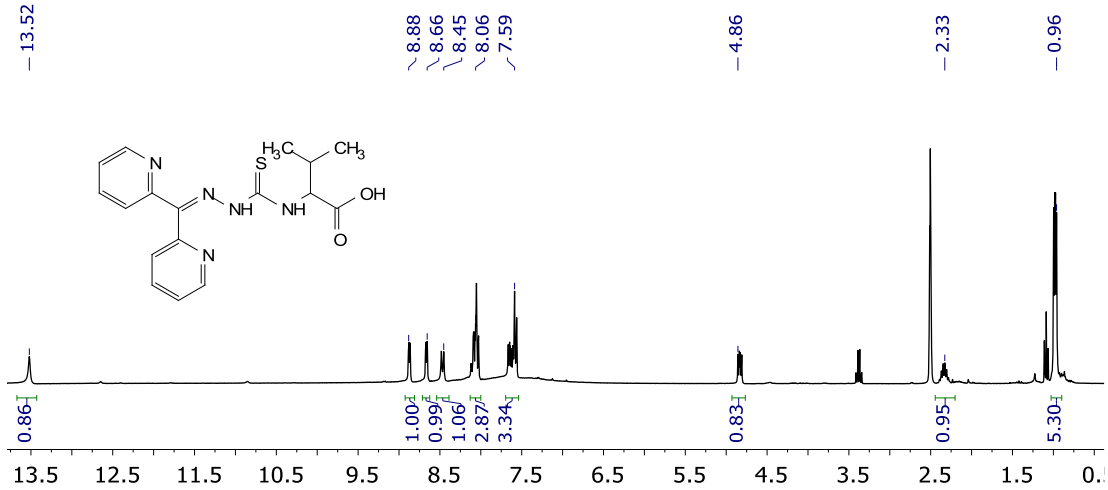


Figure 222. ^{1}H NMR spectrum of 2-(1-[Bis(2-pyridyl)methylene]thiosemicarbazido)-3-methylbutyric acid in DMSO-d_6 at 499 MHz.

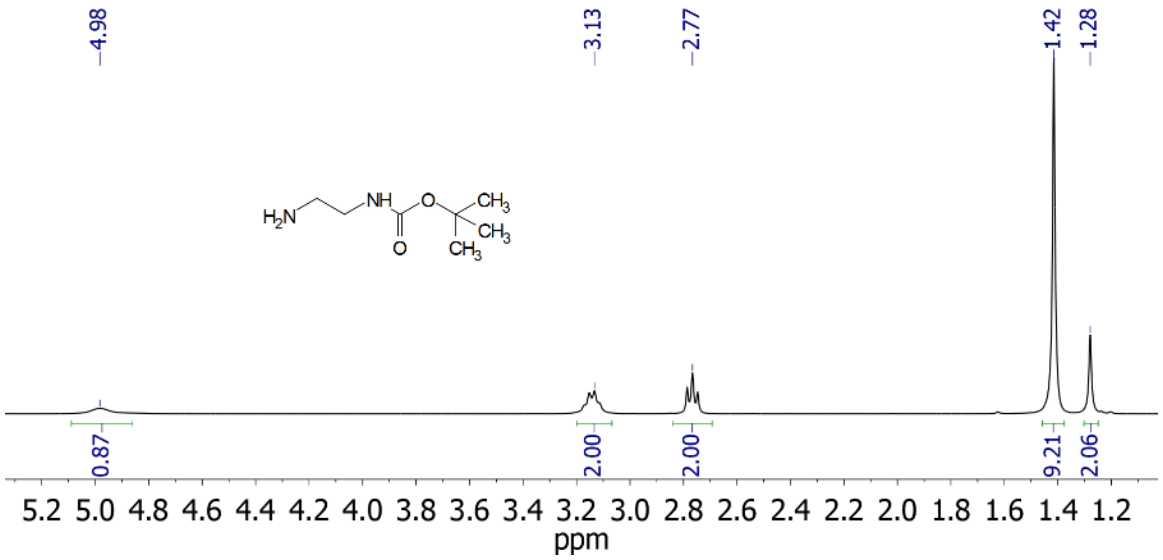


Figure 223. ^{1}H NMR spectrum of *tert*-butyl *N*-(2-aminoethyl)carbamate in $CDCl_3$ at 300 MHz.

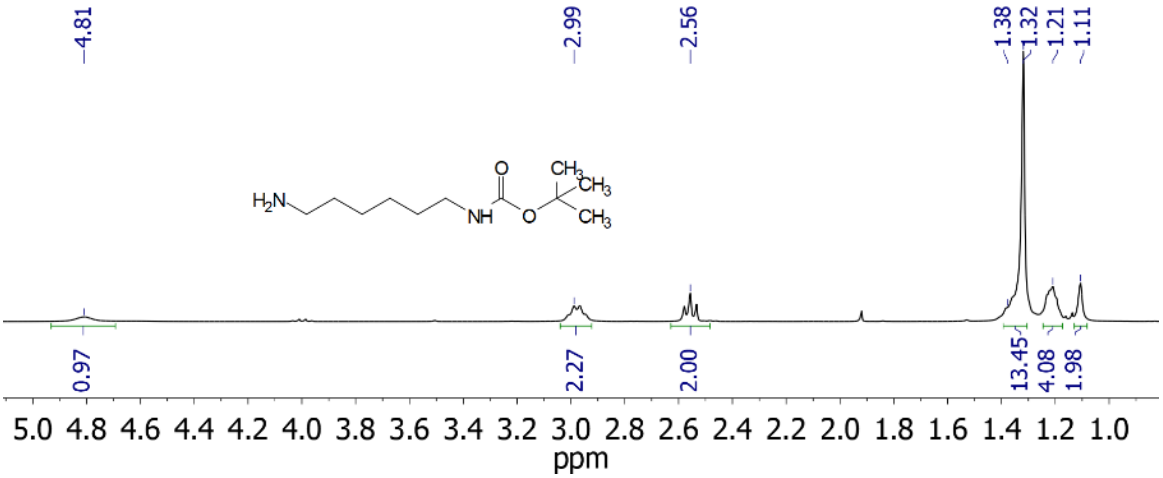


Figure 224. ^{1}H NMR spectrum of *tert*-butyl *N*-(6-aminohexyl)carbamate in $CDCl_3$ at 300 MHz.

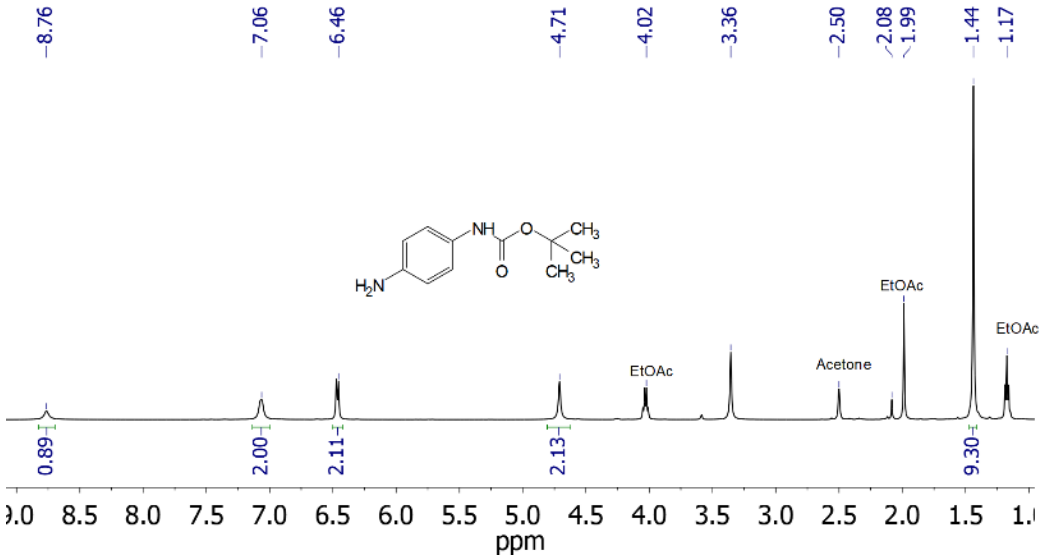


Figure 225. ^{1}H NMR spectrum of *tert*-butyl (4-aminophenyl)carbamate in DMSO-d_6 at 499 MHz.

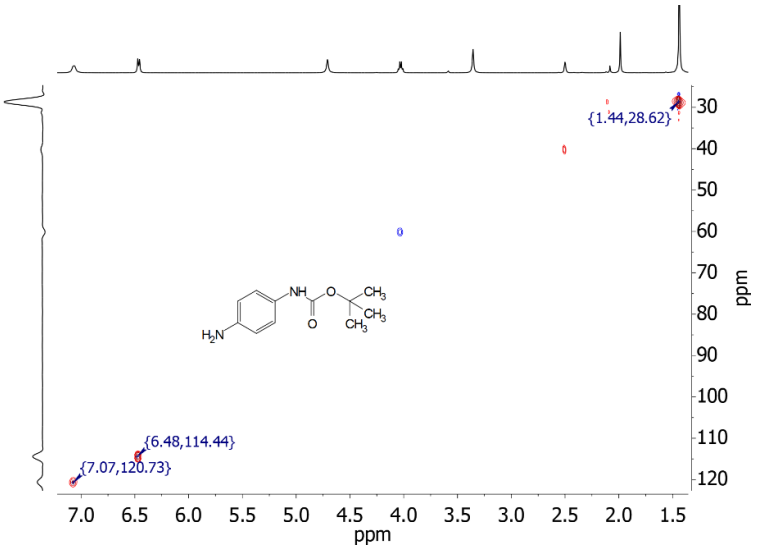


Figure 226. $^{1}H,^{13}C$ HMQC/HSQC NMR spectrum of *tert*-butyl (4-aminophenyl)carbamate in DMSO-d_6 at 499 MHz.

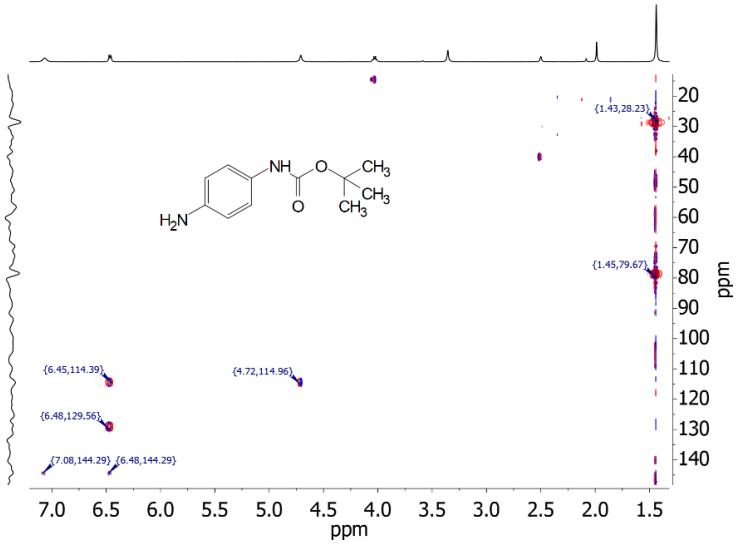


Figure 227. $^{1}H,^{13}C$ HMBC NMR spectrum of *tert*-butyl (4-aminophenyl)carbamate in DMSO-d_6 at 499 MHz.

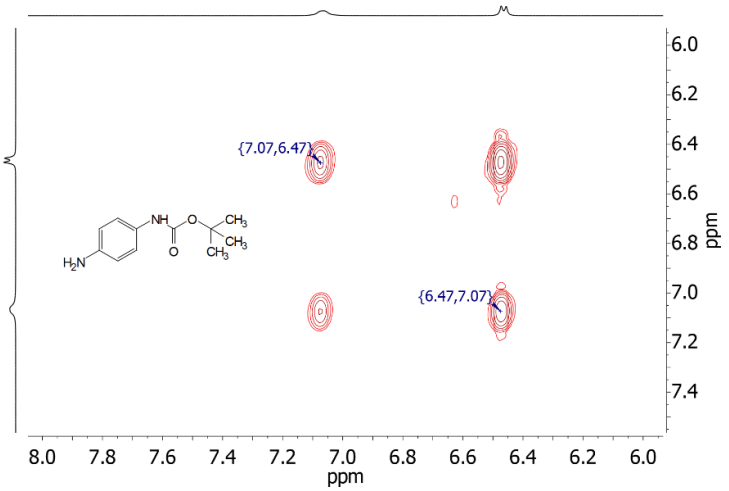


Figure 228. $^{1}H,^{1}H$ COSY NMR spectrum of *tert*-butyl (4-aminophenyl)carbamate in DMSO-d_6 at 499 MHz.

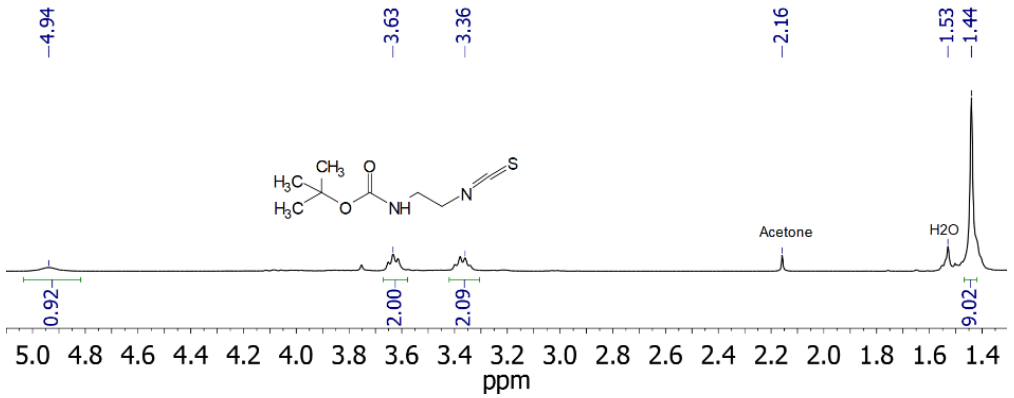


Figure 229. ^{1}H NMR spectrum of *tert*-butyl(2-isothiocyanatoethyl)carbamate in $CDCl_3$ at 300 MHz.

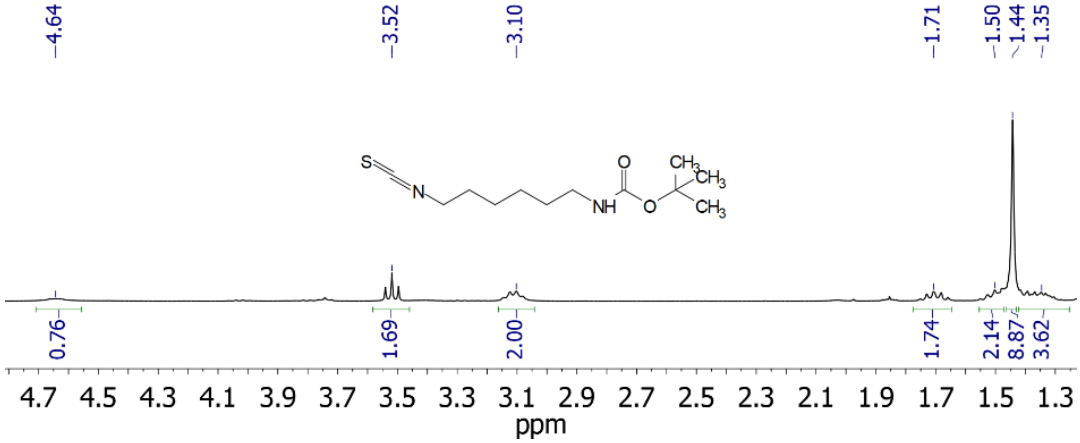


Figure 230. ^{1}H NMR spectrum of *tert*-butyl(6-isothiocyanatohexyl)carbamate in $CDCl_3$ at 300 MHz.

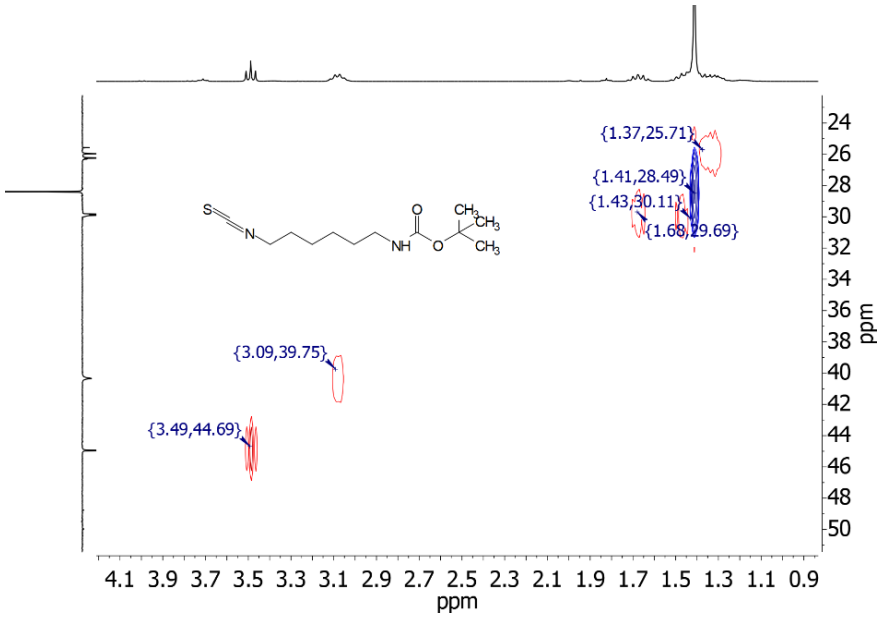


Figure 231. $^{1}H,^{13}C$ HSQC NMR spectrum of *tert*-butyl(6-isothiocyanatohexyl)carbamate in $CDCl_3$ at 300 MHz.

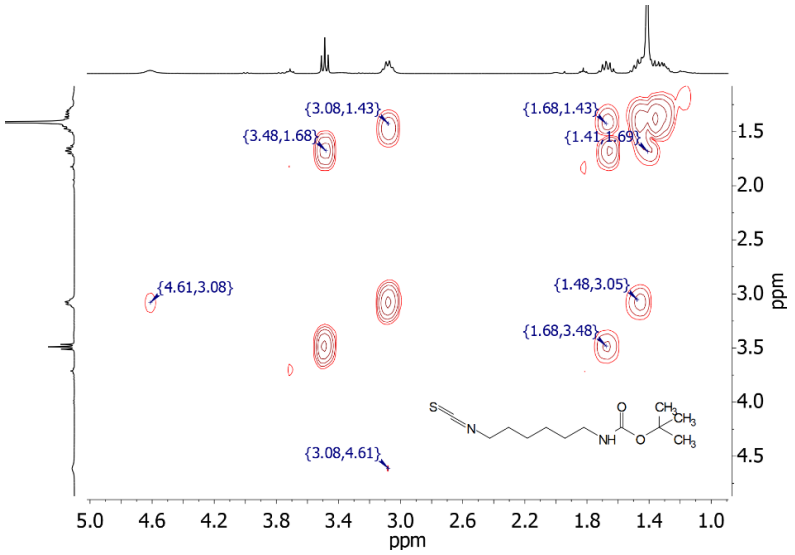


Figure 232. $^{1}H,^{1}H$ COSY NMR spectrum of *tert*-butyl(6-isothiocyanatohexyl)carbamate in $CDCl_3$ at 300 MHz.

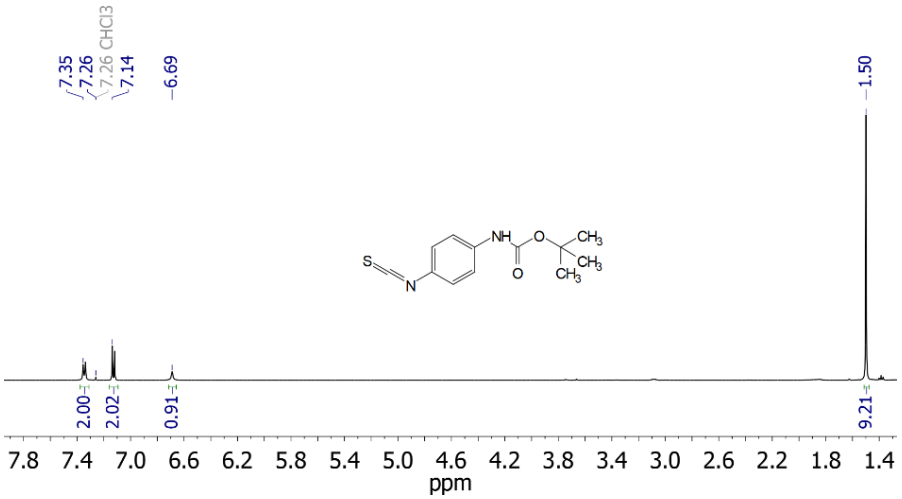


Figure 233. ^{1}H NMR spectrum of *tert*-butyl(4-isothiocyanatophenyl)carbamate in $CDCl_3$ at 499 MHz.

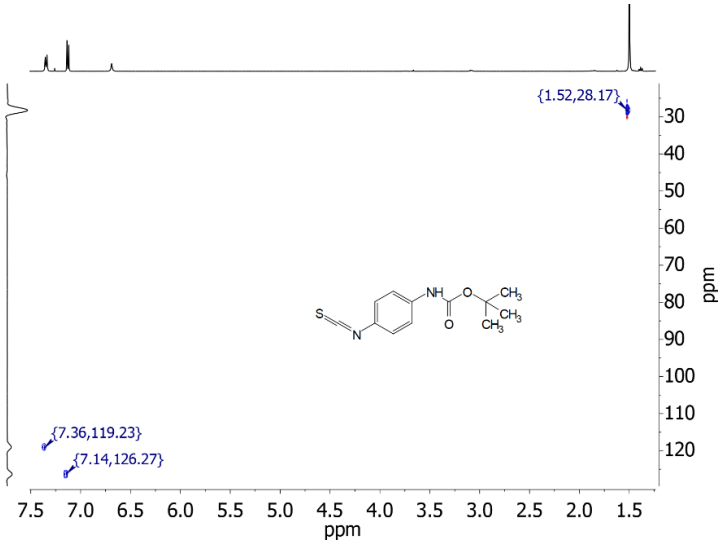


Figure 234. $^{1}H,^{13}C$ HMQC/HSQC NMR spectrum of *tert*-butyl(4-isothiocyanatophenyl)carbamate in $CDCl_3$ at 499 MHz.

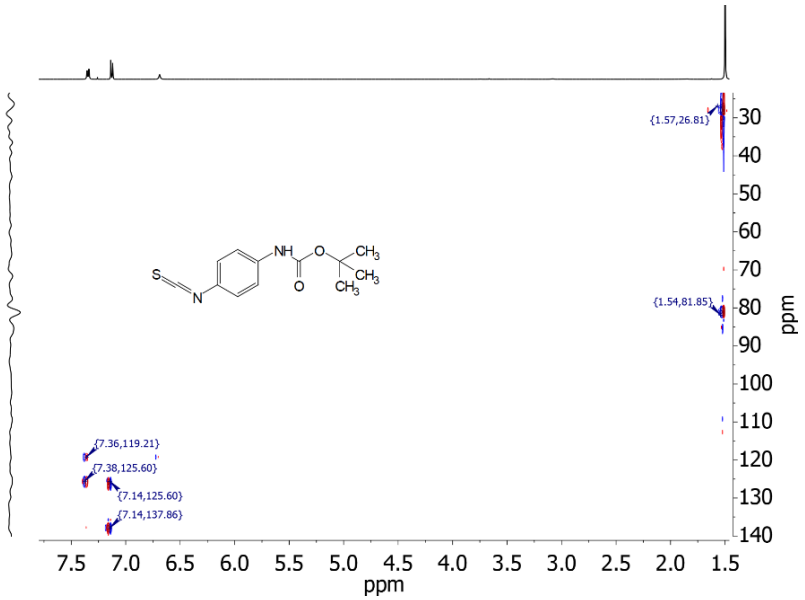


Figure 235. $^{1}H,^{13}C$ HMBC NMR spectrum of *tert*-butyl(4-isothiocyanatophenyl)carbamate in $CDCl_3$ at 499 MHz.

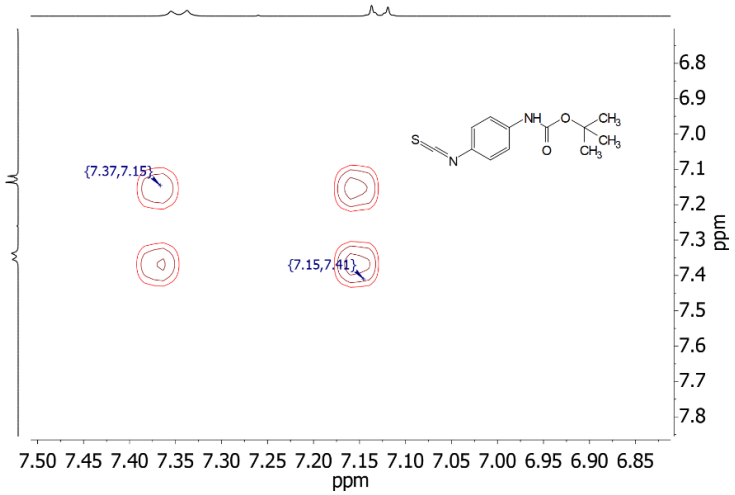


Figure 236. $^{1}H,^{1}H$ COSY NMR spectrum of *tert*-butyl(4-isothiocyanatophenyl)carbamate in $CDCl_3$ at 499 MHz.

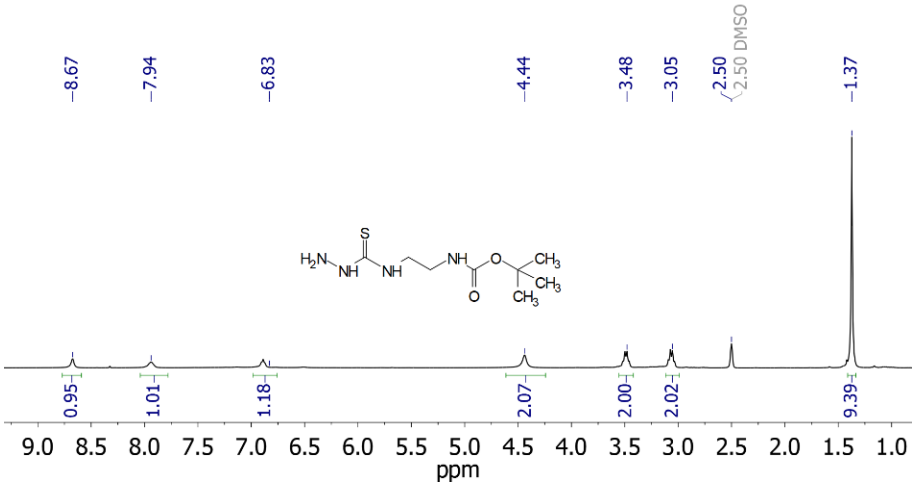


Figure 237. ^{1}H NMR spectrum of 4-(2-*tert*-butoxycarbonylamino-ethyl)thiosemicarbazide in DMSO-d_6 at 300 MHz.

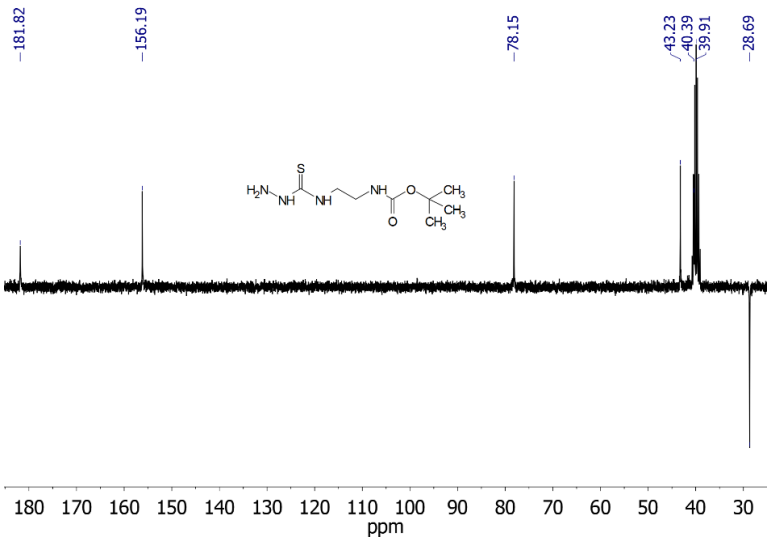


Figure 238. ^{13}C DEPTQ NMR spectrum of 4-(2-*tert*-butoxycarbonylamino-ethyl)thiosemicarbazide in DMSO-d_6 at 300 MHz.

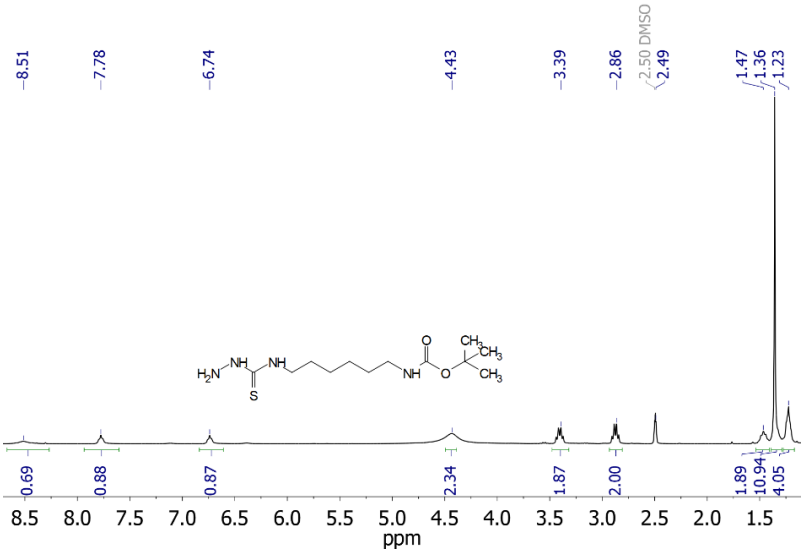


Figure 239. ^{1}H NMR spectrum of 4-(6-*tert*-butoxycarbonylamino-hexyl)thiosemicarbazide in DMSO-d_6 at 300 MHz.

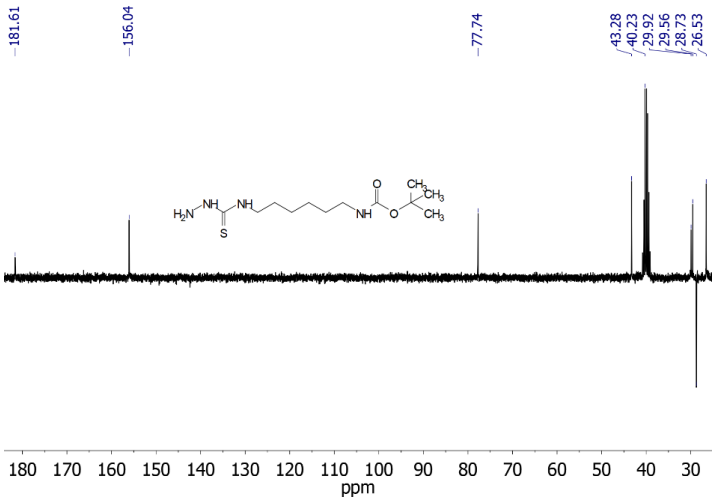


Figure 240. ^{13}C DEPTQ NMR spectrum of 4-(6-*tert*-butoxycarbonylamino-hexyl)thiosemicarbazide in DMSO-d_6 at 300 MHz.

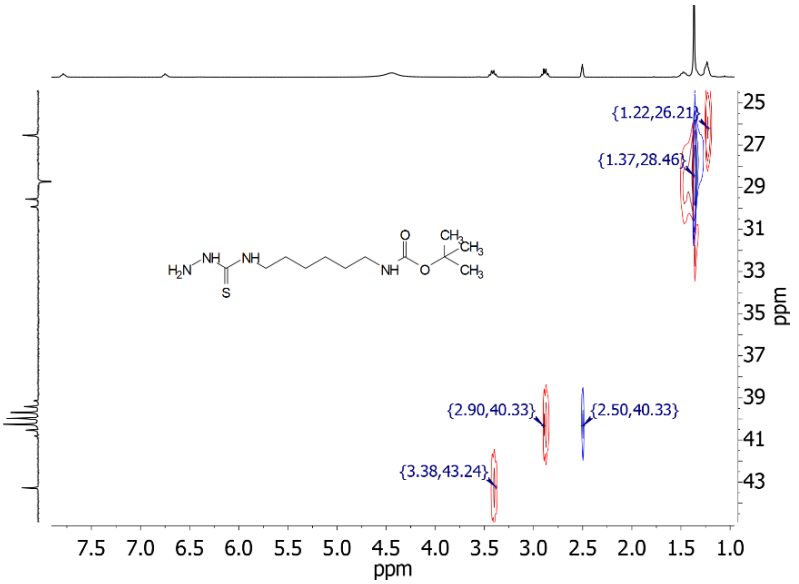


Figure 241. $^{1}H,^{13}C$ HSQC NMR spectrum of 4-(6-*tert*-butoxycarbonylamino-hexyl)thiosemicarbazide in DMSO-d_6 at 300 MHz.

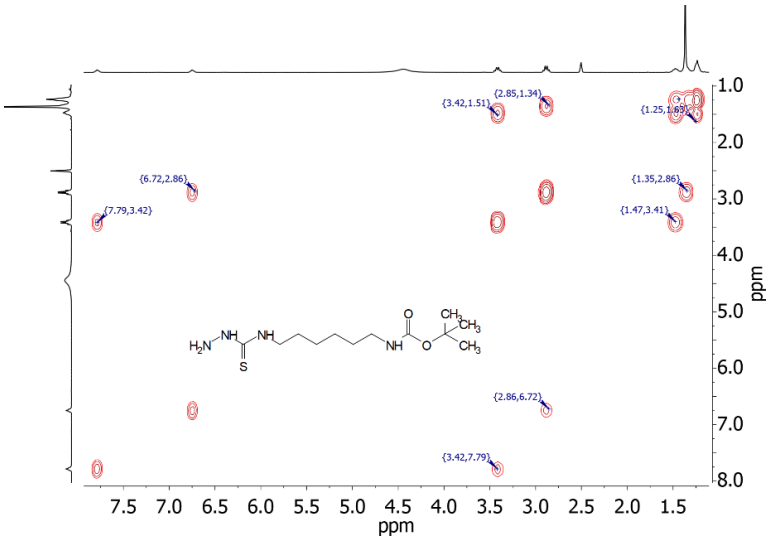


Figure 242. $^{1}H,^{1}H$ COSY NMR spectrum of 4-(6-*tert*-butoxycarbonylamino-hexyl)thiosemicarbazide in DMSO-d_6 at 300 MHz.

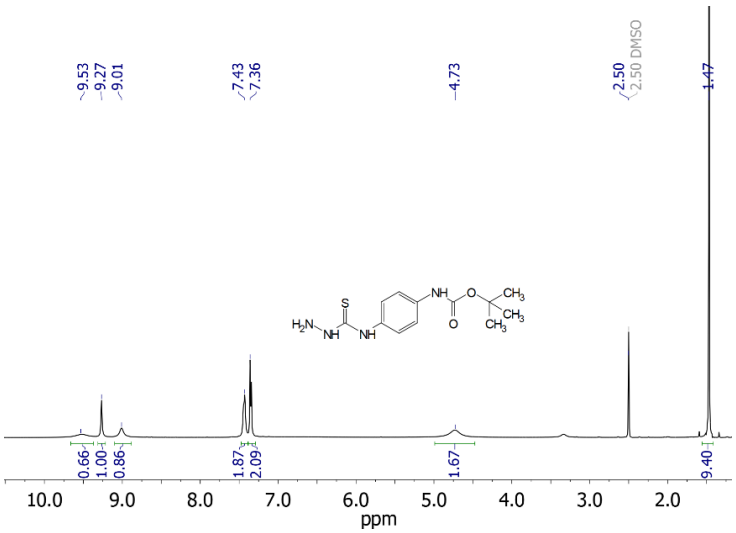


Figure 243. ^{1}H NMR spectrum of 4-(4-*tert*-butoxycarbonylamino-phenyl)thiosemicarbazide in DMSO-d_6 at 499 MHz.

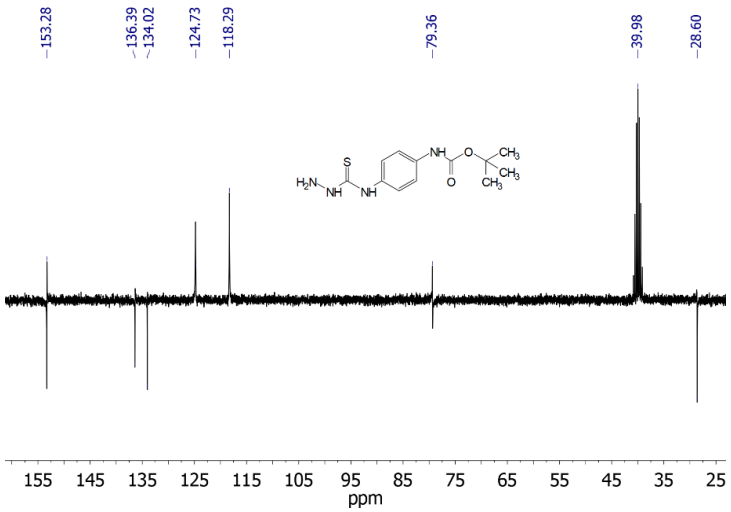


Figure 244. ^{13}C DEPTQ NMR spectrum of 4-(4-*tert*-butoxycarbonylamino-phenyl)thiosemicarbazide in DMSO-d_6 at 300 MHz.

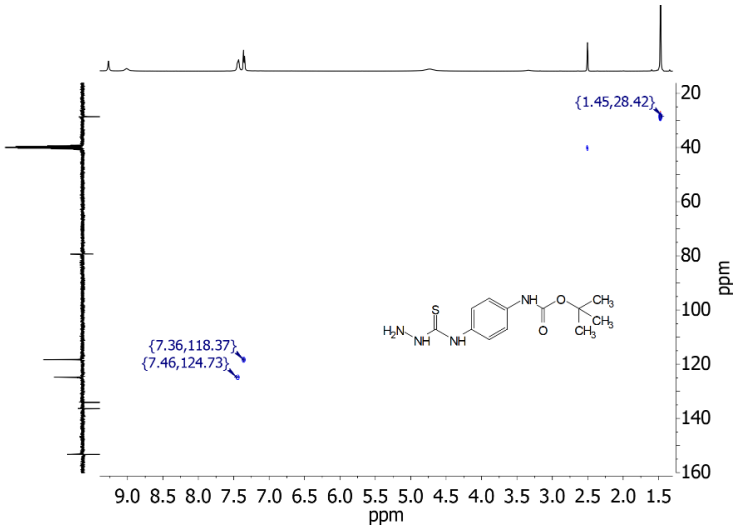


Figure 245. ^{1}H,^{13}C HMQC/HSQC NMR spectrum of 4-(4-*tert*-butoxycarbonylamino-phenyl) thiosemicarbazide in DMSO-d_6 at 499 MHz.

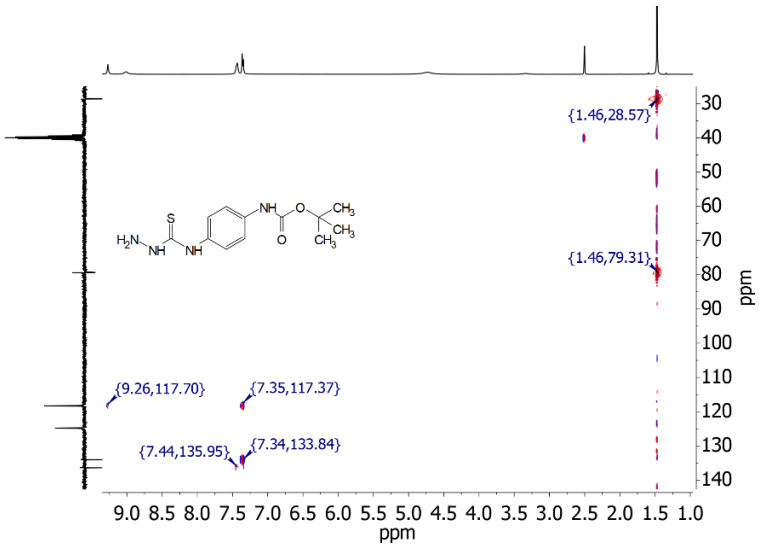


Figure 246. ^{1}H,^{13}C HMBC NMR spectrum of 4-(4-*tert*-butoxycarbonylamino-phenyl)thiosemi-carbazide in DMSO-d_6 at 499 MHz.

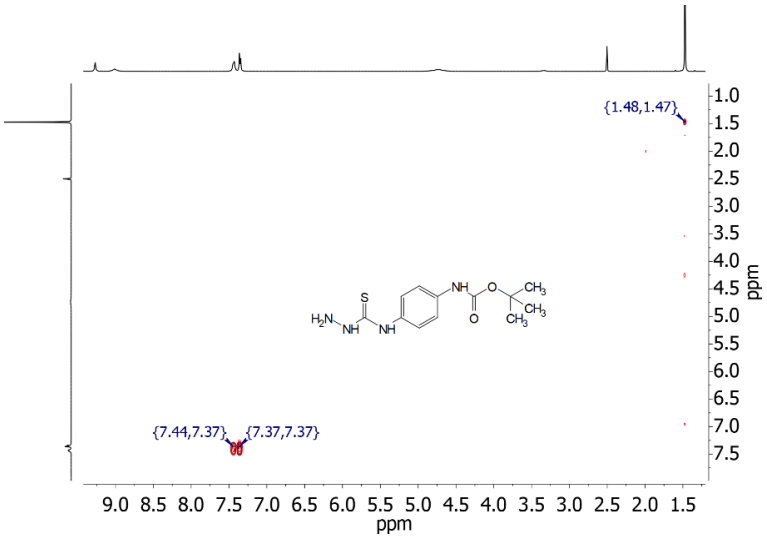


Figure 247. $^{1}H,^{1}H$ COSY NMR spectrum of 4-(4-*tert*-butoxycarbonylamino-phenyl)thiosemicarbazide in DMSO-d_6 at 499 MHz.

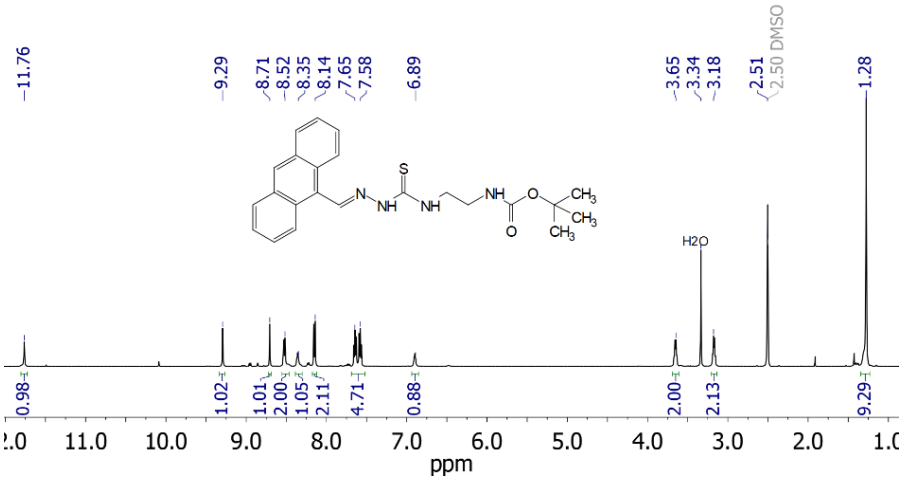


Figure 248. ^{1}H NMR spectrum of 9-anthraldehyde-4-(2-*tert*-butoxycarbonylamino-ethyl)-3-thiosemicarbazone in DMSO-d_6 at 499 MHz.

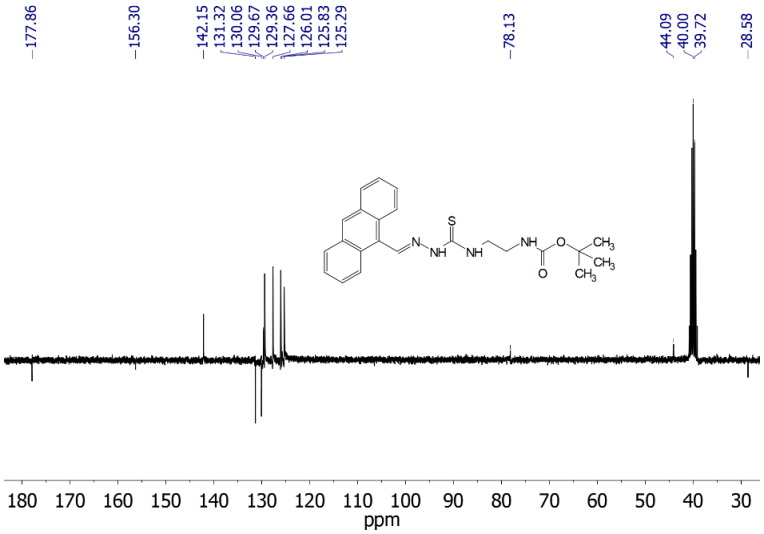


Figure 249. ^{13}C DEPTQ NMR spectrum of 9-anthraldehyde-4-(2-*tert*-butoxycarbonylamino-ethyl)-3-thiosemicarbazone in DMSO-d_6 at 300 MHz.

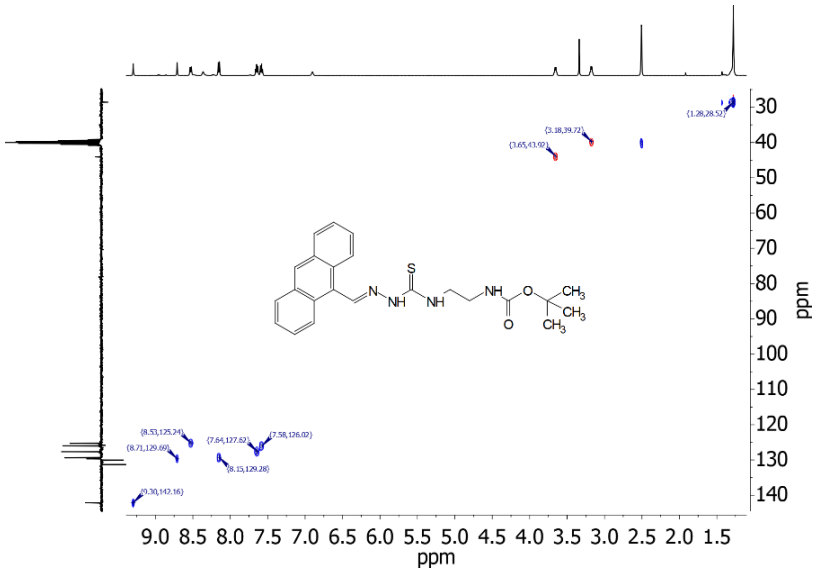


Figure 250. $^{1}H,^{13}C$ HMQC/HSQC NMR spectrum of 9-anthraldehyde-4-(2-*tert*-butoxycarbonylamino-ethyl)-3-thiosemicarbazone in DMSO-d_6 at 499 MHz.

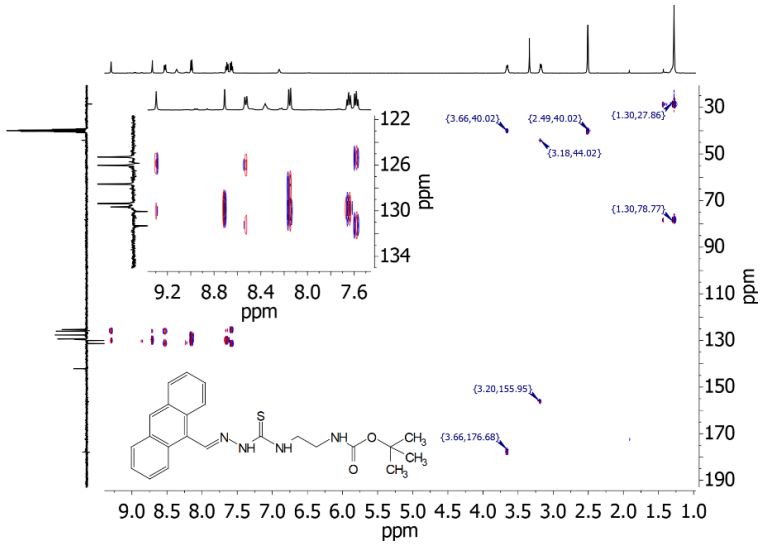


Figure 251. $^{1}H,^{13}C$ HMBC NMR spectrum of 9-anthraldehyde-4-(2-*tert*-butoxycarbonylamino-ethyl)-3-thiosemicarbazone in DMSO-d_6 at 499 MHz.

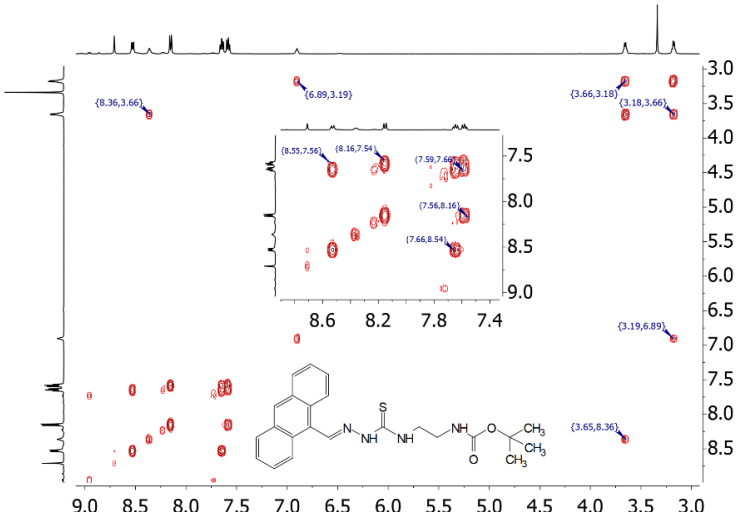


Figure 252. $^{1}H,^{1}H$ COSY NMR spectrum of 9-anthraldehyde-4-(2-*tert*-butoxycarbonylamino-ethyl)-3-thiosemicarbazone in DMSO-d_6 at 499 MHz.

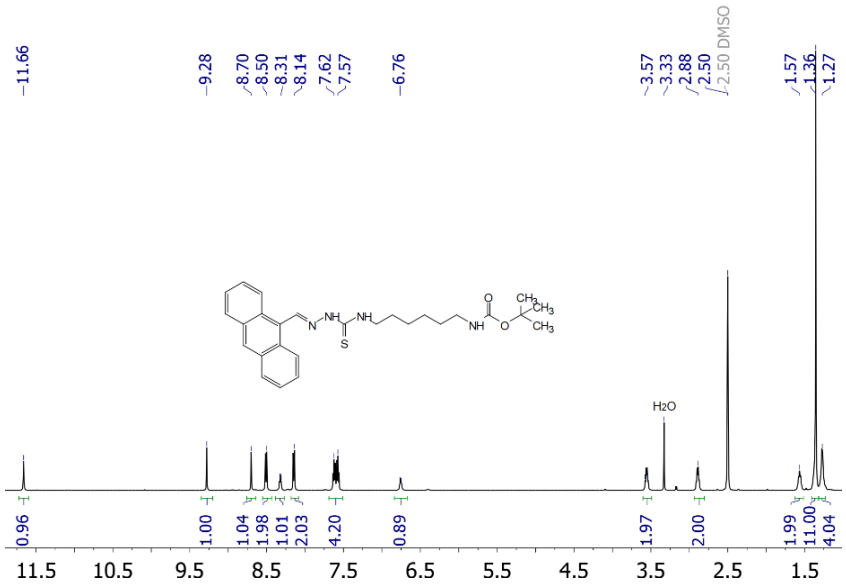


Figure 253. ^{1}H NMR spectrum of 9-anthraldehyde-4-(6-*tert*-butoxycarbonylamino-hexyl)-3-thiosemicarbazone DMSO-d_6 at 499 MHz.

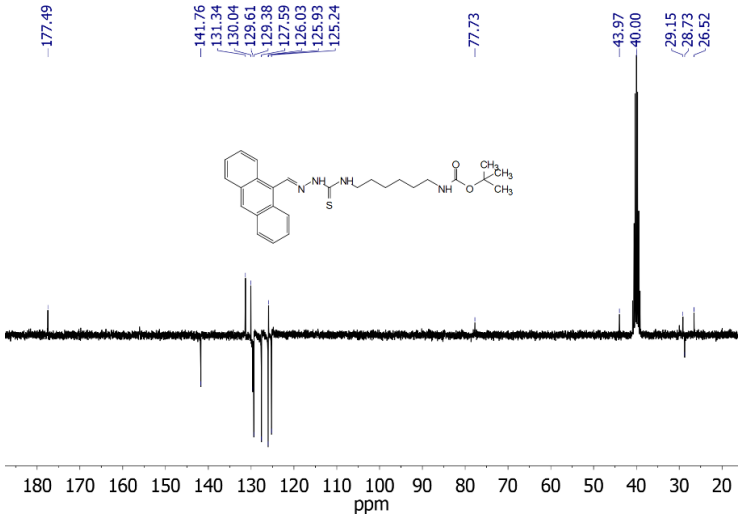


Figure 254. ^{13}C DEPTQ NMR spectrum of 9-anthraldehyde-4-(6-*tert*-butoxycarbonylamino-hexyl)-3-thiosemicarbazone in DMSO-d_6 at 300 MHz.

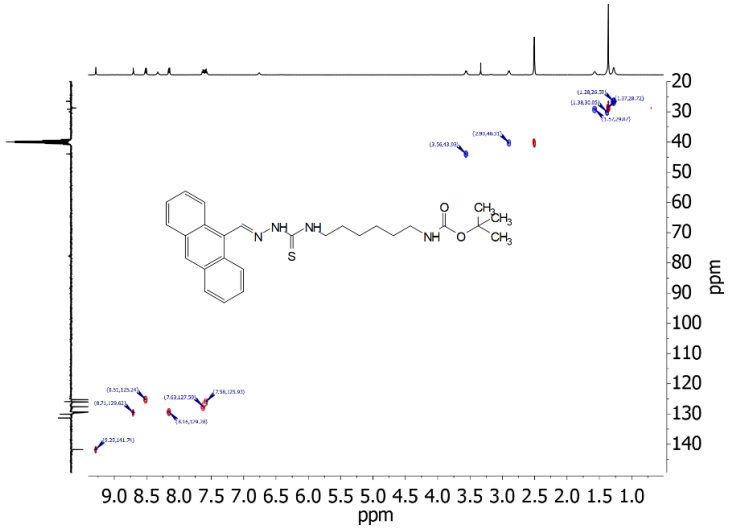


Figure 255. ^{1}H,^{13}C HMQC/HSQC NMR spectrum of 9-anthraldehyde-4-(6-*tert*-butoxycarbonylamino-hexyl)-3-thiosemicarbazone in DMSO-d_6 at 499 MHz.

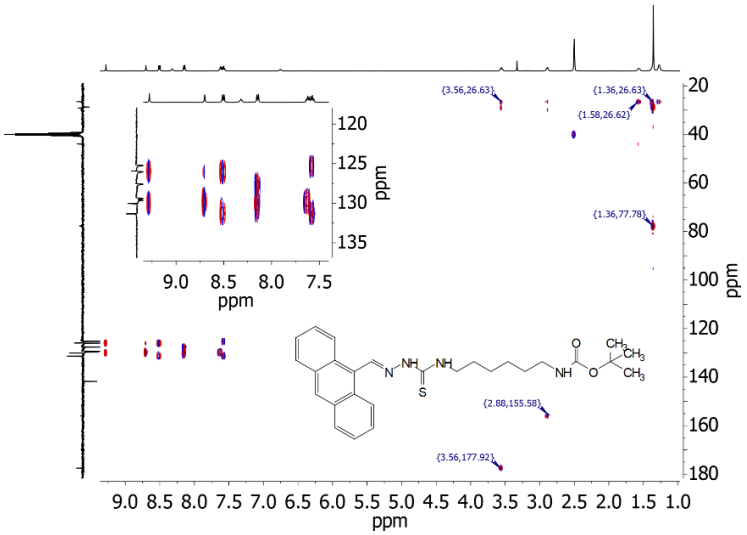


Figure 256. $^{1}H,^{13}C$ HMBC NMR spectrum of 9-anthraldehyde-4-(6-*tert*-butoxycarbonylamino-hexyl)-3-thiosemicarbazone in DMSO-d_6 at 499 MHz.

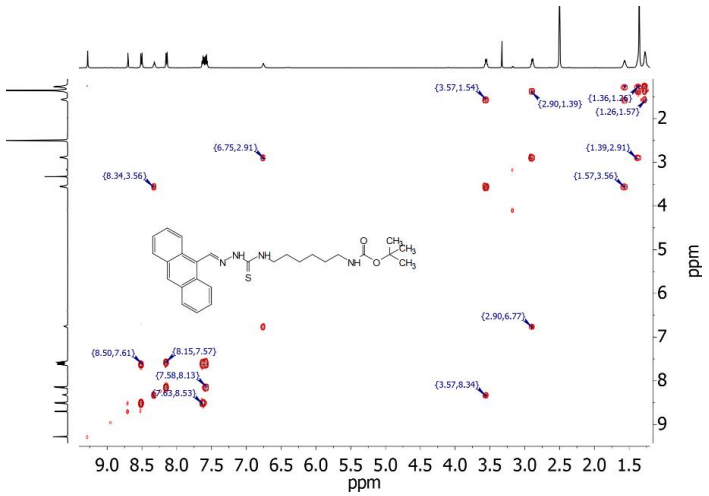


Figure 257. $^{1}H,^{1}H$ COSY NMR spectrum of 9-anthraldehyde-4-(6-*tert*-butoxycarbonylamino-hexyl)-3-thiosemicarbazone in DMSO-d_6 at 499 MHz.

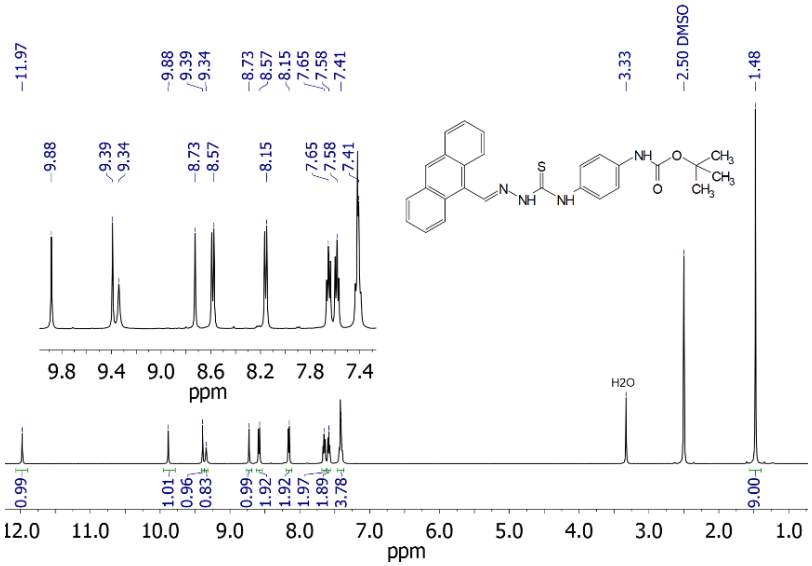


Figure 258. ^{1}H NMR spectrum of 9-anthraldehyde-4-(4-*tert*-butoxycarbonylamino-phenyl)-3-thiosemicarbazone in DMSO-d_6 at 499 MHz.

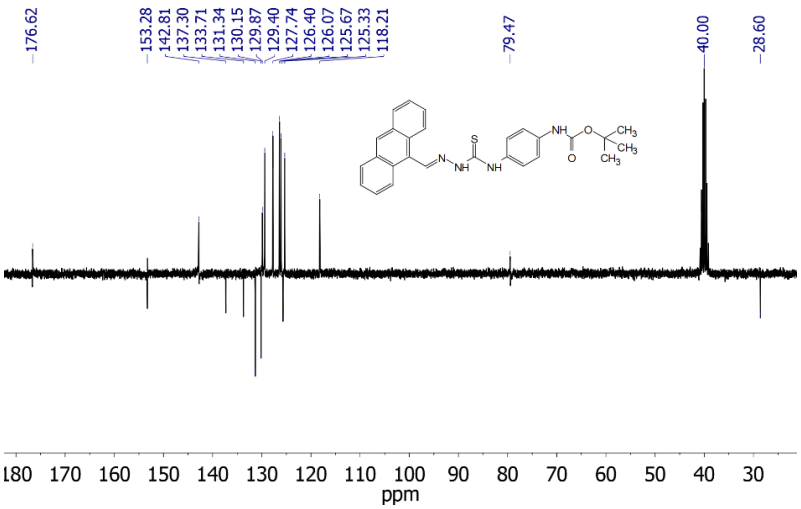


Figure 259. ^{13}C DEPTQ NMR spectrum of 9-anthraldehyde-4-(4-*tert*-butoxycarbonylamino-phenyl)-3-thiosemicarbazone in DMSO-d_6 at 300 MHz.

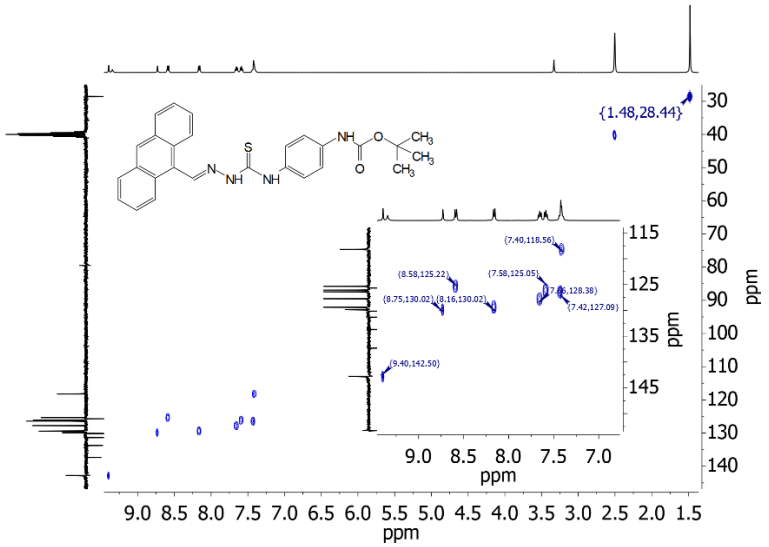


Figure 260. $^{1}H,^{13}C$ HMQC/HSQC NMR spectrum of 9-anthraldehyde-4-(4-*tert*-butoxycarbonylamino-phenyl)-3-thiosemicarbazone in DMSO-d_6 at 499 MHz.

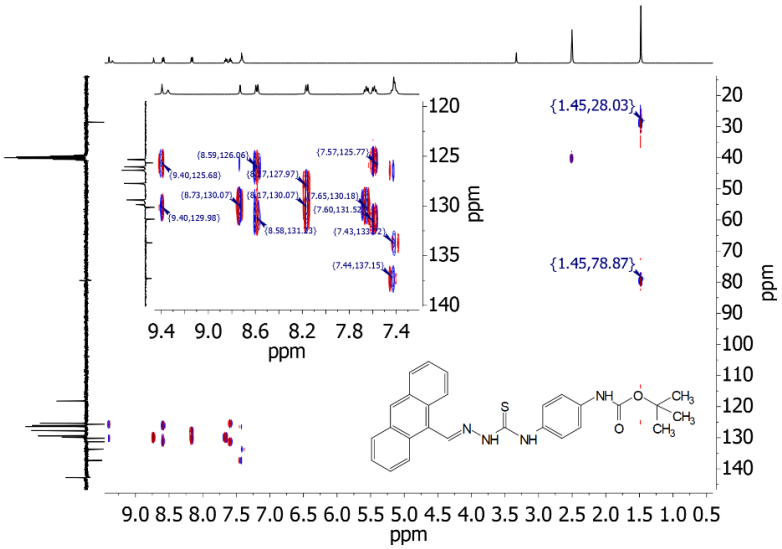


Figure 261. $^{1}H,^{13}C$ HMBC NMR spectrum of 9-anthraldehyde-4-(4-*tert*-butoxycarbonylamino-phenyl)-3-thiosemicarbazone in DMSO-d_6 at 499 MHz.

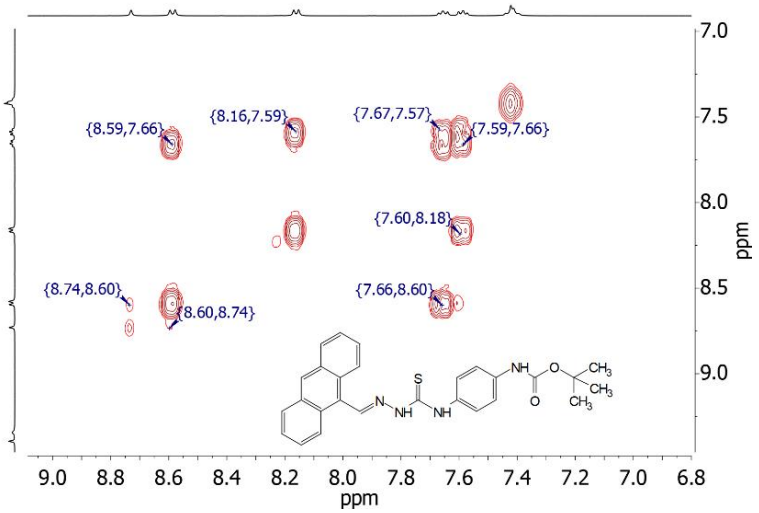


Figure 262. $^{1}H,^{1}H$ COSY NMR spectrum of 9-anthraldehyde-4-(4-*tert*-butoxycarbonylamino-phenyl)-3-thiosemicarbazone in DMSO-d_6 at 499 MHz.

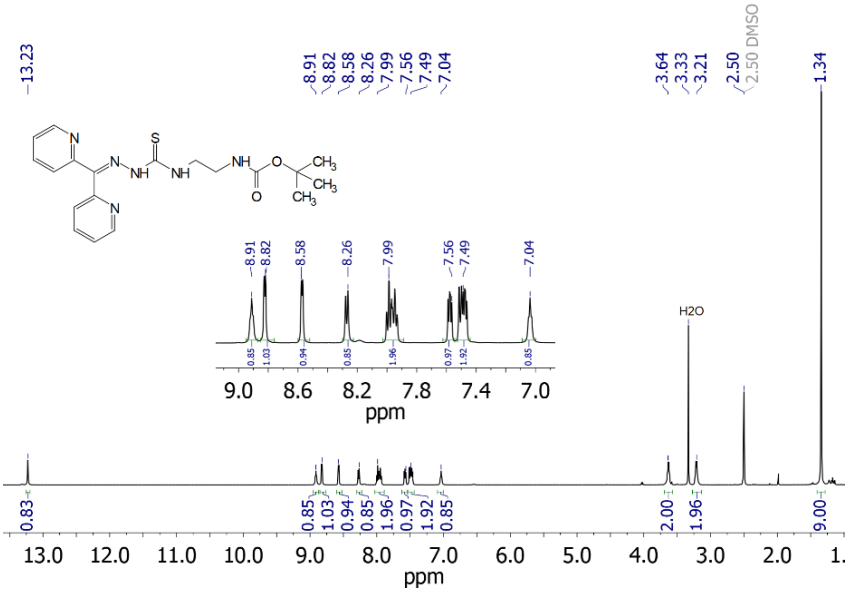


Figure 263. ^{1}H NMR spectrum of di-2-pyridylketone-4-(2-*tert*-butoxycarbonylamino-ethyl)-3-thiosemicarbazone in DMSO-d_6 at 499 MHz.

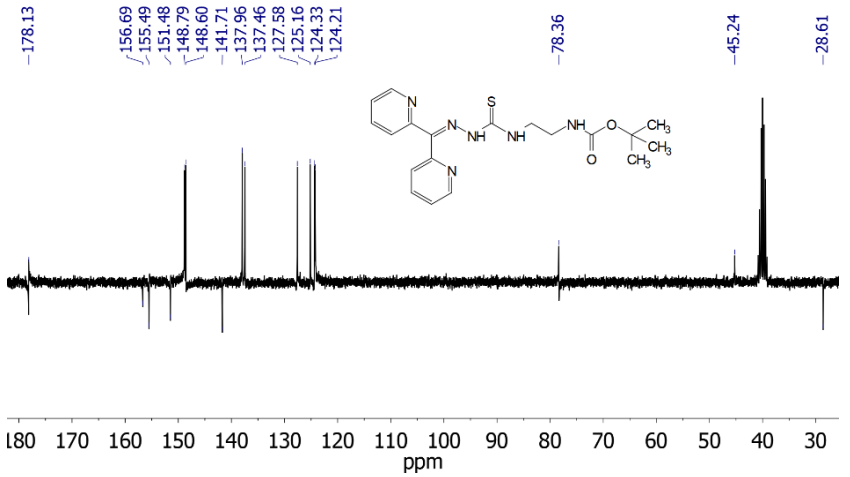


Figure 264. ^{13}C DEPTQ NMR spectrum of di-2-pyridylketone-4-(2-*tert*-butoxycarbonylamino-ethyl)-3-thiosemicarbazone in DMSO-d_6 at 300 MHz.

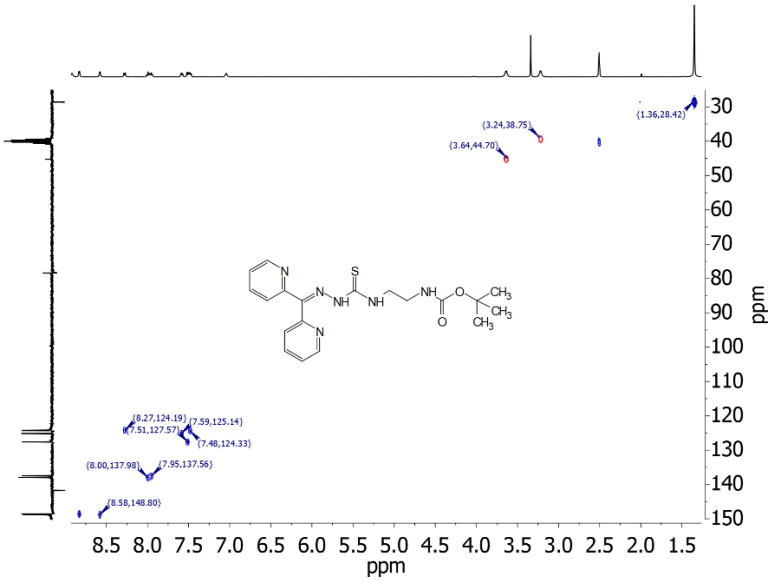


Figure 265. $^{1}H,^{13}C$ HMQC/HSQC NMR spectrum of di-2-pyridylketone-4-(2-*tert*-butoxycarbonyl-amino-ethyl)-3-thiosemicarbazone in DMSO-d_6 at 499 MHz.

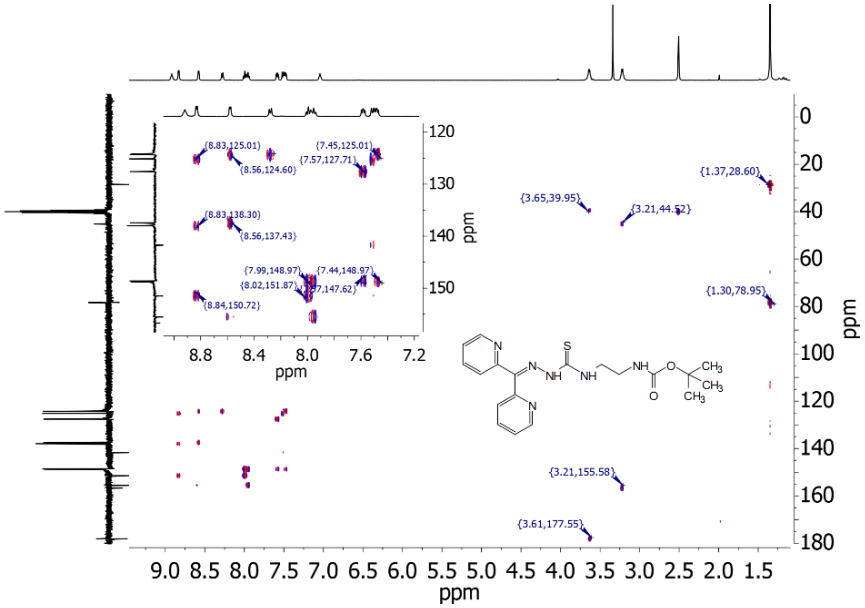


Figure 266. $^{1}H,^{13}C$ HMBC NMR spectrum of di-2-pyridylketone-4-(2-*tert*-butoxycarbonylamino-ethyl)-3-thiosemicarbazone in DMSO-d_6 at 499 MHz.

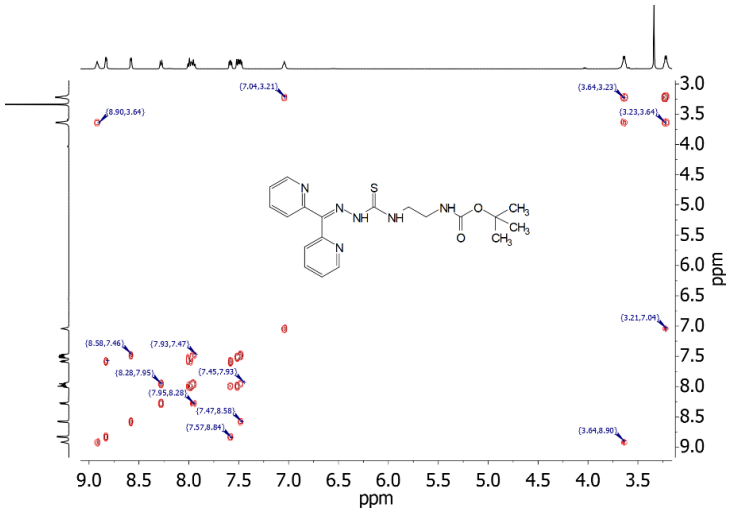


Figure 267. $^{1}H,^{1}H$ COSY NMR spectrum of di-2-pyridylketone-4-(2-*tert*-butoxycarbonylamino-ethyl)-3-thiosemicarbazone in DMSO-d_6 at 499 MHz.

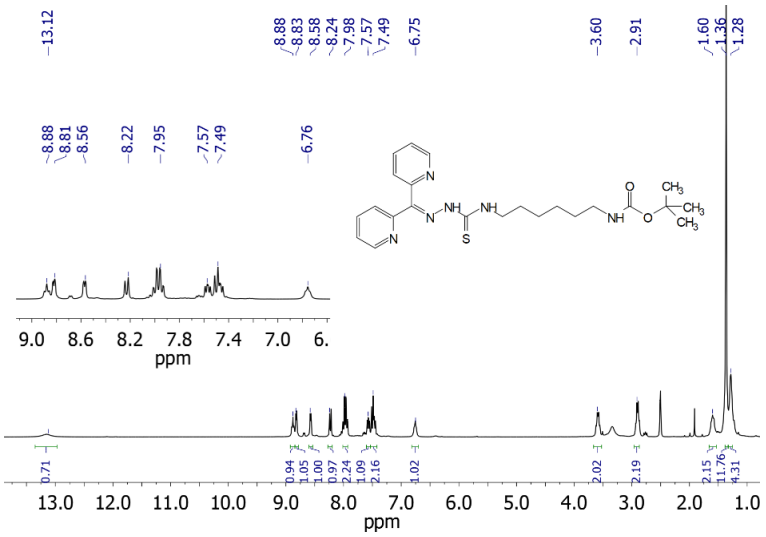


Figure 268. ^{1}H NMR spectrum of di-2-pyridylketone-4-(6-*tert*-butoxycarbonylamino-hexyl)-3-thiosemicarbazone in DMSO-d_6 at 499 MHz.

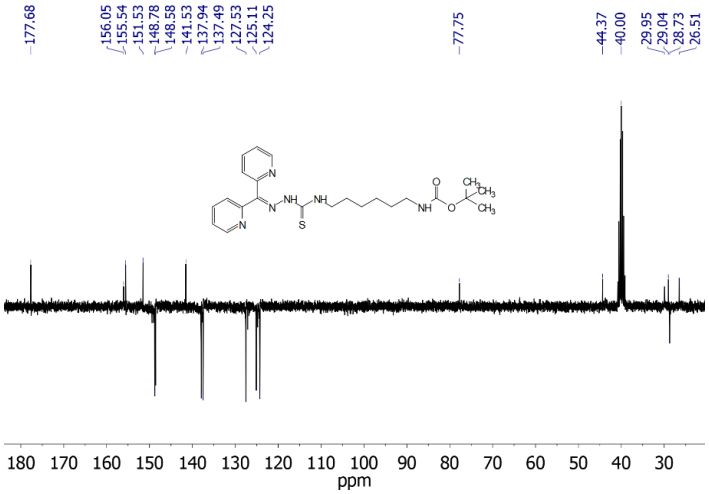


Figure 269. ^{13}C DEPTQ NMR spectrum of di-2-pyridylketone-4-(6-*tert*-butoxycarbonylamino-hexyl)-3-thiosemicarbazone in DMSO-d_6 at 300 MHz.

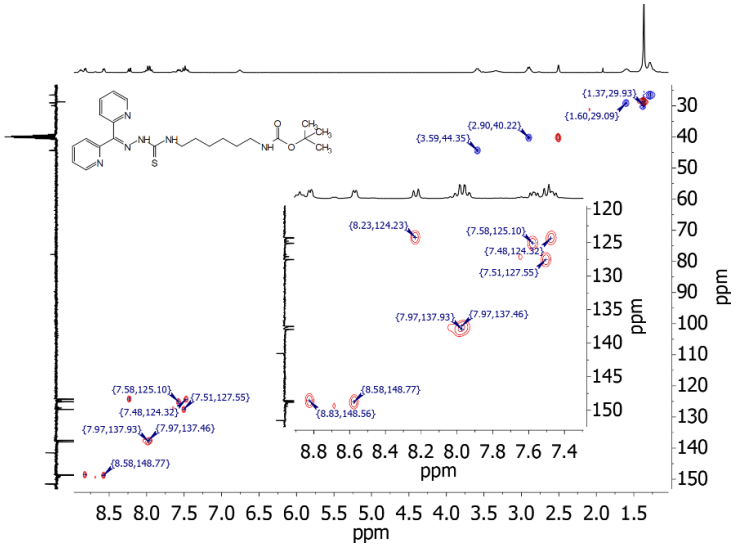


Figure 270. ^{1}H,^{13}C HMQC/HSQC NMR spectrum of di-2-pyridylketone-4-(6-*tert*-butoxycarbonyl-amino-hexyl)-3-thiosemicarbazone in DMSO-d_6 at 499 MHz.

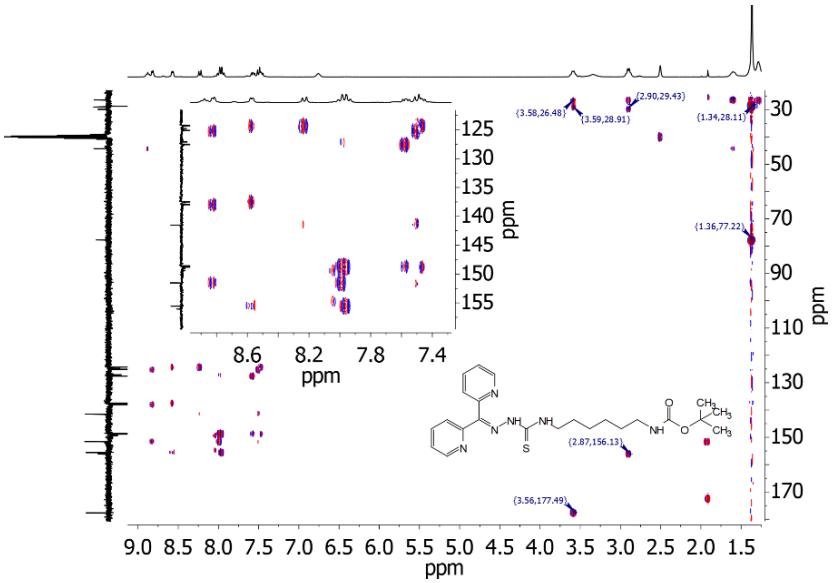


Figure 271. $^{1}H,^{13}C$ HMBC NMR spectrum of di-2-pyridylketone-4-(6-*tert*-butoxycarbonylamino-hexyl)-3-thiosemicarbazone in DMSO-d_6 at 499 MHz.

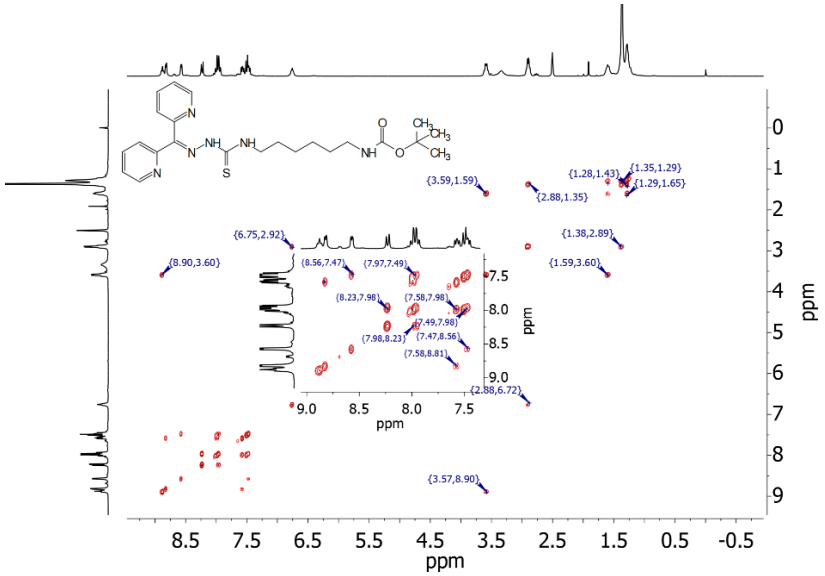


Figure 272. $^{1}H,^{1}H$ COSY NMR spectrum of di-2-pyridylketone-4-(6-*tert*-butoxycarbonylamino-hexyl)-3-thiosemicarbazone in DMSO-d_6 at 499 MHz.

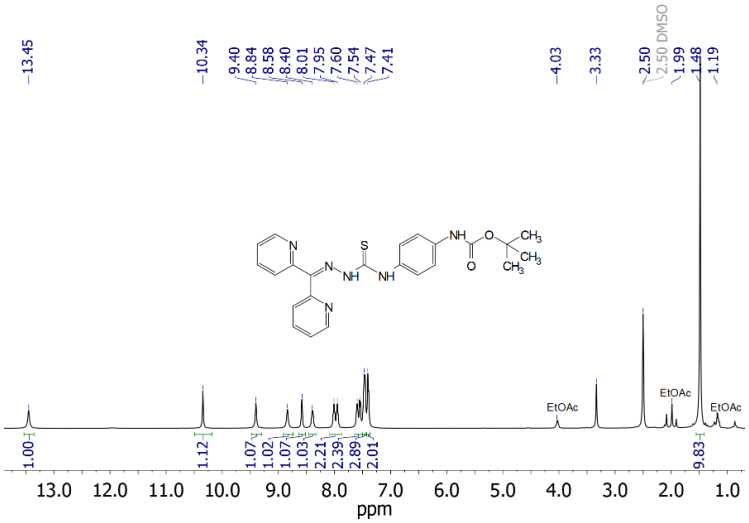


Figure 273. ^{1}H NMR spectrum of di-2-pyridylketone-4-(4-*tert*-butoxycarbonylamino-phenyl)-3-thiosemicarbazone in DMSO-d_6 at 499 MHz.

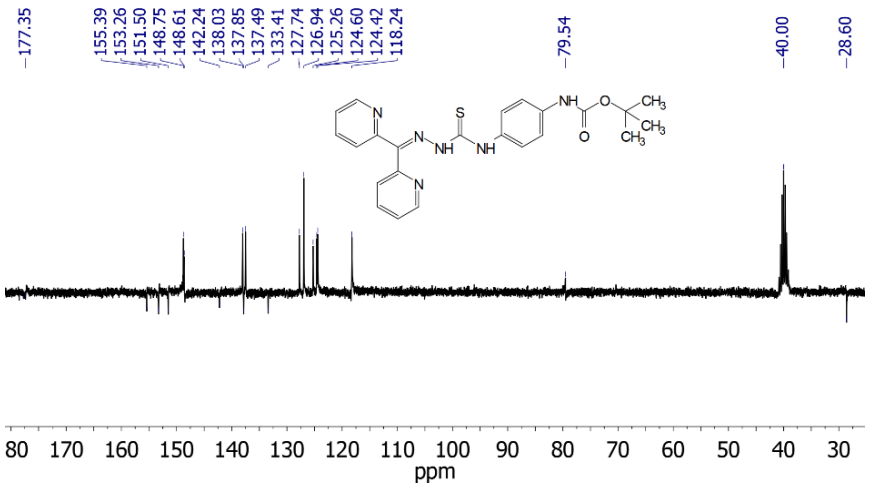


Figure 274. ^{13}C DEPTQ NMR spectrum of di-2-pyridylketone-4-(4-*tert*-butoxycarbonylamino-phenyl)-3-thiosemicarbazone in DMSO-d_6 at 300 MHz.

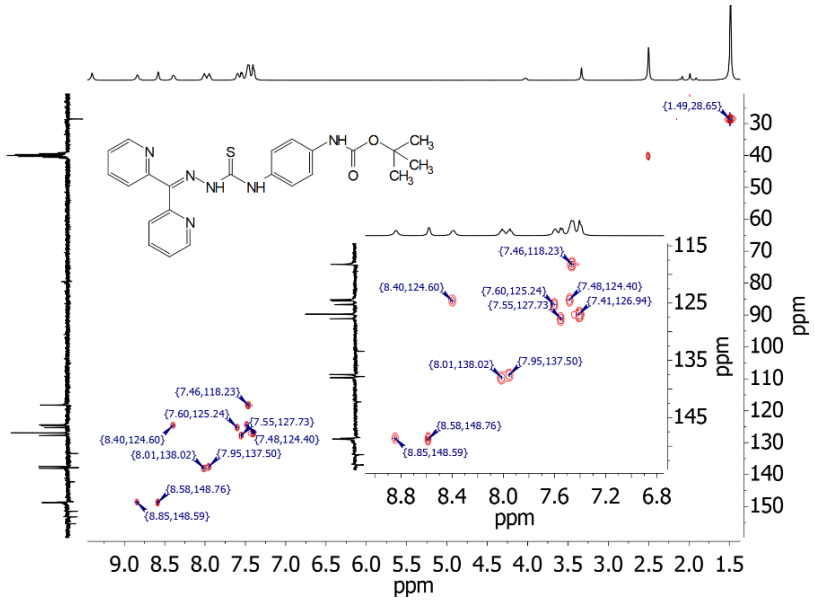


Figure 275. $^{1}H,^{13}C$ HMQC/HSQC NMR spectrum of di-2-pyridylketone-4-(4-*tert*-butoxycarbonyl-amino-phenyl)-3-thiosemicarbazone in DMSO-d_6 at 499 MHz.

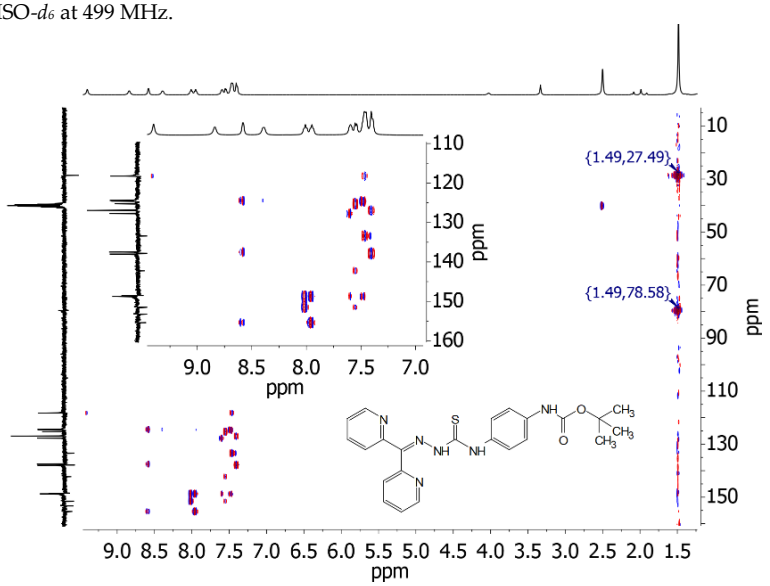


Figure 276. $^{1}H,^{13}C$ HMBC NMR spectrum of di-2-pyridylketone-4-(4-*tert*-butoxycarbonylamino-phenyl)-3-thiosemicarbazone in DMSO-d_6 at 499 MHz.

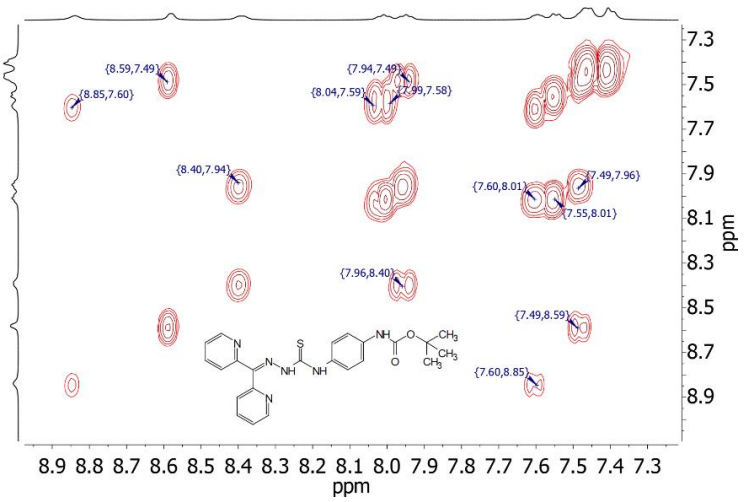


Figure 277. $^{1}H,^{1}H$ COSY NMR spectrum of di-2-pyridylketone-4-(4-*tert*-butoxycarbonylamino-phenyl)-3-thiosemicarbazone DMSO-d_6 at 499 MHz.

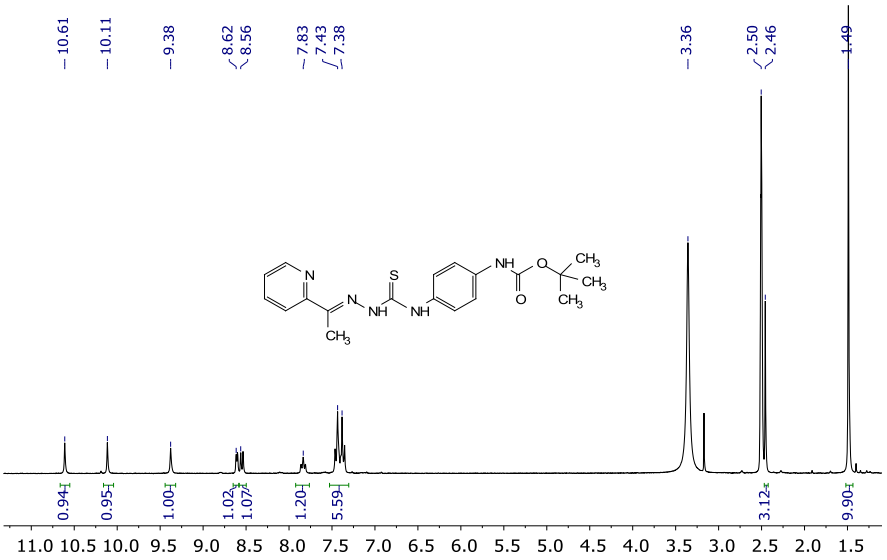


Figure 278. ^{1}H NMR spectrum of *p*-[(*E*)-1-[1-(2-Pyridyl)ethylidene]thiosemicarbazido]phenyl 2-methyl-2-propanecarbamate in DMSO-d_6 at 300 MHz.

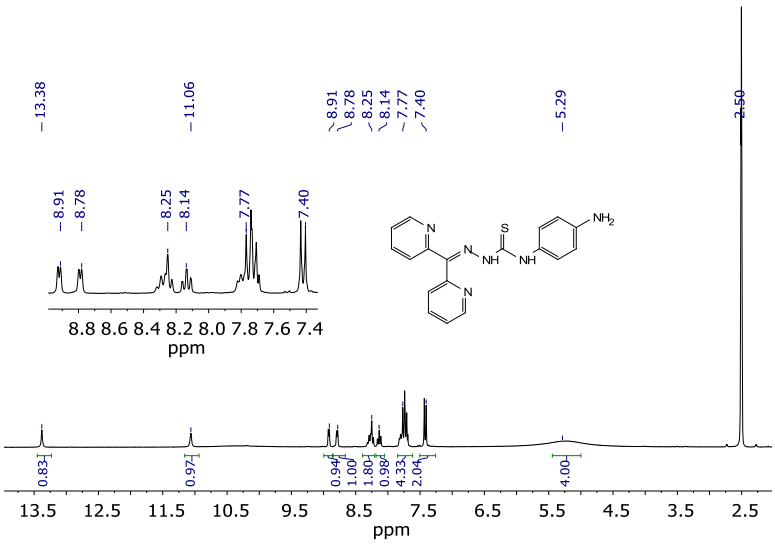


Figure 279. ^{1}H NMR spectrum of *p*-(1-[Bis(2-pyridyl)methylene]thiosemicarbazido)aniline in DMSO-d_6 at 300 MHz.

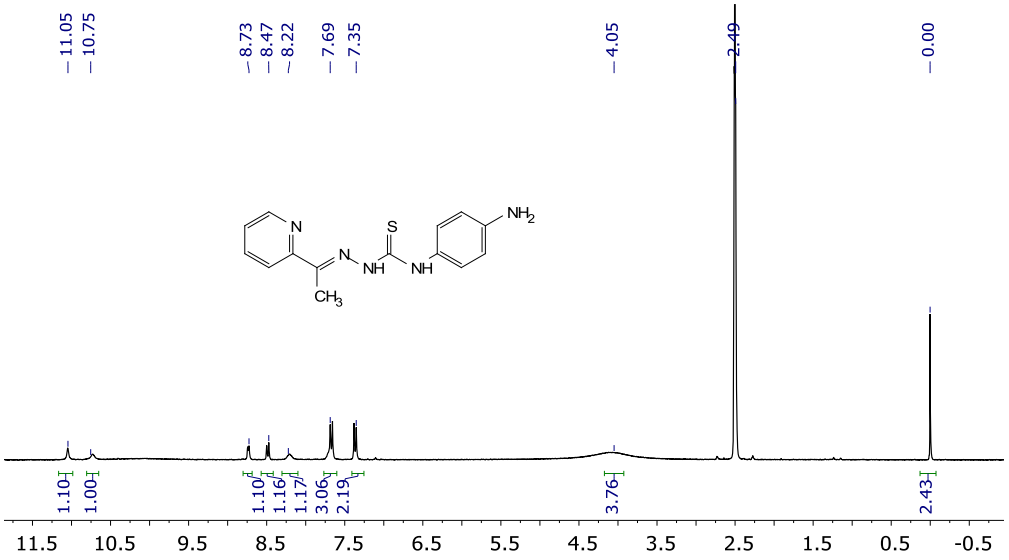


Figure 280. [1]H NMR spectrum of *p*-[(*E*)-1-[1-(2-pyridyl)ethylidene]thiosemicarbazido]aniline in DMSO-d_6 at 300 MHz.

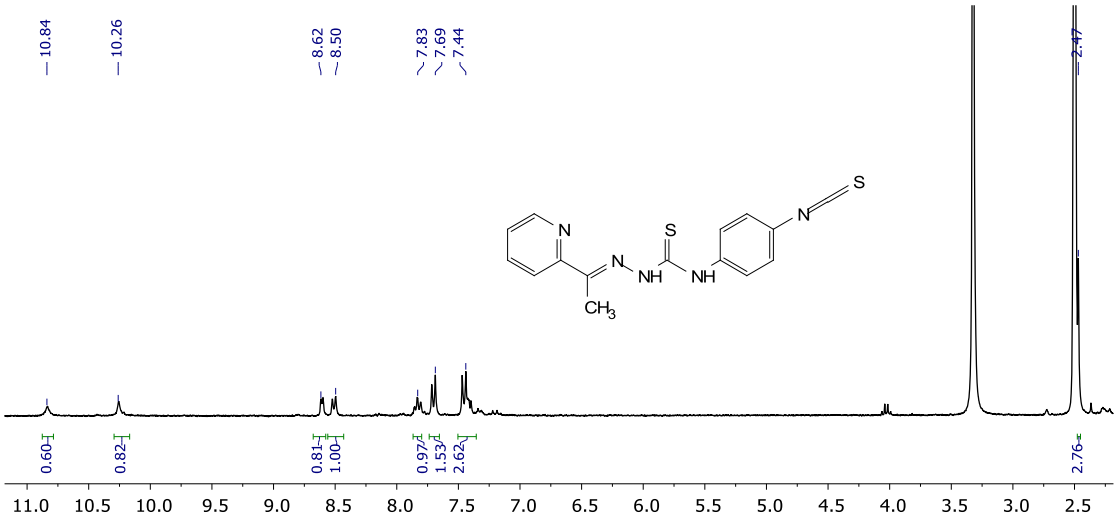


Figure 281. [1]H NMR spectrum of (*E*)-4-(*p*-Isothiocyanatophenyl)-1-[1-(2-pyridyl)ethylidene]thiosemicarbazide in DMSO-d_6 at 300 MHz.

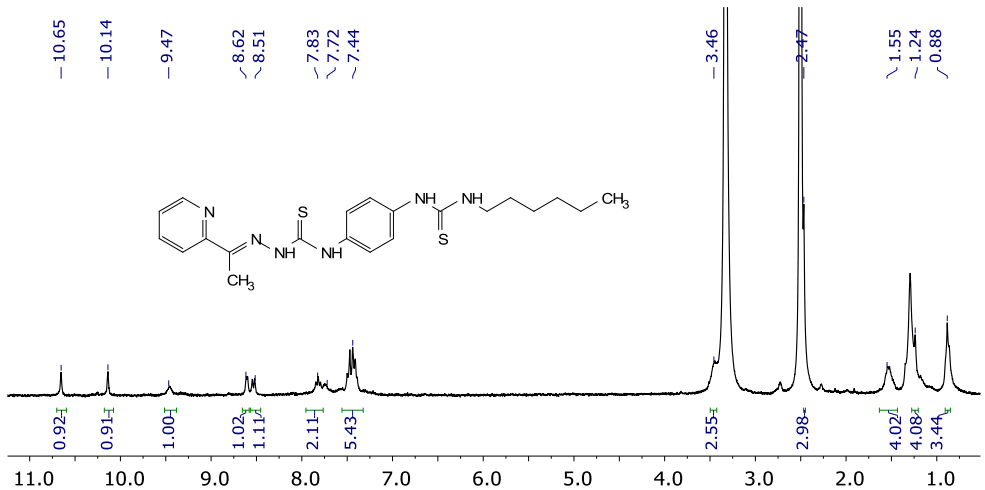


Figure 282. [1]H NMR spectrum of 1-[bis(2-pyridyl)methylene]-4-[*p*-(3-hexylthioureido)phenyl]thiosemicarbazide in DMSO-d_6 at 300 MHz.

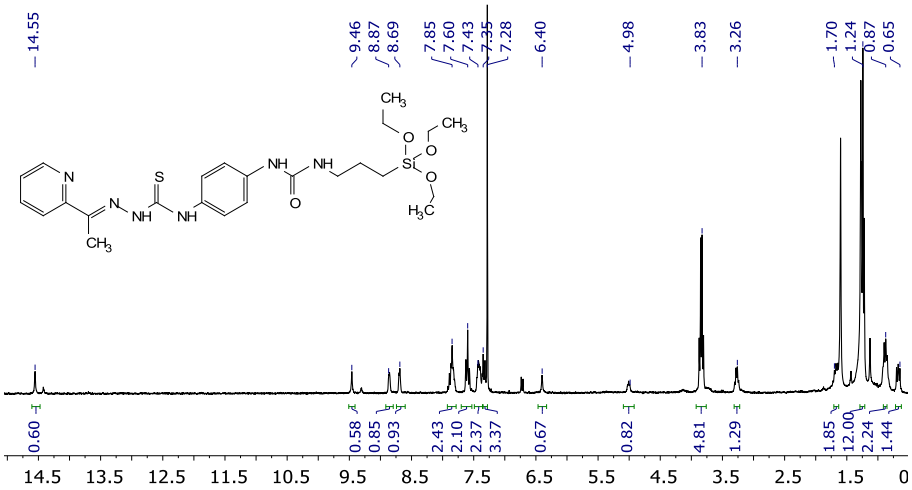


Figure 283. ^{1}H NMR spectrum of (3-[3-(*p*-(1-[Bis(2-pyridyl)methylene]thiosemicarbazido)phenyl)ureido]propyl) triethoxysilane in DMSO-d_6 at 300 MHz.

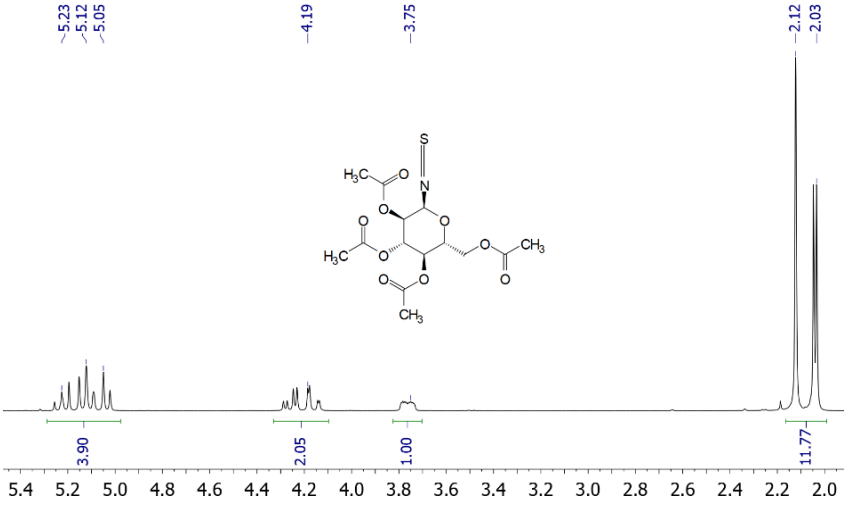


Figure 284. ^{1}H NMR spectrum of β-D-Glucopyranosyl isothiocyanate in $CDCl_3$ at 300 MHz.

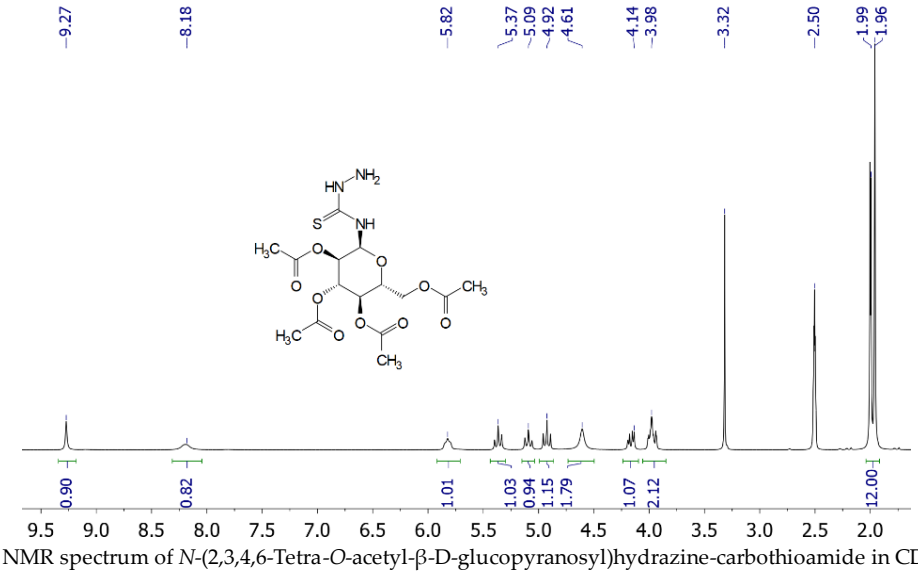


Figure 285. ^{1}H NMR spectrum of *N*-(2,3,4,6-Tetra-*O*-acetyl-β-D-glucopyranosyl)hydrazine-carbothioamide in $CDCl_3$ at 300 MHz.

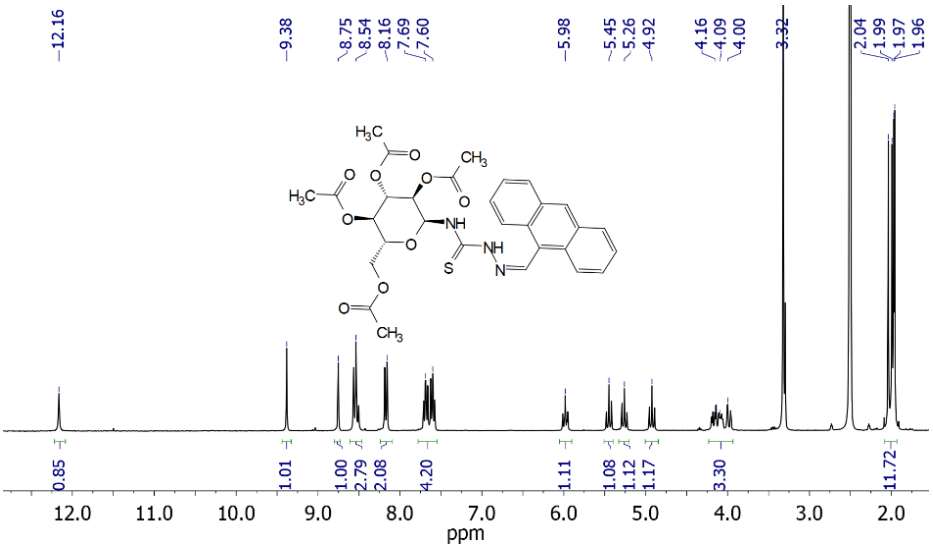


Figure 286. [1]H NMR spectrum of 9-anthraldehyde-4-(2,3,4,6-Tetra-*O*-acetyl-β-D-glucopyranosyl)-3-thiosemicarbazone in DMSO-d_6 at 499 MHz.

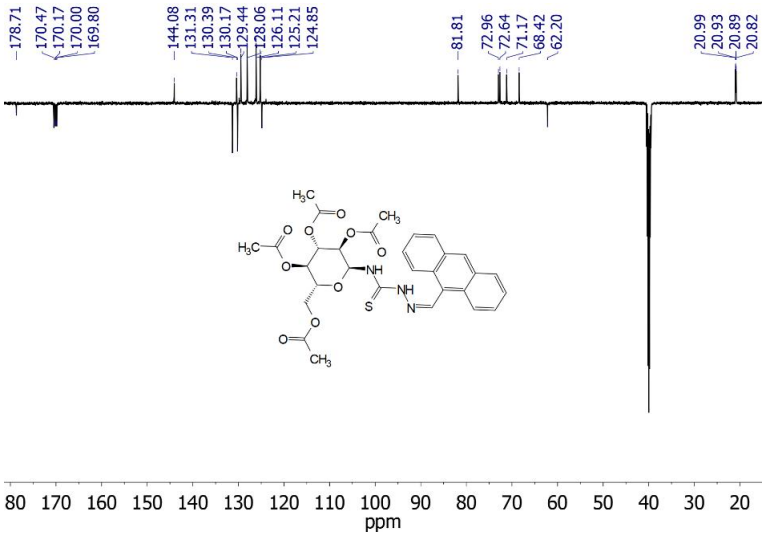


Figure 287. [13]C APT NMR spectrum of 9-anthraldehyde-4-(2,3,4,6-tetra-*O*-acetyl-β-D-glucopyranosyl)-3-thiosemicarbazone in DMSO-d_6 at 499 MHz.

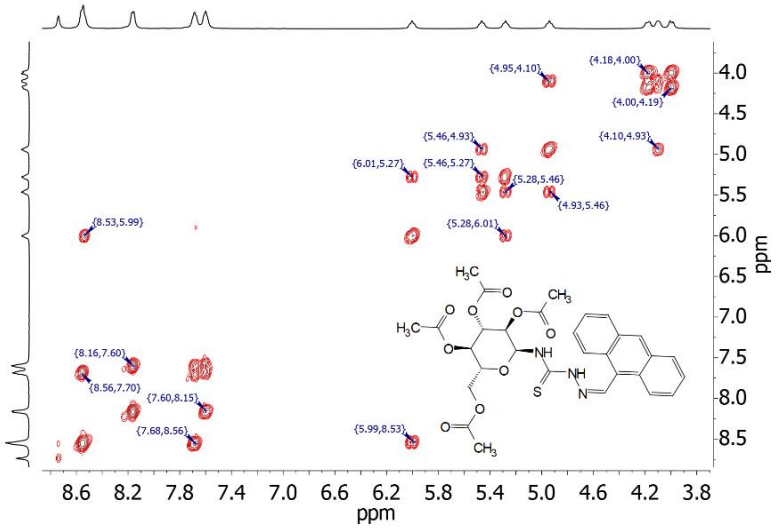


Figure 288. [1]H,[1]H COSY NMR spectrum of 9-anthraldehyde-4-(2,3,4,6-tetra-*O*-acetyl-β-D-glucopyranosyl)-3-thiosemicarbazone in DMSO-d_6 at 499 MHz.

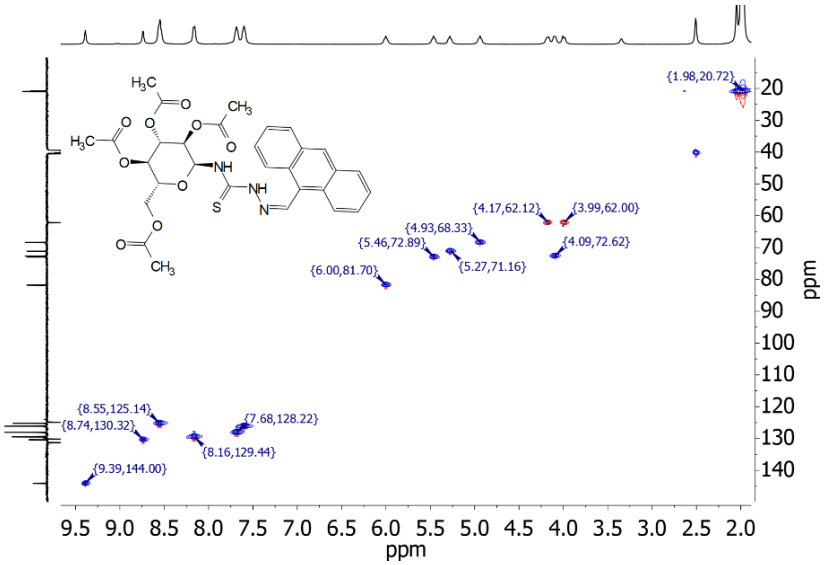


Figure 289. $^{1}H,^{13}C$ HMQC/HSQC NMR spectrum of 9-anthraldehyde-4-(2,3,4,6-tetra-*O*-acetyl-β-D-glucopyranosyl)-3-thiosemicarbazone in DMSO-d_6 at 499 MHz.

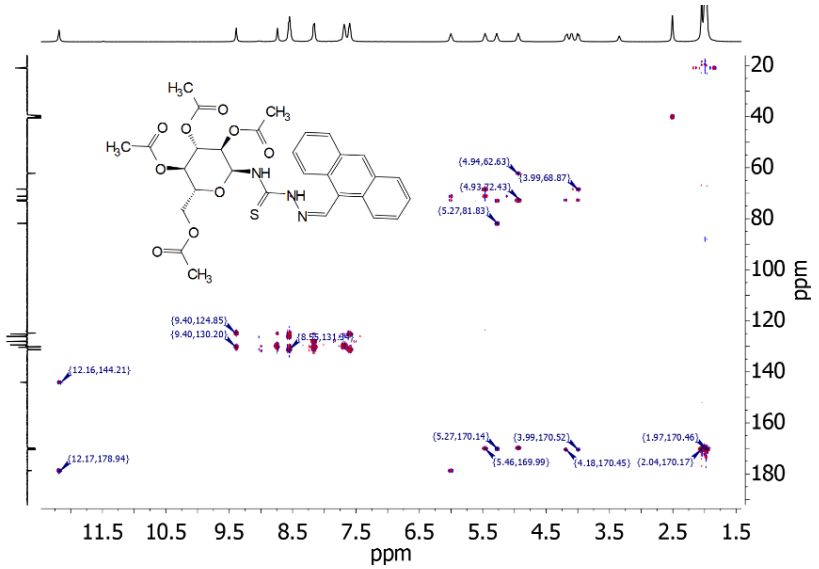


Figure 290. $^{1}H,^{13}C$ HMBC NMR spectrum of 9-anthraldehyde-4-(2,3,4,6-tetra-*O*-acetyl-β-D-glucopyranosyl)-3-thiosemicarbazone in DMSO-d_6 at 499 MHz.

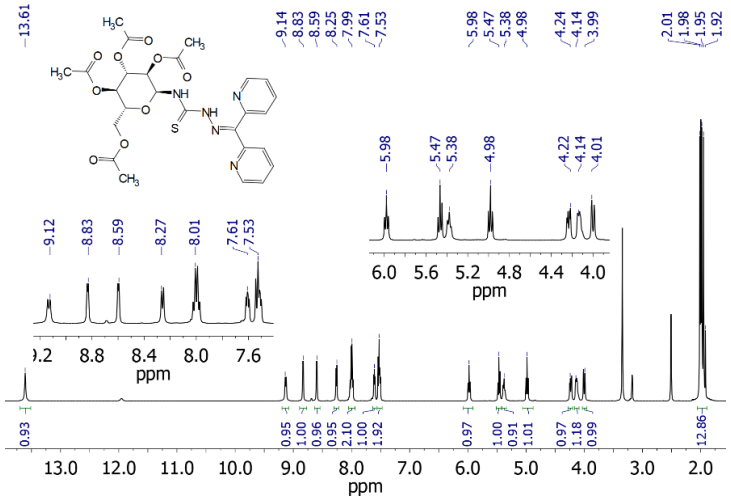


Figure 291. ^{1}H NMR spectrum of di-2-pyridylketone-4-(2,3,4,6-tetra-*O*-acetyl-β-D-glucopyranosyl)-3-thiosemicarbazone in DMSO-d_6 at 499 MHz.

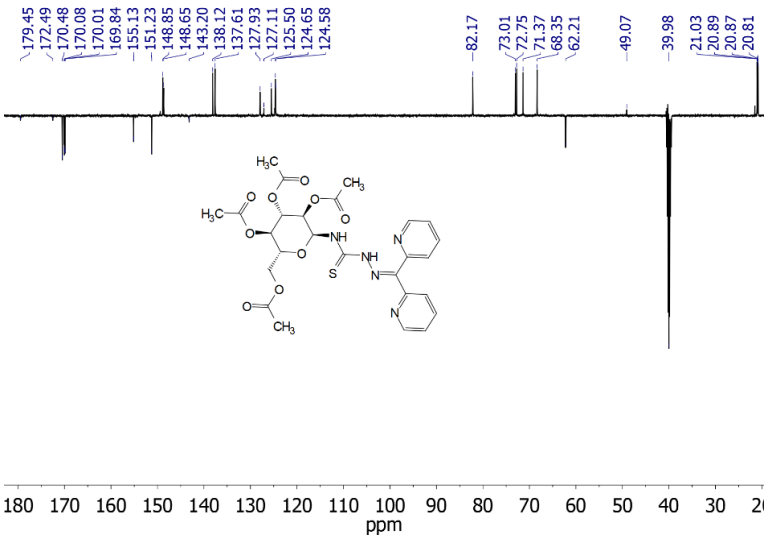


Figure 292. ^{13}C APT NMR spectrum of di-2-pyridylketone-4-(2,3,4,6-tetra-*O*-acetyl-β-D-glucopyranosyl)-3-thiosemicarbazone in DMSO-d_6 at 499 MHz.

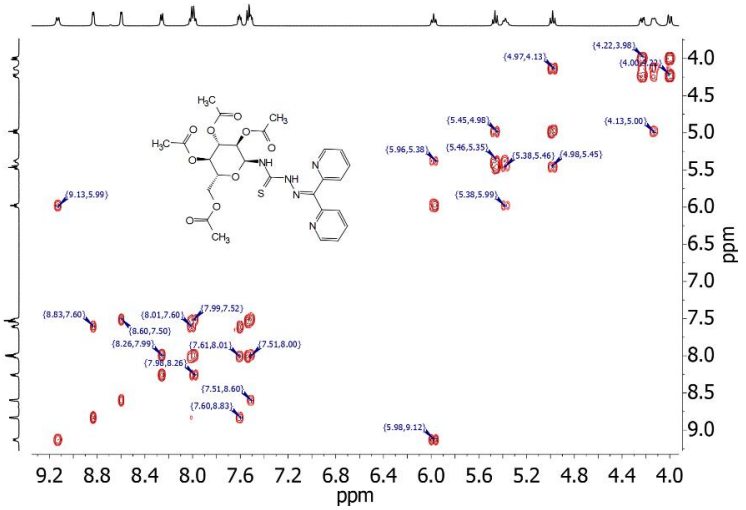


Figure 293. $^{1}H,^{1}H$ COSY NMR spectrum of di-2-pyridylketone-4-(2,3,4,6-tetra-*O*-acetyl-β-D-glucopyranosyl)-3-thiosemicarbazone in DMSO-d_6 at 499 MHz.

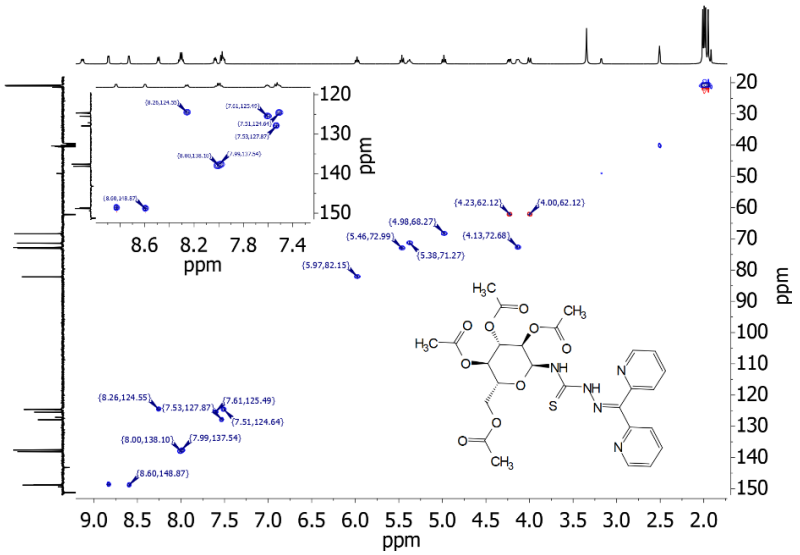


Figure 294. $^{1}H,^{13}C$ HMQC/HSQC NMR spectrum of di-2-pyridylketone-4-(2,3,4,6-tetra-*O*-acetyl-β-D-glucopyranosyl)-3-thiosemicarbazone in DMSO-d_6 at 499 MHz.

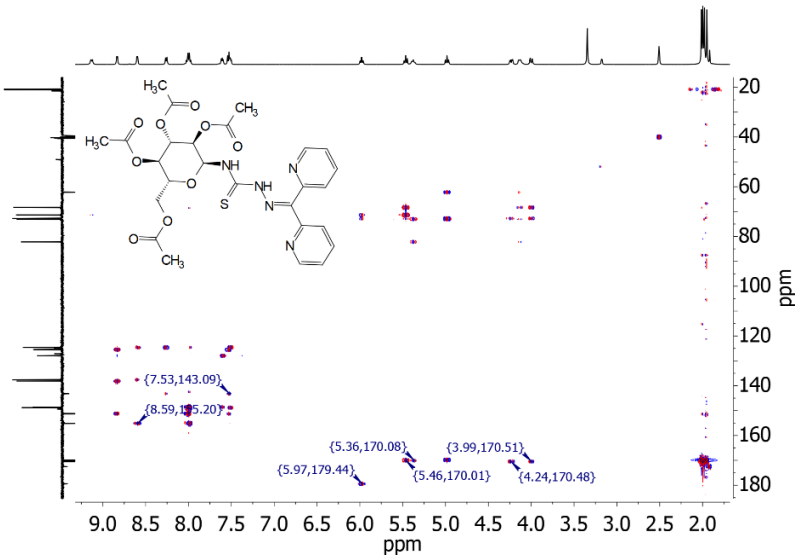


Figure 295. $^{1}H,^{13}C$ HMBC NMR spectrum of di-2-pyridylketone-4-(2,3,4,6-tetra-*O*-acetyl-β-D-glucopyranosyl)-3-thiosemicarbazone in DMSO-d_6 at 499 MHz.

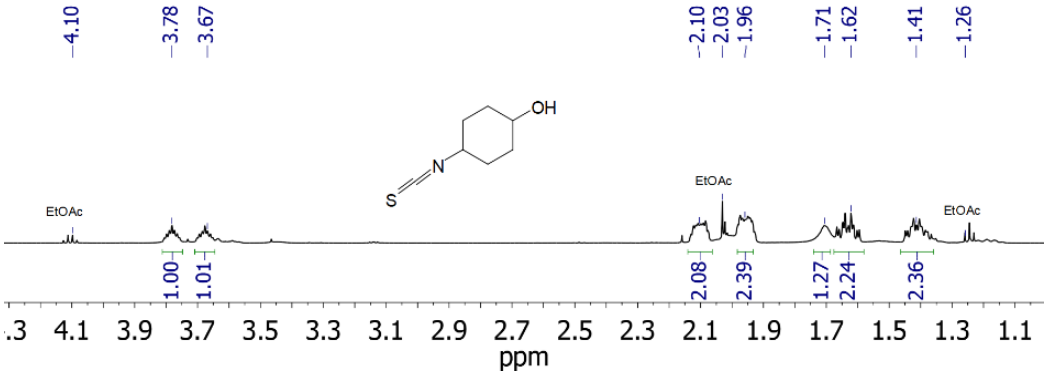


Figure 296. ^{1}H NMR spectrum of *trans*-4-hydroxycyclohexyl isothiocyanate in $CDCl_3$ at 499 MHz.

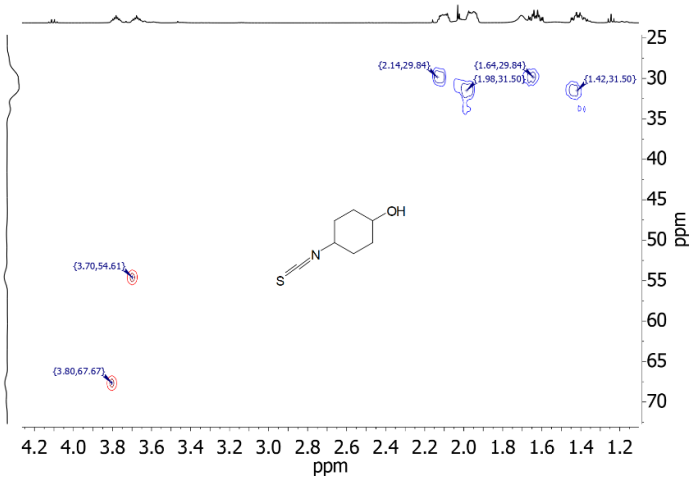


Figure 297. $^{1}H,^{13}C$ HMQC/HSQC NMR spectrum of *trans*-4-hydroxycyclohexyl isothiocyanate in $CDCl_3$ at 499 MHz.

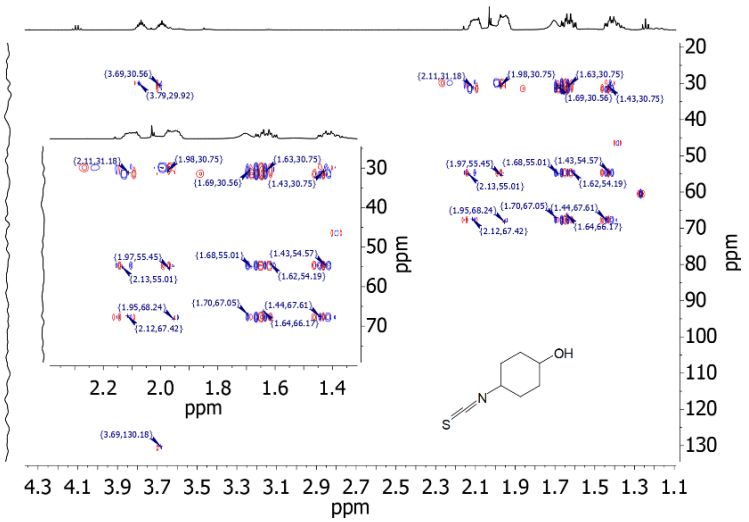


Figure 298. $^{1}H,^{13}C$ HMBC NMR spectrum of *trans*-4-hydroxycyclohexyl isothiocyanate in $CDCl_3$ at 499 MHz.

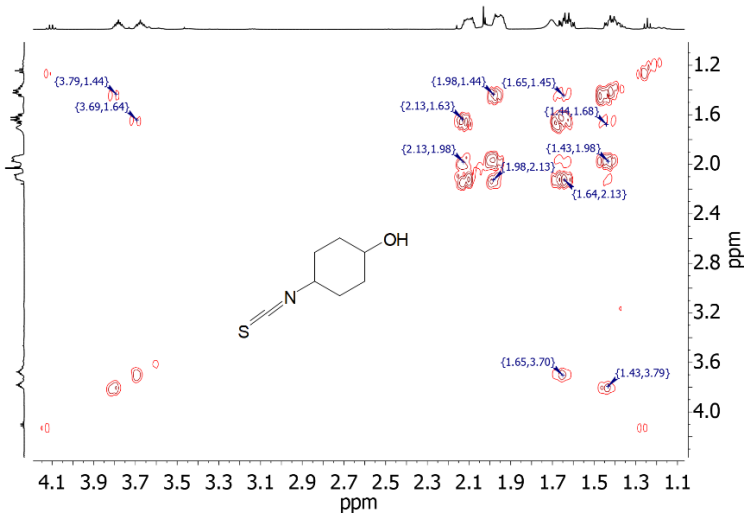


Figure 299. $^{1}H,^{1}H$ COSY NMR spectrum of *trans*-4-hydroxycyclohexyl isothiocyanate in $CDCl_3$ at 499 MHz.

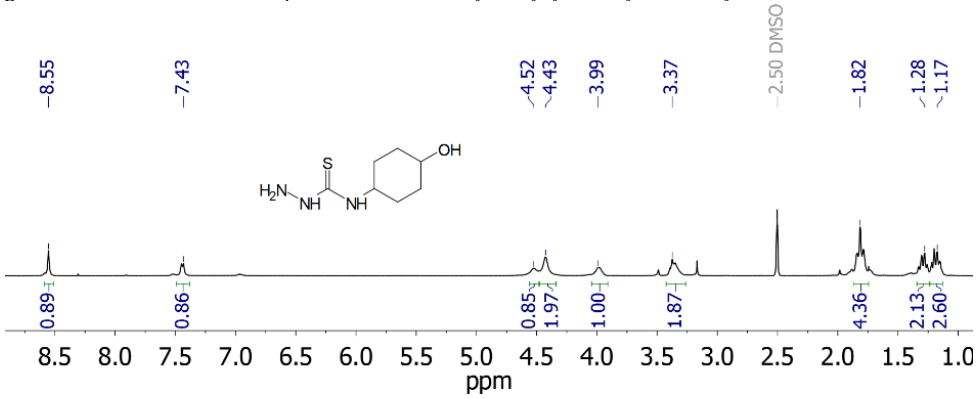


Figure 300. ^{1}H NMR spectrum of 4-(trans-4-hydroxycyclohexyl)-thiosemicarbazide in DMSO-d_6 at 499 MHz.

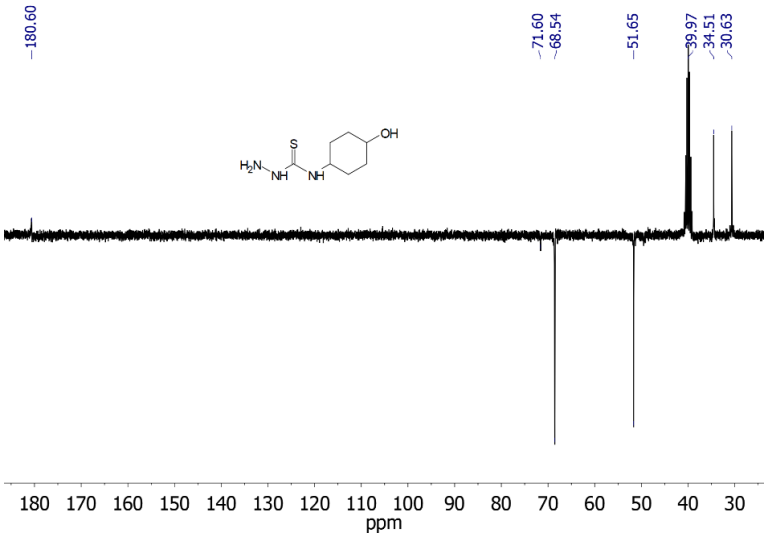


Figure 301. ^{13}C DEPTQ NMR spectrum of 4-(trans-4-hydroxycyclohexyl)-thiosemicarbazide in DMSO-d_6 at 300 MHz.

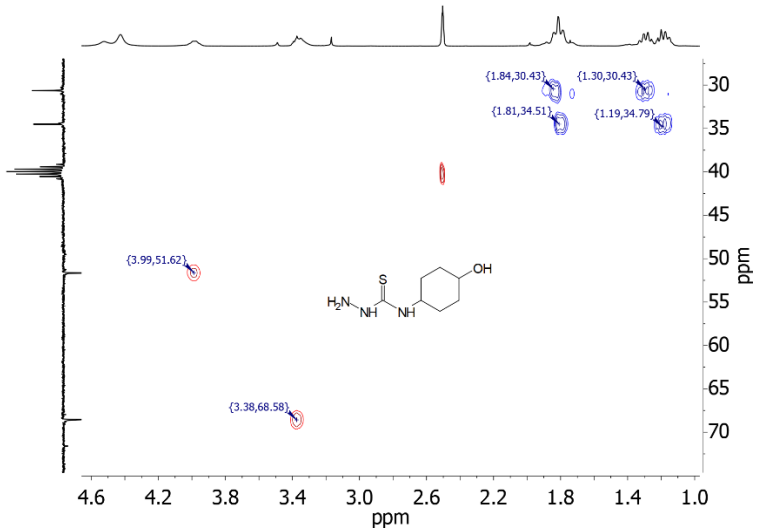


Figure 302. ^{1}H,^{13}C HMQC/HSQC NMR spectrum of 4-(trans-4-hydroxycyclohexyl)-thiosemicarbazide in DMSO-d_6 at 499 MHz.

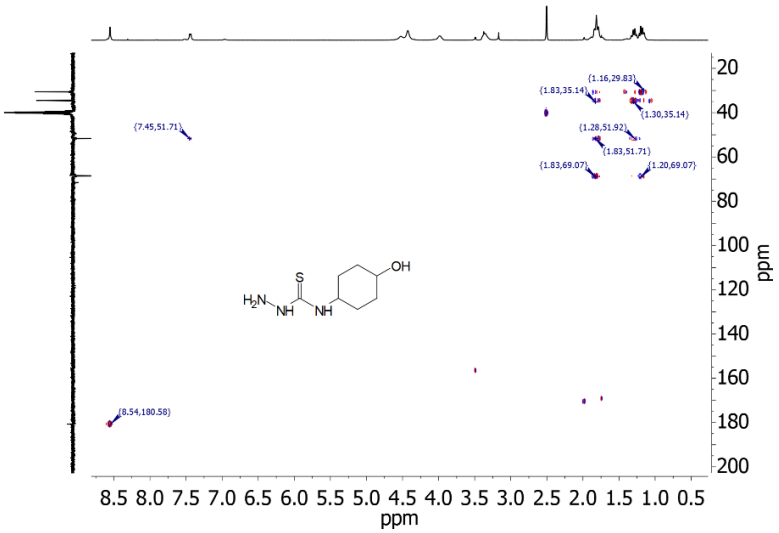


Figure 303. ^{1}H,^{13}C HMBC NMR spectrum of 4-(trans-4-hydroxycyclohexyl)thiosemicarbazide in DMSO-d_6 at 499 MHz.

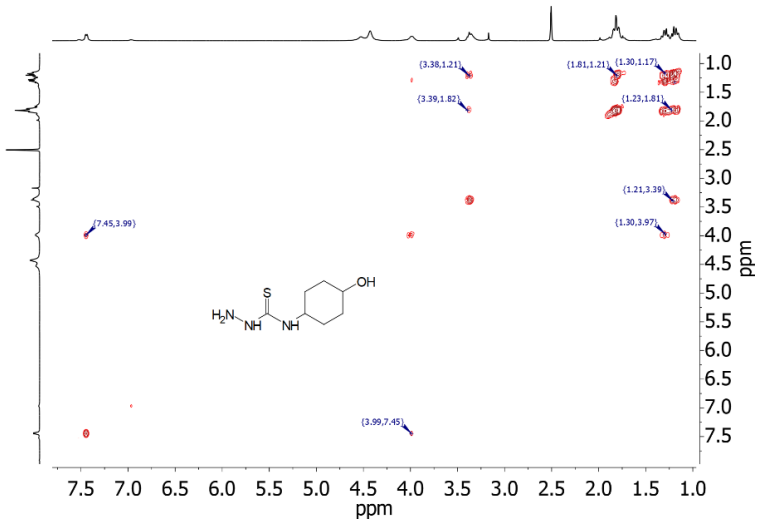


Figure 304. $^{1}H,^{1}H$ COSY NMR spectrum of 4-(trans-4-hydroxycyclohexyl)-thiosemicarbazide in DMSO-d_6 at 499 MHz.

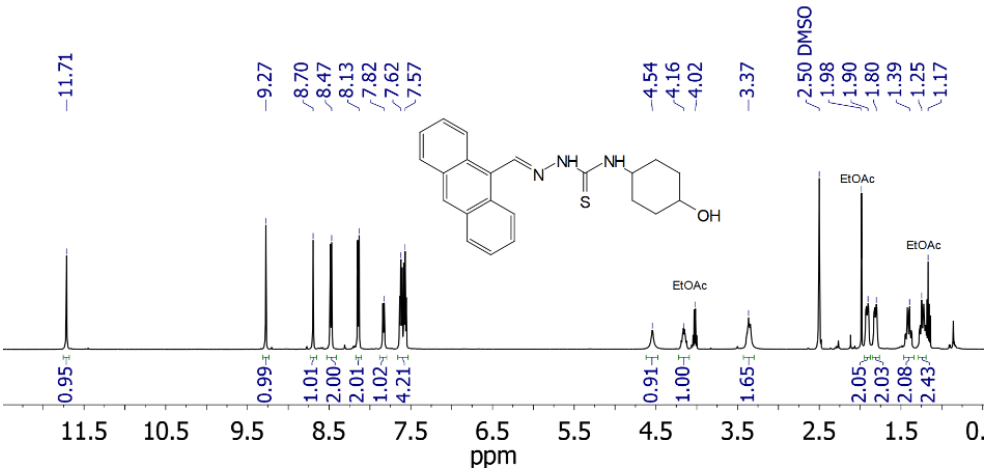


Figure 305. ^{1}H NMR spectrum of 9-anthraldehyde-4-(*trans*-4-hydroxycyclohexyl)-3-thiosemi-carbazone in DMSO-d_6 at 499 MHz.

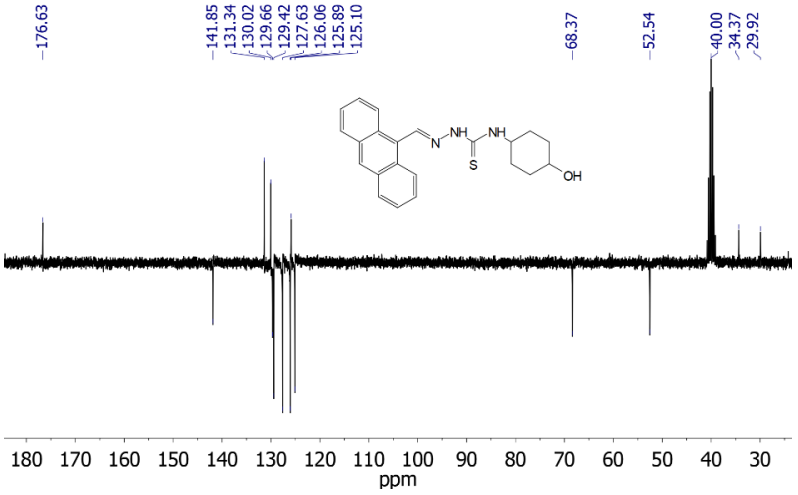


Figure 306. ^{13}C DEPTQ NMR spectrum of 9-anthraldehyde-4-(*trans*-4-hydroxycyclohexyl)-3-thiosemicarbazone in DMSO-d_6 at 300 MHz.

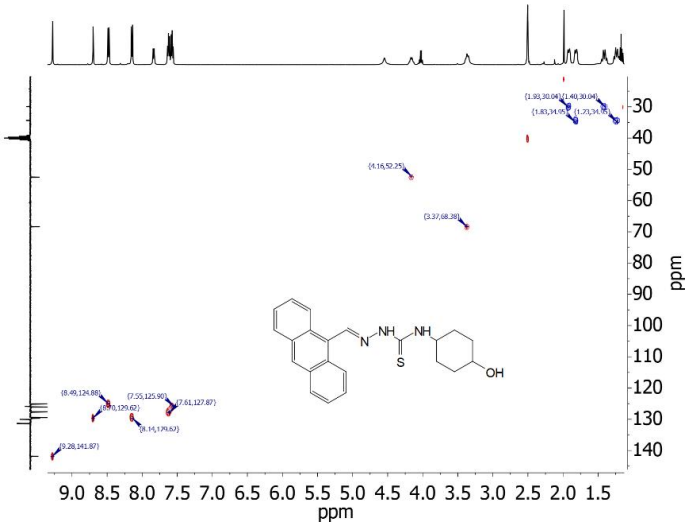


Figure 307. $^{1}H,^{13}C$ HMQC/HSQC NMR spectrum of 9-anthraldehyde-4-(*trans*-4-hydroxycyclohexyl)-3-thiosemicarbazone in DMSO-d_6 at 499 MHz.

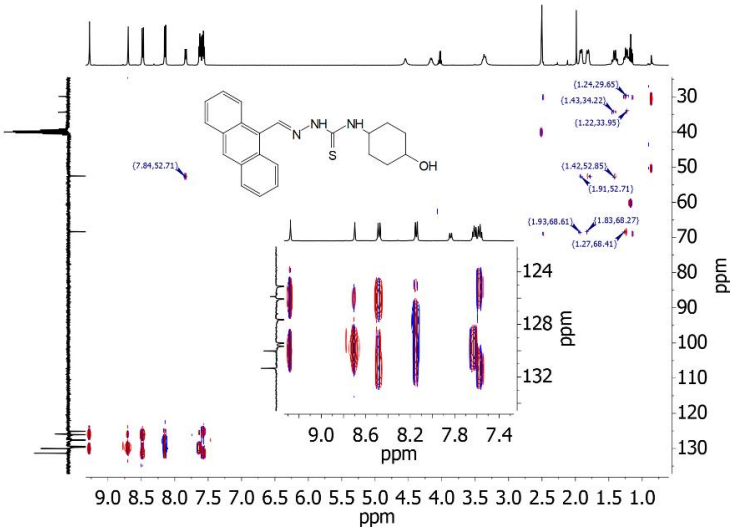


Figure 308. $^{1}H,^{13}C$ HMBC NMR spectrum of 9-anthraldehyde-4-(*trans*-4-hydroxycyclohexyl)-3-thiosemicarbazone in DMSO-d_6 at 499 MHz.

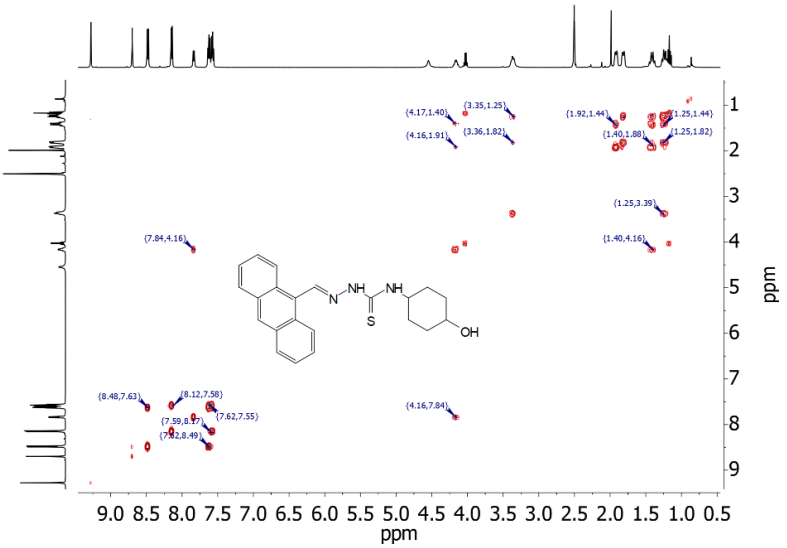


Figure 309. $^{1}H,^{1}H$ COSY NMR spectrum of 9-anthraldehyde-4-(*trans*-4-hydroxycyclohexyl)-3-thiosemicarbazone in DMSO-d_6 at 499 MHz.

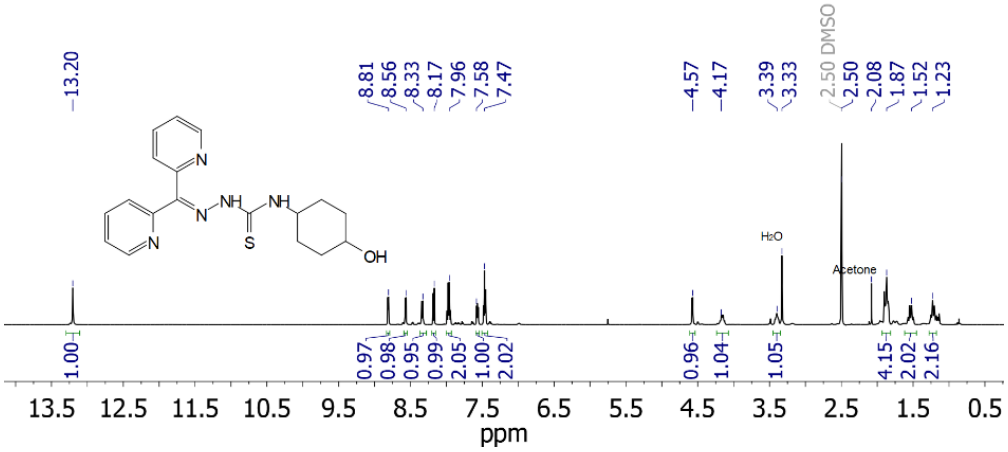


Figure 310. [1]H NMR spectrum of di-2-pyridylketone-4-(*trans*-4-hydroxycyclohexyl)-3-thiosemi-carbazone DMSO-d_6 at 499 MHz.

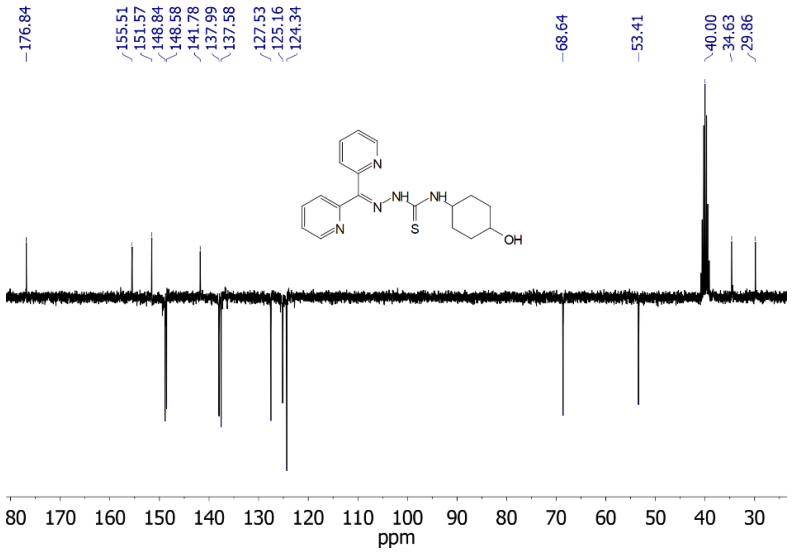


Figure 311. [13]C DEPTQ NMR spectrum of di-2-pyridylketone-4-(*trans*-4-hydroxycyclohexyl)-3-thiosemicarbazone in DMSO-d_6 at 300 MHz.

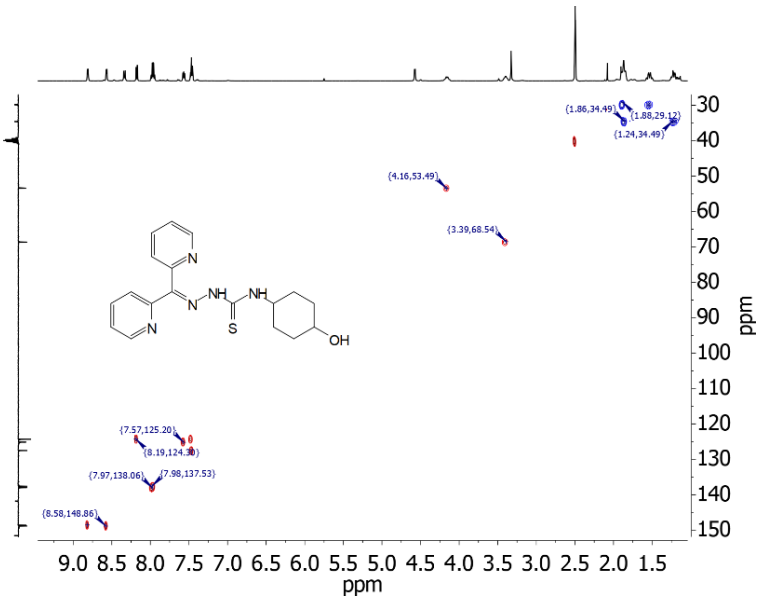


Figure 312. [1]H,[13]C HMQC/HSQC NMR spectrum of di-2-pyridylketone-4-(*trans*-4-hydroxy-cyclohexyl)-3-thiosemicarbazone in DMSO-d_6 at 499 MHz.

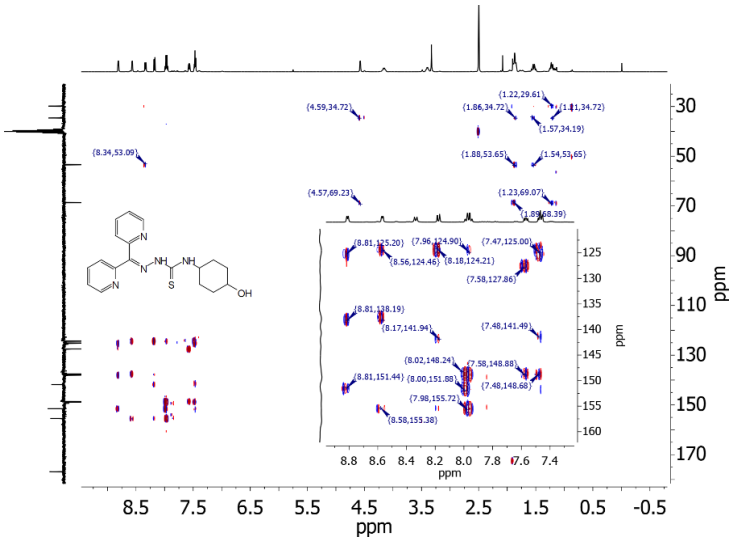


Figure 313. $^{1}H,^{13}C$ HMBC NMR spectrum of di-2-pyridylketone-4-(*trans*-4-hydroxycyclohexyl)-3-thiosemicarbazone in DMSO-d_6 at 499 MHz.

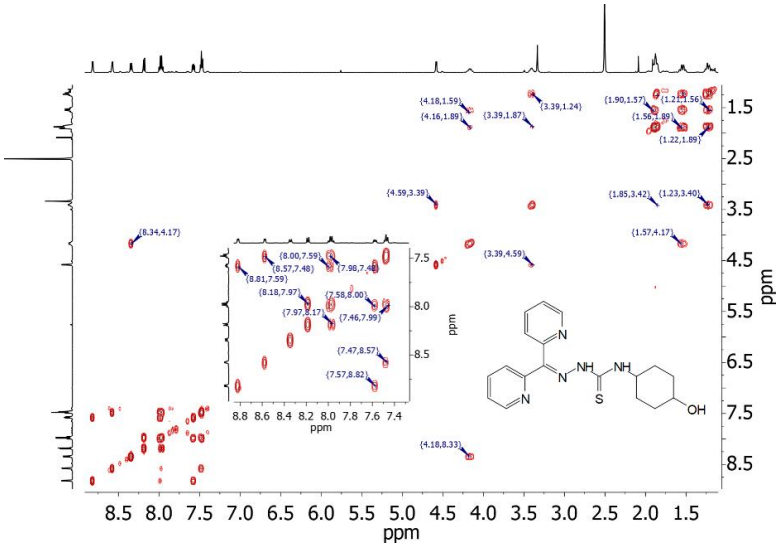


Figure 314. $^{1}H,^{1}H$ COSY NMR spectrum of di-2-pyridylketone-4-(*trans*-4-hydroxycyclohexyl)-3-thiosemicarbazone in DMSO-d_6 at 499 MHz.

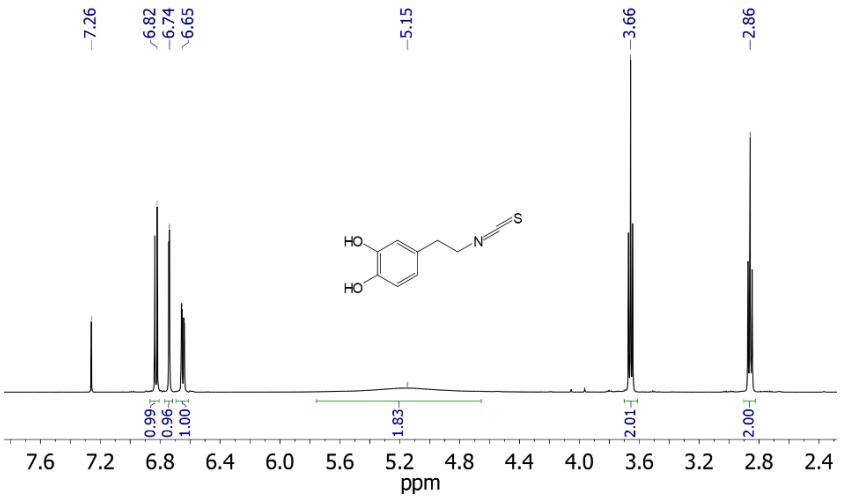


Figure 315. ^{1}H NMR spectrum of 4-(2-isothiocyanatoethyl)benzene-1,2-diol in $CDCl_3$ at 499 MHz.

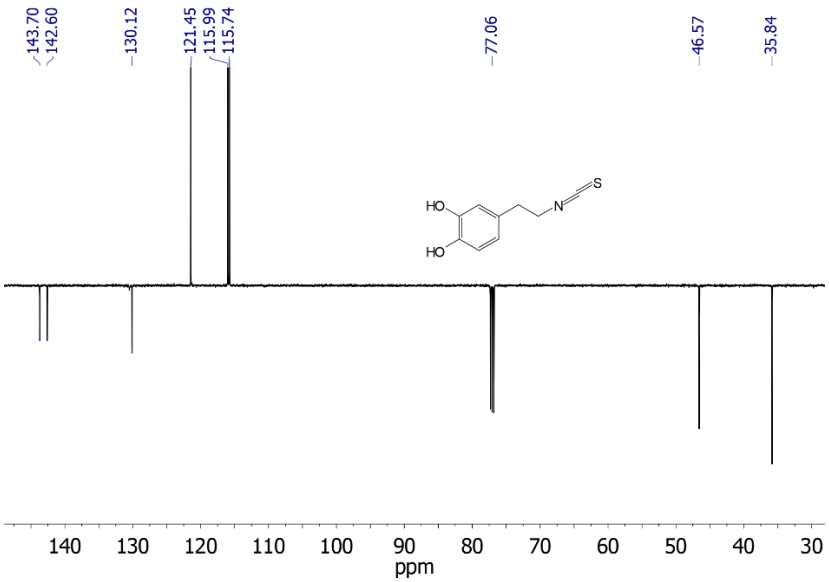


Figure 316. ^{13}C APT NMR spectrum of 4-(2-isothiocyanatoethyl)benzene-1,2-diol in $CDCl_3$ at 499 MHz.

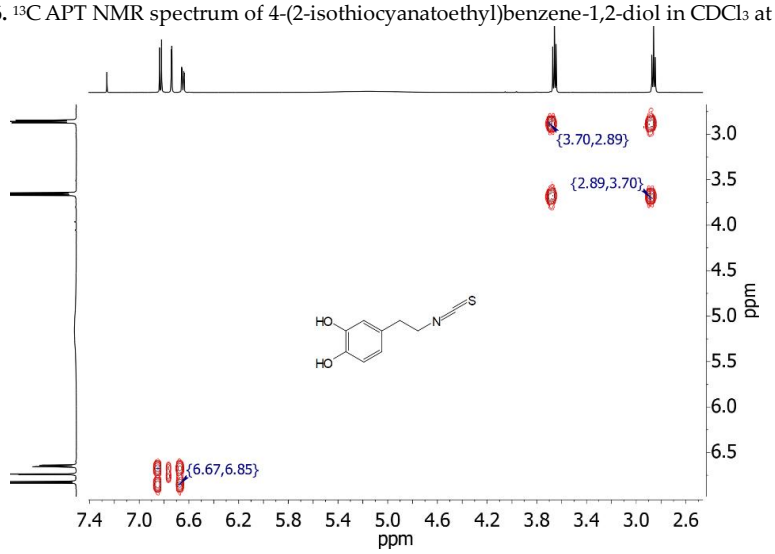


Figure 317. $^{1}H,^{1}H$ COSY NMR spectrum of 4-(2-isothiocyanatoethyl)benzene-1,2-diol in $CDCl_3$ at 499 MHz.

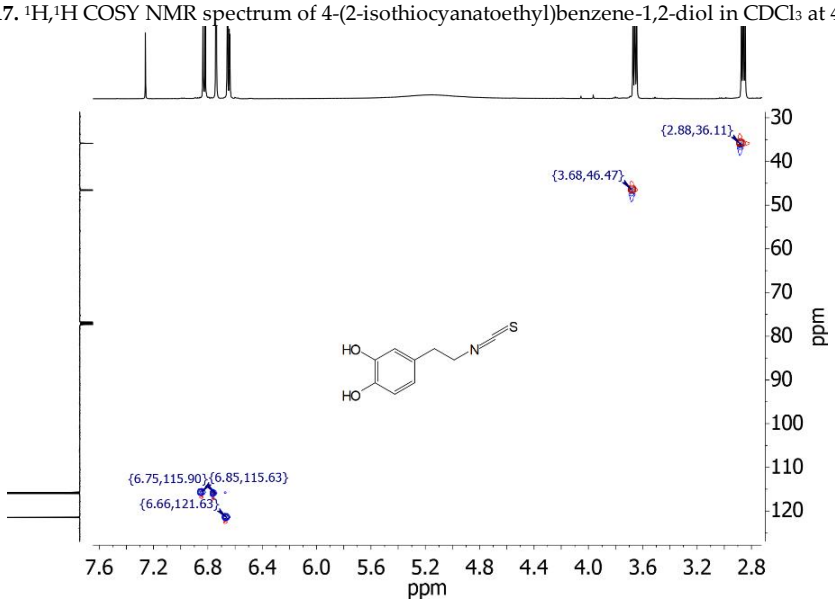


Figure 318. $^{1}H,^{13}C$ HMQC/HSQC NMR spectrum of 4-(2-isothiocyanatoethyl)benzene-1,2-diol in $CDCl_3$ at 499 MHz.

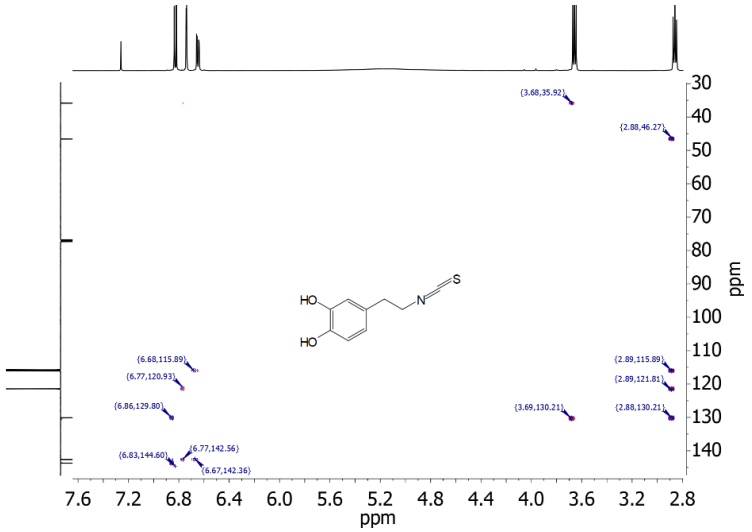


Figure 319. $^{1}H,^{13}C$ HMBC NMR spectrum of 4-(2-isothiocyanatoethyl)benzene-1,2-diol in $CDCl_3$ at 499 MHz.

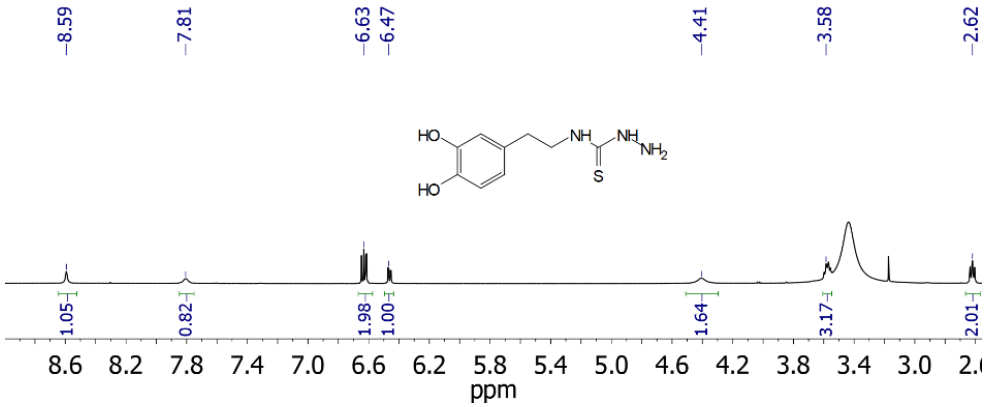


Figure 320. ^{1}H NMR spectrum of 4-[2-(hydrazidecarbothioamino)ethyl]benzene-1,2-diol in DMSO-d_6 at 499 MHz.

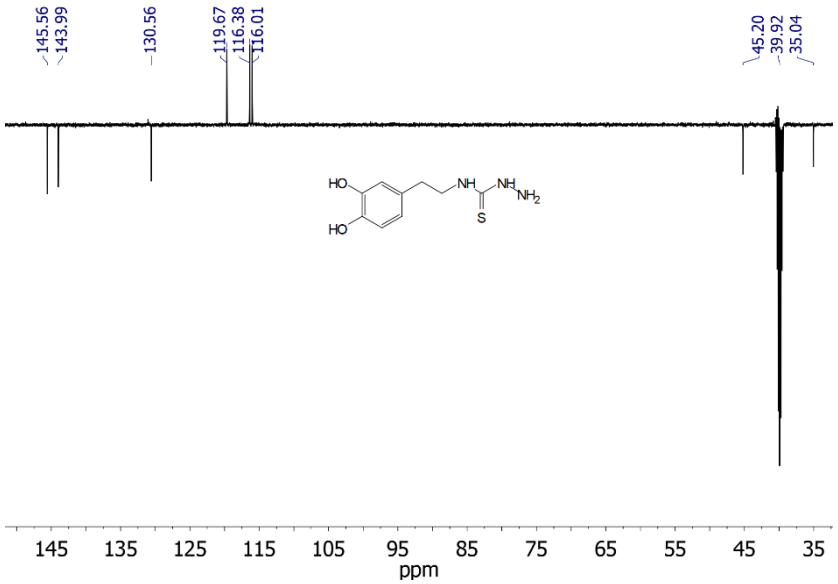


Figure 321. ^{13}C APT NMR spectrum of 4-[2-(hydrazidecarbothioamino)ethyl]benzene-1,2-diol in DMSO-d_6 at 499 MHz.

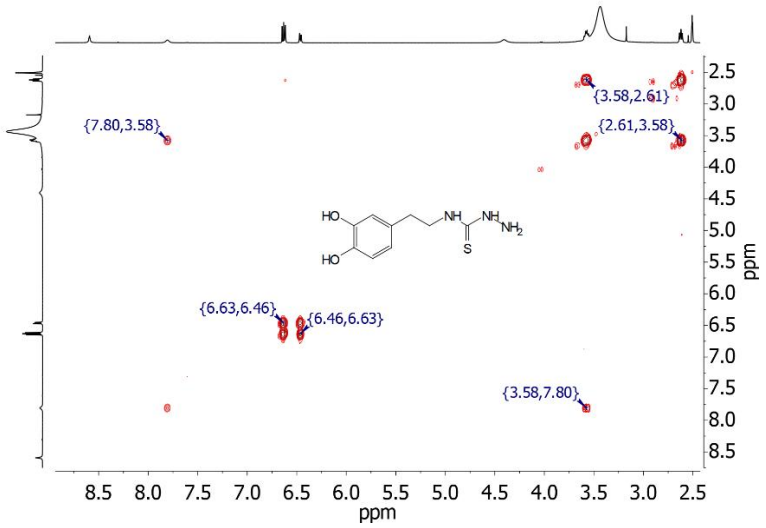


Figure 322. $^{1}H,^{1}H$ COSY NMR spectrum of 4-[2-(hydrazidecarbothioamino)ethyl]benzene-1,2-diol in DMSO-d_6 at 499 MHz.

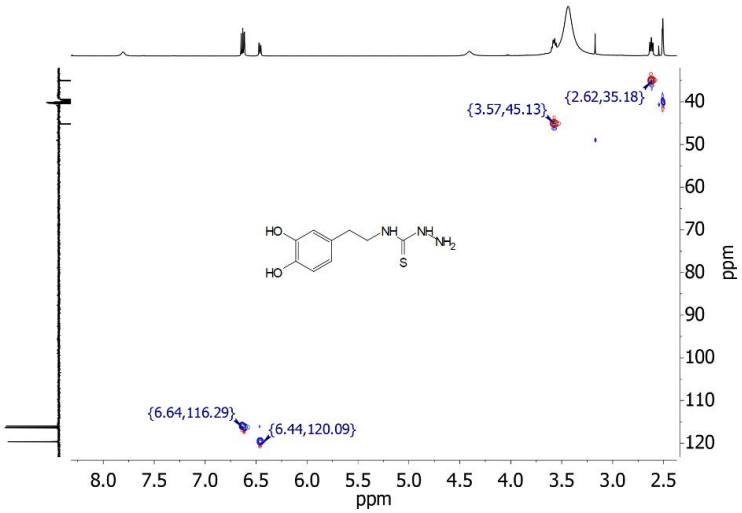


Figure 323. $^{1}H,^{13}C$ HMQC/HSQC NMR spectrum of 4-[2-(hydrazidecarbothioamino)ethyl]benzene-1,2-diol in DMSO-d_6 at 499 MHz.

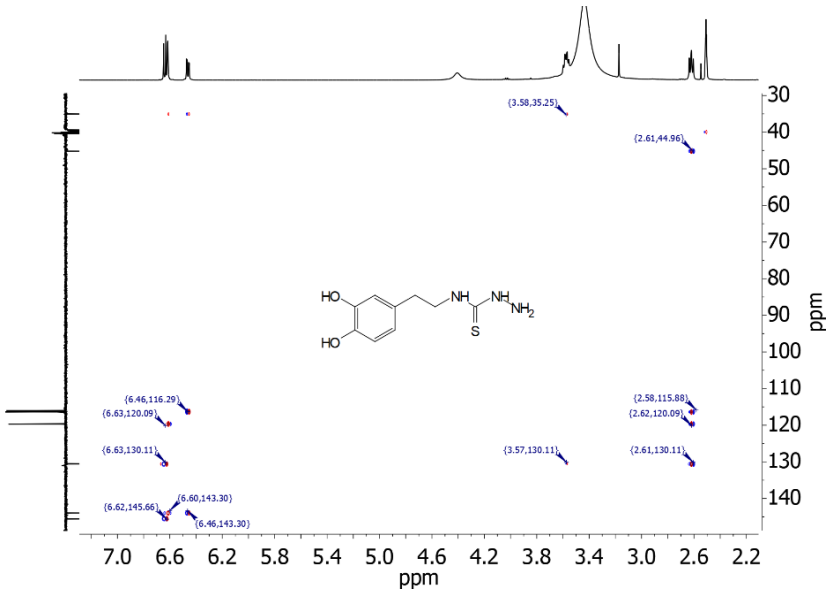


Figure 324. $^{1}H,^{13}C$ HMBC NMR spectrum of 4-[2-(hydrazidecarbothioamino)ethyl]benzene-1,2-diol in DMSO-d_6 at 499 MHz.

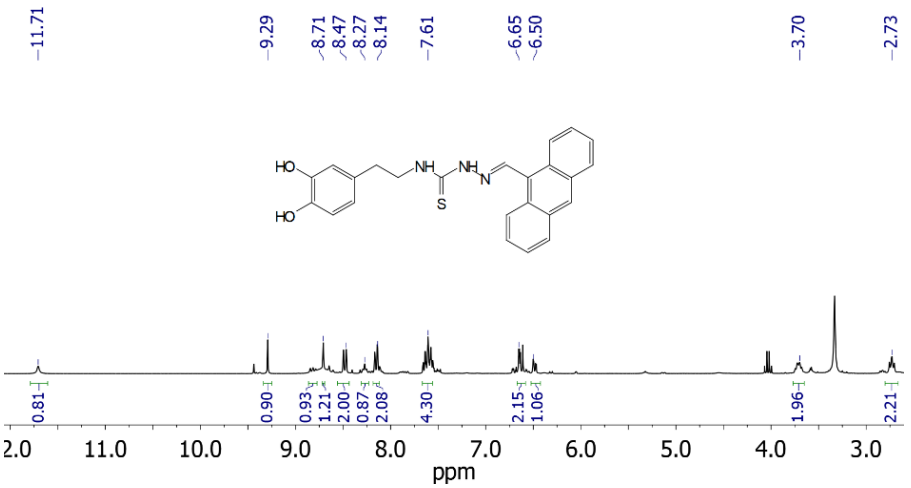


Figure 325. ^{1}H NMR spectrum of [(1*E*)-(anthracen-9-yl)methylideneamino][2-(3,4 dihydroxyphenyl) ethylamino] carbothioamide in DMSO-d_6 at 300 MHz.

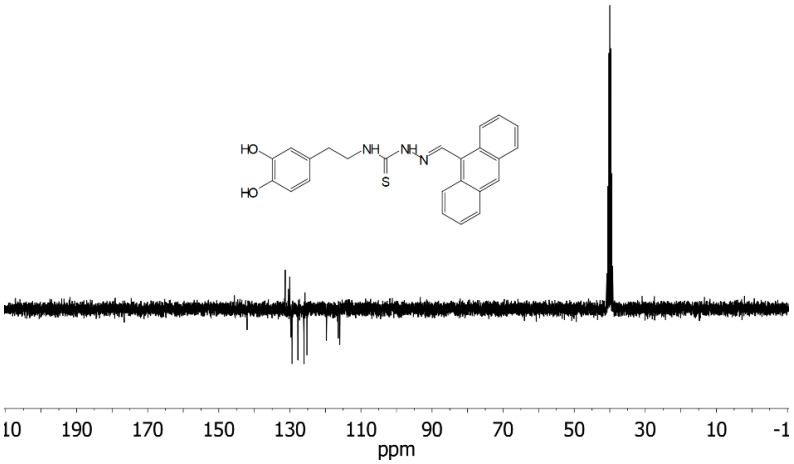


Figure 326. ^{13}C DEPTQ NMR spectrum of [(1*E*)-(anthracen-9-yl)methylideneamino][2-(3,4 dihydroxyphenyl)ethylamino] carbothioamide in DMSO-d_6 at 300 MHz.

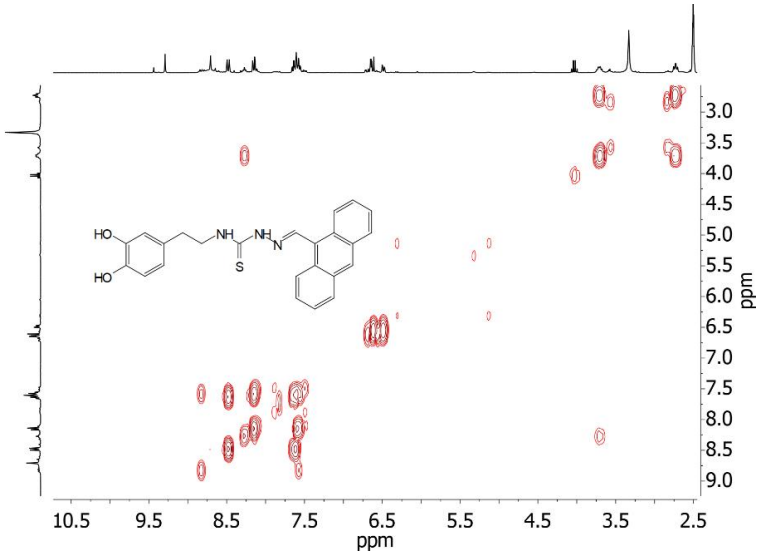


Figure 327. ^{1}H,^{1}H COSY NMR spectrum of [(1*E*)-(anthracen-9-yl)methylideneamino][2-(3,4 dihydroxyphenyl)ethylamino] carbothioamide in DMSO-d_6 at 300 MHz.

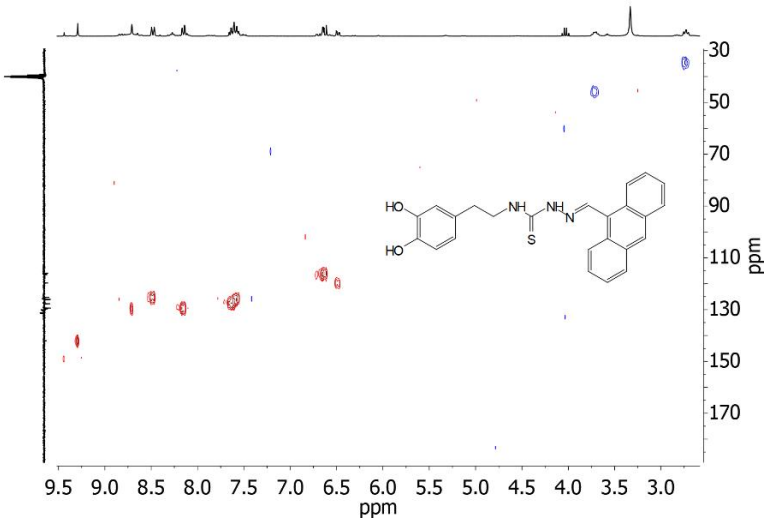


Figure 328. $^{1}H,^{13}C$ HMQC/HSQC NMR spectrum of [(1*E*)-(anthracen-9-yl)methylideneamino][2-(3,4 dihydroxyphenyl) ethylamino]carbothioamide in DMSO-d_6 at 300 MHz.

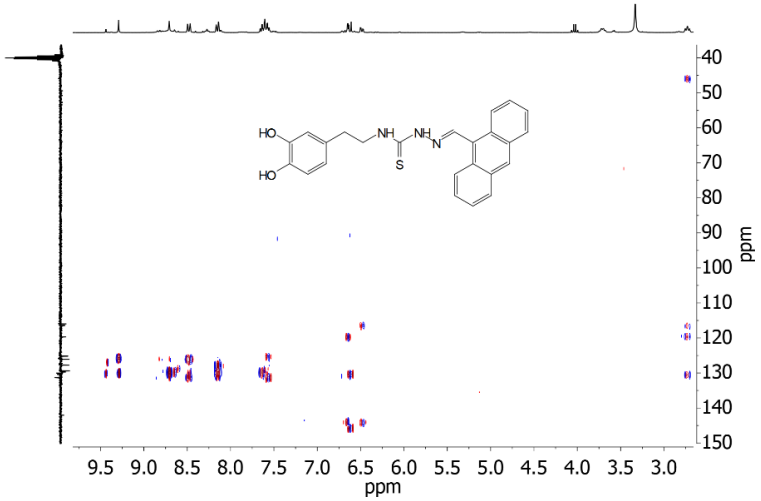


Figure 329. $^{1}H,^{13}C$ HMBC NMR spectrum of [(1*E*)-(anthracen-9-yl)methylideneamino][2-(3,4 dihydroxyphenyl)ethylamino] carbothioamide in DMSO-d_6 at 300 MHz.

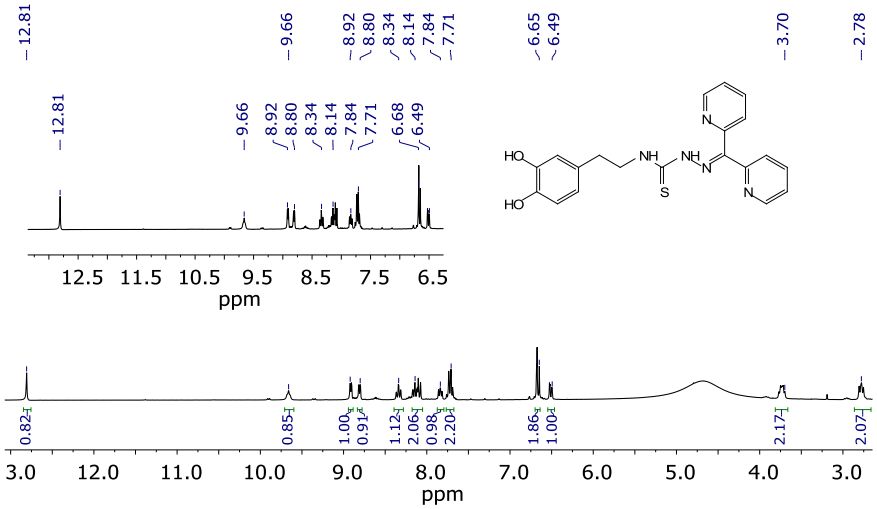


Figure 330. ^{1}H NMR spectrum of [bis(pyridin-2-yl)methylideneamino][2-(3,4dihydroxyphenyl)ethylamino]carbothioamide in DMSO-d_6 at 300 MHz.

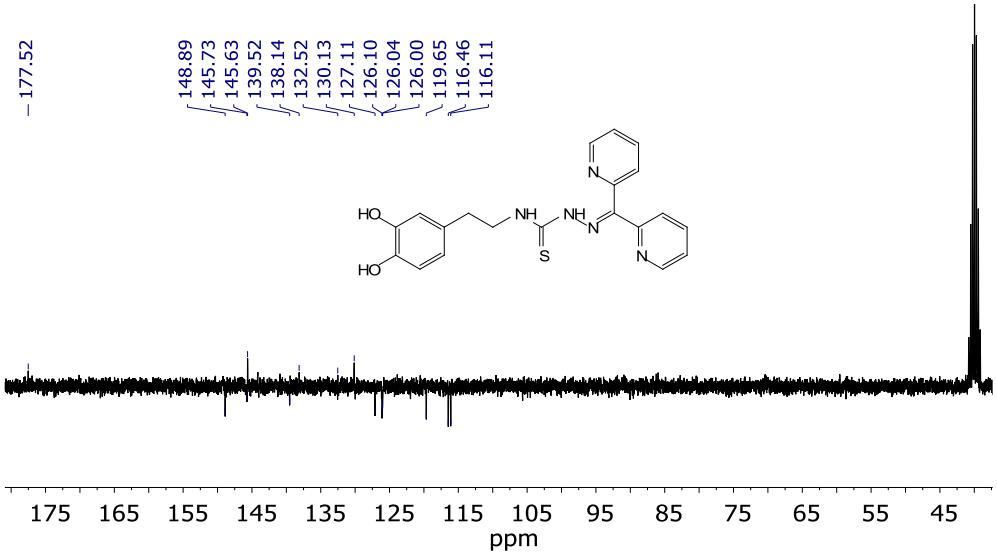


Figure 331. ^{13}C NMR spectrum of [bis(pyridin-2-yl)methylideneamino][2-(3,4 dihydroxyphenyl) ethylamino] carbothioamide in DMSO-d_6 at 300 MHz.

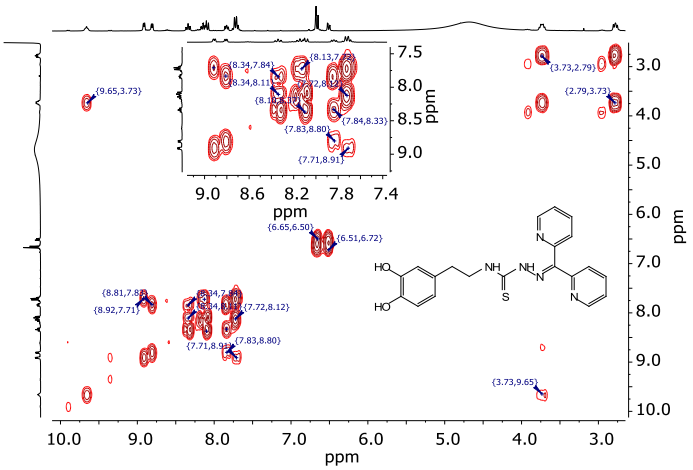


Figure 332. ^{1}H,^{1}H COSY NMR spectrum of [bis(pyridin-2-yl)methylideneamino][2-(3,4-dihydroxy phenyl)ethylamino] carbothioamide in DMSO-d_6 at 300 MHz.

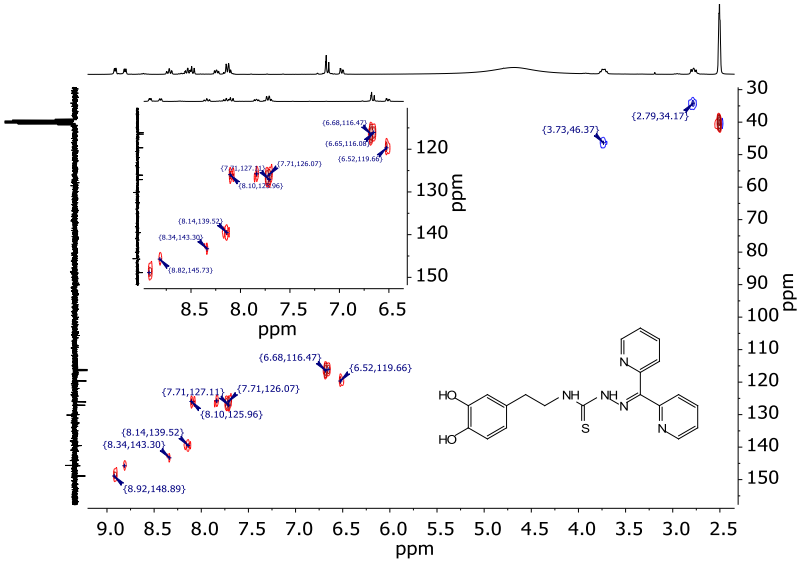


Figure 333. ^{1}H,^{13}C HMQC/HSQC NMR spectrum of [bis(pyridin-2-yl)methylideneamino][2-(3,4 dihydroxyphenyl)ethylamino] carbothioamide in DMSO-d_6 at 300 MHz.

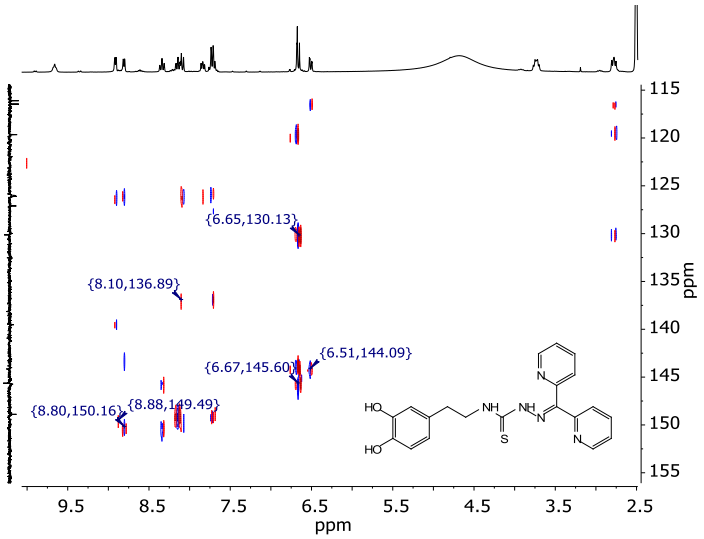


Figure 334. $^{1}H,^{13}C$ HMBC NMR spectrum of [bis(pyridin-2-yl)methylideneamino][2-(3,4 dihydroxyphenyl)ethylamino] carbothioamide in DMSO-d_6 at 300 MHz.

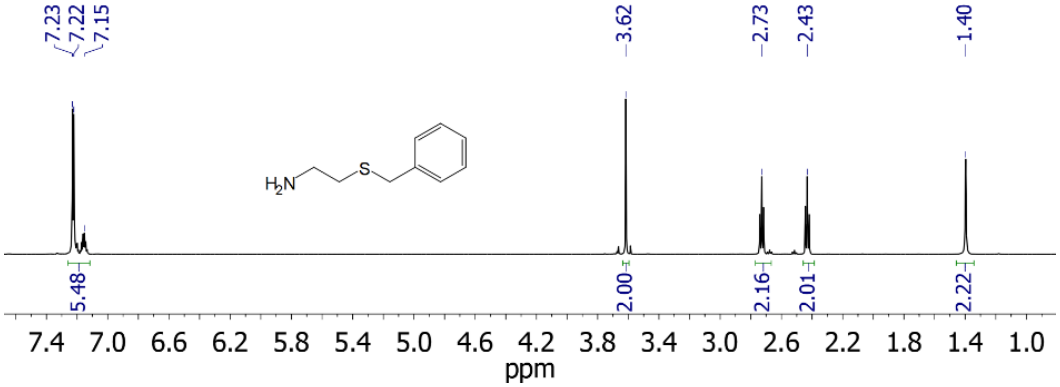


Figure 335. ^{1}H NMR spectrum of 2-benzylsulfanyl ethylamine in $CDCl_3$ at 499 MHz.

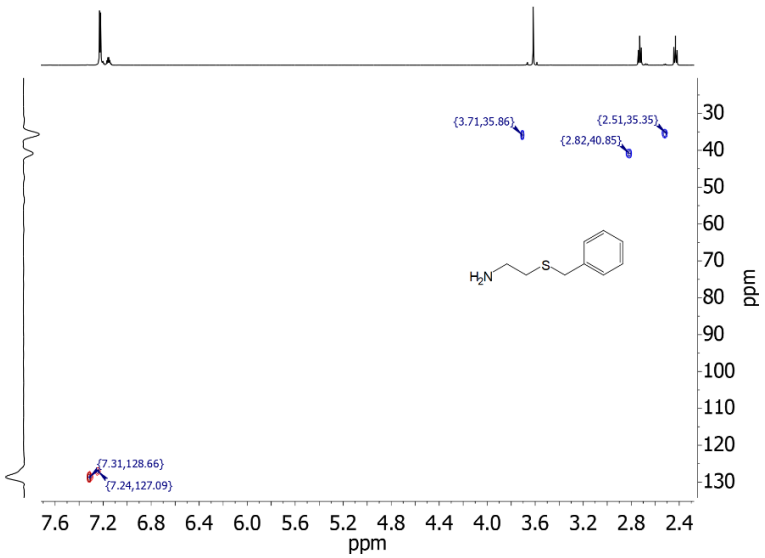


Figure 336. $^{1}H,^{13}C$ HMQC/HSQC NMR spectrum of 2-benzylsulfanyl ethylamine in $CDCl_3$ at 499 MHz.

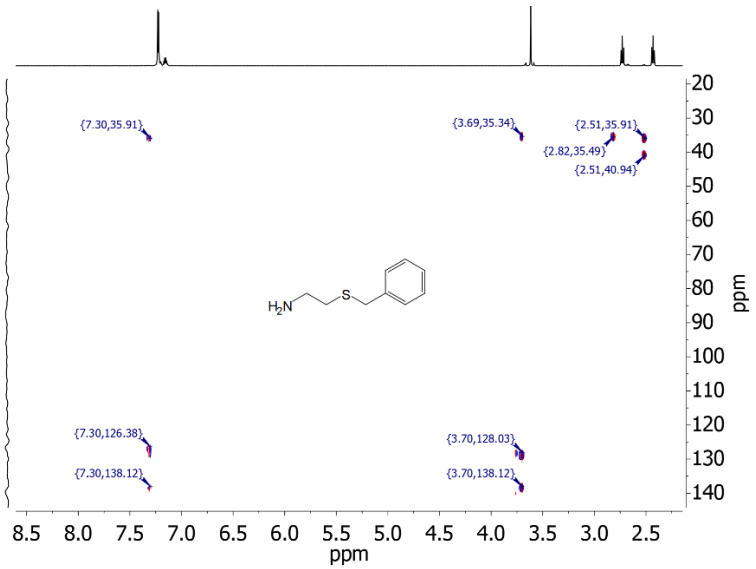


Figure 337. $^{1}H,^{13}C$ HMBC NMR spectrum of 2-benzylsulfanyl ethylamine in $CDCl_3$ at 499 MHz.

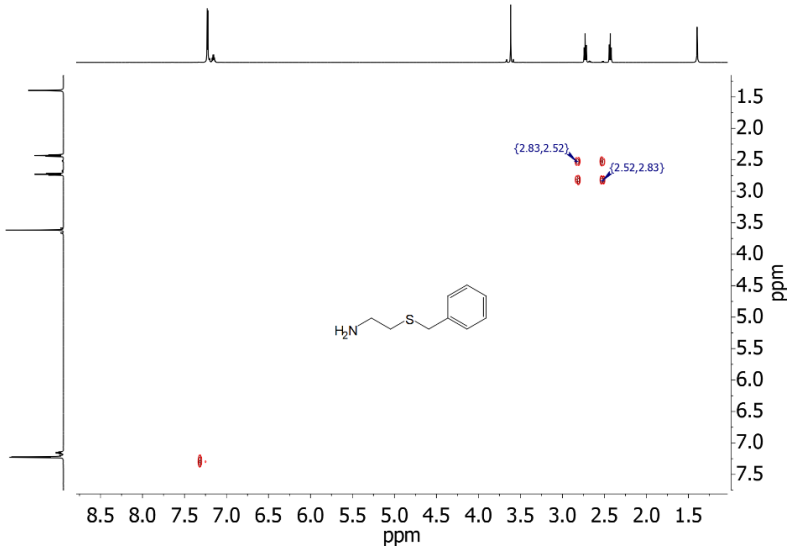


Figure 338. $^{1}H,^{1}H$ COSY NMR spectrum of 2-benzylsulfanyl ethylamine in DMSO-d_6 at 499 MHz.

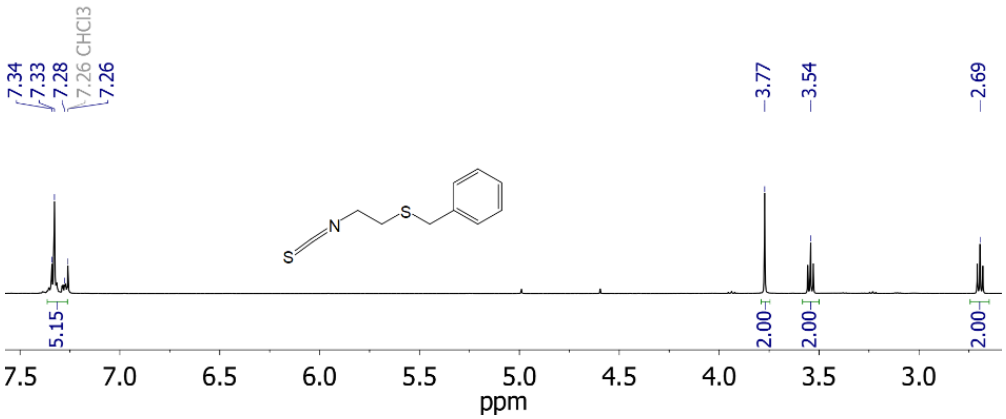


Figure 339. ^{1}H NMR spectrum of 2-benzylsulfanylethyl isothiocyanate in $CDCl_3$ at 499 MHz.

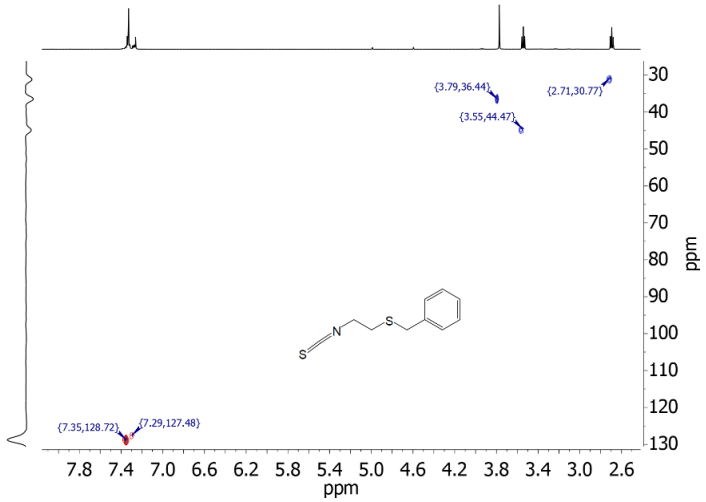


Figure 340. $^{1}H,^{13}C$ HMQC/HSQC NMR spectrum of 2-benzylsulfanylethyl isothiocyanate in $CDCl_3$ at 499 MHz.

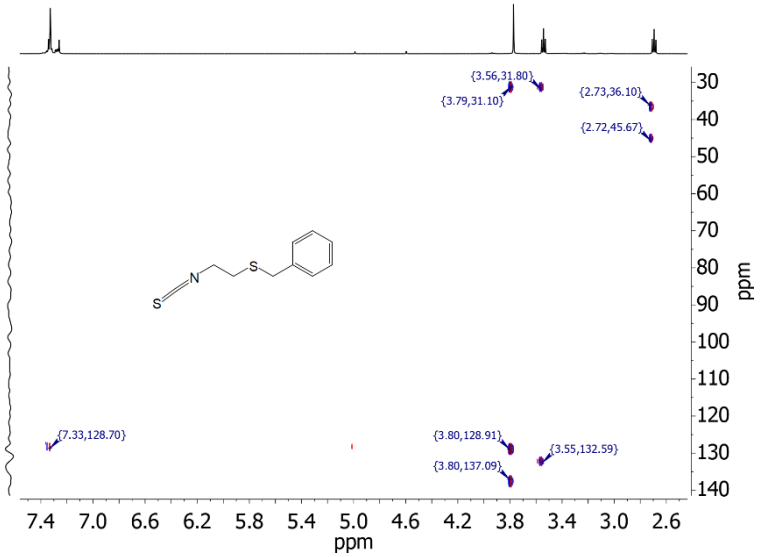


Figure 341. $^{1}H,^{13}C$ HMBC NMR spectrum of 2-benzylsulfanylethyl isothiocyanate in $CDCl_3$ at 499 MHz.

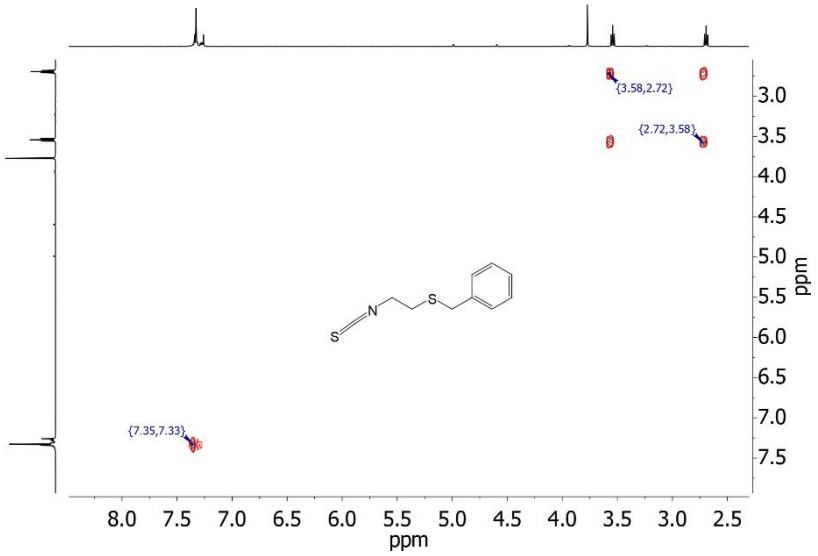


Figure 342. $^{1}H,^{1}H$ COSY NMR spectrum of 2-benzylsulfanylethyl isothiocyanate in DMSO-d_6 at 499 MHz.

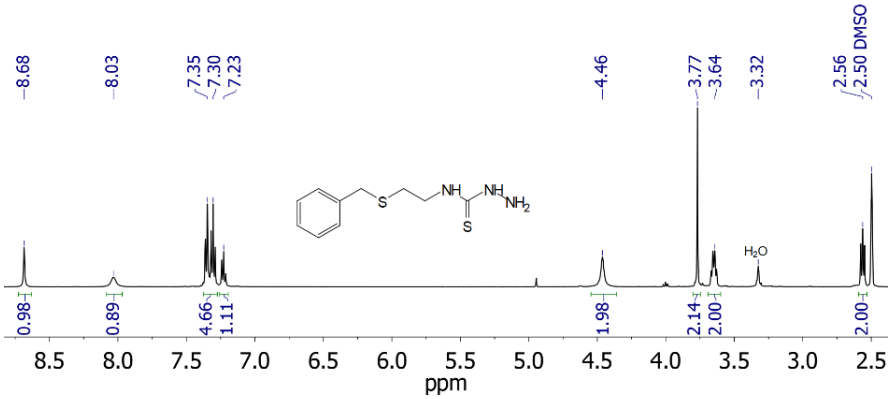


Figure 343. [1]H NMR spectrum of 4-(2-benzylsulfanylethyl)-thiosemicarbazide in DMSO-*d*$_6$ at 499 MHz.

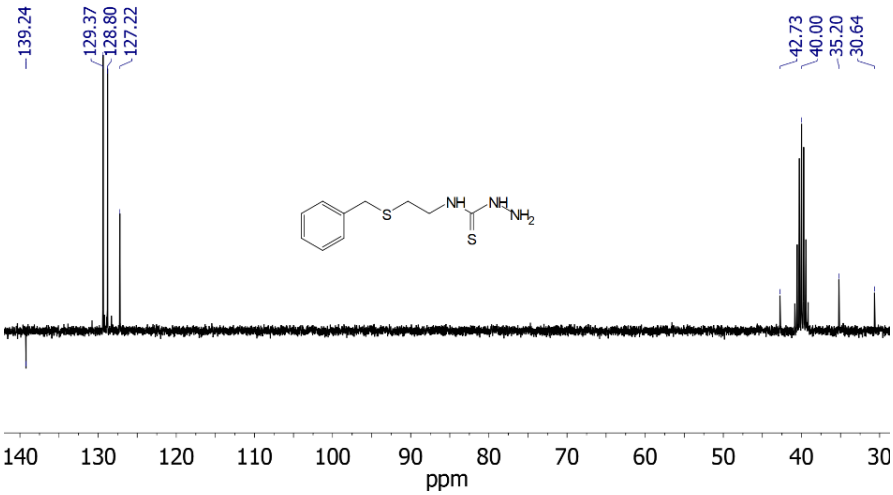


Figure 344. [13]C DEPTQ NMR spectrum of 4-(2-benzylsulfanylethyl)-thiosemicarbazide in DMSO-*d*$_6$ at 300 MHz.

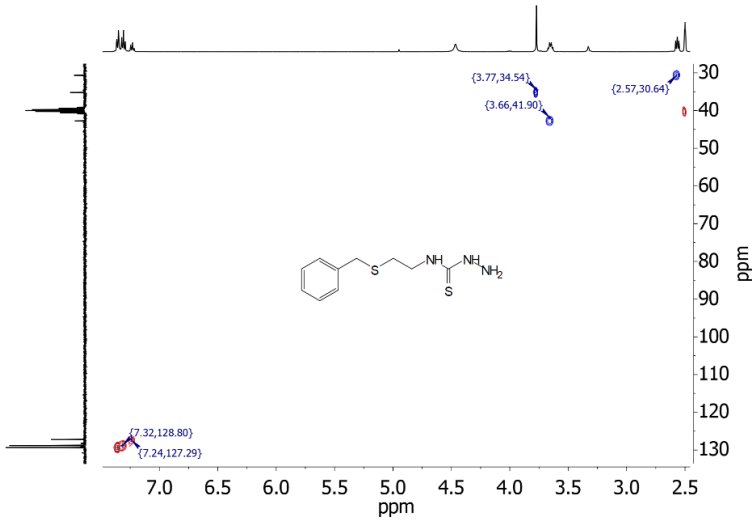


Figure 345. [1]H,[13]C HMQC/HSQC NMR spectrum of 4-(2-benzylsulfanylethyl)-thiosemicarbazide in DMSO-*d*$_6$ at 499 MHz.

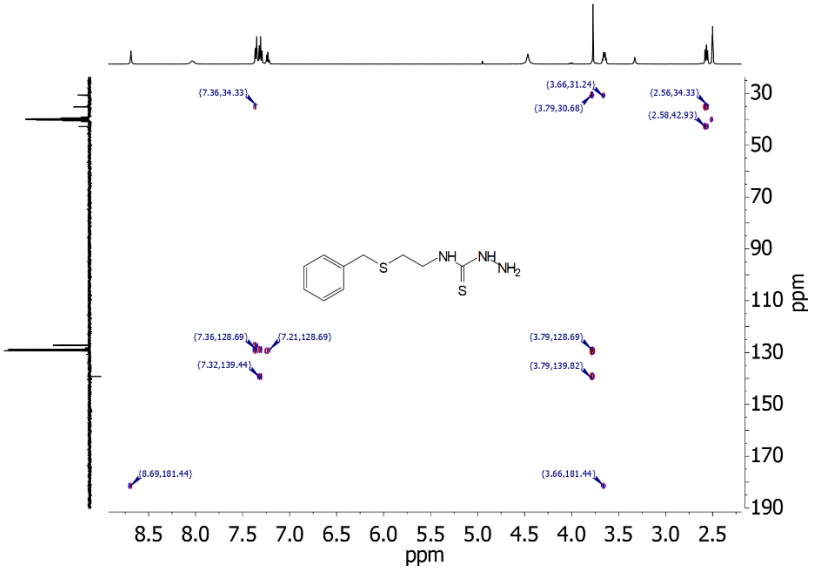


Figure 346. $^{1}H,^{13}C$ HMBC NMR spectrum of 4-(2-benzylsulfanylethyl)-thiosemicarbazide in DMSO-d_6 at 499 MHz.

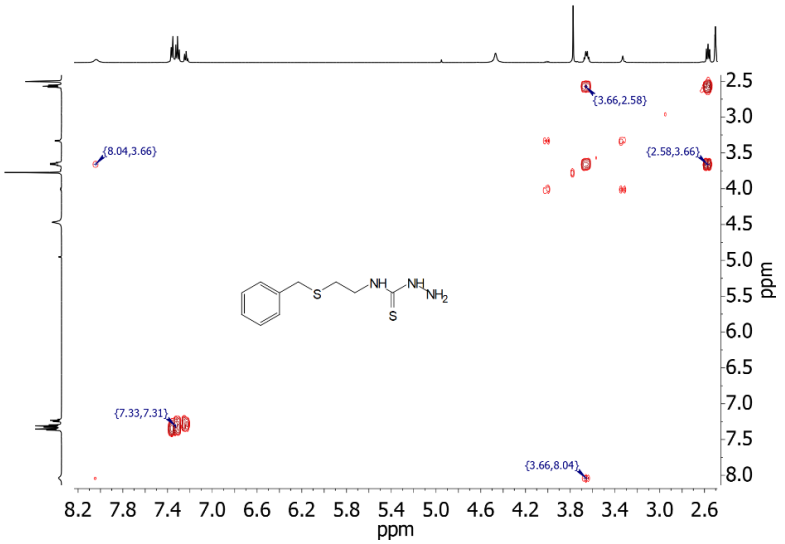


Figure 347. $^{1}H,^{1}H$ COSY NMR spectrum of 4-(2-benzylsulfanylethyl)-thiosemicarbazide in DMSO-d_6 at 499 MHz.

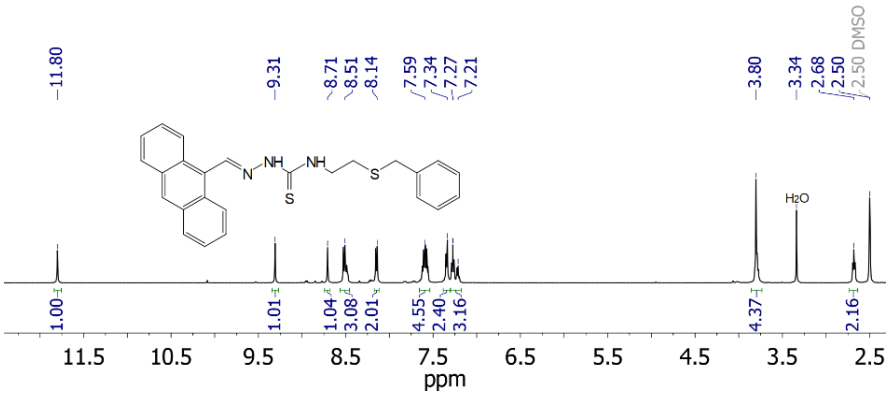


Figure 348. ^{1}H NMR spectrum of 9-anthraldehyde-4-(2-benzylsulfanylethyl)-3-thiosemicarbazone in DMSO-d_6 at 499 MHz.

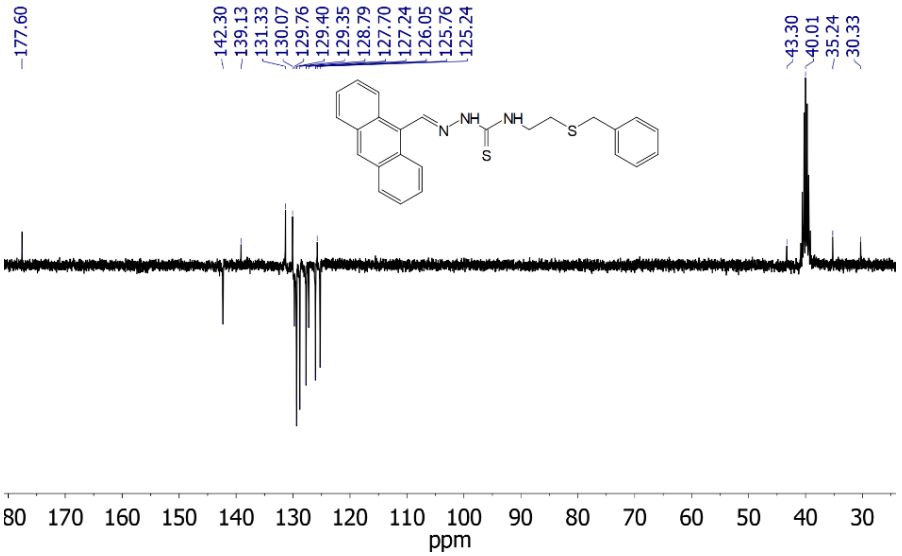


Figure 349. ^{13}C DEPTQ NMR spectrum of 9-anthraldehyde-4-(2-benzylsulfanylethyl)-3-thiosemicarbazone in DMSO-d_6 at 300 MHz.

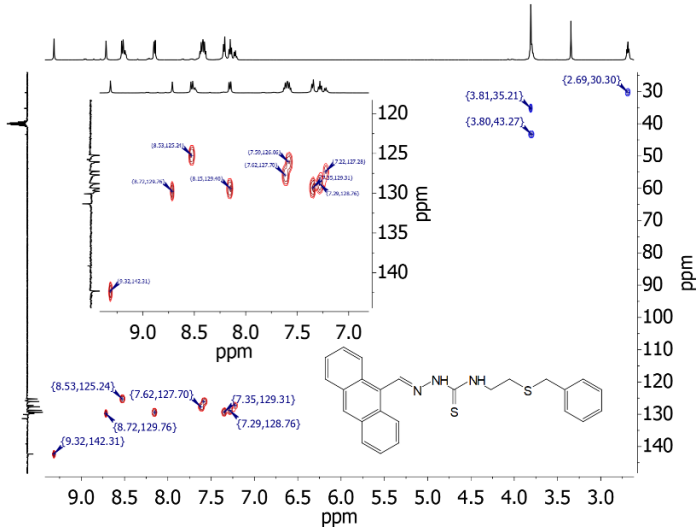


Figure 350. $^{1}H,^{13}C$ HMQC/HSQC NMR spectrum of 9-anthraldehyde-4-(2-benzylsulfanylethyl)-3-thiosemicarbazone in DMSO-d_6 at 499 MHz.

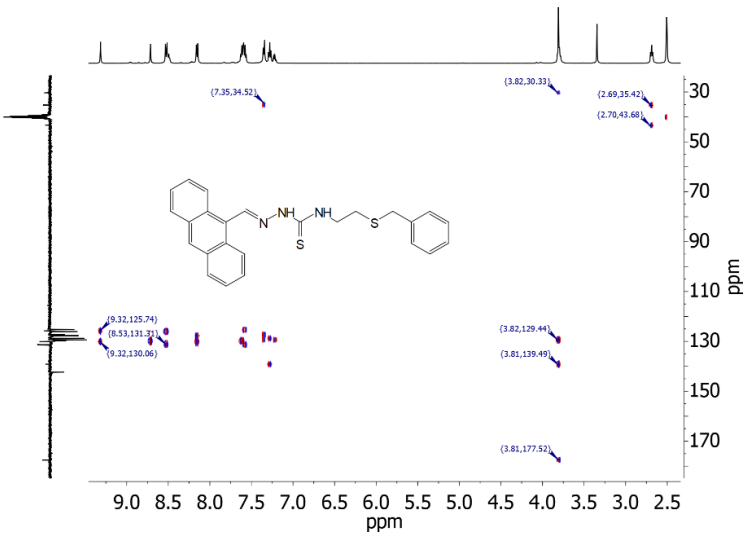


Figure 351. $^{1}H,^{13}C$ HMBC NMR spectrum of 9-anthraldehyde-4-(2-benzylsulfanylethyl)-3-thiosemicarbazone in DMSO-d_6 at 499 MHz.

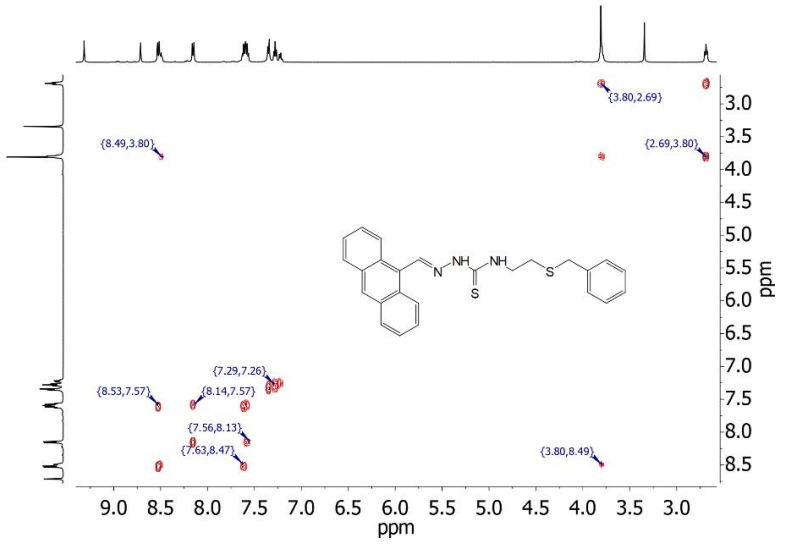


Figure 352. $^{1}H,^{1}H$ COSY NMR spectrum of 9-anthraldehyde-4-(2-benzylsulfanylethyl)-3-thiosemicarbazone in DMSO-d_6 at 499 MHz.

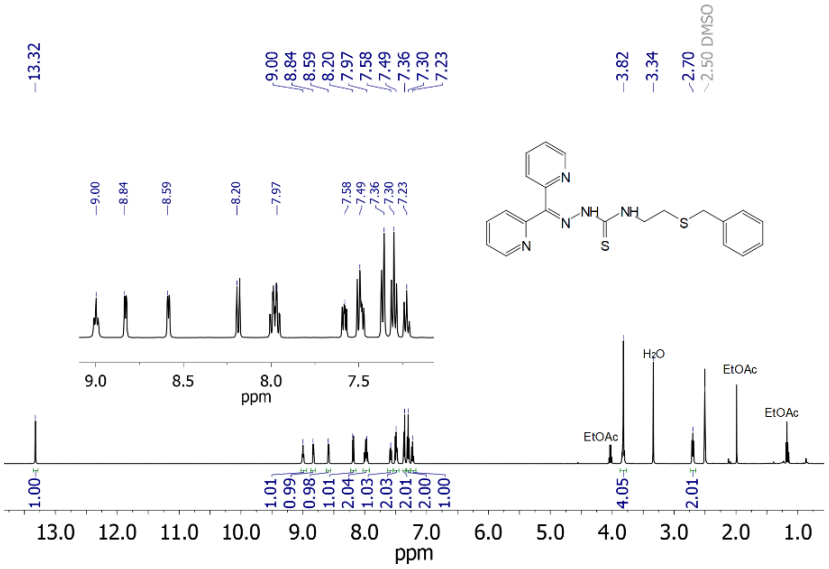


Figure 353. ^{1}H NMR spectrum of di-2-pyridylketone-4-(2-benzylsulfanylethyl)-3-thiosemicarbazone in DMSO-d_6 at 499 MHz.

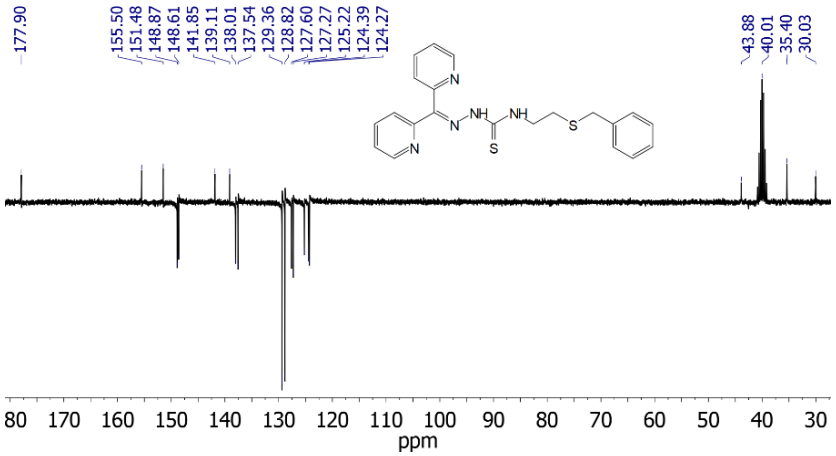


Figure 354. ^{13}C DEPTQ NMR spectrum of di-2-pyridylketone-4-(2-benzylsulfanylethyl)-3-thiosemicarbazone in DMSO-d_6 at 300 MHz.

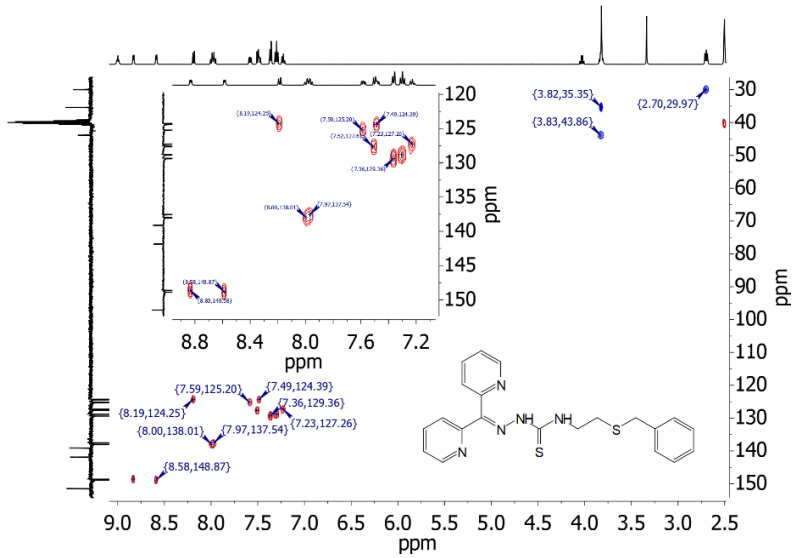


Figure 355. $^{1}H,^{13}C$ HMQC/HSQC NMR spectrum of di-2-pyridylketone-4-(2-benzylsulfanylethyl)-3-thiosemicarbazone in DMSO-d_6 at 499 MHz.

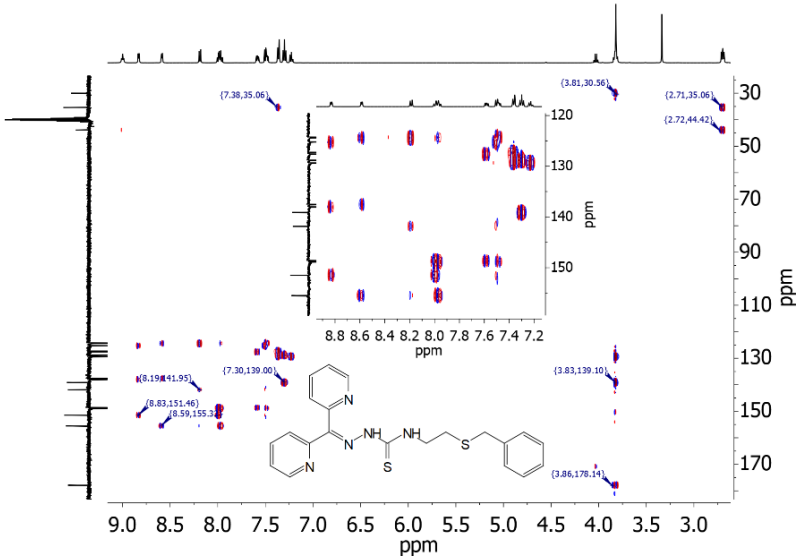


Figure 356. $^{1}H,^{13}C$ HMBC NMR spectrum of di-2-pyridylketone-4-(2-benzylsulfanylethyl)-3-thiosemicarbazone in DMSO-d_6 at 499 MHz.

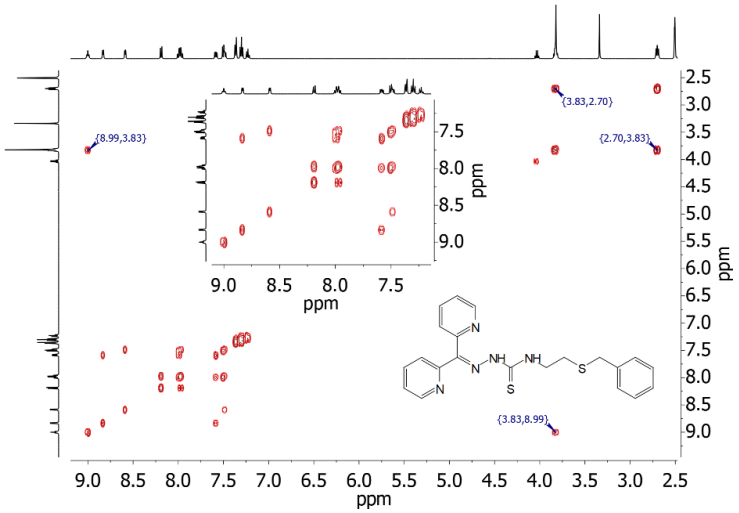


Figure 357. $^{1}H,^{1}H$ COSY NMR spectrum of di-2-pyridylketone-4-(2-benzylsulfanylethyl)-3-thiosemicarbazone in DMSO-d_6 at 499 MHz.

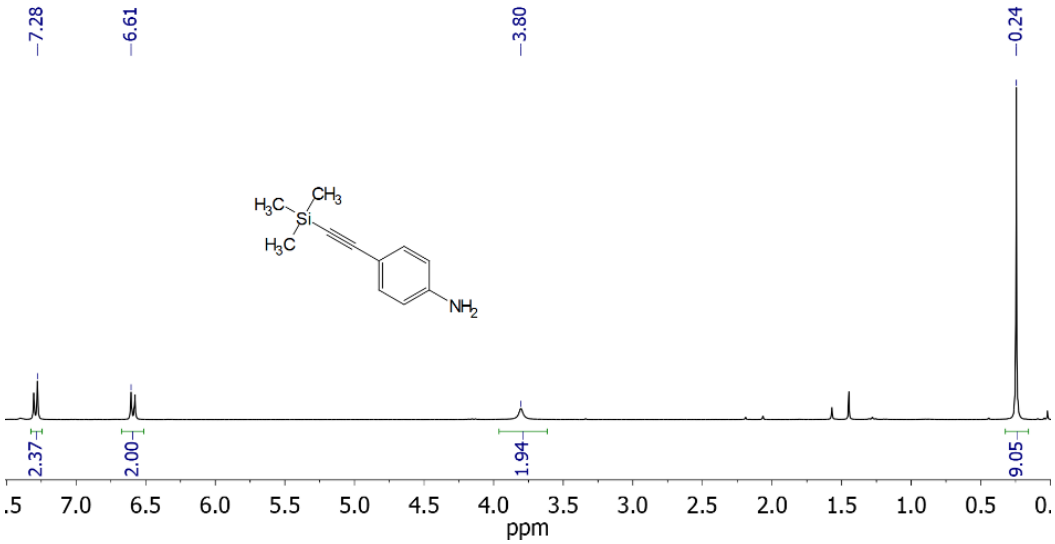


Figure 358. ^{1}H NMR spectrum of 4-[(2-trimethylsilyl) ethynyl] aniline in $CDCl_3$ at 300 MHz.

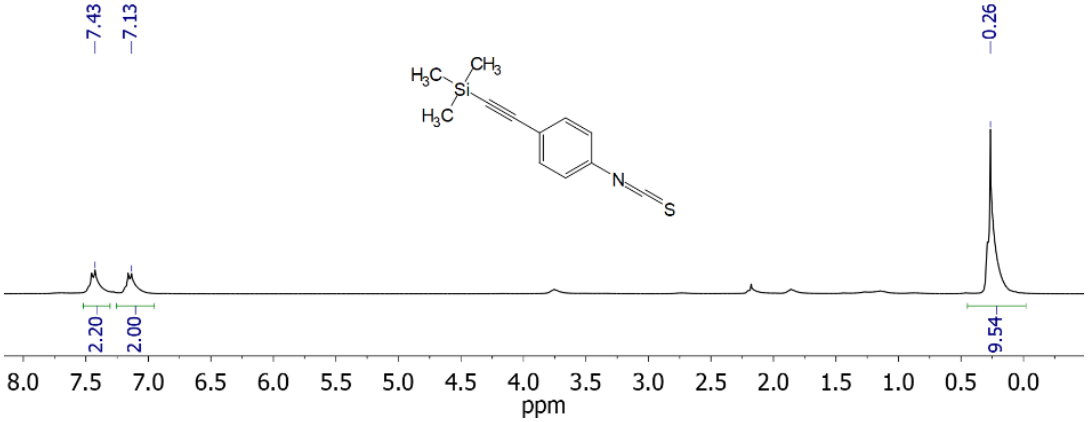


Figure 359. ^{1}H NMR spectrum of 4-[(trimethylsilyl)ethynyl] phenyl isothiocyanate in $CDCl_3$ at 300 MHz.

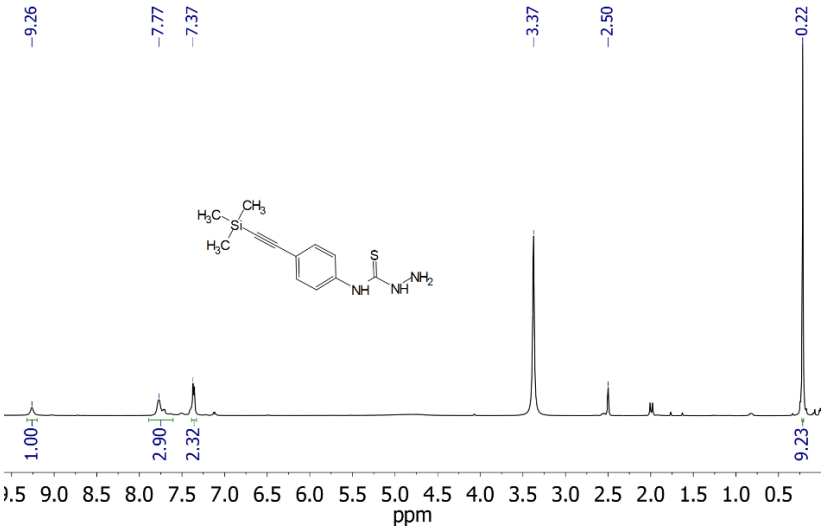


Figure 360. ^{1}H NMR spectrum of *N*-hydrazidecarbothio[4-(trimethylsilyl)ethynylphenyl]amine in DMSO-d_6 at 300 MHz.

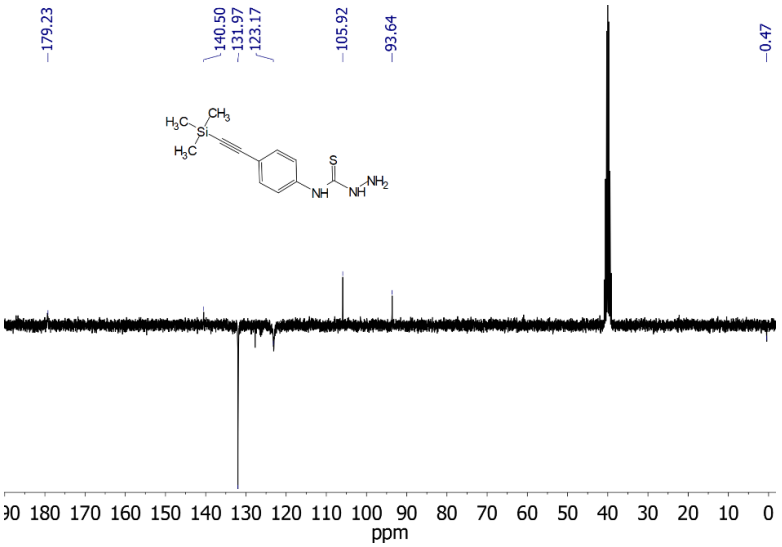


Figure 361. ^{13}C DEPTQ NMR spectrum of *N*-hydrazidecarbothio[4-(trimethylsilyl)ethynylphenyl] amine in DMSO-d_6 at 300 MHz.

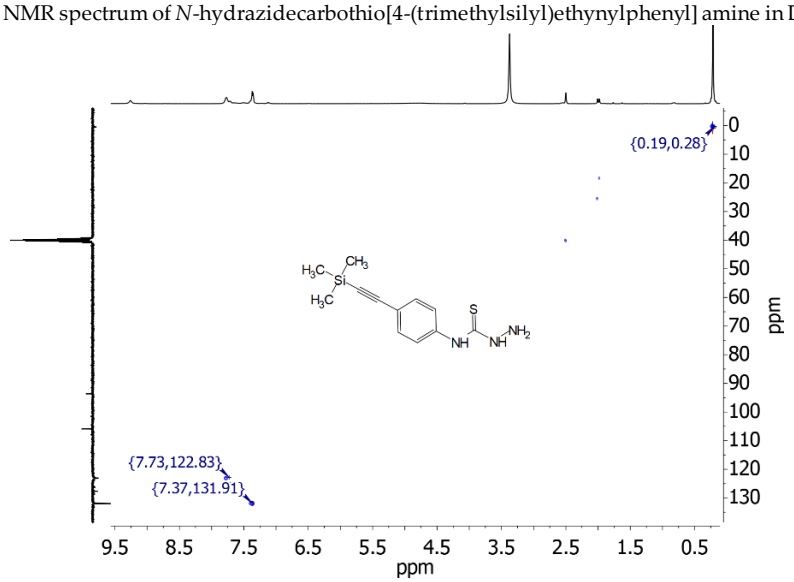


Figure 362. $^{1}H,^{13}C$ HMQC/HSQC NMR spectrum of *N*-hydrazidecarbothio[4-(trimethylsilyl)ethynyl phenyl]amine in DMSO-d_6 at 300 MHz.

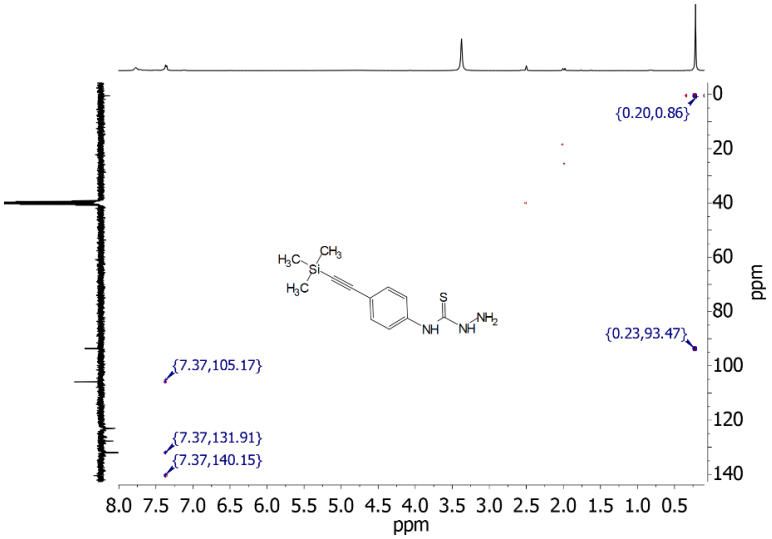


Figure 363. $^{1}H,^{13}C$ HMBC NMR spectrum of *N*-hydrazidecarbothio[4-(trimethylsilyl)ethynylphenyl] amine in DMSO-d_6 at 300 MHz.

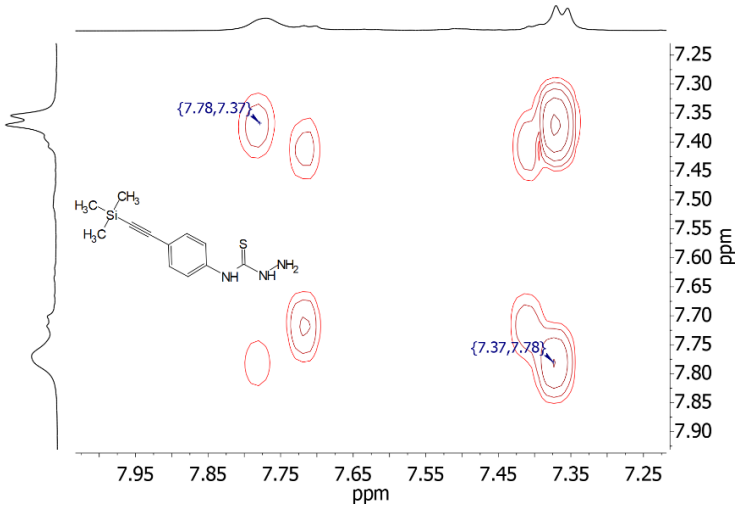


Figure 364. $^{1}H,^{1}H$ COSY NMR spectrum of *N*-hydrazidecarbothio[4-(trimethylsilyl)ethynylphenyl] amine in DMSO-d_6 at 300 MHz.

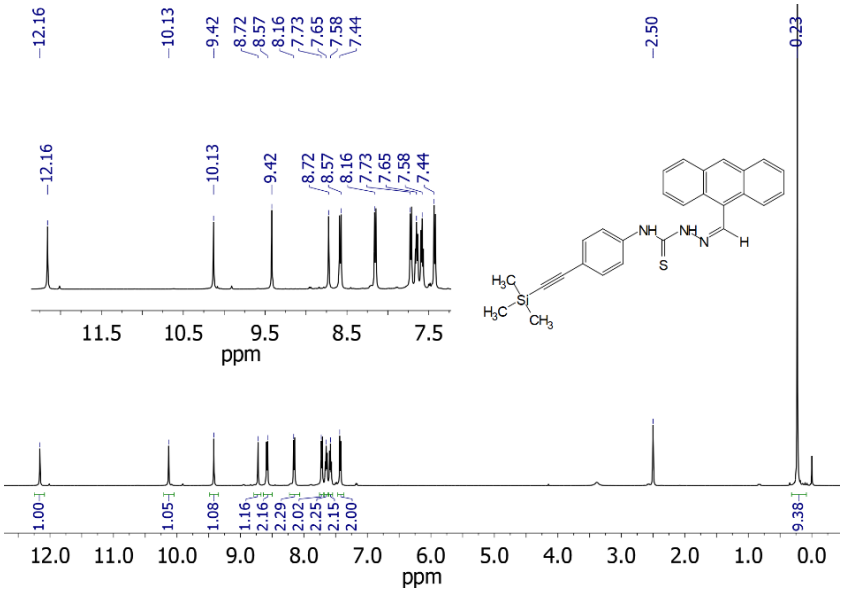


Figure 365. ^{1}H NMR spectrum of [(1*E*)-(anthracen-9-yl)methylideneamino][4-(trimethylsilyl)ethynyl-phenylamino] carbothioamide in DMSO-d_6 at 499 MHz.

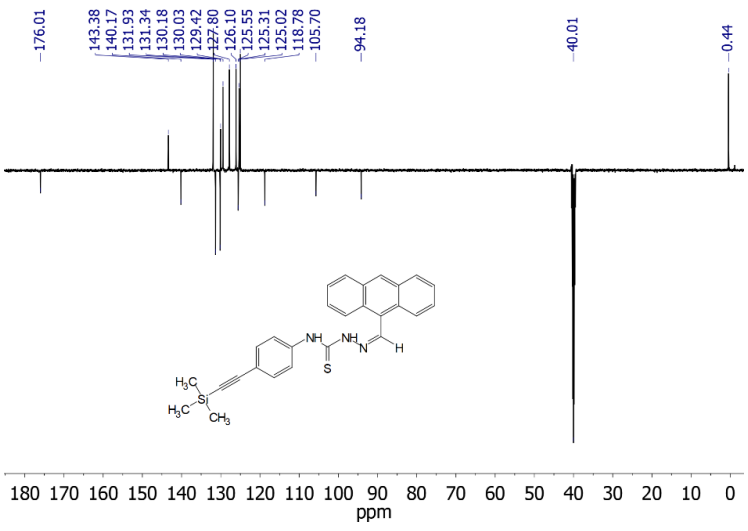


Figure 366. ^{13}C APT NMR spectrum of [(1*E*)-(anthracen-9-yl)methylideneamino][4-(trimethylsilyl)-ethynylphenylamino] carbothioamide in DMSO-d_6 at 499 MHz.

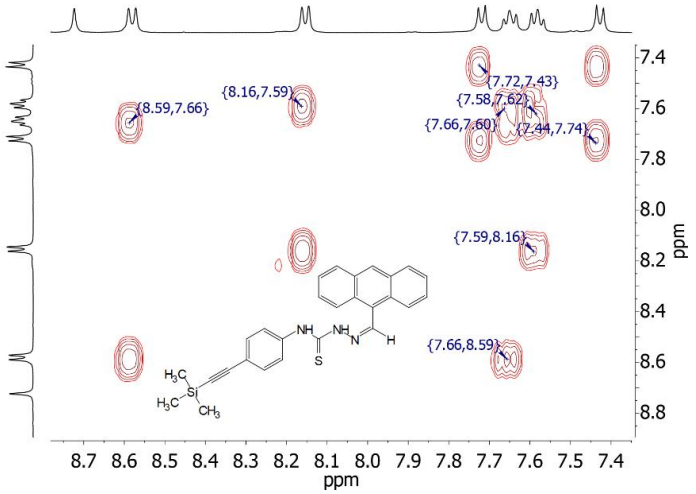


Figure 367. $^{1}H,^{1}H$ COSY NMR spectrum of [(1*E*)-(anthracen-9-yl)methylideneamino][4-(trimethylsilyl)ethynylphenylamino] carbothioamide in DMSO-d_6 at 499 MHz.

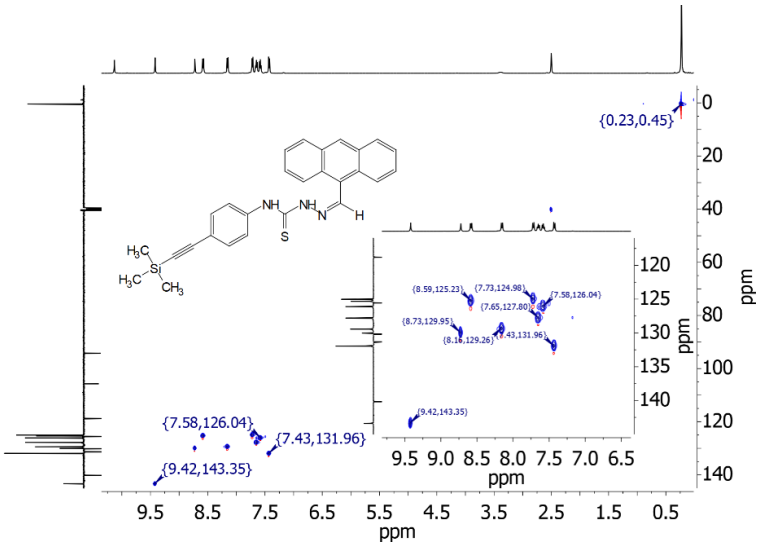


Figure 368. $^{1}H,^{13}C$ HMQC/HSQC NMR spectrum of [(1*E*)-(anthracen-9-yl)methylideneamino][4-(trimethylsilyl)ethynyl phenylamino] carbothioamide in DMSO-d_6 at 499 MHz.

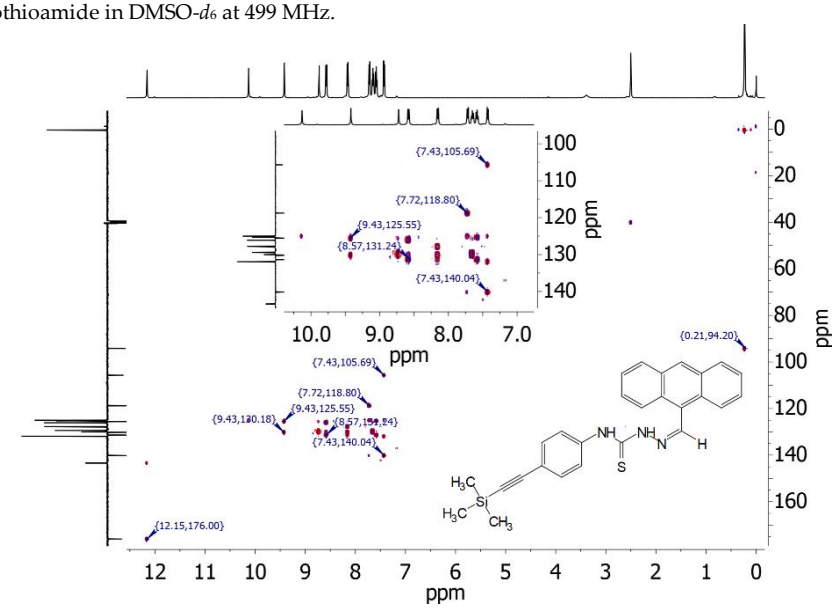


Figure 369. $^{1}H,^{13}C$ HMBC NMR spectrum of [(1*E*)-(anthracen-9-yl)methylideneamino][4-(trimethylsilyl)ethynylphenylamino] carbothioamide in DMSO-d_6 at 499 MHz.

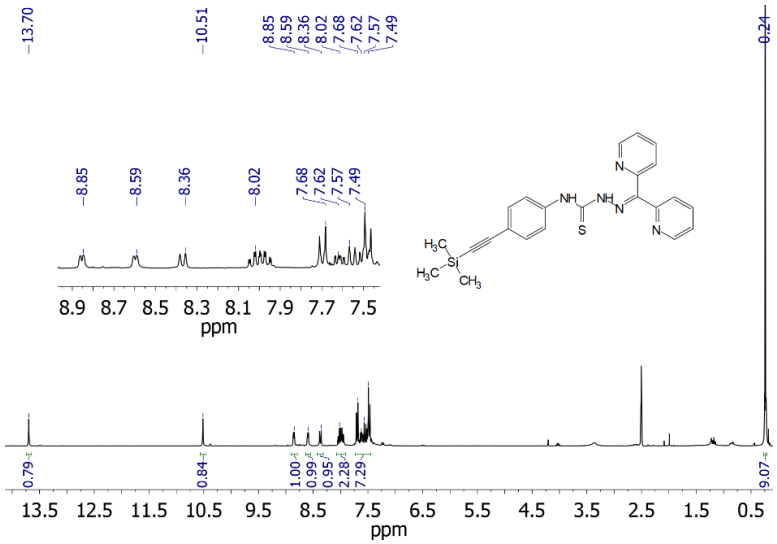


Figure 370. [1]H NMR spectrum of [bis(pyridin-2-yl)methylideneamino][4-(trimethylsilyl) ethynylphenylamino]carbothioamide in DMSO-d_6 at 300 MHz.

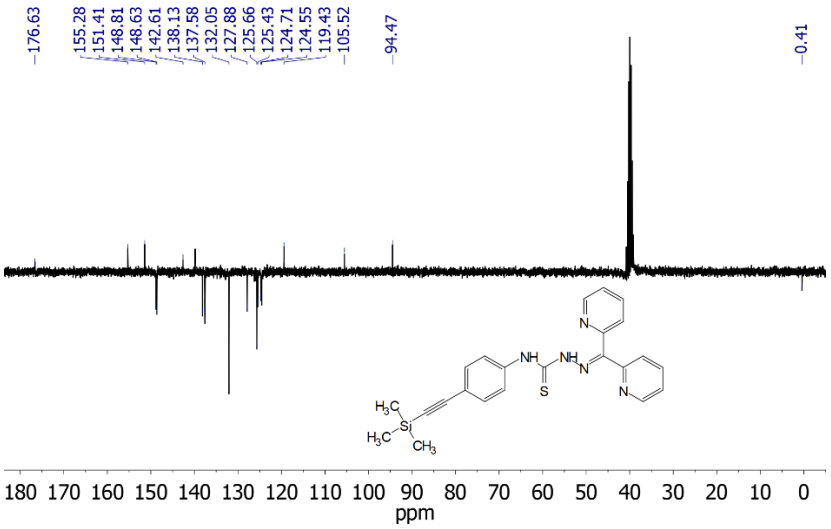


Figure 371. [13]C DEPTQ NMR spectrum of [bis(pyridin-2-yl)methylideneamino][4-(trimethylsilyl) ethynylphenylamino] carbothioamide in DMSO-d_6 at 300 MHz.

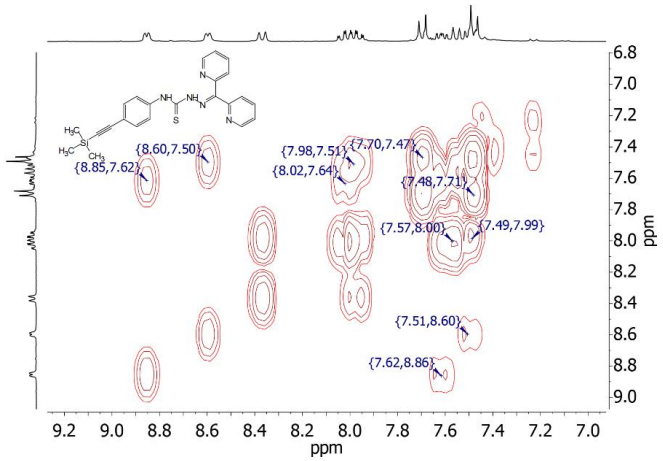


Figure 372. [1]H,[1]H COSY NMR spectrum of [bis(pyridin-2-yl)methylideneamino][4-(trimethylsilyl) ethynylphenylamino] carbothioamide in DMSO-d_6 at 300 MHz.

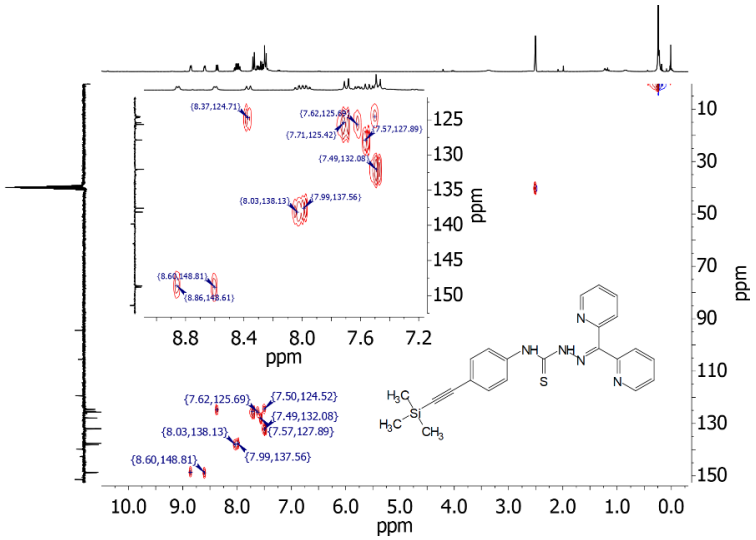


Figure 373. $^{1}H,^{13}C$ HMQC/HSQC NMR spectrum of [bis(pyridin-2-yl)methylideneamino][4-(trimethylsilyl)ethynylphenylamino] carbothioamide in DMSO-d_6 at 300 MHz.

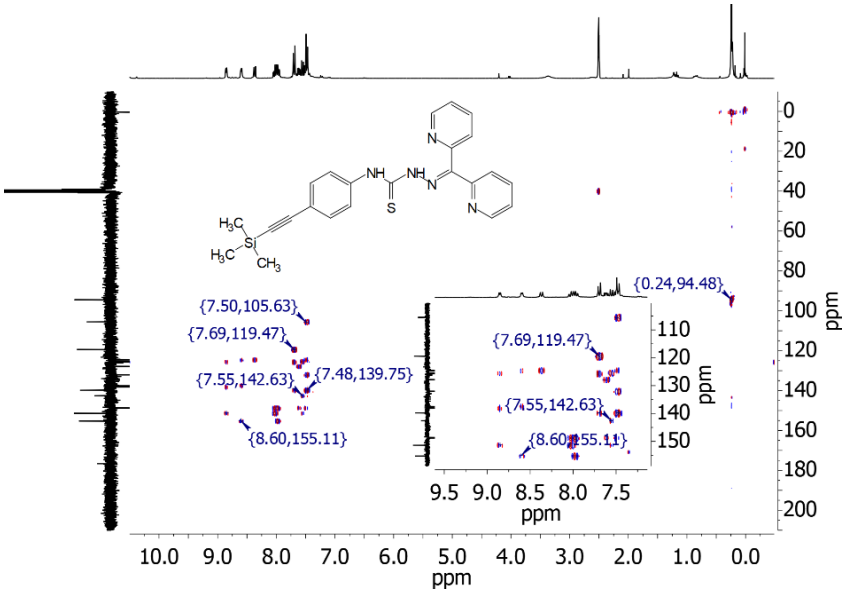


Figure 374. $^{1}H,^{13}C$ HMBC NMR spectrum of [bis(pyridin-2-yl)methylideneamino][4-(trimethylsilyl)ethynylphenylamino] carbothioamide in DMSO-d_6 at 300 MHz.

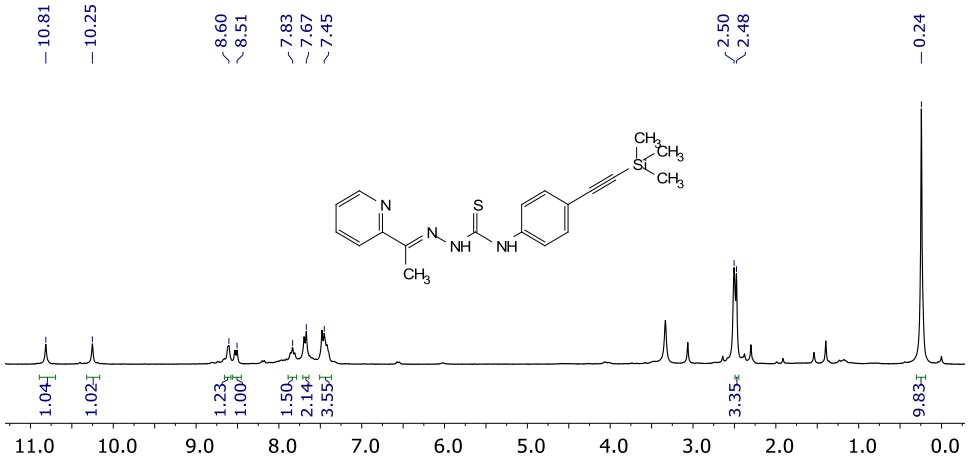


Figure 375. ^{1}H NMR spectrum of trimethyl(2-(*p*-[(*E*)-1-[1-(2-pyridyl)ethylidene]thiosemicarbazido]phenyl) ethynyl)silane in DMSO-d_6 at 300 MHz.

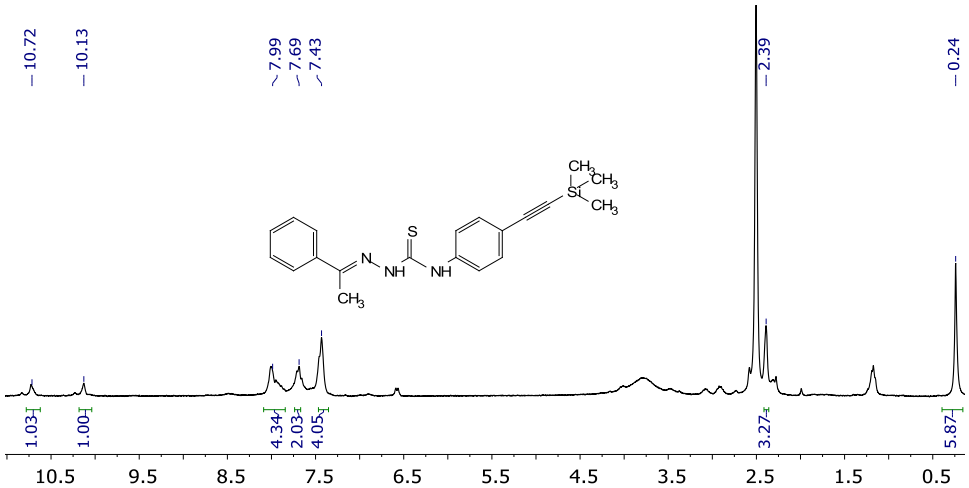


Figure 376. [1]H NMR spectrum of [(1*E*)-1-phenyleth-1-ylideneamino][4-(trimethylsilyl)ethynylphenylamino] carbothioamide in DMSO-*d*6 at 300 MHz.

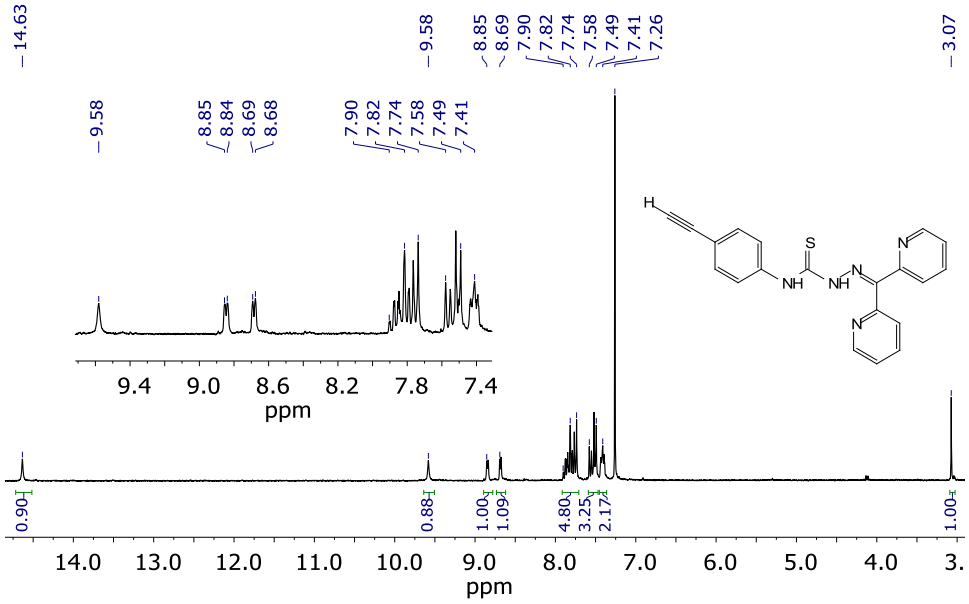


Figure 377. [1]H NMR spectrum of 1-[bis(2-pyridyl)methylene]-4-(*p*-ethynylphenyl)thiosemicarbazide in DMSO-*d*6 at 300 MHz.

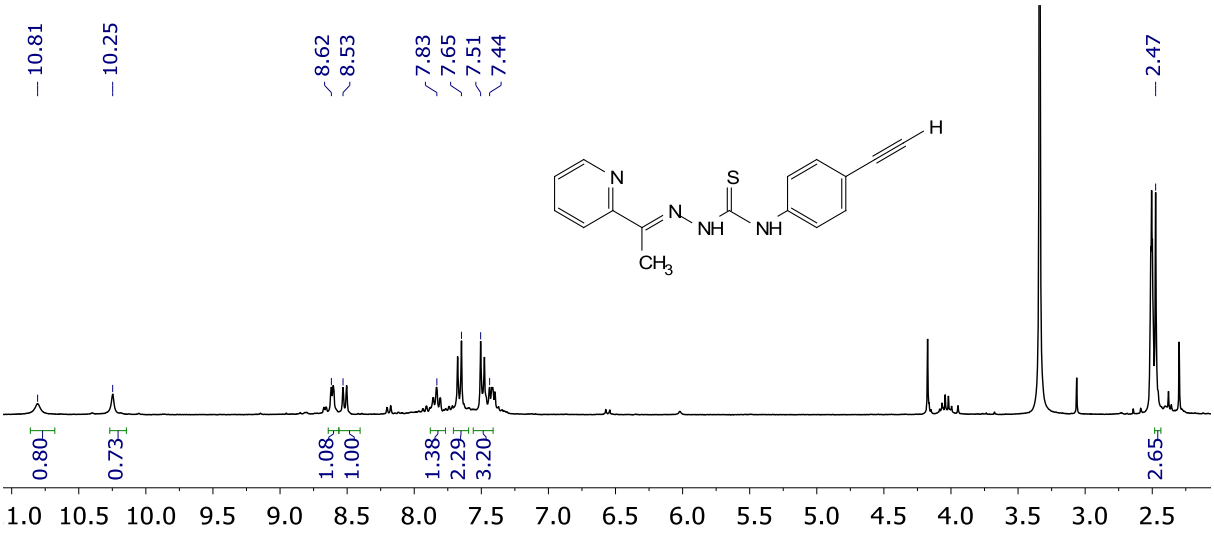


Figure 378. [1]H NMR spectrum of (*E*)-4-(*p*-ethynylphenyl)-1-[1-(2-pyridyl)ethylidene]thiosemicarbazide in DMSO-*d*6 at 300 MHz.

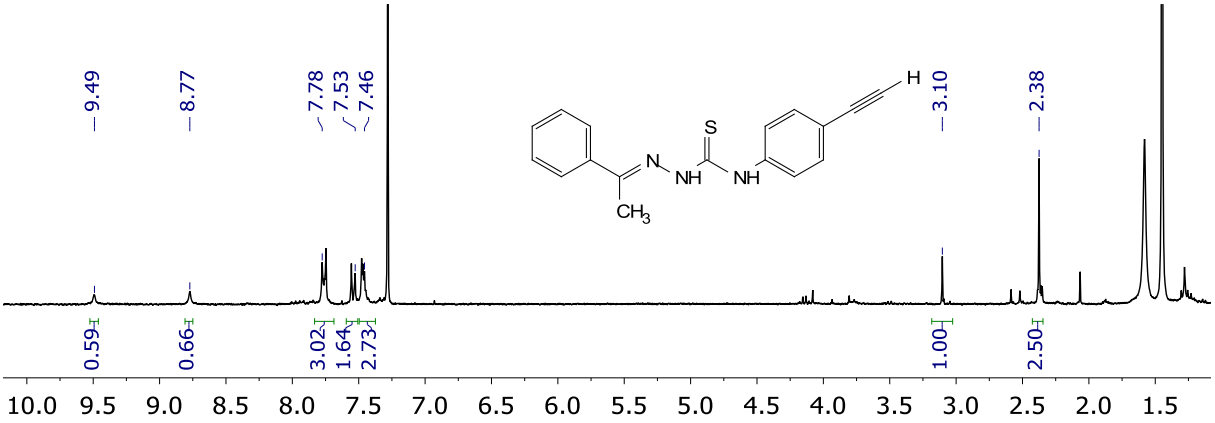


Figure 379. [1]H NMR spectrum of (*E*)-4-(*p*-ethynylphenyl)-1-(1-phenylethylidene)thiosemicarbazide in DMSO-d_6 at 300 MHz.

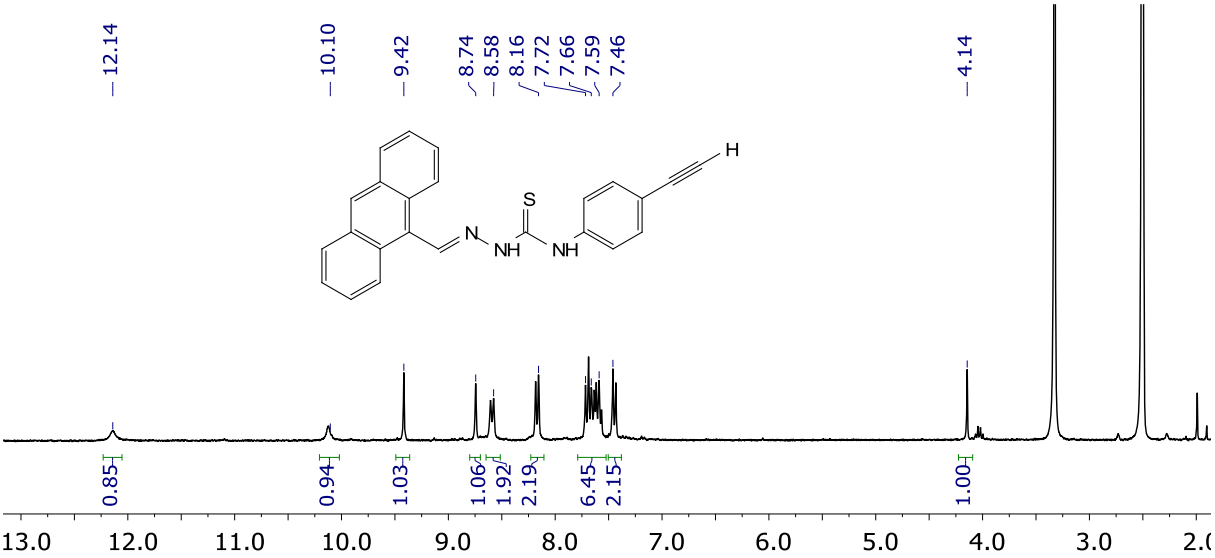


Figure 380. [1]H NMR spectrum of (*E*)-1-[(9-anthryl)methylene]-4-(*p*-ethynylphenyl)thiosemicarbazide in DMSO-d_6 at 300 MHz.

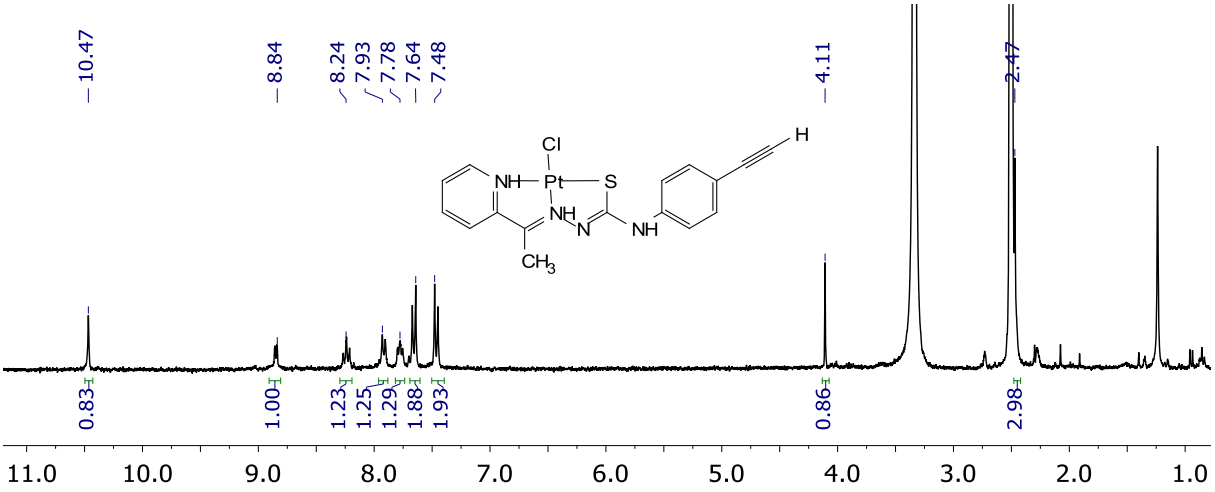


Figure 381. [1]H NMR spectrum of [Pt(MePy(TSC)PhC≡CH)Cl] in DMSO-d_6 at 300 MHz.

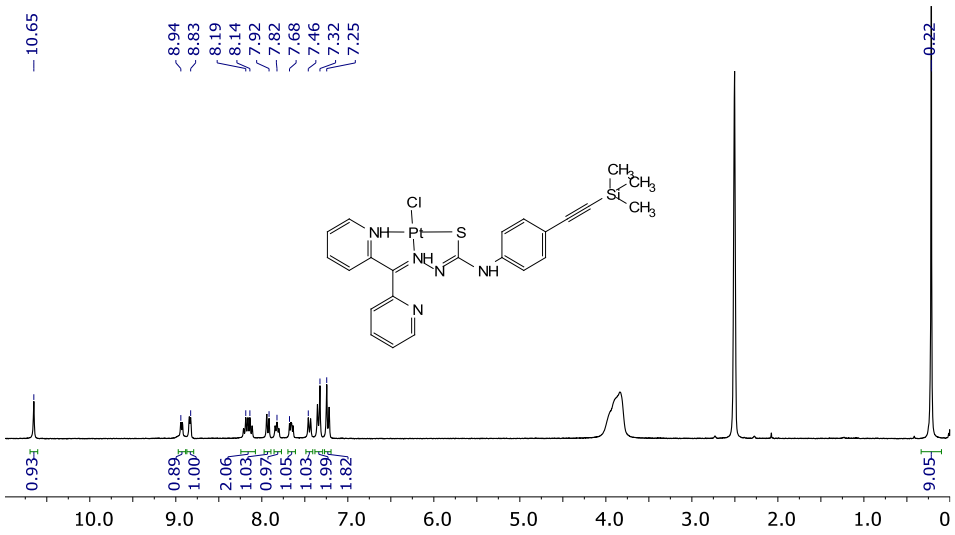


Figure 382. [1]H NMR spectrum of [Pt(Dipy(TSC)PhC≡CTMS)Cl] in DMSO-d_6 at 300 MHz.

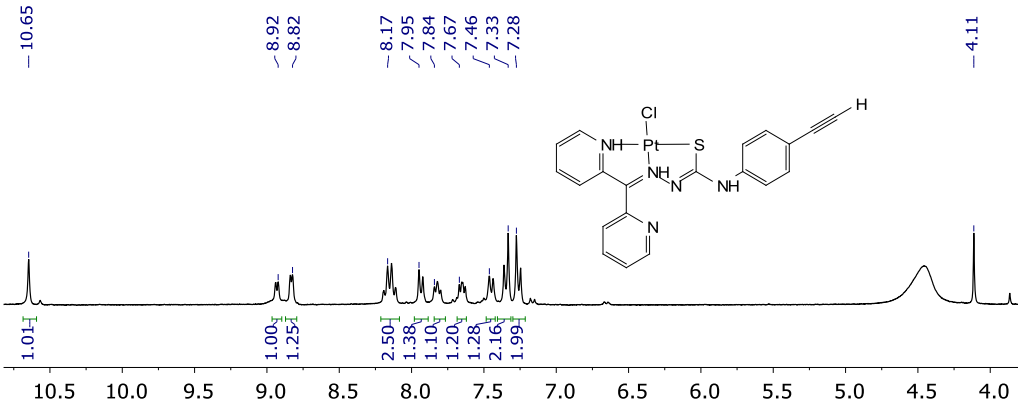


Figure 383. [1]H NMR spectrum of [Pt(Dipy(TSC)PhC≡CH)Cl] in DMSO-d_6 at 300 MHz.

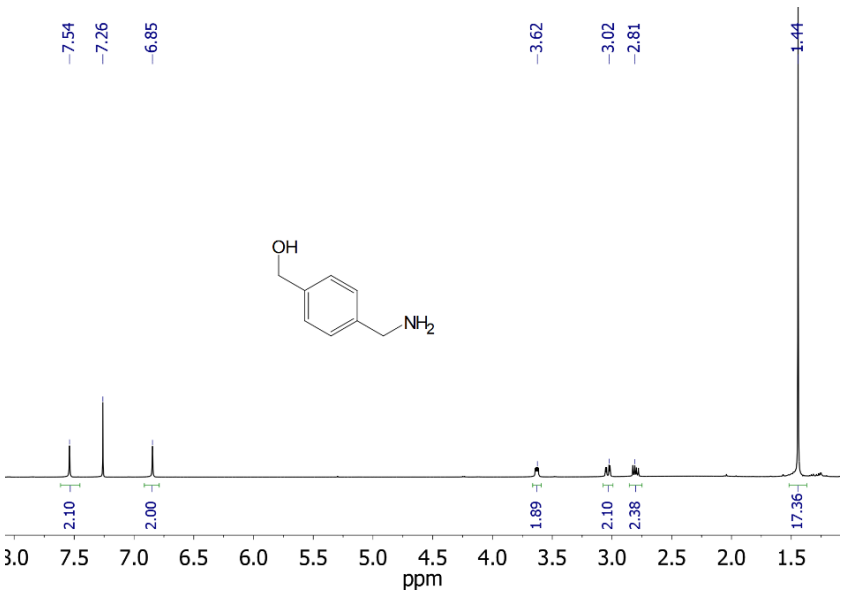


Figure 384. [1]H NMR spectrum of 4-(aminomethyl)benzyl alcohol in $CDCl_3$ at 499 MHz.

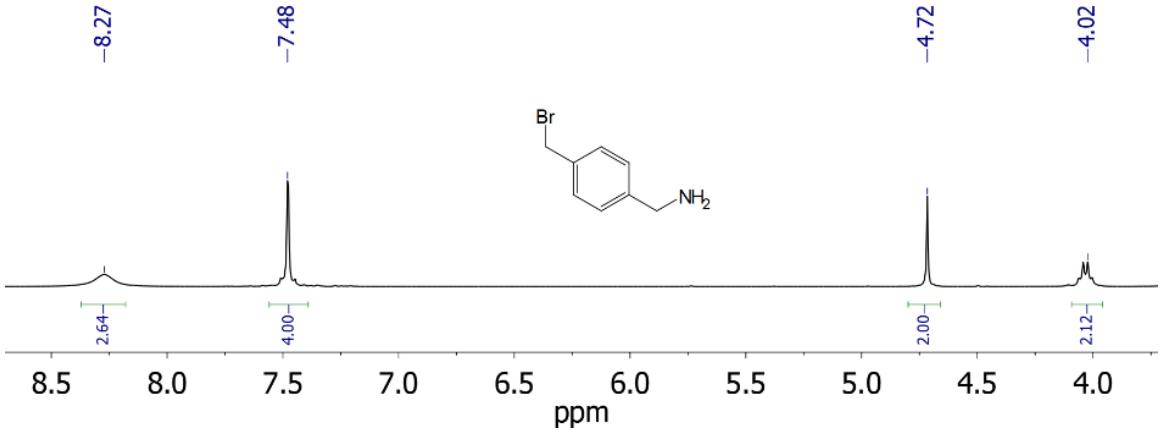


Figure 385. [1]H NMR spectrum of 4-(bromomethyl)benzylamine hydrobromide in DMSO-d_6 at 300 MHz.

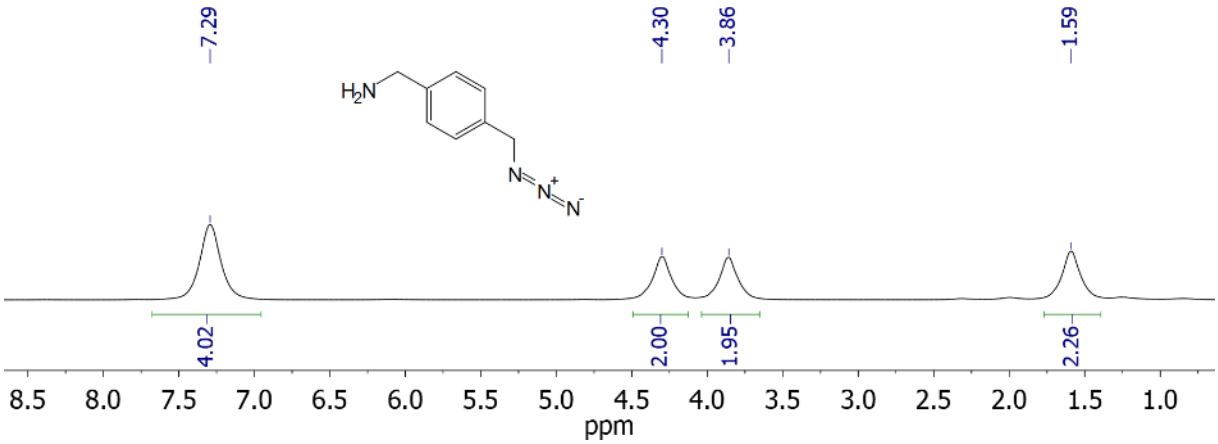


Figure 386. [1]H NMR spectrum of 4-(azidomethyl)benzylamine in DMSO-d_6 at 300 MHz.

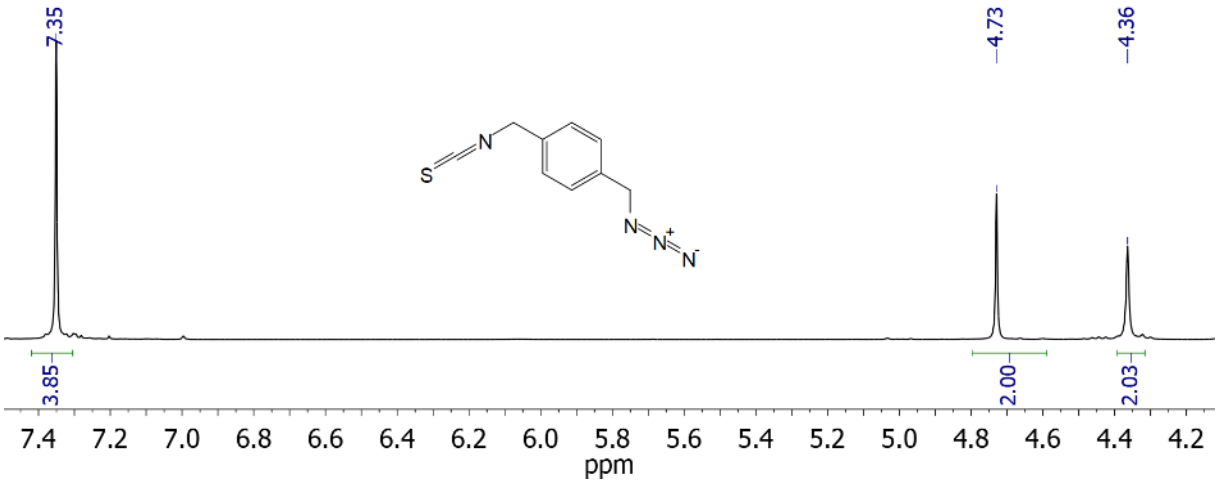


Figure 387. [1]H NMR spectrum of 1-(azidomethyl)-4-(isothiocyanatomethyl)benzene in DMSO-d_6 at 300 MHz.

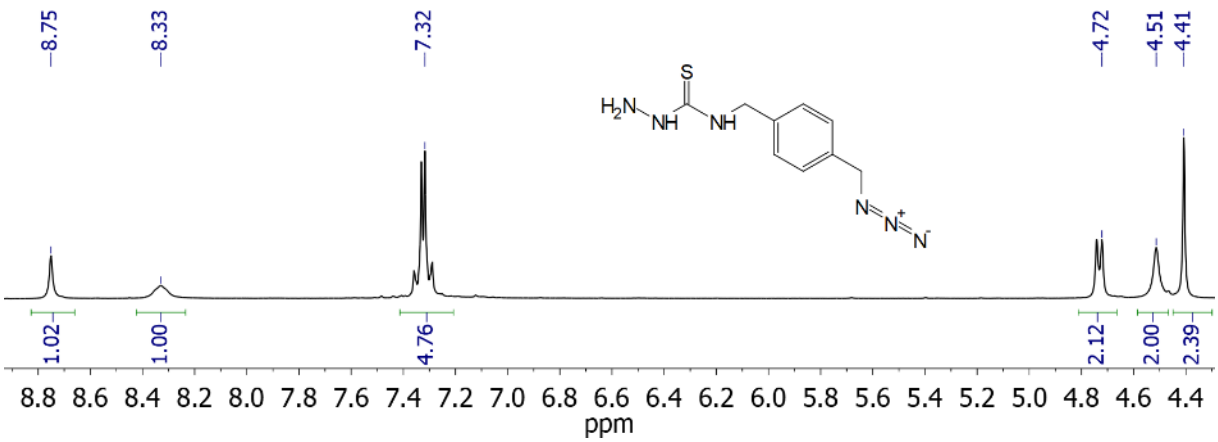


Figure 388. [1]H NMR spectrum of 4-([*p*-(azidomethyl)phenyl]methyl)thiosemicarbazide in DMSO-*d*6 at 499 MHz.

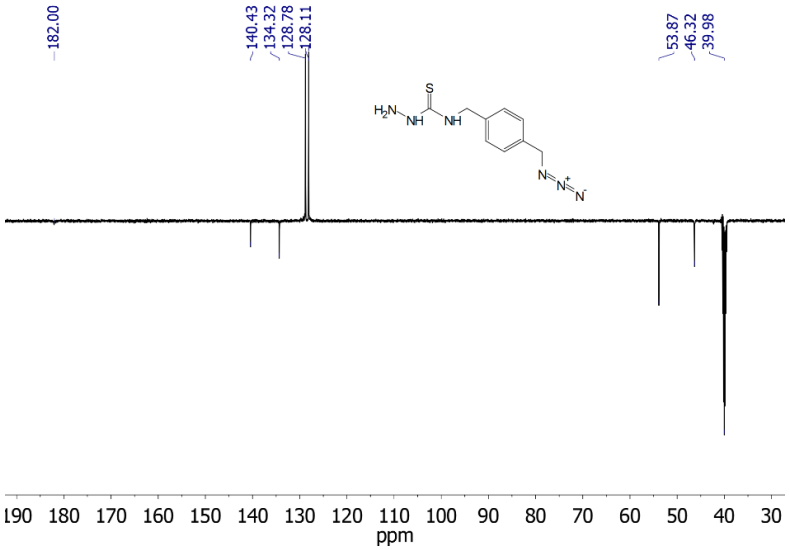


Figure 389. [13]C APT NMR spectrum of 4-([*p*-(azidomethyl)phenyl]methyl)thiosemicarbazide in DMSO-*d*6 at 499 MHz.

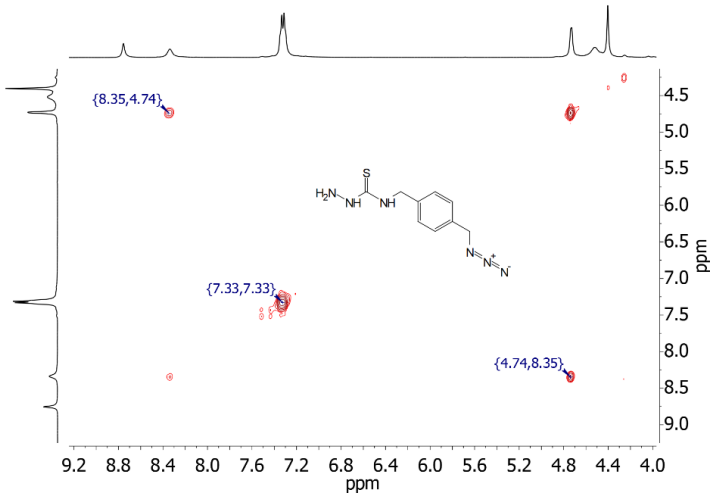


Figure 390. [1]H,[1]H COSY NMR spectrum of 4-([*p*-(azidomethyl)phenyl]methyl)thiosemicarbazide in DMSO-*d*6 at 499 MHz.

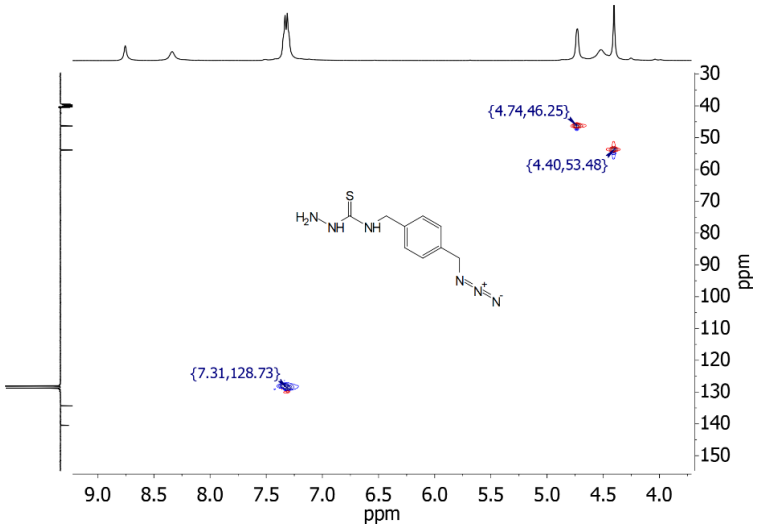


Figure 391. $^{1}H,^{13}C$ HMQC/HSQC NMR spectrum of 4-([*p*-(azidomethyl)phenyl]methyl) thiosemicarbazide in DMSO-d_6 at 499 MHz.

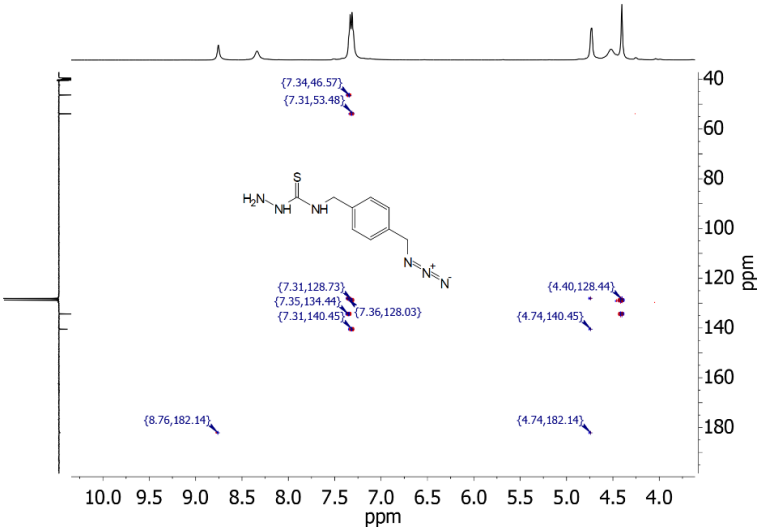


Figure 392. $^{1}H,^{13}C$ HMBC NMR spectrum of 4-([*p*-(azidomethyl)phenyl]methyl)thiosemicarbazide in DMSO-d_6 at 499 MHz.

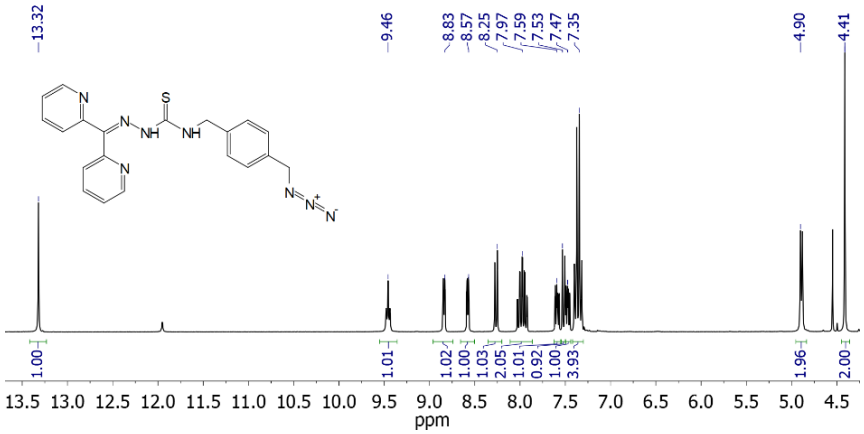


Figure 393. ^{1}H NMR spectrum of (2-[bis(pyridin-2-yl)methylidene]hydrazine)-[4-(azidomethyl) phenyl]ethanethioamide in DMSO-d_6 at 499 MHz.

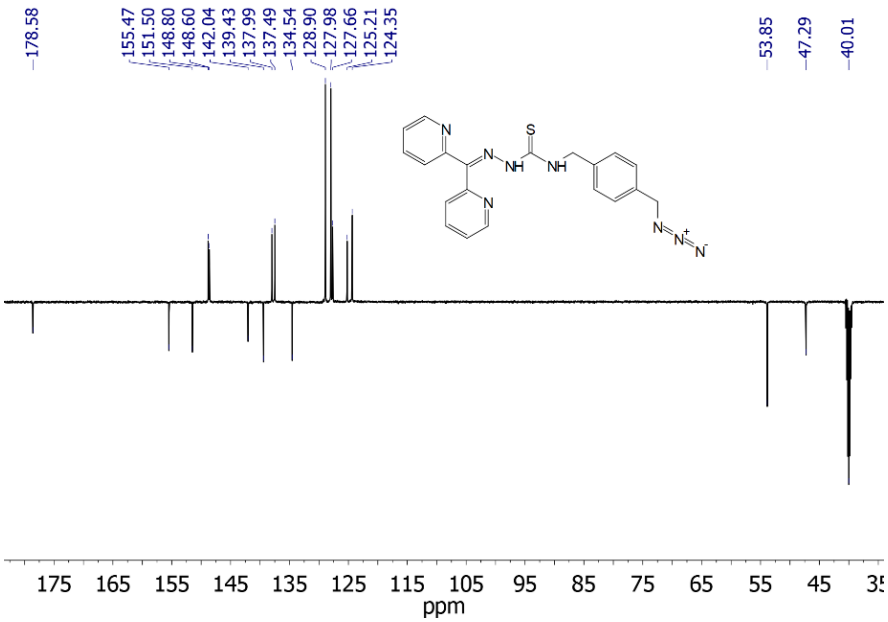


Figure 394. ^{13}C APT NMR spectrum of (2-[bis(pyridin-2-yl)methylidene]hydrazine)-[4-(azidomethyl) phenyl]ethanethioamide in DMSO-d_6 at 499 MHz.

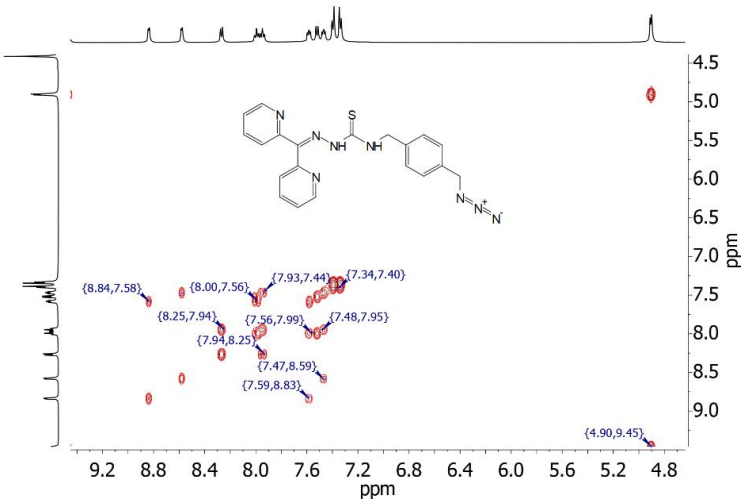


Figure 395. $^{1}H,^{1}H$ COSY NMR spectrum of (2-[bis(pyridin-2-yl)methylidene]hydrazine)-[4-(azidomethyl)phenyl]ethane thioamide in DMSO-d_6 at 499 MHz.

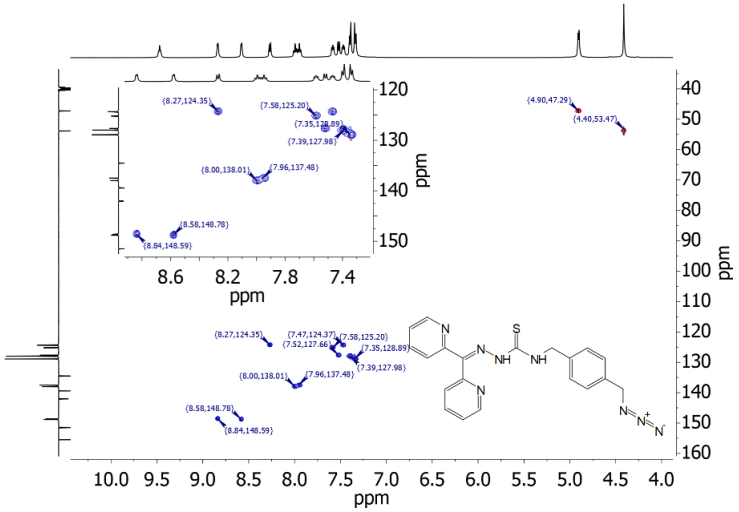


Figure 396. $^{1}H,^{13}C$ HMQC/HSQC NMR spectrum of (2-[bis(pyridin-2-yl)methylidene]hydrazine)-[4-(azidomethyl)phenyl]ethane thiolamide in DMSO-d_6 at 499 MHz.

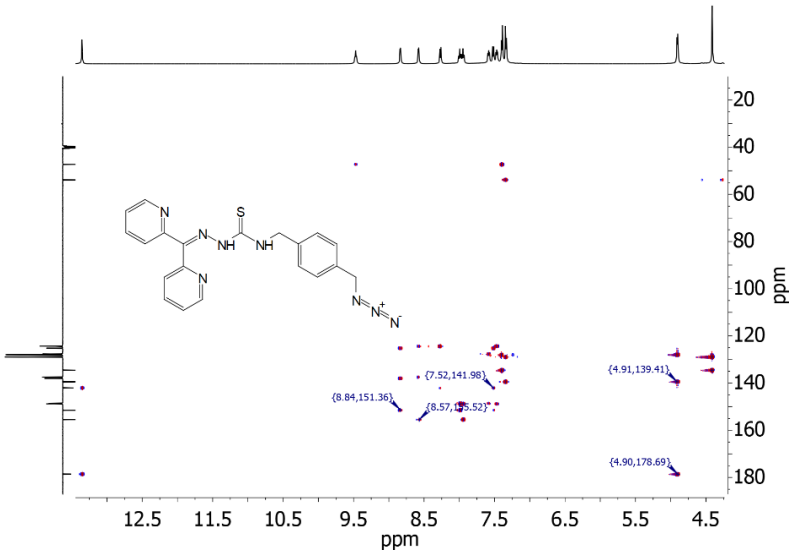


Figure 397. $^{1}H,^{13}C$ HMBC NMR spectrum of (2-[bis(pyridin-2-yl)methylidene]hydrazine)-[4-(azidomethyl)phenyl]ethane thioamide in DMSO-d_6 at 499 MHz.

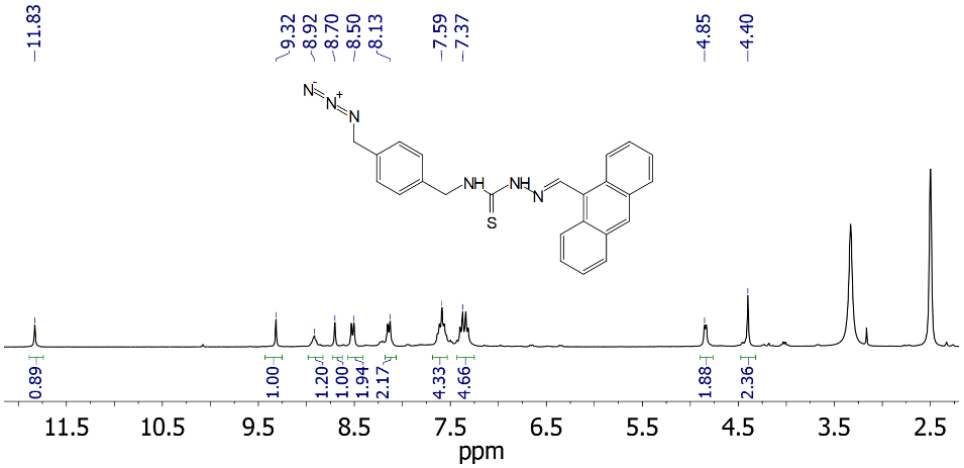


Figure 398. ^{1}H NMR spectrum of [(2*E*)-2-[(anthracen-9-yl)methylidene]hydrazino]-[4-(azidomethyl) phenyl]ethanethioamide in DMSO-d_6 at 300 MHz.

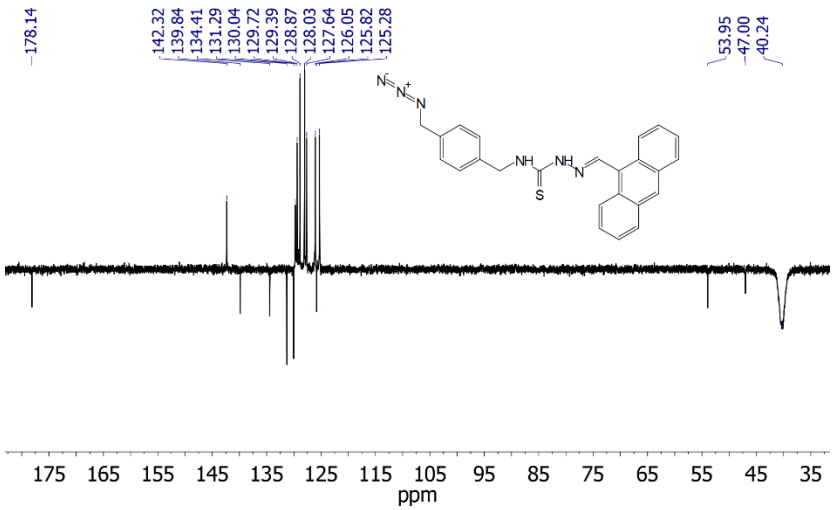


Figure 399. ^{13}C DEPTQ NMR spectrum of [(2*E*)-2-[(anthracen-9-yl)methylidene]hydrazino]-[4-(azidomethyl)phenyl]ethane thioamide in DMSO-d_6 at 300 MHz.

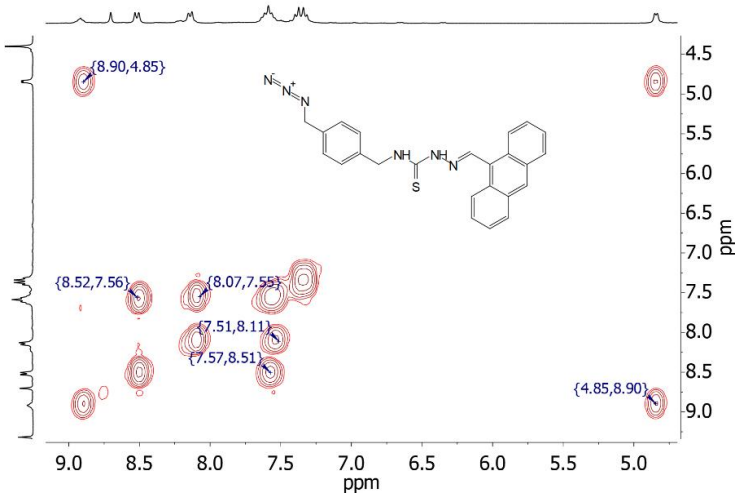


Figure 400. $^{1}H,^{1}H$ COSY NMR spectrum of [(2*E*)-2-[(anthracen-9-yl)methylidene]hydrazino]-[4-(azidomethyl)phenyl]ethane thioamide in DMSO-d_6 at 300 MHz.

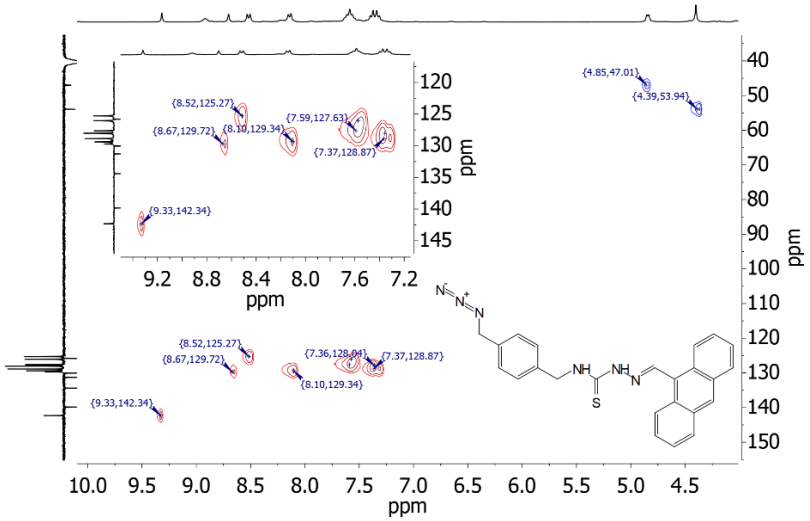


Figure 401. $^{1}H,^{13}C$ HMQC/HSQC NMR spectrum of [(2*E*)-2-[(anthracen-9-yl)methylidene] hydrazino]-[4-(azidomethyl)phenyl] ethanethioamide in DMSO-d_6 at 300 MHz.

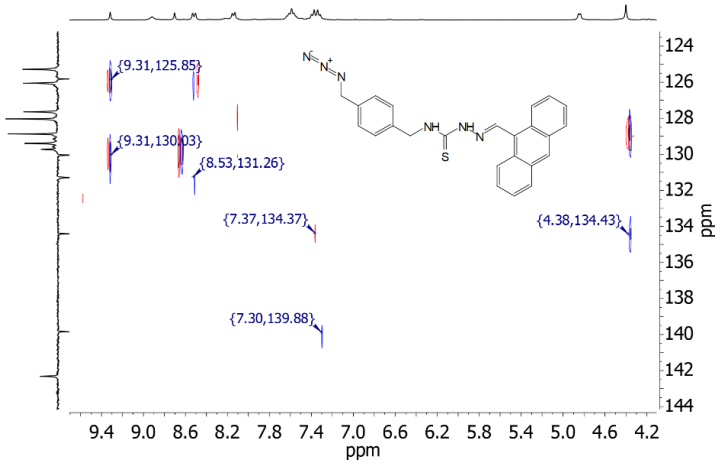


Figure 402. $^{1}H,^{13}C$ HMBC NMR spectrum of [(2*E*)-2-[(anthracen-9-yl)methylidene]hydrazino]-[4-(azidomethyl)phenyl]ethane thioamide in DMSO-d_6 at 300 MHz.

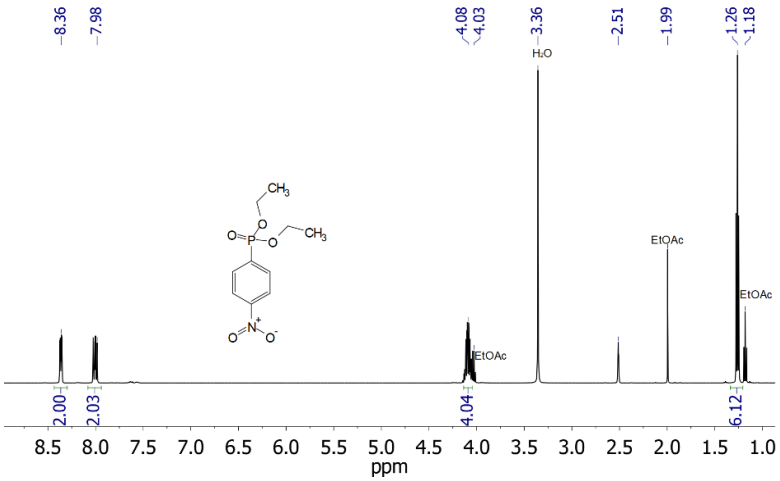


Figure 403. [1]H NMR spectrum of diethyl(4-nitrophenyl)phosphonate in DMSO-*d*6 at 499 MHz.

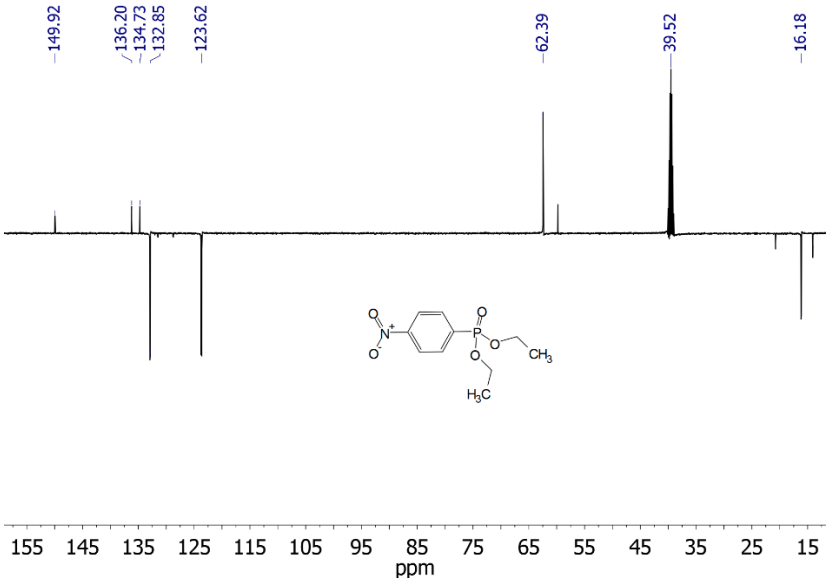


Figure 404. [13]C APT NMR spectrum of diethyl(4-nitrophenyl)phosphonate in DMSO-*d*6 at 499 MHz.

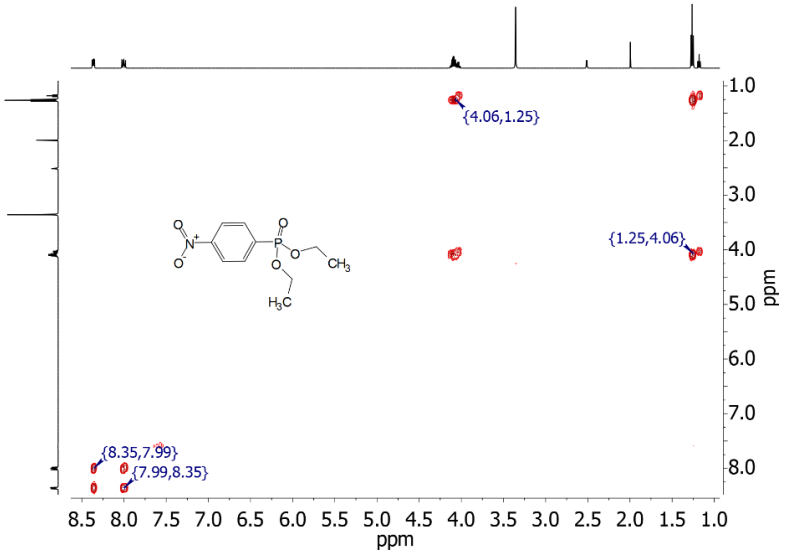


Figure 405. [1]H,[1]H COSY NMR spectrum of diethyl(4-nitrophenyl)phosphonate DMSO-*d*6 at 499 MHz.

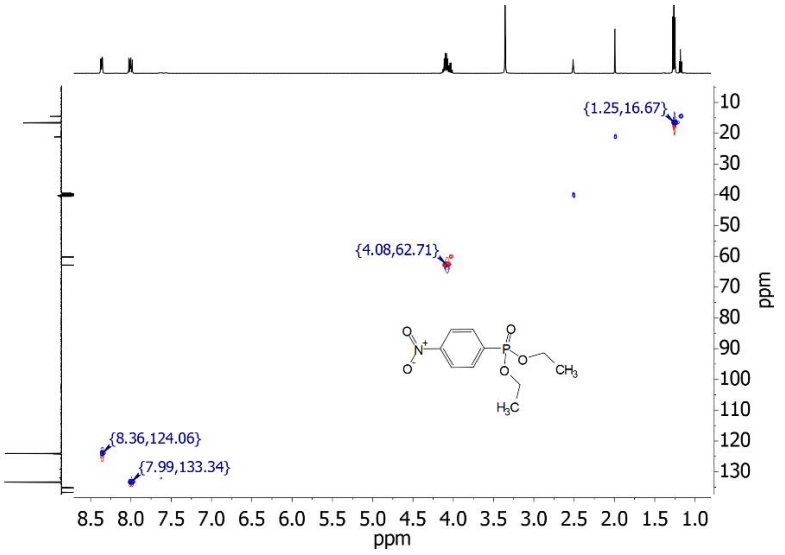


Figure 406. $^{1}H,^{13}C$ HMQC/HSQC NMR spectrum of diethyl(4-nitrophenyl)phosphonate in DMSO-d_6 at 499 MHz.

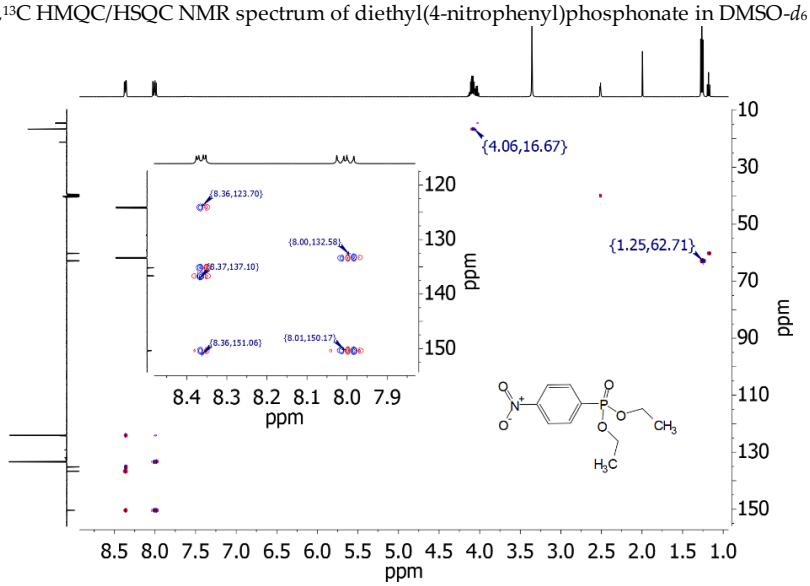


Figure 407. $^{1}H,^{13}C$ HMBC NMR spectrum of diethyl(4-nitrophenyl)phosphonate in DMSO-d_6 at 300 MHz.

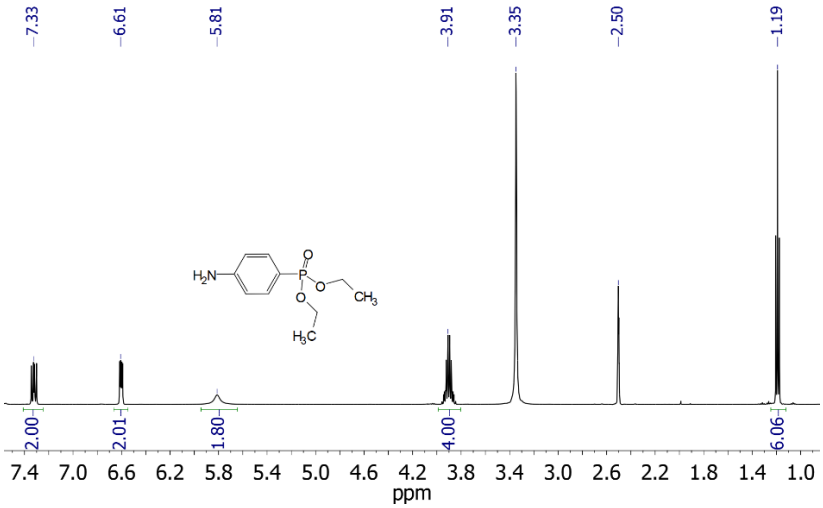


Figure 408. ^{1}H NMR spectrum of diethyl(4-aminophenyl)phosphonate in DMSO-d_6 at 499 MHz.

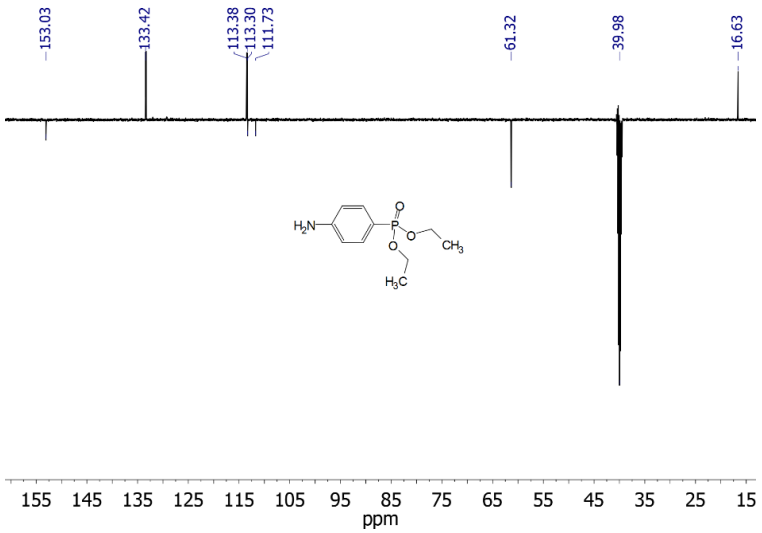


Figure 409. ^{13}C APT NMR spectrum of diethyl(4-aminophenyl)phosphonate in DMSO-d_6 at 499 MHz.

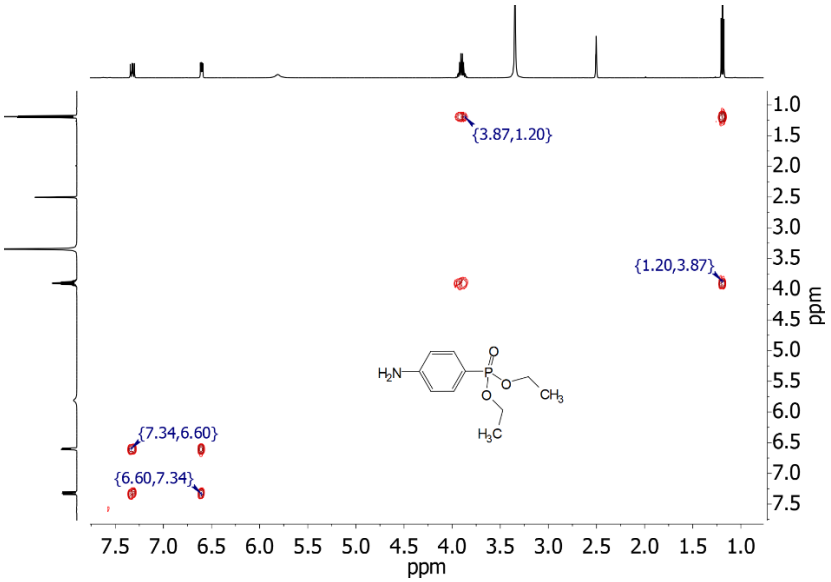


Figure 410. $^{1}H,^{1}H$ COSY NMR spectrum of diethyl(4-aminophenyl)phosphonate in DMSO-d_6 at 499 MHz.

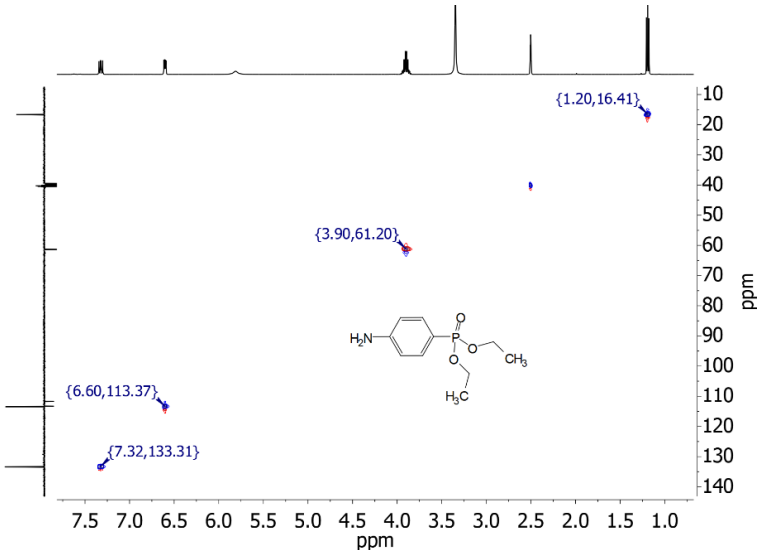


Figure 411. $^{1}H,^{13}C$ HMQC/HSQC NMR spectrum of diethyl(4-aminophenyl)phosphonate in DMSO-d_6 at 499 MHz.

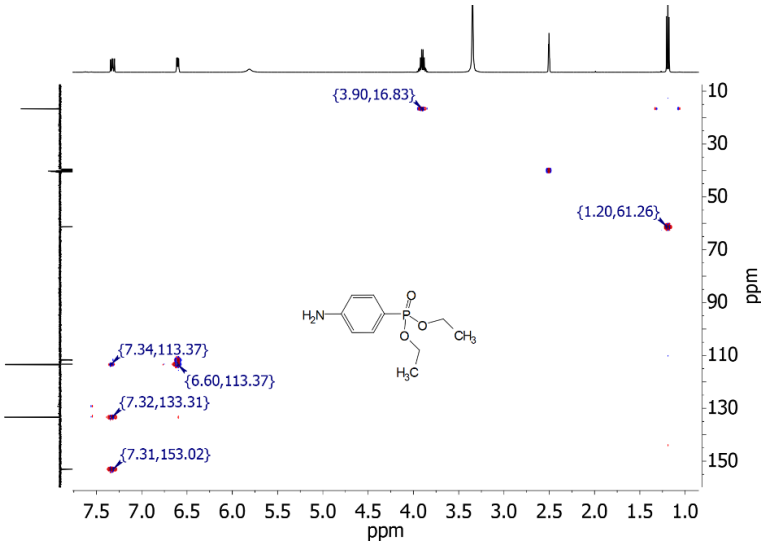


Figure 412. $^{1}H,^{13}C$ HMBC NMR spectrum of diethyl(4-aminophenyl)phosphonate in DMSO-d_6 at 499 MHz.

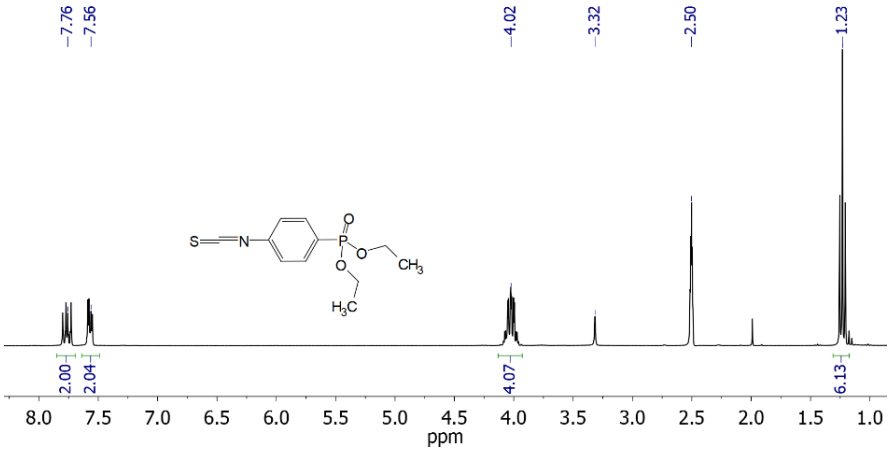


Figure 413. ^{1}H NMR spectrum of diethyl (4-isothiocyanatophenyl)phosphonate in DMSO-d_6 at 300 MHz.

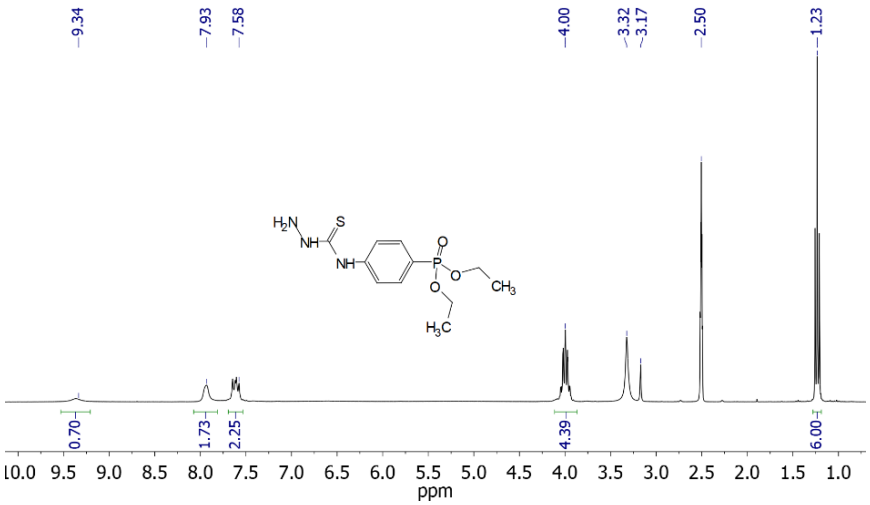


Figure 414. ^{1}H NMR spectrum of diethyl [4-(hydrazidecarbothioamino)phenyl] phosphonate in DMSO-d_6 at 300 MHz.

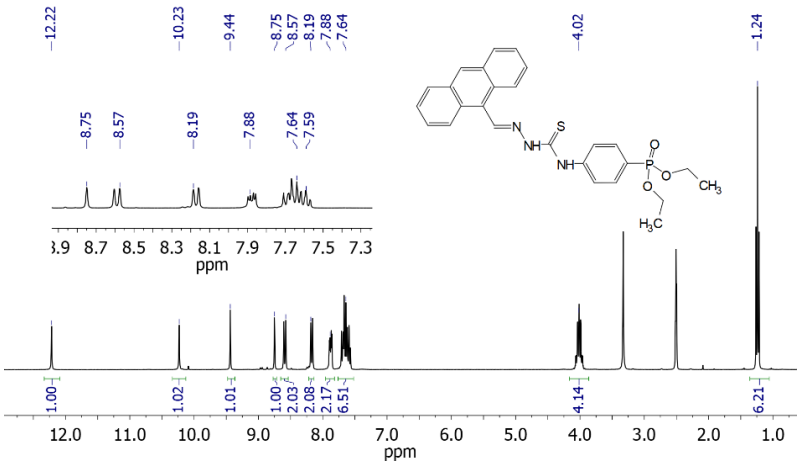


Figure 415. [1]H NMR spectrum of [(2*E*)-2-[(anthracen-9-yl)methylidene]hydrazino]-4-(diethoxy-phosphoryl)benzene-1-carbothioamide in DMSO-d_6 at 499 MHz.

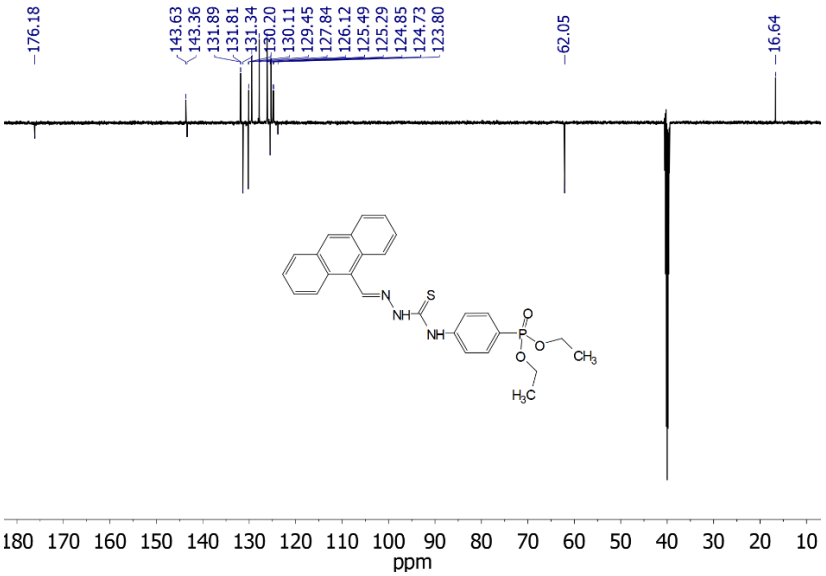


Figure 416. [13]C APT NMR spectrum of [(2*E*)-2-[(anthracen-9-yl)methylidene]hydrazino]-4-(diethoxyphosphoryl)benzene-1-carbothioamide in DMSO-d_6 at 499 MHz.

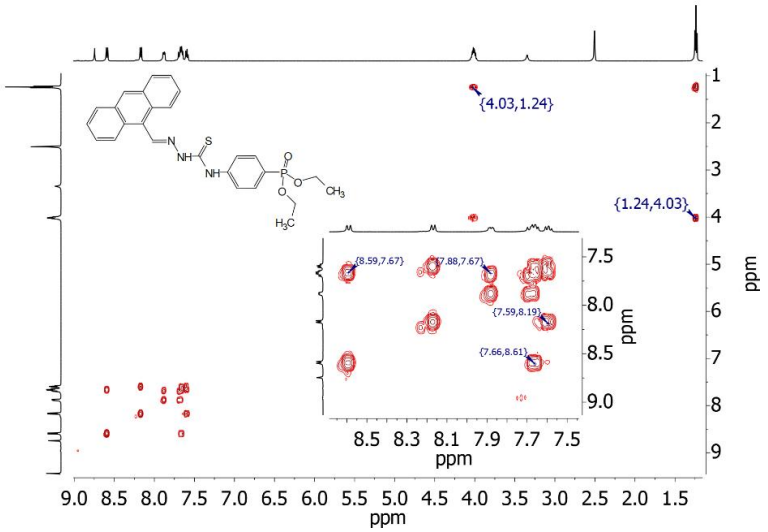


Figure 417. [1]H,[1]H COSY NMR spectrum of [(2*E*)-2-[(anthracen-9-yl)methylidene]hydrazino]-4-(diethoxyphosphoryl)benzene-1-carbothioamide in DMSO-d_6 at 499 MHz.

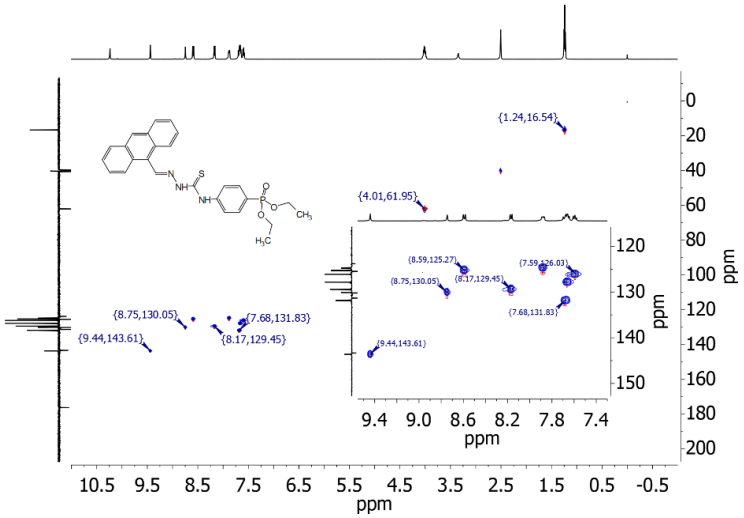


Figure 418. $^{1}H,^{13}C$ HMQC/HSQC NMR spectrum of [(2*E*)-2-[(anthracen-9-yl)methylidene] hydrazino]-4-(diethoxyphosphoryl) benzene-1-carbothioamide in DMSO-d_6 at 499 MHz.

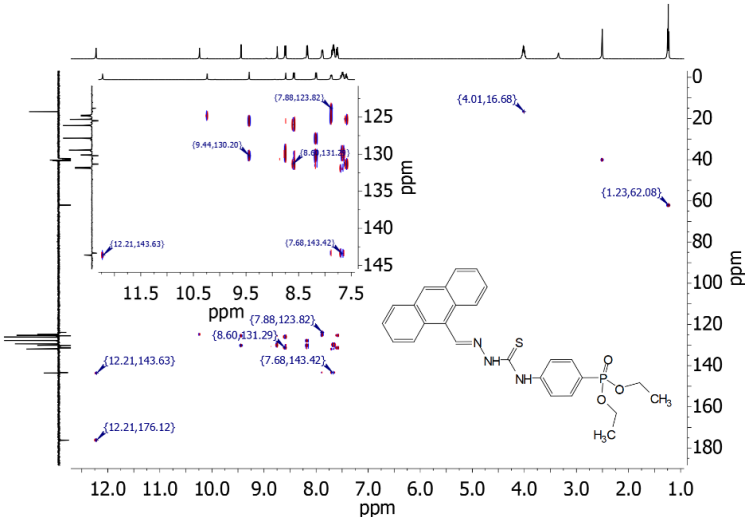


Figure 419. $^{1}H,^{13}C$ HMBC NMR spectrum of [(2*E*)-2-[(anthracen-9-yl)methylidene]hydrazino]-4-(diethoxyphosphoryl)benzene-1-carbothioamide in DMSO-d_6 at 499 MHz.

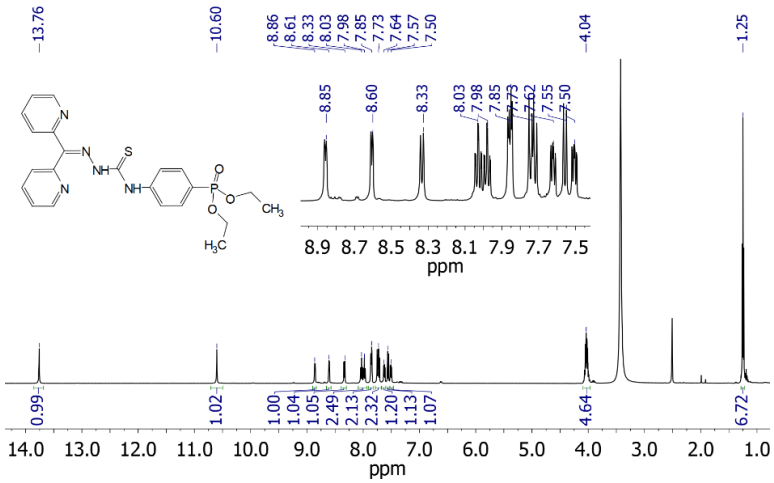


Figure 420. ^{1}H NMR spectrum of (2-[bis(pyridin-2-yl)methylidene]hydrazine)-4-(diethoxy phosphoryl)benzene-1-carbothio amide in DMSO-d_6 at 499 MHz.

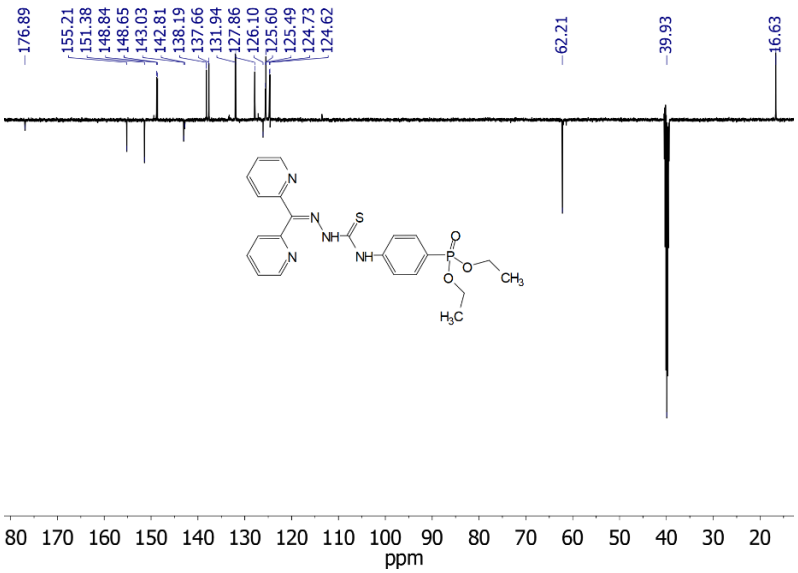


Figure 421. ^{13}C APT NMR spectrum of (2-[bis(pyridin-2-yl)methylidene]hydrazine)-4-(diethoxy-phosphoryl)benzene-1-carbothio amide in DMSO-d_6 at 499 MHz.

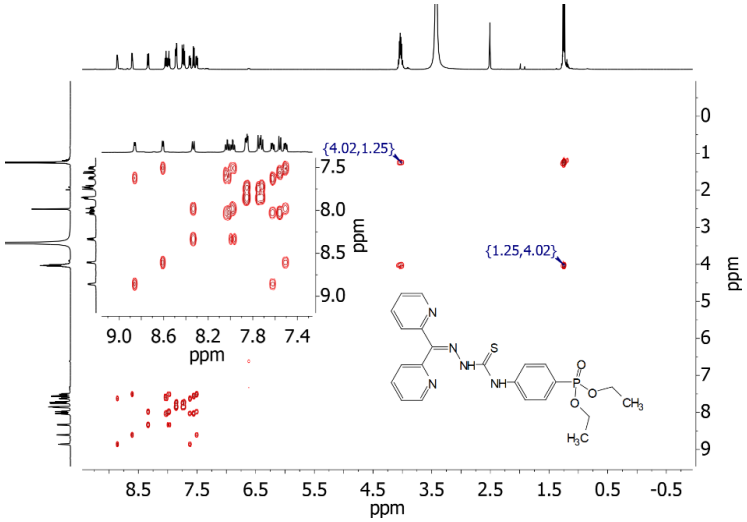


Figure 422. $^{1}H,^{1}H$ COSY NMR spectrum of (2-[bis(pyridin-2-yl)methylidene]hydrazino)-4-(diethoxy-phosphoryl)benzene-1-carbothioamide in DMSO-d_6 at 499 MHz.

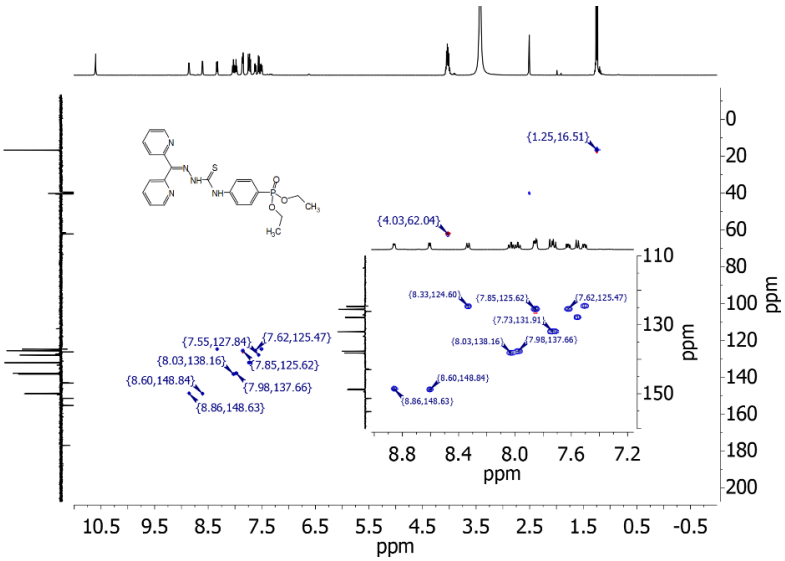


Figure 423. $^{1}H,^{13}C$ HMQC/HSQC NMR spectrum of (2-[bis(pyridin-2-yl)methylidene]hydrazino)-4-(diethoxyphosphoryl) benzene-1-carbothioamide in DMSO-d_6 at 499 MHz.

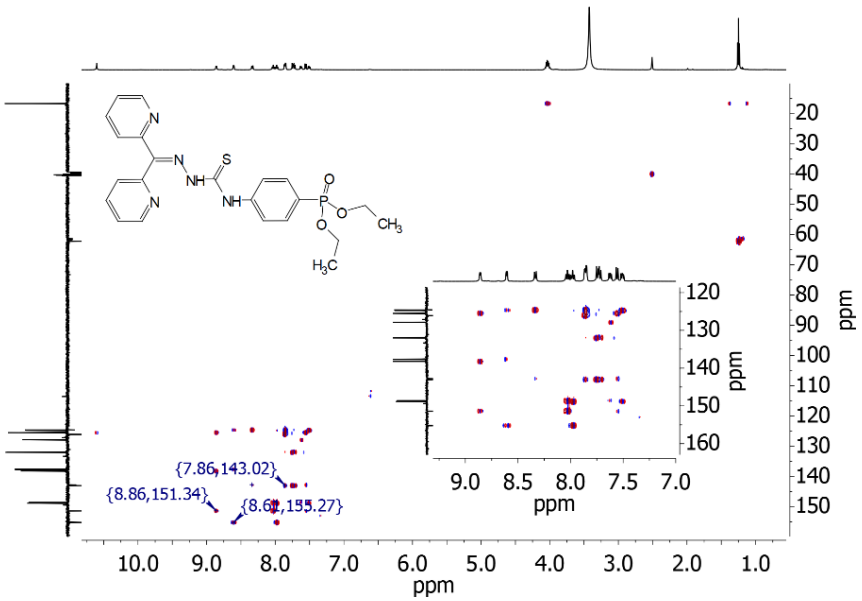


Figure 424. $^{1}H,^{13}C$ HMBC NMR spectrum of (2-[bis(pyridin-2-yl)methylidene]hydrazino)-4-(diethoxyphosphoryl)benzene-1-carbothioamide in DMSO-d_6 at 499 MHz.

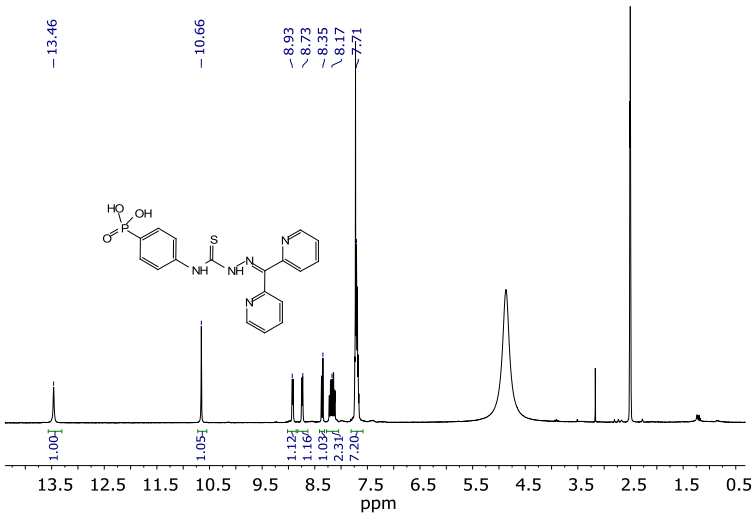


Figure 425. ^{1}H NMR spectrum of (4-([bis(pyridin-2yl)methylideneaminocarbamthioyl]amino)phenyl) phosphonic acid in DMSO-d_6 at 300 MHz.

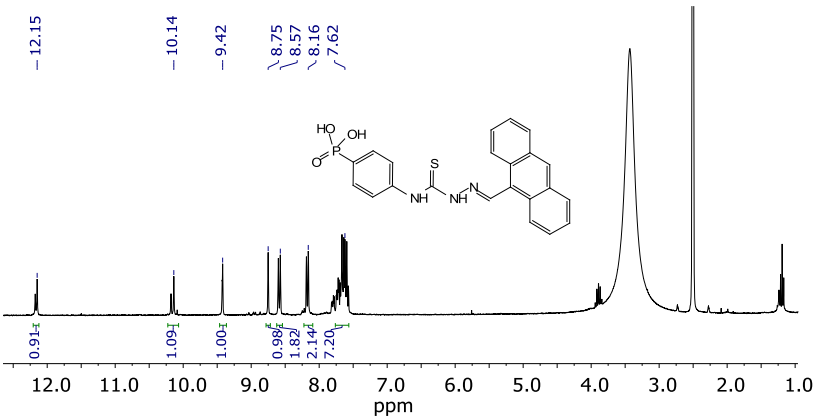


Figure 426. ^{1}H NMR spectrum of [(2*Z*)-2-[(anthracen-9-yl)methylidene]hydrazino]-4-phosphono benzene-1-carbothioamide in DMSO-d_6 at 300 MHz.

7.1.2 NMR data of the Ru(II) photosensitizer

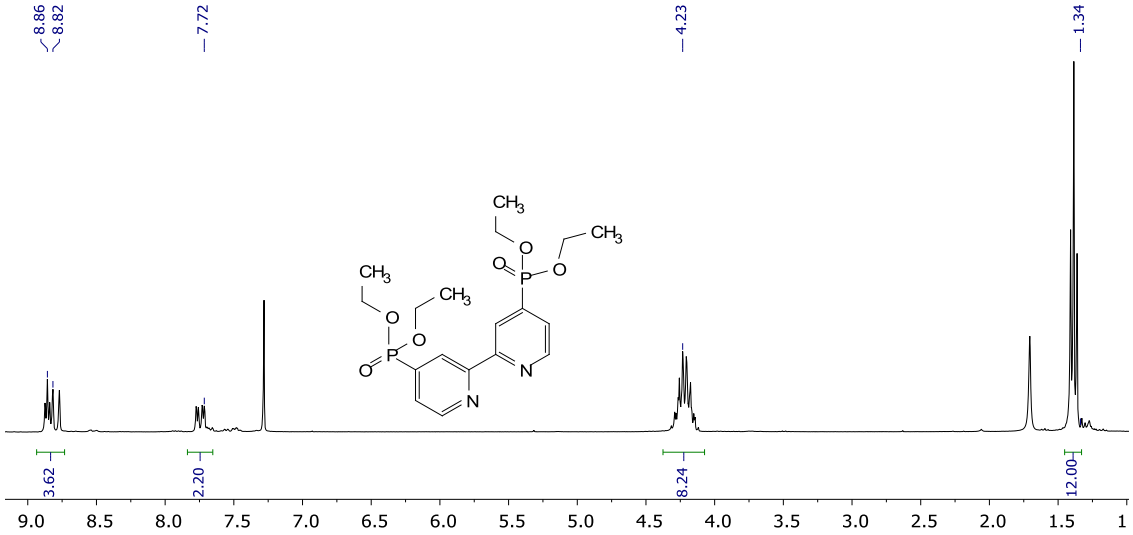


Figure 427. ^{1}H NMR spectrum of di(diethylphosphonate)bispyridine in $CDCl_3$ at 300 MHz.

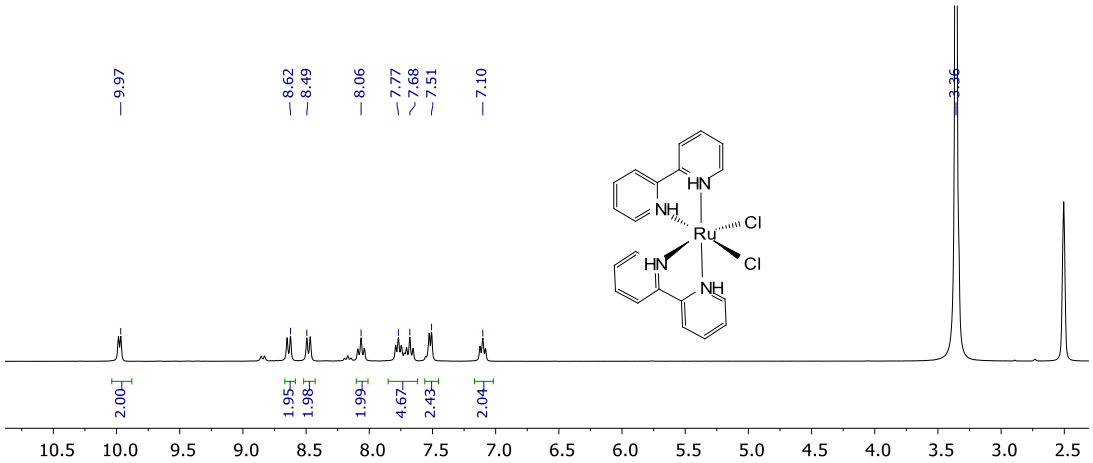


Figure 428. ^{1}H NMR spectrum of *cis*-dichlorobis(bipyridine)ruthenium(II) in DMSO-d_6 at 300 MHz.

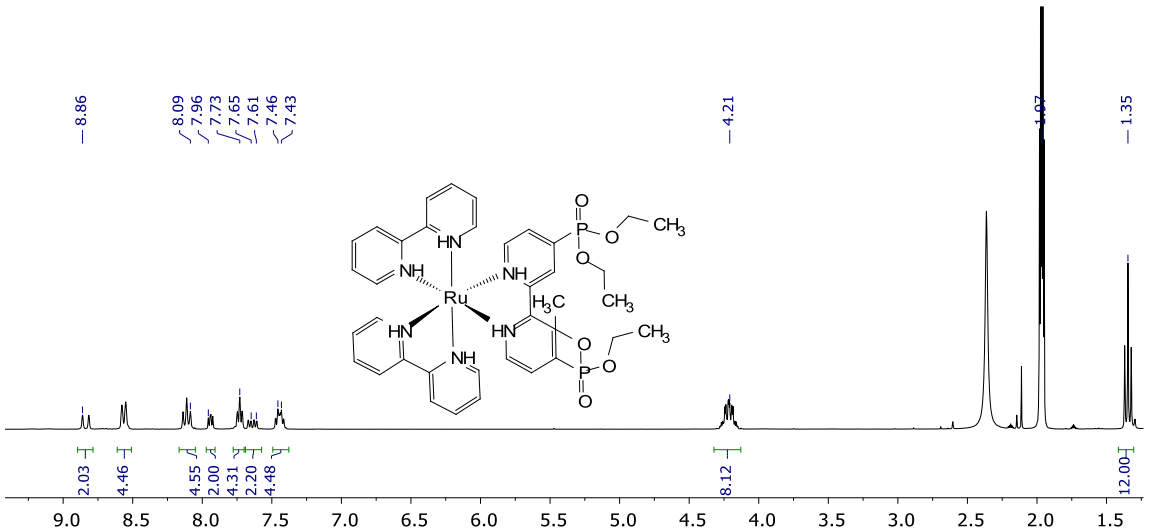


Figure 429. ^{1}H NMR spectrum of Tribis(bipyridine)ruthenium(II)di(diethyl)phosphonate in acetonitrile-d_3 at 300 MHz.

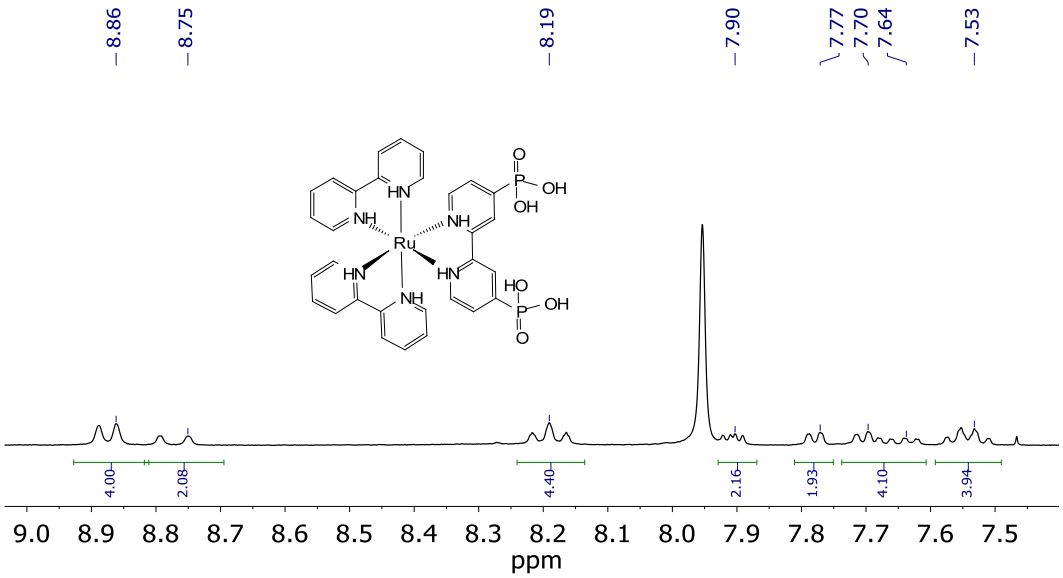


Figure 430. [1]H NMR spectrum of Tribis(bipyridine)ruthenium(II)diphosphonate in DMSO-d_6 at 300 MHz.

7.1.3 NMR data of the tagged TSCs and their Pt(II) complexes

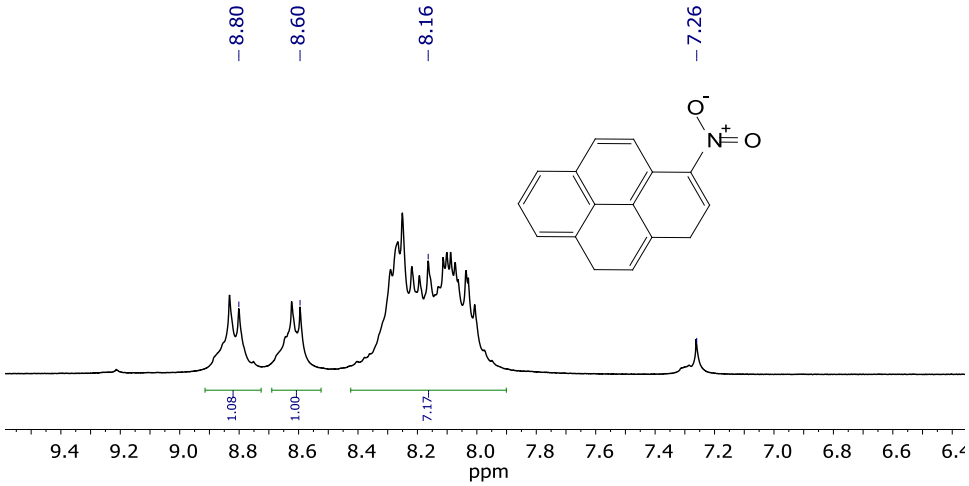


Figure 431. [1]H NMR spectrum of 1-nitropyrene in $CDCl_3$ at 300 MHz.

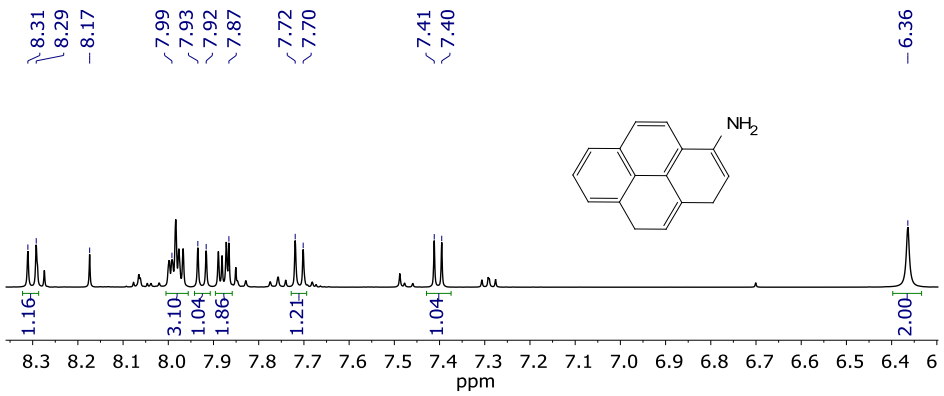


Figure 432. [1]H NMR spectrum of 1-aminopyrene in DMSO-d_6 at 499 MHz.

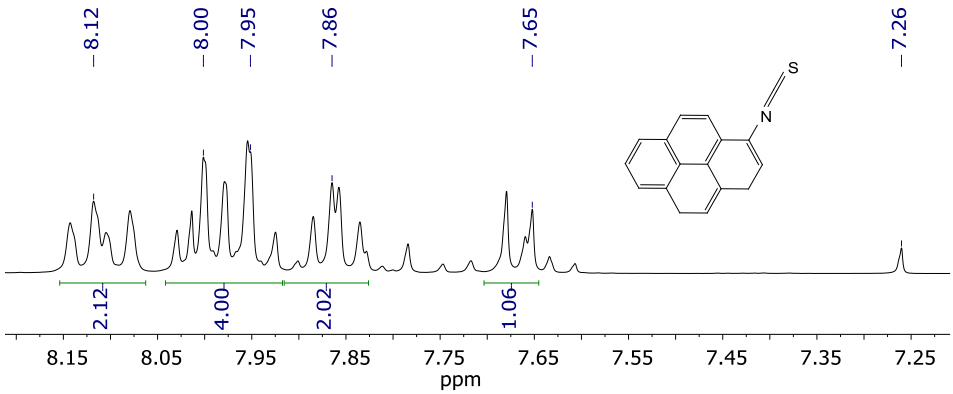


Figure 433. [1]H NMR spectrum of 1-isothiocyanatopyrene in $CDCl_3$ at 300 MHz.

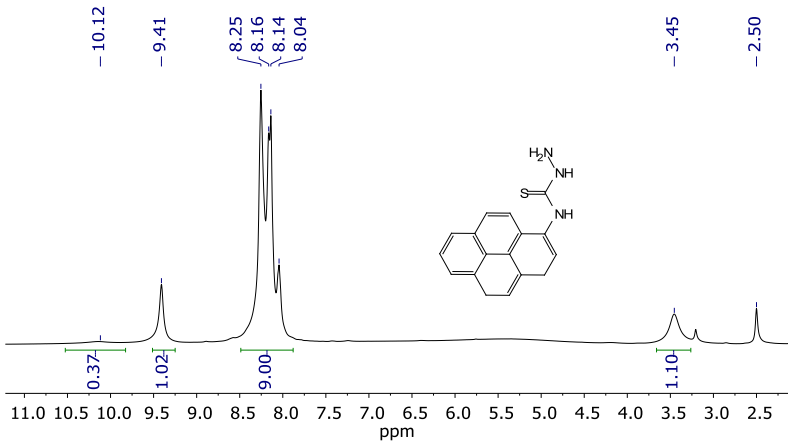


Figure 434. [1]H NMR spectrum of 4-(3,6-dihydro-1-pyrenyl)thiosemicarbazide in DMSO-d_6 at 499 MHz.

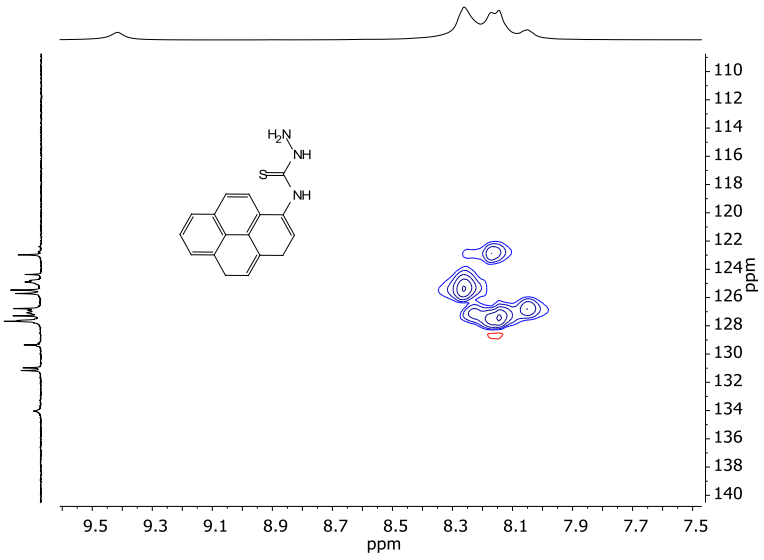


Figure 435. [1]H,[13]C HMQC/HSQC NMR spectrum of 4-(3,6-dihydro-1-pyrenyl)thiosemicarbazide in DMSO-d_6 at 499 MHz.

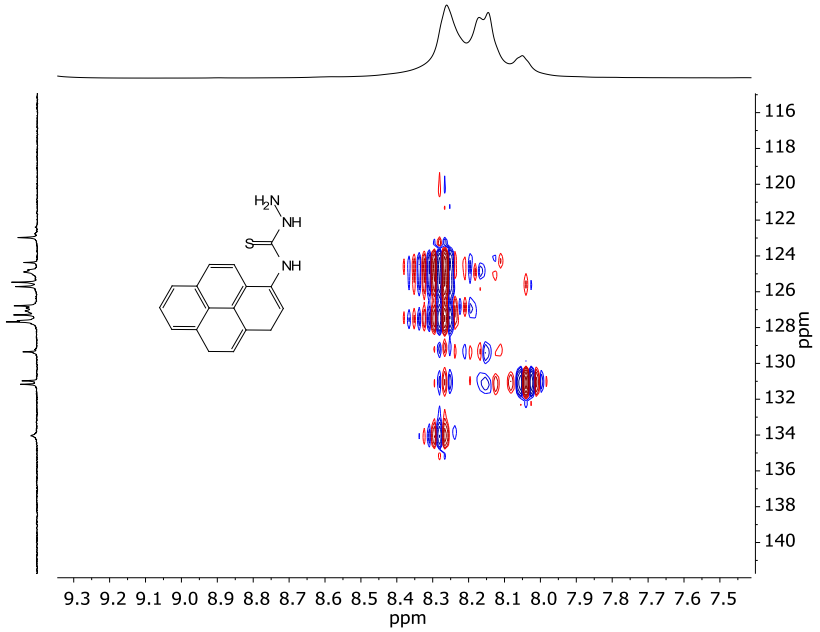


Figure 436. $^{1}H,^{13}C$ HMBC NMR spectrum of 4-(3,6-dihydro-1-pyrenyl)thiosemicarbazide in DMSO-d_6 at 499 MHz.

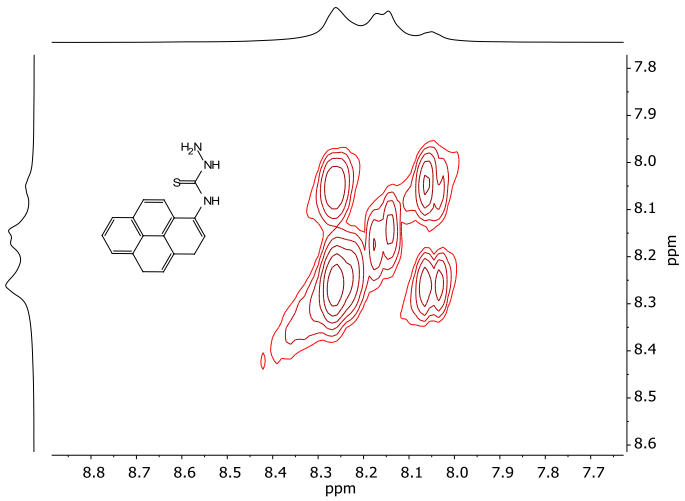


Figure 437. $^{1}H,^{1}H$ COSY NMR spectrum of 4-(3,6-dihydro-1-pyrenyl)thiosemicarbazide in DMSO-d_6 at 499 MHz.

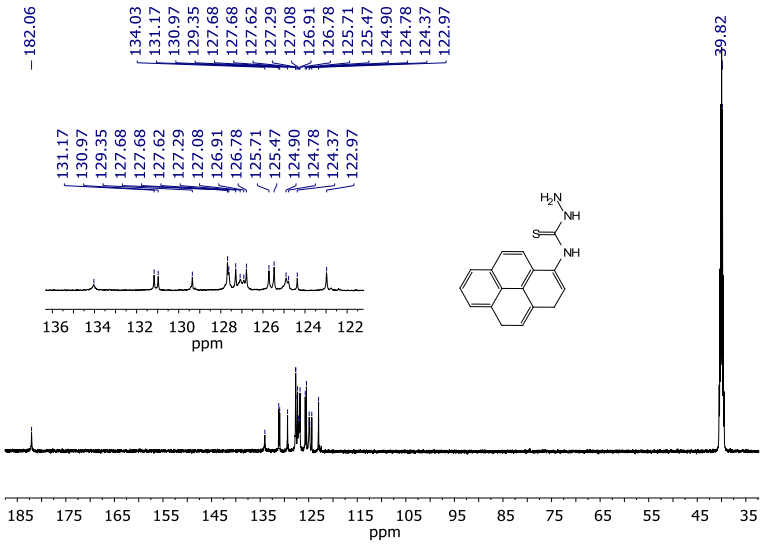


Figure 438. ^{13}C NMR spectrum of 4-(3,6-dihydro-1-pyrenyl)thiosemicarbazide in DMSO-d_6 at 499 MHz.

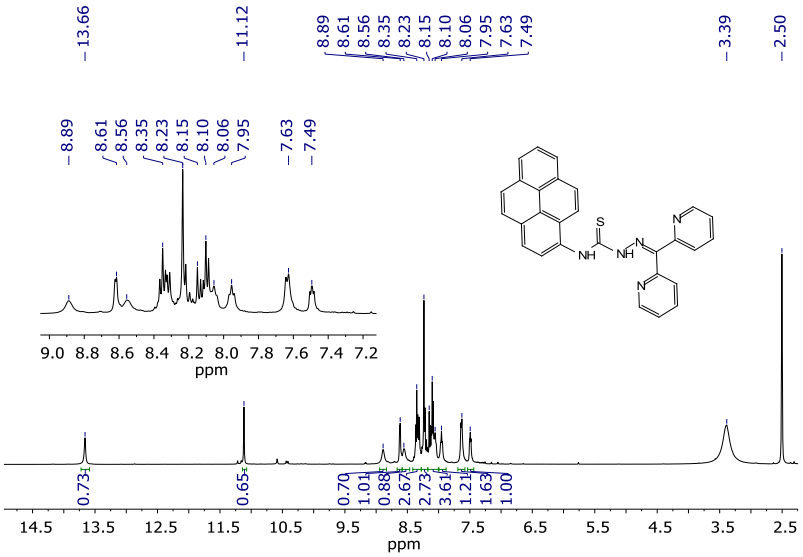


Figure 439. [1]H NMR spectrum of 1-[bis(2-pyridyl)methylene]-4-(4,8-dihydro-1-pyrenyl)thiosemicarbazide in DMSO-*d*$_6$ at 300 MHz.

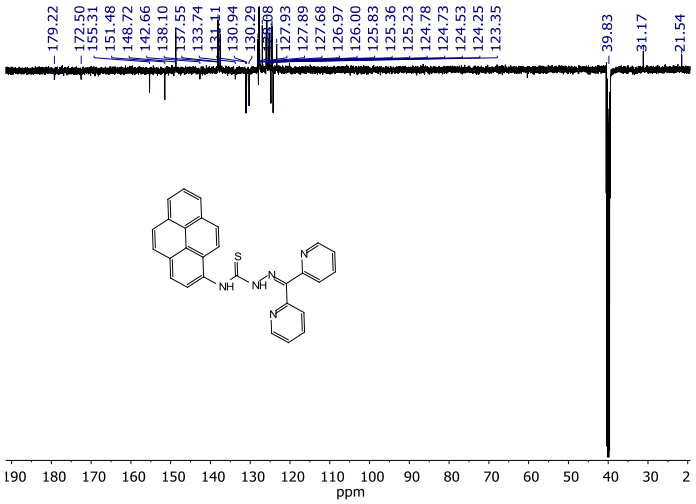


Figure 440. [13]C APT NMR spectrum of 1-[bis(2-pyridyl)methylene]-4-(4,8-dihydro-1-pyrenyl)thiosemicarbazide in DMSO-*d*$_6$ at 499 MHz.

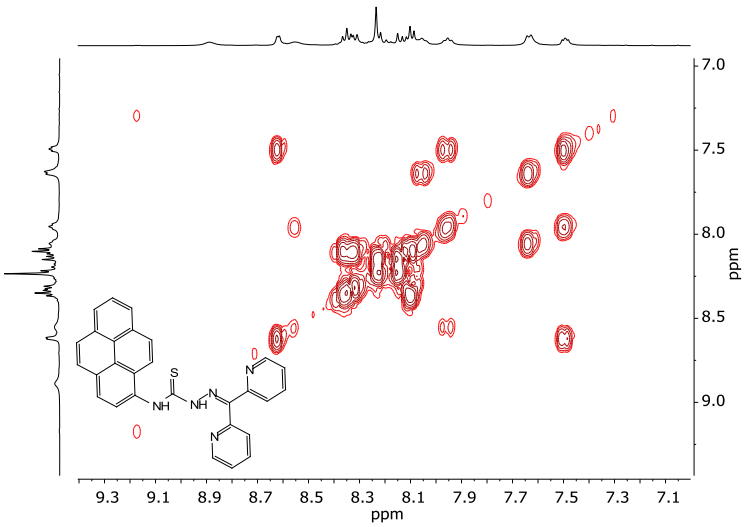


Figure 441. [1]H,[1]H COSY NMR spectrum of 1-[bis(2-pyridyl)methylene]-4-(4,8-dihydro-1-pyrenyl)thiosemi-carbazide in DMSO-*d*$_6$ at 499 MHz.

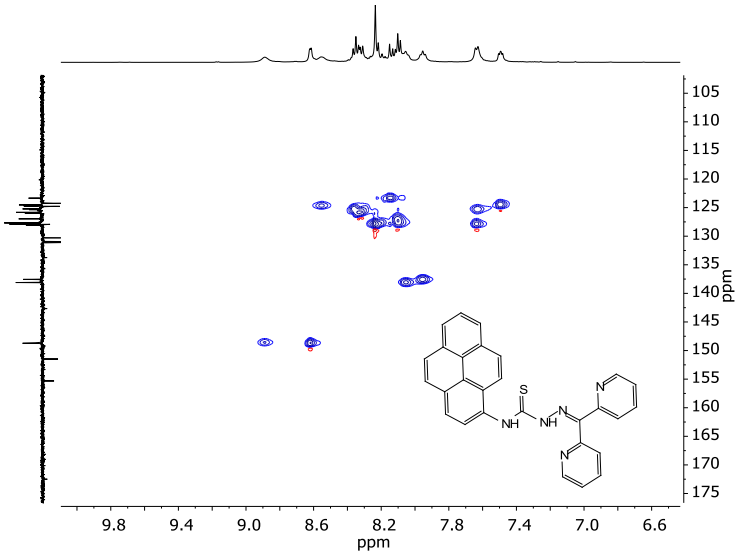


Figure 442. $^{1}H,^{13}C$ HMQC/HSQC NMR spectrum of 1-[bis(2-pyridyl)methylene]-4-(4,8-dihydro-1-pyrenyl)thiosemi carbazide in DMSO-d_6 at 499 MHz.

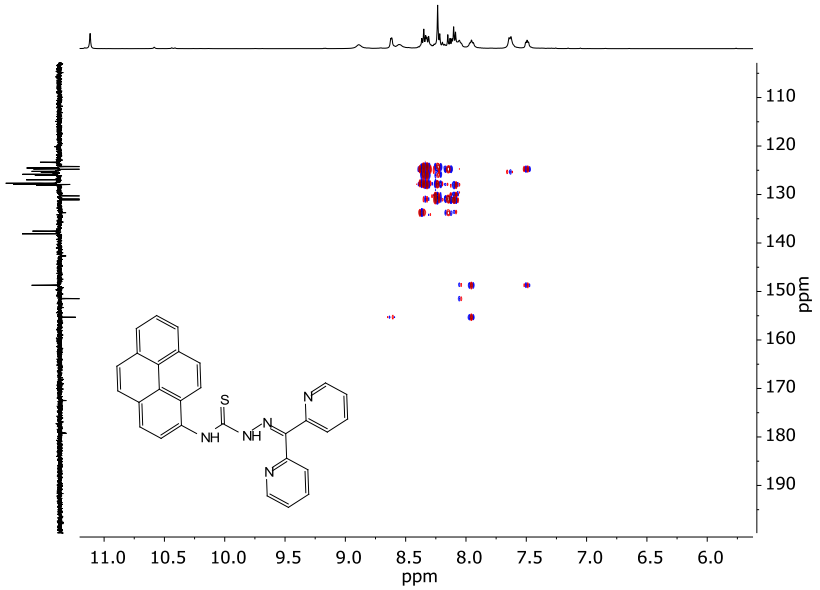


Figure 443. $^{1}H,^{13}C$ HMBC NMR spectrum of 1-[bis(2-pyridyl)methylene]-4-(4,8-dihydro-1-pyrenyl)thiosemi-carbazide in DMSO-d_6 at 499 MHz.

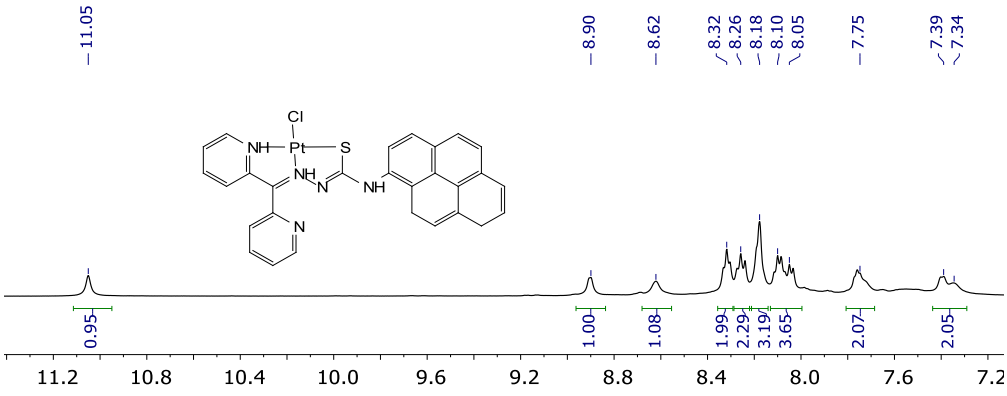


Figure 444. ^{1}H NMR spectrum of [Pt(Dipy(TSC)Pyr)Cl] in DMSO-d_6 at 300 MHz.

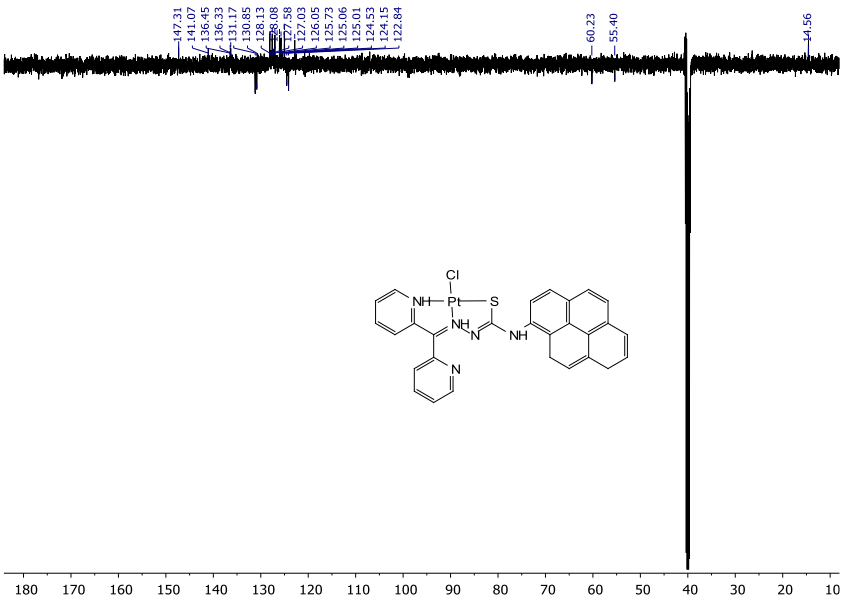


Figure 445. ^{13}C APT NMR spectrum of [Pt(Dipy(TSC)Pyr)Cl] in DMSO-d_6 at 499 MHz.

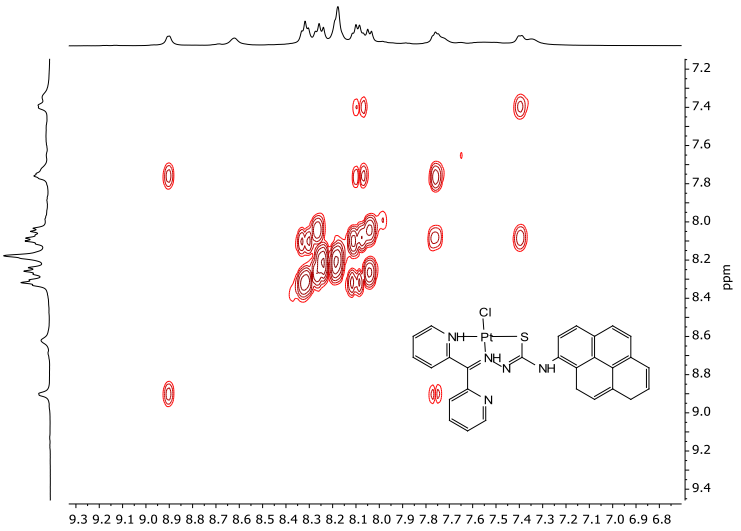


Figure 446. ^{1}H,^{1}H COSY NMR spectrum of [Pt(Dipy(TSC)Pyr)Cl] in DMSO-d_6 at 499 MHz.

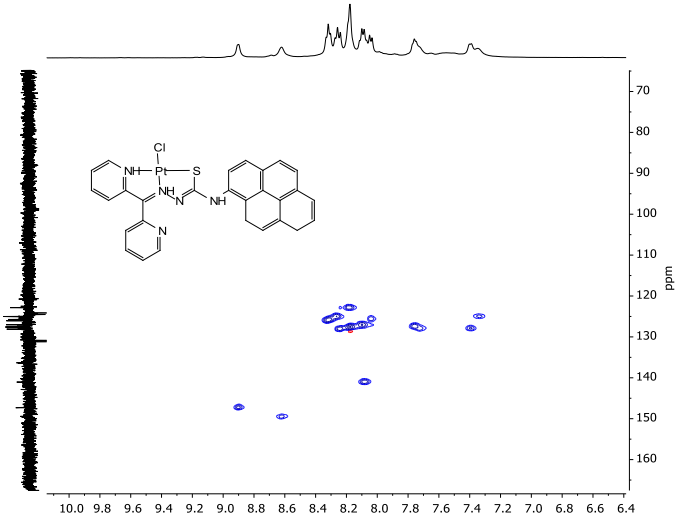


Figure 447. ^{1}H,^{13}C HMQC/HSQC NMR spectrum of [Pt(Dipy(TSC)Pyr)Cl] in DMSO-d_6 at 499 MHz.

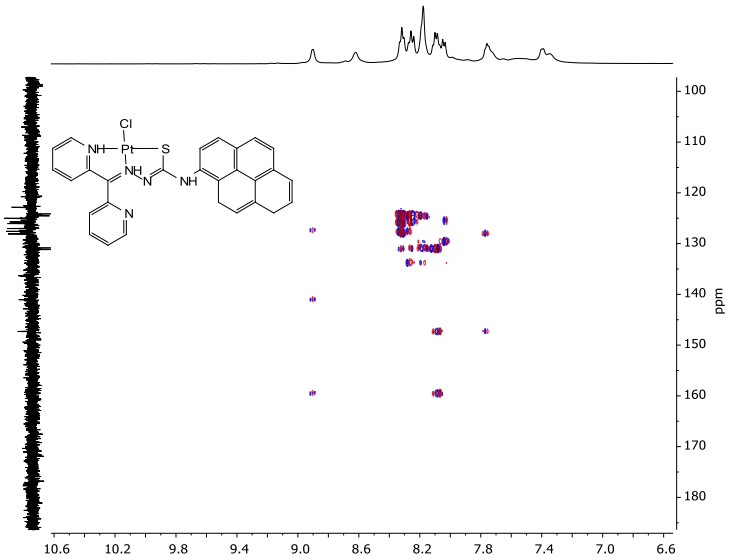


Figure 448. $^{1}H,^{13}C$ HMBC NMR spectrum of [Pt(Dipy(TSC)Pyr)Cl] in DMSO-d_6 at 499 MHz.

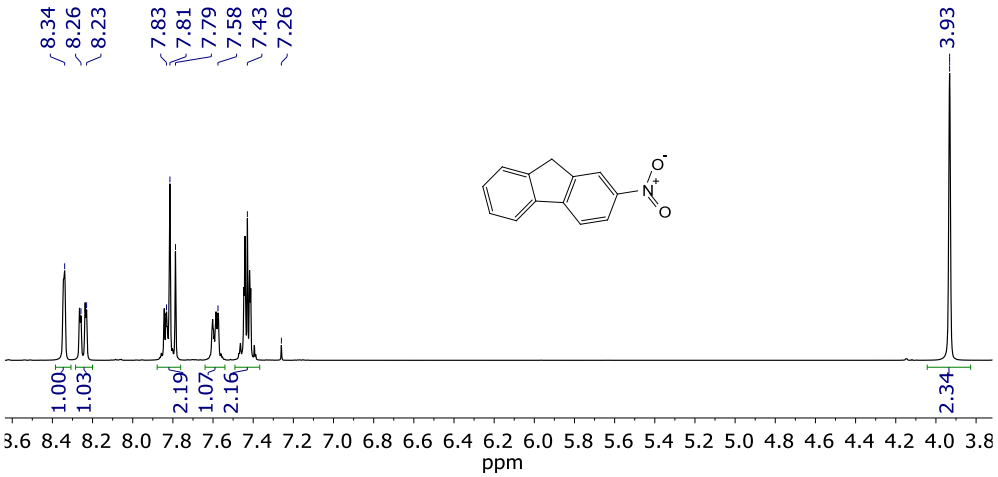


Figure 449. ^{1}H NMR spectrum of 2-nitrofluorene in $CDCl_3$ at 300 MHz.

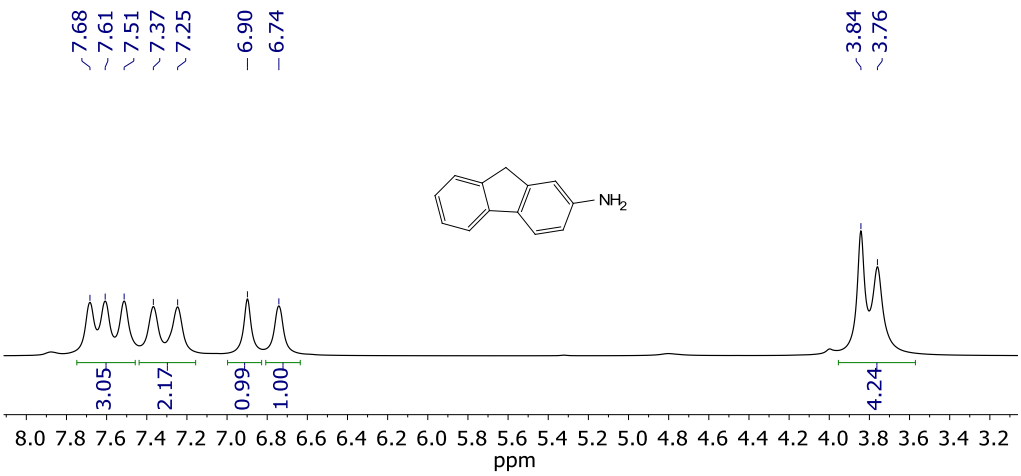


Figure 450. ^{1}H NMR spectrum of 2-aminofluorene in $CDCl_3$ at 499 MHz.

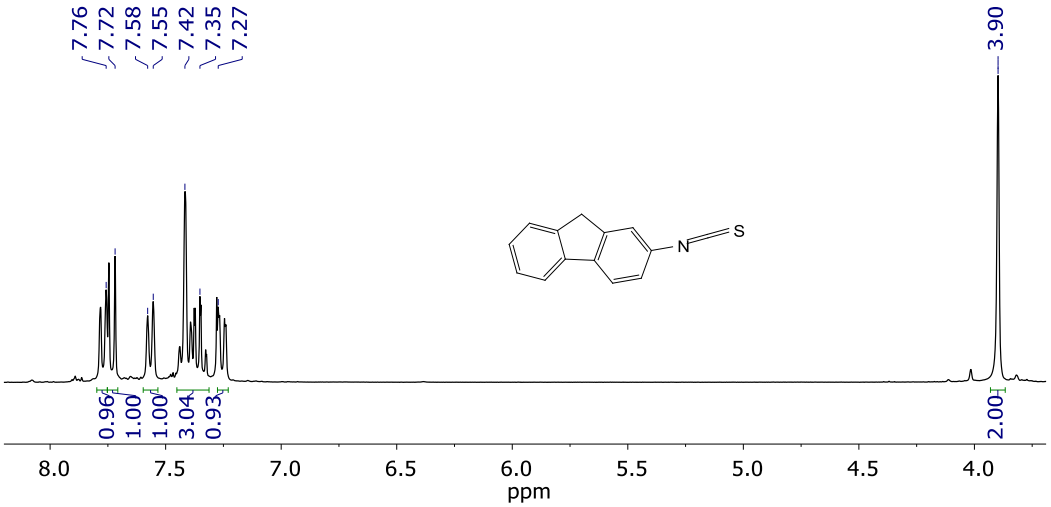


Figure 451. [1]H NMR spectrum of 2-isothiocyanatofluorene in $CDCl_3$ at 300 MHz.

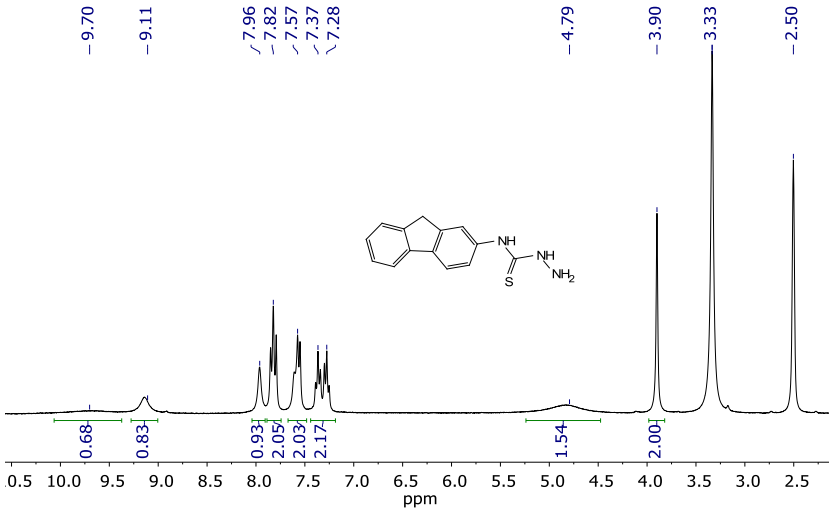


Figure 452. [1]H NMR spectrum of 4-(9*H*-Fluoren-2-yl)thiosemicarbazide in DMSO-d_6 at 300 MHz.

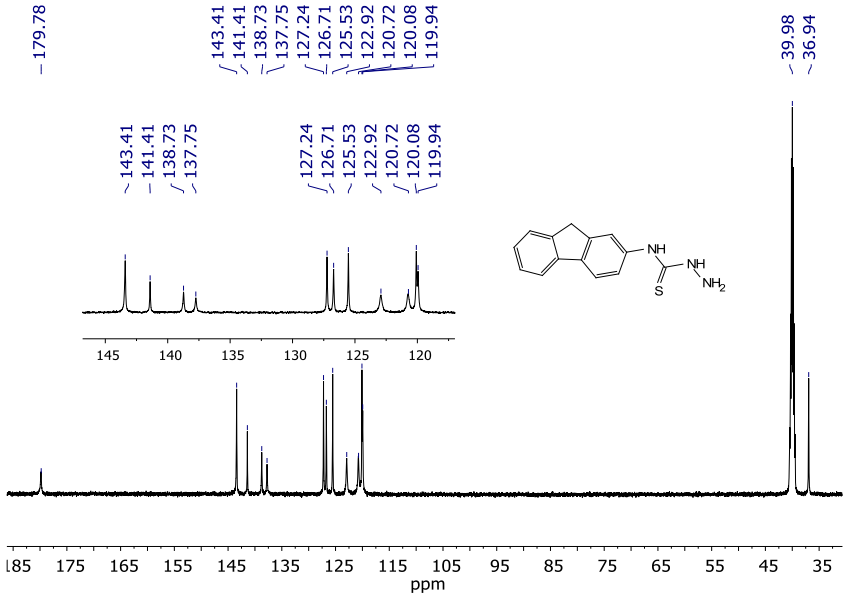


Figure 453. [13]C NMR spectrum of 4-(9*H*-Fluoren-2-yl)thiosemicarbazide in DMSO-d_6 at 499 MHz.

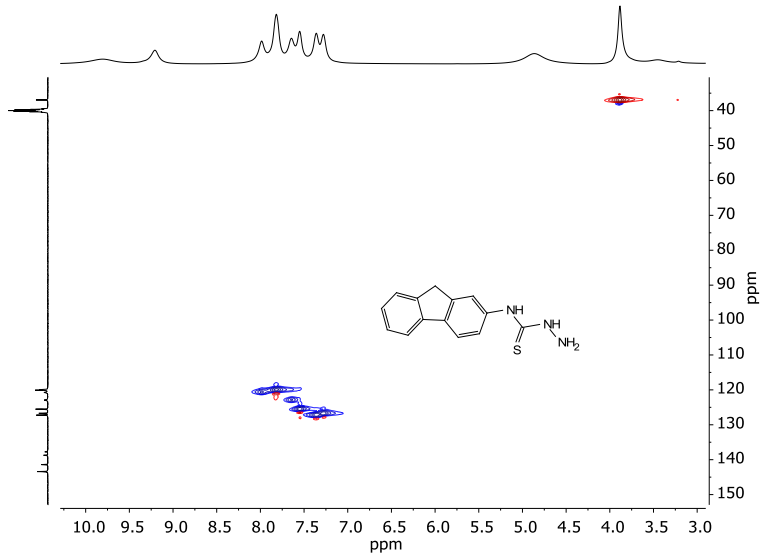


Figure 454. $^{1}H,^{13}C$ HMQC/HSQC NMR spectrum of 4-(9*H*-Fluoren-2-yl)thiosemicarbazide in DMSO-d_6 at 499 MHz.

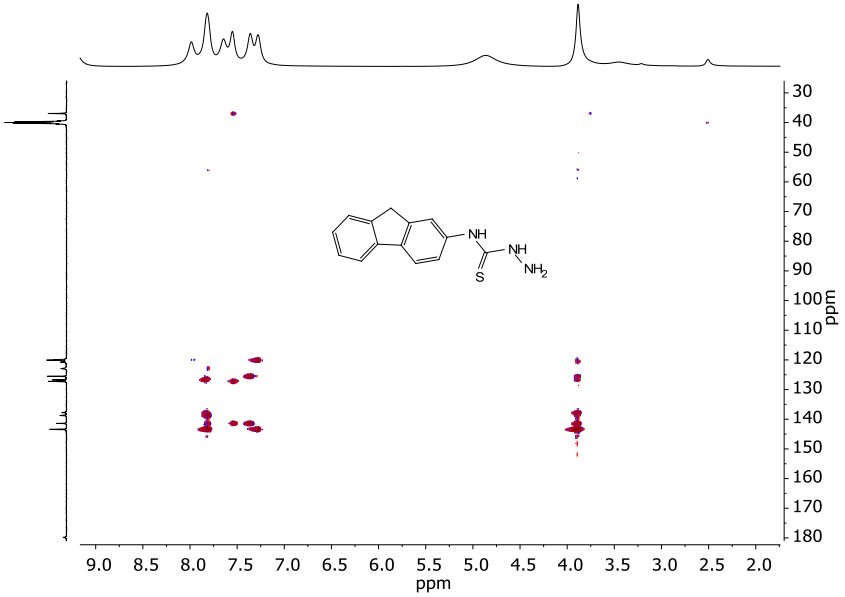


Figure 455. $^{1}H,^{13}C$ HMBC NMR spectrum of 4-(9*H*-Fluoren-2-yl)thiosemicarbazide in DMSO-d_6 at 499 MHz.

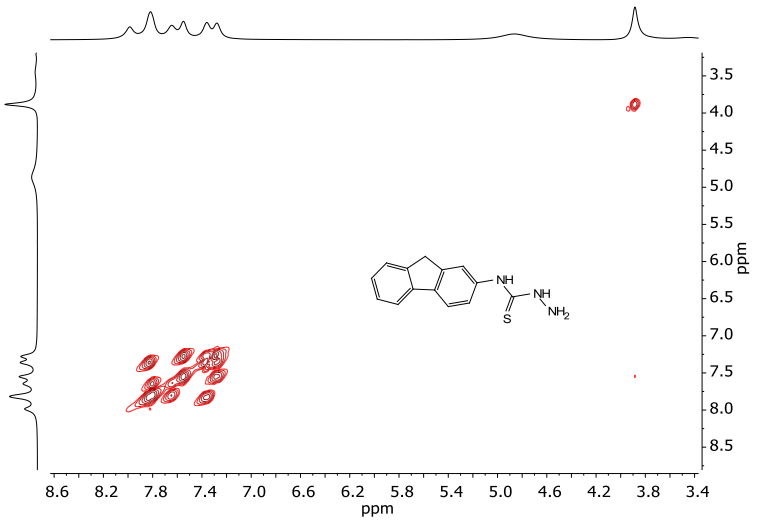


Figure 456. $^{1}H,^{1}H$ COSY NMR spectrum of 4-(9*H*-Fluoren-2-yl)thiosemicarbazide in DMSO-d_6 at 499 MHz.

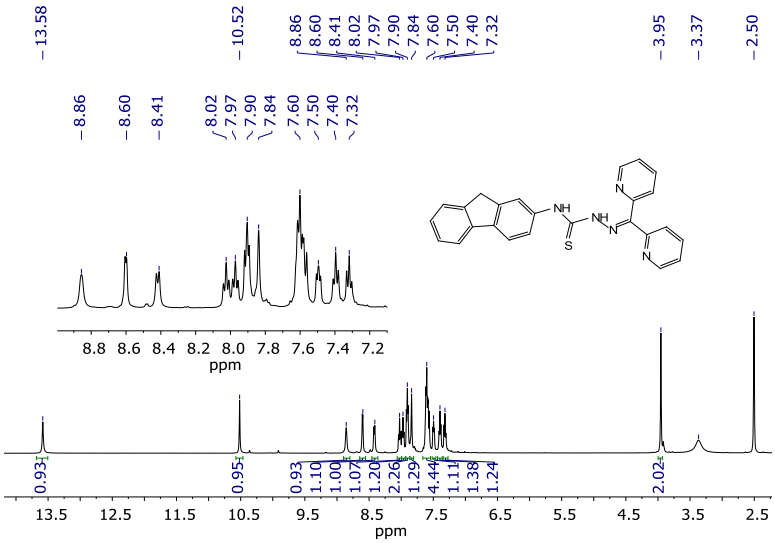


Figure 457. ^{1}H NMR spectrum of 1-[bis(2-pyridyl)methylene]-4-(9*H*-fluoren-2-yl)thiosemicarbazide in DMSO-d_6 at 300 MHz.

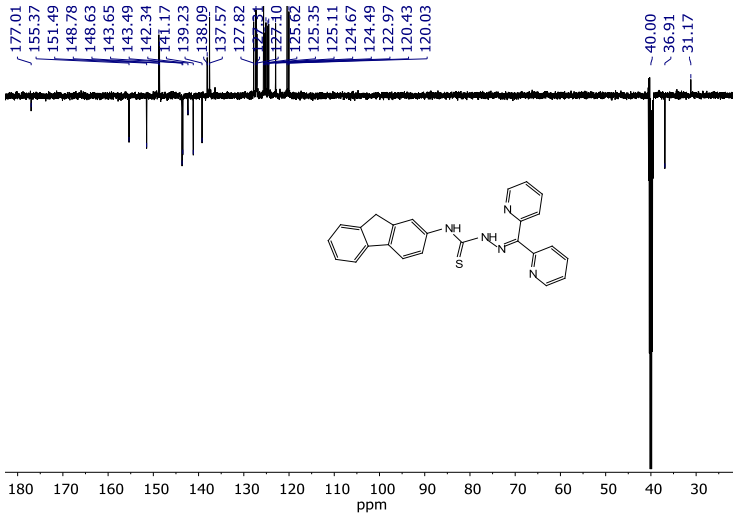


Figure 458. ^{13}C DEPTQ NMR spectrum of 1-[bis(2-pyridyl)methylene]-4-(9*H*-fluoren-2-yl)thiosemicarbazide in DMSO-d_6 at 499 MHz.

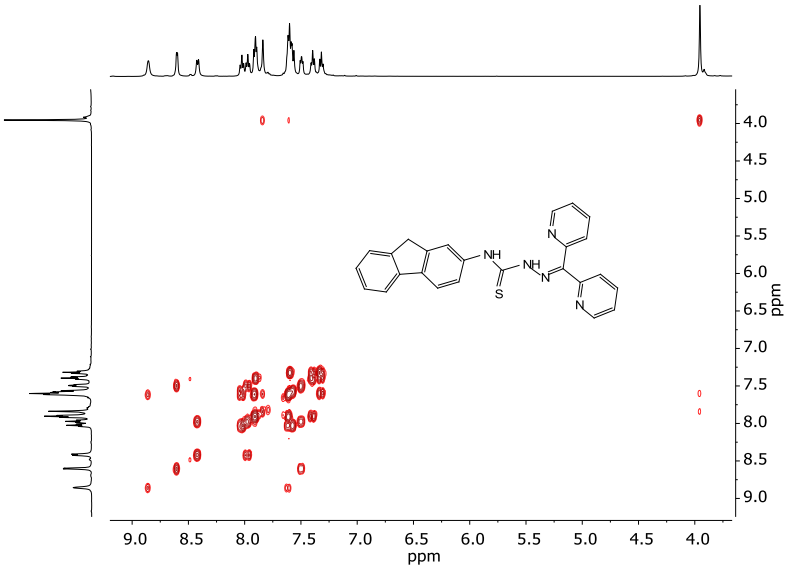


Figure 459. ^{1}H,^{1}H COSY NMR spectrum of 1-[bis(2-pyridyl)methylene]-4-(9*H*-fluoren-2-yl)thiosemicarbazide in DMSO-d_6 at 499 MHz.

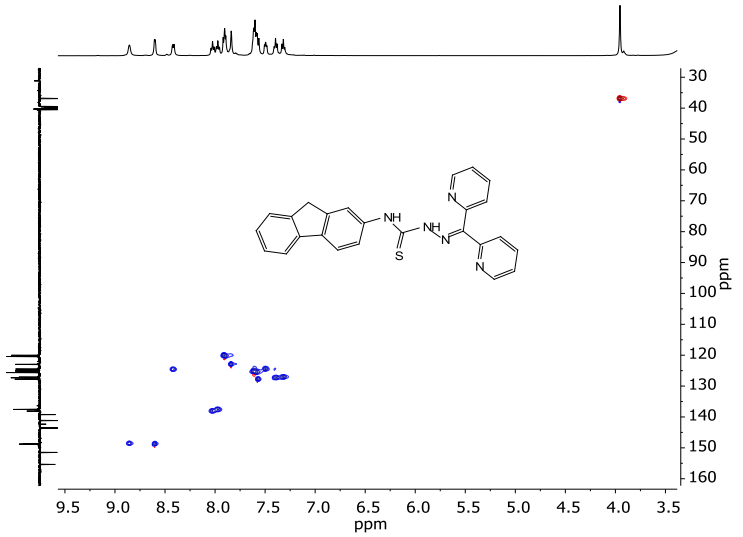


Figure 460. $^{1}H,^{13}C$ HMQC/HSQC NMR spectrum of 1-[bis(2-pyridyl)methylene]-4-(9*H*-fluoren-2-yl) thiosemicarbazide in DMSO-d_6 at 499 MHz.

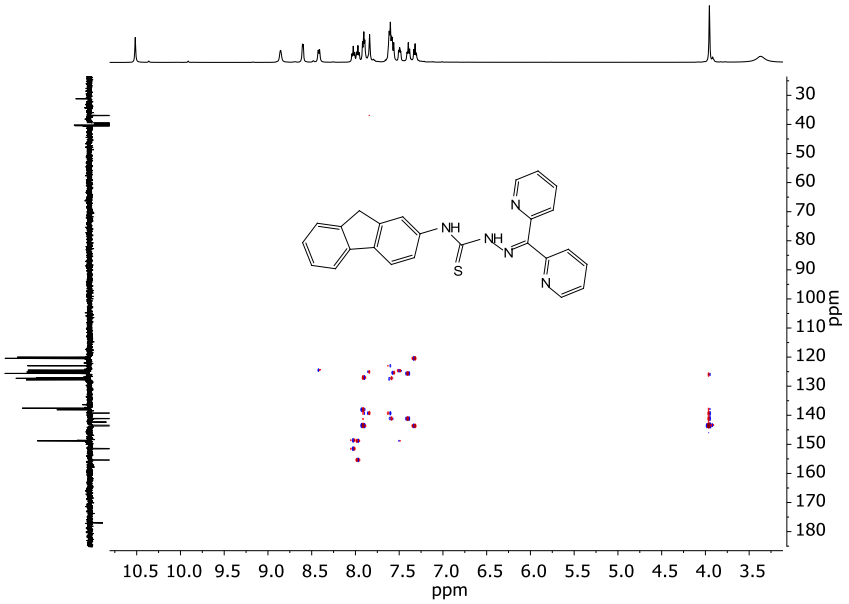


Figure 461. $^{1}H,^{13}C$ HMBC NMR spectrum of 1-[bis(2-pyridyl)methylene]-4-(9*H*-fluoren-2-yl)thiosemicarbazide in DMSO-d_6 at 499 MHz.

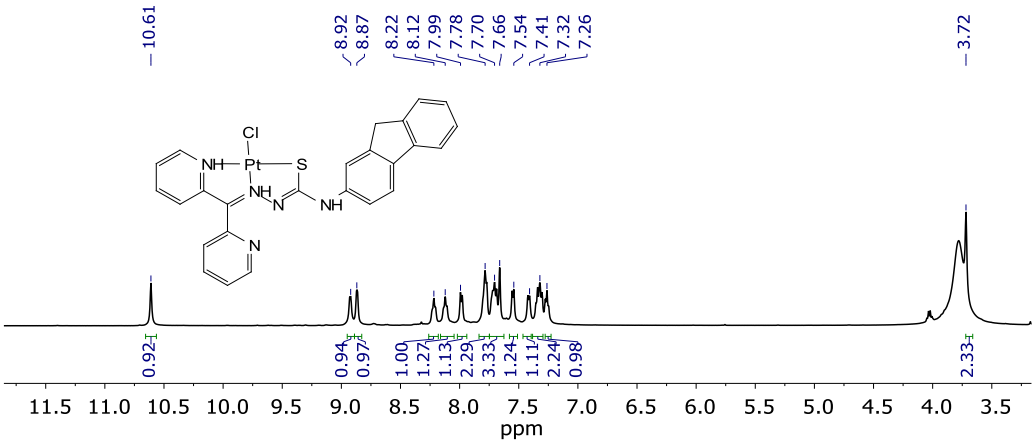


Figure 462. ^{1}H NMR spectrum of [Pt(Dipy(TSC)Flu)Cl] in DMSO-d_6 at 300 MHz.

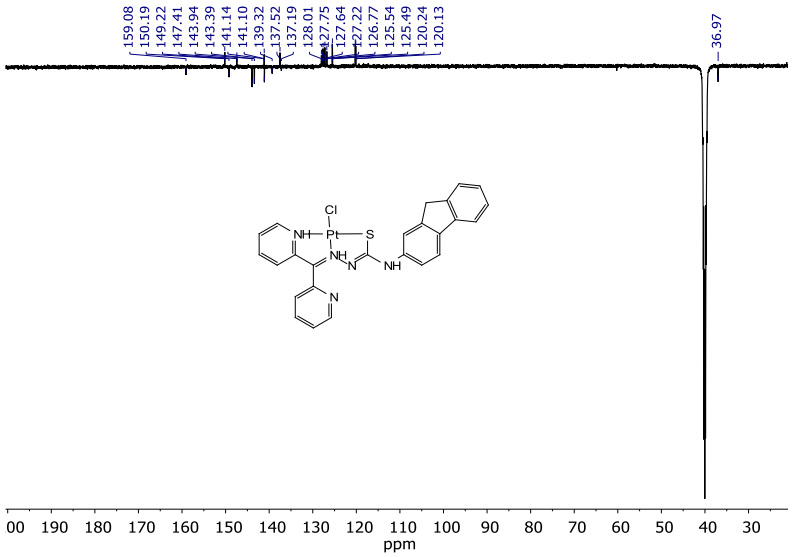


Figure 463. ^{13}C APT NMR spectrum of [Pt(Dipy(TSC)Flu)Cl] in DMSO-d_6 at 499 MHz.

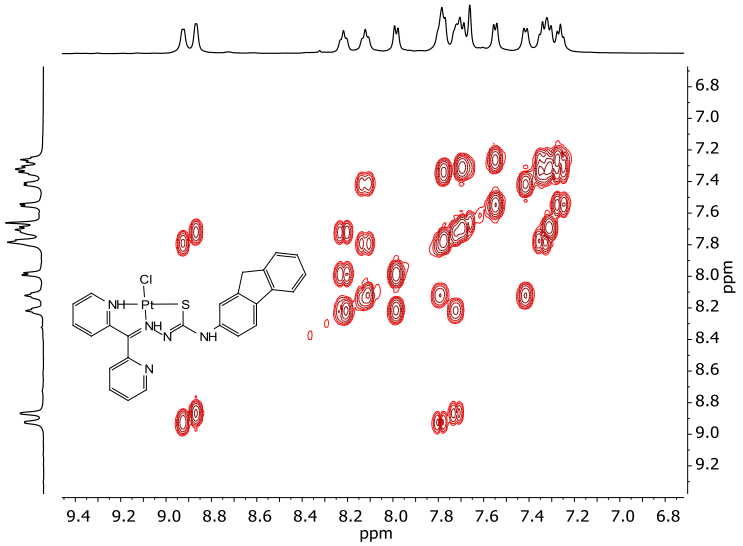


Figure 464. ^{1}H,^{1}H COSY NMR spectrum of [Pt(Dipy(TSC)Flu)Cl] in DMSO-d_6 at 499 MHz.

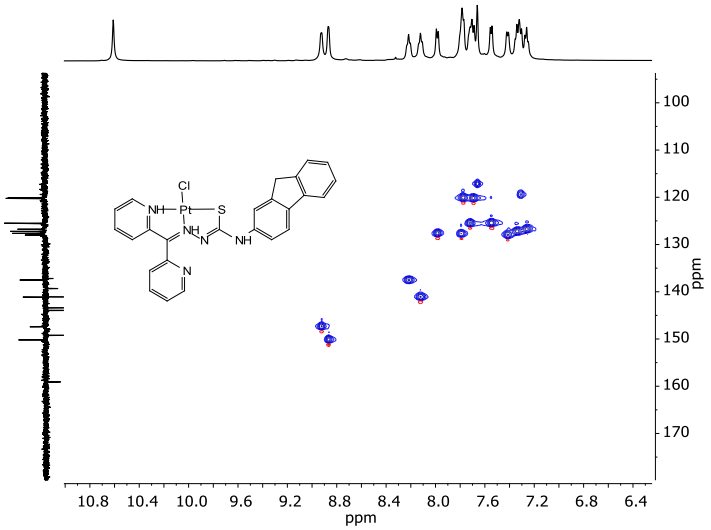


Figure 465. ^{1}H,^{13}C HMQC/HSQC NMR spectrum of [Pt(Dipy(TSC)Flu)Cl] in DMSO-d_6 at 499 MHz.

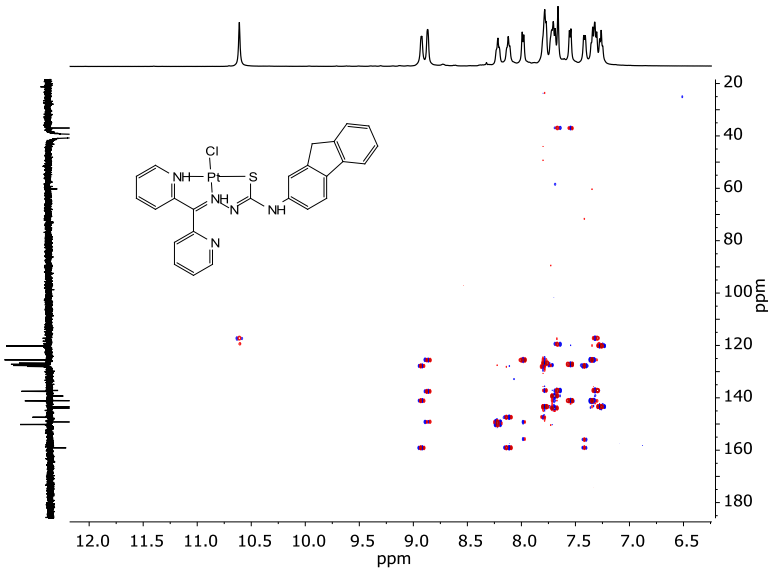


Figure 466. $^{1}H,^{13}C$ HMBC NMR spectrum of [Pt(Dipy(TSC)Flu)Cl] in DMSO-d_6 at 499 MHz.

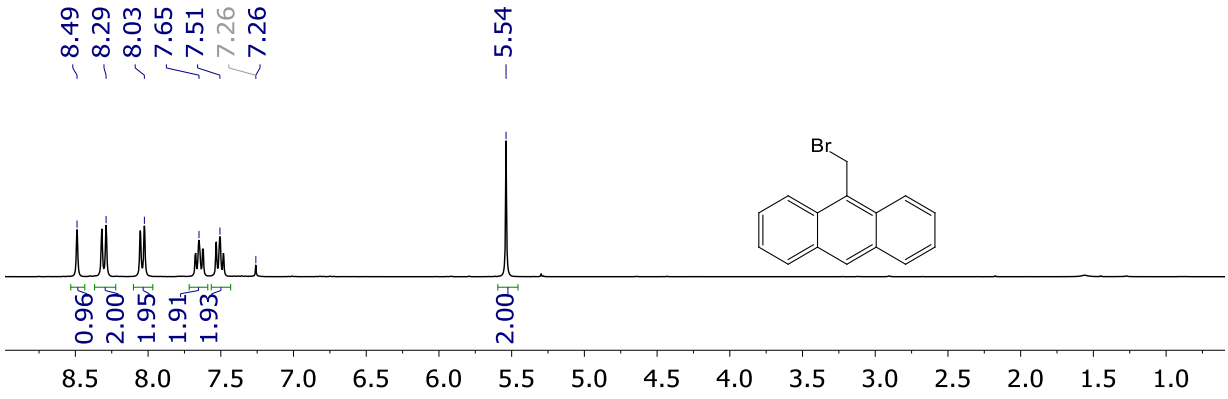


Figure 467. ^{1}H NMR spectrum 9-bromoethylanthracene in $CDCl_3$ at 300 MHz.

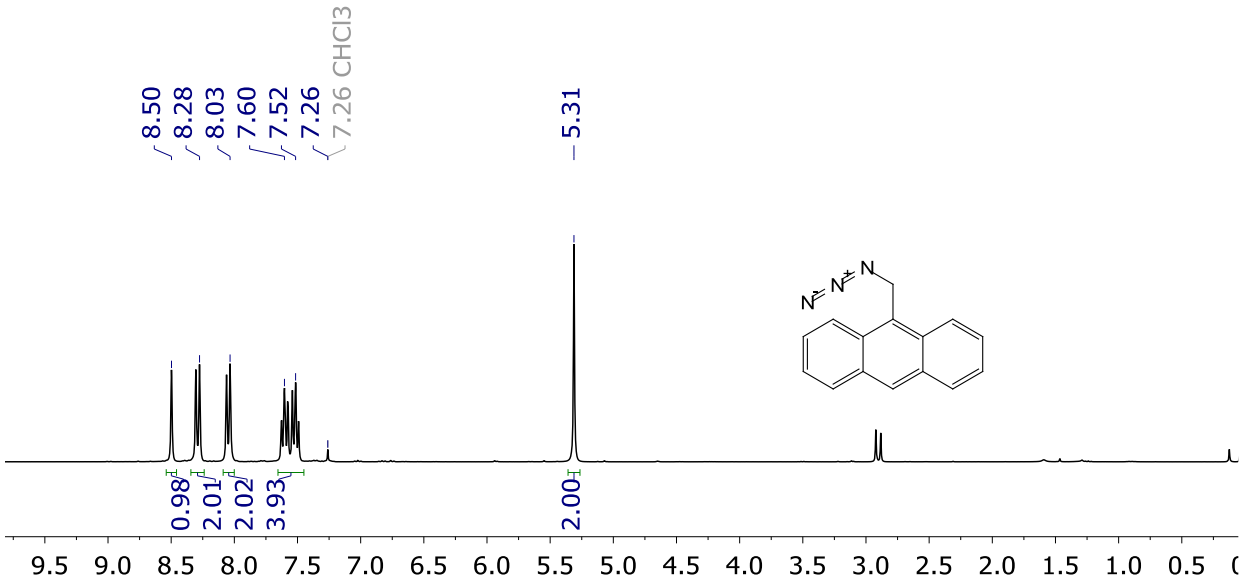


Figure 468. ^{1}H NMR spectrum of 9-(azidomethyl)anthracene in $CDCl_3$ at 300 MHz.

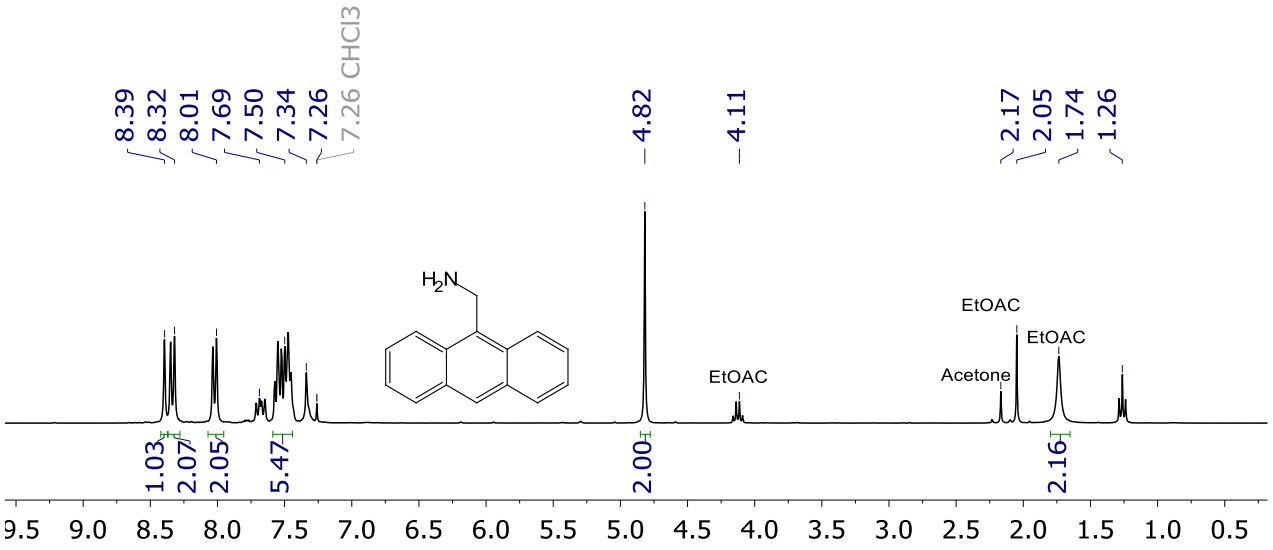


Figure 469. [1]H NMR spectrum 9-(aminomethyl)anthracene in $CDCl_3$ at 300 MHz.

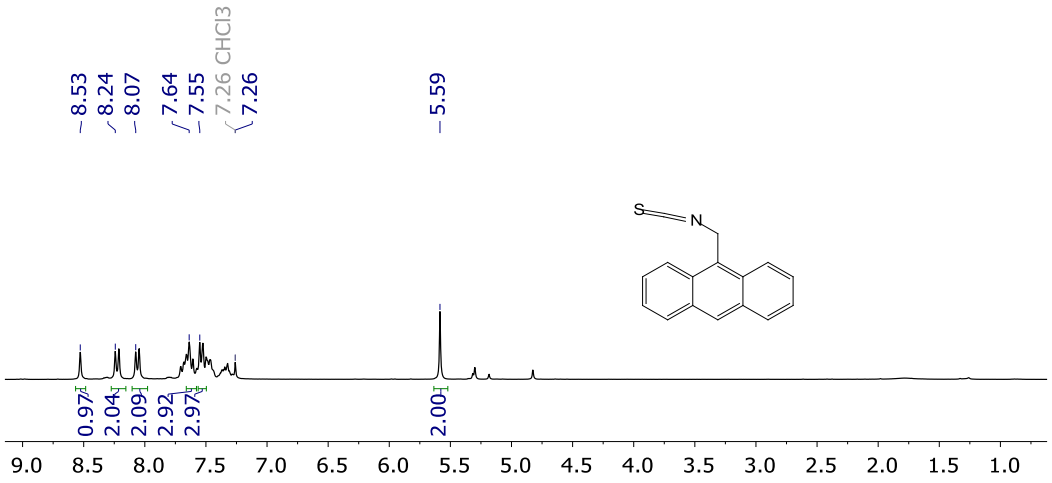


Figure 470. [1]H NMR spectrum of 9-(isothiocyanatomethyl)anthracene in $CDCl_3$ at 300 MHz.

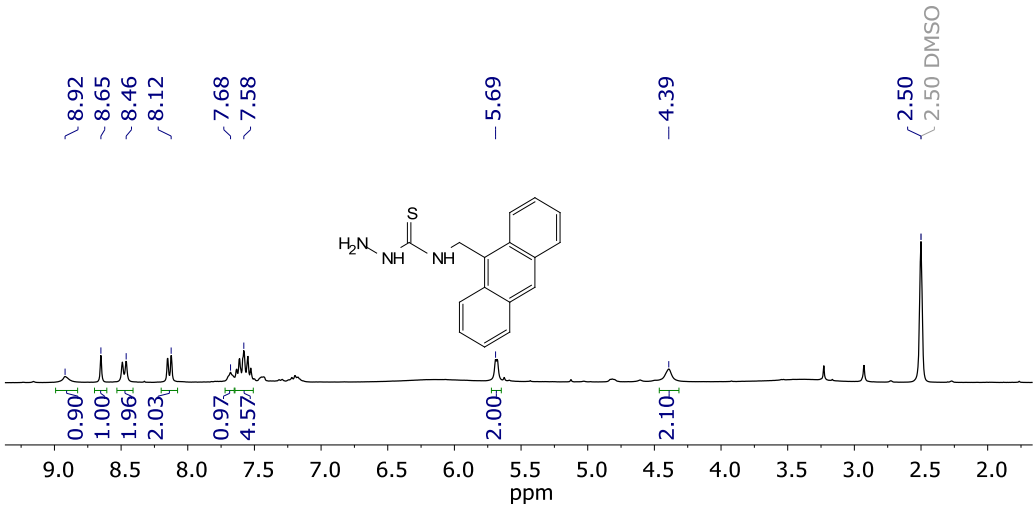


Figure 471. [1]H NMR spectrum of *N*4-9-metyhlantracene thiosemicarbazide in DMSO-d_6 at 300 MHz.

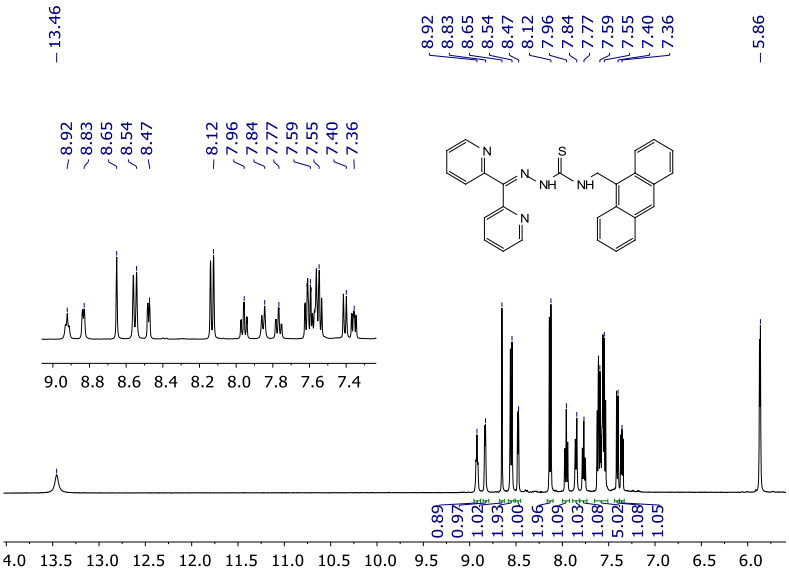


Figure 472. ^{1}H NMR spectrum of di-2-pyridylketone-4-methyl-9-antracene-3-thiosemicarbazone in DMSO-d_6 at 499 MHz.

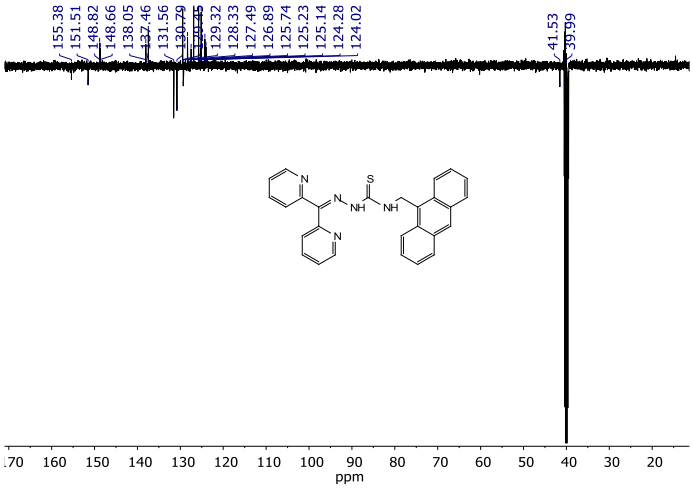


Figure 473. ^{13}C APT NMR spectrum of di-2-pyridylketone-4-methyl-9-antracene-3-thiosemicarbazone in DMSO-d_6 at 499 MHz.

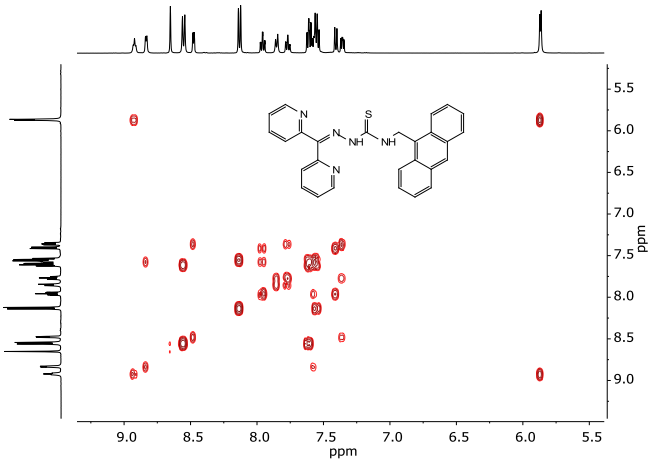


Figure 474. ^{1}H,^{1}H COSY NMR spectrum of di-2-pyridylketone-4-methyl-9-antracene-3-thiosemicarbazone in DMSO-d_6 at 499 MHz.

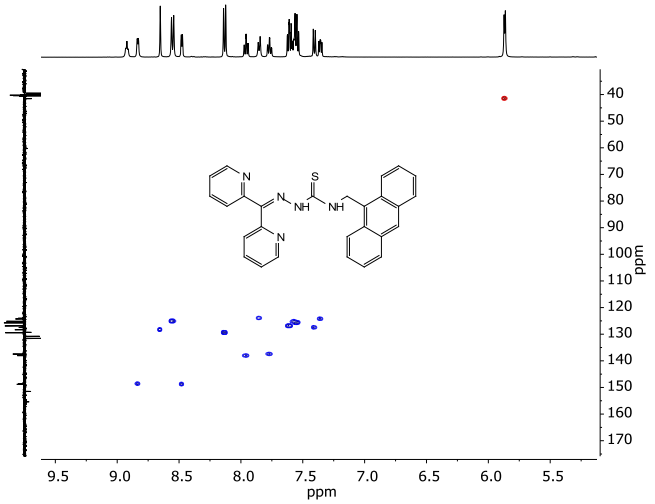


Figure 475. $^{1}H,^{13}C$ HMQC/HSQC NMR spectrum of di-2-pyridylketone-4-methyl-9-antracene-3-thiosemicarbazone in DMSO-d_6 at 499 MHz.

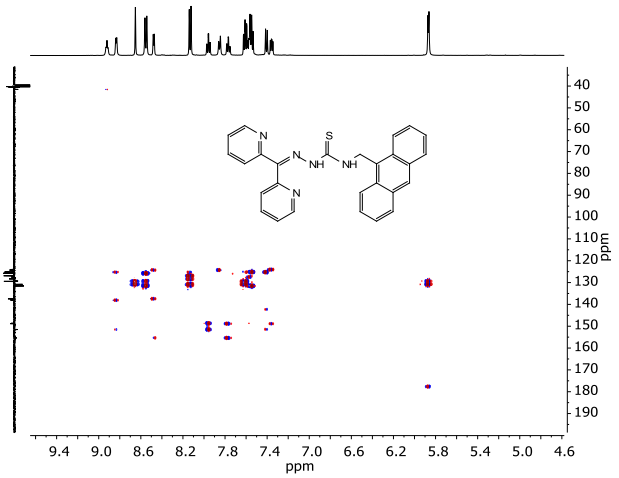


Figure 476. $^{1}H,^{13}C$ HMBC NMR spectrum of di-2-pyridylketone-4-methyl-9-antracene-3-thiosemicarbazone in DMSO-d_6 at 499 MHz.

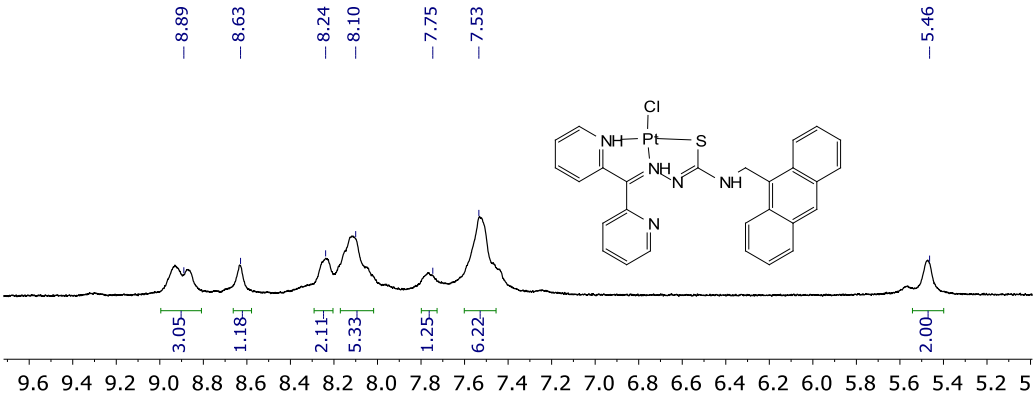


Figure 477. ^{1}H NMR spectrum of [Pt(Dipy(TSC)Ant)Cl] in DMSO-d_6 at 300 MHz.

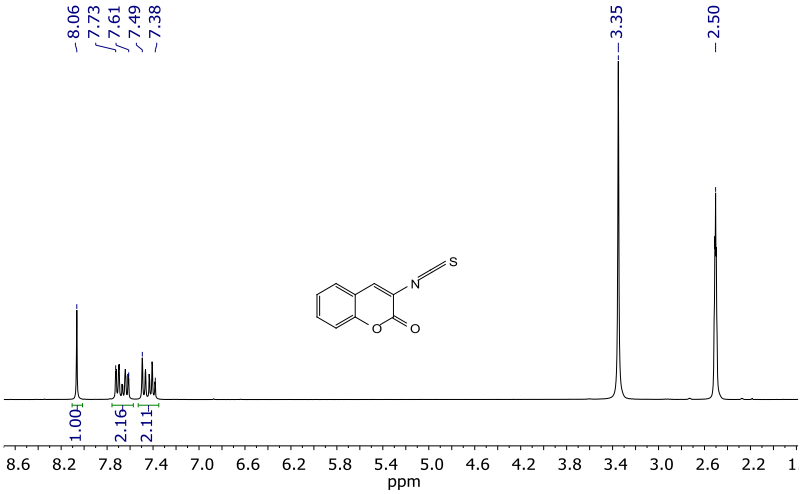


Figure 478. [1]H NMR spectrum of 3-isothiocyanatocumarine in DMSO-d_6 at 300 MHz.

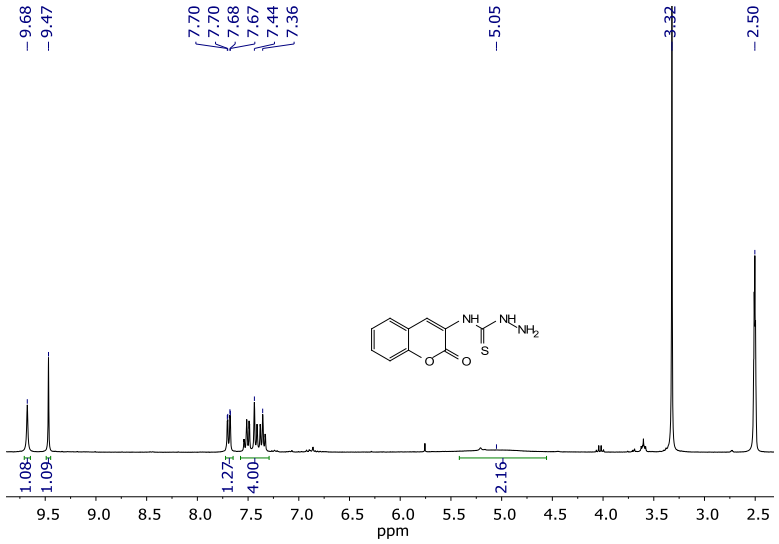


Figure 479. [1]H NMR spectrum of 4-(3-coumarinyl)thiosemicarbazide in DMSO-d_6 at 300 MHz.

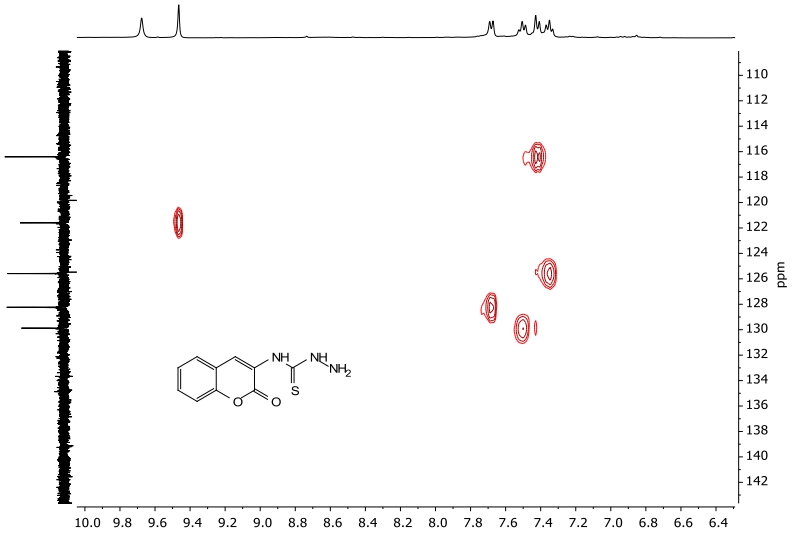


Figure 480. [1]H,[1]H COSY NMR spectrum of 4-(3-coumarinyl)thiosemicarbazide in DMSO-d_6 at 499 MHz.

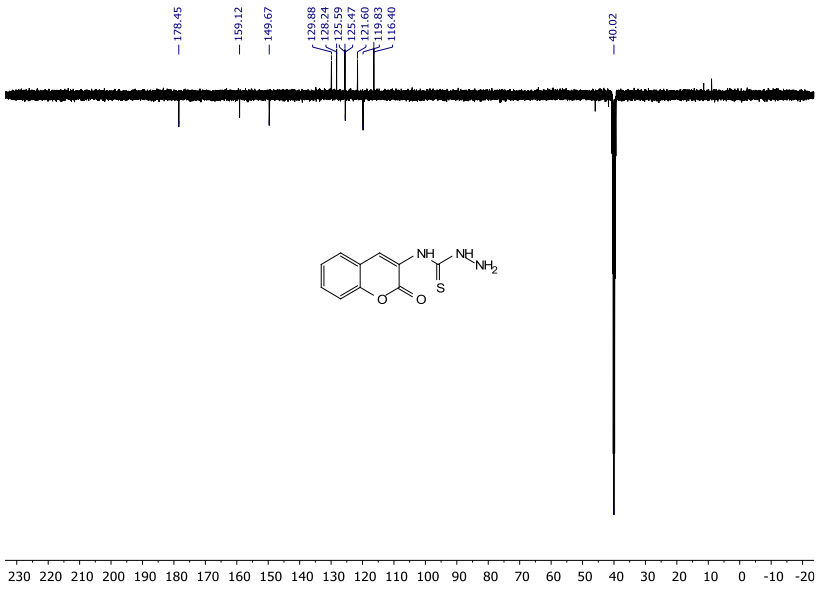


Figure 481. ^{13}C APT NMR spectrum of 4-(3-coumarinyl)thiosemicarbazide in DMSO-d_6 at 499 MHz.

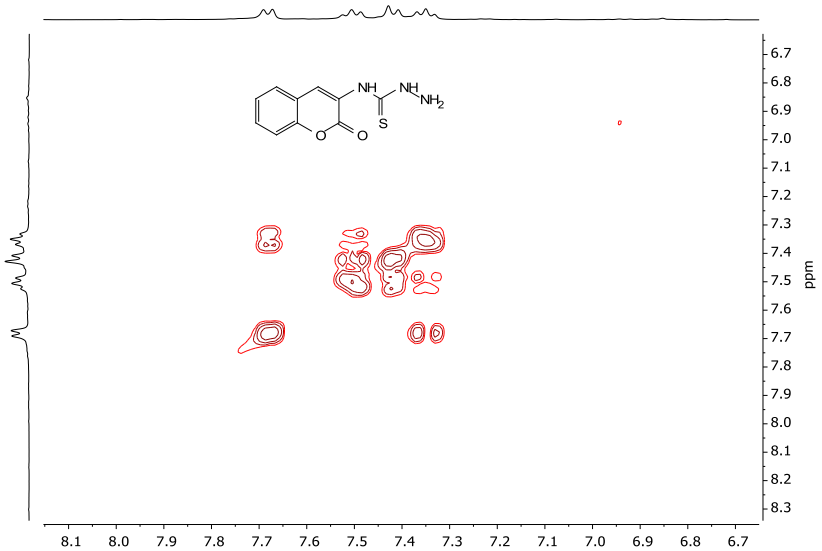


Figure 482. ^{1}H,^{1}H COSY NMR spectrum of 4-(3-coumarinyl)thiosemicarbazide in DMSO-d_6 at 499 MHz.

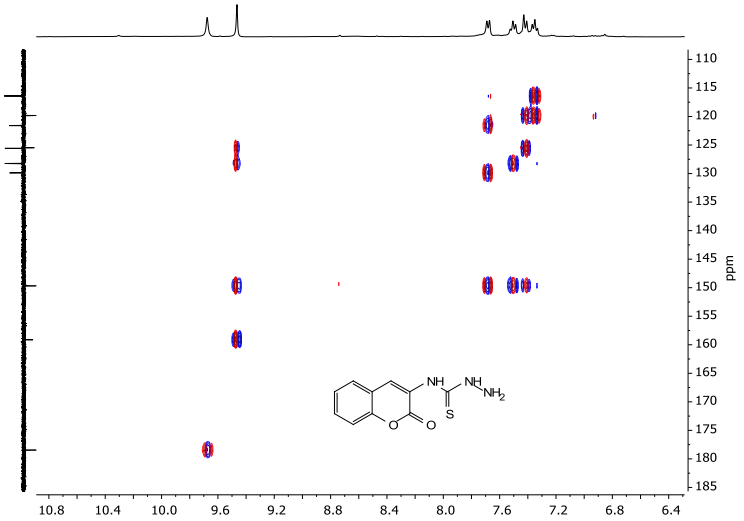


Figure 483. ^{1}H NMR spectrum of 4-(3-coumarinyl)thiosemicarbazide in DMSO-d_6 at 300 MHz.

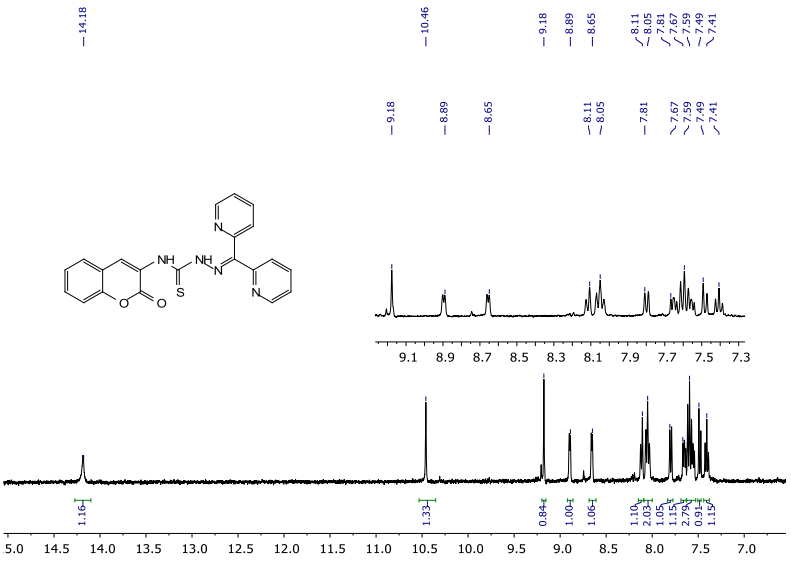


Figure 484. [1]H NMR spectrum of 1-[bis(2-pyridyl)methylene]-4-(3-coumarinyl)thiosemicarbazide in DMSO-d_6 at 300 MHz.

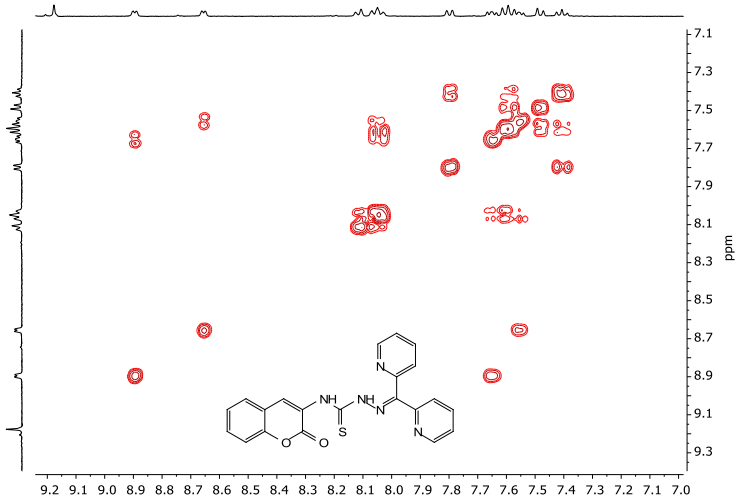


Figure 485. [1]H,[1]H COSY NMR spectrum of 1-[bis(2-pyridyl)methylene]-4-(3-coumarinyl)thiosemicarbazide in DMSO-d_6 at 499 MHz.

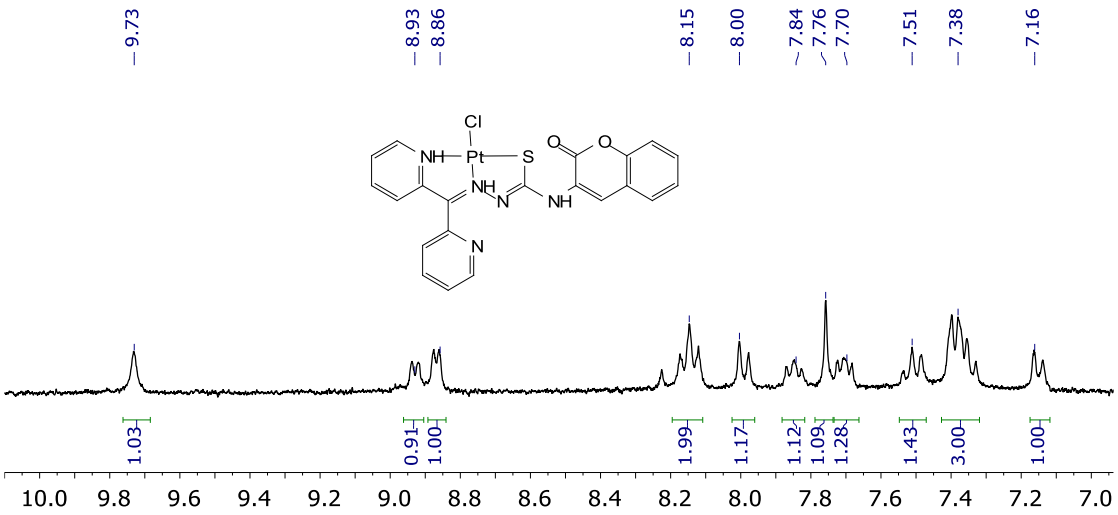


Figure 486. [1]H NMR spectrum of [Pt(Dipy(TSC)Coum)Cl] in DMSO-d_6 at 300 MHz.

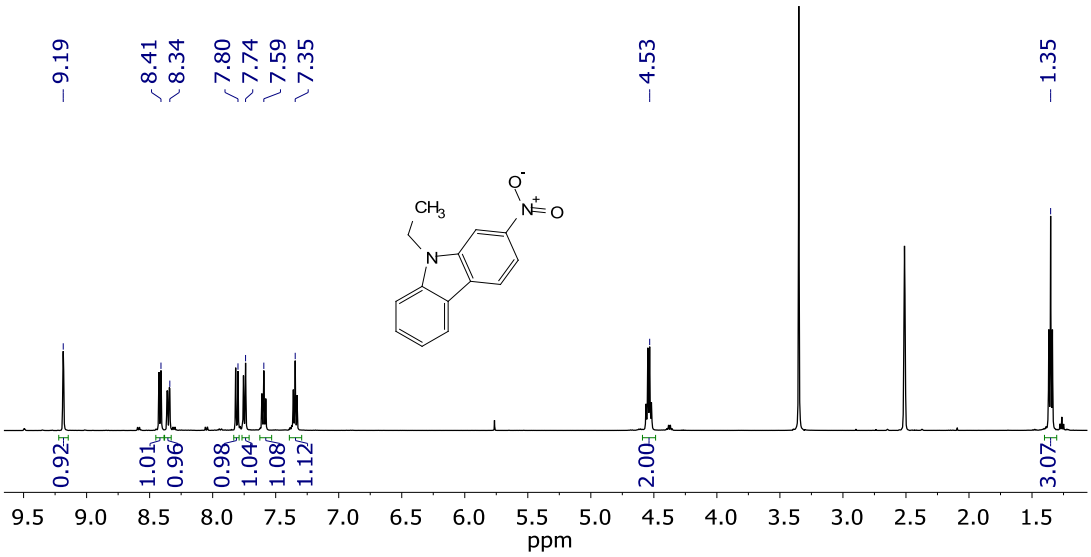


Figure 487. [1]H NMR spectrum of 2-nitro-9-ethylcarbazole in DMSO-*d*6 at 300 MHz.

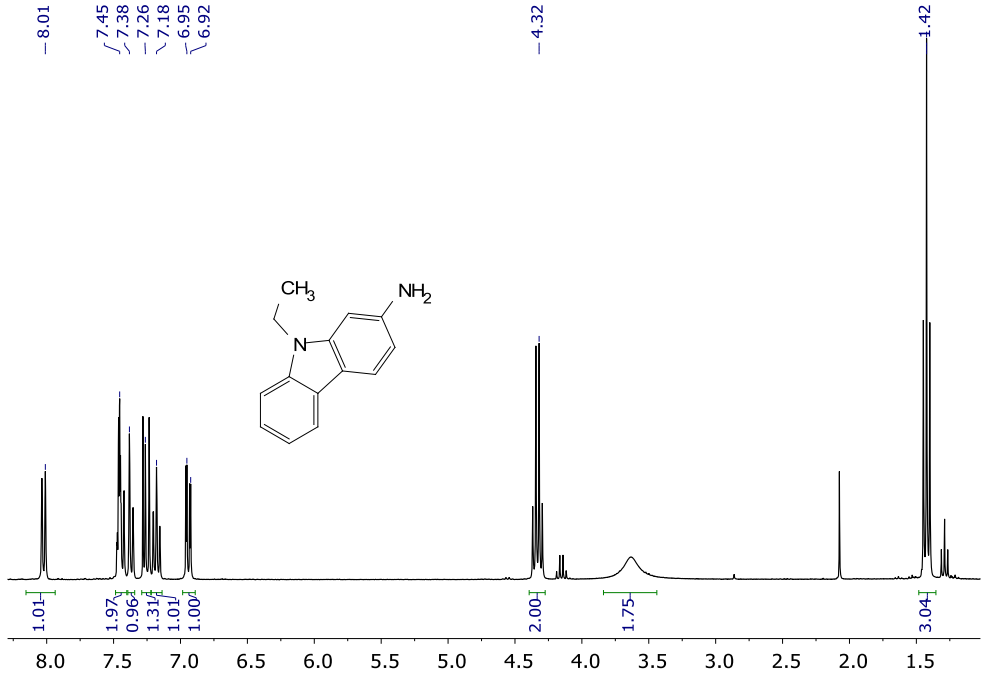


Figure 488. [1]H NMR spectrum of 2-amino-9-ethylcarbazole in DMSO-*d*6 at 300 MHz.

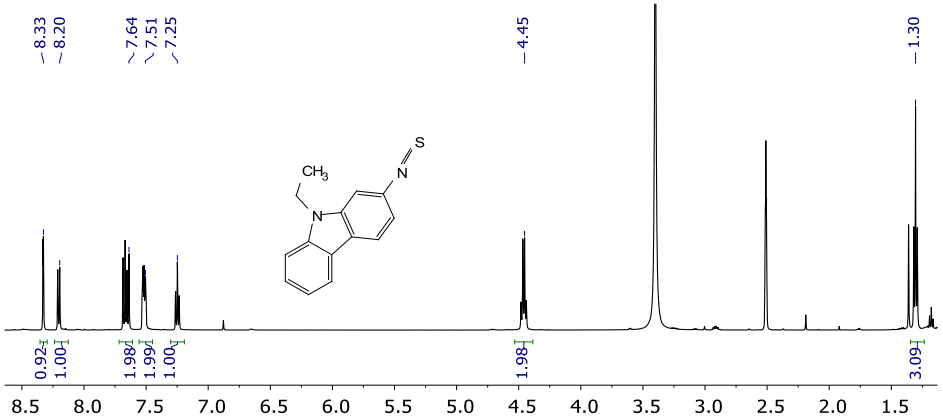


Figure 489. [1]H NMR spectrum of 2-isothiocyanato-9-ethylcarbazole in DMSO-*d*6 at 300 MHz.

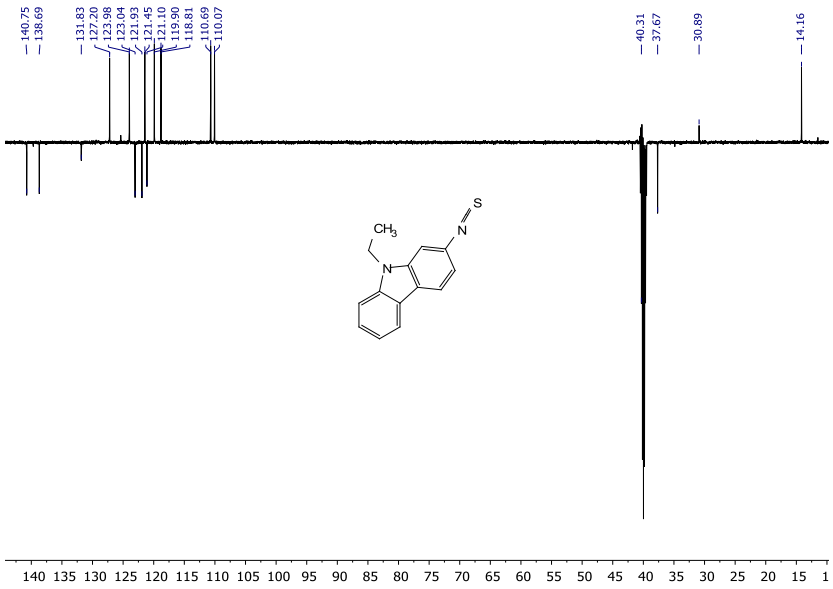


Figure 490. ^{13}C APT NMR spectrum of 2-isothiocyanato-9-ethylcarbazole in DMSO-d_6 at 499 MHz.

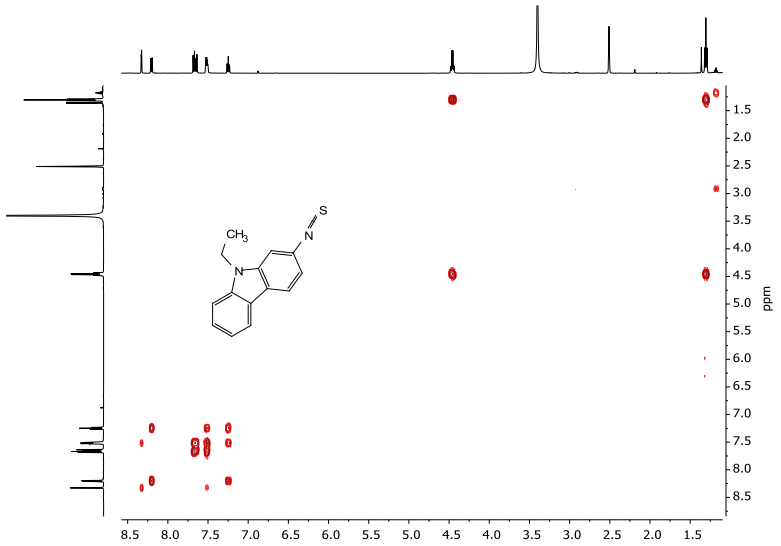


Figure 491. ^{1}H,^{1}H COSY NMR spectrum of 2-isothiocyanato-9-ethylcarbazole in DMSO-d_6 at 499 MHz.

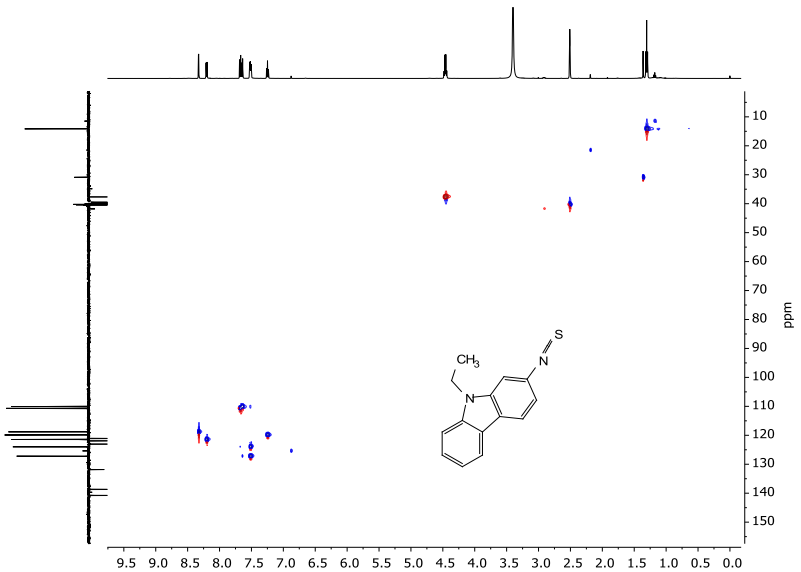


Figure 492. ^{1}H,^{13}C HMQC/HSQC NMR spectrum of 2-isothiocyanato-9-ethylcarbazole in DMSO-d_6 at 499 MHz.

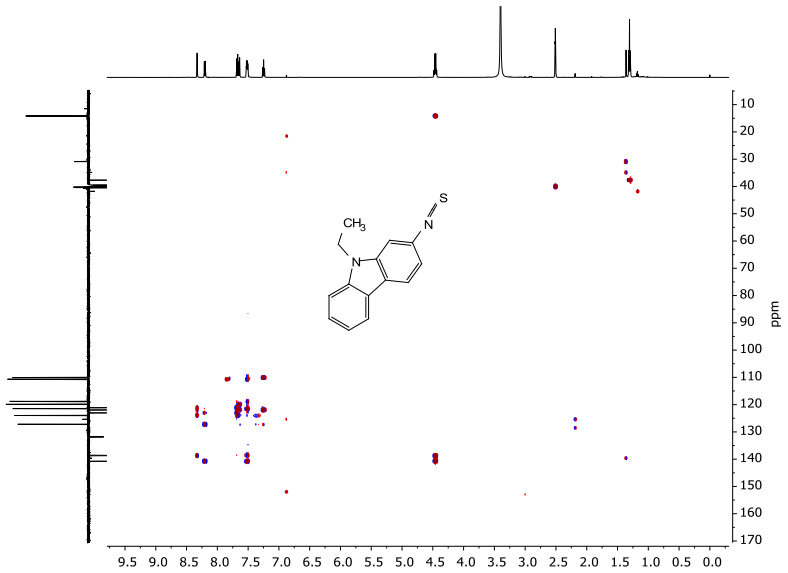


Figure 493. $^{1}H,^{13}C$ HMBC NMR spectrum of 2-isothiocyanato-9-ethylcarbazole in DMSO-d_6 at 499 MHz.

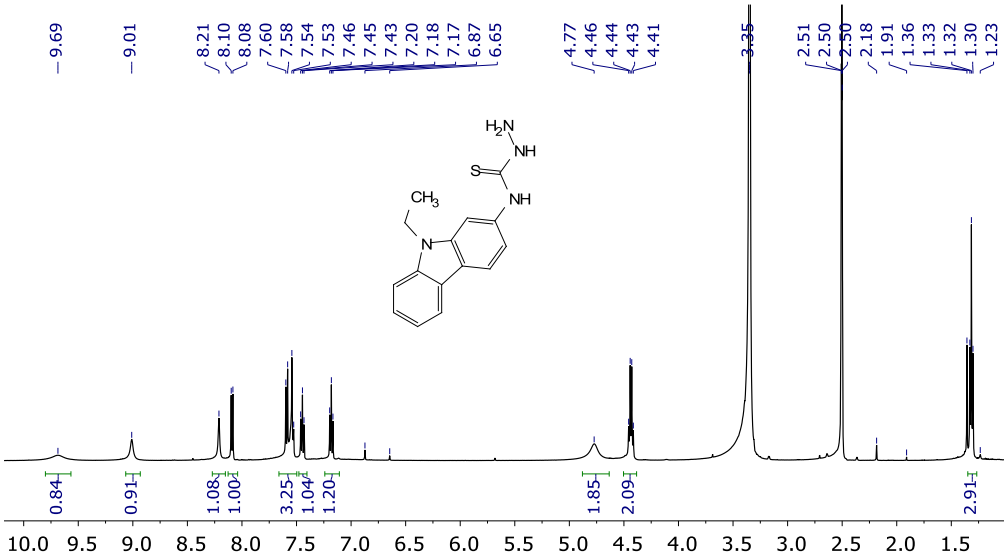


Figure 494. ^{1}H NMR spectrum of 4-(9-ethyl-2-carbazolyl)thiosemicarbazide in DMSO-d_6 at 300 MHz.

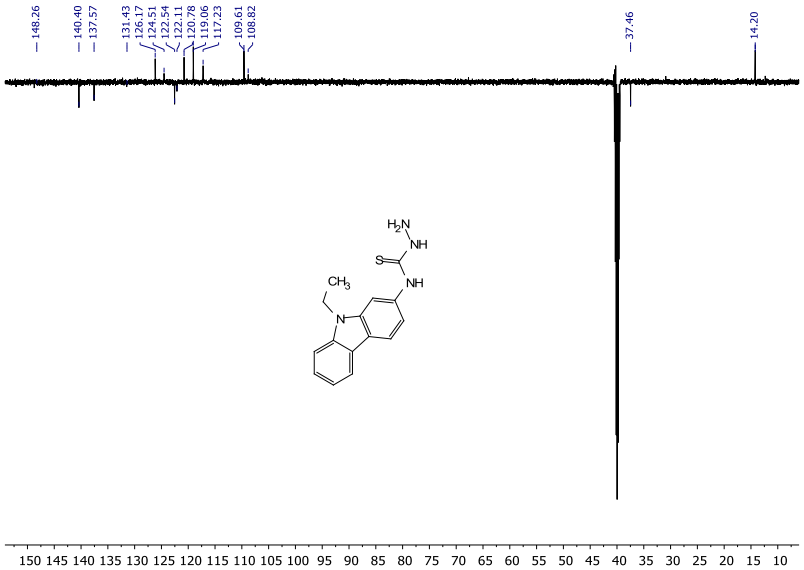


Figure 495. ^{13}C APT NMR spectrum of 4-(9-ethyl-2-carbazolyl)thiosemicarbazide in DMSO-d_6 at 499 MHz.

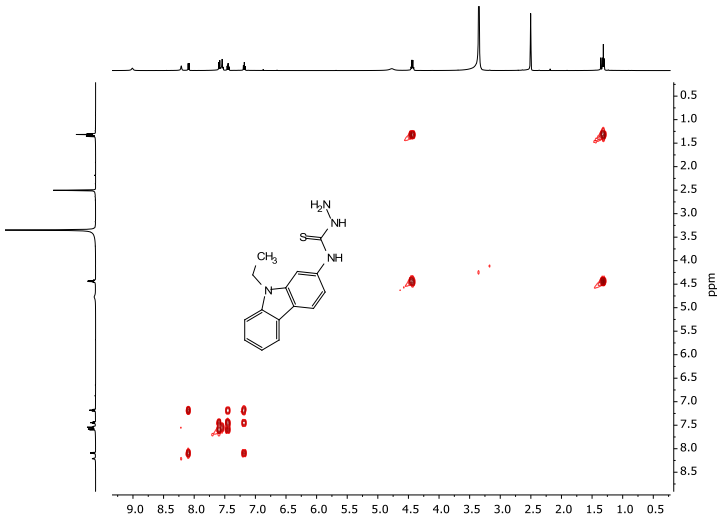


Figure 496. $^{1}H,^{1}H$ COSY NMR spectrum of 4-(9-ethyl-2-carbazolyl)thiosemicarbazide in DMSO-d_6 at 499 MHz.

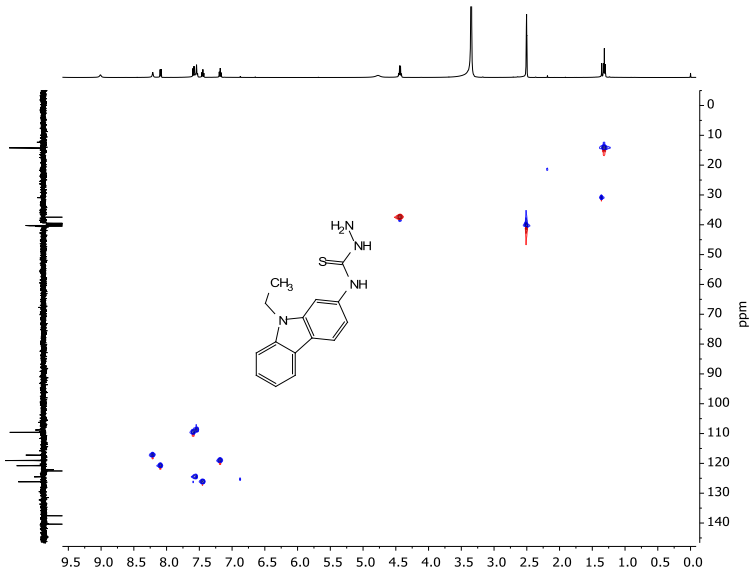


Figure 497. $^{1}H,^{13}C$ HMQC/HSQC NMR spectrum of 4-(9-ethyl-2-carbazolyl)thiosemicarbazide in DMSO-d_6 at 499 MHz.

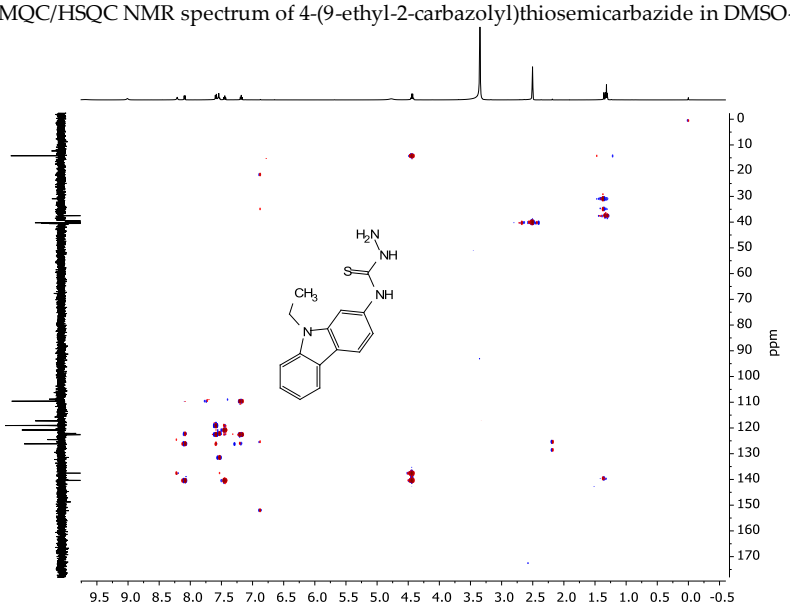


Figure 498. $^{1}H,^{13}C$ HMBC NMR spectrum of 4-(9-ethyl-2-carbazolyl)thiosemicarbazide in DMSO-d_6 at 499 MHz.

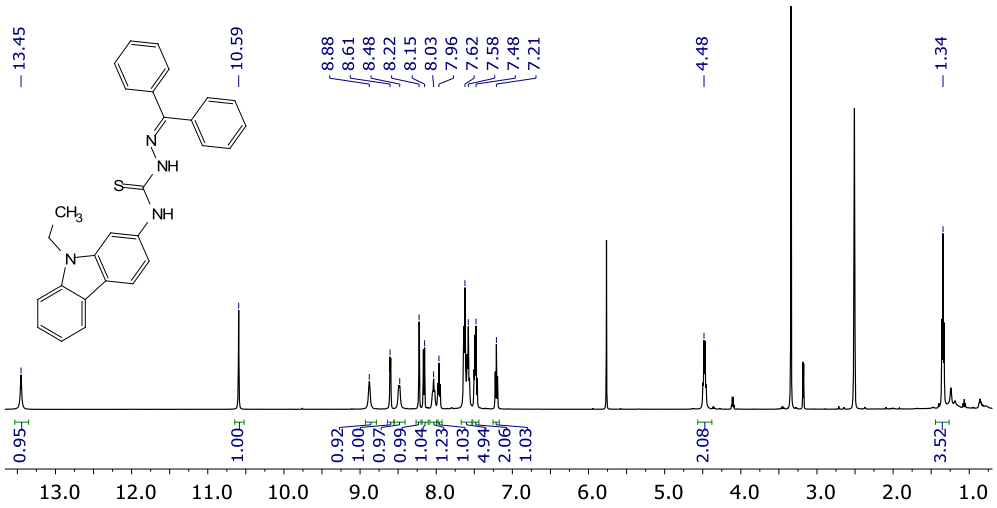


Figure 499. [1]H NMR spectrum of 1-[bis(2-pyridyl)methylene]-4-(9-ethyl-2-carbazolyl)thiosemicarbazide in DMSO-d_6 at 300 MHz.

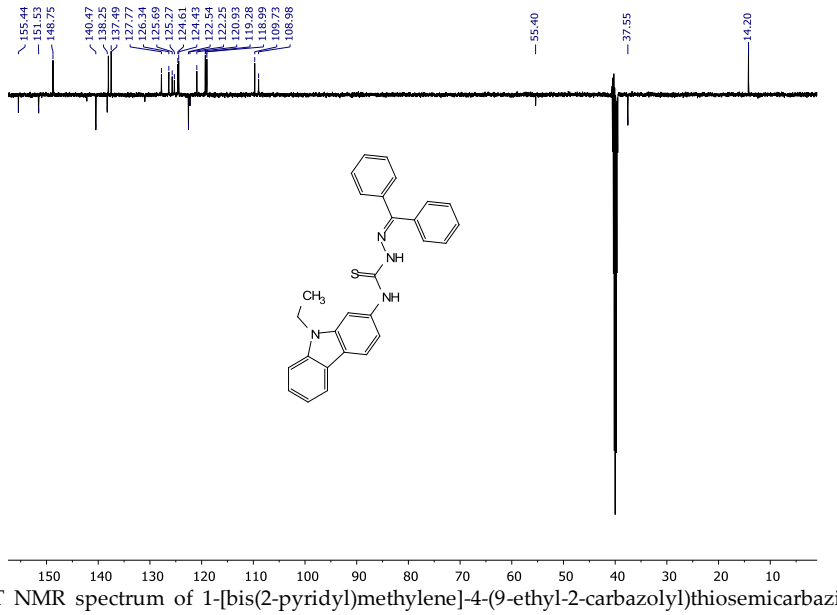


Figure 500. [13]C APT NMR spectrum of 1-[bis(2-pyridyl)methylene]-4-(9-ethyl-2-carbazolyl)thiosemicarbazide in DMSO-d_6 at 499 MHz.

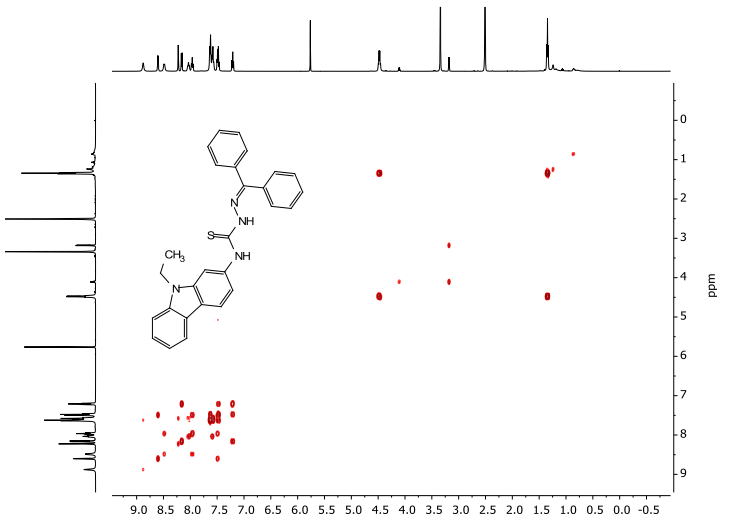


Figure 501. [1]H,[1]H COSY NMR spectrum of 1-[bis(2-pyridyl)methylene]-4-(9-ethyl-2-carbazolyl)thiosemicarbazide in DMSO-d_6 at 499 MHz.

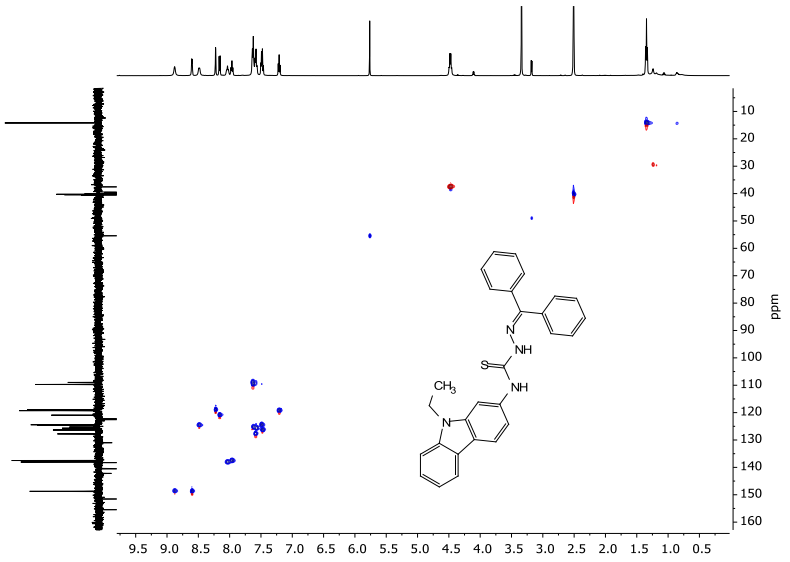


Figure 502. $^{1}H,^{13}C$ HMQC/HSQC NMR spectrum of 1-[bis(2-pyridyl)methylene]-4-(9-ethyl-2-carbazolyl)thiosemicarbazide in DMSO-d_6 at 499 MHz.

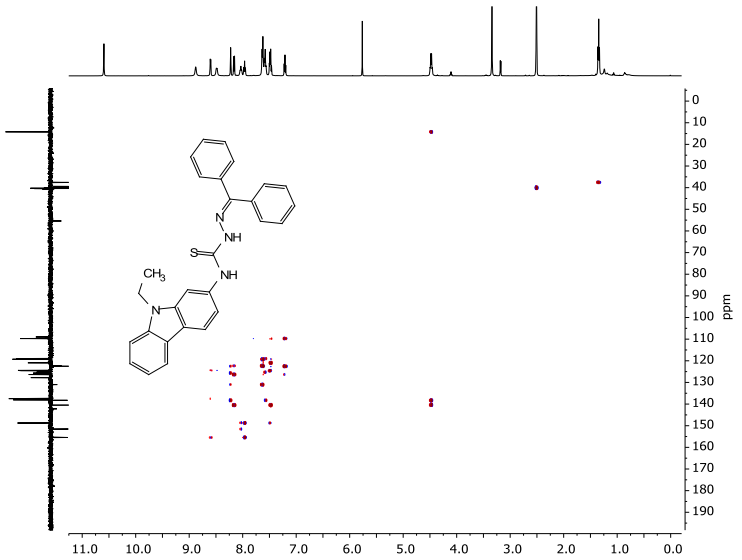


Figure 503. $^{1}H,^{13}C$ HMBC NMR spectrum of 1-[bis(2-pyridyl)methylene]-4-(9-ethyl-2-carbazolyl)thiosemicarbazide in DMSO-d_6 at 499 MHz.

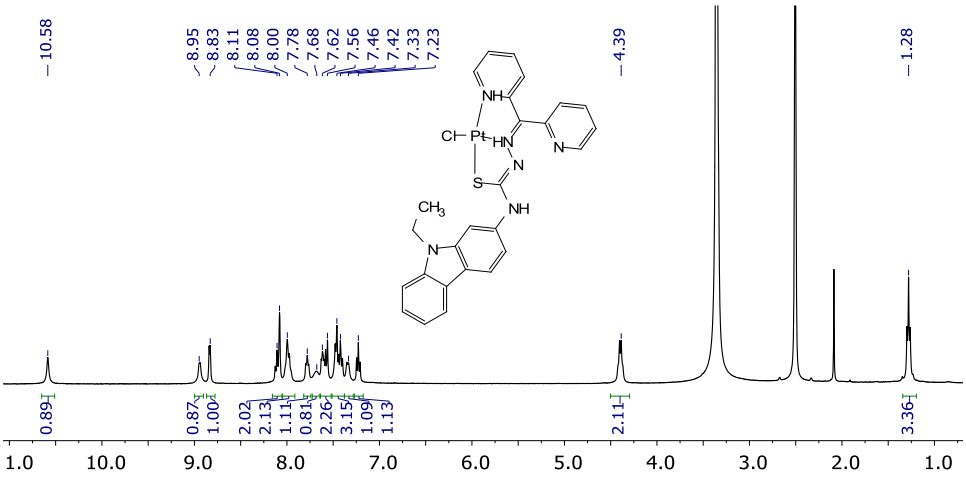


Figure 504. ^{1}H NMR spectrum of [Pt(Dipy(TSC)Carb)Cl] in DMSO-d_6 at 300 MHz.

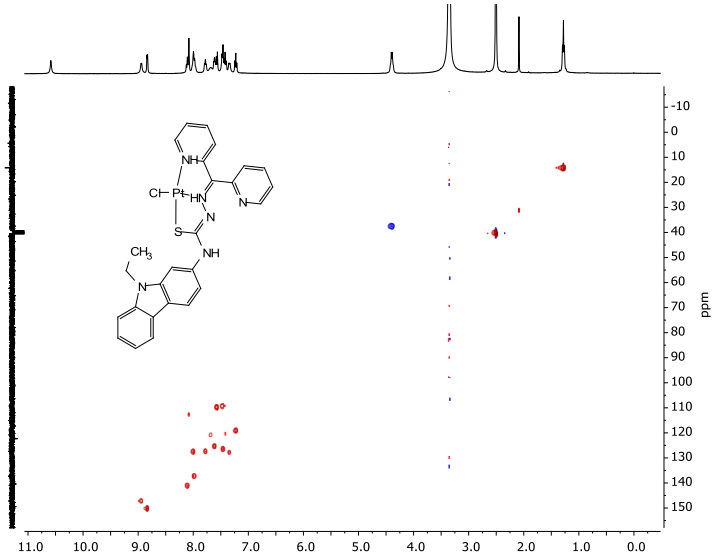


Figure 505. $^{1}H,^{13}C$ HMQC/HSQC NMR spectrum of [Pt(Dipy(TSC)Carb)Cl] in DMSO-d_6 at 499 MHz.

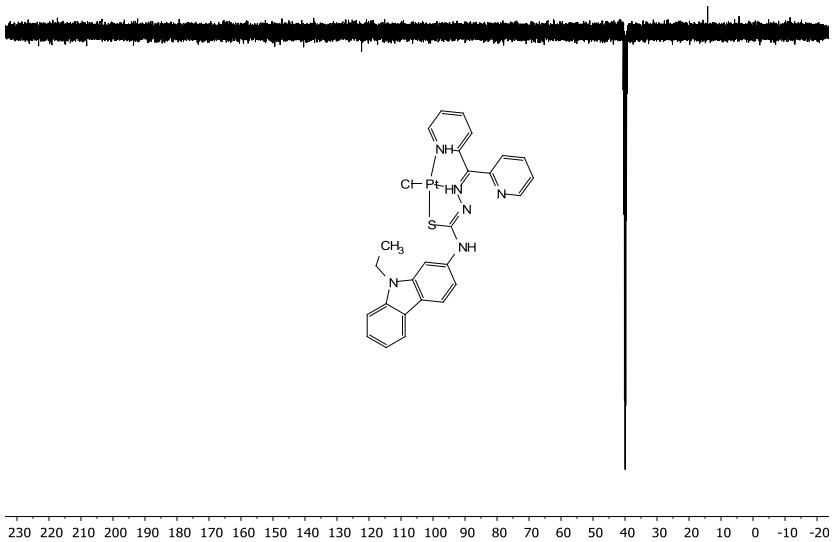


Figure 506. ^{13}C APT NMR spectrum of [Pt(Dipy(TSC)Carb)Cl] in DMSO-d_6 at 499 MHz.

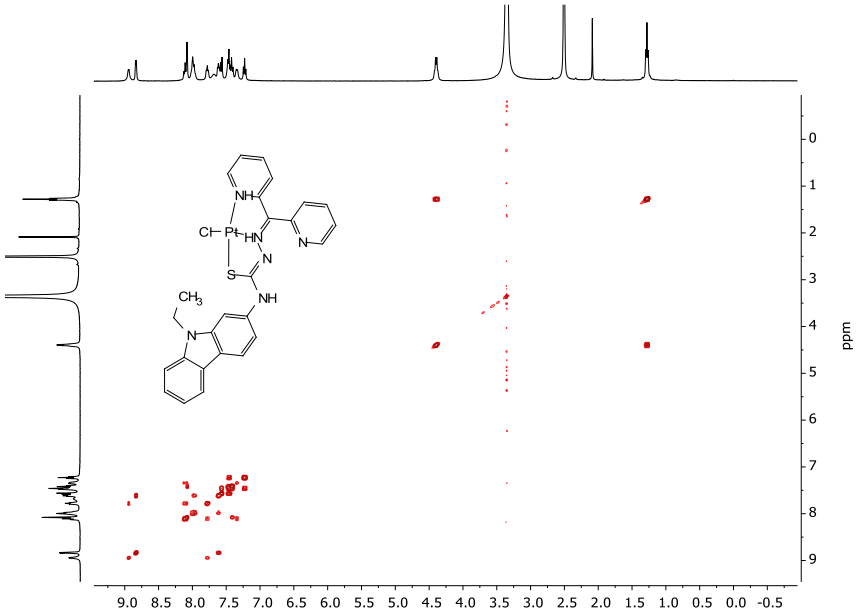


Figure 507. $^{1}H,^{1}H$ COSY NMR spectrum of [Pt(Dipy(TSC)Carb)Cl] in DMSO-d_6 at 499 MHz.

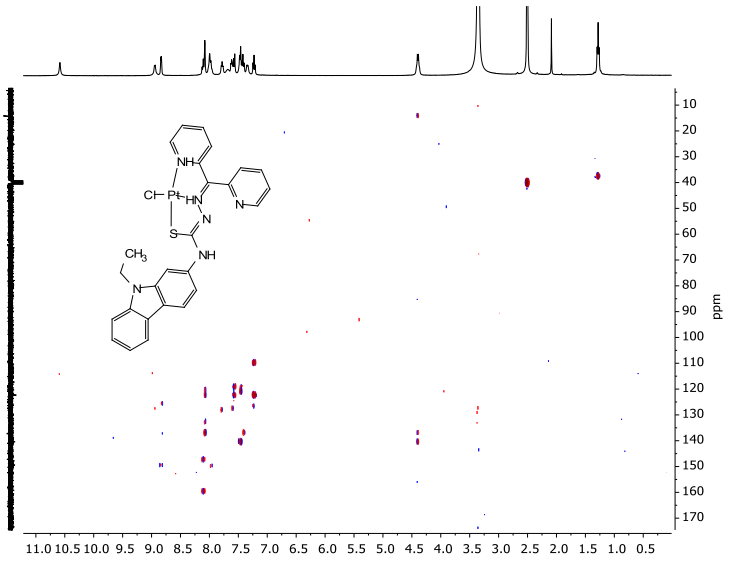


Figure 508. $^{1}H,^{13}C$ HMBC NMR spectrum of [Pt(Dipy(TSC)Carb)Cl] in DMSO-d_6 at 499 MHz.

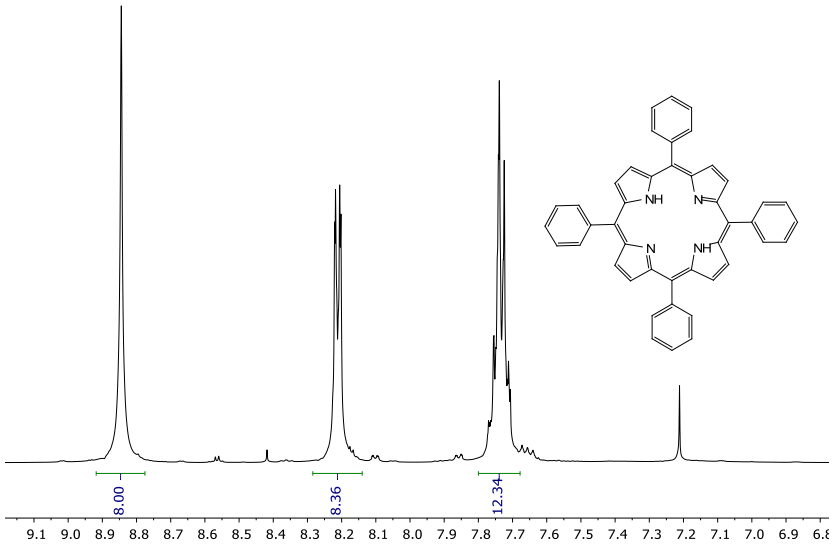


Figure 509. ^{1}H NMR spectrum of tetraphenylporphyrin in DMSO-d_6 at 300 MHz.

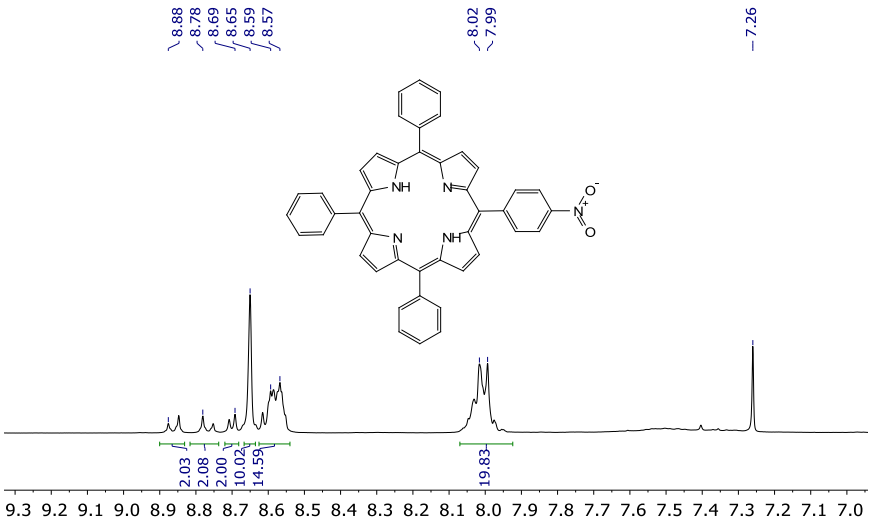


Figure 510. ^{1}H NMR spectrum of 5-(p-nitrophenyl)-10,15,20-triphenylporphyrin in DMSO-d_6 at 300 MHz.

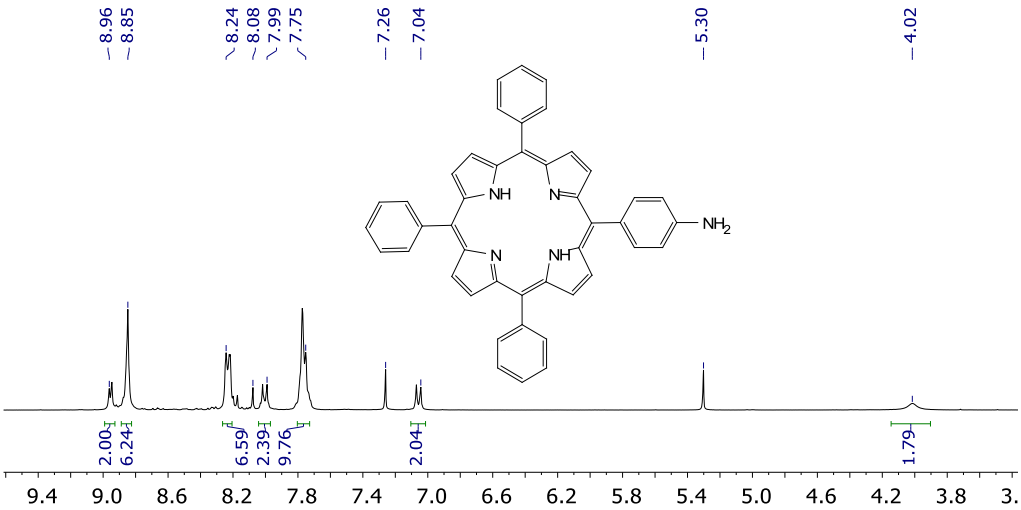


Figure 511. [1]H NMR spectrum of 5-(4-aminophenyl)-10,15,20-triphenylporphyrin in DMSO-d_6 at 300 MHz.

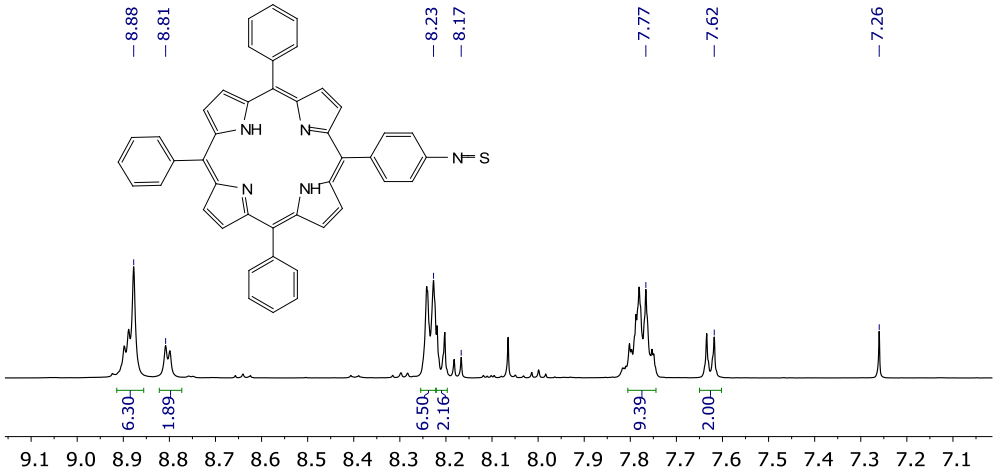


Figure 512. [1]H NMR spectrum of 5-(4-isothiocyanatophenyl)-10,15,20-triphenylporphyrin in DMSO-d_6 at 300 MHz.

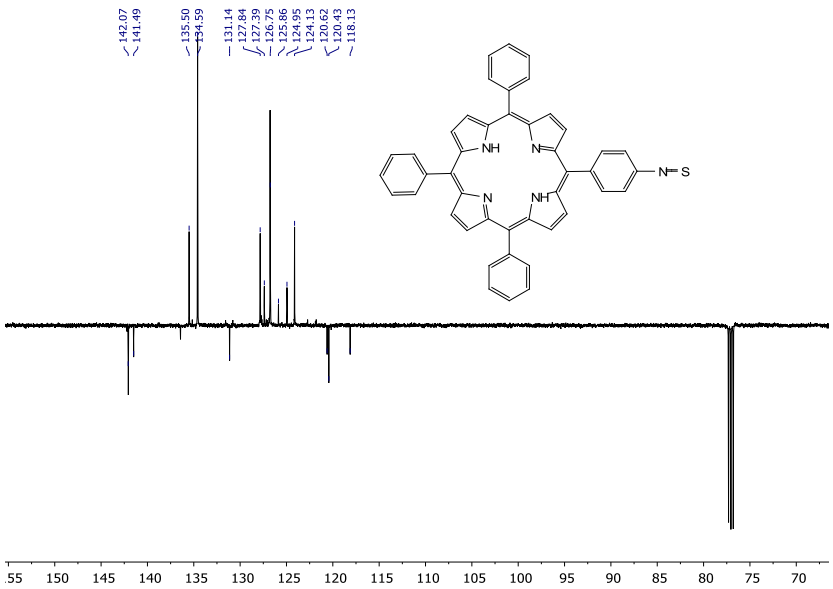


Figure 513. [13]C APT NMR spectrum of 5-(4-isothiocyanatophenyl)-10,15,20-triphenylporphyrin in DMSO-d_6 at 499 MHz.

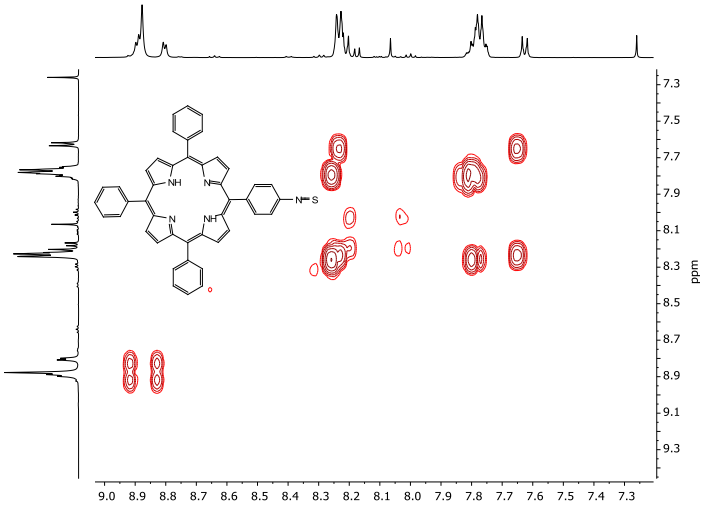


Figure 514. $^{1}H,^{1}H$ COSY NMR spectrum of 5-(4-isothiocyanatophenyl)-10,15,20-triphenylporphyrin in DMSO-d_6 at 499 MHz.

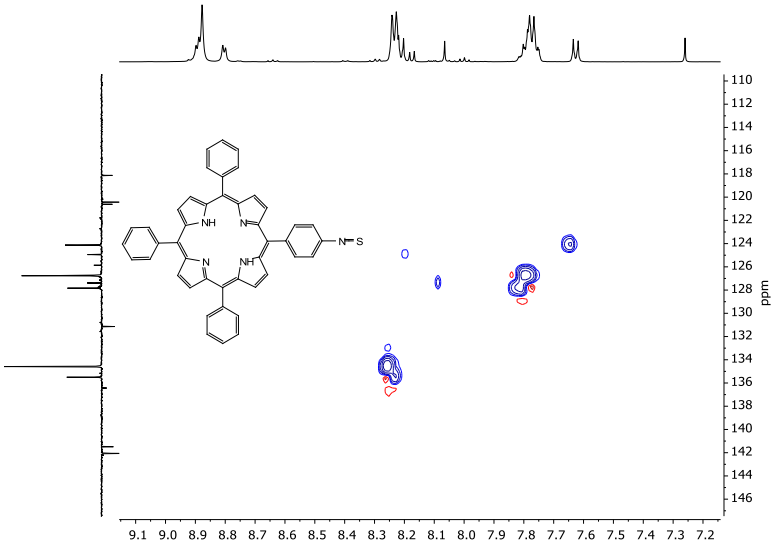


Figure 515. $^{1}H,^{13}C$ HMQC/HSQC NMR spectrum of 5-(4-isothiocyanatophenyl)-10,15,20-triphenylporphyrin in DMSO-d_6 at 499 MHz.

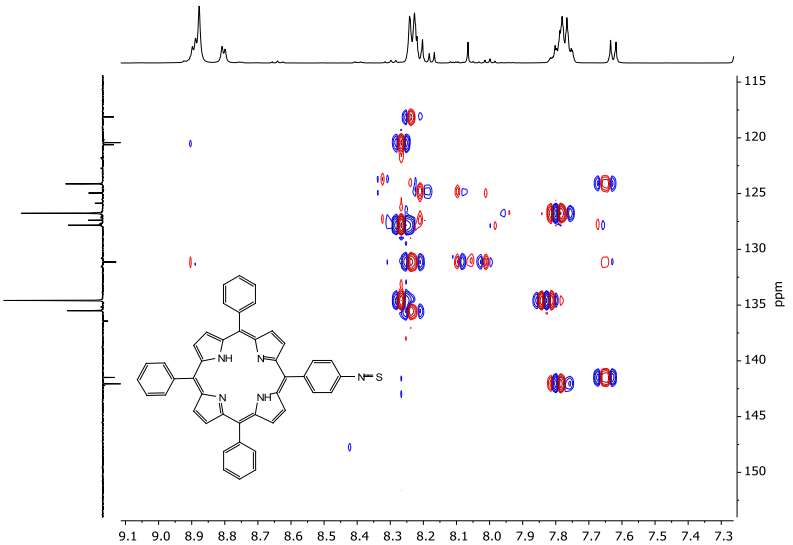


Figure 516. $^{1}H,^{13}C$ HMBC NMR spectrum of 5-(4-isothiocyanatophenyl)-10,15,20-triphenylporphyrin in DMSO-d_6 at 499 MHz.

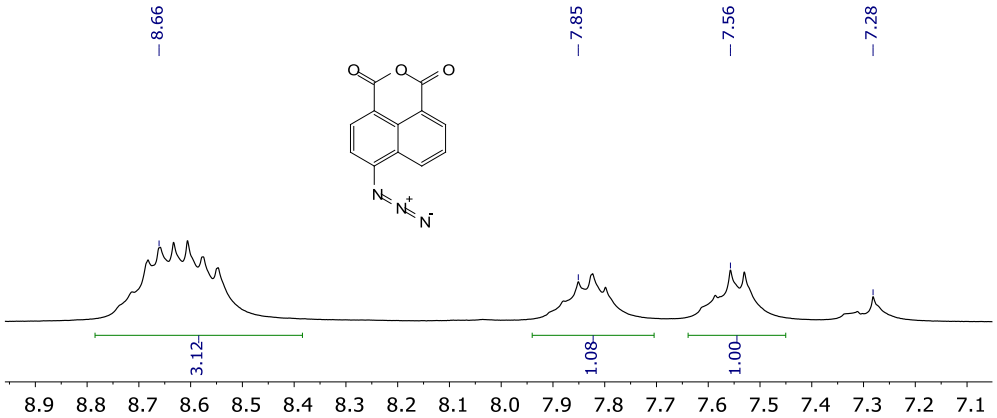


Figure 517. [1]H NMR spectrum of 4-nitro-1,8-naphthalic anhydride in DMSO-*d*6 at 300 MHz.

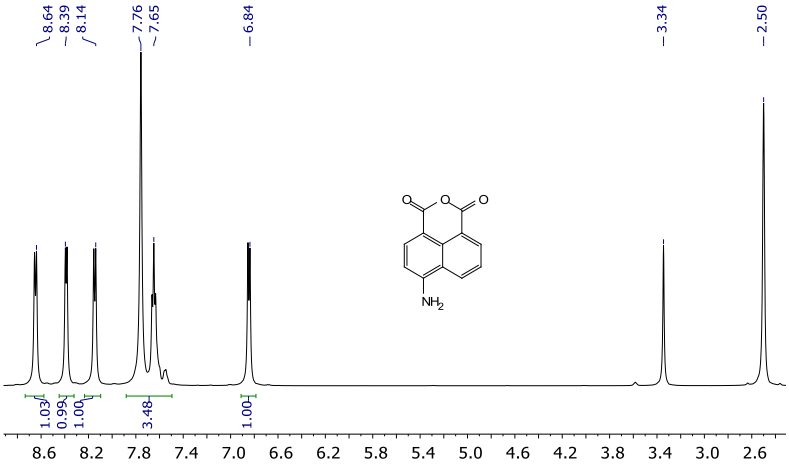


Figure 518. [1]H NMR spectrum of 4-amino-1,8-naphthalic anhydride in DMSO-*d*6 at 300 MHz.

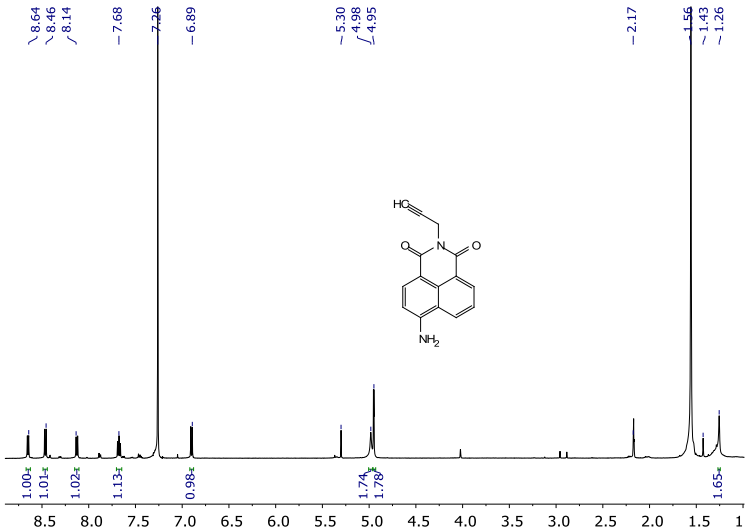


Figure 519. [1]H NMR spectrum of 6-amino-2-(prop-2-ynyl)-2-aza-1*H*-phenalene-1,3(2*H*)-dione in DMSO-*d*6 at 300 MHz.

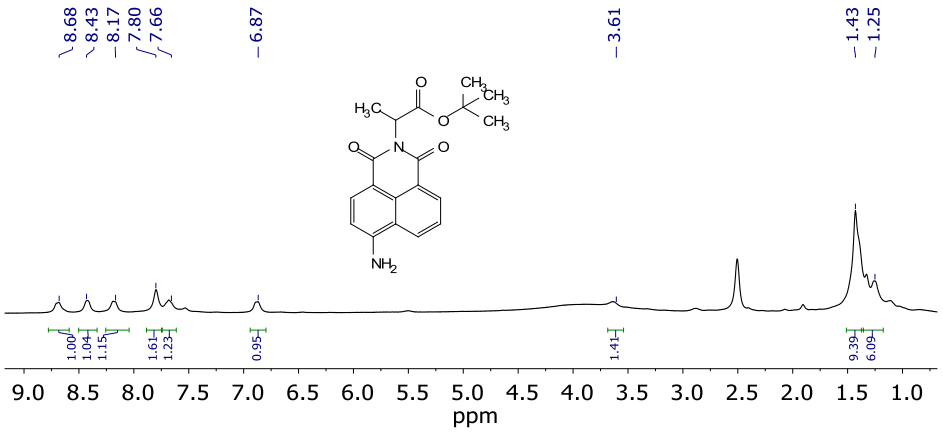


Figure 520. [1]H NMR spectrum of *tert*-butyl 2-[6-amino-1,3-dioxo-2-aza-3*H*-phenalen-2(1*H*)-yl]propanoate in DMSO-d_6 at 300 MHz.

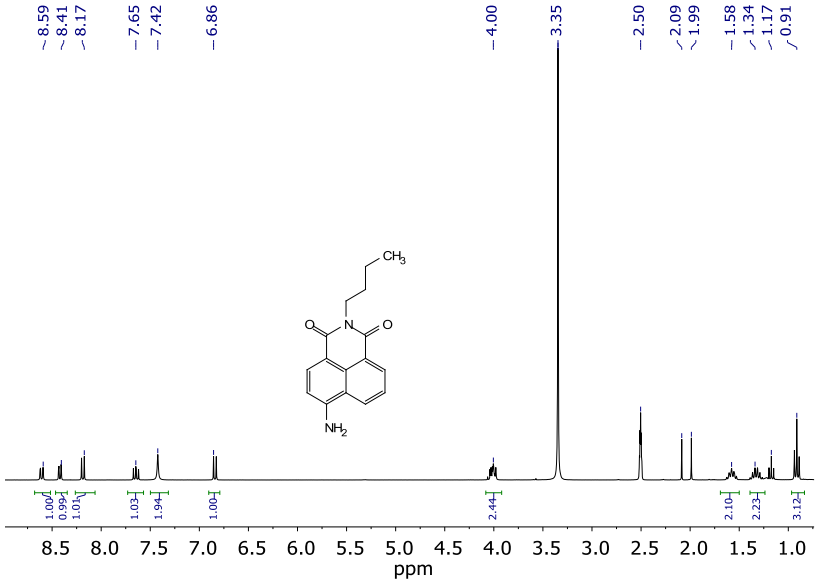


Figure 521. [1]H NMR spectrum of 6-amino-2-butyl-2-aza-1*H*-phenalene-1,3(2*H*)-dione in DMSO-d_6 at 300 MHz.

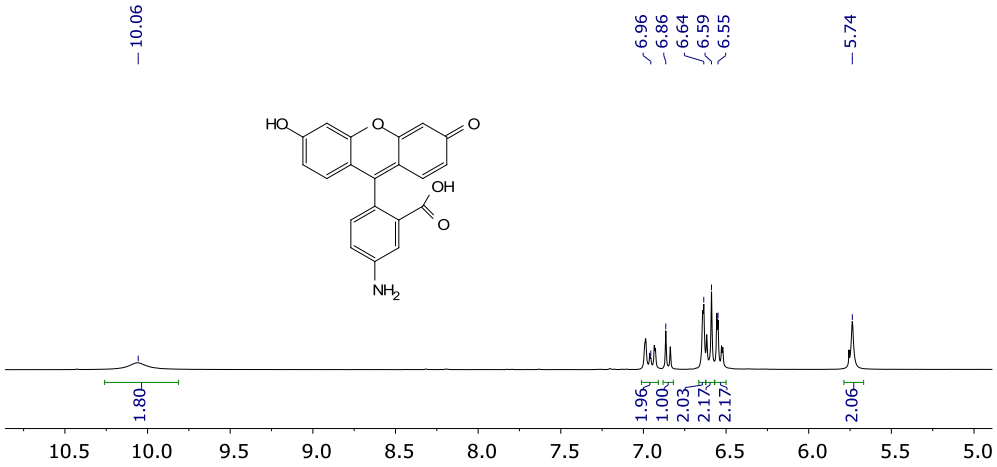


Figure 522. [1]H NMR spectrum of 5-aminoflourescein in DMSO-d_6 at 300 MHz.

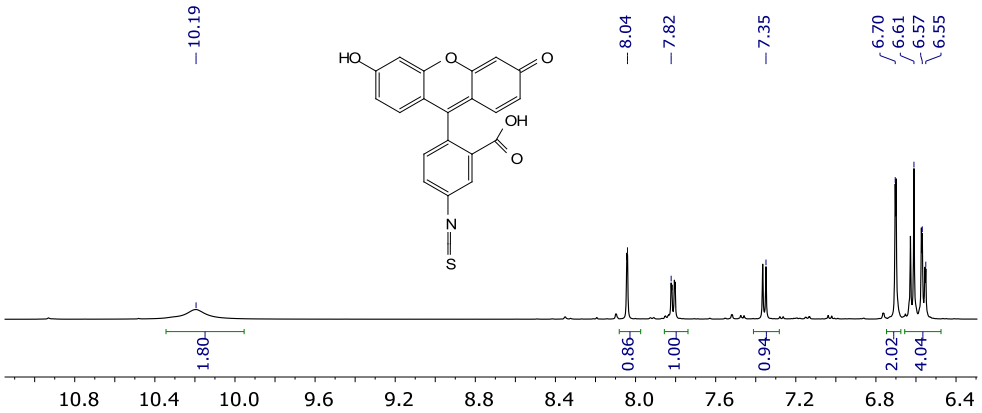


Figure 523. [1]H NMR spectrum of fluoresceine-5-isothiocyanate in DMSO-*d*6 at 300 MHz.

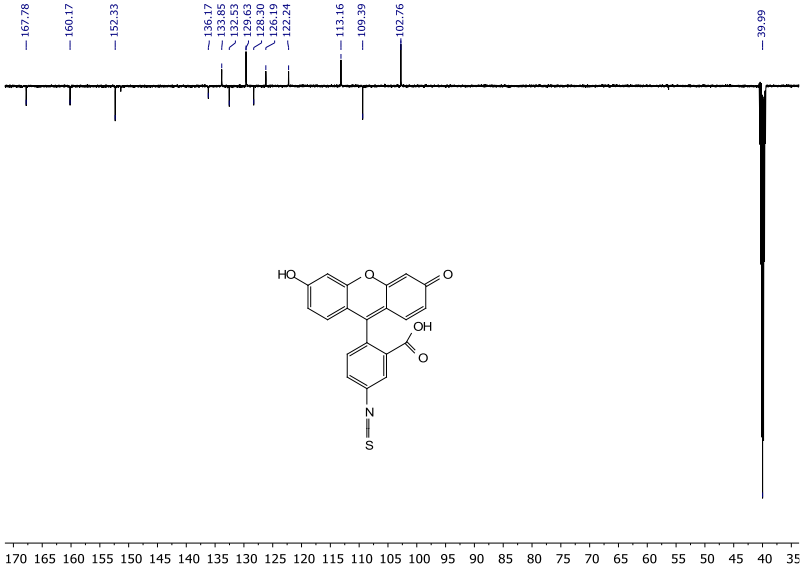


Figure 524. [13]C APT NMR spectrum of fluoresceine-5-isothiocyanate in DMSO-*d*6 at 499 MHz.

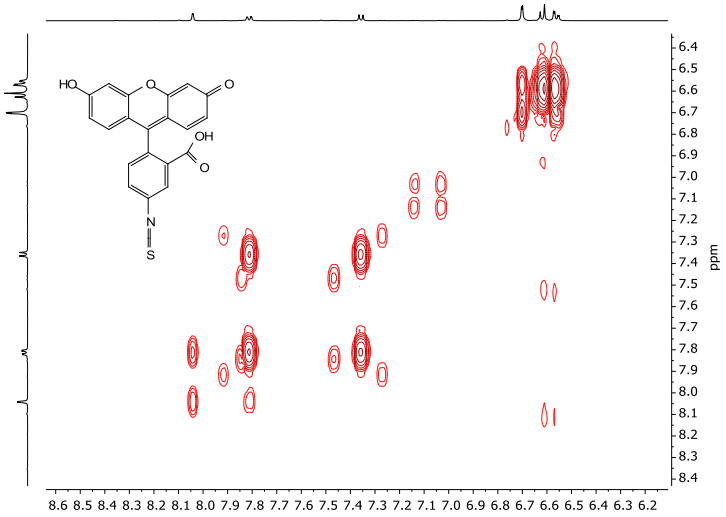


Figure 525. [1]H,[1]H COSY NMR spectrum of fluoresceine-5-isothiocyanate in DMSO-*d*6 at 499 MHz.

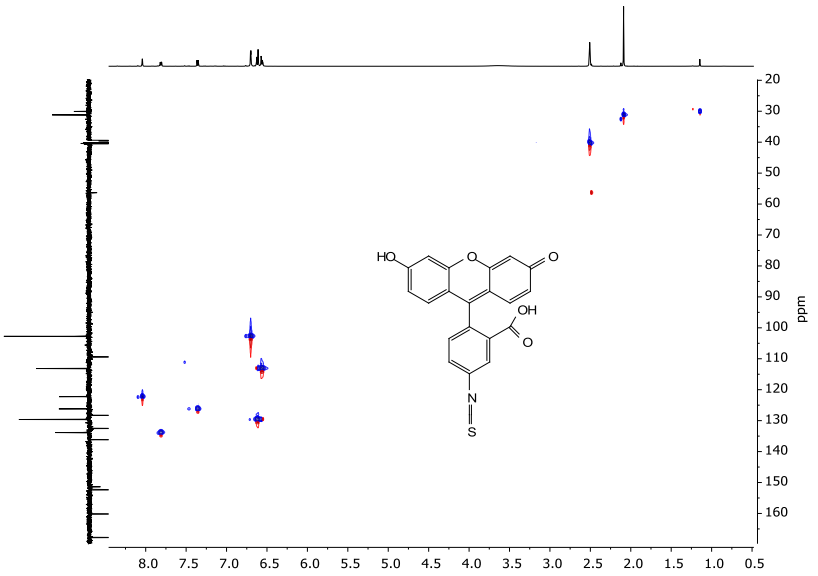


Figure 526. $^{1}H,^{13}C$ HMQC/HSQC NMR spectrum of fluoresceine-5-isothiocyanate in DMSO-d_6 at 499 MHz.

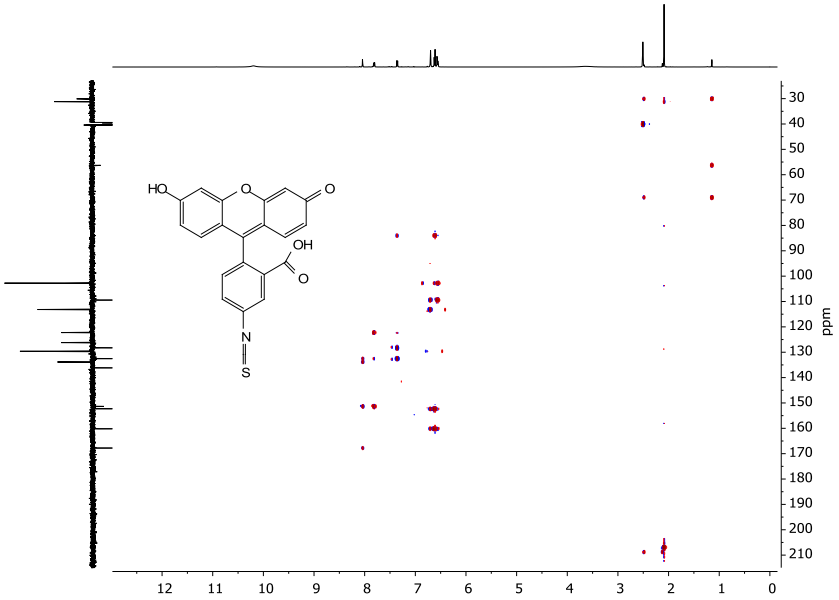


Figure 527. $^{1}H,^{13}C$ HMBC NMR spectrum of fluoresceine-5-isothiocyanate in DMSO-d_6 at 499 MHz.

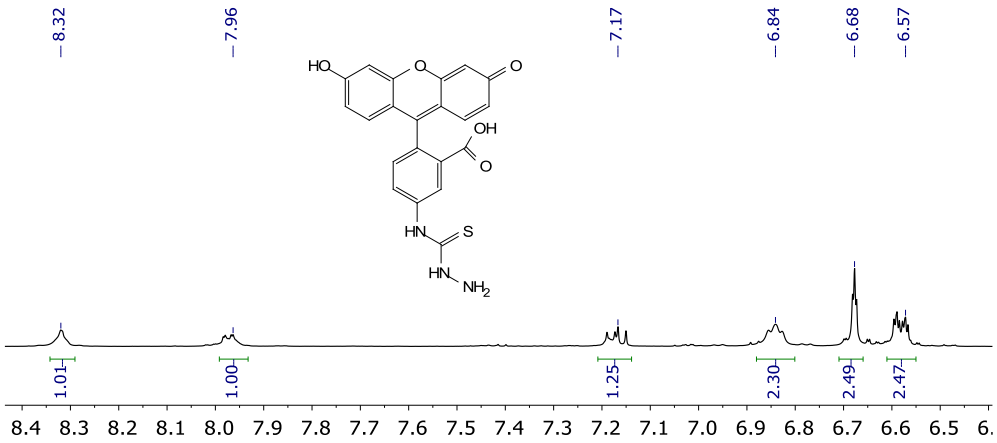


Figure 528. ^{1}H NMR spectrum of 2-(6-hydroxy-3-oxo-3*H*-xanthen-9-yl)-5-thiosemicarbazidobenzoic acid in DMSO-d_6 at 300 MHz.

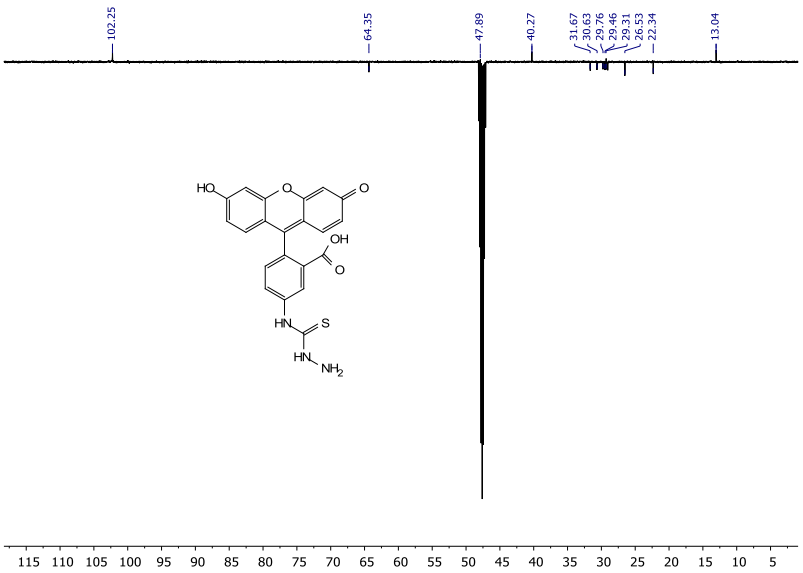


Figure 529. ^{13}C APT NMR spectrum of 2-(6-Hydroxy-3-oxo-3*H*-xanthen-9-yl)-5-thiosemicarbazidobenzoic acid in DMSO-d_6 at 499 MHz.

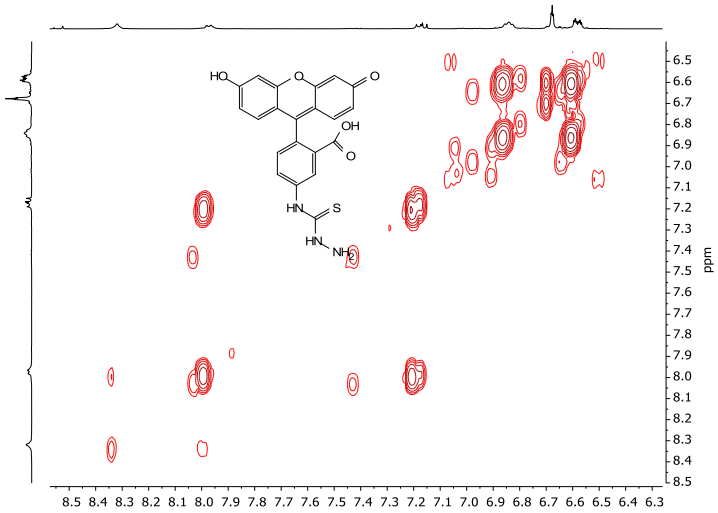


Figure 530. ^{1}H,^{1}H COSY NMR spectrum of 2-(6-Hydroxy-3-oxo-3*H*-xanthen-9-yl)-5-thiosemicarbazidobenzoic acid in DMSO-d_6 at 499 MHz.

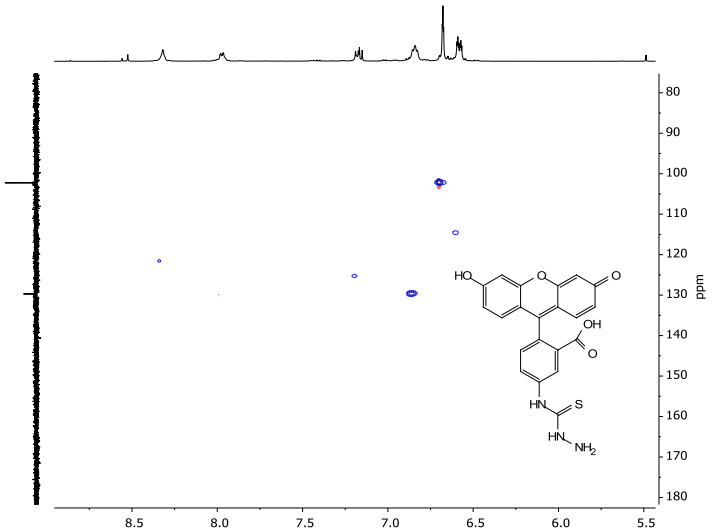


Figure 531. ^{1}H,^{13}C HMQC/HSQC NMR spectrum of 2-(6-Hydroxy-3-oxo-3*H*-xanthen-9-yl)-5-thiosemicarbazidobenzoic acid in DMSO-d_6 at 499 MHz.

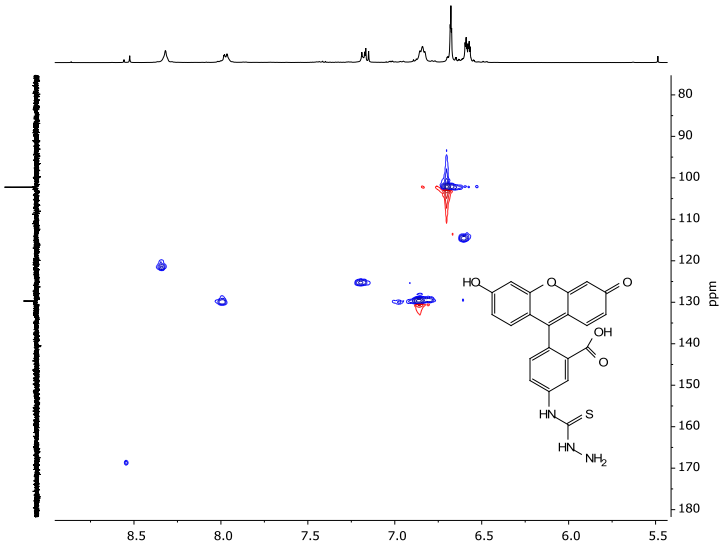


Figure 532. $^{1}H,^{13}C$ HMBC NMR spectrum of 2-(6-Hydroxy-3-oxo-3*H*-xanthen-9-yl)-5-thiosemicarbazidobenzoic acid in DMSO-d_6 at 499 MHz.

7.1.4 NMR data of hexadentate TSCs

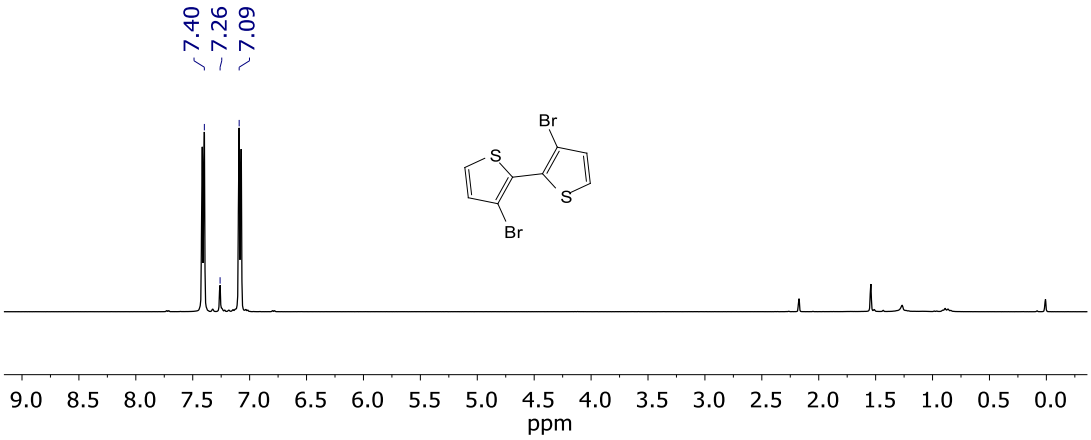


Figure 533. ^{1}H NMR spectrum of 3,3'-dibromo-2,2'-bithiophene in $CDCl_3$ at 300 MHz.

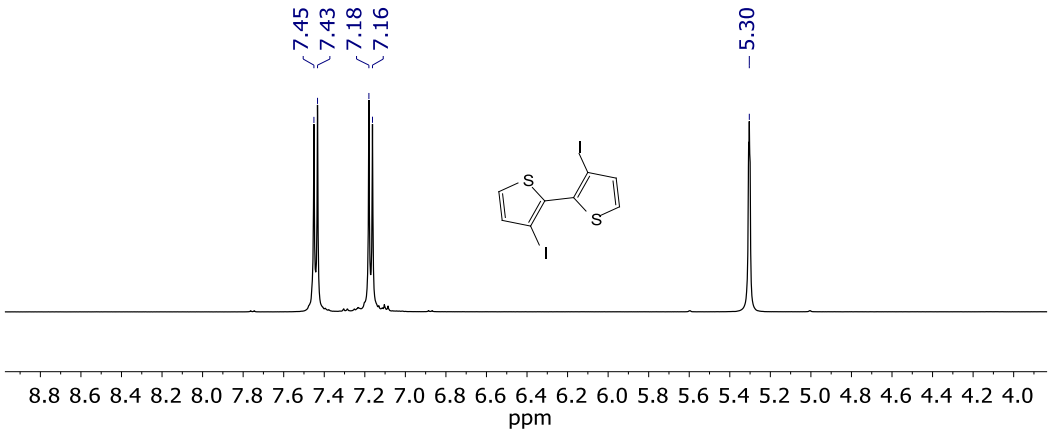


Figure 534. ^{1}H NMR spectrum of 3,3'-diiodo-2,2'-bithiophene in CD_2Cl_2 at 300 MHz.

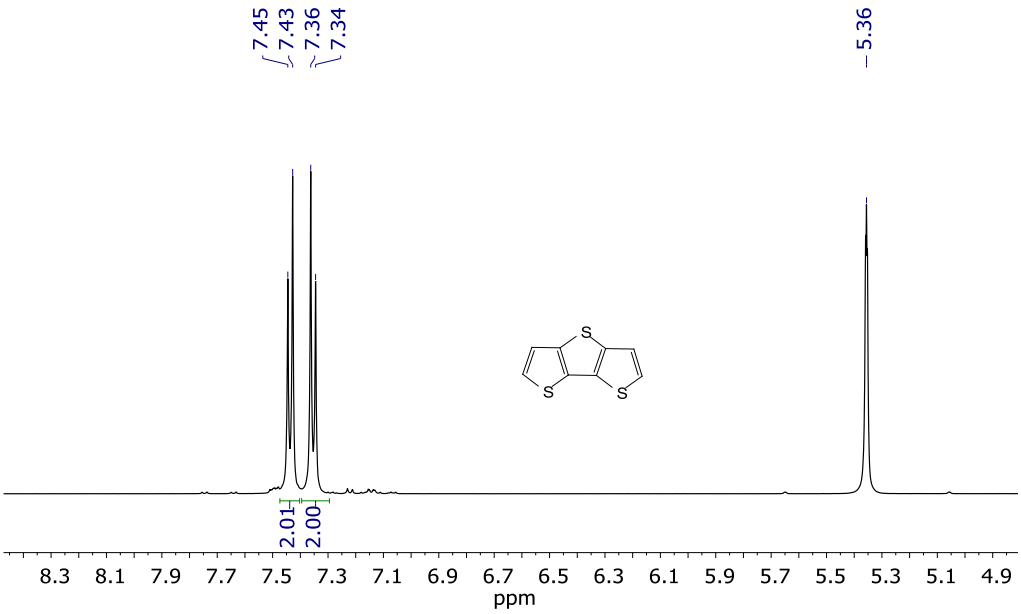


Figure 535. [1]H NMR spectrum of dithieno[3,2-b:2′,3′-d]thiophene in CD_2Cl_2 at 300 MHz.

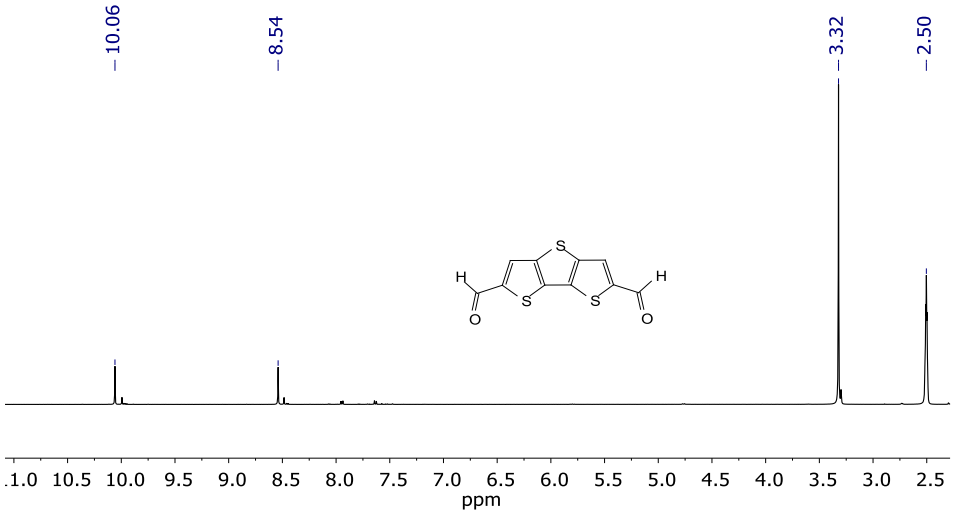


Figure 536. [1]H NMR spectrum of 3,7,11-trithiatricyclo[6.3.0.0^{2,6}]undeca-1(8),2(6),4,9-tetraene-4,10-dicarbaldehyde in DMSO-*d*$_6$ at 300 MHz.

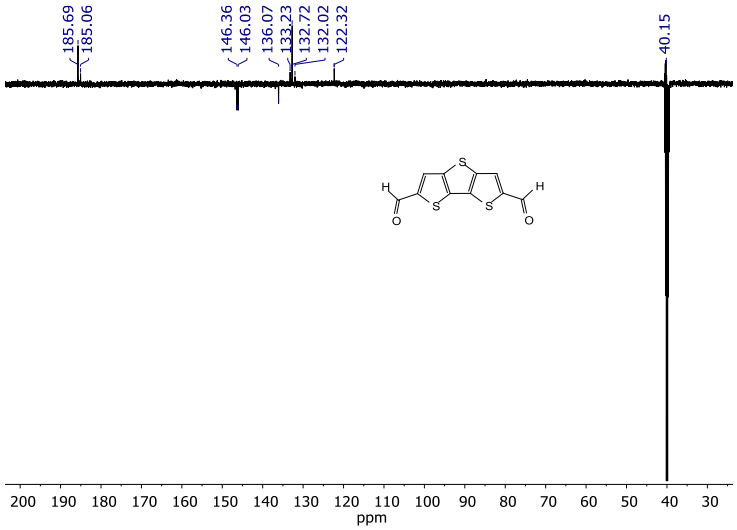


Figure 537. [13]C APT NMR spectrum of 3,7,11-trithiatricyclo[6.3.0.0^{2,6}]undeca-1(8),2(6),4,9-tetraene-4,10-dicarbaldehyde in DMSO-*d*$_6$ at 499 MHz.

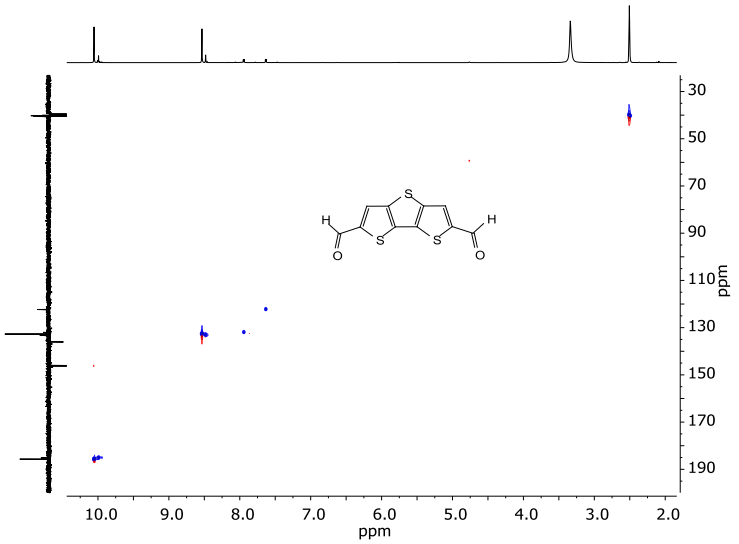


Figure 538. $^{1}H,^{13}C$ HMQC/HSQC NMR spectrum of 3,7,11-trithiatricyclo[6.3.0.0^{2,6}]undeca-1(8),2(6),4,9-tetraene-4,10-dicarbaldehyde in DMSO-d_6 at 499 MHz.

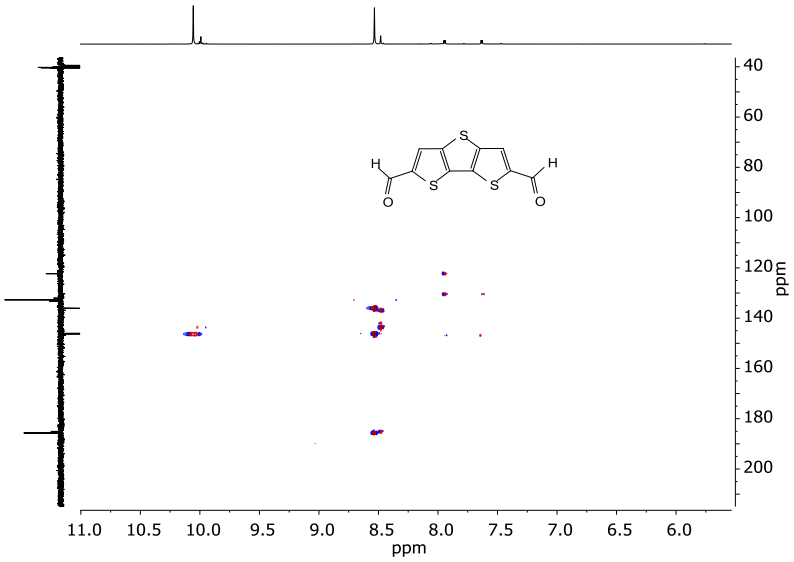


Figure 539. $^{1}H,^{13}C$ HMBC NMR spectrum of 3,7,11-trithiatricyclo[6.3.0.0^{2,6}]undeca-1(8),2(6),4,9-tetraene-4,10-dicarbaldehyde in DMSO-d_6 at 499 MHz.

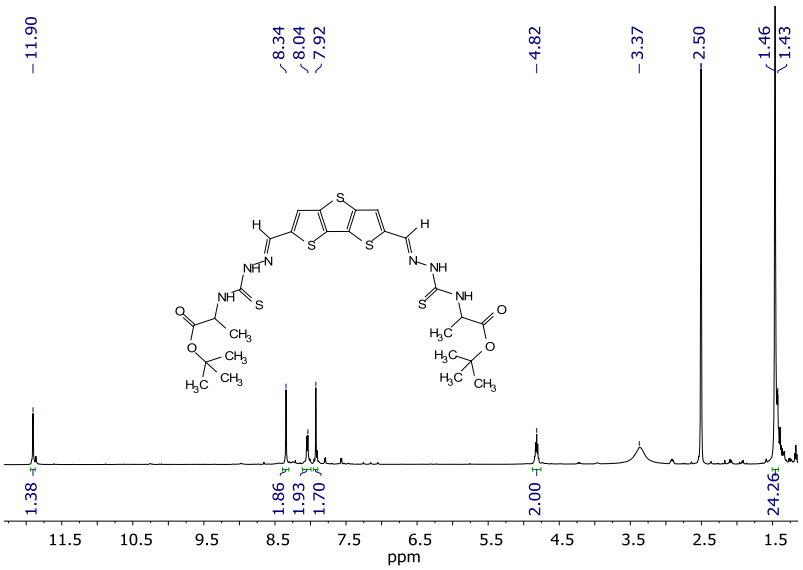


Figure 540. ^{1}H NMR spectrum of DTT(bis-TSC)Ala*t*Bu in DMSO-d_6 at 499 MHz.

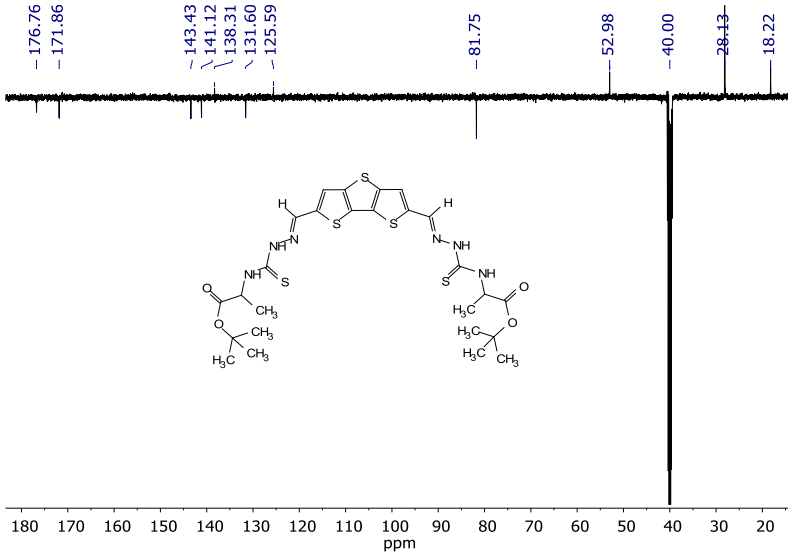


Figure 541. ^{13}C APT NMR spectrum of DTT(bis-TSC)Ala*t*Bu in DMSO-d_6 at 499 MHz.

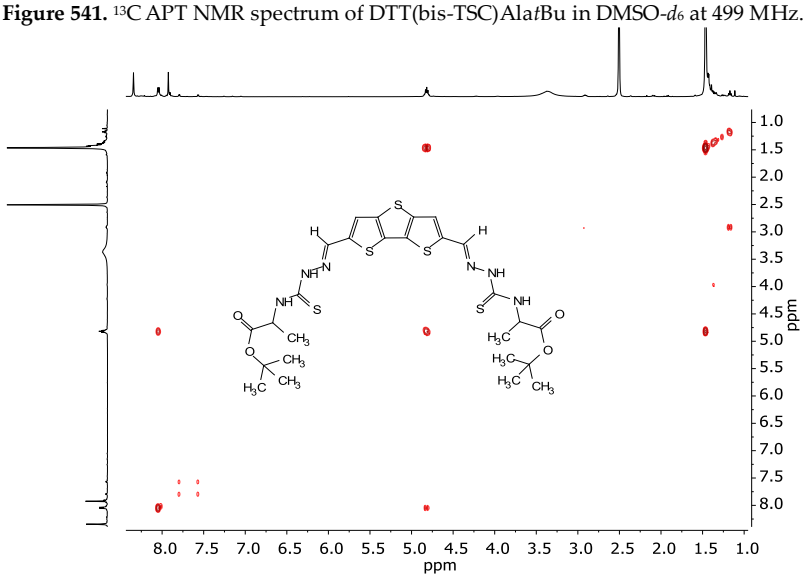


Figure 542. ^{1}H,^{1}H COSY NMR spectrum of DTT(bis-TSC)Ala*t*Bu in DMSO-d_6 at 499 MHz.

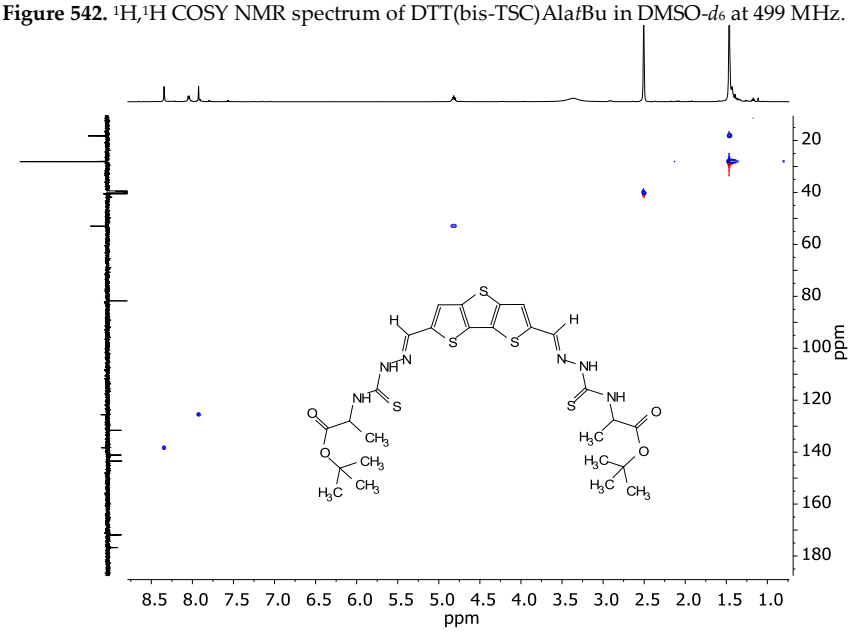


Figure 543. ^{1}H,^{13}C HMQC/HSQC NMR spectrum of DTT(bis-TSC)Ala*t*Bu in DMSO-d_6 at 499 MHz.

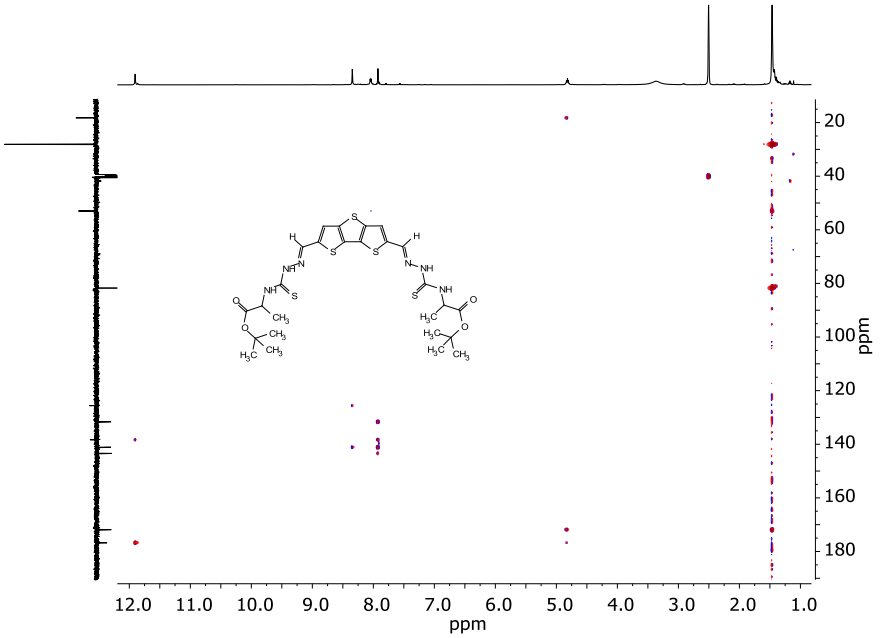


Figure 544. $^{1}H,^{13}C$ HMBC NMR spectrum of DTT(bis-TSC)Ala*t*Bu in DMSO-d_6 at 499 MHz.

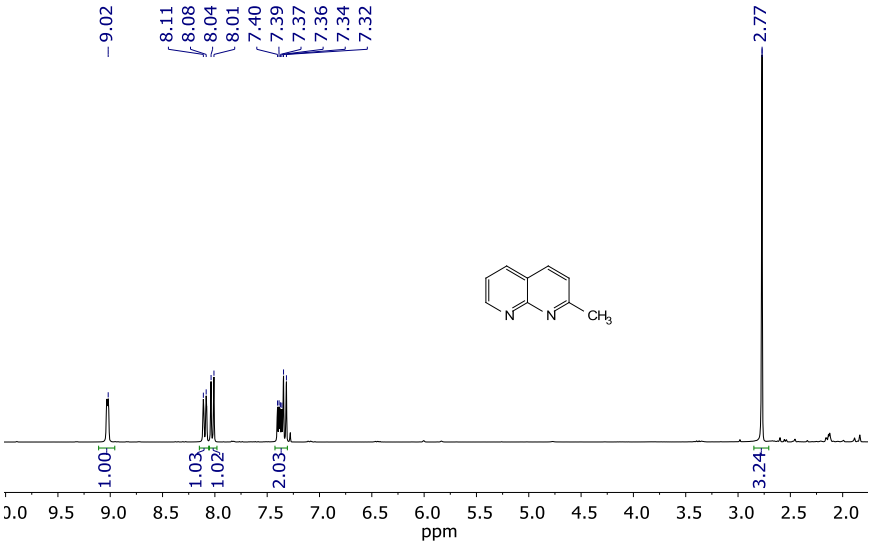


Figure 545. ^{1}H NMR spectrum of 2-methyl-1,8-naphthyridine in $CDCl_3$ at 300 MHz.

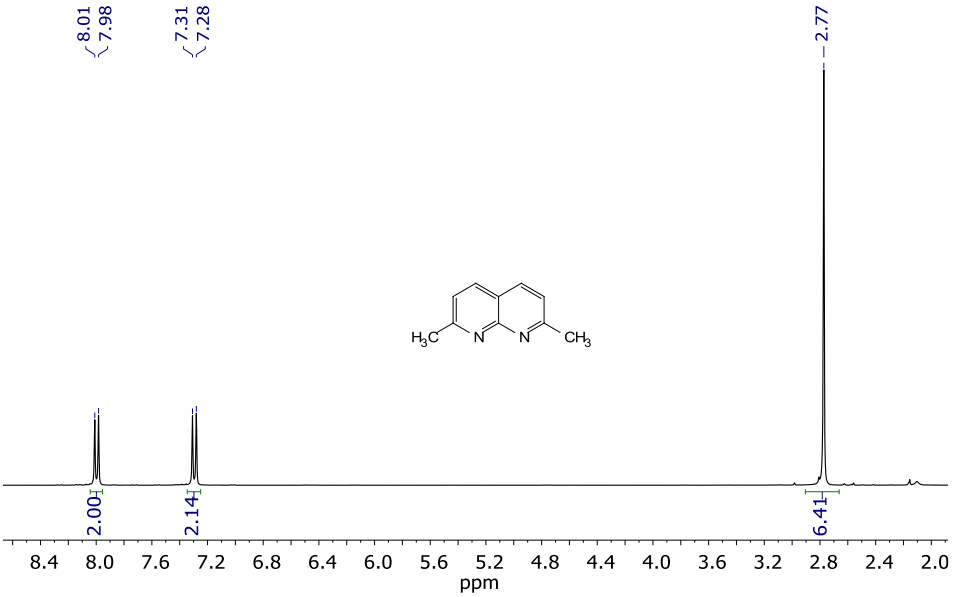


Figure 546. ^{1}H NMR spectrum of 2,7-dimethyl-1,8-naphthyridine in $CDCl_3$ at 300 MHz.

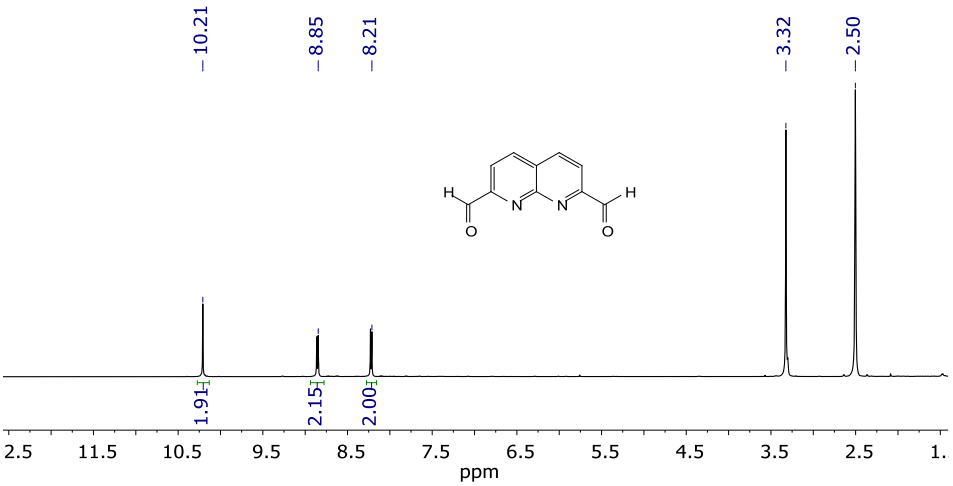


Figure 547. [1]H NMR spectrum of 1,8-diazanaphthalene-2,7-dicarbaldehyde in DMSO-*d*$_6$ at 499 MHz.

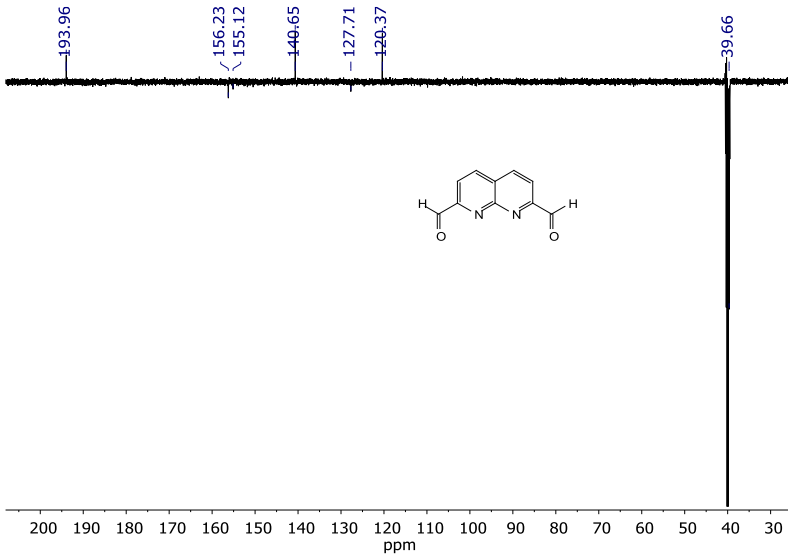


Figure 548. [13]C APT NMR spectrum of 1,8-diazanaphthalene-2,7-dicarbaldehyde in DMSO-*d*$_6$ at 499 MHz.

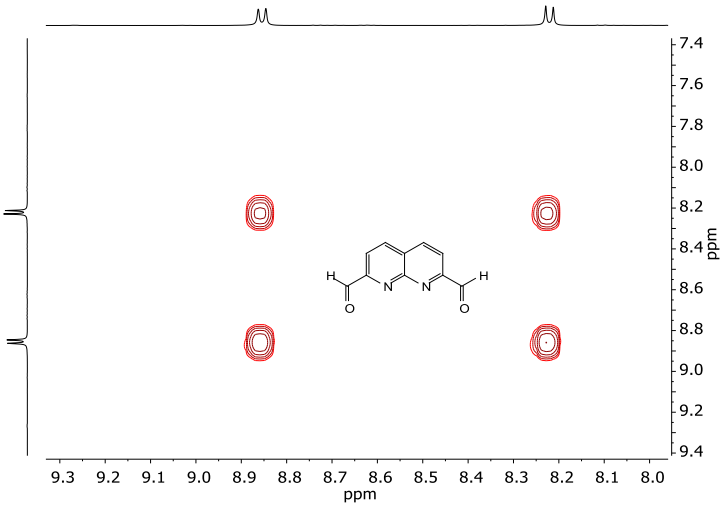


Figure 549. [1]H,[1]H COSY NMR spectrum of 1,8-diazanaphthalene-2,7-dicarbaldehyde in DMSO-*d*$_6$ at 499 MHz.

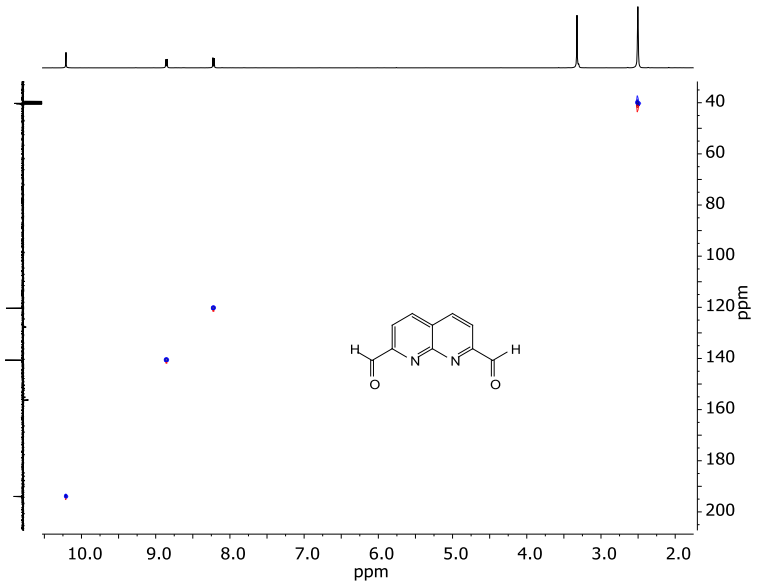


Figure 550. $^{1}H,^{13}C$ HMQC/HSQC NMR spectrum of 1,8-diazanaphthalene-2,7-dicarbaldehyde in DMSO-d_6 at 499 MHz.

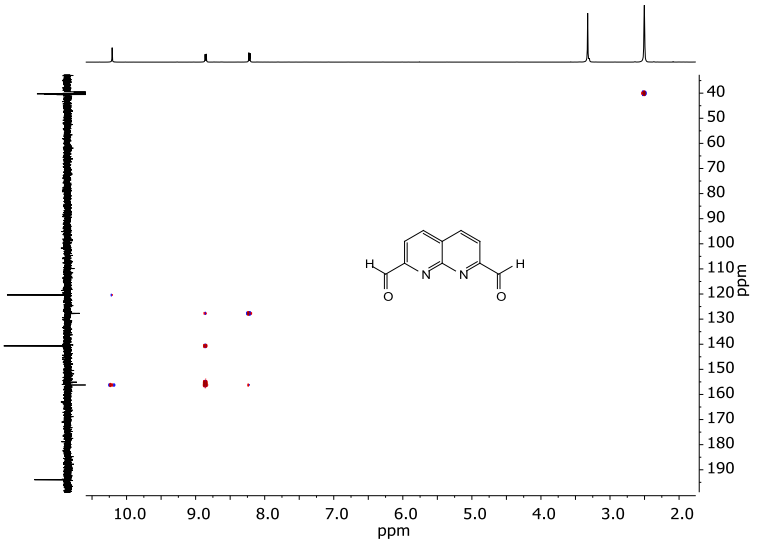


Figure 551. $^{1}H,^{13}C$ HMBC NMR spectrum of 1,8-diazanaphthalene-2,7-dicarbaldehyde in DMSO-d_6 at 499 MHz.

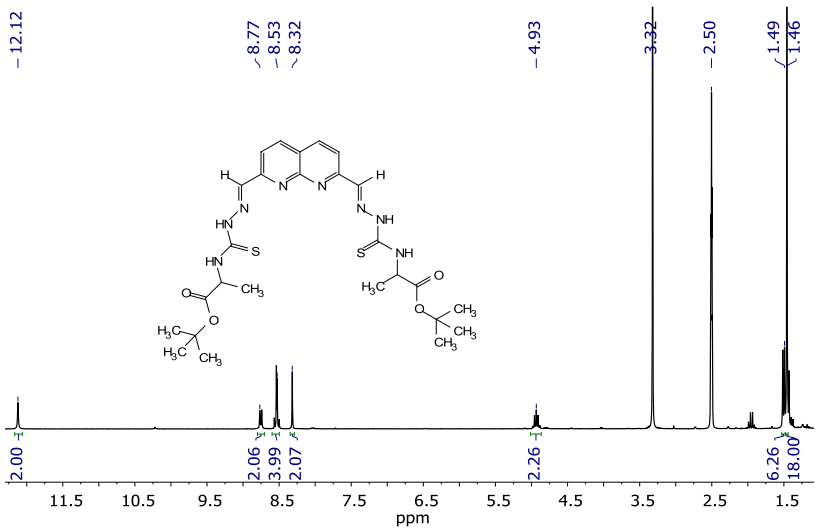


Figure 552. ^{1}H NMR spectrum of naph(bis-TSC)Ala*t*Bu in DMSO-d_6 at 300 MHz.

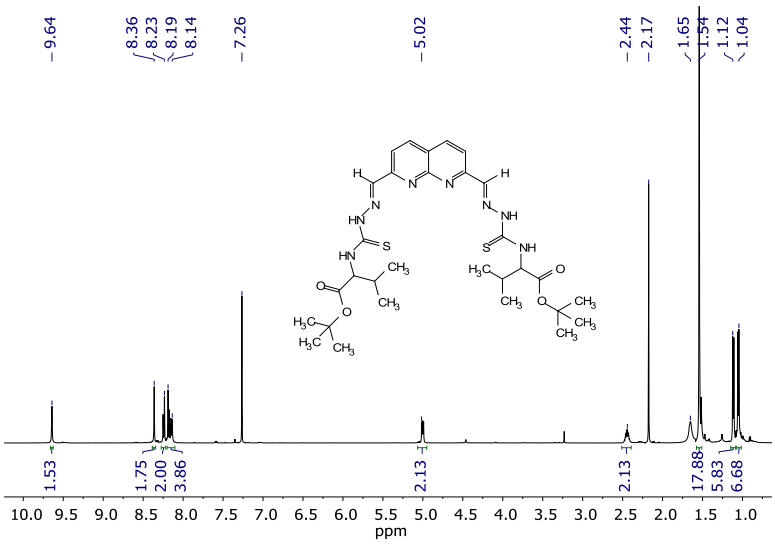


Figure 553. [1]H NMR spectrum of naph(bis-TSC)Val*t*Bu in DMSO-d_6 at 499 MHz.

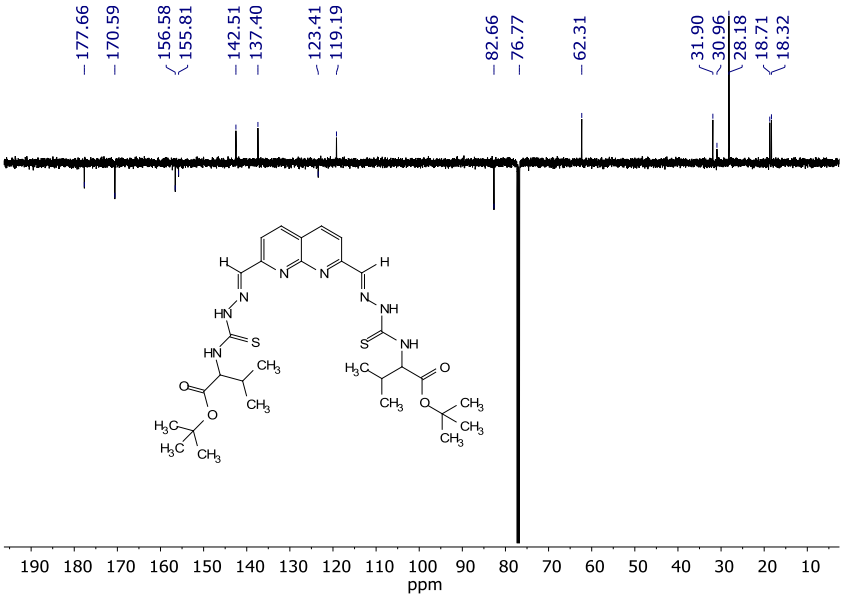


Figure 554. [13]C APT NMR spectrum of naph(bis-TSC)Val*t*Bu naph(bis-TSC)Ala*t*Bu in DMSO-d_6 at 499 MHz.

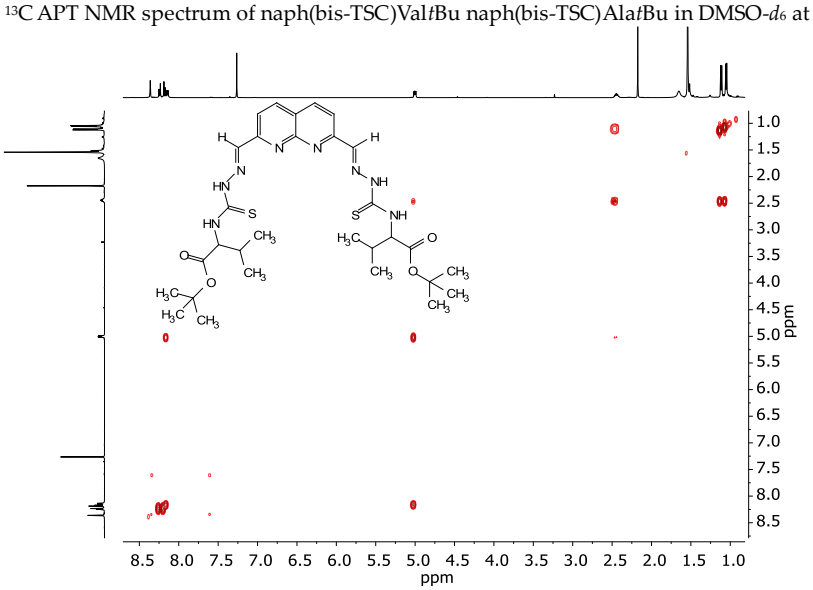


Figure 555. [1]H,[1]H COSY NMR spectrum of naph(bis-TSC)Val*t*Bu in DMSO-d_6 at 499 MHz.

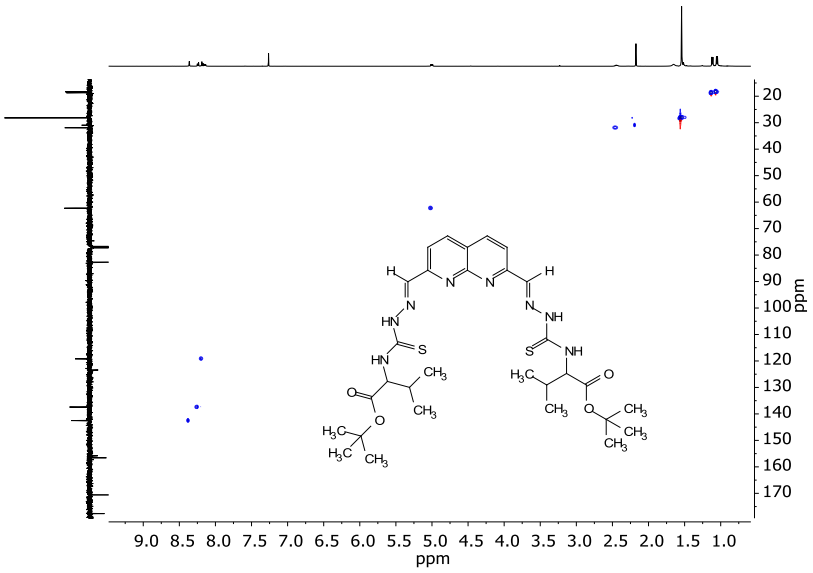


Figure 556. $^{1}H,^{13}C$ HMQC/HSQC NMR spectrum of naph(bis-TSC)Val*t*Bu in DMSO-d_6 at 499 MHz.

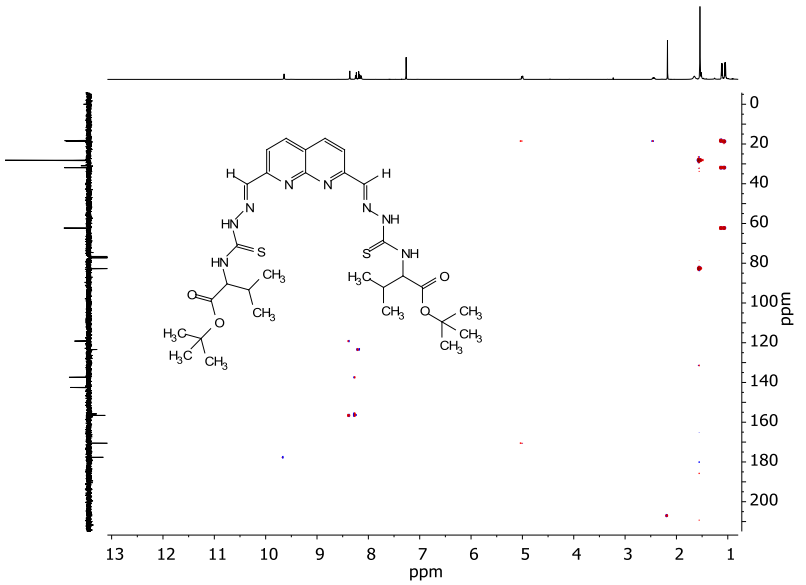


Figure 557. $^{1}H,^{13}C$ HMBC NMR spectrum of naph(bis-TSC)Val*t*Bu in DMSO-d_6 at 499 MHz.

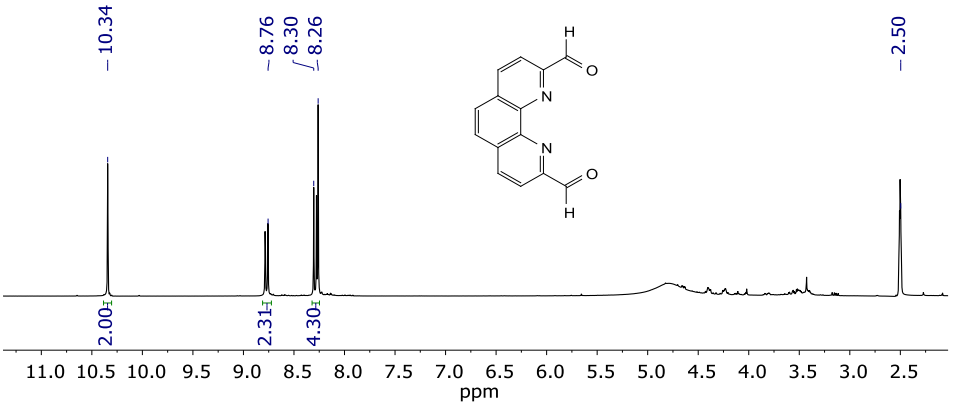


Figure 558. ^{1}H NMR spectrum of 4,5-diazaphenanthrene-3,6-dicarbaldehyde in DMSO-d_6 at 499 MHz.

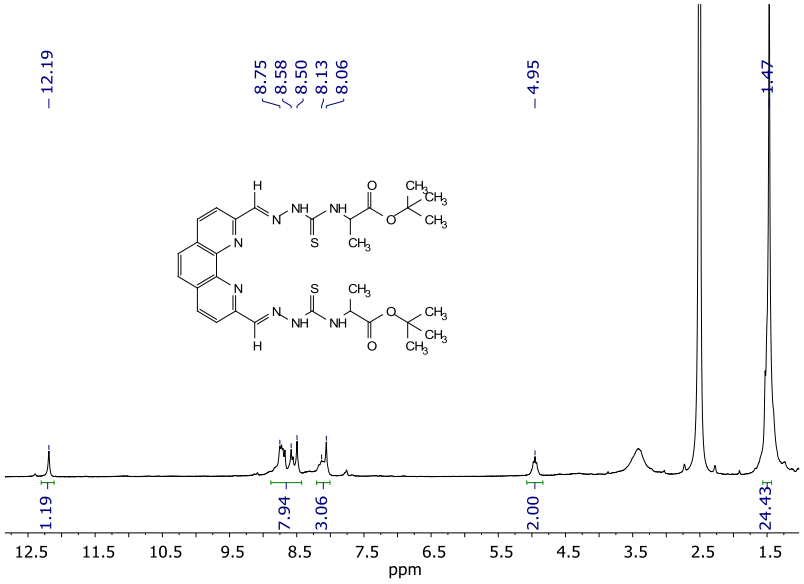


Figure 559. ^{1}H NMR spectrum of phen(bis-TSC)Ala*t*Bu in DMSO-d_6 at 499 MHz.

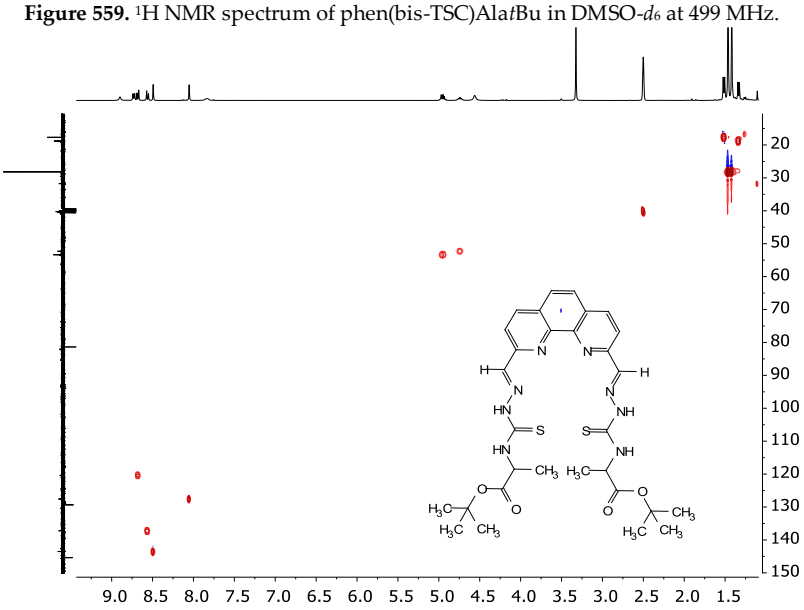


Figure 560. ^{1}H,^{13}C HMQC/HSQC NMR spectrum of phen(bis-TSC)Ala*t*Bu in DMSO-d_6 at 499 MHz.

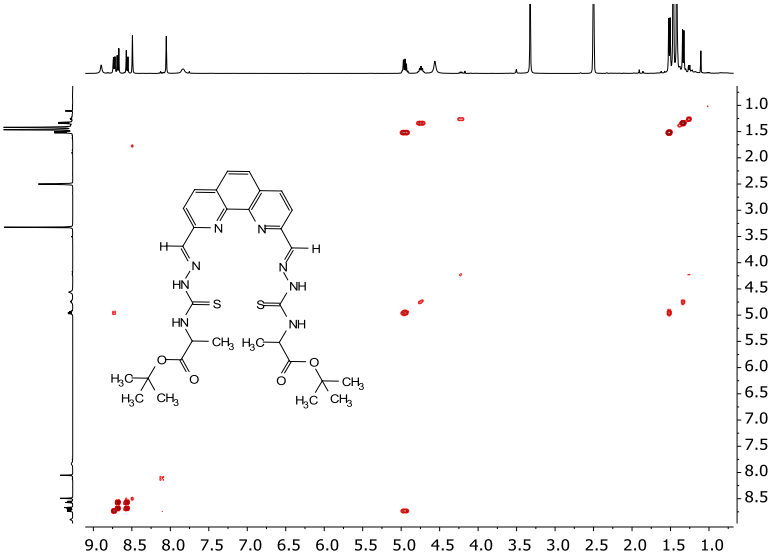


Figure 561. ^{1}H,^{1}H COSY NMR spectrum of phen(bis-TSC)Ala*t*Bu in DMSO-d_6 at 499 MHz.

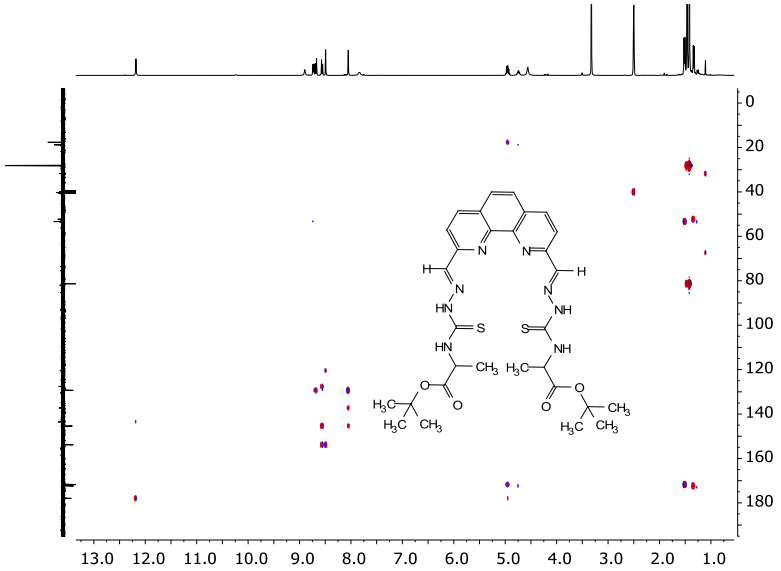


Figure 562. $^{1}H,^{13}C$ HMBC NMR spectrum of phen(bis-TSC)Ala*t*Bu in DMSO-d_6 at 499 MHz.

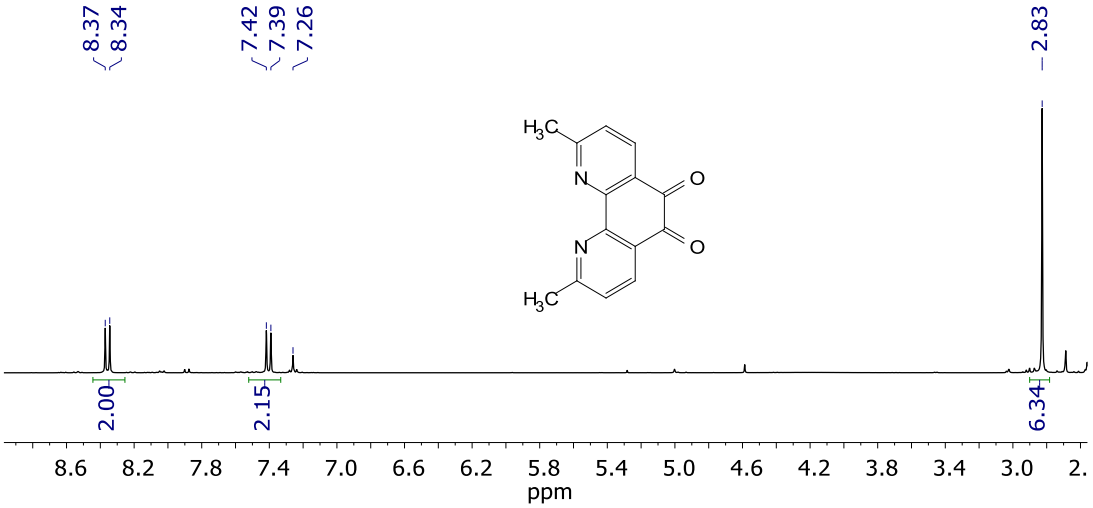


Figure 563. ^{1}H NMR spectrum of 2,9-dimethyl-1,10-phenanthroline-5,6-dione in $CDCl_3$ at 300 MHz.

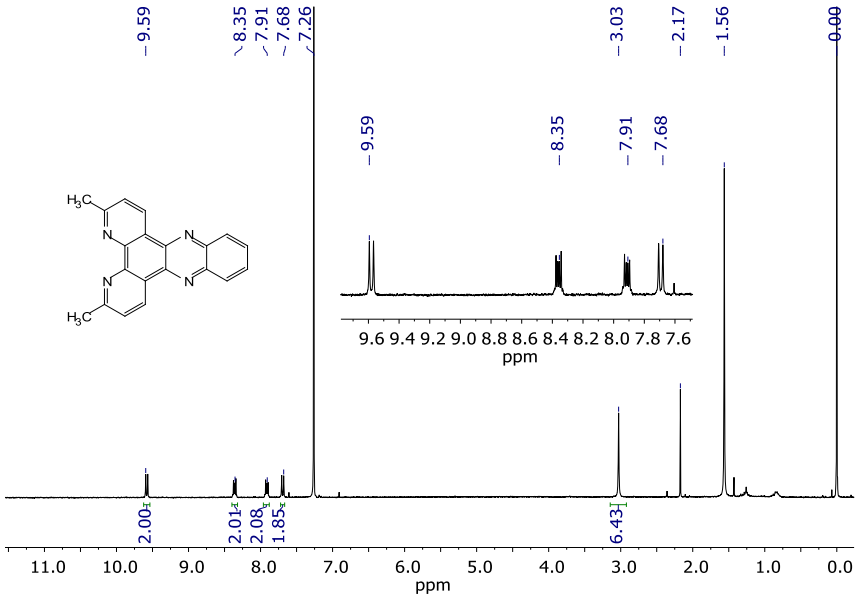


Figure 564. ^{1}H NMR spectrum of 3,6-dimethyldipyrido[3,2-a:2,3-c]phenazine in $CDCl_3$ at 300 MHz.

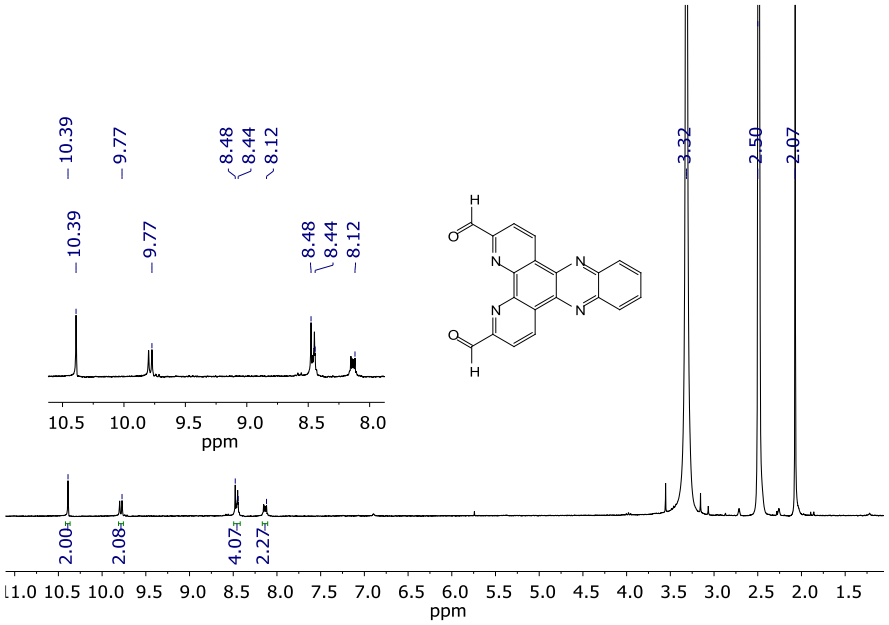


Figure 565. ^{1}H NMR spectrum of 4,5-diazaphenanthrene-3,6-dicarbaldehyde in DMSO-d_6 at 300 MHz.

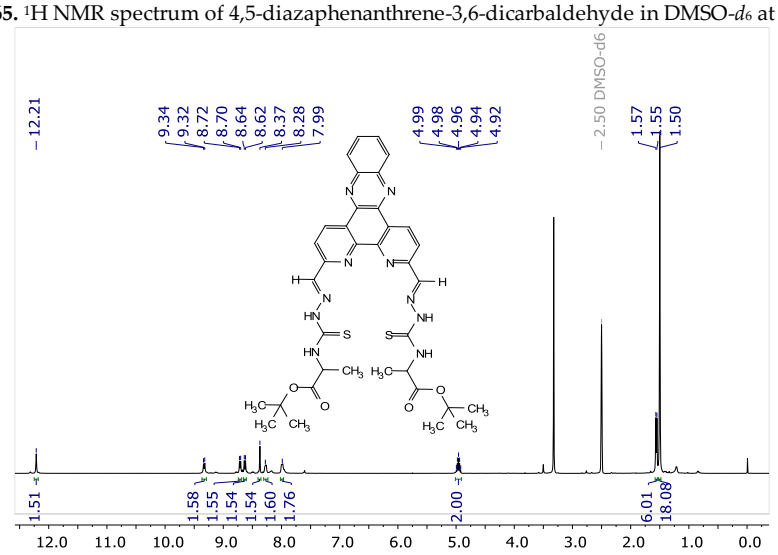


Figure 566. ^{1}H NMR spectrum of DPPZ(bis-TSC)Ala*t*Bu in DMSO-d_6 at 499 MHz.

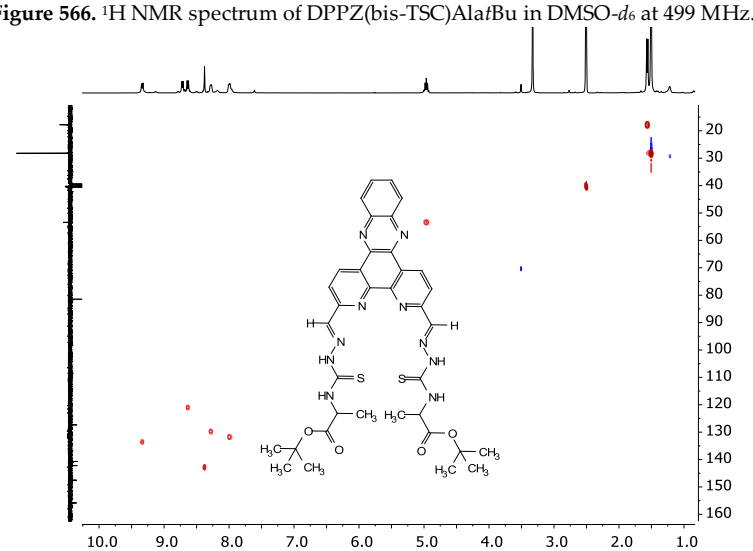


Figure 567. ^{1}H,^{13}C HMQC/HSQC NMR spectrum of DPPZ(bis-TSC)Ala*t*Bu in DMSO-d_6 at 499 MHz.

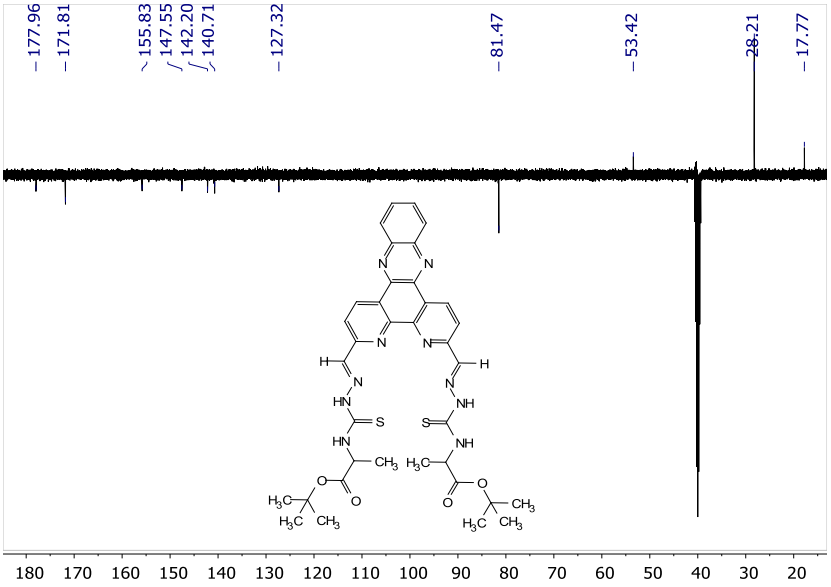


Figure 568. ^{13}C APT NMR spectrum of DPPZ(bis-TSC)Ala*t*Bu in DMSO-*d*$_6$ at 499 MHz.

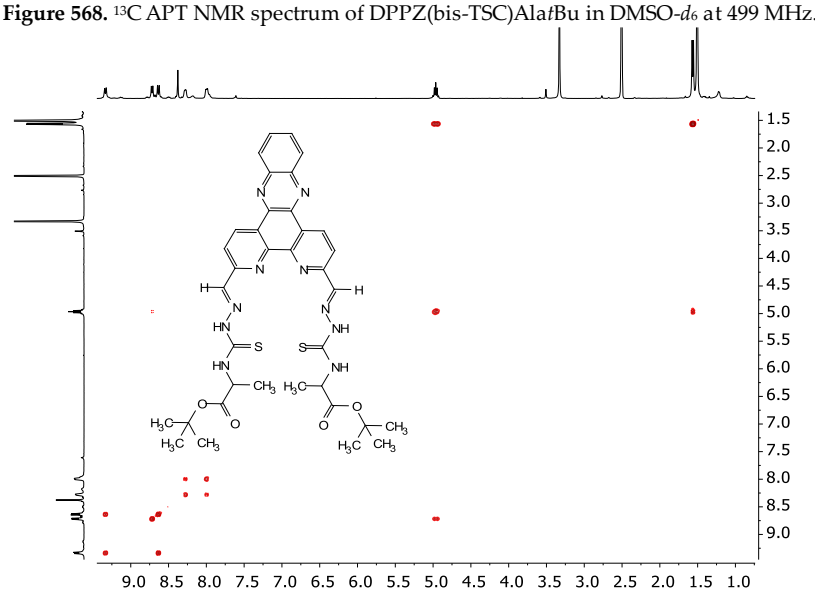


Figure 569. ^{1}H,^{1}H COSY NMR spectrum of DPPZ(bis-TSC)Ala*t*Bu in DMSO-*d*$_6$ at 499 MHz.

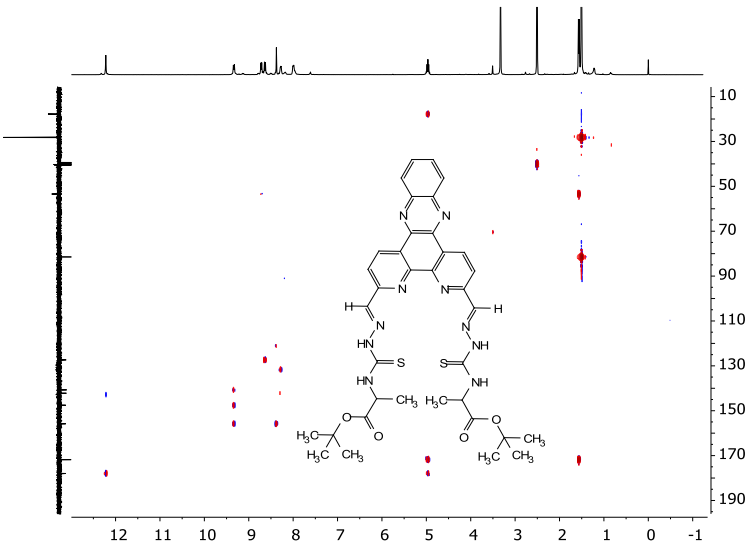


Figure 570. ^{1}H,^{13}C HMBC NMR spectrum of phen(bis-TSC)Ala*t*Bu in DMSO-*d*$_6$ at 499 MHz.

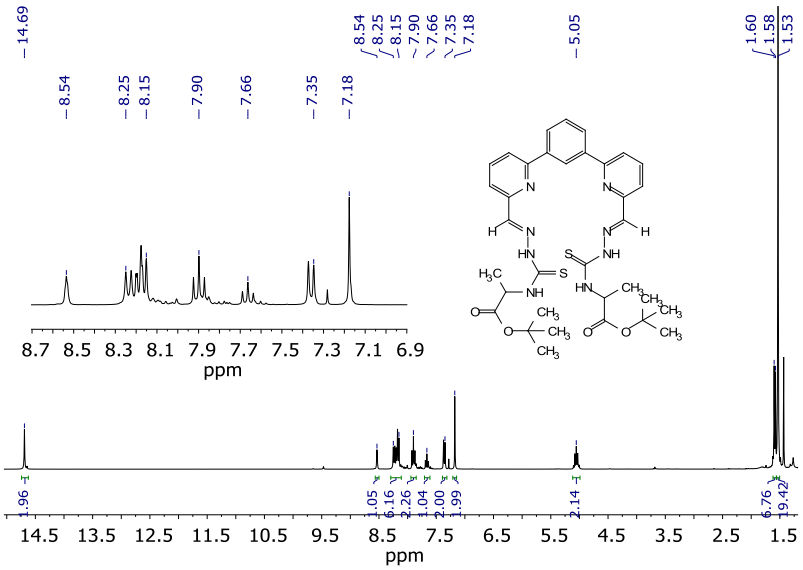


Figure 571. ^{1}H NMR spectrum of DPPZ(bis-TSC)Ala*t*Bu in DMSO-d_6 at 499 MHz.

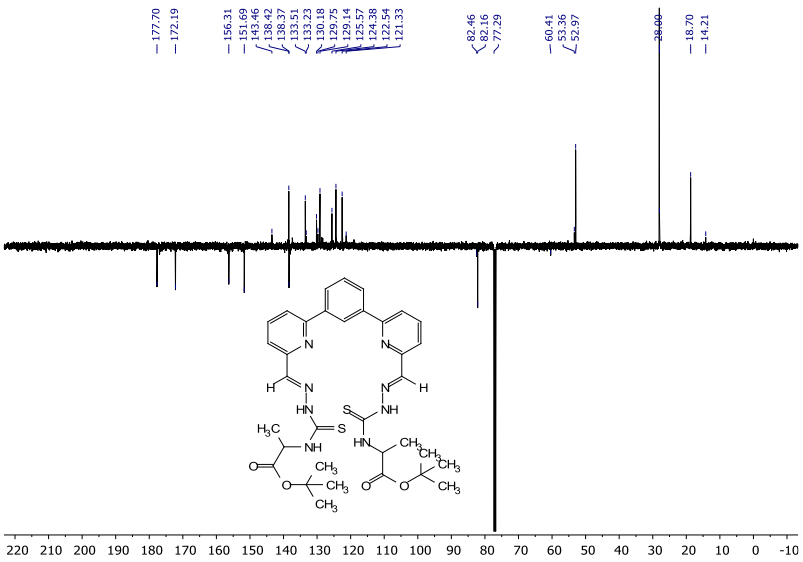


Figure 572. ^{13}C APT NMR spectrum of NCN(bis-TSC)Ala*t*Bu in DMSO-d_6 at 499 MHz.

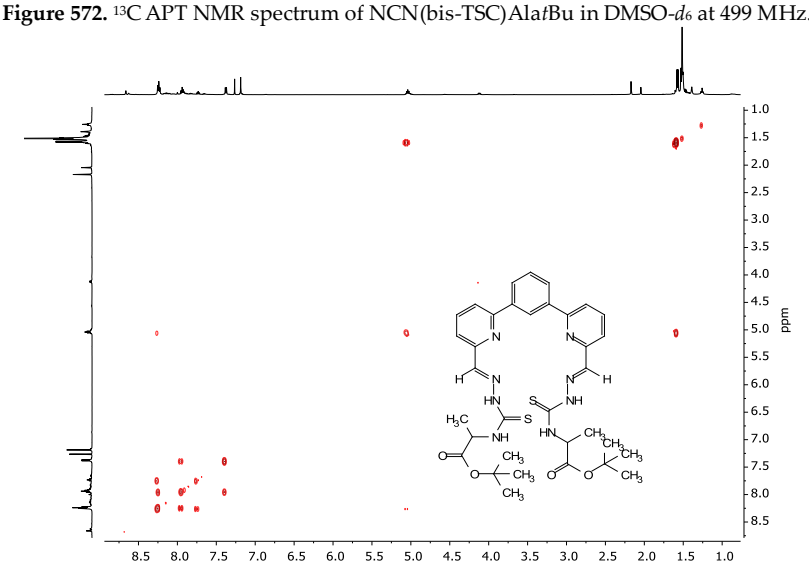


Figure 573. ^{1}H,^{1}H COSY NMR spectrum of NCN(bis-TSC)Ala*t*Bu in DMSO-d_6 at 499 MHz.

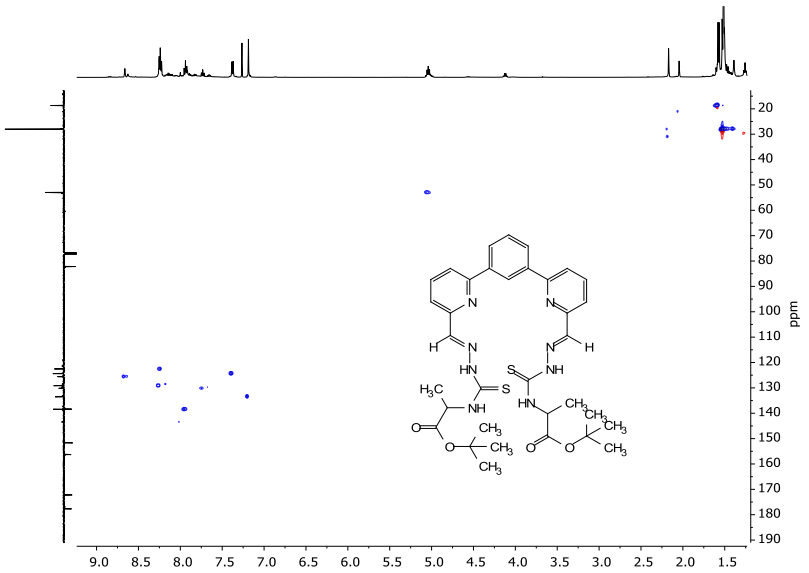


Figure 574. $^{1}H,^{13}C$ HMQC/HSQC NMR spectrum of NCN(bis-TSC)Ala*t*Bu in DMSO-d_6 at 499 MHz.

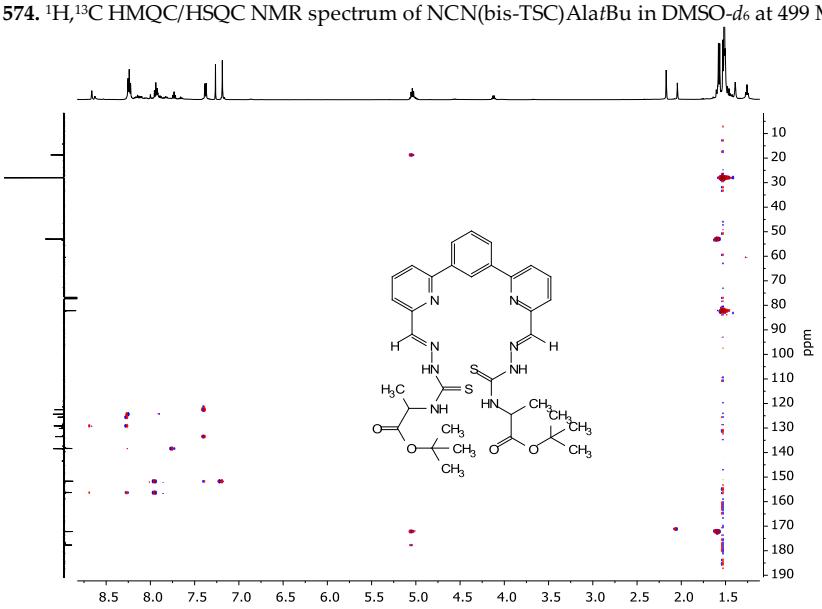


Figure 575. $^{1}H,^{13}C$ HMBC NMR spectrum of NCN(bis-TSC)Ala*t*Bu in DMSO-d_6 at 499 MHz.

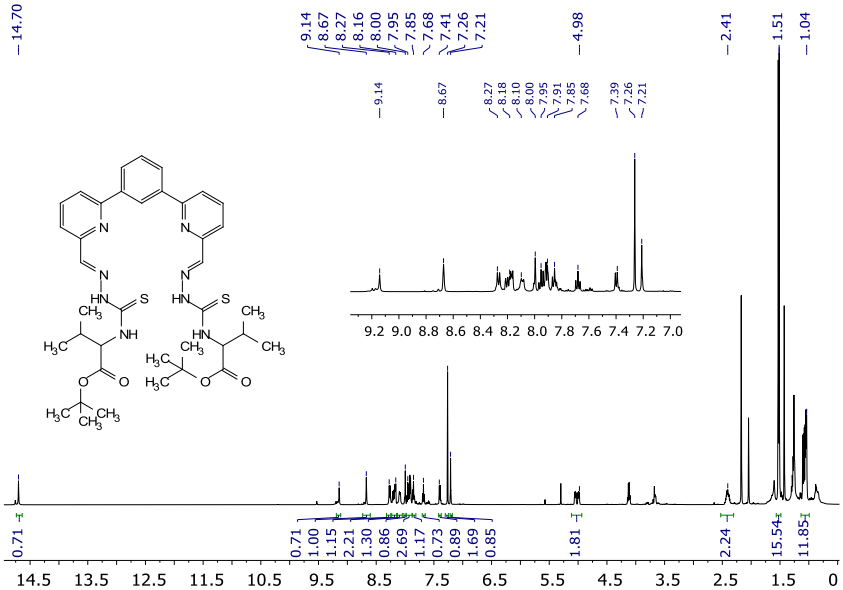


Figure 576. ^{1}H NMR spectrum of NCN(bis-TSC)Val*t*Bu in DMSO-d_6 at 300 MHz.

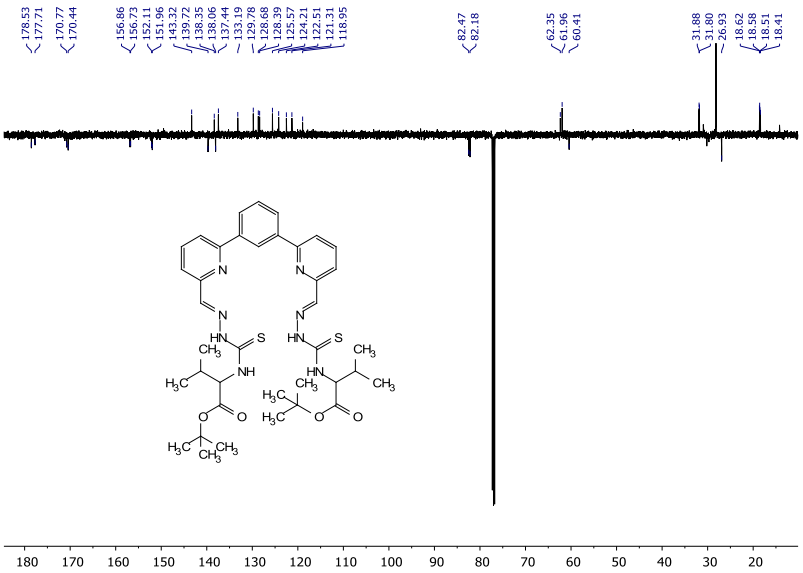


Figure 577. ^{13}C APT NMR spectrum of NCN(bis-TSC)Val*t*Bu in DMSO-*d*$_6$ at 499 MHz.

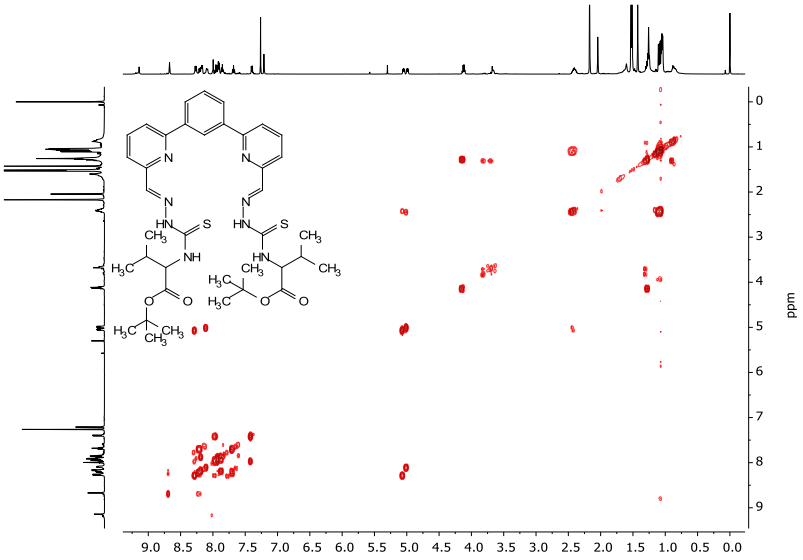


Figure 578. ^{1}H,^{1}H COSY NMR spectrum of NCN(bis-TSC)Val*t*Bu in DMSO-*d*$_6$ at 499 MHz.

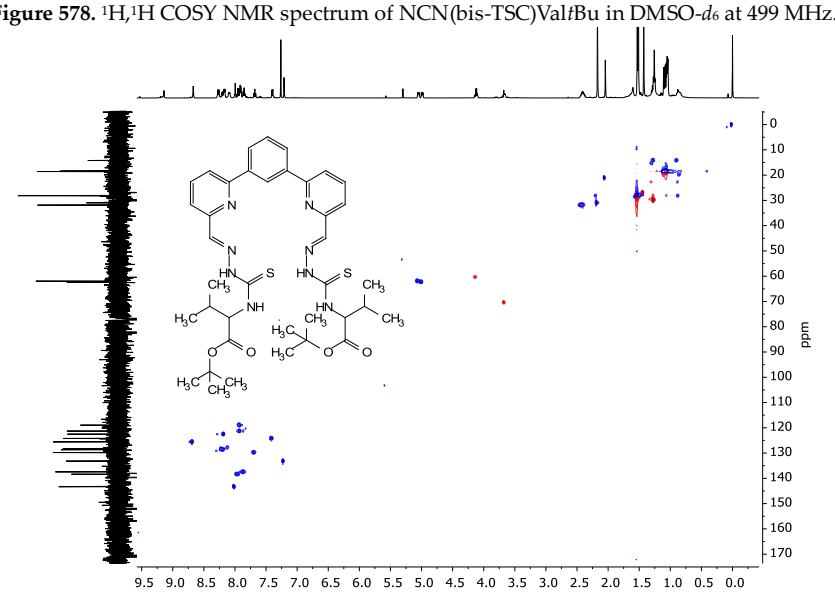


Figure 579. ^{1}H,^{13}C HMQC/HSQC NMR spectrum of NCN(bis-TSC)Val*t*Bu in DMSO-*d*$_6$ at 499 MHz.

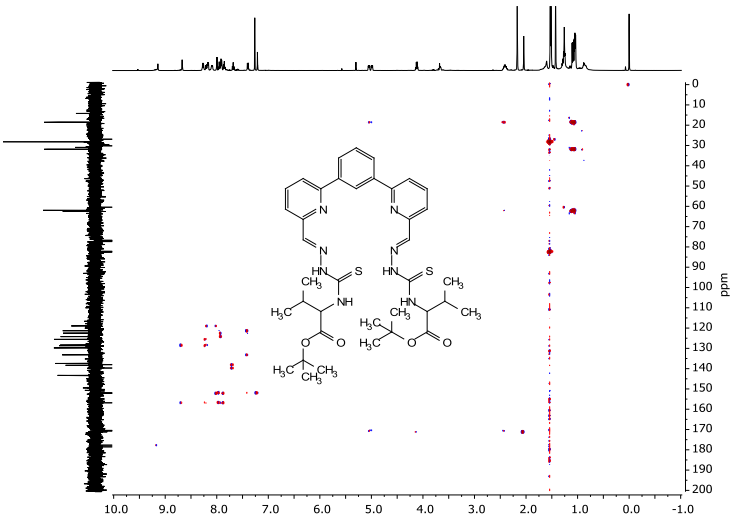


Figure 580. $^{1}H,^{13}C$ HMBC NMR spectrum of NCN(bis-TSC)Val*t*Bu in DMSO-d_6 at 499 MHz.

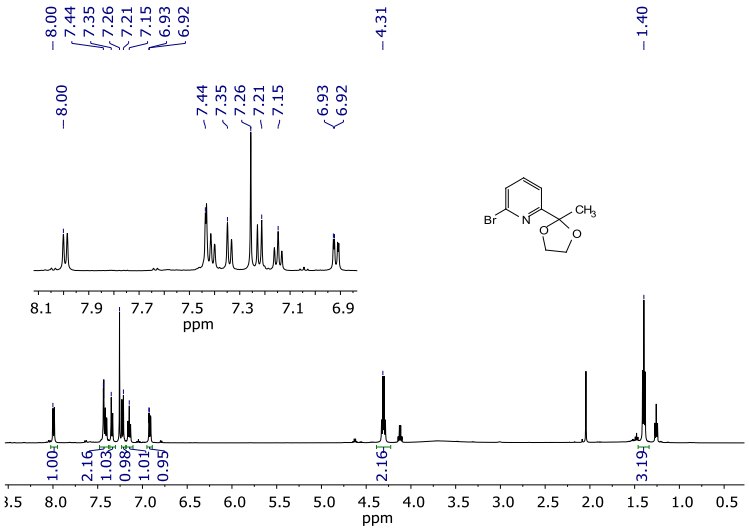


Figure 581. ^{1}H NMR spectrum of 2-bromo-6-(2- methyl-1,3-dioxolan-2-yl)pyridine in $CDCl_3$ at 499 MHz.

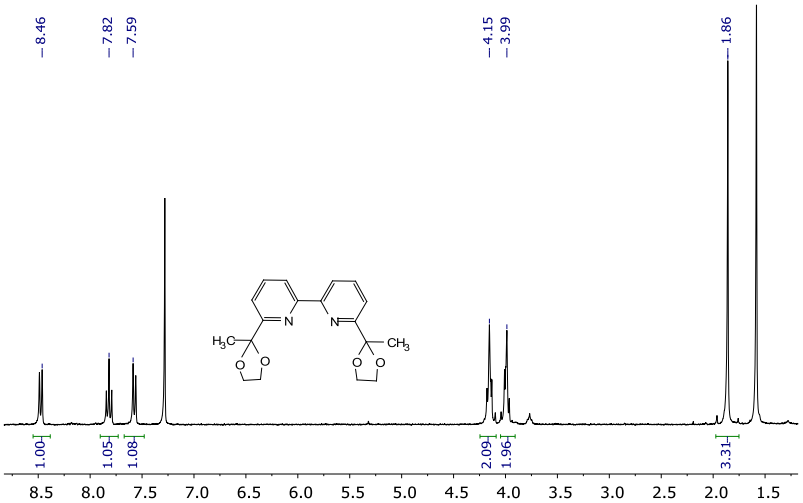


Figure 582. ^{1}H NMR spectrum of 6,6′-bis(2-methyl-1,3- dioxolan-2-yl)-2,2′-bipyridine in DMSO-d_6 at 300 MHz.

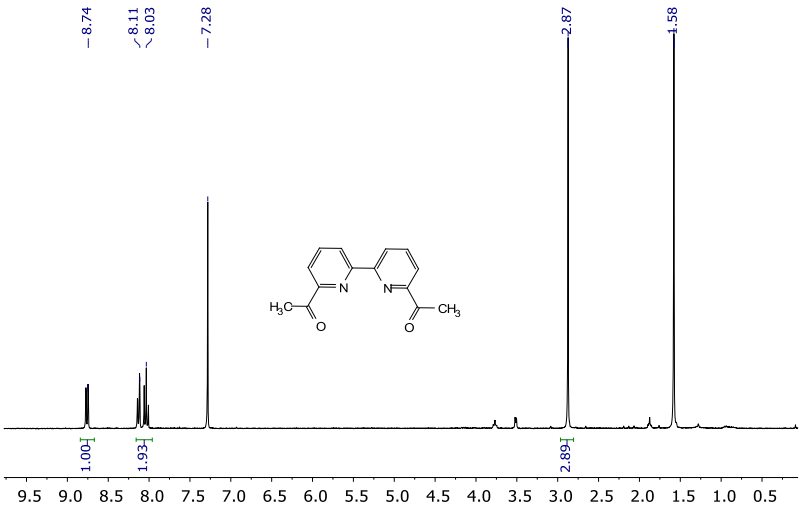


Figure 583. ^{1}H NMR spectrum of 6,6′-bis(2-acetyl)-2,2′- bipyridine in DMSO-d_6 at 300 MHz.

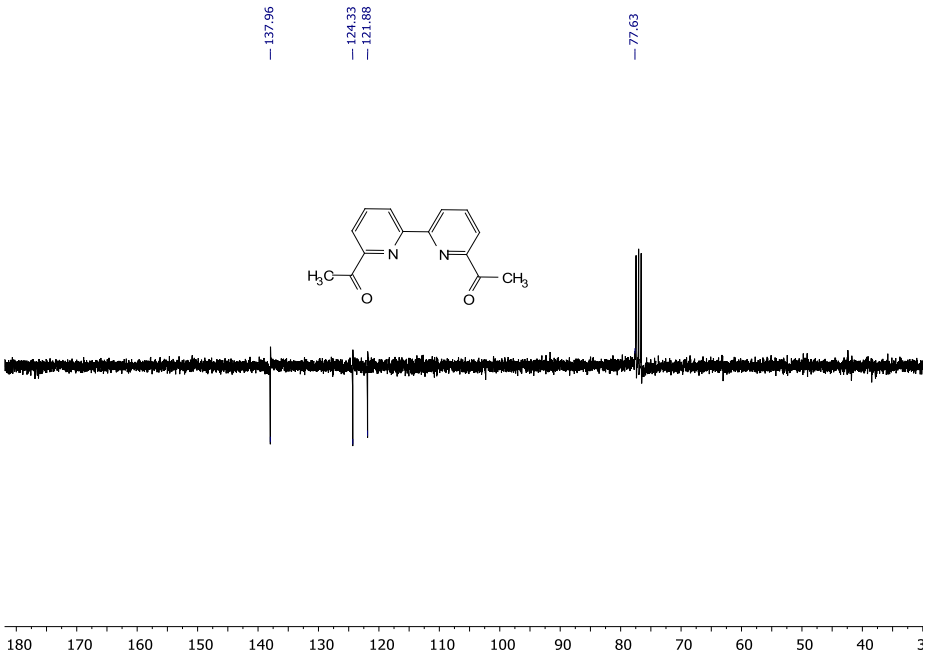


Figure 584. ^{13}C APT NMR spectrum of 6,6′-bis(2-acetyl)-2,2′- bipyridine in DMSO-d_6 at 499 MHz.

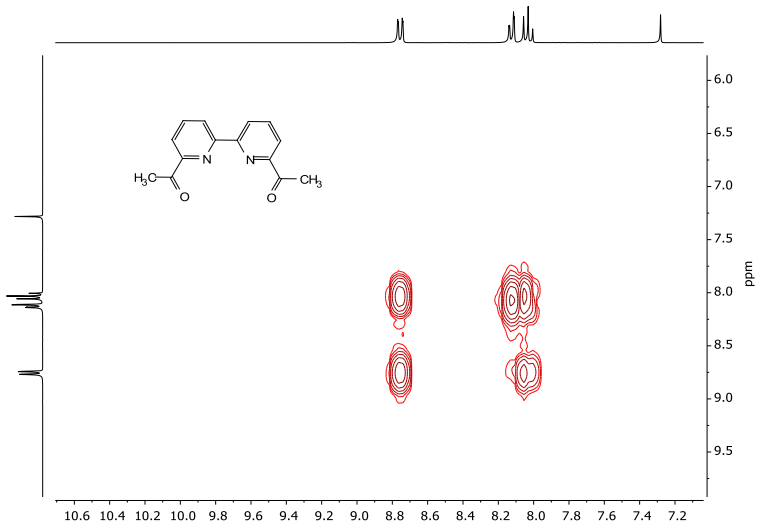


Figure 585. ^{1}H,^{1}H COSY NMR spectrum of 6,6′-bis(2-acetyl)-2,2′- bipyridine in DMSO-d_6 at 499 MHz.

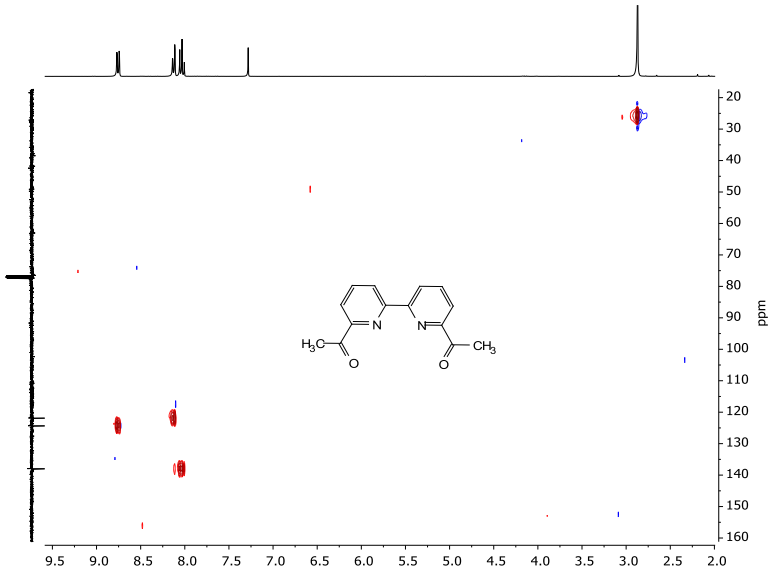


Figure 586. $^{1}H,^{13}C$ HMQC/HSQC NMR spectrum of 6,6′-bis(2-acetyl)-2,2′- bipyridine in DMSO-d_6 at 499 MHz.

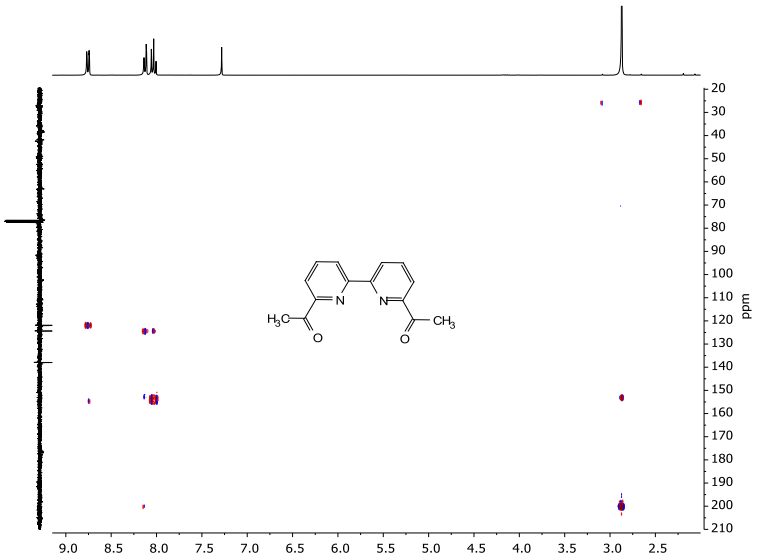


Figure 587. $^{1}H,^{13}C$ HMBC NMR spectrum of 6,6′-bis(2-acetyl)-2,2′- bipyridine in DMSO-d_6 at 499 MHz.

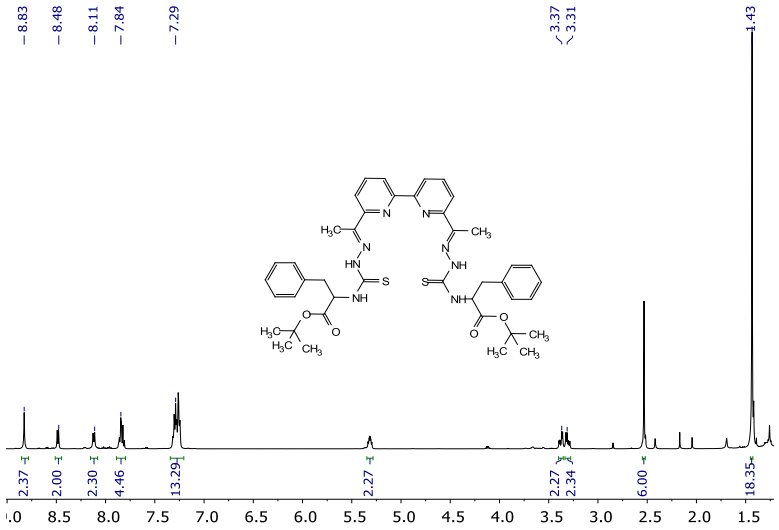


Figure 588. ^{1}H NMR spectrum of bpy(bis-TSC)Phe*t*Bu in DMSO-d_6 at 300 MHz.

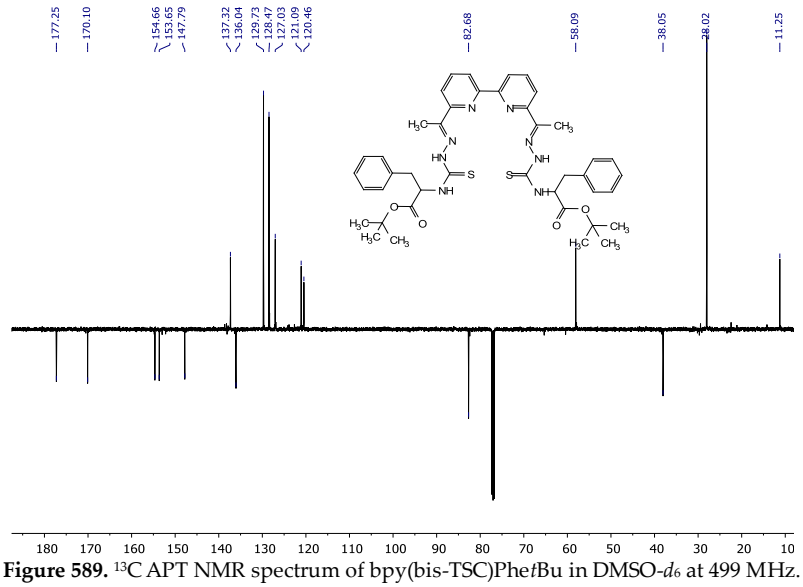


Figure 589. ^{13}C APT NMR spectrum of bpy(bis-TSC)Phe*t*Bu in DMSO-d_6 at 499 MHz.

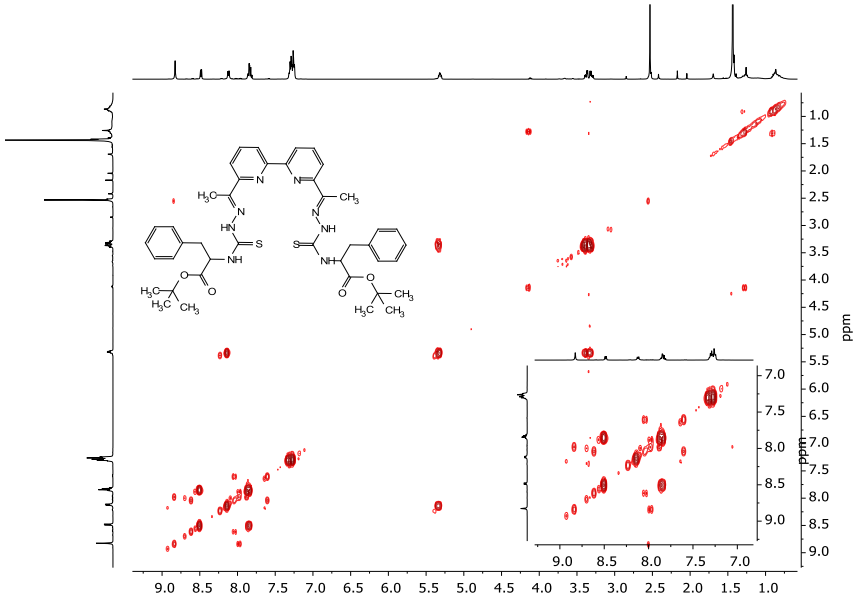


Figure 590. ^{1}H,^{1}H COSY NMR spectrum of bpy(bis-TSC)Phe*t*Bu in DMSO-d_6 at 499 MHz.

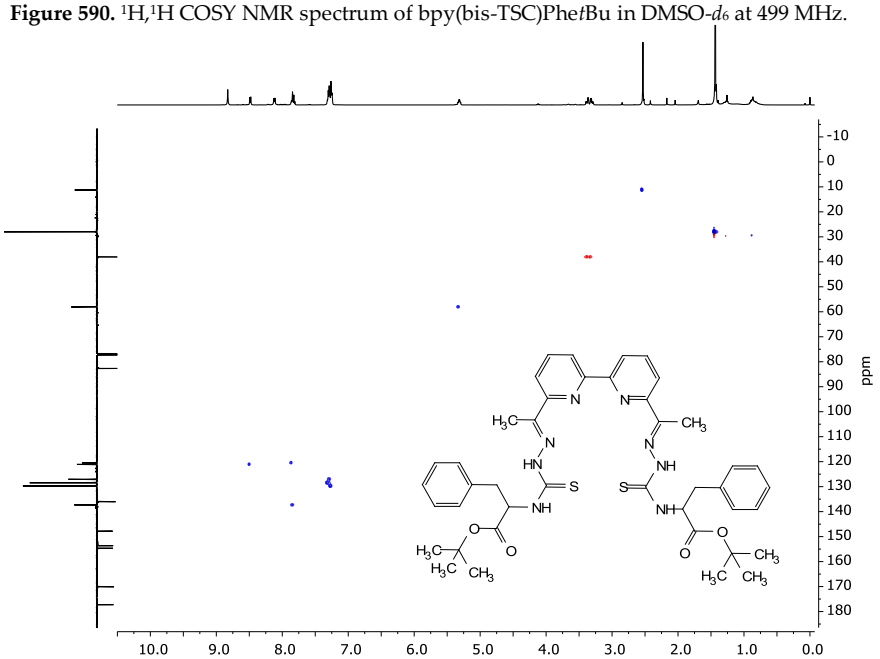


Figure 591. ^{1}H,^{13}C HMQC/HSQC NMR spectrum of bpy(bis-TSC)Phe*t*Bu in DMSO-d_6 at 499 MHz.

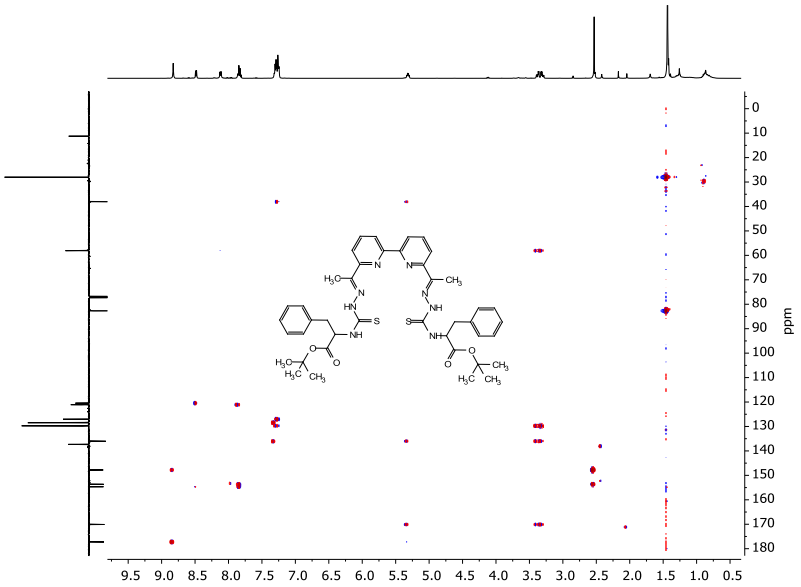


Figure 592. $^{1}H,^{13}C$ HMBC NMR spectrum of bpy(bis-TSC)Phe*t*Bu in DMSO-d_6 at 499 MHz.

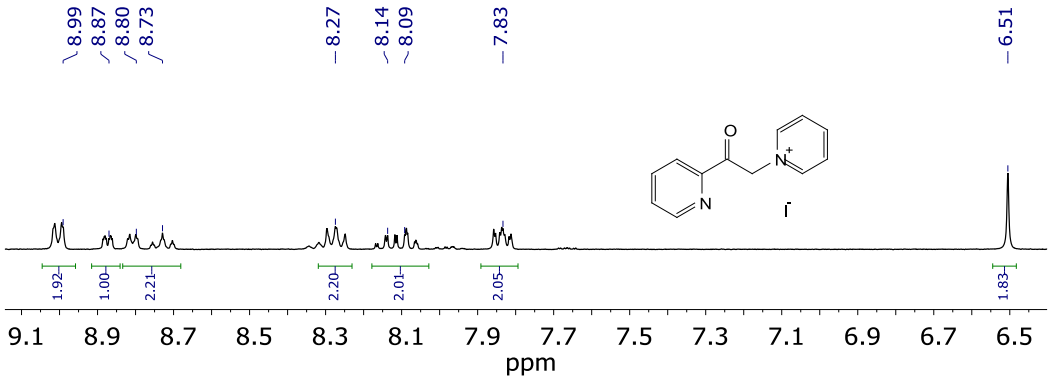


Figure 593. ^{1}H NMR spectrum of 1-[2-oxo-2-(2-pyridyl)ethyl]-1-pyridinium iodide in DMSO-d_6 at 300 MHz.

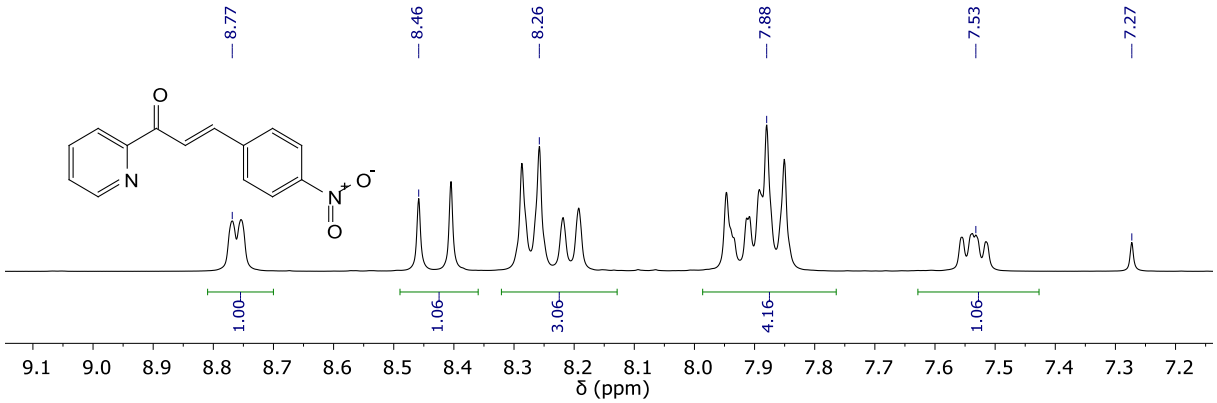


Figure 594. ^{1}H NMR spectrum of 3-(4-nitrophenyl)-1-(2-pyridyl)-2-propen-1-one in DMSO-d_6 at 300 MHz.

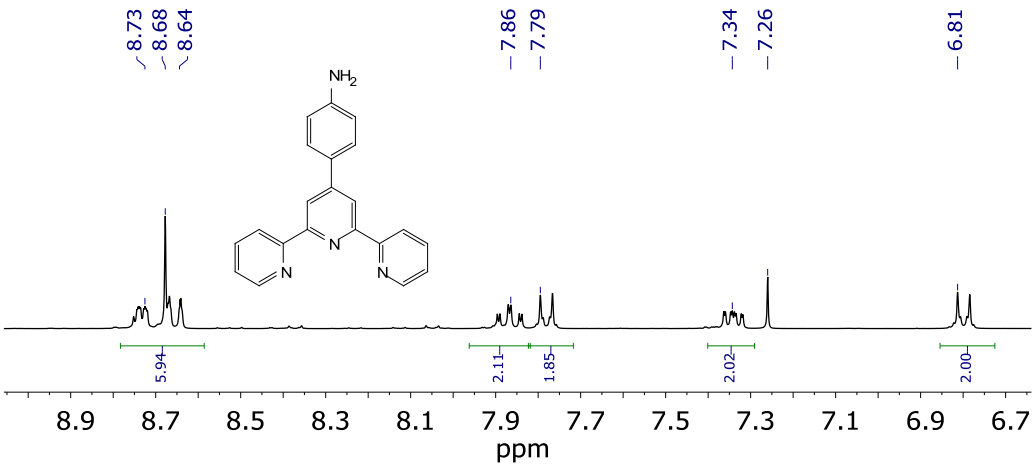


Figure 595. ^{1}H NMR spectrum of 4-([2,2':6',2''-terpyridin]-4'-yl)phenylamine in DMSO-d_6 at 300 MHz.

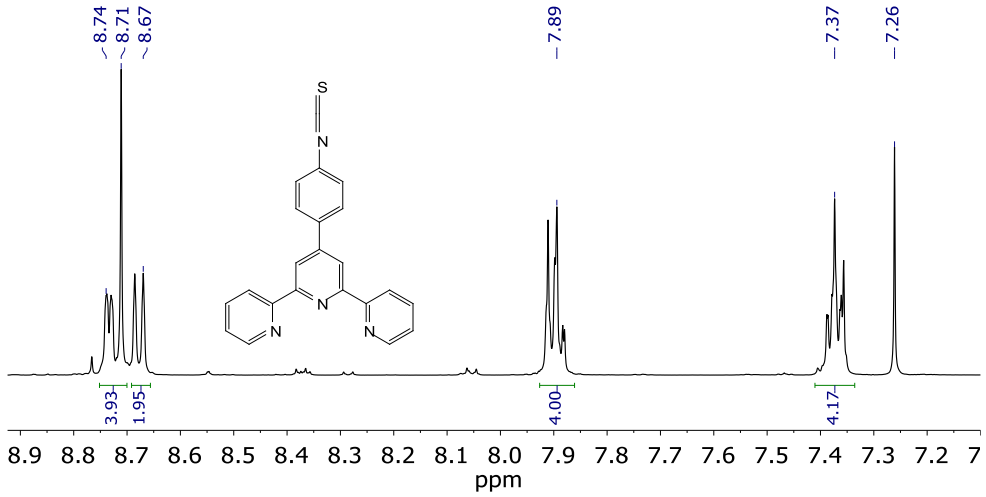


Figure 596. ^{1}H NMR spectrum of 4'-(4-isothiocyanatophenyl)-2,2':6',2''-terpyridine in DMSO-d_6 at 300 MHz.

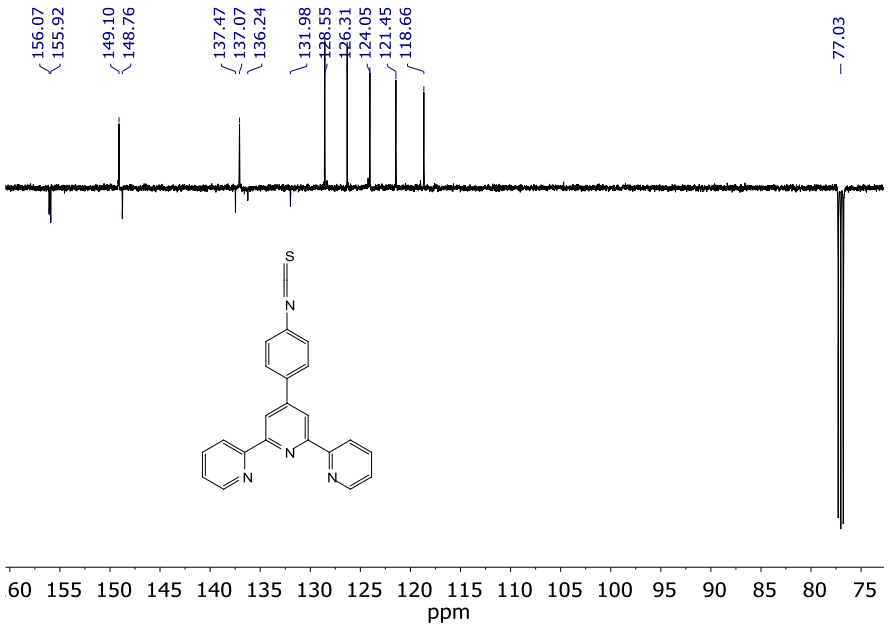


Figure 597. ^{13}C APT NMR spectrum of 4'-(4-isothiocyanatophenyl)-2,2':6',2''-terpyridine in DMSO-d_6 at 499 MHz.

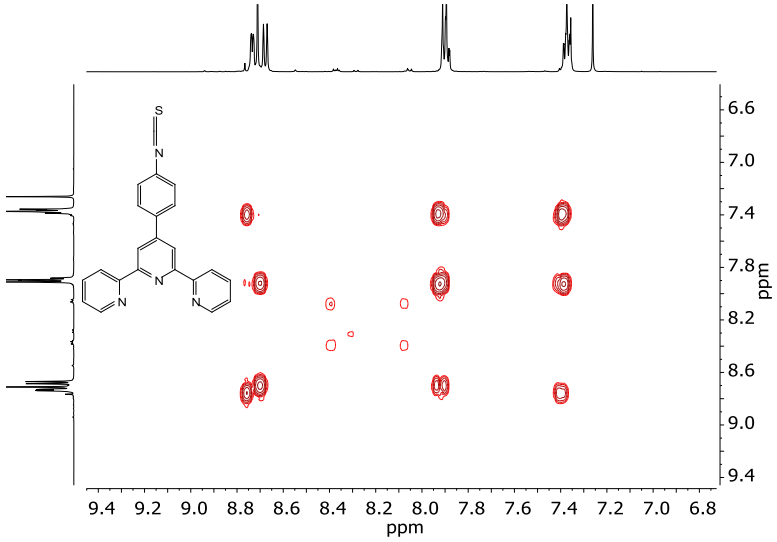


Figure 598. $^{1}H,^{1}H$ COSY NMR spectrum of 4'-(4-isothiocyanatophenyl)-2,2':6',2''-terpyridine in DMSO-d_6 at 499 MHz.

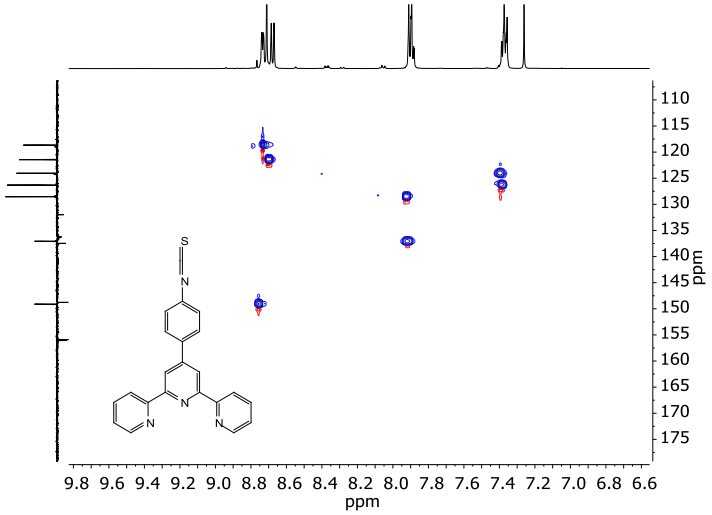


Figure 599. $^{1}H,^{13}C$ HMQC/HSQC NMR spectrum of 4'-(4-isothiocyanatophenyl)-2,2':6',2''-terpyridine in DMSO-d_6 at 499 MHz.

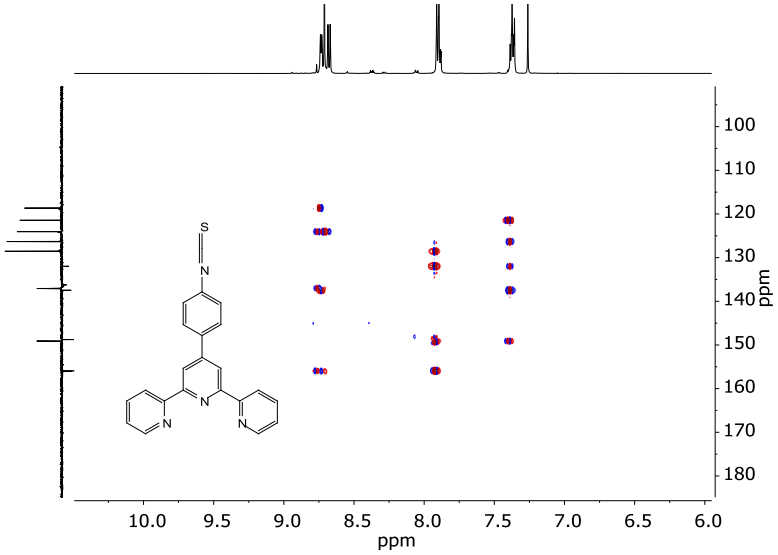


Figure 600. $^{1}H,^{13}C$ HMBC NMR spectrum of 4'-(4-isothiocyanatophenyl)-2,2':6',2''-terpyridine in DMSO-d_6 at 499 MHz.

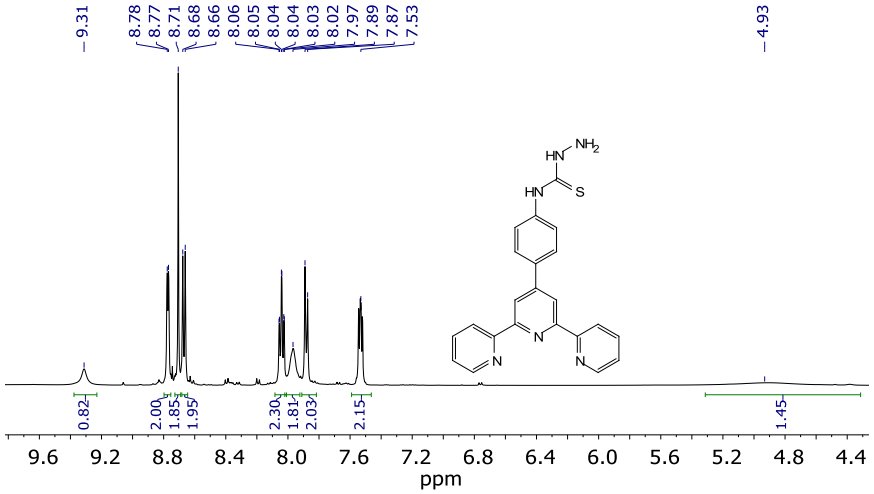


Figure 601. ^{1}H NMR spectrum of *N*-hydrazidecarbothio[4-([2,2':6',2''-terpyridin]-4'-yl)phenyl]amine in DMSO-d_6 at 300 MHz.

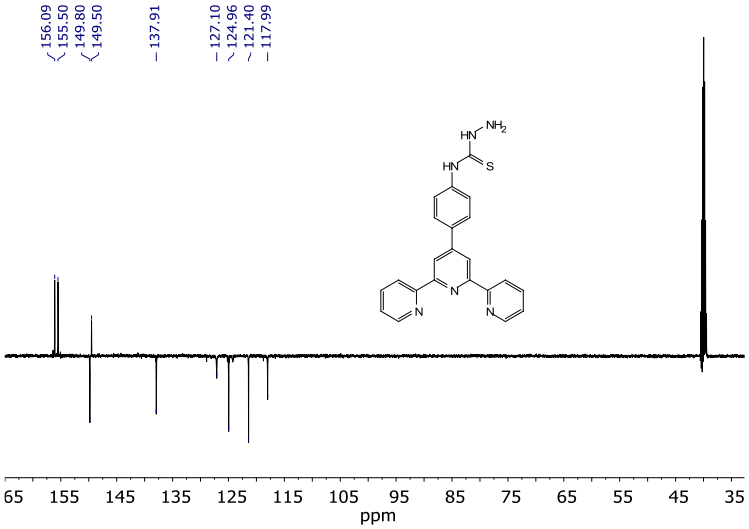


Figure 602. ^{13}C APT NMR spectrum of *N*-hydrazidecarbothio[4-([2,2':6',2''-terpyridin]-4'-yl)phenyl]amine in DMSO-d_6 at 499 MHz.

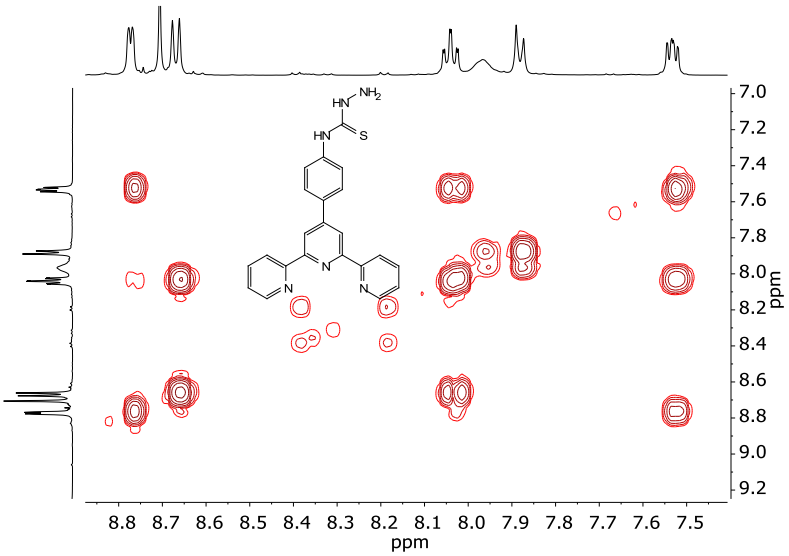


Figure 603. ^{1}H,^{1}H COSY NMR spectrum of *N*-hydrazidecarbothio[4-([2,2':6',2''-terpyridin]-4'-yl)phenyl]amine in DMSO-d_6 at 499 MHz.

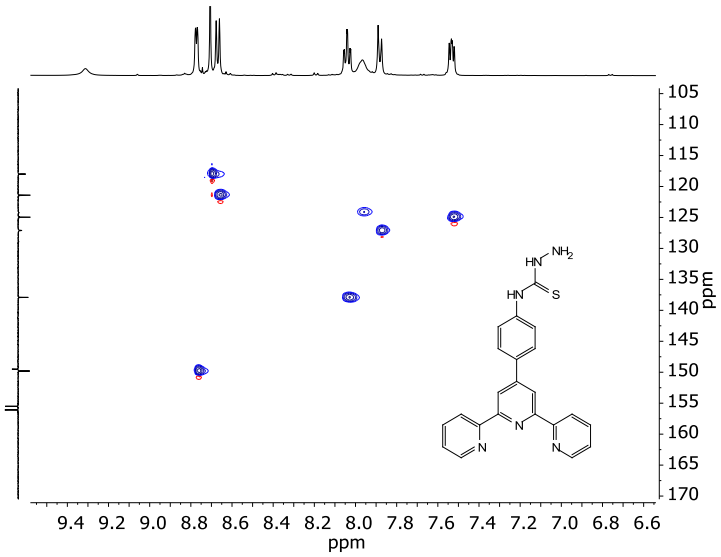


Figure 604. $^{1}H,^{13}C$ HMQC/HSQC NMR spectrum of *N*-hydrazidecarbothio[4-([2,2':6',2''-terpyridin]-4'-yl)phenyl]amine in DMSO-d_6 at 499 MHz.

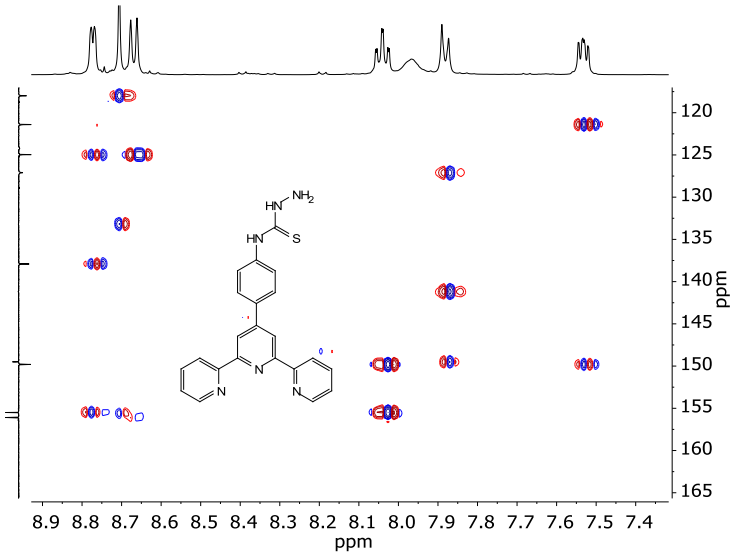


Figure 605. $^{1}H,^{13}C$ HMBC NMR spectrum of *N*-hydrazidecarbothio[4-([2,2':6',2''-terpyridin]-4'-yl)phenyl]amine in DMSO-d_6 at 499 MHz.

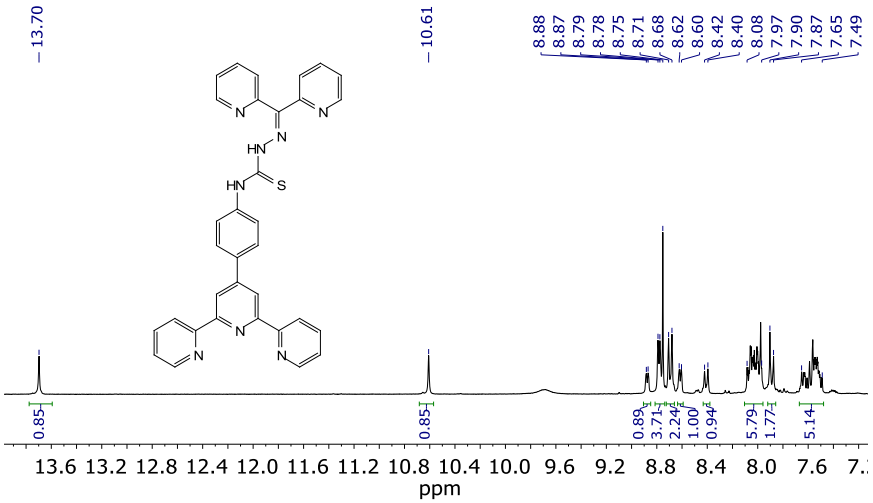


Figure 606. ^{1}H NMR spectrum of 4'-(4-([bis(pyridin-2-yl)methylideneaminocarbamthioyl]amino)phenyl)-2,2':6',2''-terpyridine in DMSO-d_6 at 300 MHz.

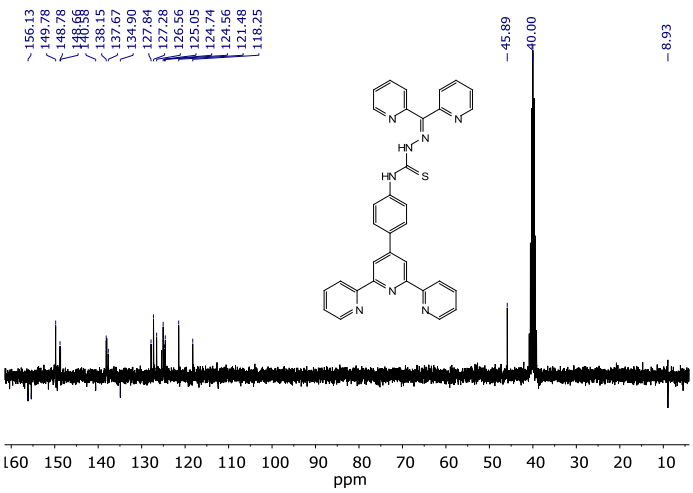


Figure 607. ^{13}C APT NMR spectrum of 4'-(4-([bis(pyridin-2-yl)methylideneaminocarbamthioyl]amino)phenyl)-2,2':6',2''-terpyridine in DMSO-d_6 at 499 MHz.

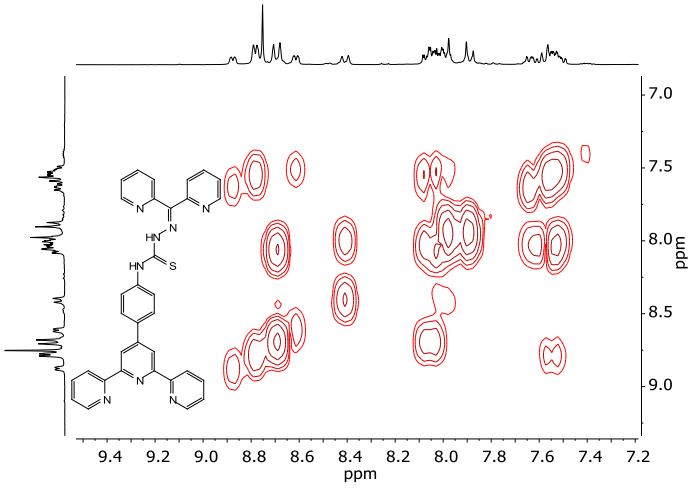


Figure 608. $^{1}H,^{1}H$ COSY NMR spectrum of 4'-(4-([bis(pyridin-2-yl)methylideneaminocarbamthioyl]amino) phenyl)-2,2':6',2''-terpyridine in DMSO-d_6 at 499 MHz.

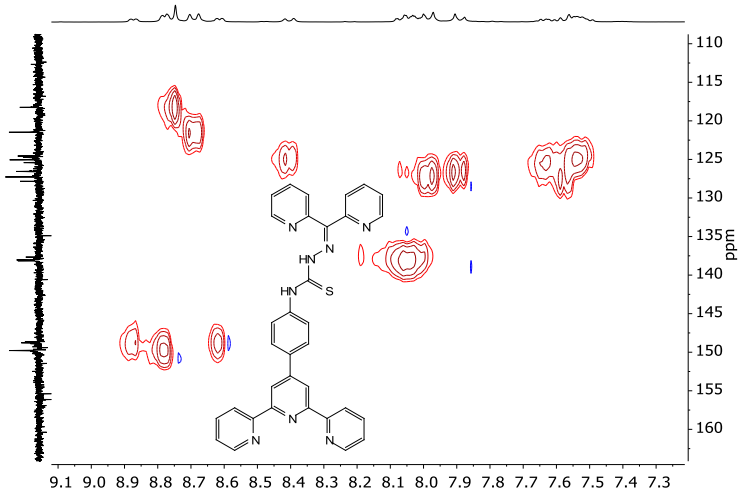


Figure 609. $^{1}H,^{13}C$ HMQC/HSQC NMR spectrum of 4'-(4-([bis(pyridin-2-yl)methylideneaminocarbamthioyl] amino) phenyl)-2,2':6',2''-terpyridine in DMSO-d_6 at 499 MHz.

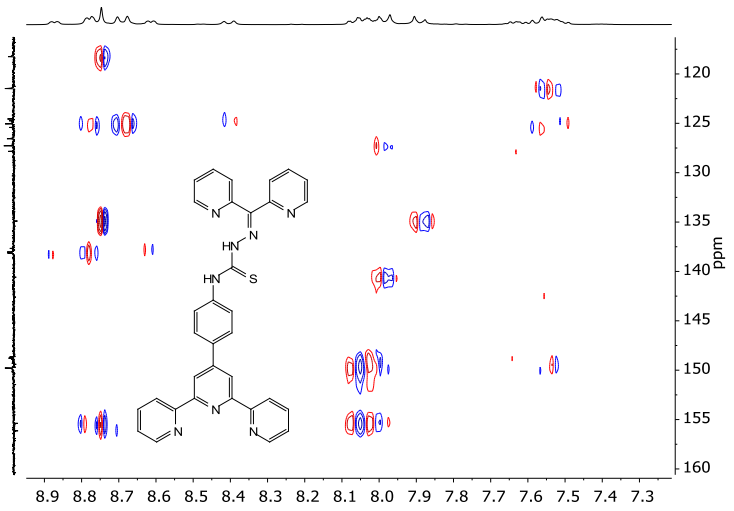


Figure 610. $^{1}H,^{13}C$ HMBC NMR spectrum of 4'-(4-([bis(pyridin-2-yl)methylideneaminocarbamthioyl]amino) phenyl)-2,2':6',2''-terpyridine in DMSO-d_6 at 499 MHz.

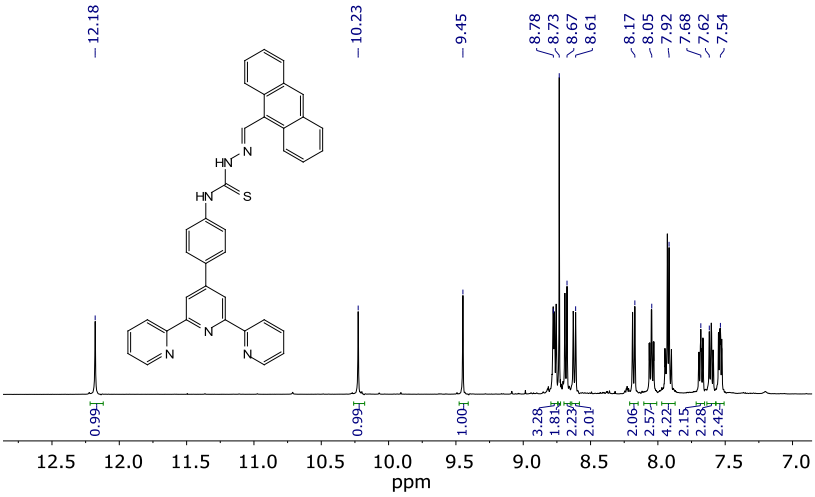


Figure 611. ^{1}H NMR spectrum of (*E*)-1-[(9-anthryl)methylene]-4-[*p*-(2,2':6',2''-terpyridin-4'-yl)phenyl] thiosemicarbazide in DMSO-d_6 at 300 MHz.

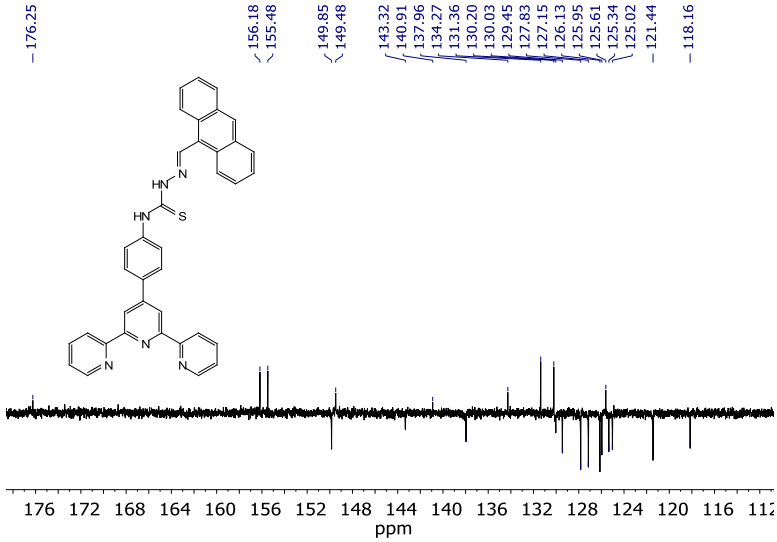


Figure 612. ^{13}C APT NMR spectrum of (*E*)-1-[(9-anthryl)methylene]-4-[*p*-(2,2':6',2''-terpyridin-4'-yl)phenyl]thiosemicarbazide in DMSO-d_6 at 499 MHz.

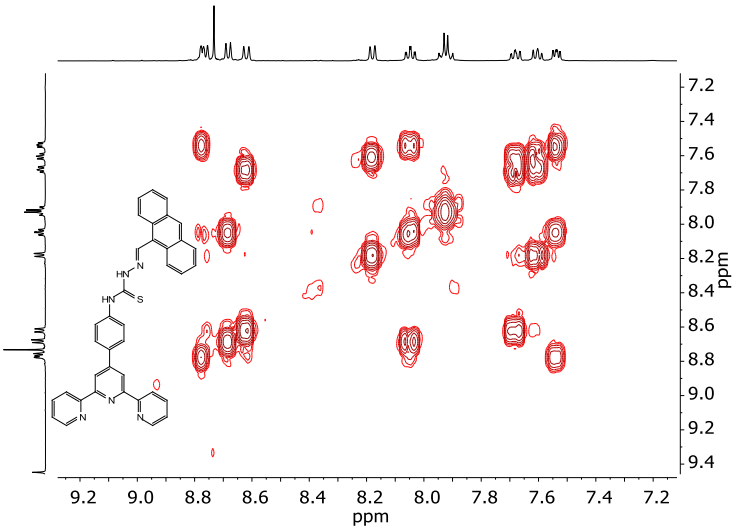


Figure 613. $^{1}H,^{1}H$ COSY NMR spectrum of (*E*)-1-[(9-anthryl)methylene]-4-[*p*-(2,2':6',2''-terpyridin-4'-yl)phenyl]thiosemicarbazide in DMSO-d_6 at 499 MHz.

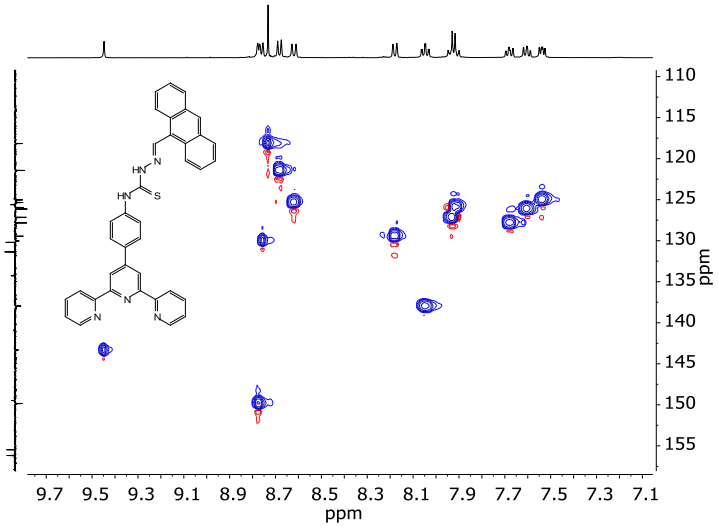


Figure 614. $^{1}H,^{13}C$ HMQC/HSQC NMR spectrum of (*E*)-1-[(9-anthryl)methylene]-4-[*p*-(2,2':6',2''-terpyridin-4'-yl)phenyl] thiosemicarbazide in DMSO-d_6 at 499 MHz.

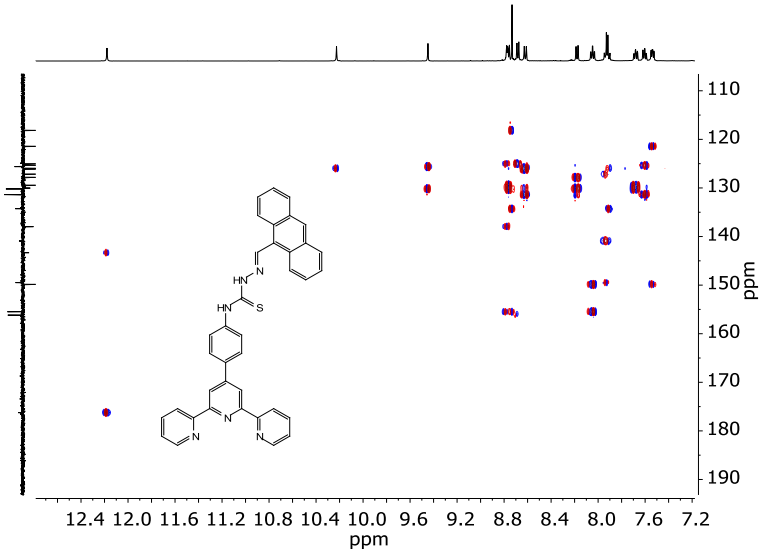


Figure 615. $^{1}H,^{13}C$ HMBC NMR spectrum of (*E*)-1-[(9-anthryl)methylene]-4-[*p*-(2,2':6',2''-terpyridin-4'-yl)phenyl] thiosemicarbazide in DMSO-d_6 at 499 MHz.

7.1.5 NMR data of α-pyridyl TSCs

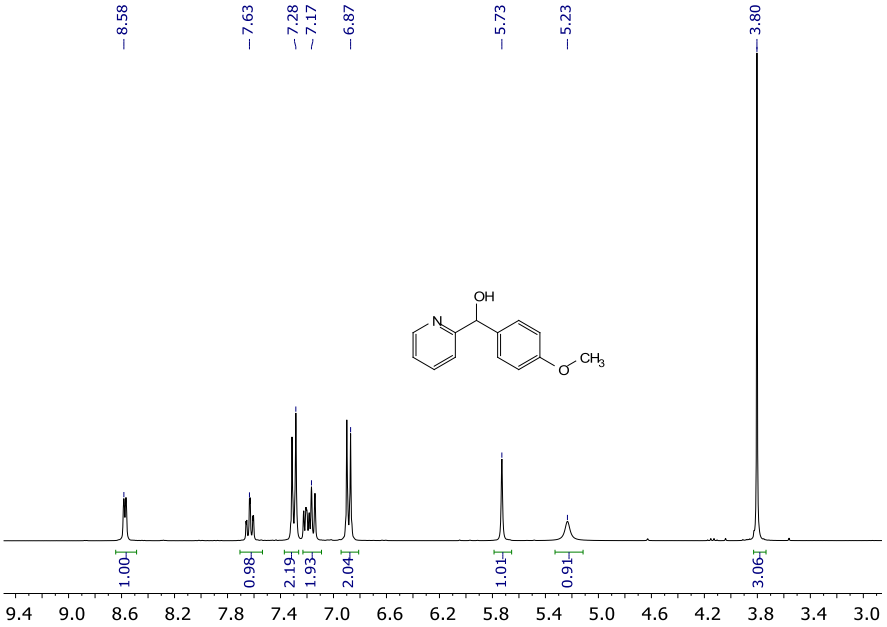


Figure 616. ^{1}H NMR spectrum of α-(4-methoxyphenyl)-2-pyridinemethanol in DMSO-d_6 at 300 MHz.

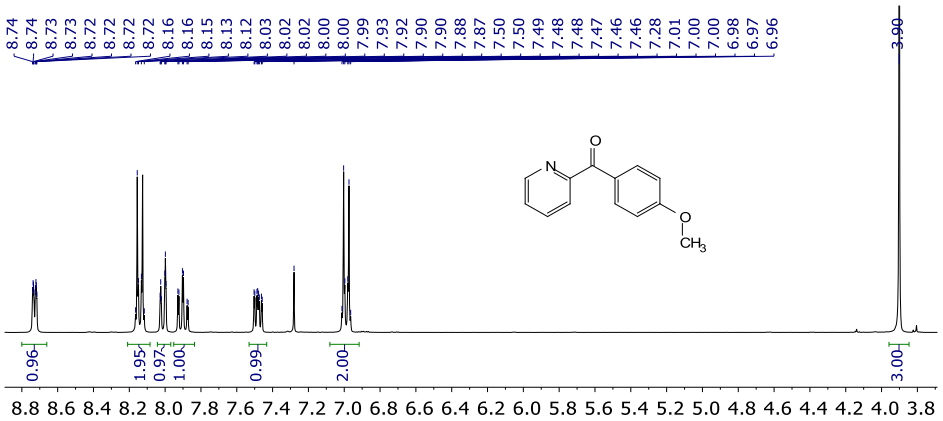


Figure 617. ^{1}H NMR spectrum of (4-methoxyphenyl)(pyridin-2-yl)methanone in DMSO-d_6 at 300 MHz.

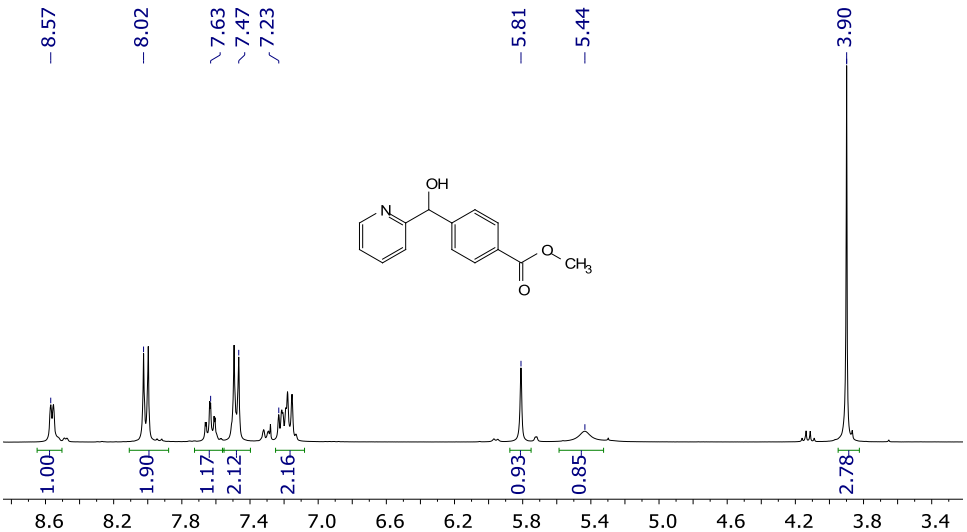


Figure 618. ^{1}H NMR spectrum of 4-[hydroxy(pyridin-2-yl)methyl]benzene-1-carboxylate in DMSO-d_6 at 300 MHz.

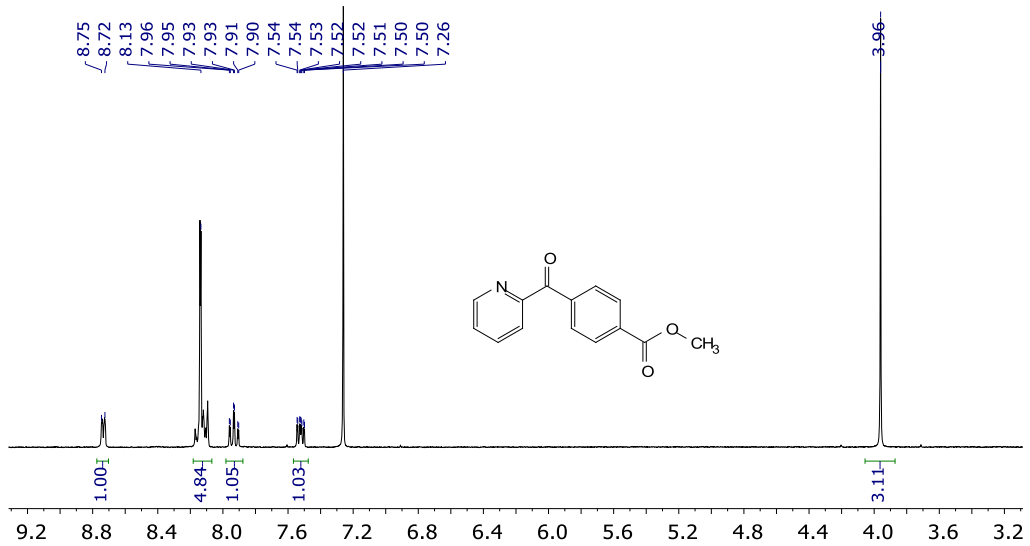


Figure 619. [1]H NMR spectrum of 4-[(pyridin-2-yl)methanoyl]benzene-1-carboxylate in DMSO-*d*6 at 300 MHz.

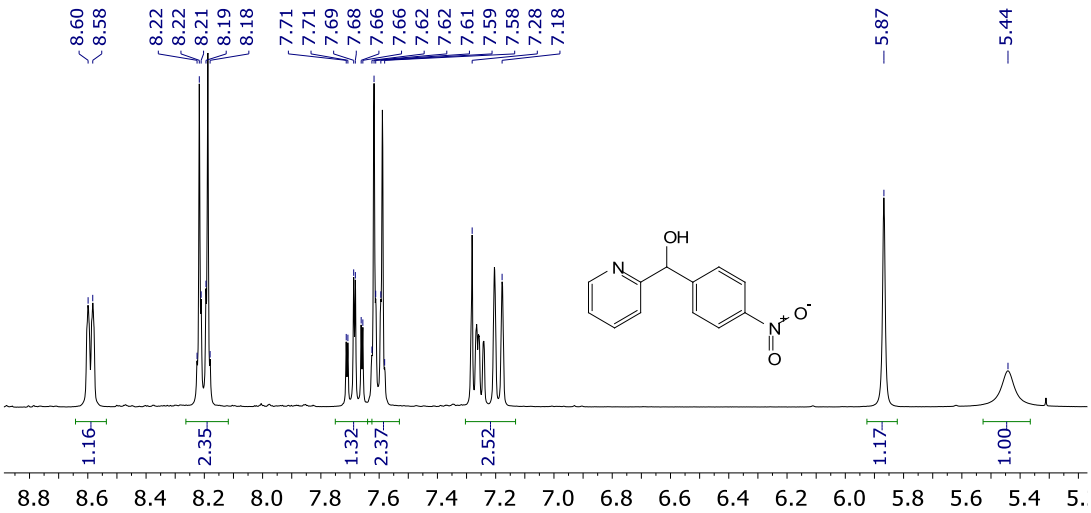


Figure 620. [1]H NMR spectrum of (4-nitrophenyl)(pyridin-2-yl)methanol in DMSO-*d*6 at 300 MHz.

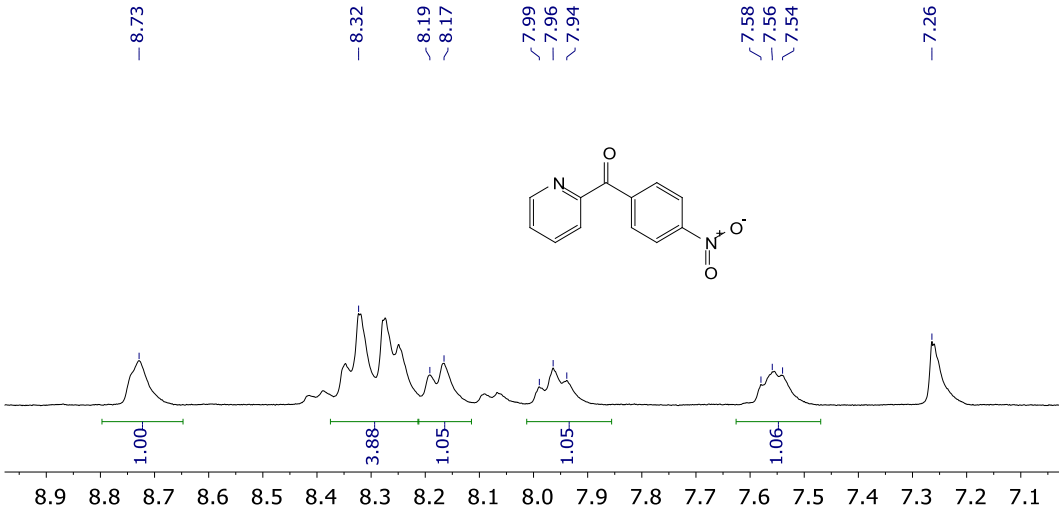


Figure 621. [1]H NMR spectrum of (4-nitrophenyl)(pyridin-2-yl)methanone in DMSO-*d*6 at 300 MHz.

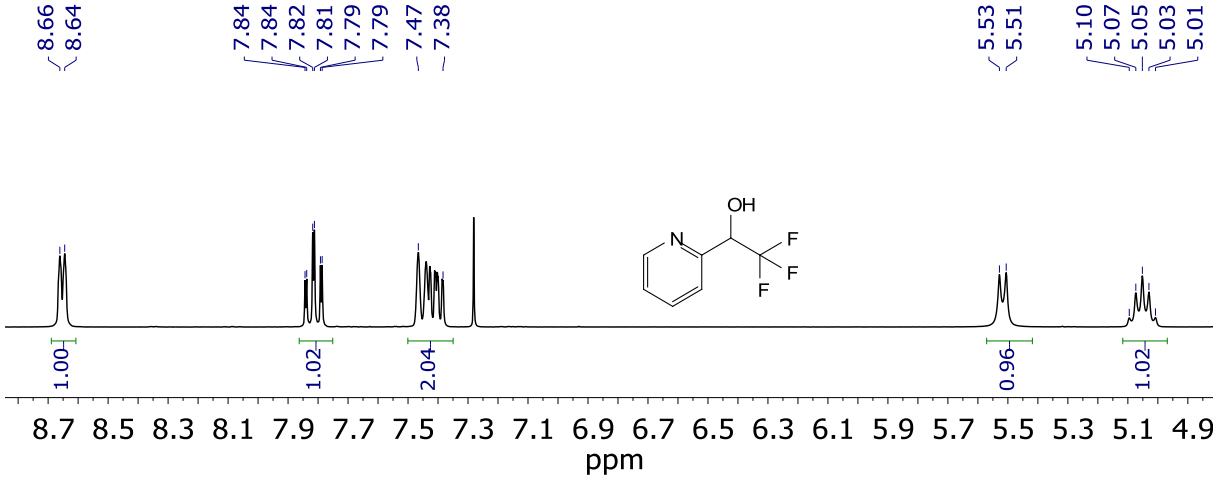


Figure 622. [1]H NMR spectrum of 2,2,2-trifluoro-1-(pyridin-2-yl)ethan-1-ol in DMSO-d_6 at 300 MHz.

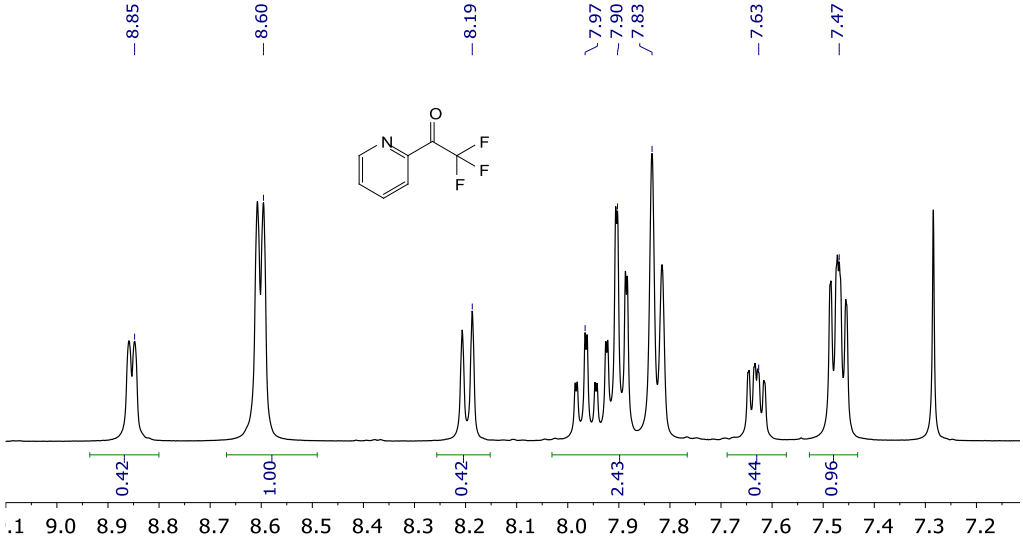


Figure 623. [1]H NMR spectrum of 2,2,2-trifluoro-1-(pyridin-2-yl)ethan-1-one in DMSO-d_6 at 300 MHz.

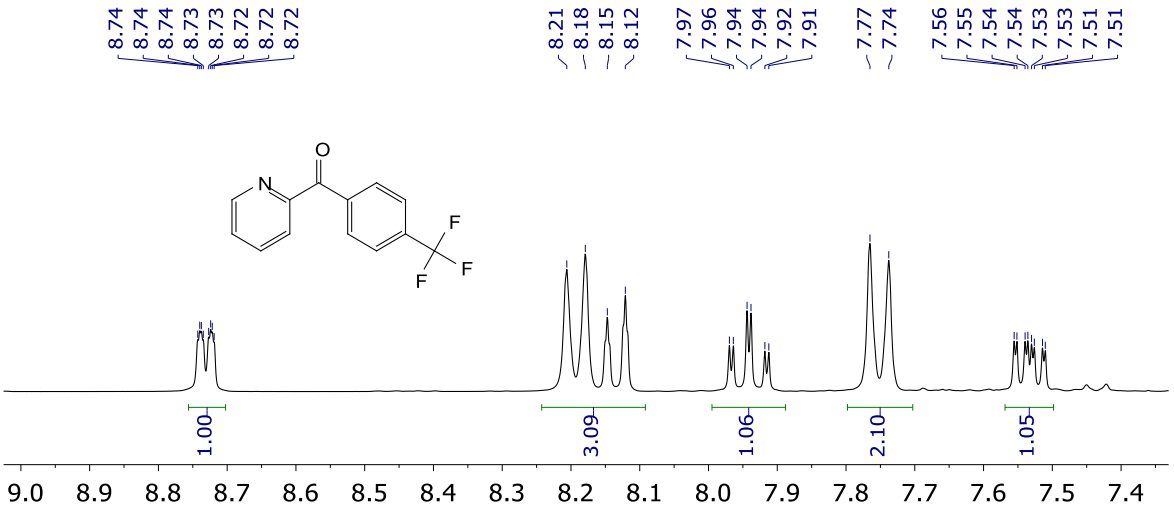


Figure 624. [1]H NMR spectrum of 2,2,2-trifluoro-1-(pyridin-2-yl)ethan-1-one in DMSO-d_6 at 300 MHz.

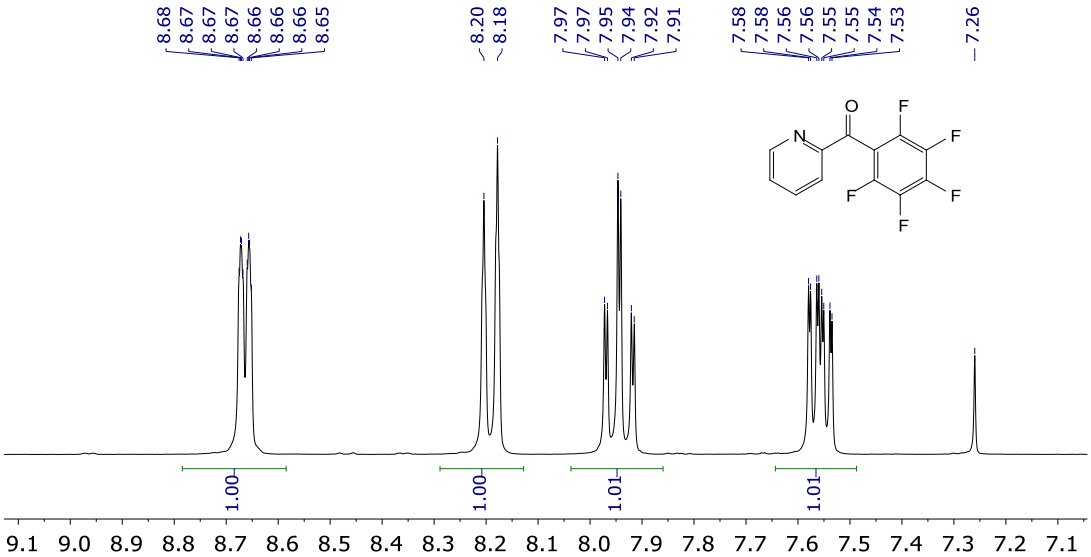


Figure 625. [1]H NMR spectrum of pentafluorophenyl(pyridin-2-yl)methanone in DMSO-*d*6 at 300 MHz.

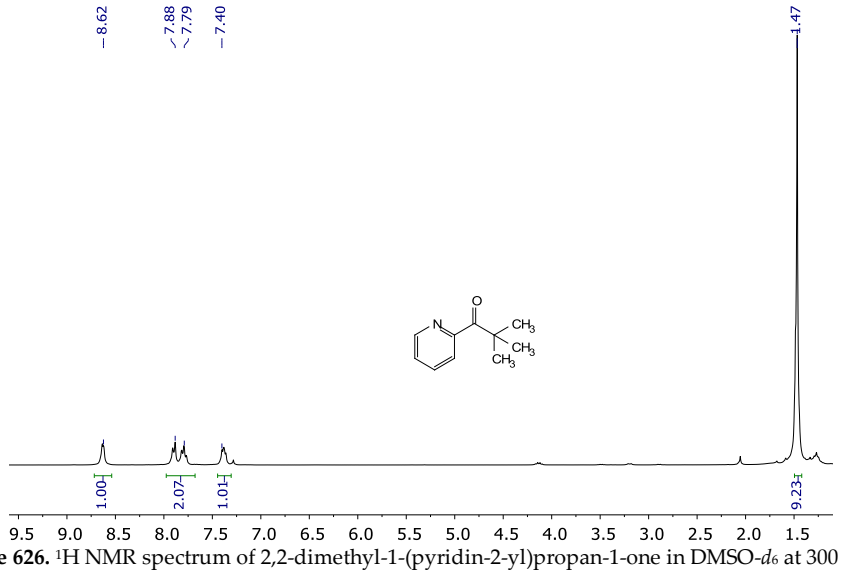


Figure 626. [1]H NMR spectrum of 2,2-dimethyl-1-(pyridin-2-yl)propan-1-one in DMSO-*d*6 at 300 MHz.

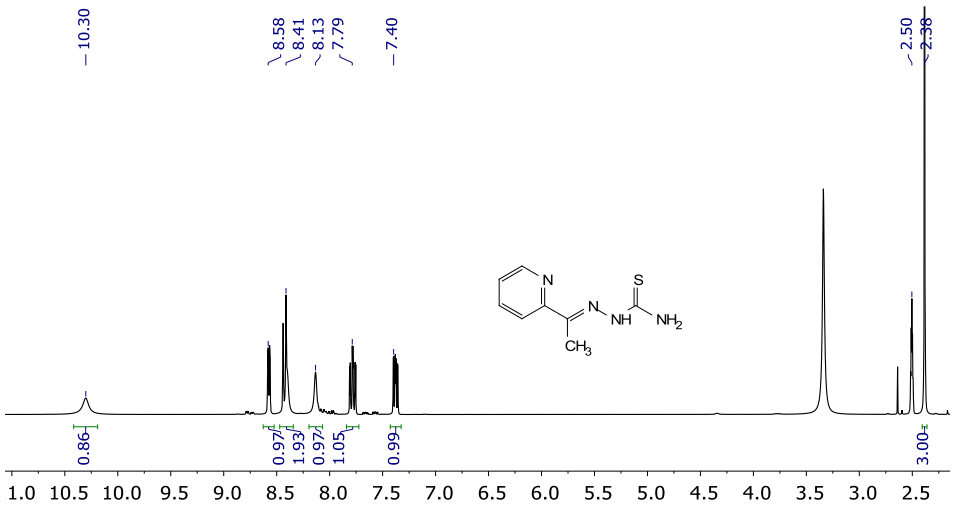


Figure 627. [1]H NMR spectrum of (*E*)-1-[1-(2-pyridyl)ethylidene]thiosemicarbazide in DMSO-*d*6 at 300 MHz.

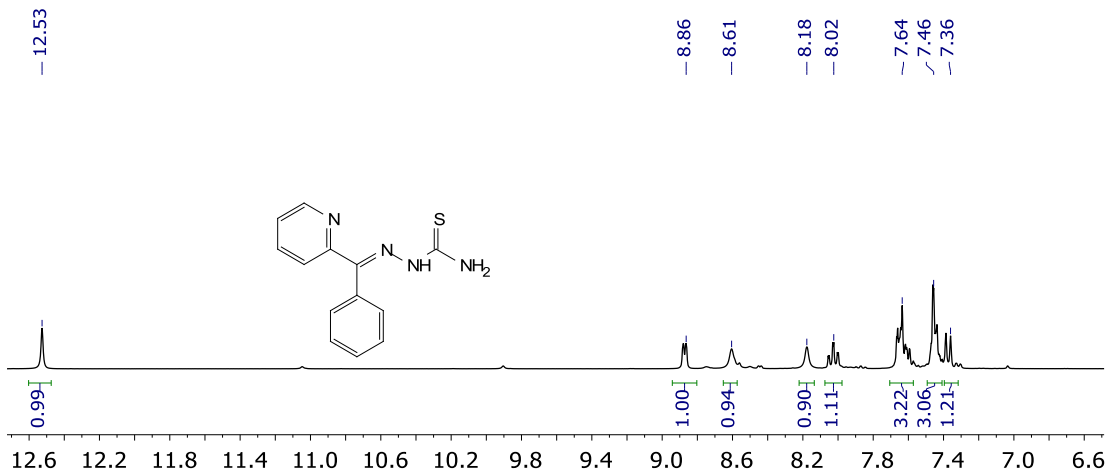


Figure 628. [1]H NMR spectrum of (*E*)-1-[phenyl(2-pyridyl)methylene]thiosemicarbazide in DMSO-d_6 at 300 MHz.

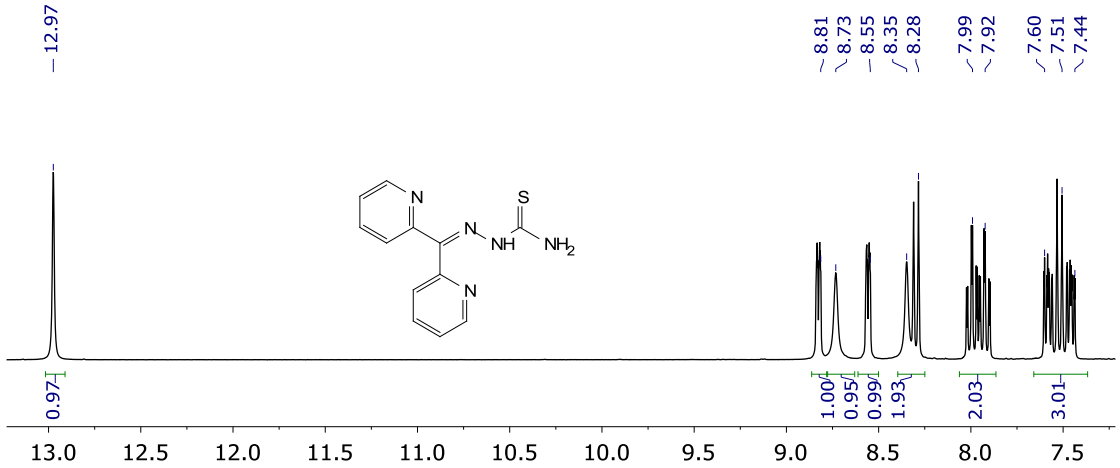


Figure 629. [1]H NMR spectrum of 1-[Bis(2-pyridyl)methylene]thiosemicarbazide in DMSO-d_6 at 300 MHz.

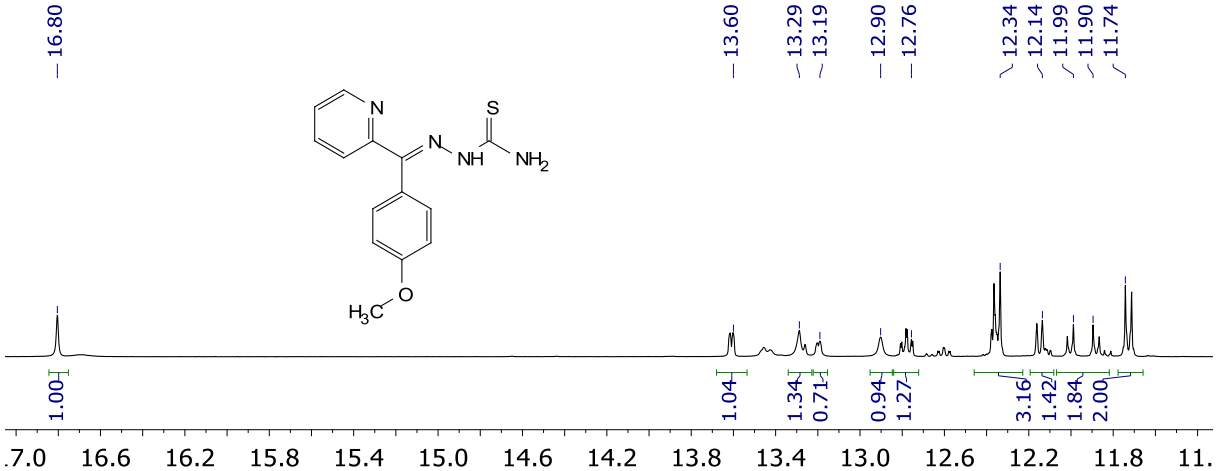


Figure 630. [1]H NMR spectrum of (*E*)-1-[(*p*-methoxyphenyl)(2-pyridyl)methylene]thiosemicarbazide in DMSO-d_6 at 300 MHz.

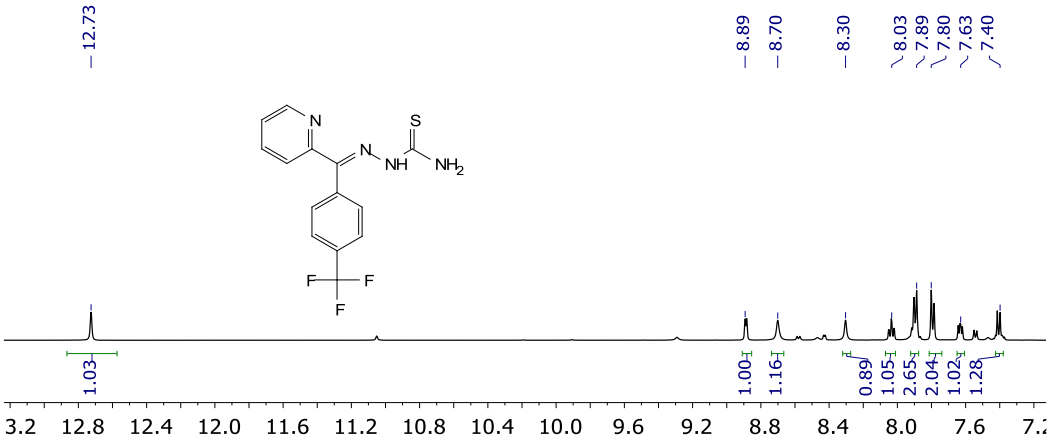


Figure 631. ^{1}H NMR spectrum of (*E*)-1-[(2-pyridyl)[*p*-(trifluoromethyl)phenyl]methylene]thiosemicarbazide in DMSO-d_6 at 300 MHz.

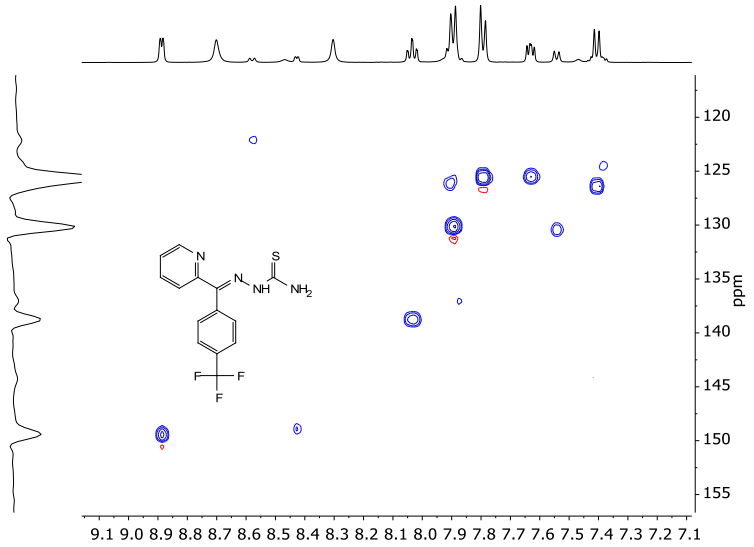


Figure 632. ^{1}H,^{13}C HMQC/HSQC NMR spectrum of (*E*)-1-[(2-pyridyl)[*p*-(trifluoromethyl)phenyl]methylene] thiosemicarbazide in DMSO-d_6 at 499 MHz.

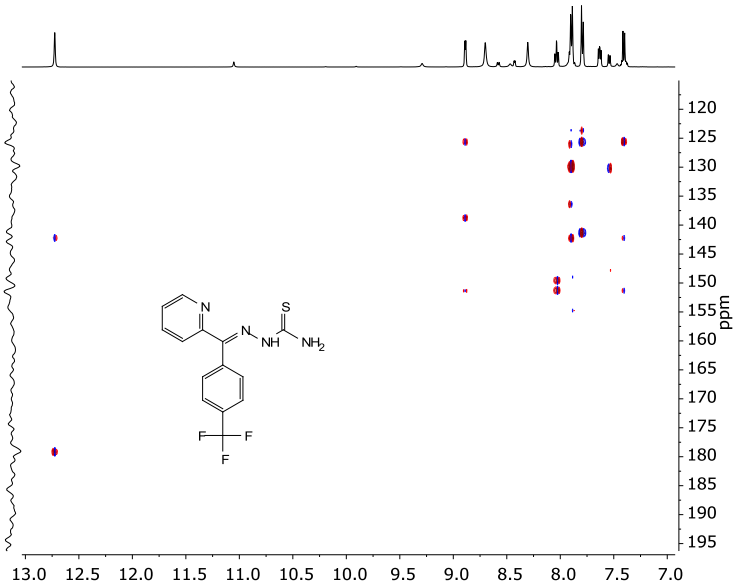


Figure 633. ^{1}H,^{13}C HMBC NMR spectrum of (*E*)-1-[(2-pyridyl)[*p*-(trifluoromethyl)phenyl]methylene] thiosemicarbazide in DMSO-d_6 at 499 MHz.

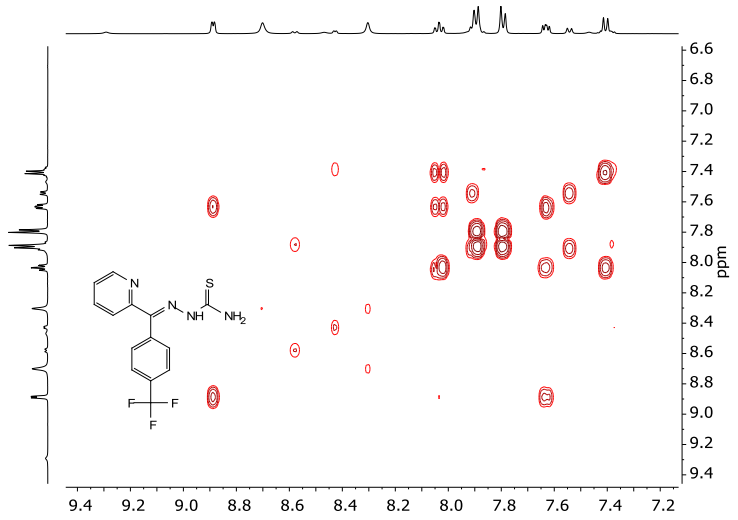


Figure 634. $^{1}H,^{1}H$ COSY NMR spectrum of (*E*)-1-[(2-pyridyl)[*p*-(trifluoromethyl)phenyl]methylene] thiosemicarbazide in DMSO-d_6 at 499 MHz.

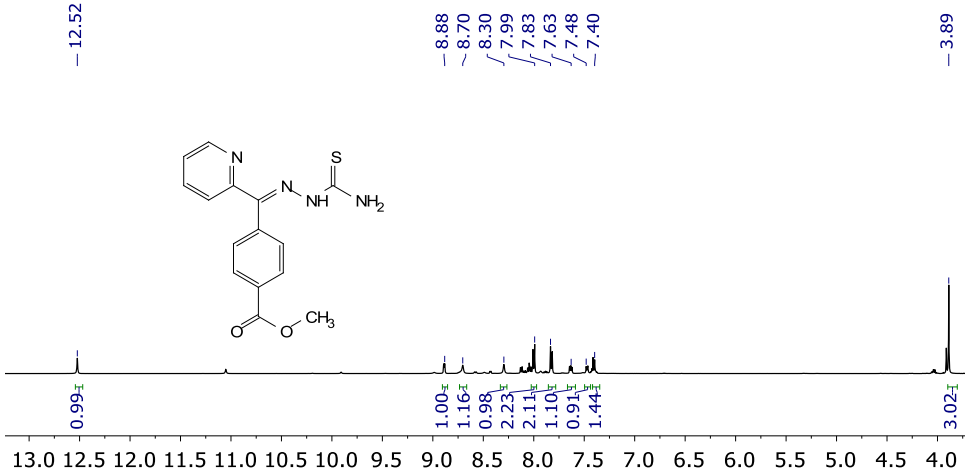


Figure 635. ^{1}H NMR spectrum of methyl *p*-[(*E*)-(2-pyridyl)thiosemicarbazidoidenemethyl]benzoate in DMSO-d_6 at 300 MHz.

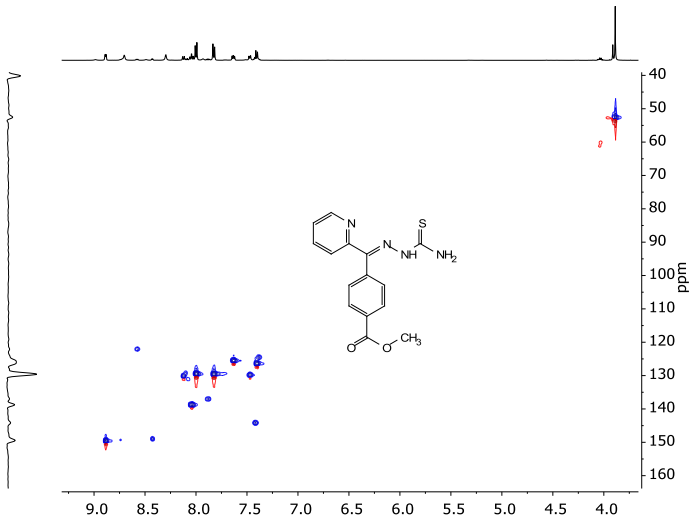


Figure 636. $^{1}H,^{13}C$ HMQC/HSQC NMR spectrum of *p*-[(*E*)-(2-pyridyl)thiosemicarbazidoidenemethyl]benzoate in in DMSO-d_6 at 499 MHz.

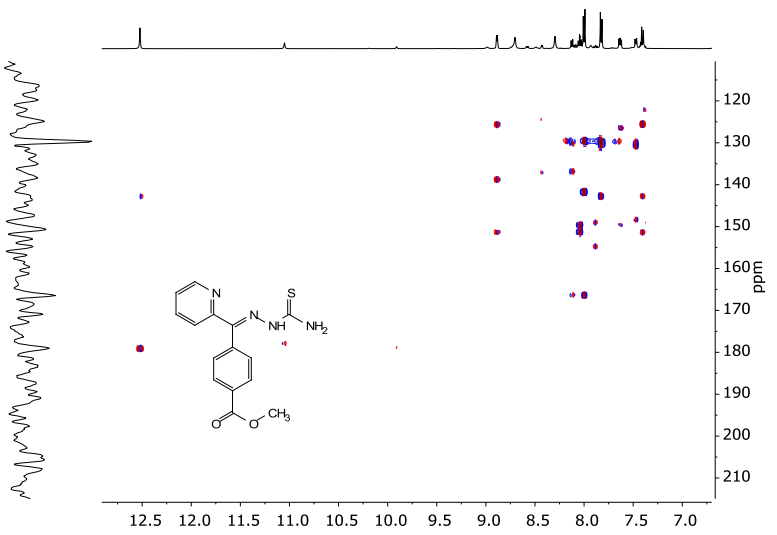


Figure 637. $^{1}H,^{13}C$ HMBC NMR spectrum of *p*-[(*E*)-(2-pyridyl)thiosemicarbazidoidenemethyl]benzoate in in DMSO-d_6 at 499 MHz.

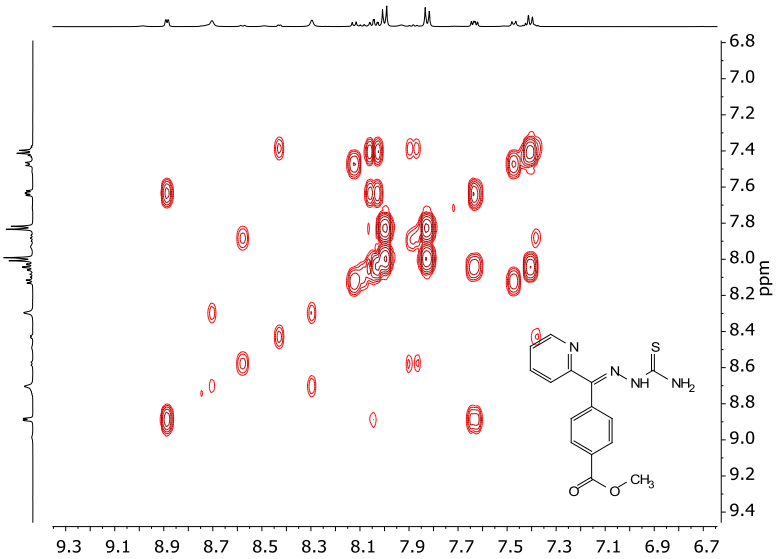


Figure 638. $^{1}H,^{1}H$ COSY NMR spectrum of *p*-[(*E*)-(2-pyridyl)thiosemicarbazidoidenemethyl]benzoate in in DMSO-d_6 at 499 MHz.

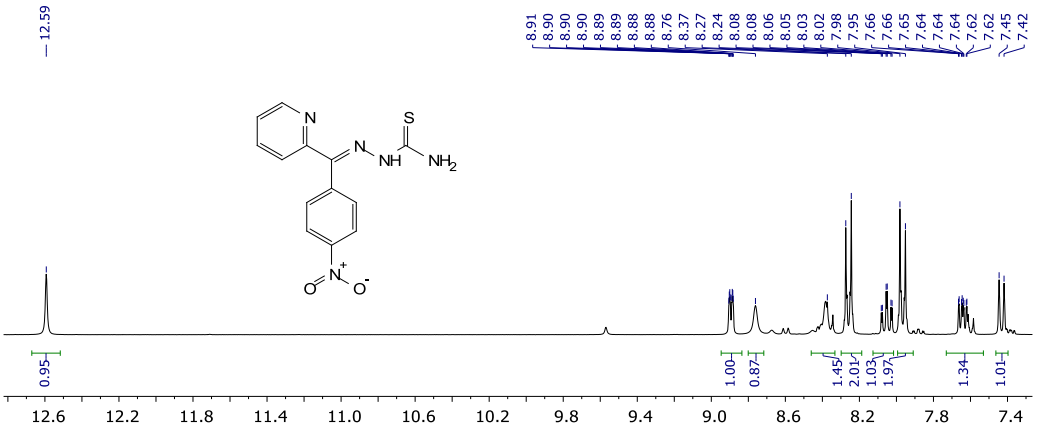


Figure 639. ^{1}H NMR spectrum of (*E*)-1-[(*p*-nitrophenyl)(2-pyridyl)methylene]thiosemicarbazide in DMSO-d_6 at 300 MHz.

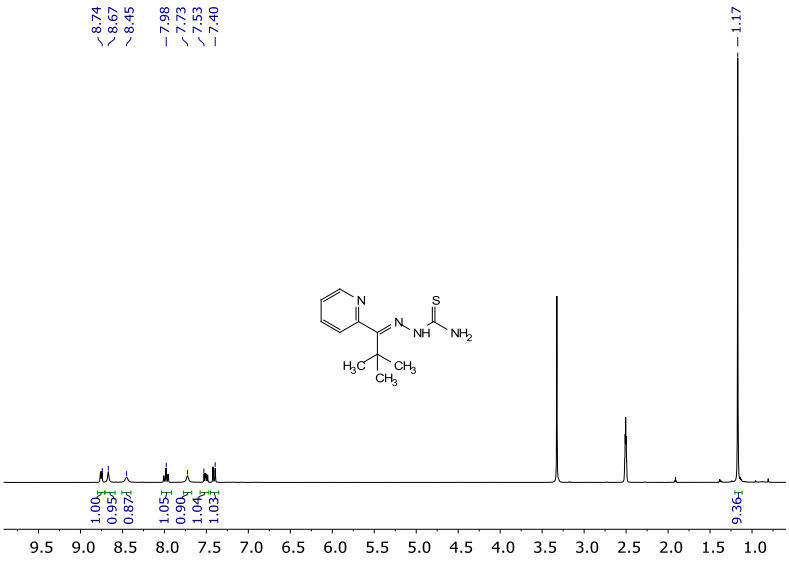


Figure 640. ^{1}H NMR spectrum of (*E*)-1-[2,2-dimethyl-1-(2-pyridyl)propylidene]thiosemicarbazide in DMSO-d_6 at 300 MHz.

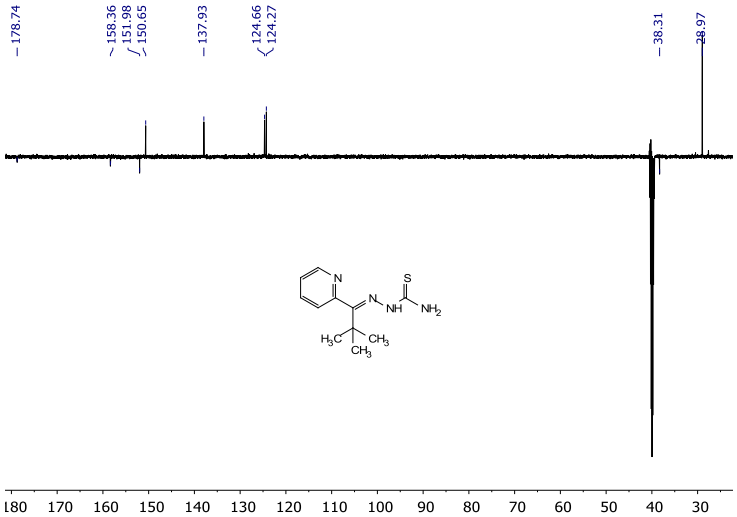


Figure 641. ^{13}C APT NMR spectrum of (*E*)-1-[2,2-dimethyl-1-(2-pyridyl)propylidene]thiosemicarbazide in DMSO-d_6 at 499 MHz.

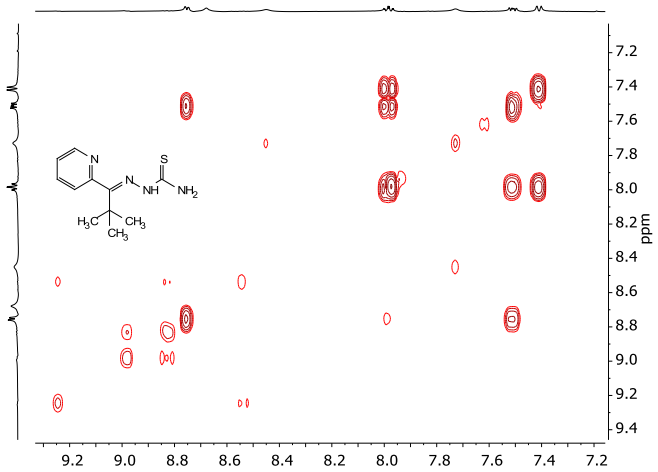


Figure 642. ^{1}H,^{1}H COSY NMR spectrum of (*E*)-1-[2,2-dimethyl-1-(2-pyridyl)propylidene]thiosemicarbazide in DMSO-d_6 at 499 MHz.

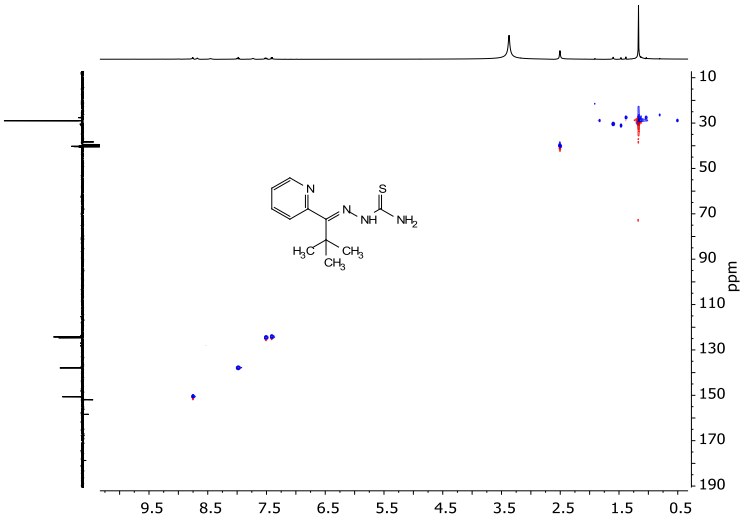


Figure 643. $^{1}H,^{13}C$ HMQC/HSQC NMR spectrum of (*E*)-1-[2,2-dimethyl-1-(2-pyridyl)propylidene] thiosemicarbazide in DMSO-d_6 at 499 MHz.

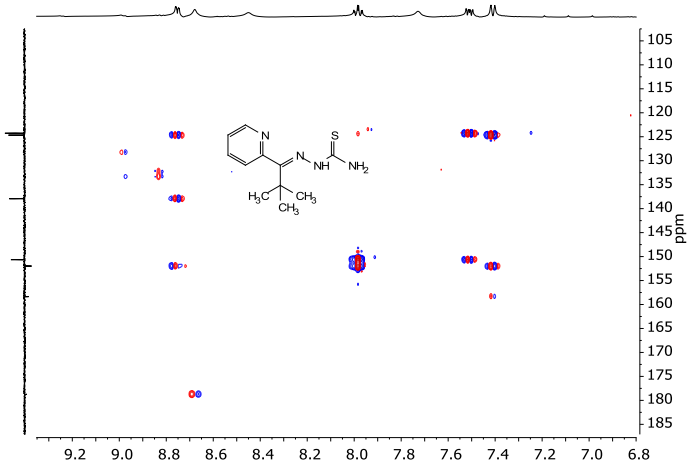


Figure 644. $^{1}H,^{13}C$ HMBC NMR spectrum of (*E*)-1-[2,2-dimethyl-1-(2-pyridyl)propylidene]thiosemicarbazide in DMSO-d_6 at 499 MHz.

7.1.6 NMR data of amphiphile TSCs

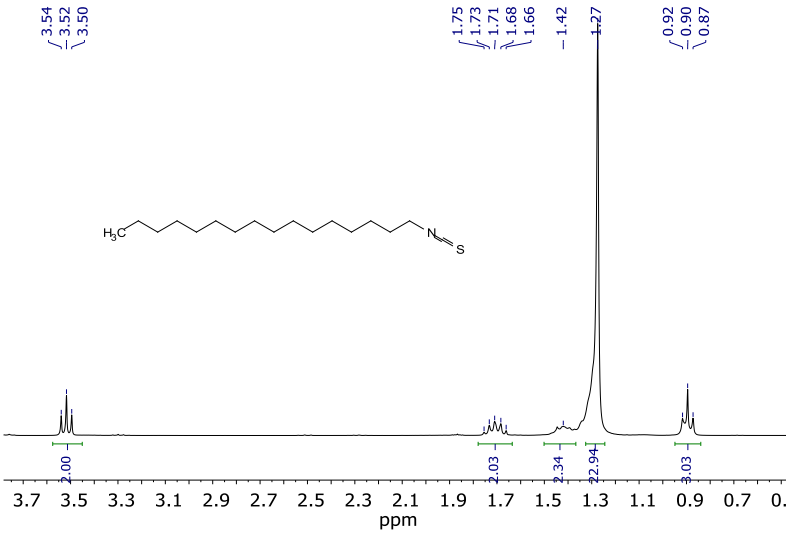


Figure 645. ^{1}H NMR spectrum of 1-isothiocyanatohexadecane in DMSO-d_6 at 300 MHz.

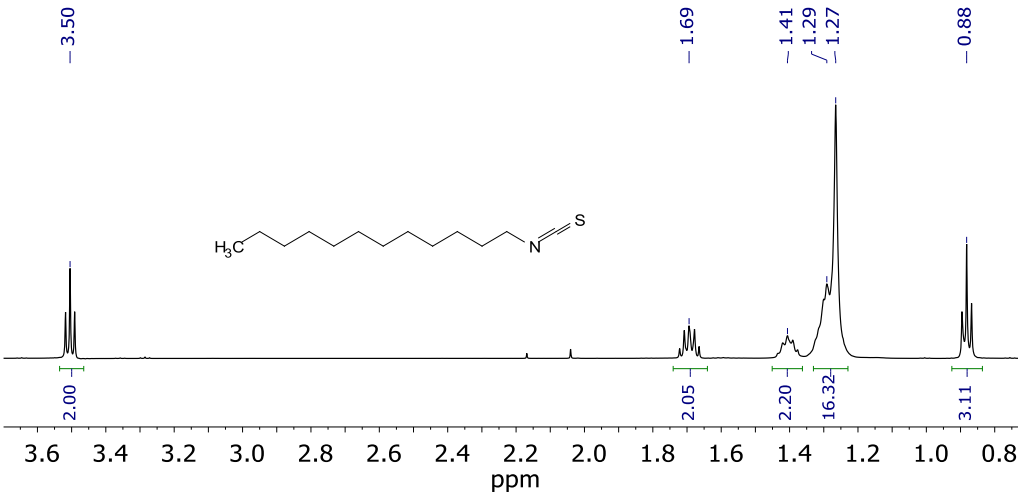


Figure 646. [1]H NMR spectrum of 1-isothiocyanatododecane in DMSO-*d*$_6$ at 300 MHz.

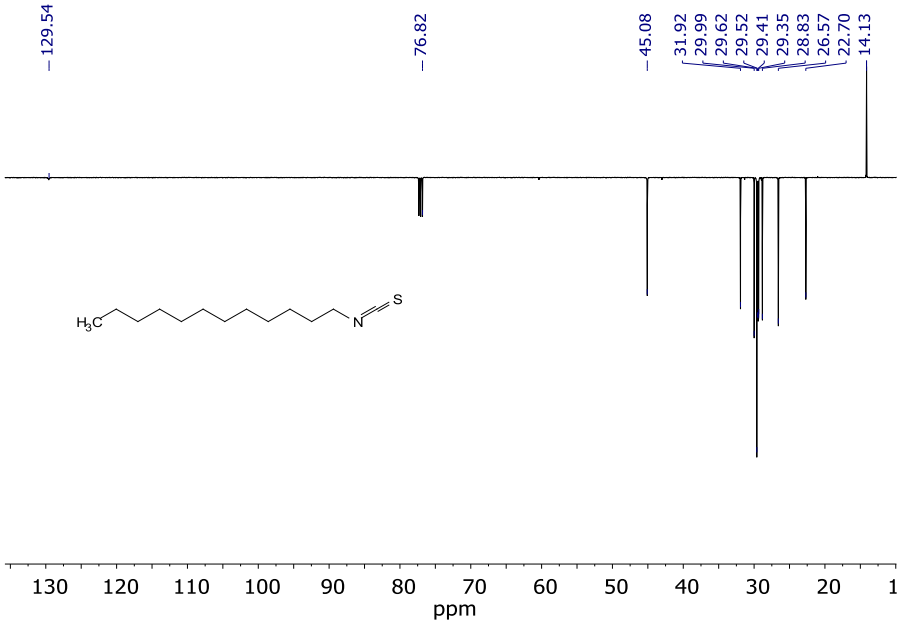


Figure 647. [13]C APT NMR spectrum of 1-isothiocyanatododecane in DMSO-*d*$_6$ at 499 MHz.

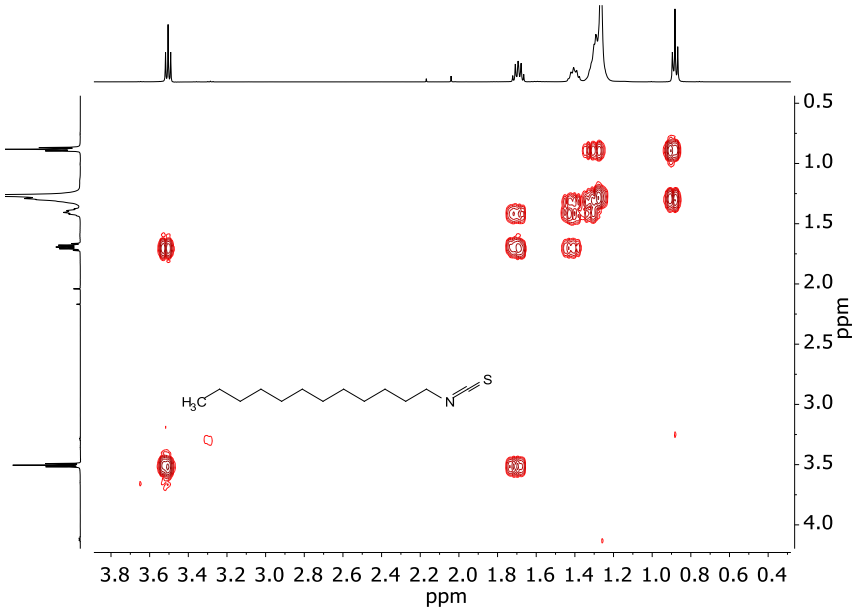


Figure 648. [1]H,[1]H COSY NMR spectrum of 1-isothiocyanatododecane in DMSO-*d*$_6$ at 499 MHz.

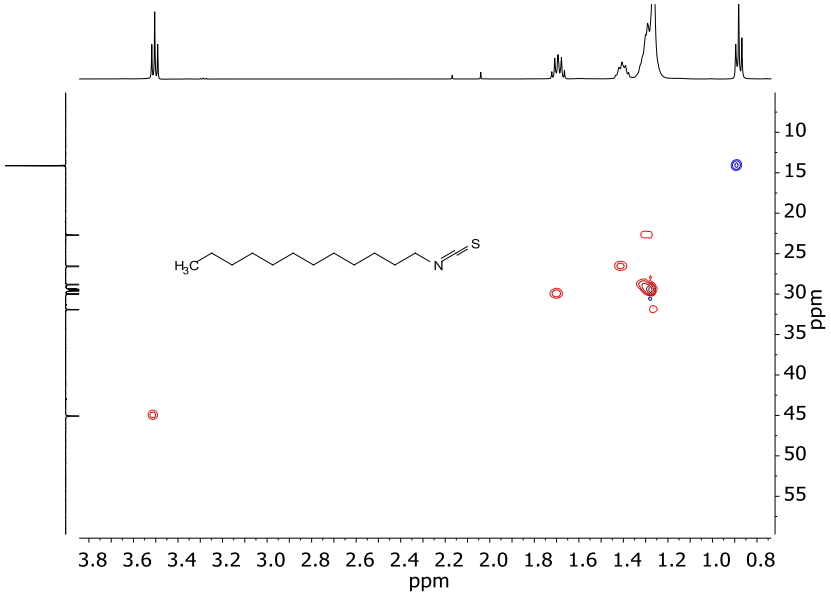


Figure 649. $^{1}H,^{13}C$ HMQC/HSQC NMR spectrum of 1-isothiocyanatododecane in DMSO-d_6 at 499 MHz.

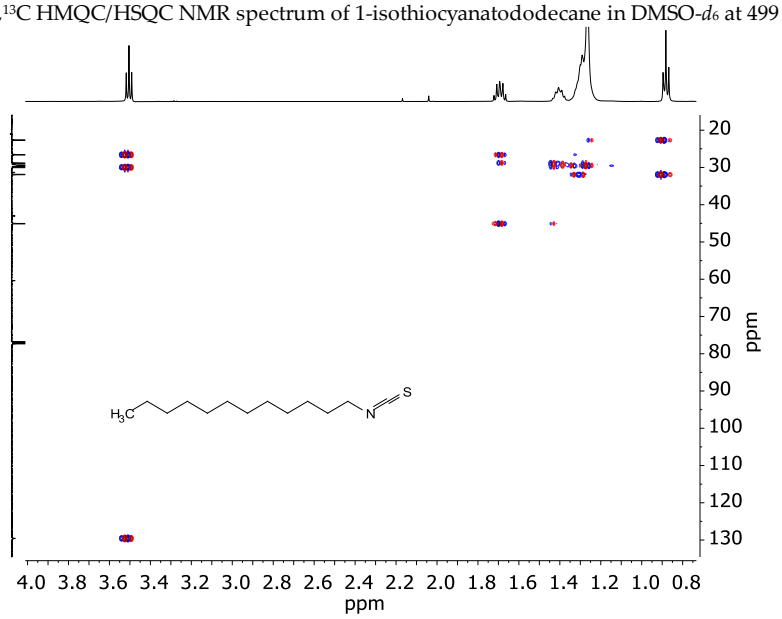


Figure 650. $^{1}H,^{13}C$ HMBC NMR spectrum of 1-isothiocyanatododecane in DMSO-d_6 at 499 MHz.

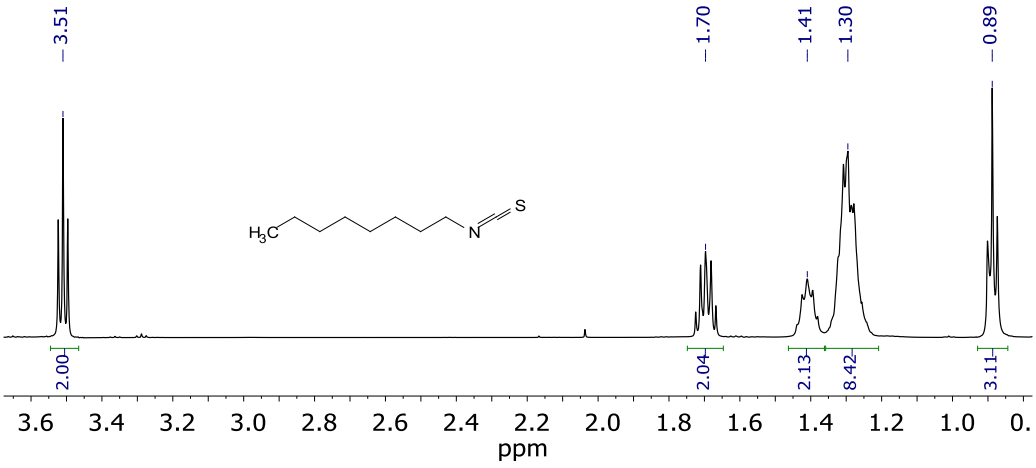


Figure 651. ^{1}H NMR spectrum of 1-isothiocyanatooctane in DMSO-d_6 at 300 MHz.

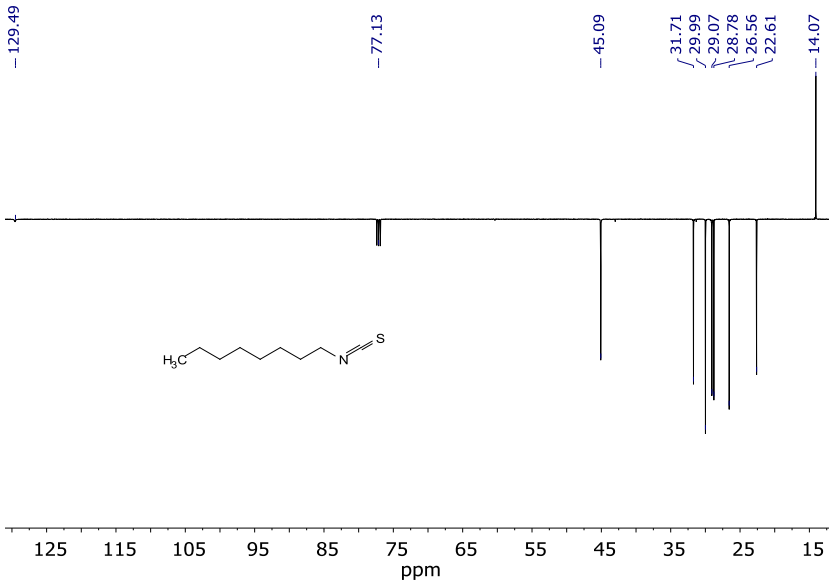


Figure 652. ^{13}C APT NMR spectrum of 1-isothiocyanatooctane in DMSO-*d*$_6$ at 499 MHz.

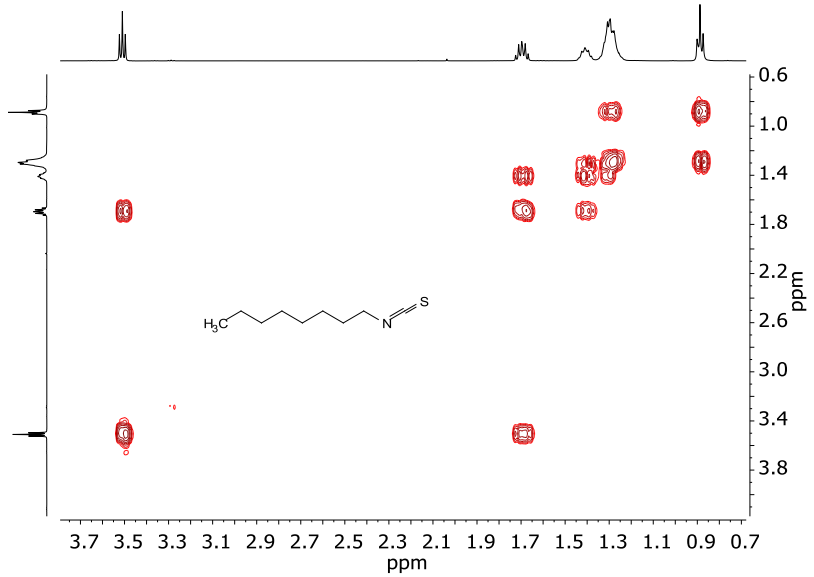


Figure 653. ^{1}H,^{1}H COSY NMR spectrum of 1-isothiocyanatooctane in DMSO-*d*$_6$ at 499 MHz.

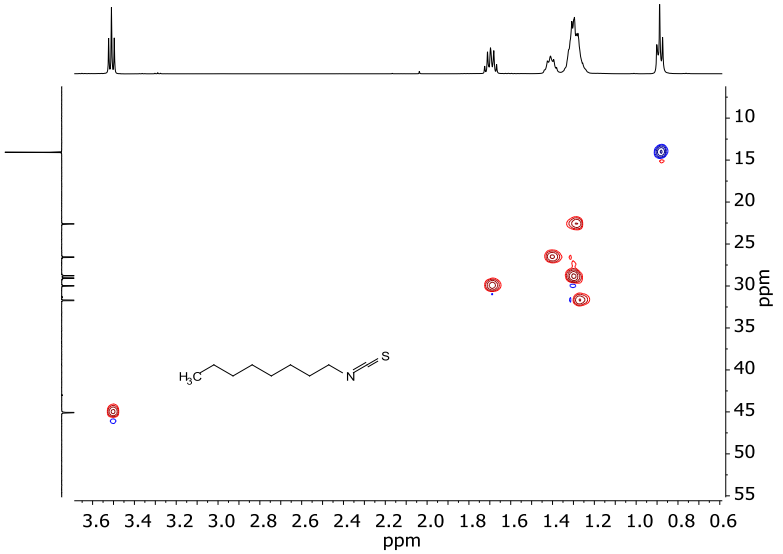


Figure 654. ^{1}H,^{13}C HMQC/HSQC NMR spectrum of 1-isothiocyanatooctane in DMSO-*d*$_6$ at 499 MHz.

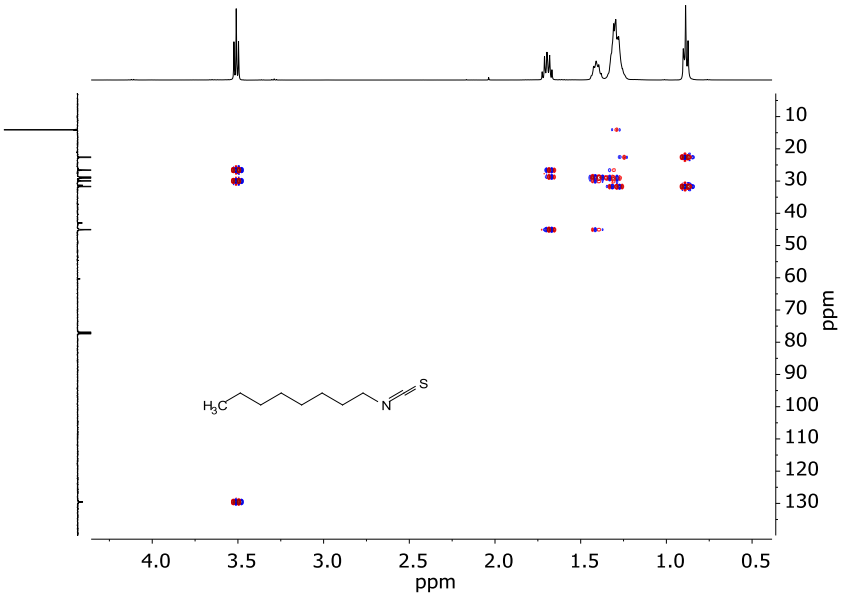


Figure 655. $^{1}H,^{13}C$ HMBC NMR spectrum of 1-isothiocyanatooctane in DMSO-d_6 at 499 MHz.

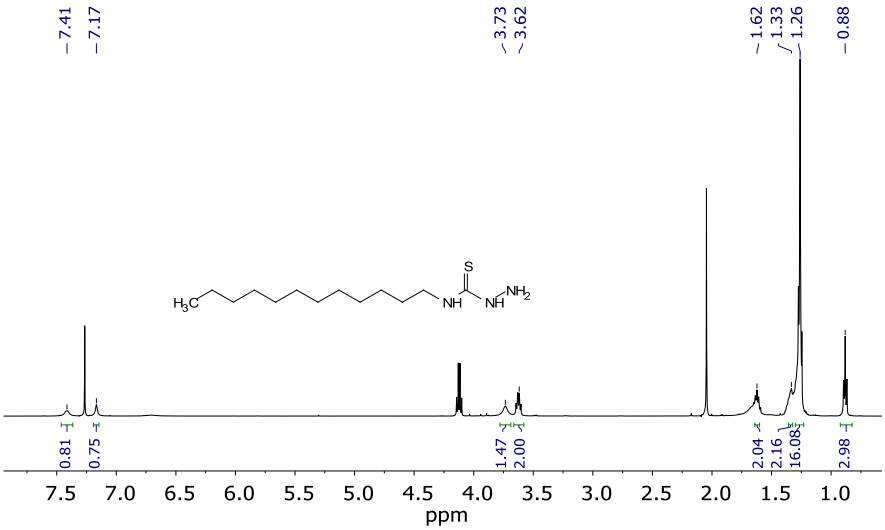


Figure 656. ^{1}H NMR spectrum of 4-dodecylthiosemicarbazide in DMSO-d_6 at 300 MHz.

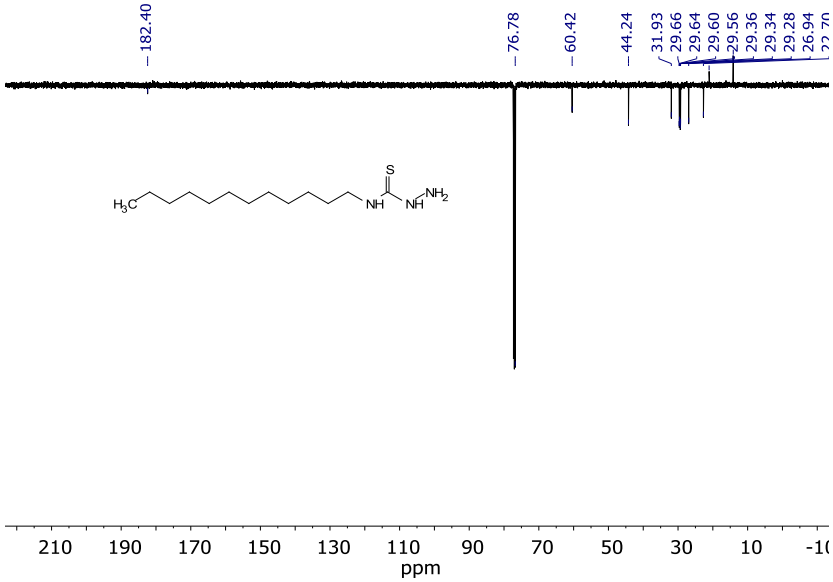


Figure 657. ^{13}C APT NMR spectrum of 4-dodecylthiosemicarbazide in DMSO-d_6 at 499 MHz.

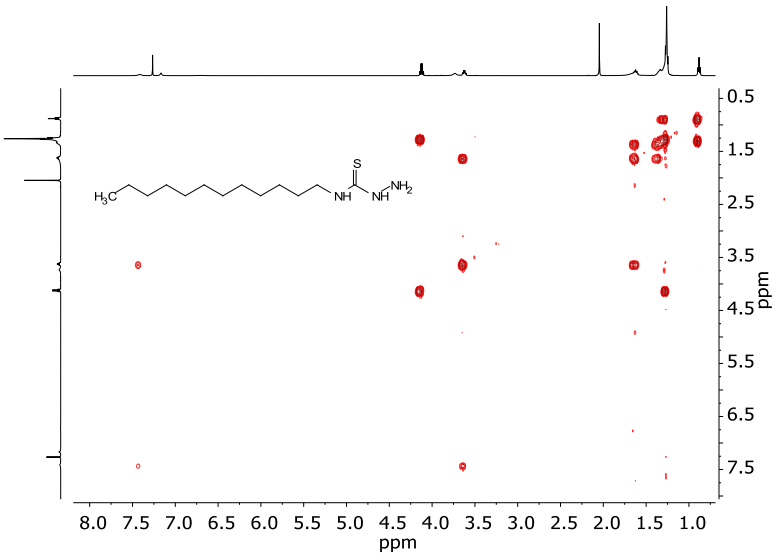


Figure 658. $^{1}H,^{1}H$ COSY NMR spectrum of 4-dodecylthiosemicarbazide in DMSO-d_6 at 499 MHz.

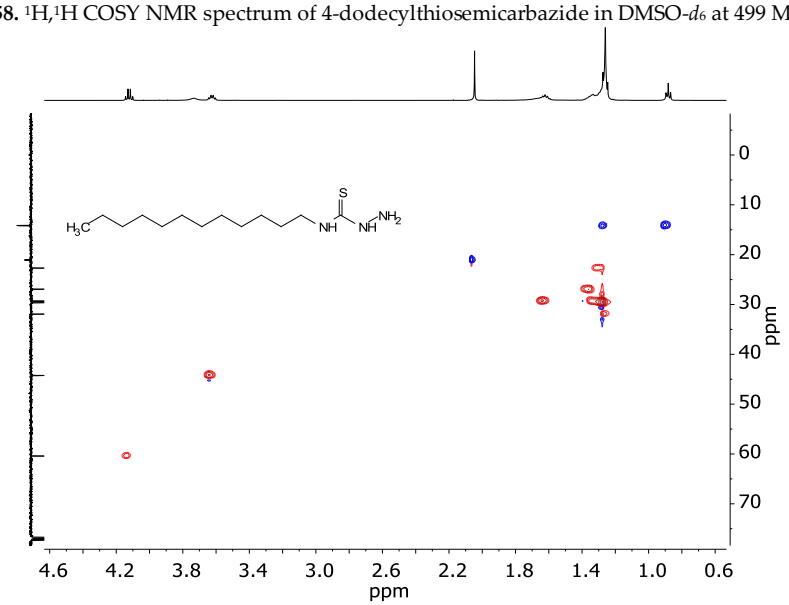


Figure 659. $^{1}H,^{13}C$ HMQC/HSQC NMR spectrum of 4-dodecylthiosemicarbazide in DMSO-d_6 at 499 MHz.

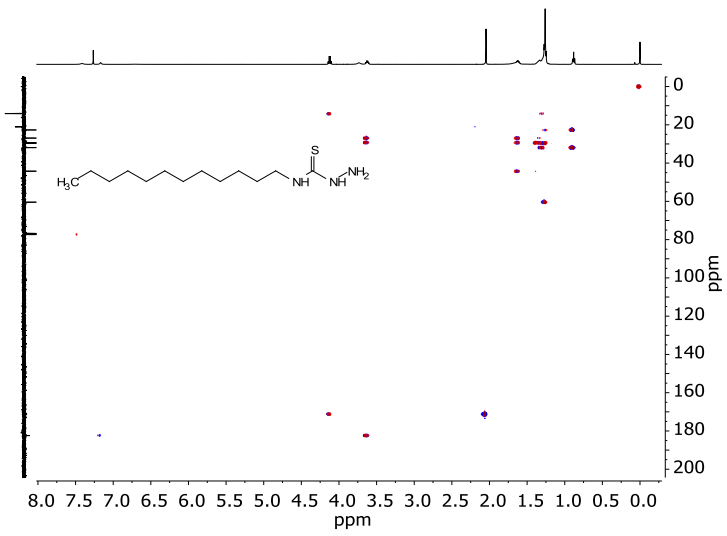


Figure 660. $^{1}H,^{13}C$ HMBC NMR spectrum of 4-dodecylthiosemicarbazide in DMSO-d_6 at 499 MHz.

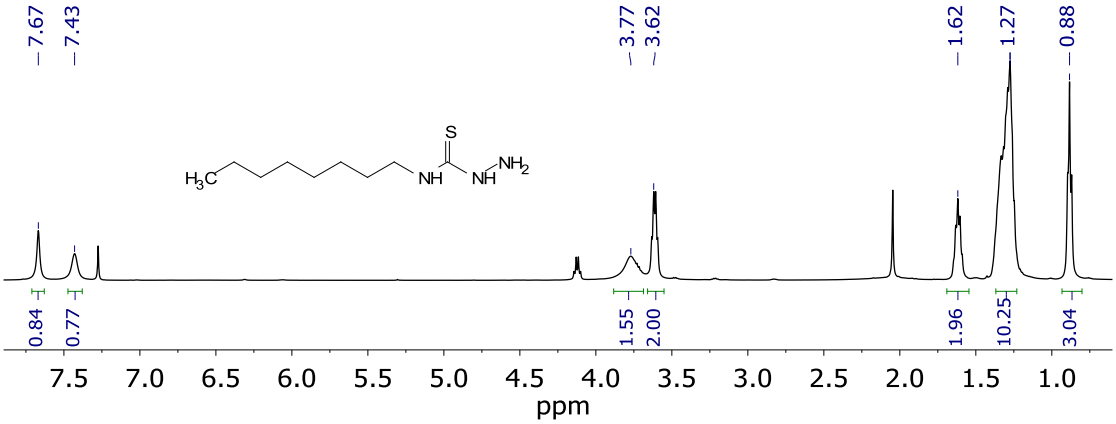


Figure 661. [1]H NMR spectrum of 4-octylthiosemicarbazide in DMSO-*d*6 at 300 MHz.

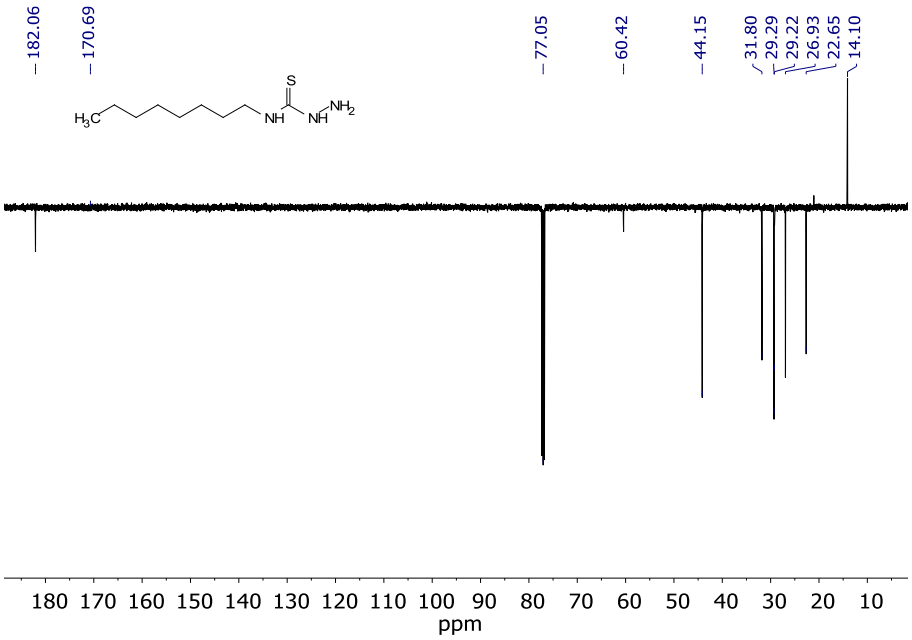


Figure 662. [13]C APT NMR spectrum of 4-octylthiosemicarbazide in DMSO-*d*6 at 499 MHz.

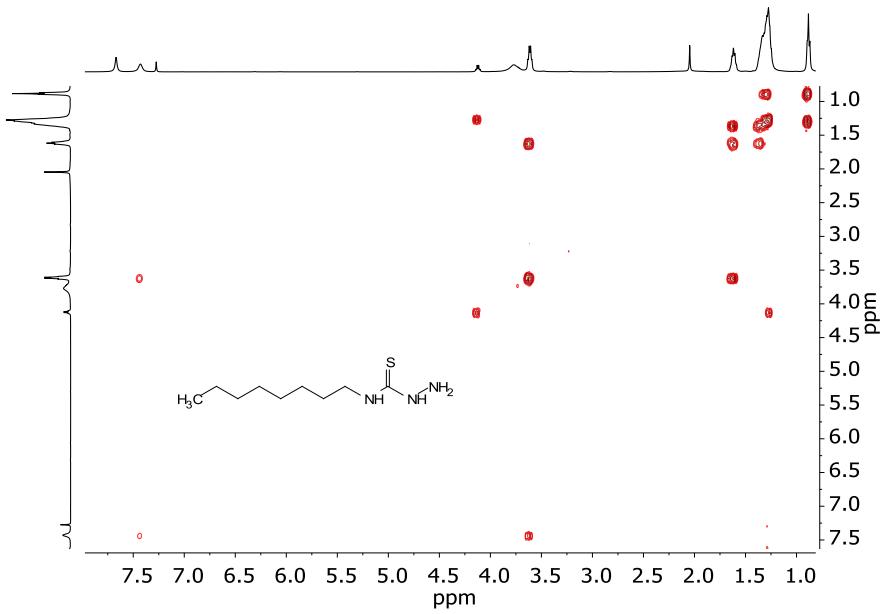


Figure 663. [1]H,[1]H COSY NMR spectrum of 4-octylthiosemicarbazide in DMSO-*d*6 at 499 MHz.

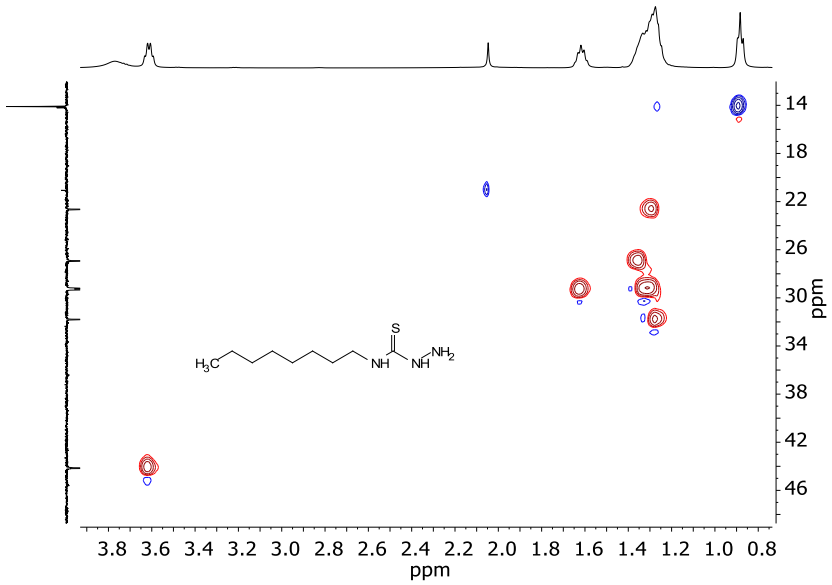


Figure 664. $^{1}H,^{13}C$ HMQC/HSQC NMR spectrum of 4-octylthiosemicarbazide in DMSO-d_6 at 499 MHz.

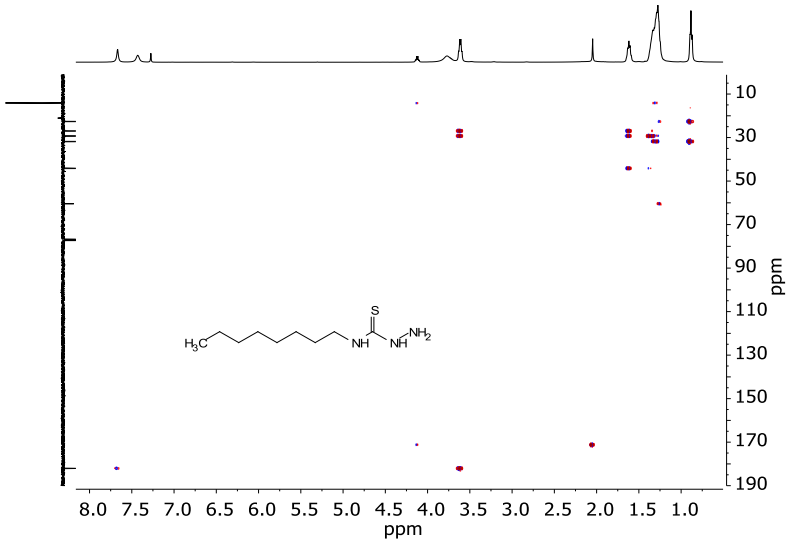


Figure 665. $^{1}H,^{13}C$ HMBC NMR spectrum of 4-octylthiosemicarbazide in DMSO-d_6 at 499 MHz.

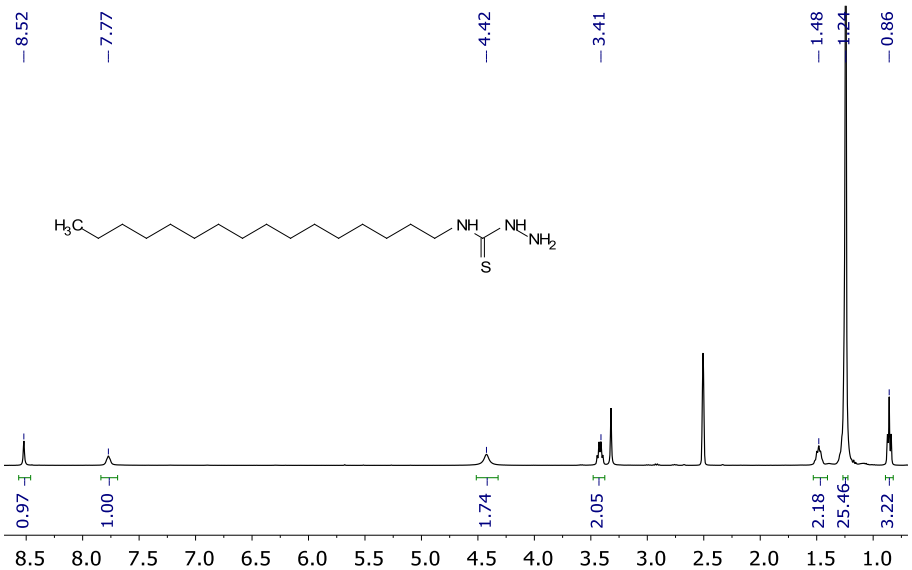


Figure 666. ^{1}H NMR spectrum of 4-hexadecylthiosemicarbazide in DMSO-d_6 at 300 MHz.

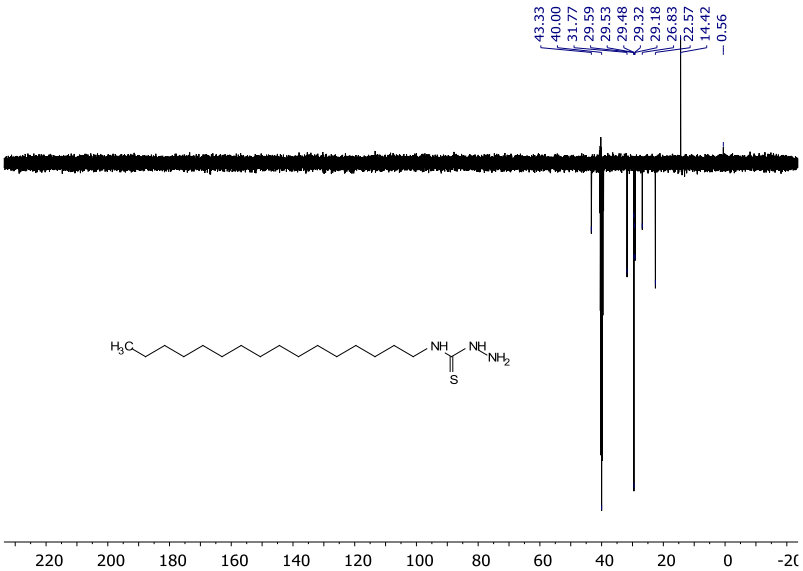


Figure 667. ^{13}C APT NMR spectrum of 4-hexadecylthiosemicarbazide in DMSO-d_6 at 499 MHz.

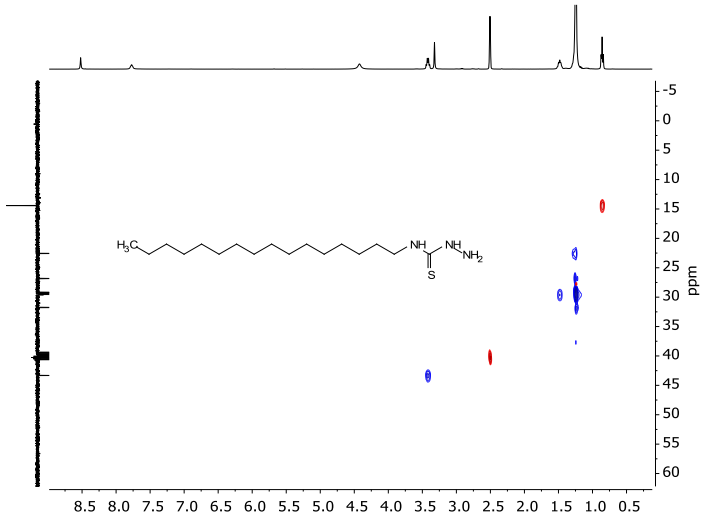


Figure 668. ^{1}H,^{13}C HMQC/HSQC NMR spectrum of 4-hexadecylthiosemicarbazide in DMSO-d_6 at 499 MHz.

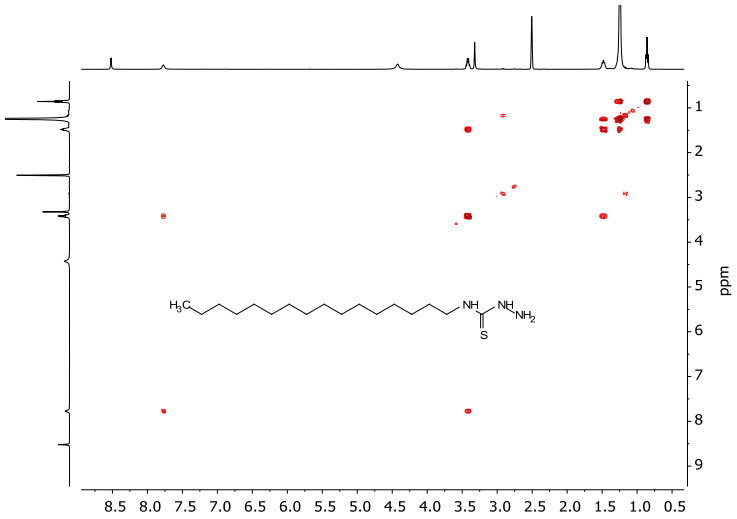


Figure 669. ^{1}H,^{1}H COSY NMR spectrum of 4-hexadecylthiosemicarbazide in DMSO-d_6 at 499 MHz.

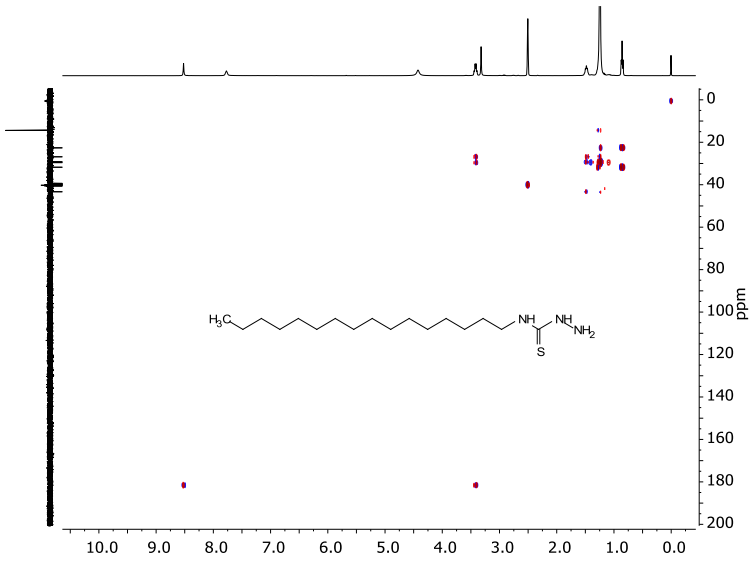


Figure 670. $^{1}H,^{13}C$ HMBC NMR spectrum of 4-hexadecylthiosemicarbazide in DMSO-d_6 at 499 MHz.

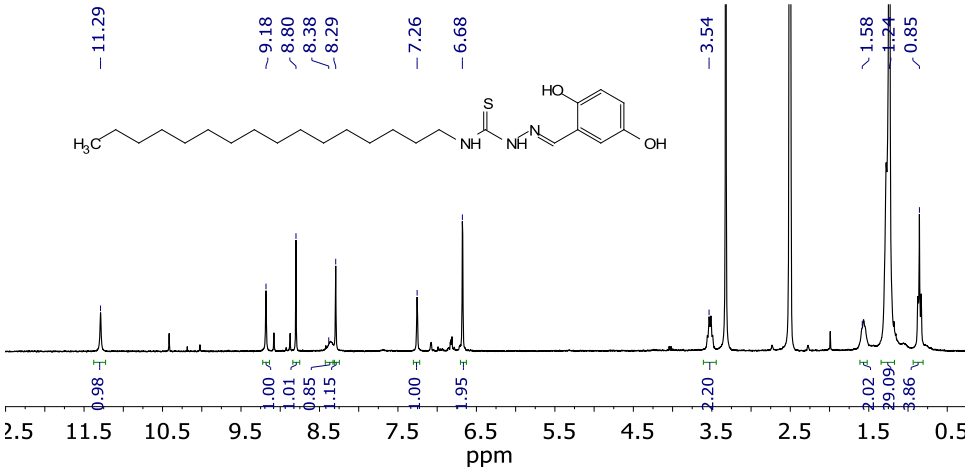


Figure 671. ^{1}H NMR spectrum of 2-[(*E*)-(4-hexadecylthiosemicarbazidoidene)methyl]hydroquinone in DMSO-d_6 at 300 MHz.

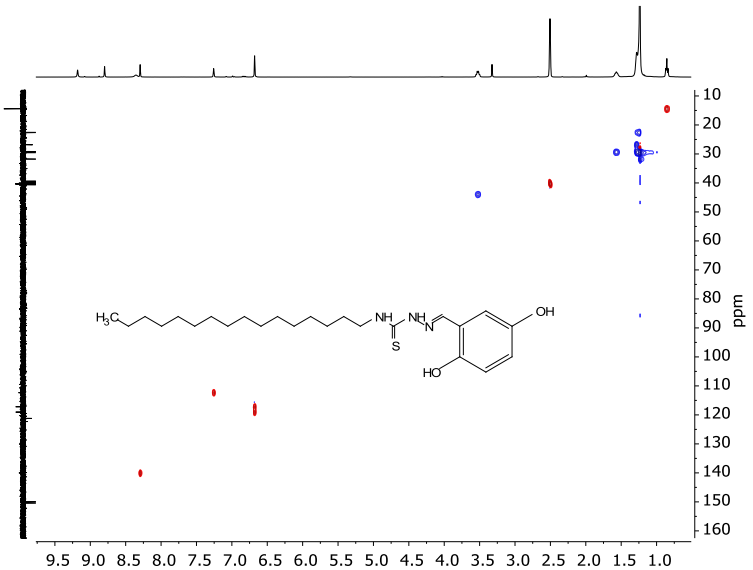


Figure 672. $^{1}H,^{13}C$ HMQC/HSQC NMR spectrum of 2-[(*E*)-(4-hexadecylthiosemicarbazidoidene)methyl] hydroquinone in DMSO-d_6 at 499 MHz.

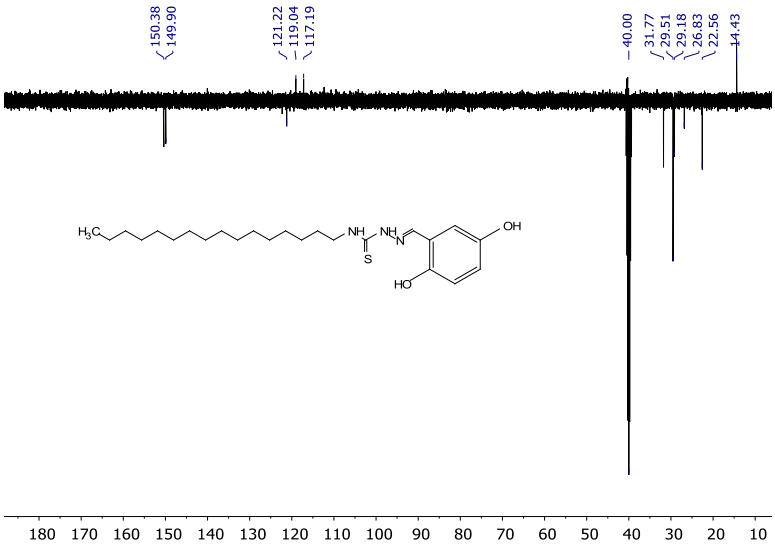


Figure 673. ^{13}C APT NMR spectrum of 2-[(*E*)-(4-hexadecylthiosemicarbazidoidene)methyl] hydroquinone in DMSO-d_6 at 499 MHz.

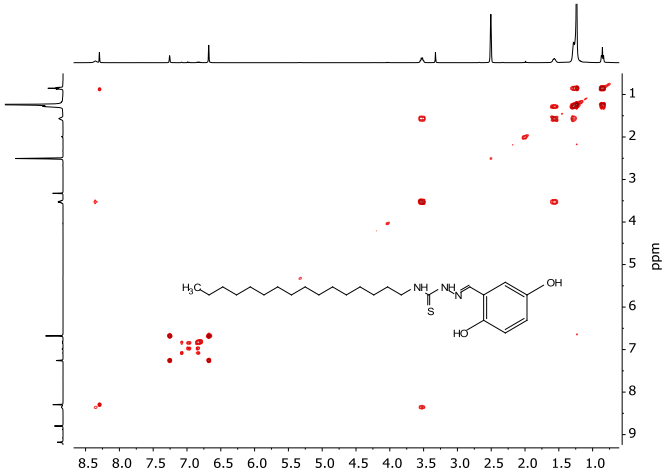


Figure 674. ^{1}H,^{1}H COSY NMR spectrum of 2-[(*E*)-(4-hexadecylthiosemicarbazidoidene)methyl] hydroquinone in DMSO-d_6 at 499 MHz.

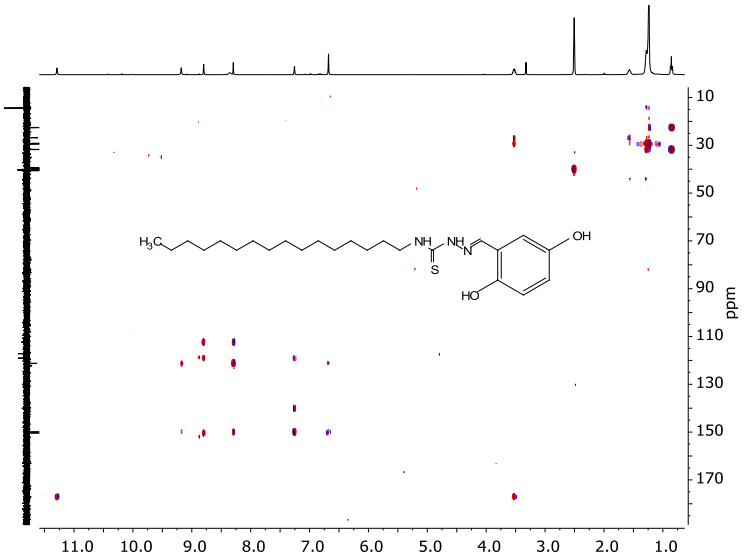


Figure 675. ^{1}H,^{13}C HMBC NMR spectrum of 2-[(*E*)-(4-hexadecylthiosemicarbazidoidene)methyl] hydroquinone in DMSO-d_6 at 499 MHz.

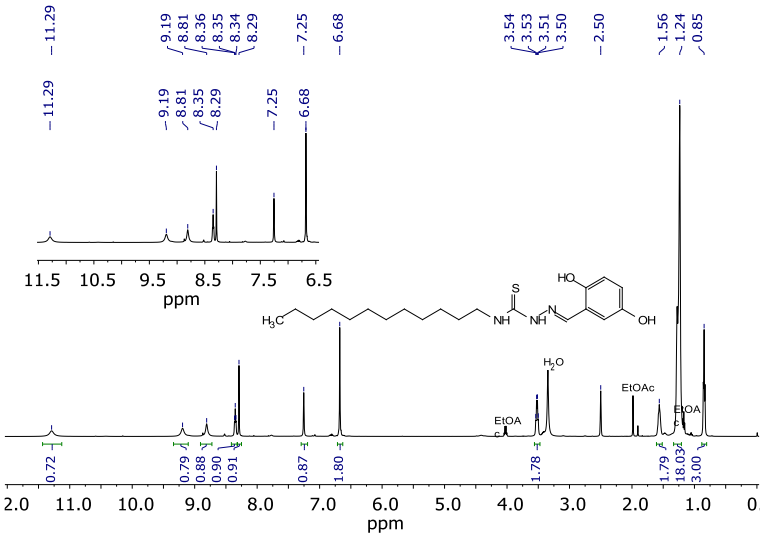


Figure 676. ^{1}H NMR spectrum of 2-[(*E*)-(4-dodecylthiosemicarbazidoidene)methyl]hydroquinone in DMSO-*d*$_6$ at 300 MHz.

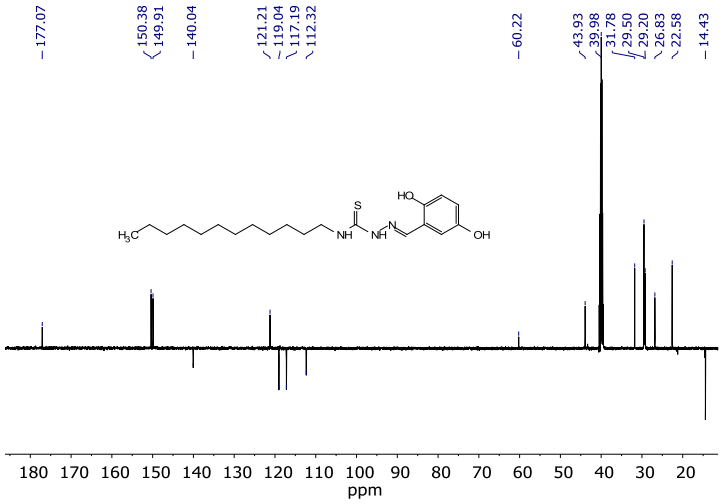


Figure 677. ^{13}C APT NMR spectrum of 2-[(*E*)-(4-dodecylthiosemicarbazidoidene)methyl]hydroquinone in DMSO-*d*$_6$ at 499 MHz.

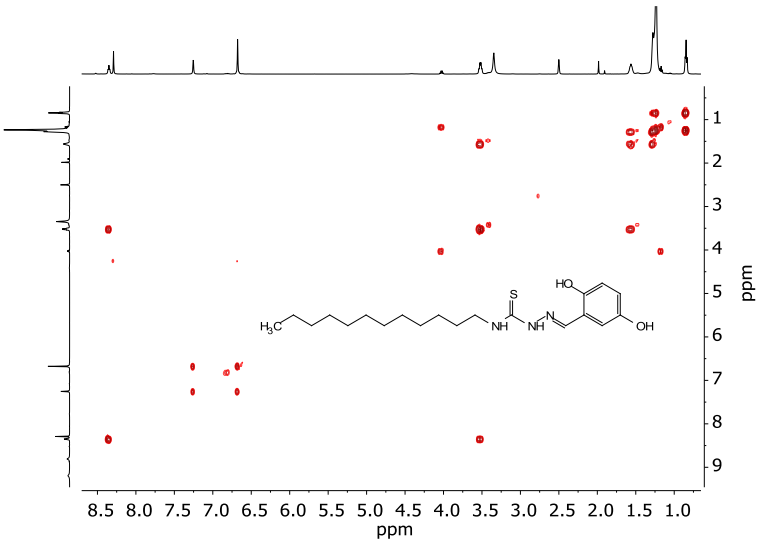


Figure 678. ^{1}H,^{1}H COSY NMR spectrum of 2-[(*E*)-(4-dodecylthiosemicarbazidoidene)methyl]hydroquinone in DMSO-*d*$_6$ at 499 MHz.

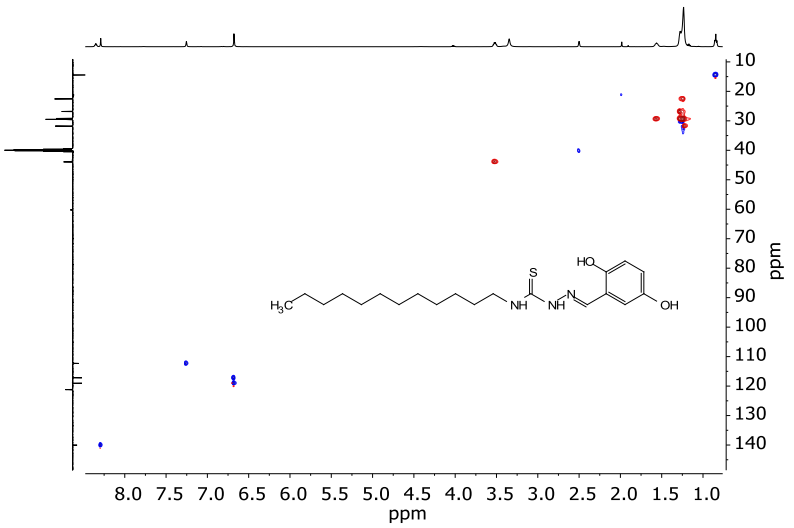


Figure 679. $^{1}H,^{13}C$ HMQC/HSQC NMR spectrum of 2-[(*E*)-(4-dodecylthiosemicarbazidoidene) methyl]hydroquinone in DMSO-d_6 at 499 MHz.

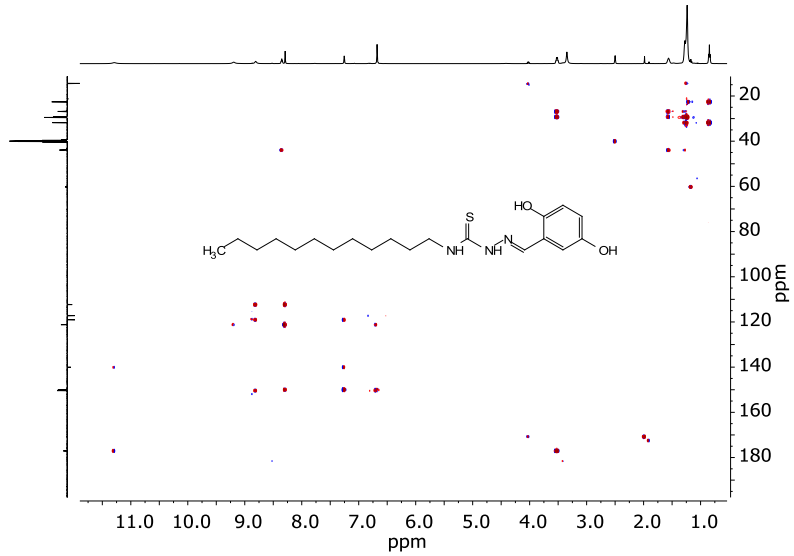


Figure 680. $^{1}H,^{13}C$ HMBC NMR spectrum of 2-[(*E*)-(4-dodecylthiosemicarbazidoidene)methyl]hydroquinone in DMSO-d_6 at 499 MHz.

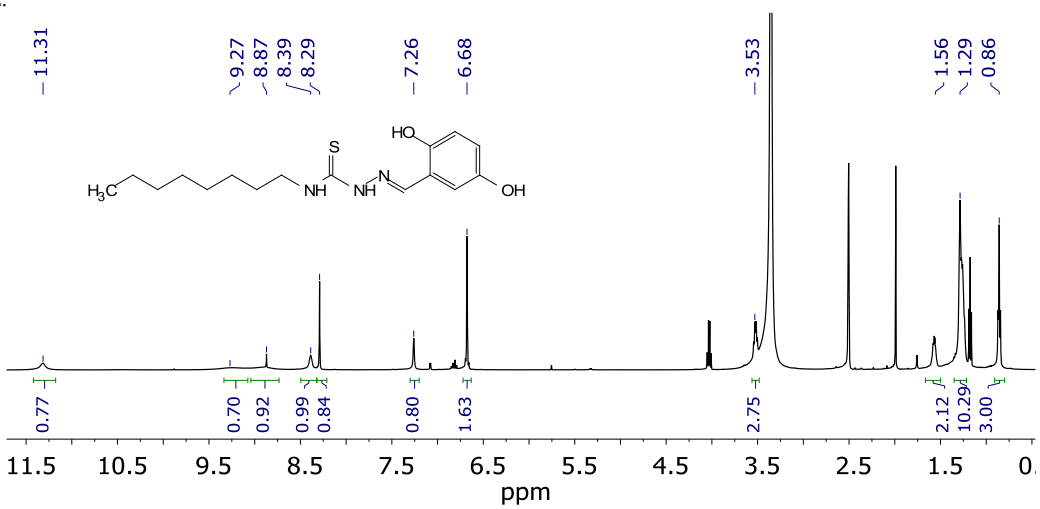


Figure 681. ^{1}H NMR spectrum of 2-[(*E*)-(4-octylthiosemicarbazidoidene)methyl]hydroquinone in DMSO-d_6 at 300 MHz.

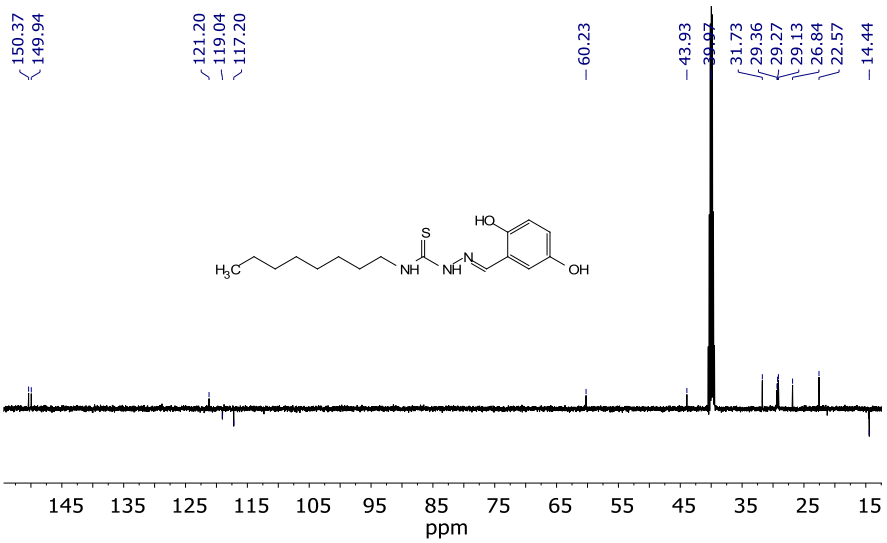


Figure 682. ^{13}C APT NMR spectrum of 2-[(*E*)-(4-octylthiosemicarbazidoidene)methyl]hydroquinone in DMSO-d_6 at 499 MHz.

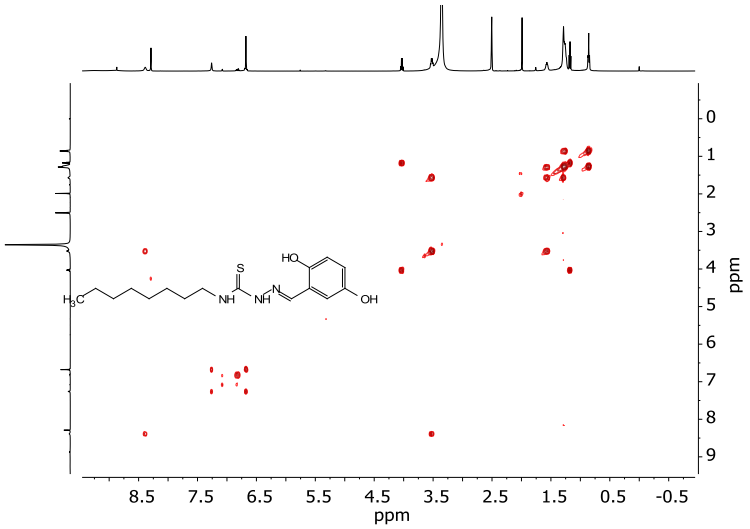


Figure 683. ^{1}H,^{1}H COSY NMR spectrum of 2-[(*E*)-(4-octylthiosemicarbazidoidene)methyl]hydroquinone in DMSO-d_6 at 499 MHz.

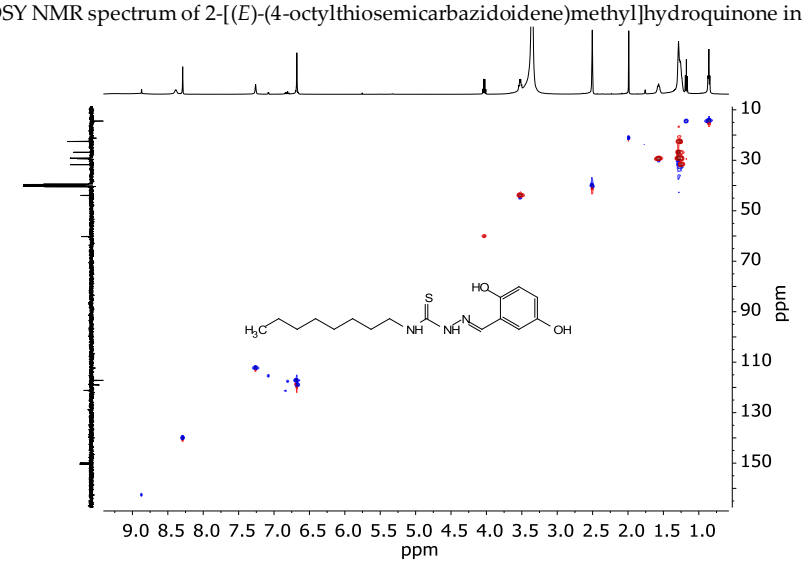


Figure 684. ^{1}H,^{13}C HMQC/HSQC NMR spectrum of 2-[(*E*)-(4-octylthiosemicarbazidoidene)methyl]hydroquinone in DMSO-d_6 at 499 MHz.

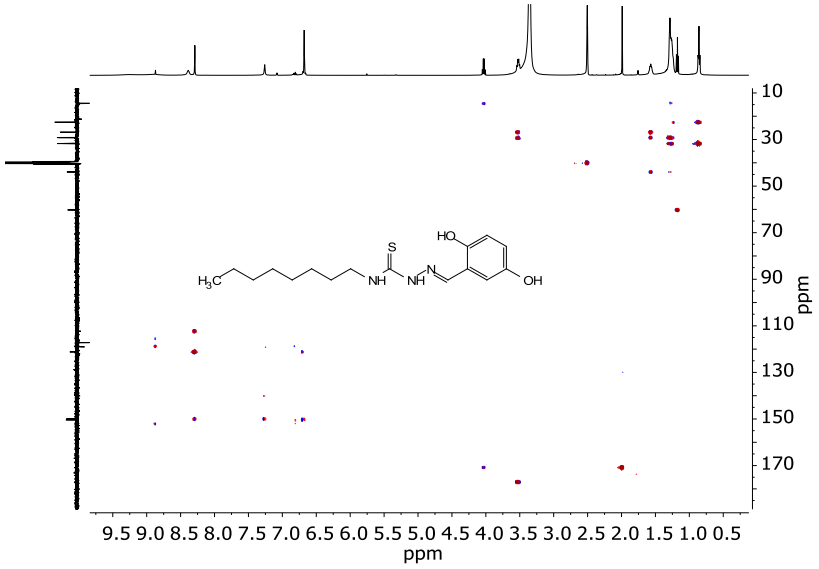


Figure 685. $^{1}H,^{13}C$ HMBC NMR spectrum of 2-[(*E*)-(4-octylthiosemicarbazidoidene)methyl]hydroquinone in DMSO-d_6 at 499 MHz.

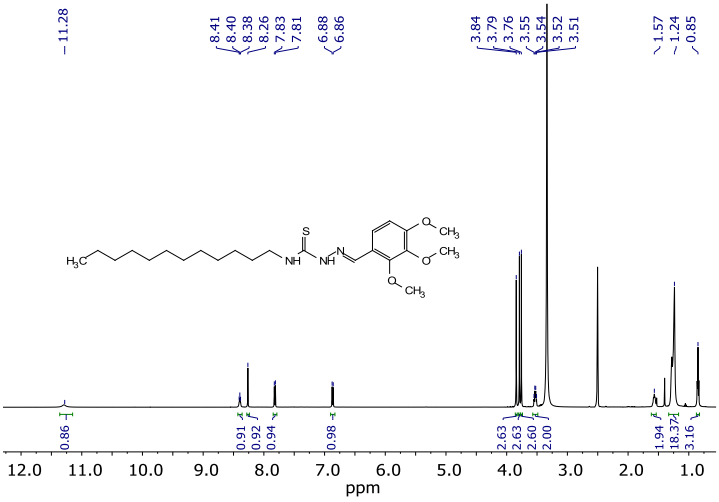


Figure 686. ^{1}H NMR spectrum of (*E*)-4-dodecyl-1-[(2,3,4-trimethoxyphenyl)methylene]thiosemicarbazide in DMSO-d_6 at 300 MHz.

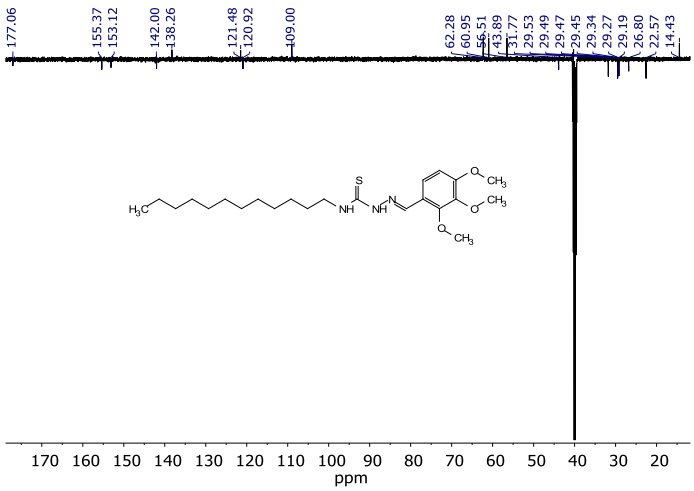


Figure 687. ^{13}C APT NMR spectrum of (*E*)-4-dodecyl-1-[(2,3,4-trimethoxyphenyl)methylene]thiosemicarbazide in DMSO-d_6 at 499 MHz.

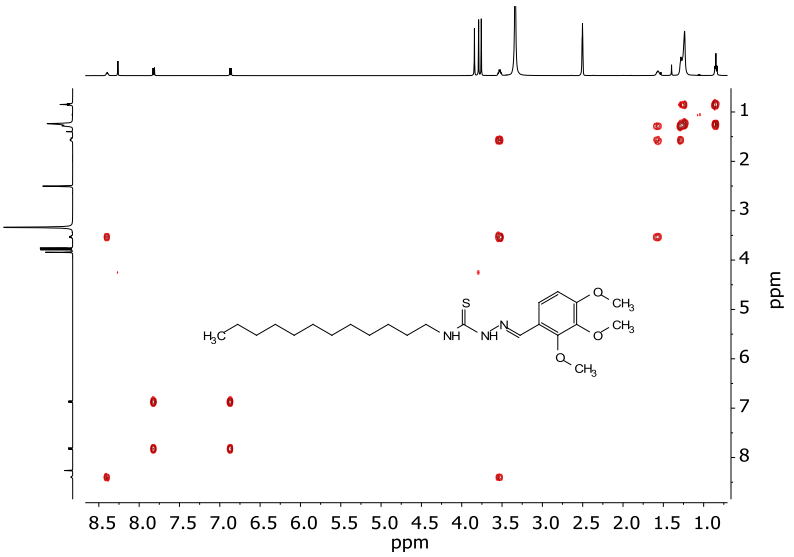


Figure 688. $^{1}H,^{1}H$ COSY NMR spectrum of (*E*)-4-dodecyl-1-[(2,3,4-trimethoxyphenyl)methylene]thiosemicarbazide in DMSO-d_6 at 499 MHz.

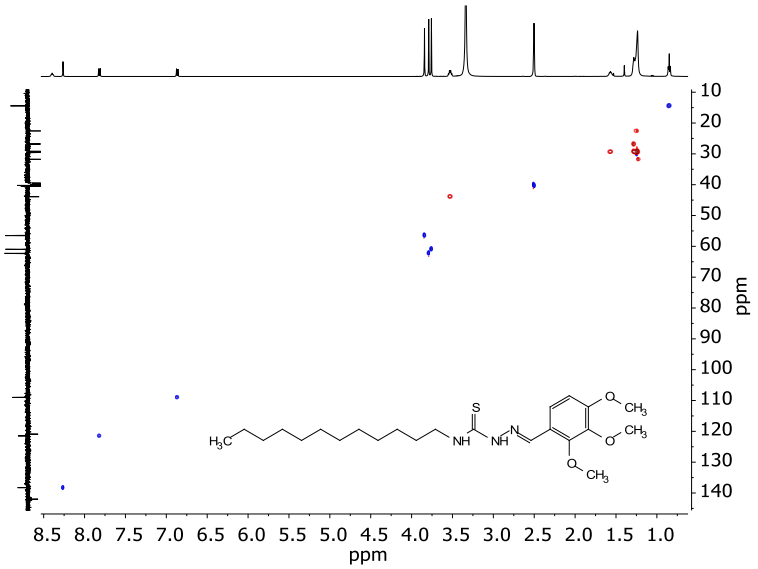


Figure 689. $^{1}H,^{13}C$ HMQC/HSQC NMR spectrum of (*E*)-4-dodecyl-1-[(2,3,4-trimethoxyphenyl)methylene] thiosemicarbazide in DMSO-d_6 at 499 MHz.

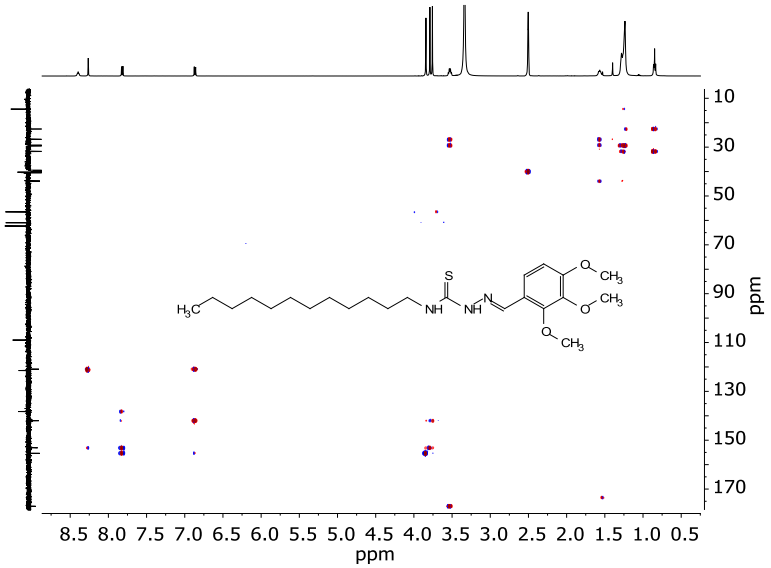


Figure 690. $^{1}H,^{13}C$ HMBC NMR spectrum of (*E*)-4-dodecyl-1-[(2,3,4-trimethoxyphenyl)methylene] thiosemicarbazide in DMSO-d_6 at 499 MHz.

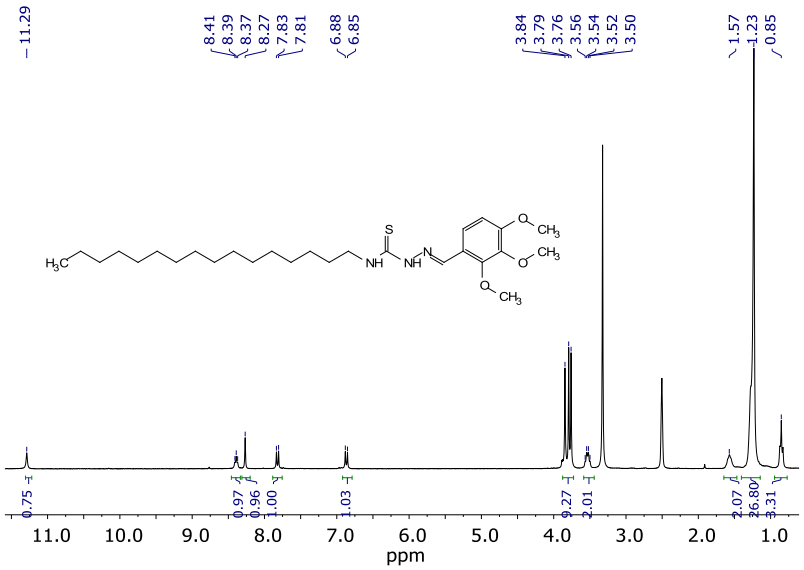


Figure 691. ^{1}H NMR spectrum of (*E*)-4-hexadecyl-1-[(2,3,4-trimethoxyphenyl)methylene]thiosemicarbazide in DMSO-*d*$_6$ at 300 MHz.

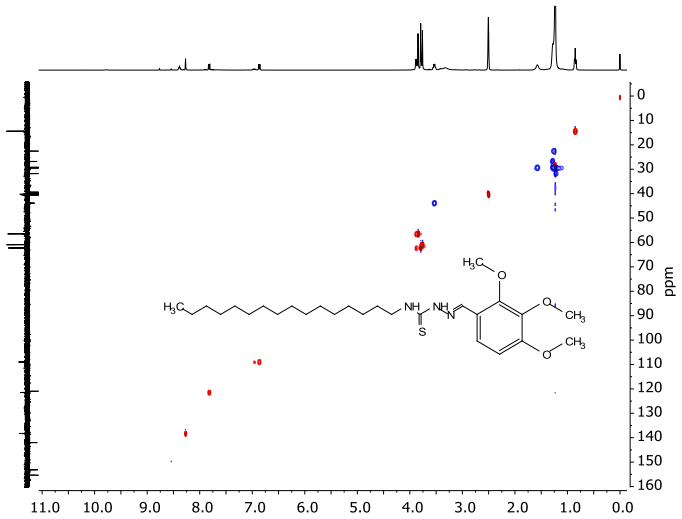


Figure 692. ^{1}H,^{13}C HMQC/HSQC NMR spectrum of (*E*)-4-hexadecyl-1-[(2,3,4-trimethoxyphenyl)methylene] thiosemicarbazide in DMSO-*d*$_6$ at 499 MHz.

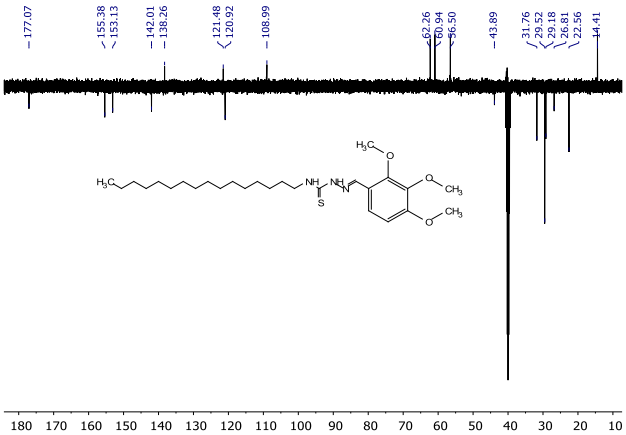


Figure 693. ^{13}C APT NMR spectrum of (*E*)-4-hexadecyl-1-[(2,3,4-trimethoxyphenyl)methylene]thiosemicarbazide in DMSO-*d*$_6$ at 499 MHz.

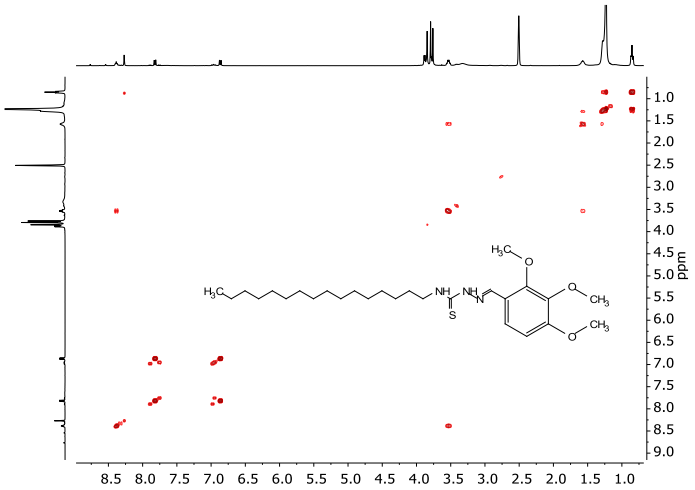


Figure 694. $^{1}H,^{1}H$ COSY NMR spectrum of (*E*)-4-hexadecyl-1-[(2,3,4-trimethoxyphenyl)methylene] thiosemicarbazide in DMSO-d_6 at 499 MHz.

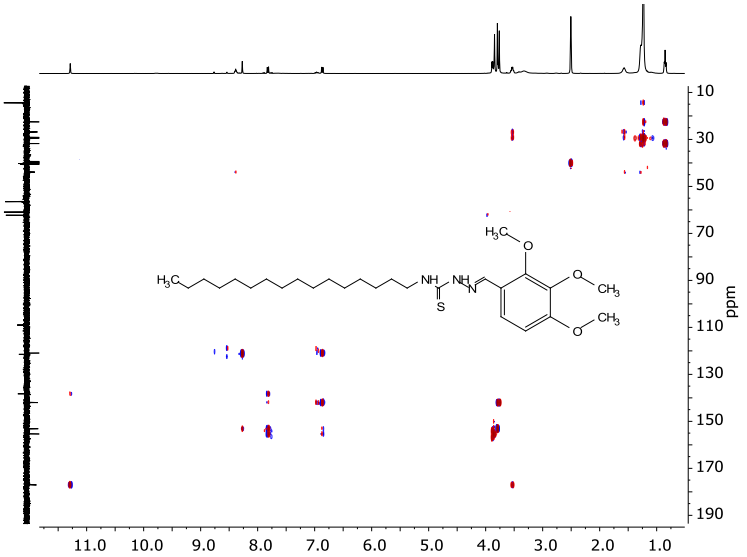


Figure 695. $^{1}H,^{13}C$ HMBC NMR spectrum of (*E*)-4-hexadecyl-1-[(2,3,4-trimethoxyphenyl)methylene] thiosemicarbazide in DMSO-d_6 at 499 MHz.

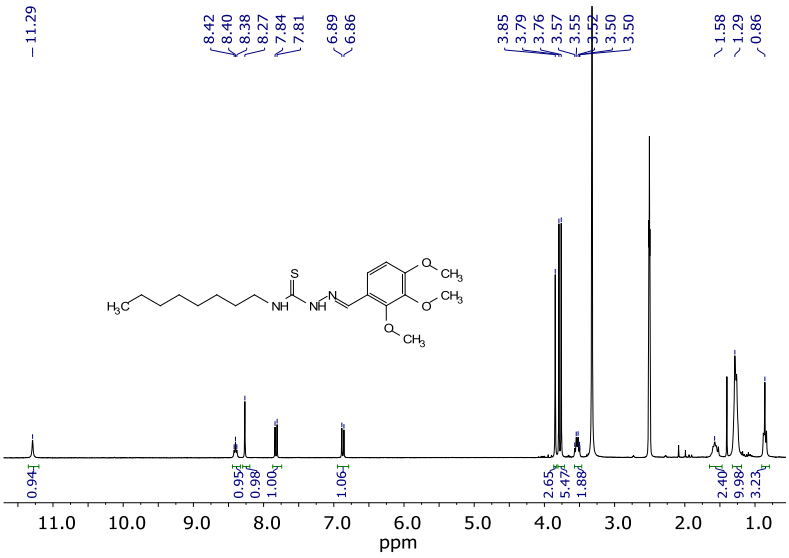


Figure 696. ^{1}H NMR spectrum of (*E*)-4-octyl-1-[(2,3,4-trimethoxyphenyl)methylene]thiosemicarbazide in DMSO-d_6 at 300 MHz.

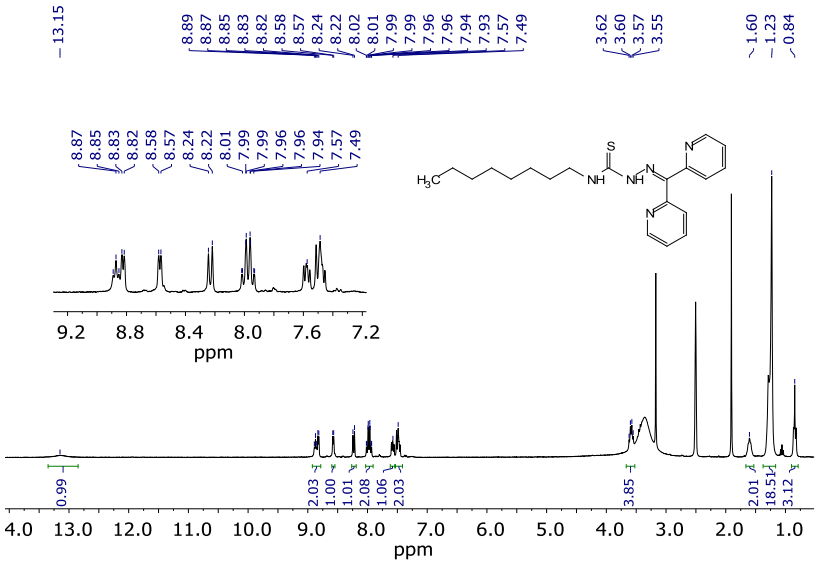


Figure 697. [1]H NMR spectrum of 1-[bis(2-pyridyl)methylene]-4-octylthiosemicarbazide in DMSO-d_6 at 300 MHz.

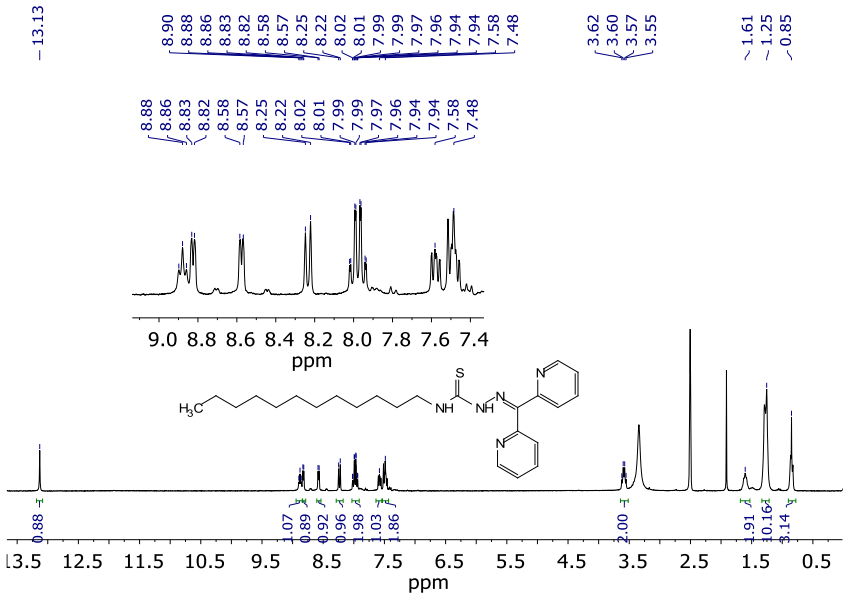


Figure 698. [1]H NMR spectrum of 1-[bis(2-pyridyl)methylene]-4-dodecylthiosemicarbazide in DMSO-d_6 at 300 MHz.

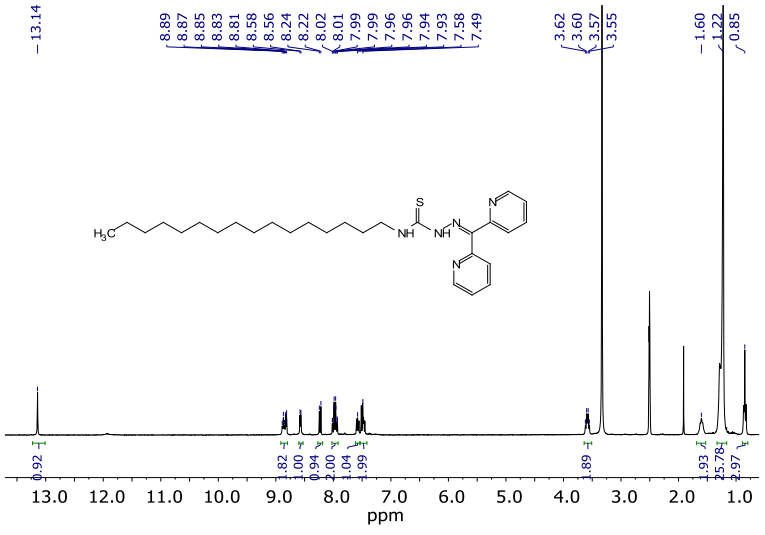


Figure 699. [1]H NMR spectrum of 1-[bis(2-pyridyl)methylene]-4-hexadecylthiosemicarbazide in DMSO-d_6 at 300 MHz.

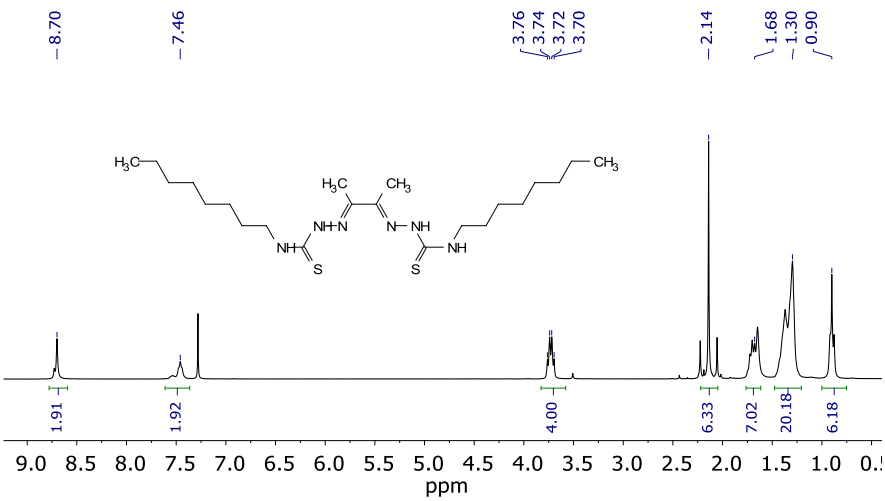


Figure 700. [1]H NMR spectrum of (*E*)-1-[1-methyl-2-(4-octylthiosemicarbazidoidene)propylidene]-4-octyl thiosemicarbazide in DMSO-*d*6 at 300 MHz.

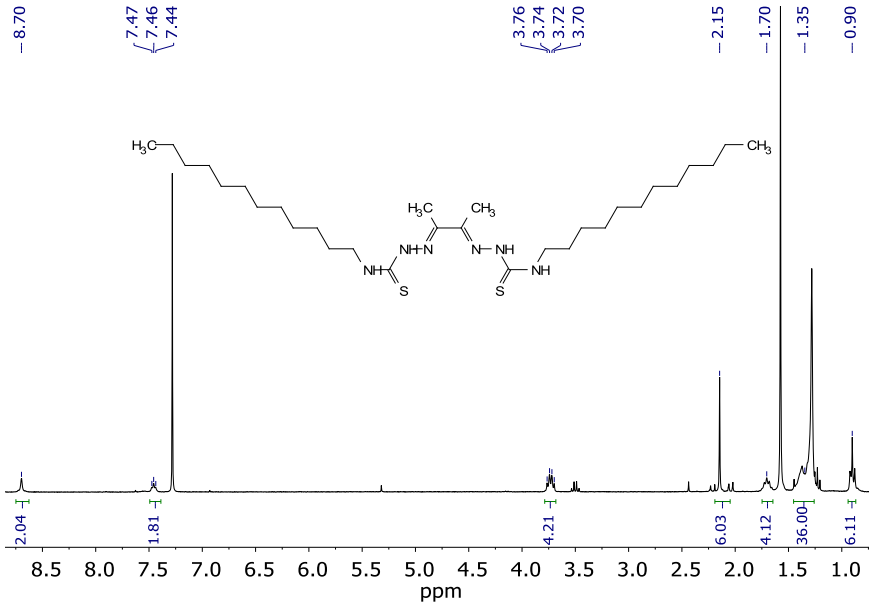


Figure 701. [1]H NMR spectrum of (*E*)-1-[1-methyl-2-(4-dodecylthiosemicarbazidoidene)propylidene]-4-dodecylthiosemicarbazide in DMSO-*d*6 at 300 MHz.

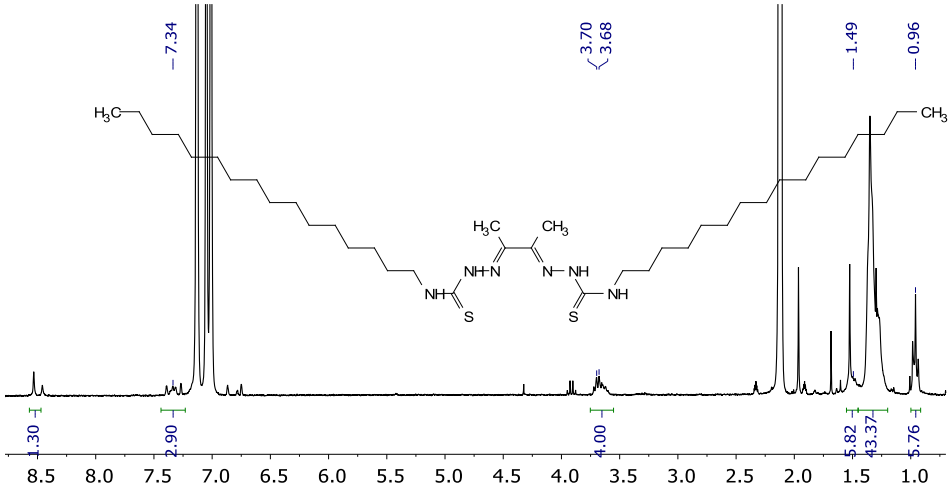


Figure 702. [1]H NMR spectrum of (*E*)-1-[1-methyl-2-(4-hexadecylthiosemicarbazidoidene)propylidene]-4-hexadecyl-thiosemicarbazide in DMSO-*d*6 at 300 MHz.

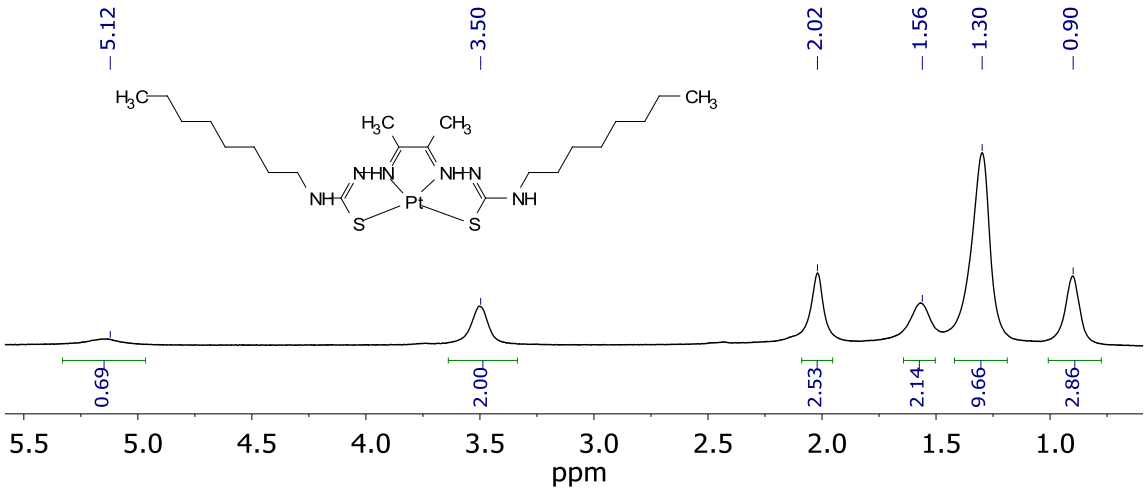


Figure 703. [1]H NMR spectrum of [Pt(dime(bis-TSC)oct)] in DMSO-d_6 at 300 MHz.

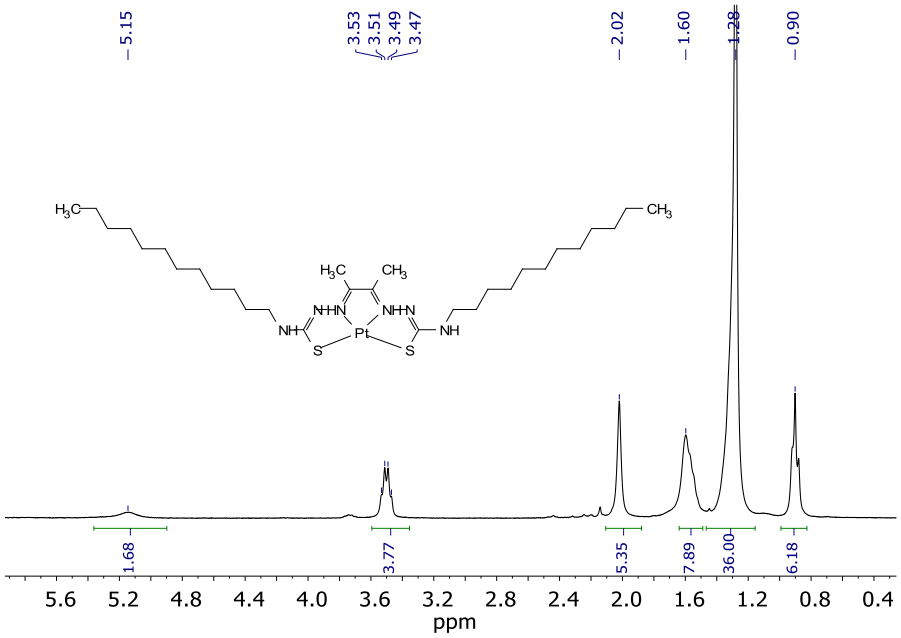


Figure 704. [1]H NMR spectrum of [Pt(dime(bis-TSC)dode)] in DMSO-d_6 at 300 MHz.

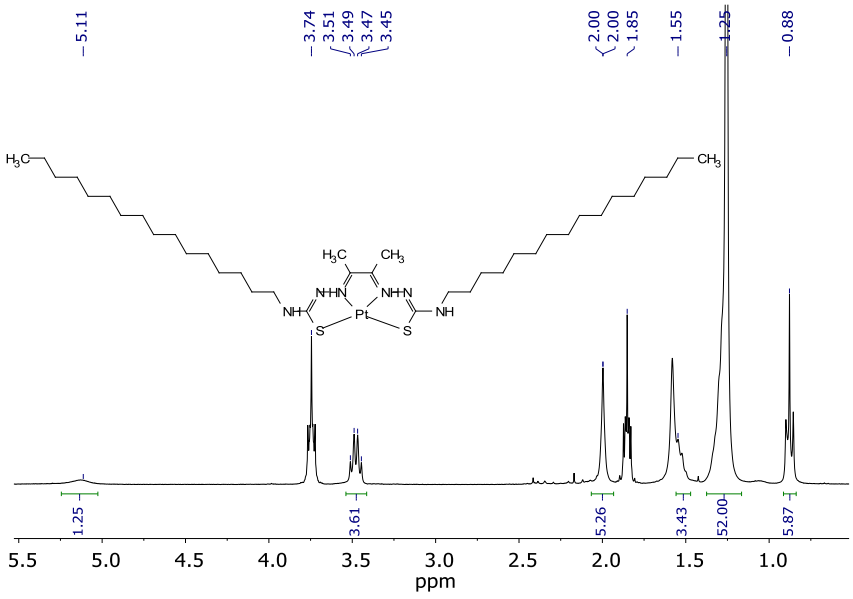


Figure 705. [1]H NMR spectrum of [Pt(dime(bis-TSC)hexde)] in DMSO-d_6 at 300 MHz.

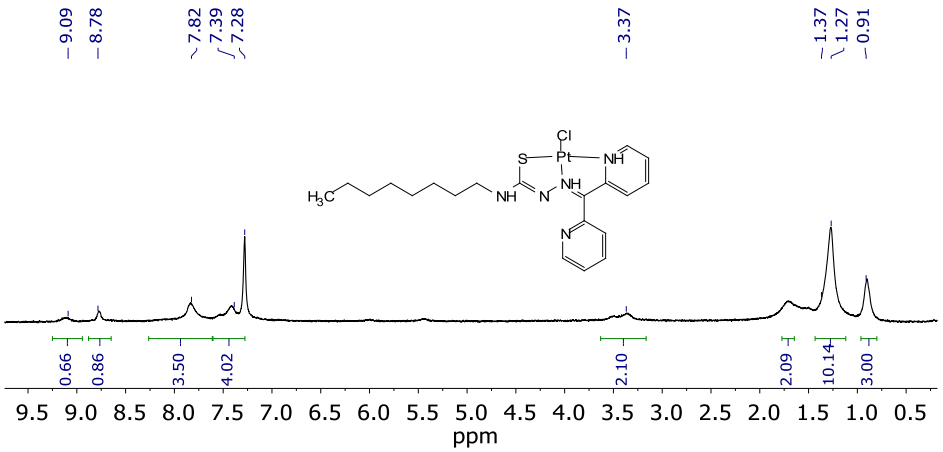


Figure 706. [1]H NMR spectrum of [Pt(dipy(TSC)oct)Cl] in DMSO-*d*$_6$ at 300 MHz.

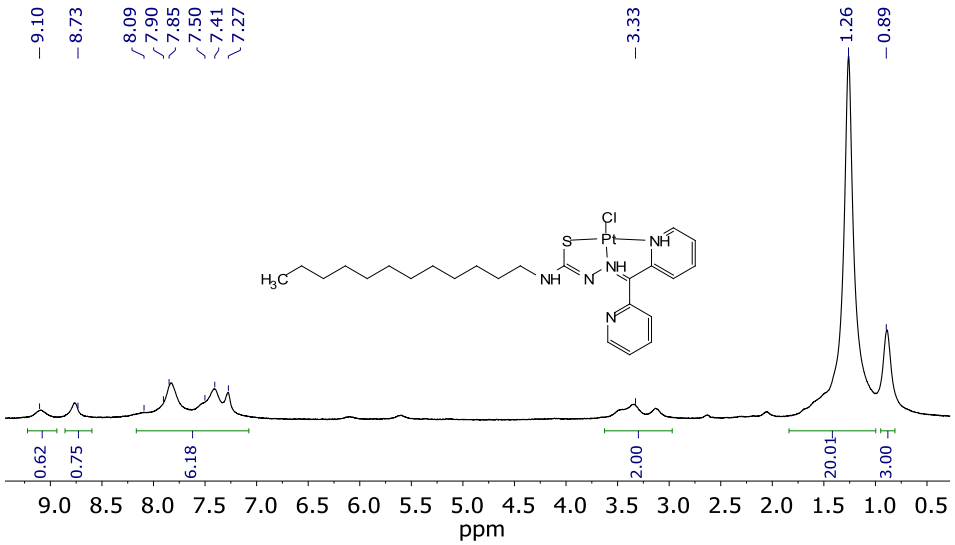


Figure 707. [1]H NMR spectrum of [Pt(dipy(TSC)dode)Cl] in DMSO-*d*$_6$ at 300 MHz.

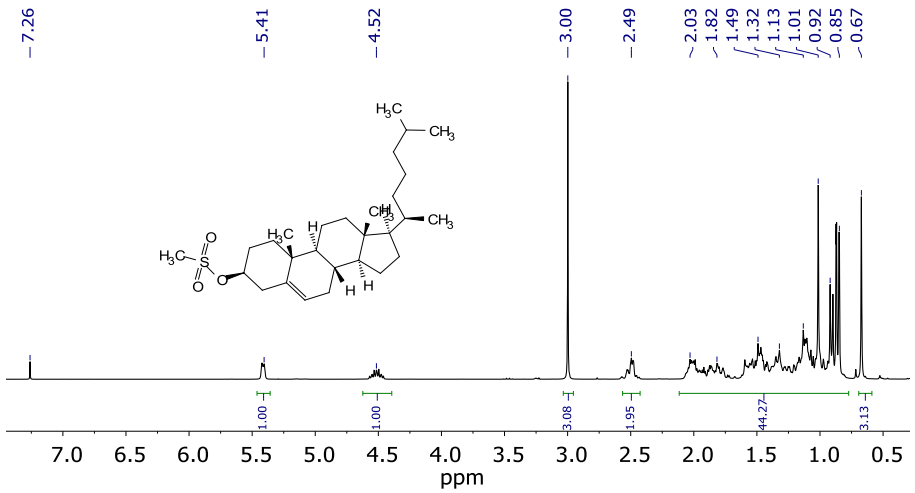


Figure 708. [1]H NMR spectrum of (1*S*,2*R*,5*S*,10*S*,11*S*,14*R*,15*R*)-14-[(1*R*)-1,5-dimethylhexyl]-5-(methanesulfonyloxy)-2,15-dimethyltetracyclo[8.7.0.0^{2,7}.0^{11,15}]heptadec-7-ene in DMSO-*d*$_6$ at 300 MHz.

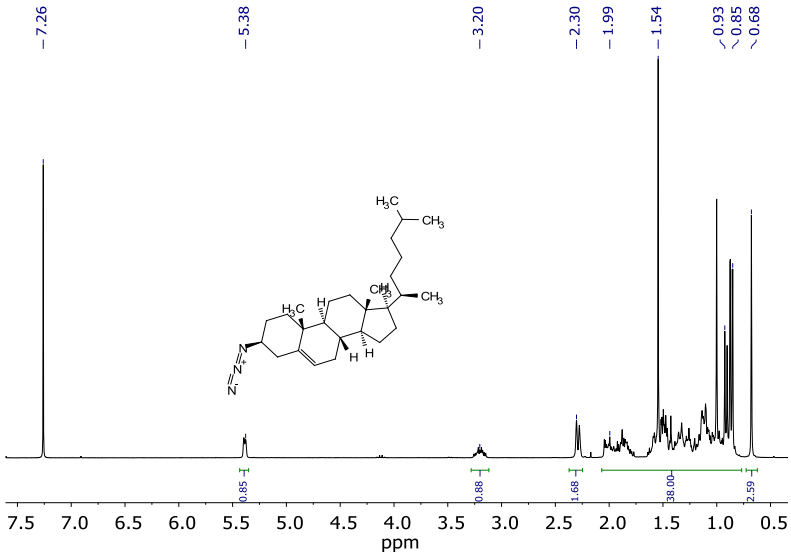


Figure 709. ^{1}H NMR spectrum of (1*S*,2*R*,5*S*,10*S*,11*S*,14*R*,15*R*)-5-azido-14-[(1*R*)-1,5-dimethylhexyl]-2,15-dimethyltetracyclo [8.7.0.0^{2,7}.0^{11,15}]heptadec-7-ene in DMSO-*d*$_6$ at 300 MHz.

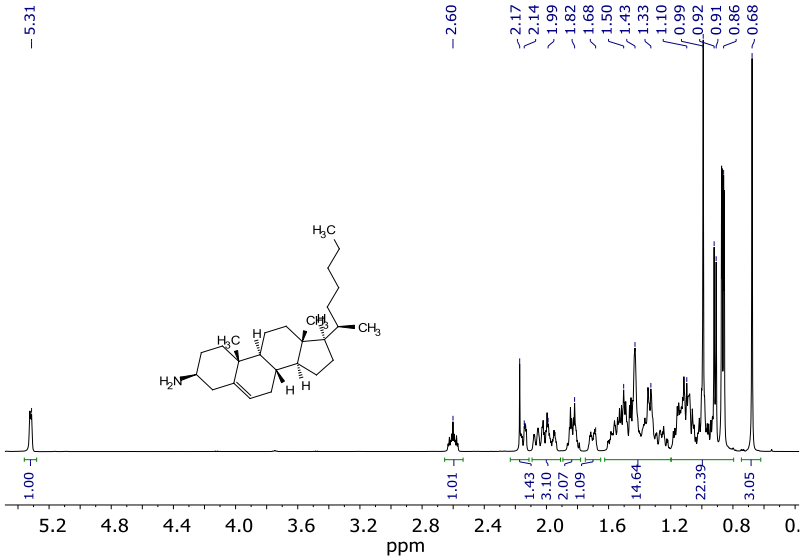


Figure 710. ^{1}H NMR spectrum of (1*S*,2*R*,5*S*,10*S*,11*S*,14*R*,15*R*)-14-[(1*R*)-1,5-dimethylhexyl]-2,15-dimethyltetracyclo [8.7.0.0^{2,7}.0^{11,15}]heptadec-7-en-5-ylamine in DMSO-*d*$_6$ at 300 MHz.

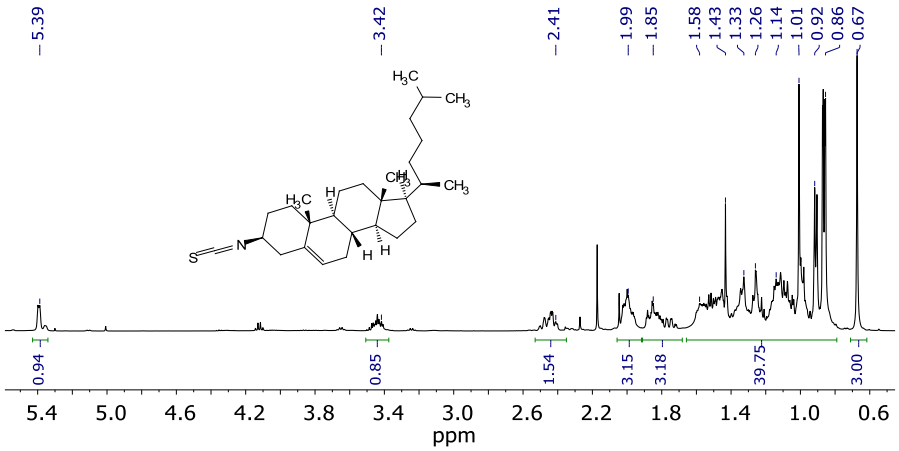


Figure 711. ^{1}H NMR spectrum of (1*S*,2*R*,5*S*,10*S*,11*S*,14*R*,15*R*)-14-[(1*R*)-1,5-dimethylhexyl]-5-isothiocyanato-2,15-dimethyl tetracyclo[8.7.0.0^{2,7}.0^{11,15}]heptadec-7-ene in DMSO-*d*$_6$ at 300 MHz.

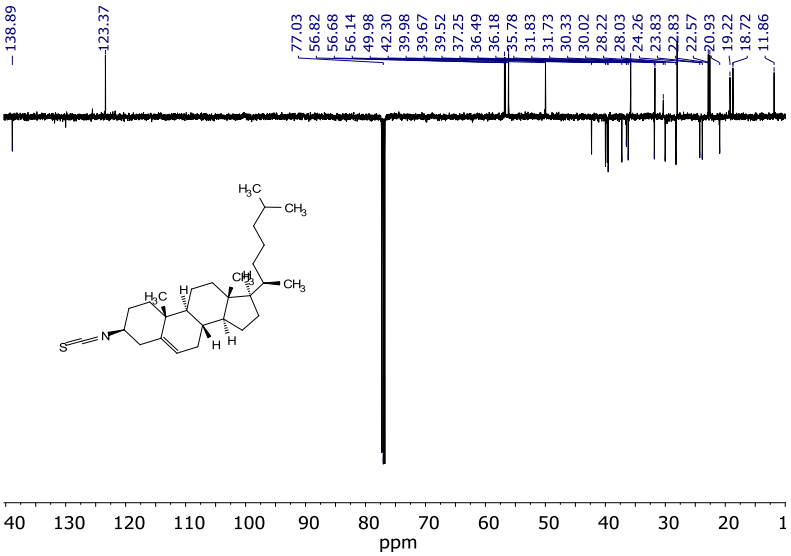


Figure 712. ^{13}C APT NMR spectrum of (1*S*,2*R*,5*S*,10*S*,11*S*,14*R*,15*R*)-14-[(1*R*)-1,5-dimethylhexyl]-5-isothiocyanato-2,15-dimethyl tetracyclo[8.7.0.0^{2,7}.0^{11,15}]heptadec-7-ene in DMSO-*d*$_6$ at 499 MHz.

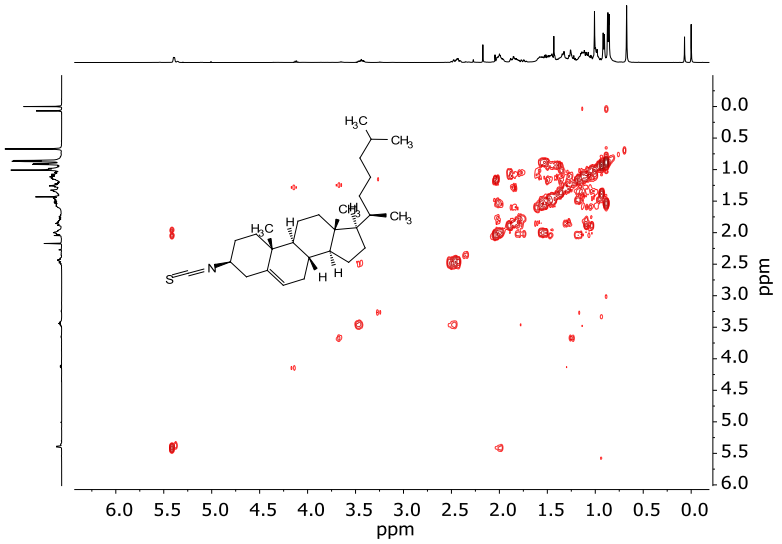


Figure 713. $^{1}H,^{1}H$ COSY NMR spectrum of (1*S*,2*R*,5*S*,10*S*,11*S*,14*R*,15*R*)-14-[(1*R*)-1,5-dimethylhexyl]-5-isothiocyanato-2,15-dimethyl tetracyclo[8.7.0.0^{2,7}.0^{11,15}]heptadec-7-ene in DMSO-*d*$_6$ at 499 MHz.

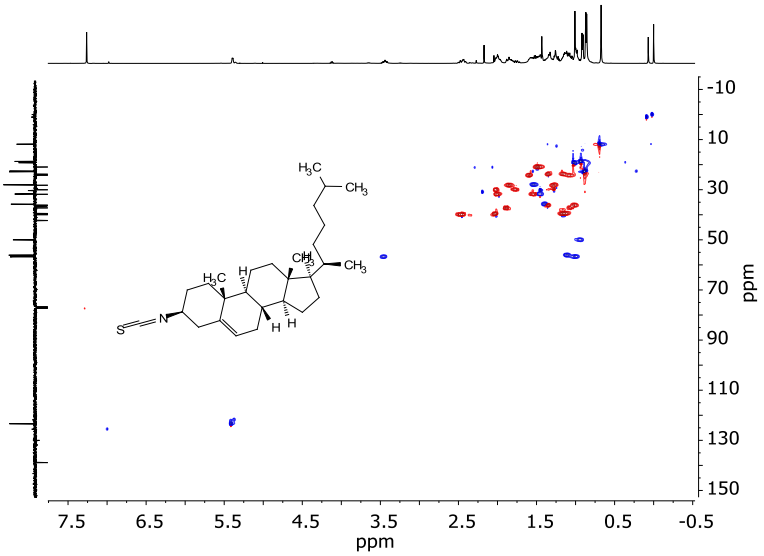


Figure 714. $^{1}H,^{13}C$ HMQC/HSQC NMR spectrum of (1*S*,2*R*,5*S*,10*S*,11*S*,14*R*,15*R*)-14-[(1*R*)-1,5-dimethylhexyl]-5-isothiocyanato-2,15-dimethyl tetracyclo[8.7.0.0^{2,7}.0^{11,15}]heptadec-7-ene in DMSO-*d*$_6$ at 499 MHz.

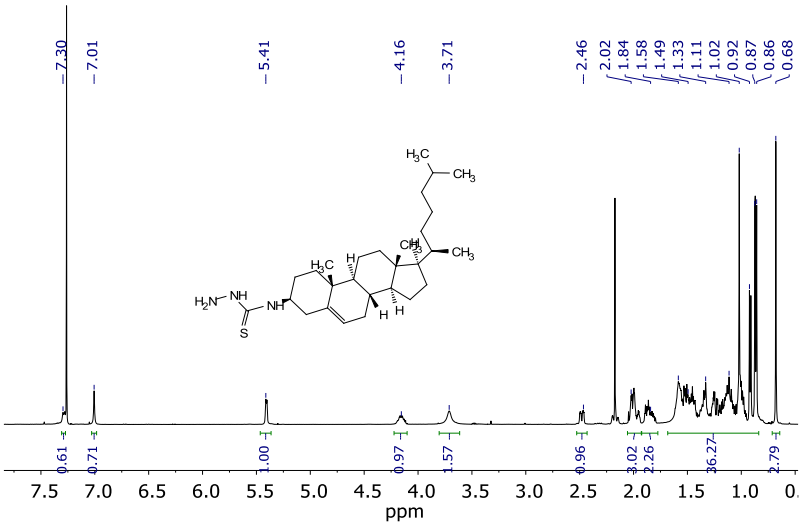


Figure 715. ^{1}H NMR spectrum of *N*-hydrazidecarbothio[(1*S*,2*R*,5*S*,10*S*,11*S*,14*R*,15*R*)-14-[(1*R*)-1,5-dimethylhexyl]-2,15-dimethyltetracyclo[8.7.0.0^{2,7}.0^{11,15}]heptadec-7-en-5-yl]amine in DMSO-*d*$_6$ at 300 MHz.

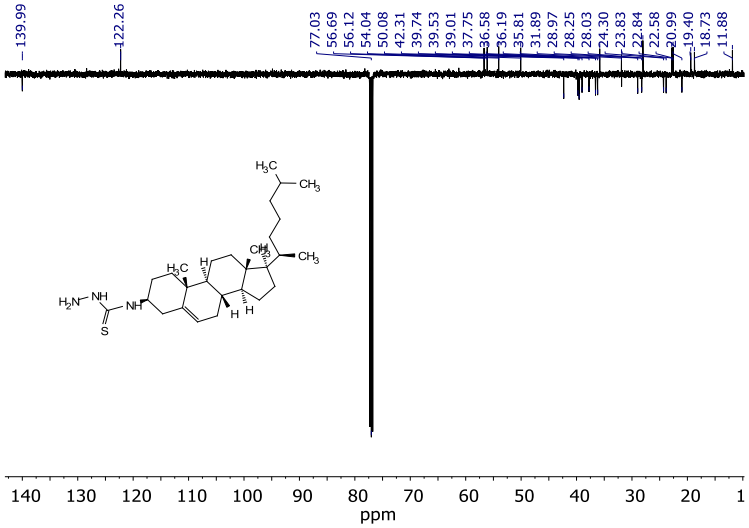


Figure 716. ^{13}C APT NMR spectrum of *N*-hydrazidecarbothio[(1*S*,2*R*,5*S*,10*S*,11*S*,14*R*,15*R*)-14-[(1*R*)-1,5-dimethylhexyl]-2,15-dimethyltetracyclo[8.7.0.0^{2,7}.0^{11,15}]heptadec-7-en-5-yl]amine in DMSO-*d*$_6$ at 499 MHz.

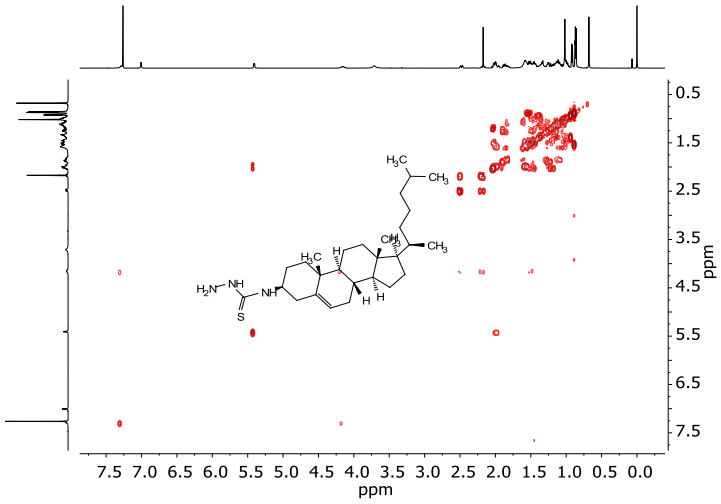


Figure 717. ^{1}H,^{1}H COSY NMR spectrum of ^{13}C APT NMR spectrum of *N*-hydrazidecarbothio [(1*S*,2*R*,5*S*,10*S*,11*S*,14*R*,15*R*)-14-[(1*R*)-1,5-dimethylhexyl]-2,15dimethyltetracyclo[8.7.0.0^{2,7}.0^{11,15}] heptadic-7-en-5-yl]amine in DMSO-*d*$_6$ at 499 MHz.

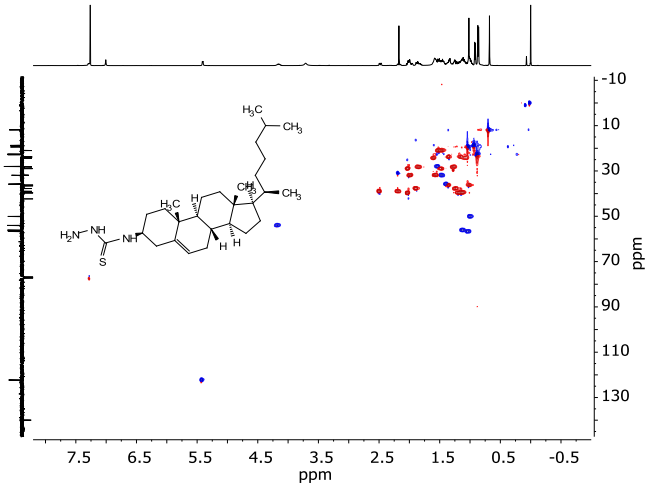


Figure 718. $^{1}H,^{13}C$ HMQC/HSQC NMR spectrum of ^{13}C APT NMR spectrum of *N*-hydrazidecarbothio [(1*S*,2*R*,5*S*,10*S*,11*S*,14*R*,15*R*)-14-[(1*R*)-1,5-dimethylhexyl]-2,15-dimethyltetracyclo[8.7.0.0^{2,7}.0^{11,15}]heptadec-7-en-5-yl]amine in DMSO-d_6 at 499 MHz.

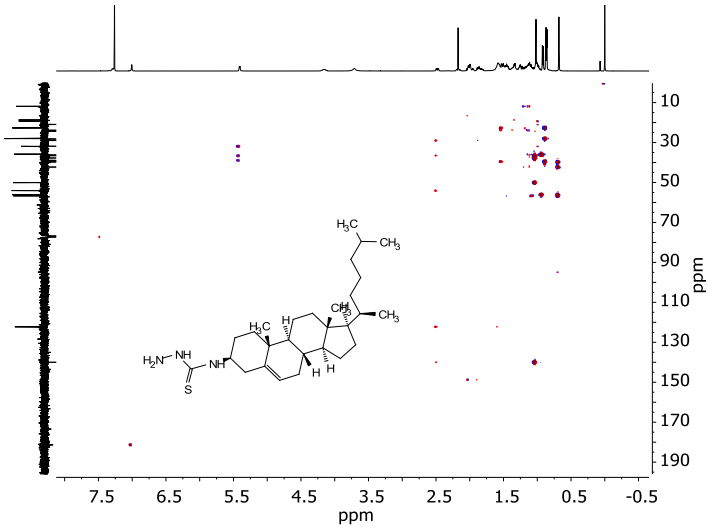


Figure 719. $^{1}H,^{13}C$ HMBC NMR spectrum of ^{13}C APT NMR spectrum of *N*-hydrazidecarbothio[(1*S*,2*R*,5*S*,10*S*,11*S*,14*R*,15*R*)-14-[(1*R*)-1,5-dimethylhexyl]-2,15-dimethyltetracyclo [8.7.0.0^{2,7}.0^{11,15}]heptadec-7-en-5-yl]amine in DMSO-d_6 at 499 MHz.

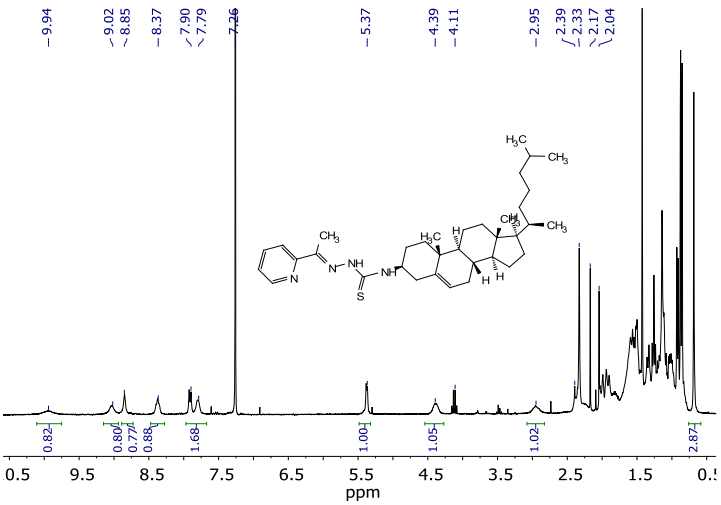


Figure 720. ^{1}H NMR spectrum of [(1*S*,2*R*,5*S*,10*S*,11*S*,14*R*,15*R*)-14-[(1*R*)-1,5-dimethylhexyl]-2,15-dimethyltetracyclo [8.7.0.0^{2,7}.0^{11,15}]heptadec-7-en-5-ylamino][(1*Z*)-1-(pyridin-2-yl)eth-1-ylideneamino]carbothioamide in DMSO-d_6 at 300 MHz.

7.2 High resolution electron spray ionization mass spectrometry (HR-ESI-MS)

7.2.1 HR-ESI-MS of TSCs with functional groups at the *N*4 position

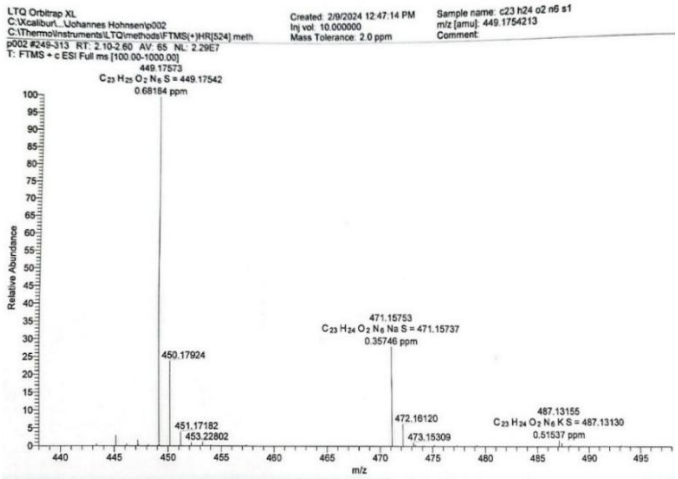


Figure 721. HR-ESI-MS of di-2-pyridylketone-4-(4-*tert*-butoxycarbonylamino-phenyl)-3-thiosemicarbazone.

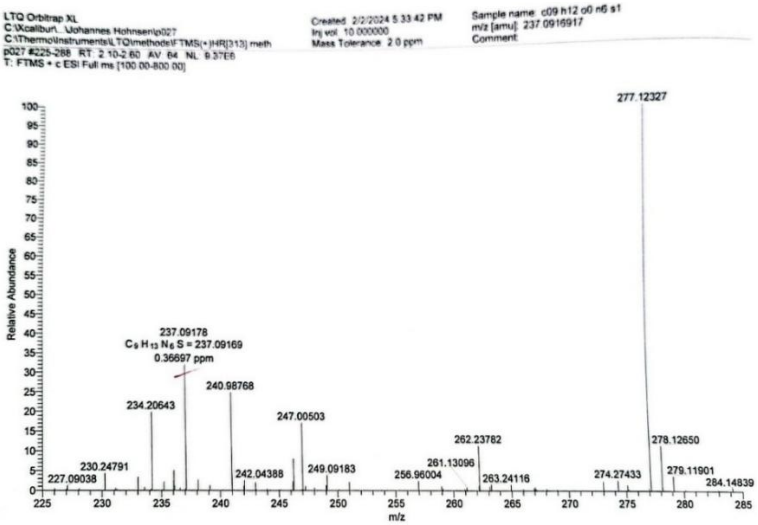


Figure 722. HR-ESI-MS of 4-([*p*-(azidomethyl)phenyl]methyl)thiosemicarbazide.

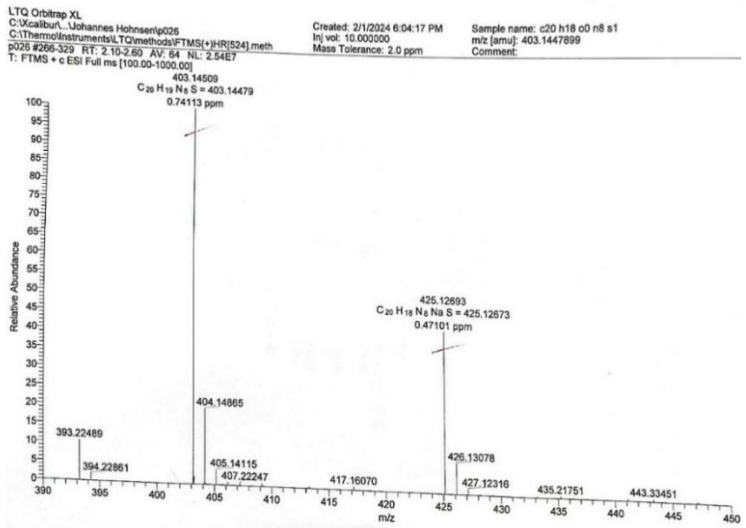


Figure 723. HR-ESI-MS of (2-[bis(pyridin-2-yl)methylidene]hydrazino)-[4-(azidomethyl)phenyl]ethanethioamide.

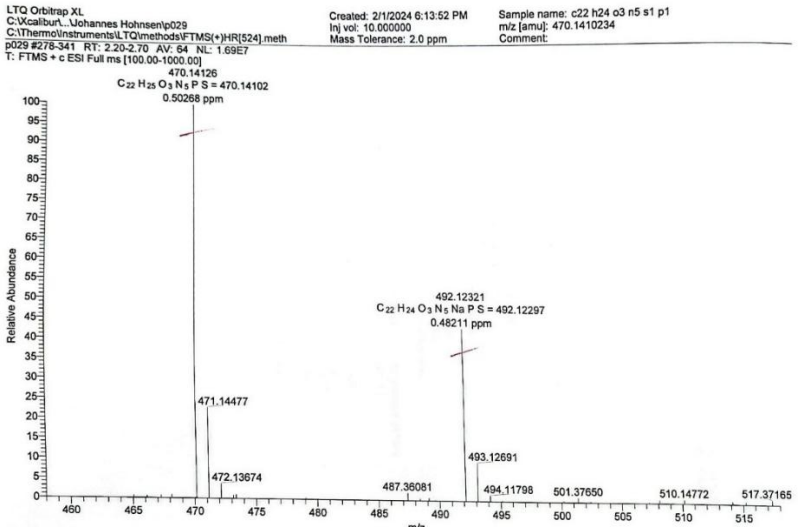


Figure 724. HR-ESI-MS of (2-[bis(pyridin-2-yl)methylidene]hydrazino)-4-(diethoxyphosphoryl)benzene-1-carbothioamide.

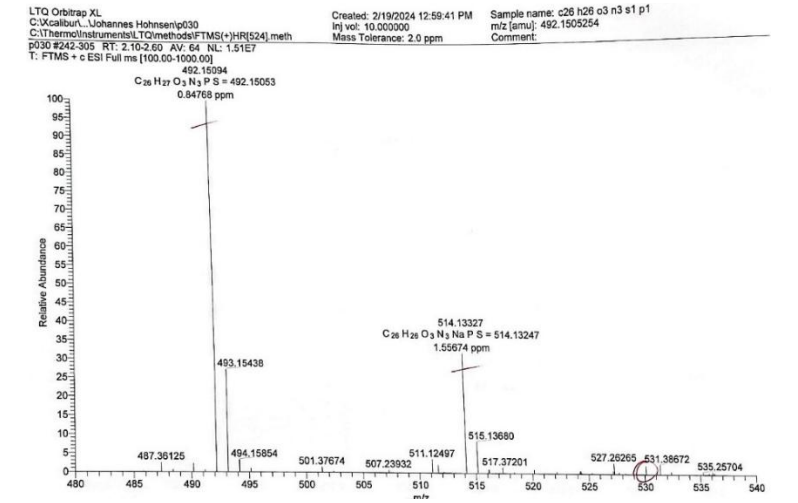


Figure 725. HR-ESI-MS of [(2*E*)-2-[(anthracen-9-yl)methylidene]hydrazino]-4-(diethoxyphosphoryl)benzene-1-carbothioamide.

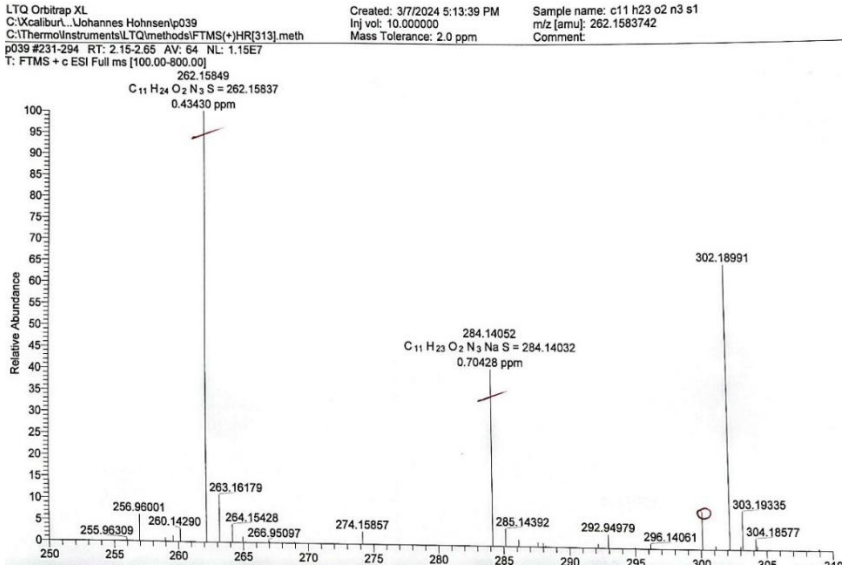


Figure 726. HR-ESI-MS of 4-((*S*)-*tert*-butyl 4-methylpentonate)thiosemicarbazide.

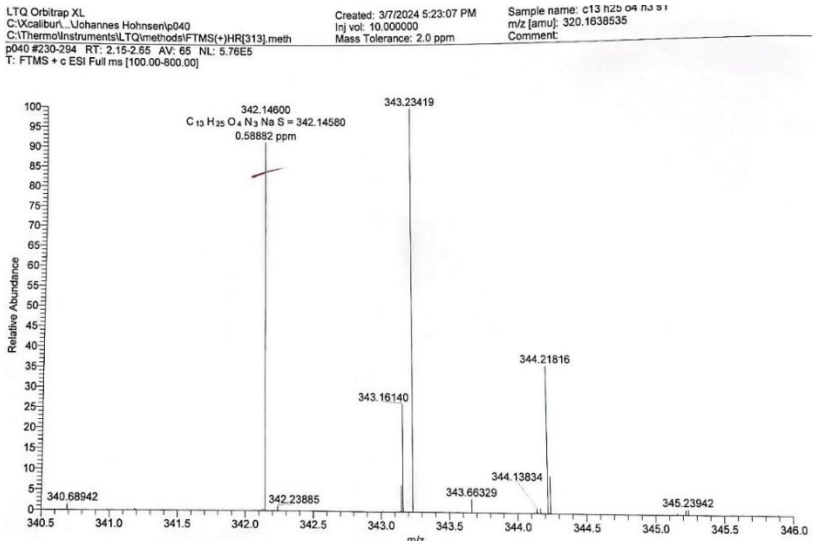


Figure 727. HR-ESI-MS of (*S*)-di-*tert*-butyl 2-(hydrazidecarbothioamino)butanedioate.

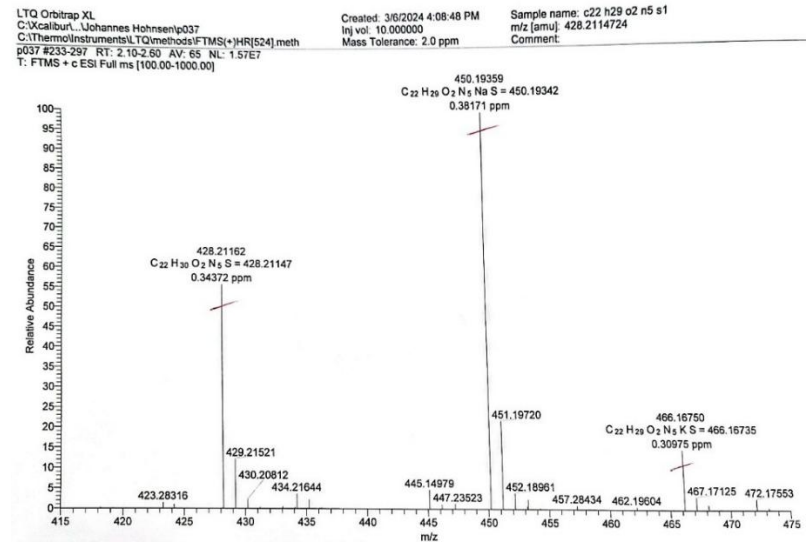


Figure 728. HR-ESI-MS of di-2-pyridylketone-4-((*S*)-*tert*-butyl-4-methylpentanoate)-3-thiosemicarbazone.

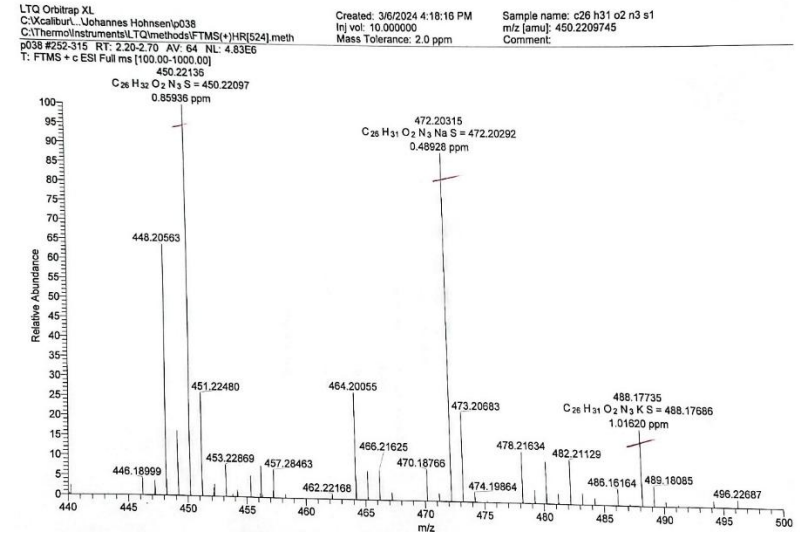


Figure 729. HR-ESI-MS of 9-anthraldehyde-4-((*S*)-*tert*-butyl 4-methylpentonate)-3-thiosemicarbazone.

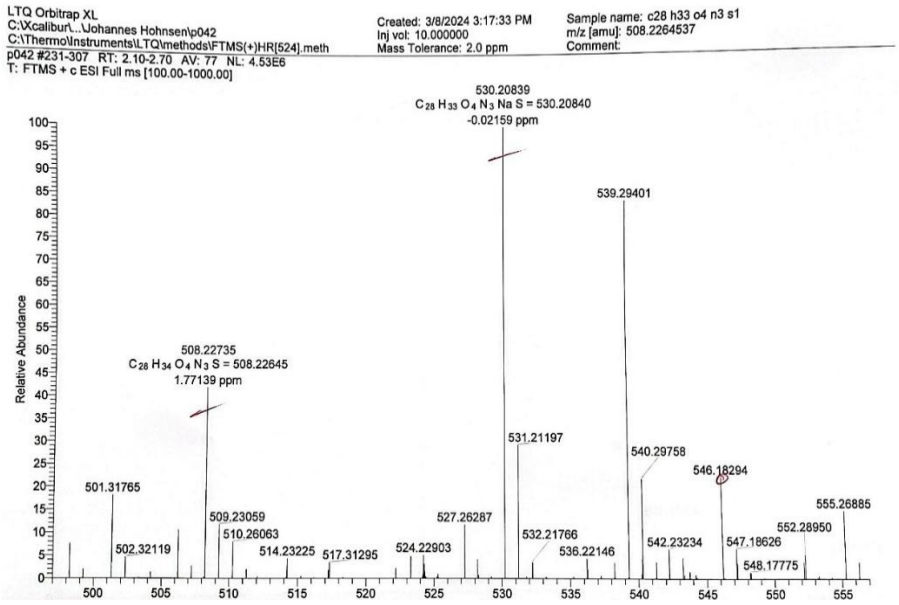


Figure 730. HR-ESI-MS of di-*tert*-butyl-2-([(1*E*)-(anthracen-9-yl)methylideneaminocarbamthioyl]amino) butanedioate.

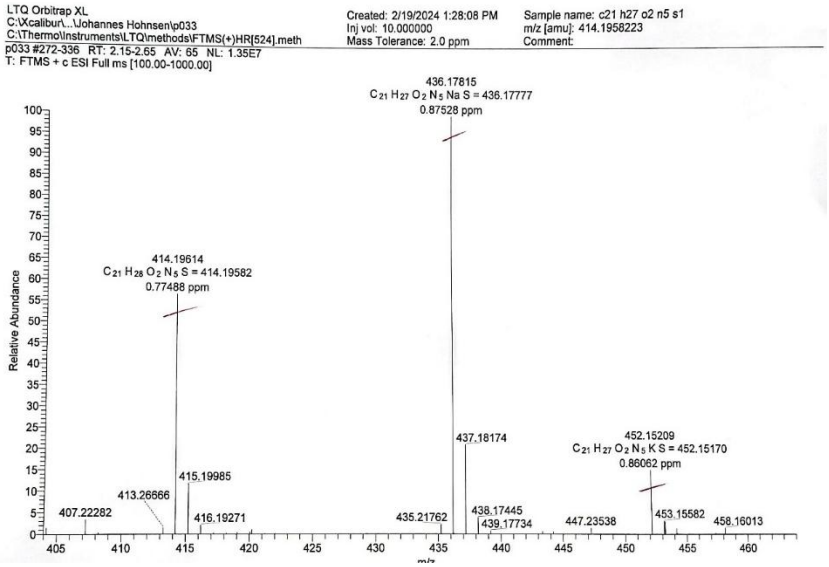


Figure 731. HR-ESI-MS of di-2-pyridylketone-4-((*S*)-*tert*-butyl 3-metylbutanoate)-3-thiosemicarbazone.

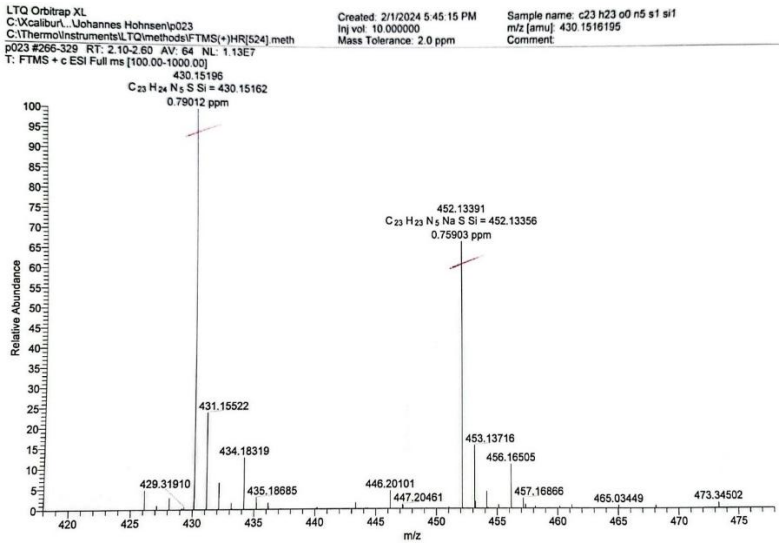


Figure 732. HR-ESI-MS of [bis(pyridin-2-yl)methylideneamino][4-(trimethylsilyl)ethynylphenylamino] carbothioamide.

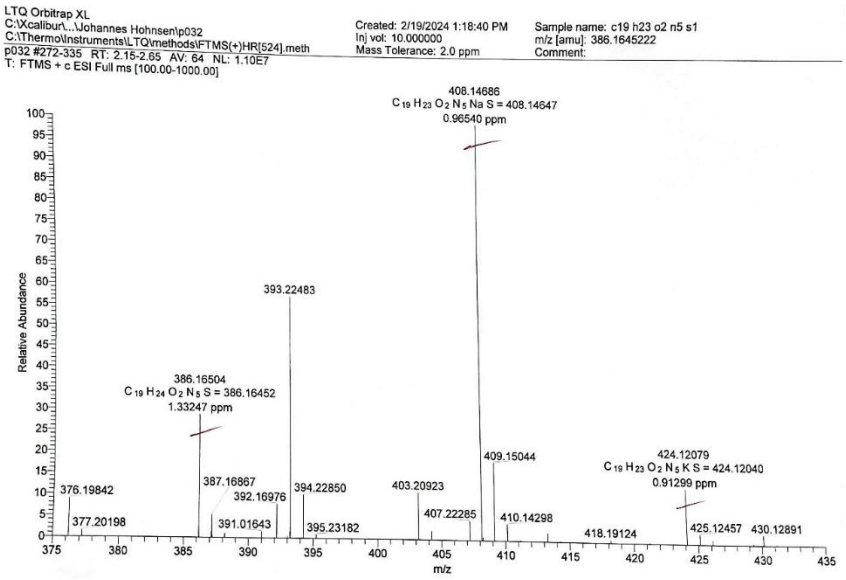


Figure 733. HR-ESI-MS of di-2-pyridylketone-4-((*S*)-*tert*-butyl propanoate)-3-thiosemicarbazone.

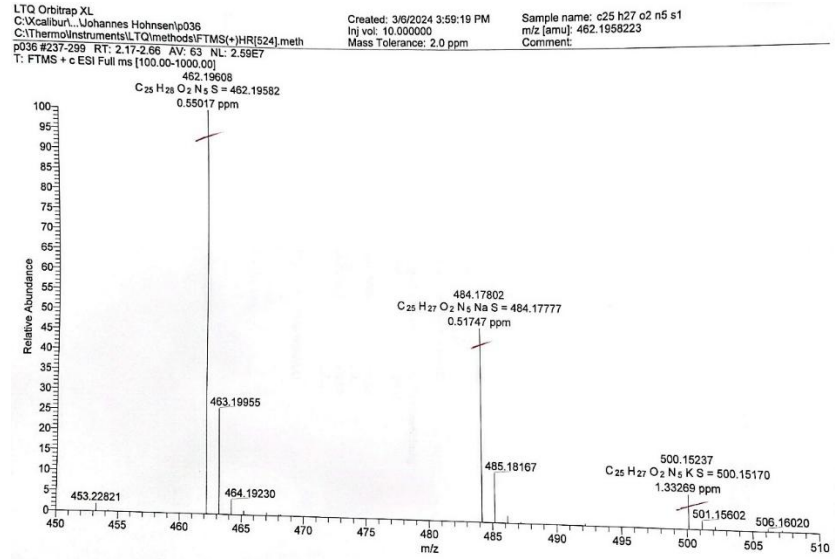


Figure 734. HR-ESI-MS of di-2-pyridylketone-4-((*S*)-*tert*-butyl 3-phenylbutanoate)-3-thiosemicarbazone.

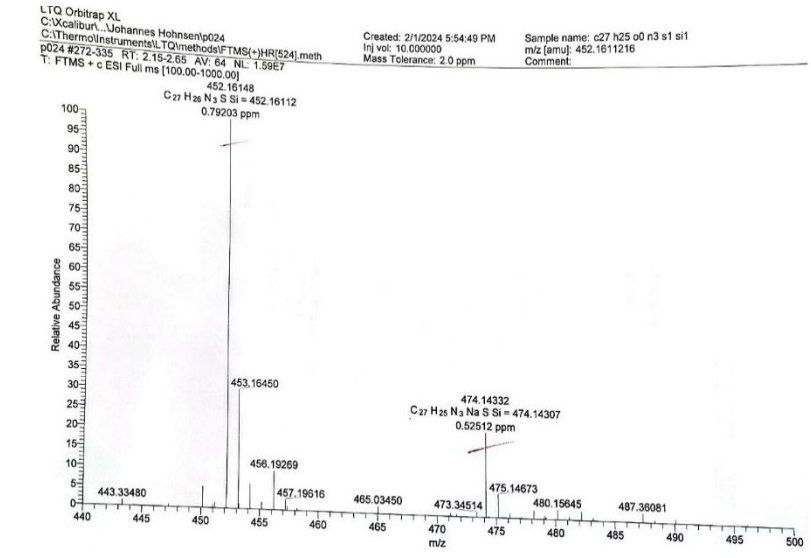


Figure 735. HR-ESI-MS of [(1*E*)-(anthracen-9-yl)methylideneamino][4-(trimethylsilyl)ethynylphenylamino]carbothioamide.

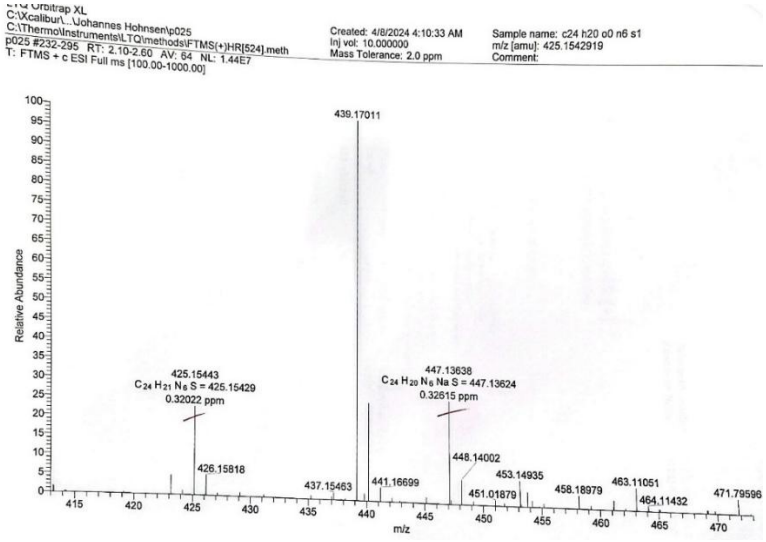


Figure 736. HR-ESI-MS of [(2*E*)-2-[(anthracen-9-yl)methylidene]hydrazino]-[4-(azidomethyl)phenyl] ethanethioamide.

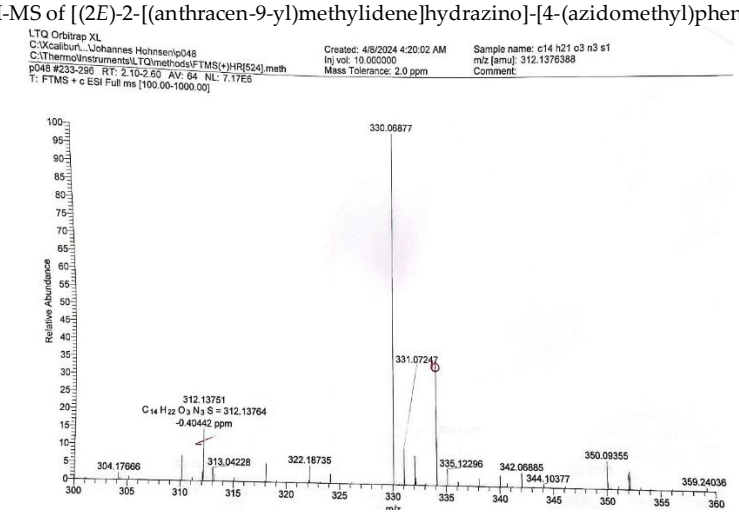


Figure 737. HR-ESI-MS of (*S*)-*tert*-butyl 2-(hydrazidecarbothioamino)-3-(4-hydroxyphenyl)propanoate.

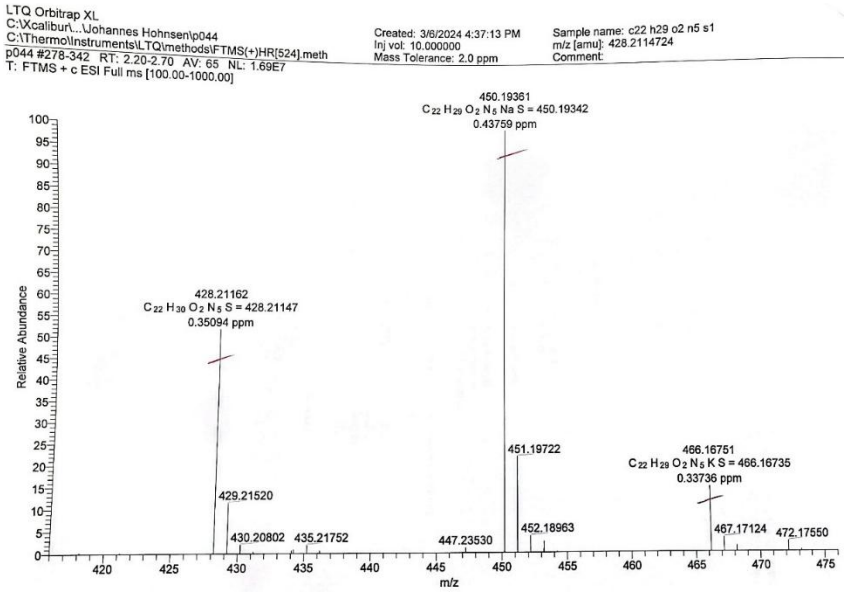


Figure 738. HR-ESI-MS of *tert*-butyl 2-(2-[bis(pyridin-2-yl)methylidene]hydrazinocarbamthioyl)-3-methylpentanoate.

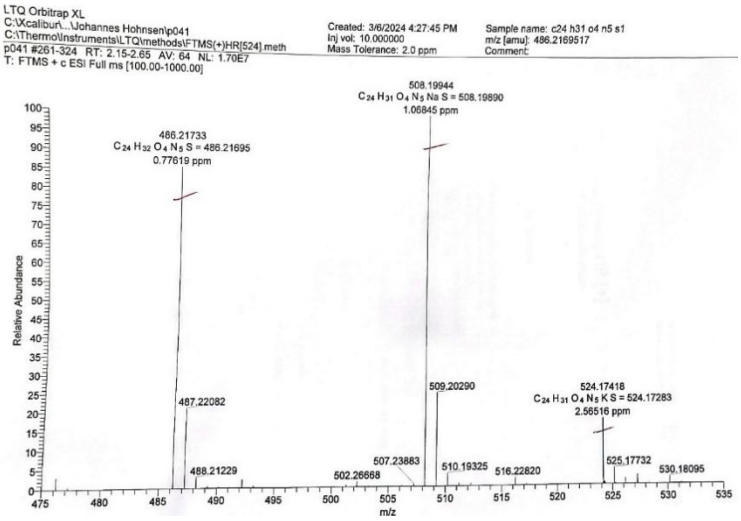


Figure 739. HR-ESI-MS of di-*tert*-butyl 2-([bis(pyridin-2-yl)methylideneaminocarbamthioyl]amino)butanedioate.

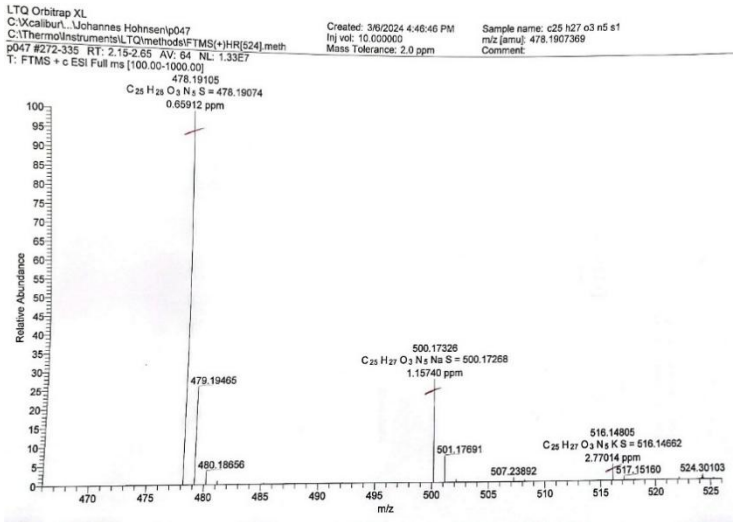


Figure 740. HR-ESI-MS of *tert*-butyl 2-(2-[bis(pyridin-2-yl)methylidene]hydrazinocarbamthioyl)-3-(4-hydroxyphenyl)-propanoate.

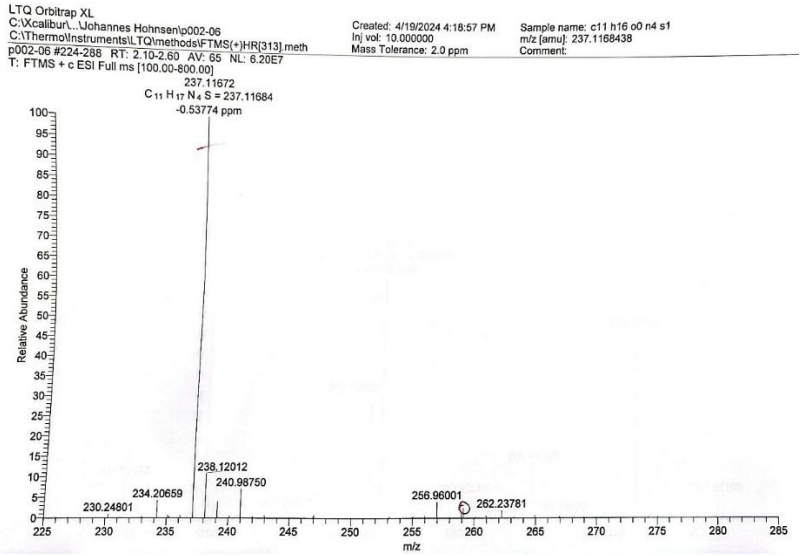


Figure 741. HR-ESI-MS of (*E*)-1-[2,2-dimethyl-1-(2-pyridyl)propylidene]thiosemicarbazide.

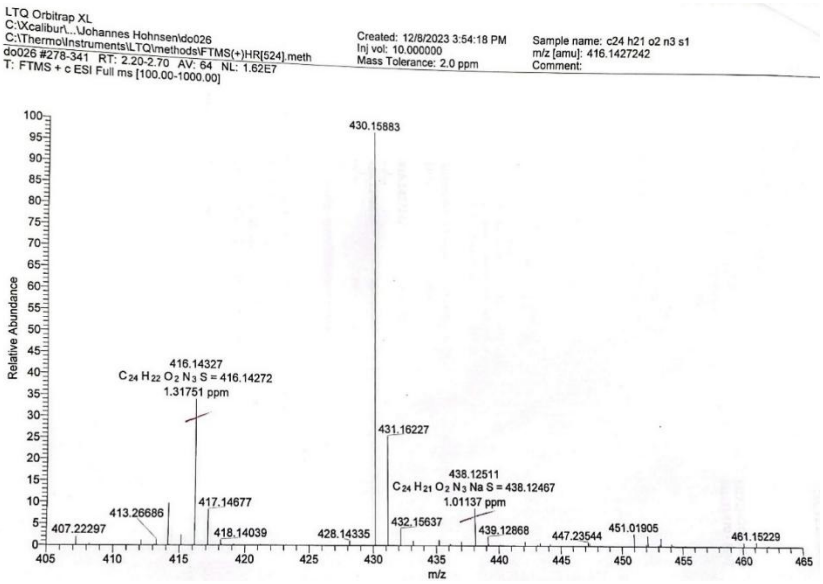


Figure 742. HR-ESI-MS of [(1*E*)-(anthracen-9-yl)methylideneamino][2-(3,4 dihydroxyphenyl)ethylamino] carbothioamide.

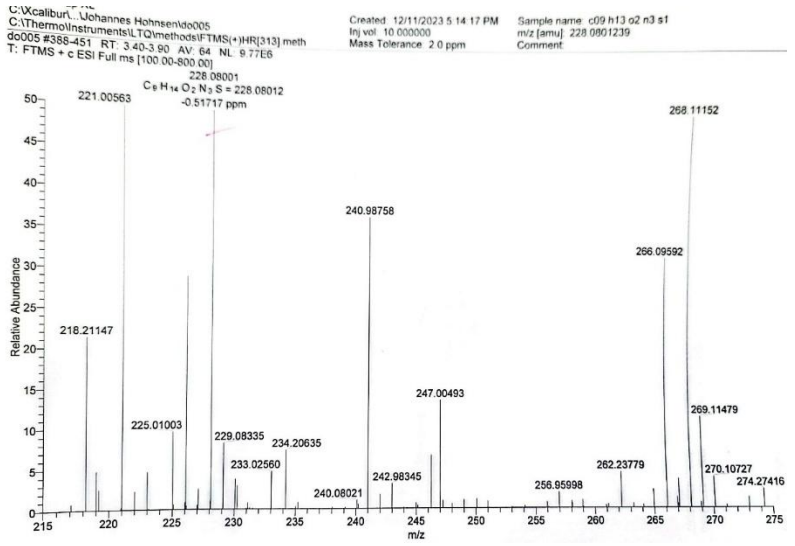


Figure 743. HR-ESI-MS of 4-[2-(hydrazidecarbothioamino)ethyl]benzene-1,2-diol.

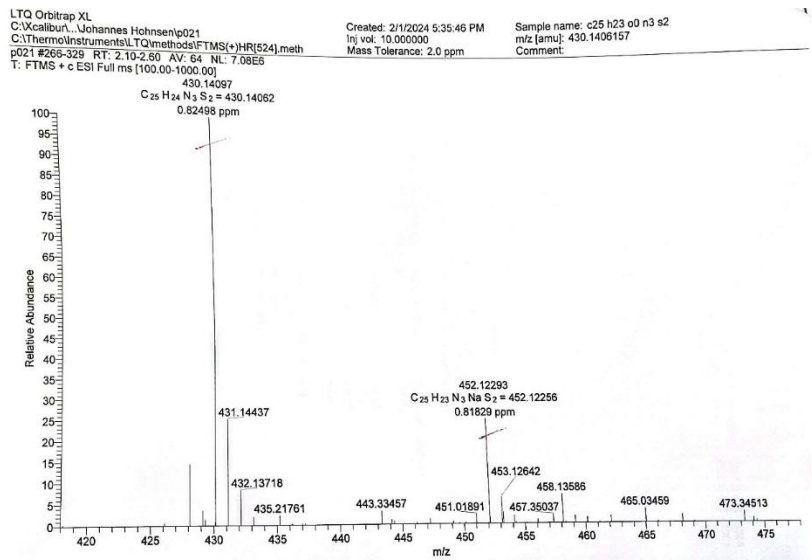


Figure 744. HR-ESI-MS of 9-anthraldehyde-4-(2-benzylsulfanylethyl)-3-thiosemicarbazone.

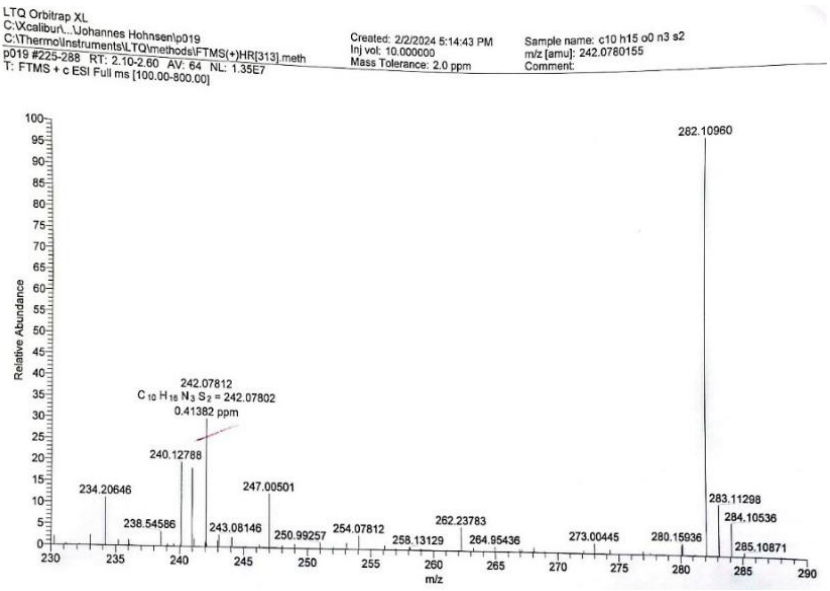


Figure 745. HR-ESI-MS of 4-(2-benzylsulfanylethyl)thiosemicarbazide.

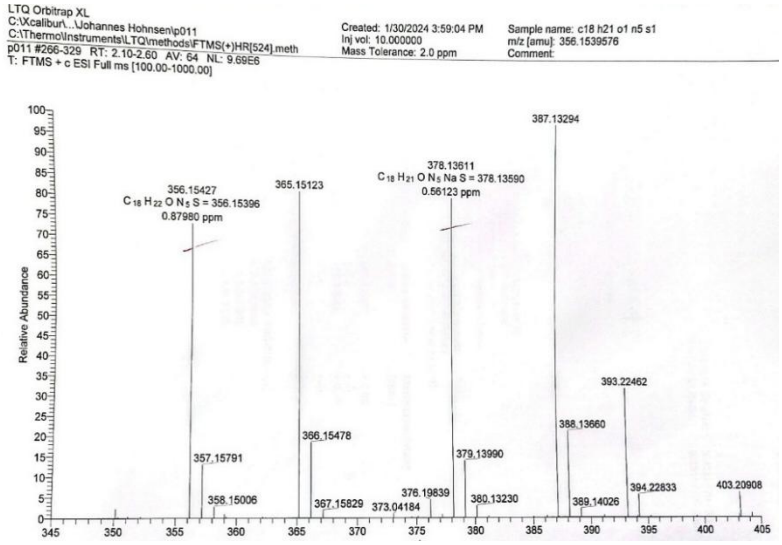


Figure 746. HR-ESI-MS of di-2-pyridylketone-4-(*trans*-4-hydroxycyclohexyl)-3-thiosemicarbazone.

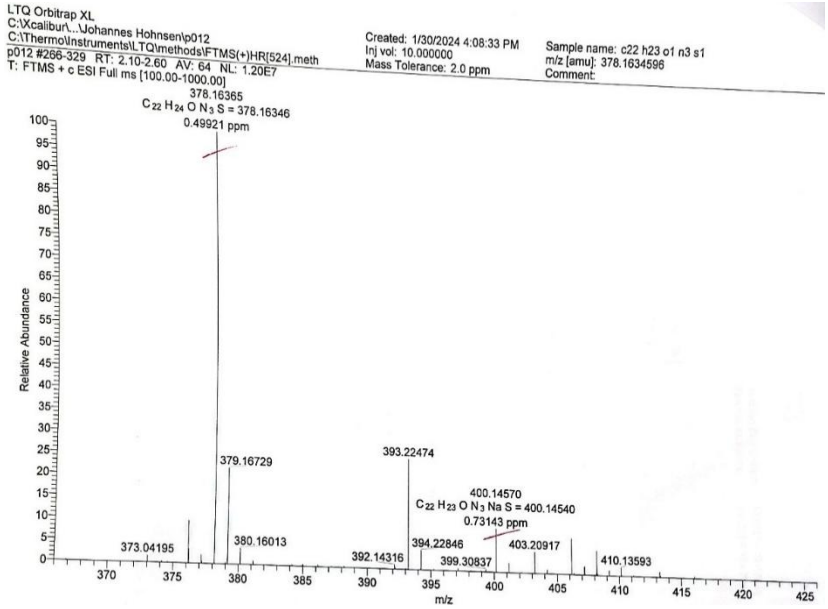


Figure 747. HR-ESI-MS of 9-anthraldehyde-4-(*trans*-4-hydroxycyclohexyl)-3-thiosemicarbazone.

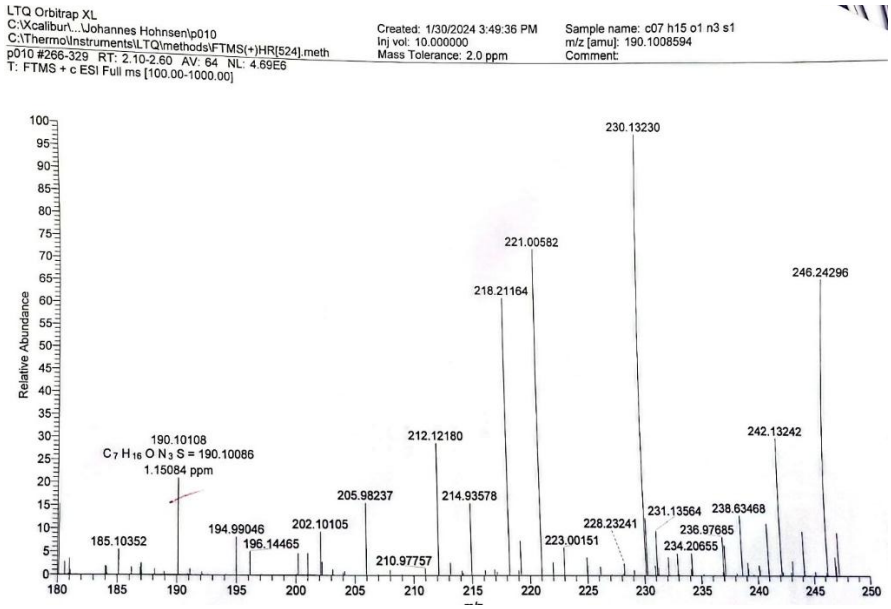


Figure 748. HR-ESI-MS of 4-(trans-4-hydroxycyclohexyl)-thiosemicarbazide.

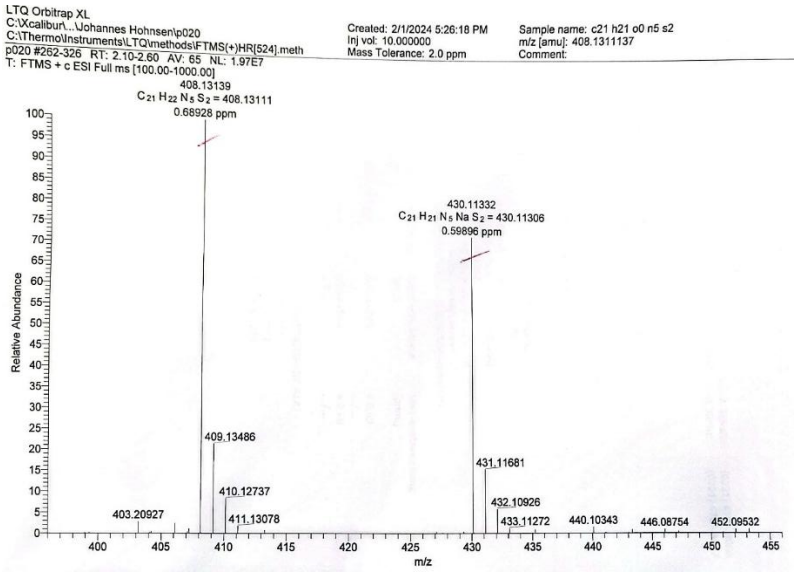


Figure 749. HR-ESI-MS of di-2-pyridylketone-4-(2-benzylsulfanylethyl)-3-thiosemicarbazone.

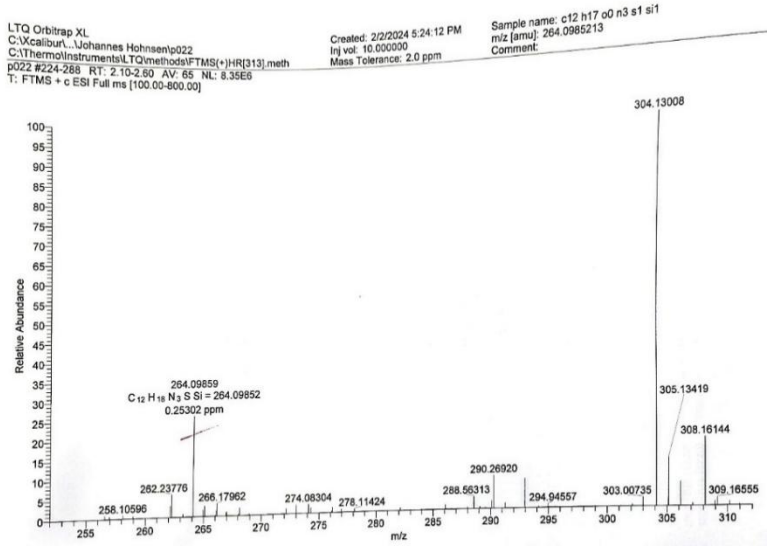


Figure 750. HR-ESI-MS of *N*-hydrazidecarbothio[4-(trimethylsilyl)ethynylphenyl]amine.

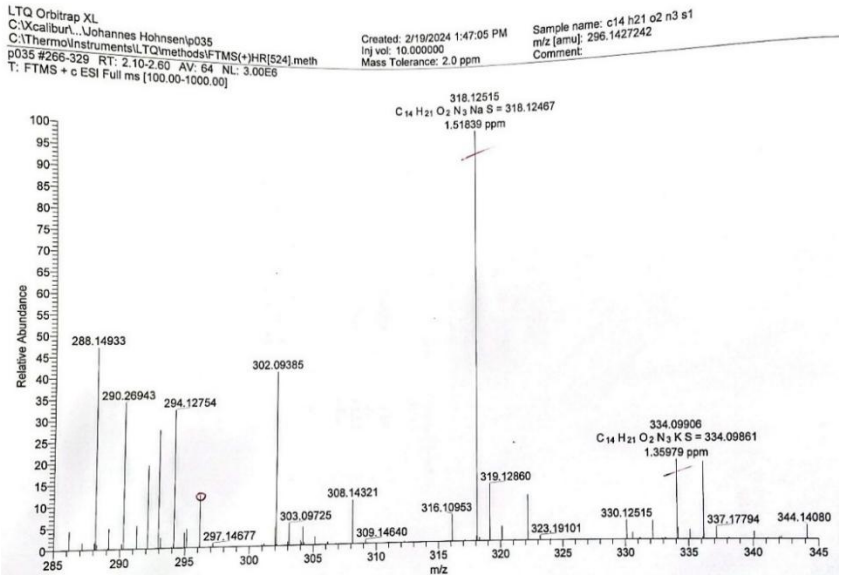


Figure 751. HR-ESI-MS of (*S*)-*tert*-butyl 2-(hydrazidecarbothioamino)-3-(4-hydroxyphenyl)propanoate.

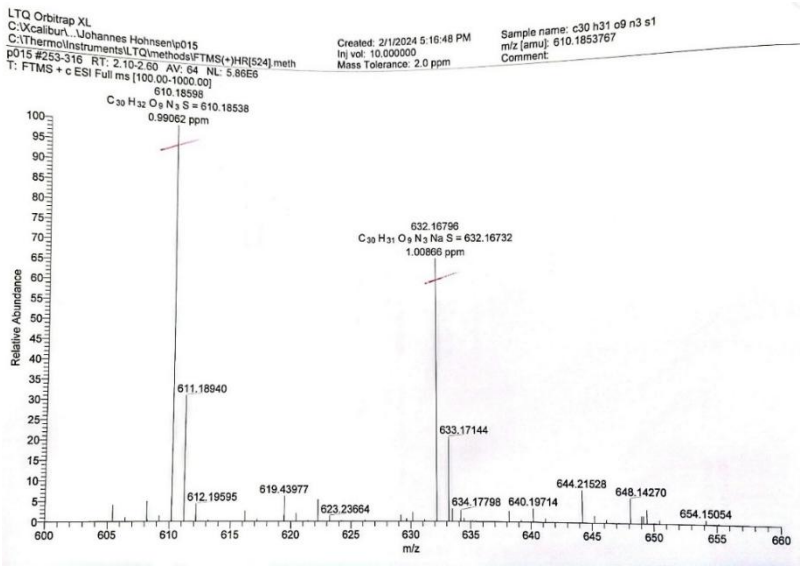


Figure 752. HR-ESI-MS of 9-anthraldehyde-4-(2,3,4,6-Tetra-*O*-acetyl-β-D-glucopyranosyl)-3-thiosemicarbazone

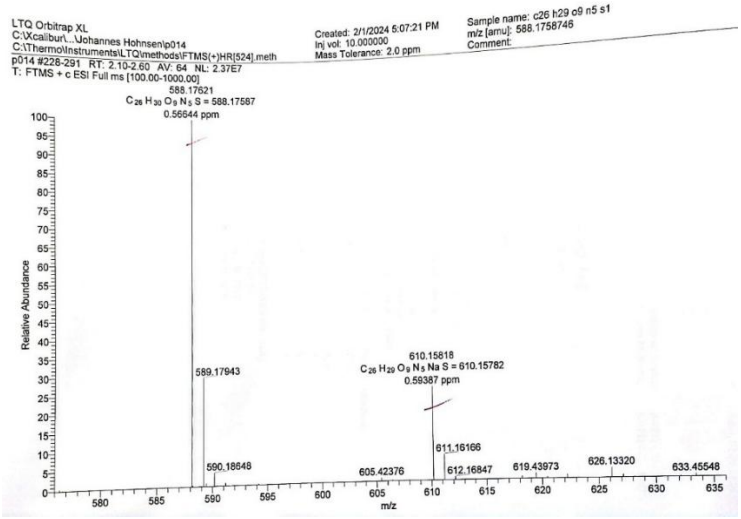


Figure 753. HR-ESI-MS of di-2-pyridylketone-4-(2,3,4,6-tetra-*O*-acetyl-β-D-glucopyranosyl)-3-thiosemicarbazone.

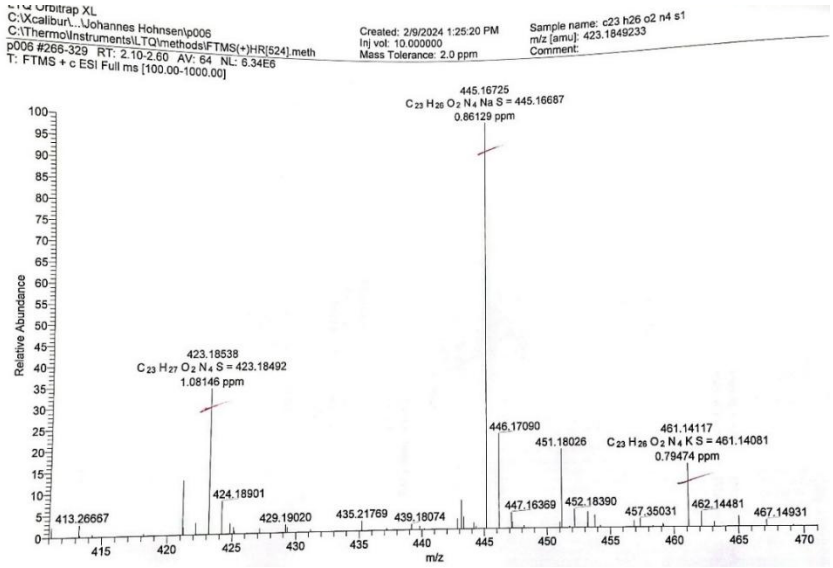


Figure 754. HR-ESI-MS of 9-anthraldehyde-4-(2-*tert*-butoxycarbonylamino-ethyl)-3-thiosemicarbazone.

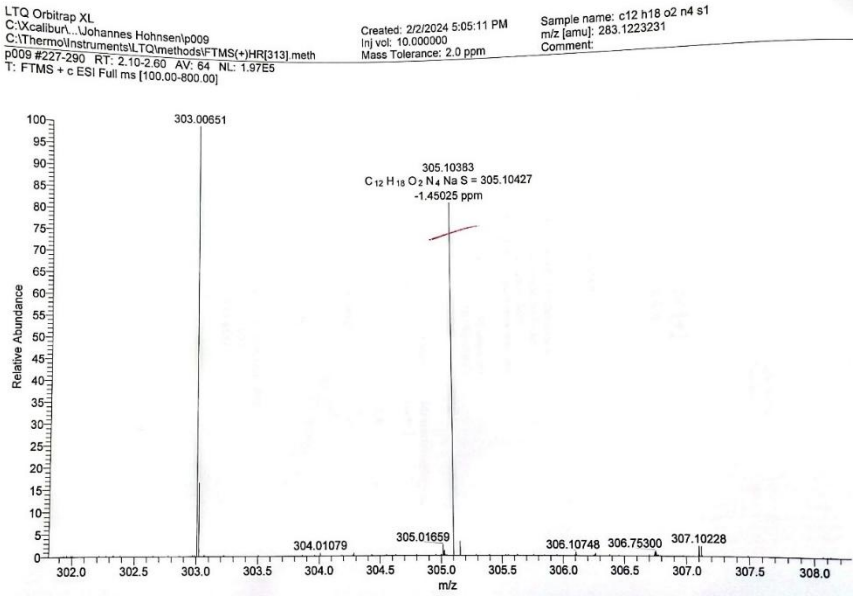


Figure 755. HR-ESI-MS of 4-(4-*tert*-butoxycarbonylamino-phenyl)thiosemicarbazide.

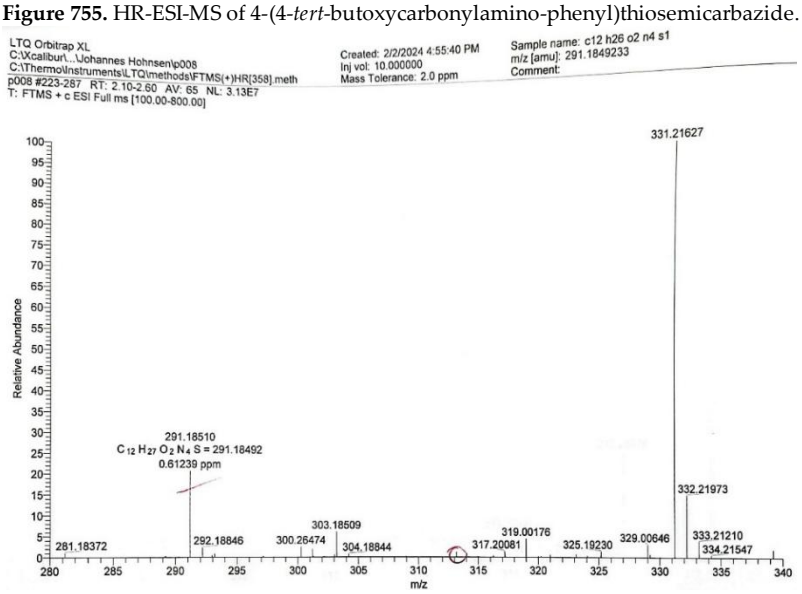


Figure 756. HR-ESI-MS of 4-(6-*tert*-butoxycarbonylamino-hexyl)thiosemicarbazide.

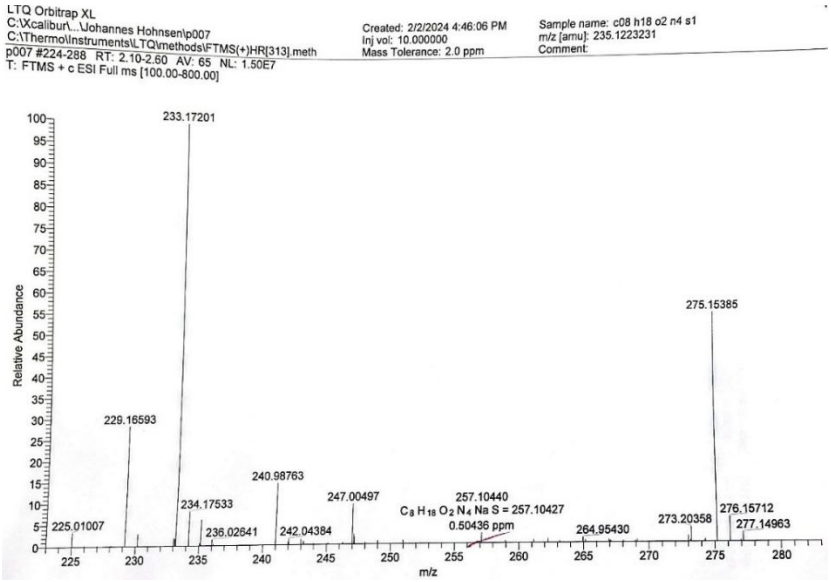


Figure 757. HR-ESI-MS of 4-(2-*tert*-butoxycarbonylamino-ethyl)thiosemicarbazide.

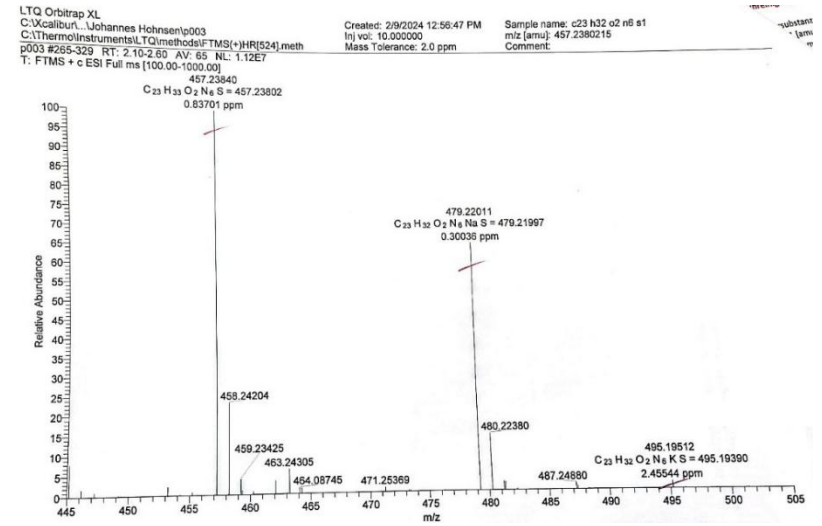


Figure 758. HR-ESI-MS of di-2-pyridylketone-4-(6-*tert*-butoxycarbonylamino-hexyl)-3-thiosemicarbazone.

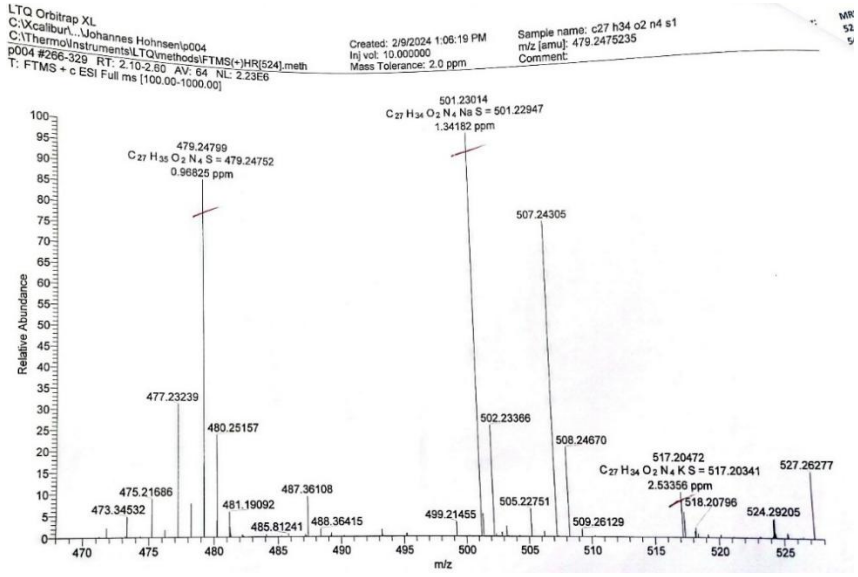


Figure 759. HR-ESI-MS of 9-anthraldehyde-4-(6-*tert*-butoxycarbonylamino-hexyl)-3-thiosemicarbazone.

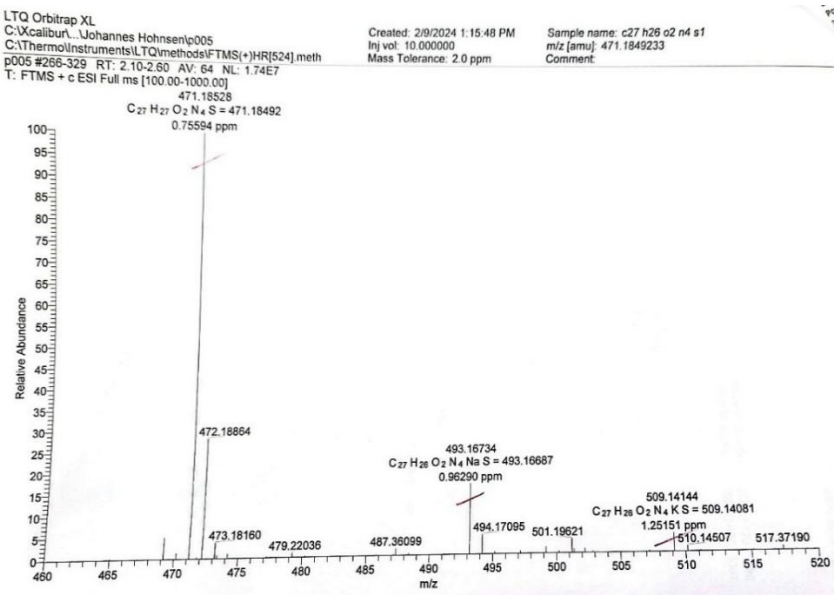


Figure 760. HR-ESI-MS of 9-anthraldehyde-4-(4-*tert*-butoxycarbonylamino-phenyl)-3-thiosemicarbazone.

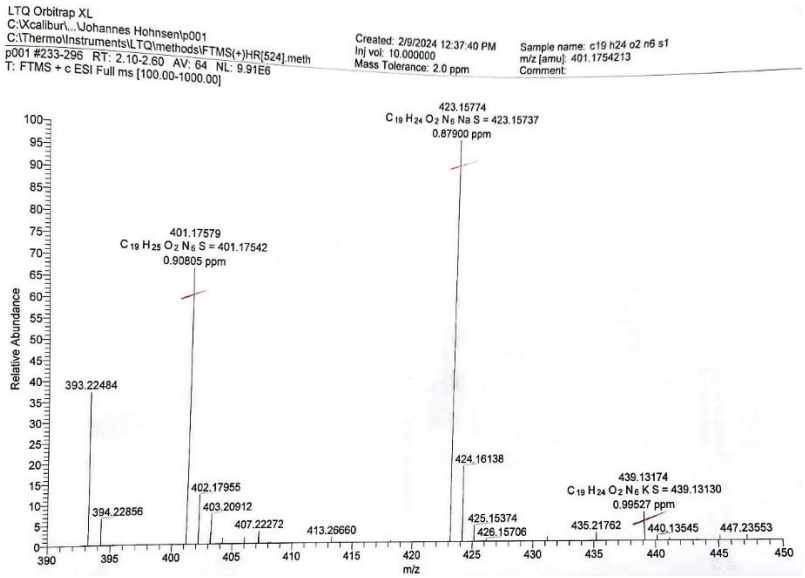


Figure 761. HR-ESI-MS of di-2-pyridylketone-4-(2-*tert*-butoxycarbonylamino-ethyl)-3-thiosemicarbazone.

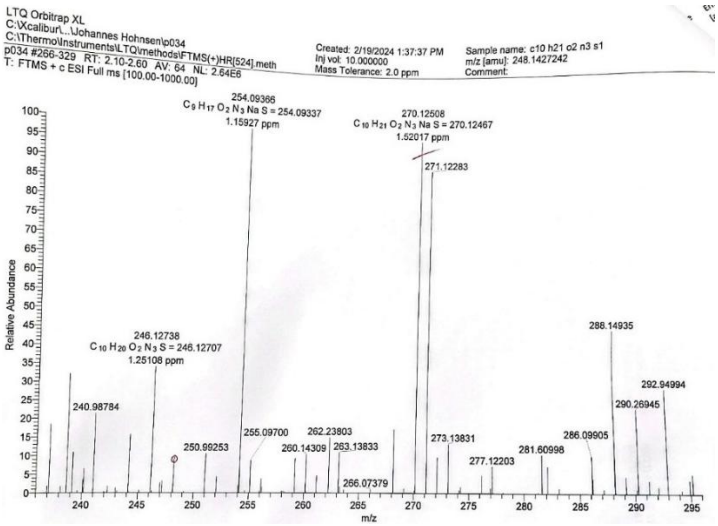


Figure 762. HR-ESI-MS of 4-((*S*)-*tert*-butyl 3-metylbutanoate)thiosemicarbazide.

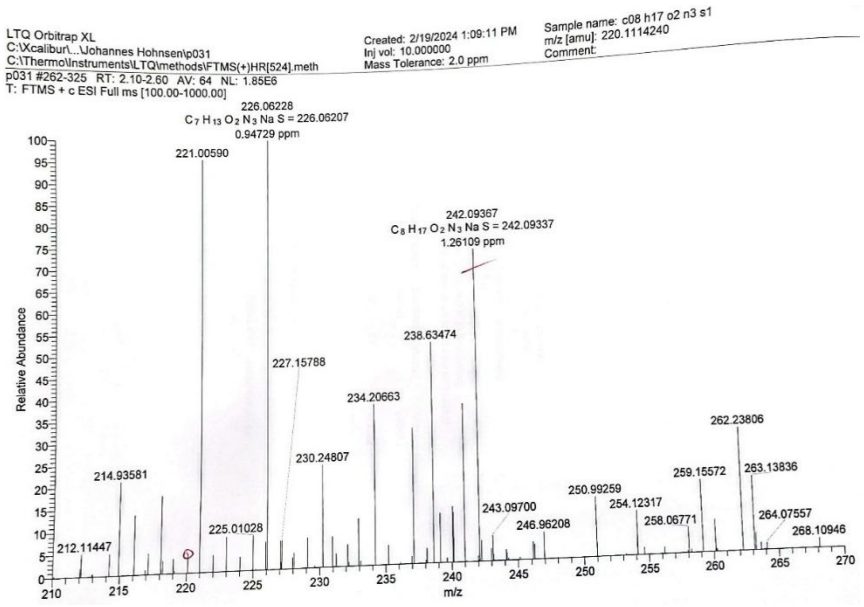


Figure 763. HR-ESI-MS of 4-((*S*)-*tert*-butyl propanoate)thiosemicarbazide.

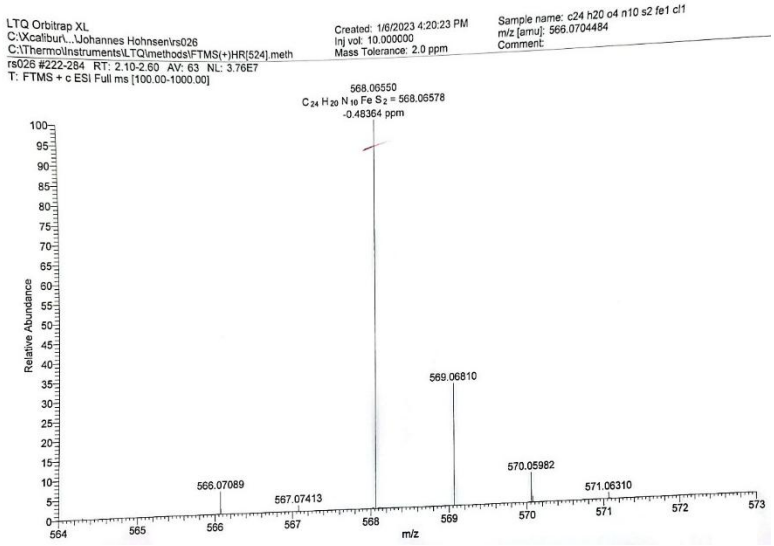


Figure 764. HR-ESI-MS of [(1*E*)-(anthracen-9-yl)methylideneamino][2-(3,4-dihydroxyphenyl)ethylamino] carbothioamide.

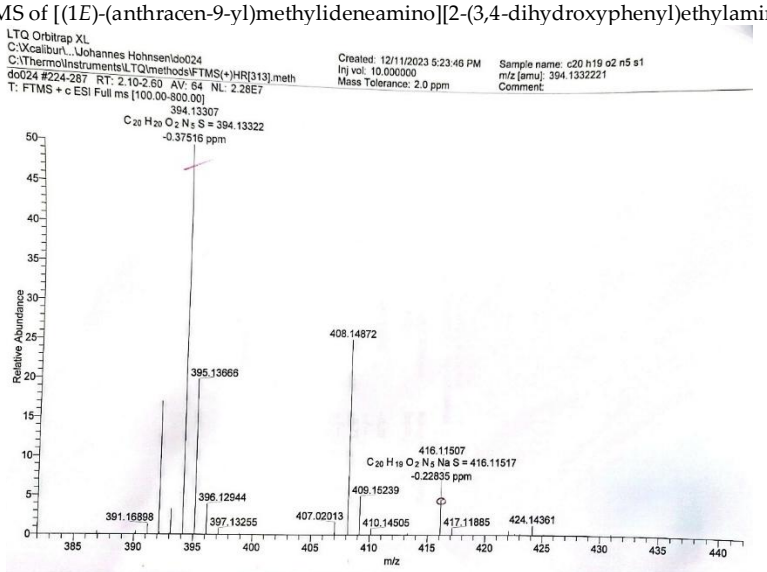


Figure 765. HR-ESI-MS of [bis(pyridin-2-yl)methylideneamino][2-(3,4-dihydroxyphenyl)ethylamino] carbothio amide.

7.2.2 HR-ESI-MS of hexadentate TSCs

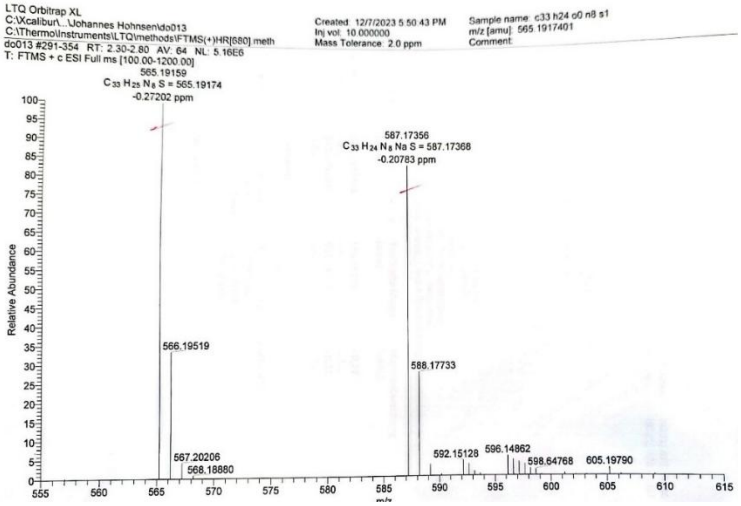


Figure 766. HR-ESI-MS of 4'-(4-([bis(pyridin-2-yl)methylideneaminocarbamthioyl]amino)phenyl)-2,2':6',2''-terpyridine.

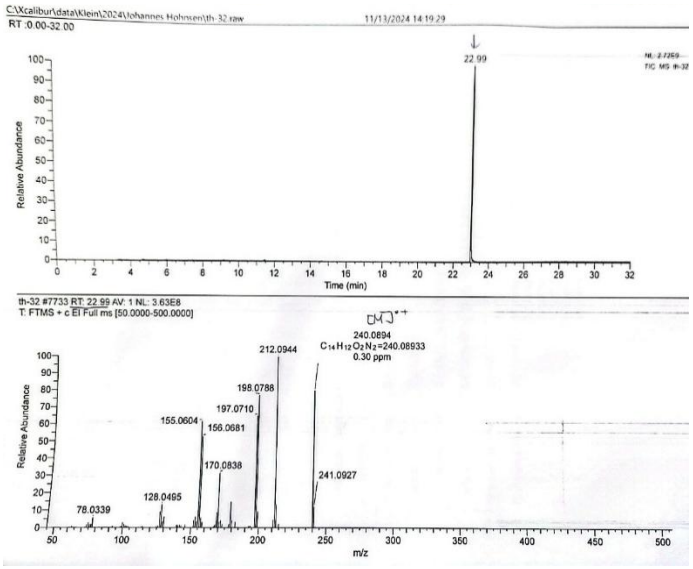


Figure 767. HR-ESI-MS of 6,6′-bis(2-acetyl)-2,2′- bipyridine.

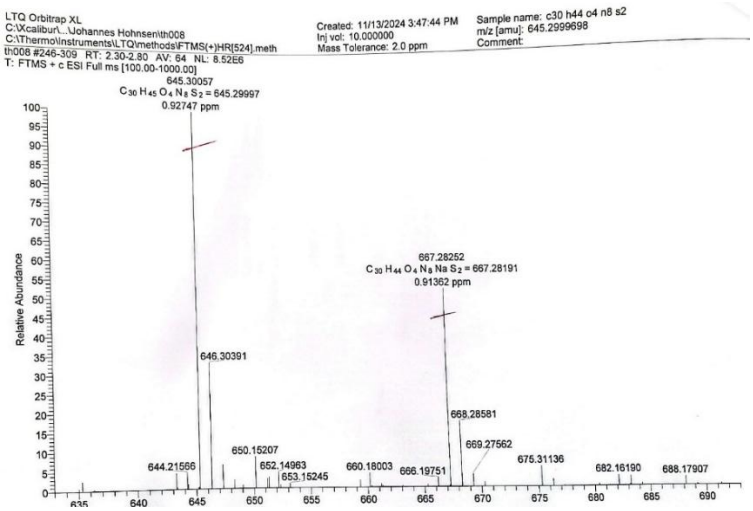


Figure 768. HR-ESI-MS of naph(bis-TSC)Val*t*Bu.

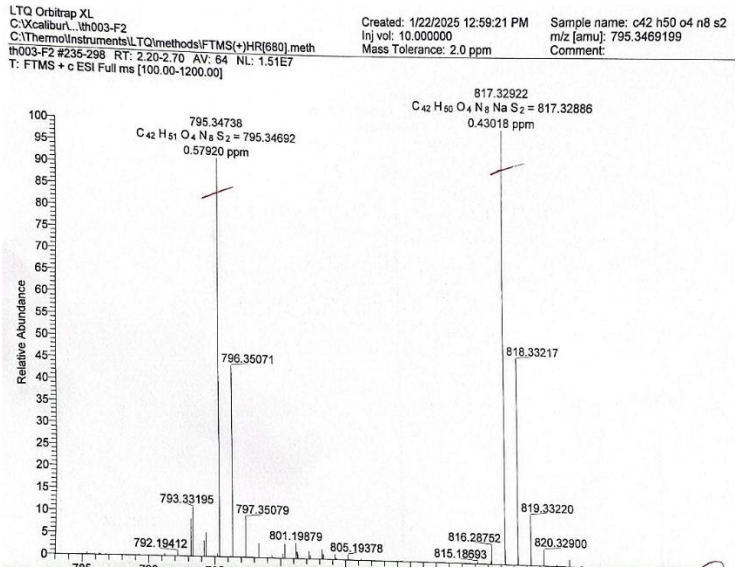


Figure 769. HR-ESI-MS of bpy(bis-TSC)Ala*t*Bu.

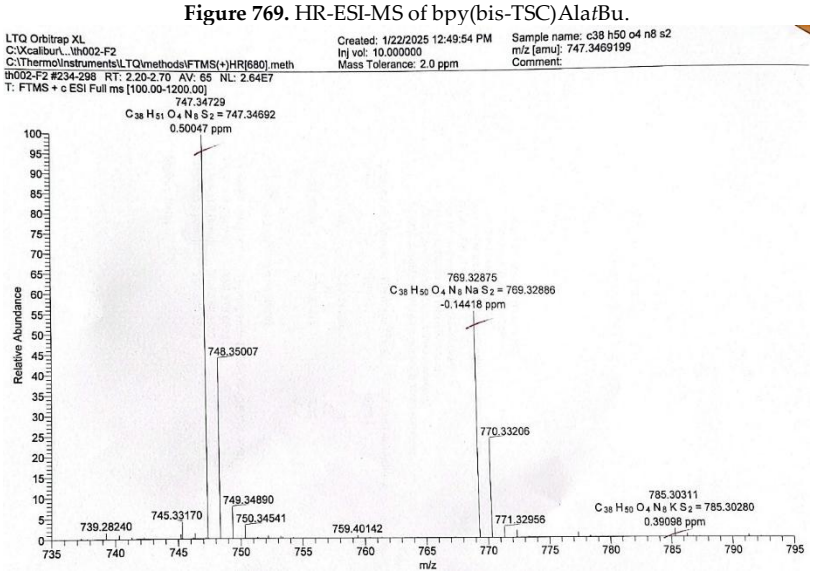


Figure 770. HR-ESI-MS of N^C^N(bis-TSC)Ala*t*Bu.

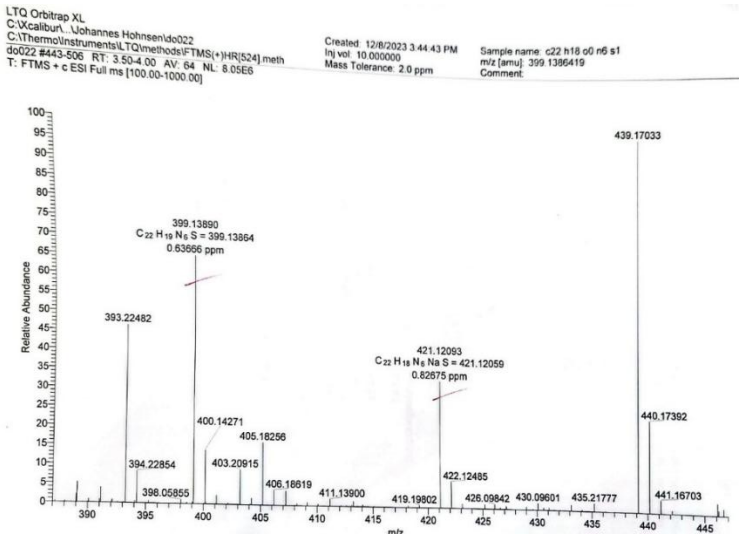


Figure 771. HR-ESI-MS of *N*-hydrazidecarbothio[4-([2,2':6',2''-terpyridin]-4'-yl)phenyl]amine.

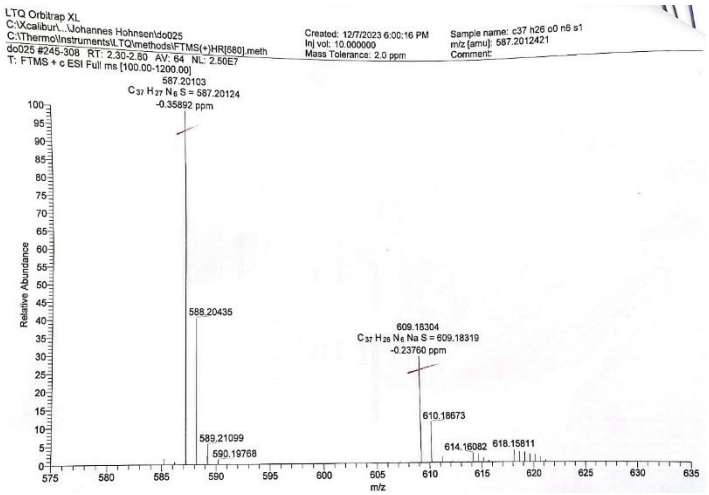


Figure 772. HR-ESI-MS of (*E*)-1-[(9-anthryl)methylene]-4-[*p*-(2,2':6',2''-terpyridin-4'-yl)phenyl]thiosemicarbazide.

7.2.3 HR-ESI-MS of α-pyridyl TSCs and their Fe(III) complexes

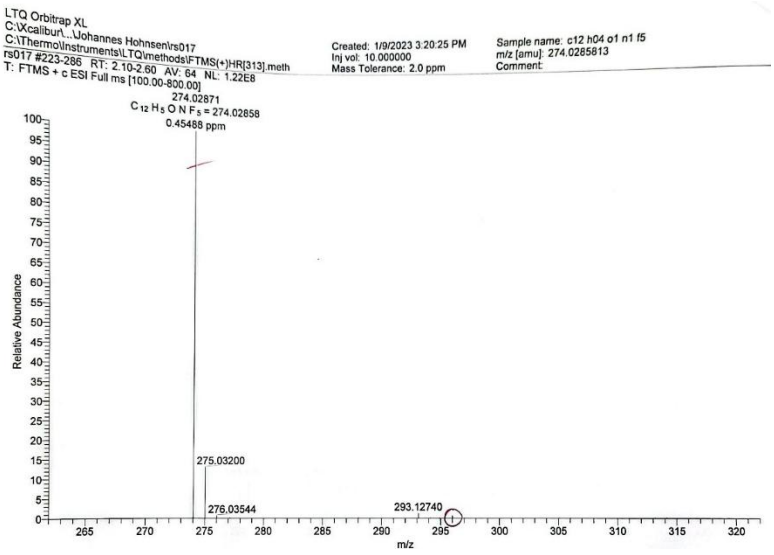


Figure 773. HR-ESI-MS of pentafluorophenyl(pyridin-2-yl)methanone.

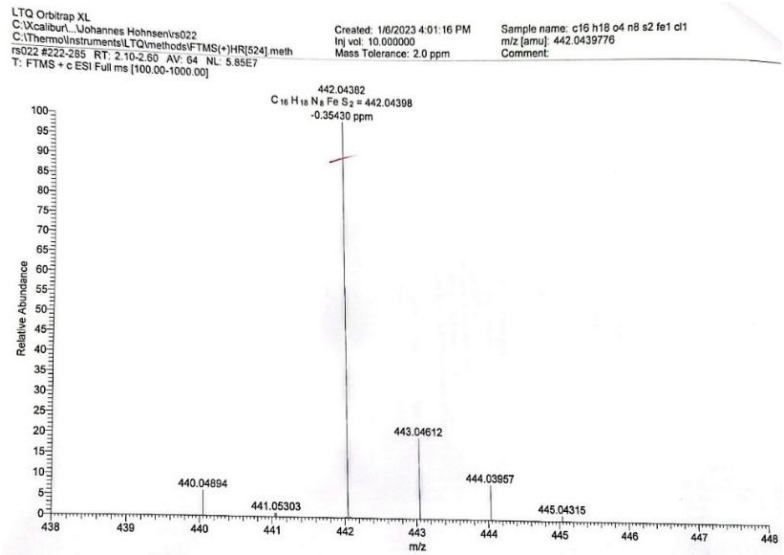


Figure 774. HR-ESI-MS of [Fe(MePy(TSC)H$_2$].

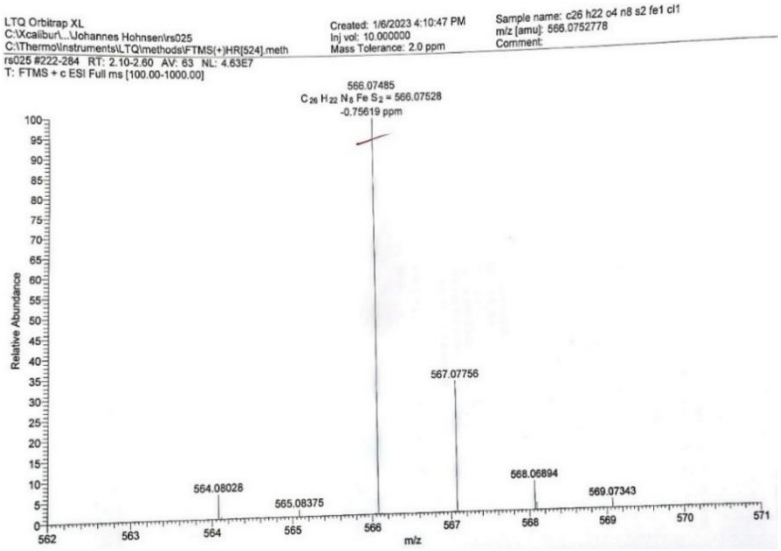


Figure 775. HR-ESI-MS of [Fe(PhPy(TSC)H_2].

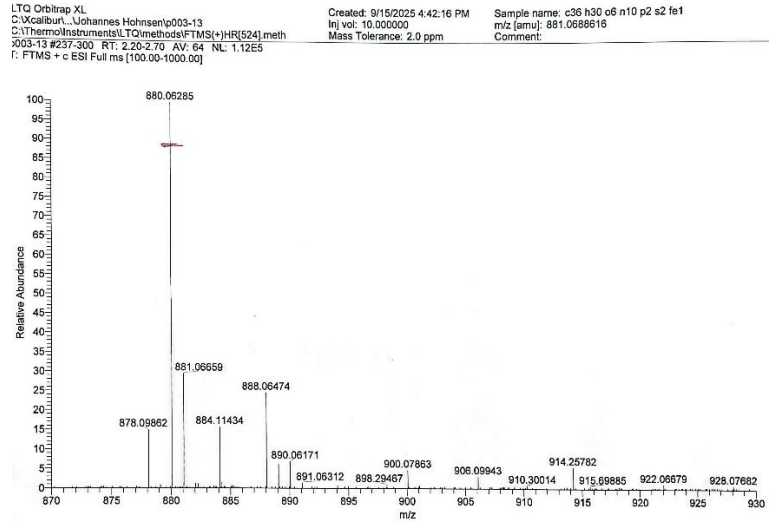


Figure 776. HR-ESI-MS of [Fe(Dipy(TSC)PhPO(OH)$_2$)$_2$]ClO_4

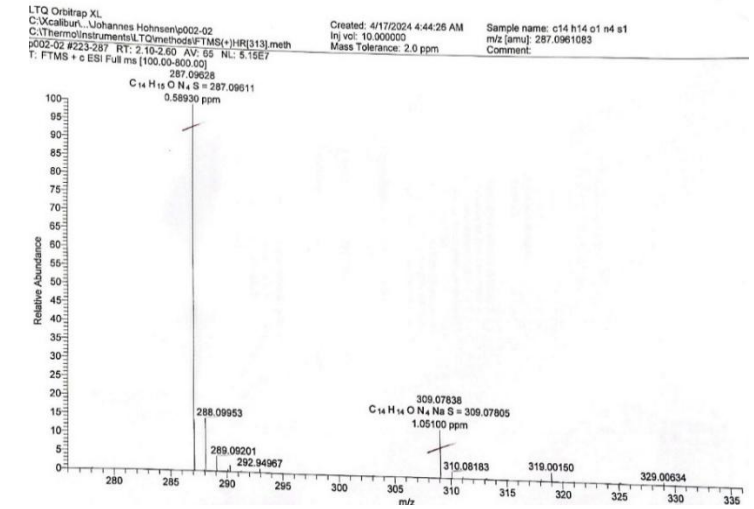


Figure 777. HR-ESI-MS of (*E*)-1-[(*p*-methoxyphenyl)(2-pyridyl)methylene]thiosemicarbazide.

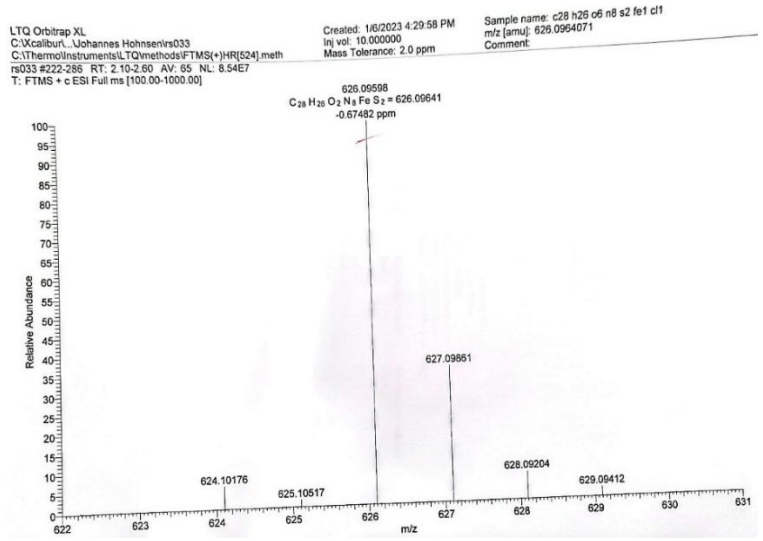


Figure 778. HR-ESI-MS of [Fe(MeOPhPy(TSC)H$_2$)$_2$].

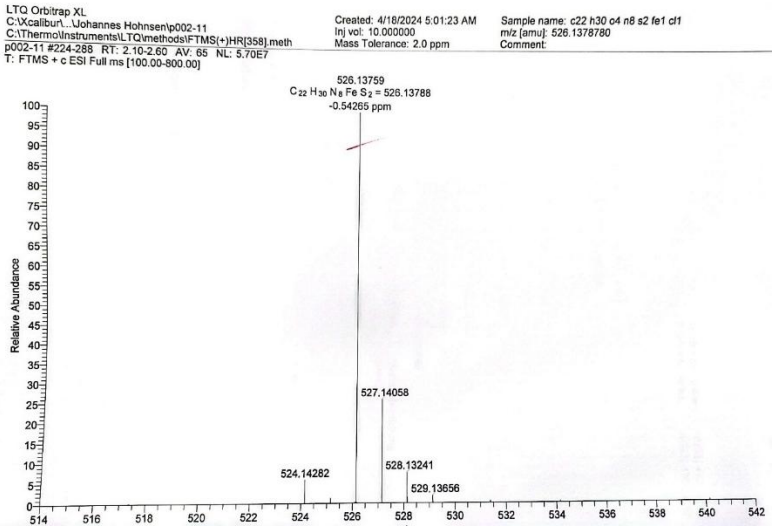


Figure 779. HR-ESI-MS of [Fe(*t*BuPy(TSC)H$_2$)]ClO$_4$.

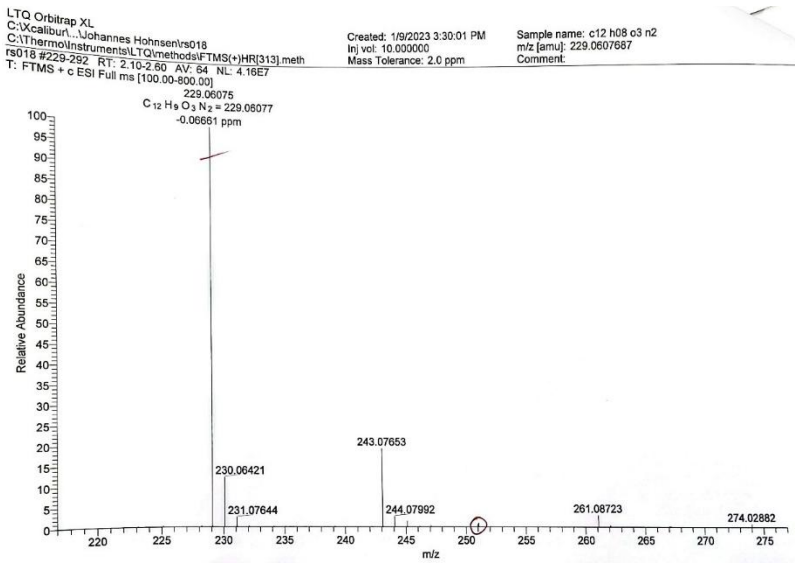


Figure 780. HR-ESI-MS of (4-nitrophenyl)(pyridin-2-yl)methanone

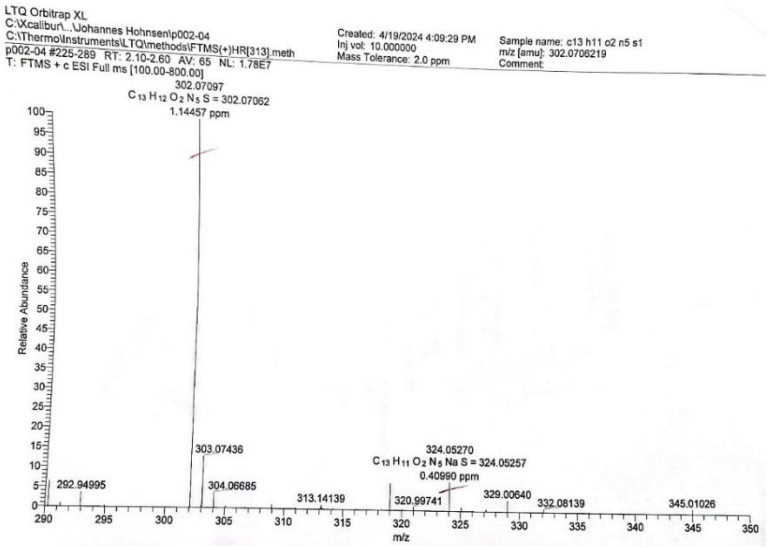


Figure 781. HR-ESI-MS of (*E*)-1-[(*p*-*N*-nitrophenyl)(2-pyridyl)methylene]thiosemicarbazide.

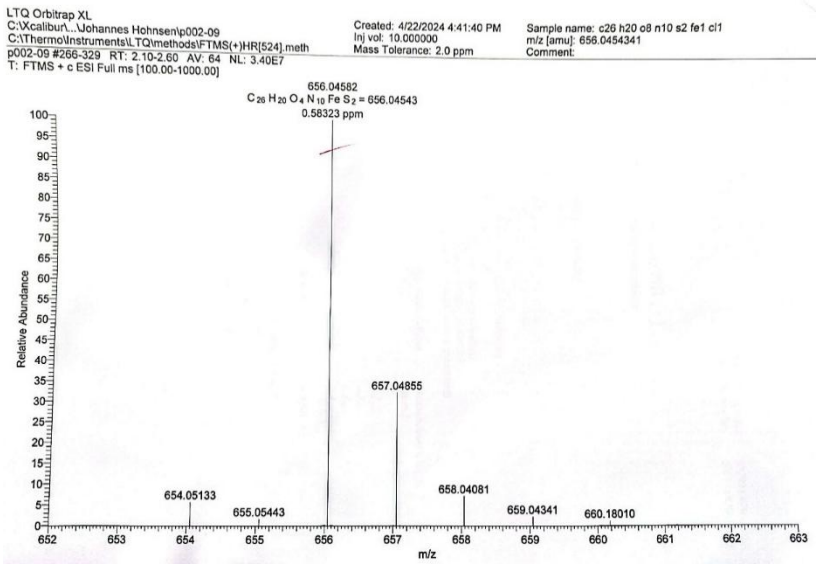


Figure 782. HR-ESI-MS of [Fe(NO$_2$PhPy(TSC)H$_2$)]ClO$_4$.

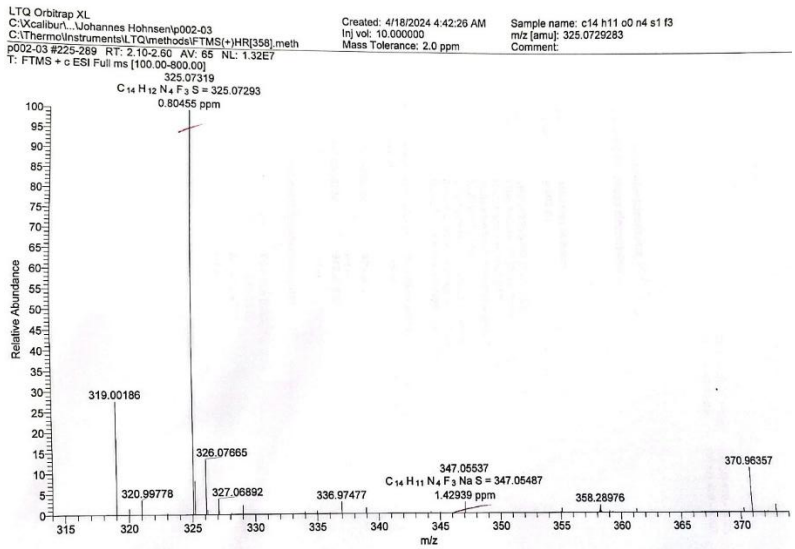


Figure 783. HR-ESI-MS of (*E*)-1-[(2-pyridyl)[*p*-(trifluoromethyl)phenyl]methylene]thiosemicarbazide.

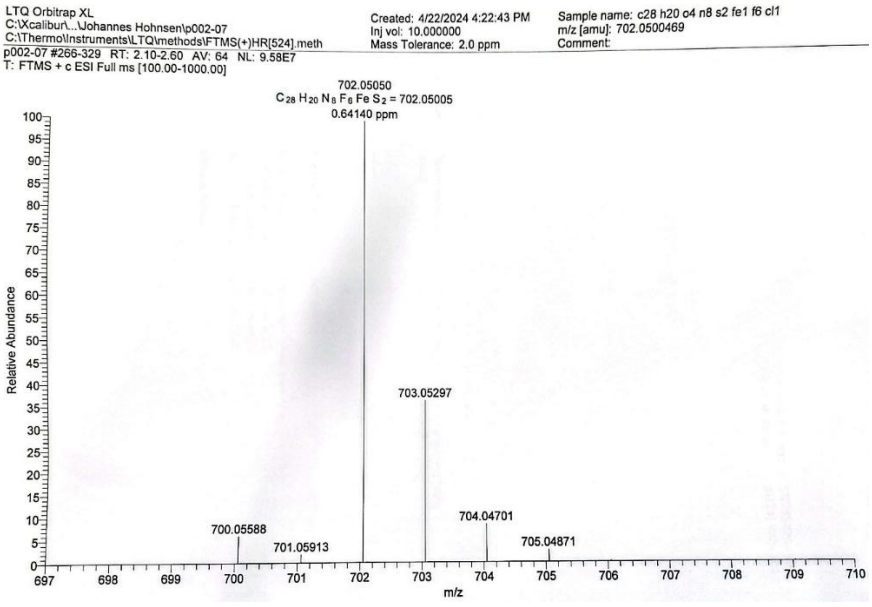


Figure 784. HR-ESI-MS of [Fe(CF_3PhPy(TSC)H_2)]ClO_4.

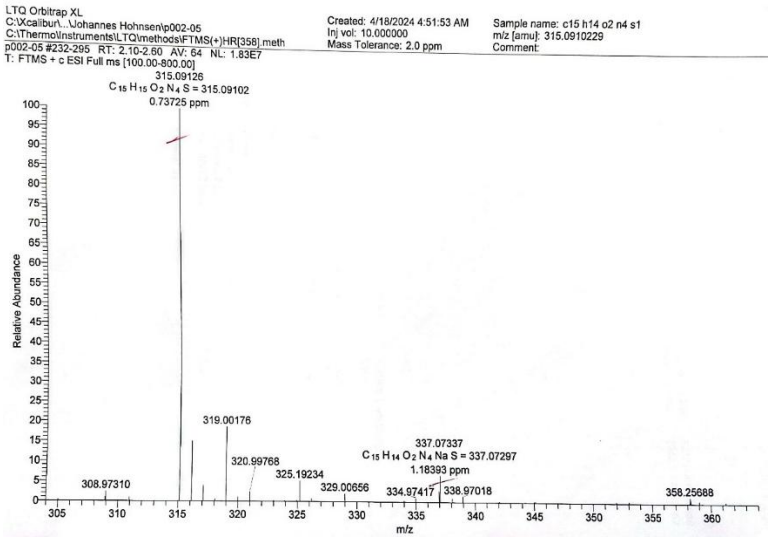


Figure 785. HR-ESI-MS of methyl *p*-[(*E*)-(2-pyridyl)thiosemicarbazidoidenemethyl]benzoate.

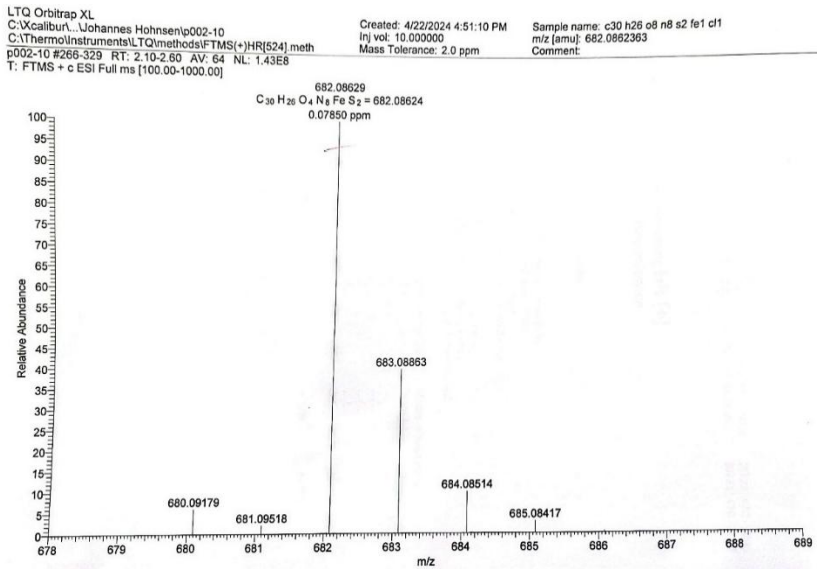


Figure 786. HR-ESI-MS of [Fe(COOMePhPy(TSC)H_2)]ClO_4.

7.2.4 HR-ESI-MS of tagged TSCs

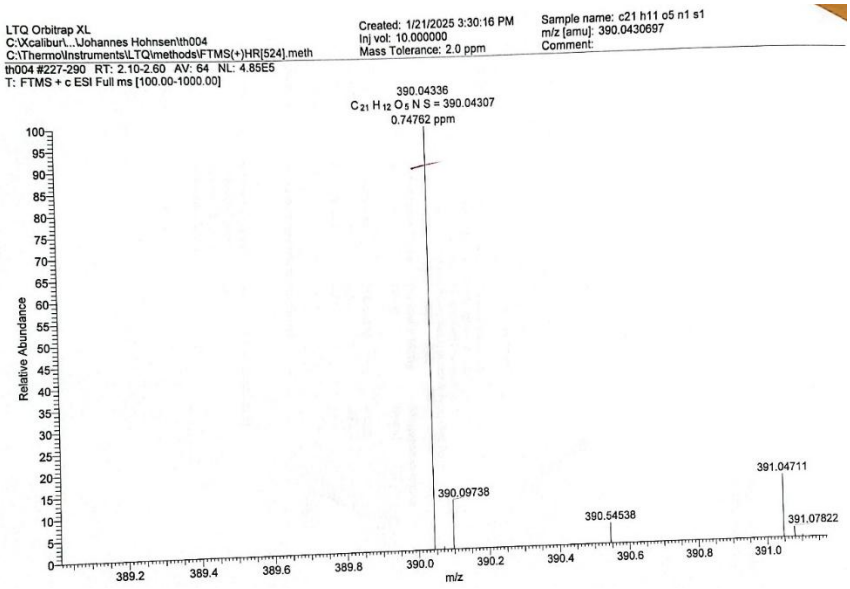


Figure 787. HR-ESI-MS of fluoresceine-5-isothiocyanate.

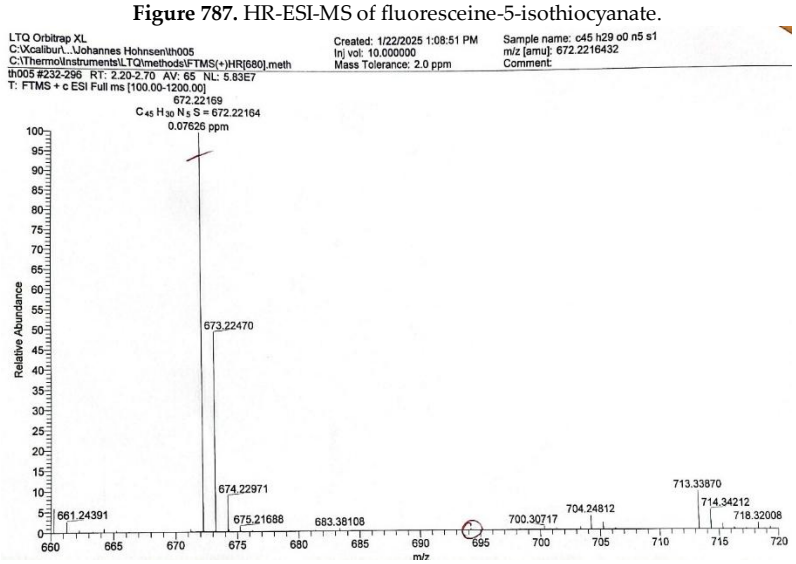


Figure 788. HR-ESI-MS of 5-(4-isothiocyanatophenyl)-10,15,20- triphenylporphyrin.

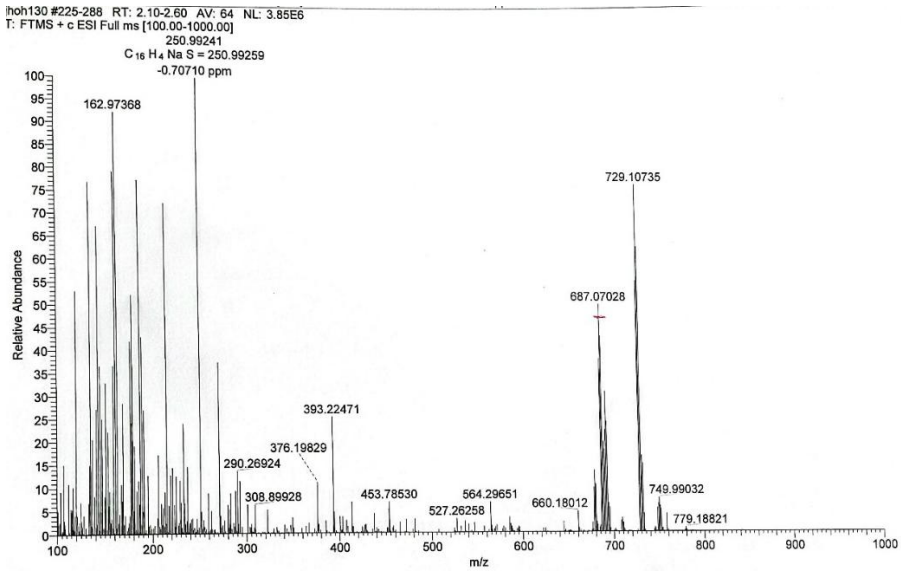


Figure 789. HR-ESI-MS of [Pt(Dipy(TSC)Pyr)Cl].

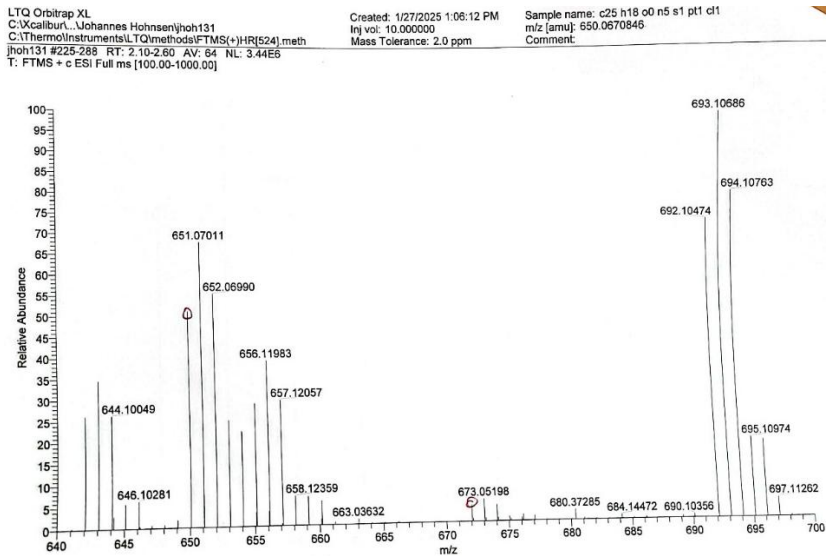


Figure 790. HR-ESI-MS of [Pt(Dipy(TSC)Flu)Cl].

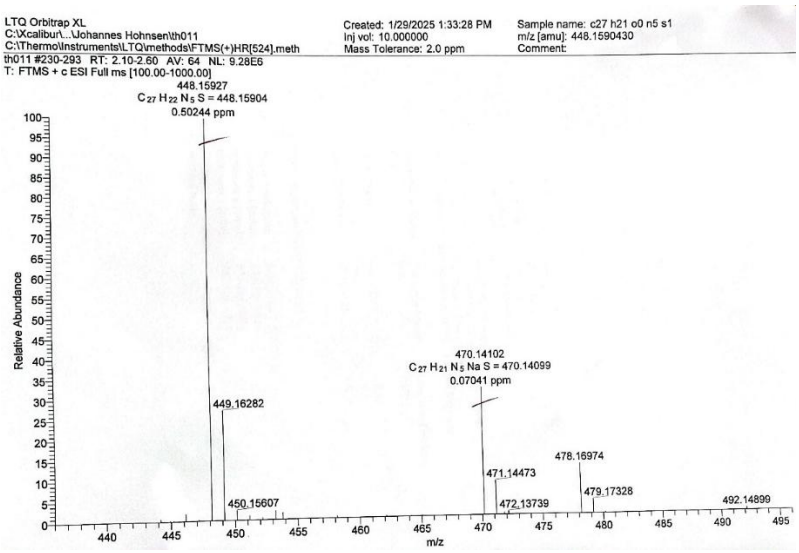


Figure 791. HR-ESI-MS of Dipy(TSC)Ant.

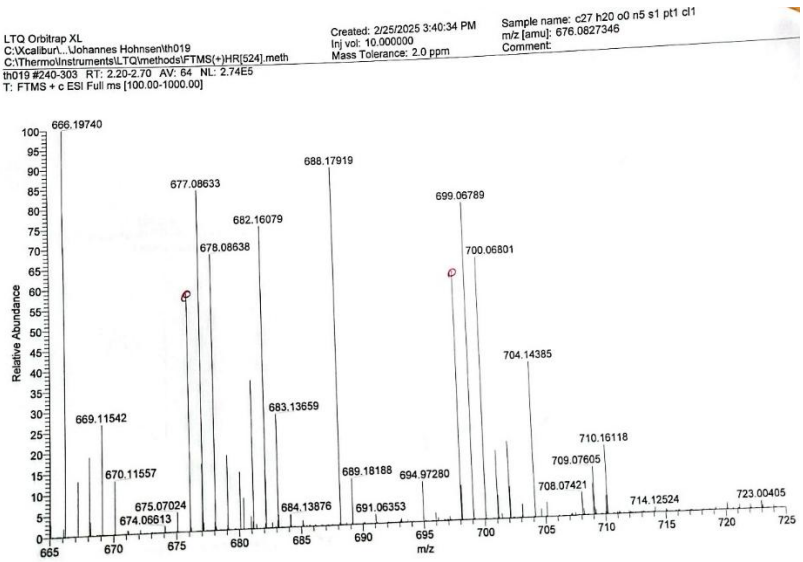


Figure 792. HR-ESI-MS of [Pt(Dipy(TSC)Ant)Cl].

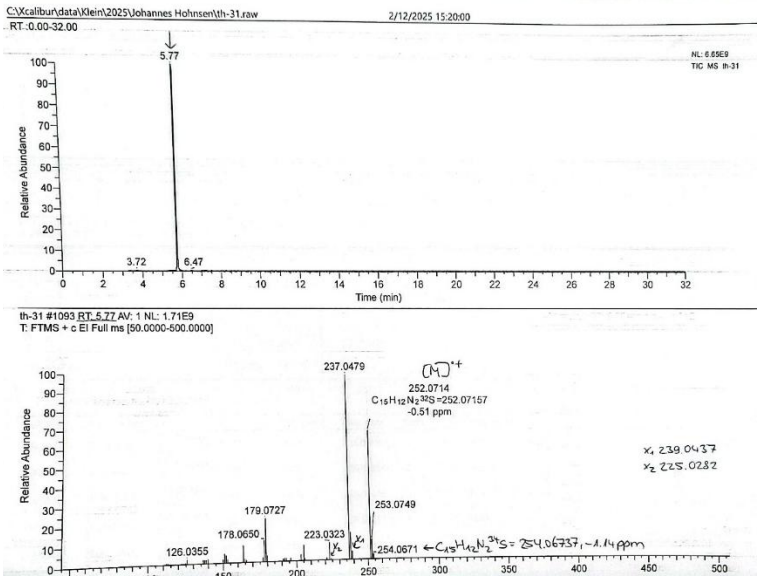


Figure 793. HR-ESI-MS of 2-isothiocyanato-9-ethylcarbazole.

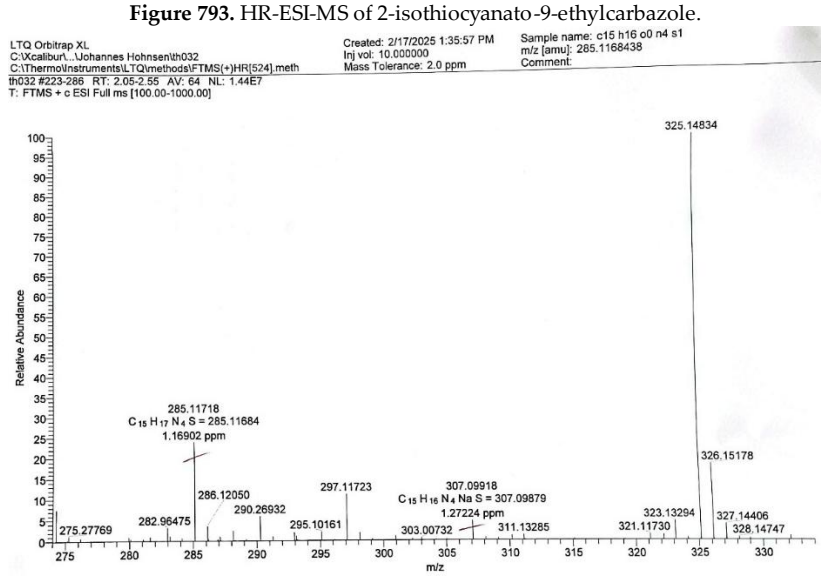


Figure 794. HR-ESI-MS of 4-(9-ethyl-2-carbazolyl)thiosemicarbazide.

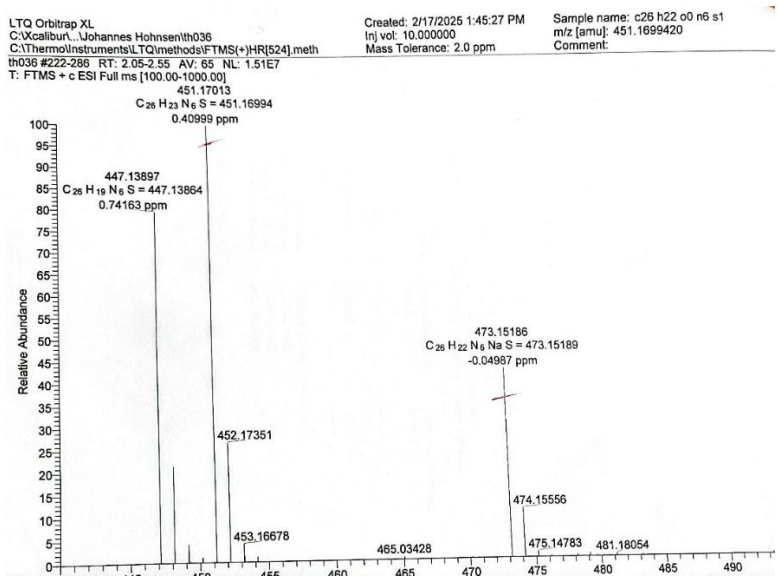


Figure 795. HR-ESI-MS of Dipy(TSC)Cbz.

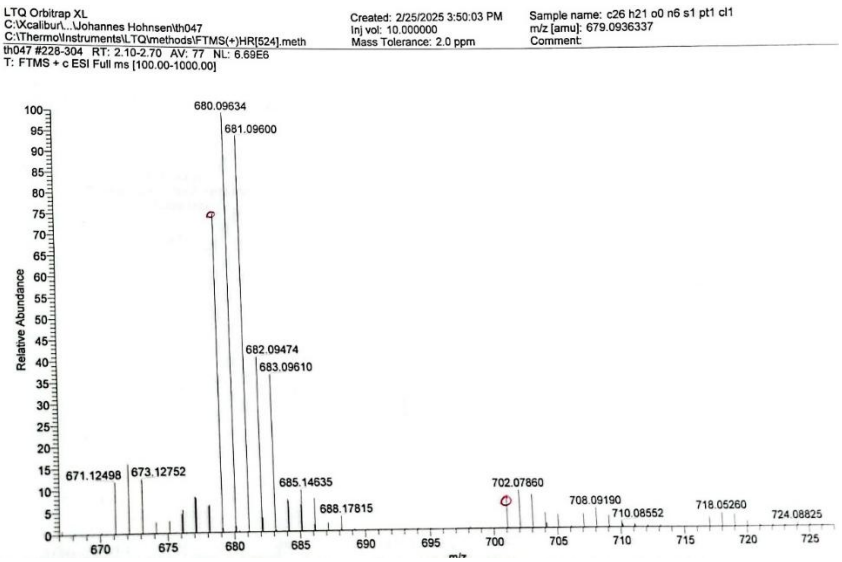


Figure 796. HR-ESI-MS of [Pt(Dipy(TSC)Cbz)Cl].

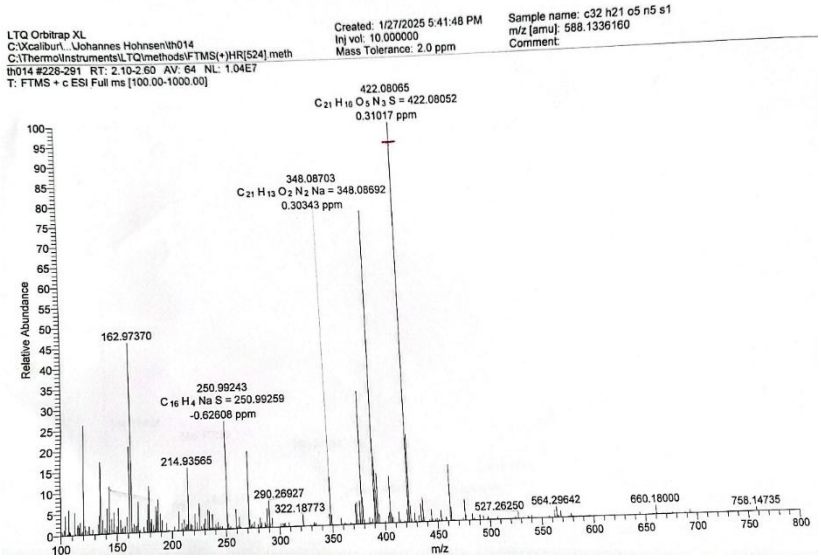


Figure 797. HR-ESI-MS of 2-(6-Hydroxy-3-oxo-3*H*-xanthen-9-yl)-5-thiosemicarbazidobenzoic acid.

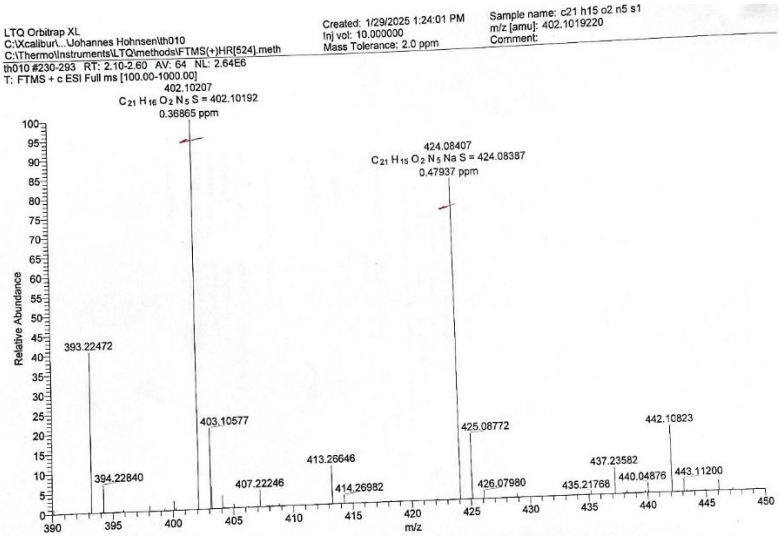


Figure 798. HR-ESI-MS of Dipy(TSC)Cou.

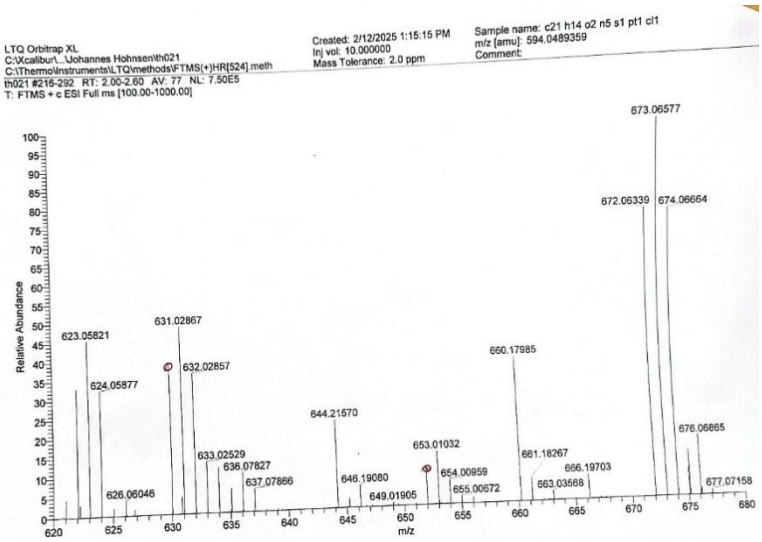


Figure 799. HR-ESI-MS of [Pt(Dipy(TSC)Cou)Cl].

7.2.5 HR-ESI-MS of amphiphilic TSCs

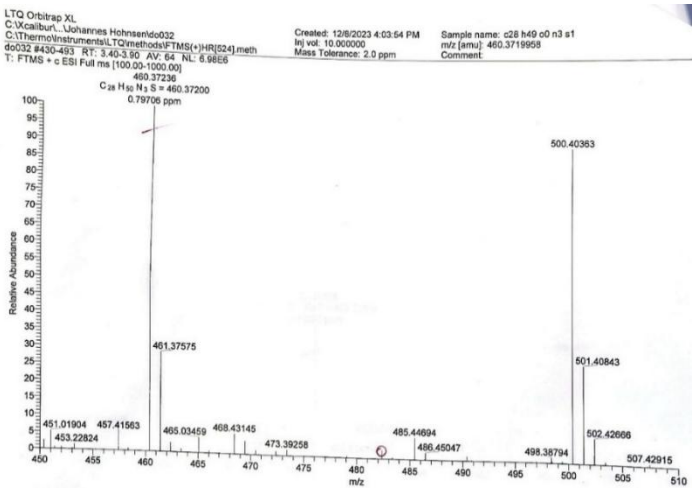


Figure 800. HR-ESI-MS of *N*-hydrazidecarbothio[(1*S*,2*R*,5*S*,10*S*,11*S*,14*R*,15*R*)-14-[(1*R*)-1,5-dimethylhexyl]-2,15-dimethyltetracyclo [8.7.0.0^{2,7}.0^{11,15}]heptadec-7-en-5-yl]amine.

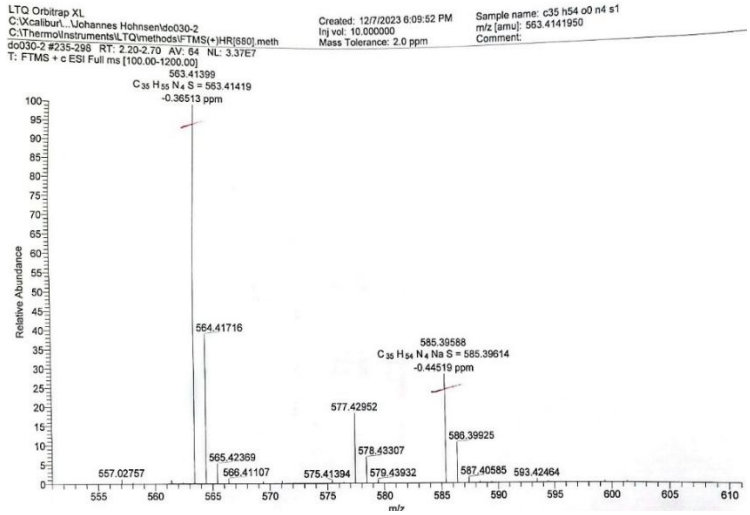


Figure 801. HR-ESI-MS of [(1*S*,2*R*,5*S*,10*S*,11*S*,14*R*,15*R*)-14-[(1*R*)-1,5-dimethylhexyl]-2,15-dimethyltetracyclo [8.7.0.0^{27}.0^{11,15}] heptadec-7-en-5-ylamino][(1*Z*)-1-(pyridin-2-yl)eth-1-ylideneamino]carbothioamide.

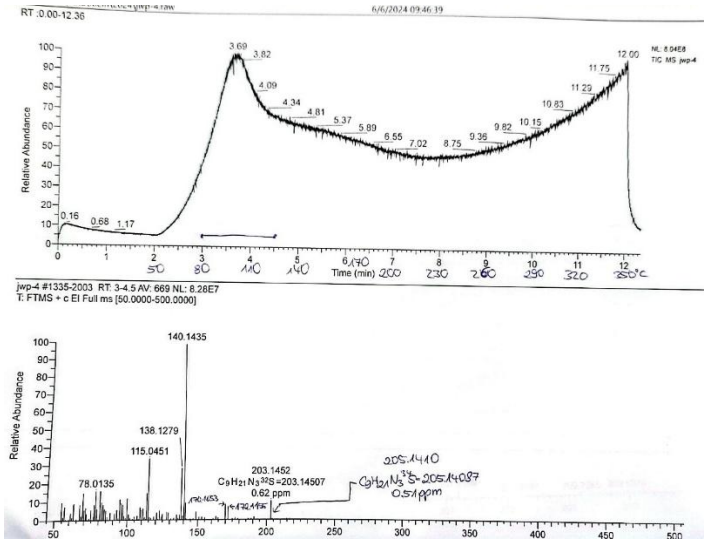


Figure 802. HR-ESI-MS of 4-octylthiosemicarbazide.

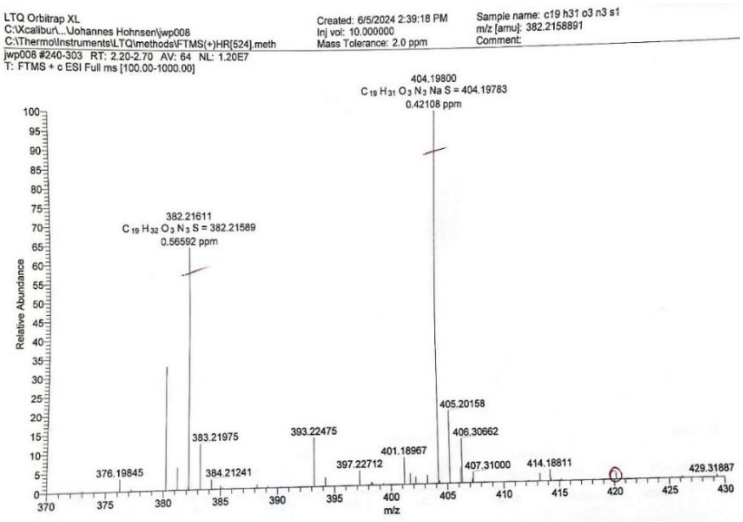


Figure 803. HR-ESI-MS of (*E*)-4-octyl-1-[(2,3,4-trimethoxyphenyl)methylene]thiosemicarbazide.

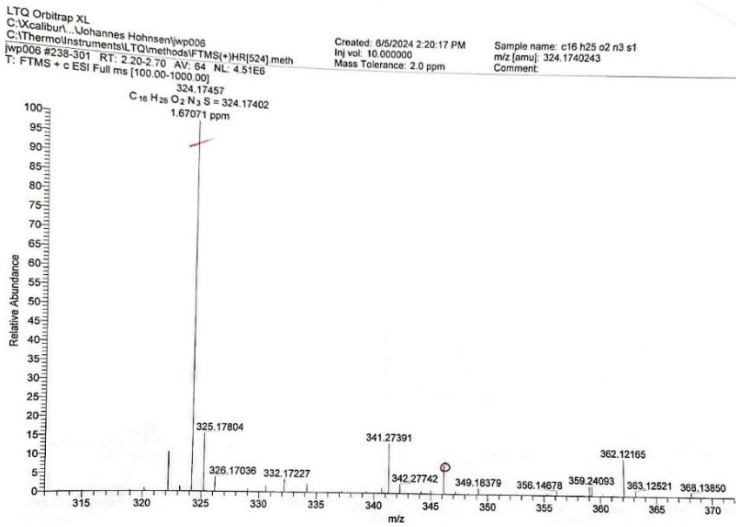


Figure 804. HR-ESI-MS of 2-[(*E*)-(4-octylthiosemicarbazidoidene)methyl]hydroquinone.

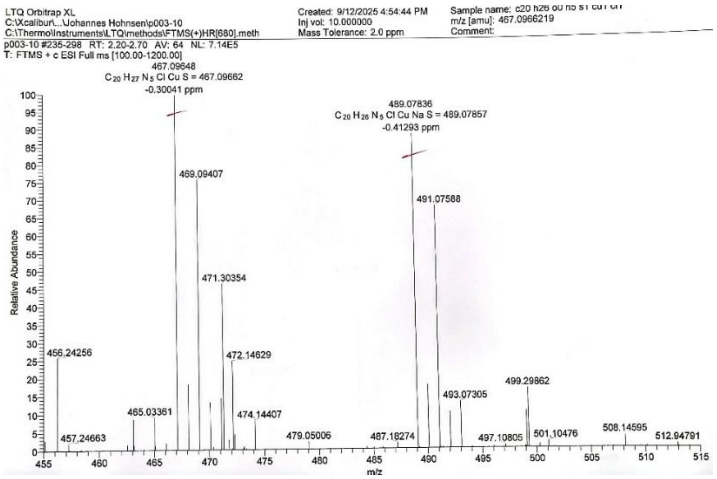


Figure 805. HR-ESI-MS of [Cu(Dipy(TSC)Oct)Cl].

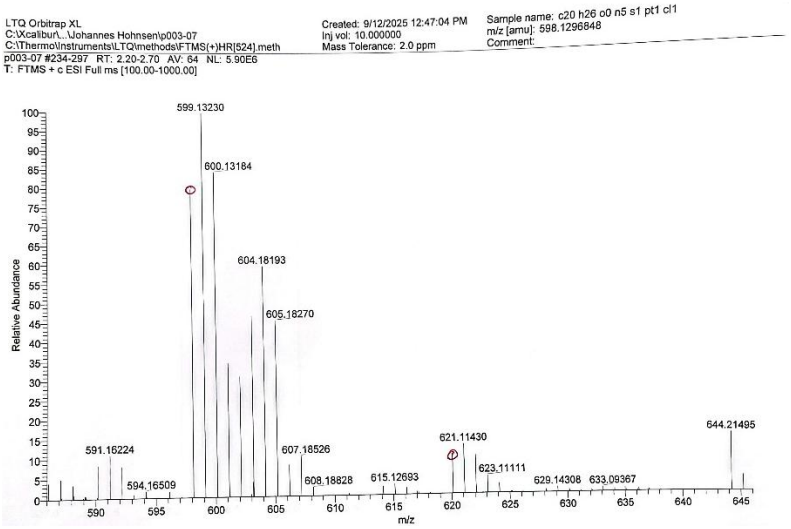


Figure 806. HR-ESI-MS of [Pt(Dipy(TSC)Oct)Cl]

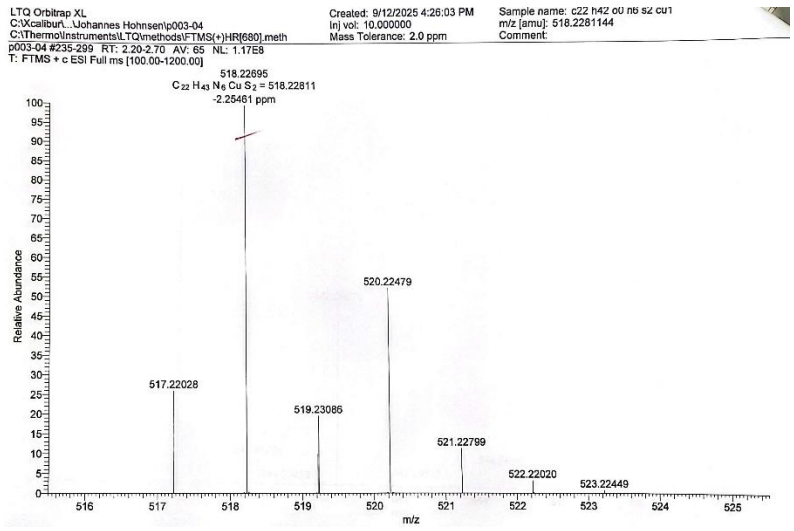


Figure 807. HR-ESI-MS of [Cu(dime(bis-TSC)Oct)].

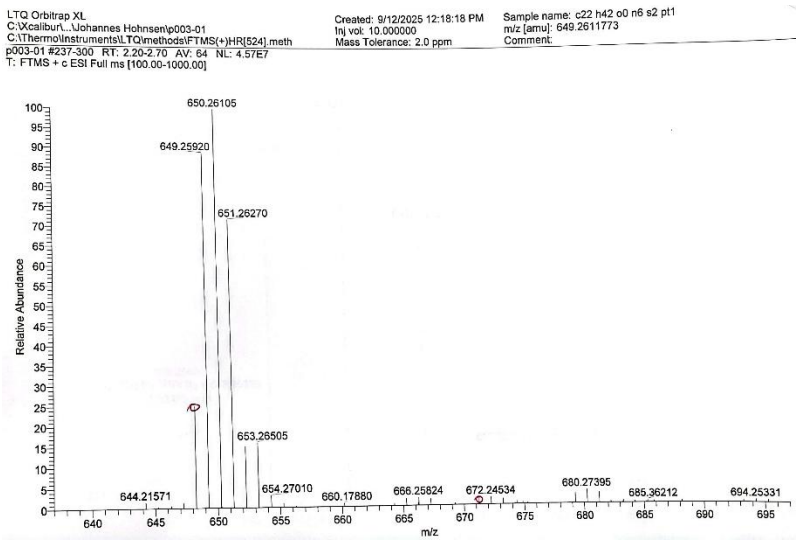


Figure 808. HR-ESI-MS of [Pt(dime(bis-TSC)Oct)].

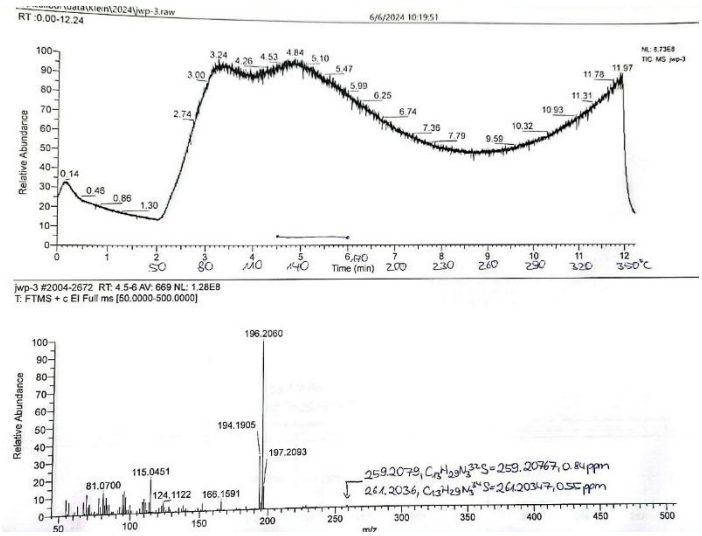


Figure 809. HR-ESI-MS of 4-dodecylthiosemicarbazide.

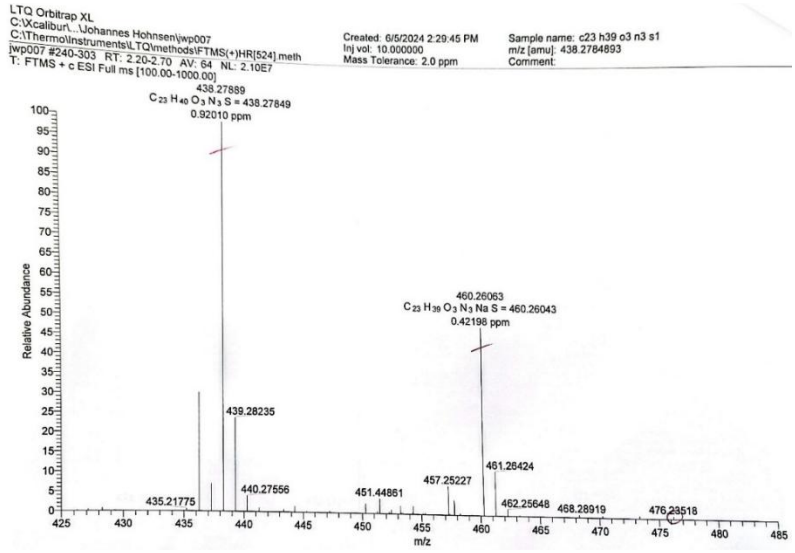


Figure 810. HR-ESI-MS of (*E*)-4-dodecyl-1-[(2,3,4-trimethoxyphenyl)methylene]-thiosemicarbazide.

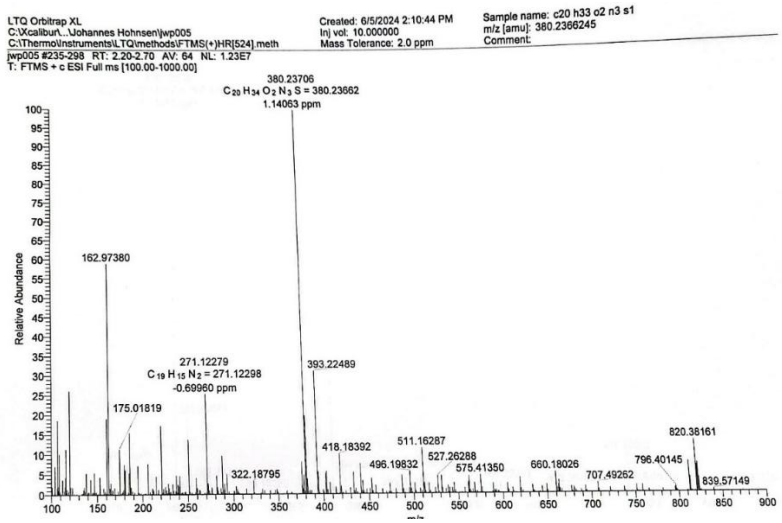


Figure 811. HR-ESI-MS of 2-[(*E*)-(4-dodecylthiosemicarbazidoidene)methyl]hydroquinone.

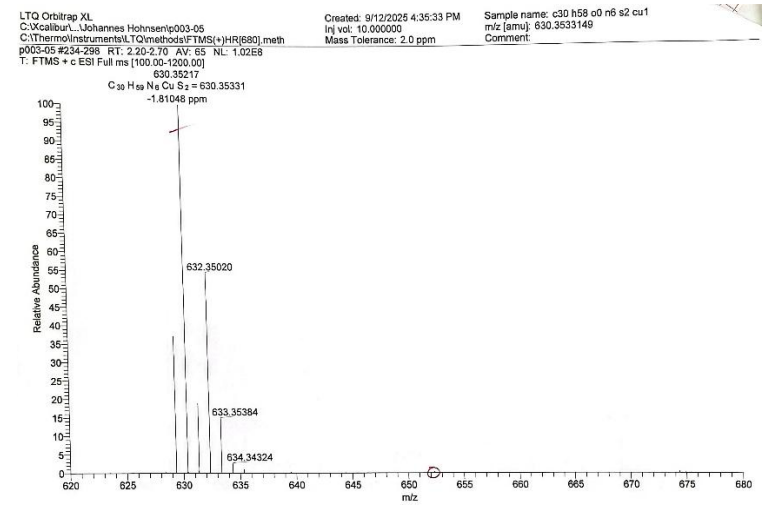


Figure 812. HR-ESI-MS of [Cu(dime(bis-TSC)Dode)].

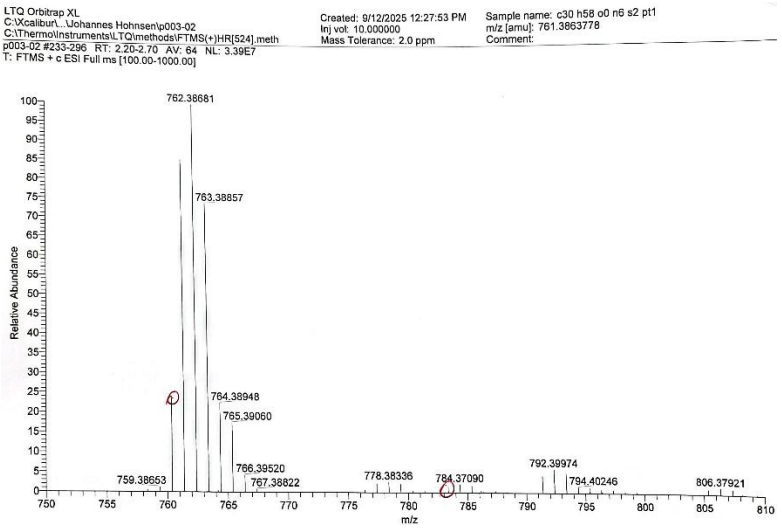


Figure 813. HR-ESI-MS of [Pt(dime(bis-TSC)Dode)].

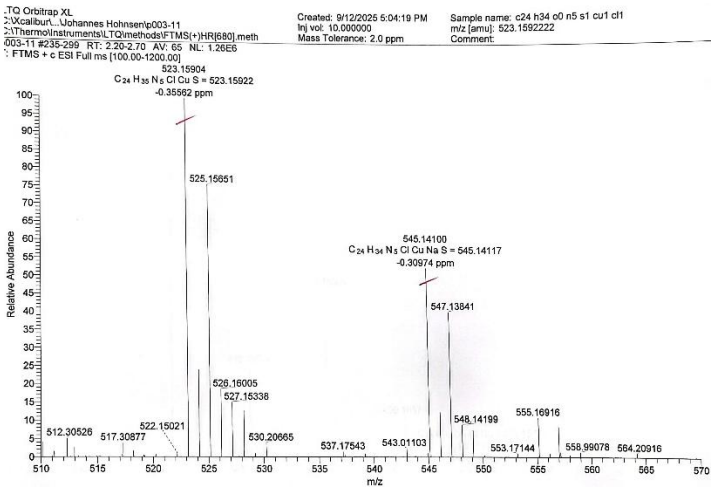


Figure 814. HR-ESI-MS of [Cu(Dipy(TSC)Dode)Cl].

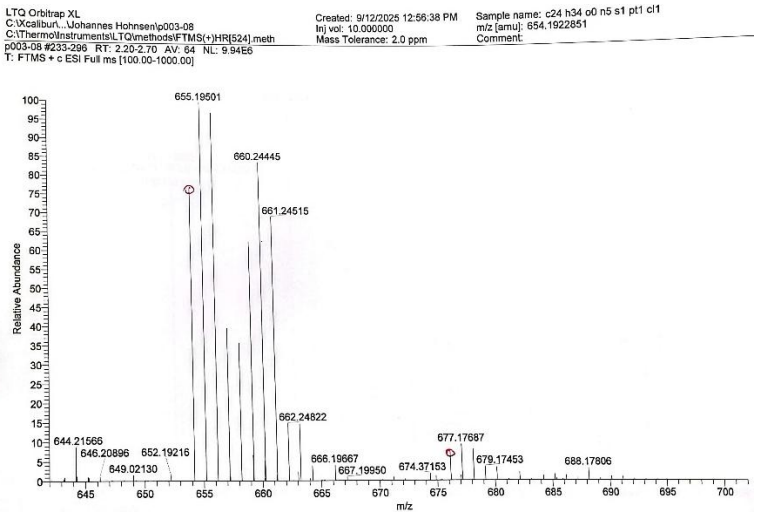


Figure 815. HR-ESI-MS of [Pt(Dipy(TSC)Dode)Cl].

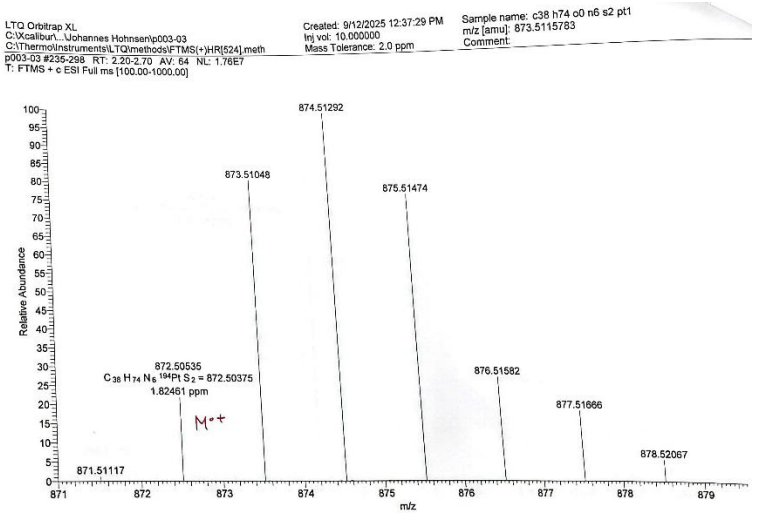


Figure 816. HR-ESI-MS of [Pt(dime(bis-TSC)Hexde)].

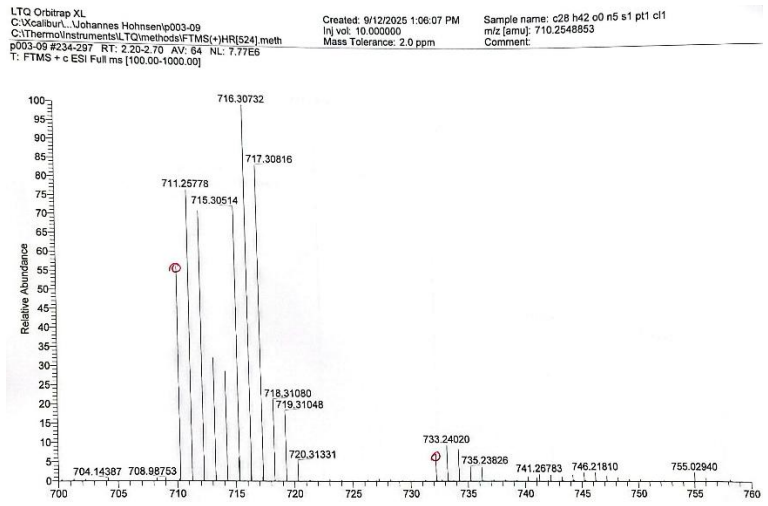


Figure 817. HR-ESI-MS of [Pt(Dipy(TSC)Hexde)Cl].

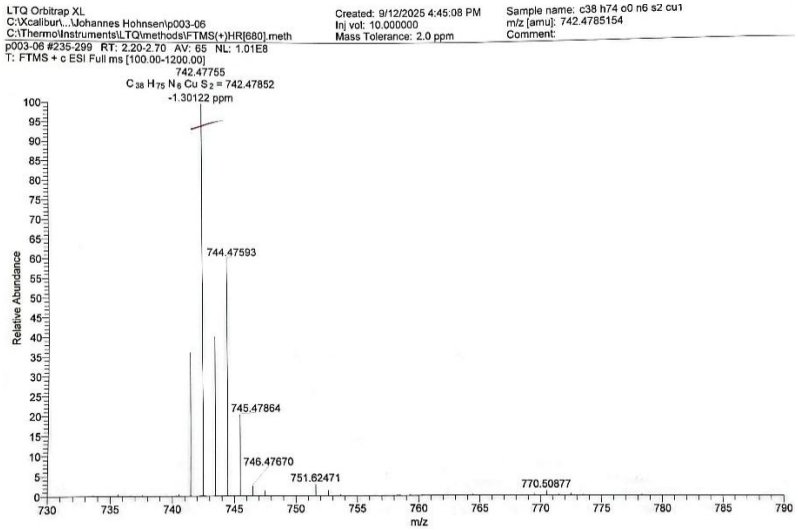


Figure 818. HR-ESI-MS of [Cu(dime(bis-TSC)Hexde)].

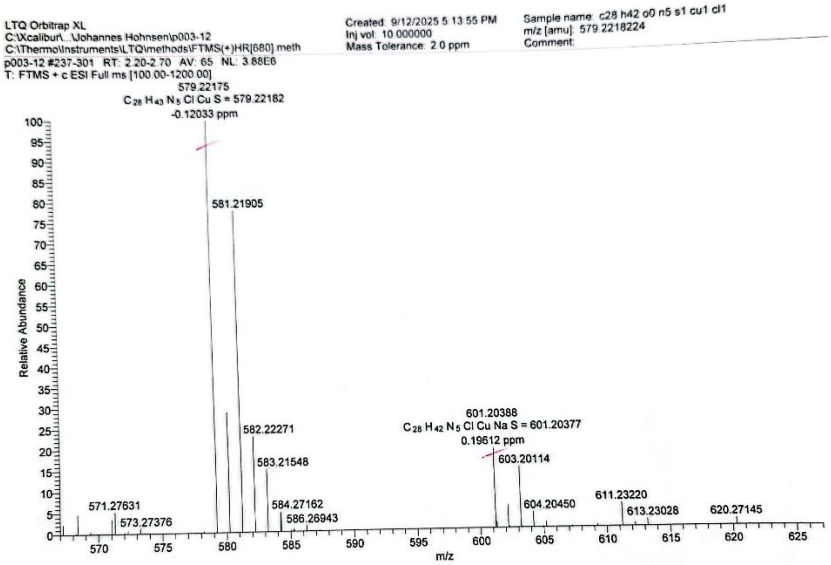


Figure 819. HR-ESI-MS of [Cu(Dipy(TSC)Hexde)Cl].

7.3 UV/Vis absorption spectroscopy

7.3.1 UV/Vis absorption spectra of *N*4 functionalized TSC with anchor groups for nano -and bioconjugation

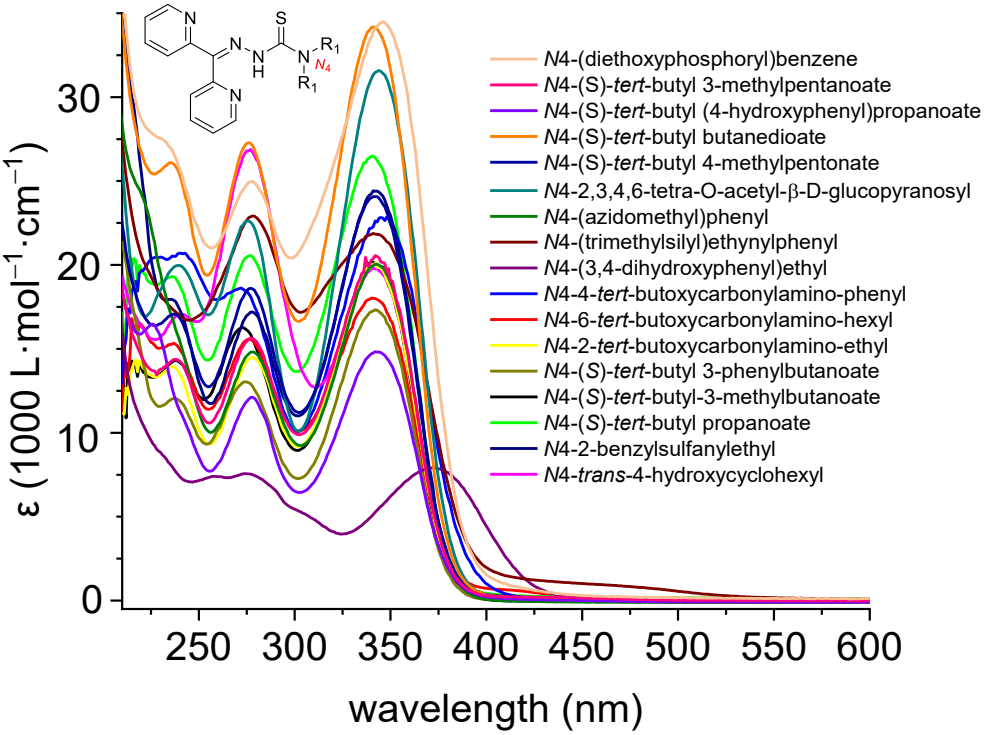


Figure 820. UV/Vis absorption spectra of dipyridyl ketone TSCs measured in MeCN.

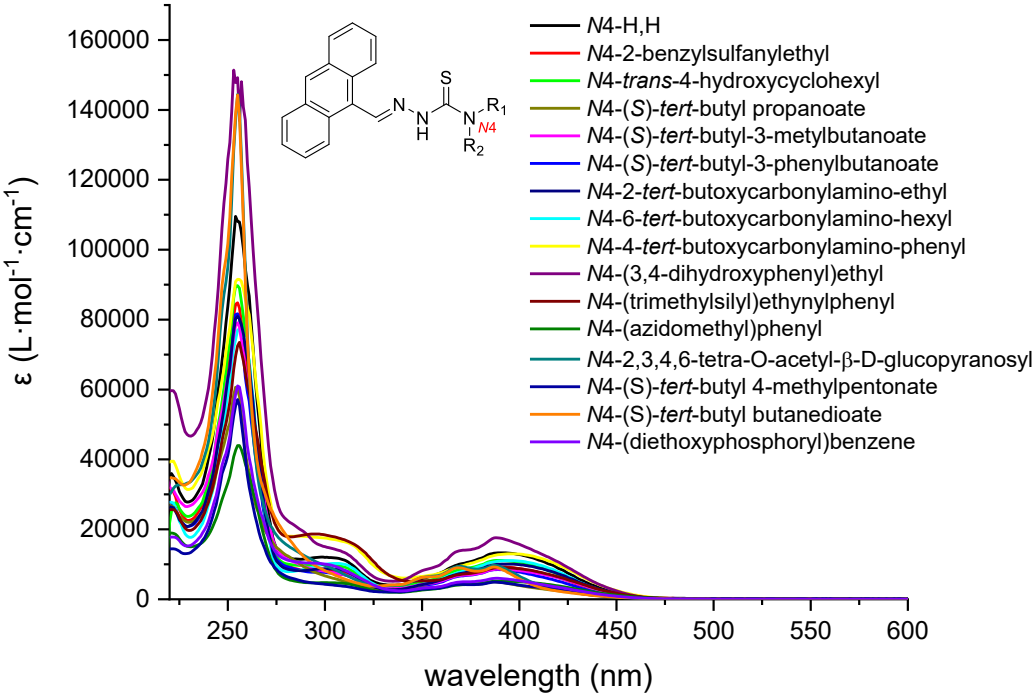


Figure 821. UV/Vis absorption spectroscopy of 9-anthraaldehyde TSCs measured in MeCN.

7.3.2 UV/Vis absorption spectra of amphiphilic TSCs

In MeOH:

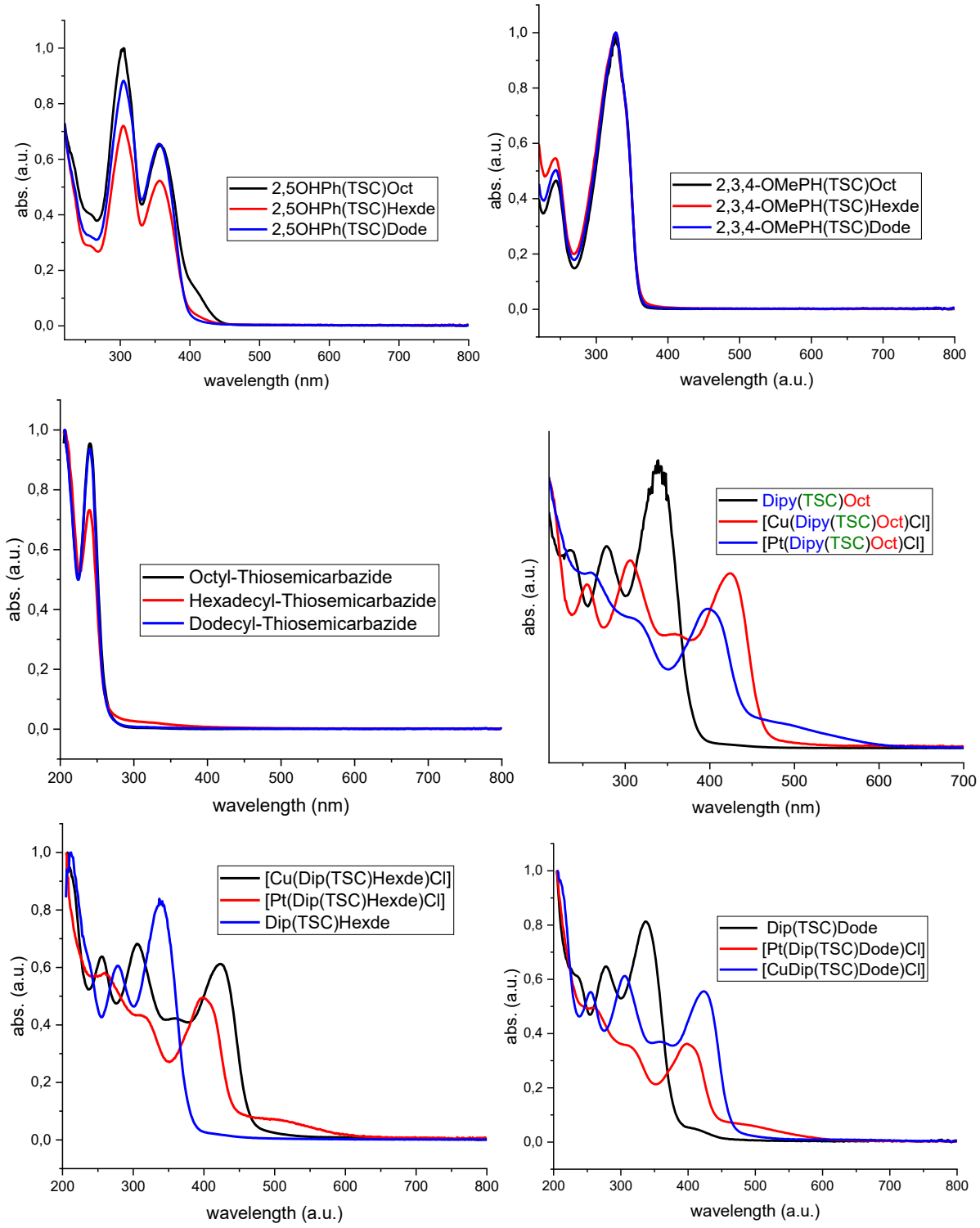


Figure 822. UV/Vis absorption spectra of amphiphilic TSCs measured in MeOH. Top, left: 2,5-OHPh(TSC)Oct/Dode/Hexde. Top, right: 2,3,4-OMePh(TSC)Oct/Dode/Hexde. Middle, left: Octyl/dodecyl/hexadecyl thiosemicarbazides. Middle, right: Dipy(TSC)oct and the Cu(II) and Pt(II) complexes. Bottom, left: Dipy(TSC)Hexde and the Cu(II) and Pt(II) complexes. Bottom, right: Dipy(TSC)Dode and the Cu(II) and Pt(II) complexes

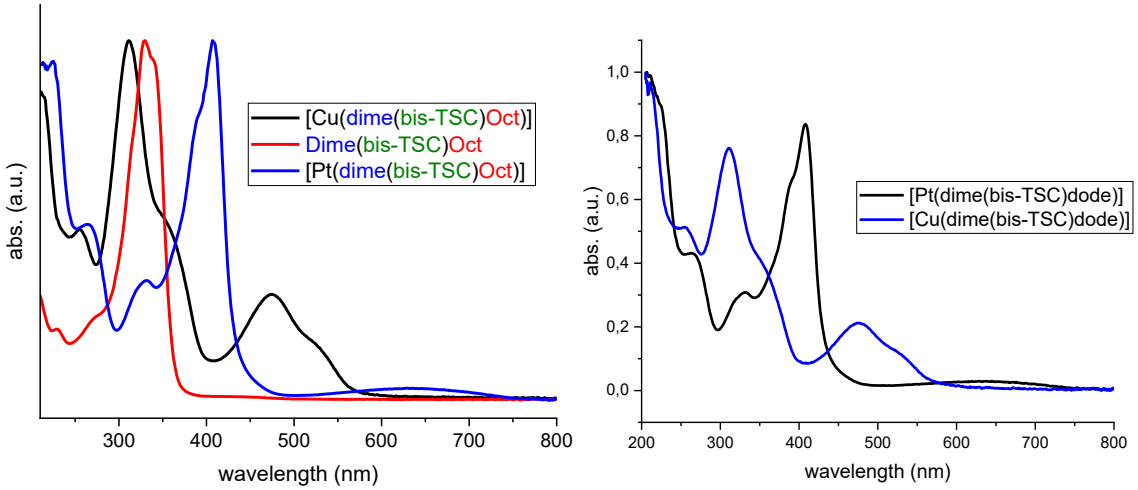


Figure 823. UV/Vis absorption spectra of amphiphilic TSCs measured in MeOH. Left: Dime(bis-TSC)Oct and the Cu(II) and Pt(II) complex. Right: [Pt(dime(bis-TSC)Dode)] and [Cu(dime(bis-TSC)Dode)].

In pentane:

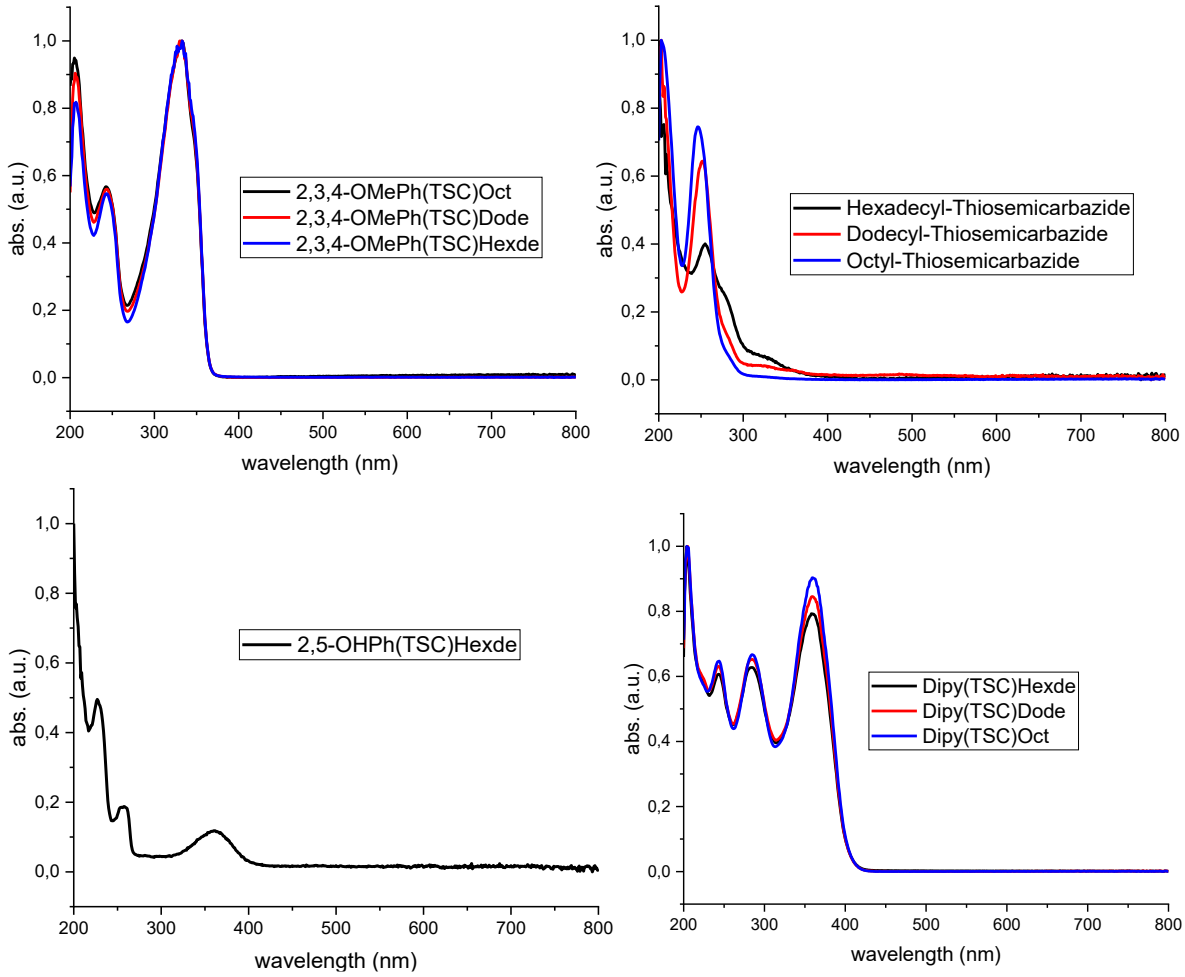


Figure 824. UV/Vis absorption spectra of amphiphilic TSCs measured in pentane. Up, left: 2,3,4-OMePh(TSC)Oct/Dode/Hexde. Up, right: Octyl/dodecyl/hexadecyl thiosemicarbazides. Down, left: 2,5-OhPh(TSC) Hexde. Down, right: Dipy(TSC)Oct/Dode/Hexde.

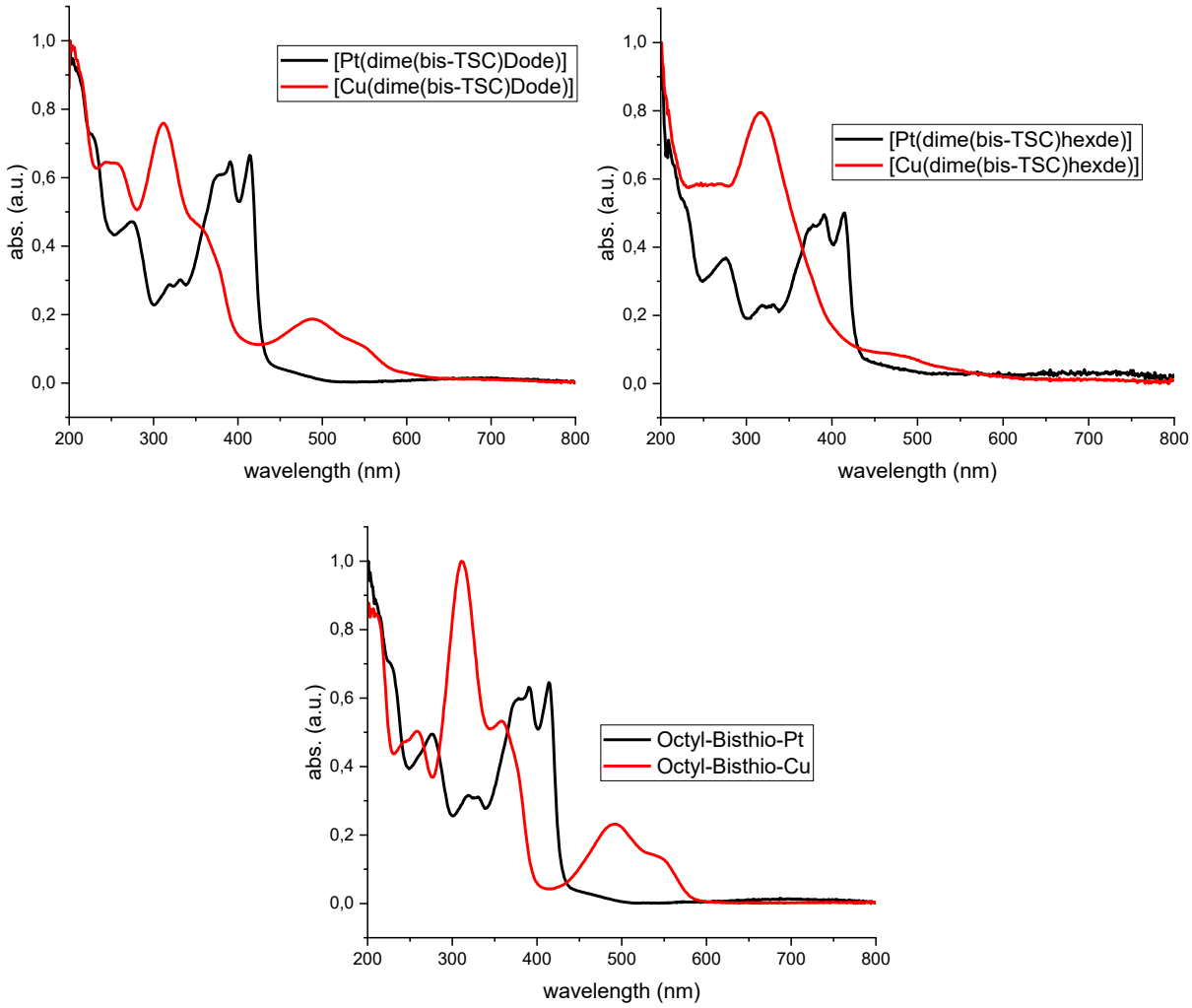


Figure 825. UV/Vis absorption spectra of amphiphilic TSCs measured in pentane. Up, left: [Pt(dime(bis-TSC)Dode)] and [Cu(dime(bis-TSC)Dode)]. Up, right: [Pt(dime(bis-TSC)Hexde)] and [Cu(dime(bis-TSC)Hexde)]. Down: [Pt(dime(bis-TSC)Oct)] and [Cu(dime(bis-TSC)Oct)].

In toluene

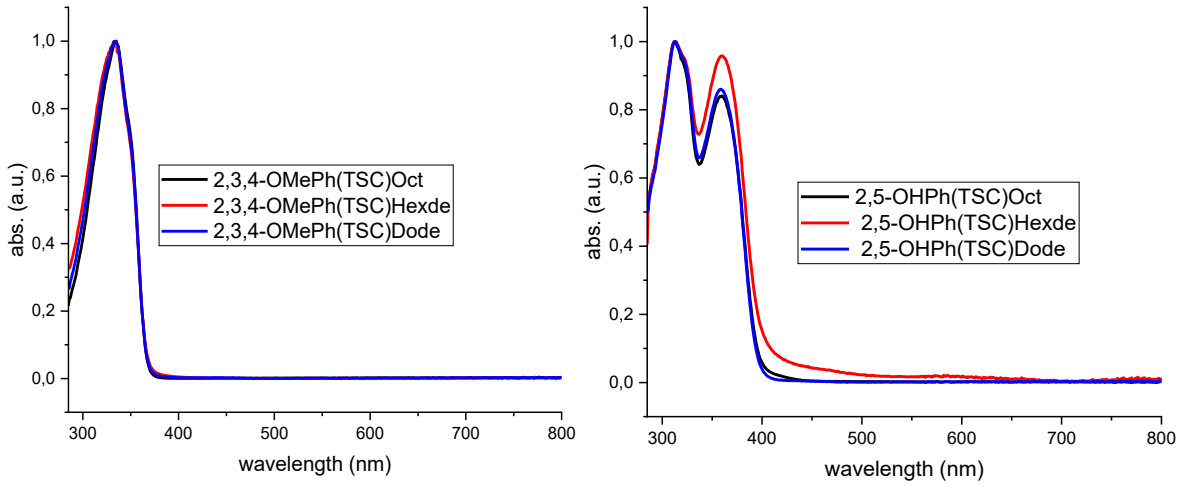


Figure 826. UV/Vis absorption spectra of amphiphilic TSCs measured in toluene. Left: 2,3,4-OMePh(TSC)Oct/Dode/Hexde. Right: 2,5-OHPh(TSC)Oct/Dode/Hexde.

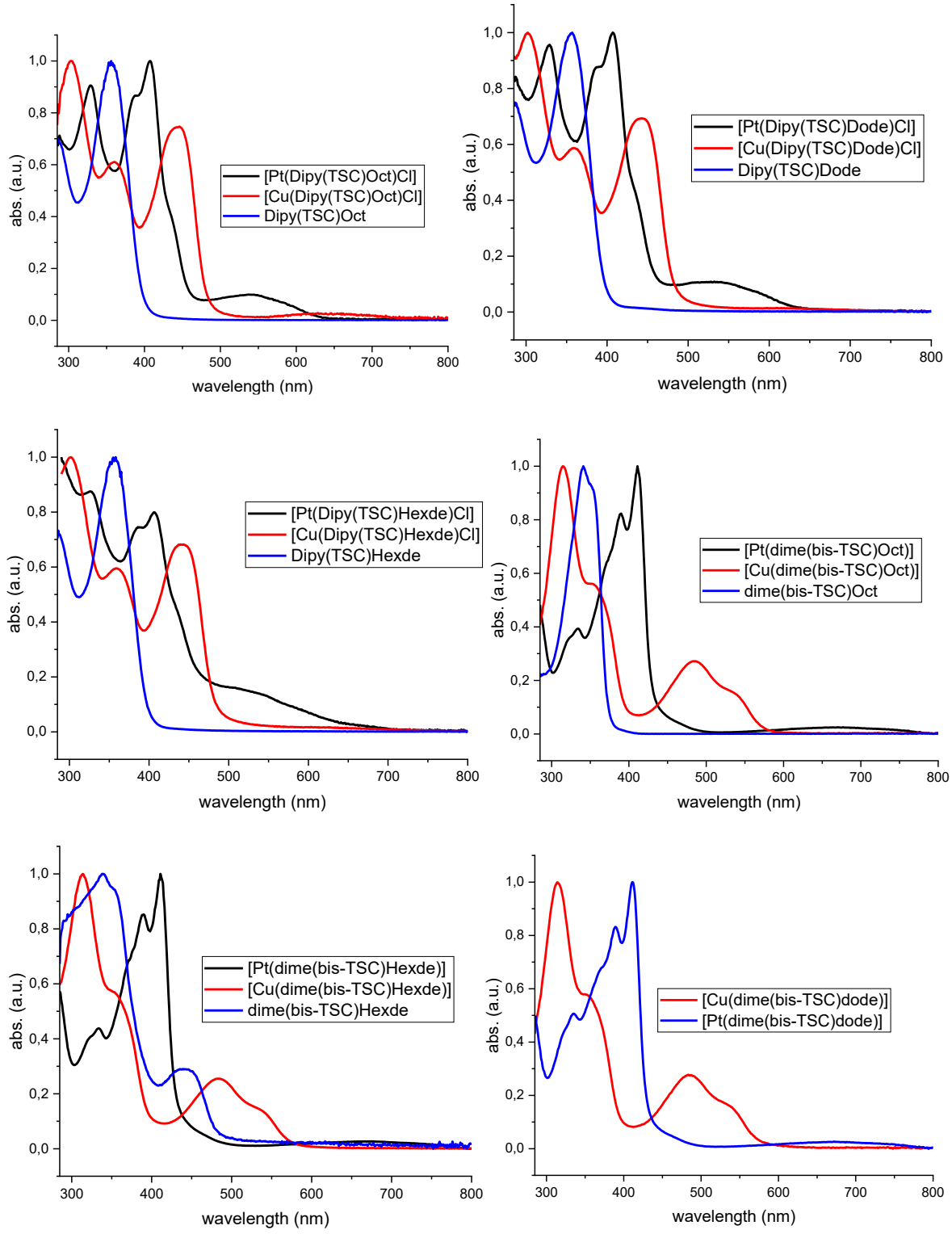


Figure 827. UV/Vis absorption spectra of amphiphilic TSCs measured in toluene. Up, left: Dipy(TSC)Oct and the Pt(II) and Cu(II) complex. Up, right: Dipy(TSC)Dode and the Pt(II) and Cu(II) complex. Middle, left: Dipy(TSC)Hexde and the Pt(II) and Cu(II) complex. Middle right: Dime(bis-TSC)Oct and the Pt(II) and Cu(II) complex. Bottom, left: Dime(bis-TSC)Hexde and the Pt(II) and Cu(II) complex. Dime(bis-TSC)Dode and the Pt(II) and Cu(II) complex.

In water:

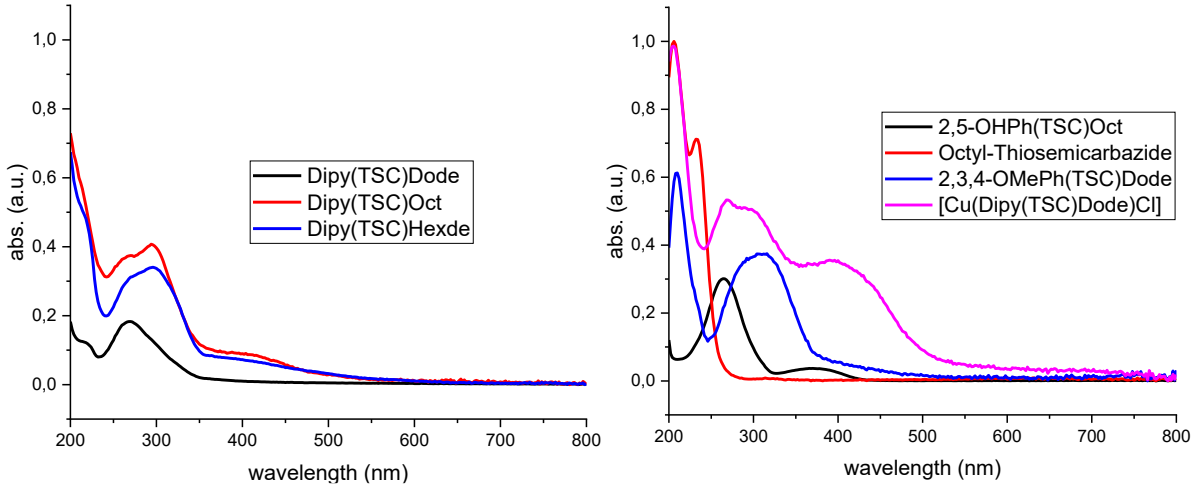


Figure 828. UV/Vis absorption spectra of amphiphilic TSCs measured in water. Left: Dipy(TSC)Oct/Dode/Hexde. Right 2,5-OhPh(TSC)Oct, Octly-Thiosemicarbazide, 2,3,4-OMePh(TSC)Dode, [Cu(dipy(TSC)Dode)Cl]

7.3.3 UV/Vis absorption spectrum of tagged TSCs

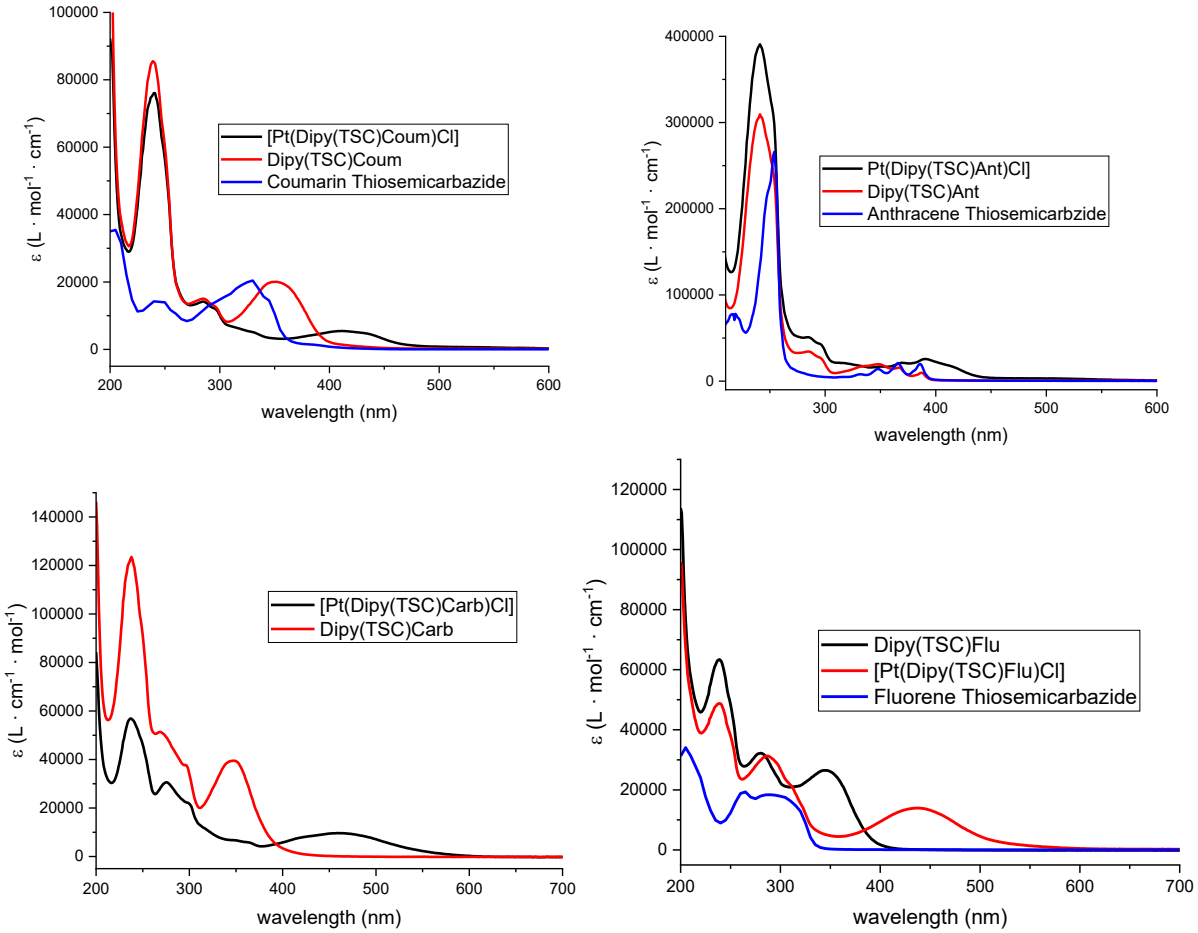


Figure 829. UV/Vis absorption spectrum of tagged TSCs and their corresponding Pt(II) complexes and thiosemicarbazized (derived from coumarin, anthracene, carbazole and fluorene). Measured in MeCN.

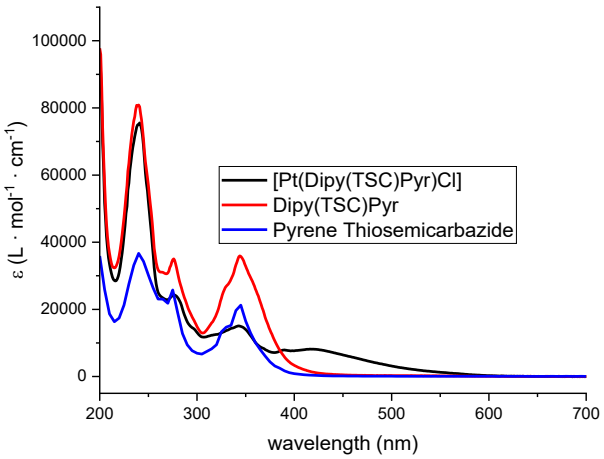


Figure 830. UV/Vis absorption spectra of Dipy(TSC)Pyr and the corrwsponding Pt(II) complex and thiosemicarbazide. Measured in MeCN.

7.3.4 UV/Vis absorption spectra of α-pyridyl TSCs and their Fe(III) complexes

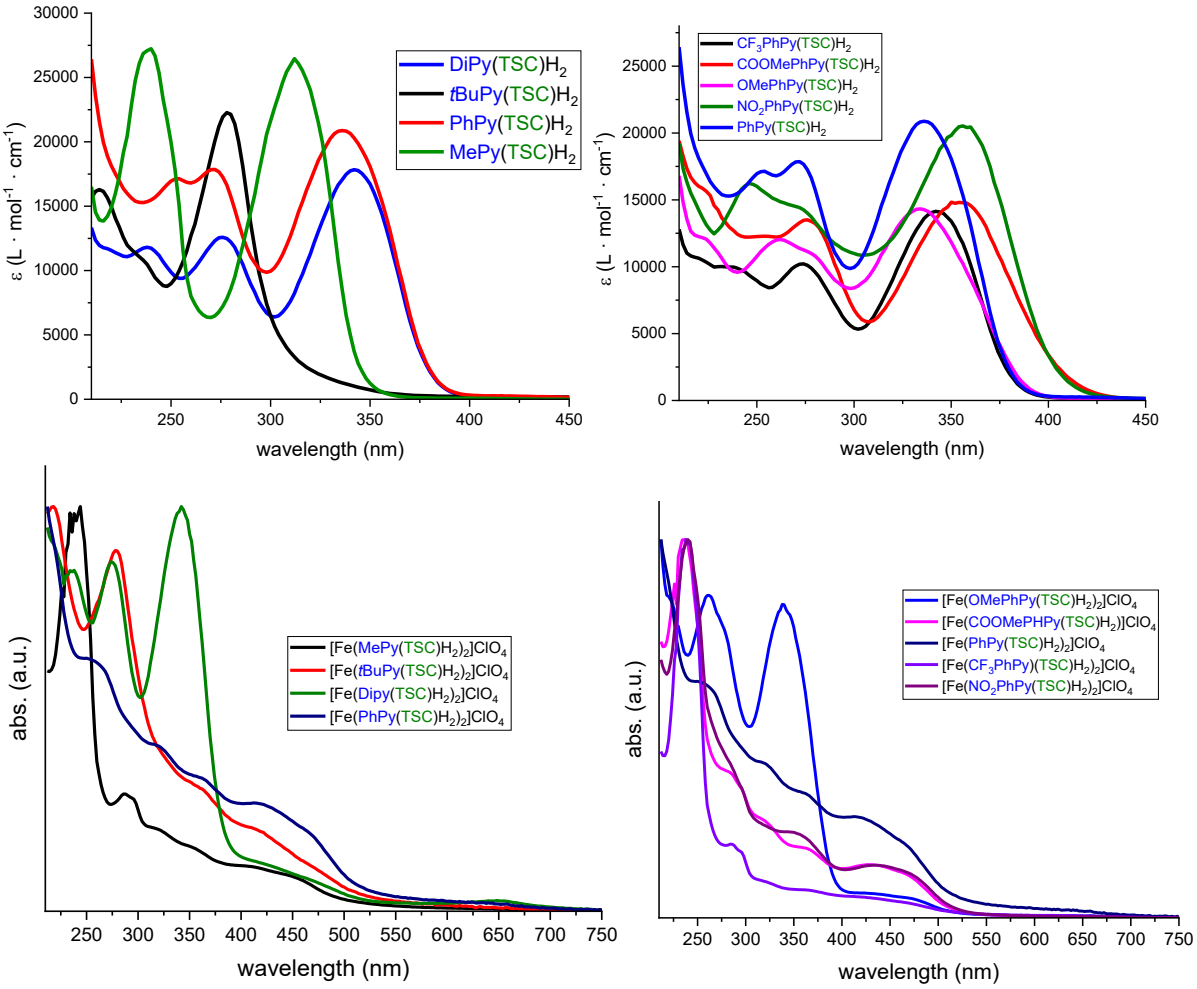


Figure 831. UV/Vis absorption spectra measured in MeCN. Up: α-pyridyl TSC; Down: the corresponding Fe(III) complexes.

7.3.5 UV/Vis absorption spectra of hexadentate TSCs

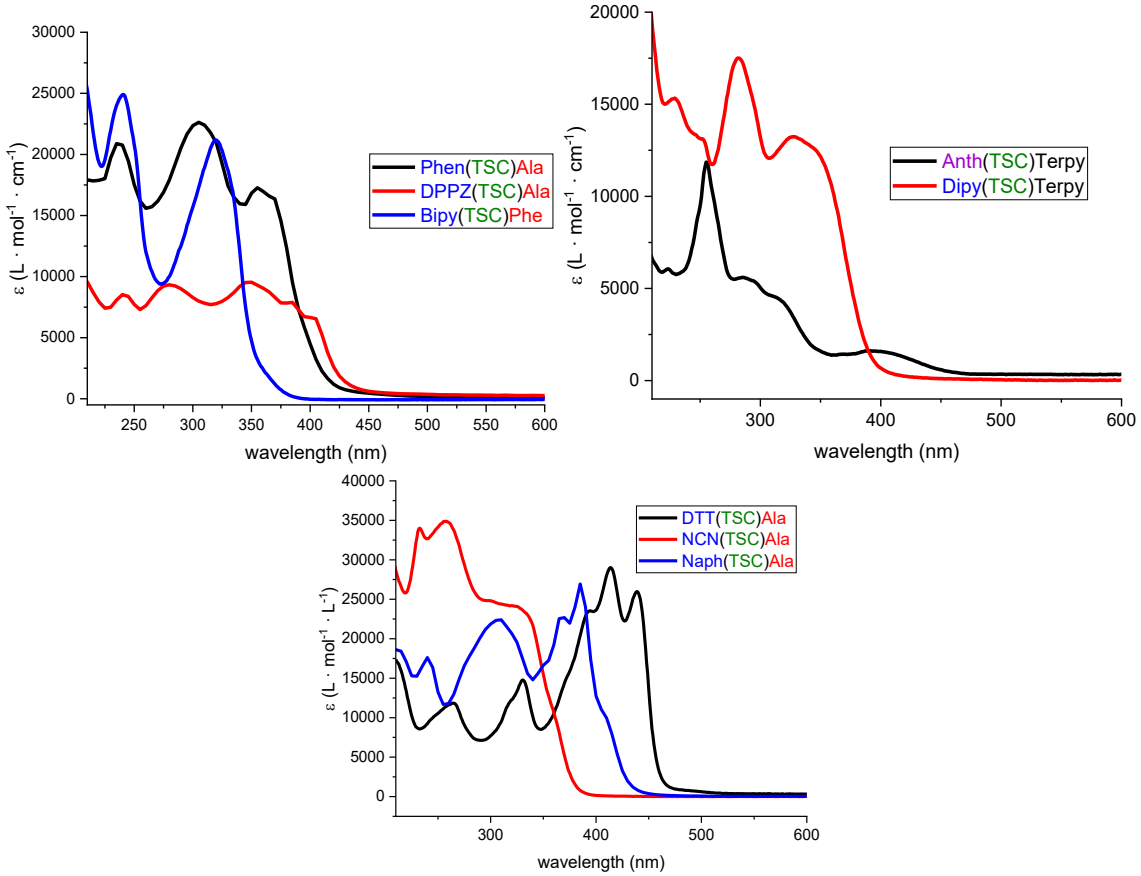


Figure 832. UV/Vis absorption spectra of hexadentate TSCs measured in MeCN.

7.4 Emission spectroscopy

7.4.1 UV/Vis emission spectroscopy of *N*4 functionalized TSC for nano -and bioconjugation

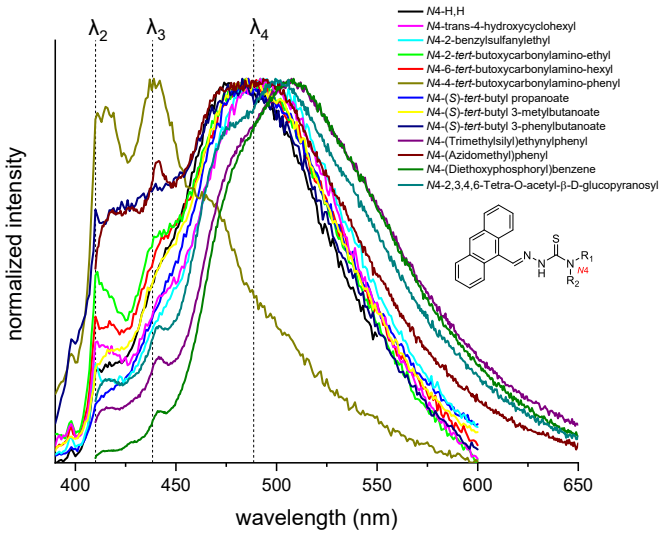


Figure 833. Normalized emission spectra of the 9-antraldehyde TSCs in MeCN upon irradiation at 365 nm. Concentrations are arbitrarily chosen.

7.4.2 UV/Vis emission spectroscopy of tagged TSCs

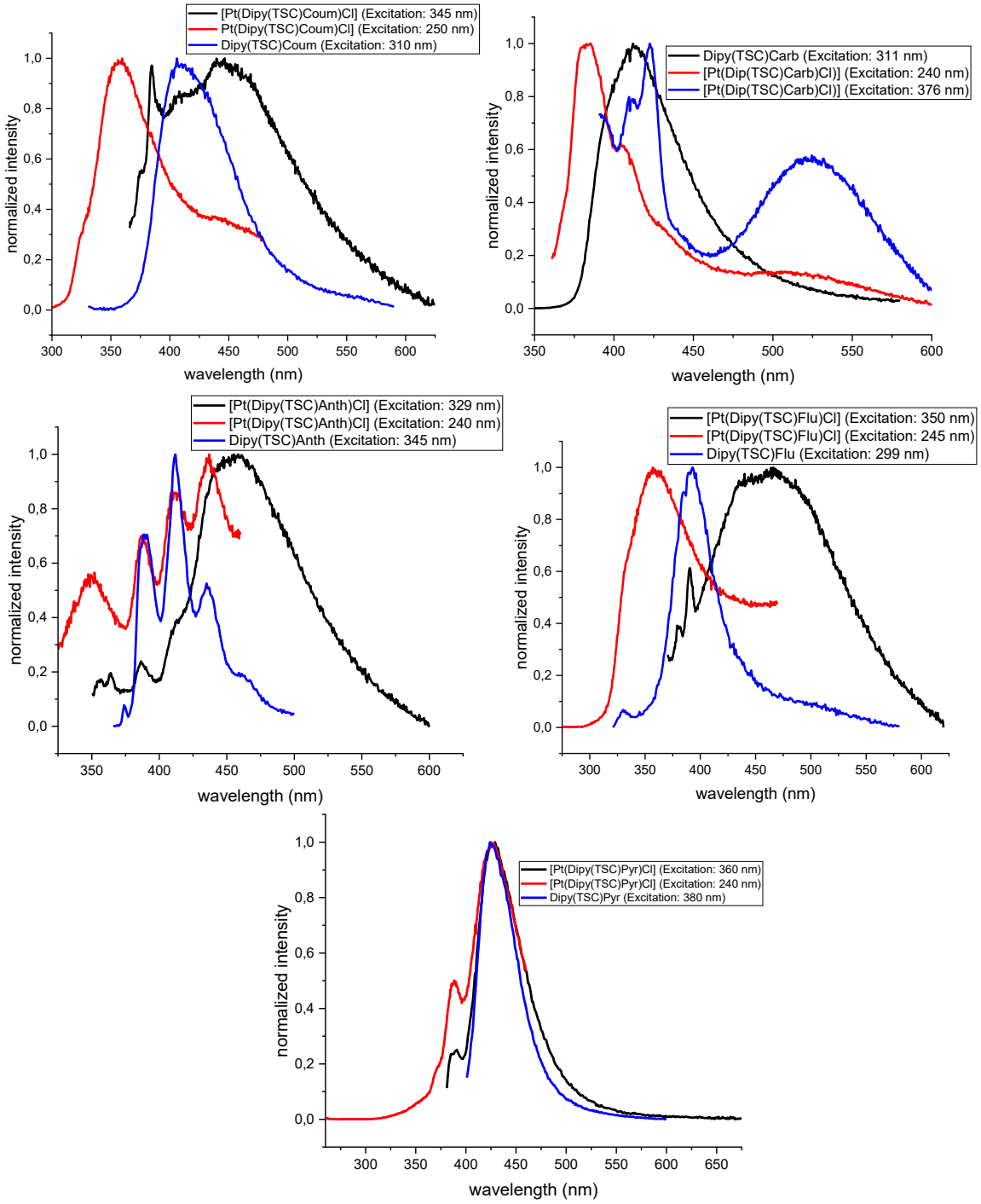


Figure 834. Normalized emission spectra of the tagged TSCs and their Pt(II) complex in MeCN at room temperature. The excitation wavelengths are given in the Figures. Concentrations are arbitrarily chosen.

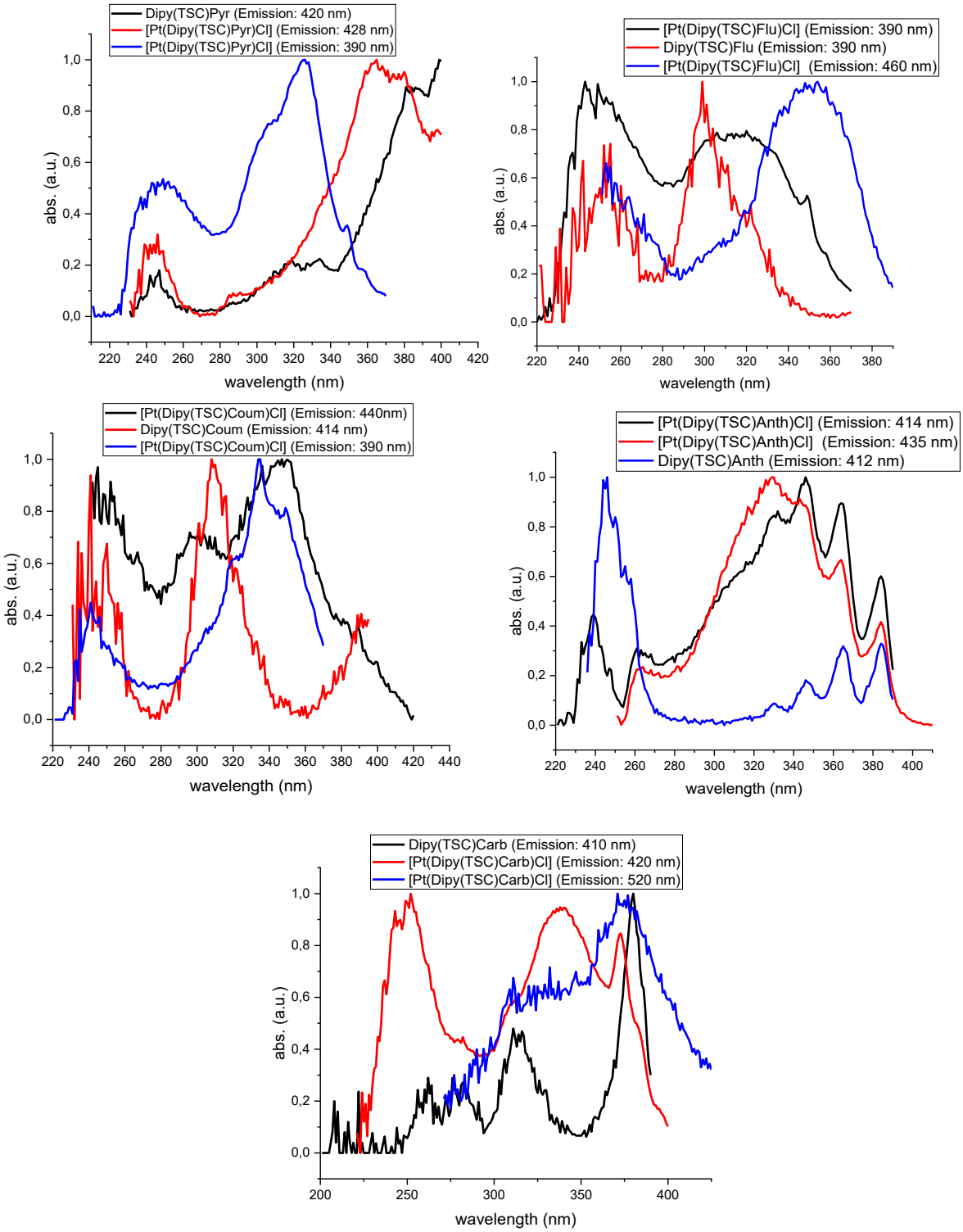


Figure 835. Normalized excitation spectra of the tagged TSCs and their Pt(II) complex in MeCN. The emission wavelengths are given in the Figures.

7.4.3 UV/Vis emission spectroscopy of hexadentate TSCs

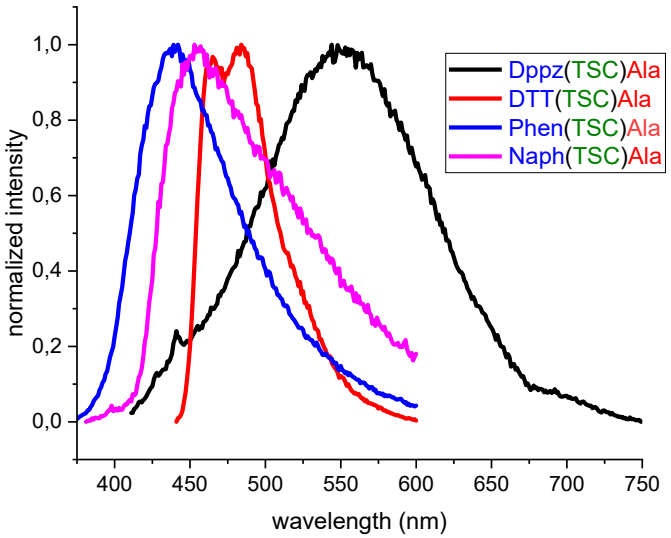


Figure 836. Normalized emission spectra of DPPZ(TSC)Ala (Excitation: 390 nm), DTT(TSC)Ala (Excitation: 420 nm), Phen(TSC)Ala (Excitation: 340 nm) and Naph(TSC)Ala (Ecitation: 365 nm) in MeCN at room temperature. Concentrations are arbitrarily chosen.

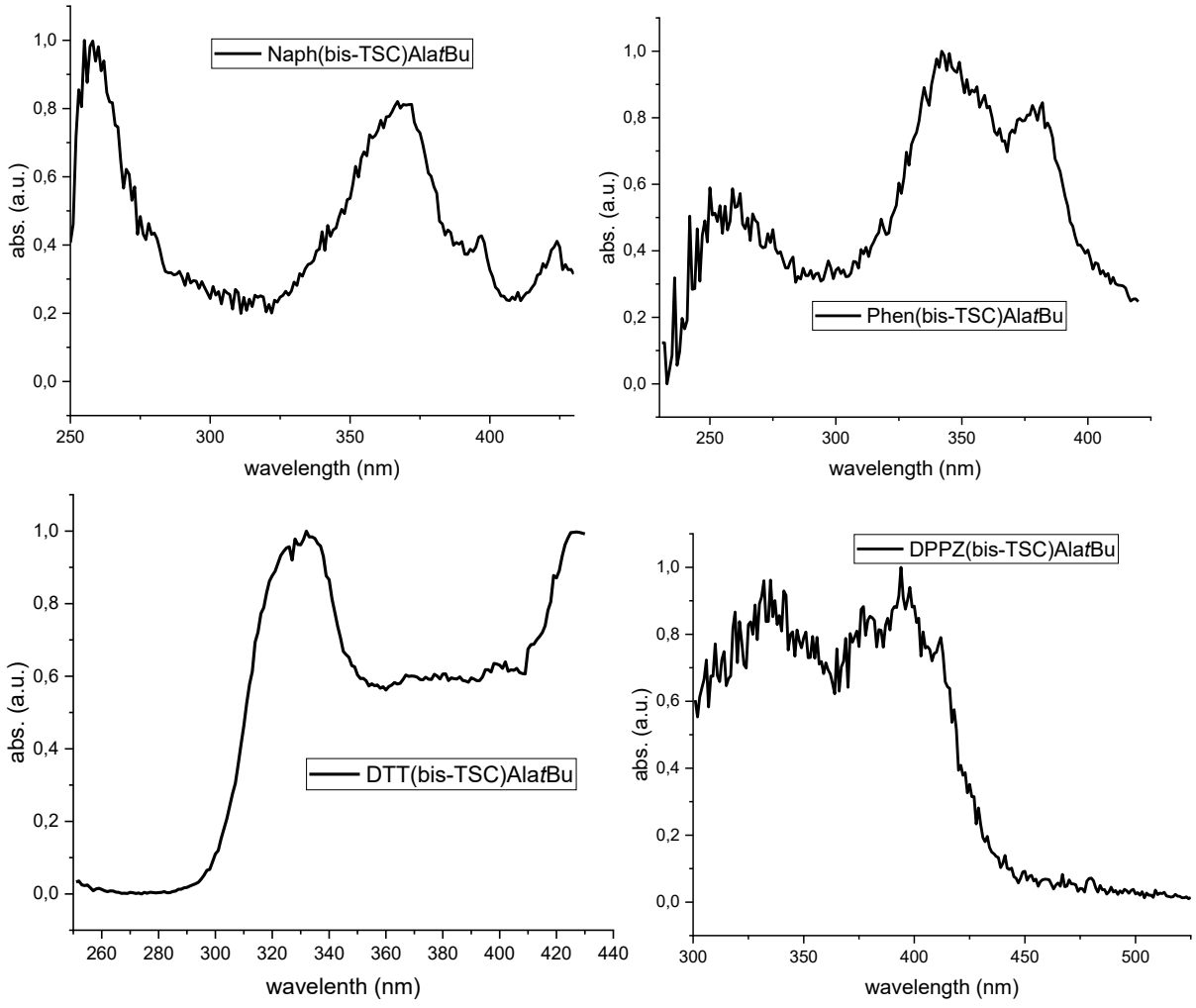


Figure 837. Normalized excitation spectra of DPPZ(TSC)Ala (Emission: 560 nm), DTT(TSC)Ala (Emission: 465 nm), Phen(TSC)Ala (Emission: 440 nm) and Naph(TSC)Ala (Emission: 450 nm) in MeCN at room temperature.

7.5 Cyclic voltammetry (CV)

7.5.1 CV of α-pyridyl TSCs and their Fe(III) complexes

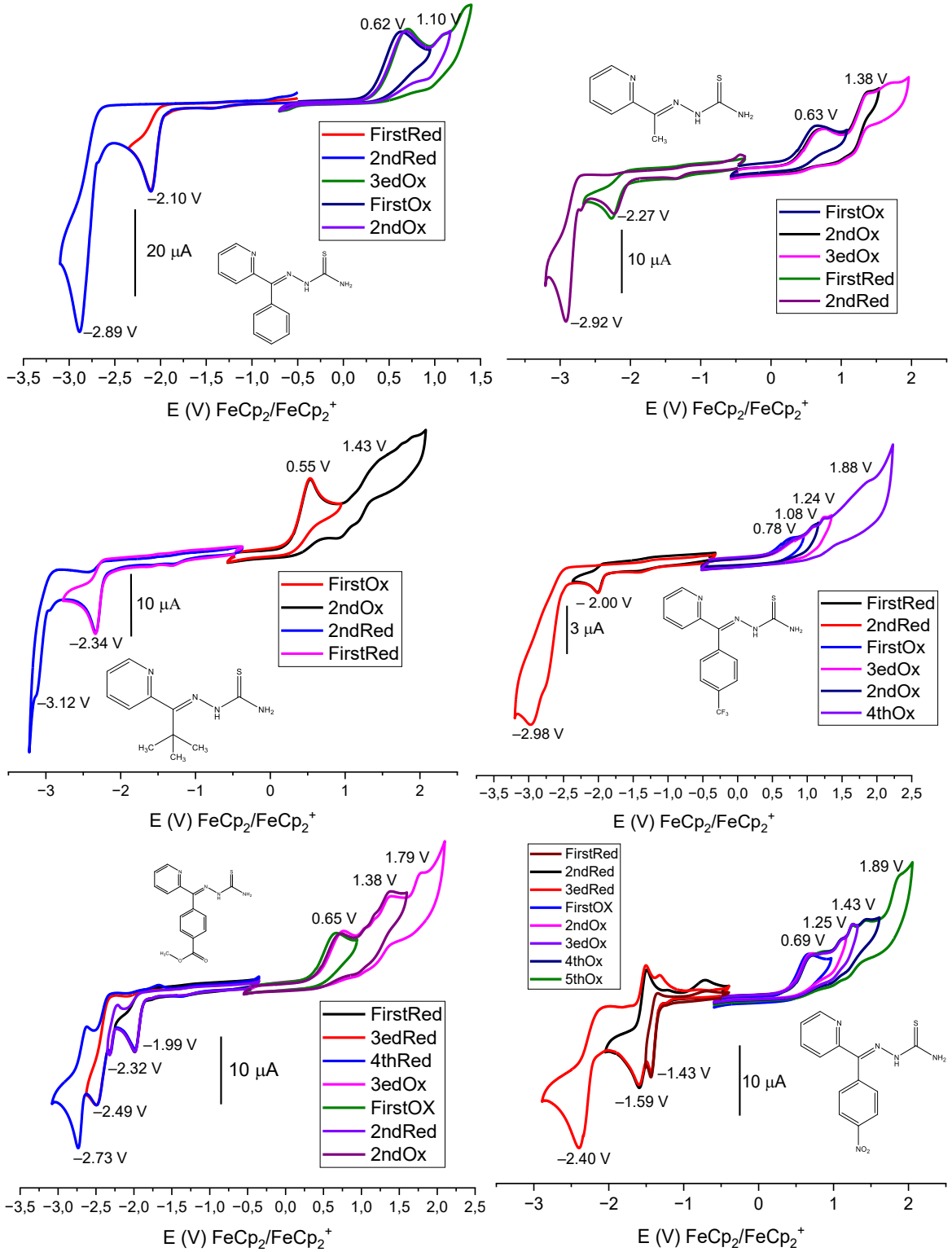


Figure 838. CVs of PhPy(TSC)H2, MePy(TSC)H2, *t*BuPy(TSC)H2, CF3PhPy(TSC)H2, COOMePhPy(TSC)H2 and NO2PhPy(TSC)H2 measured in 0.1 M solution of N(Bu)4PF6 in MeCN at a scan rate of 0.1 V/s.

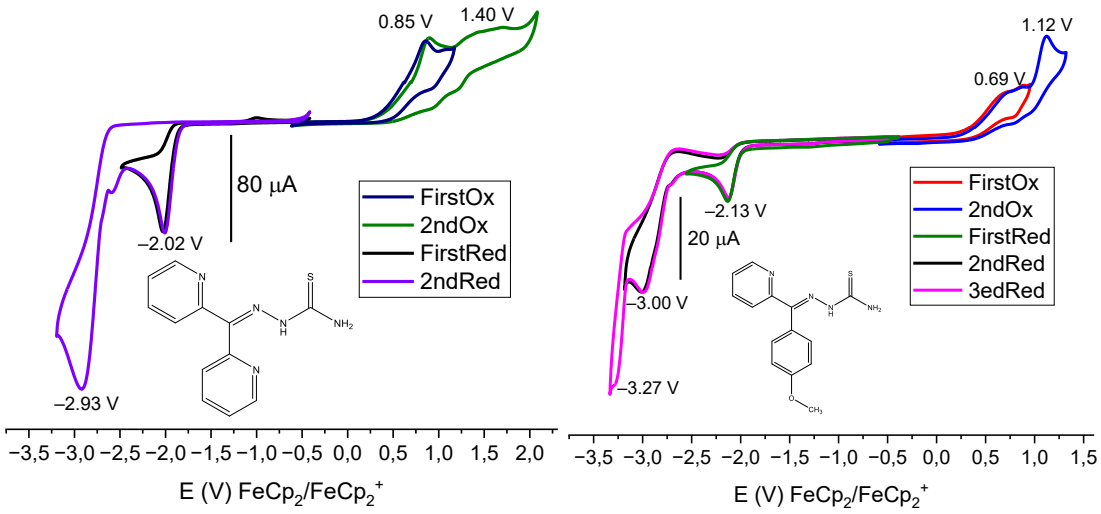


Figure 839. CVs of Dipy(TSC)H_2 and OMePhPy(TSC)H_2 measured in 0.1 M solution of $N(Bu)_4PF_6$ in MeCN at a scan rate of 0.1 V/s.

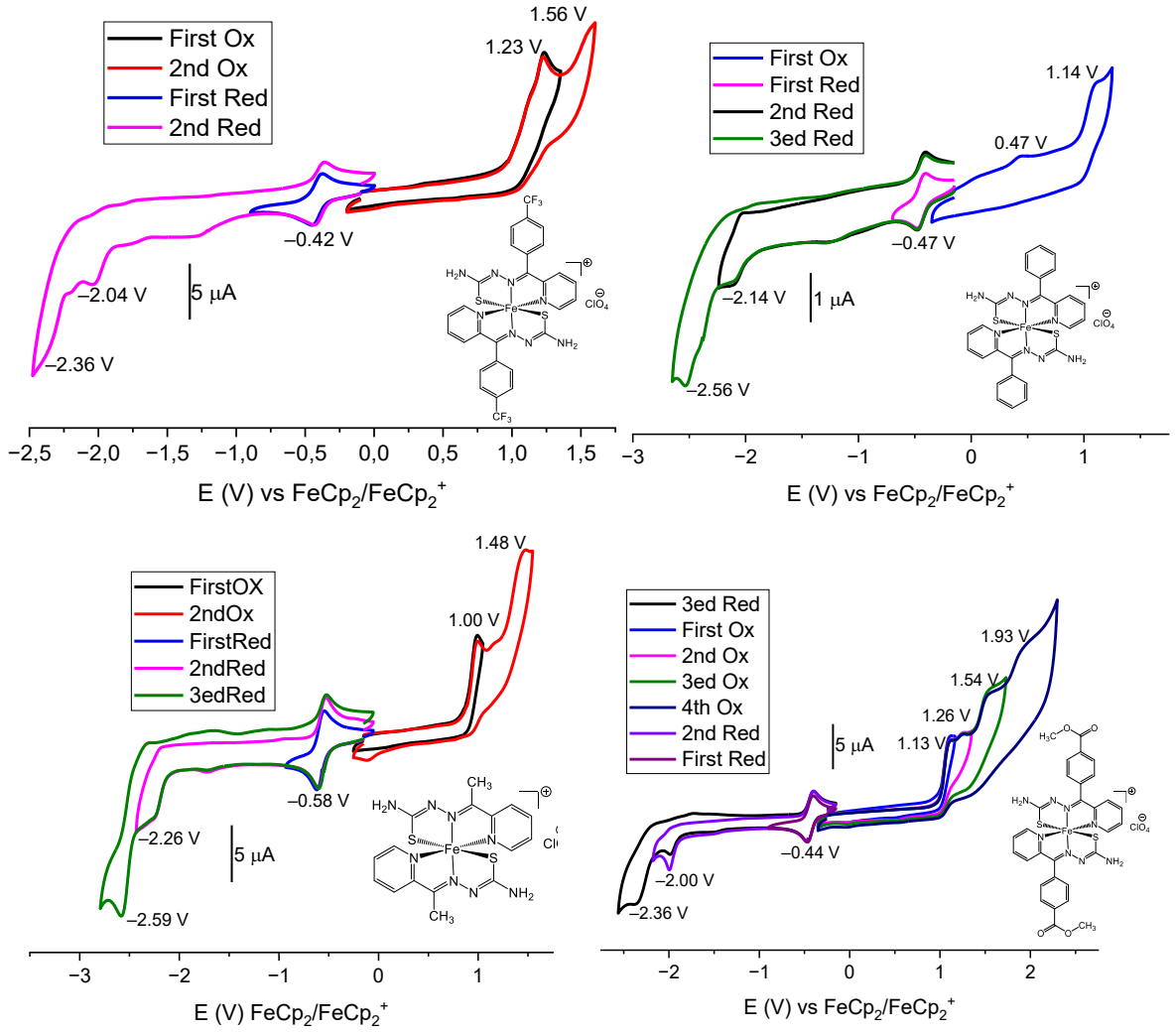


Figure 840. CVs of [Fe(CF_3PhPy(TSC)H_2)$_2$]ClO_4, [Fe(PhPy(TSC)H_2)$_2$]ClO_4, [Fe(MePy(TSC)H_2)$_2$]ClO_4 and [Fe(COOMePhPy(TSC)H_2)$_2$]ClO_4, measured in 0.1 M solution of $N(Bu)_4PF_6$ in MeCN at a scan rate of 0.1 V/s.

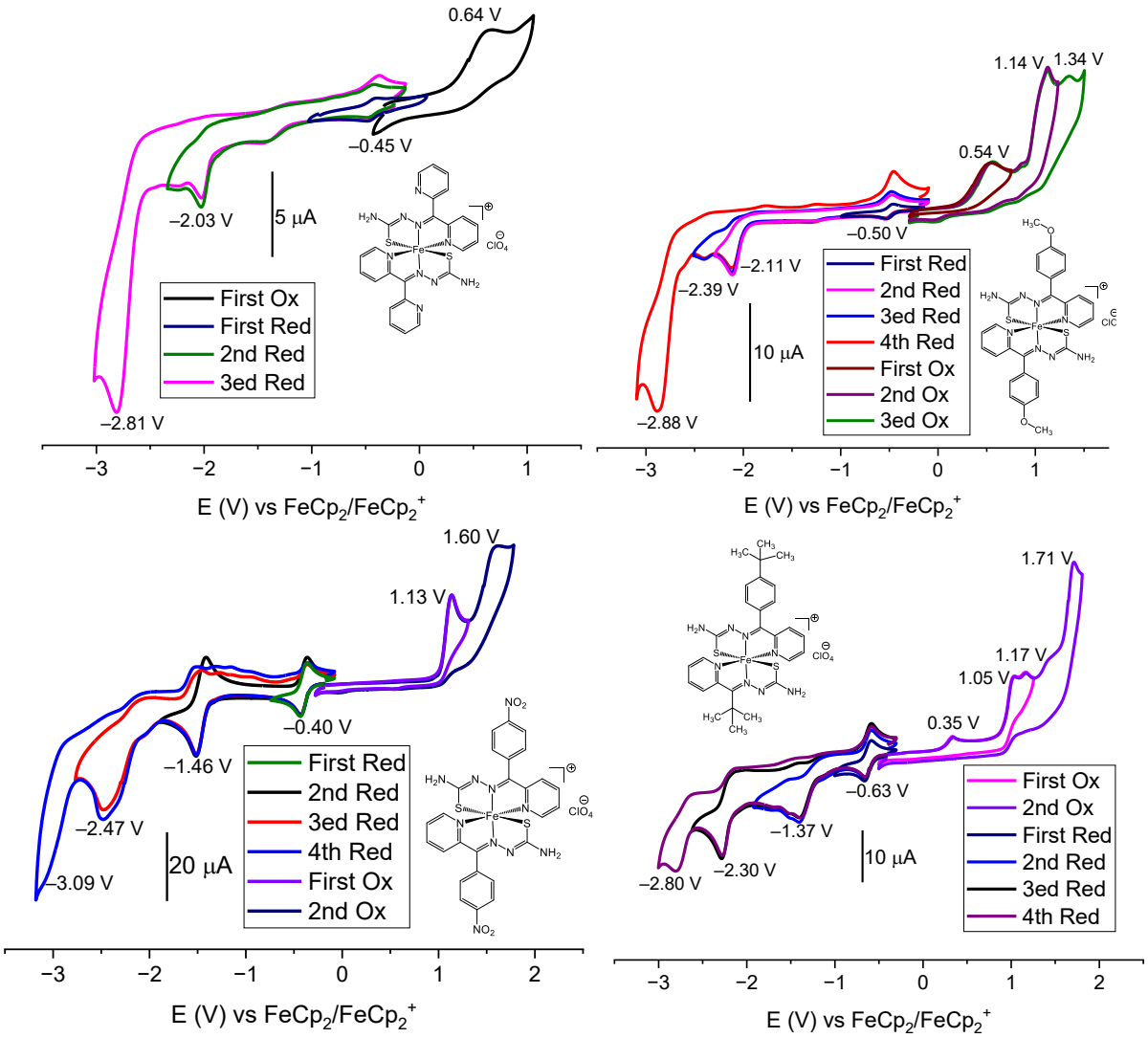


Figure 841. CVs of [Fe(Dipy(TSC)H$_2$)$_2$]ClO$_4$, [Fe(OMePhPy(TSC)H$_2$)$_2$]ClO$_4$, [Fe(NO$_2$PhPy(TSC)H$_2$)$_2$]ClO$_4$ and [Fe(*t*BuPy(TSC)H$_2$)$_2$]ClO$_4$, measured in 0.1 M solution of N(Bu)$_4$PF$_6$ in MeCN at a scan rate of 0.1 V/s.

7.5.2 CV of tagged TSCs and their Pt(II) complexes

In MeCN

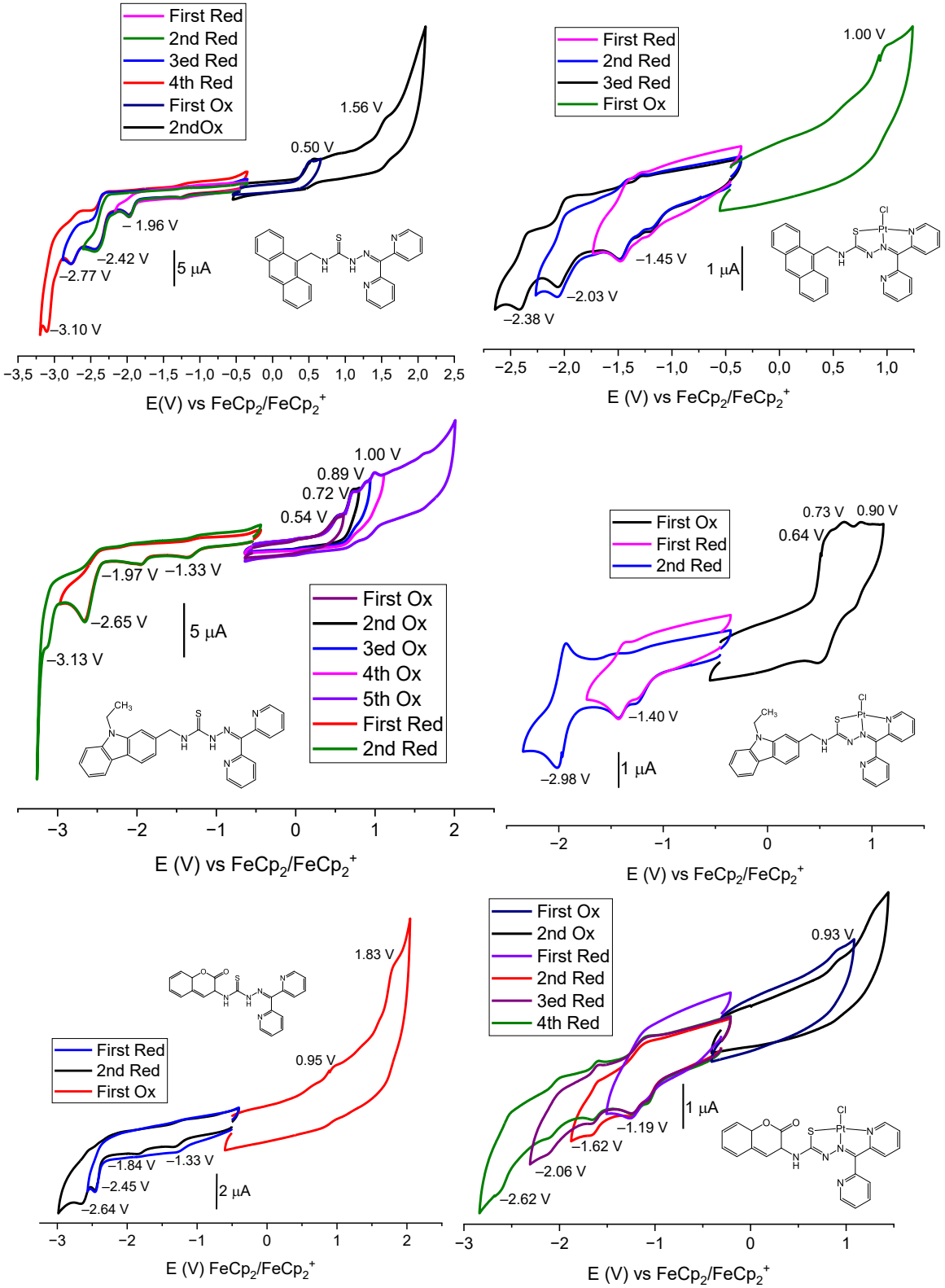


Figure 842. CVs of tagged TSCs (anthracene, carbazole, coumarin) and their corresponding Pt(II) complexes, measured in 0.1 M solution of $N(Bu)_4PF_6$ in MeCN at a scan rate of 0.1 V/s.

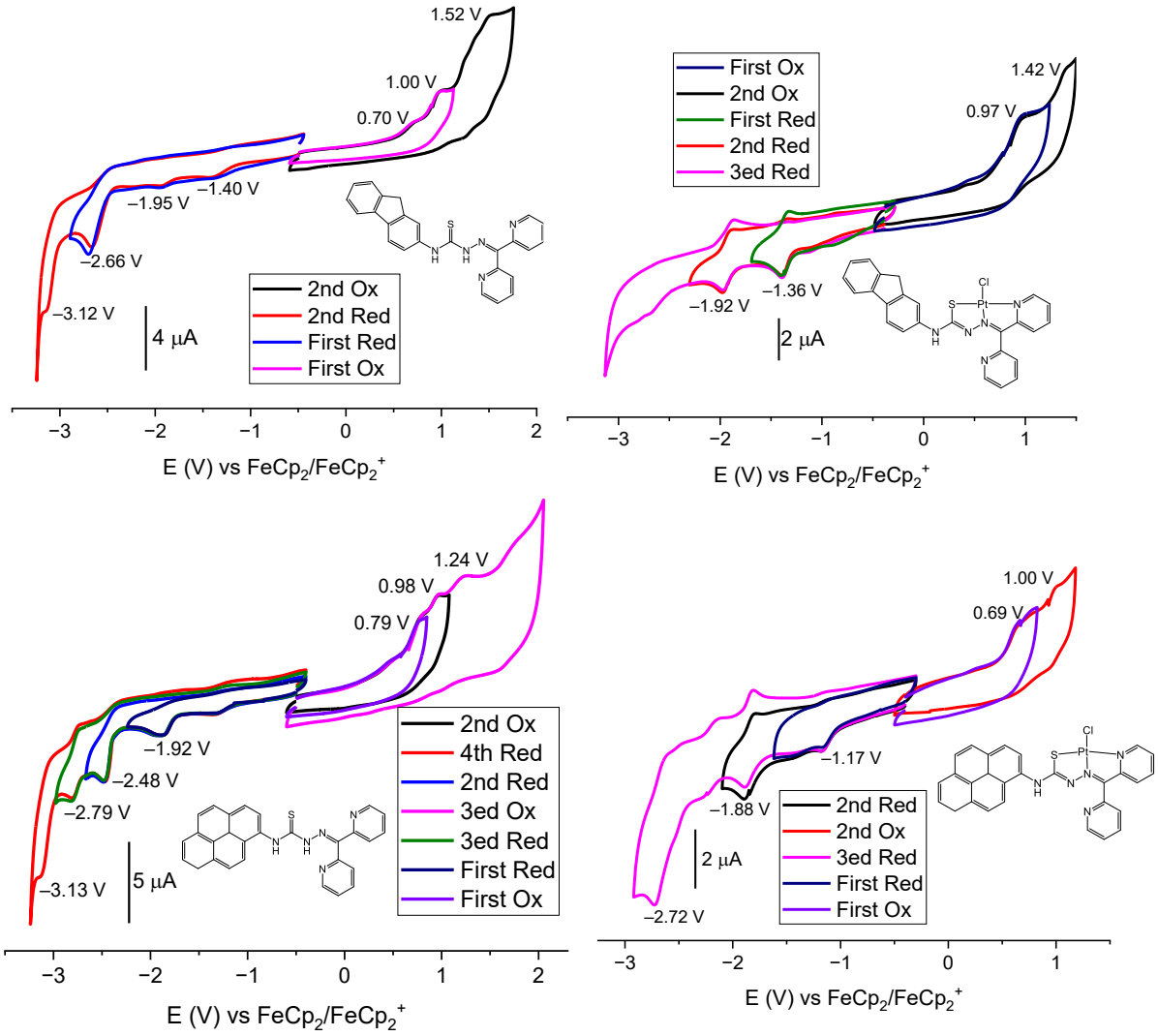


Figure 843. CVs of tagged TSCs (fluorene, pyrene) and their corresponding Pt(II) complexes, measured in 0.1 M solution of $N(Bu)_4PF_6$ in MeCN at a scan rate of 0.1 V/s.

Table 35. Redox potential of the tagged TSCs and the corresponding Pt(II) complexes in MeCN at 0.1 V/s.

	Red 4 (V)	Red 3 (V)	Red 2 (V)	Red 1 (V)	Ox 1 (V)	Ox 2 (V)	Ox 3 (V)	Ox 4 (V)
Dipy(TSC)Ant	–3.10	–2.77	–2.42	–1.96	0.50	1.56	-	-
[Pt(Dipy(TSC)Ant)Cl]	-	–2.38	–2.03	–1.45	1.00	-	-	-
Dipy(TSC)Carb	-	-	–3.13	–2.62	0.54	0.72	0.89	1.00
[Pt(Dipy(TSC)Carb)Cl]	-	-	–2.98	–1.40	0.64	0.73	0.90	-
Dipy(TSC)Coum	-	-	–2.64	–2.45	0.95	-	-	-
[Pt(Dipy(TSC)Coum)Cl]	–2.62	–2.06	–1.62	–1.19	0.93	-	-	-
Dipy(TSC)Flu	-	-	–3.12	–2.66	0.70	1.00	1.52	-
[Pt(Dipy(TSC)Flu)Cl]	-	-	–1.92	–1.36	0.97	1.42	-	-
Dipy(TSC)Pyr	–3.13	–2.79	–2.48	–1.92	0.79	0.98	1.24	-
[Pt(Dipy(TSC)Pyr)Cl]	-	–2.72	–1.88	–1.17	0.69	1.00	-	-

In THF:

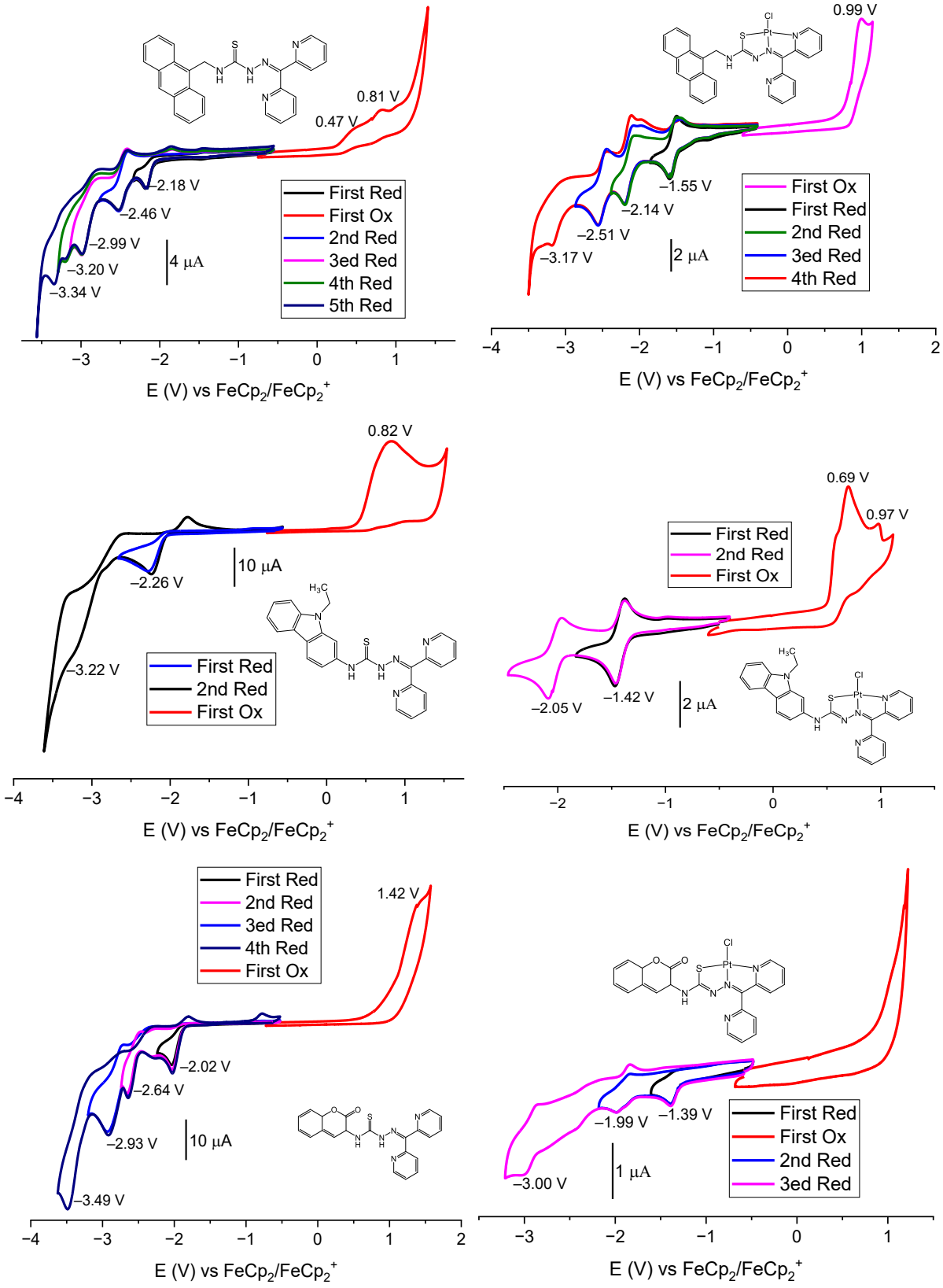


Figure 844. CVs of tagged TSCs (anthracene, carbazole, coumarin) and their corresponding Pt(II) complexes, measured in 0.1 M solution of $N(Bu)_4PF_6$ in THF at a scan rate of 0.1 V/s.

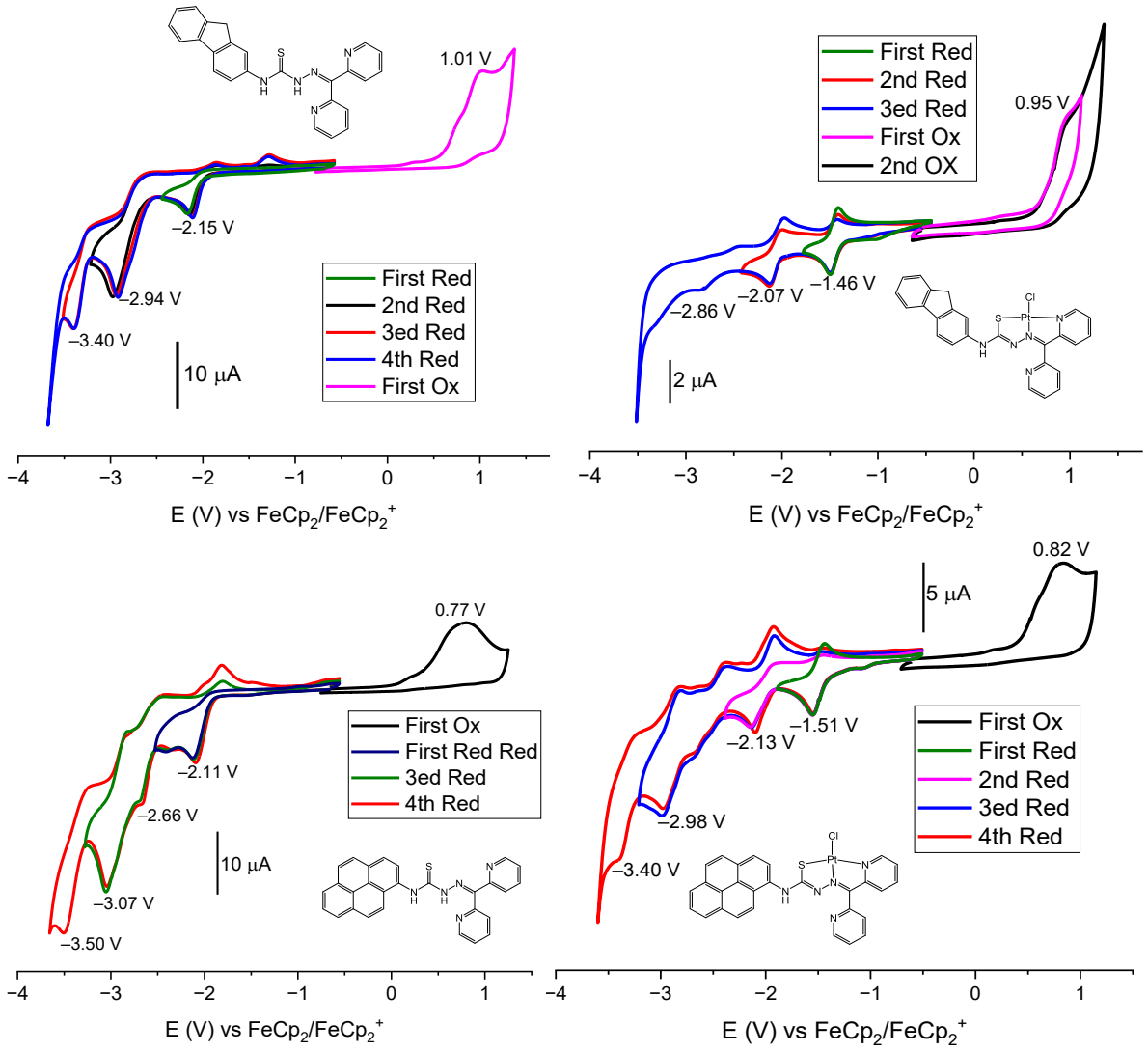


Figure 845. CVs of tagged TSCs (fluorene, pyrene) and their corresponding Pt(II) complexes, measured in 0.1 M solution of $N(Bu)_4PF_6$ in THF at a scan rate of 0.1 V/s.

Table 36. Redox potential of the tagged TSCs and the corresponding Pt(II) complexes in THF at 0.1 V/s.

	Red 5 (V)	Red 4 (V)	Red 3 (V)	Red 2 (V)	Red 1 (V)	Ox 1 (V)	Ox 2 (V)
Dipy(TSC)Ant	–3.34	–3.17	–2.51	–2.14	–1.55	0.99	-
[Pt(Dipy(TSC)Ant)Cl]	-	–3.20	–2.99	–2.46	–2.18	0.47	0.81
Dipy(TSC)Carb	-	-	-	–3.22	–2.26	0.82	-
[Pt(Dipy(TSC)Carb)Cl]	-	-	-	–2.05	–1.42	0.69	0.97
Dipy(TSC)Coum	-	–3.49	–2.93	–2.64	–2.02	1.42	-
[Pt(Dipy(TSC)Coum)Cl]	-	-	–3.00	–1.99	–1.39	-	-
Dipy(TSC)Flu	-	-	–3.40	–2.94	–2.15	1.01	-
[Pt(Dipy(TSC)Flu)Cl]	-	-	–2.86	–2.07	–1.46	0.95	-
Dipy(TSC)Pyr	-	–3.50	–3.07	–2.66	–2.11	0.77	-
[Pt(Dipy(TSC)Pyr)Cl]	-	–3.40	–2.98	–2.13	–1.51	0.82	-

7.5.3 CV of amphiphilic TSCs

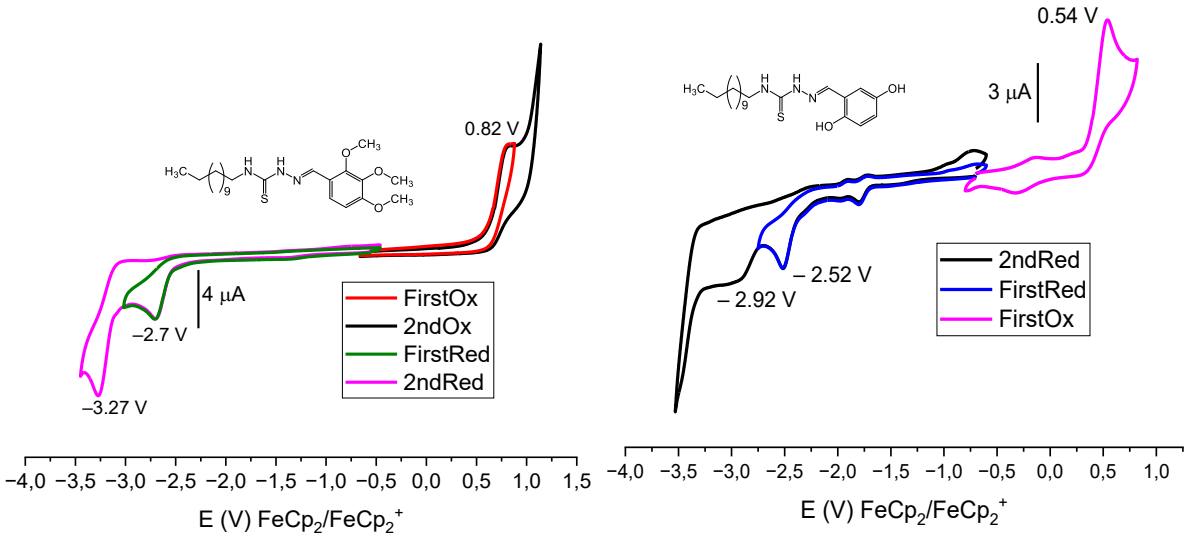


Figure 846. CVs of 1,2,4-OMePh(bis-TSC)Dode and 2,5-OHPh(bis-TSC)Dode measured in 0.1 M solution of $N(Bu)_4PF_6$ in THF at a scan rate of 0.1 V/s.

7.6 DLS/Zeta potential measurements

Name	Mean	Standard Deviation	RSD	Minimum	Maximum
Attenuator	6	-	-	6	6
Zeta Potential (mV)	-35,65	-	-	-35,65	-35,65
Zeta Deviation (mV)	5,583	-	-	5,583	5,583

Name	Mean	Standard Deviation	RSD	Minimum	Maximum
Attenuator	7	-	-	7	7
Intercept	0,9743	-	-	0,9743	0,9743
Z-Average (nm)	215	-	-	215	215
Polydispersity Index (PI)	0,1817	-	-	0,1817	0,1817
Peak 1 Mean by Intensity ordered by area (nm)	202,6	-	-	202,6	202,6
Peak 1 Area by Intensity ordered by area (%)	100	-	-	100	100
Peak 1 Mean by Volume ordered by area (nm)	206,1	-	-	206,1	206,1
Peak 1 Area by Volume ordered by area (%)	100	-	-	100	100
Peak 1 Mean by Number ordered by area (nm)	178,5	-	-	178,5	178,5
Peak 1 Area by Number ordered by area (%)	100	-	-	100	100

Figure 847. Zeta and DLS measurement of SiO_2 in water at pH 7 and room temperature.

Name	Mean	Standard Deviation	RSD	Minimum	Maximum
Z-Average (nm)	230,1	-	-	230,1	230,1
Polydispersity Index (PI)	0,3492	-	-	0,3492	0,3492
Peak 1 Mean by Intensity ordered by area (nm)	172,1	-	-	172,1	172,1
Peak 1 Area by Intensity ordered by area (%)	100	-	-	100	100

Name	Mean	Standard Deviation	RSD	Minimum	Maximum
Zeta Potential (mV)	51,16	-	-	51,16	51,16
Conductivity (mS/cm)	0,02012	-	-	0,02012	0,02012
Wall Zeta Potential (mV)	-4,671	-	-	-4,671	-4,671
Quality Factor	6,595	-	-	6,595	6,595
Zeta Peak 1 Mean (mV)	51,16	-	-	51,16	51,16

Figure 848. Zeta and DLS measurement of SiO_2@APTMS in water at pH 7 and room temperature.

Name	Mean	Standard Deviation	RSD	Minimum	Maximum
Z-Average (nm)	141,4	-	-	141,4	141,4
Polydispersity Index (PI)	0,1574	-	-	0,1574	0,1574
Peak 1 Mean by Intensity ordered by area (nm)	146,9	-	-	146,9	146,9
Peak 1 Area by Intensity ordered by area (%)	100	-	-	100	100

Name	Mean	Standard Deviation	RSD	Minimum	Maximum
Zeta Potential (mV)	44,48	-	-	44,48	44,48
Conductivity (mS/cm)	0,02079	-	-	0,02079	0,02079
Wall Zeta Potential (mV)	35,59	-	-	35,59	35,59
Quality Factor	7,25	-	-	7,25	7,25
Zeta Peak 1 Mean (mV)	44,48	-	-	44,48	44,48

Figure 849. Zeta and DLS measurement of SiO_2@APTMS@GA in water at pH 7 and room temperature.

Name	Mean	Standard Deviation	RSD	Minimum	Maximum
Z-Average (nm)	261,2	-	-	261,2	261,2
Polydispersity Index (PI)	0,3661	-	-	0,3661	0,3661
Peak 1 Mean by Intensity ordered by area (nm)	258,9	-	-	258,9	258,9
Peak 1 Area by Intensity ordered by area (%)	100	-	-	100	100

Name	Mean	Standard Deviation	RSD	Minimum	Maximum
Zeta Potential (mV)	22,94	-	-	22,94	22,94
Conductivity (mS/cm)	0,03455	-	-	0,03455	0,03455
Wall Zeta Potential (mV)	14,28	-	-	14,28	14,28
Quality Factor	2,933	-	-	2,933	2,933
Zeta Peak 1 Mean (mV)	22,94	-	-	22,94	22,94

Figure 850. Zeta and DLS measurement of SiO_2@APTMS@GA@ThioAnt in water at pH 7 and room temperature.

Name	Mean	Standard Deviation	RSD	Minimum	Maximum
Attenuator	6	-	-	6	6
Intercept	0,9744	-	-	0,9744	0,9744
Z-Average (nm)	289,4	-	-	289,4	289,4
Polydispersity Index (PI)	0,6565	-	-	0,6565	0,6565
Peak 1 Mean by Intensity ordered by area (nm)	509,3	-	-	509,3	509,3
Peak 1 Area by Intensity ordered by area (%)	80,88	-	-	80,88	80,88
Peak 2 Mean by Intensity ordered by area (nm)	58,77	-	-	58,77	58,77
Peak 2 Area by Intensity ordered by area (%)	19,12	-	-	19,12	19,12
Peak 1 Mean by Volume ordered by area (nm)	557,1	-	-	557,1	557,1
Peak 1 Area by Volume ordered by area (%)	55,21	-	-	55,21	55,21
Peak 2 Mean by Volume ordered by area (nm)	57,19	-	-	57,19	57,19
Peak 2 Area by Volume ordered by area (%)	44,79	-	-	44,79	44,79
Peak 1 Mean by Number ordered by area (nm)	469,1	-	-	469,1	469,1
Peak 1 Area by Number ordered by area (%)	0,1759	-	-	0,1759	0,1759
Peak 2 Mean by Number ordered by area (nm)	55,39	-	-	55,39	55,39
Peak 2 Area by Number ordered by area (%)	99,82	-	-	99,82	99,82

Name	Mean	Standard Deviation	RSD	Minimum	Maximum
Attenuator	4	-	-	4	4
Zeta Potential (mV)	20,61	-	-	20,61	20,61
Zeta Deviation (mV)	4,046	-	-	4,046	4,046

Figure 851. Zeta and DLS measurement of SiO_2@APTMS@Dipy(TSC)PhNCS in water at pH 7 and room temperature.

Name	Mean	Standard Deviation	RSD	Minimum	Maximum
Z-Average (nm)	537	-	-	537	537
Polydispersity Index (PI)	0.7177	-	-	0.7177	0.7177
Peak 1 Mean by Intensity ordered by area (nm)	1091	-	-	1091	1091
Peak 1 Area by Intensity ordered by area (%)	49.97	-	-	49.97	49.97
Peak 2 Mean by Intensity ordered by area (nm)	262.8	-	-	262.8	262.8
Peak 2 Area by Intensity ordered by area (%)	39.82	-	-	39.82	39.82

Name	Mean	Standard Deviation	RSD	Minimum	Maximum
Attenuator	4	-	-	4	4
Zeta Potential (mV)	-10,02	-	-	-10,02	-10,02
Zeta Deviation (mV)	3,339	-	-	3,339	3,339

Figure 852. Zeta and DLS measurement of TiO_2 in water at pH 7 and room temperature.

Name	Mean	Standard Deviation	RSD	Minimum	Maximum
Z-Average (nm)	275.4	-	-	275.4	275.4
Polydispersity Index (PI)	0.252	-	-	0.252	0.252
Peak 1 Mean by Intensity ordered by area (nm)	311.7	-	-	311.7	311.7
Peak 1 Area by Intensity ordered by area (%)	98.25	-	-	98.25	98.25
Peak 2 Mean by Intensity ordered by area (nm)	5149	-	-	5149	5149
Peak 2 Area by Intensity ordered by area (%)	1.746	-	-	1.746	1.746

Name	Mean	Standard Deviation	RSD	Minimum	Maximum
Zeta Potential (mV)	-35.73	-	-	-35.73	-35.73
Conductivity (mS/cm)	0.006474	-	-	0.006474	0.006474
Wall Zeta Potential (mV)	-36.37	-	-	-36.37	-36.37
Quality Factor	8.621	-	-	8.621	8.621
Zeta Peak 1 Mean (mV)	-35.73	-	-	-35.73	-35.73

Figure 853. Zeta and DLS measurement of TiO_2@Ant(TSC)PhPO$(OH)_2$ in water at pH 7 and room temperature.

Name	Mean	Standard Deviation	RSD	Minimum	Maximum
Z-Average (nm)	185	-	-	185	185
Polydispersity Index (PI)	0.2666	-	-	0.2666	0.2666
Peak 1 Mean by Intensity ordered by area (nm)	230.8	-	-	230.8	230.8
Peak 1 Area by Intensity ordered by area (%)	94.88	-	-	94.88	94.88
Peak 2 Mean by Intensity ordered by area (nm)	3930	-	-	3930	3930
Peak 2 Area by Intensity ordered by area (%)	5.12	-	-	5.12	5.12

Name	Mean	Standard Deviation	RSD	Minimum	Maximum
Zeta Potential (mV)	-19.4	-	-	-19.4	-19.4
Conductivity (mS/cm)	0.00526	-	-	0.00526	0.00526
Wall Zeta Potential (mV)	-12.18	-	-	-12.18	-12.18
Quality Factor	7.505	-	-	7.505	7.505
Zeta Peak 1 Mean (mV)	-19.4	-	-	-19.4	-19.4

Figure 854. Zeta and DLS measurement of TiO_2@Dipy(TSC)PhPO$(OH)_2$ in water at pH 7 and room temperature.

7.7 EDX/SEM measurements

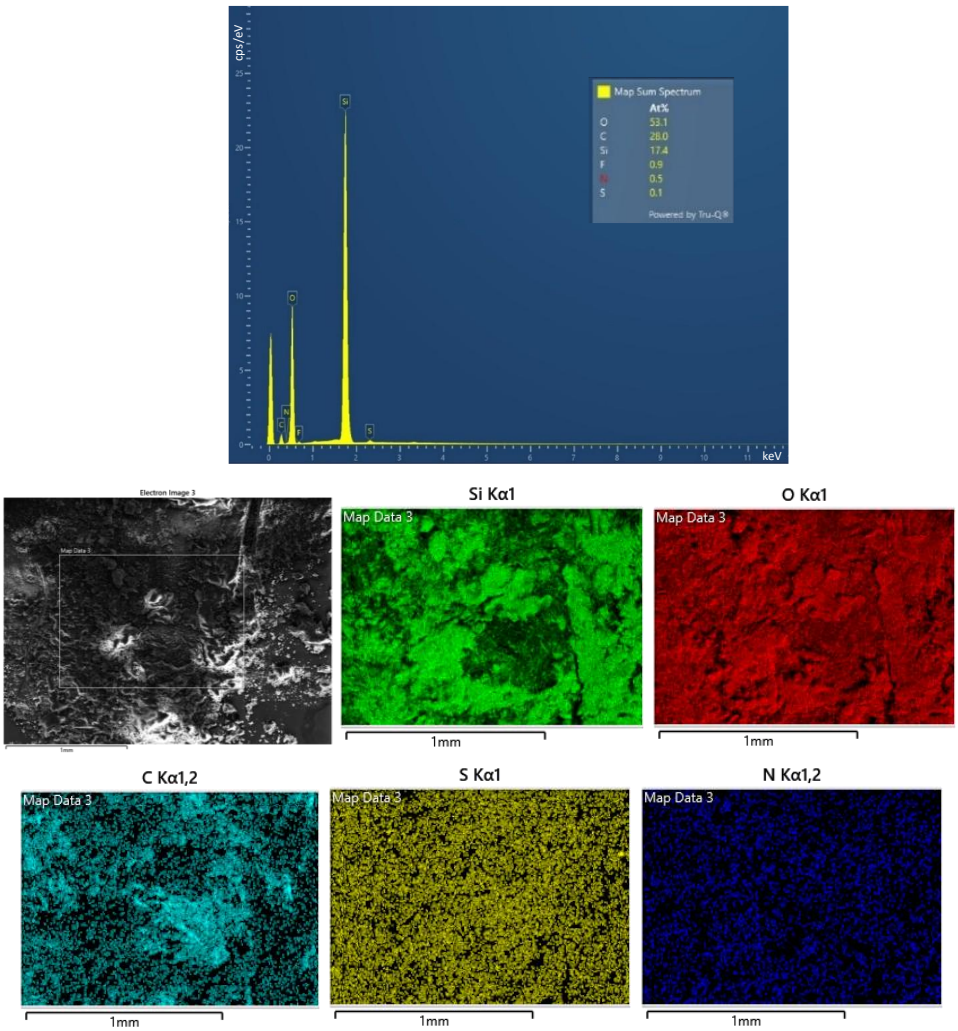


Figure 855. EDX spectrum and the corresponding EDX elemental mapping of SiO_2@APTMS@Dipy(TSC)PhNCS. The particles were spread onto a carbon tape, and the measurement was performed on large nanoaggregates to get a reliable intensity of the elements.

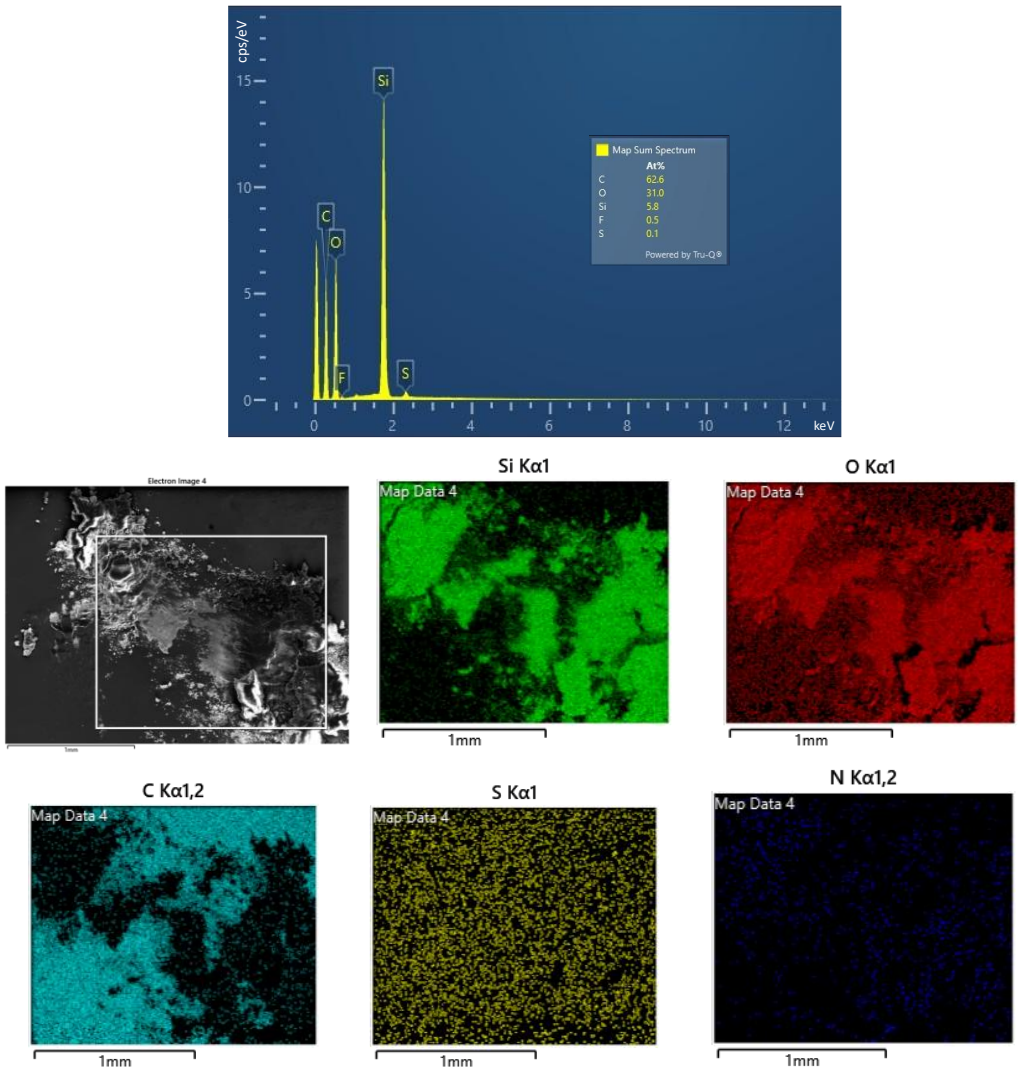


Figure 856. EDX spectrum and the corresponding EDX elemental mapping of SiO_2@APTMS@GA@AntThio. The particles were spread onto a carbon tape, and the measurement was performed on large nanoaggregates to get a reliable intensity of the elements.

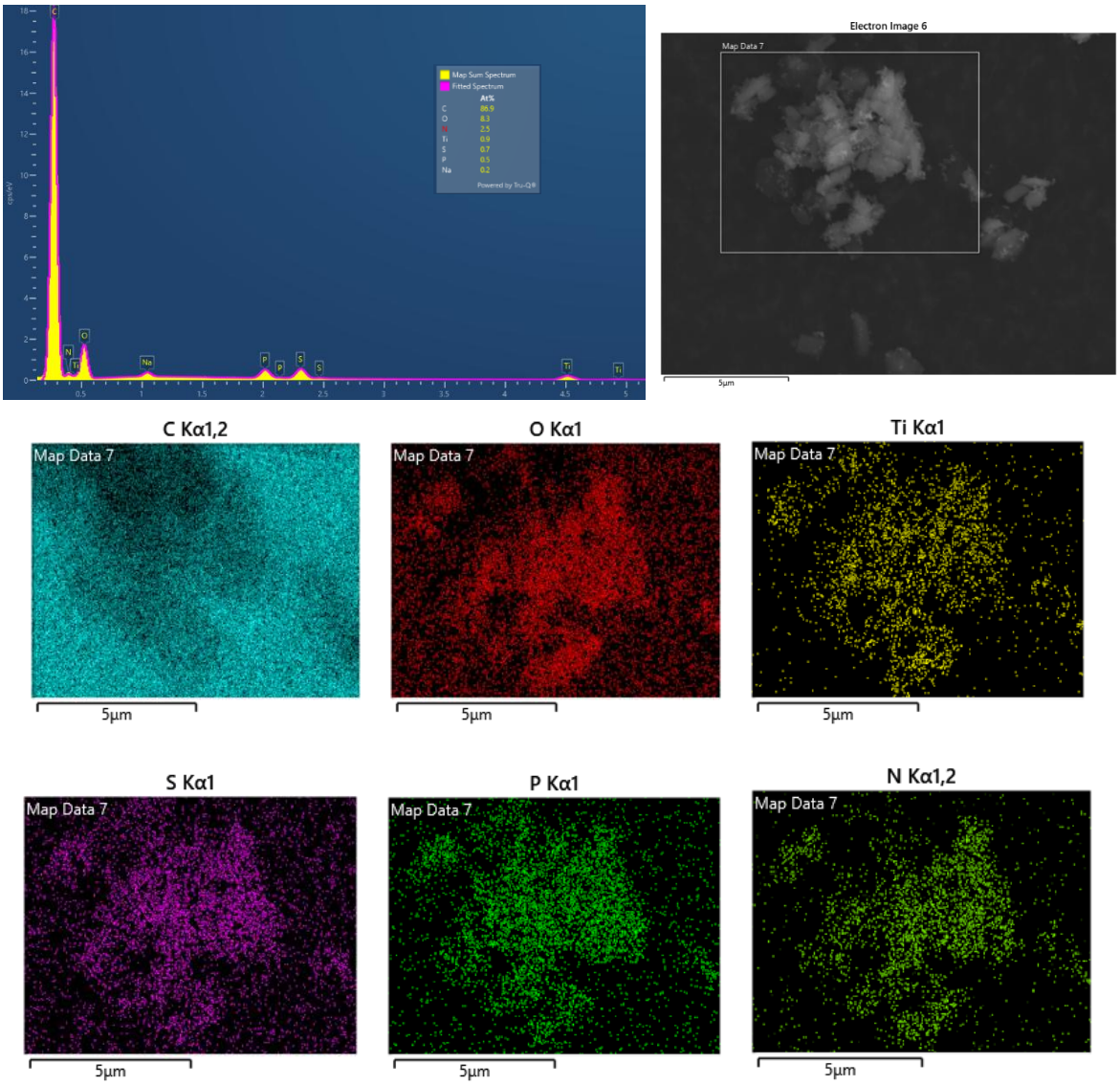


Figure 857. EDX spectrum and the corresponding EDX elemental mapping of TiO_2@Dipy(TSC)PhPO(OH)$_2$. The particles were spread onto a carbon tape, and the measurement was performed on large nanoaggregates to get a reliable intensity of the elements.

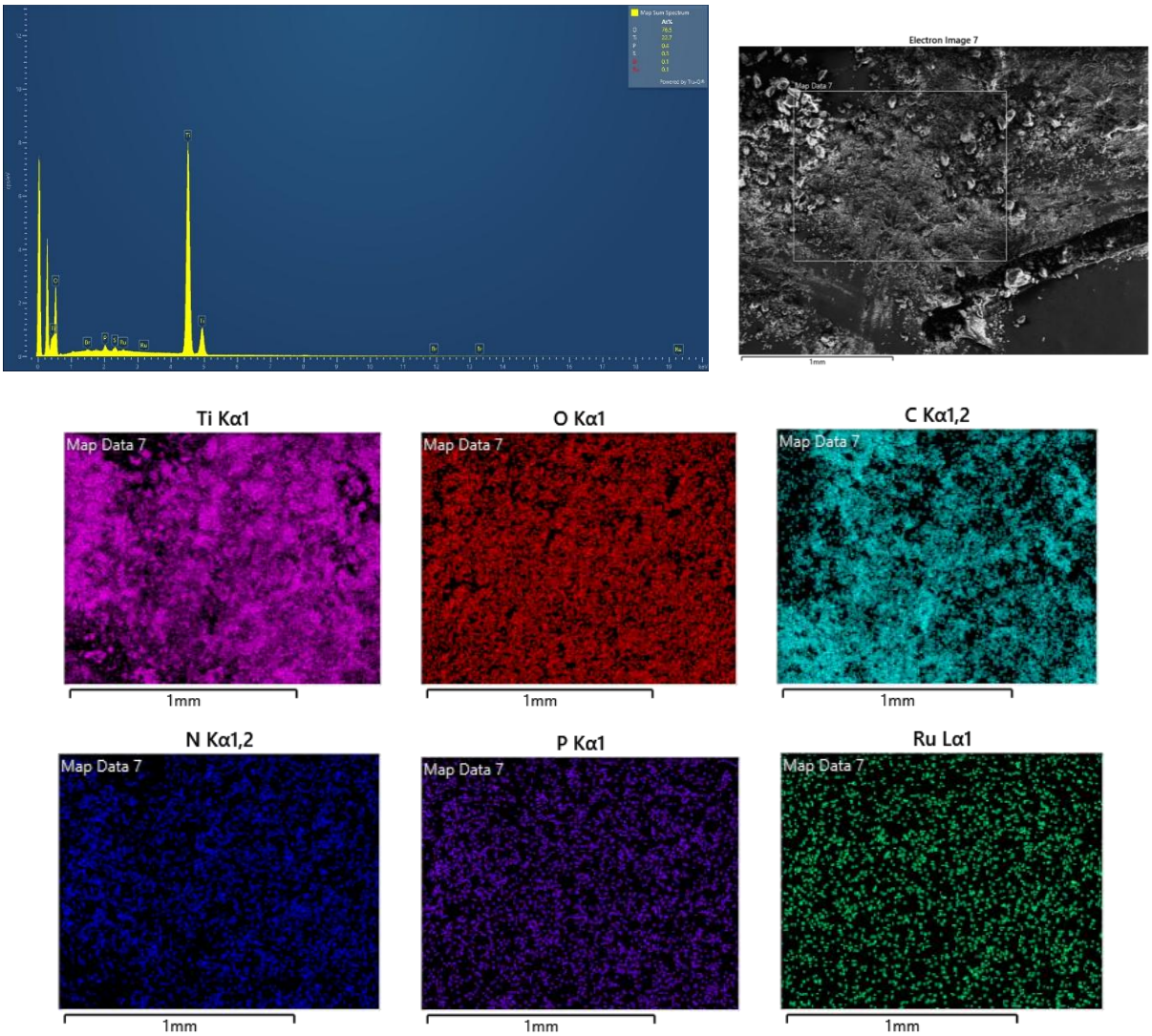


Figure 858. EDX spectrum and the corresponding EDX elemental mapping of TiO_2@[Ru(bpy)$_3$]. The particles were spread onto a carbon tape, and the measurement was performed on large nanoaggregates to get a reliable intensity of the elements.

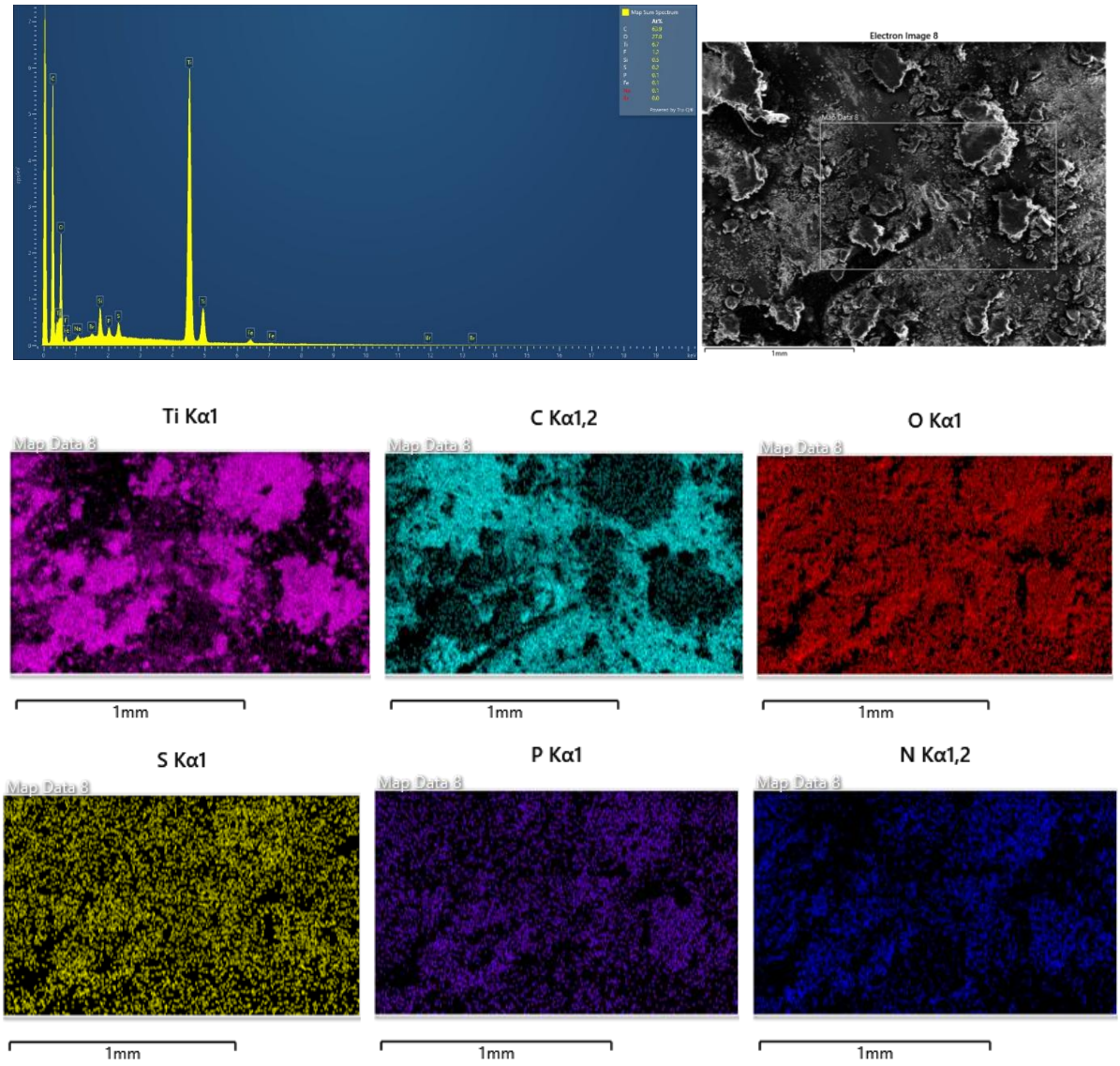


Figure 859. EDX spectrum and the corresponding EDX elemental mapping of TiO_2@[$Fe(TSC)_2$]. The particles were spread onto a carbon tape, and the measurement was performed on large nanoaggregates to get a reliable intensity of the elements.

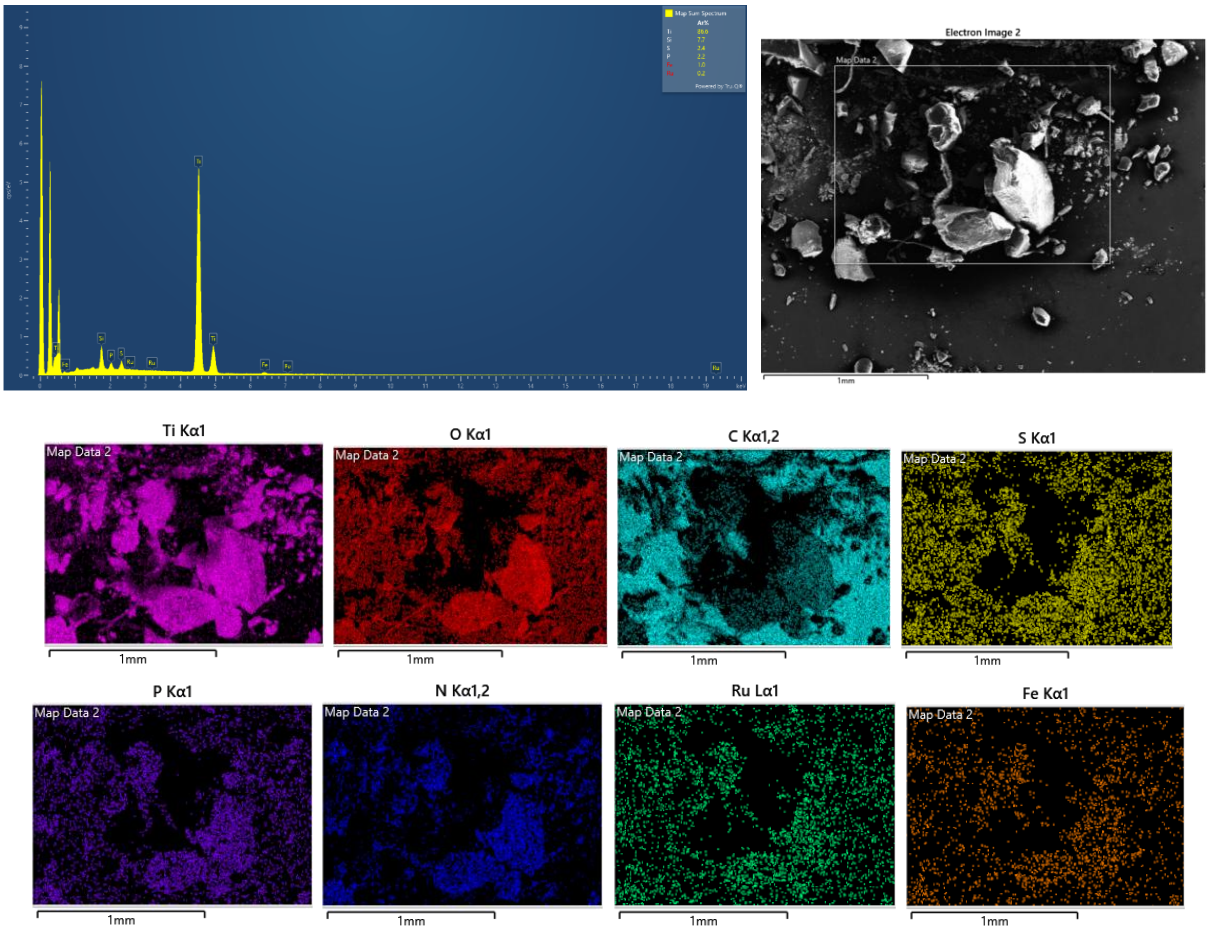


Figure 860. EDX spectrum and the corresponding EDX elemental mapping of TiO_2@[Ru(bpy)$_3$]/[Fe(TSC)$_2$]. The particles were spread onto a carbon tape, and the measurement was performed on large nanoaggregates to get a reliable intensity of the elements.